Selma Supek
Cheryl J. Aine *Editors*

Magnetoencephalography

From Signals to Dynamic Cortical Networks

Springer

Magnetoencephalography

Selma Supek · Cheryl J. Aine
Editors

Magnetoencephalography

From Signals to Dynamic Cortical Networks

Springer

Editors
Selma Supek
Department of Physics, Faculty of Science
University of Zagreb
Zagreb
Croatia

Cheryl J. Aine
Department of Radiology,
School of Medicine
University of New Mexico
Albuquerque, NM
USA

ISBN 978-3-642-33044-5 ISBN 978-3-642-33045-2 (eBook)
DOI 10.1007/978-3-642-33045-2
Springer Heidelberg New York Dordrecht London

Library of Congress Control Number: 2014943122

Printed on acid-free paper

Springer is part of Springer Science+Business Media (www.springer.com)

Preface

Magnetoencephalography (MEG), an invaluable functional brain imaging technique, provides direct, real-time monitoring of neuronal activity which is necessary for gaining insight into dynamic cortical networks. One distinct advantage of measuring weak extracranial neuromagnetic fields is that there is little attenuation in amplitude and/or smearing of the signals since they are primarily generated by primary current sources and are minimally perturbed by the intervening tissues of brain, skull, and scalp. MEG permits spatiotemporal tracking of cortical pathways with sub-millisecond temporal resolution. Over the last four decades families of analysis approaches have been developed and, to various degrees, evaluated for their accuracy and effectiveness while corroboration of results from independent methods such as intracranial recordings or combined fMRI/EEG confirms that MEG is able to provide novel insights and details of mechanisms mediating the functional organization of the human brain.

The field of MEG resulted from a merger of two lines of curiosity-driven research in physics and biophysics. One aimed to explore quantum phenomena related to low-temperature superconductivity which led to the development of the most sensitive magnetic field sensors, *Superconducting Quantum Interference Devices* (SQUIDs). The other aimed to understand physiological processes by measuring the weak magnetic fields they generate. This merger was driven by physicist David Cohen and electrical engineer/physicist James E. Zimmerman, respectively. The fortuitous timing of their research programs was capitalized on by Edgar Edelsack from the Office of Naval Research. By funding both of their projects he brought them together which resulted in the first measurements of biomagnetic signals generated by the human heart in the MIT shielded room. Their joint paper published on April 1, 1970 suggested "medical uses of SQUIDs" and marked the beginning of the field of biomagnetism. Only two years later (1972), David Cohen published the first MEG paper and since then the field of neuromagnetism has been growing steadily. The excitement of being able to reliably measure weak magnetic signals generated by the human brain led to intensive instrumentation development for two decades, with a goal of capturing the entire extracranial distribution of neuromagnetic fields via whole-head systems with hundreds of sensors. Hardware development was accompanied by algorithm development with the goal to identify the neuronal substrates of human perceptual

and cognitive processes as well as the functional connectivity between brain regions.

Although MEG developed in the laboratories of physicists and biomedical engineers it quickly spread to include researchers with varied backgrounds including those interested in imaging brains in health and disease. The range of both basic and clinical applications of MEG is impressive and growing exponentially; this book provides many examples of these research achievements. The pace of acceptance of MEG methods was stymied some by the realization of the need to apply inverse procedures to the field measurements. However, in actuality all noninvasive methods apply reconstruction algorithms to the signals measured. In contrast with other noninvasive functional imaging methods, the signals measured in MEG are direct measures of neural activity, not a correlate of it. Hemodynamic measures, for example, will always be limited in temporal resolution due to the sluggishness of the hemodynamic response itself (e.g., seconds for fMRI and tens of seconds for PET). Additional advantages of MEG are: (1) single subject analyses are conducted which are necessary for clinical applications while averaging of data across subjects can also be accomplished if desired; (2) subtraction techniques between experimental conditions is not necessary; (3) excellent spatiotemporal resolution can be achieved without the burden of using complex head models as in EEG; and (4) it is an absolute measure and thus does not require a reference as in EEG.

Our intentions for this book are to cover the richness and transdisciplinary nature of the MEG field, make it more accessible to newcomers and experienced researchers, and to stimulate growth in the MEG area. The book presents a comprehensive overview of MEG basics and the latest developments in methodological, empirical, and clinical research, and is directed toward master and doctoral students, as well as senior researchers. There are three levels of contributions: (1) tutorials on instrumentation, measurements, modeling, and experimental design; (2) topical reviews providing extensive coverage of relevant research topics; and (3) short contributions on open, challenging issues, future developments, and novel applications. The topics range from neuromagnetic measurements, signal processing, and source localization techniques to dynamic functional networks underlying perception and cognition in both health and disease. Topical reviews cover, among others: development on SQUID-based and novel sensors, multi-modal integration (low field MRI and MEG; EEG and fMRI), Bayesian approaches to multi-modal integration, direct neuronal imaging, novel noise reduction methods, source-space functional analysis, decoding of brain states, dynamic brain connectivity, sensory-motor integration, MEG studies on perception and cognition, thalamocortical oscillations, fetal and neonatal MEG, pediatric MEG studies, cognitive development, clinical applications of MEG in epilepsy, presurgical mapping, stroke, schizophrenia, stuttering, traumatic brain injury, posttraumatic stress disorder, depression, autism, cognitive neuropharmacology, aging and neurodegeneration, and an overview of the major open-source analysis tools.

The book is divided into six parts. Part I includes tutorials on MEG measurements, physical and physiological foundations of MEG, and experimental design.

The remaining parts include topical review chapters and short contributions written by leading MEG researchers. They are grouped around important MEG thrust areas on source analysis and multi-modal integration, functional connectivity and oscillatory activity, neurodevelopment across lifespan, and basic and clinical studies. The book concludes with a range of emerging technologies which offer a bright future for the field of neuromagnetism including combining MEG with ultra-low field MRI, a prospect for direct neuronal current imaging, exciting developments in magnetic relaxometry, and advances in a new generation of sensors.

While we aimed to combine didactic and academic elements in this book, a systematic synthesis was beyond our scope. The authors were asked to introduce particular topics, including an extensive review of the relevant research area, and to inject their own insights into their selected topic. All chapters were reviewed by the two editors. However, no effort was made to achieve strict standardization of symbols across contributions. There is some degree of overlap between certain chapters, left intentionally for the benefit of the reader, which present aspects of a given topic from differing viewpoints or by authors of differing backgrounds.

We hope that this book will be useful as a textbook for advanced master and doctoral students as well as a valuable resource for new and experienced researchers and practitioners. Since in quite a few chapters MEG is discussed in the context of other major functional brain imaging methods and multi-modal integration, the book may be of interest to researchers currently outside of MEG research as well. The general aim of the book was to foster the development of the MEG field by introducing most of the relevant concepts and topics, bringing the latest cutting-edge MEG research results to the forefront as well as passing on our enthusiasm and excitement for this field which is steadily advancing and growing in relevance and applicability.

We had a great time interacting with so many friends and colleagues that we have known for years, including pioneers in this field. This experience was most pleasant, gratifying, and inspiring. We appreciate their support of this book project and we are thankful for their contributions. Collaboration with Springer editor Dr. Christoph Baumann was both pleasant and constructive. We appreciate his guidance and assistance as well as the support of all the staff at Springer-Verlag that made this project a pleasurable experience. We also acknowledge several grants that supported our efforts on working on the book: a bilateral agreement between the University Zagreb and University of New Mexico, the Croatian Ministry of Science, Education, and Sport (grant 199-1081870-1252), NIH grants from the National Institute on Aging (R01 AG029495), and the National Institute of General Medical Sciences (8P20 GM103472-06). Regarding NIH support, the content is solely the responsibility of the editors and chapter authors and does not necessarily represent the official view of the National Institutes of Health.

May 2014

Selma Supek
Cheryl J. Aine

Contents

Part I Tutorials on Measurement, Physical Basis of Analysis, and Experimental Design

Instrumentation for Measuring MEG Signals 3
Yong-Ho Lee and Kiwoong Kim

Novel Noise Reduction Methods 35
Samu Taulu, Juha Simola, Jukka Nenonen and Lauri Parkkonen

Electric and Magnetic Fields of the Brain 73
Leon Heller and Petr Volegov

Forward Modeling and Tissue Conductivities 107
Jens Haueisen and Thomas R. Knösche

Designing MEG Experiments 129
Julia M. Stephen

Part II Source Analysis and Multi-Modal Integration

Magnetoencephalographic Imaging 163
Srikantan Nagarajan and Kensuke Sekihara

MEG and Multimodal Integration 183
Seppo P. Ahlfors

MEG/EEG Data Analysis Using EEGLAB 199
John R. Iversen and Scott Makeig

Fusing Concurrent EEG and fMRI Intrinsic Networks 213
David Bridwell and Vince Calhoun

MRIVIEW: A Software Package for the Analysis and Visualization of Brain Imaging Data 237
Doug Ranken

NUTMEG: Open Source Software for MEG/EEG Source Reconstruction 255
Johanna M. Zumer, Daniel D. E. Wong, Adrian G. Guggisberg, Srikantan S. Nagarajan and Sarang S. Dalal

Recent Developments in MEG Network Analysis 263
Arjan Hillebrand and Cornelis J. Stam

Non-parametric Statistical Analysis of Map Topographies on the Epoch Level 279
Michael Wagner

MEG-SIM Web Portal: A Database of Realistic Simulated and Empirical MEG Data for Testing Algorithms 285
Lori Sanfratello, Julia Stephen, Elaine Best, Doug Ranken and Cheryl Aine

Analyzing MEG Data with Granger Causality: Promises and Pitfalls 309
Mingzhou Ding and Chao Wang

Part III Functional Connectivity and Oscillatory Activity

An Introduction to MEG Connectivity Measurements 321
Matthew J. Brookes, Mark W. Woolrich and Darren Price

Human Brain Oscillations: From Physiological Mechanisms to Analysis and Cognition 359
Ole Jensen, Eelke Spaak and Johanna M. Zumer

Studying Dynamic Neural Interactions with MEG 405
Jan-Mathijs Schoffelen and Joachim Gross

Thalamocortical Network Dynamics: A Framework for Typical/Atypical Cortical Oscillations and Connectivity 429
Urs Ribary, Sam M. Doesburg and Lawrence M. Ward

Temporal and Spectral Signatures of the Default Mode Network 451
Francesco de Pasquale and Laura Marzetti

Methods to Estimate Functional and Effective Brain Connectivity from MEG Data Robust to Artifacts of Volume Conduction 477
Guido Nolte and Laura Marzetti

Neural Decoding and Brain Machine Interfaces Based on Electromagnetic Oscillatory Activities: A Challenge for MEG 503
Masayuki Hirata

Part IV Neurodevelopment Across Lifespan

Fetal Magnetoencephalography (fMEG) 509
Jana Muenssinger, Hari Eswaran and Hubert Preissl

Pediatric MEG: Investigating Spatio-Temporal Connectivity of Developing Networks 525
Kristina R. Ciesielski and Julia M. Stephen

MEG and Cognitive Developmental Studies 557
Margot J. Taylor and Elizabeth W. Pang

Language Processing in Atypical Development: Looking Below the Surface with MEG 579
Maria Mody

Whole-Head Child MEG System and Its Applications 599
Yoshiaki Adachi and Yasuhiro Haruta

Towards the Understanding of Healthy and Pathological Aging Through MEG 609
Fernando Maestú, Elena Solesio-Jofre and Ricardo Bajo

Current Status and Future Prospects of Perinatal MEG 641
Ronald T. Wakai

Technological Challenges of Pediatric MEG and Potential Solutions: The Aston Experience 645
Caroline Witton, Paul L. Furlong and Stefano Seri

Cognitive Decline Associated with Aging, Alzheimer's Disease and Cerebrovascular Risk: Advantages of Dynamic Imaging with MEG 657
Cheryl J. Aine, John C. Adair, Janice E. Knoefel, Lori Sanfratello and Julia M. Stephen

Part V Basic and Clinical Studies

MEG Auditory Research 679
Alexander Gutschalk

MEG Studies on Music 713
Sibylle C. Herholz and Christo Pantev

Sensorimotor Integration 727
Toshiaki Wasaka and Ryusuke Kakigi

Organizational Neuroscience: A New Frontier for Magnetoencephalography? 743
Sven Braeutigam

Pain- and Itch-Related Magnetic Fields 749
Hideki Mochizuki, Koji Inui and Ryusuke Kakigi

Selection of Stimulus Parameters for Visual MEG Studies of Sensation and Cognition 767
Cheryl J. Aine, Selma Supek, Lori Sanfratello and Julia M. Stephen

MEG Imaged Pathways of Stuttering 801
Susan M. Bowyer and Jennifer Peacock

MEG in Epilepsy and Pre-surgical Functional Mapping 821
Masaki Iwasaki and Nobukazu Nakasato

Towards Brain Connectivity in Epilepsy Using MEG 843
Seung-Hyun Jin and Chun Kee Chung

Review of Schizophrenia Research Using MEG 849
Donald C. Rojas

Neuropsychopharmacology: Recent MEG Investigations 875
Ksenija Marinković

Food Meets Brain 901
Maike A. Hege, Krunoslav T. Stingl and Hubert Preissl

Presurgical MEG to Forecast Pediatric Cortical Epilepsies 921
Douglas F. Rose and Hisako Fujiwara

Future Developments in Clinical MEG and Its Combination with nTMS 933
Jyrki P. Mäkelä

Part VI Emerging Technologies

Ultra-Low-Field MRI and Its Combination with MEG 941
Lauri Parkkonen, Risto J. Ilmoniemi, Fa-Hsuan Lin and Michelle Espy

Neuronal Current Imaging with Ultra-Low-Field NMR Techniques 973
Rainer Körber, Martin Burghoff and Lutz Trahms

Magnetic Relaxometry: A Comparison to Magnetoencephalography . . . 979
Edward R. Flynn

Optically-Pumped Magnetometers for MEG 993
Svenja Knappe, Tilmann Sander and Lutz Trahms

Spin Electronics Based Magnetic Sensors for Biomagnetic Measurements 1001
M. Pannetier-Lecoeur, C. Fermon, P. Campiglio, Q. Herreros and G. Jasmin-Lebras

Index 1007

Contributors

Yoshiaki Adachi Applied Electronics Laboratory, Kanazawa Institute of Technology, Ishikawa, Japan

John C. Adair Neurology, University of New Mexico School of Medicine, Albuquerque, NM, USA

Seppo P. Ahlfors Department of Radiology, MGH/HST Athinoula A. Martinos Center for Biomedical Imaging, Massachusetts General Hospital, Charlestown, MA, USA; Harvard-MIT Division of Health Sciences and Technology, Cambridge, MA, USA

Cheryl J. Aine Department of Radiology, University of New Mexico School of Medicine, Albuquerque, NM, USA

Ricardo Bajo Laboratory of Cognitive and Computational Neuroscience, Center for Biomedical Technology, Madrid, Spain

Elaine Best The Mind Research Network, Albuquerque, NM, USA

Susan M. Bowyer Departments of Neurology and Speech Pathology, Henry Ford Health systems, Detroit, MI, USA

Sven Braeutigam Oxford Centre for Human Brain Activity, University of Oxford, Oxford, UK

David Bridwell Mind Research Network, Albuquerque, NM, USA

Matthew J. Brookes Sir Peter Mansfield Magnetic Resonance Centre, School of Physics, University of Nottingham, Nottingham, UK

Martin Burghoff Physikalisch-Technische Bundesanstalt, Berlin, Germany

Vince Calhoun Electrical and Computer Engineering, University of New Mexico, Albuquerque, NM, USA

P. Campiglio DSM/IRAMIS/SPEC, CEA Saclay and CNRS URA 2464, Gif sur Yvette, France

Chun Kee Chung Department of Neurosurgery, Seoul National University Hospital, Jongno-gu, Seoul, Republic of Korea; Department of Neurosurgery, Seoul National University College of Medicine, Jongno-gu, Seoul, Republic of Korea; Department of Brain and Cognitive Sciences, Seoul National University College of Natural Sciences, Gwanak-gu, Seoul, Republic of Korea

Kristina R. Ciesielski Department of Radiology, Athinoula A. Martinos Center for Biomedical Imaging, Massachusetts General Hospital, Harvard Medical School, Charlestown, MA, USA; Department of Psychology, University of New Mexico, Albuquerque, NM, USA

Sarang S. Dalal Department of Psychology, University of Konstanz, Konstanz, Germany; Zukunftskolleg, University of Konstanz, Konstanz, Germany

Francesco De Pasquale Department of Neuroscience and Imaging, "G. d'Annunzio" University Chieti-Pescara, Chieti, Italy; Institute for Advanced Biomedical Technologies, "G. d'Annunzio" University Foundation, Chieti, Italy

Mingzhou Ding The J. Crayton Pruitt Family Department of Biomedical Engineering, University of Florida, Gainesville, USA

Sam M. Doesburg Behavioral and Cognitive Neuroscience Institute, Simon Fraser University, Burnaby, BC, Canada; Hospital for Sick Children, Toronto, ON, Canada; University of Toronto, Toronto, ON, Canada

Michelle Espy Los Alamos National Laboratory, Los Alamos, NM, USA

Hari Eswaran Department of Obstetrics and Gynecology, University of Arkansas for Medical Sciences, Little Rock, USA

C. Fermon DSM/IRAMIS/SPEC, CEA Saclay and CNRS URA 2464, Gif sur Yvette, France

Edward R. Flynn Senior Scientific LLC, Albuquerque, NM, USA

Hisako Fujiwara Division of Neurology, MEG Center, Cincinnati Children's Hospital Medical Center, University of Cincinnati, Cincinnati, OH, USA

Paul L. Furlong School of Life and Health Sciences, Aston Brain Centre, Wellcome Trust Laboratory for MEG Studies, Aston University, Birmingham B4 7ET, UK

Joachim Gross Department of Psychology, Centre for Cognitive Neuroimaging (CCNi), University of Glasgow, Glasgow, UK

Adrian G. Guggisberg Division of Neurorehabilitation, Department of Clinical Neurosciences, University Hospital Geneva, Geneva, Switzerland

Alexander Gutschalk Department of Neurology, University of Heidelberg, Heidelberg, Germany

Yasuhiro Haruta Applied Electronics Laboratory, Kanazawa Institute of Technology, Ishikawa, Japan; Department of MEG, Yokogawa Electric Corporation, Tokyo, Japan

Jens Haueisen Institute of Biomedical Engineering and Informatics, Ilmenau University of Technology, Ilmenau, Germany

Maike A. Hege Institute of Medical Psychology and Behavioral Neurobiology, fMEG Center, University of Tübingen, Tübingen, Germany

Leon Heller Applied Modern Physics Group, P-21, Los Alamos National Laboratory, Los Alamos, NM, USA

Sibylle C. Herholz Deutsches Zentrum für Neurodegenerative Erkrankungen e.V. (DZNE), Bonn, Germany

Q. Herreros DSM/IRAMIS/SPEC, CEA Saclay and CNRS URA 2464, Gif sur Yvette, France

Arjan Hillebrand Department of Clinical Neurophysiology and Magnetoencephalography Center, Neuroscience Campus Amsterdam, VU University Medical Center, Amsterdam, The Netherlands

Masayuki Hirata Department of Neurosurgery, Osaka University Medical School, Suita, Osaka, Japan

Risto J. Ilmoniemi Department of Biomedical Engineering and Computational Science, Aalto University School of Science, Espoo, Finland

Koji Inui Department of Integrative Physiology, National Institute for Physiological Sciences, Okazaki, Japan

John R. Iversen Swartz Center for Computational Neuroscience, Institute for Neural Computation, University of California San Diego, La Jolla, CA, USA

Masaki Iwasaki Department of Neurosurgery, Tohoku University Graduate School of Medicine, Sendai, Japan

G. Jasmin-Lebras DSM/IRAMIS/SPEC, CEA Saclay and CNRS URA 2464, Gif sur Yvette, France

Ole Jensen Radboud University Nijmegen, Donders Institute for Brain, Cognition and Behaviour, Centre for Cognitive Neuroimagin, Nijmegen, The Netherlands

Seung-Hyun Jin Department of Neurosurgery, Seoul National University Hospital, Jongno-gu, Seoul, Republic of Korea

Ryusuke Kakigi Department of Integrative Physiology, National Institute for Physiological Sciences, Okazaki, Aichi, Japan

Kiwoong Kim Center for Biosignals, Korea Research Institute of Standards and Science, Daejeon, Korea

Svenja Knappe National Institute of Standards and Technology, Boulder, CO, USA

Janice E. Knoefel Internal Medicine, University of New Mexico School of Medicine, Albuquerque, NM, USA

Thomas R. Knösche Institute of Biomedical Engineering and Informatics, Ilmenau University of Technology, Ilmenau, Germany

Rainer Körber Physikalisch-Technische Bundesanstalt, Berlin, Germany

Yong-Ho Lee Center for Biosignals, Korea Research Institute of Standards and Science, Daejeon, Korea

Fa-Hsuan Lin Department of Biomedical Engineering and Computational Science, Aalto University School of Science, Espoo, Finland; Institute of Biomedical Engineering, National Taiwan University, Taipei, Taiwan

Fernando Maestú Laboratory of Cognitive and Computational Neuroscience, Center for Biomedical Technology, Madrid, Spain; Department of Basic Psychology II, Complutense University of Madrid, Madrid, Spain

Scott Makeig Swartz Center for Computational Neuroscience, Institute for Neural Computation, University of California San Diego, La Jolla, CA, USA

Jyrki P. Mäkelä BioMag Laboratory, HUS Medical Imaging Center, Helsinki University Central Hospital, Helsinki, Finland

Ksenija Marinković Radiology Department, University of California at San Diego, La Jolla, CA, USA

Laura Marzetti Department of Neuroscience and Imaging, Institute for Advanced Biomedical Technologies, G. D'Annunzio University Foundation, G. D'Annunzio University, Chieti, Italy

Hideki Mochizuki Department of Integrative Physiology, National Institute for Physiological Sciences, Okazaki, Japan

Maria Mody Athinoula A. Martinos Center for Biomedical Imaging, Harvard Medical School and Massachusetts General Hospital, Harvard-MIT Division of Health Sciences and Technology, Charlestown, MA, USA

Jana Muenssinger Institute for Medical Psychology and Behavioral Neurobiology, fMEG Center, University of Tuebingen, Tuebingen, Germany

Srikantan S. Nagarajan Biomagnetic Imaging Laboratory, Department of Radiology and Biomedical Imaging, University of California, San Francisco, CA, USA

Nobukazu Nakasato Department of Epileptology, Tohoku University Graduate School of Medicine, Sendai, Japan

Jukka Nenonen Elekta Oy, Helsinki, Finland

Guido Nolte Department of Neurophysiology and Pathophysiology, University Medical Center Hamburg-Eppendorf, Hamburg, Germany

Elizabeth W. Pang Neuroscience and Mental Health Programme, The Hospital for Sick Children, University of Toronto, Toronto, ON, Canada; Neurology, The Hospital for Sick Children, University of Toronto, Toronto, ON, Canada

M. Pannetier-Lecoeur DSM/IRAMIS/SPEC, CEA Saclay and CNRS URA 2464, Gif sur Yvette, France

Christo Pantev Institut für Biomagnetismus und Biosignalanalyse, Westfälische Wilhelms- Universität, Münster, Germany

Lauri Parkkonen Elekta Oy, Helsinki, Finland; Department of Biomedical Engineering and Computational Science, Aalto University School of Science, Espoo, Finland

Jennifer Peacock Departments of Neurology and Speech Pathology, Henry Ford Health systems, Detroit, MI, USA

Hubert Preissl Institute of Medical Psychology and Behavioral Neurobiology, fMEG Center, University of Tübingen, Tübingen, Germany

Darren Price Sir Peter Mansfield Magnetic Resonance Centre, School of Physics, University of Nottingham, Nottingham, UK

Doug Ranken Los Alamos National Laboratory, Los Alamos, NM, USA

Urs Ribary Behavioral and Cognitive Neuroscience Institute, Simon Fraser University, Burnaby, BC, Canada; University of British Columbia, Vancouver, BC, Canada; Brain Research Centre, UBC, Vancouver, BC, Canada

Donald C. Rojas University of Colorado Denver, Anschutz Medical Campus, Denver, USA

Douglas F. Rose Division of Neurology, MEG Center, Cincinnati Children's Hospital Medical Center, University of Cincinnati, Cincinnati, OH, USA

Tilmann Sander Physikalisch-Technische Bundesanstalt, Berlin, Germany

Lori Sanfratello Department of Radiology, University of New Mexico School of Medicine, Albuquerque, NM, USA

Jan-Mathijs Schoffelen Centre for Cognitive Neuroimaging, Donders Institute for Brain, Cognition and Behaviour, Radboud University Nijmegen, Nijmegen, The Netherlands; Max Planck Institute for Psycholinguistics, Nijmegen, The Netherlands

Kensuke Sekihara Department of Systems Design & Engineering, Tokyo Metropolitan University, Hino, Tokyo, Japan

Stefano Seri School of Life and Health Sciences, Aston Brain Centre, Wellcome Trust Laboratory for MEG Studies, Aston University, Birmingham B4 7ET, UK; Department of Clinical Neurophysiology and Pediatric Epilepsy Surgery Program, The Birmingham Children's Hospital NHS Foundation Trust, Birmingham, UK

Juha Simola Elekta Oy, Helsinki, Finland

Elena Solesio-Jofre Motor Control Laboratory, Research Centre for Movement Control and Neuroplasticity Department of Biomedical Kinesiology, Katholieke Universiteit Leuven, Leuven, Belgium

Eelke Spaak Radboud University Nijmegen, Donders Institute for Brain, Cognition and Behaviour, Centre for Cognitive Neuroimagin, Nijmegen, The Netherlands

Cornelis J. Stam Department of Clinical Neurophysiology and Magnetoencephalography Center, Neuroscience Campus Amsterdam, VU University Medical Center, Amsterdam, The Netherlands

Julia M. Stephen The Mind Research Network and Lovelace Biomedical and Environmental Research Institute, Albuquerque, NM, USA

Krunoslav T. Stingl Institute of Medical Psychology and Behavioral Neurobiology, fMEG Center, University of Tübingen, Tübingen, Germany

Selma Supek Department of Physics, Faculty of Science, Zagreb, Croatia

Margot J. Taylor Diagnostic Imaging, The Hospital for Sick Children, University of Toronto, Toronto, ON, Canada; Neuroscience and Mental Health Programme, The Hospital for Sick Children, University of Toronto, Toronto, ON, Canada

Lutz Trahms Physikalisch-Technische Bundesanstalt, Berlin, Germany

Petr Volegov Applied Modern Physics Group, P-21, Los Alamos National Laboratory, Los Alamos, NM, USA

Samu Taulu Elekta Oy, Helsinki, Finland

Michael Wagner Compumedics Germany GmbH, Hamburg, Germany

Ronald T. Wakai Department of Medical Physics, University of Wisconsin-Madison, Madison, WI, USA

Chao Wang The J. Crayton Pruitt Family Department of Biomedical Engineering, University of Florida, Gainesville, USA

Lawrence M. Ward Behavioral and Cognitive Neuroscience Institute, Simon Fraser University, Burnaby, BC, Canada; University of British Columbia, Vancouver, BC, Canada; Brain Research Centre, UBC, Vancouver, BC, Canada

Toshiaki Wasaka Nagoya Institute of Technology, Nagoya, Aichi, Japan; Department of Integrative Physiology, National Institute for Physiological Sciences, Okazaki, Aichi, Japan

Caroline Witton School of Life and Health Sciences, Aston Brain Centre, Wellcome Trust Laboratory for MEG Studies, Aston University, Birmingham B4 7ET, UK

Daniel D. E. Wong Department of Psychology, University of Konstanz, Konstanz, Germany

Mark W. Woolrich Oxford Centre for Human Brain Activity, University of Oxford, Oxford, UK

Johanna M. Zumer Radboud University Nijmegen, Donders Institute for Brain Cognition and Behaviour, Centre for Cognitive Neuroimaging, Nijmegen, The Netherlands

Part I
Tutorials on Measurement, Physical Basis of Analysis, and Experimental Design

Instrumentation for Measuring MEG Signals

Yong-Ho Lee and Kiwoong Kim

Abstract To measure weak magnetoencephalography (MEG) signals, two basic technical requirements are sensitive magnetic sensors and reduction of environmental noises. Until now, magnetic field sensors based on superconducting quantum interference devices (SQUIDs) made from low-temperature superconductors are the main sensors used for measuring MEG signals. For effective reduction of strong environmental magnetic noise, combination of magnetic shielding and gradiometers (hardware and/or software) are typically used. Since SQUIDs are very sensitive devices, care should be taken in handling them and in using them for multichannel MEG sensor arrays. Electrostatic shocks or strong magnetic fields can damage the normal operation of SQUIDs. Cooling of the SQUIDs needs a helmet-shape dewar which should provide reliable operation for longer than 1 year in vacuum tightness, and boil-off of the liquid He should be optimized to have refill interval longer than 1 week. For economic MEG systems, the SQUID array should be simple in the manufacturing process, and the structure of the sensor array should be compact. For the MEG system to be operated easily, the process for signal acquisition and signal processing devices needs to be simple, using a single personal computer. A magnetically shielded room (MSR) is mandatory for urban hospitals or downtown laboratory environments. Considering the high cost of magnetic alloy used in the construction of a MSR, optimization and cost-effective construction is needed. Even if the MEG measurements are done in a quiet or well-shielded environment, the signal-to-noise ratio of MEG signals are not sufficiently high, and signal processing is needed to remove some artifacts generated from the human body. This chapter presents basic technical issues for MEG instrumentation, especially in fabricating and operating economic MEG systems. In the later part of this chapter, atomic magnetometers for future non-cryogenic MEG systems, and brain magnetic resonance based on low-field nuclear magnetic resonance for visualizing brain functional activity are described.

Y.-H. Lee (✉) · K. Kim
Center for Biosignals, Korea Research Institute of Standards and Science, Daejeon, Korea
e-mail: yhlee@kriss.re.kr

S. Supek and C. J. Aine (eds.), *Magnetoencephalography*,
DOI: 10.1007/978-3-642-33045-2_1,

Keywords MEG · SQUID · Magnetometer · Flux-locked loop · Analog signal processing · Data acquisition · Cooling · Dewar · Magnetically shielded room · Nonmagnetic stimuli · Digital signal processing · Low-field MRI · Atomic magnetometer · Cryocooler · High-temperature SQUID

1 Introduction

Measuring weak MEG signals in the background of strong environmental noise, having a noise level of several orders of magnitude larger than the MEG signals, is a challenging task. Since typical amplitudes of MEG signals are less than 1 pT, sensitive magnetometers using SQUIDs are presently used. By using a helmet shaped MEG system, mapping of neural currents with high temporal and spatial accuracy can be done (Hämäläinen et al. 1993; Del Gratta et al. 2001; Knuutila 2007). Up to now, several types of MEG systems having different SQUID sensor types were developed and have been used in the hospitals or brain research institutes. To collect the weak brain magnetic signals from the presence of strong environmental noise, effective combination of MSR and SQUID pickup coils is needed. A standard MEG system consists of helmet-type sensor array inside a liquid He dewar, MSR, readout and control electronics, acquisition, stimulus devices, signal processing and analysis computer. Figure 1 shows a typical block diagram for the components of MEG systems.

Considering the high price of Ni-alloy materials used for the magnetic shielding, it is desirable to use gradiometers than magnetometers to reduce the amount of Ni-alloy. Currently two types of hardware gradiometers are used, that is, axial or planar gradiometer, either in wire-wound or thin film structure. Alternatively, software gradiometers having reference sensors located at some distance from the signal sensors and software optimization to have best signal-to-noise ratio can be used.

A SQUID is basically a converter from magnetic flux to voltage. However, amplitudes of SQUID voltage output are quite small for typical input range of MEG signals, requiring a low-noise preamplifier to readout the SQUID output. To simplify the readout electronics of a multichannel SQUID system, the SQUID output voltage should be large enough, otherwise a rather complex readout scheme is needed (Drung 1996; Pizzella et al. 2001).

To increase the field detection area of a SQUID magnetometer or gradiometer, flux transformer is used where a larger pickup coil, typically about 20 mm diameter, picks up the magnetic field and converts it into flux through the input coil. The intrinsic flux noise of SQUID increases with the increase of SQUID inductance, thus the loop size of SQUID needs to be minimized. However, for effective coupling of magnetic flux with the input coil, the SQUID loop size has a certain practical limit, typically about 100 μm.

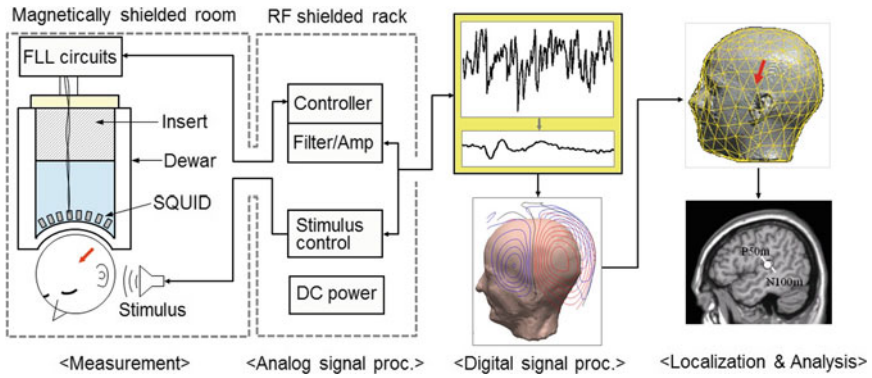

Fig. 1 Block diagram of MEG measurement system

2 SQUID Sensors

2.1 SQUID as a Magnetic Field Sensor

In the operation of a SQUID, four basic superconducting phenomena are used: (i) complete loss of electric resistance at temperatures below the critical temperature, (ii) perfect diamagnetism having no magnetic flux inside the superconductor, (iii) quantization of magnetic flux in a superconducting ring, (iv) Josephson effect. Most of the present MEG systems use low-temperature Nb-based SQUIDs. Nb has a superconductive transition temperature of about 9.2 K, and is a refractory and reliable material against repeated thermal cycling between 4.2 K and room temperature. And the noise characteristics of SQUIDs made from Nb/AlO_x/Nb Josephson junction show low leakage current in the low frequency range, which is an important requirement for measuring low-noise MEG measurement. The fabrication technology of Nb SQUID sensors is now well established and fabrication of many sensors on Si-wafers can be done (Lee et al. 1999). The typical size of the SQUID chip is about 10 mm^2, including pads for wire bonding (Al and Nb).

Figure 2 shows the principle of measuring an MEG signal using a SQUID. For the effective pickup of magnetic field signal, a superconductive flux transformer is used, consisting of a pickup coil of a much larger diameter than the SQUID loop and a multi-turn input coil integrated directly on the SQUID loop. When a magnetic field is applied to the pickup coil, a screening current is generated in the superconductive flux transformer circuit, and this current is converted into magnetic flux through the input coil and magnetic coupling with the SQUID loop. In a typical design of flux transformer and SQUID, about 0.5 nT of magnetic field in the pickup coil corresponds to flux transfer of 1 Φ_0 into the SQUID loop.

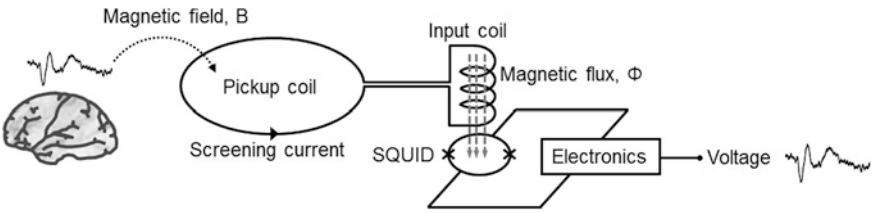

Fig. 2 Principle of measuring MEG signal using SQUID

2.2 Pickup Coil

Typical dimensions of SQUID loops are about 0.1 mm. Thus, to increase the detection efficiency, pickup coils of a diameter larger than 10 mm is usually needed. Among various types of pickup coils, magnetometers or hardware first-order gradiometers are now used in present MEG systems. Figure 3 shows examples of pickup coils.

Magnetometers have the best sensitivity to both deep and shallow sources. At the same time, however, it is more vulnerable to external noises. The optimum choice of a pickup coil depends on the details of the measurement condition; thickness of the MSR, strength of environmental noises, and signals to be measured. Inside a thick MSR or in a quiet location, magnetometers as the sensing element are preferable. In urban clinics or laboratories, there is often a limitation in the thickness or weight of the MSR. Thus, moderate or medium-thickness MSRs, in combination with gradiometers, is the best combination. Generally speaking, axial gradiometers have longer baselines than planar gradiometers, so that it has better sensitivity to deep sources than planar gradiometers. For shallow sources, planar gradiometers have better sensitivity when the axis of current dipole (y-axis in Fig. 3c) is perpendicular to the field derivative direction of the gradiometers (x-axis in Fig. 3c).

A planar gradiometer can be made on a single wafer, that is, the planar pickup coil can be integrated on the same wafer as the SQUID loop. For example, in the Neuromag system, 2 perpendicular planar gradiometers and magnetometer are integrated on the same element (wafer) (Parkkonen 2010).

A possible disadvantage of the axial gradiometer is the relative complex process in assembling the axial gradiometer, and it needs superconductive connection (bonding) between pickup coil wires and input coil pads. For the superconductive connection between the pickup coil and the input coil, usually superconducting Nb blocks or strips with screw terminals are used. To eliminate pickup area of the magnetic field due to the superconducting connection structure, Nb blocks are sometimes shielded using a superconducting tube (Ketchen 1987; ter Brake et al. 1992; Dössel et al. 1993). Since this superconducting block and tube introduces distortion of magnetic fields, and they are installed at a sufficiently large distance from the compensation coil of the gradiometer to maintain the balancing of the gradiometer against the external fields, as shown in Fig. 4a. Increased length of the

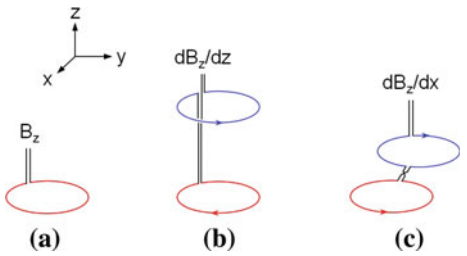

Fig. 3 Typical pickup coils used in MEG measurements. **a** Magnetometer, **b** axial first-order gradiometer, and **c** planar first-order gradiometer

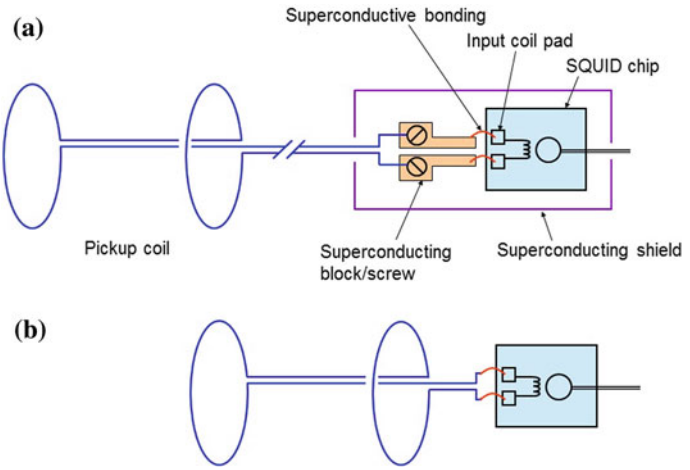

Fig. 4 Structure of axial gradiometer. **a** Conventional axial gradiometer having Nb block and screw inside a superconducting shield. **b** Simplified axial gradiometer structure with direct bonding between pickup coil and input coil

gradiometer requires higher level of liquid He to keep both SQUID and pickup coil superconducting. In order to increase the refill interval of liquid He, it is desirable to position the SQUIDs as close as possible to the gradiometers. Recently, some improvements were made to remove the shielding tube, so that the SQUID is positioned at about 20 mm from the compensation coil. But, the stray pickup area due to the superconducting connection structure generates imbalance of roughly few percent. A novel method to simplify the superconductive connection method and to reduce the stray pickup area is direct bonding of Nb wire between pickup coil wires and input coil pads. Thus, the fabrication process of the gradiometer became simpler and the total length of the gradiometer can be shortened (Lee et al. 2009). Considering that the residual fields inside the MSR are not highly homogenous, the intrinsic balancing of the gradiometers needs to be as large as possible with simple fabrication process.

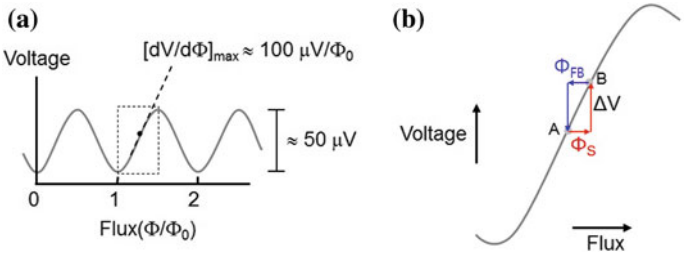

Fig. 5 Response curve of the SQUID to magnetic flux. **a** SQUID output voltage as a function of flux signal. **b** Principle of flux-locked loop operation. Change of signal flux (Φ_S) is compensated by a negative feedback flux (Φ_{FB}) applied to the SQUID loop. Φ_0 is the flux quantum ($=2.07 \times 10^{-15}$ Wb)

3 SQUID Electronics

3.1 Flux-Locked Loop Electronics

The voltage output of a SQUID is periodic like a sinusoidal function and nonlinear with respect to the input flux as shown in Fig. 5a. To get a linear response against the input flux signal, a special operation scheme, called flux-locked loop (FLL), is used. In the FLL operation (Fig. 5b), the flux in the SQUID loop is locked at a constant point using a negative feedback circuit, and the feedback voltage (or feedback flux through the feedback coil) is measured as the final output. Figure 6 shows a schematic circuit diagram of standard-type FLL operation. Since the amplitude of SQUID output against input MEG signals is small, care should be taken in detecting the SQUID output. For example, a typical MEG signal, say, 100 fT corresponds to about 0.2 $m\Phi_0$ in the SQUID loop, which generates a voltage signal of 20 nV (for a typical flux-to-voltage transfer of 100 $\mu V/\Phi_0$). To detect this level of voltage signal, careful design of a room-temperature preamplifier is needed. For economic operation of multi-channel SQUIDs for MEG systems, simple and compact room-temperature readout electronics are required. For the simple structure of the FLL circuits, output voltages and flux-to-voltage transfers of the SQUIDs should be large enough so that the contribution of preamplifier input noise is negligible in direct readout mode (Drung 1996; Drung and Mück 2004). A double relaxation oscillation SQUID (DROS), based on the relaxation oscillation of a hysteretic SQUID and a reference junction, provides large flux-modulated voltage output and a steep flux-voltage transfer coefficient (Adelerhof et al. 1994; Lee et al. 1999; 2005). One example of a DROS design is shown in Fig. 7, which enables direct measurement of SQUID output using room-temperature preamplifiers, and makes the FLL circuits compact using DC bias current. In the FLL or internal feedback scheme, there is crosstalk between adjacent pickup coils. Induced current in the flux transformer generates a magnetic field, which can be picked up by nearby pickup coils. This stray coupling can be eliminated by using the feedback scheme

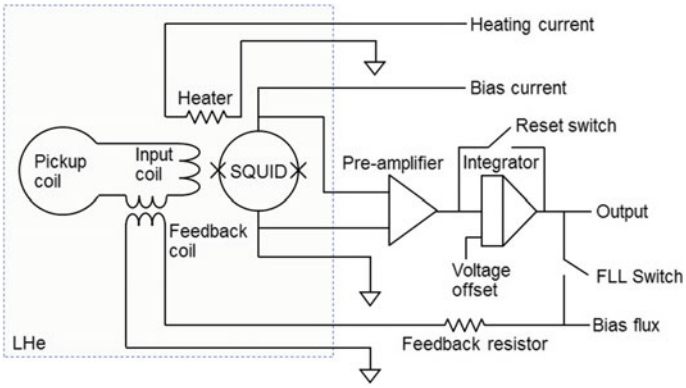

Fig. 6 Schematic diagram of the standard flux-locked loop circuit. When the feedback current is applied to the flux transformer circuit, the total flux in it is maintained constant

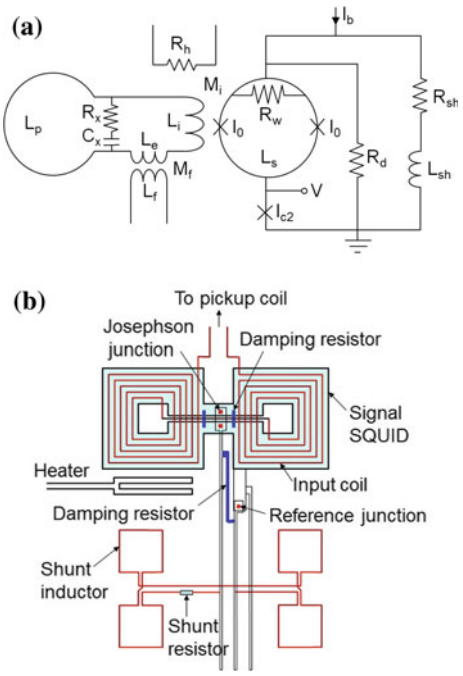

Fig. 7 Design of double relaxation oscillation SQUID (DROS). **a** Schematic circuit diagram of DROS. **b** Design layout of DROS in the SQUID loop area

called external feedback or current feedback loop, in which the current in the flux transfer circuit is kept constant (ter Brake et al. 1986).

Superconductivity is maintained under critical condition, that is, below critical temperature, critical current, and critical field. If the SQUID is exposed to high magnetic field or transient electric pulses, magnetic flux can be trapped in the thin film SQUID. Trapped flux can deteriorate the performance of the SQUID or even

make normal SQUID operation difficult. Trapped fluxes can be removed by applying a current pulse of about 1 W, typically 0.1 ~ 1 s duration, to the SQUID. The heater is placed close to the SQUID loop. During heating, the temperature of SQUID temporarily rises to just above its superconductive transition temperature, at the expense of temporary slight evaporation of liquid He.

3.2 Analog Signal Processing

The voltage output of a FLL circuit is too small to be measured directly by analog-to-digital converter using a computer. Thus, intermediate amplifier and filters are used which consist of high pass, low pass, power-line elimination filter and amplifier. Typical cutoff frequencies for high and low pass filters are 0.01 ~ 0.1 and 100 Hz, respectively. Amplification is 100 or 1,000 times. Use of analog filters makes acquisition easier and real-time monitoring of the acquisition process easier. However, analog filters can change the shape of the signal waveforms and introduce phase distortions. In addition to the separate space needed to house the analog signal processing (ASP) circuits, an ASP usually consumes more electrical power than the FLL circuit does. Recent MEG systems digitize the output of FLL directly, and measure signals through optical fibers. Advantages of using optical readout are (i) reduced power consumption, (ii) compact electronics and reduced installation space by eliminating the ASP box, (iii) elimination of electric interference from outside of MSR, and (iv) increased dynamic range of FLL output. Figure 8 shows the comparison of SQUID output measurement systems with conventional ASP circuits (Fig. 8a) and ASP-free readout system (Fig. 8b).

4 Dewar

Modern MEG systems have helmet-shaped dewars covering the whole head. Depending on the populations to be measured, there is slight variation in the shape of the helmet. For example, a dewar for Caucasian people has a longer dimension along the frontal-occipital direction than the dewars for Asian population. The size of the dewar should be large enough to accommodate most of the population, but too large of a helmet size increases the distance between the sensor surface (measurement points) and the head surface at room temperature (Vrba et al. 2002). This distance is about 20 mm or less. SQUID sensors can be installed either in the liquid He reservoir or the vacuum space with tight thermal contact with the He reservoir (coil-in-vacuum).

He dewar is made of fiberglass reinforced plastic, which is non-magnetic and mechanically strong with low thermal expansion coefficient. Between the inner and outer vessel, multiple (around 50) layers of superinsulation (SI) and vapor-cooled thermal shields are installed. The SI is made from thin aluminum film

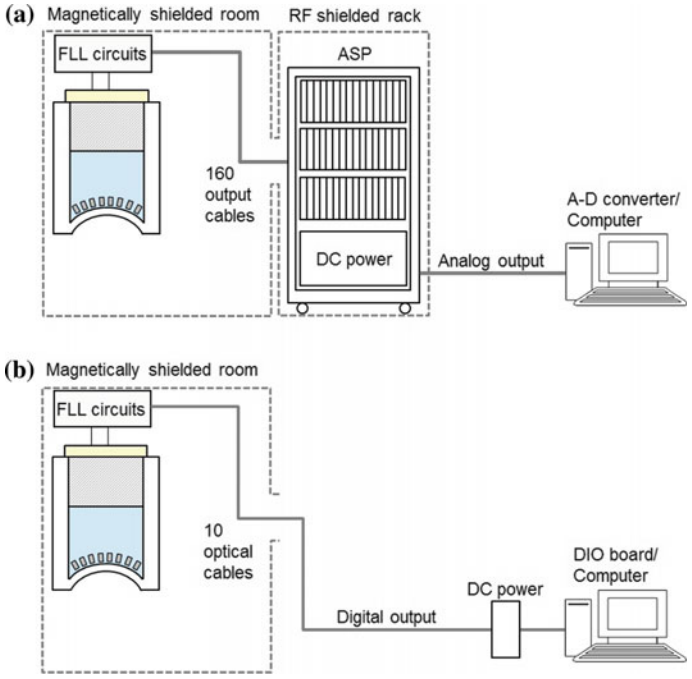

Fig. 8 Schematic diagrams of the SQUID output measurement systems. **a** Conventional type with ASP circuit and analog-to-digital converters. **b** ASP-free readout with signal transmission using optical cables

deposited on flexible insulating substrate. To minimize the thermal magnetic noise induced from the metallic film, the surface area of the aluminum is reduced by dividing it into an island structure or by crinkling it. The thermal shield also should be made to minimize the thermal noise. It is made of copper coil foil, which is a woven fabric, made of thin enameled copper wires. Improper installation of SI and the thermal shield at the helmet can increase the white noise of the SQUID system. The white noise of the modern dewars is in the range of $1 \sim 2$ $fT_{rms}/\sqrt{Hz}$. Further reduction of dewar thermal noise can be done with smaller sized aluminum islands or thinner metallic layers at the expense of slight increase of boil-off rate. Figure 9 shows the structure of a typical dewar.

5 Magnetically Shielded Room

Depending on the noise conditions of the MEG site, an optimum combination of magnetically shielded room (MSR) and pickup coil is needed. In rural or magnetically quiet sites, the requirement for MSR is lowered. In a usual urban hospital

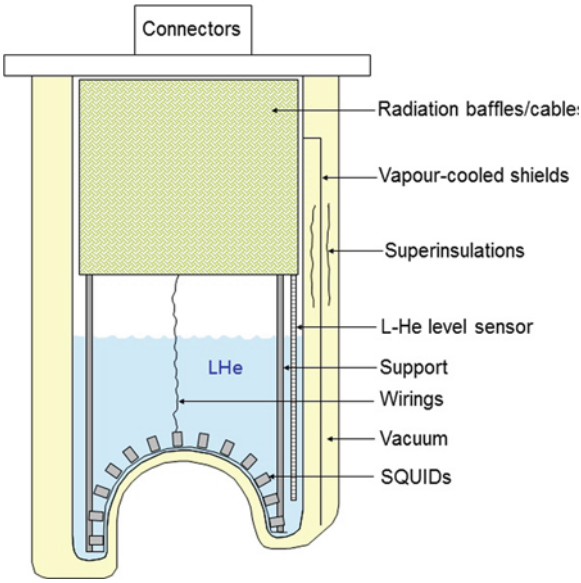

Fig. 9 Schematic structure of a helmet-shape liquid-He dewar

or laboratory environment, reliable reduction of environmental noise is a key step for successful acquisition of MEG signals. The most effective and reliable method of reducing environmental noise is magnetic shielding (Nowak 1998; Kelhä et al. 1982). Typical environmental noise spectrum in an urban site is shown in Fig. 10. In an ordinary laboratory environment, low-frequency drift of the earth's magnetic field is in the range of 100 ~ 1,000 nT, with variation frequency of about 0.1 Hz. Main sources of this low-frequency drift are operation (DC power supplied or movement) of subway (tram), public transportation and elevators, etc. By using high-pass filtering, this low-frequency drift does not affect the signal quality of MEG. But, if this drift is too large, the dynamic range of FLL could be reached, resulting in saturation of the FLL output.

The amplitude of power line noise is in the range of 10 ~ 100 nT. Use of a notch filter can reduce the noise peak at power line frequency, at the expense of phase distortion near the elimination frequency. Some subways use a power system generating strong 16.67 Hz noise peak (sub-harmonic of 50 Hz).

Mechanical vibrations of the building, MSR, gantry, and vibration of the sensor insert inside the boiling liquid He dewar, etc., generate noise peaks in the frequency range of 5 ~ 20 Hz, which overlaps with the frequency band of MEG signals.

The MSR uses a combination of ferromagnetic shielding and eddy-current shielding. For ferromagnetic shielding, high-permeability Ni-alloy, called Mumetal or Permalloy, is used. Since the permeability of Ni-alloy is sensitive to stress, care should be taken in handling the material, and the material has to be hydrogen-annealed before assembling. The magnitude of residual DC fields inside common MSRs for MEG measurements are about 10 nT. This DC field level

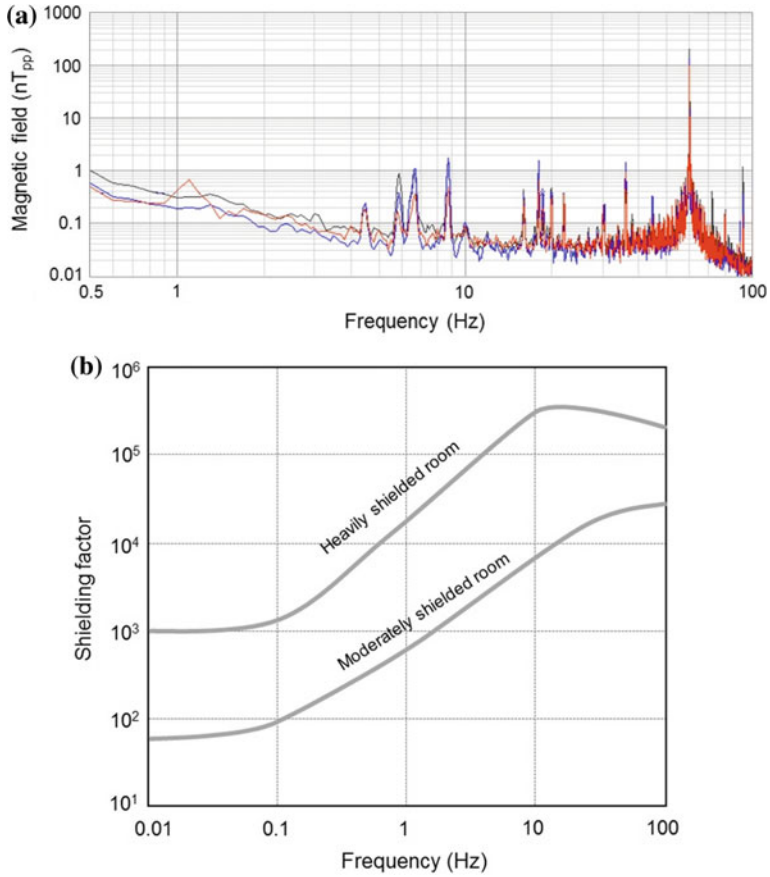

Fig. 10 Environmental noise and shielding factor of MSR. **a** Typical noise spectra of environmental noise. **b** Shielding factors as a function of frequency in moderately and heavily shielded room, respectively, used for MEG measurements

increases with time due to accumulation of stress or gradual magnetization of the soft ferromagnetic material. Thus, regular degaussing is needed to reduce the DC field, by applying a magnetic field to the ferromagnetic material with a field intensity much larger than the coercive force of the ferromagnetic material.

If the shielded room was assumed to be a cubic structure of side length L, the shielding factors of the ferromagnetic material is

$$S = 1 + 0.75\mu_r t/L,$$

where μ_r and t are the relative permeability and thickness of the magnetic layer, respectively. With a single layer, there is limitation in providing sufficient shielding factor. Thus, a multiple-layer structure is preferred, with separation between the layers.

In a 2-layer cubic structure, the shielding factor is

$$S = 1 + S_1 + S_2 + S_1 S_2 \left\{ 1 - (L_1/L_2)^3 \right\},$$

where S_1 (L_1) and S_2 (L_2) are the shielding factor (side length) of the inner and outer layer, respectively. Typically, the separation between inner and outer layer is about 20 cm, and then the term $S_1S_2\{1\text{-}(L_1/L_2)^3\}$ dominates in the above equation. In 3-layer structure, even high shielding factors can be obtained,

$$S = 1 + S_1 + S_2 + S_3 + S_1 S_2 \left\{ 1 - (L_1/L_2)^3 \right\} + S_1 S_3 \left\{ 1 - (L_1/L_3)^3 \right\} + S_2 S_3 \left\{ 1 - (L_2/L_3)^3 \right\} + S_1 S_2 S_3 \left\{ 1 - (L_1/L_2)^3 \right\} \left\{ 1 - (L_2/L_3)^3 \right\}$$

where S_1 (L_1), S_2 (L_2) and S_3 (L_3) are the shielding factor (side length) of the inner, middle and outer layer, respectively.

When the drift of the DC field is large, for example, at a measurement site near the subway, expensive ferromagnetic shielding alone does not provide sufficient shielding effect at low frequency, and an active compensation method is needed. For eddy-current shielding, effective at a frequency above 1 Hz, high-electrical-conductivity aluminum or copper plates are used (Erné 1983). Since electric conductors generate thermal magnetic noise, the inner-most part of the MSR has a ferromagnetic layer to shield the eddy-current noise from the conductive layer.

In eddy current shielding, an important parameter is skin depth δ given by

$$\delta = (\rho/\pi\mu_0 f)^{0.5},$$

where ρ is the resistivity, μ_0 is the permeability in free space, and f is frequency of the noise wave. Typically the eddy current shielding effect is effective at about 1 Hz and above, and it increases exponentially with frequency, as given by

$$S = \{(L/\delta)(1/(4\sqrt{2})\} e^{(t/\delta)},$$

where t is the thickness of the conducting plate (Sullivan et al. 1989). The total shielding factor of MSR made of ferromagnetic material and conducting material is the product of those for ferromagnetic and conducting material.

Depending on the pickup coil type, thickness of the MSR can be different. Shielding factors of typical MSRs used in MEG measurements are shown in Fig. 10. Attenuation of the DC field is in the range of 1,000 $\sim$ 10,000 times, depending on the thickness and layers of ferromagnetic plates. A heavily shielded room is used for a magnetometer array, or for gradiometers in a very noisy environment. In addition to the cost for a heavily shielded room, weight of the heavily shielded room limits the installation site to ground or basement floors. Considering both the cost and weight of the MSR, a first-order gradiometer array in combination with a moderately shielded room would be a good economic choice.

Fig. 11 A picture of a MEG system installed in a hospital. Helmet-shaped liquid He dewar mounted on a nonmagnetic gantry and inside a magnetically shielded room (MSR). Stimulation devices, acquisition, and analysis devices are outside MSR

In addition to shielding factors, homogeneity of the residual field inside the MSR is also important. If the spatial variation of field or field gradient is large, vibration of the sensor array generates noise, making the well balanced gradiometers ineffective. Thus, minimization of residual fields inside the MSR is needed, by careful installation of ferromagnetic plates and degaussing afterward.

Figure 11 shows an MEG system with a moderately shielded room installed in a downtown hospital. For easy walk-in, the doorsill of the MSR needs to be of equal height as the office floor.

6 Basic Signal Processing Methods for Magnetoencephalography

MEG signals can be easily contaminated by noises from outside of the shielded room or from the human body, such as movements of the body and heart beats (magneto-cardiograms). The outputs of flux-locked loop circuits are passed though analog filtering, and some digital filtering, such as baseline correction, and through band-pass filtering. Besides the basic band-pass analog and digital filtering, more sophisticated signal processing methods are required to improve the signal to noise ratio of the MEG recordings (Vrba et al. 2001). We can categorize such processing methods into two groups; software noise shielding and artifact rejection.

6.1 Software Noise Shielding

The software shielding includes an adaptive gradiometry with reference channels, signal space projection (SSP), signal space separation (SSS), etc. (Uusitalo and Ilmoniemi 1997; Taulu et al. 2004).

The gradiometry can be understood as spatial filtering since homogeneous magnetic fields from far-away sources are cancelled and inhomogeneous magnetic fields from near-by sources are detected. Generally, a gradiometer consists of a detection pickup coil close to the source and a reference pickup coil away from the source. The pickup coils can be replaced by separate SQUID magnetometers. Especially, the direction of a reference field component can be arbitrarily chosen by using an orthogonal three-channel vector magnetometer. By subtracting a composite reference field component of the same orientation to the detection magnetometer from the signal of the detection magnetometer, we can eliminate noise from far-away sources in a software manner; we call this method synthetic gradiometry. Here, the distance between the detection sensor and the reference sensors is called the baseline. The baseline approximately limits the spatial pass-band. By placing more reference sensors at different positions, we could form a higher-order gradiometer, which provides a sharper cut-off shoulder in the shape of the spatial pass-band.

In construction of a synthetic gradiometer, adaptive filtering can be adopted. The adaptive filtering is to find a best fitting function for the signal waveform from a linear combination of the reference waveforms. The linear combination coefficients (adaptive coefficients) can be calculated by means of linear regression methods, either in an online or in an offline manner. The adaptive coefficients correspond to a modified orientation of the reference vector magnetometer by adjusting the component gains.

We can also apply the adaptive filtering in the frequency domain. Some noise like mechanical vibration has its own characteristic frequency components; mechanical vibration of sensor mounts under the magnetic field gradient formed by magnetized walls generates magnetic vibration noise. In this case, the frequency-domain adaptive filtering is more effective. To find the frequency spectrum, short-time Fourier transforms with an adequate window are performed. Then, the same linear regression fitting process is conducted to match the linear combination of reference frequency-domain spectra to the signal spectrum.

Usually, such synthetic and adaptive filtering are quite effective to eliminate external magnetic noise; especially when the passive magnetic shielding is not sufficient. However, if your system is equipped with a high shielding factor magnetically shielded room (MSR), the performance of such software methods would have a limitation. The limitation mainly comes from the intrinsic noise of each sensor. Since the intrinsic noises of the detection sensor and reference sensors are not correlated, numerical subtraction always result in total addition of the RMS noise level of each sensor. To reduce such an effect, we suggested a compensated adaptive filtering technique which consists of a random sensor noise remover and adaptive filter. To construct the sensor noise remover, we use factor analysis (FA). The basic compensated adaptive filtering situation is illustrated in Fig. 12. The most important feature of the system is to eliminate the reference sensor's own noise. To reject the sensor noise, we utilize FA. The background noise source vector $\mathbf{s}$ and observations at the reference sensors $\mathbf{x}$ have the following linear relation,

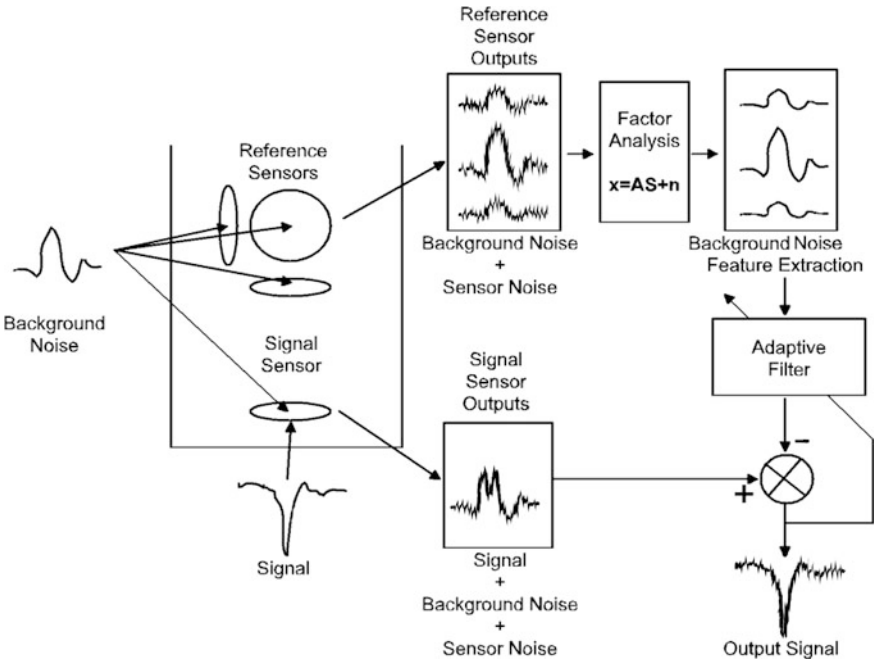

Fig. 12 Conceptual diagram of the compensated adaptive filtering system

$$\mathbf{x} = \mathbf{A}\mathbf{s} + \mathbf{n}, \tag{1}$$

where $\mathbf{A}$ is a linear mixing matrix and $\mathbf{n}$ is a real-valued sensor noise vector. We can assume that the sensor noise is random and has no correlation with other channel noises (mutually independent). That is $\mathbf{n} \sim N(0, \Xi)$, where Ξ is a diagonal variance matrix. In order to extract the feature of the background noise sources from the sensor-noise-additive observation, we have to apply a general principal component analysis (PCA) to the covariance matrix of $\mathbf{x}\mathbf{x}^{\mathbf{T}}$ but the noise variance should be taken into account. The difference between the general PCA and the FA that we have adopted is to fit only off-diagonal components of the covariance matrix. The result of the FA process, $\mathbf{y}$, can be denoted by

$$\mathbf{y} = \mathbf{R}\mathbf{x}, \tag{2}$$

where $\mathbf{R}$ is the minimum norm generalized inverse,

$$\mathbf{R} = (\hat{\mathbf{A}}^{\mathbf{T}}\hat{\Xi}^{-1}\hat{\mathbf{A}})^{-1}\hat{\mathbf{A}}^{\mathbf{T}}\hat{\Xi}^{-1}, \tag{3}$$

which can be calculated from the estimated values $\hat{\mathbf{A}}$ and $\hat{\Xi}$ of the unweighted least square method. Note that $E[\mathbf{y}\mathbf{y}^{\mathbf{T}}] = \Lambda + \mathbf{R}\Xi\mathbf{R}^{\mathbf{T}}$, where Λ is a diagonal matrix having the covariance eigenvalues of the pure background noise components.

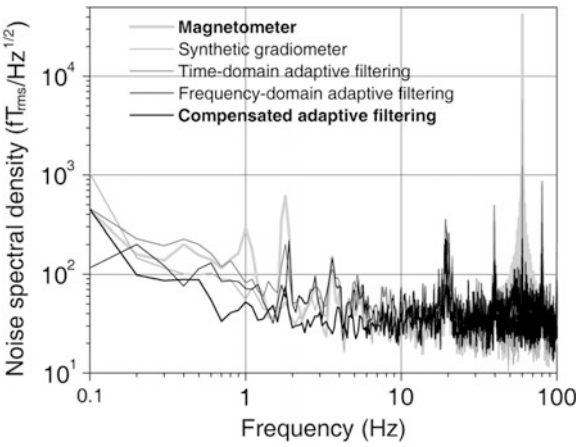

Fig. 13 Magnetic background spectra and the noise rejection effect by applying the five listed filtering methods. The thick light grey line is the original observation, the thick black line is the result of the compensated adaptive filtering, and the other thin lines are results of the conventional methods

The sensor-noise-extracted features in **y** can be projected to the observation space of **x**. Then, we apply a standard adaptive filtering process to the signal sensor input with the result of the FA.

Figure 13 shows the background noise spectra for a single detection sensor after applying the conventional methods—synthetic gradiometer, time-domain adaptive filtering, frequency-domain adaptive filtering—and the compensated adaptive filtering in the frequency range from 0.1 to 100 Hz. The baseline between the signal and the reference is more than 76 mm. The measurements are conducted in a magnetically shielded room having a shielding factor of about 200 at 0.01 Hz. In conventional methods, the noise rejection factor is about 3–15 for a low frequency environmental noise (1.8 Hz peak) and about 8–150 for the 60 Hz line-noise. In the other frequency regions, the conventional processing makes matters worse. We can see that the noise levels of conventionally processed results are even higher than that of the magnetometer in the frequency above 2 Hz. It results from adding up the reference sensor's own noise. Figure 13 also shows that the compensated adaptive filtering is helpful to lower the noise level by adding no extra reference sensor noise.

SSP is a method to separate the signal eigenspace and the noise eigenspace. The spatiotemporal recordings of a multichannel MEG system can be characterized into representative eigenvectors based on their covariance between different channel recordings so that each eigenvector (basis) describes a characteristic magnetic field distribution pattern. Once such basis eigenvectors are determined, we are able to find a projection component to the eigenvector. Generally, in order to apply SSP, we measure an environmental noise without a subject and find dominant eigenvectors which describe the external noise; that is the noise space. Afterward, in a real measurement, we calculate the projection component to the pre-acquisition noise space. By subtracting the projection component from the original MEG measurement, we can eliminate the dominant background noise components from the obtained recordings. This method is quite effective because it

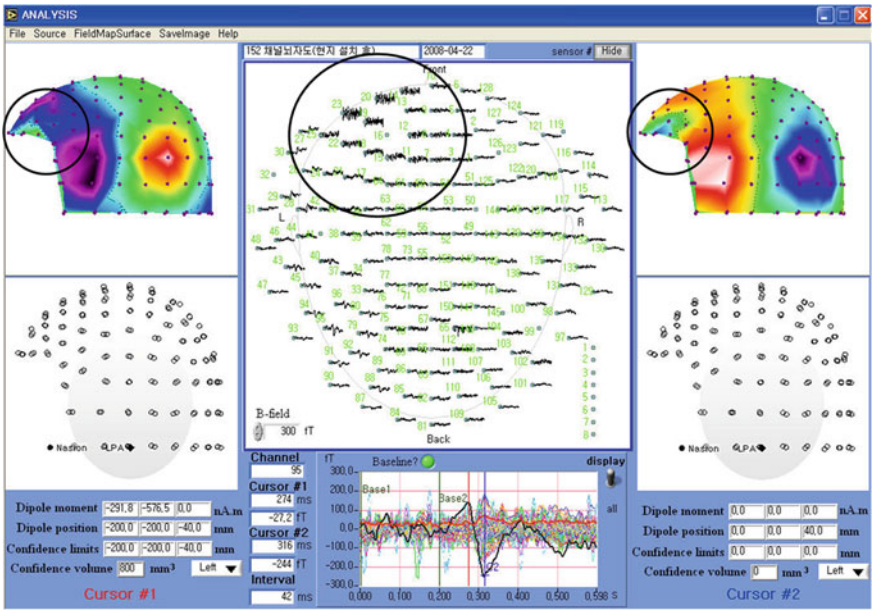

Fig. 14 Magnetic noise from a vibrating ferromagnetic particle in a cryostat. At the left frontal region, a strong magnetic oscillation has been observed, which remained strong after averaging 100 epochs for observing an auditory evoked field pattern

can be applied in real-time once the noise space matrix has been found. One interesting example is shown in Fig. 14. In this case, a tiny ferromagnetic particle was accidentally remained inside the vacuum area of the liquid helium dewar. The particle generated quite a strong magnetic vibration noise on the nearby SQUID channels. Because the location of the particle is fixed, we can expect that the spatial vibration pattern is always the same. So we could apply SSP to eliminate the artifact. Figure 15 shows the real-time rejection performance of the SSP based artifact rejection.

SSS is another spatial filtering technique based on orthogonal eigenvector basis decomposition. In SSS, spherical harmonics are used as the bases. Due to the radial dependency of each spherical harmonics function, we can categorize the field potential bases into field components from sources placed inside and field components from sources placed outside. Therefore, after separating those two categories, we can eliminate noise fields from outside sources by rejecting the outside basis components. So we could call this technique software shielding.

In practice, the number of bases is limited by the number of channels and the order of spherical harmonics is not enough to describe the signal magnetic field pattern or the noise magnetic field pattern in some cases. Another important point for the application of SSS is the shape of the sensor array. Because we have to distinguish the radial potential aspects of the eigenfunctions, if the sensors are

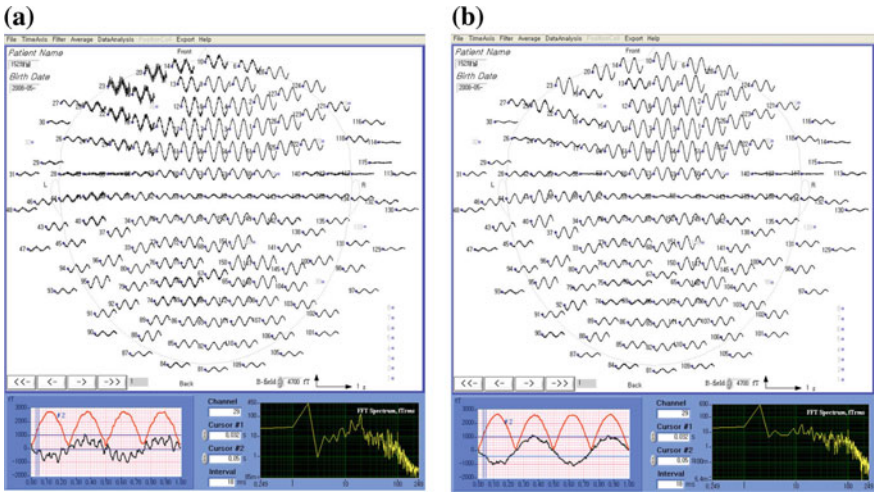

Fig. 15 **a** Magnetic noise from a vibrating ferromagnetic particle in a cryostat. **b** The noise can be eliminated by using a pre-calculated projection matrix in realtime acquisition

Fig. 16 Sensors placed on a spherical surface

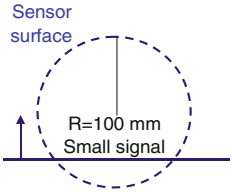

placed on a perfect sphere, the method will fail. A helmet type arrangement of the sensor array can give an affirmative result to a certain extent but a double-layer detection or more, gradiometer configuration, is desirable.

First, we examine a case of spherical arrangement of the magnetic field sensors. The sensors are assumed to be placed on a perfect sphere of 100 mm radius as in Fig. 16. A current dipole source of (100, 100, 0)(nAm) is located at (x, y, z) = (−30, 10, 60)(mm) inside of the sphere and a strong noise-generating current dipole source of (0, 0, 1)(mAm) is located at (−20, 3000, 0)(mm) outside of the sphere. In this condition, the signal source, noise source, and magnetic field sensor distributions on the sphere are depicted in Fig. 16. The result of software magnetic shielding implemented by using SSS is shown in Fig. 17. In the simulation, the number of the internal bases was nine and the number of the external bases was six.

At a spherical surface of the same radius, the same signal space will be shared by inner bases and outer bases, and consequently they cannot be distinguished. Therefore, as shown in Fig. 17d, the decomposition between the signal and noise will fail.

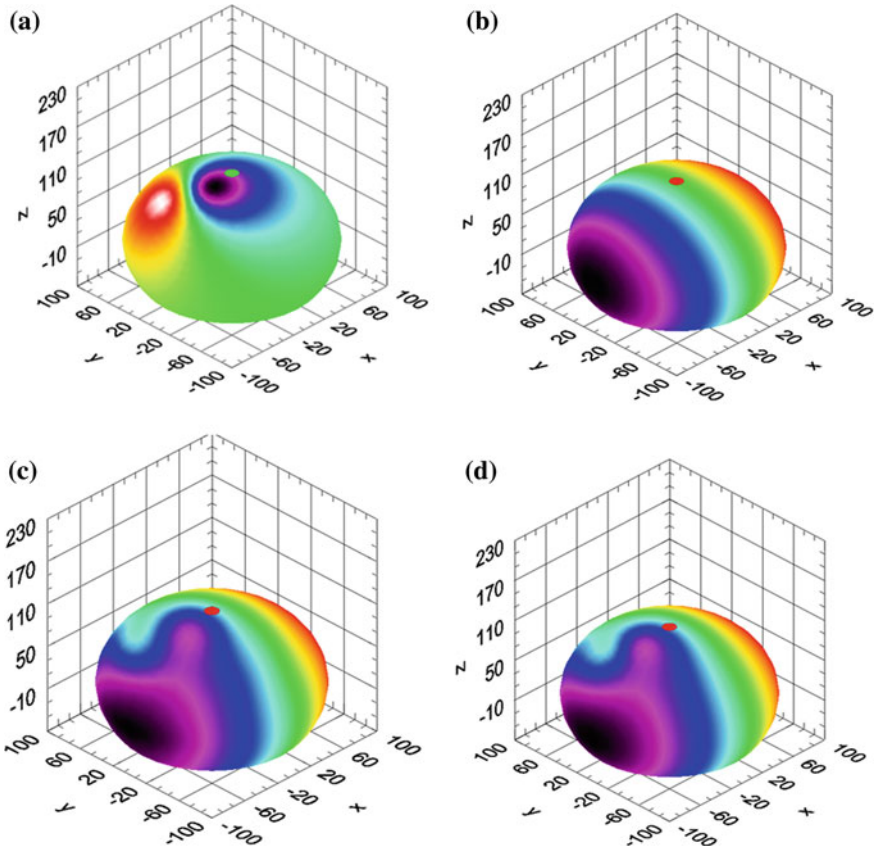

Fig. 17 **a** magnetic field pattern of the signal current source, **b** magnetic field pattern of the noise current source, **c** magnetic field pattern of the signal and noise current sources together, **d** the SSS noise reduction result in a spherical sensor array

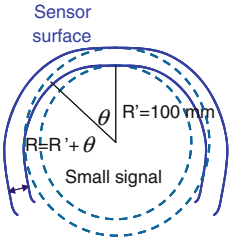

Fig. 18 Aspherical double-layered sensor arrangement (baseline: 20 mm)

As suggested in Fig. 18, we assume a double-layered arrangement of sensors on a pumpkin-like helmet plane which has an increasing radius as a function of the polar angle. The baseline, a gap between the inner and outer sensor planes, is

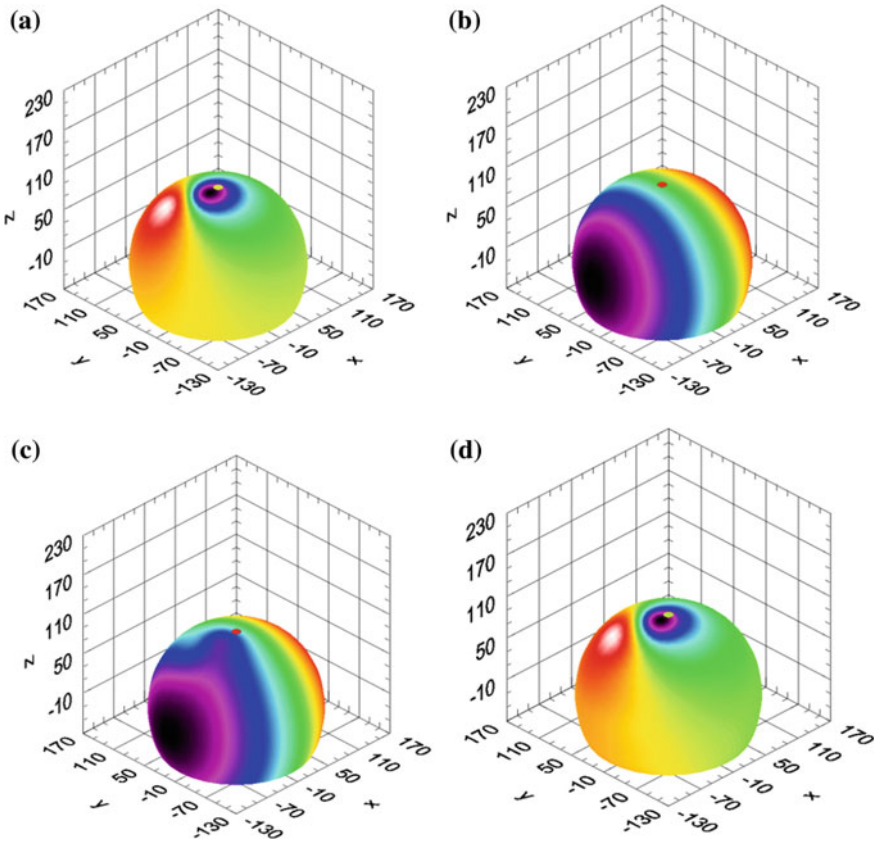

Fig. 19 **a** Signal current source **b** noise source **c** map of magnetic field formed by signal + noise source **d** Results of SSS on aspheric double-layered sensor arrangement

20 mm. A weak current dipole source of (100, 100, 0)(nAm) is located at (x, y, z) = (−30, 10, 60)(mm) inside of the sphere and a strong noise-generating current dipole source of (0, 0, 1)(mAm) is located at (−20, 3000, 0)(mm) in the external space of the sphere. In this condition, the signal source, noise source, and magnetic field sensor distribution on the modified double-layered sphere are depicted in Fig. 18.

The results of software magnetic shielding with SSS are presented in Fig. 19. In the simulation, the number of the internal bases was nine, the number of the external bases was six as assumed in the above simulations. In this case, since the inner and outer spherical harmonics bases are clearly distinguished due to the gradiometric structure of the sensor array, clear separation of the internal source signal is possible in spite of the strong external magnetic noise interference. Therefore, as shown in Fig. 19d, the decomposition between the signal and noise was performed well enough.

6.2 Artifact Rejection

Depending on the artifacts to be eliminated, different artifact rejection method can be applied; e.g., principal component analysis (PCA), factor analysis, independent component analysis (ICA), state space filtering, and morphological filter, etc.

PCA finds dominant eigenvectors to decorrelate the covariance matrix. By doing that we get dominant waveforms based on their signal variances. This method is quite effective when the magnitude of the artifact is strong enough and shows a large variance. The power line noise is a good target for the PCA-based artifact rejection method. However, PCA cannot guarantee perfect decorrelation or orthogonality between the components. Therefore, sometimes, a signal component could be mixed up with the noise component in the process to find the principal components. Then, we must use an incorrect waveform when we try to eliminate the artifacts, which results in signal baseline distortion and incorrect localization results. To reduce this risk we could use a time-delayed decorrelation method (Kim et al. 2004).

ICA finds statistically independent components and their mixing matrix. There are many kinds of ICA, mostly they separate an independent waveform based on higher-order statistics like kurtosis; the decorrelation is based on the second-order statistics. Most of ICA sequences go through a pre-whitening process and mutual information minimization process. So the ICA components are irrelevant to the magnitude of source components and have permutation uncertainty. Currently, the predominant ICA method is FastICA since its calculation speed is relatively fast and the pre-built function is equipped with a widely-used matrix calculation package. However, many authors prefer a joint approximate diagonalization of eigen-matrices (JADE) algorithm (Cardoso 1999) since JADE can deal with complex number data. For separation of spike-like components, FastICA or other methods are all satisfactory, for separation of periodic signals, however, JADE showed a more robust performance.

Target artifacts which should be rejected in MEG analysis are eye movements (Fig. 20) and heart signal (Fig. 21). Due to the permutation uncertainty of the ICA algorithm, such artifacts are basically selected visually among the separated independent components, which is a time-consuming job. For a practical use, we can utilize an expected spatial field distribution of the artifact component. For example, the power of magneto-oculogram from eye movements would be prominent on the forehead channels. The power of magnetocardiography from heart beats would be prominent on lower sensors of the helmet. Based on such power distribution, we can automatically select the independent components corresponding to the noise artifacts and we can eliminate the projection of the artifact components.

State space filtering is useful for periodic data reconstruction under low signal to noise ratio. In practice, time-series embedding is popular. According to Taken's embedding theorem, M-dimensional dynamic system can be embedded in $\Re^{2M+1}$. For $m = 2M + 1$, we can conduct time-series embedding by using equi-interval

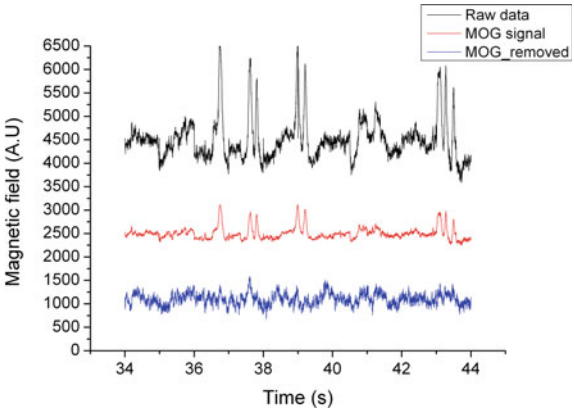

Fig. 20 Rejection of magnetooculogram (MOG) signals by using ICA. *Top* the original data, *middle* selected MOG component, *bottom* MOG removed signal

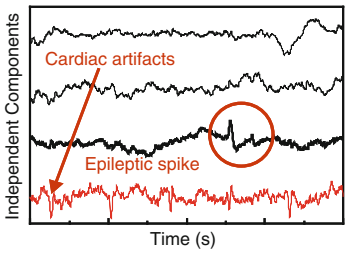

Fig. 21 Rejection of magnetocardiogram (MCG) signals by using ICA. The data were recorded from an epilepsy patient. Epileptic spikes, slow wave, and the MCG artifact are successfully separated

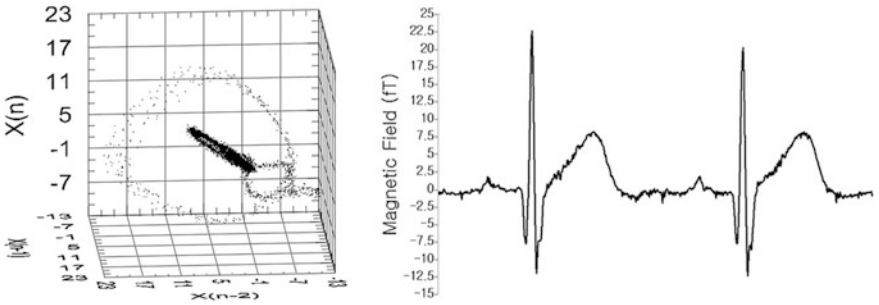

Fig. 22 State space time-series embedding of an MCG waveform. Here, the embedding space dimension is 3 and the dimension of the dynamic system is 1

time-delayed signal vector $\vec{x}_n = (x_n,\ x_{n-\tau},\ \cdots,\ x_{n-(m-1)\tau})$. Figure 22 shows an example of the time-series embedding. An MCG waveform has been embedded in a state space and it forms an attractor. The embedding time interval should be

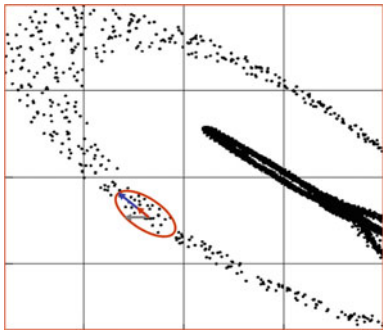

Fig. 23 Trace contraction in state space. The main axis in neighboring points is calculated by PCA and the trace is contracted to the principal orientation

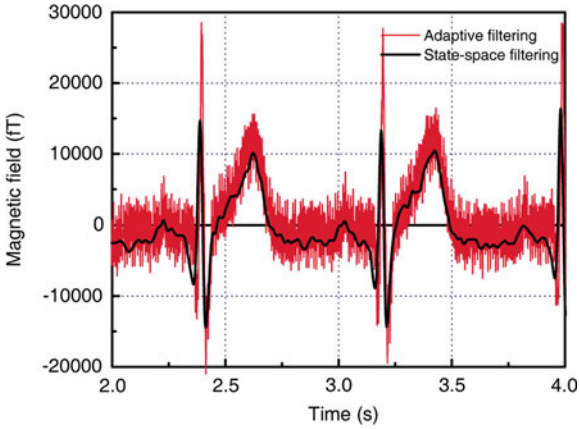

Fig. 24 Noise rejection results of adaptive filtering and state space filtering, respectively. Here, the reference sensing channel has a non-linear gain

determined carefully; if the interval is too short, then there will be a diagonally stretched attractor while when the interval is too long then there will be an attractor with no correlation. Usually, if the time series has a band-limited spectrum, the time interval can be determined as follows. $m\tau \approx \tau^* = \frac{2\pi}{\omega^*}$, where ω^* is the cutoff frequency of the spectrum.

The simplest noise reduction method in state space is to take the mean value of neighbors within a constant radius, but this is merely equivalent to triggered time-averaging. The next is trace contraction, which calculates the covariance matrix of a constant number of neighbors. Once a principle axis is determined, the orthogonal error axis components should be suppressed (Fig. 23). The other method is to use Wiener filtering, which averages neighborhoods in the Fourier space.

One good aspect of state space filtering is that we can apply this method to a data set recorded with a reference sensor of different sensitivity (even for a non-linear gain). Figure 24 shows the results of state-space filtering and adaptive filtering, respectively, for simulated MCG signals contaminated by 60 Hz power line noise. Here, the detection channel has a linear gain, but the reference channel

has a non-linear gain; a distortion in 60 Hz waveform in the reference channel. The noisy component remained in the adaptive filtering result primarily due to waveform distortion. However, the state-space filtering shows good performance.

A morphological filter is generally used for eliminating the signal baseline. Basic operators include erosion, dilation, opening, and closing. Depending on the composition and the order of applying the operators, we could make various kinds of filter characteristics. The morphological filter operation is usually adjusted by trial and error.

7 Magnetoencephalography Based on Atomic Magnetometer

MEG has been proven to be a useful brain research tool not only for clinical diagnosis but also for higher cognition studies. However, the distribution of MEG systems into the practical measurement field is not so popular. One of the reasons could be the fact that MEG systems need to be cooled down to the superconducting temperature and they consume liquid helium. In some conditions, the supply of liquid helium is burdening. Recently, optically pumped atomic magnetometer sensors are beginning to attract people's attention because they are expected to be operated in a room temperature. The basic principle of an atomic magnetometer is depicted in Fig. 25. Alkali metal vapor in a glass cell becomes polarized when the cell is illuminated by circularly-polarized light. When there is an external magnetic field, the polarization begins to tilt. The tilting changes the energy population to the probe beam direction which provides different refraction indexes for the left-circularly polarized light and right circularly polarized light, respectively. Finally, it rotates the polarization angle of the linearly polarized probe beam. By measuring the polarization angle rotation we can detect the magnetic field strength.

The sensitivity of an atomic magnetometer mainly depends on the spin relaxation or spin destruction caused by spin-spin collision or spin-wall collision, respectively. However, in a condition where the external magnetic field is very weak and the atomic density is very high at a high temperature, the spin collision happens more often than the Larmor precession. The population density of each magnetic sublevel is determined by the spin temperature and total angular momentum F_z. The slow-downed precession frequency is proportional to the torque $< S_z >/< F_z >$ and the external magnetic field. The expectation value of $< S_z >$ and $< F_z >$ can be calculated from the population density distribution. By assuming that the atoms have nonzero average orientation and the spin temperature is high, we can simply approximate the population density of M_F, magnetic quantum number, as $1 + M_F/T$. The calculation shows that the slow down factor is not so significant and the direction of precession is the same as that of a $F = I + 1/2$ free atom since the state dominates in the average spin precession

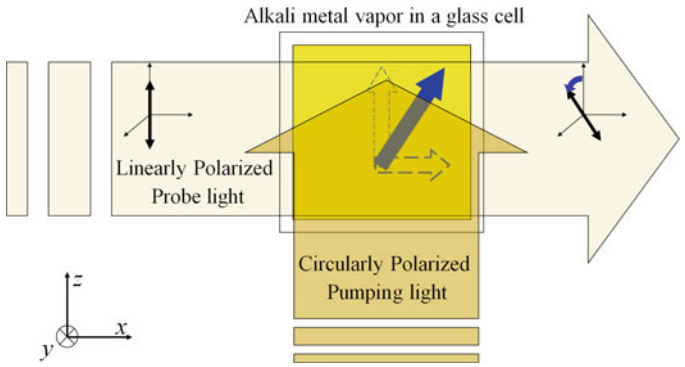

Fig. 25 Optically pumped polarization in alkali metal vapor rotates the polarization angle of linearly polarized probe light and the rotation angle is proportional to the external field strength

due to having more Zeeman sublevels. Anyway, with this scheme, there is effectively no spin exchange from the spin-spin collision, which provides a long spin coherence time and a sharp linewidth, hence the high sensitivity. By using this scheme, we could reach several fT sensitivity with an atomic magnetometer and succeed in measuring auditory evoked magnetic fields (AEF) from a human brain. The atomic magnetometer system was developed at Princeton University and Fig. 26 shows the apparatus and measurement condition for a human.

The system has 256 sensing channels and the detection area is about 3×3 cm^2.

Figure 27 shows the measurement result. For comparison, we put the same AEF experimental result with a homemade partial-coverage SQUID MEG system having 37-channel magnetometers in Fig. 27b. The signal to noise ratio is comparable to each other. However the recording of the atomic magnetometer shows only a single polarity while the SQUID MEG system shows the bipolar aspect. This result was caused by insufficient detection area of the atomic magnetometer sensor system.

Later, a wide detection area system was developed (Kim et al. 2008). The system was equipped with a wide rectangular cell, retro-reflect scheme, orthogonal tangential field component measurement, and detuned balanced pumping for the purpose of source localization (Fig. 28). The system gets rid of a blind direction in the probe beam and achieves more balanced pumping in the wide cell.

In conclusion, the atomic-magnetometer-based MEG system shows great potential as an alternative tool to a SQUID-based MEG system. As for now, there are still several practical problems that need to be solved; absolute field zeroing, compromise between sensitivity and bandwidth, phase delayed response depending on its pumping rate, etc.

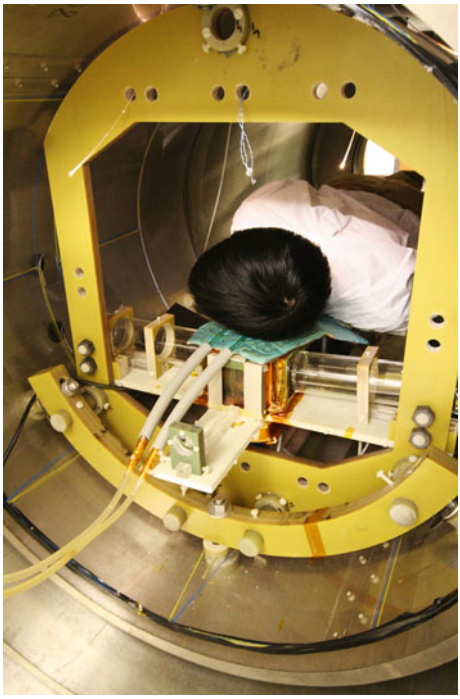

Fig. 26 Auditory evoked field measurement with the atomic brain magnetometer system. The potassium cell and a human subject are placed in a three-layered cylindrical Mu-metal shield. To block heat from the oven containing the cell, cooling water is circulating through a water bag between the head and the oven. Tone stimuli are applied to an ear through a non-magnetic pneumatic earphone (picture courtesy of K. Kim et al. in NeuroImage journal)

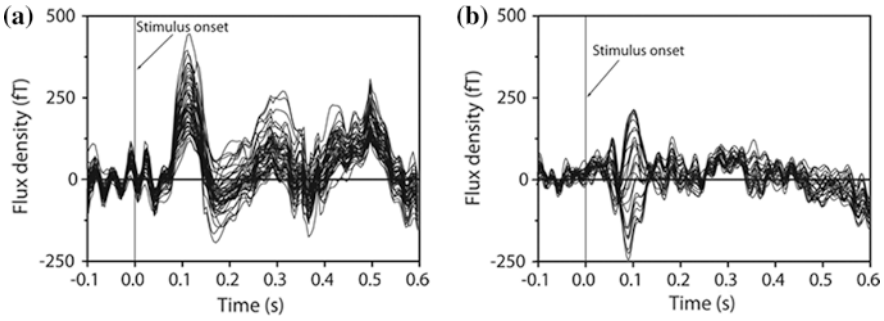

Fig. 27 **a** Auditory evoked field traces for all atomic magnetometer channels. The typical N100 m peak appears 100 ms after the sound stimulus. **b** AEF traces measured by a 37-channel SQUID MEG system (picture courtesy of K. Kim et al. in NeuroImage journal)

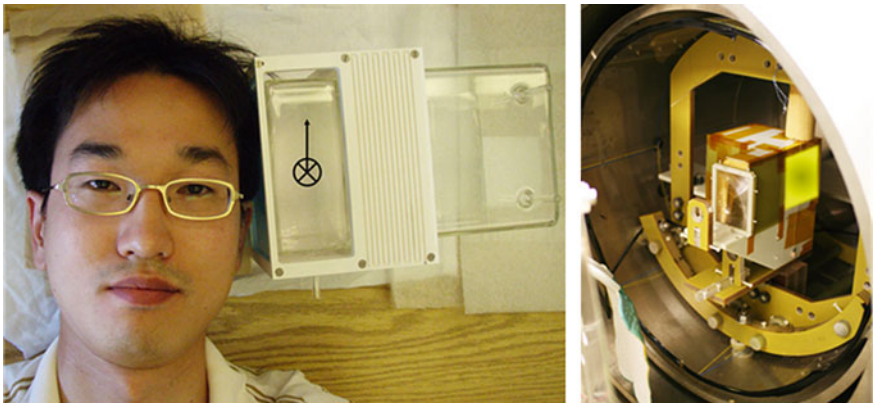

Fig. 28 A wide cell atomic brain magnetometer system for the purpose of source localization

Fig. 29 A micro-Tesla NMR/MRI system. The measurement is conducted under a micro-Tesla magnetic field. All the detection and coil systems are placed in a magnetically shielded room

8 Brain Magnetic Resonance: A Novel Modality for Visualizing Brain Functional Connectivity

Micro-Tesla nuclear magnetic resonance (NMR) technique is one of the most challenging applications based on SQUID technology. In the technique, the external magnetic field is the order of micro-Tesla and all the apparatuses including a pre-polarized sample, an imaging gradient field coil system, a low-noise SQUID detection system are placed in a magnetically shielded room (Fig. 29).

The frequency independent, high sensitivity of the SQUID magnetometer enables the measurement of weak NMR signals even for the low Larmor frequency at a micro-Tesla static field, which could provide a new application such as direct measurements of low frequency electrophysiological activity.

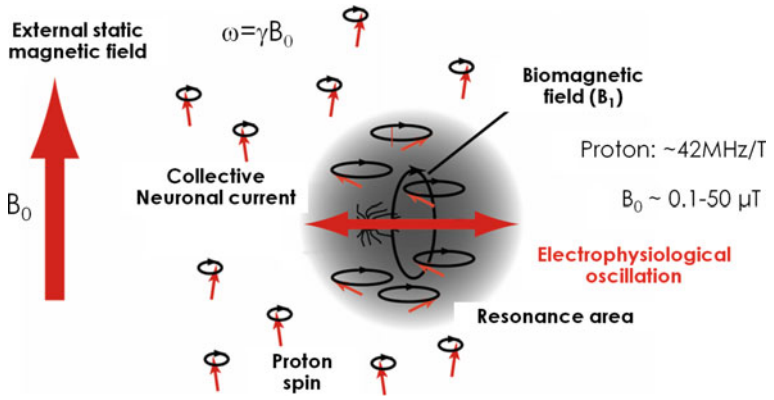

Fig. 30 The concept of biomagnetic resonance. A periodic electrophysiological oscillation can resonate nearby protons when the Larmor frequency of the external field is matched with the frequency of the electrophysiological oscillation

We suggest the new research field of SQUID NMR, be referred to as biomagnetic resonance techniques (Kim et al. 2012a). The concept of biomagnetic resonance is to conduct a direct detection of coherent bioelectric oscillation (Fig. 30).

For this purpose, we make resonance between the precession frequency of the nearby protons and the frequency of electrophysiological oscillation. The frequency range of the electrophysiological oscillation is about 1 Hz ∼ 1 kHz. As examples for the biomagnetic resonance techniques, we can think of heart magnetic resonance (HMR) and brain magnetic resonance (BMR).

HMR could be applied for development of a medical instrument localizing an abnormal myocardial excitation in hearts. In arrhythmia like atrial fibrillation or flutter, the excitation has rhythmic activity with its own characteristic frequency. The main idea of HMR is to match the NMR frequency to the specific frequency of the abnormal heart activity so that we could find the position of the reentry current generation by using the conventional magnetic resonance imaging (MRI) technique (Kim 2012).

In BMR, matching the NMR frequency to the frequency of a periodic neural oscillation like alpha- or gamma-band waves enables direct visualization of the brain functional connectivity by MRI. Especially, BMR enables localization of multiple correlated sources which has been challenging in the MEG/EEG source reconstruction.

We demonstrated the feasibility of these new ideas by conducting numerical simulations and phantom experiments with a SQUID-based micro-Tesla NMR equipment (Kim 2012c). We introduced an experimental trick named K-step, a non-adiabatic change of the external field, to decouple the NMR signal from the direct measurement of the biomagnetic fields, as well.

In the future, we expect the BMR technique could provide valuable information on neurocomputational analysis underlying higher cognitive functions of the human brain.

9 Conclusion

The technology of modern MEG systems is matured enough to measure MEG signals with sufficient signal-to-noise ratios. MEG systems using high-sensitivity SQUID sensors, either magnetometer or gradiometer (axial or planar), have system sensitivity about 3 fT/$\sqrt{}$Hz in the white frequency range. Liquid Helium dewars and MSRs are well-matured in terms of performance, but some improvements are needed to further reduce fabrication and operation costs.

Considering that liquid He is becoming more difficult to acquire, radical improvements in cooling concepts or sensor technology is needed, which do not rely on liquid He, or cooling with very-little use of liquid He. For example, cryocooler operation of low-T_c SQUID system (Sata et al. 1999), use of low-noise high-T_c SQUIDs (Faley et al. 2013) or low-noise atomic magnetometers (Sander et al. 2012) could be considered. However, cryocooler operation generates vibration noise peaks in the measurement frequency region, while mass fabrication of reliable high-sensitivity high-T_c SQUID is still an unsolved task, and the atomic magnetometer still has a technical difficulty of eliminating absolute field in the atomic vapor cells. Though the development speed of these liquid-He-free sensors is rather slow, it is worthy of watching their progress.

References

Adelerhof DJ, Nijstad H, Flokstra J, Rogalla H (1994) (Double) relaxation oscillation SQUIDs with high flux-to-voltage transfer: simulations and experiments. J Appl Phys 76:3875–3886

Cardoso JF (1999) High-order contrasts for independent component analysis. Neural Comput 11(1):157–192

Del Gratta C, Pizzella V, Tecchio F, Romani GL (2001) Magnetoencephalography—a noninvasive brain imaging method with 1 ms time resolution. Rep Prog Phys 64:1759–1814

Dössel O, David B, Fuchs M, Krüger J, Lüdeke KM, Wischmann HA (1993) A modular 31-channel SQUID system for biomagnetic measurements. IEEE Trans Appl Supercond 3:1883–1886

Drung D (1996) SQUID Sensors. In: Weinstock H (ed) Fundamentals, Fabrication and Applications. Kluwer, Dordrecht, pp 63–116

Drung D, Mück M (2004) SQUID electronics. In: Clarke J, Braginski AI (eds) The SQUID handbook. Wiley, Weinheim, pp 569–578

Erné SN (1983) Shielded rooms. In: Williamson SJ, Romani GL, Kaufman, Modena I (eds) Biomagnetism, an interdisplinary approach. Plenum Press, New York, pp 85–135

Faley MI, Poppe U, Dunin-Borkowski RE, Schiek M, Boers F, Chocholacs H, Dammers J, Eich E, Shah NJ, Ermakov AB, Slobodchikov VY, Maslennikov YV, Koshelets VP (2013) High-Tc DC SQUIDS for magnetoencephalography. IEEE Trans Appl Supercond 23(3):1600705

Hämäläinen M, Hari R, Ilmoniemi RJ, Knuutila J, Lounasmaa OV (1993) Magnetoencephalography. Theory, instrumentation and applications to the noninvasive study of human brain function. Rev Mod Phys 65:413–497

Kelhä VO, Pukki JM, Peltonen RS, Penttinen AJ, Ilmoniemi RJ, Heino JJ (1982) Design, construction, and performance of a large-volume magnetic shield. IEEE Trans Magn 18(1): 260–270

Ketchen MB (1987) Integrated thin-film dc SQUID sensors. IEEE Trans Magn 23:1650–1657

Kim K, Lee YH, Kwon H, Kim JM, Park YK, Kim IS (2004) Correction in the principal component elimination method for neuromagnetic evoked field measurements. J Korean Phys Soc 44(4):980–986

Kim K, Xia H, Lee SK, Romalis M (2008) Development of a wide-coverage atomic brain magnetometer system. In: Proceedings of 16th international conference on biomagnetism, Vancouver, BC, Canada, p 229–232

Kim K (2012) Toward cardiac electrophysiological mapping based on micro-Tesla NMR: a novel modality for localizing the cardiac reentry. Am Inst Phys Adv 2(2):022156

Kim K, Lee SJ, Kang CS, Hwang SM, Lee YH, Yu KK (2012a) Biomagnetic resonance technique based on SQUID NMR. In: Proceedings of international symposium on superconductivity, FD-6-INV:127

Kim K, Lee SJ, Kang CS, Hwang SM, Lee YH, Yu KK (2012c) Toward a novel brain functional connectivity visualization tool by direct imaging of coherent brain waves: brain magnetic resonance. In: Proceedings of 18th international conference on biomagnetism, We-89, p 389

Knuutila J (2007) Instrumentation development: from MEG recording to functional mapping. Int Congr Ser 1300:7–10

Lee YH, Kwon H, Kim JM, Park YK, Park JC (1999) Noise characteristics of double relaxation oscillation superconducting quantum interference devices with reference junction. Supercond Sci Technol 12:943–945

Lee YH, Kwon H, Kim JM, Kim K, Kim IS, Park YK (2005) Double relaxation oscillation SQUID system for biomagnetic multichannel measurements. IEICE Trans Electronic E88-C: 168–174

Lee YH, Yu KK, Kwon H, Kim JM, Kim K, Park YK, Yang HC, Chen KL, Yang SY, Horng HE (2009) A whole-head magnetoencephalography system with compact axial gradiometer structure. Supercond Sci Technol 22:045023

Nowak H (1998) Biomagnetism. In: Andrä W, Nowak H (eds) Magnetism in Medicine. Wiley, Berlin, pp 85–135

Parkkonen L (2010) Instrumentation and Data Processing. In: Hansen PC, Kringelbach ML, Salmelin R (eds) MEG: An Introduction to Methods. Oxford University Press, Oxford, pp 24–64

Pizzella V, Della Penna S, Del Gratta C, Romani GL (2001) SQUID systems for biomagnetic imaging. Supercond Sci and Technol 14: R79–R114

Sander TH, Preusser J, Mhaskar R, Kitching J, Trahms L, Knappe S (2012) Magnetoencephalography with a chip-scale atomic magnetometer. Biomed Opt Express 3(5):981–990

Sata K, Yoshida T, Fujimoto S, Miyahara S, Kang YM (1999) A Cryocooled helmet-shaped MEG measurement system. In: Proceeding of international superconductive electronics conference, p 406–408

Sullivan GW, Lewis PS, George JS, Flynn ER (1989) A magnetic shielded room designed for magnetoencephalography. Rev Sci Instrum 60(4):765–770

Taulu S, Kajola M, Simola J (2004) Suppression of interference and artifacts by the signal space separation method. Brain Topogr 16(4):269–275

ter Brake HJM, Fleuren FH, Ulfman JA, Flokstra J (1986) Elimination of flux-transformer crosstalk in multichannel SQUID magnetometers. Cryogenics 26:667–670

ter Brake HJM, Flokstra J, Houwman EP, Veldhuis D, Jaszczuk W, Stammis R, van Ancum GK, Rogalla H (1992) On the SQUID-Module for the UT Multichannel Neuromagnetometer. Superconducting Devices and Their Applications. Springer, Berlin, p 521–524

Uusitalo MA, Ilmoniemi RJ (1997) Signal-space projection method for separating MEG or EEG into components. Med Biol Eng Compu 35:135–140
Vrba J, Robinson SE (2001) Signal processing in magnetoencephalography. Methods 25:249–271
Vrba J, Robinson SE (2002) SQUID sensor array configurations for magnetoence-phalography applications. Supercond Sci Technol 15:R51–R89

Novel Noise Reduction Methods

Samu Taulu, Juha Simola, Jukka Nenonen and Lauri Parkkonen

Abstract Magnetoencephalography (MEG) is a non-invasive neuroimaging tool that offers a combination of excellent temporal and good spatial resolution, provided that the acquired signals have a high enough signal-to-noise ratio. This requirement is often compromised as MEG signals are very weak and often masked by interfering signals from environmental noise sources present at most MEG sites. Even more challenging interference is encountered if the subject carries any magnetic material attached to the body, which is sometimes inevitable in clinical settings, e.g., due to therapeutic stimulators. Therefore, to enable reliable data analysis, it is very important to reduce the contribution of noise in MEG signals as efficiently as possible. In this chapter, we review the basic characteristics of MEG signals, give a short review on traditional approaches to suppress noise, and describe some examples of modern noise reduction methods. Specifically, we emphasize the usefulness of advanced mathematical algorithms applied on the multichannel MEG data.

Keywords Noise suppression · Signal processing · Magnetic shielding · Signal space · Multichannel measurement · Interference · Calibration accuracy · Crosstalk · Signal space projection · Signal space separation · Active compensation · Principal component analysis · Independent component analysis · Spatial filtering · Artifact

S. Taulu (✉) · J. Simola · J. Nenonen · L. Parkkonen
Elekta Oy, P.O. Box 34, 00531 Helsinki, Finland
e-mail: Samu.Taulu@elekta.com

L. Parkkonen
Department of Biomedical Engineering and Computational Science, Aalto University School of Science, Espoo, Finland

S. Supek and C. J. Aine (eds.), *Magnetoencephalography*,
DOI: 10.1007/978-3-642-33045-2_2, © Springer-Verlag Berlin Heidelberg 2014

1 Introduction to Noise Reduction

1.1 Characteristics of MEG Signals and Interference

In MEG, we make inferences about neural processes based on the magnetic field produced by the associated neural currents (see, e.g., Hämäläinen et al. 1993). This magnetic field is detected outside of the head with sensors that are sensitive enough to capture those very weak signals, typically on the order of 10–1,000 fT at the usual measurement distance from the brain tissue. To date, the only technically practical and sufficiently sensitive sensor for MEG is the superconducting quantum interference device (SQUID) (see, e.g., Wikswo 2004; Clarke and Braginski 2006) although other potentially promising sensor types have also been introduced, such as atomic, or optical, magnetometers (Kominis et al. 2003) and GMR-based "mixed sensors" (Pannetier et al. 2004). Regardless of the sensor type, estimation of the neural sources underlying the MEG signals is compromised by inaccuracies posed by the MEG hardware itself and, more importantly, by magnetic interference from sources external to the brain. Due to the weakness of the brain signals, interference quite often dominates the measured MEG data and should therefore be identified and suppressed as accurately as possible. Thus, it is important to model the interference in MEG data even more precisely than the brain signal contribution. When successful, this modeling enables accurate extraction and suppression of the interference and thus facilitates reliable source analysis. However, it is quite common that source reconstruction algorithms are applied on acquired signals with the assumption of ideal hardware and ideal measurement conditions. If these assumptions were true, then one could directly fit forward models derived from Maxwell's equations to the measured data, and find the most plausible source configuration among all possible source distributions. This inverse problem, which inherently does not have a unique solution (Helmholtz 1853), only requires information about the source geometry with respect to the detected magnetic field. Yet, to obtain most accurate and reliable results, the compliance of the recorded signals with Maxwell's equations must be verified. Furthermore, the contribution of magnetic signals from sources outside of the brain should be suppressed.

Before we discuss the different types of interference that can distort the MEG signal and the approaches that can be used to suppress them, let us first review some of the basic concepts and characteristics of MEG signals. Each SQUID sensor is coupled to a pick-up loop that measures the flux of the magnetic induction field $\mathbf{B}$ through the loop. Specifically, the flux can be expressed as the surface integral of the field $\mathbf{B}$ over the area of the pick-up loop: $\phi = \int \mathbf{B} \cdot \mathbf{ds}$.

The first MEG measurements were performed with only one sensor (Cohen 1968, 1972). The number of sensors simultaneously detecting the flux at distinct locations was small until the 1980s when the size of the sensor array started to grow rapidly. Today, modern MEG systems contain hundreds of sensors (e.g. Clarke and Braginski 2006, Chap. 11). The multichannel output of these systems can be expressed as a time-varying vector in the *signal space*, a concept introduced

in the 1980s (Ilmoniemi 1981; Ilmoniemi and Williamson 1987; Ilmoniemi et al. 1987). Sampling theory (Ahonen et al. 1993) is crucial for the design of sensor arrays as well as for understanding the physical aspects of the multichannel signals, especially their spatial complexity and information content.

Various system issues in multichannel MEG systems complicate the interference suppression and signal analysis (Clarke and Braginski 2006, Chap. 7). Sensors packed close to each other in a multichannel array always suffer from crosstalk phenomena to some extent. These couplings, of the order of 1 %, typically arise from inductive coupling between the pick-up coils and feedback currents of the neighbouring MEG channels. Such cross-talk between the channels distorts the signals even in the absence of any external interference or hardware calibration errors. Therefore, cross-talk should be computationally or experimentally determined and compensated for to get an estimate of the cross-talk-free signal. Alternatively, the signals could be compensated for cross-talk in the forward model. Another major concern possibly violating our assumption of the direct applicability of Maxwell's equations on measured signals are the calibration errors. For example, the electronic components used to transform the actual magnetic flux to a voltage may contain gain errors distorting the measurement. Manufacturing of the sensors is not infinitely accurate; there may be slight variations in the surface areas of the pick-up loops, locations and orientations of the sensor may deviate from the nominal ones, and the gradiometers may exhibit small imbalances. Therefore, it is important to calibrate the system as accurately as possible before estimating any source parameters from the data with mathematical models.

In this chapter, we concentrate on interference suppression methods operating at the sensor level of a multichannel MEG system. We do not assume any specific neural source model although some source modeling approaches, such as the beamformer, may also efficiently suppress interfering signals. We will mainly describe approaches for processing of the sensor-level data that can subsequently be used for analysis with any desired source modeling method. Regarding nomenclature, although "noise" is a commonly used general term to describe all kinds of magnetic disturbance fields and artifacts, we prefer to classify different types of MEG disturbance as follows: our use of "interference" will refer to non-physiological sources that are clearly unrelated to the MEG sensor array whereas our use of "noise" will refer to sensor or radiation-shield noise caused by random processes.

1.2 Sampling of the Neuromagnetic Field

All interference suppression methods make assumptions about the separability and detectability of interference and signals of interest. Such assumptions may include *a priori* information about the spatial, temporal, or spectral features characteristic to the different signal components. One of the fundamental questions is whether

we can decompose the multichannel measurements into unique subsets of basic components, some containing only interference and others only neural signals.

In the spatial domain, the number of degrees of freedom, or the effective rank of the neuromagnetic data, has been extensively studied in the past (Ahonen et al. 1993). This spatial sampling theory for MEG is based on the fact that a multichannel MEG measurement can be considered as spatial sampling of the continuous neuromagnetic field. The theory shows that the measurable MEG signals are limited to the low end of the spatial-frequency spectrum. As a practical consequence, there is an upper limit to the number of sensors and a lower limit to the minimum distance between adjacent sensors. Specifically, it has been shown that for MEG signals measured at the minimum distance d, the contribution of spatial frequencies higher than $1/(2d)$ is below the sensor noise and therefore insignificant. Thus, the part containing biomagnetic information in the measured signals is limited in spatial complexity, which also means that the number of degrees of freedom of MEG data is limited. Although this reduces the effective rank of the data to about 100, hundreds of MEG channels are needed to reliably estimate the basis components spanning all detectable signals (e.g. Nenonen et al. 2004; Taulu and Kajola 2005).

1.3 Challenges Specific to MEG

The basic challenge of MEG stems from the fact that the neural currents are weak and aligned coherently in the brain only over a short distance, and the associated magnetic field is measured by sensors outside of the head. Additionally, with SQUID-based detectors, the sensor-to-source distance is further increased by the necessary thermal insulation layer of the helium dewar, about 20 mm. Consequently, the amplitude of the neuromagnetic signal detected in MEG is in the range from 10 to 1,000 fT.

The weakness of the signal can be overcome by increasing the sensitivity of the sensors; however, sensors that are more sensitive are also more susceptible to ambient interference fields, which may eventually exceed the dynamic range of the sensors. Clinical environments are often magnetically noisy, with a variety of electrical equipment radiating magnetic interference not only at the power line frequency and its harmonics, but also across a wide frequency range reaching from near DC up to several GHz. Interference at the lower end of the frequency range is usually due to traffic (cars, trains, trams) and large moving objects inside the building (e.g. elevators). The typical low-frequency peak-to-peak variation of the magnetic field in such an environment is a couple of μT.

To measure 10-fT signals of interest on top of 1-μT interference, one would need a sensor with a dynamic range exceeding 8 orders of magnitude. To date, no magnetic sensor exists with a linear response over such a wide dynamic range. The linearity of the sensors, on the other hand, is a necessary prerequisite for successful signal processing and source analysis. Therefore, an efficient means to reduce the

actual physical magnetic interference is necessary for feasible MEG recordings and analysis, especially in a clinical environment. When hardware-based magnetic shielding is sufficient to keep the sensors within their linear operating range, the remaining interference can be further reduced by multichannel signal processing methods, such as spatial and temporal filtering.

Another challenge specific to MEG is the possible movement of the subject's head during recording. The physical sensor array of the MEG system is stationary. Movement-related distortion of the signal biases source localization and is more challenging with MEG than with the EEG method where the electrodes are attached on the scalp and do not move with respect to brain. To fully benefit from the MEG method's better source localization capability, one must ensure that the accurate location of the head relative to the sensor array is known at all times during the MEG recording.

1.4 Sources of Interference and Noise

The largest-amplitude ambient magnetic fields usually arise from traffic outside of the building. Elevators and MRI magnets operated close to MEG, and even doors made of magnetic material are potential sources of magnetic interference inside of the building. In urban environments, cars on nearby streets, trains and metros cause low-frequency peak-to-peak variations of magnetic field which are typically in the range 1–3μT.

When a vehicle moves at a distance of D with velocity v, the frequency range of the resulting interference is around v/D. For example, cars driving at 50 km/h at a distance of 30 m or a train passing by at 200 km/h at a distance of 100 m result in low-frequency field variations at around 0.5 Hz.

In this frequency range the shielding factor of a typical magnetically shielded room (MSR) is rather low, about 100 (40 dB). Therefore, operating magnetometer sensors in an MSR with 1-μT ambient interference from traffic requires sensors with higher than 10-nT dynamic range, if no other means of interference rejection is used.

Because the shielding factor of an MSR rises steeply with increasing frequency, the low-frequency interference present in the environment will typically dictate the required hardware shielding performance at a specific MEG site. For example, interference at powerline frequencies 50/60 Hz seldom exceeds 1μT in clinical environments, and is thus sufficiently dampened by a typical MSR which easily attains a shielding factor in the range of 10^5 (100 dB) at these frequencies. An example of low- and line-frequency interference inside a magnetically shielded room is shown in Fig. 1.

At radio frequencies up to several GHz, an MSR should maintain a shielding factor of about 10^5 or higher. Although these frequencies are much higher than any brain signals and thus irrelevant for MEG, the shielding is still required because the functioning of DC SQUIDs involves intrinsic frequencies in the GHz range, related

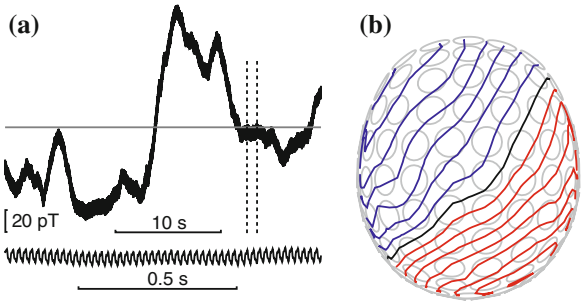

Fig. 1 **a** An example of a single magnetometer (over the occipital region) signal recorded without a subject in the magnetically shielded room. The inset shows a 1-s epoch of the data which reveals the line-frequency contamination. **b** Spatial distribution at the time of the largest amplitude of the signal shows a homogeneous field distribution. The view is from the top of the sensor array, and the *circles* indicate the locations of the 102 magnetometers of the Elekta Neuromag MEG system. *Blue* and *red lines* indicate magnetic field flux into and out of the array surface, respectively. The step between adjacent contour lines is 20 pT

to the superconducting tunnel junctions whose so-called Josephson frequency is at 4.8 GHz for a bias voltage of 10 μV (see, e.g., Clarke and Braginski 2006). Modern digital equipment may cause strong electromagnetic radiation in this frequency range, and would severely disturb unshielded SQUID-based sensors.

The sources of interference and noise mentioned above are related to the installation site of the MEG device. In addition, there are numerous interference sources that are related to the MEG technology itself. Some of them cannot be compensated for by the MSR because they stem from the MSR itself or from sources inside of the MSR. For example, the walls of the MSR are made of conductive and magnetic material, which may result in magnetic interference by two mechanisms. The thermal currents in the walls of a typical MSR generate a magnetic field noise density of about 2 fT/$\sqrt{\text{Hz}}$ (Nenonen et al. 1996). Also, small vibrations of the walls result in magnetic interference typically seen as 10–30-pT peaks in the frequency band 13–30 Hz. These peaks result from the high-Q-value eigenmodes of the MSR walls and ceiling that are driven by the vibration of the building and the infrasound due to forced ventilation.

Another vibration-related artifact in MEG signals arises from the mechanical movement of the MEG device itself in the remanence field inside of the MSR. The maximal amplitude of this type of artifact in magnetometer sensors can be estimated by multiplying the remanence field by the vibration-related rotation angle. The remanence field in a typical MSR is 100 nT. Assuming the vibrational rotation to be a 10-μm movement of the sensor helmet around an axis one meter away from the helmet, we observe 1 pT magnetic signal due to this vibration.

All metal, magnetic or conductive, components of the MEG device are potential sources of magnetic interference. Most of these sources can be eliminated by proper design of the equipment. After careful design, the dominant device-related source of magnetic interference is typically the thermal insulation (super

insulation) covering the sensor area of the dewar, which is necessary to keep the liquid helium boil-off rate below 10 l per day. In modern MEG devices this noise contribution is below 3 fT/$\sqrt{\text{Hz}}$. Any auxiliary devices such as stimulators, cameras, speakers or microphones used inside of the MSR are also potential sources of severe interference. The compatibility of these devices with the MEG method must be carefully verified case by case.

Finally, the recorded MEG signals contain sensor noise related to the SQUIDs and their readout electronics. The pick-up antennas in a modern MEG device, having about 300 sensors in total, are relatively small. Therefore, to achieve adequate field sensitivity, it is necessary to minimize the electronics-related noise contribution. This can be done, for example, by applying pre-amplifier noise cancellation based on positive feedback (Kiviranta and Seppä 1995). In this way, the noise in individual MEG channels can be kept at the level of 3–4 fT/$\sqrt{\text{Hz}}$ in the white noise range and at about (6/*f*) fT/$\sqrt{\text{Hz}}$ at low frequencies (1/*f*-noise). There are also other device-related non-idealities that manifest as distortion and bias in the recorded data. Such factors include, for example, errors in calibration, location, and orientation of individual sensors, as well as imbalance of gradiometers and cross-talk between the channels. Most of these non-idealities, often seen as a kind of "DC-interference", can be well characterized and compensated for by modern software methods that are discussed in detail in Sect. 3.

In addition to the ambient and device-related noise and interference mechanisms described above, the subject studied—or patient in case of clinical MEG—may also be a source of severe interference. This applies especially in clinical work where patients may often have dental braces, therapeutic stimulators, or magnetic residue from prior surgical operations on or inside the skull. Prior to the invention of advanced software-based methods for interference rejection, such magnetic components in the body were considered a contraindication for a meaningful MEG study. The software methods to suppress disturbances caused by magnetism in patients are discussed in detail in Sect. 3.

2 Conventional Interference Reduction Methods

2.1 Magnetic Shielding

As mentioned in the previous section, the basic method of interference reduction that has been in use since the very beginning of neuromagnetic studies (Cohen 1970) is to use a magnetically shielded room (MSR). Figure 2 illustrates the principle of magnetic shielding and shows a commercial three-layer room. MSR is a room-size metal enclosure constructed using layers of both highly conductive metal, usually aluminum or copper, and metal with high permeability (see e.g. Kelhä et al. 1982). Mu-metal is a commercial name for a variety of nickel-iron alloys having a dynamic (initial) relative permeability as high as 50,000.

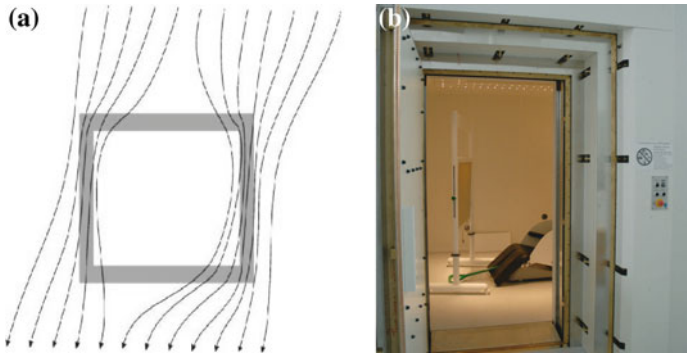

Fig. 2 **a** Principle of magnetic shielding. Layers of aluminum and mu-metal provide a path for magnetic field lines around the enclosure. **b** A three-layer magnetically shielded room (Imedco AG, Hägendorf, Switzerland) at the O.V. Lounasmaa Laboratory of Aalto University (Espoo, Finland)

The shielding performance of a MSR is usually described by a frequency-dependent shielding factor which is the ratio between the external interference field $B_{\text{ext}}(f)$ and the corresponding value of field inside of the shield $B_{\text{in}}(f)$, that is, $S(f) = B_{\text{ext}}(f)/B_{\text{in}}(f)$. The shielding effect of a metallic magnetic shield made of conducting and high-permeability material is based on two mechanisms: polarization of the high-permeability metal, and eddy currents induced by varying magnetic field. These mechanisms are demonstrated in Fig. 3 where the shielding performances of different wall compositions, with equal proportions of mu-metal and aluminum, are compared.

At frequencies below 0.1 Hz, where induction is negligible, the polarization of the high-permeability material is the only mechanism providing magnetic shielding. When the frequency increases, the induction mechanism starts to have an effect on the shielding. In this frequency range, additional shielding is provided by the "global" eddy currents induced to run in the conducting walls around the entire room. This additional shielding effect sets in at the frequency determined by the resistance of the conductive wall and the inductance related to these "global" currents. The related shielding effect grows proportional to the frequency, as shown by the lowermost $S(f)$-curve in Fig. 3. When the frequency is further increased, the induced currents on the outer surface of the wall start to shield the inner parts of the wall, and the shielding starts to grow exponentially with increasing frequency. This is the well-known skin effect, with a skin depth given by $\delta = 1/\sqrt{\pi f \mu \sigma}$. Here σ and μ are the conductivity and permeability of the wall.

Since the construction of the first room-size magnetic shield in 1962 (Patton and Fitch 1962), a variety of different multilayer MSRs have been manufactured for biomagnetic purposes. To obtain increasingly better magnetic shielding performance, the amount of metal and the number of metal layers has been increased up to the record number of eight (Bork et al. 2001). Such a huge MSR with $6 \times 6 \times 6$ m^3 external dimensions and a total of 24.3 tons of mu-metal provides

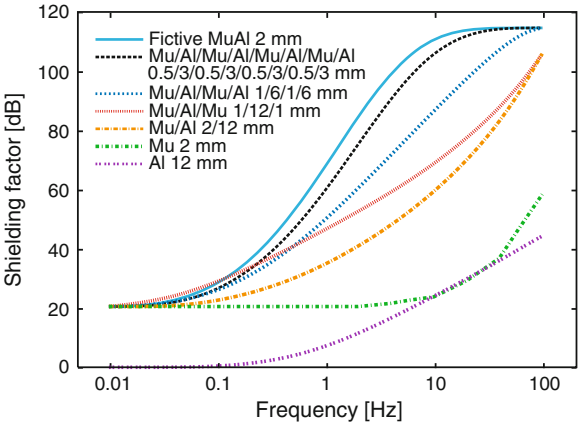

Fig. 3 Optimization of aluminum/mumetal-based MSR wall structure. Estimated shielding factors of four different Al/mu-sandwich structures are shown. The scattering matrix model for concentric spherical shells (e.g., Kelhä et al. 1982) with inside radius 1.9 m is used in the calculation. The layers in the 2-, 3-, 4-, and 8-layer sandwiches are in surface-to-surface contact, and the amount of metal is kept constant in all four structures; 2 mm of mu-metal and 12 mm of aluminum in total. For the electrical conductivity of aluminum and mu-metal, and for the relative permeability of mu-metal we have used $3.57 \times 10^7 (\Omega\mathrm{m})^{-1}$, $1.82 \times 10^6 (\Omega\mathrm{m})^{-1}$, and 16,000, respectively. For reference, the $S(f)$-curves of 12 mm of mere aluminum, and 2 mm of mere mu-metal are shown by the two lowermost *curves*. For mere aluminum, the shielding is negligible below 0.1 Hz, and above that grows proportional to f due to induced global eddy currents. The skin depth of aluminum is so long that no skin effect, that is, exponential growth of $S(f)$, is evident even at 100 Hz. This is because of the low relative permeability of aluminum. The second lowest curve is for 2-mm mu-metal showing a 20-dB shielding down to DC but no global current shielding regime, because of low electrical conductivity of mu-metal. Instead, a skin effect regime with exponential growth of $S(f)$ is starting to show up above 10 Hz. Keeping the total amount of metal constant, but increasing the number of layers in the al/mu-sandwich reduces the skin depth and the frequency at which the skin effect sets in. With an increasing number of layers in the sandwich, the shielding factor at a given frequency between 0.5 and 100 Hz increases and the $S(f)$-curves asymptotically approach the uppermost curve showing the shielding obtained with an "infinite number" of layers, that is, a 2-mm thick shell made of fictive "Al/mu-alloy" having the electrical conductivity of a 12-mm thick aluminum plate, and the relative permeability of mu-metal. The saturation of $S(f)$ at 115 dB is due to the openings in the MSR wall

excellent magnetic shielding even at very low frequencies. While this type of shielding is extremely useful in scientific research requiring magnetically disturbance free environments, it is not practical for clinical MEG use.

As a solution for the need of compact and lightweight MSRs for clinical MEG applications, designs with a total MSR weight below 5 tons and external dimensions of $3 \times 4 \times 2.5$ m^3 have been developed during the past ten years (for performance evaluations, see Parkkonen et al. (2006) and de Tiège et al. (2008)). To ensure sufficient shielding performance of these light MSRs with reduced amount of mu-metal, special attention has been paid to the joints between the metal wall elements to guarantee optimal electric and magnetic conductance

across the joints (Simola et al. 2005). Also, several conductive aluminum layers and high-permeability mu-metal layers have been interleaved to reduce the effective skin depth of the wall structure (Simola 2003). This lowers the frequency at which the skin effect and the related exponential growth of the shielding factor $S(f)$ with increasing frequency sets in, thus increasing the shielding performance at frequencies above 0.5 Hz; see Fig. 3.

To support the magnetic shielding provided by a MSR, several active shielding concepts have been proposed and realized. The simplest method to actively counteract ambient magnetic interference consists of a magnetic sensor—a three-axis fluxgate, for example—located in the vicinity of the MSR, and three orthogonal sets of coils wound on the outside of the MSR. The fluxgate records the variations of the ambient field and controls a current supply that feeds the coil sets to produce a field that counteracts the ambient field variations at the location of the MSR. This method is called feedforward active compensation. In this arrangement the fluxgate has to be located far from any local sources within the building, and at a sufficient distance from the compensation coils. The feedforward system works well against distant interference sources that produce a nearly uniform field. With this method a typical achievable shielding factor against such interference is in the range 10–50 (20–35 dB).

If the fluxgate is moved closer to or within the coil system, the arrangement turns into a feedback system that keeps the magnetic field constant at the location of the fluxgate, providing an alternative approach to construct an active compensation system. The fluxgate cannot be located inside the MSR because the inductive time constant of the MSR leads to a relatively long time delay between $B_{\text{ext}}(t)$ and $B_{\text{in}}(t)$, typically 2–3 s. A novel feedback active compensation method based on the MEG sensors and compensation coils inside the MSR will be described below in Sect. 3.5.5.

2.2 Gradiometrization

Another hardware-related interference rejection method, which has been utilized since the early days of biomagnetism, is the use of gradiometers instead of simple magnetometers. Zimmerman and Frederick (1971) used an axial gradiometer consisting of two oppositely wound co-axial coils, while Cohen (1979) utilized a planar gradiometer where the coils are on the same plane (see Fig. 4).

A first-order gradiometer has a pick-up antenna consisting of two loops that are planar, parallel, and usually identical in size and shape. The loops are oppositely wound and located in space so that one loop is translated from the other by a vector $\mathbf{h}$. The length h is called the baseline of the gradiometer. If $\mathbf{h}$ is parallel to the common normal $\mathbf{n}$ of the loops, the gradiometer is called axial. In the case of a planar gradiometer, $\mathbf{h}$ is orthogonal to $\mathbf{n}$. In principle, $\mathbf{h}$ and $\mathbf{n}$ could be at any angle relative to each other but axial and planar are the two gradiometer types most commonly used.

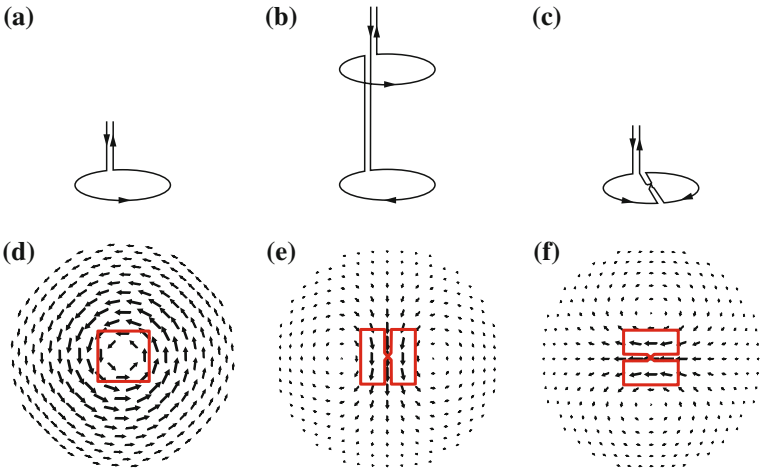

Fig. 4 Some pick-up coil geometries: **a** magnetometer, **b** co-axial first-order gradiometer, and **c** planar first-order gradiometer. The leadfield, or sensitivity, patterns of **d** magnetometer and axial gradiometer measuring B_z, **e** planar gradiometer measuring dB_z/dx, and **f** planar gradiometer measuring dB_z/dy

The signal of a gradiometer MEG channel is proportional to the net magnetic flux through the pick-up antenna. If the field contains gradients up to second order only and the gradiometer is ideal this flux is given by

$$g = A\mathbf{n}^T \begin{pmatrix} \partial B_x/\partial x & \partial B_x/\partial y & \partial B_x/\partial z \\ \partial B_y/\partial x & \partial B_y/\partial y & \partial B_y/\partial z \\ \partial B_z/\partial x & \partial B_z/\partial y & \partial B_z/\partial z \end{pmatrix} \mathbf{h} \tag{1}$$

where A is the area of one gradiometer loop.

For geometrical reasons, gradiometer antennas composed of identical oppositely-wound loops are totally insensitive to a uniform field of any direction. Consequently, they rather effectively reject interference from any sources far away from the MEG device. In practice, the interference rejection ratio of gradiometers is limited by the fact that a typical interference field is not exactly uniform, and that the geometry of the gradiometer is not ideal. The geometric non-ideality of a gradiometer is called imbalance. The signals from near-by sources, the brain signals, are highly non-uniform and therefore attenuated only slightly. Typically, for a gradiometer in a MSR, the signal-to-interference ratio for ambient interference is approximately by a factor of 100 higher than for simple magnetometers.

The interference signal in ideal gradiometers, related to relatively smooth interference fields, is well described by Eq. (1). When dealing with the signals of interest in MEG, which are related to neural current distributions, the signal in a MEG channel is better described by using the concept of a lead field $\mathbf{L}(\mathbf{r})$, defined by the expression

$$b_k = \int_{v'} \mathbf{L}_k(\mathbf{r}') \cdot \mathbf{J}(\mathbf{r}')dv' \tag{2}$$

where the output of channel k, b_k, is obtained as the projection of the current distribution $\mathbf{J}(\mathbf{r}')$ on the lead field, or sensitivity pattern, $\mathbf{L}_k(\mathbf{r}')$.

The two types of gradiometers, axial and planar, have different sensitivity patterns (Fig. 4). An axial gradiometer has a similar lead field as a magnetometer: zero for sources directly under the sensor, otherwise wide circular pattern with the maximum sensitivity some distance sideways. Thus, a single axial gradiometer can detect neuromagnetic signals from a wide region in the brain, but is also sensitive to interference caused by sources near to the sensor. Planar gradiometers in turn have very compact lead fields, which exhibit the maximum directly under the sensor.

2.3 From Single-Channel to Multichannel MEG

In the early days of biomagnetism, MEG devices were comprised of one sensor channel only. Any feature in the signal could be from the brain, environment, or electronics. Instrumentation developed during the years, and the number and size of the sensor arrays increased gradually. Figure 5 illustrates the evolution of multichannel MEG sensor array from a small-size four-channel axial gradiometer to 306-channel whole-head system combining magnetometers and planar gradiometers. Modern whole-head MEG arrays have facilitated development of effective multichannel signal processing and analysis methods, which are discussed in Sect. 3. Design of multichannel sensor arrays involves several parameters, such as the number of channels, geometry of the pick-up coils, internal noise level of the sensors and so on. Detailed comparisons of the advantages and disadvantages of the arrays of axial and planar sensor types have been presented in the literature (Ahonen et al. 1993; Vrba and Robinson 2002; Nenonen et al. 2004).

2.4 Reference Sensors

A method distantly related to the gradiometer concept is the use of reference sensors, which consists of an array of extra magnetic sensors located typically 20 cm above the MEG sensor helmet. The idea is that the reference sensors are so far from the source of interesting signals that they only detect interference. This measured interference can be modeled, either by a physical model or statistically, and then subtracted with proper weighting coefficients from the signals of the MEG channels. Because of the required extra hardware and the modeling and subtraction, the reference sensor method can be considered a combined hardware/software method.

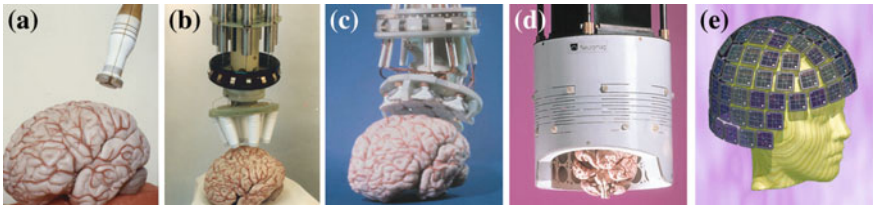

Fig. 5 Evolution of MEG devices: **a** 4-channel axial gradiometer system, **b** 7-channel axial gradiometer system, **c** 24-channel planar gradiometer array, **d** 122-channel planar gradiometer helmet, **e** 306-channel whole-head system combining 102 magnetometers and 204 planar gradiometers. (**a**–**d**: Courtesy of Dr Jukka Knuutila, Elekta Oy; **e**: Courtesy of Dr Mika Seppä, O.V. Lounasmaa Laboratory, Aalto University)

In the reference-sensor method the interference contribution at the primary MEG sensors is extrapolated from the signals in the reference sensors by expanding the magnetic field into a Taylor series about the origin at the primary sensor. Synthetic first-, second- and third-order gradiometers can be formed in this manner (Vrba and Robinson 2001). Magnetometers and gradiometers can serve both as primary and as reference sensors. Synthetic third-order gradiometers reduce the environmental interference substantially. In order to avoid increasing the sensor noise, the reference sensors should have a higher gain than the primary sensors. Synthetic gradiometers have been demonstrated to operate even without a magnetically shielded room in an environment with low magnetic interference level.

2.5 Limitations

All the traditional interference rejection methods described above are in use at many MEG sites and have proven to work and to be sufficient in most cases to enable proper functioning of the MEG device. The main problem with the passive shielding method is the large size, heavy weight and high price of the MSR. Also, the need to isolate the patient behind a closed door may hamper clinical work. Lighter passive magnetic shields would boost the clinical use of MEG.

A relatively simple way to assist passive shielding is to use feedforward active compensation. The basic problem with this method of active compensation is related to the local sources in the vicinity of the MSR and the fluxgate sensor. If there are many such sources, it is impossible to set the system up properly and the arrangement may even amplify the interference from sources close to the fluxgate.

The basic shortcoming of the reference sensor method is related to the fact that the interference inside of the MSR may still be 1,000 times higher than the brain signals. Therefore, to be able to properly subtract the interference, one should know it at the location of each sensor with an accuracy better than one per mille (0.001). This is not possible when the interference needs to be extrapolated from the signals of only 10–30 reference sensors located at a 20-cm distance from the primary MEG sensors.

The conclusion is that improved interference rejection methods are needed, specifically to develop MEG towards clinical use. For clinical installations, it is not always possible to select the magnetically most silent location in the hospital. Also, clinical patients cannot be chosen for subjects as freely as in basic neuroscientific research. Patients may also have therapeutic stimulators that are magnetic or there may be magnetic residue from previous surgery in their body. In addition, patients and healthy volunteers often show interference from biological sources such as the eyes and cardiac muscle; see Parkkonen and Salmelin (2010) for typical examples. None of the methods described above are useful against such interference.

3 Modern Approaches to Noise Reduction

3.1 Mathematical Representation of Multichannel MEG Signals

We will concentrate on mathematical noise reduction methods and start from the basic principles of computational signal representation. These basic concepts are a necessary prerequisite for the understanding of novel algorithms used in MEG today.

As explained above, a common way to express the signals of individual MEG channels is the leadfield representation of Eq. (2), which shows how the output of channel k, b_k, is obtained from the current distribution $\mathbf{J}(\mathbf{r}')$ as the projection of the current distribution to the lead field, or sensitivity pattern, $\mathbf{L}_k(\mathbf{r}')$. MEG sensors are sensitive to both neural currents and currents related to interference but usually the lead fields are computed for neural currents only with the assumption that the measured data are sufficiently clean. Figure 4 shows examples of lead fields of magnetometer and gradiometer channels. The wide-spread sensitivity pattern of the magnetometer indicates that the magnetometer picks up signal from a large portion of the source volume, including deep structures in the brain. Similarly, magnetometers are also quite sensitive to external interference signals, which are spatially relatively uniform. On the other hand, the gradiometer channels are very focal and most sensitive to the superficial parts of the brain and insensitive to homogeneous interference fields.

Modern MEG devices contain hundreds of channels and the whole sensor array discretizes the continuous field distribution into a signal vector $s(t) = [s_1(t)\, s_2(t) \ldots s_N(t)]$ at any given time t. This N-dimensional vector representation allows us to utilize linear algebra in the signal processing of MEG. From now on, we will call the set of measurable signal vectors the *signal space* of MEG and show that different subspaces can be distinguished in the signal space. The concept of signal space was first introduced in MEG already in the 1980s (Ilmoniemi 1981; Ilmoniemi and Williamson 1987; Ilmoniemi et al. 1987) and it has thereafter been the basis of several efficient signal processing algorithms.

3.2 Common Distortion Mechanisms of MEG Signals

The basis of any model applied to a multichannel MEG recording is the assumption that the sensors can be considered independent. For example, according to this assumption, a particular forward model can be computed by evaluating the magnetic flux at individual sensors merely based on the geometry of the associated source model and the sensor itself without considering the signals of other sensors. In reality, however, sensors always have some degree of coupling between each other. Therefore, instead of measuring the pure magnetic flux ϕ_i, channel i detects the distorted signal $\phi_i^{'}$ due to the coupling of all other channels through the so-called cross-talk coefficients k_{ij}, i.e.,

$$\phi_i^{'} = \phi_i + \sum_{j=1}^{N} k_{ij}\phi_j^{'}, \tag{3}$$

where $k_{ii} = 0$. Cross-talk arises e.g. from mutual inductance between sensors or electronics-based couplings. An efficient way to reduce cross-talk is to keep the current of the pick-up coils at zero by feedback, which eliminates the inductive coupling between the pick-up coils. Some cross-talk, however, always exists and it is important to estimate the coefficients k_{ij} either computationally or to measure them directly by sequentially feeding a current to each sensor and detecting the response of other channels to this test current (Taulu 2000). Computational means include a model for the mutual inductance between sensors, which can be based, e.g., on analytical formulae between wire elements of the flux transformers. Once the coefficients k_{ij} have been determined, the above equation can be written in the matrix form

$$\phi^{'} = \phi + K\phi^{'} \tag{4}$$

from which the cross-talk-corrected estimate can be computed as

$$\phi = (I - K)\phi^{'}. \tag{5}$$

In addition to the cross-talk, hardware-originating signal distortion arises due to errors in the calibration coefficients and geometrical imprecision, such as position and orientation errors of the sensors, and imbalance of gradiometers. If the expected field-to-voltage calibration coefficient of channel i is c_i and it deviates from the true calibration c_{0i} as $c_{0i} = c_{\varepsilon i}c_i$, then the corrected signals can be computed as

$$\phi_c = C\phi = C(I - K)\phi^{'}, \tag{6}$$

where C is a diagonal matrix containing the estimated relative calibration coefficients:

$$C = diag(c_{\varepsilon 1} \;\; c_{\varepsilon 2} \;\; \ldots \;\; c_{\varepsilon N}). \tag{7}$$

Thus, the hardware-based distortions such as cross-talk and scalar calibration errors can be compensated for by simple linear operations. The geometric corrections mentioned above have to be incorporated into more complex models that are applied to the acquired and compensated data ϕ_c. Several calibration algorithms have been introduced in MEG (Hall Barbosa et al. 1999; Ornelas et al. 2003; Chella et al. 2012). State-of-the-art calibration accuracy ensures a good match between the measured data and the models, such as the forward fields corresponding to neural currents or models used in interference suppression algorithms.

The distortion mechanisms described above are always present in MEG recordings, even in an ideal environment with no actual interference or noise. In addition, MEG signals always contain random sensor noise or radiation-shield noise, and almost always contain external interference. Quite often disturbances related to the subject or patient are embedded within the signal as well. In the following, we divide the interference and noise of MEG into three groups:

1. Interference from far-away sources; spatially smooth field patterns corresponding to sources relatively far from the sensor array. In an empty MSR, these sources contain currents on the walls of the MSR induced by external interference fields.
2. Interference from near-by sources; spatially complex field patterns due to the proximity of the sources.
3. Random noise intrinsic to the MEG device itself, i.e., sensor noise and sensor artifacts.

In addition to the spatial categories above, different interference types may also have specific time–frequency characteristics that can be utilized in the interference suppression approaches. MSR only attenuates interference of category 1 and therefore MEG measurements have traditionally been conducted only with cooperative subjects who are able to stay still and who have no magnetic material in their body. In clinical settings, however, it is not practical to request or rely on complete immobility of the patient. Even the slightest movements due to respiration or heart beat can cause severe movement artifacts in the presence of magnetized material related to, e.g., dental braces, tiny magnetic residues in the body, or therapeutic stimulators. Thus, signal processing methods are needed to compensate for category 2 interference. Intrinsic sensor noise (category 3) is always present in any MEG recording and its contribution is typically taken into account in the source modelling phase in the form of a covariance matrix but recently new pre-processing methods to reduce sensor noise have also been proposed.

3.3 Physics- and Statistics-Based Detection of Interference

Many interference suppression methods are based on physical or statistical models of the measured signals. The former methods typically utilize a model that aims to explain the signals in physical terms such as sources while the latter methods often consist of finding some statistical features from actual data recorded with the MEG system. In the following, we will use two signal space methods as examples of the statistical and physical approaches and explain their benefits and drawbacks.

The Signal Space Projection (SSP) (Uusitalo and Ilmoniemi 1997) and Signal Space Separation (SSS) (Taulu et al. 2004) methods utilize the ample spatial oversampling of the neuromagnetic field in a modern MEG device with hundreds of channels. At a typical brain-to-sensor distance in MEG ($\sim$3 cm), the magnetic field from neural sources has less than 100 degrees of freedom (independent geometric shapes) that can be resolved above the sensor noise.

The SSP method is based on statistical analysis of the recorded interference signal. The interference is recorded with no subject in the MEG device. A principal component analysis is made on this "empty-room recording" containing only interference and sensor noise.

In the SSP method, the signal recorded by an N-channel device from the subject is projected on the $(N - n)$-dimensional subspace that is orthogonal to the first n principal components—those with the largest eigenvalues—of the empty-room recording. Assuming that the ambient interference is a result from a reasonably stable statistical process this projection leaves us with relatively interference free $(N - n)$-dimensional MEG data. The brain signal is also slightly distorted by the projection operation but this can be taken into account in a simple manner in the subsequent signal analysis (Uusitalo and Ilmoniemi 1997).

SSP is a purely statistical method and therefore does not suffer from any calibration inaccuracy in the sensor array, as long as the calibration of the sensors and the geometry of the sensor array stays constant. Being an orthogonal projection method SSP does not increase the individual sensor noise (rather it decreases the noise slightly) but causes some distortion of the spatial pattern of the signal. Specifically, signals from very deep sources are reduced in amplitude as they have a significant projection on to typical ambient interference directions in the signal space.

Contrary to the SSP method, which is statistical, the SSS method is based on the physics of magnetic fields, i.e., Maxwell's equations (Taulu et al. 2004). In this method, the signal space is provided with a basis that encompasses all physically possible magnetic field distributions (solutions of Maxwell's equations in a space free of magnetic material). The measured signals can be uniquely represented in this basis. By simple physical arguments the field shapes can be classified into two groups: field shapes corresponding to sources inside of the sensor array, and those corresponding to sources outside of the array. In this way, two linear subspaces of the signal space can be defined: S_{in} for inside sources and S_{out} for outside sources. The external interference can now be removed from the signals by simply estimating the contributions of S_{in} and S_{out} and subsequently leaving out the signal components in S_{out}.

The advantage of SSS over SSP is its generic nature as it is based on the physics of the magnetic field rather that statistics of the recorded interference. Because of this, SSS is universal and can handle also such new interference sources that we have no prior statistics on. SSS is not an orthogonal projection, and therefore it does not change the spatial patterns of the neuromagnetic signal. On the other hand, because SSS is based on a computational model, it is rather sensitive to the calibration accuracy of the MEG system (Nurminen et al. 2008).

3.4 Noise Reduction in the Spatial, Temporal, and Spectral Domains

3.4.1 Decomposition of MEG Signals

The data acquired with N_c channels over a period of time consisting of N_t samples can be represented as an $N_c \times N_t$-dimensional matrix Φ. Modern mathematical noise reduction methods are based on a *decomposition* of the high-dimensional data into some basis components that can be used in processing the data to suppress the contribution of unwanted interference signals. We can classify the basic decomposition approaches as follows:

1. Spatial decomposition: $\underset{N_c \times N_t}{\Phi} \rightarrow \underset{n \times N_t}{X}$
2. Spectral decomposition: $\underset{N_c \times N_t}{\Phi} \rightarrow \underset{N_c \times N_F}{F}$
3. Temporal decomposition: $\underset{N_c \times N_t}{\Phi} \rightarrow \underset{N_c \times N_F}{F} \underset{N_F \times N_t}{Y}$
4. Combination of the above: for example, $\underset{N_c \times N_t}{\Phi} \rightarrow \underset{n \times N_t}{X} \rightarrow \underset{n \times N_F}{F} \rightarrow \underset{n \times N_F}{F} \underset{N_F \times N_t}{Y}$

In the following, we will describe the general mathematical models and the consequences of these operations. We will also give some examples of methods belonging to the different categories. A more detailed description of these methods will be given in Sect. 3.5.

3.4.2 Benefits and Drawbacks of the Decomposition Methods

1. In the spatial decomposition, some spatial model is applied to the data in order to extract features of interest and to suppress the contribution of interference signals. This leads to a representation $\underset{n \times N_t}{X}$, which contains the time series of the n spatially relevant features with typically $n \leq N_c$. The decomposition may be performed through a matrix operation

$$X = A\Phi, \tag{8}$$

where A is an $n \times N_c$-dimensional spatial filter matrix that may be, e.g., in the form of an orthogonal or an oblique projection matrix. In the former case, one rotates the data in the signal space into a subspace free of interfering signals (Uusitalo and Ilmoniemi 1997; Parkkonen et al. 1999a). The latter case may be used to extract the interesting from interfering signals in a mathematically unique fashion, e.g., by the SSS method. The benefit of the spatial decomposition is that it preserves the temporal information of the signals and may generally allow a robust classification of signals into interesting and interfering contributions. The drawback is that spatial operations, if not specified properly, may lead to spatial bias of the interesting signal, and measurement errors not modeled by A may spread into the decomposed result X. An example of a measurement error is a malfunctioning sensor. Methods belonging to this category include, e.g., SSP and SSS, some ICA applications, and beamformer. The last method, however, involves a specific neural source model when constructing the spatial filter matrix A.

2. In the spectral decomposition, the data are transformed into the Fourier or some other relevant temporal components by the matrix operation

$$F = \Phi B, \tag{9}$$

where B is an $N_t \times N_F$-dimensional matrix that performs the Fourier transform for each channel separately. The benefit of the spectral decomposition is that the spatial pattern is preserved and no localization bias is thus introduced. The drawback is that the signals of interest and the interference are often in the same frequency range, mixed in such a way that their reliable separation is not possible. A traditional way to use the spectral decomposition is visual investigation of the spectra of individual sensors, the rows of matrix F, and subsequent notch filtering. An example of a mathematically more advanced method is the S3P (Ramirez et al. 2011) algorithm that builds a spatial orthogonal projection matrix based on the spectral decomposition of sensor-level data.

3. In the temporal decomposition, the sensor-level signals are re-calculated from the spectral components. This is done by reconstructing the time courses from the decomposed spectral components and the corresponding temporal basis functions as

$$\Phi = F' Y, \tag{10}$$

where F' is derived from F, e.g., by leaving out spectral components expected to correspond to interference, and Y contains the corresponding temporal patterns of these selected frequency components. The benefits and drawbacks of this approach are the same as in the case of spectral decomposition. An example of

spectrum-based temporal decomposition is simple temporal filtering (low-pass, high-pass, or band-pass). However, the decomposition does not have to be based on Fourier components but it could also be derived through a direct temporal extraction such as independent component analysis (ICA).

4. The above basic formalisms can be modified and combined in several ways. An example is the spatiotemporal signal space separation method (tSSS) that utilizes both the spatial filtering properties and temporal analysis to extract and suppress interference-related temporal forms. Combinations of ICA with short-time Fourier transforms have also been proposed to decompose MEG data into neurophysiologically relevant components (Hyvärinen et al. 2010; Ramkumar et al. 2012).

3.5 Review of Selected Novel Methods

In the following, we introduce a subset of various methods that can be used for interference suppression in multichannel MEG. This list of methods is not comprehensive but it rather shows examples on what the methods are typically based on. For guidelines on recommended practical use of interference and noise suppression methods, see, e.g., the guidelines publication by Gross and colleagues (2013) and the book chapter by Parkkonen and Salmelin (2010). Below, as examples of physical and statistical methods we describe the SSS and SSP methods in more detail.

3.5.1 Multichannel MEG

The signal space in single-channel MEG devices was trivial, one-dimensional, and spatial filtering was impossible. Any feature in the signal could be from the brain, environment, or electronics. The first step taken toward spatial filtering was the adoption of gradiometric sensors described in Sect. 2.2. Instead of measuring one field component at one point in space the field is measured also at an adjacent location. By subtracting the two measurements one reduces the interference signal from distant sources by a large factor, typically 100, but the reduction in the biomagnetic signal is relatively small if a proper base length is chosen for the gradiometer. The use of a gradiometer is an elementary signal space method. The two recordings made by the two pick-up loops of the gradiometer are two measurements, subtracted from each other to reject the common mode, which is dominantly due to ambient interference. This operation could be done by software but doing it by hardware, that is, by wiring a single gradiometer pick-up coil, gives the sensor a lot of extra dynamic range against uniform interference fields. The price paid is that the dimensionality of the signal space is reduced from two (the two loops) to one.

The possibility for actual spatial filtering opened up with the first multichannel devices. Already a two-gradiometer system helps one to further resolve biomagnetic signals and possible device-based artifacts. With an increasing number of channels the estimation and rejection of both ambient and device-based interference became easier.

However, the geometric complexity of the magnetic interference field over a volume as large as a typical MEG sensor array is potentially so high that actual spatial filtering used to recognize and remove ambient interference from the signals can be efficiently realized only when the number of channels is relatively high. This is because the magnetic field is a vector field in three dimensional space with three independent uniform components, five independent first derivatives, seven second derivatives etc. To determine interference fields up to second derivatives thus requires independent measurements done with 15 sensors. So, spatial filtering by gradiometrization up to second order derivatives would cut the signal space dimensions available for the actual brain signals in a 24 channel MEG device, say, down to $24 - 15 = 9$.

This is why efficient spatial filtering in MEG data processing has become available only when the number of channels has grown upward to several hundreds. On the other hand, when such a high number of channels is available, signal space methods based on linear algebra are a better way for interference rejection than, for example, reference sensor systems, for the following reason. The interference field is usually much higher in amplitude than the neuromagnetic signal. Therefore, it must be determined with the best possible accuracy. The optimal way to do this is to use the entire set of sensors instead of the relatively few reference sensors, to record the interference. A further advantage in this approach is that the interference is now recorded at the very locations where we want to know it. No spatial extrapolation is needed, which improves accuracy of the interference estimate. In the signal space approach both interference and the biomagnetic signal are mixed up in the signals from the same set of channels but they can still be separated with appropriate signal space methods.

3.5.2 The SSP Method

The signal space projection method is set up for suppressing ambient magnetic interference by recording MEG data without a subject for a few minutes. In this situation it is certain that all recorded signal is interference. This multichannel signal is then statistically analyzed by using principal component analysis (PCA). The dominant n PCA-components give the signal space directions containing the largest-variance magnetic interference field patterns. These orthonormal signal vectors are then organized as an $N \times n$-dimensional matrix E_n and the orthogonal projection operator is formed as:

$$P_{\text{orth}} = I - E_n E_n^T, \tag{11}$$

where I is an $N \times N$-dimensional identity matrix. Then, the recorded N-channel MEG signal is projected on the $(N–n)$-dimensional signal subspace that is orthogonal to all the directions corresponding to the n dominant PCA components:

$$\phi_{\text{orth}} = P_{\text{orth}} \phi \tag{12}$$

Experience on using the SSP method at several MEG sites over 15 years has shown that the ambient interference field patterns are relatively stable over several years. SSP projection operator (with $n = 8$) determined from one 2-min recording is typically able to reduce interference amplitude in magnetometer sensors by a factor of about 300–1,000 (50–60 dB) when applied to the 2-min recording itself. In MEG recordings made at the same site even several years later, the same projection operation still suppresses interference by a factor of 100 at least.

This surprising stability of the interference patterns is partly due to the MSR. The strongest interference usually comes from distant sources which expose the MSR to relatively uniform magnetic fields. The MSR transforms these uniform fields into field patterns inside the MSR, which are not necessarily uniform but rather represent a kind of fingerprint characteristic for each room. Any new far-away source will cause a new, nearly uniform ambient field, which very closely resembles some linear combination of the interference fields due to earlier far-away sources, and thus produces a field pattern inside the MSR that approximately falls into the same interference subspace that is spanned by the dominant PCA-components in the earlier empty-room recording. We tested this MSR effect by introducing a novel interference source (an oscillating magnetic dipole 8 m from the center of the MSR) and applied the previously-determined SSP operator to suppress it; the shielding factor against this novel source was still more than 100 (40 dB) for the tested frequencies of 0.5–30 Hz (Parkkonen et al. 1999b).

SSP can be characterized as a software-based "gradiometrization" method that transforms the sensor array into a generalized gradiometer which is insensitive to those field shapes that are recognized as dominant PCA-components in a recording of ambient interference. A recently developed variant of the SSP method is the S3P algorithm (Ramirez et al. 2011) that builds the orthogonal projection operator through a spectral decomposition. This is beneficial especially for suppressing artifacts with distinct frequency characteristics; the algorithm has been shown to be useful, e.g., in the suppression of the high-frequency artifact of the deep brain stimulator (DBS).

3.5.3 The Signal Space Separation Method (SSS)

Another example of spatial filtering is the signal space separation method (SSS) that utilizes quasistatic Maxwell's equations combined with the sampling theory and geometry of the MEG array (Taulu 2008). The idea is to create a basis that

allows a device-independent representation of the data, which is capable of significantly suppressing the distortions typical to MEG, and also compensating for head movements.

At any sensor location $\mathbf{r}$ on the sensor array, the magnetic field caused by any distribution of sources is given by a series expansion

$$\mathbf{B}(\mathbf{r}) = -\mu_0 \sum_{l=1}^{\infty} \sum_{m=-l}^{l} \alpha_{lm} \frac{\boldsymbol{v}_{lm}(\boldsymbol{\theta}, \boldsymbol{\varphi})}{r^{l+2}} - \mu_0 \sum_{l=1}^{\infty} \sum_{m=-l}^{l} \beta_{lm} r^{l-1} \boldsymbol{\omega}_{lm}(\theta, \varphi), \tag{13}$$

where $\boldsymbol{v}_{lm}(\theta, \varphi) = \sqrt{(l+1)(2l+1)}\mathbf{V}_{lm}(\theta, \varphi)$ and $\boldsymbol{\omega}_{lm}(\theta, \varphi) = \sqrt{l(2l+1)}\mathbf{W}_{lm}(\theta, \varphi)$ with $\mathbf{V}$ and $\mathbf{W}$ being the vector spherical harmonic functions (VSH) defined by Hill (Hill 1954; Arfken 1985). Here the monopole term $(l = 0)$ is left out due to relation $\nabla \cdot \mathbf{B} = 0$ being valid everywhere according to the present theory of electromagnetic fields (see, e.g., Jackson 1999). In principle, an MEG device, with its data analyzed by a model including $l = 0$, could be used as a magnetic monopole detector by including $l = 0$ and estimating its contribution in the measured signal.

The infinite series of Eq. (13) is the general solution for the magnetic field in free space, expressed in the spherical coordinate system. Similar expansions based on other coordinate systems can also be used, but because of the nearly spherical shape of the sensor array it is advantageous to use this expansion for the physically possible field shapes. Using the two indices, l and m, labeling the spherical harmonics, the field shapes can be ordered according to increasing spatial complexity.

The coefficients α_{lm} and β_{lm} are called multipole moments. This expansion compactly represents the contribution of all sources generating a magnetic field. The two different parts of the expansion having different r-dependencies cover the convergence and divergence requirements of the fields produced by sources in different volumes of the physical space. Let us set the origin of the expansion somewhere in the middle of the brain volume and let $r_{\min}$ and $r_{\max}$ be the distances of the closest and most distant sensor, respectively, from this origin (see Fig. 6). The field from a source in the volume containing the origin ($r' < r_{\min}$) must be non-singular when $r' > r_{\min}$. Similarly, the field generated by a source in the outside volume ($r' > r_{\max}$) must converge when $r' < r_{\max}$. Consequently, the first sum in Eq. (13) is sufficient to describe fields generated by sources with $r' < r_{\min}$, and similarly, the second sum is all that is needed for fields from sources with $r' > r_{\max}$. As can be seen from Fig. 6, by selecting the expansion origin in a suitable way, typically at the center of the volume enclosed by the sensor array, the contributions of the brain and interference sources are separated into the first and second sum of the expansion, respectively. Here we assume that there are no sources in the volume defined by $r_{\min} < r' < r_{\max}$.

The truncation of the expansion has been investigated theoretically in (Taulu and Kajola 2005) and experimentally in (Taulu et al. 2005; Nenonen et al. 2007). The truncation of the two expansions in Eq. (13) with $l = L_{\text{in}} = 8$ and $l = L_{\text{out}} = 3$

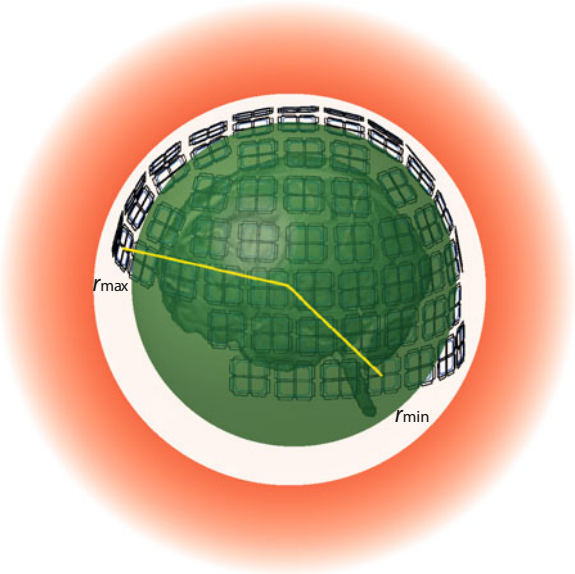

Fig. 6 Geometry of the signal space separation method

was found to be sufficient to ensure a negligible residual. Even in the case of 100 simultaneous current dipoles, $L_{\text{in}} = 8$ is enough to reconstruct the brain signal with an insignificant residual compared to sensor noise.

The basis vectors corresponding to each of the VSH functions are calculated by Eq. (13) giving us signal vectors a_{lm} and b_{lm} corresponding to the basis functions $-\mu_0 r^{-(l+2)} \boldsymbol{v}_{lm}$ and $-\mu_0 r^{l-1} \boldsymbol{\omega}_{lm}$, respectively. Thus, our linear model for any momentary signal vector ϕ, based on these basis vectors, is

$$\phi = Sx, \tag{14}$$

where the SSS basis $S = [S_{\text{in}} \;\; S_{\text{out}}]$ separates the internal and external contributions as

$$S_{\text{in}} = \left[a_{-1,1} \;\; a_{1,0} \;\; a_{1,1} \;\; \ldots \;\; a_{L_{\text{in}},L_{\text{in}}}\right] \tag{15}$$

and

$$S_{\text{out}} = \left[b_{-1,1} \;\; b_{1,0} \;\; b_{1,1} \;\; \ldots \;\; b_{L_{\text{out}},L_{\text{out}}}\right]. \tag{16}$$

The total number of spherical harmonics used in S_{in} and S_{out} must be smaller than the total number of channels. Otherwise the linear problem related to the coordinate representation in signal space becomes singular. The greater the margin (spatial oversampling) the more stable the solution of this linear problem becomes.

Since it is known that the number of measurable degrees of freedom in the neuromagnetic field—those exceeding the sensor noise—is below 100, it is usually

sufficient to map this field using spherical harmonics up to order $L_{\text{in}} = 8$. In most cases the field from external sources is sufficiently described by harmonic functions up to order $L_{\text{out}} = 3$. This corresponds to "gradiometrizing" the sensor array up to second-order derivatives of the interference field.

These relatively low expansion orders are sufficient because of the quite large distance between the sensors and sources of magnetic field in MEG. This applies to both the interesting and interfering sources. Because the series representing neural sources converges fast as a function of distance, fields with the highest spatial frequencies, corresponding to high l, are attenuated below sensor noise at the distance of the sensors when the sensor noise level of the present SQUID technology, about 3 fT/$\sqrt{\text{Hz}}$, is assumed.

In practice, modern multichannel MEG devices have a non-singular SSS basis since the sensors are located on a non-spherical surface and they are not strictly radial or tangential (Taulu 2008). Thus, we get a unique estimate for the device-independent coordinates in the form

$$\widehat{x} = S^{\dagger}\phi = \begin{bmatrix} \widehat{x}_{\text{in}} \\ \widehat{x}_{\text{out}} \end{bmatrix}, \tag{17}$$

where $S^{\dagger}$ is the pseudoinverse of S and the interference-suppressed estimate for the MEG signal can be calculated as

$$\widehat{\phi}_{\text{in}} = Re(S_{\text{in}}\widehat{x}_{\text{in}}). \tag{18}$$

By comparing Eqs. (8) and (17), we can see that SSS is a spatial filter with the model matrix $A = S^{\dagger}$.

Although the subspaces S_{in} and S_{out} are not orthogonal to each other, the contributions of the internal and external signals are not mixed in our estimated separation result, provided that our assumptions regarding sufficient values for L_{in} and L_{out} are correct and the system is calibrated accurately enough. The explanation for this is simple. Based on the theory of harmonic functions, the signal of a source in the volume $r' < r_{\text{min}}$ can be fully represented with the above expansion having non-zero α_{lm} coefficients and $\beta_{lm} = 0$. Similarly, for sources in the volume $r' > r_{\text{min}}$, the signal can be expressed with $\alpha_{lm} = 0$ and all β_{lm} being non-zero. On the other hand, the SSS basis S is linearly independent, which indicates that this obvious solution is also the only possible solution in the signal space.

Given a perfect calibration accuracy of the sensors and adequate spatial sampling, there is no mixing between the internal and external contributions because of the linear independence of the SSS basis vectors. Even with realistic calibration accuracy, this mixing is negligible if the expansion orders are sufficient.

All real measurements contain sensor noise. In MEG measurements, it is usually assumed that this noise is normally distributed and uncorrelated among the sensors, resulting in a diagonal covariance matrix. Application of SSS changes the sensor noise covariance $\mathbf{C}$ which can be taken into account if needed as shown in

(Taulu and Kajola 2005). The brain noise, which dominates over the sensor noise especially below 60 Hz, is not affected by SSS since it is produced by currents in the internal volume shown in Fig. 6.

The condition number, defined as the ratio of the largest and smallest singular value of the SSS basis, is apparently very high due to the highly different scales of the different basis functions leading to a large range of norms of the SSS basis vectors. The basis can be stabilized simply by normalizing S, which usually gives a reasonable condition number, as discussed in (Taulu et al. 2005). Further stabilization can be achieved by selecting only the basis functions that have strong enough coupling to the sensor array to exceed sensor noise (Nenonen et al. 2007). When using a normalized S, the estimated coordinates $\hat{x}_{in,lm}$ can be transformed to SI units by dividing them with the norms $||a_{lm}||$ of the non-normalized basis.

It should be noted that the numerical stability of the coordinate transformation from the recorded multichannel signal to the SSS basis depends on the degree of spatial oversampling. The noise in the SSS coordinates increases when the margin between the number of channels and the number of SSS coordinates becomes narrower. In case the values $L_{\text{in}} = 8$ and $L_{\text{out}} = 3$ are chosen, the total number of basis vectors in the SSS basis would be $(L_{\text{in}} + 1)^2 + (L_{\text{out}} + 1)^2 - 2 = 95 \ll 300$. This amount of spatial oversampling has turned out to be sufficient to prevent any significant rise in sensor noise.

As a method based on physics, SSS is sensitive to all kinds of calibration errors and cross talk between the MEG channels. For inteference sources more than 1.5 m away, the shielding performance of SSS is limited by the calibration accuracy. This effect can be utilized in the calibration of a MEG device: the orientation, sensitivity, and imbalance of gradiometers is fine-tuned by simply requiring that there is no signal left in S_{in} when SSS is applied to an empty-room recording. After fine-calibration by this method the asymptotic shielding factor against distant interference sources can be brought up to 200–300 (Taulu et al. 2005). In addition to external interference suppression and calibration adjustments, the SSS method has several important applications, such as standardization of the head position and different sensor configurations (Taulu 2008), head movement correction (Nenonen et al. 2012), and enhanced magnetic source imaging (Vrba et al. 2010). An example of the interference suppression by the SSP and SSS methods is presented in Fig. 7.

3.5.4 The Spatiotemporal Signal Space Separation Method (tSSS)

The spatial SSS performs in a satisfactory manner in typical MEG measurements. A good estimate $\hat{x}$ is guaranteed when deviations ϕ_ε of the signal from the model in Eq. (14) are insignificant. Taking the deviations into account, the model is of the form

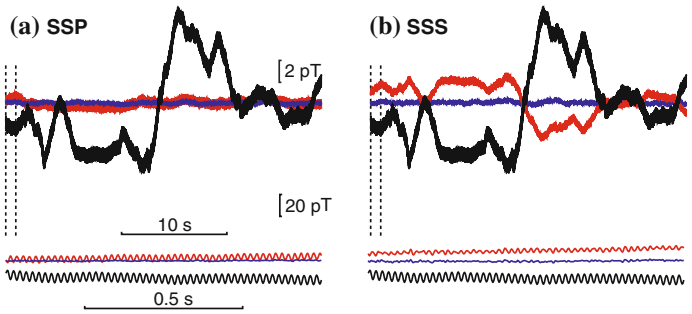

Fig. 7 Comparison of SSP and SSS with experimental data from an array with 102 magnetometers and 204 planar gradiometers. *Black curves*: raw data of a single magnetometer sensor above the occipital region recorded in an empty magnetically shielded room. **a** SSP: 5 generic SSP vectors (in *red*) and 8 SSP vectors computed from the same recording (in *blue*). **b** SSS: after SSS but without fine-calibration adjustment (in *red*) and after SSS and fine-calibration adjustment (in *blue*). The software shielding factor at the peak of the largest disturbance is 500. The *bottom* insets show a one-second epoch of the curves

$$\phi = Sx + \phi_\varepsilon \tag{19}$$

In addition to random sensor noise, such deviations can be produced by insufficient calibration accuracy of the sensor array causing erroneous elements in the basis matrix S. An additional source of deviation is the presence of sources that produce detectable magnetic fields with spatial frequencies higher than those included in the basis S, rendering the dimension of the basis matrix too small to correctly describe these fields. Such sources are typically artifactual sources in the immediate vicinity of the sensors, e.g., magnetized EEG electrodes close to the head.

From Eq. (19) we get the estimate

$$\hat{x} = S\phi = S^\dagger Sx + S^\dagger \phi_\varepsilon \equiv x + x_\varepsilon, \quad \text{where } x_\varepsilon = \begin{bmatrix} x_{\text{in},\varepsilon} \\ x_{\text{out},\varepsilon} \end{bmatrix} \tag{20}$$

Thus, the model misfit ϕ_ε leaks into the internal and external signal contribution estimated by SSS. This leakage can, however, be utilized in removing its contribution. Temporally, $x_{\text{in},\varepsilon}$ and $x_{\text{out},\varepsilon}$ contain equivalent temporal waveforms that were originally present in the signal deviation ϕ_ε. Assuming that the brain signals and external interference signals, both correctly modelled by the spatial SSS, are temporally uncorrelated, the only possible cause for temporal correlation between x_{in} and x_{out} is the above leakage phenomenon.

Removal of the contribution of ϕ_ε was developed and applied by Taulu and Simola (2006). First, the intersecting temporal waveforms are identified by a singular value decomposition (SVD)-based subspace intersection estimation method. Then, the intersecting waveforms are projected out in the time domain from the SSS estimate of the internal signal. Consequently, the recognized signal deviations, usually caused by nearby artifacts, are suppressed below the noise level

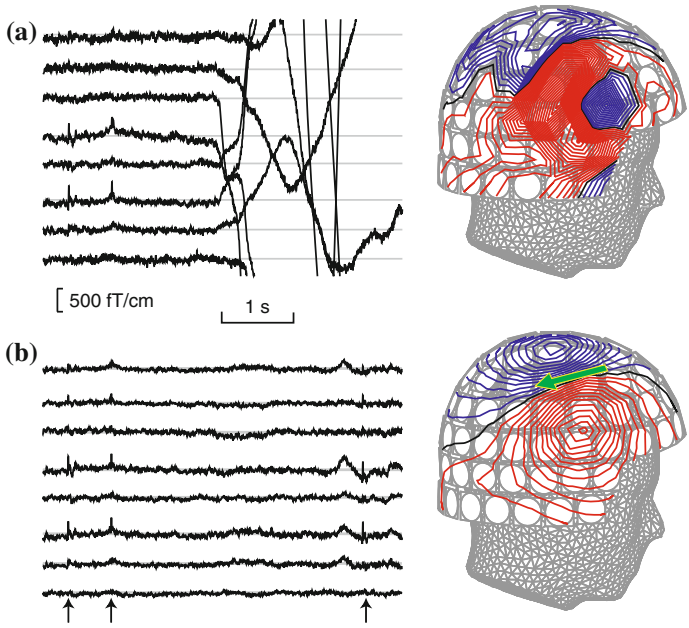

Fig. 8 An example of tSSS and movement correction. **a** *Left*: Five seconds of original raw data on six gradiometer channels above the right somatosensory cortex. The head began continuous movement approximately 3 s after the beginning of the data traces and the added magnetized piece above the somatosensory cortex emanated a very strong artifact. *Right*: The spatial MEG pattern at the N30m peak response from averaged somatosensory evoked fields (SEF). **b** The same raw data and MEG pattern after tSSS and head movement correction were employed. The *arrows* indicate single SEF responses

of the sensors. The tSSS method has been shown to work in a satisfactory manner against several different kinds of artifacts induced by magnetized pieces on the scalp (Taulu and Hari 2009), head movements (Nenonen et al. 2012), dental work (Hillebrand et al. 2013), and implanted stimulators such as DBS (Airaksinen et al. 2011) and VNS (Carrette et al. 2011; Kakisaka et al. 2012; Tanaka et al. 2009). A quite similar method utilizing reference sensors instead of SSS as the original separation method has been proposed by de Cheveigné and Simon (2007). An example of tSSS interference suppression is shown in Fig. 8 for disturbances caused by magnetized material on the scalp and head movement.

3.5.5 Feedback Active Compensation

In the feedback active compensation method, we use magnetometer sensors on the MEG helmet as null detectors in a negative feedback loop that controls currents in coils on the inside walls of the MSR. The magnetic fields from these coils counteract the ambient interference and keep the field constant at the locations of

the zero detectors. This helps keep the interference field within the dynamic range of the sensors in the entire MEG helmet. Interference rejection performance provided by this method is limited by geometry: the magnetic field is kept strictly constant at the location of the zero-detector magnetometers only. Because the counteracting field shapes obtained from the coils on the walls differ from the interference field shapes, it is not possible to exactly cancel the field in all MEG magnetometers distributed over the relatively large volume in the sensor helmet. Typically using six coils—a "Helmholz-pair" in all three principal directions of the MSR—an interference rejection ratio of about 10 can be achieved over the entire sensor array. A method to get around this geometric limitation in shielding performance and to achieve a higher shielding factor by this feedback active compensation has been described in a patent application (Simola and Taulu 2011).

An active compensation arranged in this way naturally distorts the spatial pattern of the biomagnetic signals. The method keeps also the biomagnetic signal at zero in the null-detector channels. The compensation coils, however, are simply sources of external interference and any method appropriately compensating for such interference also restores the unbiased brain signals in all sensors, including the zero-detector channels. In the present implementation of active compensation, the SSS method is used for this purpose.

3.5.6 Principal and Independent Component Analysis

Principal component analysis (PCA) decomposes data into orthogonal component vectors via a singular value decomposition of the covariance matrix. PCA is applied to compose the vectors spanning the interference subspace, typically from MEG data recorded in an empty magnetically shielded room as described in Sect. 3.5.2. PCA can also be applied to subject-based interference such as fields due to eye blinks and heartbeat. Data from a large enough number of such disturbances are extracted and few most prominent PCA vectors are selected to represent the subject interference, to be projected out from the MEG and EEG data after the recording.

Independent component analysis (ICA) is a newer technique which aims at separation of unknown sources whose unknown mixture is measured by the sensors:

$$\phi(t) = \mathbf{A}\mathbf{s}(t), \tag{21}$$

where $\phi(t)$ is the signal vector at time t, $\mathbf{s}(t)$ represents the instantaneous source activity, and matrix $\mathbf{A}$ represents the mixing. The ICA procedure provides an estimate of the unmixing matrix $\mathbf{B}$ so that the estimated source activity becomes

$$\hat{\mathbf{s}}(t) = \mathbf{B}\phi(t). \tag{22}$$

ICA belongs to the family of blind source separation methods, because the source signals are not directly observed and nothing is known about their mixture; the only

assumption is that the sources $\mathbf{s}(t)$ are statistically independent. The separation is obtained by optimizing a contrast function of some distributional property of the output $\hat{s}$. The contrast functions are based on entropy, mutual independence, high-order decorrelations, etc. (see, e.g., Cardoso 1998; Hyvärinen 1999).

ICA has been applied to MEG and EEG to mainly remove artifacts (e.g., Vigario et al. 2000). ICA has also been used to decompose MEG/EEG data into separate components (e.g., Tang et al. 2002). However, the underlying assumption of statistical independence between the activations of the different neural sources may not be valid for a physiologically plausible separation of distinct neural processes or sources. Nevertheless, applying ICA to a suitable sparsifying transformation of the MEG data may help extract relevant brain activity patterns (Hyvärinen et al. 2010; Ramkumar et al. 2012).

3.5.7 Sensor Noise Suppression

By sensor noise we mean random noise signals that are inherent to the MEG sensors and independent from other sensors. Such a noise component does not have a unique overall field pattern that could be modeled and subtracted from all sensors simultaneously. Therefore, the traditional way of addressing sensor noise is by statistical means, e.g., by estimating the noise covariance matrix of the sensors and taking it into account in source modeling.

Recently de Cheveigné and Simon (2008) proposed a sensor noise reduction approach that is based on the assumption that sensor noise is uncorrelated with brain activity and uncorrelated between sensors. In their method, PCA is applied iteratively by omitting one channel at a time. The data of the omitted channel is replaced by its regression on the subspace formed by the other channels. Computation time is saved by orthogonalizing a subset of channels selected on the basis of correlation with the omitted channel data. Even more recently, a similar approach has been proposed (Taulu et al. 2012) with the difference that the model for the spatially correlated part of the sensor signals is estimated with a physical model based on SSS instead of using statistics such as PCA. Both of the above methods decrease the random sensor noise significantly and improve the signal-to-noise ratio of the brain signals. The SSS based method was recently demonstrated to reduce the overall sensor noise level in the frequency band of 400–800 Hz by factors of 4.5 and 2.1 for gradiometers and magnetometers, respectively (Helle et al. 2012).

Denoising source separation, DSS (Särelä and Valpola 2005) is yet another way to suppress noise contributions from the sensors and background brain activity. DSS is an iterative method that refines a template filter, often seeded by ICA, applied on whitened data. The method has been demonstrated on single-trial MEG data (Karp et al. 2009). DSS was utilized also by de Cheveigné (2010) for constructing a spatiotemporal filter to partition the recorded data into signal and noise components. Time-shifted signals and PCA are utilized to construct special FIR filters, and averaged evoked responses are utilized as a contrast function to emphasize the brain activity.

3.5.8 Spatial Filtering Combined with Source Modeling

Spatial filtering methods, such as beamforming, aim at finding and characterizing the neural current sources in the brain (Vrba and Robinson 2001). A spatial filter is constructed so that it passes the activity at the target location with unit gain while suppressing the contribution from other sources. Spatial filtering can thus suppress unwanted interference, provided that the low-rank interference has spatially and temporally distinctly different characteristic from the brain signals (Sekihara et al. 2004). Typically such interference originates outside of the magnetically shielded room, but the beamformer technique has been demonstrated to successfully suppress nearby interference from a pain stimulator (Adjamian et al. 2009). However, the basic assumptions are not valid in cases where the patient-induced artifacts, e.g. due to dental braces, are huge compared to the brain signals (Hillebrand et al. 2013).

Another approach to combine source imaging and interference suppression was suggested by Mosher et al. (2009). They placed a grid of dipoles inside the MEG helmet and used their lead fields to compose the basis of the signal subspace. Its null space was then used to construct a blocking operator for removing all neural activity components from the measured data. Projection of unwanted interference waveforms is basically similar to the temporal SSS presented above, but the method can produce current source estimates for the analysis without a separate step.

3.5.9 Physiological Artifacts

While SSS can geometrically separate the brain from external interference sources by the concentric inner and outer spheres, the method does not suppress signals from physiological sources in the inner volume or the space between the spheres. Such physiological artifacts include signals from head muscles, eyes (blinks and saccades), or cardiac signals due to cardiac volume currents and pulsating blood flow within this intermediate space. If strong cardiac or eye-blink artifacts are present, a further post-processing to suppress them can be performed with the signal space projection method (Uusitalo and Ilmoniemi 1997). In this case, instead of applying PCA directly on the continuous signals, it is often beneficial to average with respect to these stereotypical artifacts to boost them relative to brain signals and then perform PCA on the average. Identification and suppression of the neck muscle artifacts could be performed utilizing methods such as independent component analysis (Vigario et al. 2000). Generally, individual variations exist between subjects with respect to the heartbeat-related residual after SSS.

4 Future Prospects

The adoption of modern signal processing methods to multi-channel MEG data has advanced the MEG interference suppression rapidly during the last few years. In addition, solely hardware-based magnetic shielding has shifted towards active

shielding methods, which are less expensive and lighter-weight than conventional passive means and thus allow more flexibility in planning the location of an MEG laboratory. These trends are likely to continue in the future to support wider adoption of MEG, not only through cost reduction but also by allowing MEG to be applied to patients with magnetic material in their body. In the following, we try to highlight some of the future opportunities and challenges of interference suppression in MEG.

4.1 MEG Without a Shielded Room

As an ultimate goal for interference suppression, one could envision an MEG system without a magnetically shielded room. Since the room constitutes roughly 20 % of the total cost of a MEG set-up, replacing the expensive passive shield altogether with an active system is tempting. However, operating an MEG system in a magnetically harsh, or even average, environment without any passive shielding is challenging for the following reasons: (i) the combination of the sensors, the active compensation system and the software-based interference suppression method should have a very large dynamic range (in excess of 140 dB) in order to cope with the largest interference signals while not elevating the sensor noise floor, (ii) the compensation system should be able to deal with the high-order field gradients due to near-by interference sources, (iii) Earth's static magnetic field (500–1,000 times stronger than the remanent field in a typical MSR) polarizes paramagnetic objects which cause additional interference when moving or vibrating within or in the vicinity of the sensor helmet, (iv) SQUIDs must be shielded against radio-frequency interference (see Sect. 1.4); a passive magnetically shielded room acts as an RF shield as well and thus a system without such a room may still require an RF-shield around it for reliable operation if the sensor elements cannot be RF-shielded locally. Despite these problems, proof-of-concept MEG measurements without a shielded room have been performed in magnetically quiet environments. However, reliable unshielded MEG operation in typical environments will become possible only after considerable advances regarding the above challenges.

4.2 Novel Sensor Technologies

Low-Tc SQUIDs have so far been the sensor of choice for serious MEG instrumentation due to their excellent noise performance and stability; however, these sensors require expensive liquid-helium cooling, and the large temperature gradient necessitates elaborate thermal insulation which introduces a considerable gap from the scalp to the sensors. New sensor technologies that may alleviate these problems have emerged recently. High-Tc SQUIDs (see the work by Öisjöen and

colleagues (2012) for a recent MEG application) and "mixed sensors" (Pannetier et al. 2004; Pannetier-Lecoeur et al. 2011) can be operated in liquid nitrogen, avoiding much of cryogenics-related costs, and brought closer to the scalp. Atomic magnetometers are based on optical detection of magnetic-field-induced light polarization changes in alkali-metal vapors; these sensor operate at +120 to +150 C and they can also be located within a few mm from the scalp. Atomic magnetometers allow a non-rigid sensor helmet that can be adapted to the head size and shape of individual subjects. Devices using liquid nitrogen may also allow some degree of geometric adaptability if the sensor array is split into multiple small dewars.

These considerable improvements in MEG instrumentation will have implications for interference suppression. Bringing the sensors closer to the scalp implies that higher spatial frequencies can be measured, which improves source reconstruction accuracy but also requires that the physics-based interference suppression methods, such as SSS, have to be adapted accordingly to work efficiently. On the other hand, an adaptable snugly-fitting sensor array is likely to deviate from a sphere more than the current fixed array, which makes the SSS transform numerically more stable and may provide a higher shielding factor. However, the adaptability of the array calls for very accurate yet quick means to determine the locations and orientations of the sensors in order to efficiently use these physics-based methods for decomposing the data to neural signals and interference. On the contrary, statistics-based adaptive methods, such as SSP, would not need the geometric information but would lack the generic nature of SSS.

4.3 Hybrid Instrumentation

Very recently, large-scale MEG has been successfully combined with ultra-low-field (ULF) MRI in the same system (Vesanen et al. 2012). This combination is attractive since the SQUID sensor array can be efficiently used for both MEG and ULF-MRI signal acquisition. However, for a decent signal-to-noise ratio in ULF-MRI, the low measurement field ($\sim$100 μT) has to be accompanied with a stronger pre-polarization field (typically 10–100 mT) that is switched on briefly before collecting the data. The SQUID sensors should be highly resistant to flux traps so that they can recover within few milliseconds from the pre-polarization field. Such field tolerance of the sensors would be beneficial also for MEG when operating the system in a very light shield or completely without a shielded room.

Similarly to MEG, the MRI mode of the hybrid MEG–MRI system benefits from efficient interference suppression. Although the MRI signals are in the kHz range where environmental interference is usually not of concern, reduction of the intrinsic sensor noise, as outlined in Sect. 3.5.7, could considerably improve image quality. In addition, noise of the MRI gradient amplifiers may propagate to the sensors via the gradient coils. Since the field pattern of such interference is constant, projection methods such as SSP should work efficiently.

5 Conclusion

The MEG measurement technology has taken huge steps forward since the early days when the number of recording channels was one or only a few. Novel interference and noise suppression methods have emerged as a kind of byproduct of the significant increase in the number of recording channels. Because at present the number of detectable degrees of freedom in the magnetic brain signal is known to be around 80 only, modern devices containing over 300 independent channels oversample the actual neuromagnetic field. This fact has enabled efficient general-purpose interference and noise reduction methods such as signal space projection (SSP) and signal space separation (SSS).

Because interfering magnetic fields—even when MEG is performed in a magnetically shielded room—may exceed the strength of the neuromagnetic signal by about a factor of thousand, it is actually necessary to record the interference with a better relative accuracy than the neuromagnetic signal itself; Only this enables sufficiently precise subtraction of the interference from the recorded raw signal. To achieve such an accuracy, it is necessary to use the entire set of MEG channels for this purpose, not only a limited set of reference channels as was done in the early 1990s. Thanks to the ample oversampling of the magnetic field, signal space methods can then be used to determine and subtract the interference signal from the recorded raw signal.

With the help of such effective "software magnetic shielding" the required hardware shielding, magnetically shielded room, can be made lighter and cheaper. This may be an effective booster for the adoption of MEG in hospitals.

References

Adjamian P, Worthen S, Hillebrand A, Furlong P, Chizh B, Hobson A, Aziz Q, Barnes G (2009) Effective electromagnetic noise cancellation with beamformers and synthetic gradiometry in shielded and partly shielded environments. J Neurosci Methods 178(1):120–127

Ahonen A, Hämäläinen M, Ilmoniemi R, Kajola M, Knuutila J, Simola J, Vilkman V (1993) Sampling theory for neuromagnetic detector arrays. IEEE Trans Biomed Eng 40:859–869

Airaksinen K, Mäkelä J, Taulu S, Ahonen A, Nurminen J, Schnitzler A, Pekkonen E (2011) Effects of DBS on auditory and somatosensory processing in Parkinson's disease. Hum Brain Mapp 32(7):1091–1099

Arfken G (1985) Mathematical methods for physicists. Academic Press, San Diego

Bork J, Hahlbohm HD, Klein R, Schnabel, A (2001) The 8-layered magnetically shielded room of the PTB: design and construction. In: Biomag2000, Proceedings of the 12th international conference on biomagnetism, Helsinki University of Technology, Espoo, Finland 2000, p 970–973

Cardoso J (1998) Blind signal separation: statistical principles. Proc IEEE 86:2009–2025

Carrette E, De Tiège X, Op De Beeck M, De Herdt V, Meurs A, Legros B, Raedt R, Deblaere K, Van Roost D, Bourguignon M, Goldman S, Boon P, Van Bogaert P, Vonck K (2011) Magnetoencephalography in epilepsy patients carrying a vagus nerve stimulator. Epilepsy Res 93(1):44–52

Chella F, Zappasodi F, Marzetti L, Della Penna S, Pizzella V (2012) Calibration of a multichannel MEG system based on the signal space separation method. Phys Med Biol 57(15):4855–4870

Clarke J, Braginski A (eds) (2006) The SQUID handbook. Wiley-VCH, Weinham

Cohen D (1968) Magnetoencephalography: evidence of magnetic fields produced by alpha-rhythm current. Science 161:784–786

Cohen D (1970) Large-volume conventional magnetic shields. Rev Phys Appl 5:53–58

Cohen D (1972) Magnetoencephalography: detection of the brain's electrical activity with a superconducting magnetometer. Science 175:664–666

Cohen D (1979) Magnetic measurement and display of current generators in the brain. Part I: the 2-d detector. In: Proceedings of the 12th international conference on medical and biological engineering, Jerusalem, pp 15–16

De Cheveigné A, Simon J (2007) Denoising based on time-shift PCA. J Neurosci Methods 165:297–305

De Cheveigné A, Simon J (2008) Sensor noise suppression. J Neurosci Methods 168(1):195–202

De Cheveigné A (2010) Time-shift denoising source separation. J Neurosci Methods 189(1):113–120

De Tiège X, Op de Beeck M, Funke M, Legros B, Parkkonen L, Goldman S, Van Bogaert P (2008) Recording epileptic activity with MEG in a light-weight magnetic shield. Epilepsy Res 82(2–3):227–231

Gross J, Baillet S, Barnes G, Henson R, Hillebrand A, Jensen O, Jerbi K, Litvak V, Maess B, Oostenveld R, Parkkonen L, Taylor J, van Wassenhove V, Wibral M, Schoffelen J (2013) Good practice for conducting and reporting MEG research. Neuroimage 65:349–363

Hall Barbosa C, Andrade Lima E, Bruno A, Ewing A, Wikswo JP Jr (1999) Flux/voltage calibration of axial SQUID gradiometers using an optimization procedure. IEEE Trans App Supercond 9:3523–3526

Hämäläinen M, Hari R, Ilmoniemi RJ, Knuutila J, Lounasmaa OV (1993) Magnetoencephalography—theory, instrumentation, and applications to noninvasive studies of the working human brain. Rev Mod Phys 65:413–498

Helle L, Parkkonen L, Taulu S. Ahonen A (2012) Suppression of uncorrelated sensor noise and artifacts: demonstration with high frequency brain signals. Abstracts of the 18th international conference on biomagnetism, Paris 2012, p 284

von Helmholtz H (1853) Ueber einige Gesetze der Vertheilung elektrischer Ströme in körperlichen Leitern, mit Anwendung auf die thierisch-elektrischen Versuche. Ann Phys Chem 89(211–233):353–377

Hill E (1954) The theory of vector spherical harmonics. Am J Phys 22:211–214

Hillebrand A, Pazio P, de Munck J, van Dijk B (2013) Feasibility of clinical magnetoencephalography (MEG) functional mapping in the presence of dental artefacts. Clin Neurophysiol 124(1):107–113

Hyvärinen A (1999) Fast and robust fixed-point algorithms for independent component analysis. IEEE Trans Neural Netw 10:626–634

Hyvärinen A, Ramkumar P, Parkkonen L, Hari R (2010) Independent component analysis of short-time Fourier transforms for spontaneous EEG/MEG analysis. Neuroimage 49:257–271

Ilmoniemi R (1981) 7-channel SQUID magnetometer for brain research. M.Sc. thesis, Helsinki University of Technology

Ilmoniemi R, Williamson S (1987) Analysis of the magnetic alpha rhythm in signal space. Soc Neurosci Abstr 13:46

Ilmoniemi R, Williamson S, Hostetler W (1987) New method for the study of spontaneous brain activity. Biomagnetism 87. Tokyo Denki University Press, Tokyo, p 182–185

Jackson J (1999) Classical electrodynamics. John Wiley & Sons, Inc, New York

Kakisaka Y, Mosher J, Wang Z, Jin K, Dubarry A, Alexopoulos A, Burgess R (2012) Utility of temporally-extended signal space separation algorithm for magnetic noise from vagal nerve stimulators. Clin Neurophysiol

Karp E, Parkkonen L, Vigário R (2009) Denoising single trial event related magnetoencephalographic recordings. In: Adali T et al (eds) Independent component analysis and signal separation, Springer, Berlin, pp 427–434

Kelhä V, Pukki J, Peltonen R, Penttinen A, Ilmoniemi R, Heino J (1982) Design, construction, and performance of a large-volume magnetic shield. IEEE Trans Magn MAG-18:260–270

Kiviranta M, Seppä H (1995) DC-SQUID electronics based on the noise cancellation scheme. IEEE Trans Appl Superconduct 5(2):2146–2148

Kominis I, Kornack T, Allred J, Romalis M (2003) A subfemtotesla multichannel atomic magnetometer. Nat London 422:596

Mosher J, Hämäläinen M, Pantazis D, Hui H, Burgess R, Leahy R (2009) Generalized sidelobe canceller for magnetoencephalography arrays. Proc IEEE Int Symp Biomed Imaging. 2009:149–152

Nenonen J, Montonen J, Katila T (1996) Thermal noise in biomagnetic measurements. Rev Sci Instr 67(6):2397–2405

Nenonen J, Kajola M, Simola J, Ahonen A (2004) Total information of multichannel MEG sensor arrays. Proceedings of the 14th international conference on biomagnetism, Biomag Ltd., Boston 2004, p 630–631

Nenonen J, Taulu S, Kajola M, Ahonen A (2007) Total information extracted from MEG measurements. Int Congr Ser 1300:245–248

Nenonen J, Nurminen J, Kičić′ D, Bikmullina R, Lioumis P, Jousmäki V, Taulu S, Parkkonen L, Putaala M, Kähkönen S (2012) Validation of head movement correction and spatiotemporal signal space separation in magnetoencephalography. Clin Neurophysiol 123(11):2180–2191

Nurminen J, Taulu S, Okada Y (2008) Effects of sensor calibration, balancing and parametrization on the signal space separation method. Phys Med Biol 53(7):1975–1987

Ornelas P, Bruno A, Hall Barbosa C, Andrade Lima E, Costa Ribeiro P (2003) A survey of calibration procedures for SQUID gradiometers. Supercond Sci Technol 16:427–431

Pannetier M, Fermon C, Goff G, Simola J, Kerr E (2004) Femtotesla magnetic field measurement with magnetoresistive sensors. Science 304:1648–1650

Pannetier-Lecoeur M, Parkkonen L, Sergeeva-Chollet N, Polovy H, Fermon C, Fowley C (2011) Magnetocardiography with sensors based on giant magnetoresistance. Appl Phys Lett 98:153705

Parkkonen L, Simola J, Tuoriniemi J, Ahonen A (1999a) An interference suppression system for multichannel magnetic field detector arrays. In: Yoshimoto T et al (eds) Recent advances in biomagnetism: proceedings of the 11th international conference on biomagnetism, pp 13–16, Tohoku University Press

Parkkonen L, Simola J, Kajola M, Hämäläinen M, Ahonen A (1999b) Experiments on interference suppression in MEG measurements. Abstracts of the human brain mapping conference, Düsseldorf 1999, #165

Parkkonen L, Simola J, Taulu S, Kajola M, Knuutila J, Kojo A, Laine P, Nenonen J, Ahonen A (2006) A light-weight magnetic shield: performance in real MEG measurements. Proceedings of the 15th International Conference on Biomagnetism, Vancouver, BC, Canada, 21–25 Aug 2006. Abstracts of the 15th International Conference on Biomagnetism, Vancouver 2006

Parkkonen L, Salmelin R (2010) Ch3: Measurements. In: Hansen P, Kringelbach M, Salmelin R (eds) MEG: an introduction to methods, Oxford University Press, New York

Patton B, Fitch J (1962) Design of a room-size magnetic shield. J Geophys Res 67(3):1117

Ramirez R, Kopell B, Butson C, Hiner B, Baillet S (2011) Spectral signal space projection algorithm for frequency domain MEG and EEG denoising, whitening, and source imaging. Neuroimage 56(1):29–78

Ramkumar P, Parkkonen L, Hari R, Hyvärinen A (2012) Characterization of neuromagnetic brain rhythms over time scales of minutes using spatial independent component analysis. Hum Brain Mapp 33:1648–1662

Särelä J, Valpola H (2005) Denoising source separation. J Mach Learn Res 6:233–327

Sekihara K, Nagarajan S, Poeppel D, Marantz A (2004) Performance of an MEG adaptive-beamformer source reconstruction technique in the presence of additive low-rank interference. IEEE Trans Biomed Eng 51(1):90–99
Simola J (2003) Wall element for magnetically shielded room and magnetically shielded room. Patent WO/2003/059030
Simola J, Laine P, Rakkolainen H (2005) Joint structure between the wall elements of a magnetically shielded room, PCT/FI05/00385
Simola J, Taulu S (2011) Method for designing coil systems for generation of magnetic fields of desired geometry, PCT/FI2011/050249
Tanaka N, Thiele E, Madsen J, Bourgeois B, Stufflebeam S (2009) Magnetoencephalographic analysis in patients with vagus nerve stimulator. Pediatr Neurol 41(5):383–387
Tang A, Pearlmutter B, Malaszenko N, Phung D, Reeb B (2002) Independent components of magnetoencephalography: localixation. Neural Comput 14:1827–1858
Taulu S (2000) M.Sc. thesis (in Finnish), Helsinki University of Technology
Taulu S, Kajola M, Simola J (2004) Suppression of interference and artifacts by the signal space separation method. Brain Topogr 16(4):269–275
Taulu S, Kajola M (2005) Presentation of electromagnetic multichannel data: the signal space separation method. J Appl Phys 97(124905):1–10
Taulu S, Simola J, Kajola M (2005) Applications of the signal space separation method. IEEE Trans Sign Proc 53:3359–3372
Taulu S, Simola J (2006) Spatiotemporal signal space separation method for rejecting nearby interference in MEG measurements. Phys Med Biol 51(7):1759–1768
Taulu S (2008) Processing of weak magnetic multichannel signals: the signal space separation method. PhD Dissertation, Helsinki University of Technology
Taulu S, Hari R (2009) Removal of magnetoencephalographic artifacts with temporal signal-space separation: demonstration with single-trial auditory-evoked responses. Hum Brain Mapp 30(5):1524–1534
Taulu S, Simola J, Kajola M, Helle L, Ahonen A, Sarvas J (2012) Suppression of uncorrelated sensor noise and artifacts in multichannel MEG data. Abstracts of the 18th international conference on biomagnetism, Paris 2012, p 285
Uusitalo M, Ilmoniemi R (1997) Signal-space projection method for separating MEG or EEG into components. Med Biol Eng Comput 35(2):135–140
Vesanen P, Nieminen J, Zevenhoven K, Dabek J, Parkkonen L, Zhdanov A, Luomahaara J, Hassel J, Penttilä J, Simola J, Ahonen A, Mäkelä J, Ilmoniemi R (2012) Hybrid ultra-low-field MRI and magnetoencephalography system based on a commercial whole-head neuromagnetometer. Magn Reson Med (2012 Jul 17, epub ahead of print)
Vigario R, Särelä J, Jousmäki V, Hämäläinen M, Oja E (2000) Independent component approach to the analysis of EEG and MEG recordings. IEEE Trans Biomed Eng 47:589–593
Wikswo J (2004) SQUIDs remain best tools for measuring brain's magnetic field. Phys Today 57(2):15
Vrba J, Robinson S (2001) Signal processing in magnetoencephalography. Methods 25:249–271
Vrba J, Robinson S (2002) SQUID sensor array configurations for magnetoencephalography applications. Supercond Sci Technol 15:R51–R89
Vrba J, Taulu S, Nenonen J, Ahonen A (2010) Signal space separation beamformer. Brain Topogr 23(2):128–133
Zimmerman J, Frederick N (1971) Miniature ultrasensitive superconducting magnetic gradiometer and its use in cardiography and other applications. Appl Phys Lett 19:16
Öisjöen F, Schneiderman J, Figueras G, Chukharkin M, Kalabukhov A, Hedström A, Elam M, Winkler D (2012) High-Tc superconducting quantum interference device recordings of spontaneous brain activity: towards high-Tc magnetoencephalography. Appl Phys Lett 100:132601

Electric and Magnetic Fields of the Brain

Leon Heller and Petr Volegov

Abstract Electroencephalography (EEG) and Magnetoencephalography (MEG) provide two noninvasive methods to learn about the spatial and temporal behavior of neuronal currents. In this tutorial chapter we present the physics and mathematics needed to interpret such measurements. The frequencies present in neuronal activity are sufficiently low that Maxwell's equations for electromagnetism can be approximated by omitting the terms involving time derivatives. In this 'quasistatic' approximation the electric and magnetic fields follow the time dependence of the neuronal current. The "Forward Problem" consists of solving for these fields on the surface of the scalp and just outside the head, for any assumed neuronal current distribution. It requires a knowledge of the 'head model', namely the shapes and electrical conductivities of the main head compartments, i.e., the brain, skull, and scalp, and possibly the cerebrospinal fluid. Analytical and numerical methods for doing this are discussed. In the "Inverse Problem" one tries to deduce the neuronal current distribution from EEG and/or MEG measurements on human subjects. The factors that contribute to the non-uniqueness of the solution are discussed, and the methods that are actually employed to obtain current distributions are described. The standard procedure is to assume one or more current distributions, solve the forward problem for each one, and compare them with the data. Various criteria for calculating how well they agree are discussed.

Keywords Electroencephalography · Magnetoencephalography · Neuronal currents · Quasistatic approximation · Forward problem · Current dipole · Head model · Inverse problem · Lead field · Maximum likelihood estimation · Source localization · Minimum norm solution

L. Heller (✉) · P. Volegov
Applied Modern Physics Group, P-21, Los Alamos National Laboratory, Los Alamos, NM 87545, USA
e-mail: lheller@lanl.gov

P. Volegov
e-mail: volegov@lanl.gov

S. Supek and C. J. Aine (eds.), *Magnetoencephalography*,
DOI: 10.1007/978-3-642-33045-2_3,

1 Introduction

Electrical currents play a variety of roles in living tissue. In this tutorial chapter, intended for graduate students and researchers entering the field, we will be concerned with currents in the brain that flow inside neurons and across their boundaries into the extracellular medium. These currents produce an electric potential that can be detected noninvasively on the surface of the scalp, and a magnetic field that can be measured outside the head. These modalities are called electroencephalography (EEG) and magnetoencephalography (MEG). Throughout the chapter we emphasize the basic physics and the associated mathematics needed to interpret experimental data obtained in MEG and EEG experiments.

Here is an outline of the material. In Sect. 2 we show how Maxwell's equations simplify for the low frequencies associated with neuronal activity. This is called the Quasistatic Approximation. Another approximation is based on the fact that the electrical conductivity of the brain is not known in any spatial detail, hence a single average value is commonly used. The same is true for each of the other major compartments of the head: cerebrospinal fluid, skull, and scalp, each with its own average value. This is discussed in Sect. 2.1.

Section 3 begins one of the two major subdivisions of the entire chapter, called the Forward Problem. In it one calculates the electric potential and the magnetic field produced by an *assumed* neuronal current. Further, the notion of a "current dipole" is introduced as the spatially simplest possible current; any more general current can be obtained as a (possibly continuous) sum of current dipoles. This is useful because Maxwell's equations are linear in the source currents, and the fields produced by a more general source can be obtained as a linear sum of the fields produced by the individual sources. This property is used a number of times in the development.

The other major subdivision of the chapter is found in Sect. 4, called the Inverse Problem. Here one tries to deduce, from experimentally measured values of the electric potential and/or the magnetic field on the head, the locations, strengths, and time courses of the electrical currents that produced those measurements. That there is no unique solution of this problem is pointed out in the Forward Problem section.

As generally used, the Inverse Problem consists of solving the Forward Problem for the electric potential and the magnetic field produced by an assumed neuronal current, and varying that current to find the best match, in a sense to be discussed, with the data. Noise in the data must be taken into account. As will be seen, even if one is only interested in magnetic field data, it is still generally necessary to solve for the electric potential.

The frequencies that are associated with neuronal activity are in the range 1–1,000 Hz, and in the next section we show how Maxwell's equations for the electric and magnetic fields simplify as a result. A review of this field as of 1993 is found in (Hämäläinen et al. 1993).

2 Low Frequency (Quasistatic) Approximation

The total electric current within the head has been written as the sum of two terms of distinctly different nature in (Geselowitz 1967), and (Barnard et al. 1967). One, called the primary current, $\mathbf{J}^p$, is the current that flows within neurons and across their membranes, and is the quantity of interest in neuroscience. Because the cells are embedded in an electrically conducting medium, the extracellular current—also called the the "return" current—follows a path that depends upon the conductivity profile of the extracellular medium. The return current $\mathbf{J}^R$ is taken to be the product of the local conductivity σ and the electric field intensity $\mathbf{E}$, i.e., it is ohmic current. The complete current becomes

$$\mathbf{J} = \mathbf{J}^p + \sigma\mathbf{E}. \tag{1}$$

Electric current either flows in closed circuits or else, if it starts or stops somewhere, electric charge builds up (or declines) at such locations. This is embedded in the fundamental principle of 'charge conservation', the mathematical statement of which is the continuity equation

$$\nabla \cdot \mathbf{J} + \frac{\partial \rho}{\partial t} = 0, \tag{2}$$

where ρ is the charge density. Equations (1) and (2) together with the Maxwell equation that embodies Gauss's Law, $\nabla \cdot \mathbf{E} = \rho/\varepsilon_0$, lead to

$$\nabla \cdot \mathbf{J}^p + \nabla\sigma \cdot \mathbf{E} + \omega_0\rho + \frac{\partial \rho}{\partial t} = 0, \tag{3}$$

where the characteristic frequency $\omega_0 = \sigma/\varepsilon_0$. Even for the skull, which is the part of the head with the smallest conductivity, ω_0 is approximately 10^9 Hz. This is orders of magnitude greater than the frequencies of neuronal activity, which are in the range 1–1,000 Hz.

2.1 Regions of Constant Conductivity

It requires many thousands of nearby neurons acting in near synchrony to produce a signal strong enough to be detected by EEG or MEG. Since the electrical conductivities of the various compartments of the head are not known in any spatial detail, it is common to assign an average value to the brain, one to the cerebrospinal fluid, one to the skull and one to the scalp.

2.1.1 The Electric Field

In any region of constant conductivity a number of conclusions follow from Eq. (3), where the term $\nabla\sigma$ drops out.

(i) Away from primary current any electric charge must fall off with time as $\exp(-\omega_0 t)$.
(ii) As mentioned above the frequencies of neuronal activity are smaller than ω_0 by many orders of magnitude in all the compartments of the head. Hence the term $\partial\rho/\partial t$ is negligible compared to $\omega_0\rho$ in Eq.(3).
(iii) At the site of primary current charge can persist for the duration of the current, and then falls off as in (i).
(iv) Electric charge can also appear at the boundary between regions of different conductivity. This will be discussed later.

With the term $\partial\rho/\partial t$ gone Eq. (3) can be rewritten as

$$\nabla \cdot (\mathbf{J}^p + \sigma\mathbf{E}) = 0. \tag{4}$$

A further approximation for $\mathbf{E}$ will follow after consideration of the magnetic field.

2.1.2 The Magnetic Field

From the Maxwell equation $\nabla \cdot \mathbf{B} = 0$, which says that there are no magnetic monopoles, it follows that $\mathbf{B}$ can be written as $\mathbf{B} = \nabla \times \mathbf{A}$, where $\mathbf{A}$ is called the vector potential. This makes use of the vector identity $\nabla \cdot \nabla\times = 0$.

From Faraday's Law comes the Maxwell equation $\nabla \times \mathbf{E} = -\partial\mathbf{B}/\partial t$, which means that the electric field can be written in terms of the scalar potential V and the vector potential as

$$\mathbf{E} = -\nabla V - \frac{\partial \mathbf{A}}{\partial t}. \tag{5}$$

The proof follows by taking the curl of both sides of Eq. (5) since $\nabla \times \nabla = 0$.

Any electric current gives rise to a magnetic field, and this is embodied in the fourth Maxwell equation

$$\nabla \times \mathbf{B} = \mu_0 \mathbf{J} + \frac{1}{c^2}\frac{\partial \mathbf{E}}{\partial t} \tag{6}$$

The final term in Eq. (6) is called the Displacement Current, and c is the speed of light. Putting that term there was Maxwell's great achievement to insure that charge is conserved, as can be checked by taking the divergence of both sides of the equation.

Since the magnetic field arises from the current, $\mathbf{A}$ and $\mathbf{B}$ follow the time dependence of $\mathbf{J}^p$. This places an approximate limit on the magnitude of the time derivative terms in Eqs. (5) and (6) since the maximum frequency of the neuronal activity of interest is $\omega \approx 1$ kHz.

For Eq. (6) the return current $\sigma\mathbf{E}$ makes the first term on the right hand side larger than the second term by the ratio ω_0/ω, which is many orders of magnitude. For Eq. (5) it takes more work to show that the magnitude of $\partial\mathbf{A}/\partial t$ is negligible compared to ∇V. After seeing what follows by neglecting that term, one can go back and verify that the neglect was justified. Combining Eq. (4) with $\mathbf{E} = -\nabla V$ gives

$$\nabla \cdot \mathbf{J}^p - \sigma \nabla^2 V = 0, \tag{7}$$

which represents the quasistatic approximation for the electric potential in any region of constant conductivity.

The electric potential is that solution of Eq. (7) which satisfies the boundary conditions that the electric potential is continuous and the normal component of the return current is continuous on the boundary separating regions with conductivities σ' and σ''. While there may be electric charges on the boundary, continuity of the potential assumes there are no electric dipoles. And continuity of the normal component of the return current assumes there is no source of primary current right on the boundary.

$$V' = V''; \quad \sigma' \mathbf{n} \cdot \nabla' V = \sigma'' \mathbf{n} \cdot \nabla'' V. \tag{8}$$

The solution of Eq. (6) without the time derivative term is given by the Biot-Savart Law

$$\mathbf{B}(\mathbf{r}) = \frac{\mu_0}{4\pi} \int \mathbf{J}(\mathbf{r}') \times \frac{\mathbf{r} - \mathbf{r}'}{|\mathbf{r} - \mathbf{r}'|^3} d^3 r' = \frac{\mu_0}{4\pi} \int \mathbf{J}(\mathbf{r}') \times \nabla' \frac{1}{|\mathbf{r} - \mathbf{r}'|} d^3 r'. \tag{9}$$

To verify that Eq. (9) satisfies Eq. (6) (without the displacement current) requires some algebra which is best handled using component notation. It is correct only if the current $\mathbf{J}$ is conserved, i.e., it must be the complete current, satisfying $\nabla \cdot \mathbf{J} = 0$. Of course the two contributions to $\mathbf{B}$ coming from the primary and return currents can be evaluated separately, but only the sum of the two is physically meaningful. They are designated as $\mathbf{B}^p(\mathbf{r})$ and $\mathbf{B}^R(\mathbf{r})$.

Equations (7), (8) and (9) together constitute the quasistatic approximation to Maxwell's equations. An essential property of Maxwell's equations is that they are linear in the source charges and currents. This means that the solution of the equations, for the electric field and the magnetic field, for the sum of two sources is the sum of the solutions for the individual sources. Naturally this property also holds for the quasistatic approximation to the equations, *and will be used throughout the chapter.*

3 The Forward Problem

A head model consists of a specification of the geometry and conductivity of the various compartments of the head, e.g., brain, cerebrospinal fluid, skull and scalp. For any assumed primary current distribution $\mathbf{J}^p(\mathbf{r})$ the 'Forward Problem' for EEG and MEG solves Eqs. (7) and (8) for the electric potential, and Eq. (9) for the magnetic field on the surface of the head and outside.

There are other applications of electromagnetic theory to the brain besides EEG and MEG. For example, if one were interested in the effect of current in the brain on MRI, which is called 'direct neural imaging', then one would need the magnetic field *inside* the brain. For a uniform sphere the solution is given in (Heller et al. 2004). In addition, brain stimulation by an external current source (known as Transcranial Magnetic Stimulation (TMS)) makes use of the electric field *induced* inside the brain.

3.1 A Current Dipole

Suppose that the primary current occupies a quite localized region, e.g., a few millimeters in size. Then for positions $\mathbf{r}$ that are not too close to that current the primary current contribution to the integral in Eq. (9), can be approximated as

$$\mathbf{p} \times \frac{\mathbf{r} - \mathbf{r_0}}{|\mathbf{r} - \mathbf{r_0}|^3} \tag{10}$$

where

$$\mathbf{p} = \int \mathbf{J}^p(\mathbf{r}')d^3r'. \tag{11}$$

This approximation amounts to concentrating all the primary current at a single position, where $\mathbf{r_0}$ is somewhere inside current. One writes $\mathbf{J}^p(\mathbf{r}) = \mathbf{p}\delta^{(3)}(\mathbf{r} - \mathbf{r_0})$, where δ is the Dirac delta function. $\mathbf{p}$ is called the current dipole moment. Note that any current whatsoever, no matter how spread out it may be, can be written as a linear combination of current dipoles. Since Maxwell's equations are linear in the sources, the solution for the fields becomes a linear sum of the solutions for the individual dipoles. In applications to experimental data it is common to represent the source as the sum of a small number of current dipoles.

3.2 Special Solutions

To solve Eqs. (7), (8) and (9) for the electric potential and the magnetic field for a general head model requires a numerical solution first for $V(\mathbf{r})$ and then for $\mathbf{B}(\mathbf{r})$

since the return current contribution to **B** needs ∇V. But for certain special geometries analytic solutions are available, and the most important one is a *spherical geometry* in which the electrical conductivity σ is assumed to depend only on the distance from the origin. Although the human head is not a sphere it is not vastly different, and one can get a fair approximation to V and **B** by treating the brain, skull and scalp as concentric spherical regions. This solution is also useful for checking the accuracy of computer programs written for more general geometries.

3.2.1 The Magnetic Field

For the magnetic field *outside* the head, where there is no electric current, from Eq. (6) (neglecting the time derivative term) $\nabla \times \mathbf{B} = 0$ and therefore **B** can be obtained as the gradient of a *scalar potential*, (Bronzan 1971). With σ a function of r it was shown in (Grynszpan and Geselowitz 1973; Cuffin and Cohen 1977; Ilmoniemi et al. 1985; Sarvas 1987) that the complete magnetic field due to a point current dipole with moment $\mathbf{p}$ at position $\mathbf{r_0}$ is

$$\mathbf{B}(\mathbf{r}) = \frac{\mu_0}{4\pi F^2}[F\mathbf{p} \times \mathbf{r_0} - (\mathbf{p} \times \mathbf{r_0} \cdot \mathbf{r})\nabla F] \tag{12}$$

where

$$F = a(\mathbf{r} \cdot \mathbf{a} + ra) \tag{13}$$

and

$$\mathbf{a} = \mathbf{r} - \mathbf{r_0}. \tag{14}$$

Written in this form Eq. (12) is called the 'Sarvas formula' (Sarvas 1987). Note that it is completely independent of the conductivity function, provided that it depends only on the radial distance from the origin!

Another consequence of considerable importance can be read off Eq. (12). If the dipole moment $\mathbf{p}$ points in the same radial direction as its position $\mathbf{r_0}$, then $\mathbf{p} \times \mathbf{r_0} = 0$, and hence there is no magnetic field *outside* the head. Such a 'radial dipole' is the simplest example of what is called a "magnetically silent source", i.e., an electric current that produces no magnetic field outside the head. A radial dipole does produce a non-zero magnetic field *inside* the head, however (Heller et al. 2004).

The existence of silent sources poses a difficulty for the *Inverse Problem*, which is discussed in Sect. 4. It consists of trying to deduce the electric currents in the brain that produce an experimentally observed magnetic field and/or electric potential. While an actual current dipole might have both radial and tangential components only the tangential component can be determined. Even though the

head is not a sphere a considerable remnant of this uncertainty persists in a realistic head model.

3.2.2 The Electric Potential

Unlike the magnetic field case, the electric potential in a spherical geometry does depend on the values of the conductivity in each concentric region, (Rush and Driscoll 1969). For a uniform sphere an analytic formula for the potential $V(\mathbf{r})$ due to a current dipole moment $\mathbf{p}$ located at position $\mathbf{r}_1$ is given in (Heller and van Hulsteyn 1992):

$$\begin{gathered} V(\mathbf{r}) = \mathbf{p} \cdot \nabla_1 H(\mathbf{r}, \mathbf{r}_1) \\ H(\mathbf{r}, \mathbf{r}_1) = \frac{1}{4\pi\sigma}\left[\frac{2}{|\mathbf{r}-\mathbf{r}_1|} - \frac{1}{r}\ln\frac{\mathbf{r}\cdot(\mathbf{r}-\mathbf{r}_1)+r|\mathbf{r}-\mathbf{r}_1|}{2r^2}\right], (r \geq R, r_1 \leq R) \end{gathered} \tag{15}$$

where R is radius of the sphere. This difference between the two modalities MEG and EEG, has the following consequence. Suppose the skull, which has a small electrical conductivity, did not conduct current at all. Then there would be no such thing as EEG because no current, and hence no electric field or potential, would be present at the scalp. The magnetic field, on the other hand, penetrates through regions that have no electrical conductivity.

3.3 Realistic Head Models

We now discuss how to solve for the electric potential and the magnetic field in a realistic head model obtained from magnetic resonance imaging of an actual head, together with the assumed conductivity values for the various compartments of the head.

3.3.1 The Electric Potential

The most useful method to solve Eq. (7) for the electric potential in a realistic head model, subject to the boundary conditions in Eq. (8), was given by (Geselowitz 1967). It consists of converting the linear partial differential Eq. (7) to a *linear integral equation* on the boundaries that separate regions of different conductivity. As shown below, it has the advantage that the boundary conditions are built right in! The starting point is an identity

$$\nabla' \cdot \left(V(\mathbf{r}')\nabla' \frac{1}{|\mathbf{r}-\mathbf{r}'|} - \frac{1}{|\mathbf{r}-\mathbf{r}'|}\nabla' V(\mathbf{r}') \right) = V(\mathbf{r}')\nabla^{2'} \frac{1}{|\mathbf{r}-\mathbf{r}'|} - \frac{1}{|\mathbf{r}-\mathbf{r}'|}\nabla^{2'} V(\mathbf{r}'), \tag{16}$$

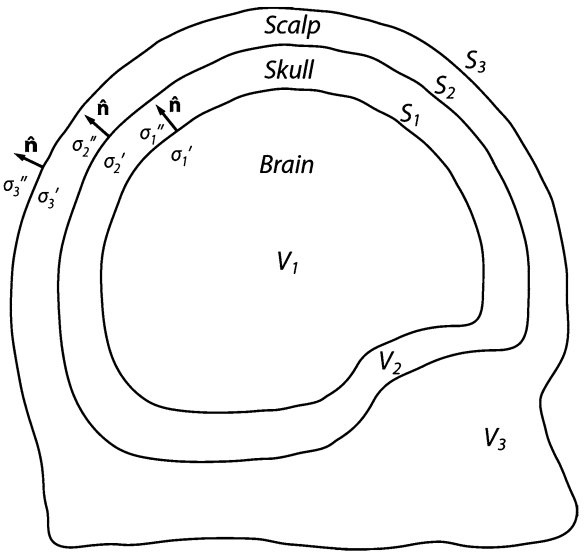

Fig. 1 A schematic diagram showing three head regions with their respective volumes V_j, surfaces, S_j, and normal vectors **n**. In the literature the conductivities of the respective regions are called σ_j', and a second set of labels, designated σ_j'' is introduced for notational reasons. They are related as follows. $\sigma_1'' = \sigma_2'$; $\sigma_2'' = \sigma_3'$; and σ_3'', being the conductivity of the space surrounding the head, is zero

which is then integrated throughout the entire volume of the head model, *one conductivity region at a time*. Vector **r** is a position anywhere inside the head model. On the left side of Eq. (16) one makes use of the divergence theorem, which says that the integral of the divergence of a vector throughout a volume V is equal to the integral over the surface S of that volume of the component of the vector along the direction of the *outward* pointing normal vector. On the right hand side of Eq. (16) one can make use of Eq. (7) to replace $\nabla^2 V = \nabla \cdot \mathbf{J}^p/\sigma$. Also, $\nabla^2 1/|\mathbf{r} - \mathbf{r}'| = -4\pi\delta(\mathbf{r} - \mathbf{r}')$.

Figure 1 shows the notation for the case of three regions, brain, skull, and scalp. The normal vector on each surface is chosen to point outward from that region. It is straightforward to apply Eq. (16) to the innermost (brain) region with volume V_1, surface S_1, and conductivity σ_1' (see Fig. 1). Multiplying Eq. (16) by σ_1' and integrating it throughout region 1 yields

$$\begin{aligned} &\int_{S_1} dS_1' \mathbf{n}(\mathbf{r}') \cdot \left(\sigma_1' V_1(\mathbf{r}') \nabla' \frac{1}{|\mathbf{r} - \mathbf{r}'|} - \frac{1}{|\mathbf{r} - \mathbf{r}'|} \sigma_1' \nabla_1' V_1(\mathbf{r}') \right) \\ &\quad = -\int_{V_1} d^3 r' \left[4\pi\sigma_1' V(\mathbf{r}')\delta(\mathbf{r} - \mathbf{r}') + \frac{1}{|\mathbf{r} - \mathbf{r}'|} \nabla' \cdot \mathbf{J}^p(\mathbf{r}') \right] \end{aligned} \tag{17}$$

In this equation the normal vector $\mathbf{n}(\mathbf{r}')$ points outward from the region with conductivity σ_1'. Furthermore, the quantities $V_1(\mathbf{r}')$ and $\nabla_1' V_1(\mathbf{r}')$ are the values of those quantities as S_1 is approached from the interior of volume V_1.

When Eq. (16) is integrated throughout region V_2 with conductivity σ_2', there are two surfaces that contribute to the left side of the equation, S_1 and S_2. The contribution from surface S_2 looks just like the left side of Eq. (17) with the subscript 1 replaced everywhere with 2. But because we have already chosen the normal vector on S_1 to point *outward* from region 1, which makes it *inward* pointing to region 2, the contribution of S_1 to the left side of the equation requires an overall minus sign.

When the equations for conductivity regions 1 and 2 are summed over the contribution from S_1 contains $(\sigma_1' V_1(\mathbf{r}') - \sigma_2' V_2(\mathbf{r}'))$ and $(\sigma_1' \nabla_1' V_1(\mathbf{r}') - \sigma_2' \nabla_2' V_2(\mathbf{r}'))$. Applying the boundary conditions Eq. (8) on S_1, $V_1(\mathbf{r}') = V_2(\mathbf{r}')$ and $\mathbf{n} \cdot (\sigma_1' \nabla_1' V_1(\mathbf{r}') - \sigma_2' \nabla_2' V_2(\mathbf{r}')) = 0$. This confirms the statement earlier that the integral equation has the advantage over the differential equation that the boundary conditions are built in.

After integrating Eq. (16) over the complete volume of the head the result is, (Geselowitz 1967)

$$\sigma(\mathbf{r})V(\mathbf{r}) = \frac{1}{4\pi}\Sigma_j(\sigma_J' - \sigma_j'') \int_{S_j} dS_j' \mathbf{n}(\mathbf{r}') \cdot \frac{\mathbf{r}' - \mathbf{r}}{|\mathbf{r}' - \mathbf{r}|^3} V(\mathbf{r}') + \frac{1}{4\pi} \int_V d^3 r' \mathbf{J}^{\mathbf{p}}(\mathbf{r}') \cdot \frac{\mathbf{r} - \mathbf{r}'}{|\mathbf{r}' - \mathbf{r}|^3}. \tag{18}$$

In Eq. (18) the position $\mathbf{r}$ is anywhere in the volume, and $\sigma(\mathbf{r})$ is the value of the conductivity in the head compartment containing that position. The final integral on the right side is obtained by once again using the divergence theorem on $\nabla \cdot (\mathbf{J}^{\mathbf{p}}(\mathbf{r}')/|\mathbf{r} - \mathbf{r}'|)$ and noting that there is no contribution from the surface integral on the surface of the head because there is no primary current there.

Equation (18) determines the value of the potentlal at position $\mathbf{r}$ only if one already knows its values on all the surfaces of discontinuity of the conductivity. To obtain those values let the point $\mathbf{r}$ approach a position $\mathbf{r_k}$ on one of the surfaces, S_k. Care must be taken because the denominator of the surface integral vanishes there.

There is a geometric meaning of the integrand which reveals the problem and points to the solution. Apart from the function $V(\mathbf{r}')$ the rest of the integrand in the surface integral in Eq. (18) is just the element of solid angle $d\Omega'(\mathbf{r}, \mathbf{r}')$ subtended at the position $\mathbf{r}$ by an element of surface area dS' at position $\mathbf{r}'$, i.e.,

$$d\Omega'(\mathbf{r}, \mathbf{r}') = dS' \mathbf{n}(\mathbf{r}') \cdot \frac{\mathbf{r}' - \mathbf{r}}{|\mathbf{r}' - \mathbf{r}|^3}. \tag{19}$$

Now the *total* solid angle subtended at any position $\mathbf{r}$ *inside* a closed surface (with outward pointing normal) is 4π; if $\mathbf{r}$ is *outside* the surface the total is zero, and if $\mathbf{r}$ is *on* the surface the total is 2π. *It is a discontinuous function*. It is equally true with any function $V(\mathbf{r})$ in Eq. (18) that the limit of the surface integral as $\mathbf{r}$ approaches a position $\mathbf{r_k}$ on the surface is not equal to the value of the integral with $\mathbf{r} = \mathbf{r_k}$; there is an extra term (Vladimirov 1971)

$$\lim_{\mathbf{r}\to\mathbf{r_k}} \int\limits_{S_k} dS'_k \mathbf{n}(\mathbf{r}') \cdot \frac{\mathbf{r}' - \mathbf{r}}{|\mathbf{r}' - \mathbf{r}|^3} V(\mathbf{r}') = \int\limits_{S_k} dS'_k \mathbf{n}(\mathbf{r}') \cdot \frac{\mathbf{r}' - \mathbf{r_k}}{|\mathbf{r}' - \mathbf{r_k}|^3} V(\mathbf{r}') + 2\pi V(\mathbf{r_k}). \quad (20)$$

For the final step, in Eq. (18) let $\mathbf{r}$ approach $\mathbf{r_k}$ from the σ'_k side, and replace the limit of the surface integral on surface S_k according to Eq. (20). Then there will be an additional term on the right side of $(1/4\pi)(\sigma'_k - \sigma''_k)(2\pi V(\mathbf{r_k}))$. When this term is brought over to the left side of the equation, which consists of $\sigma'_k V(\mathbf{r_k})$, and the two terms combined, the result is, (Sarvas 1987)

$$\frac{\sigma'_k + \sigma''_k}{2} V(\mathbf{r_k}) = \frac{1}{4\pi} \Sigma_j (\sigma'_j - \sigma''_j) \int\limits_{S_j} dS'_j \mathbf{n}(\mathbf{r}') \cdot \frac{\mathbf{r}' - \mathbf{r_k}}{|\mathbf{r}' - \mathbf{r_k}|^3} V(\mathbf{r}') + \frac{1}{4\pi} \int\limits_V d^3 r' \mathbf{J^p}(\mathbf{r}') \cdot \frac{\mathbf{r_k} - \mathbf{r}'}{|\mathbf{r_k} - \mathbf{r}'|^3} \quad (21)$$

The reader can check that it does not matter if the point $\mathbf{r}$ approaches $\mathbf{r_k}$ from the σ'_k side or the σ''_k side; Eq. (21) results either way. [Recall that the normal vector on the σ'' side has the opposite sign.]

Equation (21) is a set of coupled linear integral equations for the electric potential, one equation for each surface. A standard method for numerically solving Eq. (21) for the electric potential on those surfaces is to approximate each surface separating different conductivity regions by a set of small triangles, noting that there is an analytic formula for the solid angle subtended by a triangle at an arbitrary position, (van Oosterom and Strackee 1983). Some treatments choose the vertices of the triangles as the locations for evaluating the potential, and some choose the centers of the triangles. See, for example, (Schlitt et al. 1995). When this is done the continuous integral equation is replaced by a set of ordinary coupled linear algebraic equations, which are solved by standard matrix techniques. Figure 2 shows a mesh of triangles on the brain-skull interface, and the outlines of the skull-scalp interface and the scalp-air interface, used for solving Eq. (21).

When doing this it is important to make sure *numerically* that the total solid angle subtended by all the triangles on a given surface at an interior point is 4π, and zero at an exterior point. And if the point in question is on one of those triangles the total is 2π. Consequently, since a flat triangle subtends *zero* solid angle at any point on itself, all the other triangles on that same surface must subtend a total of 2π at any point located on a triangle.

As mentioned above, once the potential has been found on the surfaces of discontinuity, it can then be evaluated at any other position using Eq. (18).

3.3.2 The Magnetic Field

The starting point for evaluating the magnetic field in a realistic head model is Eq. (9), the Biot-Savart Law. For the primary current contribution simply insert $\mathbf{J^p}$ into that equation,

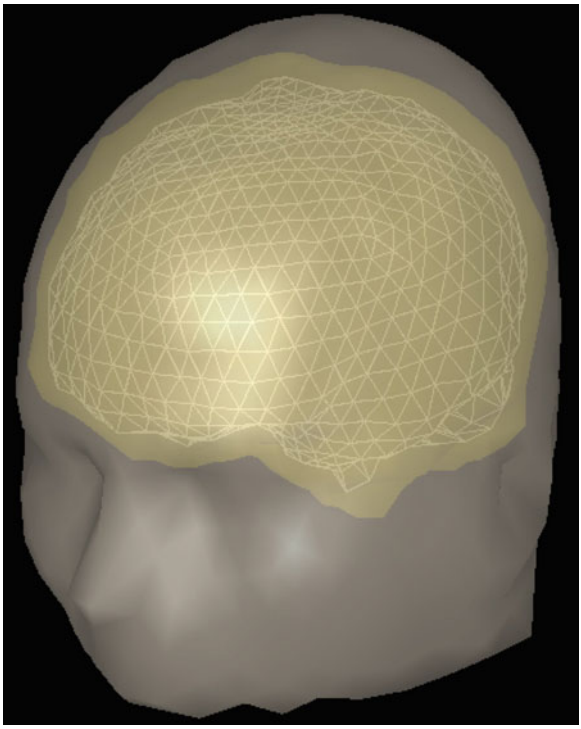

Fig. 2 A mesh of triangles on the brain-skull interface used to numerically solve Eq. (21) for the electric potential. There are similar meshes on the skull-scalp interface and the scalp-air interface, which are not shown. The values of the potential at every triangle vertex are the unknowns being solved for, given an assumed primary current

$$\mathbf{B}^{\mathbf{p}}(\mathbf{r}) = \frac{\mu_0}{4\pi} \int_V \mathbf{J}^{\mathbf{p}}(\mathbf{r}') \times \nabla' \frac{1}{|\mathbf{r} - \mathbf{r}'|} d^3 r', \tag{22}$$

where V is the complete volume of the head.

For the return current one must have already solved for electric potential $V(\mathbf{r})$. Since $\mathbf{J}^R = -\sigma \nabla V$, its contribution to the magnetic field is

$$\mathbf{B}^R(\mathbf{r}) = -\frac{\mu_0}{4\pi} \sum_i \sigma_i \int_{V_i} \nabla' V(\mathbf{r}') \times \nabla' \frac{1}{|\mathbf{r} - \mathbf{r}'|} d^3 r', \tag{23}$$

where the sum is over all compartments of the head. Here one makes use of the identity $\nabla V \times \nabla(1/|\mathbf{r} - \mathbf{r}'|) = \nabla \times [V \nabla(1/|\mathbf{r} - \mathbf{r}'|)]$, together with Stokes's theorem. It says that the integral of the curl of a vector $\mathbf{N}$ throughout a volume is equal to the integral over the surface of that volume of $\mathbf{n} \times \mathbf{N}$, where $\mathbf{n}$ is the outward pointing normal vector. In the present case $\mathbf{N}$ is chosen to be $[V(\mathbf{r}')\nabla'(1/|\mathbf{r} - \mathbf{r}'|)]$.

Just as in the case of the electric potential the contributions from the two compartments that share surface S_j will contribute with opposite signs because the normal vector is chosen to point from the region with conductivity σ'_j into the

region with conductivity σ_j''. The final result for the return current contribution to the magnetic field is, (Geselowitz 1970).

$$\mathbf{B}^R(\mathbf{r}) = -\frac{\mu_0}{4\pi}\Sigma_j(\sigma_j' - \sigma_j'')\int_{S_j} dS_j'\mathbf{n}(\mathbf{r}') \times V(\mathbf{r}')\nabla'\frac{1}{|\mathbf{r}-\mathbf{r}'|}. \tag{24}$$

Since all the equations above for the electric potential and the magnetic field are linear, their solutions for an arbitrary primary current, say a sum of point current dipoles, are just the sum of the solutions for the individual dipoles.

3.3.3 Conductivity Values

In order to actually solve Eq. (21) for the electric potential in a given head model it is necessary to know the actual values of the conductivity in each compartment of the head. These measurements are made in a number of ways. In one, current is injected into the head and the resulting potential distribution on the scalp is measured; a best fit of assumed conductivity values to the data is then made. Here, the injected current plays the role of the primary current $\mathbf{J}^p$ in Eq. (21). With patients about to undergo surgery, e.g., for epilepsy, electrodes can be placed right on the surface of the brain, both to inject current and detect the resulting potential.

Since the assumption of a constant isotropic conductivity in each head region is somewhat crude, it is not surprising that there is considerable variation from person to person when these measurements are made. Some approximate values obtained are as follows. σ (skull) = 0.015 S/m; and σ (brain):σ(skull):σ(scalp) = 1:1/15:1, (Oostendorp et al. 2000). This value for the skull conductivity is much larger than that found in older literature. A separate measurement of the conductivity of human cerebrospinal fluid gives the value 1.79 S/m at body temperature and a somewhat smaller value at room temperature, (Baumann et al. 1997).

4 Inverse Problem

An inverse problem is generally understood as methods or techniques used to obtain information about a physical object or system using indirect measurements. In the context of EEG/MEG the inverse problem deals with reconstructing current sources, i.e. current distribution $\mathbf{J}^p(\mathbf{r})$, using measured magnetic fields and/or electric potentials generated by those currents. We will start to discuss the inverse problem considering only MEG sensors. Given that we have a number of MEG sensors we can write the MEG inverse problem in general as a set of integral equations:

$$f_i(t) = \int_V \mathbf{M}_i(\mathbf{r}') \cdot \mathbf{J}^p(\mathbf{r}', t) d^3 r' + \xi_i(t), i = 1, .., N \tag{25}$$

Here $f_i(t)$ is the signal recorded in the i-th sensor, $\xi_i(t)$ is noise present in the i-th channel, N is number of the sensors, and the integration is over the volume occupied by neuronal currents. Vector function $\mathbf{M}_i(\mathbf{r})$, called "lead field", describes a response of the i-th sensor to a unit current dipole at position $\mathbf{r}$. Specifically $(\mathbf{M}_i(\mathbf{r}))_x$ is magnetic field flux through the pick-up coil of i-th sensor generated by a unit current dipole aligned along x-axis, correspondingly $(\mathbf{M}_i(\mathbf{r}))_y$, $(\mathbf{M}_i(\mathbf{r}))_z$ are magnetic field flux due to dipoles aligned along y- and z- axis. It is important to note that lead field function $\mathbf{M}_i(\mathbf{r})$ describes effects of both the primary and return currents. In order to obtain lead field function one first must compute the magnetic field due to primary current consisting of a unit current dipole, see Eq. (22, and the magnetic field due to the return current associated with this dipole (Eq. (24)). For the latter one must have first solved for electrical potential according to Eqs. (18) and (21). Then the total magnetic field is integrated over the area of a sensor pick-up coil to compute the magnetic field flux. Often times in practice the lead field function is approximated by sampling the field at several points over the area of a sensor pick-up coil:

$$\mathbf{M}(\mathbf{r}) \approx \frac{1}{N_p} \sum_{k=1}^{N_p} \{(\mathbf{B}_x(\mathbf{r}_k, \mathbf{r}) \cdot \hat{\mathbf{n}}_k)\hat{\mathbf{e}}_x + (\mathbf{B}_y(\mathbf{r}_k, \mathbf{r}) \cdot \hat{\mathbf{n}}_k)\hat{\mathbf{e}}_y + (\mathbf{B}_z(\mathbf{r}_k, \mathbf{r}) \cdot \hat{\mathbf{n}}_k)\hat{\mathbf{e}}_z\} \Delta S_k \tag{26}$$

Here N_p is number of the sampling points, ΔS_k and $\hat{\mathbf{n}}_k$ are respectively the area of a pick-up coil and the unit vector normal to a pick-up coil associated with a sampling point $\mathbf{r}_k$, $\mathbf{B}_x(\mathbf{r}_k, \mathbf{r})$, is magnetic field at the sampling point $\mathbf{r}_k$ generated by total current associated with a unit current dipole positioned at $\mathbf{r}$ and aligned along x-axis, correspondingly $\mathbf{B}_y(\mathbf{r}_k, \mathbf{r})$ and $\mathbf{B}_z(\mathbf{r}_k, \mathbf{r})$ are fields generated by dipoles aligned along y- and z-axis.

Equation (25) being Fredholm integral equations of the first kind for the current $\mathbf{J}^p$, constitute a notoriously ill-posed problem. The term "ill-posed" in the context of the inverse problem points to the presence of one of the following three problems: (a) the solution may not exist, i.e. that there is no current distribution $\mathbf{J}^p(\mathbf{r})$ which corresponds to the measured data, (b) the solution is not unique, meaning that there are several different current distributions $\mathbf{J}^p(\mathbf{r})$ which give the same observed data, and, finally, (c) the solution changes dramatically with slight changes in the measured data.

An EEG/MEG inverse problem demonstrates all of the three aforementioned conditions. First due to corruption of the measurements by omnipresent noise it is quite possible that no current distribution can explain the observed data. Second, as early as in 1853 it was shown by Helmholtz (1853) that a current distribution inside a conducting body can not be uniquely reconstructed knowing only the

electromagnetic field outside this body. There are possible current distributions inside a conductor which produce no magnetic field outside the conductor, or produce no electrical potentials on the surface of the conductor. Such current distributions are called magnetically silent and electrically silent, respectively. An example of magnetically silent current is a current dipole placed inside a conducting sphere and aligned along the radius. Due to symmetry of the problem, see Eq. (12), the field outside of the sphere is identically zero. An example of an electrically silent current is a loop current inside a conductor, which produces a magnetic field outside the conductor, but does not contribute to the electrical potential on the surface of the conductor. There are also current distributions which produce no magnetic field outside the conductor nor electrical potentials on the surface of the conductor. Finally if the current is limited to an area located far from the surface of the conductor, then quite different current distributions inside this area will result in about the same magnetic and electrical field outside the conductor, thus giving the possibility that a solution will change drastically with a slight change in the measured data.

This suggests that special attention should be paid to how we define a solution of an EEG/MEG problem and how we obtain it.

4.1 Formulation of the Problem

The first step in estimating neuronal currents is to somehow describe it in terms of known sources. This can be done in many ways, provided that the selected sources can represent the function $\mathbf{J}^p(\mathbf{r})$ reasonably well, but for the purposes of this book we assume that the primary current $\mathbf{J}^p(\mathbf{r})$ can be represented by a finite sum of current dipoles:

$$\mathbf{J}^p(\mathbf{r}) = \sum_{j=1}^{M} \mathbf{p}_j \delta^3(\mathbf{r} - \mathbf{r}_j) \tag{27}$$

where $\mathbf{p}_j$ and $\mathbf{r}_j$ define direction and position of the j-th dipole. Substituting this last formula into Eq. (25) we obtain a set of equation for the unknown parameters of dipoles:

$$f_i(t) = \sum_{j=1}^{M} \mathbf{M}_i(\mathbf{r}_j) \cdot \mathbf{p}_j(t) + \xi_i(t), i = 1, .., N \tag{28}$$

Here $\mathbf{M}_i(\mathbf{r}_j)$, which is the lead field function of the i-th sensor, represents the response of the i-th MEG sensor to a unit current dipole at position $\mathbf{r}_j$. In this last equation position of the dipoles, i.e. $\mathbf{r}_j$, could be defined from anatomical MRI data, or left undefined. In the first case, we only need to find dipole vectors $\mathbf{p}_j$ by solving a system of linear equations, but in the second case we also need to find the

positions of the dipoles $\mathbf{r}_j$ along with their vectors $\mathbf{p}_j$ to specify the current source, which makes the problem non-linear. One must remember not to include silent current dipoles, such as, for example, a radial dipole inside a conducting sphere, because there is no way we can attribute strength to such a dipole.

Here it is convenient to introduce matrix notation which is ubiquitous in the literature, both textbooks and research, dedicated to MEG/EEG. Using matrix notation equation (28) can be written as:

$$\mathbf{f} = \mathbf{K}\mathbf{q} + \xi \tag{29}$$

where the measured data are represented by column vectors: $\mathbf{f} \equiv (f_1, \ldots, f_N)^T$, $\xi \equiv (\xi_1, \ldots, \xi_N)^T$ (here and later the superscript T denotes a transposed matrix/vector), column vector $\mathbf{q}$ comprises components of the all dipole vectors $\mathbf{p}_j$:

$$\mathbf{q} \equiv \left((\mathbf{p}_1)_x, (\mathbf{p}_1)_y, (\mathbf{p}_1)_z, (\mathbf{p}_2)_x, (\mathbf{p}_2)_y, (\mathbf{p}_2)_z, \ldots, (\mathbf{p}_M)_x, (\mathbf{p}_M)_y, (\mathbf{p}_M)_z\right)^T \tag{30}$$

and components of the lead field functions $\mathbf{M}_i(\mathbf{r}_j)$ form matrix $\mathbf{K}$ usually called a "gain" matrix:

$$\mathbf{K} \equiv \mathbf{K}(\mathbf{r}_1, \mathbf{r}_2, \ldots, \mathbf{r}_M) \equiv \begin{bmatrix} (\mathbf{M}_1(\mathbf{r}_1))_x & (\mathbf{M}_1(\mathbf{r}_1))_y & (\mathbf{M}_1(\mathbf{r}_1))_z & \ldots & (\mathbf{M}_1(\mathbf{r}_M))_x & (\mathbf{M}_1(\mathbf{r}_M))_y & (\mathbf{M}_1(\mathbf{r}_M))_z \\ (\mathbf{M}_2(\mathbf{r}_1))_x & (\mathbf{M}_2(\mathbf{r}_1))_y & (\mathbf{M}_2(\mathbf{r}_1))_z & \ldots & (\mathbf{M}_2(\mathbf{r}_M))_x & (\mathbf{M}_2(\mathbf{r}_M))_y & (\mathbf{M}_2(\mathbf{r}_M))_z \\ \ldots & \ldots & \ldots & \ldots & \ldots & \ldots & \ldots \\ (\mathbf{M}_N(\mathbf{r}_1))_x & (\mathbf{M}_N(\mathbf{r}_1))_y & (\mathbf{M}_N(\mathbf{r}_1))_z & \ldots & (\mathbf{M}_N(\mathbf{r}_M))_x & (\mathbf{M}_N(\mathbf{r}_M))_y & (\mathbf{M}_N(\mathbf{r}_M))_z \end{bmatrix} \tag{31}$$

Recalling the rules of matrix multiplication it is easy to see that the matrix Eq. (29) constitutes exactly the set of Eq. (28).

So far we have only discussed MEG data, but without changing anything we can add measured EEG data to the data vector $\mathbf{f}$ and "gain" matrix of the EEG channels, i.e. matrix elements which describe responses of a EEG channels to a unit current dipole, to the matrix $\mathbf{K}$, thus consider Eq. (29) describing the complete EEG/MEG problem.

Now we can formulate the MEG/EEG inverse problem as follows: estimate current source parameters $\boldsymbol{\Theta} \equiv \{\mathbf{p}_j, \mathbf{r}_j\}$, given a MEG/EEG data set $\mathbf{f}$ measured with some statistical errors ξ. This is obviously a parameter estimation problem.

4.2 Maximum Likelihood Approach

A very common method of estimating the parameters of a statistical model is maximum-likelihood estimation (MLE). In general the method gives the model parameters $\boldsymbol{\Theta}$ which give the observed data $\mathbf{f}$ the greatest probability:

$$\mathbf{\Theta}_{MLE} = \arg\max_{\mathbf{\Theta}}(p(\mathbf{f}|\mathbf{\Theta})) \tag{32}$$

Here $p(\mathbf{f}|\Theta)$ is the probability density, i.e. $p(\mathbf{f}|\Theta)\Delta\mathbf{f}$ is the probability to measure MEG/EEG signals in the interval $(\mathbf{f}, \mathbf{f}+\Delta\mathbf{f})$, provided the actual source was defined by parameters $\mathbf{\Theta}$, and $\mathbf{\Theta}_{MLE}$, called a maximum likelihood estimation, is that value of $\mathbf{\Theta}$ which maximize $p(\mathbf{f}|\mathbf{\Theta})$ considered as a function of $\mathbf{\Theta}$. The probability density function considered as a function of the $\mathbf{\Theta}$ instead of $\mathbf{f}$ is called the likelihood function: $L(\mathbf{\Theta}) \equiv p(\mathbf{f}|\mathbf{\Theta})$. Usually it is more convenient to maximize the logarithm of the likelihood function:

$$\mathbf{\Theta}_{MLE} = \arg\max_{\mathbf{\Theta}}(l(\mathbf{\Theta})) \tag{33}$$

where $l(\mathbf{\Theta}) \equiv \ln(L(\mathbf{\Theta})) \equiv \ln(p(\mathbf{f}|\mathbf{\Theta}))$ is called a log-likelihood function.

Naturally, the MLE approach requires knowing the statistical properties of the noise. One simple, but plausible, assumption is that the noise ξ_i obeys the Gaussian distribution with zero mean. In this case for each measurement channel we can write the probability density to observe value x, which can be a magnetic field or electric potential, in a measurement channel:

$$p_i(x|\mathbf{\Theta}) = \frac{1}{\sqrt{2\pi\sigma_i^2}} e^{-\frac{(x-\widetilde{f}_i)^2}{2\sigma_i^2}} \tag{34}$$

where $p_i(x|\mathbf{\Theta})$ is the conditional probability density for the i-th measurement channel, i.e. $p_i(x|\mathbf{\Theta})\Delta x$ is the probability to observe signal in the i-th channel in the interval $(x, x+\Delta x)$, provided the current source was defined by parameters $\mathbf{\Theta}$, $\widetilde{f}_i \equiv \sum_{j=1}^{M} K_{i,j} q_j$ is the expected value for model parameters $\mathbf{\Theta}$, and σ_i^2 is the noise variance for the i-th measurement channel respectively. Further assuming that the noise in the different channels is independent, i.e. the combined probability for all the measurement channels is a product of probabilities of the individual channels: $p(f_1, \ldots, f_N|\mathbf{\Theta}) = p_1(f_1|\mathbf{\Theta})p_2(f_2|\mathbf{\Theta})\ldots p_N(f_N|\mathbf{\Theta})$, we will get the likelihood function for this noise model:

$$L(\mathbf{\Theta}) = \prod_{i=1}^{M} \frac{1}{\sqrt{2\pi\sigma_i^2}} e^{-\frac{(f_i-\widetilde{f}_i)^2}{2\sigma_i^2}} \tag{35}$$

Taking the logarithm of this last expression we will get a log-likelihood function, i.e. the function we seek to minimize to find the current distribution most consistent with the measurements, in the case of uncorrelated Gaussian noise:

$$l(\Theta) = -\frac{1}{2}\sum_{i=1}^{N} \frac{(f_i - \widetilde{f}_i)^2}{\sigma_i^2} + const \tag{36}$$

It should be noted that in practice the noise in different channels is more often correlated, than not, because it is caused by common ambient noise sources. Still assuming that the noise obeys a Gaussian distribution we can generalize formula (36) as:

$$l(\Theta) = -\frac{1}{2}(\mathbf{f} - \widetilde{\mathbf{f}})^T \mathbf{C}^{-1}(\mathbf{f} - \widetilde{\mathbf{f}}) + const \tag{37}$$

where $\widetilde{\mathbf{f}} = \mathbf{Kq}$ is the vector of expected values of the measured signals for the model parameters $\mathbf{\Theta}$, $\mathbf{C} \equiv [C_{i,j}]$ is the covariance matrix of noise in the measurement channels, and $\mathbf{C}^{-1}$ denotes the inverse of this matrix, i.e. $\mathbf{C}^{-1}\mathbf{C} = \mathbf{C}\mathbf{C}^{-1} = \mathbf{I}$, where $\mathbf{I}$ is an identity matrix. By definition elements of a covariance matrix $C_{i,j}$ are expectation values of product of noise signals in the different channels:

$$C_{i,j} = E\{(\xi_i - \overline{\xi}_i)(\xi_j - \overline{\xi}_j)\} \tag{38}$$

Here $E\{\ldots\}$ denotes the expectation value of an expression in the brackets, ξ_i is noise present in the channel i, the bar over a quantity, to shorten the notation, also denotes the expectation value of quantity, i.e. $\overline{\xi}_i \equiv E\{\xi_i\}$ is the mean value of noise in i-th channel. Note that Eq. (38) can be written in matrix notation as:

$$\mathbf{C} = E\{(\xi - \overline{\xi})(\xi - \overline{\xi})^T\} \tag{39}$$

In the case of uncorrelated noise considered above, see Eq. (36), all non-diagonal elements of the correlation matrix are equal to zero, and the diagonal elements, i.e. $C_{i,i}$, are simply variance of the measurement channels.

$$\mathbf{C} = \begin{bmatrix} \sigma_1^2 & 0 & 0 & \ldots & 0 \\ 0 & \sigma_2^2 & 0 & \ldots & 0 \\ & & \ldots & & \\ 0 & \ldots & 0 & \sigma_{N-1}^2 & 0 \\ 0 & \ldots & 0 & 0 & \sigma_N^2 \end{bmatrix} \tag{40}$$

Respectively the inverse matrix of this diagonal matrix is also a diagonal matrix, the diagonal elements are the inverse variance of the corresponding measurement channels:

$$\mathbf{C}^{-1} = \begin{bmatrix} 1/\sigma_1^2 & 0 & 0 & \ldots & 0 \\ 0 & 1/\sigma_2^2 & 0 & \ldots & 0 \\ & & \ldots & & \\ 0 & \ldots & 0 & 1/\sigma_{N-1}^2 & 0 \\ 0 & \ldots & 0 & 0 & 1/\sigma_N^2 \end{bmatrix} \tag{41}$$

It is easy to see that by substituting (41) into (37) we will get exactly formula (36).

4.3 Chi-Square Criteria

Before we proceed to describe techniques for finding solutions according to (33), let us qualitatively analyze the properties of the MLE.

First, by solving the problem (29) in some sense we estimate both the source parameters $\boldsymbol{\Theta}$ and the noise ξ. Second, if the problem (29) has an exact solution, i.e. if $\boldsymbol{\Theta}$ exists such that $\mathbf{Kq} = \mathbf{f}$, where $\mathbf{f}$ is the measured data, then this solution is a MLE solution. This means that in this case the estimated noise is identically zero, which is very hard to believe. This leads to a paradox: the better we fit the data $\mathbf{f}$ by adjusting the source parameters $\boldsymbol{\Theta}$, the higher the probability that the source generates the data, but if we fit the data too well it becomes very unlikely that the data are generated by the source. This situation is usually referenced to as "overfitting" the data.

These considerations lead us to the necessity to characterize somehow the difference between the measured data and the model, i.e. between $\mathbf{f}$ and $\widetilde{\mathbf{f}} \equiv \mathbf{Kq}$. This difference describes how well the model describes the data. If the variance of the noise is known this difference can be characterized by a quantity denoted as χ^2 and defined by the following equation:

$$\chi^2 = \sum_{i=1}^{N} \frac{(f_i - \widetilde{f}_i)^2}{\sigma_i^2} \equiv (\mathbf{f} - \widetilde{\mathbf{f}})^T \Sigma^{-1} (\mathbf{f} - \widetilde{\mathbf{f}}) \tag{42}$$

where elements of the diagonal matrix Σ^{-1} are the inverse variance of the corresponding measurement channels (compare with Eq. (41)). From the definition (42) it is obvious that if the parameters of a true model are somehow known, the expectation value of χ^2 is equal to the number of the measurement channels N. In the case the noise in different measurement channels is uncorrelated and normally distributed with zero mean, the quantity χ^2 defined according to (42) obeys a probability distribution known as "chi-square" distribution (hence the notation) with v degrees of freedom. This distribution has the expectation equal to the number of degrees of freedom v and the variance twice this number $2v$. In the limiting case $v \to \infty$ chi-square distribution converges to a normal distribution.

The notion of "number of degrees of freedom" deserves some explanation. Usually it is assumed that $v = N - M$, where N is the dimension of the data vector, i.e. the number of measurement channels, and M is the number of model parameters. This reflects the fact that if we estimate M model parameters minimizing (42) and using N measurements, then we can expect that on average the value of χ^2 will be about $N - M$ with the variance twice this number, provided our model allows for the exact solution of the model equation (Eq. (29) in our case). In the limiting case when the number of the estimated model parameters (including the ones estimated implicitly) is equal to the number of available data points, then we can expect the difference χ^2 is identically zero. This approach helps to answer the questions about fidelity of the model: "can it describe the data set?", "are M

parameters enough to account for the complexity of the data?", "do we have any redundant model parameters?". However if we formulate the question as "is it plausible that the model in question generated the observed data set?" then we need to assume that the number of degrees of freedom is equal to the number of the data points: $v = N$.

In practice it is convenient to use the normalized chi-square (or reduced chi-square) criteria—χ^2_n, which is χ^2 per degree of freedom:

$$\chi^2_n = \chi^2 / v \tag{43}$$

Obviously the expectation value of χ^2_n is always 1, and the variance is $2/v$, which makes it easy to interpret: if χ^2_n is about 1 within, say, a variance, then our model is consistent with the data, if $\chi^2_n << 1$, then our model captures not only the signal but also the noise (or the noise is overestimated), and finally if $\chi^2_n >> 1$, then our model is not adequate to describe the signal (or the noise is underestimated). Naturally, one must not forget that in order to apply these rules the variance of the noise should be very reliably estimated.

These simple rules may be formalized by introducing P- and Q-values. Given a particular value we can calculate the probabilities obtaining an experimental value of χ^2 that is less (P-value) and greater (Q-Value) than this value. The most widely accepted critical value is Q=0.05, meaning that only in 5 % of trials the higher value of χ^2 would be observed if the model under consideration is true. In MEG sometimes a solution is considered to be acceptable if its Q-value is greater than 0.001.

Similar to (37) definition of the χ^2 (42) can be generalized using a complete covariance matrix $\mathbf{C}$, which in the general case is not a diagonal:

$$\chi^2 = (\mathbf{f} - \widetilde{\mathbf{f}})^T \mathbf{C}^{-1} (\mathbf{f} - \widetilde{\mathbf{f}}) \tag{44}$$

Here if the matrix $\mathbf{C}$ has full rank, then the χ^2 defined according to (44) is chi-squared distributed.

Concluding the discussion of characterizing the difference between the model and the measurement we would like to reiterate that characterizing the validity of the model and the validity of the solution of the inverse problem in MEG/EGG is of paramount importance.

4.4 Imaging Versus Localization

Now let us proceed to find estimations of the current sources according to Eq. (33). It is generally accepted, see for example (Baillet et al. 2001), that depending on how we select the current dipoles in the decomposition (27) the estimation of

current sources can be broadly divided into two classes: (1) "localization" and (2) "imaging".

In the first case we assume that the current source under study is limited to a few small areas. Naturally here the basis sources are selected to be a few current dipoles, positions and magnitudes of which are considered to be unknown parameters of the model to be estimated by fitting the model to the data.

In the second case the current source is assumed to be of distributed nature. In this case the basis functions typically constitute a large number of current dipoles distributed according to some rule over the target surface or volume. The positions and orientations of those dipoles are assumed to be known, and the amplitudes of the dipoles are considered to be the model parameters to be estimated.

In addition to the two classes described above one can also distinguish "beamforming" techniques, which are somewhat intermediate between the localization and imaging techniques. The main idea of this approach is to design a filter, which being applied to the data vector $\mathbf{f}$ emphasize the signals resulting from some selected spatial area, while suppressing the signals from the rest of the target volume.

4.4.1 Single/Multiple Dipole Localization

Early studies of the fields generated by evoked somatosensory responses (Brenner et al. 1978) revealed a dipolar character of both the magnetic field around a head and the electrical potential on head surface. An example of such fields is shown in Fig. 3 where the dipolar and complementary nature of the MEG/EEG signals is clearly visible. This leads to the simplest model of neuronal current source as an equivalent current dipole (ECD): $\mathbf{J}^p(\mathbf{r}) = \mathbf{p}_d\delta^3(\mathbf{r} - \mathbf{r}_d)$.

It is straightforward to find parameters of the dipole, i.e. its position $\mathbf{r}_d$ and vector $\mathbf{p}_d$, by maximizing log-likelihood function (37), or, which is equivalent, minimizing χ^2 (44), with respect to $\mathbf{r}_d$ and $\mathbf{p}_d$ using the following relation for the model $\widetilde{\mathbf{f}}$:

$$\widetilde{\mathbf{f}} = \mathbf{K}(\mathbf{r}_d)\mathbf{p}_d \tag{45}$$

with an iterative optimization procedure. The most popular techniques for this problem are Levenberg-Marquart (Levenberg 1944; Marquardt 1963) and Nelder-Mead downhill simplex (Nelder and Mead 1965). It should be noted that as a rule iterative optimization techniques require specifying an initial guess of what the solution may be. In our case that means one needs to specify the initial position of the dipole.

As the number of parameters of this model is small, i.e. 3 for dipole position and 3 for the dipole vector, compared to the number of data channels, typically modern EEG/MEG systems have a few hundred measurement channels, the risk of overfitting the data is practically non-existent. However due to non-linearity of the

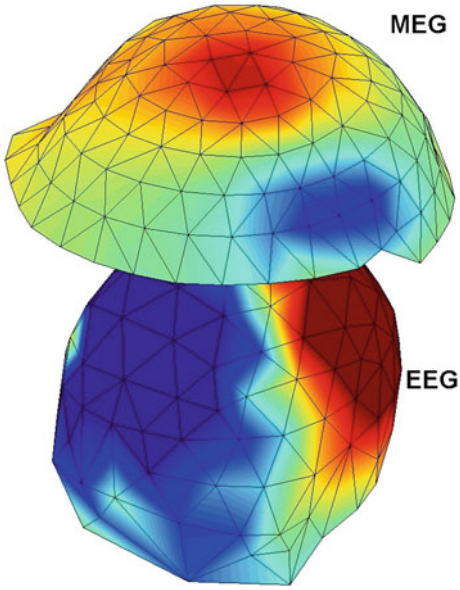

Fig. 3 An example of combined MEG/EEG data for median nerve stimulation experiment. MEG/EEG sensors were positioned at the vertices of the corresponding meshes, and then the data were interpolated to the corresponding surface to enhance visualization (the MEG surface is shifted relative to the EEG surface to provide a better view of the EEG data). MEG data were obtained using 149 channel LANL SIS system (Kraus et al. 2002) and EEG data were collected with a 128 channel Geodesic Sensor Net (Tucker 1993)

problem, even in this simplest model, there is a possibility, albeit small, that the optimization algorithm will converge to a local, but not to the global extremum of the likelihood function. To avoid being trapped at the local extremum, the localization procedure it typically repeated several times each time using a different starting point (i.e. the initial position of a dipole) and selecting the solution giving the best fit.

Let us illustrate this approach using MEG data obtained during a simple median nerve stimulation experiment. Under the protocol of the median nerve test, see for example (Huang et al. 2004), the left or/and right median nerves are stimulated by application of electrical current strong enough to cause robust twitches of a thumb, and magnetic fields generated by neuronal currents associated with such stimulation are recorded by a MEG acquisition system. Figure 4 shows a typical pattern of the recorded signals due to right hand stimulation, where the left panel shows the time course of magnetic field for all the MEG channels and right panel shows spatial pattern of the evoked response field at 33.5 ms after application of the stimulus. The magnitude of the fields is about 200 fT. The dipolar nature of the evoked response is obvious, so we can try to use an equivalent current dipole model to fit the obtained measurements. To obtain the location and the strength of the ECD which describes best the measurements, we need to specify the head

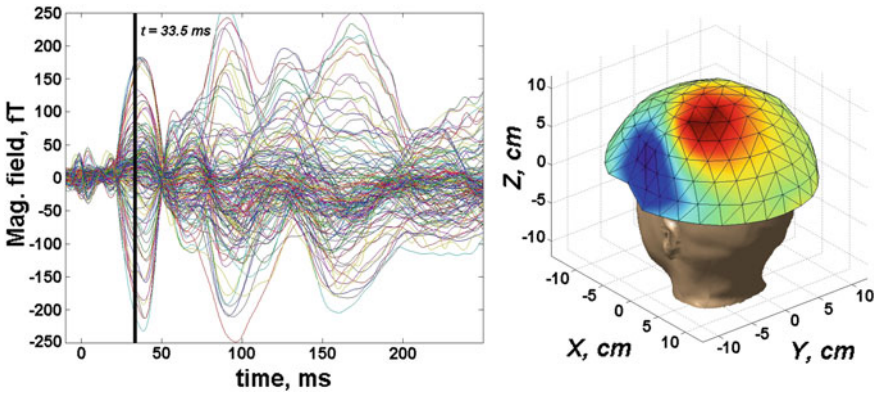

Fig. 4 Evoked somatosensory response field after electrical stimulation of the right median nerve

model, i.e. the way we compute the return currents. In this example we will use the simplest model—a conducting sphere. The conductivity of the sphere, as follows from the Eq. (12), has no effect of the magnetic fields generated by return currents, so to use this model we only need to specify the center of the sphere and its size which can be done by fitting the sphere to the inner scull surface obtained from anatomical MRI data. It is important to note that when considering a spherical head model, a current dipole aligned along a radius of the sphere—a "radial" dipole—produces no magnetic field outside the sphere, i.e. such a dipole is magnetically silent. Since we are using only MEG data to locate the ECD in the current, we need to exclude such radial current dipoles from the solution. To do this we need to impose the condition $(\mathbf{p}_d \cdot \mathbf{r}_d) = 0$ for dipole parameters $\mathbf{r}_d$ and $\mathbf{p}_d$ while searching for the best fit. This can be done by decomposing a dipole vector $\mathbf{p}_d$ into two tangential components at the dipole position $\mathbf{r}_d$:

$$\mathbf{p}_d = \widehat{\mathbf{e}}_1(\mathbf{r}_d)p_1 + \widehat{\mathbf{e}}_2(\mathbf{r}_d)p_2 \equiv \mathbf{R}(\mathbf{r}_d)\mathbf{p}_\perp \tag{46}$$

where unit vectors $\widehat{\mathbf{e}}_1(\mathbf{r}_d)$ and $\widehat{\mathbf{e}}_2(\mathbf{r}_d)$ are defined by conditions $(\widehat{\mathbf{e}}_{1,2}(\mathbf{r}_d) \cdot \mathbf{r}_d) = 0$. Equation (45) needs to be accordingly modified:

$$\begin{aligned} \widetilde{\mathbf{f}} &= \mathbf{K}_\perp(\mathbf{r}_d)\mathbf{p}_\perp \\ \mathbf{K}_\perp(\mathbf{r}_d) &= \mathbf{K}(\mathbf{r}_d)\mathbf{R}(\mathbf{r}_d) \end{aligned} \tag{47}$$

where $\mathbf{R}(\mathbf{r}_d) \equiv [\,\widehat{\mathbf{e}}_1(\mathbf{r}_d) \quad \widehat{\mathbf{e}}_2(\mathbf{r}_d)\,]$, and $\mathbf{p}_\perp \equiv (p_1 1, p_2)^T$. Note that excluding radial dipoles from the solution resulted in the reduction of unknown parameters.

Figure 5 summarizes results of this exercise, where the top-left panel shows the measured field and the top-right panel shows the best fit, i.e. the field generated by an equivalent current dipole which is closest to the measured data in the maximum

likelihood sense. The position of the dipole, mapped on anatomical MRI data, is shown in the bottom-left panel of Fig. 5. The strength of the dipole was found to be 31.3 nAm. The bottom-right panel in Fig. 5 shows the difference between the measured data and the model data, which is about 20 fT.

As we can see from this example even the simplest head model gives rather good agreement with the experimental data. However it is important to estimate what possible localization errors associated with this simple approximation. This problem was exhaustively studied (see for example Cohen and Cuffin 1991; Hamalainen and Sarvas 1989; Tomita et al. 1996; Huang et al. 1999). The general consensus is that the spherical model is more accurate for the MEG than for EEG. In the case of MEG using a simplistic head model instead of a realistic boundary element model (BEM) could result in dipole localization errors from a few millimeters if a dipole is close to the head surface, up to 10 mm if a dipole is located deep inside the head.

Finding parameters of the model is only part of the solution, next we need to estimate confidence intervals of the solution. Once again, the non-linear nature of the problem complicates the task. The straightforward approach is to employ a Monte-Carlo type technique (e.g. Medvick et al. 1989): starting with the localized dipole $\{\mathbf{r}_d, \mathbf{p}_d\}$ to generate the model data, i.e. vector $\mathbf{f}$, then add some noise to this vector using a plausible noise model, and finally find new dipole parameters $\{\mathbf{r}'_d, \mathbf{p}'_d\}$ using this new synthetic dataset. After repeating this procedure several times we can estimate the spread of the parameters of the dipole.

Another approach is based on the assumption that the localization error is not too large, so that the gain matrix can be approximated in the vicinity of the dipole parameters $\{\mathbf{r}_d, \mathbf{p}_d\}$ using only the first terms in Taylor decomposition:

$$\mathbf{K}(\mathbf{r})\mathbf{p} \approx \mathbf{K}(\mathbf{r}_d)\mathbf{p}_d + \mathbf{K}(\mathbf{r}_d)\Delta\mathbf{p} + (\Delta\mathbf{r}\cdot\nabla)\mathbf{K}(\mathbf{r})|_{\mathbf{r}=\mathbf{r}_d}\mathbf{p}_d \tag{48}$$

where $\Delta\mathbf{r} \equiv \mathbf{r} - \mathbf{r}_d$, $\Delta\mathbf{p} \equiv \mathbf{p} - \mathbf{p}_d$ are localization errors, and differential operator $(\Delta\mathbf{r}\cdot\nabla) \equiv \Delta x\frac{\partial}{\partial x} + \Delta y\frac{\partial}{\partial y} + \Delta z\frac{\partial}{\partial z}$ is applied to each element of the matrix $\mathbf{K}(\mathbf{r})$. Now Eq. (29) can be written in the linear form with respect to the localization errors $\Delta\mathbf{r}$ and $\Delta\mathbf{p}$:

$$\mathbf{f} = \mathbf{K}(\mathbf{r}_d)\mathbf{p}_d + \mathbf{G}(\mathbf{r}_d)\Delta\Theta + \xi \tag{49}$$

Here $\Delta\Theta = (\Delta x, \Delta y, \Delta z, \Delta p_x, \Delta p_y, \Delta p_z)^T$ is a vector of the localization error, and $\mathbf{G}$ is the matrix of the derivatives of the gain matrix $\mathbf{K}$ which can be explicitly written as:

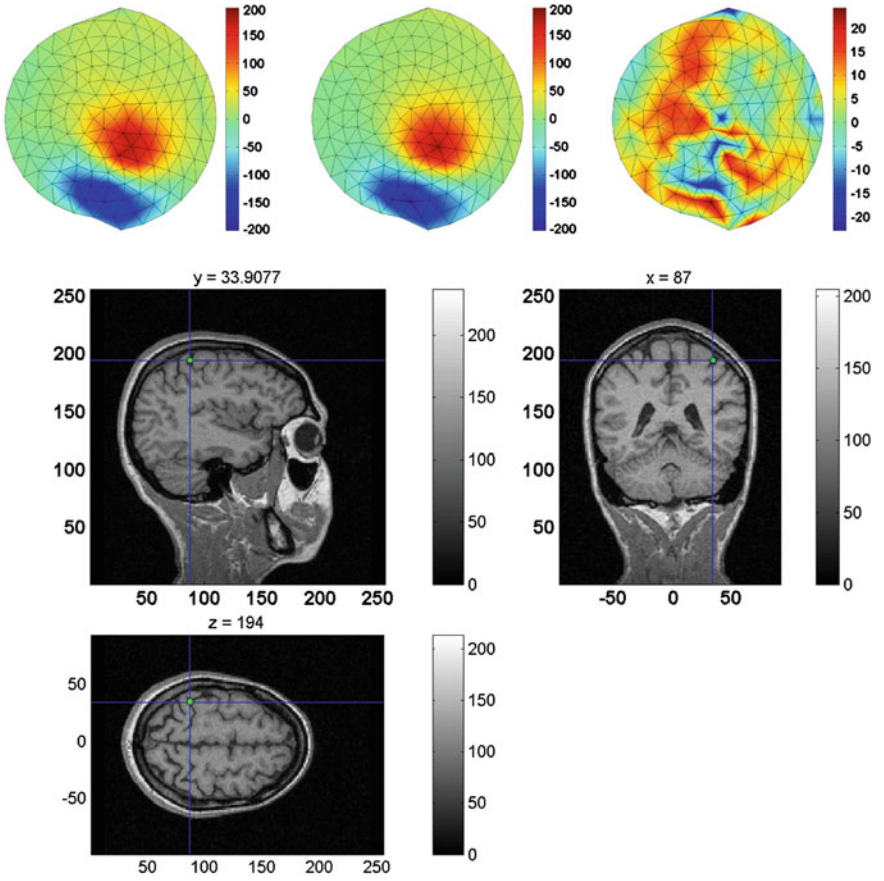

Fig. 5 Localization of an equivalent current dipole in a right median nerve stimulation experiment. *Top row left*—measured data, *middle*—model fit, *right*—residual. *Bottom row* position of the localized dipole (*green* marker), mapped on anatomical MRI data

$$\mathbf{G}(\mathbf{r}_d) = \begin{bmatrix} \frac{\partial}{\partial x}(\mathbf{M}_1\mathbf{p}_d) & \frac{\partial}{\partial y}(\mathbf{M}_1\mathbf{p}_d) & \frac{\partial}{\partial z}(\mathbf{M}_1\mathbf{p}_d) & (\mathbf{M}_1)_x & (\mathbf{M}_1)_y & (\mathbf{M}_1)_z \\ \frac{\partial}{\partial x}(\mathbf{M}_2\mathbf{p}_d) & \frac{\partial}{\partial y}(\mathbf{M}_2\mathbf{p}_d) & \frac{\partial}{\partial z}(\mathbf{M}_2\mathbf{p}_d) & (\mathbf{M}_2)_x & (\mathbf{M}_2)_y & (\mathbf{M}_2)_z \\ \cdots & \cdots & \cdots & \cdots & \cdots & \cdots \\ \frac{\partial}{\partial x}(\mathbf{M}_N\mathbf{p}_d) & \frac{\partial}{\partial y}(\mathbf{M}_N\mathbf{p}_d) & \frac{\partial}{\partial z}(\mathbf{M}_N\mathbf{p}_d) & (\mathbf{M}_N)_x & (\mathbf{M}_N)_y & (\mathbf{M}_N)_z \end{bmatrix} \tag{50}$$

where matrix elements are evaluated at $\mathbf{r} = \mathbf{r}_d$.

Solving Eq. (49) in the maximum likelihood sense, i.e. minimizing expression (37), we will get the following formula for the localization errors:

$$\Delta\Theta = (\mathbf{G}^T\mathbf{C}^{-1}\mathbf{G})^{-1}\mathbf{G}^T\mathbf{C}^{-1}\xi \tag{51}$$

Here $\Delta\Theta$ is a random vector of the localization errors which we would like to characterize by the corresponding correlation matrix:

$$\mathbf{C}_{\Delta\Theta} = E\{(\Delta\Theta - \overline{\Delta\Theta})(\Delta\mathbf{Q} - \overline{\Delta\Theta})^T\} \tag{52}$$

Recall that ξ is a random variable described by the correlation matrix $\mathbf{C}$, so substituting (51) into (52) and carrying out matrix multiplications will finally result in a simple expression for the correlation matrix of localization errors:

$$\mathbf{C}_{\Delta\Theta} = (\mathbf{G}^T\mathbf{C}^{-1}\mathbf{G})^{-1} \tag{53}$$

It should be noted that formula (53) is actually a lower bound for localization errors. According to the Cramer-Rao inequality theorem (Rao 1945; Cramer 1946) the covariance matrix of the errors between the true ψ and estimated $\tilde{\psi}$ parameters is bounded from below by the inverse of the Fisher information matrix:

$$\mathbf{C}_{\psi\psi} \equiv E\{(\psi - \tilde{\psi})(\psi - \tilde{\psi})^T\} \geq \mathbf{F}^{-1} \tag{54}$$

where the Fisher information matrix is defined as

$$\mathbf{F} = E\{[\frac{d}{d\psi}\ln p(\mathbf{f}|\psi)][\frac{d}{d\psi}\ln p(\mathbf{f}|\psi)]^T\} \tag{55}$$

Here $\frac{d}{d\psi}\ln p(\mathbf{f}|\psi)$ denotes a column vector of partial derivatives of log-likelihood function:

$$\frac{d}{d\psi}\ln p(\mathbf{f}|\psi) \equiv (\frac{\partial}{\partial\psi_1}\ln p(\mathbf{f}|\psi), \ldots, \frac{\partial}{\partial\psi_k}\ln p(\mathbf{f}|\psi))^T \tag{56}$$

Using Eqs. (37) and (45) to compute Fisher information matrix for a single dipole model we will get:

$$\mathbf{F} = \mathbf{G}^T\mathbf{C}^{-1}\mathbf{G} \tag{57}$$

where again the matrix $\mathbf{G}$ is defined by Eq. (50) and matrix $\mathbf{C}$ is the correlation matrix according to (39). From this last formula it is easy to see that estimation of the localization errors (53) is indeed the Cramer-Rao lower bound (CRLB).

Analysis of the localization errors using CRLB approach, see for example (Mosher et al. 1992, Plis et al. 2007), reveals that even when using quite favorable assumptions about the noise level the localization errors are quite large reaching $\sim$1 cm for dipoles located just a few centimeters below a head surface (see

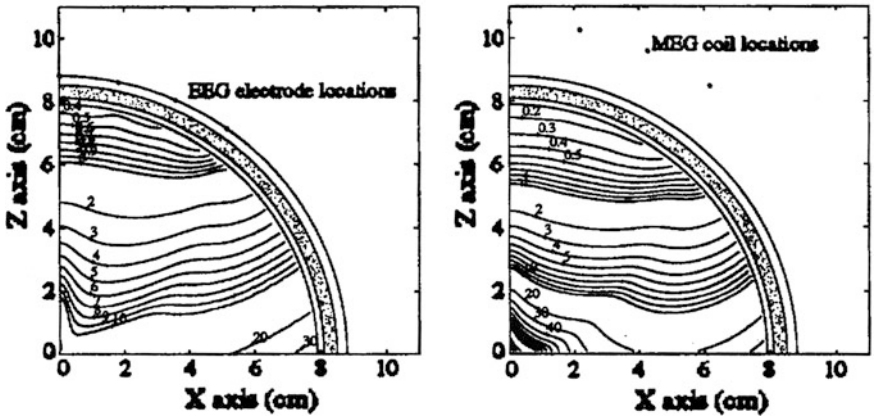

Fig. 6 Average error lower bound for a single dipole. *Left panel* EEG, *right panel* MEG. (Mosher et al. 1992)

Fig. 6), thus emphasizing the inherent ill-posed nature of a MEG/EEG inverse problem.

A single equivalent current dipole model considered so far nicely illustrates the methods used to find a dipole location. However, in practice this simple model may not be adequate to describe a more complicated current source. An example of such a situation is shown in Fig. 7. It is obvious that the pattern can not be fitted with a single dipole model, so it is quite natural to expand the model to assume that the current source contains several equivalent current dipoles.

The first question here one must ask is "how many dipoles?". The straightforward approach to answer this question is a systematic search across increasing number of dipoles (Supek and Aine 1993). The main idea is starting with a model consisting of one ECD or some small number of dipoles and conduct a search across model orders by increasing the number of dipoles to determine if the model adequately describes the observed data using, say, χ^2 criteria. The model which adequately describes the observed data using minimal number of dipoles is considered to be the answer.

Another approach to estimate the number of dipoles is based on the assumption that dipoles are not correlated in time, i.e. the time courses of dipoles are linearly independent. To outline this approach let us write the recorded data as a matrix:

$$\mathbf{D} \equiv \begin{bmatrix} f_1(t_1) & f_1(t_2) & \dots & f_1(t_M) \\ f_2(t_1) & f_2(t_2) & \dots & f_2(t_M) \\ \dots & \dots & \dots & \dots \\ f_N(t_1) & f_N(t_2) & \dots & f_N(t_M) \end{bmatrix} \tag{58}$$

where $f_i(t_j)$ is the signal in the i-th sensor at time t_j, so each row of the matrix $\mathbf{D}$ constitutes recorded time signal of the corresponding sensor. If we assume that

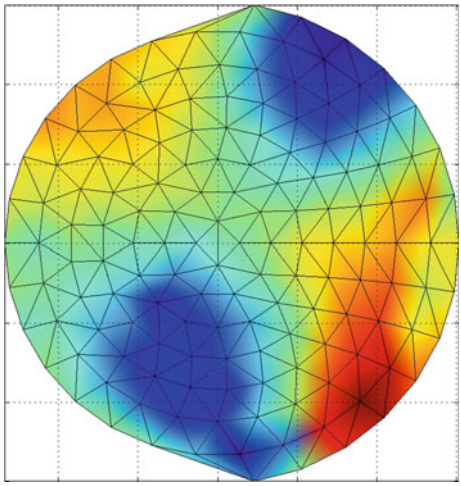

Fig. 7 Auditory evoked response demonstrating 2-dipole like features of the MEG signals

these signals are generated by a certain number of linearly independent sources, the number of linearly independent rows is equal to the number of these sources. So to estimate the number of dipoles we need to estimate the number of linearly independent rows in the matrix **D**, which can be done using a singular value decomposition (SVD) of this matrix (see Chen et al. 1991 for details). It should be noted that this approach gives a *minimum* number of dipoles, because, as it is easy to see, if some current sources are active synchronously, then under this approach, they will be counted as one source even if they are spatially distinct.

As we have mentioned before, parameters of the dipoles are obtained by maximizing the likelihood function. However for a model consisting of multiple current dipoles one is likely to encounter difficulties in finding the global extremum. As it was shown in a number of publications, see for example (Achim et al. 1991; Supek and Aine 1993), if the number of dipoles is greater than one, the result strongly depends on the initial guess of the dipoles' positions. This is due to the very high probability that the optimization procedure will converge to a local extremum. A way to overcome this is to repeat the procedure several time each time using different initial guess of the dipoles' positions. As the number of dipoles grows, selecting initial parameters of dipoles becomes tedious and time consuming, so there is a need to automate this step. One straightforward approach is randomly select initial positions of dipoles inside the head volume, and then select the solution giving the best fit. It was shown (Huang et al. 1998) that this approach in combination with the downhill simplex method is effective in finding the global extremum within a reasonable computation time. Subsequent approaches were developed to further optimize the computation time by: (1) using a two-stage simplex procedure to first rule out sub-optimal solutions (i.e., it uses a coarse convergence criterion in the simplex procedure) and then refines the remaining solutions using a fine convergence setting; and (2) using a MUSIC-seeded approach (Ranken et al. 2002, 2004).

4.4.2 Imaging Techniques

In this case we assume that locations of the current dipoles—and usually orientations—are fixed and known. Typically it is assumed that the dipoles are distributed over the cortex surface and their orientations are orthogonal to this surface. As for the positions of current dipoles, Eq. (29) is reduced to a linear equation with respect to unknown dipole vectors, which can be solved using a maximum likelihood approach.

If the number of unknowns is less than the number of linearly independent rows in $\mathbf{K}$, i.e. the number of independent equations in (28), then the MLE solution according to formula (33) is unique and is given by:

$$\mathbf{q} = (\mathbf{K}^T\mathbf{C}^{-1}\mathbf{K})^{-1}(\mathbf{K}^T\mathbf{C}^{-1})\mathbf{f} \equiv (\breve{\mathbf{K}}^T\breve{\mathbf{K}})^{-1}\breve{\mathbf{K}}^T\breve{\mathbf{f}} \tag{59}$$

Here, to shorten the notation, we introduced so the called "whitened" data and gain matrices:

$$\begin{aligned} \breve{\mathbf{f}} &\equiv \mathbf{C}^{-1/2}\mathbf{f} \\ \breve{\mathbf{K}} &\equiv \mathbf{C}^{-1/2}\mathbf{K} \end{aligned} \tag{60}$$

where $\mathbf{C}^{-1/2}\mathbf{C}^{-1/2} = \mathbf{C}^{-1}$. It is easy to see that the noise covariance matrix of the "whitened" data—$\breve{\mathbf{C}}$—is an identity matrix:

$$\begin{aligned} \breve{\mathbf{C}} &\equiv E\{(\breve{\mathbf{f}} - \overline{\breve{\mathbf{f}}})(\breve{\mathbf{f}} - \overline{\breve{\mathbf{f}}})^T\} \\ &= E\{\mathbf{C}^{-1/2}(\mathbf{f} - \overline{\mathbf{f}})(\mathbf{f} - \overline{\mathbf{f}})^T\mathbf{C}^{-1/2}\} = \mathbf{C}^{-1/2}E\{(\mathbf{f} - \overline{\mathbf{f}})(\mathbf{f} - \overline{\mathbf{f}})^T\}\mathbf{C}^{-1/2} = \mathbf{C}^{-1/2}\mathbf{C}\mathbf{C}^{-1/2} \equiv \mathbf{I} \end{aligned} \tag{61}$$

where $\mathbf{I}$ denotes an identity matrix.

In the opposite case which is more likely to be encountered in practice, the number of unknowns is greater than the number of independent equations and the MLE solution is not unique. This means that there are an infinite number of different vectors $\mathbf{q}$, i.e. sets of dipole victors $\mathbf{p}_i$, which deliver a maximum to the likelihood function (37). In this case we need to make an additional assumption about the solution to select one set, which we consider to be a plausible solution. The simplest, and the most widely used, approach to achieve this is to require that the sum of the squares of the current dipole magnitudes be minimal. As it turns out, a solution in such sense, which called a minimum norm solution, is unique. This solution can be written in a closed form as:

$$\mathbf{q} = \breve{\mathbf{K}}^T(\breve{\mathbf{K}}\breve{\mathbf{K}}^T)^{-1}\breve{\mathbf{f}} \tag{62}$$

Here it is very important to realize that the solution obtained by straightforward application of this last formula will almost certainly result in unacceptable noisy images due to magnification of the noise present in the experimental data. This noise magnification is inherent to the MEG/EEG inverse problem due to properties of the gain matrix $\mathbf{K}$. So to get a meaningful solution we need somehow to limit this noise propagation. One way to do this is to use a Tikhonov regularization (Tikhonov and Arsenin 1977). Under this approach the formula (62) is modified as following:

$$\mathbf{q} = \breve{\mathbf{K}}^T(\breve{\mathbf{K}}\breve{\mathbf{K}}^T + \lambda^2\mathbf{I})^{-1}\breve{\mathbf{f}} \equiv \breve{\mathbf{W}}\breve{\mathbf{f}} \tag{63}$$

where λ^2 is a regularization parameter, and $\breve{\mathbf{W}} \equiv \breve{\mathbf{K}}^T(\breve{\mathbf{K}}\breve{\mathbf{K}}^T + \lambda^2\mathbf{I})^{-1}$. The correct scale of this regularization parameter can be estimated using the following formula:

$$\lambda \sim \frac{\sqrt{trace(\breve{\mathbf{K}}\breve{\mathbf{K}}^T)/N}}{SNR} \tag{64}$$

where N is the number of measurement channels, and SNR is signal to noise ratio.

As we mentioned before it is very important to estimate errors of the solution. The measurement data $\breve{\mathbf{f}}$ contains random noise, that means the solution (63) also exhibits stochastic behavior, which can be characterized by a covariance matrix $\mathbf{C_q}$:

$$\mathbf{C_q} \equiv E\{(\mathbf{q} - \overline{\mathbf{q}})(\mathbf{q} - \overline{\mathbf{q}})^T\} = \breve{\mathbf{W}}\breve{\mathbf{W}}^T \tag{65}$$

This last equation is easy to obtain recalling that the covariance matrix of whitened data is an identity matrix (see Eq. (61)).

Let us again illustrate this approach using MEG data obtained during a median nerve stimulation experiment. We use the same data set we used to demonstrate an equivalent dipole localization technique, see top-left panel on Fig. 5. We started with extracting cortex surface from the volume MRI data using MRIView tool (Ranken and George 1993). This resulting tesselated cortical surface is shown in the top left panel of Fig. 8. The mesh constituting the cortical surface consists of about 90,000 triangular faces. Next the gain matrix was computed according to Eq. (31) using unit current dipoles placed in the centers of the triangular faces, and the dipole vector were computed according to formula (63). The results are shown in Fig. 8. The focal character of the neuronal activity is evident. The residuals, i.e. the difference between the measured data and the model, shown in bottom-right panel in Fig. 8 demonstrated good agreement of the model with the measurements across almost the whole sensor array. A few sensors placed directly above the

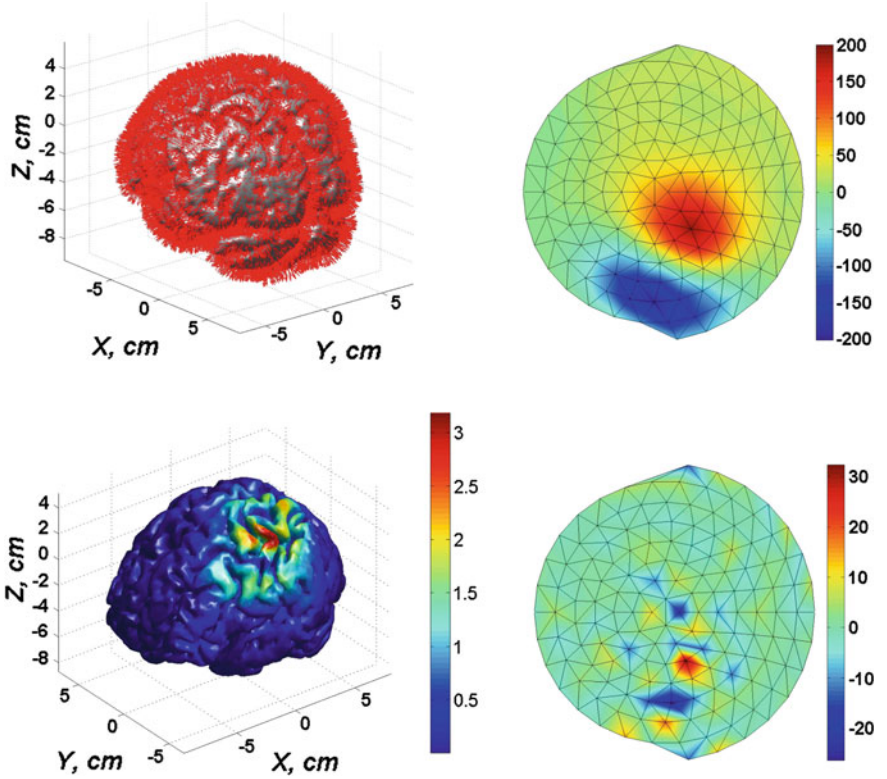

Fig. 8 A minimum-norm solution. *Top-left* Tesselated cortical surface, *red arrows* represent unit current dipoles placed at the centers of mesh *triangles* and *orthogonal* to the surface. *Bottom-left* amplitude of the dipoles. *Top-right* model fit. *Bottom-right* residual

focus of neural activity exhibit relatively high residuals, ±30 fT. This is explained by the fact that in this model the current dipoles' positions are fixed, and it happens that there are no dipole placed close enough to the true position of the actual evoked neuronal current dipole.

Acknowledgments Authors (L. H. and P. V.) thank D. M. Ranken for Fig. 2, extraction of the cortical surface from the MRI data and fruitful discussions with respect to multiple dipole localization techniques.

References

Achim A, Recher F, Saint-Hilaire J-M (1991) Methodical consideration for the evaluation of spatio-temporal source models. Electroenceph. Clin. Neurophysiol 79:227–240

Baillet S, Mosher JC, Leahy RM (2001) Electromagnetic brain mapping. IEEE Signal Process Mag 18(6):14–30

Barnard A, Duck I, Lynn M (1967) The application of electromagnetic theory to electrocardiology. I. derivation of the integral equations. Biophys J 7:443–462

Baumann S, Wozny D, Kelly S, Meno F (1997) The electrical conductivity of human cerebrospinal fluid at body temperature. IEEE Trans Biomed Eng 44(3):220–223

Brenner D, Lipton J, Kaufman L, Williamson S (1978) Somatically evoked magnetic fields of the human brain. Science 199:81–83

Bronzan J (1971) The magnetic scalar potential. Amer J Phys 39:1357–1359

Chen W, Wong KM, Reilly JP (1991) Detection of number of signals: a predicted eigen-threshold approach. IEEE Signal Process 39:1088–1098

Cohen D, Cuffin BN (1991) EEG versus MEG localization accuracy: theory and experiment. Brain Topogr 4:95–103

Cramer H (1946) Mathematical methods of statistics. Princeton University Press, Princeton

Cuffin BN, Cohen D (1977) Magnetic fields of a dipole in special volume conductor shapes. IEEE Trans Biomed Eng 24:372–381

Geselowitz D (1967) On bioelectric potentials in an inhomogeneous volume conductor. Biophys J 7(1):1–11

Geselowitz D (1970) On the magnetic field generated outside an inhomogeneous volume conductor by internal current sources. IEEE Trans Magn 6(2):346–347

Grynszpan F, Geselowitz DB (1973) Model studies of the magnetocardiogram. Biophys J 13:911–925

Hämäläinen M, Hari R, Ilmoniemi RJ, Knuutila J, Lounasmaa OV (1993) Magnetoencephalography—theory, instrumentation, and applications to noninvasive studies of the working human brain. Revs Mod Phys 65(2):413–497

Hämäläinen M, Sarvas J (1989) Realistic conductivity geometry model of the human head for interpretation of neuromagnetic data. IEEE Trans Biomad Eng 36:165–171

Heller L, Ranken DM, Best E (2004) The magnetic field inside special conducting geometries due to internal current. IEEE Trans Biomed Eng 51:1310–1318

Heller L, van Hulsteyn D (1992) Brain stimulation using electromagnetic sources: theoretical aspects. Biophys J 63(1):129–138

Helmholtz HV (1853) Uber einige gesetze der vertheilung elektrischer strome in korperlichen leitern, mit anwendung auf die thierisch-elektrischen versuche. Ann Phys Chem 89:211–233, 353–377

Huang M, Aine CJ, Supek S, Best E, Ranken D, Flynn ER (1998) Multi-start downhill simplex method for spatio-temporal source localization in magnetoencephalography. Electroencephalogr Clin Neurophysiol 108:32–44

Huang M, Davis LE, Aine C, Weisend M, Harrington D, Christener R, Stephen J, Edgar JC, Herman M, Meyer J, Paulson K, Martin K, Lee RR (2004) MEG response to median nerve stimulation correlates with recovery of sensory and motor function after stroke. Clin Neurophysiol 115:820–833

Huang MX, Mosher JC, Leahy RM (1999) A sensor-weighted overlapping-sphere head model and exhaustive head model comparison for MEG. Phys Med Biol 44:423–440

Ilmoniemi R, Hamalainen MS, Knuutila J (1985) The forward and inverse problems in the spherical model. In: Weinberg H, Stroink G, Katila T (eds) Proceedings of biomagnetism: applications and theory journal, Pergamon, New York, pp 278–282

Kraus RH, Volegov P, Maharajh K, Espy MA, Matlashov AN, Flynn ER (2002) Performance of a novel squid-based superconducting imaging-surface magnetoencephalography system. Physica C 368:18–23

Levenberg K (1944) A method for the solution of certain problems in least squares. Quart Appl Math 2:164–168
Marquardt DW (1963) An algorithm for least-squares estimation of nonlinear parameters. SIAM J Appl Math 11:431–441
Medvick P, Lewis P, Aine C, Flynn E (1989) Monte carlo analysis of localization errors in magnetoencephalography. In: Williamson SJ, Hoke M, Stroink G, Kotani M (eds) Advances in biomagnetism. Plenum, New York, pp 543–546
Mosher JC, Spencer ME, Leahy RM, Lewis PC (1992) Error bounds for MEG and EEG source localization. Electroencephalogr Clin Neurophysiol 86:303–321
Nelder JA, Mead RA (1965) A simplex method for function minimization. Comput J 7:308–313
Oostendorp T, Delbeke J, Stegman D (2000) The conductivity of the human skull: results of in vivo and in vitro measurements. IEEE Trans Biomed Eng 47(11):1487–1492
Plis SM, George JS, Jun SC, Ranken DM, Volegov PL, Schmidt DM (2007) Probabalistic forward model for electroencephalography source analysis. Phys Med Biol 52:5309–5327
Ranken D, Best E, Schmidt D, George J, Wood C, Huang M (2002) MEG/EEG forward and inverse modeling using mri view. In: Nowak H, Haueisen J, Giebler F, Juonker R (Eds.) Proceedings of the 13th international conference on biomagnetism, pp 324–331
Ranken D, Stephen J, George J (2004) MUSIC seeded multii-dipole MEG modeling using the constrained start spatio-temporal modeling procedure. Neurol Clin Neurophysiol 80:1–6
Ranken DM, George J (1993) MRIVIEW: an interactive computational tool for investigation of brain structure and function. In: Proceedings of IEEE visualization '93, IEEE Computer Society Press, p 324–331
Rao R (1945) Information and the accuracy attainable in the estimation of statistical parameters. Bull Calcutta Math Soc 37:81–91
Rush S, Driscoll D (1969) EEG electrode sensitivity–an application of reciprocity. IEEE Trans Biomed Eng 16(1):15–22
Sarvas J (1987) Basic mathematical and electromagnetic concepts of the biomagnetic inverse problem. Phys Med Biol 32(1):11–22
Schlitt HA, Heller L, Aaron R, Best E, Ranken DM (1995) Evaluation of boundary element methods for the eeg forward problem: effect of linear interpolation. IEEE Trans Biomed Eng 42(1):52–58
Supek S, Aine CJ (1993) Simulation studies of multiple dipole neuromagmetic source localization: model order and limits of source resolution. IEEE Trans Biomed Eng 40:459–540
Tikhonov AN, Arsenin VY (1977) Solution of Ill-posed Problems. Winston & Sons, Washington
Tomita S, Kajihara S, Kondo Y, Yoshida Y, Shibata K, Kado H (1996) Influence of head model in biomagnetic source localization. Brain Topog 8:337–340
Tucker DM (1993) Spatial sampling of head electrical fields: the geodesic sensor net. Electroencephalogr Clin Neurophysiol 87(3):154–163
van Oosterom A, Strackee J (1983) The solid angle of a plane triangle. IEEE Trans Biomed Eng 30:125
Vladimirov VS (1971) Equations of mathematical Physics. Marcel Dekker, New York

Forward Modeling and Tissue Conductivities

Jens Haueisen and Thomas R. Knösche

Abstract The neuroelectromagnetic forward model describes the prediction of measurements from known sources. It includes models for the sources and the sensors as well as an electromagnetic description of the head as a volume conductor, which are discussed in this chapter. First we give a general overview on the forward problem and discuss various simplifications and assumptions that lead to different analytical and numerical methods. Next, we introduce important analytical models which assume simple geometries of the head. Then we describe numerical models accounting for realistic geometries. The most important numerical methods for head modeling are the boundary element method (BEM) and the finite element method (FEM). The boundary element method describes the head by a small number of compartments, each with a homogeneous isotropic conductivity. In contrast, the finite element method discretizes the 3D distribution of the anisotropic conductivity tensor with the help of small volume elements. Subsequently, we discuss in some detail how electrical conductivity information is measured and how it is used in forward modeling. Finally, we briefly introduce the lead field concept.

Keywords Volume conduction · Field computation · EEG/MEG modeling · BEM · FEM

J. Haueisen (✉)
Institute of Biomedical Engineering and Informatics, Ilmenau University of Technology, Gustav-Kirchhoff-Str. 2, 98684 Ilmenau, Germany
e-mail: jens.haueisen@tu-ilmenau.de

T. R. Knösche
Max Planck Institute for Human Cognitive and Brain Sciences, Stephanstraße 1A, 04103 Leipzig, Germany
e-mail: knoesche@cbs.mpg.de

S. Supek and C. J. Aine (eds.), *Magnetoencephalography*,
DOI: 10.1007/978-3-642-33045-2_4,

1 Introduction

A crucial part in any source reconstruction procedure is the computation of the bioelectromagnetic field generated by known sources. This computation is known as the forward problem or direct problem and includes the mathematical description of the sources and sensors, as well as the description of the relationship between the source parameters and the simulated data at the sensors. The material (tissue) properties and the distribution of tissues within the volume conductor[1] are highly complex. This complexity makes the transfer function between sources and measurements non-trivial. Thus, approaches to the forward problem are mainly characterized by the degree of simplification they apply.

First we consider the description of the sources. Microscopically, currents across cell membranes are impressed by chemical processes and concentration gradients. In the pyramidal cells of the cortex, these currents are mainly arranged in a radially symmetric manner around the axes of the dendrites, which causes a cancellation of their far field and therefore invisibility to EEG/MEG. These impressed currents give rise to local ohmic currents inside and outside the cells, governed by a complex interplay of chemical and electrical processes at the microscopic level (involving voltage-gated ion channels, second messenger chains, barriers like cell membranes, etc.). However, these functional and structural details at the cellular level are usually not taken into account when modeling EEG/MEG. Instead, the source area is considered as a black box. All currents within that box, including impressed and passive ohmic currents inside and outside the cells, are represented by a single *primary current*, usually modeled by means of an *equivalent current dipole*. The far field of this current is probably dominated by intracellular ohmic currents flowing along the longitudinal axis of the apical dendrites of the pyramidal cells (i.e., perpendicular to the cortical surface). It is assumed that at least a few ten thousands of neurons need to be simultaneously active to produce a measurable effect at the head surface (Murakami and Okada 2006). The extent of the box is implicitly determined by the spatial resolution of the measurement. More specifically, the primary current is normally described as point-like. Under this constraint, the extent of that black box must be small compared to the distance to the sensors. All currents outside the box are defined as volume currents (secondary currents). Thus, the total current density is the sum of primary and secondary current densities: $\vec{J}(\vec{r}') = \vec{J}_p(\vec{r}') + \vec{J}_v(\vec{r}')$. Since often multiple source components[2] are active at the same time, the measured magnetic fields and electric potentials represent a superposition of all contributions. Each source component can be characterized by a set of parameters (see below) and by the signals it produces at sensor level. These signals are often termed components

[1] The term **volume conductor** denotes the part of the biological tissue, in which the relevant volume currents are flowing (e.g. the head for MEG).

[2] A **source component** combines primary currents which react to experimental manipulation as a whole or which depend uniformly on observable environmental variables.

of the signal (Donchin 1966; Kayser and Tenke 2005). In the literature on source separation the term "source" is often used synonymously for the signal the source component is producing, whereas in the literature on source reconstruction it is used to describe the parameterized source model.

The primary current density $\vec{J}_p(\vec{r}', t)$ is a spatially continuous function. In order to describe it with a finite vector of parameters, two approaches exist. The discretization approach divides the space into sections, within each of which the current density is replaced by the integral over the volume of that section:

$$\vec{d}_i(t) = \int_{V_i} \vec{J}_p(\vec{r}', t) dv \tag{1}$$

where $\vec{d}_i(t)$ denotes the dipole moment typically given in nanoamperemeters [nAm]. The discretization approach is based on the topology of the source space. For example, the entire brain volume can be discretized in hexahedral voxels, or the cortical sheet can be discretized into prisms (triangles representing the cortical surface plus a predefined thickness). In each of these elements, the primary current density is modeled by one current dipole.

In many practical applications the primary current density is relatively focal, such that it can be satisfactorily described by a few current dipoles at the centers of activity leading to the multiple dipoles model. The second approach parameterizes the primary current density with the help of a series expansion. The series can also describe extended source configurations centered at the expansion point. Often, the electric potential at the measurement location $\vec{r}$expressed by a Taylor series expansion with the origin at position $\vec{r}'$:

$$\varphi(\vec{r}) = \frac{1}{4\pi\sigma}\left[\frac{m}{|\vec{r}-\vec{r}'|} + \frac{\vec{d}(\vec{r}-\vec{r}')}{|\vec{r}-\vec{r}'|^3} + \frac{1}{|\vec{r}-\vec{r}'|^3}\left(\frac{3}{|\vec{r}-\vec{r}'|^2}(\vec{r}-\vec{r}')^T\bar{q}(\vec{r}-\vec{r}') - tr(\bar{q})\right) + \cdots\right] \tag{2}$$

Here, m is the electric monopole moment, which vanishes due to the charge conservation law:

$$m = -\int_V \nabla\vec{J}_p(\vec{r}')dv, \tag{3}$$

$\vec{d}$ is the dipole moment according to Eq. (1) and $\bar{q}$ is the quadrupole tensor:

$$\bar{q} = \int_V \vec{J}_p(\vec{r}')\vec{r}'^T dv \tag{4}$$

Table 1 Full and quasi-static Maxwell equations

	Faraday's law	Amperè's law	Gauß's law	Gauß's law for mag.	Material equations
Full	$\nabla \times \vec{E} = -\dot{\vec{B}}$	$\nabla \times \vec{H} = \vec{J} + \dot{\vec{D}}$	$\nabla \vec{D} = \rho_f$	$\nabla \vec{B} = 0$	$\vec{J} = \bar{\sigma}\vec{E}$
Quasi-static	$\nabla \times \vec{E} = 0$	$\nabla \times \vec{H} = \vec{J}$	$\nabla \vec{D} = \rho_f$	$\nabla \vec{B} = 0$	$\vec{D} = \bar{\varepsilon}\vec{E}$ $\vec{B} = \bar{\mu}\vec{H}$

The vectorial state variables comprise the electric field strength $\vec{E}$, the magnetic field strength $\vec{H}$, the electric current density $\vec{J}$, the magnetic induction $\vec{B}$ and the electric displacement current density $\vec{D}$. The material tensorial parameters are the electrical conductivity $\bar{\sigma}$, the permittivity $\bar{\varepsilon}$ and the permeability $\bar{\mu}$. The scalar parameter ρ_f denotes the free volume charge density

A truncation of this series, after the dipole term, results in the equivalent current dipole model which represents the entire current density as a point-like current element. Extending this approach to multiple partial volumes yields the same multiple dipoles model, which was derived from the discretization approach above.

The sensor model describes how a sensor transforms a physical quantity into an accessible output. For biomagnetic measurements this typically involves first the transformation of the magnetic flux density into a magnetic flux by integration over the area of a pickup coil. Next this magnetic flux is often combined across several coils in order to suppress far field disturbances. Finally, the magnetic flux is converted into a voltage. Important parameters of this model are the position, orientation, geometrical form, and number of windings of the coils. The exact integration of the flux density over the coil area would be computationally demanding. Thus, often the flux density at the center point of the coil is assumed to represent the constant value over the entire coil area. More accurate approaches involve a weighted average of the flux density at a small number of integration points within the coil area. Magnetic recordings do not require a reference, which is an advantage compared to electric recordings.

Next we consider the description of the relationship between source parameters and the simulated data at the sensors. Maxwell's equations are the basis for this transfer function. For most non-invasively measured electric and magnetic biosignals, frequencies are below 1,000 Hz and the spatial dimension is below 1 m. Consequently, the temporal derivatives in the Maxwell equations can be omitted (Plonsey and Heppner 1967), yielding the quasi-static Maxwell equations that disregard capacitive and inductive effects (Table 1). The free volume charge density is not relevant here, since we consider the electric flow field only, which is uncoupled from the electrostatic field due to the vanishing derivative of D in the quasistatic approximation of Ampère's law (Table 1). The only remaining relevant material parameter is the electrical conductivity.

From the definition of the scalar electric potential $\vec{E} = -\nabla\varphi$ (based on the quasi-static law of Faraday) and Ohm's law $\vec{J} = \bar{\sigma} \cdot \vec{E}$, one can derive Poisson's equation (Eq. 5), while the quasi-static law of Ampère allows (under the

assumption of a scalar magnetic permeability $\bar{\mu} = \mu$) for computing the magnetic field from the electric potential (Eq. 6).

$$\nabla \bar{\sigma} \nabla \varphi = -\nabla \vec{J}_p \tag{5}$$

$$\nabla \times \vec{B} = -\mu \left(\bar{\sigma} \nabla \varphi + \vec{J}_p \right). \tag{6}$$

This leads to expressions for the electric potential φ and the magnetic induction $\vec{B}$ at position $\vec{r}$, arising from N dipoles at positions $\vec{r}_i'$ with moments $\vec{d}_i$, in an infinite volume with homogeneous and isotropic conductivity.

$$\vec{B}_\infty(\vec{r}) = \frac{\mu}{4\pi} \sum_{i=1}^{N} \vec{d}_i \times \frac{(\vec{r} - \vec{r}_i')}{|\vec{r} - \vec{r}_i'|^3} \quad \varphi_\infty(\vec{r}) = \frac{1}{4\pi\sigma} \sum_{i=1}^{N} \vec{d}_i \frac{(\vec{r} - \vec{r}_i')}{|\vec{r} - \vec{r}_i'|^3} \tag{7}$$

These equations, however, do not provide an acceptable solution for the situation in real biological tissue as they do not take into account the effects of conductivity inhomogeneities. If very simplifying assumptions about the distribution of conductivities are made, analytical or semi-analytical solutions can be used. The human head can be modeled with the help of a series of spherical or ellipsoidal layers (Cuffin and Cohen 1977; Sarvas 1987; de Munck 1988, 1989; Kariotou 2004; Giapalaki and Kariotou 2006). Such models allow for easy computations, but can yield significant errors (Cuffin and Cohen 1977).

More realistic conductivity profiles can be modeled using numerical methods. These methods can be classified into differential and integral methods depending on whether derivatives or integrals are to be approximated. Additionally, methods can be classified according to their basic assumptions and simplifications. A crucial property of the head is the fact that a relatively low-conducting skull encloses the relatively well-conducting brain. In turn, the skull is surrounded by a relatively well-conducting remainder of the head (scalp, muscles, eyes, etc.). This leads to the compartment assumption. Typically, 3 compartments with homogeneous and isotropic conductivity are defined: scalp, skull and brain. The brain compartment subsumes all tissues inside the skull. The skull compartment includes both compact and spongy bone. The scalp compartment summarizes all tissues outside the skull. The compartment approach necessitates the use of an integral-based method.

Alternatively, the compartment assumption can be replaced by a 3D volume discretization. Here, the volume is divided into small elements. The size and number of elements governs the achievable accuracy and is limited by computational resources. Volume discretization approaches are usually treated with differential methods.

The boundary element method (BEM) is an integral method based on the compartment assumption (Barnard et al. 1967a, b; Geselowitz 1967, 1970; Sarvas 1987; Hämäläinen and Sarvas 1989; Stenroos et al. 2007). An alternative approach is the multiple multipole method (MMP) (Haueisen et al. 1996). Here, multipole

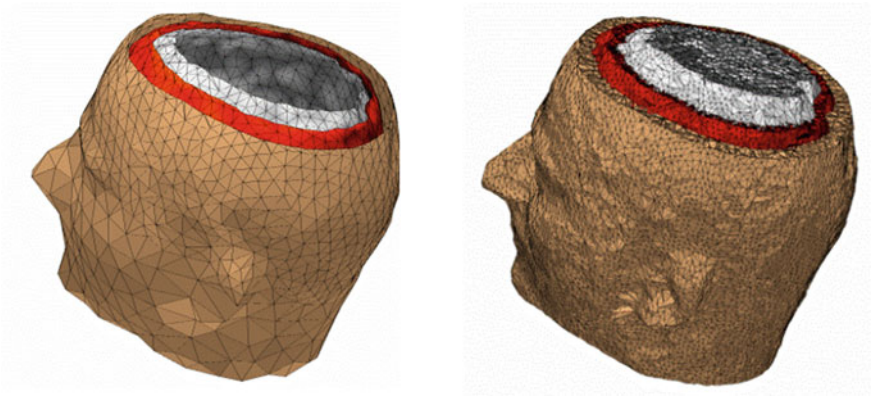

Fig. 1 Examples for head models. *Left* boundary element model with the most important conductivity boundaries (inner and outer skull surface, outer surface of the head) described by triangular meshes. *Right* finite element model built with tetrahedral elements. *Colors* represent tissue types

expansions are used to describe the neuroelectromagnetic field and the expansion coefficients may be computed based on a matching of the boundary conditions at a set of boundary points representing the major conductivity jumps. For modeling the 3D or anisotropic conductivity profile of the head, the finite element method (FEM) (Witwer et al. 1972; Haueisen et al. 1995; Wolters et al. 2004; Hallez et al. 2005) or the finite difference method (FDM) (Witwer et al. 1972; Haueisen et al. 1995; Wolters et al. 2004; Hallez et al. 2005) can be used. Both are differential methods. The entire volume is discretized into small elements and each volume element is assigned a separate conductivity tensor. While FDM is easier to implement, FEM allows for a smoother geometry description of conductivity boundaries. For a review including the FEM and FDM see e.g. (Hallez et al. 2007).

In the following, we will treat analytical methods, BEM, and FEM in more detail, since these methods are most frequently used. Figure 1 shows an example model for BEM and FEM.

2 Analytical and Semi-Analytical Methods

In order to obtain analytical or semi-analytical formulations of the forward problem, the geometry of the head and the conductivity distribution have to be described in terms of simple shapes, such as concentric spherical or ellipsoidal shells. In the simplest case, the volume conductor is assumed to be a sphere, which is more or less adapted to the actual head geometry. Under this assumption, for MEG it can be shown that the predicted magnetic field outside the head depends solely on the origin of the sphere as well as the positions and orientations of the

sources and the sensors. The conductivity profile including the outer radius, as long as it is spherically symmetric, plays no role. According to Sarvas (1987), the magnetic induction $\vec{B}$ at sensor position $\vec{r}$ due to N dipoles at positions $\vec{r}_i'$ with dipole moments $\vec{q}_i$ ($i = 1 \ldots N$) is computed as follows:

$$\vec{a}_i = \vec{r} - \vec{r}_i' \tag{8}$$

$$F_i = |\vec{a}_i|\left(|\vec{r}||\vec{a}_i| + |\vec{r}|^2 - \vec{r}_i'\vec{r}\right) \tag{9}$$

$$\nabla F_i = \left(|\vec{r}|^{-1}|\vec{a}_i|^2 + |\vec{a}_i|^{-1}\vec{a}_i\vec{r} + 2\vec{a}_i + 2\vec{r}\right)\vec{r} - \left(\vec{a}_i + 2\vec{r} + |\vec{a}_i|^{-1}\vec{a}_i\vec{r}\right)\vec{r}_i' \tag{10}$$

$$\vec{B}(\vec{r}) = \frac{\mu}{4\pi}\sum_{i=1}^{N}\frac{F_i\vec{q}_i \times \vec{r}_i' - \vec{q}_i \times \vec{r}_i'\vec{r}\nabla F_i}{F_i^2} \tag{11}$$

Another important property of this volume conductor model can be seen from the formula above: a dipole with radial orientation does not contribute to the measured field. Its effect is completely compensated for by the Ohmic return currents.

In contrast, the predicted EEG on the surface of a spherical volume conductor does depend on sources of all orientations, as well as on the conductivities and radii of the different tissue layers. A semi-analytical solution based on Legendre polynomials is given by de Munck (1989). It allows for the inclusion of tissue compartments with different conductivities, bounded by concentric spherical surfaces. It even allows for a simple form of tissue anisotropy, namely the distinction between radial and tangential conductivities.

Although spherical models reflect the basic geometric properties of the head, such as its round shape and the concentric arrangement of the tissue layers, the deviations from the real head shape may lead to substantial errors (Cuffin and Cohen 1977). There are a number of possibilities to improve this situation without giving up the advantages of an analytical solution. One option is the use of ellipsoidal instead of spherical shells, as proposed, for example, by Fieseler (Fieseler 1999) and Kariotou (Kariotou 2004; Giapalaki and Kariotou 2006).

Alternatively, one can use a separate spherical volume conductor model for each sensor. One way to find these local spheres is to fit them locally to a patch of the head (or brain) surface near the respective sensor (Ilmoniemi 1985; Lütkenhöner et al. 1990). This assumes that the description of the tissue boundaries in the immediate vicinity of the respective sensor is most crucial for the accuracy of the forward computation. A more principled, but also computationally more expensive, way to find the best spherical models on a sensor-to-sensor basis was proposed by Huang et al. (1999). They first used a realistic 3-shell boundary element model (see below) to compute solutions in each sensor for a large number of dipoles located in the entire brain (i.e., a leadfield computation, see below). Then, for each sensor, the solutions for the same dipoles were computed using a

spherical head model, and the parameters of that spherical model were optimized such that the difference between the boundary element method solution and the spherical solution became minimum. For MEG, a single-compartment boundary element model can be used alternatively. The resulting spheres can then be used to calculate forward solutions for arbitrary dipoles. In principle, this method can be seen as a sophisticated way for interpolating leadfields computed using numerical methods, such as BEM. For a review and evaluation of different methods using multiple spheres, see Lalancette et al. (2011).

Finally, Nolte (2003) proposed an approach, where the solution for a spherical volume conductor is corrected by a superposition of basis functions constructed from spherical harmonics and fitted to the boundary conditions. It can be shown that this approach yields good approximations for non-spherical volume conductors such as the prolate spheroid (Nolte 2003) and even for realistically shaped volume conductors (Stenroos et al. 2012).

3 Numerical Methods

3.1 Boundary Element Method

The BEM is an important and popular field calculation method used in biomagnetism. It can describe the head as an isotropic and piecewise homogeneous volume conductor of realistic shape. In practice, the compartments are designed such that their boundaries represent the most prominent conductivity jumps in the head. These are most often the head surface as well as the outer and inner bounds of the skull. For MEG, the volume currents outside the interior of the skull contribute relatively little to the measurements and therefore the respective compartments (skull, scalp) are often neglected (Hämäläinen and Sarvas 1989). However, it was recently shown that the inclusion of the skull and scalp compartments allows for a relevant improvement in accuracy (Stenroos et al. 2012).

Mathematically, the solution is derived from Poisson's equation (Eq. 5) and the appropriate Cauchy boundary conditions: (1) the potential has to be continuous across the boundary: $\varphi^+ = \varphi^-$, and (2) the perpendicular component of the current has to be continuous across the boundary[3]: $\sigma^+(\nabla_\perp \varphi)^+ = \sigma^-(\nabla_\perp \varphi)^-$, where the superscripts $()^+$ and $()^-$ refer to the values on either side of the boundary and $\nabla_\perp$ is the derivative with respect to the normal direction of the boundary. There are two different approaches to the solution: direct and indirect BEM. In the direct approach one sets up and solves an equation system for both the potentials and their normal derivatives (Boemmel et al. 1993; Fletcher et al. 1995). A specific variant of direct BEM is the symmetric BEM approach (Kybic et al. 2005). In the

[3] Note that for the outer boundary of the head this means that the perpendicular current component is zero.

indirect approach the potential function is first derived analytically, before applying the BEM (Brebbia et al. 1984; Mosher et al. 1999). This leads to the following expressions for the electric potential and the magnetic induction (Geselowitz 1967, 1970):

$$\frac{\sigma_k^+ + \sigma_k^-}{2}\varphi(\vec{r}) = \sigma_s\varphi_\infty(\vec{r}) - \sum_{j=1}^{N}\frac{\sigma_j^- - \sigma_j^+}{4\pi}\int_{S_j}\varphi(\vec{r}')\vec{n}(\vec{r}')\frac{\vec{r}-\vec{r}'}{|\vec{r}-\vec{r}'|^3}dS' \tag{12}$$

$$\vec{B}(\vec{r}) = \vec{B}_\infty(\vec{r}) - \frac{\mu}{4\pi}\sum_{j=1}^{N}\left(\sigma_j^- - \sigma_j^+\right)\int_{S_j}\varphi(\vec{r}')\vec{n}(\vec{r}')\times\frac{\vec{r}-\vec{r}'}{|\vec{r}-\vec{r}'|^3}dS' \tag{13}$$

Here, σ_s refers to the conductivity in the source compartment, $\vec{n}$ is the normal vector of the boundary, $\vec{r}$ and $\vec{r}'$ denote the positions where the potential is calculated, S_j is the j-th boundary between compartments with different conductivity, N is the number of compartments, and k is the index of the boundary on which the potential is calculated. Both, the magnetic induction and the electric potential are computed as a sum of the respective term for the infinite volume conductor (Eq. 7) and a correction term accounting for the geometry. For the electric potential, Eq. (12) is implicit, since the correction term depends on the potential itself. Equations (12 and 13) can also be interpreted in the following way (Gencer and Acar 2004): in addition to primary sources, causing the infinite volume potential/field, so-called secondary sources are placed on the boundaries, their orientations being perpendicular to the boundaries and their strength being proportional to the electric potential and the size of the conductivity step.

For the numerical implementation of BEM, the potential has to be approximated on the realistically shaped compartment boundaries. This leads to the necessity to discretize these boundaries into small elements and to express the potential on each element. The elements can have different shapes, the most common one being the triangle. The potential can be assumed to be constant on each boundary element or to vary linearly (or, in some cases, quadratically) between the vertices (basis function). The most basic method for the formulation of the resulting problem is the collocation method, where the residual is minimized in all discretization points (i.e., the centroid of elements for constant and the vertices for linear basis functions). Alternatively, one can use the Galerkin method, where the integral of the residual over the surface is approximated by means of the basis functions and then minimized. Numerical simulation with single-shell models have shown that the Galerkin method using linear basis functions usually performs better than the collocation method or the Galerkin method with constant basis functions. However, these differences are generally small (Tissari and Rahola 2003; Stenroos and Haueisen 2008). Although the benefit of the Galerkin is expected to increase with several and closely spaced surfaces, with nowadays frequently used higher mesh densities (>4,000 nodes per surface) the numerical errors due to the use of collocation BEM are smaller than errors due to model

simplifications or geometrical errors, assuming that the sources are not too close to the boundary (Mosher et al. 1999; Stenroos and Nenonen 2012).

An important question when practically constructing boundary element models is the discretization of the boundaries, which was shown to critically influence the accuracy of the solution (Haueisen et al. 1997). More precisely, it was shown that when using the collocation method with constant basis functions, the size of triangular elements should not exceed 10 mm or the minimal distance between sources and boundary, whichever is the smaller. When using linear basis functions, the size of the triangles can be up to twice the distance between sources and boundary. These rules also apply to secondary sources, which account for the conductivity discontinuities at the boundaries (see above). Thus, the thickness of tissue layers (e.g., skull compartment) and triangle size is linked in an analogous way. Due to the fact that the distribution of the secondary sources is fairly smooth, the consequences are less severe.

The relatively low conductivity of the skull tends to cause the resulting equation systems to be ill-posed. This is usually ameliorated by the isolated source approach, which first solves the problem assuming a perfectly insulating skull and then applies a correction term (Hämäläinen and Sarvas 1989; Stenroos and Sarvas 2012).

3.2 Finite Element Method

In contrast to the BEM, the FEM principally allows for accounting for the full three-dimensional tensor-valued conductivity function. In practice, of course, this is limited by the chosen discretization. The discretization means the subdivision of the volume into small elements, each endowed with a separate conductivity tensor. Within each element, the electric potential is described by a three-dimensional parameterized function, the so-called Ansatz function. For each element, a Laplace equation is approximated by deriving the Ansatz function twice. For those elements with sources, the Laplace equation turns into a Poisson equation, with an additional term accounting for the source divergence. Since the sources are usually modeled as point-like, a numerical singularity arises, which has to be treated suitably. Finally, the Cauchy boundary conditions between the elements have to be considered. This all leads to a high-dimensional sparse linear system of equations. The sparsity of the system allows, in spite of its large size, for a relatively time and memory efficient solution using dedicated algorithms. Finally, by numerical derivation of the potential, a current is computed, which is then used to compute the magnetic induction at the sensors using the law of Biot-Savart.

The two main types of discretization elements are tetrahedra and hexahedra. While hexahedra perfectly match the shape of medical imaging voxels, which form the main source of information on volume conductor geometry, tetrahedra are especially versatile when it comes to approximating arbitrarily shaped tissue boundaries. However, the node shifting technique largely compensates for this

latter disadvantage of the hexahedra approach (Wolters et al. 2007). The representation of the head can be done with uniform elements of the same size (e.g. 1 mm^3 voxels) or with elements of varying sizes depending on the segmentation of the tissues and the expected potential gradient. In addition, it is possible to adaptively change the discretization depending on metrics which are derived from intermediate solutions (Schimpf 2007). For example, in hexahedral elements the potential of one element e is given as:

$$\varphi^{\mathrm{e}}(\mathrm{x},\mathrm{y},\mathrm{z}) = \sum_{\mathrm{j}=1}^{8} \mathrm{N}_{\mathrm{j}}^{\mathrm{e}}(\mathrm{x},\mathrm{y},\mathrm{z})\varphi_{\mathrm{j}}, \tag{14}$$

where φ_j are the potentials of the nodes adjacent to the element e, and N_j^e are the shape functions describing the parameterized approximation used for each element. Most often, tri-linear shape functions are used (first-order FEM). However, also tri-quadratic functions may be used (second-order FEM). Zhang et al. (2004) suggest that for a relatively low number of elements ($\sim$150,000) and high dipole eccentricity second-order FEM provides higher accuracy compared to first order FEM. However, the results of van Uitert et al. (2001) indicate that for small element sizes (less than 2 mm side length) there is no significant advantage of second-order FEM.

Source modeling often assumes a point-like dipole. Although this model is an idealization, it forms the starting point of most source representations in EEG/MEG volume conductor modeling. However, this idealization poses a problem for FEM, as it causes a singularity. Three major approaches were put forward to treat this singularity. First, it is possible to replace the effect of the point-like dipole by making appropriate assumptions on the voltages and/or currents at the surrounding nodes of the dipole. This is equivalent to the introduction of Dirichlet and/or Neumann boundary conditions at nodes in the immediate neighborhood of the dipole. For example, a current dipole can be represented by a number of current monopoles in its surrounding. The entire group of methods can be seen as a variant of *Saint-Venant*'s principle (blurred dipole representation). In literature, however, the *Saint-Venant*'s principle only refers to current monopole representations. The second principal approach separates the problem into a source-free numerical problem governed by the Laplace equation and a Poisson problem in the infinite homogeneous space, for which an analytical solution exists. This approach is often called *subtraction method* (van den Broek et al. 1996; Drechsler et al. 2009). In the third principal approach, the *partial integration* method, the divergence of the current is projected onto the Ansatz functions and integrated over the volume. By making use of the fact that the current perpendicular to the surface is zero, one can eliminate the derivative of the primary current density and hence the singularity. Comparisons of two or three of the above dipole modeling approaches are given e.g. in (Schimpf et al. 2002; Hallez et al. 2007; Wolters et al. 2007). Although evaluations of all methods in larger studies are still missing, the Saint-Venant's principle dipole representation seems a suitable choice especially in high

resolution FEM models (Haueisen et al. 1995; Schimpf et al. 2002; Wolters et al. 2007). This is supported by the fact that brain activity is characterized by distributed current sources and sinks. Note that for the validity of the approach it is necessary that all sources and sinks are actually located within the tissue of the source areas (e.g. grey matter).

While earlier FEM studies mainly used successive over-relaxation (SOR) and Jacobi preconditioned conjugate gradient methods (Haueisen et al. 2002), multigrid methods nowadays provide a computationally more efficient way of solving the large system of equations. A recent paper showed that high resolution FEM models of the human head can also be computed within reasonable time and memory bounds (Wolters et al. 2007). This makes FEM models suitable for application in clinical studies.

4 Electric Conductivity

4.1 Introduction

A crucial piece of information for all models described above is the distribution of the electric conductivity in the head. Therefore, the determination of conductivity values is of great importance. Electric current flow in the human head is based on the movement of ions. Thus, the electric conductivity is largely determined by the concentration of these ions and the anatomical microstructure representing the restrictions and hindrances to the movement of these ions. Consequently, conductivity is a continuous function of location, i.e. inhomogeneous. Additionally, at each point the conductivity can be different in different directions (e.g. in white matter, the conductivity is higher along the fibers and lower across the fibers). This leads to the concept of anisotropic conductivity, which is mathematically represented by the conductivity tensor $\bar{\sigma}$. In order to practically handle the tensor-valued continuous function of conductivity, a discretization is required. Naturally, the single elements in full 3D methods like FEM provide a discretization. Here, each element is assigned a value representing the mean conductivity tensor for this element. The conductivity discretization thus depends on the chosen resolution of the model. Often, anisotropic conductivity information is not available. In these cases the tensor is replaced by a scalar conductivity value for each element. Moreover, elements are grouped together and assigned the same scalar conductivity value. This leads, in the simplest case, to a compartment style representation of conductivity in full 3D methods like FEM. Lumped scalar conductivity values are also assigned to entire compartments, such as the skull, the brain, the cerebrospinal fluid (CSF) or the skin, in analytical sphere and ellipsoid models as well as in BEM models.

4.2 Measurement of Electric Conductivity

Measurements of in vivo electrical conductivity values are difficult to perform for any level of discretization needed in the different types of forward models. The most common direct conductivity measurement approach is the four-electrode method. Here, two electrodes supply a current yielding a current density distribution in the specimen under investigation. The other two electrodes are used to measure a voltage drop within the specimen. From the measured voltage and the given current density, the unknown conductivity can be calculated. Alternatively, a voltage can be impressed and a current can be measured. Assuming a homogeneous specimen, four point-like electrodes can be placed in a row on the specimen, where the outer two supply the current and the inner two measure the voltage. In order to increase the accuracy of the model assumptions and to reduce the sensitivity towards local inhomogeneities of the tissue, the two current supplying electrodes might be extended in two dimensions (e.g. plate electrodes). Sources of error in such measurements are related to the positioning and the polarization of the electrodes as well as the violation of the homogeneity assumption for the specimen. The latter can be partially avoided by using an appropriate model to describe the inhomogeneous structure of the specimen. Moreover, if electrodes are put into tissue, damage is unavoidable. Besides other consequences, this leads to impressed current flow both in the intra- and extracellular space. Thus, the measured conductivity reflects both parts to a varying degree, referred to as *apparent conductivity* (Ranck 1963; Okada 1994). Another source of error lies in the fact that there is intrinsic electric activity in biological tissue, which interacts with the applied current. The interplay of these sources of error depends on the type of tissue under investigation and on the size and spacing of the electrodes.

For practical and ethical reasons, in vivo conductivity measurements on humans are rarely possible, which leads to the necessity to employ in vitro preparations. However, the conductivity values differ significantly between in vivo and in vitro situations depending on the applied preparation protocol (Galeotti 1902; Crile et al. 1922; Geddes and Baker 1967; Akhtari et al., 2000, 2002). For example, the selection of the tissue samples, the exposure to air and the temperature control during the experiment are critical parameters (Hoekema et al. 2003). Moreover, significant differences in measured conductivity values exist across species (Geddes and Baker 1967; Gabriel et al., 1996). There is inter- and intra-subject variability which can be related to age (Wendel et al. 2010), diseases, environmental factors, and personal constitution (Crile et al. 1922). It was argued that natural heterogeneity and sample–sample variability dominate the measurement uncertainty (Gabriel et al. 2009).

Alternative conductivity measurement methods impress a current and measure the induced magnetic field. For example, in magnetic resonance electric impedance tomography (MREIT) electrodes are used to impress currents into the human body and the induced magnetic flux densities are measured with the help of an MRI scanner (Seo and Woo 2011). The conductivity values are subsequently

reconstructed. It is also possible to impress currents with the help of magnetic fields and measure the resulting magnetic field.

Another class of conductivity estimation techniques uses measured electric and/or magnetic data during the source localization procedure. For very simple source configurations, such as the first cortical somatosensory evoked activity, not only the unknown source parameters are estimated in the inverse procedure but also the unknown conductivity values. Naturally, this approach can only be applied for very few unknowns, for example the conductivities of the scalp, skull, and brain compartments. The advantage of this method lies in the direct estimation of the relevant model parameters (Fuchs et al. 1998; Goncalves et al. 2003; Baysal and Haueisen 2004; Gutierrez et al. 2004; Lai et al. 2005). The disadvantage is rooted in the strong model assumptions, also concerning the source configuration.

The direction dependence of the electric conductivity can be estimated based on the measurement of direction dependent water diffusion using diffusion weighted MRI (Basser et al. 1994). With the help of the effective-medium approach, the tensor of the electric conductivity is estimated from the tensor of the measured water diffusion (Tuch et al. 2001), which was successfully validated in (Oh et al. 2006; Bangera et al. 2010) and refined in (Wang et al. 2008). However, this approach is limited due to the complex and unknown relationship between ion mobility and water diffusion.

In spite of all effort so far, getting exact, detailed and reliable conductivity information for head models is still a challenge and will require substantial research effort in the future.

4.3 Conductivity of Single Tissue Types

The following Table 2 gives an account of the conductivity values for single tissues based on existing literature. Tissue conductivity depends, among other factors, on frequency and temperature. Thus, only conductivity values measured at or near body temperature and at low frequencies (d.c. up to 100 kHz) were taken into account. Among the relevant literature, two reviews are most often cited: (Geddes and Baker 1967; Gabriel et al. 1996) (and its more recent extension Gabriel et al. 2009).

4.4 Compartment Conductivities

Since most often three or four compartments are used to describe the volume conductor, these compartment conductivities of the brain, CSF, skull, and scalp are most relevant and considered here. Each compartment-conductivity depends on the complex geometrical arrangement of the tissues determining the compartment. Furthermore, since the compartment conductivity is merely a model for the real

Table 2 Isotropic conductivity values of single tissue types used in human head volume conductor modeling

Tissue	Conductivity in S/m	References
Brain gray matter	0.3	Gabriel et al. (1996, 2009)
Brain white matter	0.2	Gabriel et al. (1996, 2009)
Spinal cord and cerebellum	0.16	Haueisen et al. (1995)
Cerebrospinal fluid	1.79	Baumann et al. (1997)
Hard bone (compact bone)	0.004	Tang et al. (2008)
Soft bone (spongiform bone)	0.02	Akhtari et al. (2002)
Blood	0.6	Gabriel et al. (2009)
Muscle	0.1	Gabriel et al. (1996, 2009)
Fat	0.08	Gabriel et al. (2009)
Eye	1.6	Pauly and Schwan (1964), Lindenblatt and Silny (2001)
Scalp	0.43	Geddes and Baker (1967)
Soft tissue	0.17	Haueisen et al. (1995)
Internal air	0.0001	Haueisen et al. (1995)

conductivity profile, the source configuration also has an influence on the choice of this value. In principle, there are three ways to estimate a compartment conductivity: (i) based on the measurement of single tissues an average for a compartment is computed (either model based or model free); (ii) the conductivity of an entire compartment is directly measured (bulk conductivity); and (iii) the compartment model (conductivity as free parameter) is fitted to purposely performed measurements (e.g. EEG, MEG, DTI), see above.

A number of studies report bulk conductivity measurements. Akhtari et al. (2006) measured freshly excised human neocortex and subcortical white matter in 21 neurosurgical patients and found values of 0.066–0.156 S/m. CSF, as indicated above, has 1.79 S/m. The conductivity values for the skull compartment show large variation. Akhtari et al. (2002) found 0.0085–0.0114 S/m bulk conductivity for live human skull at room temperature, while in an earlier study on a cadaver skull the values ranged from 0.0023 to 0.00584 S/m (Akhtari et al. 2000). Hoekema et al. (2003) found values between 0.032 and 0.08 S/m in a very well controlled study of live human skull in 5 neurosurgical patients. The most comprehensive study on 3 layer live human skull at body temperature was performed by Tang et al. (2008). They demonstrated that the conductivity value largely depends on the local structure of the skull. They distinguished (besides other criteria) between normal and thin spongiform layers and found conductivity values for the 3 layer skull of 0.0126 S/m and 0.00691 S/m, respectively. The standard deviation was about 20 %. Using electric impedance tomography and the model fit approach, Gonçalves et al. (2003) estimated the conductivity of the brain and skull compartment in six subjects to be 0.33 S/m and 0.0082 S/m with a standard deviation of 13 and 18 %, respectively.

For separate EEG or MEG analysis only compartment conductivity ratios are needed. For the often used 3-compartment model this is the ratio of scalp:skull:-brain. In the past, the most often used ratio was 1:1/80:1, which was derived from a study by Rush and Driscoll (1968), who measured the impedance of a dry half-skull in fluid and proposed values of 0.33, 0.0042 and 0.33 S/m. Recently, this ratio was questioned by a number of researchers. Oostendorp et al. (2000) performed both measurement on cadaver skull and in vivo on volunteers using electric stimulation and found a ratio of 1:1/15:1. Baysal and Haueisen (2004) used combined MEG/EEG measurements and estimated a ratio of 1:1/22:1. Lai et al. (2005) suggested a ratio of 1:1/25:1. Based on the measurements of Hoekema et al. (2003), a ratio of 1:1/8:1 can be considered. Zhang et al. (2006) estimated 1:1/20:1 based on measurement in two epilepsy patients. The values of Tang et al. (2008) indicate approximate ratios between 1:1/25:1 and 1:1/50:1 and the values of Gonçalves et al. (2003) approximately 1:1/40:1. Dannhauer et al. (2011) report a ratio of 1:1/25:1 to 1:1/47:1 based on the measurements of Akhtari et al. (2002) and a model fit. Although the recent studies show some degree variability, they all agree on the fact that the value of 80 in the long standing ratio of 1:1/80:1 is too high.

5 Leadfield Concept

Results from the forward calculation can be used in inverse procedures directly (e.g., in spatio-temporal dipole fitting) or stored in so-called leadfield matrices. Such matrices represent the forward solutions for sources on a predefined grid. The term *leadfield* (originally derived from "lead" that stands for a single EEG channel) refers to a function describing the sensitivity of the output of one sensor to the parameters of the source model. For example when using the dipole model, the leadfield is a function of the position and the orientation of a unit strength dipole. Usually, the leadfield is discretized, e.g. the dipoles are positioned on the nodes of a regular grid with canonical orientations (e.g. x, y, z). These leadfield vectors are combined into a leadfield matrix, describing the influence of each unit dipole on each sensor. Accordingly, this matrix is also sometimes called influence matrix or gain matrix. In such a matrix, each row refers to one sensor (one leadfield) and each column describes the influence of one unit dipole (e.g. one unit dipole per canonical direction) on the sensor array. In general, the leadfield matrix is a discretized representation of the forward problem. The discretization has to be such that it adequately approximates the leadfield. When using dipoles in the brain, spatial sampling of 3-10 mm is common. Any dipole orientation can be represented by the superposition of 3 canonical orientations.

6 Conclusion and Outlook

Source localization is increasingly applied in neuroscientific research and clinical studies. The accuracy of source reconstruction depends on the accuracy of the solution of the forward problem. Finite element models are more elaborate compared to boundary element models and can, in principle, account for the anisotropic distribution of connectivity at any level of detail. Until recently, there were three major obstacles for the use of this kind of forward modeling in source reconstruction schemes. (1) The computation was computationally too costly to allow for a repetitive computation of forward solutions as required by inverse algorithms. (2) The possibility to account for the anisotropic conductivity on a voxel basis turns from an advantage to a drawback, if reliable information on these material properties at this level of detail is missing. (3) At the position of the dipoles, singularities occur, which were difficult to treat numerically. While reasons (1) and (3) can be considered to be mostly solved (Wolters et al. 2004; Lew et al. 2009), reason (2) still requires substantial research. Especially diffusion weighted MR imaging promises to offer new ways to estimate material properties at a fine level of detail (Güllmar et al. 2010; Dannhauer et al., 2011; Sengül and Baysal 2012). If there is no reliable information on anisotropic volume conduction BEM can be the method of choice in realistic volume conductor modeling.

References

Akhtari M, Salamon N, Duncan R, Fried I, Mathern GW (2006) Electrical conductivities of the freshly excised cerebral cortex in epilepsy surgery patients; Correlation with pathology, seizure duration, and diffusion tensor imaging. Brain Topogr 18:281–290

Akhtari M, Bryant HC, Mamelak AN, Heller L, Shih JJ, Mandelkern M, Matlachov A, Ranken DM, Best ED, Sutherling WW (2000) Conductivities of three-layer human skull. Brain Topogr 13:29–42

Akhtari M, Bryant HC, Marnelak AN, Flynn ER, Heller L, Shih JJ, Mandelkern M, Matlachov A, Ranken DM, Best ED, DiMauro MA, Lee RR, Sutherling WW (2002) Conductivities of three-layer live human skull. Brain Topogr 14:151–167

Bangera N, Schomer D, Dehghani N, Ulbert I, Cash S, Papavasiliou S, Eisenberg S, Dale A, Halgren E (2010) Experimental validation of the influence of white matter anisotropy on the intracranial EEG forward solution. J Comput Neurosci 29:371–387

Barnard ACL, Duck IM, Lynn MS (1967a) Application of electromagnetic theory to electrocardiology I. Derivation of integral equations. Biophys J 7:443–462

Barnard ACL, Duck IM, Lynn MS, Timlake WP (1967b) Application of electromagnetic theory to electrocardiology II. Numerical solution of integral equations. Biophys J 7:463–491

Basser PJ, Mattiello J, LeBihan D (1994) MR diffusion tensor spectroscopy and imaging. Biophys J 66:259–267

Baumann S, Wozny D, Kelly S, Meno F (1997) The Electrical Conductivity of Human Cerebrospinal Fluid at Body Temperature. IEEE Trans Biomed Eng 44:220–223

Baysal U, Haueisen J (2004) Use of a priori information in estimating tissue resistivities—application to human data in vivo. Physiol Meas 25:737–748

Boemmel F, Roeckelein R, Urankar L (1993) Boundary element solution of biomagnetic problems. IEEE Trans Magn 29:1395–1398
Brebbia C, Telles J, Wrobel L (1984) Boundary element techniques. Springer, Berlin
Crile GW, Hosmer HR, Rowland AF (1922) The electrical conductivity of animal tissues under normal and pathological conditions. Am J Physiol 60:59–106
Cuffin BN, Cohen D (1977) Magnetic fields of a dipole in special volume conductor shapes. IEEE Trans Biomed Eng 24:372–381
Dannhauer M, Lanfer B, Wolters CH, Knösche TR (2011) Modeling of the human skull in EEG source analysis. Hum Brain Mapp 32:1383–1399
de Munck JC (1988) The potential distribution in a llayered anisotropic spheroidal volume conductor. J Appl Phys 64:464–470
de Munck JC (1989) A mathematical and physical interpretation of the electromagnetic field of the brain. In: University of Amsterdam, The Netherlands
Donchin E (1966) A multivariate approach to analysis of average evoked potentials. IEEE Trans Biomed Eng BM13:131–139
Drechsler F, Wolters CH, Dierkes T, Si H, Grasedyck L (2009) A full subtraction approach for finite element method based source analysis using constrained Delaunay tetrahedralisation. Neuroimage 46:1055–1065
Fieseler T (1999) Analytic source and volume conductor models for biomagnetic fields. University Jena, Germany
Fletcher D, Amir A, Jewett D, Fein G (1995) Improved method for computation of potentials in a realistic head shape model. IEEE Trans Biomed Eng 42(11):1094–1104
Fuchs M, Wagner M, Wischmann HA, Kohler T, Theissen A, Drenckhahn R, Buchner H (1998) Improving source reconstructions by combining bioelectric and biomagnetic data. Electroencephalogr Clin Neurophysiol 107:93–111
Gabriel C, Gabriel S, Corthout E (1996) The dielectric properties of biological tissues. 1. Literature survey. Phys Med Biol 41:2231–2249
Gabriel C, Peyman A, Grant EH (2009) Electrical conductivity of tissue at frequencies below 1 MHz. Phys Med Biol 54:4863–4878
Galeotti G (1902) The electric conductibility of animal tissues. Zeitschrift für Biologie 43:289–340
Geddes LA, Baker LE (1967) Specific resistance of biological material - a compendium of data for the biomedical engineer and physiologist. Medical & Biological Engineering 5:271–293
Gencer NG, Acar CE (2004) Sensitivity of EEG and MEG measurements to tissue conductivity. Phys Med Biol 49:701–717
Geselowitz D (1967) On bioelectric potentials in an inhomogeneous volume conductor. Biophys J 7:1–11
Geselowitz D (1970) On magnetic field generated outside an inhomogeneous volume conductor by internal current sources. IEEE Trans Magn 6:346–347
Giapalaki SN, Kariotou F (2006) The complete ellipsoidal shell-model in EEG imaging. Abstr Appl Anal 2006:1–18
Goncalves S, de Munck JC, Verbunt JPA, Heethaar RM, da Silva FHL (2003) In vivo measurement of the brain and skull resistivities using an EIT-based method and the combined analysis of SEF/SEP data. IEEE Trans Biomed Eng 50:1124–1128
Güllmar D, Haueisen J, Reichenbach JR (2010) Influence of anisotropic electrical conductivity in white matter tissue on the EEG/MEG forward and inverse solution. A high resolution whole head simulation study. Neuroimage 51:145–163
Gutierrez D, Nehorai A, Muravchik CH (2004) Estimating brain conductivities and dipole source signals with EEG arrays. IEEE Trans Biomed Eng 51:2113–2122
Hallez H, Vanrumste B, Van Hese P, D'Asseler Y, Lemahieu I, Van de Walle R (2005) A finite difference method with reciprocity used to incorporate anisotropy in electroencephalogram dipole source localization. Phys Med Biol 50:3787–3806

Hallez H, Vanrumste B, Grech R, Muscat J, De Clercq W, Vergult A, D'Asseler Y, Camilleri KP, Fabri SG, Van Huffel S, Lemahieu I (2007) Review on solving the forward problem in EEG source analysis. J Neuroeng Rehabil 4:46

Hämäläinen MS, Sarvas J (1989) Realistic conductivity geometry model of the human head for interpretation of neuromagnetic data. IEEE Trans Biomed Eng 36:165–171

Haueisen J, Ramon C, Czapski P, Eiselt M (1995) On the influence of volume currents and extended sources on neuromagnetic fields: a simulation study. Ann Biomed Eng 23:728–739

Haueisen J, Hafner C, Nowak H, Brauer H (1996) Neuromagnetic field computation using the multiple multipole method. Int J Numer Model 9:144–158

Haueisen J, Bottner A, Funke M, Brauer H, Nowak H (1997) The influence of boundary element discretization on the forward and inverse problem in electroencephalography and magnetoencephalography. Biomed Tech 42:240–248

Haueisen J, Tuch DS, Ramon C, Schimpf PH, Wedeen VJ, George JS, Belliveau JW (2002) The influence of brain tissue anisotropy on human EEG and MEG. Neuroimage 15:159–166

Hoekema R, Wieneke GH, Leijten FSS, van Veelen CWM, van Rijen PC, Huiskamp GJM, Ansems J, van Huffelen AC (2003) Measurement of the conductivity of skull, temporarily removed during epilepsy surgery. Brain Topogr 16:29–38

Huang MX, Mosher JC, Leahy RM (1999) A sensor-weighted overlapping-sphere head model and exhaustive head model comparison for MEG. Phys Med Biol 44:423–440

Ilmoniemi R (1985) Neuromagnetism: theory, techniques, and measurements. Helsinki University of Technology, Finland

Kariotou F (2004) Electroencephalography in ellipsoidal geometry. J Math Anal Appl 290:324–342

Kayser J, Tenke CE (2005) Trusting in or breaking with convention: towards a renaissance of principal components analysis in electrophysiology. Clin Neurophysiol 116:1747–1753

Kybic J, Clerc M, Abboud T, Faugeras O, Keriven R, Papadopoulo T (2005) A common formalism for the integral formulations of the forward EEG problem. IEEE Trans Med Imaging 24:12–28

Lai Y, van Drongelen W, Ding L, Hecox KE, Towle VL, Frim DM, He B (2005) Estimation of in vivo human brain-to-skull conductivity ratio from simultaneous extra- and intra-cranial electrical potential recordings. Clin Neurophysiol 116:456–465

Lalancette M, Quraan M, Cheyne D (2011) Evaluation of multiple-sphere head models for MEG source localization. Phys Med Biol 56:5621–5635

Lew S, Wolters CH, Dierkes T, Röer C, Macleod RS (2009) Accuracy and run-time comparison for different potential approaches and iterative solvers in finite element method based EEG source analysis. Appl Numer Math 59:1970–1988

Lindenblatt G, Silny J (2001) A model of the electrical volume conductor in the region of the eye in the ELF range. Phys Med Biol 46:3051–3059

Lütkenhöner B, Pantev C, Hoke M (1990) Comparison between different methods to approximate an area of the human head by a sphere. In: Grandori F, Hoke M, Romani GL (eds) Advances in audiology, pp 103–118

Mosher JC, Leahy RM, Lewis PS (1999) EEG and MEG: Forward solutions for inverse methods. IEEE Trans Biomed Eng 46:245–259

Murakami S, Okada Y (2006) Contributions of principal neocortical neurons to magnetoencephalography and electroencephalography signals. J Physiol-Lond 575:925–936

Nolte G (2003) The magnetic lead field theorem in the quasi-static approximation and its use for magnetoencephalography forward calculation in realistic volume conductors. Phys Med Biol 48:3637–3652

Oh S, Lee S, Cho M, Kim T, Kim I (2006) Electrical conductivity estimation from diffusion tensor and T2: a silk yarn phantom study. Proc Int Soc Magn Reson Med 14:3034

Okada Y (1994) Origin of the apparent tissue conductivity in the molecular and granular layers of the in vitro turtle cerebellum and the interpretation of current source-density analysis. J Neurophysiol 72:742–753

Oostendorp TF, Delbeke J, Stegeman DF (2000) The conductivity of the human skull: Results of in vivo and in vitro measurements. IEEE Trans Biomed Eng 47:1487–1492
Pauly H, Schwan H (1964) The dielectric properties of the bovine eye lens. IEEE Trans Biomed Eng 11:103–109
Plonsey R, Heppner DB (1967) Considerations of quasi-stationarity in electrophysiological systems. Bull Math Biophys 29:657–664
Ranck JB (1963) Analysis of specific impedance of rabbit cerebral cortex. Exp Neurol 7:153–174
Rush S, Driscoll DA (1968) Current distribution in the brain from surface electrodes. Anesth Analg Curr Res 47:717–723
Sarvas J (1987) Basic mathematical and electromagnetic concepts of the biomagnetic inverse problem. Phys Med Biol 32:11–22
Schimpf PH (2007) Application of quasi-static magnetic reciprocity to finite element models of the MEG lead-field. IEEE Trans Biomed Eng 54:2082–2088
Schimpf PH, Ramon C, Haueisen J (2002) Dipole models for the EEG and MEG. IEEE Trans Biomed Eng 49:409–418
Sengül G, Baysal U (2012) An extended Kalman filtering approach for the estimation of human head tissue conductivities by using EEG data: a simulation study. Physiol Meas 33:571–586
Seo JK, Woo EJ (2011) Magnetic resonance electrical impedance tomography (MREIT). Siam Rev 53:40–68
Stenroos M, Haueisen J (2008) Boundary element computations in the forward and inverse problems of electrocardiography: comparison of collocation and Galerkin weightings. IEEE Trans Biomed Eng 55:2124–2133
Stenroos M, Sarvas J (2012) Bioelectromagnetic forward problem: isolated source approach revis(it)ed. Phys Med Biol 57:3517–3535
Stenroos M, Nenonen J (2012) On the accuracy of collocation and Galerkin BEM in the EEG/MEG forward problem. Int J Bioelectromagn 14:29–33
Stenroos M, Mantynen V, Nenonen J (2007) A Matlab library for solving quasi-static volume conduction problems using the boundary element method. Comput Methods Programs Biomed 88:256–263
Stenroos M, Hunold A, Eichardt R, Haueisen J (2012) Comparison of three- and single-shell volume conductor models in magnetoencephalography. Biomedical Engineering-Biomedizinische Technik 57:311
Tang C, You F, Cheng G, Gao D, Fu F, Yang G, Dong X (2008) Correlation between structure and resistivity variations of the live human skull. IEEE Trans Biomed Eng 55:2286–2292
Tissari S, Rahola J (2003) Error analysis of a Galerkin method to solve the forward problem in MEG using the boundary element method. Comput Methods Programs Biomed 72:209–222
Tuch DS, Wedeen VJ, Dale AM, George JS, Belliveau JW (2001) Conductivity tensor mapping of the human brain using diffusion tensor MRI. Proc Natl Acad Sci U.S.A 98:11697–11701
van den Broek SP, Zhou H, Peters MJ (1996) Computation of neuromagnetic fields using finite-element method and Biot-Savart law. Med Biol Eng Compu 34:21–26
van Uitert R, Weinstein D, Johnson C, Zhukov L (2001) Finite element EEG and MEG simulations for realistic head models: quadratic versus linear approcimations. In: International conference on non-invasive functional source imaging, Innsbruck, 2001
Wang K, Li J, Zhu S, Mueller B, Lim K, Liu Z, He B (2008) A new method to derive white matter conductivity from diffusion tensor MRI. IEEE Trans Biomed Eng 55:2481–2486
Wendel K, Vaisanen J, Seemann G, Hyttinen J, Malmivuo J (2010) The influence of age and skull conductivity on surface and subdermal bipolar EEG leads. Comput Intell Neurosci 2010:397272
Witwer JG, Trezek GJ, Jewett DL (1972) Effect of media inhomogeneities upon intracranial electrical fields. IEEE Trans Biomed Eng BM19:352–362
Wolters C, Köstler H, Möller C, Härdtlein J, Anwander A (2007) Numerical approaches for dipole modeling in finite element method based source analysis. Int Congr Ser 1300:189–192
Wolters CH, Grasedyck L, Hackbusch W (2004) Efficient computation of lead field bases and influence matrix for the FEM-based EEG and MEG inverse problem. Inverse Prob 20:1099–1116

Zhang YC, Zhu SA, He B (2004) A second-order finite element algorithm for solving the three-dimensional EEG forward problem. Phys Med Biol 49:2975–2987
Zhang YC, van Drongelen W, He B (2006) Estimation of in vivo brain-to-skull conductivity ratio in humans. Appl Phys Lett 89:223903

Designing MEG Experiments

Julia M. Stephen

Abstract With well-designed experiments, the exquisite temporal resolution of MEG allows investigators to track the temporal progression of cortical activity throughout the brain during sensory and cognitive tasks and further allows investigators to capture the interplay between the nodes of the cortical network activity underlying brain function. Because of this high temporal resolution, a number of considerations must be considered to obtain good quality MEG data. These considerations include: recording parameters, participant considerations, stimulus equipment and timing reliability, stimulus parameters and temporal sensitivity of the response. This chapter reviews the common instrumentation parameters, peripheral equipment that provides the precise timing needed for MEG experiments, and participant-monitoring equipment that provides complementary information for data quality and data interpretation purposes. Modality-specific (auditory, visual, tactile and motor) factors to consider during data collection are also discussed.

Keywords Magnetoencephalography (MEG) · Experimental design · Visual · Auditory · Somatosensory · Motor · Timing parameters · Peripheral equipment

1 Introduction

The goal of this chapter is to provide an overview of the parameters that should be considered when setting up and conducting MEG experiments. MEG provides an incredibly rich dataset from which to study brain function and dysfunction. In particular, MEG provides high temporal resolution at the time resolution that brain

J. M. Stephen (✉)
The Mind Research Network, Albuquerque, NM, USA
e-mail: jstephen@mrn.org

S. Supek and C. J. Aine (eds.), *Magnetoencephalography*,
DOI: 10.1007/978-3-642-33045-2_5,

activity occurs (Kandel et al. 2000). In addition, MEG signals are not distorted by the skull, providing improved spatial resolution relative to EEG (Flemming et al. 2005). Therefore, one can obtain exquisite sensitivity to cortical network oscillations and the interplay between different cortical areas. However, this richness comes with multiple challenges. One of the biggest challenges of MEG is to identify task related activity in the presence of background brain activity. Resting brain activity, including resting brain rhythms such as occipital alpha and sensorimotor mu rhythms are 10–100 times greater in amplitude than evoked responses (e.g. the magnetic field generated by the presentation of an auditory stimulus). That is, the signal to noise ratio for a single presentation of a stimulus is <1. Therefore, a common method to identify stimulus related activity is to present multiple trials of the same stimulus to allow for signal averaging in the time, frequency or time/frequency domain. Further challenges include minimizing magnetic artifact from both internal and external sources of magnetic fields and capturing complementary data that can better guide interpretation of the results. MEG experimental design is therefore focused on optimizing all parameters to ensure that the high temporal resolution is maintained and signal to noise is optimized despite the challenges of background brain activity and other artifacts.

2 Instrumentation

2.1 Recording Parameters

The magnetic fields that are generated by the brain oscillate with the onset and offset of local brain activity (Hamalainen et al. 1993). Based on in vivo and in vitro characterization of neuronal activity, we know that the temporal profile of brain activity that generates these magnetic fields changes on the order of milliseconds (Kandel et al. 2000). This suggests that in order to properly capture the rapid changes in magnetic field associated with brain activity; data must be sampled at or around one sample per ms or 1,000 Hz. Furthermore, to capture the ongoing network interactions, it is important to capture this activity synchronously from around the head to allow investigators to characterize the interplay of cortical activity during task performance or during rest.

Therefore, current MEG systems record data synchronously from hundreds of MEG channels at digitization rates of between 100–5,000 Hz. This provides a temporal resolution of between 10 and 0.2 ms, respectively. This high sampling rate and the rapid neuronal response underlie the high temporal resolution of MEG. Table 1 shows the parameters that one must choose before beginning data collection on a standard MEG system. The choice of sampling rate depends on the required temporal resolution and spectral content of the data of interest. There are trade-offs between high and low sampling rates. While a high sampling rate may always appear to be better, long experiments may lead to prohibitively large data sets (a 10 min continuous dataset including 306 sensors sampled at 1,000 Hz is

Table 1 Recording parameters

Channels to record	MEG, EEG, A/D channels, trigger channels
Digitization rate	100–5,000 Hz
Online filter settings	High pass filter, anti-aliasing filter $< \frac{sampling\,frequency}{2}$
Trigger settings	Choose triggers, averaging epoch for online averaging display

approximately 1 GB in size). The typical sampling rate for visual, auditory and cognitive studies is between 300–1,000 Hz. A sampling rate of 300–400 Hz is often sufficient for averaged evoked responses for cognitive studies, where most of the spectral content in an averaged response is less than 60 Hz. However, median nerve stimulation requires a sampling rate of at least 1,000 Hz to capture the temporal profile of the M20 response. Also, recent interest in high frequency activity, which has been found in the somatosensory modality (Curio et al. 1997), during cognitive tasks (Uhlhaas et al. 2011) and in patients with epilepsy (Engel et al. 2009), may require a sampling rate or $\geq$2,000 Hz. Some systems allow for higher data acquisition rates when subsets of channels are chosen.

In conjunction with the sampling rate, an online anti-aliasing filter must be applied to ensure that higher frequency signals do not appear as an aliased low frequency signal. The anti-aliasing filter should be set at a frequency less than the sampling frequency/2. That is, if your sampling frequency is 300 Hz the online low-pass filter should be less than 150 Hz. In addition to the anti-aliasing filter, one can also choose a high pass filter setting on most MEG systems. This choice is left to the discretion of the investigator. The relevant question is whether there is any low frequency activity that might be relevant to the study. If one is interested in delta wave activity, it is best to choose the lowest cutoff option (generally 0.01 or 0.03 Hz). On the other hand, if the system is located in an environment with considerable low frequency noise, it may be desirable to eliminate low-frequency noise at the point of data collection.

2.2 Other Recording Channels

MEG systems also have additional channels that are recorded simultaneously with the MEG data. This option for simultaneous recording is critical to ensure that peripheral devices are truly synchronized with the MEG data. Trigger channels are supplementary channels that allow one to simultaneously record the timing of stimulus presentations. These channels accept transistor-transistor logic (TTL) pulses, which are standard binary pulses denoting on/off status. The width of the TTL pulse should be brief to allow for multiple triggers in short periods of time and it must be long enough that the sampling rate can sufficiently capture the onset and offset of the TTL pulse. Within these constraints the normal duration is

Table 2 Other recording channels

Trigger channels	Collect TTL pulse triggers (5–10 ms) from stimulus computer/equipment
Referenced EEG	Collect 1–128 channels of referenced EEG
Bipolar EEG	Electro-oculogram (EOG), electromyogram (EMG), electrocardiogram (ECG)
A/D channels	Allows collection of miscellaneous ±10 V analog signal

between 5 and 10 ms. These TTL trigger pulses can be generated by stimulus delivery software (e.g. NBS Presentation, Neuroscan StimII, Eprime) or by custom-built equipment. Additionally, some MEG systems provide an option to set periodic internal triggers (independent of external stimuli) to allow for epoching of the data (breaking the data into equal sized bins) if no stimulus triggers are present. These are often used to generate averaged spectra for noise runs or spectral analysis of resting-state MEG data.

Current MEG systems offer at least 64-channel referenced EEG capabilities allowing for simultaneous MEG/EEG recordings. In addition, at least 4 bipolar EEG channels are available for recording eye blinks and muscle movement. Our standard adult studies use two bipolar EEG channels to capture horizontal and vertical eye movements, respectively and one bipolar channel to collect ECG.

Finally, A/D channels accept any type of analog data generally within a ±10 V range. This allows one to collect any type of supplementary continuous data that is within the appropriate amplitude range. Examples of analog data that we have collected in MEG studies include: pressure transducer amplitude from a squeeze device to evaluate the strength of the squeeze (Berchicci et al. 2011), eye position and pupilometry data obtained from an MEG compatible eye-tracking system (Coffman et al. 2013), and voice recordings during task completion. A BNC connector is generally required to interface with the MEG electronics (Table 2).

2.3 Peripheral Devices

Since the high temporal resolution (∼1 ms) of MEG is one of its strengths, it is critical that temporal resolution is not compromised due to peripheral equipment. Most off-the-shelf equipment (e.g. computer sound cards, visual projectors or computer screens) is not tested for millisecond timing accuracy. Therefore, when choosing new equipment it is recommended to contact other MEG labs or the MEG manufacturer to obtain information about recommended devices. While MRI-compatible equipment available for fMRI studies is useful to control magnetic artifacts from peripheral devices, these devices are not always tested for high temporal resolution due to the lower temporal resolution of fMRI. In addition, it is recommended that you work with a representative of the company who has sufficient technical expertise of the peripheral equipment to determine the temporal

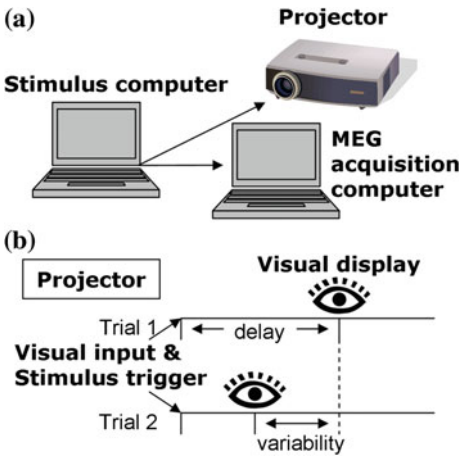

Fig. 1 **a** Basic visual setup. **b** Schematic of different timing parameters for evaluating an MEG visual setup

characteristics. In some cases, the companies are willing and able to allow on-site demonstration of the equipment. In this case it is recommended that you measure the temporal characteristics directly. Finally, it is important to test the timing of the final setup to ensure that the timing of the complete setup is accounted for (e.g. stimulus computer, amplifiers, peripheral equipment).

In accounting for timing, it is important to understand what factors may or may not introduce delays. Any signal that is transmitted at the speed of light is effectively transmitted instantaneously over the distances considered for MEG data collection. That is, signal is transferred along a 5 m long cable in $\sim$0.00001 ms at the speed of light leading to no measurable delay. However, electronic equipment (sound cards, electronic circuits, etc.) can introduce delays in the transfer of signal and should be tested. Furthermore, the speed of sound is considerably slower than the speed of light and any distance from the generation of the sound wave to the participants' ears should be accounted for in the delay calculation. The delay can be calculated based on the speed of sound in air ($\sim$0.344 m/ms). So for every 1/3 of a meter traveled in air, sound is delayed by 1 ms. All other signals need to be tested empirically.

Generally, the trigger is sent from the stimulus computer to the MEG electronics at the same time that the signal is sent to the peripheral equipment (see Fig. 1a). Therefore, the parameters to be tested are the *delay* of the peripheral device (defined as the time from when the signal was sent to the peripheral device to the time the stimulus reaches the participant) and the variability in this transfer time (*jitter*). If there is variability in the presentation time of the peripheral device, meaning that one presentation may occur 5 ms after the projector received the signal and a second presentation may occur 50 ms after the projector received the signal, this will not be captured by the trigger sent in parallel to the MEG acquisition computer. A delay in the peripheral equipment can be measured and accounted for in post-processing steps, however, jitter cannot easily be addressed based on triggers alone. The variability in the onset times can be large depending

on the equipment. This introduces a significant shift in latencies across trials thereby blurring the temporal resolution of the measured cortical response (leading to peak broadening and/or reduced amplitude due to cancellation across trials). Therefore, the optimal jitter is <1 ms. In some cases, one can still account for jitter (described in more detail below). However, experiments that require precise timing between stimuli (e.g. testing the ability to predict the next stimulus) or experiments that require multiple stimuli to be presented synchronously (e.g. multisensory integration studies) require consistent timing (jitter <1 ms) across trials to provide the required timing between stimuli.

The other significant challenge with peripheral equipment is identifying equipment that does not introduce artifact (strong magnetic fields) during data collection. This is often addressed by placing electrical equipment outside of the magnetically shielded room (MSR) and passing the signal/stimulus into the room through non-magnetic stimulus delivery systems. These can include shielded and properly grounded wires and fiber optic cables. Fiber optic cables are ideal for two primary reasons. First the signal travels at the speed of light, introducing no measurable delay in transfer of the signal. Second, the fiber optic cables are made of non-ferromagnetic materials (plastic sheathing and glass), thereby introducing no magnetic artifacts into the MSR. All other peripheral equipment including screens, response buttons, etc. should be built with non-ferromagnetic materials which include plastic, wood and brass. The prevalence of fMRI has made acquisition of non-ferromagnetic stimulus equipment more readily available. However, as mentioned throughout this chapter, not all MRI-safe equipment is suitable for MEG.

2.3.1 Bipolar EEG Channels

Bipolar EEG channels are used to monitor muscle activity. The most common use is to monitor eye blinks. It is important to have a set policy for eye blinks when providing your participant with instructions prior to beginning data collection for the MEG study. This however, can be difficult. If too much emphasis is placed on not blinking, the participants will almost invariably blink more (e.g., their eyes become dry which causes involuntary blinking). It is generally recommended that you tell the participants when they can blink rather than informing them that they cannot blink. “When you need to blink please blink after you’ve responded or blink between the stimuli.” Some studies (e.g. Tesche and Karhu 2000) have explicitly set aside a blink period between stimuli.

Regardless, it is important to use eye blink detection channels in most if not all MEG experiments. The magnetic fields generated by the muscles around the eyes are significantly larger than the magnetic fields of interest. This leads to two problems. First, eye blinks can completely swamp any signal that you are interested in measuring. Second, eye blinks are large amplitude events with a consistent field pattern so that there is very little chance that they will average out across trials. It is also the case that many subjects will blink in response to a stimulus (partially time-synched), making it even more likely that you will obtain a large

amplitude eye blink artifact. There are a number of different configurations that can be used to monitor eye blinks and eye movement. It is generally best to incorporate a setup that can monitor both vertical and horizontal eye movements. With two sets of electrooculogram (EOG) electrodes it is best to place one set of electrodes on the superior and inferior orbital ridges of one eye to monitor eye blinks and vertical eye movement and the second set of electrodes on the left and right outer canthi to monitor horizontal eye movements. With one set of EOG electrodes, one electrode can be placed on the superior orbital ridge of one eye and the other on the outer canthi of the other eye to incorporate both horizontal and vertical eye movements into one EOG channel.

Bipolar EEG channels are also useful for monitoring heartbeat. While it is highly recommended to monitor heart beat in clinical cases, it is not as critical to monitor in basic research studies. However, there are some subjects that exhibit significant heart beat artifact in their MEG. By recording the electrocardiogram (ECG), it is much easier to confirm and eliminate heart beat artifact from the MEG signal than if the data are simply not acquired. A standard placement of two EEG leads just below the left and right clavicle generally provides a good ECG recording. Heart beat artifact can be removed from the signal using projection methods described in Sect. 4.1.

Another common use of bipolar EEG channels is to monitor other muscle movement. These can be used with standard electromyogram (EMG) placements to monitor specific muscle activity to confirm or disprove mirror movements that may occur in cases of brain injury such as Cerebral Palsy or Stroke (Grosse et al. 2002). EMG channels have now been widely used to quantify coherence of brain oscillations with oscillations measured in the EMG to better understand the mechanisms associated with Parkinson's Disease (Timmermann et al. 2003, 2004).

2.3.2 Visual Equipment

Currently, projectors are the standard equipment used to present visual stimuli (often with the projector located outside the MSR such that it can project onto a rear-projection screen located within the MSR). Most off-the-shelf projectors do not provide reliable timing. The timing profile of a projector can be tested by collecting MEG data with the visual stimulus trigger and a photosensor attached to the screen. The photosensor signal should be routed to one of the analog-to-digital (A/D) channels and timing of the photosensor signal relative to the visual triggers can then be measured (see Fig. 2). Depending on the type of projector, timing may also vary across the screen (e.g. cathode ray tube (CRT) monitors) so timing parameters should be tested at the location of the visual stimuli. To test the timing parameters, a separate visual stimulus at the desired screen location should be used such that the stimulus changes from black to white (or vice versa) at the onset of the stimulus to provide a clear change in photo luminance for the photosensor. Collect approximately 30 trials to determine the variability in this timing measurement. If the maximum variability of this timing is low ($\sim$3 ms or less), then

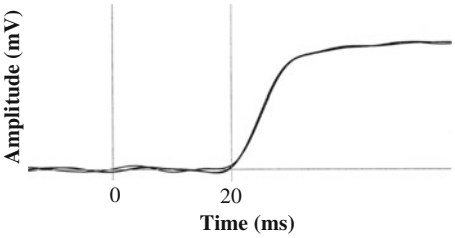

Fig. 2 Photo diode recording on an A/D channel. Time 0 is the time the trigger pulse reached the MEG data acquisition system. Time 20 ms is the onset of the photodiode response. This 20 ms delay denotes the delay from when the projector was signaled to present the stimulus to the time the stimulus was actually presented. Three trials are overlaid showing no difference in timing and represents <1 ms jitter. When jitter is present the onset of the individual trials is variable relative to time 0

one can record the absolute timing difference (delay) and use this as a correction factor for the timing of the visual response after data processing. If the variability is high, then one should incorporate the photo-diode in your studies and use the photo-diode signal as the visual stimulus onset trigger for averaging across trials. Variability in visual stimulus presentation can also be minimized by optimizing the timing of stimulus presentation relative to the projector refresh rate. The stimulus onset for visual studies should be a multiple of the refresh rate of your projector so that the signal is received by the projector at the same phase in the refresh cycle (e.g. a 60 Hz refresh rate means stimuli should be presented at multiples of 16 ms). This is also relevant if you are trying to present carefully timed stimuli such as characterizing the frequency response of the visual system. Again, it is best to confirm the actual projector oscillation rate with a photo-diode.

There are two primary types of projectors that are currently being used for MEG studies, liquid-crystal display (LCD) and digital light processing (DLP) projectors. DLP projectors have the best temporal characteristics for MEG studies (low variability (<1 ms), and synchronous color presentation for 3-chip DLP projectors). However, the price of these projectors is often prohibitive. Some LCD projectors also have low variability in stimulus onset from trial-to-trial. Both of these projectors often have a 20–40 ms delay from the time the projector receives the signal to the time the stimulus is presented. A few MEG systems are compatible with using monitors for displaying visual stimuli directly. However, LCD monitors have not been well characterized in terms of timing parameters. Some measurements from our lab suggest that timing jitter can be high in LCD monitors and should be carefully tested.

Another important projector variable to consider is brightness. Many commercially available projectors are designed to project tens to hundreds of feet. The path length from the projector to the screen is ~ 3 m for MEG rooms. This leads to intense lighting for visual studies which can produce significant eye strain. The projector menu may allow for brightness control. An additional option is to buy a neutral density filter that reduces the brightness across all projector settings. While one of the

motivations behind reducing eye strain is to make the experience comfortable for the participants, reducing eye strain also reduces eye movement artifacts and tearing during task performance.

2.3.3 Auditory Equipment

Ear Inserts: MEG labs often use foam ear inserts connected by tubing to Etymotic sound transducers placed between 0.5 and 3 m from the MEG helmet. These sound transducers can be placed within the MSR and generate minimal noise. One advantage of these devices is that the signal is transferred at the speed of light until it reaches the sound transducer. The slower speed of sound ($\sim$0.344 m/ms) will introduce delays in the auditory signal, which need to be accounted for based on the distance to the participant once the signal is converted into a sound wave (length of the tubing from transducer to participant). Other delays and jitter in the auditory stimulus timing can arise from the stimulus computer sound card or speaker electronics. Another consideration with presenting sounds via tubing is that the manufacturer characterizes the sound quality for a specified tube length (the sound will be attenuated with longer tube lengths). Tubing also acts as a filter, thereby limiting the frequency range of the stimuli that can be presented through this setup. Etymotic sound transducers are supplied with a frequency response curve that is calibrated to a recommended tube length and tube characteristic. If different lengths, diameter or rigidity of the tubing are employed additional sound characteristic testing would be required. Unfortunately, MRI-compatible headphones are not feasible for MEG systems because headphones generally do not fit within the MEG helmet.

Speakers: Standard speakers are used in some MEG studies, e.g. (Stephen et al. 2012). However, sound is generated from standard speakers through movement of magnets, therefore, they are not artifact free. Some flat panel speakers generate minimal artifact relative to traditional speakers and maximizing the distance between the speakers and the MEG helmet also reduces the amplitude of the noise. With significant artifact it is important to recognize that speakers are active for the full duration of the auditory stimulus, therefore, it is important to ensure that one can eliminate speaker-generated artifact from MEG data through data processing if the stimuli will be longer than $\sim$50 ms. Finally, speakers within a closed room do not provide the same characteristics as open field sound sources. Sound dampening material on the walls can improve sound characteristics within the confined space.

2.3.4 Somatosensory Equipment

Electrical Stimulation: Direct electrical stimulation of a nerve (e.g. median or tibial nerves) provides temporally precise somatosensory stimulation. Timing of the system can be tested by recording the electrical output used to stimulate the nerves relative to the stimulus trigger. However, electrical stimulation can introduce artifacts. Twisting the wires that travel from the stimulator to the nerve helps to minimize artifact from signal traveling through the wires. Despite these artifacts,

stimulation of nerves provides a reliable stimulus and a very short duration pulse (0.5 ms) can be used to obtain a robust cortical response. Therefore, artifact is limited to a brief period before cortical activation. Finally it is important to recognize that the distance traveled along the peripheral nerve (from the location that the nerve is stimulated to the brain) will induce delays in cortical activation. Unlike auditory and visual systems where differences in the length of the peripheral nerves are, negligible, there is considerable variation in height across participants with systematic differences in height by gender leading to potential group differences. Therefore, recording height from study participants is useful to ensure height differences do not account for group latency differences.

Vibration Stimuli: Tactile devices can be driven with an oscillatory electrical signal to generate a vibration stimulus when placed directly on the skin. This stimulus can provide precise timing for the somatosensory stimulus since the electrical signal is converted directly to vibratory motion. However, these devices generally require that the electrical motor be located close to the skin, again causing varying levels of artifact from the device.

Pneumatic Stimuli: Pneumatic stimuli are often generated by an air puff presented directly to the skin to activate hair sensory receptors or a puff of air filling a balloon to generate a pressure stimulus. The pneumatic stimulus provides a non-threatening somatosensory stimulus for pediatric populations and is artifact-free, if the air regulating device is located outside of the MSR. However a pressure stimulus introduces a significant time delay based on the time that it takes for a pressure stimulus to travel along the plastic tubing from the external air regulator to the participant (approximately the speed of sound). This requires that a pressure transducer be available to assess the time delay of the stimulus relative to the trigger. Also, rigid tubing is essential to preserve the pressure profile across the 3–5 m distance.

2.3.5 Motor Equipment

Equipment used to assess motor function is primarily designed to capture the onset of motor activation. The different types of equipment used in motor paradigms are described below.

Finger lift device (Fig. 3): A finger lift device is often comprised of fiber optic tubing connected to a light source at one end and a photo diode at the other with a break in the middle. Both the light source and the photo diode are located outside the MSR. The trigger is generated either when the light beam is broken or when the light beam is allowed to pass to the photo diode. In any case, breaking or connecting the light beam provides a rapid transition that the photodiode registers and is then converted to a TTL pulse acting as a stimulus trigger. Many systems are designed to trigger either at the time the light beam is interrupted or at the time the light beam passes through unimpeded.

Squeeze ball: A squeeze ball has been used to obtain a larger motor response than the finger lift task and it allows certain patients to perform a motor task who may not have sufficient manual dexterity to perform the finger lift task (e.g. patients

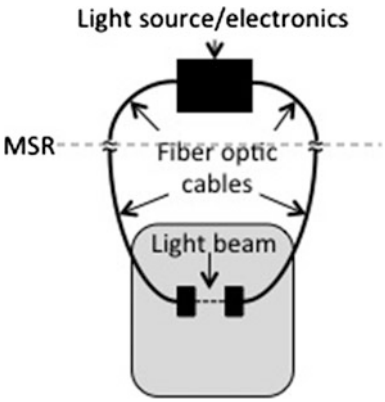

Fig. 3 Example Fiber Optic Motor Apparatus. The light source and electronics that identify triggers are located outside the MSR. The light source is connected to one side of the fiber optic cable loop and the light is delivered back to the electronics through the other side. The hand rests on the motor pad (*grey* platform) and the finger is aligned such that it interrupts the light beam when it is lowered to the motor pad. The electronics can be set to trigger based on the interruption or completion of the light beam across the space on the motor pad

who have suffered a stroke). Onset of motor function in this case, is registered when the ball is squeezed. Release of air or water from the squeeze ball can push an object that in turn breaks a beam of light (e.g. fiber optic cable) or through a sudden change in pressure registered by a pressure transducer (generally located outside the MSR). However, the delay in registering the squeeze can be quite long if the signal is measured by a pressure transducer at the end of the tube located outside the MSR due to the slow speed of a pressure stimulus traveling along a tube. Furthermore, the pressure profile can be quite variable depending on the strength of the squeeze, thereby making it challenging to define a trigger with low jitter.

EMG signal: As mentioned above, bipolar EEG channels can be used to collect EMG signals by placing them on the muscle group of interest (with an appropriate reference location for the second electrode) to capture onset of muscle movement. EMG signal that is recorded simultaneously with the MEG data provides signal with no equipment induced delay or jitter. However, EMG signal can be contaminated by muscle activity that is not of primary interest to the specified task, if the electrodes are not placed correctly or if the participant cannot isolate the movement for task purposes only. Furthermore, the EMG signal needs to be converted to a trigger signal using post-processing methods to indicate movement onset. Varying levels of movement quality (slow vs. fast onset) may also lead to ambiguous movement onset for trigger creation.

Response Devices: MEG systems are generally equipped with artifact-free response devices that record the participant's response during cognitive tasks to collect behavioral reaction times and accuracy. These devices can also be used to signify onset of motion in a finger lift task. See Sect. 2.3.6.

2.3.6 Behavioral Response Devices

It is important to have some type of behavioral response device which is compatible with the MEG system. This allows one to not only obtain behavioral information about how individual participants performed the task, but also provides some confidence that the participants are performing the task, as instructed. While many of the MEG manufacturers provide four button response pads, it is often useful to develop a reaction time device that allows for responses from all fingers. One example of this type of device has been developed by Michael Doty at the Mind Research Network (http://www.mrn.org/collaborate/imaging-equipment/). This is a fully optical system with non-metallic buttons and is also fully compatible with MRI. One particular challenge in developing a noise free response device is finding reliable response buttons that do not have ferromagnetic springs. Yet, it is critically important to ensure that response pads do not generate any noise due to the variability in responses that can and will generate artifacts throughout much of your data set. Also, there should be no significant delay between when the response button is pressed and when the information is registered to the stimulus or acquisition computer. It is also useful to have an ergonomically comfortable device to ensure that participants do not tense their shoulders or become uncomfortable, leading to potential muscle artifacts in the MEG data.

3 Experimental Design Considerations

3.1 Interstimulus Interval (ISI)

One of the important factors to consider when designing an MEG study is determining the rate at which stimuli will be presented. The interstimulus interval (ISI) defines the time between stimuli. This timing parameter must be balanced between keeping the interval between stimuli short to decrease overall task duration and minimize participant fatigue, while optimizing the cortical response for the proposed task. Numerous studies have described the impact of different ISIs on brain function. Rapid ISIs tend to decrease secondary and higher order brain activity and emphasize primary sensory activity (Wikstrom et al. 1996). However, primary sensory activity also decreases with rapid presentation of repetitive stimuli (Hari et al. 1982). In contrast, designing experiments with long ISIs will increase the overall duration of data collection, thereby contributing to participant fatigue. Therefore, a number of factors should be considered when choosing ISI.

1. It is important that stimuli are sufficiently separated in time such that the cortical processing associated with the previous stimulus has ended prior to the presentation of the next trial. For example, the cortical response to median nerve stimulation is complete by $\sim$400 ms after stimulus onset (see Fig. 4).

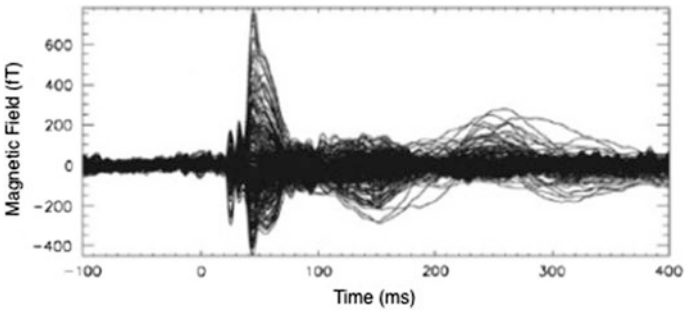

Fig. 4 Somatosensory response to median nerve stimulation. The median nerve stimulation was presented at time (t = 0 ms). The MEG channels are overlaid to show the response across the MEG array. A baseline time interval (−100, 0) is shown prior to stimulus presentation. The response has returned to baseline levels by 400 ms post-stimulus

Therefore, stimuli can be presented every 0.5 s. On the other hand, language stimuli for example evoke a more protracted cortical response (Aine et al. 2005) requiring that the time between stimuli be longer. Therefore, ISI should be determined based on the previous literature or empirical testing of the response across a range of ISIs.

2. The ISI must also include sufficient time to provide a baseline time interval between the offset of the cortical response to the previous stimulus and the onset of the stimulus for the following trial. Due to the natural drift in MEG channel amplitude over time, most MEG studies employ baseline correction during data processing. Therefore, the ISI should be chosen such that the interstimulus interval is greater than the (baseline time interval) + (duration of the cortical response). The duration of the baseline time interval varies depending on the paradigm and the analysis to be performed. Following the example provided in Fig. 4, the baseline time interval chosen for median nerve stimulation is often 100 ms.
3. The duration of stimuli is an important consideration when determining ISI. If a visual stimulus is presented for 1 second, the onset of subsequent visual stimuli must be separated by approximately 1.5 s. This provides sufficient time for the visual off-response and a baseline time interval between stimuli prior to the onset of the next visual stimulus.
4. Varying ISI across trials also helps eliminate anticipatory responses such as the contingent negative variation (CNV) response first identified in EEG studies (Rohrbaugh et al. 1986). Furthermore, introducing variability in the ISI also helps to limit anticipatory behavioral responses during repetitive tasks (participants may respond with a button press prior to stimulus presentation). However, some paradigms require a constant ISI (e.g. studies that specifically focus on understanding the ability to predict stimulus timing). Finally, by varying the ISI, one may help reduce habituation of responses (i.e., a reduction in amplitude across time to a repetitive stimulus presented at a constant ISI).

5. During cognitive tasks it is also important to take reaction times into consideration when determining ISI. It is important to provide sufficient time for the participant to respond prior to the onset of the next trial so that brain activity in the following trial is not contaminated by motor responses from the previous trial. Slower reaction times often associated with patient populations should also be considered. One approach is to allow for dynamic changes in ISI by initiating the next trial as soon as a response is made. However, this may introduce systematic group differences in ISI if a patient group is consistently slower than the control group, leading to an experimental confound as described above.
6. Finally, the number of trials per condition is also a consideration when determining ISI. As described in the signal averaging section below, most stimuli in MEG studies are presented 10–100 s of times to allow for noise reduction through signal averaging. However, the number of trials per condition and the ISI interact to determine the duration of the task. For example, a study with 2 conditions with 100 trials per condition and an average ISI of 1 s will take 3.3 min. If the ISI is doubled, the data collection time will also double (6.6 min). Balancing the number of trials with the ISI helps to optimize signal quality and task duration to ensure participants can provide good quality data and attentive responses throughout data collection.

In summary, it is important to balance timing parameters with other considerations such as participant fatigue and task complexity to obtain high quality MEG data based on the constraints of the experimental paradigm.

3.2 Training the Participant

It is important to allow time for the participant to practice the task for a number of reasons. Once data collection has begun, it is important that the participant feel comfortable with task instructions to minimize the likelihood that data collection needs to be stopped due to confusion over the task. Starting and stopping data collection is problematic and can lead to participant fatigue and frustration as well as introducing variability in data acquisition time across participants. Therefore, it is best to get the participant comfortable with the setup and the stimuli and the required responses prior to data collection. If the experiment is incorporating a behavioral task, one might set a percent correct criterion during the practice session to decide how long the subject practices the task. Depending on access to the machine, practice can occur in the MSR or at a practice computer.

3.3 Habituation

It is also useful to randomize different conditions within an experiment for a number of reasons. First, cortical responses are largest in response to changing stimuli. Using visual stimuli for demonstration purposes, if a participant is expected to look at the exact same visual stimulus over a long period of time, the salience of the stimulus will fade due to the physiology of the visual system. Therefore, if you are testing both left and right visual fields it is best to randomize the left and right stimuli within blocks. This randomization also helps to prevent a shift in gaze away from the fixation point. While it is most common to place a small cross-hair at the location that the participant is supposed to maintain visual fixation, if all of the stimuli are below the visual fixation, for example, participant gaze will tend to shift below the intended fixation point. Randomizing stimuli, such that the average location is at the fixation point, helps to minimize fixation drift. If the experimental design does not allow for full randomization of the location of the stimuli, then it is best to block the stimuli in relatively small blocks and present different locations in blocks of ~ 30 stimuli per location, while presenting as many blocks in a randomized fashion to allow for the desired number of averages. Randomizing the conditions across the entire data collection period also helps to ensure that differences in responses between conditions are not simply due to changes in attention across time. Similar habituation considerations are important for auditory, somatosensory, motor and cognitive paradigms.

3.4 Subject Positioning

It is important to consider the primary areas of interest when positioning the participant in the MEG dewar. For participants with large heads, placement within the dewar will not be a consideration. However, a large number of subjects have significant room to move their head both front and back and side-to-side in the current MEG helmets. It is generally best to try to center the head as much as possible from left to right, unless your hypothesis focuses specifically on a well-documented lateralized response. However, for a basic visual study, you should encourage the participant to move their head back as far as possible and perhaps tilt the head forward a bit to provide additional coverage below the occipital cortex. On the other hand, if you want to focus on orbital frontal cortex, moving the head forward and tilting the head back would be most ideal for optimal coverage of the area of interest.

Furthermore, when the subject has sufficient room in the helmet to move their head around, it is important to provide some mechanism to help maintain head position within the dewar. Placing covered foam pieces on either side of the head near the cheekbones generally works well both in providing the subject with tactile feedback while also maintaining head position. Another alternative for head

stabilization sometimes provided by the MEG manufacturer is an inflatable bladder placed around the head where different sections may be independently inflated. These systems sometimes make the participant hot or uncomfortable.

3.5 Artifact Prevention

Artifacts are one of the most challenging aspects of collecting good quality MEG data. The sources of artifacts include both external and internal factors. External factors include any large ferromagnetic object that moves close (up to 0.5 km away) to the MEG system. That is, elevators, cars, gurneys, chairs, etc. can all generate noise in the MEG system. Fortunately, the noise generated by these examples is very low frequency. This type of noise is problematic if the MEG amplifiers become saturated and leads to data loss. Identification of these artifacts is generally performed by working as a team to monitor MEG activity while another individual observes external activity.

There are also a large number of artifacts that can be associated with the participant. Clearly, it is important that the participant remove all electronic devices before entering the MSR, including cell phones, pagers, watches, etc. The largest problem is with dental work. Permanent bridges are almost invariably too noisy for good quality data. Unfortunately, the frequency range of noise generated from dental work directly overlaps with physiological signal. Therefore, it is challenging to eliminate this noise from the signal without also losing signal of interest. It is also heterogeneous across data collection, making projection techniques such as that used for eyeblinks and heart beat artifact unusable. It is important to ask the participant to take out all removable dental work. Sometimes de-gaussing will work in removing magnetization from permanent dental work. If the participant is a member of a difficult-to-recruit study group, it is important to attempt de-gaussing at least a couple of times. While participants with removable dentures may seem to be ideal subjects, the absence of dentures may lead to more mouth movement and muscle artifact.

Muscle artifact is the next largest contaminant to MEG data. Both eye and mouth movements affect the MEG signal. In general, the magnetic fields generated by muscle movement are much larger than the magnetic fields generated by brain activity. Therefore, necessary muscle movements, such as eye blinks, present a constant problem for MEG. The participant may also have habits that lead to artifacts that include muscle movement such as tensing the jaw or shoulders. Mouth movements can be particularly difficult for MEG since the jaw muscles extend posteriorly across much of the head. This artifact is best identified by asking the subject to consciously tense their jaw or shoulders and then asking the subject to consciously relax while one is observing the continuous MEG signal. Some subjects are tense when they first start a study, but relax once the study begins. If this is a possibility, it is useful to let the subject practice the task to help them settle into the environment.

The other main source of artifacts originates from participant clothing and other accessories. All piercings should be removed prior to data collection unless it is known that the piercing is non-ferromagnetic. Some mascara, makeup, hair dye and finger nail polish can have metallic ingredients. Mascara can generate amplified eye blink artifacts. Breathing artifacts can be seen from a number of different sources. (1) T-shirts with metallic ink in the silk screen; (2) underwire bras; (3) clothes with metallic dyes; and (4) belts. While it is best to encourage participants to come dressed in plain metal-free clothes, an alternative is to provide metal free clothes (e.g. medical scrubs) to participants.

4 Data Preprocessing

4.1 Artifact Removal

The first priority with MEG artifacts is to minimize the contribution of artifacts that contaminate MEG data. As mentioned above, a number of sources of artifacts can be eliminated prior to data collection. However, there are a number of artifacts that cannot be eliminated entirely (e.g. flux jumps, eye blinks, movement artifact, etc.). For the artifacts that remain, there are two competing goals when removing artifacts from data. If the artifact is a large amplitude, rare event, then it is necessary to eliminate it from the signal by removing the trial, since it is very unlikely to be reduced by signal averaging. On the other hand, it is important to maintain as many trials for each condition so that one gains the advantage of signal averaging for low amplitude noise.

The most reliable method for eliminating artifacts (i.e., guarantees that the artifact will be removed without removing any signal of interest) is to eliminate any trials that contain artifacts. If you are able to collect more trials than needed, then trial removal can be performed either using automated or manual methods. For example, eye-blink rejection is often performed by eliminating any trials that contain a signal that exceeds 75 μV in the EOG channel. Additional criteria may be included which only eliminate blinks in the eye channel within a certain time range relative to the stimulus trigger (e.g. eye blinks that occur after the signal of interest). This approach can also be used for large movement artifacts (e.g. cough or shifting position). Often these trials are identified by setting an upper bound on the magnetic field strength ($\sim$2,000 fT) and eliminating trials that exceed that value. However, if one channel is noisy throughout the entire recording, then it is recommended that the channel not be used (turned off/marked bad) for the analysis rather than eliminating bad trials based on this channel.

Additional methods for artifact rejection provide mathematical solutions to artifact rejection. However, these techniques run the risk of eliminating signal as well as noise in the artifact removal process. For example, eye blinks can be identified by using an eye blink template. Whenever a sufficient match is made with the template the magnetic field associated with the template eye blink is

projected out of the data (Uusitalo and Ilmoniemi 1997). This technique can be very useful when eye blinks are relatively homogeneous to maximize the number of trials retained in the average.

Independent components analysis (ICA) has also been used to eliminate artifacts from MEG data. The advantage of ICA is that artifacts should be independent of the brain signal of interest. Therefore the underlying assumption of the method is valid. This technique has been used by many MEG groups (e.g. Vigario et al. 2000; Iwaki et al. 2004; Mantini et al. 2007). However, there are a number of different forms of ICA. Some of the ICA programs separate the data into many components as decided upon by the user. Others separate the data into the same number of components as number of input channels. Either way the actual assignment to any particular independent component is random. Therefore, it is necessary for the investigator to determine a method that identifies artifact versus signal components. Depending on the artifact, this may or may not be obvious.

4.2 Removal of Bad Channels

The choice to remove bad channels is based on two factors. If the channel is bad because of technical difficulties with the SQUID, the noise is clearly not physiological with multiple square wave jumps throughout the dataset. These channels should be eliminated since they do not provide any useful information regarding brain activity and yet can dramatically bias source modeling. The other factor is physiologic noise. Sometimes eye blinks can be found throughout the entire dataset. If none of the above artifact removal options appear to solve the problem, it may be more useful to delete channels that are largely affected by eye blinks. This is done, for example, if you are not interested in activity in brain areas near the eyes. Most, if not all, MEG analysis programs allow you to toggle bad channels on and off. So the data is not deleted, it is just not marked for display and analysis purposes. Again, it is important to balance the two factors of retaining as much information as possible, while also eliminating as much noise from the signal as possible.

4.3 Filtering

The choice of filter settings should be carefully considered. Historically, ERP recording equipment limited the dynamic range of the signal leading to narrow filter settings. Some MEG studies have followed these filter settings since this facilitates direct comparisons with previous ERP work. However, the acquisition equipment for both EEG and MEG is far advanced at this time. Filter settings can be adjusted during post-processing steps and it is recommended that acquisition filters be set as wide as possible. Due to these early filtering restrictions, both slow wave activity and high frequency gamma were not initially reported in ERPs (filtering was often

set with a bandpass of 5–30 Hz). Our results have described the importance of slow wave activity in cognitive tasks (Aine et al. 2003, 2005). Recent EEG and MEG studies have also identified the role of high gamma oscillations in cognitive tasks (Engel et al. 2009; Uhlhaas et al. 2011).

4.4 Averaging

Signal averaging is still the norm for obtaining reliable evoked responses in MEG studies. This requires a trigger from which to average the signals. As described above, these triggers can either be generated by a program that delivers the stimuli to the subject (e.g. trigger pulse sent from Presentation program) or by a device that measures when the stimulus is presented to the subject (e.g. photo-diode). After eliminating any noise sources from individual trials, the trials for each condition are then averaged together. This allows for an increase in signal to noise ratio (SNR) that is approximately equal to $\sqrt{N}$ where N is the number of trials. This relationship is exact in the case of truly Gaussian white noise. It is only approximate in cases where the noise is not truly random as is the case with brain noise. Therefore, if there is a consistent noise source that is time-locked to the stimulus (e.g. the participant always blinks with the presentation of a visual stimulus or artifact from a stimulation device), the signal will not average out.

It is important to check various factors when performing signal averaging. For example, it is useful to compare the averages between the 1st and 2nd half of the recording session or the average of the even versus odd trials. This can be easily automated. It ensures that the average is not biased by the presentation of the first few trials (as in the case of habituation) or by a random noise event that was not eliminated using other artifact removal techniques. It is also important to define a unique trigger for each stimulus condition. It is easy to automate averaging across conditions. However, it is not easy to separate out different conditions after data acquisition, if one does not provide unique triggers for these conditions at the outset. The generally accepted number of averages that are needed to obtain good SNR in most MEG studies is a minimum of 100 trials/condition. This number may be larger or smaller based on the amplitude of the signal of interest. For example the high frequency activity reported by Curio et al. (1997) required thousands of trials to obtain the necessary SNR. On the other hand, inter-ictal epileptic spike activity provides sufficient SNR for single trial analysis in many cases.

Signal averaging has some disadvantages because it assumes that the signal of interest is exactly time-locked to the stimulus and identical on each trial. If these assumptions are not true, the variability from trial to trial will be lost in the averaging process. Time-frequency analysis has provided an additional means to look at activity that is related to the signal and yet not perfectly time-locked with the stimulus (Tallon-Baudry et al. 1996). This method of analysis is especially relevant for high frequency signals such as gamma activity (>30 Hz), since without perfect time-locking this activity will average out based on the rapid oscillation rate.

5 Visual Experiments

5.1 Stimulus Parameters

Stimulus parameters for visual experiments are discussed in more detail in the chapter describing visual studies (Aine et al. this volume). These parameters include but are not limited to: visual stimulus characteristics such as visual contrast, luminance, spatial frequency, size and timing. Below we describe the parameters that one must consider with respect to designing a visual study to provide consistent visual stimulus presentation across participants.

5.2 Ambient Lighting

During visual experiments it is important to maintain similar ambient lighting conditions across participants. Most MSRs include a dialed light switch that allows one to choose a consistent setting across participants for each experiment. The difference in ambient light is important since it changes perceived contrast levels. Differences in contrast cause differences in onset latencies with higher contrast visual stimuli leading to shorter onset latencies (Robson 1966; Campbell and Kulikowski 1972; Okada et al. 1982). It is also important to consider ambient light with regards to stimulus brightness. If the background lighting is turned down, then the perceived brightness will be greater.

5.3 Calculating the Visual Angle

The visual angle of a stimulus can be calculated by measuring the size of the stimulus (size) and the distance from the stimulus to the participant's eyes (dist). Generally, one can use the distance from the stimulus to the participant's nasion as a good approximation. It is important to use identical units when measuring size and distance as well as being aware of whether the output of the inverse tangent function is reported in radians or degrees. Use the following equation for the calculation:

$$\theta = 2 \cdot \tan^{-1}\left(\frac{size}{2 \cdot dist}\right)$$

5.4 Calculating the Cortical Magnification Factor

In order to activate similar amounts of primary visual cortex across different eccentricities, it is important to apply the cortical magnification correction factor. More cortical cells are devoted to the central visual field than to the peripheral visual field. Therefore, to activate equivalent patches of cortex, the peripheral visual stimuli need to be larger than the central visual stimuli. The human cortical magnification factor was most precisely mapped out by Rovamo and Virsu (1979). They provided a cortical magnification factor for stimuli in peripheral field in the nasal, superior, temporal, and inferior directions. They suggest linear interpolation between these four equations when trying to equate activation along other meridians. Horton and Hoyt (1991) derived an equation based on fMRI and occipital lesion studies in humans that provides an approximation for all directions:

$$M_{\mathbf{linear}} = \frac{17.3}{E + 0.75},$$

where, E is the eccentricity in degrees and M is the linear correction factor in mm/degree. This equation agrees well with the dimensions determined for non-human primates while accounting for the larger size of the visual cortex in humans. Horton and Hoyt also provide an areal correction with the assumption that the cortical magnification is isotropic. While this deviates from the results of Rovamo and Virsu, it is perhaps a reasonable approximation for neuroimaging studies as suggested by the agreement of these results with PET and phosphene mapping.

5.5 Measuring Luminance

Matching luminance of the stimuli and background is important to ensure that differences in responses are not generated based on simple luminance changes throughout the experiment. Luminance measures are performed using a light meter and are a measure of the total light output for a part of a stimulus for a given period of time. A full description of how one measures luminance and mean luminance for complex stimuli such as visual gratings is described in detail by Brigell et al. (1998).

5.6 Vision Correction

It is important to have a method to correct for differences in visual acuity across participants since blurred images tend to produce lower amplitude responses and differences in the ability to see the stimuli will lead to differences in task difficulty.

Although vision correction is generally only considered when performing visual studies, it is also advisable to offer vision correction during a nonvisual MEG scan since some individuals get a headache without their glasses. Vision correction can be a challenge in MEG because in adults eyeglass frames do not fit in the MEG dewar and most eyeglasses contain ferrous screws, including glasses with titanium frames. Unless an individual has MRI-safe glasses, wearing glasses will likely cause artifacts. If the participant needs vision correction there are three standard options.

Contact lenses. One option is for the individual to wear contact lenses. However, many individuals blink more frequently with their contact lenses in place. Therefore, it is advisable to have other vision correction options.

Pinhole glasses. A simple option for vision correction is pinhole glasses. If the individual only needs to fixate on a chosen point throughout the task, a single pinhole, in a piece of paper for each eye can be created. This approach addresses difficulties with nearsightedness, farsightedness and astigmatisms. Despite its wide-ranging use, the challenge of attaching the pieces of paper to the participant in such a way that the pinhole remains in place throughout the experiment remains. Often tape is the best option. The drawbacks of this approach are that it can be annoying to participants since it severely limits their field of view and it may be viewed by participants as a low-tech approach to vision correction.

Optical lenses. A complete set of optical corrective lenses can be purchased. These sets include lenses to help account for myopia, hyperopia and astigmatism. The lenses can either be taped to the subject or a device compatible with the MEG system can be designed to hold the lenses in front of the subject. These corrective lenses are also compatible with MRI systems. MRI compatible glasses with interchangeable lenses are also an option; however, they should be tested prior to purchase due to the space limitations of the MEG dewar. The clear advantage of these lenses is that one can match the individual's eyeglass prescription.

5.7 Eye-Tracking

MEG compatible eye-tracking systems are now available commercially. These systems can be an important complement to MEG data collection by providing confirmation of experimental compliance (participant fixates as instructed), testing emotional responses to stimuli by capturing the pupillary diameter, analyzing the participant's eye-movements throughout a task (e.g. quantifying eye-position during a face processing task), or for understanding the eye-control network (saccades). It is important to acquire an MEG-compatible eye-tracker since standard eye-tracking systems use a head-mounted device that does not fit within the MEG helmet. The MEG-compatible systems perform eye-tracking through a remote camera. A couple of factors to consider while designing a study with an eye-tracking system are:

(1) These systems currently require that head position relative to the eye-tracker camera remain constant. These systems require highly restricted head movement similar to MEG systems that do not have head movement compensation.
(2) Vision correction options (e.g. contact lenses) generally eliminate the ability to perform eye-tracking experiments since the corneal reflection is used to quantify the eye-movements and additional reflections interfer with capturing the corneal reflection.
(3) Eye-tracking will fail in a certain number of participants due to a number of factors that inhibit the ability to capture the corneal reflection (e.g. droopy eyelid, amblyopia, etc.).

Therefore, careful selection of participant group and task design is important prior to requiring eye-tracking for a study.

6 Auditory Experiments

6.1 Stimulus Parameters

All auditory parameters can be manipulated using currently available software. In light of the fast temporal processing that occurs in the auditory system including at the cochlear, brainstem and cortical levels, it is important to understand the characteristics of the stimuli that are being presented. Simple tones represent one frequency and can easily be generated in Matlab. However, any sudden onset of a sound represents a square-wave transition and thereby activates frequencies across the frequency spectrum. Therefore, when testing tonotopy or simply reporting that a simple tone was presented, it is important to increase the volume gradually over a short period of time to reduce the 'click' associated with a sudden onset/offset of a sound. This is commonly performed by applying a 10–20 ms amplitude taper to the onset and offset of the tone (e.g. Hanning window). More complex auditory stimuli can also be characterized through a spectrogram to characterize the contribution of an array of frequencies to the sound. To ensure good matching of stimuli across conditions, it is good to match stimuli on the basis of duration, mean amplitude and frequency content.

6.2 Auditory Threshold Testing

Auditory threshold testing should be performed to account for differential hearing loss across participants. This can vary widely in participants at all ages. The testing should be performed at frequencies that characterize the auditory stimuli in the study. If you are using auditory inserts for presenting auditory stimuli, these should be inserted just prior to data collection and auditory thresholding should be performed with the ear inserts in place. The placement of the ear inserts influences the

perceived volume and auditory threshold testing is sensitive to minor adjustments to this placement. If there is a large difference in auditory threshold between ears, it may be related to poor placement in one of the ears. Repositioning and retesting of the auditory threshold is recommended in this case. With a speaker setup, auditory threshold testing can occur at a prior visit, assuming that the volume can be carefully controlled from one visit to the next. The general approach for auditory threshold testing is to present volumes that are well above and well below threshold and have the participant respond to every sound they hear. This requires an adaptive program that continually decreases the interval between the above and below threshold sounds. Randomly presenting tones of different volumes and randomizing the time between stimuli, while working toward the ultimate goal of identifying the threshold helps to eliminate the possibility of false reports.

6.3 Volume Assessment

Volume can be measured using a sound meter. Volume should also be tested with the stimulus program and any sound equipment used, to determine if the actual sound volume is consistent with the expected volume output. For example, the volume increases/decreases by a specified dB level based on programming parameters in the Neurobehavioral systems Presentation software. We have found our system to track well with the expected increases and decreases in sound volume, although the absolute volume is larger than reported. Furthermore, the length of the tubing from the sound transducers/distance from speakers will change the volume level accordingly. The volume should be measured to emulate the conditions of the stimulus. Therefore, if sounds are being presented through ear inserts, the ear inserts should be connected to the sound meter with a piece of tubing at a distance approximately equivalent to the distance to the tympanic membrane. The volume from speakers should be measured with open air access to the sound meter sensor at the approximate location of the participant.

7 Somatosensory Experiments

7.1 Stimulus Parameters

There are three different types of somatosensory stimulation that have been employed in MEG studies: direct nerve stimulation with electric pulse, pressure stimulus generated by a balloon, and vibration stimuli. There are six different tactile receptors in the skin and each of them responds to different types of tactile stimuli (Kandel et al., 2000). Vibration stimuli primarily activate Pacinian corpuscles, whereas multiple receptors likely respond to a pressure stimulus such as a

balloon inflating next to the skin, e.g. Ruffini corpuscles and Merkel receptors, which respond to skin stretch and pressure, respectively.

7.1.1 Direct Nerve Stimulation

Direct nerve stimulation requires that one ensure that the nerve is properly activated by the electrical pulse. Due to differences in skin conductance and other factors, the most common method to ensure proper electrode placement is to position the electrodes and increase the voltage until a known reflex to nerve stimulation occurs (e.g. median nerve stimulation evokes a natural thumb twitch). Some median nerve studies choose a voltage setting relative to the onset of the thumb twitch, whereas other studies simply increase the voltage until the current is first perceived by the participant. The interstimulus interval can be very brief with median nerve stimulation (down to 0.5 s) although shorter ISIs decrease the strength of the later components and longer ISIs lead to a larger contribution from secondary somatosensory cortex (Wikstrom et al. 1996).

7.1.2 Tactile Stimulation

Tactile stimulation is most commonly performed with an air puff achieved by filling an air bladder that is placed directly on the skin. The compressed air must be connected to a device that can control the duration and pressure of the stimulus. There are two parameters that must be considered when designing a tactile experiment: pressure and duration. The pressure is often set around 40 PSI with duration of 20–50 ms to provide time for the balloon to inflate, provide a pressure stimulus, and deflate again (Lauronen et al. 2006). Activation of the somatosensory system through a pressure stimulus takes longer than direct nerve stimulation. Therefore, longer ISIs are recommended ($\geq$1 s).

7.1.3 Vibration Stimulation

Vibration stimuli require a longer duration stimulus and are often used in a pseudo-steady-state design. This is related to the natural oscillatory nature of the stimulus requiring that a sufficient number of cycles are presented to provide a robust response. Rate of oscillation is another variable to consider to ensure that the stimulus is comfortable for the participant.

7.2 Paradigms

Most somatosensory paradigms include simple sensory designs. However, it is good to alternate left and right median nerve stimulation to reduce habituation effects. Additional studies have explored the utility of MEG for further understanding somatosensory processing including: mapping somatotopy (Inoue et al. 2013; Jamali and Ross 2013), understanding the interaction between sensory and motor functioning (Cheyne 2013; Piitulainen et al. 2013), linking pain perception with somatosensory processing (May et al. 2012; Rossiter et al. 2013) and exploring cognitive aspects to somatosensory processing (Moseley et al. 2013; Sun et al. 2013).

8 Motor Assessment

8.1 Stimulus Parameters

An important consideration when designing motor experiments is minimizing motor related artifact. Tasks as simple as pressing a button with an index finger activate a complex set of muscles that can introduce significant stimulus-locked muscle artifact in the MEG dataset. Furthermore, muscle tension from holding the hand or arm in position for movement can lead to muscle tension related artifact. It is advisable to achieve ergonomic positions for the participant to reduce muscle tension during data collection. It is also advisable to ask the participant to remain relaxed throughout data collection. A common approach to identify shoulder tension is to ask the participant to raise their shoulders into a shrug and then relax.

8.2 Paradigms

Motor paradigms focus on capturing the onset of motion with the goal of capturing the activity that initiates the movement. In many cases, it is advisable to cue the participant to initiate movement (e.g. every time the circle appears on the screen, lift your right index finger). Without pacing provided by external stimuli, participants tend to decrease the ISI over time and may decrease it to the point that the motor activity is not easily distinguishable across trials. It is also important to provide concise instructions and allow the participant to practice. Better synchronization across trials is obtained with a precise and rapid finger lift as opposed to slowly lifting the finger. However, other motor tasks may introduce too much muscle artifact and head motion with rapid onset movement. Pilot testing helps to provide guidance on developing novel motor paradigms.

9 Cognitive Paradigms

Due to the large number of cognitive paradigms employed in MEG studies, specific paradigms are not discussed here. However, there are common considerations to keep in mind when developing cognitive paradigms that are described below.

First, it is important to match sensory properties across cognitive conditions to allow one to properly assess cognitive function independent of stimulus parameter differences (as discussed in the chapter by Aine et al. in this volume). For example, in Aine et al. (2006) we performed a passive viewing task and a spatial working memory task using Walsh stimuli. Although the visual stimuli were complex and changed in complexity across trials, the presentation of these stimuli during a passive viewing task allowed us to identify the visual processing components that were independent of the spatial working memory task. Maintaining stimulus characteristics ensures that contrasts between the control and the cognitive condition are not simply related to sensory differences.

Second, cognitive tasks generally require confirmation that the participant is performing the task to a specified accuracy level. Therefore, it is important to find a way to assess whether the participant is performing the task, as instructed. Many investigators require some type of response using a button press, for example. This provides a behavioral correlate (reaction time and percent correct) to the neurophysiological response as well as allowing the investigator to assess whether the participant understands the task and is performing the task throughout data collection. If a behavioral response confounds the task, one strategy is to perform a pre-scan training session and a post-scan questionnaire to determine task compliance. Another strategy is to require the participant to count the number of target stimuli (rare stimuli designed to test compliance).

Third, the timing of the stimuli and the likely variability of the response must be considered, to determine if the cognitive process that one is most interested in studying can be assessed using an MEG study. For example, sentence comprehension occurs over a prolonged time window and comprehension may not occur at the same time relative to the onset of the sentence. One strategy that has been employed is to complete the sentence with a coherent or nonsense word and trigger off of the final word of the sentence (e.g. Maess et al. 2006). This helps to minimize the variability of the cortical response across time, trial and participants.

Finally, a number of strategies have been employed to reduce artifacts that may contaminate the brain response of interest. For example, Tesche and Karhu (2000) employed a fixed temporal pattern during a working memory task. Included in the experimental design was a ‘blink’ command to ensure participant did not contaminate the remainder of the trial with eye blinks. Other strategies include imposing a delayed response to ensure that motor responses do not contaminate cognitive responses to different stimuli. In that case, it is also important to recognize that imposing a delayed response (respond when you hear the ‘beep’ cue) also introduces additional cognitive load into the experiment.

In summary, high temporal resolution provides an exquisite view into the cortical dynamics underlying brain function. However, the variability in cortical response during cognitive tasks can inhibit interpretation. Careful design of the experiment is important to capitalize on the strengths of MEG.

10 Good Practices

There are a number of good practices outlined below that will facilitate good quality data collection. Before beginning a study it is important to pilot test the paradigm to ensure that the behavioral results are as expected. Behavioral testing in a small group of participants is inexpensive and increases the likelihood that the MEG results will be meaningful. The question to be answered is whether the patient group or age group can perform the task to the desired accuracy level. Once the paradigm is established and the stimulus computer has been programmed to present the desired task, stimulus timing evaluation should be performed. Empty room MEG data collection can be performed to test the relative timing of triggers, to verify the number of triggers/condition is correct and to establish the timing of all peripheral devices. One should also check that data is being collected for all relevant channels (including MEG, EEG, bipolar EEG, trigger, and A/D channels), the correct sampling rate is being used, and the correct filter settings are chosen. This is a necessary step that will help prevent the loss of data due to incorrect settings. Finally, it is important to run one or a few pilot test participants to ensure that the expected evoked responses are attained with the paradigm (e.g. auditory M100 is observed when an auditory stimulus is presented, etc.). Once the paradigm is established, it is important to maintain identical stimulus parameters across participants to ensure that sufficiently powered statistical comparisons can be performed at the end of the study. It is also recommended that a naming convention be established at the beginning of the study to ensure consistency across subjects. Our current naming convention includes the SubjectNumber_studyName_Run#_visit#_cont/ave, where studyName is a descriptive name of the paradigm (e.g. audMMN, visP300, spatwm), Run# is the number of a series of runs with the same stimulus conditions if the study population requires breaks during data collection, visit# accounts for longitudinal studies where the same paradigm is collected over multiple time points and cont/ave refers to either a continuous data file or the online average data file. Consistency facilitates auto-analysis pipelines and compilation of data across studies. Finally, record all stimulus settings and data acquisition parameters to ensure that the same conditions can be replicated across participants. This is particularly important in labs where multiple study teams use the same equipment.

Prior to each data collection session it is important to perform a simple test to ensure that the equipment is in the same state as recorded above. For example, confirm stimuli are being presented as expected (you can hear the sound through the auditory inserts, the visual system is functional, etc.). Also, test triggers in the

MEG data to ensure the program is sending triggers through to the data acquisition system. Finally, check the participant response device and confirm that the signals are being received by the stimulus presentation computer and the MEG data acquisition computer.

11 Summary

There are a number of critical factors to consider in properly designing and implementing MEG studies to produce high quality data and to eliminate artifacts that can mislead the interpretation of the results or mask the signal(s) of interest. Identifying sources of artifact and confounding factors prior to data collection can simplify post-processing thereby reducing the number of processing steps needed to obtain good SNR. Being able to reliably identify when stimuli are presented or when events of interest occurred and characterizing confounding activity provides the best means to understand the cortical networks involved in brain function. Finally, establishing good data acquisition procedures to ensure reliable and consistent data collection across participants is imperative to developing generalizable knowledge. With proper experimental design and participant monitoring novel MEG analysis techniques will continue to be developed to capitalize on the rich spatio-temporal datasets obtained with MEG.

References

Aine C, Stephen J, Christner R, Hudson D, Best E (2003) Task relevance enhances early transient and late slow-wave activity of distributed cortical sources. J Comput Neurosci 15:203–221

Aine CJ, Adair JC, Knoefel JE et al (2005) Temporal dynamics of age-related differences in auditory incidental verbal learning. Brain Res Cogn Brain Res 24(1):1–18

Aine CJ, Woodruff CC, Knoefel JE et al (2006) Aging: compensation or maturation? Neuroimage 32(4):1891–1904

Berchicci M, Zhang T, Romero L et al (2011) Development of mu rhythm in infants and preschool children. Dev Neurosci 33(2):130–143

Brigell M, Bach M, Barber C, Kawasaki K, Kooijman A (1998) Guidelines for calibration of stimulus and recording parameters used in clinical electrophysiology of vision. Calibration Standard Committee of the International Society for Clinical Electrophysiology of Vision (ISCEV). Doc Ophthalmol 95(1):1–14

Campbell FW, Kulikowski JJ (1972) The visual evoked potential as a function of contrast of a grating pattern. J Physiol 222(2):345–356

Cheyne DO (2013) MEG studies of sensorimotor rhythms: a review. Exp Neurol 245:27–39

Coffman BA, Kodituwakku P, Kodituwakku EL, et al (2013) Primary visual response (M100) delays in adolescents with FASD as measured with MEG. Hum Brain Mapp 34(11): 2852–2862

Curio G, Mackert BM, Burghoff M et al (1997) Somatotopic source arrangement of 600 Hz oscillatory magnetic fields at the human primary somatosensory hand cortex. Neurosci Lett 234(2–3):131–134

Engel J Jr, Bragin A, Staba R, Mody I (2009) High-frequency oscillations: what is normal and what is not? Epilepsia 50(4):598–604

Flemming L, Wang Y, Caprihan A, Eiselt M, Haueisen J, Okada Y (2005) Evaluation of the distortion of EEG signals caused by a hole in the skull mimicking the fontanel in the skull of human neonates. Clin Neurophysiol 116(5):1141–1152

Grosse P, Cassidy MJ, Brown P (2002) EEG-EMG, MEG-EMG and EMG-EMG frequency analysis: physiological principles and clinical applications. Clin Neurophysiol Off J Int Fed Clin Neurophysiol 113(10):1523–1531

Hamalainen M, Hari R, Ilmoniemi RJ, Knuutila J, Lounasmaa OV (1993) Magnetoencephalography—theory, instrumentation, and applications to noninvasive studies of the working human brain. Rev Mod Phys 65(2):413–497

Hari R, Kaila K, Katila T, Tuomisto T, Varpula T (1982) Interstimulus interval dependence of the auditory vertex response and its magnetic counterpart: implications for their neural generation. Electroencephalogr Clin Neurophysiol 54(5):561–569

Horton JC, Hoyt WF (1991) The representation of the visual field in human striate cortex. A revision of the classic Holmes map. Arch Ophthalmol 109(6):816–824

Inoue K, Nakanishi K, Hadoush H et al (2013) Somatosensory mechanical response and digit somatotopy within cortical areas of the postcentral gyrus in humans: an MEG study. Hum Brain Mapp 34(7):1559–1567

Iwaki S, Yamamoto C, Tonoike M, Yamamoto T (2004) Rejection of stimulus-related MEG artifacts using independent component analysis. Neurol Clin Neurophysiol NCN 2004:17

Jamali S, Ross B (2013) Somatotopic finger mapping using MEG: toward an optimal stimulation paradigm. Clin Neurophysiol 124(8):1659–1670

Kandel E, Schwartz J, Jessell T (2000) Principles of Neural Science, 4th edn. McGraw-Hill, New York

Lauronen L, Nevalainen P, Wikstrom H, Parkkonen L, Okada Y, Pihko E (2006) Immaturity of somatosensory cortical processing in human newborns. Neuroimage 33(1):195–203

Maess B, Herrmann CS, Hahne A, Nakamura A, Friederici AD (2006) Localizing the distributed language network responsible for the N400 measured by MEG during auditory sentence processing. Brain Res 1096(1):163–172

Mantini D, Franciotti R, Romani GL, Pizzella V (2007) Improving MEG source localizations: an automated method for complete artifact removal based on independent component analysis. Neuroimage 34:598–607

May ES, Butz M, Kahlbrock N, Hoogenboom N, Brenner M, Schnitzler A (2012) Pre- and post-stimulus alpha activity shows differential modulation with spatial attention during the processing of pain. Neuroimage 62(3):1965–1974

Moseley RL, Pulvermuller F, Shtyrov Y (2013) Sensorimotor semantics on the spot: brain activity dissociates between conceptual categories within 150 ms. Sci Rep 3:1928

Okada YC, Kaufman L, Brenner D, Williamson SJ (1982) Modulation transfer functions of the human visual system revealed by magnetic field measurements. Vis Res 22(2):319–333

Piitulainen H, Bourguignon M, De Tiege X, Hari R, Jousmaki V (2013) Coherence between magnetoencephalography and hand-action-related acceleration, force, pressure, and electromyogram. Neuroimage 72:83–90

Robson J (1966) Spatial and temporal contrast-sensitivity functions of the visual system. J Opt Soc Am 56:1141–1142

Rohrbaugh JW, McCallum WC, Gaillard AW, Simons RF, Birbaumer N, Papakostopoulos D (1986) ERPs associated with preparatory and movement-related processes. A review. Electroencephalogr Clin Neurophysiol Suppl 38:189–229

Rossiter HE, Worthen SF, Witton C, Hall SD, Furlong PL (2013) Gamma oscillatory amplitude encodes stimulus intensity in primary somatosensory cortex. Front Hum Neurosci 7:362

Rovamo J, Virsu V (1979) An estimation and application of the human cortical magnification factor. Exp Brain Res 37:495–510

Stephen J, Kodituwakku P, Kodituwakku EL et al (2012) Delays in auditory processing identified in preschool children with FASD. Alcohol Clin Exp Res 36(10):1720–1727

Sun ZY, Wang JH, Sun JL et al (2013) Magnetoencephalography assessment of evoked magnetic fields and cognitive function in subcortical ischemic vascular dementia patients. Neurosci Lett 532:17–22

Tallon-Baudry C, Bertrand O, Delpuech C, Pernier J (1996) Stimulus specificity of phase-locked and non-phase-locked 40 Hz visual responses in human. J Neurosci 16(13):4240–4249

Tesche C, Karhu J (2000) Theta oscillations index human hippocampal activation during a working memory task. Proc Natl Acad Sci USA 97(2):919–924

Timmermann L, Gross J, Butz M, Kircheis G, Haussinger D, Schnitzler A (2004) Pathological oscillatory coupling within the human motor system in different tremor syndromes as revealed by magnetoencephalography. Neurol Clin Neurophysiol 2004:26

Timmermann L, Gross J, Dirks M, Volkmann J, Freund HJ, Schnitzler A (2003) The cerebral oscillatory network of parkinsonian resting tremor. Brain 126(Pt 1):199–212

Uhlhaas PJ, Pipa G, Neuenschwander S, Wibral M, Singer W (2011) A new look at gamma? High-(>60 Hz) gamma-band activity in cortical networks: function, mechanisms and impairment. Prog Biophys Mol Biol 105(1–2):14–28

Uusitalo MA, Ilmoniemi RJ (1997) Signal-space projection method for separating MEG or EEG into components. Med Biol Eng Comput 35(2):135–140

Vigario R, Sarela J, Jousmaki V, Hamalainen M, Oja E (2000) Independent component approach to the analysis of EEG and MEG recordings. IEEE Trans Bio-Med Eng 47(5):589–593

Wikstrom H, Huttunen J, Korvenoja A et al (1996) Effects of interstimulus interval on somatosensory evoked magnetic fields (SEFs): a hypothesis concerning SEF generation at the primary sensorimotor cortex. Electroencephalogr Clin Neurophysiol 100(6):479–487

Part II
Source Analysis and Multi-Modal Integration

Magnetoencephalographic Imaging

Srikantan Nagarajan and Kensuke Sekihara

Abstract Non-invasive and dynamic imaging of brain activity in the sub-millisecond time-scale is enabled by measurements on or near the scalp surface using an array of sensors that measure magnetic fields (magnetoencephalography (MEG)) or electric potentials (electroencephalography (EEG)). Algorithmic reconstruction of brain activity from MEG data is referred to as magnetoencephalographic imaging (MEGI). Reconstructing the actual brain response to external events and distinguishing unrelated brain activity has been a challenge for many existing algorithms in this field. Furthermore, even under conditions where there is very little interference, accurately determining the spatial locations and timing of brain sources from MEG data is a challenging problem because it involves solving for unknown brain activity across thousands of voxels from just a few sensors ($\sim$300). In recent years, our research group has developed a suite of novel and powerful algorithms for MEGI that we have shown to be considerably superior to existing benchmark algorithms. Specifically, these algorithms can solve for many brain sources, including sources located far from the sensors, in the presence of large interference from unrelated brain sources. Our algorithms efficiently model interference contributions to sensors, accurately estimate sparse brain source activity using fast and robust probabilistic inference techniques. Here, we review some of these algorithms and illustrate their performance in simulations and real MEG/EEG data. We also briefly how functional connectivity approaches have evolved and are being applied in conjunction with MEG imaging.

Keywords MEG · EEG · Source reconstruction · Forward models · Inverse algorithms · Bayesian methods · Functional connectivity · Group statistics

S. Nagarajan (✉)
Department of Radiology and Biomedical Imaging, University of California,
513 Parnassus Avenue, S362, San Francisco, CA 94143, USA
e-mail: sri@ucsf.edu

K. Sekihara
Department of Systems Design & Engineering, Tokyo Metropolitan University,
Asahigaoka 6-6, Hino, Tokyo 191-0065, Japan

S. Supek and C. J. Aine (eds.), *Magnetoencephalography*,
DOI: 10.1007/978-3-642-33045-2_6, © Springer-Verlag Berlin Heidelberg 2014

1 Introduction

Multiple modalities of non-invasive functional brain imaging have made a tremendous impact in improving our understanding of human auditory cortex. Ever since its advent in 1991, functional magnetic resonance imaging (fMRI) has emerged as the predominant modality for imaging of the functioning brain, for several reasons (Belliveau et al. 1992; Ogawa et al. 1992; Tank et al. 1992). fMRI uses MRI to measure changes in blood oxygenation level-dependent (BOLD) signals due to neuronal activation. It is a safe, non-invasive method that allows for whole-brain coverage, including the ability to examine activity in deep brain structures. Importantly, the widespread availability of commercial and open-source tools for analysis of fMRI data has enabled many researchers to easily embrace this technology. However, since the BOLD signal is only an indirect measure of neural activity and is fundamentally limited by the rate of oxygen consumption and subsequent blood flow mechanism, fMRI lacks the temporal resolution required to image the dynamic and oscillatory spatiotemporal patterns that are associated with cognitive processes. The temporal resolution limitations of fMRI particularly constrain auditory studies because auditory stimuli and responses have inherently fast dynamics that cannot be readily assessed with fMRI. Furthermore, since the BOLD signal is only an approximate, indirect measure of neural activity, it might not accurately reflect true neuronal processes especially in regions of altered vasculature. In fact the exact frequency-band of neuronal processes that corresponds to the BOLD signal is still being actively debated (Logothetis et al. 2001; Niessing et al. 2005). Finally, in the context of auditory studies of speech and language, because fMRI measurements involve loud scans, caused by fast forces on MR gradient coils, the scans themselves will invoke auditory responses that have to be deconvolved from the signals in order to examine external stimulus related activity. Hence, to non-invasively image brain activity on a neurophysiologically relevant timescale and to observe neurophysiological processes more directly, silent imaging techniques are needed that have both high temporal and adequate spatial resolution.

Temporal changes can be non-invasively measured using methods with high (e.g. millisecond) temporal resolution, namely magnetoencephalography (MEG) and electroencephalography (EEG). MEG measures tiny magnetic fields outside of the head that are generated by neural activity. EEG is the measurement of electric potentials generated by neural activity using an electrode array placed directly on the scalp. In contrast to fMRI, both MEG and EEG directly measure electromagnetic (EM) fields emanating from the brain with excellent temporal resolution (<1 ms) and allow the study of neural oscillatory processes over a wide frequency range (at least 1–600 Hz). MEG and EEG also provide complementary information about brain activity because of their differing sensitivity to current sources within the brain. While MEG is primarily sensitive to tangential currents in the brain closer to the surface and insensitive to poor conductive properties of the skull, EEG is primarily sensitive to radial sources while being highly sensitive to

the conductive properties of the brain, skull, and scalp. Since bioelectric currents produced by neurons also generate magnetic fields, which are not distorted by the heterogeneous environment, measurements of these magnetic fields using MEG can be considered to give rise to an undistorted signature of underlying cortical activity. Therefore, MEG and EEG can be viewed as being complementary in terms of the sensitivity to underlying neural activity. In this chapter, a review is initially presented on how brain activity can be reconstructed from MEG measurements with implications for spatial and temporal resolution of such reconstructions.

2 Sensing the Brain's Magnetic Fields

Biomagnetic fields detected by MEG are extremely small, in the tens-to-hundreds of femto-Tesla (fT) range—seven orders of magnitude smaller than the earth's magnetic field, and as a result, appropriate data collection necessitates a magnetically shielded room and highly sensitive detectors—Superconducting quantum interference devices (SQUIDs). The fortuitous anatomical arrangement of cortical pyramidal cells allows the noninvasive detection of their activity by MEG. The long apical dendrites of these cells are arranged perpendicularly to the cortical surface and parallel to each other, allowing their electromagnetic fields to often sum up to magnitudes large enough to detect at the scalp. Synchronously fluctuating dendritic currents result in electric and magnetic dipoles that produce these electromagnetic fields (Nunez and Srinivasan 2006). These dendritic currents from the brain are typically sensed using detection coils called flux transformers or magnetometers, which are positioned closely to the scalp and connected to SQUIDS. SQUIDS act as a magnetic-field-to-voltage converter, and its typically non-linear response is linearized by flux-locked loop electronic circuits, and have a sensitivity of $\sim$10 femto-Tesla per square root of Hz which is adequate for detection of brain's magnetic fields (Vrba and Robinson 2002).

MEG sensors are often configured for differential magnetic field measurements to reduce ambient noise in measurements—which are also referred to as gradiometers, although some MEG systems are also built out of magnetometers and rely on magnetic shielding and clever electronics for noise cancellation. The two commonly used gradiometer configurations are axial and planar gradiometers. Axial gradiometers consist of two coils that share an axis, whereas planar gradiometers measure gradients (or differences) of magnetic fields in a given plane. The sensitivity profile of planar gradiometer sensors is somewhat similar to EEG, whereby a sensor is maximally sensitive to a source closest to it on the cortical surface In contrast however, the sensitivity profile of an axial gradiometer can be somewhat counterintuitive because it is not maximally sensitive to sources closest to the sensors. Both planar and axial gradiometers are sensitive to the orientation of the sources in a counterintuitive manner, similar to EEG sensors.

Modern MEG systems often consist of simultaneous recordings from many differential sensors that cover the whole head, and the total number of sensors varies from 100–300. The advent of such array systems has significantly advanced MEG studies. Typical MEG systems have sensors that are spaced approximately 2.2–3.6 cm apart. Although the maximum sampling rate for many MEG systems is approximately 12 kHz, most MEG data is usually recorded at about 1,000 Hz, thereby still providing excellent temporal resolution for measuring the dynamics of cortical neuronal activity at the millisecond level.

There are many reasons why neuroscientists have embraced MEG. First, MEG setup time is very short and convenient for both experimenters and subjects. A participant or patient can be in the scanner within 10–15 min from entering the laboratory because—unlike EEG—the lengthy time necessary to apply and check electrodes is obviated. Second, the anatomical location of large parts of primary sensory cortices in sulci makes MEG ideally suited for electrophysiological studies in audition. Furthermore, with whole-head sensor arrays, MEG is also well-suited to investigate hemispheric lateralization effects based on sensor waveforms. In contrast to evoked responses measured with EEG, which are maximal at midline electrodes making hemispheric effects difficult to characterize, MEG responses are well lateralized. Distinct groups of MEG sensors are sensitive to lateralized temporal lobe activity that allows for hemisphere-specific assessments.

3 From Sensing to Imaging: The Prerequisites

MEG sensor data analysis only provides qualitative information about underlying brain regions whose activity is observed on the sensor array based on experienced users' intuitions about the sensitivity profile of the sensors. To more precisely interpret observed sensor data in terms of the underlying brain activity, it is possible to reconstruct brain activity from MEG data. Reconstruction of brain activity from MEG data typically involves two major components—a forward model and an inverse model.

3.1 Forward Models Describing Brain Activity and Measurements

The forward model consists of three sub-components—a source model, a volume conductor, and a measurement model. Typical source models assume that the MEG measurements outside the head are generated primarily by electric current dipoles located in the brain. This model is consistent with available measurements of coherent synaptic and intracellular currents in cortical columns that are thought to be major contributors to MEG and EEG signals. Although several more

complex source models have been proposed recently, the equivalent current dipole is still the dominant source model in the literature (Jerbi et al. 2002; Mosher et al. 1999b; Nolte and Curio 2000; von Ellenrieder et al. 2005). Given the distance between the sources in the brain and the sensors outside the head, the dipole is still a reasonable approximation of the sources.

Volume conductor models refer to the equations that govern the relation between the source model and the sensor measurements—i.e. the electric potentials or the magnetic fields. These surface integral equations, obtained by solving Maxwell's equations under quasi-static conditions, can be solved analytically for special geometries of the volume conductor, such as a sphere and ellipsoids. For realistic volume conductors, various numerical techniques such as finite-element and boundary-element methods are employed. These methods are very time consuming and their use may appear impractical in many settings because of the lack of knowledge about specific parameters used in these models (Mosher et al. 1999b).

Measurement models refer to the specific measurement systems used in EEG and MEG including the position of the sensors relative to the head. For instance, different MEG systems measure axial versus planar gradients of the magnetic fields with respect to different locations of reference sensors. The measurement model incorporates such information about the type of measurement and the geometry of the reference sensors. Since MEG sensor arrays are fixed relative to the head of a subject, it is necessary to measure the position of head relative to the sensor array. Typically this is accomplished by attaching head-localization coils to fiducial landmarks on the scalp, passing current through these coils, measuring the magnetic field created by the currents passed, and triangulating to locate the head-position relative to the sensor array. In many MEG systems, head localization is accomplished every 5–10 min because it disrupts normal data collection. Within a block of 10 min, with subjects in a supine position with their heads securely positioned in the array, typically head-movements are found to be less than 5 mm. However, more modern systems are sometimes equipped with continuous head-localization procedures that enable constant updating of sensor locations relative to the head and also correction for subjects' head movements.

The source, volume conductor and measurement models are typically combined and embodied in the idea called the "forward-field" that describes a linear relationship between sources and the measurements. Usually, we assume that the forward-field matrix is known. We can easily calculate the forward field for equivalent electric current dipoles in a spherical volume conductor model for a whole-head axial gradiometer MEG system. In this model, MEG is sensitive only to the tangential component of the primary current dipoles, whereas EEG is sensitive to all components but sensitive to uncertainties in the head model. Simultaneous MEG and EEG can be acquired in most modern MEG systems and require some modification to the forward-field matrix for combined MEG/EEG measurements especially for more realistic source, volume conductor and measurement models.

Co-registration is an integral part of forward model construction. Co-registration involves defining three fiducial points on an individual subject's head surface, which creates a coordinate system that includes the brain and the position of the MEG sensors relative to it. Based on these fiducial landmarks, a transformation matrix is obtained that enables co-registration with the subjects MRI. This allows for the source locations and sensors to be defined in MRI coordinates and enables interpretation of inverse model reconstructions in terms of the underlying brain anatomy provided by MRI.

3.2 Identifying and Reducing Influences from Sources of Noise in MEG

An enduring problem in MEG-based imaging is that the brain responses to sensory or cognitive events is small when compared to the large number of sources of noise, artifacts (biological and non-biological) and interference from spontaneous brain activity unrelated to the sensory or cognitive task of interest. All existing methods for brain source localization are hampered by these many sources of noise present in MEG data. For example, the magnitude of the stimulus-evoked auditory cortical sources are on the order of noise on a single trial, and so typically 75–200 averaged trials are at least needed in order to clearly distinguish the sources above noise. This limits the type of questions that can be asked, and is prohibitive for examining processes such as learning that can occur over just one or several trials. Averaging across trials is time-consuming and therefore difficult for a subject or patient to hold still or pay attention through the duration of the experiment. Gaussian thermal noise or Gaussian electrical noise is also present at the MEG or EEG sensors themselves. Background room interference from power lines and electronic equipment, for example, can be problematic. Biological noise such as heartbeat, eye blink or other muscle artifact can also be present. Ongoing brain activity itself, including the drowsy-state alpha ($\sim$10 Hz) rhythm can drown out evoked brain sources.

Noise in MEG and EEG data is typically reduced by a variety of preprocessing algorithms before being used by source localization algorithms. Simple forms of preprocessing include filtering out frequency bands not containing a brain signal of interest. Additionally and more recently, Independent Component Analysis (ICA) (Delorme and Makeig 2004; Makeig et al. 1997) as well as other blind source separate methods (Parra et al. 2002, 2005; Tang et al. 2002a, b) have been used to remove artifactual components, such as eye blinks. More sophisticated techniques have also recently been developed using graphical models for preprocessing prior to source localization (Nagarajan et al. 2006, 2007). Therefore, algorithms for source localization from MEG and EEG data typically use a two-stage procedure—the first for noise/interference removal and the second for source localization. However, more recent algorithms that integrate interference suppression with source reconstructions have also been proposed and provide for robust source reconstruction (Wipf et al. 2010; Zumer et al. 2007).

4 Inverse Algorithms for Magnetoencephalographic Imaging

Inverse algorithms are used to solve the bioelectromagnetic inverse problem i.e. estimating neural source model parameters from MEG and EEG measurements obtained outside the human head. In general, there are no unique solutions to the inverse problem because there are many source configurations that could result in the sensor observations, even in the absence of noise and infinite spatial or temporal sampling. This non-uniqueness is referred to as the ill-posed nature of the inverse problem. Nevertheless, to get around this non-uniqueness, various estimation procedures incorporate prior knowledge and constraints about source characteristics such as possible source locations, the source spatial extent, the total number of sources or the source frequency/time-frequency characteristics.

Inverse algorithms can be broadly classified into two categories—parametric dipole fitting and non-parametric whole-brain imaging methods. Parametric dipole fitting methods assume that a small set of current dipoles (usually 2–5) can adequately represent some unknown source distribution. In this case, the dipole locations and moments form a set of unknown parameters which are typically found using either a non-linear least square fit or multiple signal classification algorithms (MUSIC) or maximum likelihood estimation methods (Mosher et al. 1999a). Parametric dipole fitting has been successfully used clinically for localization of early sensory responses in somatosensory and auditory cortices. Figure 1 shows an example of parametric dipole localization in the context of somatosensory evoked responses, and shows that responses to early somatosensory peaks can often be localized to activity arising from primary somatosensory cortex located in the central sulcus.

Two major problems exist in dipole fitting procedures. First, due to non-linear optimization there are problems of local minima when more than two dipole parameters are estimated and this is usually manifested by sensitivity to initialization (Huang et al. 1998). Brute-force search methods have a huge computational burden—exponential in the number of parameters (Mosher et al. 1992, 1993). A second, more difficult problem in parametric methods is that often these methods require a priori knowledge of the number of dipoles. Often, such information about model order is not known a priori, especially for complex brain mapping conditions, and the resulting localization of higher-order cortical functions can sometimes be unreliable. Although information theoretic or Bayesian estimation criteria have been proposed to address this problem, the success of these approaches is less clear as these are not widely used (Campi et al. 2011; Kiebel et al. 2008; Sorrentino et al. 2009; Wolters et al. 1999). Nevertheless, many basic neuroscience and clinical studies to date have successfully used dipole-fitting procedures to gain important insights (Aine et al. 2010; Salmelin et al. 1994; Susac et al. 2009).

Non-parametric whole brain imaging is an alternative approach to estimate the inverse problem. The relevant localization problem can be posed as follows. The measured signal is a $d_b \times n$ matrix B, where d_b equals the number of sensors and

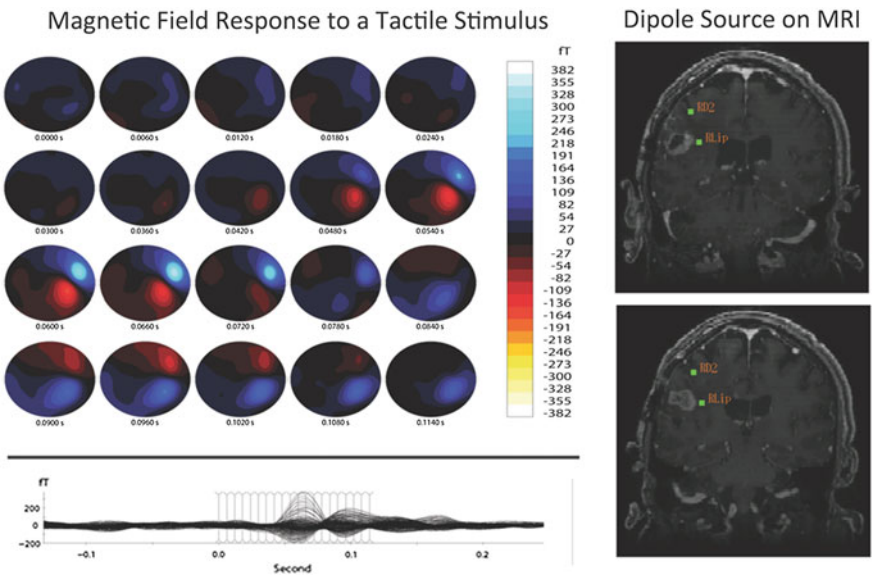

Fig. 1 Example case of parametric dipole localization of separate somatosensory stimulation of the right lip (RLip) and right index finger (RD2). Multiple stimulus trials are performed for each skin stimulation site during MEG recordings. The trials are averaged and a single dipole is reconstructed for each site using the non-linear fit method. The resulting dipoles are then displayed on a co-registered, T1-weighted post-gadolinium coronal MR slice

n is the number of time points at which measurements are made and the unknown sources are given by a $d_s \times n$ matrix S which is the (discretized) amplitude of the source activity at d_s candidate locations obtained from the forward model calculations. In this case, B and S are related by the generative model

$$B = LS + E$$

where L is the composite forward-field matrix that captures the relationship between unit sources all over the brain and the expected pattern of magnetic field measurement on the sensor array. The number of candidate source locations is much larger than the number of sensors ($d_s >> d_b$). Therefore, the problem reduces to estimation of the activity in each source regions, which are reflected by the non-zero rows of the source estimate matrix $\hat{S}$. E is a noise or interference term discussed earlier.

Many whole-brain imaging algorithms impose constraints on source locations i.e. the candidate locations for sources based on anatomical and functional information obtained from other brain imaging modalities. Such constraints within a Bayesian framework are embedded in a prior distribution $p(S)$ either implicitly or explicitly. If under a given experimental or clinical paradigm this $p(S)$ were

somehow known exactly, then the posterior distribution can be computed via Bayes rule:

$$p(S|B) = p(B|S)p(S)/p(B).$$

This distribution contains all possible information about the unknown S conditioned on the observed data B. Two fundamental problems prevent using $p(S|B)$ for source localization. First, for most priors $p(S)$, the normalization distribution $p(B)$ given by

$$p(B) = \int p(B|S)p(S)ds$$

cannot be computed analytically. If only a point estimate for S is desired, rather than a full distribution, then this normalizing distribution may not be needed. For example, a popular estimator is the minimum-norm estimator which involves finding the value of S by assuming that prior $p(S)$ has a Gaussian distribution with a single scalar variance term. This variance is related to the regularization constant in many implementations of the minimum-norm estimator and can be obtained by maximizing the posterior distribution (a.k.a. the MAP estimate) of $p(S|B)$ which is invariant to $p(B)$. Second, and more importantly, we do not actually know the prior $p(S)$ and so some appropriate distribution must be assumed, perhaps based on neurophysiological constraints or computational considerations. In fact, it is this choice, whether implicitly or explicitly specified, that differentiates a wide variety of localization methods (Phillips et al. 1997; Wipf and Nagarajan 2009).

While seemingly quite different in many respects, we recently presented a generalized framework that encompasses different whole-brain imaging methods for source localization and points to intimate connections between algorithms. We showed that many seemingly disparate algorithms for source imaging can be unified using a hierarchical Bayesian modeling framework with a general form of prior distribution, called Gaussian scale mixture, with flexible covariance components, and two different types of inferential procedures. The wide variety of Bayesian source localization methods that fall under this framework can be differentiated by the following factors: (1) selection of covariance component regularization terms; (2) choice of initial covariance component set; (3) optimization method/update rules; and (4) approximation to the lower bound on the marginal likelihood of the data. Bayesian source localization methods demonstrate a number of surprising similarities or out-right equivalences between what might otherwise appear to be very different algorithms. Specifically, from the vantage point of a simple Gaussian scale mixture model with flexible covariance components, our initial work in this area analyzed and extended several broad categories of Bayesian inference directly applicable to source localization including empirical Bayesian approaches, standard MAP estimation, and variational Bayesian (VB) approximations. This perspective leads to explicit connections between many established algorithms and suggests natural extensions for handling unknown dipole orientations, extended

source configurations, correlated sources, temporal smoothness, and computational expediency. Specific imaging methods elucidated under this paradigm include weighted minimum L2-norm, FOCUSS, minimum-L1 norm (also called minimum-current estimation (MCE)), VESTAL, sLORETA, ReML and covariance component estimation, beamforming, Variational Bayes, and Automatic relevance determination (ARD) with multiple sparse priors (MSP). Perhaps surprisingly, all of these methods can be formulated as particular cases of covariance component estimation using different concave regularization terms and optimization rules, making general theoretical analyses and algorithmic extensions/improvements particularly relevant.

These ideas help to bring an insightful perspective to Bayesian source imaging methods, reduce confusion about how different techniques relate to one another, and expand the range of feasible applications. Additionally, there are numerous promising directions for future research, including time-frequency extensions, alternative covariance component parameterizations, and integration with robust interference suppression. These insights allow for continued development of novel algorithms for whole-brain imaging in relation to prior efforts in this enterprise. Figure 2 shows performance in simulations using one such novel algorithm, called Champagne, as well as reconstructions from popular benchmark algorithms for comparisons that highlight their poorer spatial resolution and sensitivity to correlated sources and noise (Owen et al. 2012; Wipf et al. 2010). When compared to ground-truth it can be seen that Champagne is the algorithm that is able to reconstruct the source configuration. Figure 3 shows source reconstructions of auditory evoked responses using called Champagne, and benchmarks algorithms. Auditory evoked responses are challenging datasets because of high degree of correlations between bilateral auditory cortices. In these real datasets from three different subjects, it can also be seen that Champagne is the only algorithm able to reliably reconstruct bilateral auditory cortical activity.

Instead of simultaneous estimation of all sources a popular alternative is to scan the brain and estimate source amplitude at each source location independently. It can be shown that such scanning methods are closely related to whole-brain imaging methods, and the most popular scanning algorithms are adaptive spatial filtering techniques, more commonly referred to as “adaptive beamformers” or just “beamformers” (Sekihara and Nagarajan 2008). Adaptive beamformers have been shown to be quite simple to implement and are powerful techniques for characterizing cortical oscillations and are closely related to other whole-brain imaging methods. However, one major problem with adaptive beamformers is that they are extremely sensitive to the presence of strongly correlated sources. Although they are robust to moderate correlations, in the case of auditory studies, since auditory cortices are largely synchronous in their activity across the two hemisphere, these algorithms tend to perform poor for auditory evoked datasets without workarounds), and many modifications have been proposed for reducing the influence of correlated sources (Dalal et al. 2006). The simplest such work-around is to use half the sensors corresponding to each hemisphere separately, and this approach works surprisingly well for cross-hemispheric interactions. Other

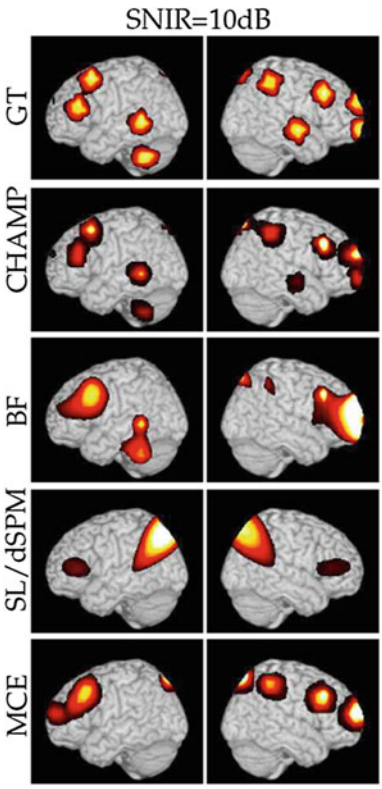

Fig. 2 Localization performance in simulations. A single example of the localization results for 10 clusters (each with 10 dipoles) at SNIR = 10 dB with the vector lead field and real brain-noise. The ground truth (*GT*) location of the clusters are shown for comparison, first *row*. The results with Champagne (*CHAMP*) are shown in the second *row* and the comparison algorithms, minimum-variance adaptive beamformer (*BF*), sLORETA or dSPM (*SL/dSPM*), and generalized minimum-current estimation (*MCE*) are shown in the subsequent *rows*. We project the source power to the surface of a template brain

modifications to the original algorithms have been proposed in the literature that require some knowledge about the location of the correlated source region (Dalal et al. 2006; Quraan and Cheyne 2010). Recently, we have shown that significant improvements in performance can be achieved by modern Bayesian inference algorithms that are closely related to minimum-variance adaptative beamformers and these extensions allow for accurate reconstructions of a large number of sources from typical configurations of MEG sensors (Wipf et al. 2010; Zumer et al. 2007, 2008).

5 Temporal and Spatial Resolution of MEG Imaging

Since MEG data can be acquired at sub-millisecond time-scale, temporal resolution of MEG imaging is only limited by the sampling rate, typically $\sim$1 kHz, and in principle, cortical oscillations can be observed up to 500 Hz. In contrast to its temporal resolution, determining the spatial resolution of MEG imaging is challenging because it is highly dependent on the reconstruction algorithm chosen, as

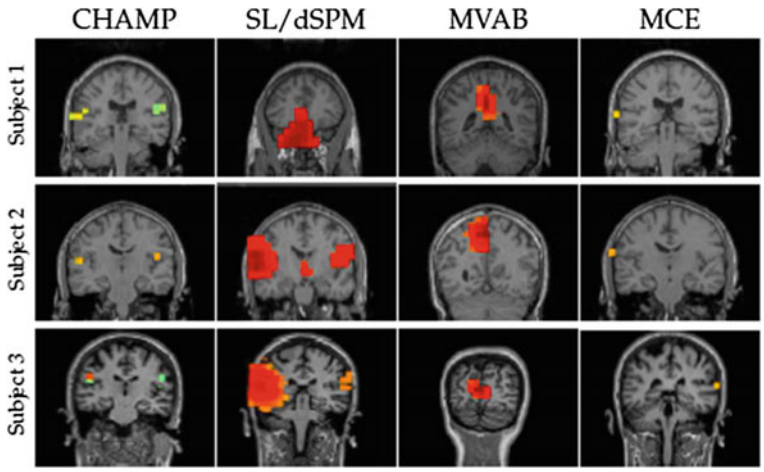

Fig. 3 Auditory evoked field results for 3 subjects for four different benchmark algorithms. Champagne is able to reliably reconstruct bilateral auditory cortex activity in all subjects. SLORETA is only able to do so in two of the three subjects. MVAB fails because of the high-degree of correlations between the two sources. MCE is another sparse reconstruct algorithm that only finds auditory cortex in one hemisphere in each subject

well as a variety of factors such as signal-to-noise and interference-ratio, model formulation, forward-model accuracy, co-registration errors and accuracy of priors (Owen et al. 2012; Wipf et al. 2010). In general, it can be easily shown that the spatial resolution of MEG reconstruction is not limited by sensor spacing, because many adaptive methods can perform better than estimates based on spatial sampling criteria. For instance, while sensor spacing in many axial gradiometer systems is 2.2 cm, reconstruction accuracy can in some cases be as small as 3 mm! In general, co-registration errors alone can be on the order of 3 mm (Roberts et al. 2000). While whole-brain imaging algorithms, such as minimum-norm methods, have poor spatial resolution on the order of a few centimeters, the spatial resolution of adaptive spatial filtering methods, and more recent whole-brain reconstruction methods based on machine learning techniques, are difficult to generally compute because these estimates depend on the data and factors contributing to data quality etc. As a rule of thumb, for typical datasets, these newer methods can reconstruct tens-to-hundreds of sources about 0.5 cm apart (assuming time-frequency separation and detectability) and this can be considered an approximate spatial resolution for MEG, keeping in mind that under certain circumstances the spatial resolution can be even greater (Owen et al. 2012; Wipf et al. 2010).

A common myth, related to the spatial resolution of MEG, is its lack of sensitivity to gyral crown activity and relative insensitivity to deep sources. While it is a fact that for single spherical volume conductor models MEG sensors are insensitive to radially pointing dipoles, this does not necessarily translate to gyral sources. It has been shown that, using realistic volume conductor models (such as

boundary element methods or multiple local-sphere models), some sensitivity to radial sources can be recovered, and that there is no predominant loss of sensitivity to gyral sources (Hillebrand and Barnes 2002). Furthermore, while there is a significant drop in sensitivity to deeper sources because their contributions will fall by approximately the square of the distance to the sensors, recovery of deep sources is an issue of the signal to noise ratio. In general, if high signal-to-noise ratio data are recorded, there is no inherent problem in recovery of deep sources with some of the newer Bayesian reconstruction methods. However, mid-brain sources have two additional problems. First, they may not have dipolar organization due to the architectures and second, the uncertainties in the lead-field increases for deep brain sources, thereby making them more difficult to reconstruct.

6 From Single Subject Reconstructions to Group Level Inference

While the power of MEG imaging is its ability to reconstruct the timing of activation across different frequency bands in single subjects, inferences across subjects require group level statistical analyses (Dalal et al. 2008). The most ubiquitous form of group analysis of MEG studies of auditory cortex are based on parameters, obtained from dipole fitting of typical component peaks in the response, such as timing, amplitude, location and sometimes orientation. For the less common whole-brain imaging and scanning based algorithms, group analysis of data across subjects have typically paralleled similar procedures for whole-brain analysis based on fMRI and PET studies (Singh et al. 2003, 2002). These procedures include spatial normalization to template brains, general-linear modeling of experimental effects, parametric and non-parametric inference procedures, and corrections for multiple comparisons. It is to be noted that group level statistical corrections for multiple comparisons are not yet as well developed for MEG imaging studies as they are for fMRI, and fMRI correction procedures such as family wise error FWE can sometimes be too conservative for MEG reconstructions for a variety of reasons, including the fact that spatial correlations in reconstructed images are higher than in fMRI (Dalal et al. 2008; Darvas et al. 2004; Owen et al. 2012).

7 From Source Activity Imaging to Functional Connectivity Imaging

It is now well recognized in systems and cognitive neuroscience that it is necessary to examine not only activity within an area during an active or inactive state, but also how the brain integrates information *across* multiple regions. The term

functional connectivity essentially defines the complex functional interaction between local and more remote brain areas. Although a common approach is to examine functional connectivity by using hemodynamic measures of brain activity (such as fMRI), MEG directly measures changes in the magnetic field induced by underlying neuronal currents, and is better suited for modeling these types of interactions. Decomposition of information across, space, time, and oscillatory domains yields complex information about how sources in the brain interact across many levels.

Despite the advantage of MEG (and EEG) in the temporal domain over fMRI, there have been relatively few publications that assess event-related or resting-state functional connectivity using MEG or EEG as compared to fMRI. There are two genres of metrics used in MEG functional connectivity: bivariate quantities are calculated in a pair-wise fashion between pairs of voxels and multivariate techniques model the interactions between several regions of interest. Likewise, functional connectivity metrics in MEG data analyses can be applied either in sensor-space or in source-space. Although many metrics have been proposed for functional connectivity in MEG, no careful comparisons have been made for the same dataset across bivariate and multivariate metrics.

7.1 Bivariate Metrics of Functional Connectivity in MEGI

Bivariate metrics can be applied to MEG/EEG data in two ways. Since these metrics are computed between two time courses, they can either be computed between target sensors/voxels or they can be computed between all sensors/voxels and then an average connectivity value can be calculated for every sensor/voxel. The first of these methods is used when there is knowledge about the areas involved and can be considered a "hypothesis-driven" approach. The second, in contrast, can be described as a "data-driven" approach and is applicable when there is not a priori knowledge about which areas should exhibit high or changed connectivity. Correlation and its frequency domain analog, coherence, are the two most commonly used bivariate metrics in the literature (Nunez et al. 1997). An extension of using coherence on sensor time courses, a source localization algorithm called DICS, is particularly designed to construct coherent activity by estimating time course and calculating magnitude coherence (Gross et al. 2001). There are also phase difference-based bivariate metrics that can be applied in similar fashion to the metrics described above. The difference in instantaneous phase between two time courses can be calculated using the Hilbert transform. There are different subsequent calculations that can be performed with the phase difference, e.g. phase coherence (PC), phase synchronization, index of synchronization.

All types of bivariate metrics are susceptible to spurious interactions that arise from volume conduction artifacts in MEG and EEG recordings. The magnetic field or electric potential generated by a single neuronal source is picked up by not only the nearest sensor to the source, but the neighboring sensors also pick up the signal

with a zero-time lag. This creates instantaneous blurring across the sensors. As such, the time courses of many sensors can contain overlapping information due to this electromagnetic phenomenon, which can produce spurious interactions. Some bivariate metrics used for MEG and EEG functional connectivity analyses have been designed to overcome this blurring by isolating the non-zero-time-lag interactions from the zero-time-lag interactions, namely imaginary coherence (IC) and phase lag index (PLI). Both metrics are designed to assess only non-zero time lagged interactions in source or sensor data in order to cancel out the effects of cross-talk across the detection sensors.

Imaginary coherence is calculated by only considering the imaginary component of the complex-valued coherence. The imaginary part of the coherence is produced by non-instantaneous interactions between waveforms. It was found to be a better measure of coupling than the magnitude of coherence in an EEG experiment of voluntary finger movement (Nolte et al. 2004). PLI is similar to IC in that it includes only information that is transmitted at a non-zero time lag; any two signals that are instantaneously coupled and therefore have a phase difference of zero, are not included in the calculation of PLI. PLI and PC of EEG and MEG data were more sensitive than IC to increasing levels of true synchronization in the simulated data, but IC and PLI were less susceptible to spurious correlations in the data due to common sources (Stam et al. 2007). In addition, PLI and IC were better able to detect beta band connectivity and uncovered a different spatial pattern of connectivity in the MEG data. IC has also revealed significant changes in the over all resting-state connectivity induced by brain lesions (de Pasquale et al. 2010, 2012; Guggisberg et al. 2007; Martino et al. 2011; Marzetti et al. 2013; Tarapore et al. 2012; Hipp et al. 2011, 2012) (Fig. 4).

7.2 Multivariate Connectivity Metrics in MEG

In contrast to bivariate metrics, which compute relationships between elements in a pair-wise fashion, multivariate metrics are able to model interactions between multiple areas in a single model (Astolfi et al. 2005). While powerful, computational complexity is an issue when performing a multivariate analysis. While all areas can be modeled simultaneously, the limitation of these methods lies in maintaining the necessary condition that the number of parameters fit in the model does not exceed the number of time points. This is done by considering fewer areas or voxels or by limiting the number of lags the model will analyze. Multivariate autoregressive models (MVAR) can be applied in the time domain, or in the frequency domain, as is the case with partial directed coherence and direct transfer function methods. Although some of these methods have been demonstrated to be powerful in determining neural networks associated with basic sensory processing (Porcaro et al. 2009). Future studies will determine how these metrics can be extended to examinations of impairments in cognitive function in a variety of clinical populations.

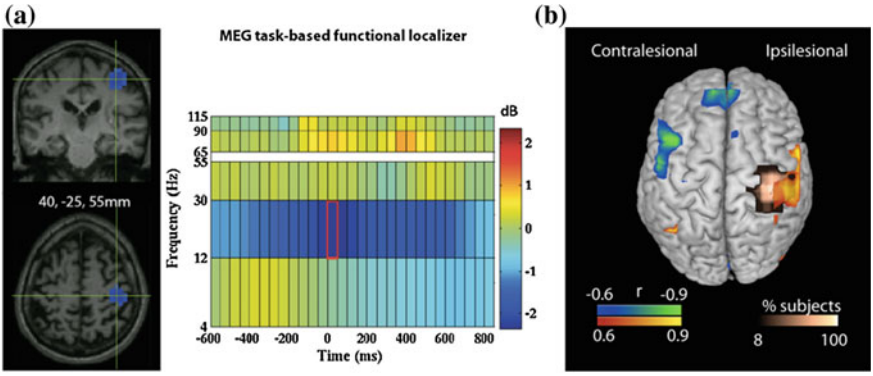

Fig. 4 Activation and Functional Connectivity in Stroke. **a** Activation of motor cortex and its associated time-frequency plot of the voxel of maximal power change in the beta frequency band during affected finger button press. **b** Results of the correlation analysis between baseline resting MEGI functional connectivity and recovery scores. *Gold* indicates the location of the lesion and activated motor cortex. *Blue* indicates negative correlations. *Red* indicates positive correlations. Strong ipsilesional connectivity predicts recovery (Westlake et al. 2012)

Nevertheless, already in these early days of functional connectivity analyses, it has been shown to have profound clinical significance as disturbances in networks as manifested as abnormalities in functional connecting even during resting state. Recent studies have shown this to be the case in many clinical conditions such as brain tumor, schizophrenia, stroke, and developmental disorders (Bartolomei et al. 2006a, b; Bosma et al. 2008a, b). For example, neurocognitive effects are correlated with functional connectivity changes in brain tumor patients, especially in patients with low-grade gliomas (Douw et al. 2008, 2009, 2010; van Dellen et al. 2012). Similarly, combining activation mapping and resting-state functional connectivity can help predict functional recovery in stroke. Therefore, mapping functional connectivity and combining this information with brain activation studies may be an important component in surgical planning and clinical diagnosis in a variety of disorders (Martino et al. 2011; Tarapore et al. 2012).

8 Conclusions

Great strides have occurred in the development of novel and powerful algorithms for MEG imaging. These algorithmic approaches not only enable more accurate reconstruction of brain activity, their time courses and spectral power fluctuations, but also enable us to examine functional connectivity between different brain regions from MEG data. These efforts pave the way novel and powerful applications for MEG imaging in many basic and clinical neuroscience studies of neural oscillations in the human brain.

References

Aine CJ, Bryant JE, Knoefel JE, Adair JC, Hart B, Donahue CH, Montano R, Hayek R, Qualls C, Ranken D, Stephen JM (2010) Different strategies for auditory word recognition in healthy versus normal aging. Neuroimage 49:3319–3330

Astolfi L, Cincotti F, Mattia D, Babiloni C, Carducci F, Basilisco A, Rossini PM, Salinari S, Ding L, Ni Y, He B, Babiloni F (2005) Assessing cortical functional connectivity by linear inverse estimation and directed transfer function: simulations and application to real data. Clin Neurophysiol 116:920–932

Bartolomei F, Bosma I, Klein M, Baayen JC, Reijneveld JC, Postma TJ, Heimans JJ, Van Dijk BW, De Munck JC, De Jongh A, Cover KS, Stam CJ (2006a) Disturbed functional connectivity in brain tumour patients: evaluation by graph analysis of synchronization matrices. Clin Neurophysiol 117:2039–2049

Bartolomei F, Bosma I, Klein M, Baayen JC, Reijneveld JC, Postma TJ, Heimans JJ, Van Dijk BW, De Munck JC, De Jongh A, Cover KS, Stam CJ (2006b) How do brain tumors alter functional connectivity? A magnetoencephalography study. Ann Neurol 59:128–138

Belliveau JW, Kwong KK, Kennedy DN, Baker JR, Stern CE, Benson R, Chesler DA, Weisskoff RM, Cohen MS, Tootell RB et al (1992) Magnetic resonance imaging mapping of brain function. Human visual cortex. Invest Radiol 27(Suppl 2):S59–S65

Bosma I, Douw L, Bartolomei F, Heimans JJ, Van Dijk BW, Postma TJ, Stam CJ, Reijneveld JC, Klein M (2008a) Synchronized brain activity and neurocognitive function in patients with low-grade glioma: a magnetoencephalography study. Neuro Oncol 10:734–744

Bosma I, Stam CJ, Douw L, Bartolomei F, Heimans JJ, Van Dijk BW, Postma TJ, Klein M, Reijneveld JC (2008b) The influence of low-grade glioma on resting state oscillatory brain activity: a magnetoencephalography study. J Neurooncol 88:77–85

Campi C, Pascarella A, Sorrentino A, Piana M (2011) Highly automated dipole estimation (HADES). Comput Intell Neurosci 2011:982185

Dalal SS, Guggisberg AG, Edwards E, Sekihara K, Findlay AM, Canolty RT, Berger MS, Knight RT, Barbaro NM, Kirsch HE, Nagarajan SS (2008) Five-dimensional neuroimaging: localization of the time-frequency dynamics of cortical activity. Neuroimage 40:1686–1700

Dalal SS, Sekihara K, Nagarajan SS (2006) Modified beamformers for coherent source region suppression. IEEE Trans Biomed Eng 53:1357–1363

Darvas F, Pantazis D, Kucukaltun-Yildirim E, Leahy RM (2004) Mapping human brain function with MEG and EEG: methods and validation. Neuroimage 23(Suppl 1):S289–S299

De Pasquale F, Della Penna S, Snyder AZ, Lewis C, Mantini D, Marzetti L, Belardinelli P, Ciancetta L, Pizzella V, Romani GL, Corbetta M (2010) Temporal dynamics of spontaneous MEG activity in brain networks. Proc Natl Acad Sci U S A 107:6040–6045

De Pasquale F, Della Penna S, Snyder AZ, Marzetti L, Pizzella V, Romani GL, Corbetta M (2012) A cortical core for dynamic integration of functional networks in the resting human brain. Neuron 74:753–764

Delorme A, Makeig S (2004) EEGLAB: an open source toolbox for analysis of single-trial EEG dynamics including independent component analysis. J Neurosci Methods 134:9–21

Douw L, Baayen H, Bosma I, Klein M, Vandertop P, Heimans J, Stam K, De Munck J, Reijneveld J (2008) Treatment-related changes in functional connectivity in brain tumor patients: a magnetoencephalography study. Exp Neurol 212:285–290

Douw L, Baayen JC, Klein M, Velis D, Alpherts WC, Bot J, Heimans JJ, Reijneveld JC, Stam CJ (2009) Functional connectivity in the brain before and during intra-arterial amobarbital injection (Wada test). Neuroimage 46:584–588

Douw L, Van Dellen E, Baayen JC, Klein M, Velis DN, Alpherts WC, Heimans JJ, Reijneveld JC, Stam CJ (2010) The lesioned brain: still a small-world? Front Hum Neurosci 4:174

Gross J, Kujala J, Hamalainen M, Timmermann L, Schnitzler A, Salmelin R (2001) Dynamic imaging of coherent sources: studying neural interactions in the human brain. Proc Natl Acad Sci U S A 98:694–699

Guggisberg AG, Honma SM, Findlay AM, Dalal SS, Kirsch HE, Berger MS, Nagarajan SS (2007) Mapping functional connectivity in patients with brain lesions. Ann Neurol 63(2):193–203

Hillebrand A, Barnes GR (2002) A quantitative assessment of the sensitivity of whole-head MEG to activity in the adult human cortex. Neuroimage 16:638–650

Hipp JF, Engel AK, Siegel M (2011) Oscillatory synchronization in large-scale cortical networks predicts perception. Neuron 69:387–396

Hipp JF, Hawellek DJ, Corbetta M, Siegel M, Engel AK (2012) Large-scale cortical correlation structure of spontaneous oscillatory activity. Nat Neurosci 15:884–890

Huang M, Aine CJ, Supek S, Best E, Ranken D, Flynn ER (1998) Multi-start downhill simplex method for spatio-temporal source localization in magnetoencephalography. Electroencephalogr Clin Neurophysiol 108:32–44

Jerbi K, Mosher JC, Baillet S, Leahy RM (2002) On MEG forward modelling using multipolar expansions. Phys Med Biol 47:523–555

Kiebel SJ, Daunizeau J, Phillips C, Friston KJ (2008) Variational Bayesian inversion of the equivalent current dipole model in EEG/MEG. Neuroimage 39:728–741

Logothetis NK, Pauls J, Augath M, Trinath T, Oeltermann A (2001) Neurophysiological investigation of the basis of the fMRI signal. Nature 412:150–157

Makeig S, Jung TP, Bell AJ, Ghahremani D, Sejnowski TJ (1997) Blind separation of auditory event-related brain responses into independent components. Proc Natl Acad Sci U S A 94:10979–10984

Martino J, Honma SM, Findlay AM, Guggisberg AG, Owen JP, Kirsch HE, Berger MS, Nagarajan SS (2011) Resting functional connectivity in patients with brain tumors in eloquent areas. Ann Neurol 69:521–532

Marzetti L, Della Penna S, Snyder AZ, Pizzella V, Nolte G, De Pasquale F, Romani GL, Corbetta M (2013) Frequency specific interactions of MEG resting state activity within and across brain networks as revealed by the multivariate interaction measure. Neuroimage 79:172–183

Mosher JC, Baillet S, Leahy RM (1999a) EEG source localization and imaging using multiple signal classification approaches. J Clin Neurophysiol 16:225–238

Mosher JC, Leahy RM, Lewis PS (1999b) EEG and MEG: forward solutions for inverse methods. IEEE Trans Biomed Eng 46:245–259

Mosher JC, Lewis PS, Leahy RM (1992) Multiple dipole modeling and localization from spatio-temporal MEG data. IEEE Trans Biomed Eng 39:541–557

Mosher JC, Spencer ME, Leahy RM, Lewis PS (1993) Error bounds for EEG and MEG dipole source localization. Electroencephalogr Clin Neurophysiol 86:303–321

Nagarajan SS, Attias HT, Hild KE 2nd, Sekihara K (2006) A graphical model for estimating stimulus-evoked brain responses from magnetoencephalography data with large background brain activity. Neuroimage 30:400–416

Nagarajan SS, Attias HT, Hild KE 2nd, Sekihara K (2007) A probabilistic algorithm for robust interference suppression in bioelectromagnetic sensor data. Stat Med 26(21):3886–3910

Niessing J, Ebisch B, Schmidt KE, Niessing M, Singer W, Galuske RA (2005) Hemodynamic signals correlate tightly with synchronized gamma oscillations. Science 309:948–951

Nolte G, Bai O, Wheaton L, Mari Z, Vorbach S, Hallett M (2004) Identifying true brain interaction from EEG data using the imaginary part of coherency. Clin Neurophysiol 115:2292–2307

Nolte G, Curio G (2000) Current multipole expansion to estimate lateral extent of neuronal activity: a theoretical analysis. IEEE Trans Biomed Eng 47:1347–1355

Nunez PL, Srinivasan R (2006) A theoretical basis for standing and traveling brain waves measured with human EEG with implications for an integrated consciousness. Clin Neurophysiol 117:2424–2435

Nunez PL, Srinivasan R, Westdorp AF, Wijesinghe RS, Tucker DM, Silberstein RB, Cadusch PJ (1997) EEG coherency. I: statistics, reference electrode, volume conduction, Laplacians, cortical imaging, and interpretation at multiple scales. Electroencephalogr Clin Neurophysiol 103:499–515

Ogawa S, Tank DW, Menon R, Ellermann JM, Kim SG, Merkle H, Ugurbil K (1992) Intrinsic signal changes accompanying sensory stimulation: functional brain mapping with magnetic resonance imaging. Proc Natl Acad Sci U S A 89:5951–5955

Owen JP, Wipf DP, Attias HT, Sekihara K, Nagarajan SS (2012) Performance evaluation of the Champagne source reconstruction algorithm on simulated and real M/EEG data. Neuroimage 60:305–323

Parra L, Alvino C, Tang A, Pearlmutter B, Yeung N, Osman A, Sajda P (2002) Linear spatial integration for single-trial detection in encephalography. Neuroimage 17:223–230

Parra LC, Spence CD, Gerson AD, Sajda P (2005) Recipes for the linear analysis of EEG. Neuroimage 28:326–341

Phillips JW, Leahy RM, Mosher JC, Timsari B (1997) Imaging neural activity using MEG and EEG. IEEE Eng Med Biol Mag 16:34–42

Porcaro C, Zappasodi F, Rossini PM, Tecchio F (2009) Choice of multivariate autoregressive model order affecting real network functional connectivity estimate. Clin Neurophysiol 120:436–448

Quraan MA, Cheyne D (2010) Reconstruction of correlated brain activity with adaptive spatial filters in MEG. Neuroimage 49:2387–2400

Roberts TP, Ferrari P, Perry D, Rowley HA, Berger MS (2000) Presurgical mapping with magnetic source imaging: comparisons with intraoperative findings. Brain Tumor Pathol 17:57–64

Salmelin R, Hari R, Lounasmaa OV, Sams M (1994) Dynamics of brain activation during picture naming. Nature 368:463–465

Sekihara K, Nagarajan SS (2008) Adaptive spatial filters for electromagnetic brain imaging Springer, Heidelberg

Singh KD, Barnes GR, Hillebrand A (2003) Group imaging of task-related changes in cortical synchronisation using nonparametric permutation testing. Neuroimage 19:1589–1601

Singh KD, Barnes GR, Hillebrand A, Forde EM, Williams AL (2002) Task-related changes in cortical synchronization are spatially coincident with the hemodynamic response. Neuroimage 16:103–114

Sorrentino A, Parkkonen L, Pascarella A, Campi C, Piana M (2009) Dynamical MEG source modeling with multi-target Bayesian filtering. Hum Brain Mapp 30:1911–1921

Stam CJ, Nolte G, Daffertshofer A (2007) Phase lag index: assessment of functional connectivity from multi channel EEG and MEG with diminished bias from common sources. Hum Brain Mapp 28:1178–1193

Susac A, Ilmoniemi RJ, Pihko E, Nurminen J, Supek S (2009) Early dissociation of face and object processing: a magnetoencephalographic study. Hum Brain Mapp 30:917–927

Tang AC, Pearlmutter BA, Malaszenko NA, Phung DB (2002a) Independent components of magnetoencephalography: single-trial response onset times. Neuroimage 17:1773–1789

Tang AC, Pearlmutter BA, Malaszenko NA, Phung DB, Reeb BC (2002b) Independent components of magnetoencephalography: localization. Neural Comput 14:1827–1858

Tank DW, Ogawa S, Ugurbil K (1992) Mapping the brain with MRI. Curr Biol 2:525–528

Tarapore PE, Martino J, Guggisberg AG, Owen J, Honma SM, Findlay A, Berger MS, Kirsch HE, Nagarajan SS (2012) Magnetoencephalographic imaging of resting-state functional connectivity predicts postsurgical neurological outcome in brain gliomas. Neurosurgery 71:1012–1022

Van Dellen E, Douw L, Hillebrand A, Ris-Hilgersom IH, Schoonheim MM, Baayen JC, De Witt Hamer PC, Velis DN, Klein M, Heimans JJ, Stam CJ, Reijneveld JC (2012) MEG network differences between low- and high-grade glioma related to epilepsy and cognition. PLoS ONE 7:e50122

Von Ellenrieder N, Muravchik CH, Nehorai A (2005) MEG forward problem formulation using equivalent surface current densities. IEEE Trans Biomed Eng 52:1210–1217

Vrba J, Robinson SE (2002) SQUID sensor array configurations for magnetoencephalography applications. Supercond Sci Technol 15:51–89

Westlake KP, Hinkley LB, Bucci M, Guggisberg AG, Byl N, Findlay AM, Henry RG, Nagarajan SS (2012) Resting state alpha-band functional connectivity and recovery after stroke. Exp Neurol 237:160–169

Wipf D, Nagarajan S (2009) A unified Bayesian framework for MEG/EEG source imaging. Neuroimage 44(3):947–966

Wipf DP, Owen JP, Attias HT, Sekihara K, Nagarajan SS (2010) Robust Bayesian estimation of the location, orientation, and time course of multiple correlated neural sources using MEG. Neuroimage 49:641–655

Wolters CH, Beckmann RF, Rienacker A, Buchner H (1999) Comparing regularized and non-regularized nonlinear dipole fit methods: a study in a simulated sulcus structure. Brain Topogr 12:3–18

Zumer JM, Attias HT, Sekihara K, Nagarajan SS (2007) A probabilistic algorithm integrating source localization and noise suppression for MEG and EEG data. Neuroimage 37(1):102–115

Zumer JM, Attias HT, Sekihara K, Nagarajan SS (2008) Probabilistic algorithms for MEG/EEG source reconstruction using temporal basis functions learned from data. Neuroimage 41:924–940

MEG and Multimodal Integration

Seppo P. Ahlfors

Abstract Functional brain imaging methods provide measures of various physiological processes with a range of spatial and temporal scales. Because the sensitivity properties of the imaging modalities differ, combining multimodal data is expected to provide more information about the brain activity than is available by a single method. In direct data fusion, multimodal data can be described as complementary or supportive. Complementary modalities have the same type of sources, such as electroencephalography (EEG) and magnetoencephalography (MEG), which are both generated by cortical primary currents, but with different sensitivity characteristics. Combination of EEG and MEG data can resolve ambiguities in data from only one of the modalities. In a supportive role data from one imaging modality guides the analysis and interpretation of another modality. Structural magnetic resonance imaging (MRI) provides supportive data for MEG source estimation, e.g., by indicating allowable locations and orientations of MEG source currents. Functional MRI (fMRI) can be used in a supportive role to suggest a likely source distribution for MEG among multiple alternatives. MEG and fMRI can also be considered complementary if the different source types, i.e., primary currents for MEG and blood oxygenation level dependent (BOLD) contrast for fMRI, are both derived from a common physiological model.

Keywords Magnetoencephalography (MEG) · Electroencephalography (EEG) · Functional magnetic resonance imaging (fMRI) · Multimodal · Data fusion

S. P. Ahlfors (✉)
Department of Radiology, MGH/HST Athinoula A. Martinos Center for Biomedical Imaging, Massachusetts General Hospital, 149, 13th Street, Mail Code 149-2301, Charlestown, MA 02129, USA
e-mail: seppo@nmr.mgh.harvard.edu

S. P. Ahlfors
Harvard-MIT Division of Health Sciences and Technology, Cambridge, MA, USA

S. Supek and C. J. Aine (eds.), *Magnetoencephalography*,
DOI: 10.1007/978-3-642-33045-2_7,

1 Introduction

Different functional neuroimaging methods, often called imaging modalities, provide information about a variety of physiological processes related to brain activity, and have a range of spatial and temporal sensitivity characteristics (He and Liu 2008). Magnetoencephalography (MEG) and electroencephalography (EEG) detect electrical activity in the brain with millisecond temporal spatial resolution, but the inverse problem of determining the spatial distribution of the activity is challenging, and the accuracy depends among other things on the overall pattern of activity (Michel et al. 2009; Hansen et al. 2010). Functional magnetic resonance imaging (fMRI), positron emission tomography (PET), single-photon emission computed tomography (SPECT), and optical near infrared spectroscopy (NIRS) detect hemodynamic phenomena; the time-resolution of these methods is limited by the relatively slow hemodynamic response. However, fMRI can provide millimeter-scale spatial resolution across the whole brain, without the kind of ambiguities inherent in the MEG and EEG source localization. The different sensitivity properties of the imaging modalities suggest that multimodal imaging can provide more information about brain function than is attainable by any single method alone.

In MEG, superconducting quantum interference device (SQUID) sensors are used to measure extracranial magnetic fields generated by neuroelectric currents in the brain (Cohen 1972). The main sources of the MEG signals are post-synaptic dendritic currents in cortical pyramidal cells (Lopes da Silva 2010). From the measured spatial pattern for the magnetic field outside the head, the spatiotemporal pattern of sources within the brain can be estimated (Ahlfors and Hämäläinen 2012). Both MEG and EEG originate from the same type of physiological sources, described as primary currents (Tripp 1983). The spatial sensitivity patterns to the primary currents are different for MEG and EEG, allowing them to provide complementary information about the same type of sources. In contrast, the physiological sources of fMRI (commonly the blood oxygenation level depend or BOLD contrast) and other hemodynamic signals are of a different type from those of MEG and EEG, thereby presenting various opportunities and challenges for multimodal imaging.

According to Horwitz and Poeppel (2002), three main approaches to combining data from multiple neuroimaging modalities are: converging evidence, direct data fusion, and computational neural modeling. Comparison of separately obtained results from different modalities to establish converging spatial or temporal patterns of brain activation is useful for the assessment of the obtained results, e.g., in clinical pre-surgical mapping studies. Many studies have examined the convergence of MEG and fMRI results, including (Beisteiner et al. 1995; Morioka et al. 1995; Sanders et al. 1996; Stippich et al. 1998; Inoue et al. 1999; Woldorff et al. 1999; Del Gratta et al. 2002; Mathiak et al. 2002; Singh et al. 2002; Moradi et al. 2003; Tuunanen et al. 2003; Rossini et al. 2004; Vartiainen et al. 2011; Swettenham et al. 2013); see also the reviews (Mathiak and Fallgatter 2005; Poline et al. 2010).

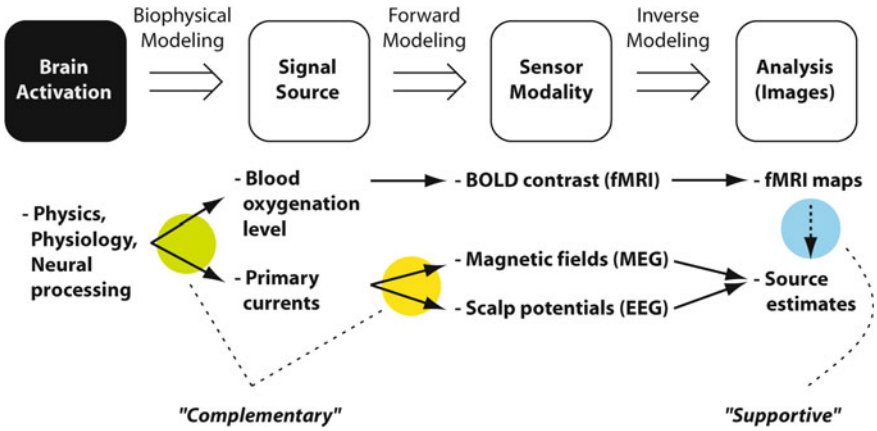

Fig. 1 Schematic diagram of stages involved in the construction of functional brain images. Biophysical modeling can be used to relate the physical and physiological neural processes associated with brain activation to the underlying sources of the brain imaging signals. Forward modeling describes the signal patterns generated by a given source distribution. Inverse modeling involves the estimation of the source distribution on the basis of the recorded signals. MEG and EEG record "complementary" (*yellow circle*) information about the same sources, i.e., primary currents. Functional MRI can be used in a "supportive" role (*blue*) in MEG source analysis. MEG/EEG and fMRI can also be considered complementary (*green*) since the sources of both signals originate from common neural processes

In direct fusion, data from different modalities are combined mathematically to estimate the sources of the measured signals (George et al. 1995; Dale and Halgren 2001). In computational neural modeling, different functional imaging modalities can be modeled within a common framework and the experimental multimodal data can be used to determine parameters of the computation model of the brain networks underlying cognitive tasks (Horwitz et al. 1999; David and Friston 2003; Riera et al. 2005; Babajani and Soltanian-Zadeh 2006; Valdes-Sosa et al. 2009; Plis et al. 2010; Bojak et al. 2011). Here we focus on the combination of MEG with EEG, anatomical MRI, and fMRI, mainly from the point of view of direct data fusion.

We suggest that in the direct data fusion approach, imaging modalities can be conceptually described as "complementary" or "supportive", depending on the nature of the signal sources and the role of the modalities in the interpretation of the multimodal data (Fig. 1). Complementary modalities provide information about the same type of sources. EEG and MEG are complementary modalities, which both detect the primary current distribution related to neural activity. A common source model greatly facilitates the fusion of complementary multimodal data. In a supportive role, data from one modality is used to guide and influence the analysis of the data from another modality. In the analysis of MEG (and/or EEG) signals, anatomical MRI provides important supportive data to constrain the allowable MEG source space. Functional MRI data can be combined with MEG in both supportive and complementary way. In a supportive role fMRI activation can be used, e.g., to constrain the locations of the MEG sources. However, special

considerations are necessary when the sources of signals are of different type. Since both fMRI and MEG signals ultimately have their origin in brain activity, linked via neurovascular coupling, they can also be treated as complementary modalities.

2 MEG and EEG

Since the physiological sources underlying both MEG and EEG are of the same type, the benefits of combining MEG and EEG are based on the different sensitivity properties of these modalities. The spatial sensitivity patterns of MEG and EEG sensors are called lead fields. The set of lead fields is one way to express the forward model, which incorporates the available physical and structural information about the head and the instrumentation to establish the signal patterns that primary currents generate in a sensor array. The structure of the lead fields forms the basis on which source estimates (inverse solution) are constructed. The lead fields of MEG and EEG sensors differ in a non-trivial way from each other, thereby providing complementary information about the underlying primary current distribution in the brain (Cuffin and Cohen 1979; Cohen and Cuffin 1983; Malmivuo and Plonsey 1995; Mosher et al. 1999; Riera et al. 2006). The complementary properties of MEG and EEG can enhance the detection, dissociation, and localization of the neural sources of interest (Wood et al. 1985).

Two major differences between MEG and EEG lead fields are related to the orientation and the depth of the sources (Cuffin and Cohen 1979). Regarding the source orientation, MEG sensors are insensitive to radial source currents, whereas EEG sensors are sensitive to both radial and tangential sources. In the spherical head model, the sensitivity of MEG to radially oriented sources is zero (Baule and McFee 1965; Grynszpan and Geselowitz 1973). The insensitivity of MEG to one source orientation occurs also for realistic, non-spherical head models (Melcher and Cohen 1988; Haueisen et al. 1995; Ahlfors et al. 2010a). In a simulation study using a boundary element model for the head, the median value over cortical locations for the relative signal magnitude for the source orientation with the lowest versus the highest sensitivity was found to be 0.06 for MEG and 0.6 for EEG (Ahlfors et al. 2010a). The selective sensitivity of MEG to tangential source components can be helpful for the dissociation of multiple time-varying sources.

Regarding the source depth, both MEG and EEG are generally more sensitive to superficially located sources than to deep sources. However, the relative sensitivity of MEG diminishes faster as a function of depth than that of EEG (Cuffin and Cohen 1979; Hillebrand and Barnes 2002). In the spherical head model, the sensitivity of MEG is zero at the center of the sphere, whereas EEG signal can be generated by sources at any location. Assuming the primary currents are oriented perpendicular to the cortical surface, only very narrow strips at the crest of gyri are expected to have the radial orientation that the MEG cannot detect; therefore, the depth-dependency appears more important in the comparison of sensitivity patterns of MEG and EEG than the orientation dependence (Hillebrand and Barnes 2002).

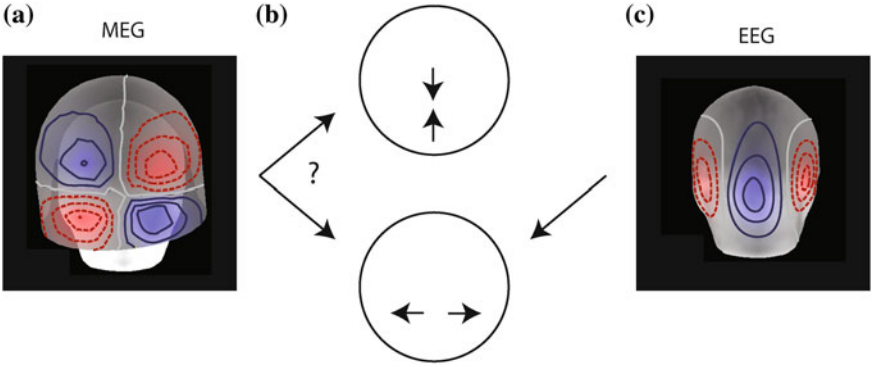

Fig. 2 An example of complementary properties of MEG and EEG signals that can, in combination, help disambiguate the source distribution. The quadrupolar pattern of the extracranial magnetic fields (MEG) (**a**) could be generated either by two near-midline dipoles in the parietal and occipital regions (**b**, *top*) or by two bilaterally located occipital dipoles (**b**, *bottom*). However, the corresponding topography of scalp potentials (EEG) would be quite different for these two configurations; here the EEG pattern for the two occipital bilateral dipoles is illustrated (**c**). Thus, the combination of MEG and EEG can resolve source configurations that can be ambiguous in one of the modalities. Analogous examples can be easily constructed in which MEG resolves source patterns that are ambiguous on the basis of EEG topography only. Adapted from (Ahlfors et al. 2010b)

Selective cancellation of signals from tangential source components on opposite walls of a sulcus or a gyrus tends to make extended source patches look radial (Eulitz et al. 1997; Freeman et al. 2009; Ahlfors et al. 2010b), with potentially important implications to the relative signal-to-noise ratio (SNR) of MEG and EEG and the detectability of e.g., epileptic activity (Goldenholz et al. 2009; Ebersole and Ebersole 2010).

Several studies have demonstrated complementary properties of EEG and MEG in detecting epileptic discharges, such that some are detectable in EEG only or in MEG only, but not necessarily in both (Sutherling et al. 1991; Yoshinaga et al. 2002; Zijlmans et al. 2002; Lin et al. 2003; Rodin et al. 2004; Knake et al. 2006; Ramantani et al. 2006; Ossenblok et al. 2007). Differences in source detectability can be understood in terms of the expected SNR for different sources, which depends on the sensor lead fields, signal noise, the source magnitude, and the background brain activity (de Jongh et al. 2005; Goldenholz et al. 2009; Huiskamp et al. 2010). Prominent differences between MEG and EEG have also been demonstrated, for example, in sleep data (Dehghani et al. 2010).

Combining MEG and EEG data can sometimes be useful for resolving source configurations that are ambiguous on the basis of the signal topography in a single modality. Figure 2 shows simulated MEG data from a bilateral pair of occipital current dipoles. In this case, the quadrupolar MEG topography (Fig. 2a) is consistent in the presence of uncertainty due to measurement noise with two very different two-dipole models, either laterally located horizontal dipoles or medially located vertical dipoles (Fig. 2b). The EEG topography, however, would be very different

for these two scenarios: the EEG map shown in Fig. 2c suggests horizontally oriented dipoles. Bilateral activation of auditory cortices is a well-know example of topographies that can be potentially ambiguous in terms of source areas: two tangential supra-temporal lobe dipoles typically generate a large mid-frontal maximum in EEG that could be mis-interpreted as being due to a radial frontal source (Vaughan 1982), whereas in MEG the two auditory cortex sources are typically readily dissociable (Mäkelä et al. 1993); however, these sources may also generate a dipolar looking MEG signal pattern over the parietal lobe (Hämäläinen et al. 1995).

Combined MEG and EEG inverse modeling is facilitated by the common source model. Indeed, incorporating signals from both EEG and MEG sensors is not different, in principle, from incorporating different types of MEG sensors, such as gradiometers and magnetometers. An important practical issue is how to adjust the relative weighting of the different sensors in the source estimation procedures to take into account the expected SNR for each sensor (Fuchs et al. 1998; Baillet et al. 1999). Determining the SNR is challenging, however, because of the various types of uncertainties that should be incorporated, such as those related to co-registration, head model, sensor calibration, and background physiological noise. Enhanced source estimation results obtained by combining EEG and MEG data have been demonstrated in several studies of experimental and simulated data (Stok et al. 1990; Mosher et al. 1993; Phillips et al. 1997; Fuchs et al. 1998; Muravchik et al. 2000; Pflieger et al. 2000; Babiloni et al. 2001; Liu et al. 2002; Sharon et al. 2007; Molins et al. 2008).

3 MEG and Structural MRI

MEG source estimates are commonly visualized by superimposing them on high-resolution structural MRI, thereby relating the MEG results to brain anatomy. Structural MRI also provides essential supportive information for the inverse modeling of MEG signals. Anatomical information from MRI can be used to determine the permissible MEG source locations (often called the source space) to be within the cranial volume or the cortical gray matter (George et al. 1991; Dale and Sereno 1993). In addition, the source orientation can be constrained to be strictly or nearly perpendicular to the cortical surface (Dale and Sereno 1993; Lin et al. 2006; Chang et al. 2013). Typically, anatomical constraints are imposed on the individual subject level, but atlas-based approaches are possible as well (Hillebrand et al. 2012).

4 MEG and Functional MRI

Functional MRI and other hemodynamic imaging data can be used in a supportive role in MEG (and EEG) data analysis to suggest a likely spatial distribution for the sources of MEG signals (George et al. 1995; Simpson et al. 1995; Dale and

Halgren 2001). One possibility is to place equivalent dipoles at the locations of foci of fMRI activation (Heinze et al. 1994; Ahlfors et al. 1999; Korvenoja et al. 1999; Torquati et al. 2005). A powerful application of fMRI-guided MEG source estimation is to use information from fMRI-based mapping of the retinotopic representation of the visual field to constrain the locations of equivalent dipoles in multiple visual areas (Hagler et al. 2009). For distributed MEG source models, such as the minimum-norm estimate (MNE) (Hämäläinen and Ilmoniemi 1994), fMRI can be used as an a priori weighting for the inverse solution (Liu et al. 1998; Dale et al. 2000). This is implemented by adjusting the diagonal elements of the source covariance matrix (Liu et al. 1998).

Because of the different physiological nature of the origin of fMRI and MEG signals, it is important to minimize potential adverse effects from a mismatch between the locations of activity seen in fMRI and the actual source locations of the MEG signals (Dale and Halgren 2001). "False positive" fMRI locations refer to cases in which activation in fMRI does not correspond to an MEG source, whereas "false negative" fMRI refers to the lack of fMRI activity at the location of a true MEG source (Liu et al. 1998; Ahlfors and Simpson 2004; Im et al. 2005; Im and Lee 2006; Liu et al. 2006). In general, both of these types of mismatches can be due to the differing physiological properties of the signal generation in the two modalities. There is encouraging experimental evidence of the BOLD contrast typically observed in fMRI being closely correlated with post-synaptic currents (Logothetis et al. 2001). However, it is likely that details of the local neural circuitry and the neural and vascular morphology can result in differences in the properties of the signals in the different imaging modalities. Mismatches may also be caused by differences in the experimental design in fMRI and MEG data acquisition and analysis. Event-related fMRI paradigms make it possible to use similar cognitive task designs that are commonly used in MEG (Rosen et al. 1998). However, it is important to critically evaluate the similarity of the baseline conditions and design contrasts used in each modality. In addition, false negative fMRI locations can result from susceptibility artifacts or partial-only coverage of the head in the fMRI data. False positive fMRI can occur when MEG is insensitive to some activity, e.g., when the corresponding primary currents are radially oriented or located deep in the brain. Furthermore, false positive fMRI is bound to happen in the analysis of individual time points of the MEG data: because of the slow time course of the hemodynamic response, a single fMRI map usually shows areas whose activity in the millisecond time scale may only partially overlap in time, and therefore only a subset of the activated areas in fMRI is expected to contribute to the MEG signal at any given time instant.

Ideally, an approach for incorporating a priori constraints from a supportive modality would give improved source estimates when the a priori information is compatible with the actual source distribution, while also being insensitive to incompatible priors (Liu et al. 1998; Vauhkonen et al. 1998; Ahlfors and Simpson 2004). False positive fMRI constraints in MEG source modeling are typically well-behaving, i.e., the contribution to the MEG inverse estimates is usually small for the false positive fMRI locations, especially if the true and false locations are far

apart from each other (Liu et al. 1998; Fujimaki et al. 2002). False negative fMRI constraints are expected to be more problematic than false positive ones (Liu et al. 1998; Ahlfors and Simpson 2004; Im et al. 2005), although simple false negative fMRI may actually have only little effect (Babiloni et al. 2003). In particular, if the assumed MEG sources are strictly restricted at the locations of fMRI activation only, MEG signals originating from other locations may be erroneously assigned to the assumed source locations (Liu et al. 1998; Ahlfors and Simpson 2004). Therefore, it is important that the source estimation algorithm allows the MEG sources to be also at non-fMRI locations.

The possibility of a mismatch in the spatial distribution of activation detected by MEG and fMRI raises a dilemma concerning the use of fMRI in a supportive role to guide the MEG source estimation. On the one hand, if we cannot be certain that the underlying patterns of activity are the same, the fMRI may provide an erroneous bias to the MEG source estimate. On the other hand, if the source analysis of MEG without the fMRI constraint indicates that the source locations of a particular set of MEG data indeed are identical to those seen in the corresponding fMRI, then there would be no need for the fMRI constraint. In other words, converging evidence of source locations from the comparison of MEG and fMRI data is useful in confirming MEG source localization results, but once this has been established, fMRI does not provide additional information for the supportive data fusion. The suggested resolution to this dilemma is that fMRI data should be used to indicate likely solutions among the set of all possible solutions allowed by the non-uniqueness of the inverse problem. The Bayesian approach provides a general formalism for these types of problems (Baillet and Garnero 1997; Friston et al. 2002; Jun et al. 2008; Auranen et al. 2009; Wipf and Nagarajan 2009; Henson et al. 2010). The principle can also be expressed geometrically in the source space (Ahlfors and Simpson 2004), leading to the same weighted MNE solution in which fMRI information is incorporated in the diagonal elements of the a priori source covariance matrix (Liu et al. 1998).

Figure 3 illustrates an example of visual motion related activity in which fMRI data suggested a likely solution among two possible ones for an ambiguous MEG topography (Ahlfors et al. 1999). The averaged visual evoked MEG signal showed a spatial pattern with four extremes (Fig. 3a). This topography suggests at least two sources, one occipitotemporal and one frontal (Fig. 3b, top). However, the dipolar pattern formed by the pair of extremes in the middle raises the question whether a third source, located in between the other two contributed to these MEG data (Fig. 3b, bottom). The fMRI data obtained using a similar stimulus paradigm indeed showed activity in the posterior part of the superior temporal sulcus, in accordance with the location of the putative third source (Fig. 3c). Thus, the fMRI suggests that a three-source model may be more likely here for the MEG than the two-source model. However, it is important to acknowledge that both solutions are consistent with the observed experimental MEG data. Note the difference between the case of combining EEG and MEG in Fig. 2, where the complementary data about the same type of sources was able to disambiguate between the two possible models for the MEG-only data because the EEG data was inconsistent with one of the models.

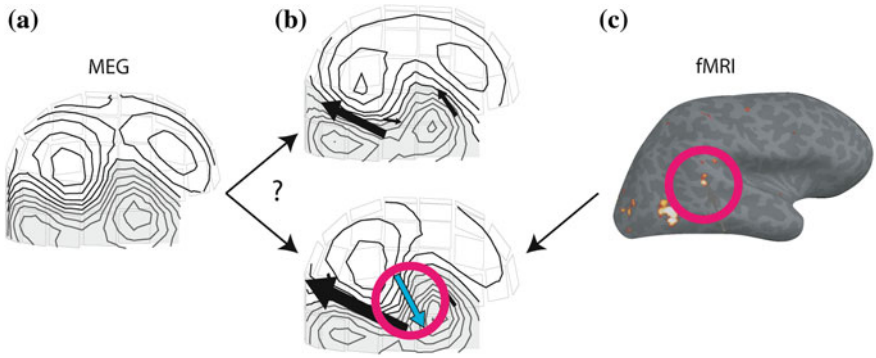

Fig. 3 An example of how fMRI data can suggest a likely MEG inverse solution among possible solutions. Averaged visual evoked MEG response at the latency of 170 ms after the reversal of the direction of the motion of concentric *circles* showed an ambiguous topography with four local extremes (**a**). This topography suggest two underlying dipole sources (*black arrows*), one at the visual motion sensitive middle temporal area and one near the frontal eye field (**b**, *top*). However, the measured topography would also be consistent with a third source in between the other two, contributing to the dipolar pattern of the two extremes in the middle of the topography (**b**, *bottom*). FMRI data recorded on the same subject indicated activation in posterior superior temporal sulcus (*red circle*) that matches the hypothesized third source location for the MEG (**c**). Thus, the fMRI suggested that the three-dipole model may be more likely that the two-dipole model; however, both models are possible solutions for the observed MEG topography. Adapted from (Ahlfors et al. 1999)

Examples of specific situations in which combining fMRI and MEG could provide helpful qualitative information about the neural activation patterns are illustrated in Fig. 4. The source currents of MEG and EEG are vector quantities, whose orientation and direction, in addition to the magnitude, can provide useful information that is not obtainable by fMRI. MEG is well suited to detect accurately the physical orientation of the tangential component of a source, because the whole topographic map of the extracranial signal will rotate if the source rotates tangentially. A change in the source orientation indicates that the neural sources contributing to the measured signals are not constant over time. This property may be useful for the detection of the presence of more than one neural population, even if the fMRI shows only a single extended focus of activity (Fig. 4a).

Since the primary currents generating the MEG signals are expected to be oriented locally perpendicular to the cortical surface, the physiological direction of the source can be described as inward (towards the white matter) or outward (Lopes da Silva 2010). However, the physical orientation, as detected by MEG and EEG, can be highly variable for a source within the convoluted cerebral cortex. In determining the physiological direction of the source current, fMRI can be particularly helpful in suggesting from which side of a sulcus or a gyrus the source is located. Figure 4b depicts a case in which uncertainty in the MEG source localization allows both walls of a sulcus as possible sites of the source. MEG can reliably determine the physical direction of the source, but the physiological

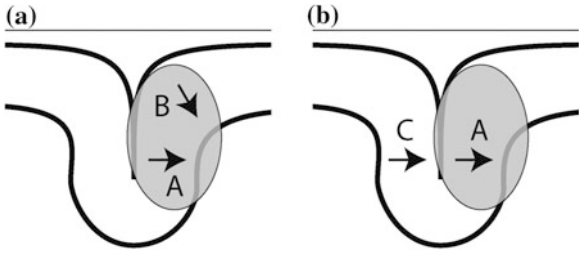

Fig. 4 Schematic illustration of helpful information that can be obtained by combining MEG and fMRI data. **a** A change in the MEG source orientation over time (from "*A*" to "*B*") reveals the presence of more than one neural population contributing to the activity, even when the spatial resolution of MEG as such may not be high enough to dissociate the locations of the source components, and the fMRI may show a single extended region of activation (*gray region*). **b** Uncertainty in the exact location of the source of the MEG signals can result in erroneous physiological interpretation of the source current direction if the source is mis-localized into the opposite wall of a sulcus. Using fMRI to identify the location of activity within the sulcus can help to determine the physiological direction of the MEG source. Here, the physical direction of both "*A*" and "*C*" is the same; however, the physiological direction is inward for "*A*" but outward for "*C*" with respect to the cortical surface

direction (outward vs. inward) depends on which side of the sulcus the source is located. Thus, using fMRI information to identify the likely location of the source will also help to determine the physiological direction of the source.

MEG and fMRI can also be considered complementary modalities, if the sources of both types of signals are taken to be related to a common pattern of neural activation. In this case, computational neural modeling is essential to relate the pattern of activity within brain networks capable of performing the cognitive task under study, as well as of generating the multimodal neuroimaging signals (Horwitz et al. 1999; David and Friston 2003; Riera et al. 2005; Babajani and Soltanian-Zadeh 2006; Daunizeau et al. 2007; Valdes-Sosa et al. 2009; Plis et al. 2010; Bojak et al. 2011).

5 Summary and Future Prospects

Multimodal data can provide information about brain activation patterns that is not attainable by a single method alone. In the analysis of MEG data, the role of other imaging modalities in the direct data fusion approach can be described as complementary or supportive, depending on whether the sources of the signals in the different modalities can be considered to be of the same type or not. This framework can encompass also other existing and emerging imaging modalities. Simultaneous acquisition of multimodal data has obvious advantages over sequential recordings, e.g., by ensuring that the state of the brain was the same for each modality, and enabling multimodal recording of events that are difficult to

repeat in a controlled way, such as epileptic activity. MEG and scalp EEG are commonly recorded simultaneously. Because EEG is better suited than MEG for simultaneous data acquisition with hemodynamic imaging modalities, the similarity of the state of the brain during sequential recordings of MEG and other modalities can be evaluated by examining the concomitantly recorded EEG data. Promising prospects for multimodal integration in the future are expected from further developments in computational neural modeling of the brain processes that underlie the signals of all the imaging modalities.

References

Ahlfors SP, Hämäläinen MS (2012) MEG and EEG: source estimation. In: Brette R, Destexhe A (eds) Handbook of neural activity measurement. Cambridge University Press, Cambridge, pp 257–286

Ahlfors SP, Han J, Belliveau JW, Hämäläinen MS (2010a) Sensitivity of MEG and EEG to source orientation. Brain Topogr 23:227–232

Ahlfors SP, Han J, Lin FH, Witzel T, Belliveau JW, Hämäläinen MS, Halgren E (2010b) Cancellation of EEG and MEG signals generated by extended and distributed sources. Hum Brain Mapp 31:140–149

Ahlfors SP, Simpson GV (2004) Geometrical interpretation of fMRI-guided MEG/EEG inverse estimates. NeuroImage 22:323–332

Ahlfors SP, Simpson GV, Dale AM, Belliveau JW, Liu AK, Korvenoja A, Virtanen J, Huotilainen M, Tootell RB, Aronen HJ, Ilmoniemi RJ (1999) Spatiotemporal activity of a cortical network for processing visual motion revealed by MEG and fMRI. J Neurophysiol 82:2545–2555

Auranen T, Nummenmaa A, Vanni S, Vehtari A, Hämäläinen MS, Lampinen J, Jääskeläinen IP (2009) Automatic fMRI-guided MEG multidipole localization for visual responses. Hum Brain Mapp 30:1087–1099

Babajani A, Soltanian-Zadeh H (2006) Integrated MEG/EEG and fMRI model based on neural masses. IEEE Trans Biomed Eng 53:1794–1801

Babiloni F, Babiloni C, Carducci F, Romani GL, Rossini PM, Angelone LM, Cincotti F (2003) Multimodal integration of high-resolution EEG and functional magnetic resonance imaging data: a simulation study. NeuroImage 19:1–15

Babiloni F, Carducci F, Cincotti F, Del Gratta C, Pizzella V, Romani GL, Rossini PM, Tecchio F, Babiloni C (2001) Linear inverse source estimate of combined EEG and MEG data related to voluntary movements. Hum Brain Mapp 14:197–209

Baillet S, Garnero L (1997) A Bayesian approach to introducing anatomo-functional priors in the EEG/MEG inverse problem. IEEE Trans Biomed Eng 44:374–385

Baillet S, Garnero L, Marin G, Hugonin JP (1999) Combined MEG and EEG source imaging by minimization of mutual information. IEEE Trans Biomed Eng 46:522–534

Baule G, McFee R (1965) Theory of magnetic detection of the heart's electrical activity. J Appl Phys 36:2066–2073

Beisteiner R, Gomiscek G, Erdler M, Teichtmeister C, Moser E, Deecke L (1995) Comparing localization of conventional functional magnetic resonance imaging and magnetoencephalography. Eur J Neurosci 7:1121–1124

Bojak I, Oostendorp TF, Reid AT, Kötter R (2011) Towards a model-based integration of co-registered electroencephalography/functional magnetic resonance imaging data with realistic neural population meshes. Phil Trans R Soc A 369:3785–3801

Chang WT, Ahlfors SP, Lin FH (2013) Sparse current source estimation for MEG using loose orientation constraints. Hum Brain Mapp 34:2190–2201

Cohen D (1972) Magnetoencephalography: detection of the brain's electrical activity with a superconducting magnetometer. Science 175:664–666
Cohen D, Cuffin BN (1983) Demonstration of useful differences between magnetoencephalogram and electroencephalogram. Electroencephalogr Clin Neurophysiol 56:38–51
Cuffin BN, Cohen D (1979) Comparison of the magnetoencephalogram and electroencephalogam. Electroencephalogr Clin Neurophysiol 47:132–146
Dale AM, Halgren E (2001) Spatiotemporal mapping of brain activity by integration of multiple imaging modalities. Curr Opin Neurobiol 11:202–208
Dale AM, Liu AK, Fischl BR, Buckner RL, Belliveau JW, Lewine JD, Halgren E (2000) Dynamic statistical parametric mapping: combining fMRI and MEG for high-resolution imaging of cortical activity. Neuron 26:55–67
Dale AM, Sereno MI (1993) Improved localization of cortical activity by combining EEG and MEG with MRI cortical surface reconstruction: a linear approach. J Cogn Neurosci 5:162–176
Daunizeau J, Grova C, Marrelec G, Mattout J, Jbabdi S, Pelegrini-Issac M, Lina JM, Benali H (2007) Symmetrical event-related EEG/fMRI information fusion in a variational Bayesian framework. NeuroImage 36:69–87
David O, Friston KJ (2003) A neural mass model for MEG/EEG: coupling and neuronal dynamics. NeuroImage 20:1743–1755
de Jongh A, de Munck JC, Goncalves SI, Ossenblok P (2005) Differences in MEG/EEG epileptic spike yields explained by regional differences in signal-to-noise ratios. J Clin Neurophysiol 22:153–158
Dehghani N, Cash SS, Chen CC, Hagler DJ Jr, Huang M, Dale AM, Halgren E (2010) Divergent cortical generators of MEG and EEG during human sleep spindles suggested by distributed source modeling. PLoS ONE 5:e11454
Del Gratta C, Della Penna S, Ferretti A, Franciotti R, Pizzella V, Tartaro A, Torquati K, Bonomo L, Romani GL, Rossini PM (2002) Topographic organization of the human primary and secondary somatosensory cortices: comparison of fMRI and MEG findings. NeuroImage 17:1373–1383
Ebersole JS, Ebersole SM (2010) Combining MEG and EEG source modeling in epilepsy evaluations. J Clin Neurophysiol 27:360–371
Eulitz C, Eulitz H, Elbert T (1997) Differential outcomes from magneto- end electroencephalography for the analysis of human cognition. Neurosci Lett 227:185–188
Freeman WJ, Ahlfors SP, Menon V (2009) Combining fMRI with EEG and MEG in order to relate patterns of brain activity to cognition. Int J Psychophysiol 73:43–52
Friston KJ, Glaser DE, Henson RN, Kiebel S, Phillips C, Ashburner J (2002) Classical and Bayesian inference in neuroimaging: applications. NeuroImage 16:484–512
Fuchs M, Wagner M, Wischmann HA, Kohler T, Theissen A, Drenckhahn R, Buchner H (1998) Improving source reconstructions by combining bioelectric and biomagnetic data. Electroencephalogr Clin Neurophysiol 107:93–111
Fujimaki N, Hayakawa T, Nielsen M, Knosche TR, Miyauchi S (2002) An fMRI-constrained MEG source analysis with procedures for dividing and grouping activation. NeuroImage 17:324–343
George JS, Aine CJ, Mosher JC, Schmidt DM, Ranken DM, Schlitt HA, Wood CC, Lewine JD, Sanders JA, Belliveau JW (1995) Mapping function in the human brain with MEG, anatomical MRI and functional MRI. J Clin Neurophysiol 12:406–431
George JS, Lewis PS, Ranken DM, Kaplan L, Wood CC (1991) Anatomical constraints for neuromagnetic source models. SPIE Med Imaging V Image Phys 1443:37–51
Goldenholz DM, Ahlfors SP, Hämäläinen MS, Sharon D, Ishitobi M, Vaina LM, Stufflebeam SM (2009) Mapping the signal-to-noise-ratios of cortical sources in magnetoencephalography and electroencephalography. Hum Brain Mapp 30:1077–1086
Grynszpan F, Geselowitz DB (1973) Model studies of the magnetocardiogram. Biophys J 13:911–925
Hagler DJ Jr, Ahmadi ME, Kuperman J, Holland D, McDonald CR, Halgren E, Dale AM (2009) Automated white-matter tractography using a probabilistic diffusion tensor atlas: Application to temporal lobe epilepsy. Hum Brain Mapp 30:1535–1547

Hämäläinen M, Hari R, Lounasmaa OV, Williamson SJ (1995) Do auditory stimuli activate human parietal brain regions? NeuroReport 6:1712–1714

Hämäläinen MS, Ilmoniemi RJ (1994) Interpreting magnetic fields of the brain: minimum norm estimates. Med Biol Eng Comput 32:35–42

Hansen P, Kringelbach M, Salmelin R (2010) MEG: an introduction to methods. Oxford University Press, New York

Haueisen J, Ramon C, Czapski P, Eiselt M (1995) On the influence of volume currents and extended sources on neuromagnetic fields: a simulation study. Ann Biomed Eng 23:728–739

He B, Liu Z (2008) Multimodal functional neuroimaging: integrating functional MRI and EEG/MEG. IEEE Rev Biomed Eng 1:23–40

Heinze HJ, Mangun GR, Burchert W, Hinrichs H, Scholz M, Münte TF, Gös A, Scherg M, Johannes S, Hundeshagen H, Gazzaniga MS, Hillyard SA (1994) Combined spatial and temporal imaging of brain activity during visual selective attention in humans. Nature 372:543–546

Henson RN, Glandin G, Friston KJ, Mattout J (2010) A parametric empirical Bayesian framework for fMRI-constrained MEG/EEG source reconstruction. Hum Brain Mapp 31:1512–1531

Hillebrand A, Barnes GR (2002) A quantitative assessment of the sensitivity of whole-head MEG to activity in the adult human cortex. NeuroImage 16:638–650

Hillebrand A, Barnes GR, Bosboom JL, Berendse HW, Stam CJ (2012) Frequency-dependent functional connectivity within resting-state networks: an atlas-based MEG beamformer solution. NeuroImage 59:3909–3921

Horwitz B, Poeppel D (2002) How can EEG/MEG and fMRI/PET data be combined? Hum Brain Mapp 17:1–3

Horwitz B, Tagamets MA, McIntosh AR (1999) Neural modeling, functional brain imaging, and cognition. Trends Cogn Sci 3:91–98

Huiskamp G, Agirre-Arrizubieta Z, Leijten F (2010) Regional differences in the sensitivity of MEG for interictal spikes in epilepsy. Brain Topogr 23:159–164

Im CH, Jung HK, Fujimaki N (2005) fMRI-constrained MEG source imaging and consideration of fMRI invisible sources. Hum Brain Mapp 26:110–118

Im CH, Lee SY (2006) A technique to consider mismatches between fMRI and EEG/MEG sources for fMRI-constrained EEG/MEG source imaging: a preliminary simulation study. Phys Med Biol 51:6005–6021

Inoue T, Shimizu H, Nakasato N, Kumabe T, Yoshimoto T (1999) Accuracy and limitation of functional magnetic resonance imaging for identification of the central sulcus: comparison with magnetoencephalography in patients with brain tumors. NeuroImage 10:738–748

Jun SC, George JS, Kim W, Pare-Blagoev J, Plis S, Ranken DM, Schmidt DM (2008) Bayesian brain source imaging based on combined MEG/EEG and fMRI using MCMC. NeuroImage 40:1581–1594

Knake S, Halgren E, Shiraishi H, Hara K, Hamer HM, Grant PE, Carr VA, Foxe D, Camposano S, Busa E, Witzel T, Hämäläinen MS, Ahlfors SP, Bromfield EB, Black PM, Bourgeois BF, Cole AJ, Cosgrove GR, Dworetzky BA, Madsen JR, Larsson PG, Schomer DL, Thiele EA, Dale AM, Rosen BR, Stufflebeam SM (2006) The value of multichannel MEG and EEG in the presurgical evaluation of 70 epilepsy patients. Epilepsy Res 69:80–86

Korvenoja A, Huttunen J, Salli E, Pohjonen H, Martinkauppi S, Palva JM, Lauronen L, Virtanen J, Ilmoniemi RJ, Aronen HJ (1999) Activation of multiple cortical areas in response to somatosensory stimulation: combined magnetoencephalographic and functional magnetic resonance imaging. Hum Brain Mapp 8:13–27

Lin FH, Belliveau JW, Dale AM, Hämäläinen MS (2006) Distributed current estimates using cortical orientation constraints. Hum Brain Mapp 27:1–13

Lin YY, Shih YH, Hsieh JC, Yu HY, Yiu CH, Wong TT, Yeh TC, Kwan SY, Ho LT, Yen DJ, Wu ZA, Chang MS (2003) Magnetoencephalographic yield of interictal spikes in temporal lobe epilepsy. Comparison with scalp EEG recordings. NeuroImage 19:1115–1126

Liu AK, Belliveau JW, Dale AM (1998) Spatiotemporal imaging of human brain activity using functional MRI constrained magnetoencephalography data: Monte Carlo simulations. Proc Natl Acad Sci USA 95:8945–8950

Liu AK, Dale AM, Belliveau JW (2002) Monte Carlo simulation studies of EEG and MEG localization accuracy. Hum Brain Mapp 16:47–62

Liu Z, Ding L, He B (2006) Integration of EEG/MEG with MRI and fMRI. IEEE Eng Med Biol Mag 25:46–53

Logothetis NK, Pauls J, Augath M, Trinath T, Oeltermann A (2001) Neurophysiological investigation of the basis of the fMRI signal. Nature 412:150–157

Lopes da Silva FH (2010) Electrophysiological basis of MEG signals. In: Hansen P, Kringelbach M, Salmelin R (eds) MEG: an introduction to methods. Oxford University Press, New York, pp 1–23

Mäkelä JP, Ahonen A, Hämäläinen M, Hari R, Ilmoniemi R, Kajola M, Knuutila J, Lounasmaa OV, McEvoy L, Salmelin R, Salonen O, Sams M, Simola J, Tesche C, Vasama J-P (1993) Functional differences between auditory cortices of the two hemispheres revealed by whole-head neuromagnetic recordings. Hum Brain Mapp 1:48–56

Malmivuo J, Plonsey R (1995) Bioelectromagnetism: principles and applications of bioelectric and biomagnetic fields. Oxford University Press, New York

Mathiak K, Fallgatter AJ (2005) Combining magnetoencephalography and functional magnetic resonance imaging. Int Rev Neurobiol 68:121–148

Mathiak K, Rapp A, Kircher TT, Grodd W, Hertrich I, Weiskopf N, Lutzenberger W, Ackermann H (2002) Mismatch responses to randomized gradient switching noise as reflected by fMRI and whole-head magnetoencephalography. Hum Brain Mapp 16:190–195

Melcher JR, Cohen D (1988) Dependence of the MEG on dipole orientation in the rabbit head. Electroencephalogr Clin Neurophysiol 70:460–472

Michel CM, Koenig T, Brandeis D, Gianotti LRR, Wackermann J (2009) Electrical neuroimaging. Cambridge University Press, Cambridge

Molins A, Stufflebeam SM, Brown EN, Hämäläinen MS (2008) Quantification of the benefit from integrating MEG and EEG data in minimum l2-norm estimation. NeuroImage 42:1069–1077

Moradi F, Liu LC, Cheng K, Waggoner RA, Tanaka K, Ioannides AA (2003) Consistent and precise localization of brain activity in human primary visual cortex by MEG and fMRI. NeuroImage 18:595–609

Morioka T, Mizushima A, Yamamoto T, Tobimatsu S, Matsumoto S, Hasuo K, Fujii K, Fukui M (1995) Functional mapping of the sensorimotor cortex: combined use of magnetoencephalography, functional MRI, and motor evoked potentials. Neuroradiology 37:526–530

Mosher JC, Leahy RM, Lewis PS (1999) EEG and MEG: forward solutions for inverse methods. IEEE Trans Biomed Eng 46:245–259

Mosher JC, Spencer ME, Leahy RM, Lewis PS (1993) Error bounds for EEG and MEG dipole source localization. Electroencephalogr Clin Neurophysiol 86:303–321

Muravchik C, Bria O, Nehorai A (2000) EEG/MEG error bounds for a dynamic dipole source with a realistic head model. Methods Inf Med 39:110–113

Ossenblok P, de Munck JC, Colon A, Drolsbach W, Boon P (2007) Magnetoencephalography is more successful for screening and localizing frontal lobe epilepsy than electroencephalography. Epilepsia 48:2139–2149

Pflieger ME, Simpson GV, Ahlfors SP, Ilmoniemi RJ (2000) Superadditive information from simultaneous MEG/EEG Data. In: Aine CJ, Okada Y, Stroink G, Swithenby SJ, Wood CC (eds) BioMag96: 10th international conference on biomagnetism, vol II. Springer, Santa Fe, NM, pp 1154–1157

Phillips JW, Leahy RM, Mosher JC, Timsari B (1997) Imaging neural activity using MEG and EEG. IEEE Eng Med Biol Mag 16:34–42

Plis SM, Calhoun VD, Weisend MP, Eichele T, Lane T (2010) MEG and fMRI Fusion for Non-Linear Estimation of Neural and BOLD Signal Changes. Front Neuroinform 4:114

Poline J-P, Garnero L, Lahaue P-J (2010) Combining neuroimaging techniques: the future. In: Hansen P, Kringelbach M, Salmelin R (eds) MEG: an introduction to methods. Oxford University Press, New York, pp 273–299

Ramantani G, Boor R, Paetau R, Ille N, Feneberg R, Rupp A, Boppel T, Scherg M, Rating D, Bast T (2006) MEG versus EEG: influence of background activity on interictal spike detection. J Clin Neurophysiol 23:498–508

Riera J, Aubert E, Iwata K, Kawashima R, Wan X, Ozaki T (2005) Fusing EEG and fMRI based on a bottom-up model: inferring activation and effective connectivity in neural masses. Philos Trans R Soc Lond B Biol Sci 360:1025–1041

Riera JJ, Valdes PA, Tanabe K, Kawashima R (2006) A theoretical formulation of the electrophysiological inverse problem on the sphere. Phys Med Biol 51:1737–1758

Rodin E, Funke M, Berg P, Matsuo F (2004) Magnetoencephalographic spikes not detected by conventional electroencephalography. Clin Neurophysiol 115:2041–2047

Rosen BR, Buckner RL, Dale AM (1998) Event-related functional MRI: past, present, and future. Proc Natl Acad Sci USA 95:773–780

Rossini PM, Altamura C, Ferretti A, Vernieri F, Zappasodi F, Caulo M, Pizzella V, Del Gratta C, Romani GL, Tecchio F (2004) Does cerebrovascular disease affect the coupling between neuronal activity and local haemodynamics? Brain 127:99–110

Sanders JA, Lewine JD, Orrison WW (1996) Comparison of primary motor cortex localization using functional magnetic resonance imaging and magnetoencephalography. Hum Brain Mapp 4:47–57

Sharon D, Hämäläinen MS, Tootell RB, Halgren E, Belliveau JW (2007) The advantage of combining MEG and EEG: comparison to fMRI in focally stimulated visual cortex. NeuroImage 36:1225–1235

Simpson GV, Pflieger ME, Foxe JJ, Ahlfors SP, Vaughan HG Jr, Hrabe J, Ilmoniemi RJ, Lantos G (1995) Dynamic neuroimaging of brain function. J Clin Neurophysiol 12:432–449

Singh KD, Barnes GR, Hillebrand A, Forde EM, Williams AL (2002) Task-related changes in cortical synchronization are spatially coincident with the hemodynamic response. NeuroImage 16:103–114

Stippich C, Freitag P, Kassubek J, Soros P, Kamada K, Kober H, Scheffler K, Hopfengartner R, Bilecen D, Radu EW, Vieth JB (1998) Motor, somatosensory and auditory cortex localization by fMRI and MEG. NeuroReport 9:1953–1957

Stok CJ, Spekreijse HJ, Peters MJ, Boom HB, Lopes da Silva FH (1990) A comparative EEG/MEG equivalent dipole study of the pattern onset visual response. Electroencephalogr Clin Neurophysiol Suppl 41:34–50

Sutherling WW, Levesque MF, Crandall PH, Barth DS (1991) Localization of partial epilepsy using magnetic and electric measurements. Epilepsia 32(Suppl 5):S29–S40

Swettenham JB, Muthukumaraswamy SD, Singh KD (2013) BOLD responses in human primary visual cortex are insensitive to substantial changes in neural activity. Front Hum Neurosci 7:76

Torquati K, Pizzella V, Babiloni C, Del Gratta C, Della Penna S, Ferretti A, Franciotti R, Rossini PM, Romani GL (2005) Nociceptive and non-nociceptive sub-regions in the human secondary somatosensory cortex: an MEG study using fMRI constraints. NeuroImage 26:48–56

Tripp JH (1983) Physical concepts and mathematical models. In: Williamson SJ, Romani G-L, Kaufman L, Modena I (eds) Biomagnetism: an interdisciplinary approach. Plenum Press, New York, pp 101–139

Tuunanen PI, Kavec M, Jousmäki V, Usenius JP, Hari R, Salmelin R, Kauppinen RA (2003) Comparison of BOLD fMRI and MEG characteristics to vibrotactile stimulation. NeuroImage 19:1778–1786

Valdes-Sosa PA, Sanchez-Bornot JM, Sotero RC, Iturria-Medina Y, Aleman-Gomez Y, Bosch-Bayard J, Carbonell F, Ozaki T (2009) Model driven EEG/fMRI fusion of brain oscillations. Hum Brain Mapp 30:2701–2721

Vartiainen J, Liljeström M, Koskinen M, Renvall H, Salmelin R (2011) Functional magnetic resonance imaging blood oxygenation level-dependent signal and magnetoencephalography evoked responses yield different neural functionality in reading. J Neurosci 31:1048–1058

Vaughan HG Jr (1982) The neural origins of human event-related potentials. Ann N Y Acad Sci 388:125–138

Vauhkonen M, Vadasz D, Karjalainen PA, Somersalo E, Kaipio JP (1998) Tikhonov regularization and prior information in electrical impedance tomography. IEEE Trans Med Imaging 17:285–293

Wipf D, Nagarajan S (2009) A unified Bayesian framework for MEG/EEG source imaging. Neuroimage 44:947–966

Woldorff MG, Tempelmann C, Fell J, Tegeler C, Gaschler-Markefski B, Hinrichs H, Heinz HJ, Scheich H (1999) Lateralized auditory spatial perception and the contralaterality of cortical processing as studied with functional magnetic resonance imaging and magnetoencephalography. Hum Brain Mapp 7:49–66

Wood CC, Cohen D, Cuffin BN, Allison T (1985) Electrical sources in human somatosensory cortex: identification by combined magnetic and potential recordings. Science 227:1051–1053

Yoshinaga H, Nakahori T, Ohtsuka Y, Oka E, Kitamura Y, Kiriyama H, Kinugasa K, Miyamoto K, Hoshida T (2002) Benefit of simultaneous recording of EEG and MEG in dipole localization. Epilepsia 43:924–928

Zijlmans M, Huiskamp GM, Leijten FS, Van Der Meij WM, Wieneke G, Van Huffelen AC (2002) Modality-specific spike identification in simultaneous magnetoencephalography/electroencephalography: a methodological approach. J Clin Neurophysiol 19:183–191

MEG/EEG Data Analysis Using EEGLAB

John R. Iversen and Scott Makeig

Abstract EEGLAB (*sccn.ucsc.edu/eeglab*) is an easily extensible, highly evolved, and widely used open source environment for signal processing and visualization of electroencephalographic data running on MATLAB (The Mathworks, Inc.). Methods central to EEGLAB include time- and time-frequency analysis and visualization of individual datasets and complete studies, independent component analysis (ICA), and rich tools for connectivity analysis, brain computer interface (BCI) development, and tools for fusion and joint analysis of simultaneously recorded motion-capture and brain data. We introduce a new MEEG plug-in that enables MEG and simultaneously recorded MEG/EEG (MEEG) data to be readily analyzed using EEGLAB. Its use is demonstrated by the analysis of an MEEG dataset. Here we show a first ICA decomposition of an MEEG data set and use MEEG plotting tools to localize and evaluate maximally independent joint MEG/EEG component processes in the data. The analysis naturally recovers a range of artifact sources, as well as brain sources common to MEG and EEG, as well as sources primarily visible only to EEG.

Keywords MEG · EEG · MEEG · Independent component analysis (ICA) · EEGLAB · Localization · Radial · Tangential · Dipole · AMICA

1 Introduction

EEGLAB (*sccn.ucsd.edu/eeglab*) (Delorme and Makeig 2004) evolved from an ICA Toolbox for Electrophysiological Data Analysis released by Makeig and colleagues at The Salk Institute (La Jolla CA) in 1997. Currently EEGLAB is a

J. R. Iversen (✉) · S. Makeig
Swartz Center for Computational Neuroscience, Institute for Neural Computation,
University of California San Diego, La Jolla, CA 92093-0559, USA
e-mail: jiversen@ucsd.edu

S. Supek and C. J. Aine (eds.), *Magnetoencephalography*,
DOI: 10.1007/978-3-642-33045-2_8,

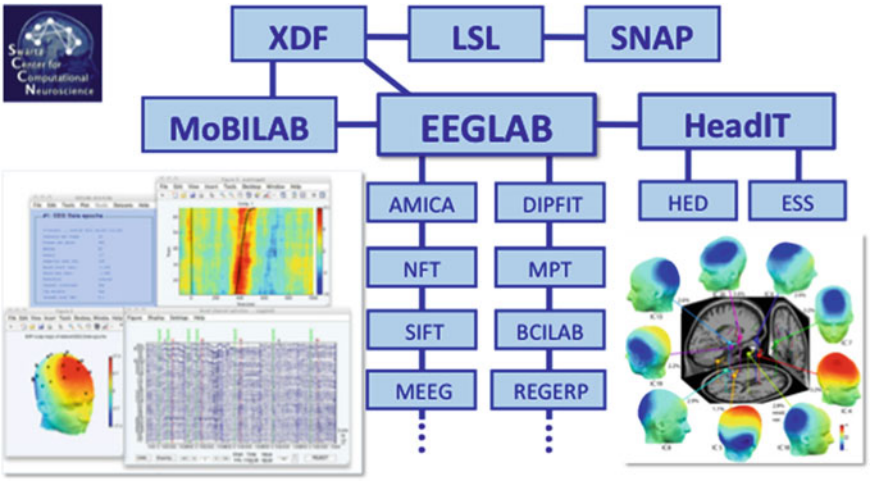

Fig. 1 The EEGLAB environment for electrophysiological signal processing is the center of a growing framework of tools developed and released by researchers at the Swartz Center for Computational Neuroscience (SCCN) at UCSD. These include software for synchronized multimodal recording (SNAP, LSL, XDF), MoBILAB, an object-oriented toolbox for analysis and visualization of multimodal data, the HeadIT data and tools resource with its associated tools (HED, ESS, etc.), and a growing set of toolboxes that operate as EEGLAB plug-ins (AMICA, DIPFIT, NFT, MPT, SIFT, BCILAB, etc.). MEEG is a new plug-in developed by the authors for analysis of MEG and MEEG (synchronized MEG plus EEG) data

mature, actively evolving open-source software environment for electrophysiological data analysis running on MATLAB (The Mathworks, Inc.) that makes freely available a range of state-of-the-art approaches to describe brain dynamics of effective cortical and non-brain EEG sources at both the individual and group levels (Delorme and Makeig 2004; Makeig et al. 2004). By a 2011 survey (Hanke and Halchenko 2011), EEGLAB may currently be the most widely used open-source toolbox for EEG analysis. EEGLAB functions comprise a broad core range of functionality accessible either through its graphic user interface (GUI) and/or directly from the MATLAB command line, plus plug-in tools and toolboxes that implement a wide range of advanced analysis and visualization methods.

User interface. EEGLAB can be controlled through its GUI (Fig. 1 lower left, panel), or more directly through MATLAB scripts and command line calls. Use of the GUI is highly convenient for data exploration. The GUI also accumulates a history of the commands to EEGLAB functions it issues, enabling processing pipelines developed using the GUI to be easily turned into a MATLAB script. Already many students (worldwide) have learned to write MATLAB data analysis scripts by combining the EEGLAB history mechanism with the extensive EEGLAB function and wiki documentation (*sccn.ucsd.edu/wiki/eeglab*).

Other tools. EEGLAB is the center of a growing ecosystem of open source software tools (Fig. 1) that have been released by researchers at the Swartz Center for Computational Neuroscience at UCSD (*sccn.ucsd.edu*). These include the

Human Electrophysiology, Anatomic Data, and Integrated tools (HeadIT) data archive and resource (*headit.org*), with its system for tagging uploaded studies (Experimental Study Schema (ESS) (Bigdely-Shamlo et al. 2013a), Hierarchical Events Descriptors (HED) (Bigdely-Shamlo et al. 2013b) and a cross-platform system for synchronized collection of data from EEG and many other devices (Lab Streaming Layer (LSL), *code.google.com/p/labstreaminglayer*) plus an extensible, XML-based data format (Extensible Data format, XDF; *code.google.com/p/XDF*) and a Python-language scripting framework for controlling simple or very complex experimental paradigms (SNAP).

MoBILAB. An object-oriented environment for analysis of multimodal data collected under the mobile brain/body imaging (MoBI) paradigm, MoBILAB (*sccn.ucsd.edu/wiki/Mobilab_software*) can export EEG data to EEGLAB for further analysis, and may in the future become our primary platform for developing and sharing multimodal data analysis methods, since the EEGLAB *EEG* data structure has limited support for different channel types and assumes all data to be recorded at the same sampling rate. For MEG/EEG data recorded at the same rate this is not much of an inconvenience, as EEGLAB provides a channel type variable that allows functions to perform EEG analysis and/or MEG analysis of the respective data channel subsets based on their specified channel types.

EEGLAB plug-ins. The growing range of EEGLAB plug-ins have been previously described (Delorme et al. 2011). Plug-ins released by SCCN itself include advanced Adaptive Mixture ICA (AMICA) for identification of maximally independent brain sources with artifact rejection (Delorme et al. 2012; Palmer 2006), the DIPFIT toolbox implementing source dipole fitting tools by Robert Oostenveld from Fieldtrip (*fieldtrip.fcdonders.nl*), the Neuroelectromagnetic Forward Head Modeling Toolbox (NFT) for creating detailed boundary element model (BEM) or finite element model (FEM) head models (Akalin Acar and Makeig 2010), the Measure Projection Toolbox (MPT) for cross-subject source-level analysis using measure projection (Bigdely-Shamlo et al. 2013c), the Source Information Flow Toolbox (SIFT) for calculation and visualization of multivariate causal source dynamics in both event-related and continuous data (Delorme et al. 2011), and BCILAB, a complete toolbox for building, running, and statistically evaluating brain-computer interface (BCI) models (Kothe and Makeig 2010). At least 20 other plug-in tools and toolboxes have been released by other research groups; these are listed on a wiki page (*sccn.ucsd.edu/wiki/EEGLAB_Plugins*). A facility for automated updating of listed plug-ins to new versions from within EEGLAB is planned for EEGLAB v13.

The MEEG plug-in. EEGLAB now includes an MEEG plug-in (*sccn.ucsd.edu/wiki/MEEG*) that expands the ability of EEGLAB users to import and analyze MEG and dual-modality MEEG (concurrent MEG and EEG) datasets, thereby opening a range of novel data analysis techniques for use by the MEG community. MEEG data handling within EEGLAB is tightly coupled to Fieldtrip, allowing the EEGLAB data structures to be readily imported from and exported to Fieldtrip. Both the EEGLAB environment and the MEEG plug-ins are ongoing efforts that we hope other MEG users and methods developers will contribute to. The MEEG

developers remain open to partnering with other methods developers to share capabilities between MEEG and other MEG toolboxes.

Data and experiment types supported. In addition to standard EEG data types, EEGLAB now supports the loading of MEG and MEEG data through its integration of the Fieldtrip *fileio* module. Individual data files can be imported as individual EEGLAB data sets, or multiple runs can be combined into a single dataset using realignment to a common sensor orientation. In addition, the new MEEG plug-in enables EEGLAB to import and export a range of Fieldtrip data structures, including raw and epoched data, as well as independent component analyses, so that EEGLAB processing can begin after partial analysis in Fieldtrip, or can be exported, allowing Fieldtrip to be used for additional processing. EEG recording systems provide a single scalar value per sensor location, in contrast to the wider variety of MEG sensor types. The scalar model easily accommodates magnetometer and radial gradiometer systems, but requires either magnetometers or the magnitude of the planar gradient to be chosen (e.g., for Yokogawa system data sets).

Source localization. ICA decomposition enables the profitable use of dipole-based inverse methods because of the characteristic resemblance of many MEG, EEG, or also MEEG independent component scalp maps to the projection of a single equivalent dipole, allowing them to be well-fit by a single equivalent dipole model (or, in some cases, to a dual-dipole model with symmetric location constraints) (Delorme et al. 2012). The DIPFIT toolbox in EEGLAB implements equivalent dipole model fitting tools by Robert Oostenveld from Fieldtrip (*fieldtrip.fcdonders.nl*). Dipole fitting tools have been integrated in the Neuroelectromagnetic Forward head modeling Toolbox (NFT) (Akalin Acar and Makeig 2010). These plus some novel distributed source localization methods will be put into a toolbox paralleling NFT, to be called the Neuroelectromagnetic Inverse Source modeling Toolbox (NIST).

Processing data from multiple subjects or sessions. EEGLAB supports across-subject analysis via a STUDY structure that points to a set of similar EEG datasets forming an experimental study. Currently, these datasets are typically epoched datasets (sets of data epochs similarly time locked to one or more sets of experimental events). EEGLAB Study software can prepare and store a user-specified set of continuous (power spectrum) and event-related (ERP, ERSP, ITC, etc.) measures for each dataset and help the user to separate these measures into conditions, sessions, and/or subject groups. Typically, each dataset is associated with an ICA decomposition and a list of 'brain' components to study, each with an equivalent dipole model. The Study functions can then prepare a pair-wise distance measure between components based on component dipole (and/or scalp map) and specified measure distances. Users then can cluster the components using at least three clustering methods, and can compute statistical contrasts across subjects/sessions using either parametric (Gaussian) or non-parametric (bootstrap) statistical methods. Clustering scalp channel signals, though less advised, is also supported.

Currently, users can create and process one or more $1 \times N$ or $N \times M$ statistical designs for a given Study. Thus, for example, given 5 different event-related

measures for each subject in an experiment, the user can specify Conditions 1–4 as forming a 2 × 2 design, and/or can also compare Conditions 2 versus 5 in another design, without needing to duplicate the STUDY structure and its associated measure files. Both within-subject and across-subject variable types are supported.

As in practice the range of experimental designs is much wider (than NxM), EEGLAB and some EEGLAB toolbox developers are now working with Cyril Pernet of the University of Glasgow to incorporate his LIMO toolbox into the core of EEGLAB study processing. It supports parametric and non-parametric statistics for a much wider range of designs (*gforge.dcn.ed.ac.uk/gf/project/limo_eeg*) (Pernet et al. 2011).

Measure projection. An alternate approach to component clustering is taken in the Measure Projection Toolbox (MPT) (Bigdely-Shamlo et al. 2013c). This toolbox focuses on comparing component source dynamics for a single measure at a time (for example, ERPs) based on the location of the equivalent source dipole in a template brain. Each component dipole location is replaced by a 3-D Gaussian blur (representing location probability) and, after populating the template brain with source dipoles across a potentially large number of subjects, two operations are applied voxel-wise (that is, template brain voxel-by-voxel). First, brain regions in which local dipole measures agree are identified, forming a measure consistency subspace. Next, voxels in this subspace are clustered using affinity clustering to form voxel domains with distinct measure time courses. Here the concept of measure domains in the template brain volume replaces the discrete component clusters produced by the default EEGLAB study processing. Users may choose either or both paths to use to characterize their study data.

CSA clustering. Arthur Tsai of Academica Sinica, Taiwan, has recently developed an advanced approach to study source clustering (Tsai et al. 2013). This applies spatiotemporal ICA decomposition using EMSICA (Tsai et al. 2006) to EEG (or as readily, MEG) data from its projection back onto to the oriented subject cortex, modeled from a subject MR head image. The cortical surface models are then inflated and co-registered using tools available in Freesurfer (Fischl et al. 1999). Finally, source clustering across subjects is performed in the 2-D cortical surface-aligned space rather than in 3-D template brain space (as in MPT and EEGLAB Study functions). A CSA (Cortical Surface Alignment) EEGLAB plug-in is envisaged that will allow users to perform this potentially more accurate analysis when MR head images are available for the individual subjects in an EEG or MEG study.

2 MEEG Data Decomposition: An Empirical Data Example

For example purposes, we will illustrate the capabilities of the MEEG plug-in and other EEGLAB features using a simultaneously recorded multimodal (MEEG) MEG plus EEG dataset (Bledowski et al. 2012) that is jointly decomposed, in a

single AMICA decomposition, to extract independent components accounting for both MEG and EEG data streams. The validity of the decomposition is based on the assumed linearity of the underlying electric and magnetic components of the electromagnetic field generated by the effective generators of the scalp-recorded (EEG) potentials and (MEG) flux. We use the NFT toolbox to create an EEG and MEG head model and use it to fit equivalent dipole models to the resulting independent component (IC) scalp maps. We focus here on describing the relations between MEG signal and EEG signal projections of the resulting ICs, including a first statistical examination using ICA of the degree to which radial EEG sources (as determined by an equivalent dipole model) are also visible in MEG.

Data loading and preprocessing. The epoched CTF dataset included time series data from 269 radial gradiometers (3rd-order synthetic) plus 56 EEG channels. Five separate runs from the same recording session were imported and merged into a single EEGLAB dataset of size 325 channels by 580 k time points. The MEEG toolbox enabled the selection of alignment across runs of the MEG data (e.g., projection onto the average across-run gradiometer locations using Fieldtrip *ft_megrealign*) as well as the choice (when appropriate) of synthetic gradiometer order. Field contributions from external sources were removed by computation of third order gradients using contributions from reference sensors (Fife 1999). The resulting EEGLAB dataset included 324 channels and 136 6-s data epochs. These data were down sampled from 1200 to 600 Hz, and the EEG channels were average referenced. One EEG channel was dropped following these procedures to keep the data full rank.

Artifact detection and rejection. A range of artifact rejection options are available in EEGLAB, both automated and interactive data rejection or cleaning, as well as ICA-based artifact rejection. For the dataset used here, epochs containing large artifacts had previously been rejected based on visual inspection.

Independent Component Analysis. The MEEG data were analyzed using AMICA to find independent components across the modalities. ICA in general proceeds from the observation that the signal measured at any sensor is a linear mixture of multiple sources within the brain (Makeig et al. 1996). The goal of the algorithm is to learn an unmixing matrix across all channels that results in a complete decomposition of the data into maximally independent components (ICs). In single-modality MEG or EEG data, many ICs have dipolar patterns of projection onto the sensors (Delorme et al. 2012). In MEEG data decompositions, both the associated MEG and EEG scalp projection maps in clearly defined components may be dipolar. In such cases, the maps are near-orthogonal and the implied equivalent dipole locations and orientations near-identical (Liu et al. 1998), showing that ICA has identified the joint electromagnetic field associated with a single source process that may be located using its well-defined MEG and EEG projection patterns also returned by ICA. The AMICA (Adaptive Mixture ICA; (Palmer et al. 2007); sccn.ucsd.edu/~jason/amica_web.html) algorithm used here is the blind source separation method that performed best in a recent comparative test of 22 linear decomposition algorithms—by both producing the greatest reduction of the strong mutual information present in the channel data, and

by finding the largest number of component processes with 'dipolar' scalp maps compatible with the projection of a single cortical area or patch (Delorme et al. 2012).

The joint analysis of MEG and EEG data using independent component analysis is novel; to our knowledge it has not been previously reported. ICA itself, as a purely statistical method, has no notion of the type of signal it is decomposing or of the types of signal sources contributing independent information to the recorded source mixtures. Thus, to perform ICA decomposition of MEEG data, the MEG and EEG channel signals are simply concatenated into a dataset (here of 324 channels). The MEG and EEG portions of the data were individually sphered (a standard procedure to remove correlations and scale from data) before decomposition (Tukey and Tukey 1981). Sphering serves both to make the MEG and EEG signals numerically identical in size (avoiding μV versus fT scaling issues), and to remove correlations between sensors (a standard step prior to ICA that speeds the convergence of the algorithm). The result of the joint decomposition is a collection of maximally independent components, each with a pair of spatial topographies (scalp maps) representing the spatial projections of the source onto the MEG and EEG sensors, respectively, and a joint MEG/EEG time course of activation across the trials.

Forward and inverse source modeling. The NFT toolbox was used to warp an MNI template 4-layer BEM model to the individual head shape defined by the EEG electrode locations. The EEG head model used the full BEM model, with forward solutions solved with METU-BEM (Akalin Acar and Gençer 2004). The MEG head model used the inner skull surface mesh of the BEM model to define a single-shell BEM model (Hämäläinen and Sarvas 1989). When individual anatomical MRIs are available, the NFT toolbox can use them to segment and create individual electrical and magnetic forward head models. NFT also generates lead field matrices for 3-D grid (FEM) source space or for a cortically constrained (BEM) source-space, e.g. constructed using the Freesurfer toolbox (*surfer.nmr.mgh.harvard.edu*). The head models and lead fields generated by the NFT toolkit can likewise be used for volumetric or cortically constrained inverse solutions in other data analysis packages. Dipoles were fit to all components automatically, with a separate dipole fit for the MEG and EEG IC topography. Each fit was characterized by its residual variance, as well as its direction with respect to the radial direction (as defined in relation to a best-fit sphere, fit to the scalp surface).

3 Results: ICA Analysis of MEEG Data

Figure 2 shows 'ERP image' plots of trial-by-trial activities of four functionally distinct ICs from this data set. Each panel shows the IC topography for EEG and MEG in the upper left. The *erpimage* function produces a raster image generated by stacking event-related trials (in any specified order) as horizontal colored lines,

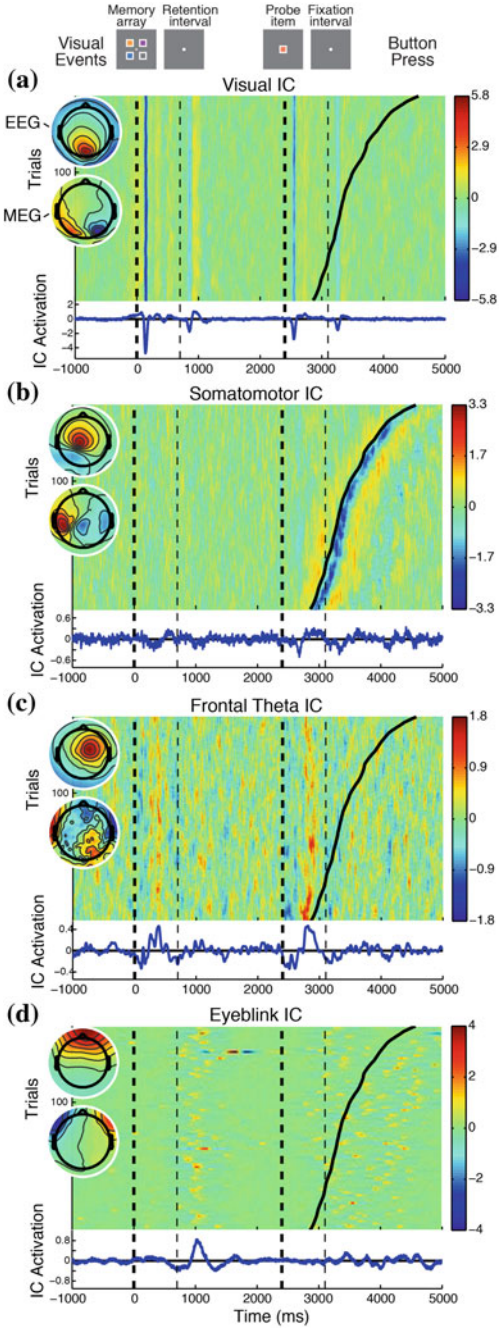
Memory array
Retention interval
Probe item
Fixation interval
Visual Events
Button Press
(a)
Visual IC
EEG
MEG
Trials
IC Activation
(b)
Somatomotor IC
(c)
Frontal Theta IC
(d)
Eyeblink IC
Time (ms)

◀**Fig. 2** Four 'ERP image' panels showing trial-by-trial activities of four MEEG independent components. The experiment trial design is depicted above panel 1: in each trial, a target array of colored squares that are to be memorized is briefly presented, then replaced by a fixation dot during a retention interval. A single colored probe square is then presented; the participant had to respond whether or not it was present in the initial color array. In each *erpimage* panel, vertical dashed black lines indicate the onset of each visual stimulus (*heavier lines* for target and probe stimuli; *lighter lines* for onsets of *fixation dots*). The large color image within each panel represents a raster image of all 136 individual trials, with IC activation coded by color. Activation units are proportional to projected rms EEG μV and MEG fT. The trials are sorted in order of descending reaction time, so the trace of button press moments (*dark solid* trace) forms a diagonal arc. In the *erpimage* panels, the trial activations have been (*vertically*) smoothed with a 10-trial moving window. Below each *erpimage* panel is the standard trial average activation ERP. EEG and MEG IC topographies are shown in the upper left of each panel. **a** A visual (occipital) IC (with clear, near-orthogonal EEG and MEG topographies) showing consistent evoked responses time-locked to presentations of visual stimuli. **b** A somatomotor IC (again with clear, near-orthogonal EEG and MEG projections) whose evoked responses are time locked primarily to button presses. **c** A near-radial right frontal theta band dominant component with weak and less clearly defined MEG projection. Response to target and probe stimuli can be modeled as a theta band burst superimposed on a lower-frequency response, and **d** an eye blink IC (with clearly defined, near-orthogonal MEG and EEG projections; 2 trial smoothing window). Separation of the signals into maximally independent component processes separates out processes that are maximally functionally distinct as well

where color represents signal value. Consistent evoked response activity across trials time locked to events with consistent trial latencies appears as vertical bands of color. Smoothing (vertically) lightly across trials can highlight these regularities. Here, the dashed black lines show the onset of visual stimulus presentations, and the trials are sorted in order of increasing participant reaction time to the cue stimulus (the curving black trace indicating the moment of the button press in each trial).

In Fig. 2, evoked responses of four components demonstrate ICAs tendency to isolate functionally distinct brain responses from the recorded mixture, and that this naturally generalizes to multimodal recordings. A visual cortex IC (a) follows onsets of visual stimuli. Note the associated dipolar and near-orthogonal MEG and EEG scalp maps. The evoked response of a somatomotor cortex IC (b) is primarily time locked to (before and after) participant button presses, and again has near-orthogonal MEG and EEG scalp maps. A right frontal-cortex IC (c), whose spectrum had a broad peak in the theta band (not shown), produces increased theta band power (not shown here) during presentation of memorandum (1st) stimuli and subsequent (3rd) probe stimuli. Some of this theta burst energy was phase locked across trials; thus, the evoked response of this IC to the memoranda (1st stimuli) resembles a theta burst superimposed on a slower ERP base. Note the near-radial scalp pattern of the EEG scalp map, and the corresponding lack of definition of the (weak) MEG IC projection (discussed further below). The ERP image plot for an IC accounting for eye blinks (d) shows that the participant blinked consistently during fixation intervals. Again, the MEG and EEG projections are well defined, consistent with sources in the eyes themselves, and are near orthogonal.

Figure 3 shows a more complete set of IC MEG and EEG topographies for (brain and non-brain process) ICs accounting for the most signal variance among

the 324 ICs returned by AMICA (pvaf = percent variance accounted for; the leftmost number above each topography). Each IC is represented as a vertical pair of head cartoons depicting the spatial projection of the IC onto the EEG (top) and MEG (bottom) sensor arrays. As usual, the ICs accounting for the most signal variance in each modality are artifactual (top row): an IC accounting for eye blinks (accounting for 12.6 % of EEG signal variance), and another accounting for cardiographic contributions (in these data accounting for 21.7 % of MEG signal variance). The relative sensitivity of each modality to different artifact types is apparent in the pvaf values: Eye blinks and muscles account for proportionally more EEG then MEG variance, while for heart-related and line-noise artifacts the reverse holds. Many of the maps show dipole-like ('dipolar') topographies. AMICA analysis produced a pair of spatially near-orthogonal topographies for the MEG and EEG projections of the identified joint electromagnetic source processes, consistent with an origin in a single cortical patch or non-brain generator. Non-brain components (top two rows) were so classified on the basis of having identifiable non-brain time courses (Eye & EKG components) or a large high-frequency spectrum consistent with myographic (or line noise) activity together with equivalent dipole localized to outside the brain volume (myographic or line noise sources). Identified Brain components have equivalent dipoles (indicated in black) located within the brain volume (here with residual variance of the dipole fit <= 20 %). Dipole localization is discussed further below.

As is well known, MEG is less sensitive to the radial component of brain current sources. In joint MEEG data ICA decompositions, this relationship falls out naturally: sources with a strong radial orientation have weak and usually less well-defined MEG projections. For example, the four brain components in the bottom row of Fig. 3 have large EEG projections, accounting for between 3.5 and 0.9 % of total signal variance (3.5 % was the largest pvaf value of any brain component). Low residual-variance dipole fits to the IC EEG scalp map return a near radial equivalent dipole (e.g. in 3 of these 4, with radial angle defined relative to a best-fit spherical head model). In contrast, the associated MEG scalp maps for these ICs have quite low pvaf (<0.2 %) and are not dipolar (residual variances, 25–70 %). To check for the presence of this pattern overall in the decomposition, in Fig. 4 we plot, for each dipolar, brain-based IC, the ratio of variance accounted for in the whole EEG and MEG signals (EEG pvaf /MEG pvaf) as a function of the angle from radial of the EEG equivalent dipole. Relative variance explained by the MEG portion of ICs is reduced 20-fold as the best fit dipole angle approaches a radial direction, and is close to 1:1 for tangential dipoles, in accordance with general expectations, and more specifically with expectations that the MEG component of a radial source dipole in a real head should be about 5–10 % of that to a tangential source dipole (Ahlfors et al. 2010; Menninghaus and Lütkenhöner 1995).

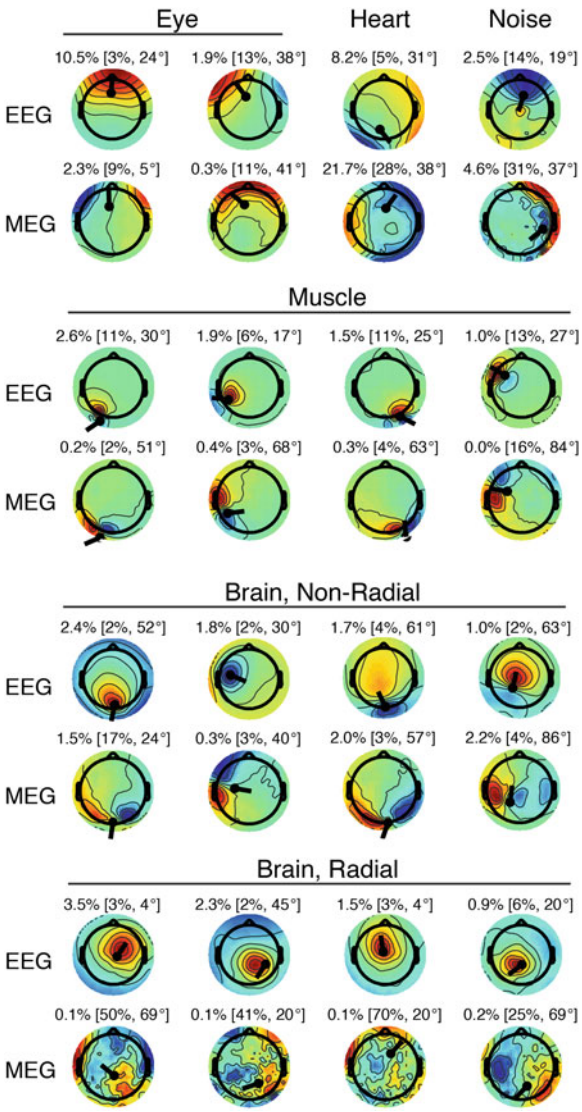

Fig. 3 Results of the MEEG data joint independent component decomposition. Joint independent component (IC) topographies representing the projection patterns of individual ICs to the EEG (*upper map*) and MEG (*lower map*) sensor arrays as viewed from above the head. Each IC is represented by a vertical pair of EEG and MEG topographies. Numbers above each sensor map indicate percentage of (EEG or MEG) data variance explained (pvaf, percent variance accounted for); in brackets, the residual variance of the equivalent dipole fit to the scalp map (shown as a *black dot* and line on the maps), and the angle (relative to radial of a best-fit sphere) of the equivalent dipole. Depicted non-brain (*top* two rows of four ICs) and brain (*bottom* two rows) ICs are the 16 (of 324) accounting for most signal variance in each category. The non-brain component processes account for eye blinks, cardiographic sources (50-Hz) line noise, and scalp muscle activity, as labeled. The pair of MEG and EEG scalp maps for most components are near orthogonal, consistent with a single cortical or non-brain source. This holds for brain ICs having more tangential EEG topographies and equivalent dipoles, while (as expected) dipoles with a near-radial EEG maps and equivalent dipoles have weak (low-pvaf), and less dipolar MEG projections (i.e., single equivalent dipole model for these MEG scalp maps have higher residual variance)

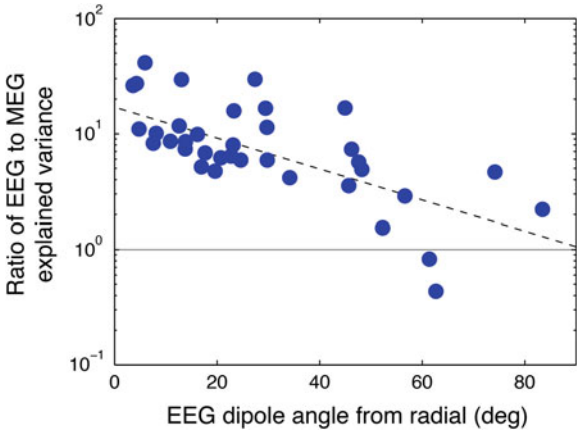

Fig. 4 Ratios of relative EEG/MEG strengths (as ratio of the percentages of MEG and EEG signal variance accounted for, on a log scale) for returned independent MEEG components with near-dipolar scalp maps (less than 20 % residual variance of the single equivalent dipole model in at least one of the modalities), as a function of the deviation of the angle from radial of the EEG-map equivalent dipole. Note the expected dominance of the EEG current projections, relative to the MEG field projections, of the ICA identified near-radial sources. Best fit line ($R^2 = 0.31$) has an EEG /MEG ratio of 18.2 for a radial source, and 1.06 for a tangential source

4 Conclusions

For EEG (Makeig et al. 1996), fMRI (McKeown et al. 1998), MEG (Ikeda and Toyama 2000), ECoG (Whitmer et al. 2010), and other biomedical data modalities, ICA has become a widely accepted approach that provides a powerful method for identifying and separating out separate *information* sources in multichannel data each of whose channel signals sums activity from more than one (often, not directly recorded) source.

Here we have demonstrated that ICA may at least complement other methods for jointly analyzing simultaneously recorded EEG and MEG data (Dale and Sereno 1993; Fuchs et al. 1998; Huang et al. 2007; Takada et al. 2000; Trujillo-Barreto et al. 2008). Its benefits may include improved source localization due to the recovery of dipole-like components with small source projections. Near-radial sources appear as those with poorly defined MEG projections, and may be better located by inverting their simultaneously recorded and subsequently ICA-recovered electrical correlate. In addition, MEEG decomposition by ICA gives direct information on the relative scaling of MEG and EEG signals projected by cortical (and other) data sources. ICA decomposition of MEEG data should also allow principled examination of claims that MEG and EEG sources may sometimes have different spatial distributions. If and when this were the case, some class or classes of independent component processes returned by ICA applied to MEEG data should have very little EEG or MEG power. Here we showed that in our sample

data set the latter was the case for EEG processes with a net radial orientation, as expected from theory.

We believe the EEGLAB environment, now augmented with the MEEG plug-in incorporating several data loading and handling functions from Fieldtrip, as well as custom handling of the MEEG data within EEGLAB, is suitable for performing a range of custom MEG data analyses using available EEGLAB tools and its growing family of plug-in toolboxes. For students and researchers exploring new data sets, the EEGLAB GUI and palette of data visualization methods offers a ready way to explore data features and data quality, while its core support for data decomposition by advanced ICA methods including AMICA, and further analyses using the IC component basis, provide a powerful platform for information- and biophysics-based data modeling and statistical testing of experimental hypotheses.

Acknowledgments The authors thank Michael Wibral and colleagues for the use of the MEG/EEG data set, and Jason Palmer, Zeynep Akalin Acar, and Arnaud Delorme for useful discussions. This work was funded by a gift from The Swartz Center (Old Field NY) and from grant R01 NS047293-09 from the National Institutes of Health USA.

References

Ahlfors SP, Han J, Belliveau JW, Hämäläinen MS (2010) Sensitivity of MEG and EEG to source orientation. Brain Topogr 23:227–232

Akalin Acar Z, Gençer NG (2004) An advanced boundary element method (BEM) implementation for the forward problem of electromagnetic source imaging. Phys Med Biol 49:5011–5028

Akalin Acar Z, Makeig SD (2010) Neuroelectromagnetic forward head modeling toolbox. J Neurosci Methods 190:258–270

Bigdely-Shamlo N, Kreutz-Delgado K, Kothe C, Makeig SD (2013a) Towards an EEG search engine. IEEE Global Conference on Signal and Information Processing (GlobalSIP), Austin, pp 25–28

Bigdely-Shamlo N, Kreutz-Delgado K, Robbins K, Miyakoshi M, Westerfield M, Bel-Bahar T, Kothe CA, His J, Makeig SD (2013b) Hierarchical Event Descriptor (HED) Tags for Analysis of Event-Related EEG Studies. IEEE Global Conference on Signal and Information Processing (GlobalSIP), Austin, pp 1–4

Bigdely-Shamlo N, Mullen T, Kreutz-Delgado K, Makeig SD (2013c) Measure projection analysis: a probabilistic approach to EEG source comparison and multi-subject inference. NeuroImage 72:287–303

Bledowski C, Kaiser J, Wibral M, Yildiz-Erzberger K, Rahm B (2012) Separable neural bases for subprocesses of recognition in working memory. Cereb Cortex 22:1950–1958

Dale AM, Sereno MI (1993) Improved localization of cortical activity by combining EEG and MEG with MRI cortical surface reconstruction: a linear approach. J Cogn Neurosci 5:162–176

Delorme A, Makeig SD (2004) EEGLAB: an open source toolbox for analysis of single-trial EEG dynamics including independent component analysis. J Neurosci Methods 134:9–21

Delorme A, Mullen T, Kothe CA, Acar ZA, Bigdely-Shamlo N, Vankov A, Makeig SD (2011) EEGLAB, SIFT, NFT, BCILAB, and ERICA: new tools for advanced EEG processing. Comput Intell Neurosci 2011:1–12

Delorme A, Palmer J, Onton J, Oostenveld R, Makeig SD (2012) Independent EEG sources are dipolar. PLoS ONE 7:e30135

Fife AA (1999) Synthetic gradiometer systems for MEG. IEEE Trans Appl Supercond 9:4063–4068

Fischl B, Sereno MI, Dale AM (1999) Cortical surface-based analysis. II: inflation, flattening, and a surface-based coordinate system. NeuroImage 9:195–207

Fuchs M, Wagner M, Wischmann HA, Köhler T, Theissen A, Drenckhahn R, Buchner H (1998) Improving source reconstructions by combining bioelectric and biomagnetic data. Electroencephalogr Clin Neurophysiol 107:93–111

Hanke M, Halchenko YO (2011) Neuroscience runs on GNU/Linux. Front Neuroinform 5:8

Hämäläinen MS, Sarvas J (1989) Realistic conductivity geometry model of the human head for interpretation of neuromagnetic data. IEEE Trans BioMed Eng 36:165–171

Huang M-X, Song T, Hagler DJ Jr, Podgorny I, Jousmaki V, Cui L, Gaa K, Harrington DL, Dale AM, Lee RR, Elman J, Halgren E (2007) A novel integrated MEG and EEG analysis method for dipolar sources. NeuroImage 37:731–748

Ikeda S, Toyama K (2000) Independent component analysis for noisy data–MEG data analysis. Neural Netw 13:1063–1074

Kothe CA, Makeig SD (2010) BCILAB: a BCI/EEG research framework. Proceedings of the fourth international brain-computer interface meeting

Liu AK, Belliveau JW, Dale AM (1998) Spatiotemporal imaging of human brain activity using functional MRI constrained magnetoencephalography data: Monte Carlo simulations. Proc Natl Acad Sci USA 95:8945–8950

Makeig SD, Bell AJ, Jung T-P (1996) Independent component analysis of electroencephalographic data. Adv Neural Info Proc Syst 8:145–151

Makeig SD, Debener S, Onton J, Delorme A (2004) Mining event-related brain dynamics. Trends Cogn Sci 8:204–210

McKeown MJ, Makeig SD, Brown GG, Jung T-P, Kindermann SS, Bell AJ, Sejnowski TJ (1998) Analysis of fMRI data by blind separation into independent spatial components. Hum Brain Mapp 6:160–188

Menninghaus E, Lütkenhöner B (1995) how silent are deep and radial sources in neuromagnetic measurements. In: Baumgartner C (ed) Biomagnetism: fundamental research and clinical applications. Elsevier Science, Vienna, pp 352–356

Palmer JA (2006) Variational and scale mixture representations of non-Gaussian densities for estimation in the Bayesian linear model: Sparse coding, independent component analysis, and minimum entropy segmentation. University of California, San Diego

Palmer JA, Kreutz-Delgado K, Rao BD, Makeig SD (2007) Modeling and estimation of dependent subspaces with non-radially symmetric and skewed densities. Independent component analysis and signal separation. Springer, Heidelberg, p 97–104

Pernet CR, Chauveau N, Gaspar C, Rousselet GA (2011) LIMO EEG: a toolbox for hierarchical LInear MOdeling of ElectroEncephaloGraphic data. Comput Intell Neurosci 2011:1–11

Takada K, Nomura K, Ono Y, Kurosawa M, Ishiyama A, Kasai N, Nakasato N (2000) MEG/EEG Hybrid Method for Source Localization of a Dipole with Radial Component. Papers of Technical Meeting on Magnetics MAG-00:23–28

Trujillo-Barreto NJ, Aubert-Vázquez E, Penny WD (2008) Bayesian M/EEG source reconstruction with spatio-temporal priors. NeuroImage 39:318–335

Tsai AC, Jung T-P, Chien V, Savastyanov AN, Makeig SD (2013) Cortical surface alignment in multi-subject spatiotemporal independent EEG source imaging. J Neurosciencce (in press):1–28

Tsai AC, Liou M, Jung T-P, Onton JA, Cheng PE, Huang C-C, Duann J-R, Makeig SD (2006) Mapping single-trial EEG records on the cortical surface through a spatiotemporal modality. NeuroImage 32:195–207

Tukey PA, Tukey JW (1981) Graphical display of data sets in three or more dimensions. In: Barnett V (ed) Interpreting Multivariate Data. Wiley, Chichester

Whitmer D, Worrell G, Stead M, Lee IK, Makeig SD (2010) Utility of independent component analysis for interpretation of intracranial EEG. Front Hum Neurosci 4:184

Fusing Concurrent EEG and fMRI Intrinsic Networks

David Bridwell and Vince Calhoun

Abstract Different imaging modalities are sensitive to different aspects of brain activity, and integrating information from multiple modalities can provide an improved picture of brain dynamics. Electroencephalography (EEG) and functional Magnetic Resonance Imaging (fMRI) are often integrated since they make up for each other's limitations. FMRI can reveal localized intrinsic networks whose BOLD signals have periods from 100 s to about 10 s. EEG recordings, in contrast, reflect cortical electrical fluctuations with periods up to 20 ms or higher. The following chapter surveys the physiological differences between EEG and fMRI recordings and the implications and results of their integration. EEG-fMRI findings are reviewed in cases where individuals do not participate in an explicit task (e.g. during "rest"). The results are discussed in the context of different methodological approaches to EEG-fMRI integration, including correlation and GLM-based analysis, and ICA decomposition of group EEG-fMRI datasets. The resulting EEG-fMRI networks capture a broader range of brain dynamics compared to EEG or fMRI alone, and can serve as a reference for studies integrating MEG and fMRI.

Keywords BOLD fMRI · EEG · ERP · Networks · Oscillations · Intrinsic connectivity · Spatiotemporal dynamics · Data fusion · Source separation

D. Bridwell (✉)
Mind Research Network, Albuquerque, NM, USA
e-mail: dbridwell@mrn.org

V. Calhoun
Electrical and Computer Engineering, University of New Mexico, Albuquerque, NM, USA
e-mail: vcalhoun@mrn.org

S. Supek and C. J. Aine (eds.), *Magnetoencephalography*,
DOI: 10.1007/978-3-642-33045-2_9,

1 Introduction and Motivation

Brain networks operate over a broad range of spatial and temporal scales. Our ability to capture brain network activity is limited by the spatial and temporal resolution of the tools that are available. The most common non-invasive imaging modalities are blood oxygenation level dependent (BOLD) functional magnetic resonance imaging (fMRI), magnetoencephalography (MEG), and electroencephalography (EEG). Each of these modalities provide a distinct, but limited, window onto brain network activity. Researchers are therefore interested in integrating information obtained from these different modalities in order to obtain a more detailed picture of true underlying brain dynamics.

The following chapter addresses some of the motivations, methodology, difficulties, and results of integrating EEG and fMRI. EEG and fMRI are widely used for multimodal integration since they make up for each other's spatial and temporal limitations. EEG is sensitive to temporal dynamics on the millisecond timescale, but has very limited spatial resolution. FMRI, in contrast, is sensitive to spatial differences on the order of millimeters, but can only capture temporal changes on the order of seconds. MEG provides comparable spatial and temporal resolution to EEG with the additional advantage that magnetic source activity is not spatially filtered by the volume conduction properties of the scalp, skull and brain. In addition, EEG and MEG are each sensitive to activity at comparable spatial scales, or volumes of cortex. However, MEG, due to the direction of magnetic field lines, is preferentially sensitive to cortical activity oriented tangential (or sulcal) to the scalp, while EEG is preferentially sensitive to radial (or gyral) activity (Cohen and Cuffin 1983). EEG and MEG each provide relatively distinct measures of cortical source activity. This motivates methodological approaches that can integrate information both between EEG-fMRI and between MEG-fMRI.

In addition to their complementary spatial and temporal sensitivities, fMRI and EEG differ in terms of the aspects of neural activity that they are most sensitive. EEG is sensitive to synchronous neural electrical potentials primarily along cortical gyri (Cohen and Cuffin 1983). BOLD fMRI, in contrast, is sensitive to neural metabolic processes via its coupling with changes in local blood oxygenation. EEG therefore provides a measure of neural activity directly along the cortical surface while fMRI provides an indirect measure of neural activity throughout the entire brain.

The different spatiotemporal and neural sensitivities of fMRI and EEG raise caution in assuming a direct one to one correspondence between the two. It is a strong assumption that fMRI responses represent the spatial location of the observed EEG directly, or that EEG responses directly reflect the temporal dynamics of responsive fMRI spatial locations. Instead EEG and fMRI are sensitive to the different aspects of neural activity that operate over their respective temporal and spatial scales. EEG may reflect the activity within only a subset of

activated voxels, or EEG may reflect the activity within brain networks that covary in a complex manner with fMRI networks.

Different analysis approaches impose different assumptions on the relationship between EEG and fMRI. One line of research assumes a direct relationship between them, for example, by constraining EEG sources or inverse solutions to BOLD fMRI activations or structural MRI locations within radially oriented cortical gyri (e.g. Ahlfors and Simpson 2004; Lin et al. 2005). Alternatively, another line of research focuses on common temporal modulations within each modality irrespective of their spatial overlap. In this instance, fMRI voxels may be associated with EEG responses measured anywhere over the scalp, and vice versa. The linked EEG-fMRI responses reveal brain networks that overlap after incorporating the broader range of spatial and temporal scales available within each modality (Siegel et al. 2012).

2 Physiological Considerations in EEG-fMRI

The sections below provide a broad overview of the physiology underlying EEG and BOLD fMRI responses. These physiological differences are an important consideration in EEG-fMRI study design and in the subsequent approach to EEG-fMRI analysis. The differences also provide important context for interpretation of the EEG-fMRI findings reviewed in the sections of the chapter that follow.

2.1 The Neural Basis of EEG

The first human EEG recordings were reported by Berger (1929) in his seminal paper. His initial observations were met with skepticism within the scientific community, and even Berger himself was wary of the findings. The initial skepticism was rightfully warranted, as it is difficult to imagine that small changes in brain activity would propagate through the head, generating measurable electrical potentials on the surface of the scalp.

EEG measures micro-volt differences in scalp electric potentials that emerge from the aggregate activity of a large number of cortical pyramidal neurons. Synaptic inputs to pyramidal cells generate small sources and sinks along the cell membrane. These sources and sinks are space averaged over cortical areas that approximate the size of cortical columns. Pyramidal neurons are aligned parallel to each other along the cortex, forming a patch of neural tissue that approximates a dipole moment vector or more realistically, a dipole *layer*. Scalp EEG is thought to reflect the average extracellular current generated from these pyramidal synaptic potentials. In order for the current to propagate to the scalp the net charge of an individual patch of tissue must be oriented perpendicular to the scalp, and must not be completely canceled out by opposing charges within neighboring tissues.

A single EEG electrode reflects dynamic fluctuations in neural activity over an at least cm^2 sized patch of cortex.[1] EEG responses can be distinguished as "local" or "global" by comparing the raw cortical potential with its spatially filtered representation (e.g. with surface Laplacian or current source density (CSD) analysis). Local sources are located underneath the electrode and are consistent with the assumption of a single dipole source. Global sources are present over many electrodes, correspond to either large areas of cortical activation or deep sources, and are inconsistent with the dipole assumptions of source localization (Nunez 2000; Srinivasan 2005).

Currents move in opposite directions at any given moment along certain locations of the scalp, forming sources and sinks. The overall current moving perpendicular in one direction along the scalp equals the current moving in the other direction. The movement of currents, and the spatial location of source and sinks, depends on the skull conductivity. Skull conductivity differs across the head due to differences in skull thickness and the nature of the bone tissue. Thus, scalp sources and sinks are more likely to appear over the locations with increased skull conductivity (Chauveau et al. 2004; Cuffin 1993; Nunez and Srinivasan 2006). These locations may not directly overlap with the location of cortical activity.

EEG responses reflect cortical potentials conducted through cerebrospinal fluid (CSF), the skull, and the scalp. The resistivity of these tissues contributes to the *volume conduction* properties of the head, effectively forming a *head transfer function* (Nunez and Srinivasan 2006). Theoretical studies suggest that these volume conduction properties emphasize large dipole layers over small dipole layers (Srinivasan et al. 1996). This low-pass spatial filtering property of the head effectively acts as a low-pass temporal filter as well, since larger areas of activation are associated with greater transmission delays and increased transmission delays render it difficult to sustain high frequency oscillations (e.g. within gamma band responses appearing at 40 Hz and above). Thus, low frequency EEG responses between 1–12 Hz (e.g. incorporating the delta, theta, and alpha bands) are often global or widespread (Nunez and Srinivasan 2006).

In summary, it should be clear that there are a number of nuances to consider along with the statement that "EEG reflects synchronous cortical electrical fluctuations". Notable nuances include the orientation of the cortical source, the degree in which cortical sources are cancelled out by neighboring tissues, the distance between the cortex and the electrode, and the choice of reference. In addition, the spatial location of EEG is influenced by differences in electrical conductivity over the skull, and the observed potentials reflect a low-pass spatially (and temporal) filtered representation of the underlying cortical sources. Some of these issues with EEG are absent in MEG recordings, and are thus an important consideration when comparing findings from EEG-fMRI and MEG-fMRI.

[1] Note that the voltage at a single electrode reflects the *difference* in potential between that electrode and a reference electrode. The electrode is commonly re-referenced to the average of all electrodes.

2.2 The Neural Basis of BOLD fMRI

Increases in neural activity within a particular brain area result in increased blood flow to that same area. For example, tapping your finger for a few seconds will result in increased blood volume within vessels that supply the motor cortex. The enhanced blood flow response carries oxygen to the activated neural tissue, although the amount of oxygen available to the tissues exceeds the tissues needs. It has been said that the excessive increase in blood volume is akin to a gardener "watering the entire garden for the sake of one thirsty flower" (Malonek and Grinvald 1996).

The mechanism and function of the large increase in blood flow is a topic of ongoing research. One hypothesis is that the large increase in blood flow may help maintain a constant tissue oxygen pressure (pO2) (Buxton 2010). This hypothesis emphasizes the importance of pO2 in oxygen metabolism, which is interesting in light of the observation that tissue pO2 appears to approximate the level of pO2 in the atmosphere when oxygen metabolism first arose on earth. Regardless of the functional role, however, there is no debate that the large increase in blood flow is fortuitous, since it is a phenomenon on which the majority of functional neuroimaging studies are based.

Blood oxygenation levels serve as a proxy for underlying changes in neural activity. The relationship between neural activity and blood oxygenation is complex and indirect. Neural activity leads to an increase in cerebral oxygen metabolism ($CMRO_2$) and an increase in cerebral blood flow (CBF). These two effects contribute to the measured fMRI response in opposite ways. A sudden increase in oxygen metabolism leads to a decrease in oxygenated hemoglobin, which, due to its magnetic properties, disrupts the magnetic field and reduces the BOLD fMRI response. The increase in CBF replaces deoxygenated hemoglobin with oxygenated hemoglobin, which reduces the magnetic field distortion and contributes to increased fMRI responses.[2] The neural mechanisms that lead to decreased $CMRO_2$ may differ somewhat from the mechanisms that lead to increased CBF. Relatedly, the ratio of $CMRO_2$ and CBF changes can differ within the same brain area across subjects, across brain areas within a single subject, and even within the same brain area in response to different stimuli. This means that the observed percent signal change can differ in situations where neural activity is the same (for a review see Buxton 2010).

The BOLD response is most sensitive to aspects of neural activity that are associated with increased aerobic metabolism. Attwell and Laughlin (2001) estimate that the majority of the brain's energy is devoted to restoring postsynaptic ion gradients. This supports the notion that BOLD fMRI more closely reflects synaptic integration than neural spike rate, as demonstrated empirically by stronger correlations between BOLD fMRI and the local field potential (LFP) than with

[2] The term "BOLD" is not technically accurate since the response depends upon *deoxygenated* hemoglobin.

microelectrode measures of spiking activity (Logothetis et al. 2001) (for exceptions see Ekstrom 2010). The sensitivity to synaptic integration means that the BOLD signal is sensitive to *inputs* to a particular area, without directly depending upon whether or not those inputs were effective at generating spikes (i.e. outputs) to other areas.

In addition, the observed BOLD response can be conceptualized as the neural metabolic process convolved with a hemodynamic response function (HRF). The HRF filter peaks about ~6 s following the onset of the initial neural/metabolic event. The ~6 s delay accounts for the sluggishness of blood flow changes in response to neural activity. It is this delay, and the limited sampling rate of fMRI, that contribute to the reduced temporal resolution of fMRI recordings.

2.3 Physiological Overlap Between EEG-fMRI

The finding that EEG and fMRI are sensitive to different aspects of neural activity does not make EEG-fMRI integration a futile endeavor. Instead, if EEG and fMRI completely overlapped in their neural and spatiotemporal sensitivities then their integration would be redundant and pointless. Instead, linking the two provides an improved window onto the brain's spatiotemporal dynamics by incorporating their non-overlapping range of spatial and temporal sensitivities. The resulting EEG-fMRI networks indicate that synaptic activity changes (coupled with metabolism and blood flow) at fMRI spatial locations are related to synchronous cortical potentials (from pyramidal cells) at certain EEG frequencies.

EEG and fMRI have many important commonalities. The sensitivity of fMRI to synaptic metabolism overlaps well with the sensitivity of EEG to synchronous cortical potentials. For example, both EEG and fMRI appear to overlap more with the low frequency spectrum of multi-unit activity (e.g. up to 250 Hz) compared to the high frequency spectrum (e.g. from 500–1,000 Hz). The low frequency spectrum (i.e. the local field potential or LFP) is thought to represent integrative perisynaptic processes, while the high frequency spectrum reflects "multi-unit" spiking activity. The processes generating LFP's thus overlap with the processes generating EEG and the metabolic processes thought to drive BOLD fMRI (for reviews see Heeger and Ress 2002; Logothetis 2008) (for exceptions see Ekstrom 2010). However, the direct relation between fMRI and LFP's is less straightforward since spiking activity is often correlated with both fMRI and LFP's. This association is strengthened by cases where correspondence is observed between fMRI and LFP in the absence of spiking activity. Similar correspondence (e.g. between spiking activity and fMRI in the absence of LFP's) is rarely observed (Goense and Logothetis 2008; Logothetis et al. 2001). With regards to EEG, the physiologically interesting frequencies observed in LFP's overlap reasonably well with the frequencies commonly studied in EEG. For example, the characteristics of the alpha frequency band (e.g. 8–12 Hz) have also been examined in visual LFP recordings (Bollimunta et al. 2011; Mo et al. 2011).

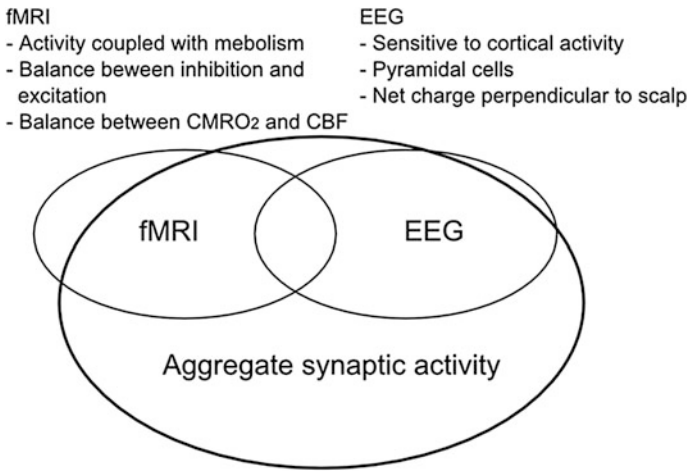

Fig. 1 EEG and fMRI are each primarily sensitive to synaptic activity. The factors that contribute to the non-overlap between EEG and fMRI are listed on *top*

An additional similarity between EEG and fMRI is that they are sensitive to responses that occur over similar volumes of brain tissue. It has been estimated that at least a cm^2 cortex must be synchronously active to generate electrical activity observable on the scalp (Nunez and Srinivasan 2006). This volume of cortex overlaps pretty well with the size of fMRI voxels, which typically range from about 27 to 64 mm^3. The voxels are subsequently smoothed with their neighbors in order to enhance the signal to noise ratio (SNR) of fMRI responses. This smoothing also brings a closer correspondence between the effective volume of fMRI voxels and the minimum volume of cortex for EEG. In either case however, EEG and fMRI each represent an *aggregate* measure of activity from the collective dynamics that emerge from millions of neurons (Fig. 1).

The aggregate window on brain activity provided by EEG and fMRI likely contributes to their utility in understanding cognition and perception. For example, cognition and perception are thought to emerge from the dynamic interactions between multiple brain areas (Siegel et al. 2012; Varela et al. 2001). These dynamic interactions likely overlap within the timescales of EEG, in the sense that the timescale of changes in our perceptual experience overlaps well with the timescales of fluctuations in EEG. EEG, for example, can separate the early visual response to sensory inputs from the subsequent visual response to the same input following reciprocal interactions with other brain areas (Lamme and Roelfsema 2000). FMRI provides a limited picture of these aspects of neural dynamics. However, fMRI is capable of measuring neural responses throughout the whole brain, providing a window on the brain areas that integrate together over second-by-second time scales.

Synchronization directly contributes to EEG and likely comprises synaptic integration processes that contribute to fMRI. The sensitivity of each measure to

synaptic integration suggests that they also provide an aggregate measure of neural excitability, since neural excitability appears to coincide with the phase of synchronous activity (Klimesch et al. 2007). These coordinated bursts of activity help ensure that neurons influence other brain areas in a coordinated, efficient manner. Thus, the spatiotemporal scales and neural sensitivities of EEG and fMRI appear relevant to understand the brain's integrative processes guiding cognition and perception.

3 Approaches to EEG-fMRI Integration

We now turn our focus to different approaches that have been utilized to integrate EEG and fMRI, and review the findings revealed through each approach. Associations between the two modalities time courses are considered, as examined by correlation or general linear modeling (GLM) of the time courses, by deconvolution of the EEG and fMRI time courses, or by independent component analysis (ICA) of multi-subject EEG and fMRI datasets. These approaches are insensitive to whether there is a direct causal relationship between EEG and fMRI. Thus, there is no implicit assumption that EEG reflects a measure of the neural activity that contributes directly to the BOLD fMRI response.

3.1 Overview of Correlation and GLM Based Findings

The most straightforward approach to integrating concurrent EEG and fMRI is by either correlating the time courses or by including the EEG time course as a predictor in a general linear model (GLM) analysis. In either case, the EEG time course is divided into non-overlapping epochs and converted to its frequency representation (e.g. by Fourier analysis), returning complex valued coefficients for each frequency and epoch. The coefficients are absolute valued, returning the amplitude of each frequency within a given epoch. The EEG epochs are chosen such that each amplitude value (within a given frequency) corresponds in time to a concurrently recorded fMRI acquisition. Broadly, this approach examines whether fluctuations within a given EEG frequency are related to fluctuations within a given fMRI voxel.

Temporal delays between the EEG and fMRI time courses are not directly accounted for in traditional correlation or general linear model (GLM) analysis, since they focus on the instantaneous relationship between variables. Therefore, the delay in the hemodynamic response must be accounted for prior to analysis. The characteristics of the hemodynamic delay are well described by the hemodynamic response function (HRF) (for review see Buxton et al. 2004). The assumption is that the BOLD fMRI response reflects a low-pass delayed representation of the underlying neural activity. The characteristics of the filter are

incorporated within the HRF shape. For example, the HRF peaks at a delay of ~6 s, which reflects the delayed increase in blood oxygenation following neural/metabolic events. The low-pass characteristic of the filter incorporates the temporal smearing that results from sluggish hemodynamics. These properties are accounted for by either convolving the EEG time course with the canonical HRF, or by deconvolving the fMRI time course with the canonical HRF.

The initial EEG-fMRI studies focused on correlations between individual fMRI voxel time courses and the amplitude time course of EEG frequencies. This approach can generate an unmanageable number of statistical comparisons if univariate tests are conducted separately for each of thousands of fMRI voxels and for dozens of EEG electrodes and frequency bands. The number of statistical comparisons is typically reduced by focusing a priori on a subset of EEG frequency bands and/or on a subset of fMRI regions of interest (i.e. ROIs). Data decomposition approaches have also been quite successful at reducing the data to a few underlying sources (Eichele et al. 2009).

Initial EEG-fMRI studies focused on fMRI responses associated with the EEG alpha band (e.g. 8–12 Hz). The emphasis on the alpha band was motivated by its robust presence in individual recordings; alpha activity can be observed by an untrained experimenter in unprocessed EEG. The robust presence of alpha activity is particularly important in concurrent EEG-fMRI since the scanner environment introduces substantial artifacts in the EEG (for review see Ritter and Villringer 2006). The salience of alpha activity in EEG recordings likely contributes to their "salience" in the EEG literature, as decades of research have been conducted on the generators and characteristics of the EEG alpha rhythm. It was appropriate that the first EEG-fMRI studies focused on the alpha band as well.

Alpha oscillations appear predominantly over occipital electrodes and demonstrate a robust increase when individuals close their eyes, are drowsy, or engage in mental arithmetic (Klimesch et al. 2007). These tasks involve a lesser degree of visual cortical activity, thus, increased occipital alpha activity is thought to reflect cortical inactivity. This inactivity reduces the ability of visual areas to influence areas of the brain that support current cognitions or tasks. For example, increases in alpha activity are associated with reduced resting-state connectivity between early visual areas and the rest of the brain (Scheeringa et al. 2012). Increased visual inactivity is also synonymous with increased synchrony across visual areas, increased dependence across areas, and an overall reduction in visual complexity (Edelman and Tononi 2000). These processes are also likely associated with reduced cortical metabolism, and the sensitivity of BOLD fMRI to metabolic processes allowed the unique ability to test this theory.

Early EEG-fMRI studies have indeed demonstrated negative relationships between alpha activity and occipital, parietal, temporal, and fontal fMRI responses (Bridwell et al. 2013; de Munck et al. 2009; Goldman et al. 2002; Laufs et al. 2003; Sadaghiani et al. 2010; Scheeringa et al. 2011), and positive relationships between alpha and the thalamus (Bridwell et al. 2013; de Munck et al. 2009; Goldman et al. 2002). The negative correlation is consistent with the idea that increased alpha activity reflects reduced cortical metabolism and a subsequent

Table 1 Main findings from select EEG-fMRI studies

Study	Rest	Frequencies examined (Hz)	Source separation	Main findings
Goldman et al. (2002)	Yes (EC: eyes closed)	Alpha (8–12)	No (fMRI)	− with alpha (occipital, temporal, frontal)
			No (EEG)	+ with alpha (thalamus)
Laufs et al. (2003)	Yes (EC)	Alpha (8–12)	No (fMRI)	− with alpha (parietal and frontal)
		Beta (17–23)	No (EEG)	+ with beta
Mantini et al. (2007)	Yes (EC)	Delta (1–4)	Yes (fMRI)	+ with multiple frequencies
		Theta (4–8)	No (EEG)	
		Alpha (8–13)		
		Beta (13–30)		
		Gamma (30–50)		
Sammer et al. (2007)	No (mental arithmetic)	Theta (3.5–7.5)	No (fMRI)	+ with theta
			Yes (EEG)	
Scheeringa et al. (2008)	Yes (EO: eyes open)	Delta	No (fMRI)	− with delta/theta ("resting state networks")
		Theta	Yes (EEG)	
de Munck et al. (2009)	Yes (EC)	Delta (0.1–4)	No (fMRI)	− with alpha (occipital, parietal)
		Theta (4.5–8)	No (EEG)	+ with alpha (thalamic)
		Alpha (8.5–12)		
		Beta (12.5–36)		
		Gamma (36.5–100)		
Sadaghiani et al. (2010)	Yes	All (1–30)	No (fMRI)	− with alpha1 and beta1 (dorsal attn. network)
			No (EEG)	+ with alpha2 and beta2 (alertness network)
Scheeringa et al. (2011)	No (attention task)	All (2.5–120)	No (fMRI)	− with alpha and beta
			Yes (EEG)	+ With gamma
Bridwell et al. (2013)	Yes (EO+EC)	All (1–35)	Yes (fMRI)	− with alpha3, alpha4, beta1
			Yes (EEG)	+ with delta, theta, beta2, gamma

reduction in the BOLD fMRI response. Equivalently, increased metabolism is associated with increased fMRI responses and a reduction in alpha. This interpretation was further supported by Moosmann et al. (2003) by demonstrating a negative relationship between changes in deoxy hemoglobin (measured by near-infrared spectroscopy (NIRS)) and alpha EEG. The main findings from selected "resting-state" EEG-fMRI studies are demonstrated in Table 1. The majority of studies demonstrate a negative relationship between fMRI and EEG alpha activity. Thus, this finding is one of the most consistent and reproduced findings in the EEG-fMRI literature. It can serve as a useful "sanity check" in EEG-fMRI.

3.2 Background and Advantages of ICA in EEG-fMRI

One of the most difficult challenges in multimodal integration is extracting meaningful information from high dimensional datasets. BOLD fMRI responses are obtained within tens of thousands of voxels and each EEG epoch contains information within multiple frequency bands over dozens of electrodes. Integrating the EEG channel by frequency information with the fMRI voxel information with the traditional correlation or GLM approach ignores the rich structure within each dataset, is computationally demanding, and generates an unmanageable number of statistical comparisons. These limitations can be alleviated with blind source separation (BSS) approaches such as spectral ICA (Bridwell et al. 2013; Wu et al. 2010), principle component analysis (PCA), and temporal ICA (for a review see Makeig et al. 2004), as well as semi-BSS approaches such as functional source separation (FSS) (Porcaro et al. 2010, 2011). These approaches decompose each observation as the linear sum of a small number of underlying sources.

Among the data decomposition techniques described above, spatial ICA has demonstrated to be particularly informative and useful in fMRI analysis. For example, ICA (implemented with the Infomax algorithm) can emphasize sparse independent spatial fMRI maps, which aligns with the assumption that cognitive activation is sparse and distributed, and with the sparse and spatially specific nature of cardiac and motion artifacts (McKeown et al. 1998). Temporal ICA is commonly utilized for EEG data, and the assumptions for temporal ICA align well with the theoretical generation of EEG. For example, the decomposition of a time course as a linear sum of independent temporal sources aligns well with the assumption that the response at a single electrode reflects a linear mixture of independent scalp sources[3] (for review see Makeig et al. 2004). ICA can also be conducted on EEG spectra, revealing spectral sources that peak within characteristic EEG frequency bands (Bridwell et al. 2013).

BSS approaches are particularly advantageous when EEG and/or fMRI are measured in the absence of an explicit task. For example, BSS algorithms such as ICA utilize the inherent structure in the data to extract underlying spatiotemporal activity patterns. These coherent patterns of activity likely result from activity within somewhat distinct brain modes or sources. The coherent nature of unique modes or sources suggests that they may also be described as distinct brain *networks*. The unique networks observed with ICA may demonstrate functionally distinct properties. For example, "resting-state" ICA can reveal sources which overlap with brain areas with greater activation during "internal" mental states (e.g. the so-called "default mode" areas). Other sources overlap with brain areas with greater activation during "external" attentive states (Corbetta et al. 2008). Of course, it is difficult or impossible to infer the functional role of networks that are

[3] "Sources" here refers to the independent sources estimated through ICA. These sources are different from the cortical "equivalent dipole sources" thought to generate EEG.

present in the absence of explicit tasks since the individuals' cognitions are unknown to the experimenter.

ICA is routinely used to extract independent spatial fMRI sources to link with concurrent EEG (for a review see Eichele et al. 2009). EEG is then associated with temporal fluctuations in fMRI spatial sources, rather than individual voxels or clusters. This is advantageous since it separates the voxel response at each point in time by the separate contribution of multiple independent sources. However, only a few EEG-fMRI studies have additionally conducted ICA on the EEG (Bridwell et al. 2013; Eichele et al. 2009; Wu et al. 2010). Thus, BOLD fMRI sources are often linked with EEG spectral information that potentially contains the combined contribution of multiple sources with overlapping frequency bands and spatial locations. A spectral EEG decomposition (with ICA) may reveal sources with distinct peaks that correspond to the traditional EEG frequency bands. This data-driven approach can validate the presence of distinct EEG frequency bands, improving the ability to link fMRI with EEG activity within each band.

It can be particularly important to decompose EEG spectra within the alpha band, as previous studies demonstrate that it contains the combined contribution of multiple distinct networks which may overlap spectrally and/or spatially. The 8–12 Hz alpha band has been subdivided by its upper and lower frequencies, and overlaps in frequency with the central mu rhythm. These different alpha sources demonstrate distinct spatial topographies, spectral peaks, and/or sensitivities to experimental manipulation (Niedermeyer 1997; Nunez et al. 2001), and the average 8–12 Hz activity represents the combined contribution of these multiple independent sources. The presence of multiple sources with overlapping spectral characteristics is also suggested by the difficulty indentifying the boundaries between EEG frequency bands within the average EEG spectrum and the presence of high correlations between the different frequency bands (de Munck et al. 2009; Mantini et al. 2007).

Conducting an independent group ICA within each modality can provide an improved measure of fMRI or EEG network activity while also helping to incorporate as much information as possible within each modality. The approach reduces the need to restrict the analysis to only a subset of fMRI networks (e.g. the default mode), or to restrict analysis to a subset of EEG electrodes or frequencies. An important consequence of this restriction is that it helps guarantee the frequency specificity of the results. Consider the negative relationship between alpha EEG and fMRI as an example. The demonstration of this relationship can be strengthened by demonstrating that similar relationships do not exist for other EEG frequency bands. For example, fluctuations in the alpha band likely reflect both broad fluctuations in the EEG spectral baseline, as well as fluctuations specific to the alpha band. This possibility can be directly addressed by including additional frequencies as covariates in a GLM (de Munck et al. 2009) or multiple linear regression (e.g. PPI) (Scheeringa et al. 2012), by reporting results obtained separately for multiple frequencies, and/or by extracting frequency specific sources with blind source separation (Bridwell et al. 2013; Scheeringa et al. 2008, 2011).

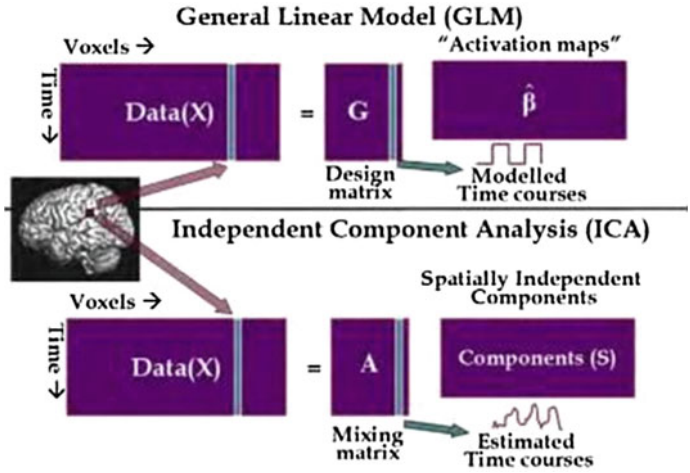

Fig. 2 Comparing the GLM and ICA for fMRI. The GLM estimates the contribution of each modeled time course to the observed data by deriving beta ($\hat{\beta}$), the "activation map". ICA models the observed data as a linear mixture of underlying spatially independent sources *S* (Adapted from Calhoun et al. 2009)

In either case, considering multiple frequency bands helps acknowledge the full constellation of fMRI and EEG networks that may be present at any given moment (Mantini et al. 2007; Siegel et al. 2012).

3.3 Multi-subject Extensions of ICA

ICA can extract spatiotemporal patterns within EEG or fMRI data when individuals are not engaged in an explicit task (i.e. "during rest"). Generalization of these results across subjects can be more challenging with ICA than a traditional GLM analysis. For example, GLM analysis can be conducted on fMRI data for each individual subject and the beta weight associated with the experimental time course is utilized as an independent observation in the second level group analysis. Generalization across subjects is straightforward since beta weights can correspond to the same experimental condition across all subjects. ICA decomposes the multivariate fMRI data into a set of independent spatial sources and their associated time courses. Thus, ICA essentially estimates the unknown time courses of functionally distinct spatial maps (in accordance with the assumptions of the ICA algorithm) (Fig. 2). Researchers are then faced with the challenge of pairing up common sources across individuals. This problem can be addressed by incorporating information from multiple subjects within a single ICA decomposition, and then examining the subject specific parts (Beckmann and Smith 2005; Calhoun et al. 2001; Esposito et al. 2005; Guo and Pagnoni 2008; Schmithorst and Holland

2004). We focus here on the group ICA technique implemented in Calhoun et al. (2001) and in the GIFT software package (http://mialab.mrn.org/software/gift/).

The typical ICA model assumes that each observation can be described as a linear mixture of independent sources. This can be demonstrated in an example with two observations represented by $\boldsymbol{X} = (x_1, x_2)^T$, begin generated from the following model:

$$X = AS.$$

$\boldsymbol{S} = (s_1, s_2)^T$ is the estimated sources and $\boldsymbol{A}$ is the estimated mixing matrix. The mixing matrix describes the contribution of each source at each observation. ICA estimates the matrix inverse of $\boldsymbol{A}$, which is denoted as the unmixing matrix $\boldsymbol{W}$. The unmixing matrix applies a spatial transformation of the observations to arrive at the estimated sources:

$$Y = WX,$$

which approximates the 'true' sources $\boldsymbol{S}$. ICA algorithms can emphasize the normality, independence, and complexity of the derived sources when estimating the unmixing matrix. For example, the infomax ICA algorithm iteratively changes the unmixing matrix in order to maximize the entropy of the estimated sources, which also maximizes their independence (Bell and Sejnowski 1995). Further details on ICA algorithms can be found in Stone (2004) and Hyvarinen et al. (2001).

Group ICA extends the ICA implementation described above in order to decompose data from multiple subjects. Group ICA estimates group sources based upon the aggregate group data and enables evaluation of individual subject differences via individual back-reconstructed components (Beckmann and Smith 2005; Calhoun et al. 2001; Erhardt et al. 2011). The individual data X_i is first compressed through principle components analysis (PCA), as expressed by:

$$Y_i = F_i^{-1} X_i.$$

F_i^{-1} is the reducing matrix derived from PCA for subject i. The reduced data from M subjects is concatenated in order to form an aggregate group matrix which, in the case of fMRI, is $[[time \times M]\ by\ voxels]$. The aggregate group matrix is compressed with PCA into the number of desired group components:

$$Y = G^{-1} \begin{bmatrix} F_1^{-1} X_1 \\ \cdots \\ F_M^{-1} X \end{bmatrix}.$$

The reducing matrix G^{-1} is a $[components\ by\ [time \times M]]$ matrix derived from PCA. The resulting matrix Y is decomposed through ICA (e.g. $Y = \hat{A}\hat{S}$) in order to

derive the [*component by voxel*] matrix of group sources $\hat{S}$. The individual subject loadings (i.e. time courses for spatial ICA) are derived by matrix multiplication of the individual partition of the PCA reducing matrix F_i by the individual partition of the aggregate reducing matrix G_i and $\hat{A}$ (Calhoun and Adali 2012; Calhoun et al. 2001; Erhardt et al. 2011).

The group ICA steps described above implement ICA on a data matrix containing the aggregate data from all of the subjects. Spatial group ICA is commonly applied to fMRI data. In this instance the data are concatenated temporally such that each column corresponds to the same spatial location across subjects. This approach assumes common aggregate spatial maps across subjects while allowing flexibility in the estimated time courses for each subject.

3.4 Group ICA Applied to EEG and fMRI

Spatial group ICA has been particularly effective with fMRI data collected in the absence of tasks (for review see Calhoun et al. 2009), or in cases where the experimental models may not necessarily be known in advance (Calhoun et al. 2002). Group ICA has recently been extended to time-locked EEG (i.e. event-related potentials (ERPs)) analysis during tasks (Eichele et al. 2011) and spatio-spectral EEG during rest. For example, Bridwell et al. (2013) decomposed 2D frequency by channel spectral maps into a set of group frequency by channel sources. The incorporation of frequency and channel information ensures that the decomposition utilizes as much of the data as possible, without restricting analysis to a single frequency band or electrode. The group sources correspond well with the characteristic frequency bands in EEG, and the temporal modulation of the group source is conceptually similar to the envelope of the response within the particular frequency band.

Group ICA can be conducted independently on EEG data and fMRI data collected concurrently. The data matrices are constructed so that the temporal modulations of the fMRI sources correspond in time with the temporal modulations of the concurrent EEG sources. EEG and fMRI can then be linked by focusing on relationships between the modulations within the two time courses. For example, the time courses may be correlated with each other after convolving the EEG time course with the canonical HRF or deconvolving the fMRI time course with a canonical HRF. This approach is less than optimal, however, as deviations in the assumption of a fixed HRF can reduce the sensitivity to instantaneous covariations between each modality. These assumptions can be relaxed by deconvolving the fMRI time course against the EEG time course, generating an estimated impulse response function (IRF). This approach treats the fMRI response as the output of the EEG response convolved with the unknown estimated filter (de Munck et al. 2009). If the neural activity measured with EEG overlaps with the neural activity that contributes to fMRI, then the estimated IRF will likely resemble the HRF.

Estimation of the IRF from the data directly can account for the variation in HRF shape observed across individuals and over different brain regions (Aguirre et al. 1998; Handwerker et al. 2004; Steffener et al. 2010).

An advantage of applying group ICA independently to fMRI and EEG is that the number of possible statistical tests reduces from *voxels* × *electrodes* × *frequencies*] to [*fMRI sources* × *EEG sources*]. Figure 3 indicates 56 group fMRI sources (in a) and 10 group EEG sources (in b). The results from all 560 comparisons are indicated in the [56 × 10] matrix in c. Positive associations (indicated by significant deviations in the estimated IRF) are indicated in white and negative associations are indicated in black. In general the majority of positive associations are present within the lower (e.g. delta and theta) and upper (e.g. high beta and low gamma) EEG frequencies, while the negative associations were primarily restricted to two of the five alpha components.

The widespread nature of the findings in Fig. 3 may be related to improved measurements of frequency specific activity by decomposing underlying EEG sources at the group level and by relaxing the assumption of a fixed relationship (e.g. the assumption of a canonical HRF) between EEG and fMRI (as in de Munck et al. 2007, 2009). This is particularly applicable for the theta band, since estimated theta IRFs less clearly resemble the canonical HRF (de Munck et al. 2007) and theta IRFs tend to be more variable across subjects compared to the alpha band (de Munck et al. 2009).

Variability in the IRF can contribute to the variability of results observed in the literature. For example, the relationship between fMRI and theta EEG is less consistent than the relationship with the alpha band. Scheeringa et al. (2008) indicates that frontal theta activity is negatively correlated with many fMRI regions during rest, including inferior frontal, medial frontal, inferior parietal, and medial temporal areas. The negative correlation with theta and medial frontal areas is also supported by (Mizuhara et al. 2004). Figure 3 primarily indicates positive associations between theta and fMRI, which agrees with positive associations that have been reported while individuals perform mental arithmetic tasks (Mizuhara et al. 2004; Sammer et al. 2007).

4 Further Considerations

4.1 The Importance of Concurrent Recording

The fMRI environment introduces substantial artifacts within EEG recordings. The fluctuating magnetic field induces electric current in EEG, which appears as EPI artifacts. Current is also induced by movement of EEG wires within the static magnetic field with each heart beat (i.e. the ballistocardiogram artifact). The EEG can also introduce artifacts within MRI (Luo and Glover 2012). Researchers must therefore consider whether the benefits of concurrent recordings outweigh the

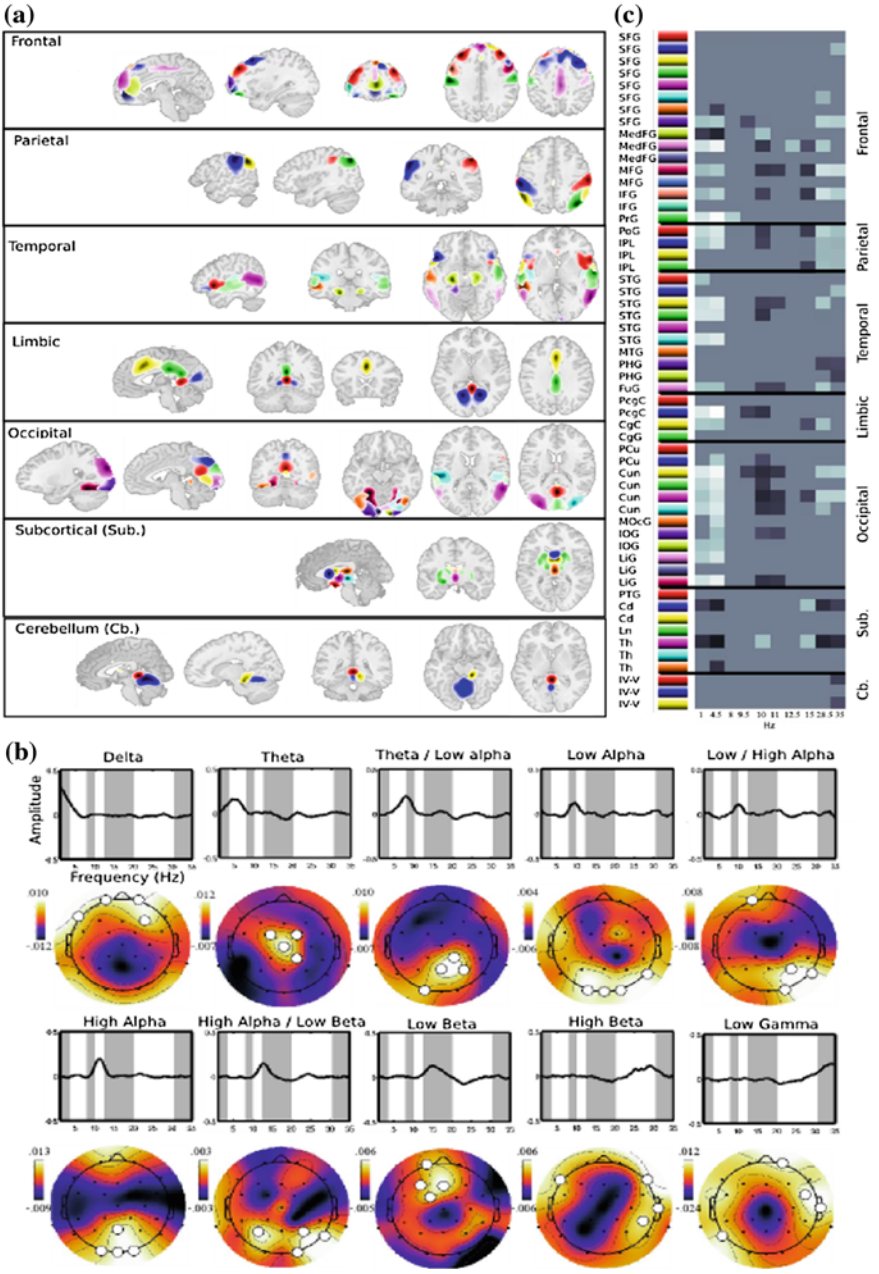

Fig. 3 Spatial fMRI components and their relationship to concurrent frequency by spatial EEG. 56 BOLD fMRI components are z-scored, thresholded and displayed in (**a**). The spectrum and topography of the 2D EEG sources are indicated in (**b**). The relationship between the sources are indicated by the [*fMRI source* $\times$ *EEG source*] matrix in (**c**). Significant positive associations are indicated along the *white grayscale* axis and significant negative associations are indicated along the *black grayscale* axis (Adapted from Bridwell et al. 2013)

costs associated with these artifacts. It may sometimes be the case that concurrent recordings are not necessary. For example, EEG responses are often averaged together after time-locking to an external event (i.e. with ERP analysis). This approach discards the trial-by-trial fluctuations within each EEG epoch, which strongly reduces the need to measure fMRI concurrently. Instead, ERPs can be measured outside of the scanner environment, and fluctuations within ERPs across subjects can be related to fluctuations in fMRI maps across subjects (Calhoun et al. 2006). Fluctuations in ERP and fMRI maps across subjects may be directly compared with results from MEG, which can further improve the ability to spatiotemporally characterize brain activity (Plis et al. 2010).

Concurrent recordings are particularly advantageous when examining the epoch-by-epoch fluctuations within each modality. For example, this approach demonstrates that fluctuations within a particular EEG frequency are associated with fluctuations within a particular fMRI spatial location. Concurrent recordings are important in this instance, since they can reveal the characteristics in which the brain dynamically integrates distant spatial locations in cognition and behavior (Debener et al. 2006).

4.2 Intrinsic Connectivity Networks

The spatiotemporal patterns that emerge from EEG or fMRI data are thought to reflect the brain's inherent structure or intrinsic connectivity. One might imagine that these networks describe a particular brain state, and that this particular state is involved in an aspect of cognition such that fluctuations within that state are associated with fluctuations in that cognition. These networks can be identified in the absence of explicit tasks (e.g. during "rest"), and research is beginning to focus on how the networks identified during rest can potentially inform individuals' ability to perform tasks (Carter et al. 2010; Deco et al. 2011).

The idea that "resting state" networks can predict performance is reasonable, since the cognitions that individuals experience during "rest" likely overlap with cognitions experienced during tasks. For example, attention is likely facilitated by enhanced activity within a subset of networks and suppressed activity within another subset. Tasks can promote attention, which promotes the ability to identify the subset of networks that facilitate attention. These same networks are likely present during "rest" since overlapping attentional processes likely occur during the "resting state".

Thus, the "resting state" should not be thought of as inherently distinct from tasks. Instead, it simply reflects the broad range of cognitions that can emerge when individuals are unconstrained by an explicit task. Broadly, this supports the idea that the intrinsic connectivity networks identified during rest might inform the degree in which individuals utilize attention and memory processes that underlie tasks.

An additional implication, however, it that the *relationship* between EEG-fMRI networks observed during rest may overlap closely with the relationship between EEG-fMRI networks identified during tasks. This brings up a distinction between the *extent* in which an area is activated, and the *coupling* of that area with other areas or modalities (O'Reilly et al. 2012). Consider the negative correlation between occipital fMRI voxels and EEG alpha. Individuals may perform tasks which suppress EEG alpha activity (e.g. reduces its extent), but the *relationship* between EEG alpha and occipital fMRI voxels would likely remain intact. In this instance, one would anticipate an overall reduction in EEG alpha and an overall increase in occipital fMRI responses. However, the relationship between alpha activity and occipital responses may remain the same, such that the two measures maintain the same correlation, and the estimated IRFs do not differ across the two conditions. This type of scenario is expected if the EEG-fMRI networks reflect the intrinsic structure of brain activity. Cognitive processes may modulate the extent in which a particular area is activated, but the inherent intrinsic structure would likely remain intact.

5 Summary

Combining the spatial information of fMRI and the spectral information of EEG can provide an improved picture of brain dynamics. These EEG-fMRI networks can be revealed even though each modality is sensitive to unique aspects of neural activity. The initial EEG-fMRI integration studies focused largely on fMRI responses associated with the EEG alpha band, and utilized correlation and GLM-based approaches. Decomposing the information within each modality (e.g. with ICA) can provide an improved ability to isolate distinct networks, which can facilitate subsequent EEG-fMRI or MEG-fMRI integration. Within this context, it can be particularly important to account for differences in the hemodynamic response across individuals and across brain areas. The resulting EEG-fMRI networks can supplement findings in MEG-fMRI. Overall, combining information within each modality provides an improved ability to isolate brain networks, which may help clarify their potentially distinct roles in cognition and behavior.

References

Aguirre GK, Zarahn E, D'Esposito M (1998) The variability of human, BOLD hemodynamic responses. NeuroImage 8:360–369

Ahlfors SP, Simpson GV (2004) Geometrical interpretation of fMRI-guided MEG/EEG inverse estimates. NeuroImage 22(1):323–332

Attwell D, Laughlin SB (2001) An energy budget for signaling in the grey matter of the brain. J Cereb Blood Flow Metab 21(10):1133–1145

Beckmann CF, Smith SM (2005) Tensorial extensions of independent component analysis for multisubject FMRI analysis. NeuroImage 25(1):294–311
Bell AJ, Sejnowski TJ (1995) An information-maximization approach to blind separation and blind deconvolution. Neural Comput 7(6):1129–1159
Berger H (1929) Uber das elektrenkephalogramm des menschen. Eur Arch Psychiatry Clin Neurosci 87:527–570
Bollimunta A, Mo J, Schroeder CE, Ding M (2011) Neuronal mechanisms and attentional modulation of corticothalamic alpha oscillations. J Neurosci 31(13):4935–4943. doi:10.1523/JNEUROSCI.5580-10.2011
Bridwell DA, Wu L, Eichele T, Calhoun VD (2013) The spatiospectral characterization of brain networks: fusing concurrent EEG spectra and fMRI maps. NeuroImage 1(69):101–111
Buxton RB (2010) Interpreting oxygenation-based neuroimaging signals: the importance and the challenge of understanding brain oxygen metabolism. Front Neuroenergetics 2:1–15
Buxton RB, Uludag K, Dubowitz DJ, Liu TT (2004) Modeling the hemodynamic response to brain activation. NeuroImage 23(Suppl 1):S220–S233
Calhoun V, Adali T (2012) Multi-subject independent component analysis of fMRI: a decade of intrinsic networks, default mode, and neurodiagnostic discovery. IEEE Rev Biomed Eng 5:60–72
Calhoun VD, Adali T, Pearlson GD, Kiehl KA (2006) Neuronal chronometry of target detection: fusion of hemodynamic and event-related potential data. NeuroImage 30(2):544–553
Calhoun VD, Adali T, Pearlson GD, Pekar JJ (2001) A method for making group inferences from functional MRI data using independent component analysis. Hum Brain Mapp 14(3):140–151
Calhoun VD, Liu J, Adalı T (2009) A review of group ICA for fMRI data and ICA for joint inference of imaging, genetic, and ERP data. NeuroImage 45(1 Suppl):S163
Calhoun VD, Pekar JJ, McGinty VB, Adali T, Watson TD, Pearlson GD (2002) Different activation dynamics in multiple neural systems during simulated driving. Hum Brain Mapp 16(3):158–167
Carter AR, Astafiev SV, Lang CE, Connor LT, Rengachary J, Strube MJ, Corbetta M (2010) Resting inter-hemispheric fMRI connectivity predicts performance after stroke. Ann Neurol 67(3):365–375
Chauveau N, Franceries X, Doyon B, Rigaud B, Morucci JP, Celsis P (2004) Effects of skull thickness, anisotropy, and inhomogeneity on forward EEG/ERP computations using a spherical three-dimensional resistor mesh model. Hum Brain Mapp 21(2):86–97
Cohen D, Cuffin BN (1983) Demonstration of useful differences between magnetoencephalogram and electroencephalogram. Electroencephalogr Clin Neurophysiol 56(1):38–51
Corbetta M, Patel G, Shulman GL (2008) The reorienting system of the human brain: from environment to theory of mind. Neuron 58(3):306–324. doi:10.1016/j.neuron.2008.04.017
Cuffin BN (1993) Effects of local variations in skull and scalp thickness on EEG's and MEG's. IEEE Trans Biomed Eng 40(1):42–48
de Munck JC, Goncalves SI, Huijboom L, Kuijer JPA, Pouwels PJW, Heethaar RM, da Lopes Silva FH (2007) The hemodynamic response of the alpha rhythm: an EEG/fMRI study. NeuroImage 35(3):1142–1151
de Munck JC, Goncalves SI, Mammoliti R, Heethaar RM, da Lopes Silva FH (2009) Interactions between different EEG frequency bands and their effect on alpha-fMRI correlations. NeuroImage 47(1):69–76
Debener S, Ullsperger M, Siegel M, Engel AK (2006) Single-trial EEG-fMRI reveals the dynamics of cognitive function. Trends Cogn Sci 10(12):558–563
Deco G, Jirsa VK, McIntosh AR (2011) Emerging concepts for the dynamical organization of resting-state activity in the brain. Nat Rev Neurosci 12(1):43–56. doi:10.1038/nrn2961
Edelman GM, Tononi G (2000) A universe of consciousness. Basic Books, New York
Eichele T, Calhoun VD, Debener S (2009) Mining EEG–fMRI using independent component analysis. Int J Psychophysiol 73(1):53–61. doi:10.1016/j.ijpsycho.2008.12.018
Eichele T, Rachakonda S, Brakedal B, Eikeland R, Calhoun VD (2011) EEGIFT: group independent component analysis for event-related EEG data. Comput Intell Neurosci 2011:9

Ekstrom A (2010) How and when the fMRI BOLD signal relates to underlying neural activity: the danger in dissociation. Brain Res Rev 62(2):233–244
Erhardt EB, Rachakonda S, Bedrick EJ, Allen EA, Adali T, Calhoun VD (2011) Comparison of multi-subject ICA methods for analysis of fMRI data. Hum Brain Mapp 32(12):2075–2095. doi:10.1002/hbm.21170
Esposito F, Scarabino T, Hyvarinen A, Himberg J, Formisano E, Comani S, Di Salle F (2005) Independent component analysis of fMRI group studies by self-organizing clustering. NeuroImage 25(1):193–205
Goense JBM, Logothetis NK (2008) Neurophysiology of the BOLD fMRI signal in awake monkeys. Curr Biol 18(9):631–640
Goldman RI, Stern JM, Engel J, Cohen MS (2002) Simultaneous EEG and fMRI of the alpha rhythm. NeuroReport 13(18):2487–2492. doi:10.1097/00001756-200212200-00022
Guo Y, Pagnoni G (2008) A unified framework for group independent component analysis for multi-subject fMRI data. NeuroImage 42(3):1078–1093
Handwerker DA, Ollinger JM, D'Esposito M (2004) Variation of BOLD hemodynamic responses across subjects and brain regions and their effects on statistical analyses. NeuroImage 21(4):1639–1651
Heeger DJ, Ress D (2002) What does fMRI tell us about neuronal activity? Nat Rev Neurosci 3:142–150
Hyvarinen A, Karhunen J, Oja E (2001) Independent component analysis. Wiley, New York
Klimesch W, Sauseng P, Hanslmayr S (2007) EEG alpha oscillations: the inhibition-timing hypothesis. Brain Res Rev 53(1):63–88. doi:10.1016/j.brainresrev.2006.06.003
Lamme VAF, Roelfsema PR (2000) The distinct modes of vision offered by feedforward and recurrent processing. Trends Neurosci 23(11):571–579
Laufs H, Krakow K, Sterzer P, Eger E, Beyerle A, Salek-Haddadi A, Kleinschmidt A (2003) Electroencephalographic signatures of attentional and cognitive default modes in spontaneous brain activity fluctuations at rest. Proc Natl Acad Sci USA 100(19):11053
Lin FH, Belliveau JW, Dale AM, Hämäläinen MS (2005) Distributed current estimates using cortical orientation constraints. Hum Brain Mapp 27(1):1–13
Logothetis NK (2008) What we can do and what we cannot do with fMRI. Nature 453(7197):869–878
Logothetis NK, Pauls J, Augath M, Trinath T, Oeltermann A (2001) Neurophysiological investigation of the basis of the fMRI signal. Nature 412(6843):150–157
Luo Q, Glover GH (2012) Influence of dense-array EEG cap on FMRI signal. Magn Reson Med 68(3):807–815
Makeig S, Debener S, Onton J, Delorme A (2004) Mining event-related brain dynamics. Trends Cogn Sci 8(5):204–210
Malonek D, Grinvald A (1996) Interactions between electrical activity and cortical microcirculation revealed by imaging spectroscopy: implications for functional brain mapping. Science 272(5261):551–554
Mantini D, Perrucci MG, Del Gratta C, Romani GL, Corbetta M (2007) Electrophysiological signatures of resting state networks in the human brain. Proc Natl Acad Sci 104(32):13170
McKeown MJ, Makeig S, Brown GG, Jung TP, Kindermann SS, Bell AJ, Sejnowski TJ (1998) Analysis of fMRI data by blind separation into independent spatial components. Hum Brain Mapp 6:160–629
Mizuhara H, Wang L-Q, Kobayashi K, Yamaguchi Y (2004) A long-range cortical network emerging with theta oscillation in a mental task. NeuroReport 15(8):1233–1238. doi:10.1097/01.wnr.0000126755.09715.b3
Mo J, Schroeder CE, Ding M (2011) Attentional modulation of alpha oscillations in macaque inferotemporal cortex. J Neurosci 31(3):878–882. doi:10.1523/JNEUROSCI.5295-10.2011
Moosmann M, Ritter P, Krastel I, Brink A, Thees S, Blankenburg F, Villringer A (2003) Correlates of alpha rhythm in functional magnetic resonance imaging and near infrared spectroscopy. NeuroImage 20(1):145–158. doi:10.1016/S1053-8119(03)00344-6

Niedermeyer E (1997) Alpha rhythms as physiological and abnormal phenomena. Int J Psychophysiol 26(1–3):31–49

Nunez PL (2000) Toward a quantitative description of large-scale neocortical dynamic function and EEG. Behav Brain Sci 23(3):371–398

Nunez P, Srinivasan R (2006) Electric fields of the brain: the neurophysics of EEG, 2nd edn. Oxford University Press, New York

Nunez P, Wingeier BM, Silbertein RB (2001) Spatial-temporal structures of human alpha rhythms: theory, microcurrent sources, multiscale measurements, and global binding of local networks. Hum Brain Mapp 13(3):125–164

O'Reilly JX, Woolrich MW, Behrens TEJ, Smith SM, Johansen-Berg H (2012) Tools of the trade: psychophysiological interactions and functional connectivity. Soc Cogn Affect Neurosci 7(5):604–609

Plis SM, Calhoun VD, Weisend MP, Eichele T, Lane T (2010) MEG and fMRI Fusion for non-linear estimation of neural and BOLD signal changes. Front Neuroinform 4:1–17. doi: 10.3389/fninf.2010.00114

Porcaro C, Ostwald D, Bagshaw AP (2010) Functional source separation improves the quality of single trial visual evoked potentials recorded during concurrent EEG-fMRI. NeuroImage 1:112–123

Porcaro C, Ostwald D, Hadjipapas A, Barnes GR, Bagshaw AP (2011) The relationship between the visual evoked potential and the gamma band investigated by blind and semi-blind methods. NeuroImage 56(3):1059–1071

Ritter P, Villringer A (2006) Simultaneous EEG-fMRI. Neurosci Biobehav Rev 30:823–838

Sadaghiani S, Scheeringa R, Lehongre K, Morillon B, Giraud A-L, Kleinschmidt A (2010) Intrinsic connectivity networks, alpha oscillations, and tonic alertness: a simultaneous electroencephalography/functional magnetic resonance imaging study. J Neurosci 30(30):10243–10250. doi:10.1523/JNEUROSCI.1004-10.2010

Sammer G, Blecker C, Gebhardt H, Bischoff M, Stark R, Morgen K, Vaitl D (2007) Relationship between regional hemodynamic activity and simultaneously recorded EEG-theta associated with mental arithmetic-induced workload. Hum Brain Mapp 28(8):793–803. doi:10.1002/hbm.20309

Scheeringa R, Bastiaansen M, Petersson KM, Oostenveld R, Norris DG, Hagoort P (2008) Frontal theta EEG activity correlates negatively with the default mode network in resting state. Int J Psychophysiol 67(3):242–251

Scheeringa R, Petersson KM, Kleinschmidt A, Jensen O, Bastiaansen MCM (2012) EEG alpha power modulation of fMRI resting state connectivity. Brain Connectivity 2:254–264

Scheeringa R, Fries P, Petersson K-M, Oostenveld R, Grothe I, Norris DG, Bastiaansen MCM (2011) Neuronal dynamics underlying high- and low-frequency EEG oscillations contribute independently to the human BOLD signal. Neuron 69(3):572–583. doi:10.1016/j.neuron.2010.11.044

Schmithorst VJ, Holland SK (2004) Comparison of three methods for generating group statistical inferences from independent component analysis of functional magnetic resonance imaging data. J Magn Reson Imaging 19(3):365–368

Siegel M, Donner TH, Engel AK (2012) Spectral fingerprints of large-scale neuronal interactions. Nat Rev Neurosci. doi:10.1038/nrn3137

Srinivasan R (2005) High-resolution EEG: theory and practice. In: Handy T (ed) Event-related potentials: a methods handbook. The MIT Press, Cambridge

Srinivasan R, Nunez PL, Tucker DM, Silberstein RB, Cadusch PJ (1996) Spatial sampling and filtering of EEG with spline Laplacians to estimate cortical potentials. Brain Topogr 8(4):355–366

Steffener J, Tabert M, Reuben A, Stern Y (2010) Investigating hemodynamic response variability at the group level using basis functions. NeuroImage 49(3):2113–2122. doi:10.1016/j.neuroimage.2009.11.014

Stone JV (2004) Independent component analysis: a tutorial introduction. MIT press, Cambridge

Varela F, Lachaux JP, Rodriguez E, Martinerie J (2001) The brainweb: phase synchronization and large-scale integration. Nat Rev Neurosci 2(4):229–239

Wu L, Eichele T, Calhoun VD (2010) Reactivity of hemodynamic responses and functional connectivity to different states of alpha synchrony: a concurrent EEG-fMRI study. NeuroImage 52(4):1252–1260

MRIVIEW: A Software Package for the Analysis and Visualization of Brain Imaging Data

Doug Ranken

Abstract MRIVIEW is a freely available, open-source software package written in IDL that is used to analyze and visualize brain imaging data. Key capabilities of MRIVIEW include a multi-start, multidipole, spatiotemporal MEG/EEG modeling program, an MEG/EEG forward simulator program, a large suite of image and volume processing for manipulating MRI or CT data, and both two dimensional and three dimensional visualization tools. Dipole-based modeling is provided by the Calibrated Start Spatial Temporal (CSST) multidipole inverse procedure that runs numerous spatiotemporal multidipole inverse fits from randomly selected sets of starting locations derived from a calibrated grid of cortical locations, to find a small number of sets of dipoles and associated timecourses that best fit the data. The MEG/EEG Forward Simulator provides an interactive environment for creating a wide range of realistic MEG/EEG forward simulations. A segmented layer of cortical voxels from a subject's MRI data is used to create cortical activity patches of arbitrary size and shape, and a tool is provided to assign individual timecourses to these patches. The head-to-sensor system geometry is used to create sensor forward values, based on the patch timecourses, and user-selected noise levels. A fully-integrated visualization environment is provided to view CSST and Forward Simulator results. MRIVIEW relies on a companion package, MEGAN, that provides extensive capabilities in signal processing and organization of MEG/EEG data.

Keywords Brain imaging · MEG · EEG · MRI · sMRI · fMRI · Spatiotemporal · Multi- start · Dipole analysis · Inverse procedures · Forward simulator · MUSIC · Cortical networks · Segmentation · Visualization

D. Ranken (✉)
Los Alamos National Laboratory, Los Alamos, NM 87545, USA
e-mail: ranken@lanl.gov

S. Supek and C. J. Aine (eds.), *Magnetoencephalography*,
DOI: 10.1007/978-3-642-33045-2_10,

1 Introduction

MRIVIEW was originally designed as a software tool for viewing and manipulating volumetric MRI head data, and for using this data as an anatomical reference in MEG studies of brain function (Ranken and George 1993). The initial MRIVIEW capabilities included methods for reading in raw MRI data, segmenting structures in the data, reconciling coordinate systems between multiple imaging modalities, viewing combinations of anatomical and functional information, and building models of structures within the head. Since its initial version, MRIVIEW has been extended in several directions, including: an MEG/EEG multi-dipole spatiotemporal modeling procedure (CSST), an MEG/EEG forward simulator, a greatly-expanded set of visualization capabilities, and additional image processing capabilities.

The Calibrated Start Spatial Temporal (CSST) multidipole inverse procedure is based on the Multi-Start Spatio-Temporal inverse procedure (MSST) (Huang et al. 1998). CSST runs multiple nonlinear simplex procedures from random combinations of MRI-derived cortical starting locations. For each set of starting locations, the simplex procedure minimizes a reduced Chi square value obtained from a linear fit of the dipole timecourses to the measured MEG or EEG sensor data. Using multiple combinations of starting locations allows the procedure to avoid local minima of the reduced Chi square error function. A parallel version of this procedure has been implemented, that uses MPI to distribute the calculation across a Linux cluster. This provides a linear speedup of the procedure on the number of processors, with very little overhead. Graphical interfaces, that are extensions of the MRIVIEW 3D Model Viewer, are used to set up CSST runs, and to view and analyze results.

The Forward Simulator (Ranken et al. 2002) allows a user to generate regions of cortical activity using ellipsoidal constraints on a segmented MRI volume, then assign separate timecourses to each of these regions. The timecourses can be sine waves, combinations of several Gaussians, or arbitrary timecourses from input files. The output is either an MEG or EEG forward calculation with user specified noise based on a sensor geometry derived from a netMEG file.

We begin by describing the computing environment for MRIVIEW, followed by discussions of the MRIVIEW interfaces for segmentation and visualization of MRI data, and for visualization of MEG/EEG analysis results. This is followed by an overview of CSST. The Forward Simulator is then described. Finally, we present a case study that uses both the Forward Simulator and CSST to investigate the feasibility of combining MEG and fMRI data to perform analyses of MEG single-pass data.

2 Computing Environment

MRIVIEW is implemented using the programming language and runtime environment IDL (Interactive Data Language), made by ExelisVIS (www.exelvis.com). IDL is an interpreted language, and can be used as an interactive data analysis and visualization environment, but it is mainly used as a fourth generation scientific programming language, and has similarities to Matlab. It supports arithmetic operations on multidimensional arrays, and has a wide range of analysis and visualization routines that typically operate on one to three dimensional arrays. IDL supports both procedural and object-oriented programming. One of its most useful features is optional keyword arguments in procedure and function argument lists. This makes it easy to extend the capabilities of existing IDL programs, while maintaining backward compatibility for codes that are already reliant on these programs. IDL also provides an Integrated Development Environment, for code development.

3 Two Dimensional Interface

When an MRI head data set is read into MRIVIEW, it is maintained as a 3 dimensional array that can be viewed in the 3 orthogonal view planes, to provide standard radiological views (sagittal, coronal and axial). MRIVIEW can read a broad range of MRI data formats. It converts these data to an MRIVIEW-standard format that relies on IDL's Save and Restore routines. The 2D Interface in MRIVIEW is used to view MRI data in the user-selected orientation, either 2- or 8 slices at a time, and allows quick paging through the MRI data volume. The 2D Interface is mostly used with the data segmenting capabilities. MRIVIEW provides semi-automated methods for labeling different structures within the head, such as the entire brain, gray matter, white matter, or the scalp. These can be used to create meshes for Boundary Element Method forward models, and labeled volumes for finite element of finite difference method models. Figure 1 shows a view of the 2D Interface, with the several head tissue classes labeled, used for a finite difference MEG forward model. Figure 2 shows a 3D rendering of this labeling on the left. MRIVIEW segmentations can also be used for visualization or location categorization purposes. A segmentation of the major brain compartments is shown in 3D on the right of Fig. 2.

4 Constrained 3D Interface

In order to localize MEG-derived brain activity on brain anatomy, it is often necessary to identify head fiducials in the MRI head data volume. The Constrained 3D Interface was initially developed to address this problem. With it, a

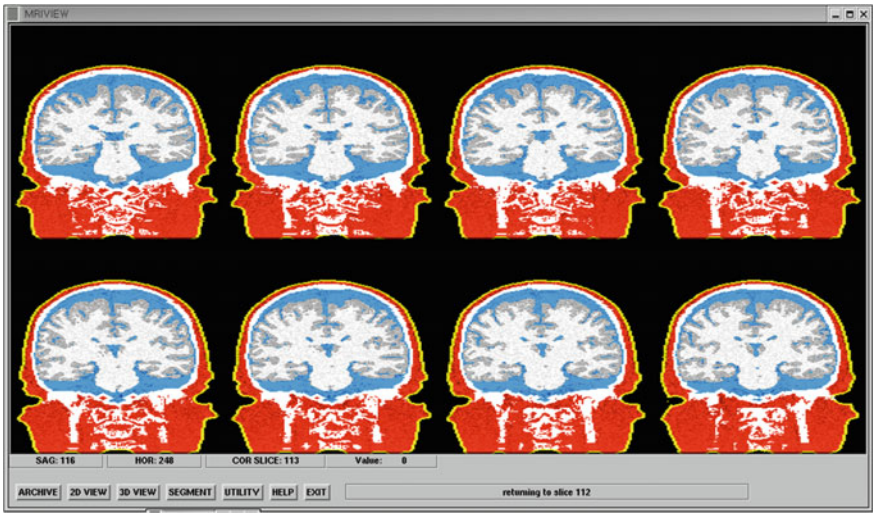

Fig. 1 The MRIVIEW 2D interface, shown here after performing a segmentation of MRI head data into 6 tissue types

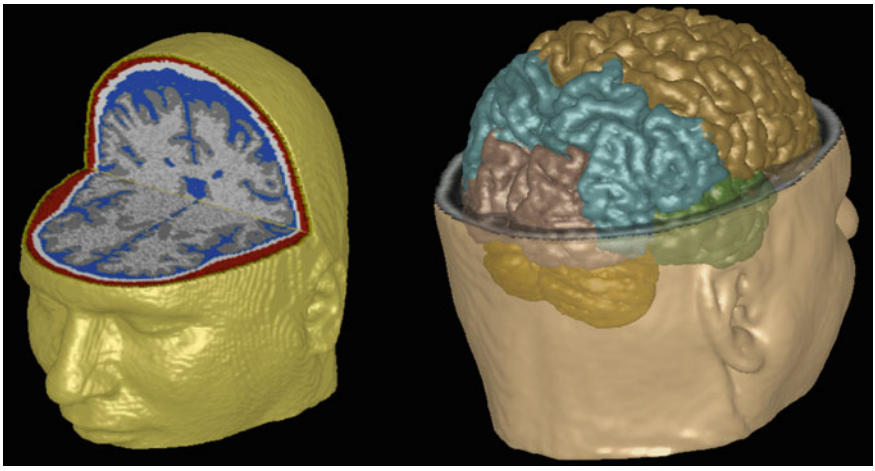

Fig. 2 The 6 tissue class segmentation is shown in 3D on the *left*. A segmentation of the major brain compartments is rendered in 3D on the *right*

user can obtain five head surface views (front, back, top, and sides), by selecting an isosurface value. A data structure links these five views to location information, so that cursoring over any of the five surfaces will select the corresponding orthogonal slice views, also shown in the interface (see Fig. 3). After the user selects fiducials corresponding to those used when obtaining MEG (or EEG) data, an MEG- (or EEG)-to-MRI coordinate transformation can be obtained, and used both

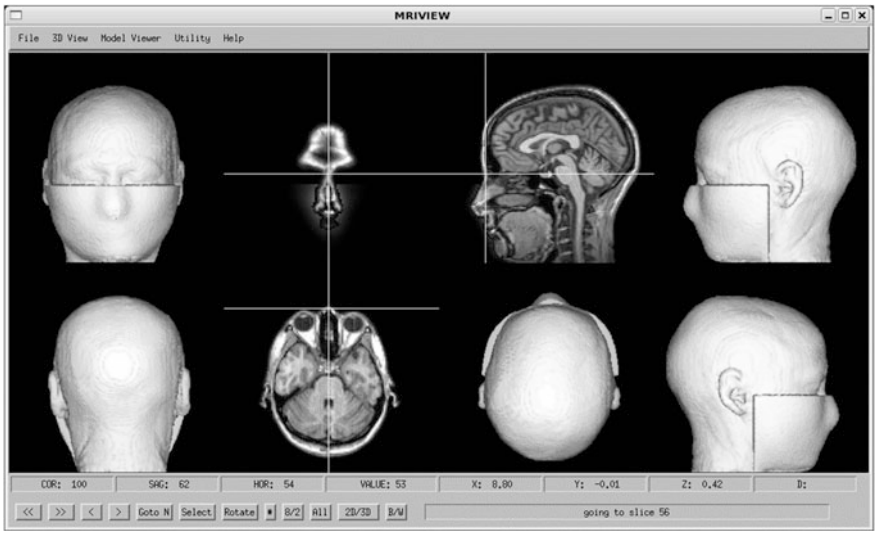

Fig. 3 The 8-panel view of the constrained 3D interface, showing selection of the nasion

for MEG (or EEG) forward (and thus inverse) calculations, and to plot representations of source activity on the MRI-based brain anatomy.

The other major use of the Constrained 3D Interface is with the MEG/EEG Forward Simulator. This will be discussed in the Forward Simulator section below.

5 Full 3D Interface

A full 3D interface, called the Model Viewer, was developed to show combinations of MRI-derived anatomy with representation of brain activity and sensor locations in a full 3D viewing environment. The Model Viewer consists of a procedural-based graphical user interface (GUI) that makes calls to an object-oriented viewing engine, which in turn utilizes many of the capabilities in the IDL Object Graphics library. The Model Viewer provides four model objects, that are used to store either volumetric or geometric data. Typically, the MRI data is loaded into Model 1, while source representations and other geometric information is loaded into Models 2 through 4. An isosurface of the MRI data can be obtained, and sliced in the 3 orthogonal directions to provide 3D reference anatomy. The slices and isosurface can each be shaded and colored independently, and are all stored in a single viewer model (Fig. 4). The Model Viewer can be used to show combinations of anatomy, sensor locations and magnetic or electric field values by using the available model containers to independently control, then combine model elements, as shown in Fig. 5.

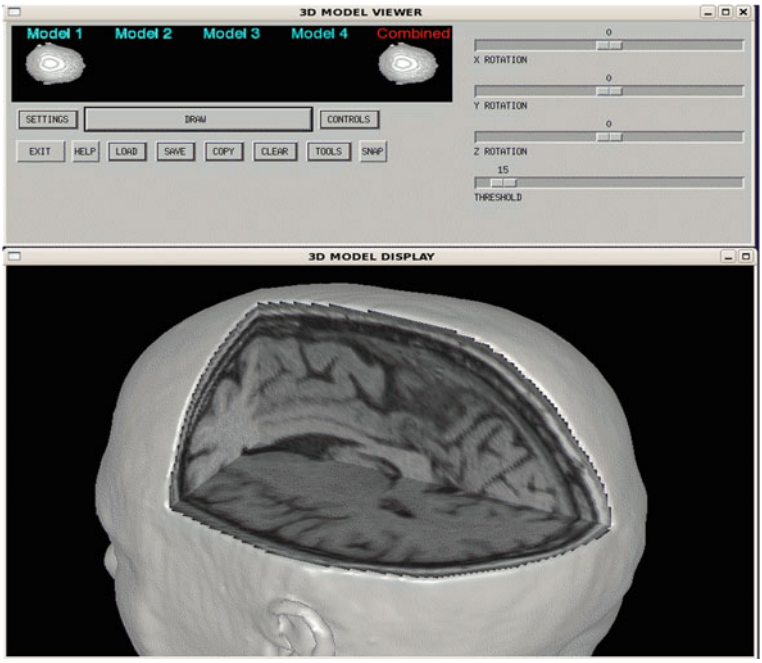

Fig. 4 3D model viewer user interface (*above*) and display window (*below*) showing orthogonal cutplanes

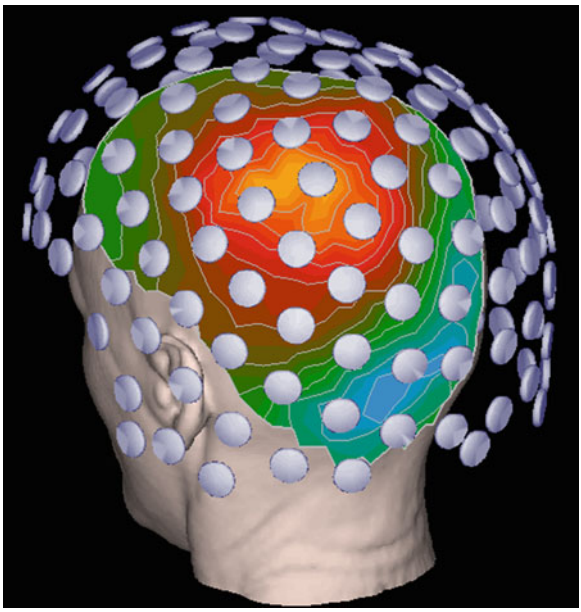

Fig. 5 MRI-based head anatomy is combined with MEG sensor geometry, and a color contour map representation of the magnetic field at the head surface

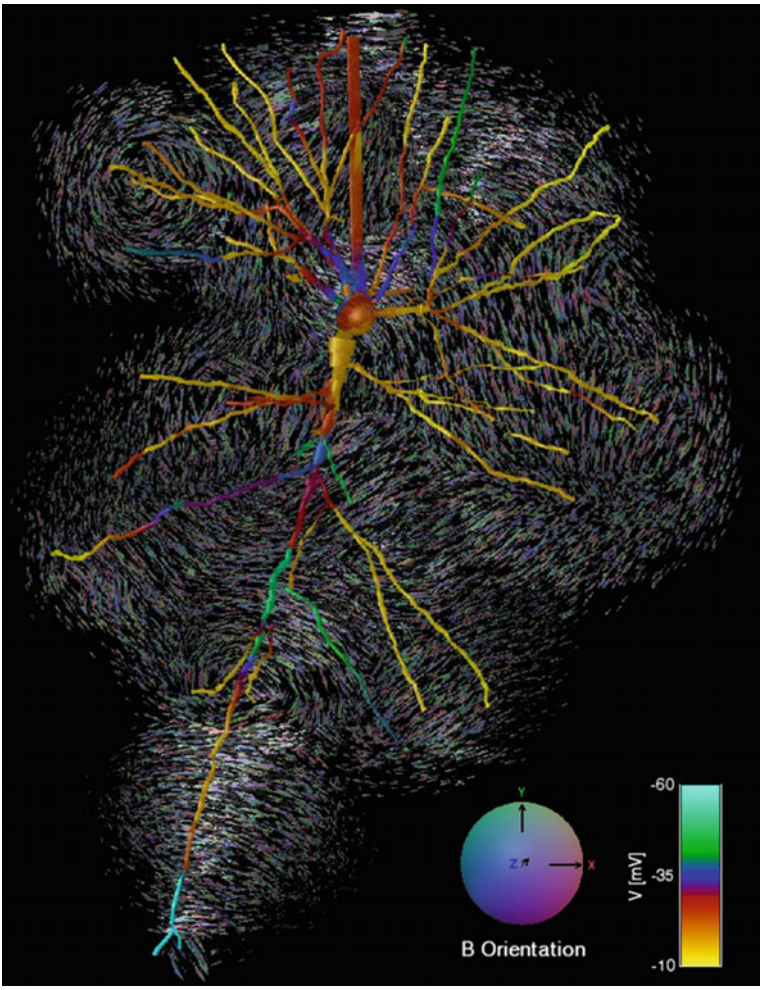

Fig. 6 A frame from a neuron electric potential and magnetic field simulation, generated using the API capabilities of the model viewer

The 3D Model Viewer has a small set of application programming interface (API) routines that can be used to perform more generalized 3D model viewing, including movie generation. The image in Fig. 6 is one frame from a neuron activation simulation movie, showing the changing electric potentials within the neuron, and corresponding magnetic fields surrounding it (Blagoev et al. 2007).

6 MEG/EEG Inverse Modeling

Inverse modeling is integrated into the Model Viewer interface of MRIVIEW, using CSST. In CSST, a multi-dipole inverse procedure is started M times, using M sets of N randomly chosen locations. M and N are user inputs, with N being the dipole model order. In CSST, the cortical voxel locations obtained with the segmentation procedures in the 2D Interface provide the set of locations from which the random starting points are selected. The segmentation procedures can be used to select different types of starting location sets, such as all the brain voxel locations, or locations from a selected area of the brain. Originally, cortical locations were typically used, because they provide good coverage of the brain using less than 40,000 points. Currently, the preferred approach uses a calibrated grid that spans the entire brain, with the grid becoming coarser for deeper regions of the brain, since brain activity in these deeper regions cannot be localized as accurately as more superficial sources, based on Cramer-Rao bounds (Mosher et al. 1993). Figure 7 shows a typical grid of starting locations. For each set of starting locations, the multi-dipole procedure implemented in CSST uses the Nelder-Mead nonlinear simplex procedure (Nelder and Mead 1965) to perform a spatial search. For each step of the simplex search, a singular value decomposition is used to obtain a linear fit to the sensor measurements, using a spherical model for MEG or a 3 sphere model for EEG, with unconstrained dipole orientations. A reduced Chi square value is calculated for this fit. This is the value that is minimized by the simplex procedure. The user selects how many of the best fits to save for a given program run. After processing, the Model Viewer in MRIVIEW can be used to display the CSST results (see Fig. 8).

For higher-dipole model orders (e.g., 5–9 dipoles) multi-start procedures become computationally intensive. For this reason, CSST, written in IDL, has been parallelized using the Message Passing Interface (MPI). The parallel version, MPI_CSST, uses a C language implementation of MPI to distribute the multiple starts across a user-selected number of processors in a Linux cluster, each running an instance of CSST. Each instance of CSST runs with its subset of the original set of starting locations. As each CSST process completes, the output is collated with the output from CSST processes that have already completed, to produce a combined output with the number of best fits requested by the user. The performance of MPI_CSST scales linearly with the number of processors used. The speed-up obtained using multiple processors makes the real-time use of MPI_CSST feasible.

6.1 Two-Stage Simplex Search

Many starting dipole configurations are far removed from an optimal solution, and end up converging on sub-optimal solutions after many iterations of the simplex minimization procedure. For this reason, a two-stage simplex approach has been

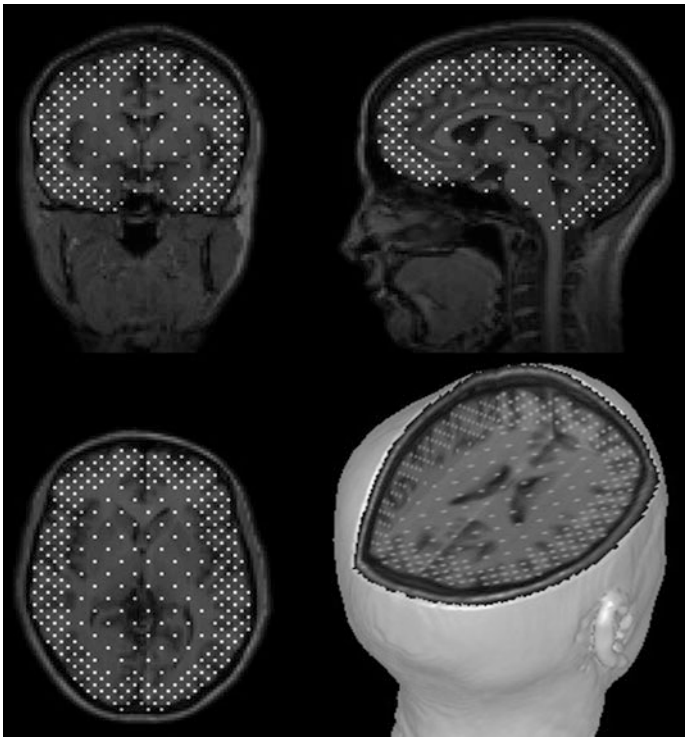

Fig. 7 Grid of brain locations from which CSST randomly selects numerous sets of initial dipole locations

added to MPI_CSST. Stage one uses a coarse convergence setting in the simplex procedure, saving a user-selected number of best solutions. A fine convergence setting is used in the second stage on these best solutions, to obtain the final results. This two-stage approach reduces the analysis time by 50 % or more, compared to the single-stage approach.

6.2 MUSIC-Seeded CSST

For difficult MEG/EEG inverse analyses (high model order, low SNR), CSST requires numerous random starts to achieve high confidence that a global minimum to the reduced Chi square function has been found. For instance, a six dipole model of MEG visual data may require 15,000 random starts with a CSST analysis. By incorporating the results of a MUSIC analysis into the selection of starting dipole configurations in CSST, the number of starting configurations needed to

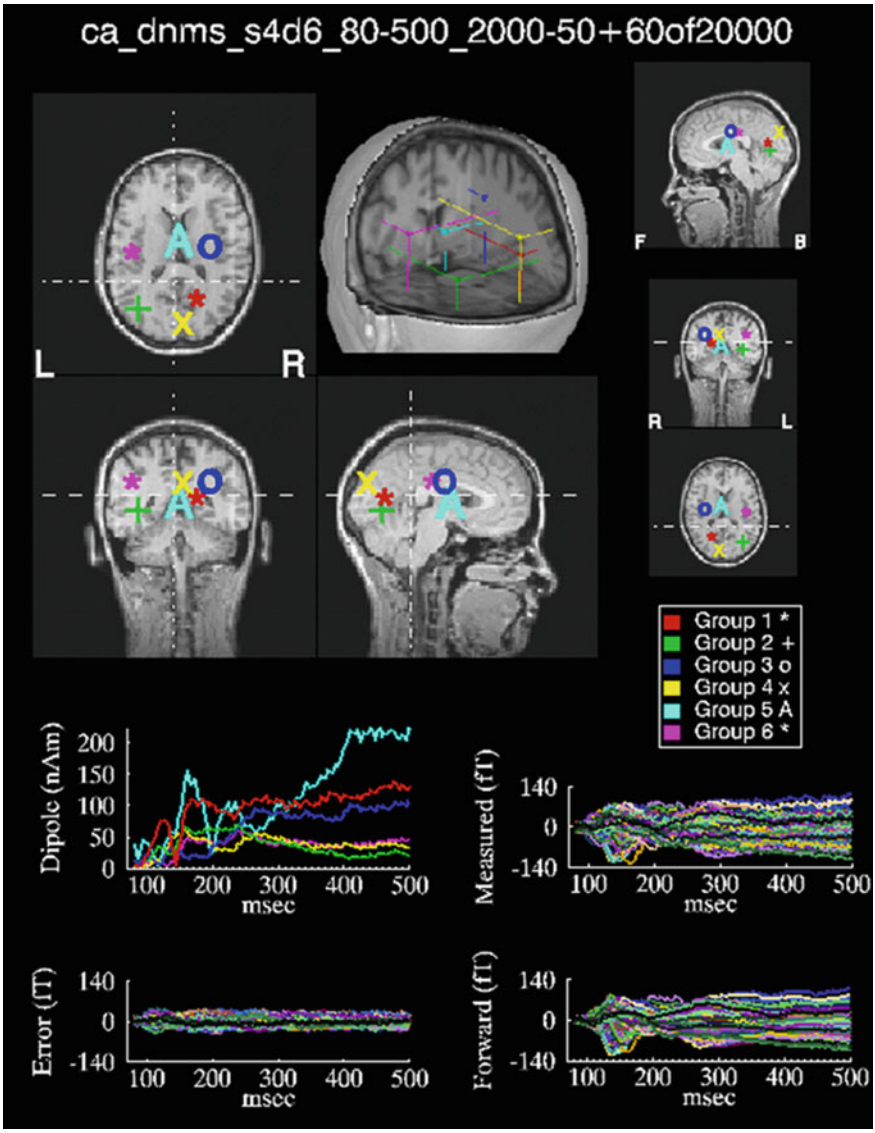

Fig. 8 CSST results for an MEG visual study, showing the best 60, 6-dipole fits from 20,000 starts

obtain accurate CSST results can be greatly reduced. The MUSIC-seeded CSST (MS-CSST) algorithm performs one MUSIC analysis on a variable density grid of approximately 7000 locations. A novel clustering approach is used to find the MUSIC peaks, saving the best 20 dipole locations in each cluster for use with CSST. Various sampling strategies can be used when mixing in these MUSIC

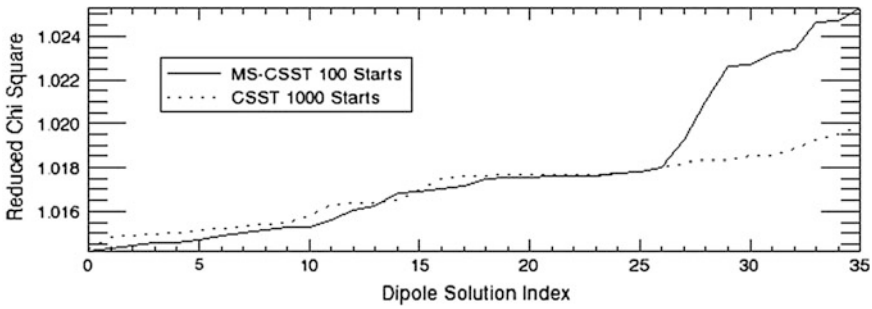

Fig. 9 This figure compares the performance of MS-CSST to regular CSST, showing the best 36 reduced Chi square values for a 5-dipole analysis of MEG data generated from 5 simulated sources. MS-CSST slightly outperformed regular CSST, when comparing the best 26 solutions from each analysis, using one-tenth as many starting dipole sets

dipole locations with randomly selected locations, while creating the CSST starting dipole sets. We illustrate results for a five dipole MEG simulation, based on an actual subject/sensor configuration with a Neuromag 122 system. The dipoles were given highly-overlapping timecourses, with low signal-to-noise, so that the MUSIC procedure would not localize all of the dipoles well. A 5-dipole MS-CSST analysis was performed, using 100 pseudo-random initial dipole configurations, creating 50 sample configurations with 2 MUSIC locations and 3 random locations, and 50 samples with 1 MUSIC location and 4 random locations. The same data was analyzed with CSST with no MUSIC seeding, using 1000 initial dipole configurations, and saving the best 100 based on reduced Chi square values. We compare the reduced Chi square results for these 2 analyses in Fig. 9. Comparing the best 26 fits from each analysis, MS-CSST outperformed regular CSST, with one tenth as many initial dipole configurations.

In analyses of simulated MEG data, MS-CSST outperforms CSST with 90 % fewer initial dipole configurations. In analyses of empirical MEG data, the performance improvement has been less, requiring 75–80 % fewer starting configurations with MS-CSST versus CSST to produce comparable results for the best 5 to 10 solution sets.

6.3 MEG/EEG Signal Processing and Data Organization Using MEGAN

All of the human subject MEG/EEG data used by CSST are first processed using MEGAN, a software package written in IDL by Elaine Best (Best et al. 1998) MEGAN provides a large suite of tools to process and view MEG/EEG sensor data. The signal processing tools provided include noise filtering, artifact rejection, pass averaging and other capabilities needed to work with MEG/EEG data.

MEGAN is graphical user interface base, and provides several interfaces for viewing raw and processed data, including overlaid multi-sensor signal time plots, signal plots on a map of the sensor locations, and colored contour plots (and movies). MEG/EEG data sets processed by MEGAN are written to a standardized format, called netMEG, that is based on netCDF. It is thus a self-describing format that can be accessed using standard libraries available for several major programming languages, including C and Fortran. Using these netMEG files to provide the MEG/EEG input data for CSST greatly simplifies reading in and setting up the data for CSST analyses.

6.4 Combining MEG and EEG

CSST provides a method for analyzing combined MEG and EEG data. This is done using the same nonlinear simplex analysis as is used for a single-modality analysis, but averaging the MEG and EEG reduced Chi square values at each step of the simplex search. The user sets a weighting that determines the relative contribution of each modality to this combined metric. Only preliminary work has been done on determining what weighting value to use for a given combined analysis. Criteria to consider include: the relative SNR of the MEG versus EEG data being analyzed (usually higher for EEG), the relative overall quality of the data (e.g. sensor count and spacing), and the fact that localization accuracy is generally better for MEG than EEG.

6.5 Combining fMRI/MEG/EEG

CSST can be used to perform combined analyses of MEG and/or EEG with fMRI or other volume based brain imaging data, using the concept of a likelihood volume (LV). An LV is used in CSST to weight the reduced Chi square values of the multi-dipole analysis using information from other functional (or volume-based) brain imaging modalities, such as fMRI, PET or structural MRI. Voxels in the LV contain a value in the interval [0, 1], representing the likelihood of cortical activity at that voxel location. If V is the value in a voxel of the LV, an error value, VE is obtained using $VE = 1.0 - V$. If AVE is the average of the VE values for a set of dipole locations, CE is the reduced Chi square value for this dipole set, and W is a user selected weighting value, then the new error measure for the simplex search is defined by: $E = W * CE + (1 - W) * AVE$. This error measure will influence the simplex search for the best-fitting dipole location sets, but still allows dipole locations in best-fitting sets that do not fall within regions of high likelihood, as determined by the LV.

As used with CSST, an LV is constructed with the same resolution as the structural MRI volume, and is registered to this MRI volume, and thus, the MEG or

EEG data. In the case of BOLD fMRI, an LV can be obtained by thresholding and scaling the T-statistic volume derived from the fMRI analysis to [0, 1], then resampling and registering this volume to the subject's sMRI volume.

A simulation-based analysis of the use of combined MEG/fMRI for analyzing single-pass MEG data is presented below. That analysis shows the possible benefits of using a combined MEG/fMRI analysis. The use of a LV has more recently been incorporated in a Bayesian combined fMRI/MEG analysis procedure (Jun et al. 2008).

7 Forward Simulator

To aid in comparing alternative MEG/EEG inverse algorithms using more realistic current distributions than single or multiple dipoles, a focal- and distributed-source forward simulator was developed within the MRIVIEW framework. Using the MRIVIEW surface viewing mode, ellipsoidal regions of the g/w matter boundary can be labeled. A user-specified oriented ellipsoid is used to create simulated regions of activity that can, for instance, lie along one bank of a sulcus. Multiple regions of arbitrary size and orientation can be created. Figure 10 shows three regions created using the forward simulator.

The simulator interface contains a table, with a row to control the activation characteristics of each region. The activation timecourses can be modeled using multiple Gaussians or a sinusoid, or they can be read from a file. For each region, a maximum timecourse current is set using table entries for either current density, or total current.

To generate EEG or MEG forward solutions, sensor geometries and other information are obtained from a netMEG file produced by the program MEGAN, usually from a human EEG or MEG study. Treating the cortical voxels in a region as oriented dipoles acting in concert, a spherical EEG or MEG forward is calculated using the timecourse for that region. The EEG forward uses the Sun algorithm (Sun 1997); the MEG forward uses the Sarvas formula (Sarvas 1987). The simulated sensor measurements are obtained by summing the forwards for all of the regions. Spatially uncorrelated Gaussian noise with a desired standard deviation can be added to the forward measurements, as can real noise from MEG/EEG experiments. Figure 11 shows the Forward Simulator interface being used to create a complex, 5-active-region simulation, showing plots of the simulated cortical activity, and the forward timecourses based on subject/sensor geometries obtained from a study using a Neuromag 122 MEG system. The MEG/EEG Simulator has been used in several MEG studies (e.g. Stephen et al. 2002), and is a key component of the MEG-SIM Portal project (Aine et al. 2012; Sanfratello et al. 2010 and see Sanfratello et al. this volume).

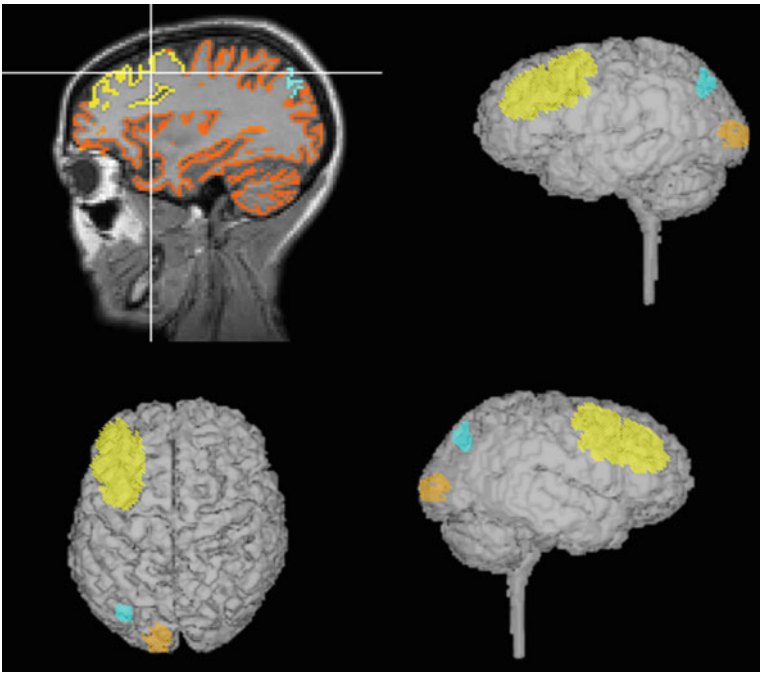

Fig. 10 The forward simulator and constrained 3D interface were used to create 3 patches of simulated cortical activity

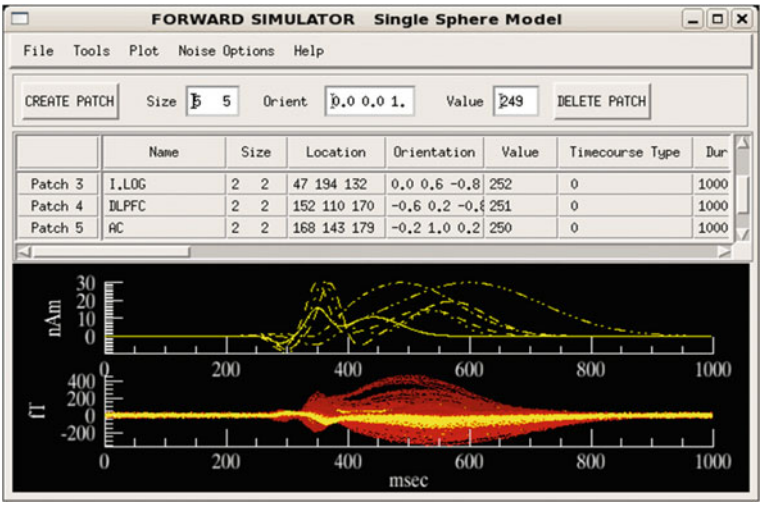

Fig. 11 The forward simulator interface, showing a 5-active-region simulation. The *upper* plot shows the simulated timecourses, the *lower* shows the resulting sensor measurements

8 Combining MEG and fMRI for Single-Pass MEG Analysis: A Simulation Study

In a typical MEG sensory response experiment, a single MEG pass measures the brain activity corresponding to a single application of a stimulus, such as the sounding of a tone. Usually, 100 or more passes are recorded for a given stimulus, and their average is used to perform location and timecourse analysis of the stimulus-induced brain activity. Because of the low single to noise ratio, inverse analysis of single pass MEG data is extremely difficult. In some cases, using information from other sources could aid in this analysis. The fMRI data in a combined MEG-fMRI experiment can complement the MEG data, in terms of providing additional brain activity location information, but it does not provide information on millisecond activity timecourses.

The MEG Forward Simulator in MRIVIEW was used to create 3 regions of brain activity, with activity timecourses similar to those shown in the upper right plot in Fig. 12, and MEG sensor timecourses shown in the two left plots. The upper left plot shows noise-free sensor timecourses, the lower left plot shows the same timecourses with added simulated noise, giving a noise level typical of single-pass MEG data.

A simulated fMRI volume was generated by applying a smoothing algorithm to the voxels of the three simulated regions, plus four additional regions having no electrical activity, to create brain activity maps similar to those obtained in an fMRI analysis. A LV was obtained for these regions by scaling the voxel values in the smoothed volume to the interval [0, 1]. This volume was registered to the MEG coordinate space. During the CSST search process, the voxel values of the LV were used to weight the MEG-only Chi square measure for a given set of locations, to produce a combined (simulated) MEG- fMRI measure. This fMRI weighting influences the simplex search in CSST, but does not constrain the dipole locations to only regions of fMRI activity.

The lower right plots in Fig. 12 show the benefits that may be realized with a combined MEG-fMRI analysis. The combined MEG-fMRI analysis demonstrates the fMRI influence on dipole locations. In the combined analysis, the fitted dipole locations are pulled toward regions of high fMRI activity, counteracting the influence of the MEG noise on the dipole fits. The dipole timecourses arising from the combined CSST analysis of the noisy simulated MEG data more closely match the low-noise analysis results, as evidenced by the shape and peak amplitudes shown in green and blue. In the MEG-only case, the peak green dipole timecourse amplitude is 50 % higher than it should be, because of complications in dipole fitting arising from the sensor noise. A similar problem can be seen with the blue dipole. For both the green and blue dipoles, the combined analysis time-course results closely match the actual timecourses. This improvement in time-course matching most likely arises from the fMRI contribution reducing the error in fitted dipole locations due to the influence of sensor noise.

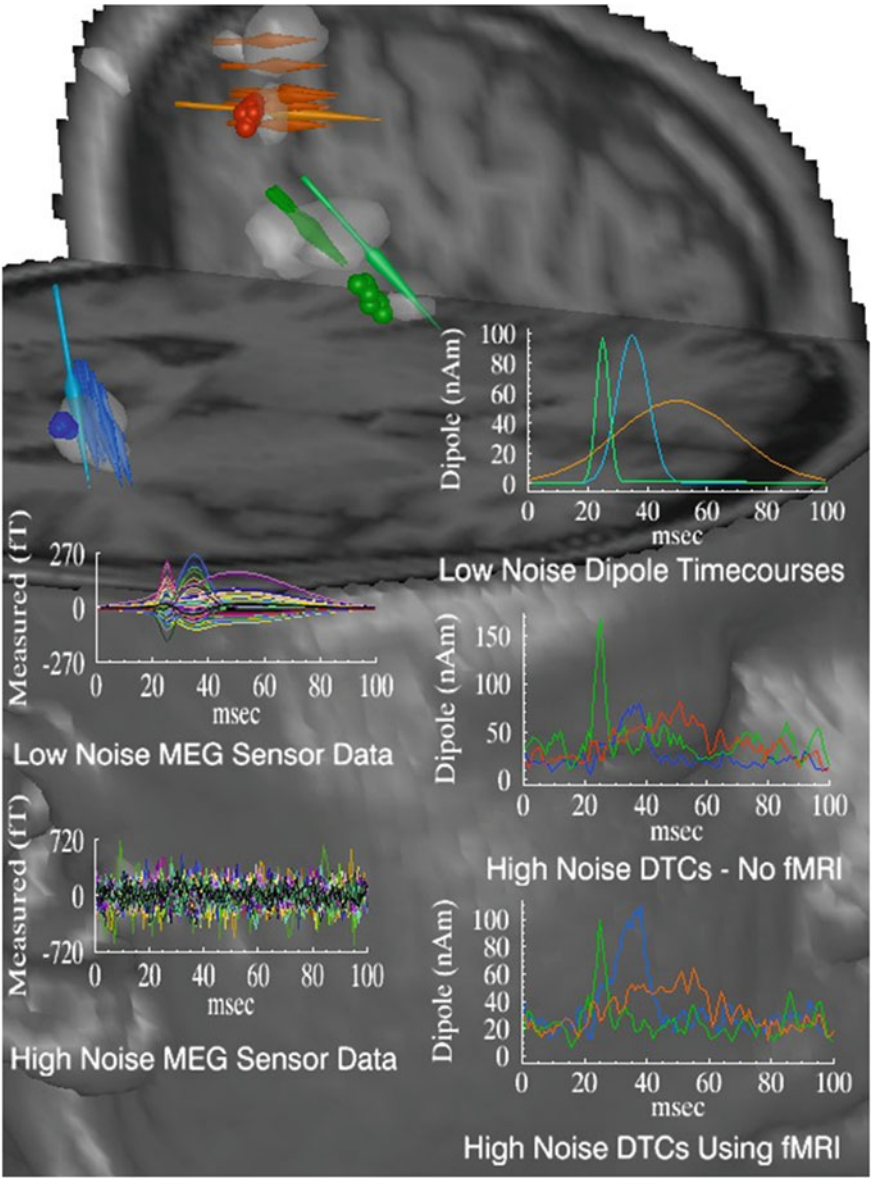

Fig. 12 The MRI head data shown in 3D was used to create simulated regions of brain activity. The *white* regions represent simulated fMRI data. The 3-dipole CSST solution for the low noise case is shown with the *larger arrows*. For the high noise analyses, the MEG-only solution locations are shown using spheres. The combined MEG, fMRI solution locations are shown using the *smaller arrows*

A LV can also be constructed by performing a CSST analysis of averaged (low-noise) MEG data obtained from the MEG data, by deriving a LV from a Monte Carlo analysis (a post-processing option in CSST) of the CSST results. The derived LV will have peaks at locations where the Monte Carlo analysis is most densely clustered. In either case, having a LV to influence the CSST fitting procedure shows promise as an approach to single-pass analysis. In cases where MEG and EEG are acquired simultaneously, the improved SNR will be even more likely to produce reasonable single-pass results using a combined MEG/EEG/LV analysis. Since this could provide spatially localized signal (time) frequency information, the results of these single pass analyses could be useful in performing reconstructions of cortical networks.

9 Conclusion

The MRIVIEW brain imaging software package provides an integrated environment for analyzing MEG/EEG data, and visualizing the results on MRI anatomy. The major components of MRIVIEW provide a wide range of capabilities, allowing a user to read in and view MRI data, segment anatomical structures, obtain MEG to MRI transformations and create MEG/EEG forward simulations. MRIVIEW includes CSST, which is used to perform multi-start, multi-dipole-based analyses of MEG/EEG data, with options for using MUSIC-based seeding or fMRI data to improve minimization performance. Solutions from fMRI analyses or averaged multi-pass MEG data can also be used to create LVs. The use of these LVs in CSST shows promise as a means of obtaining dipole location and time-course information from single-pass MEG/EEG data.

10 Obtaining MRIVIEW

MRIVIEW is freely available from this website: ftp.lanl.gov/public/ranken/mri-view. The source code is also freely available for academic research use. The software is written in IDL and requires IDL to be used. A free version of IDL, called the IDL Virtual Machine, is available from ExelisVIS at www.ExelisVis.com. The Virtual Machine can be used to run 3rd-party, GUI-based packages, such as MRIVIEW, but cannot be used for code development.

References

Aine CJ, Santratello L, Ranken DM, Best E et al (2012) MEG-SIM: a web portal for testing MEG analysis methods using realistic simulated and empirical data. Neuroinformatics 10(2):141–158

Best ED, Huang MX, Mosher JC, Ranken DM, Aine CJ, George JS (1998) MEGAN: a software package for MEG and EEG analysis and visualization. In: Proceedings of the fourth international conference on functional mapping of the human brain. Montreal, Canada

Blagoev K, Mihaila B, Travis B, Alexandrov L, Bishop A, Ranken D, Posse S, Gasparovic C, Mayer A, Aine C, Ulbert I, Morita M, Müller W, Connor J, Halgren E (2007) Modelling the magnetic signature of neuronal tissue. Neu- roImage 37:137–148

Huang M, Aine CJ, Supek S, Best E, Ranken D, Flynn ER (1998) Multi-start downhill simplex method for spatio-temporal source localization in magnetoencephalography. Electroencephalogr Clin Neurophysiol Evoked Potentials 108:32

Jun SC, George JS, Kim W, Pare-Blagoev J, Plis S, Ranken DM, Schmidt DM (2008) Bayesian brain source imaging based on combined MEG/EEG and fMRI using MCMC. NeuroImage 40(4):1581–1594

Mosher JC, Spencer M, Leahy R, Lewis P (1993) Error bounds for EEG and MEG dipole source localization. Electroencephalogr Clin Neurophysiol 86:303–321

Nelder JA, Mead R (1965) A simplex-method for function minimization. Comput J 7(4):308–313

Ranken D, George J (1993) MRIVIEW: an interactive computational tool for investigation of brain structure and function. In: Proceedings of IEEE visualization '93. IEEE Computer Society Press, pp 324–331

Ranken DM, Best ED, Stephen JM, Schmidt DM, George JS, Wood CC, Huang M (2002) MEG/EEG forward and inverse modeling using MRIVIEW. In: Proceedings of Biomag 2002, pp 785–787

Sanfratello L, Stephen JM, Ranken DM, Best ED, Wallace T, Gilliam K, Aine CJ (2010) MEG-SIM portal: reconstructions from realistic simulations of sensory and cognitive processing. In: Proceedings of the 17th international conference on biomagnetism vol 28, pp 132–135

Sarvas J (1987) Basic mathematical and electromagnetic concepts of the biomagnetic inverse problem. Phys Med Biol 32:11–22

Stephen JM, Aine CJ, Ranken DM (2002) Mutlidipole analysis of simulated epileptic spikes with real background activity. J Clin Neurophysiol 20:1–16

Sun MG (1997) An efficient algorithm for computing multishell spherical module conductor models in EEG dipole source localization. Trans Biomed Eng 44(12):1243–1252

NUTMEG: Open Source Software for MEG/EEG Source Reconstruction

Johanna M. Zumer, Daniel D. E. Wong, Adrian G. Guggisberg, Srikantan S. Nagarajan and Sarang S. Dalal

Abstract NUTMEG is an open-source MATLAB-based toolbox for MEG/EEG data. NUTMEG includes many options for source reconstruction, an easily navigable window for exploring source results, several options for source level connectivity computation, statistical evaluation of these source results, and conversion to and from formats of other toolboxes.

Keywords MEG · Source reconstruction · Beamformer · Inverse method · Time-frequency · Evoked responses · Bayesian inversion · Connectivity · Source statistics · EEG · Intracranial data

J. M. Zumer (✉)
Radboud University Nijmegen, Donders Institute for Brain Cognition and Behaviour, Centre for Cognitive Neuroimaging, Kapittelweg 29, 6525 EN Nijmegen, The Netherlands
e-mail: johanna.zumer@gmail.com

D. D. E. Wong · S. S. Dalal
Department of Psychology, University of Konstanz, Fach 905, 78457 Konstanz, Germany
e-mail: dan.wong.c@utoronto.ca

S. S. Dalal
e-mail: sarang.dalal@uni-konstanz.de

A. G. Guggisberg
Division of Neurorehabilitation, Department of Clinical Neurosciences, University Hospital Geneva, Avenue de Beau-Séjour 26, 1211 Geneva, Switzerland
e-mail: aguggis@gmail.com

S. S. Nagarajan
Biomagnetic Imaging Laboratory, Department of Radiology and Biomedical Imaging, University of California, 513 Parnassus Ave. S-362, San Francisco, CA 94143-0628, USA
e-mail: sri@ucsf.edu

S. S. Dalal
Zukunftskolleg, University of Konstanz, Fach 905, 78457 Konstanz, Germany

S. Supek and C. J. Aine (eds.), *Magnetoencephalography*,
DOI: 10.1007/978-3-642-33045-2_11,

1 Introduction

1.1 Background

NUTMEG (nutmeg.berkeley.edu) (Dalal et al. 2004, 2011) was initially developed by researchers and collaborators at the University of California San Francisco Biomagnetic Imaging Lab. The primary objective was to provide an open-source, easy-to-use toolbox for beamformer source reconstruction from MEG data, along with intuitive visualization and navigation of the source level analyses. It has since implemented a variety of other source reconstruction methods, support for EEG and, experimentally, intracranial EEG.

1.2 Data and Experiment Types Supported

NUTMEG includes custom import functions for several major MEG manufacturers, including CTF, 4D/BTi, KIT/Yokogawa, and Elekta Neuromag. In addition, all of the MEG, EEG and intracranial EEG data types that are supported with the FieldTrip *fileio* (Oostenveld et al. 2011) may also be read into the NUTMEG sensor data structure. This is achieved either via a NUTMEG graphical user interface (GUI) which calls FieldTrip functions, or by converting a dataset already loaded using standard FieldTrip into the NUTMEG data style.

Essentially all experiment and analysis types are supported in NUTMEG. Task-based evoked responses, task-based induced oscillatory changes, and task-based or resting connectivity analysis have been successfully analyzed using NUTMEG.

1.3 Integration with Other Toolboxes

NUTMEG is easily compatible with other MATLAB-based toolboxes. NUTMEG uses two primary data structures, a sensor level data structure and a source level data structure. Both may be converted to or from FieldTrip, for sharing of pre-processing, source inversion, or statistical testing steps between packages. Pre-processed data in ELAN (Aguera et al. 2011) may also be imported into NUTMEG.

Lead fields computed in other software packages, including OpenMEEG (Gramfort et al. 2011), Cartool (Brunet et al. 2011), FieldTrip (including Simbio [https://www.mrt.uni-jena.de/simbio] and FNS (Dang and Ng, 2011)), MNE (www.martinos.org/mne), EMSE (www.sourcesignal.com), SMAC (Spinelli et al. 2000), and Brainstorm (Tadel et al. 2011), may be imported for use with NUTMEG inverse solutions.

Visualization of NUTMEG source data primarily utilizes SPM8 (www.fil.ion.ucl.ac.uk/spm/software/spm8) to overlay activations on an MRI, without requiring

conversion to the SPM8 MEG/EEG data format. The NUTMEG source data may also be explicitly converted to Analyze format for further visualization or manipulation in Cartool, mri3dX (www.cubric.cf.ac.uk/Documentation/mri3dX), DataViewer3D (Gouws et al. 2009) and MRIcro (mricro.com).

1.4 Interface

NUTMEG has been designed with a graphical interface that facilitates the most common data processing workflow scenarios involving evoked responses as well as time-frequency modulations (Fig. 1a). This comprises data import, MRI coregistration, source analysis parameters, and statistical analysis. Additionally, most features of the graphical interface call underlying functions that can be manually used from the command line or batch analysis scripts. This feature allows any potentially intensive calculations, such as permutation testing or processing raw data with large filter banks, to be conveniently passed to high-performance computing clusters. Finally, the GUI features interactive visualization and navigation of the analyzed results, described in further detail below.

2 Processing Steps

2.1 Loading MEG/EEG Data

See Sect. 1.2 for which MEG and EEG data formats can be loaded and how they may be loaded. The open source format of NUTMEG allows for the seamless implementation of customized scripts from third parties to load additional file formats. During the M/EEG data loading process, sensor coordinates can also be imported for both visualization of field/potential topographies and lead field/potential calculation. This is done automatically for some MEG datasets. For EEG datasets, Polhemus-localized sensor positions are supported.

2.2 Loading Anatomical Information

Through SPM8, NUTMEG is able to load Analyze and Nifti MRI file formats for coregistration (Fig. 1b). The option of loading an additional, spatially normalized MRI allows for the computation of MNI coordinates for inter-subject comparison. For the purposes of coregistering M/EEG sensors, fiducials can be manually marked on the imported MRI, as well as imported from saved text files or CTF MEG localsphere head model files.

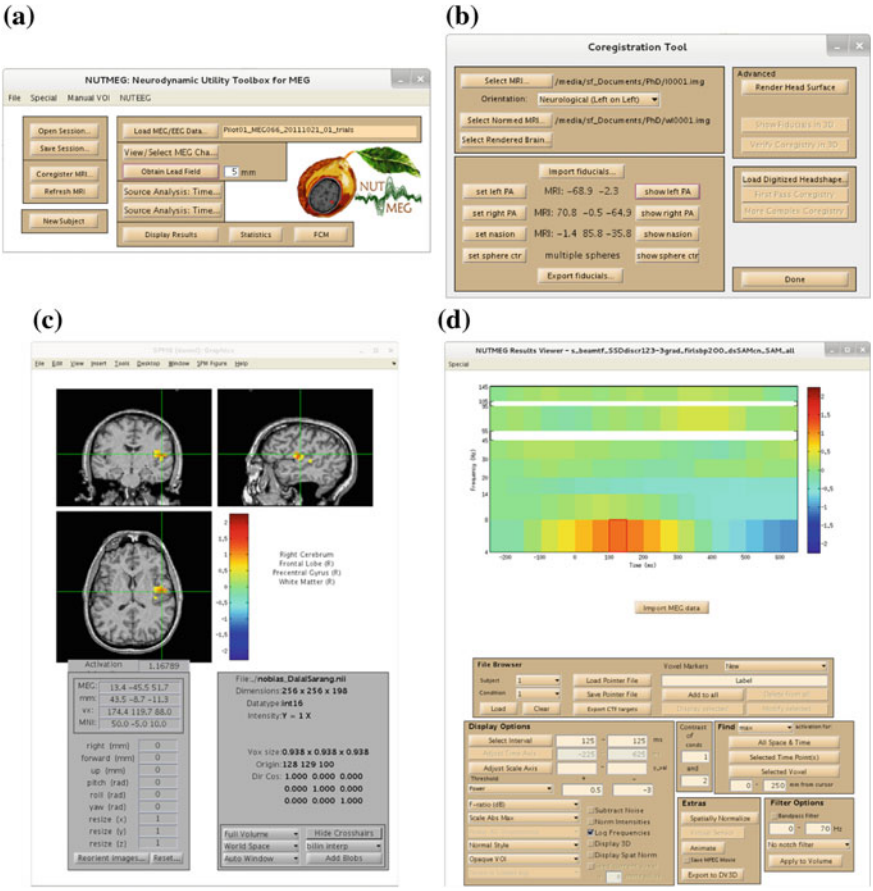

Fig. 1 Example components of the NUTMEG graphical user interfaces (GUIs). **a** The main GUI is designed to guide the user through sequential stages of the data analysis process. **b** The coregistration interface allows the user to load MRI data along with normalization data and mark the fiducial points. **c** The SPM8 window allows the user to navigate the MRI, define fiducial points, and visualize activation overlays. **d** The NUTMEG results viewer showing time-frequency data: the user can specify which frequency band and time point to visualize on the activation overlay in the dynamically linked SPM8 window. The results viewer can also display time-domain data, depending on the type of analysis used

2.3 Computation of Head Models

NUTMEG provides several options for computing the lead field. Forward fields and potentials can be computed for spherical head models using built-in functions. The sphere center can either be specified manually, or loaded from a CTF local sphere head model file. The loading of CTF multisphere head models is supported for MEG datasets. For EEG datasets, a multisphere model can be generated using a provided

function that adjusts the sphere centers to minimize the difference between the forward potentials generated for a few sparsely sampled points using the multi-sphere method and those derived using the boundary element method (BEM).

The calculation of lead fields/potentials using more computationally intensive BEM head models is provided via integration between NUTMEG and either the Helsinki BEM (Stenroos et al. 2007) or the OpenMEEG (Gramfort et al. 2010) toolboxes. NUTMEG provides the necessary tools for importing tissue surface meshes from either BrainSuite or BrainVisa MRI segmenting software, thereby presenting the user with a complete BEM pipeline. Finally, see Sect. 1.3 for loading forward lead fields computed in other software for use in NUTMEG.

2.4 Inverse Methods

Many variants of popular inverse methods are included; furthermore, NUTMEG is stylized to allow easy drop-in and incorporation of newly developed inverse methods. The use of the time-domain LCMV beamformer for localizing both the oscillatory power changes over many time-frequency windows as well as evoked responses (ERF/ERPs) is well supported in NUTMEG. Minimum-norm methods also supported include sLORETA and dSPM.

Several Bayesian methods have been developed in the research group of Prof. Nagarajan for improved source estimation and denoising. These localization methods include Champagne (Owen et al. 2012b), SAKETINI (Zumer et al. 2007), and NSEFALoc (Zumer et al. 2008), which all involve the idea of denoising and localizing data in one step, for improved spatial specificity and reduced sensitivity to correlated sources. Prior to inversion, data may also be preprocessed to remove artifacts. Several versions of Bayesian factor analysis (Nagarajan et al. 2007) are implemented which identify artifact components present in a control condition so that they can be removed from a condition of interest in the sensor data; this denoised sensor data may then be input to the beamformer or minimum-norm inverse methods.

3 Visualization

Neural activity can be visualized as a tomographic map overlaid on the MRI in SPM (Fig. 1c). Using the modified SPM orthogonal-slice navigator, the researcher can explore the source reconstructed M/EEG dataset in 3D space overlaid on the MRI, while an extra, integrated GUI allows the user to explore the dataset over time by displaying the virtual sensor time course for the voxel selected on the SPM navigator. For time-freqency analysis (Dalal et al. (2008), Fig. 7 of Dalal et al. (2011), and Fig. 1d), the virtual sensor data plot is replaced by a time-frequency image of the power for the selected voxel.

A link to SPM functions offers the ability to display the activations on a normalized rendered brain surface. Neural activity can also be projected on a 3D brain surface imported from BrainSuite. If dipole orientation vectors are provided for each voxel, this display has the option of attenuating surface projections from voxels that do not contain a dipole orientation that is orthogonal to the cortical surface.

4 Statistics

Both within-subject and across-subject parametric and non-parametric statistics are available to compute. Within-subject statistics may use the Wilcoxon signed rank test based on the variability of responses across trials in a single subject. For across-subject analyses, NUTMEG uses statistical non-parametric mapping (SnPM) (Singh et al. 2003), which has the advantage that it does not depend on an assumption of a normal distribution and that it is robust even for small populations of as few as 5 subjects (though having more subjects will allow detection of weaker effects). SnPM also allows correcting for multiple voxels, time windows, and frequency bands. Most common study designs are supported including paired and unpaired comparisons, as well as correlations with behavioral variables. It is also possible to account for confounding covariates. The computed statistical probabilities can be used to display thresholded functional images.

5 Connectivity

NUTMEG offers a functional connectivity map (FCM) toolbox that enables the localization of functional connectivity (FC) among brain areas from EEG and MEG recordings. The FCM toolbox takes advantage of the rich set of source analysis algorithms available in NUTMEG and reconstructs neural oscillations in the cortex. From this, the toolbox efficiently computes several measures of functional connectivity (FC) between voxels, including imaginary coherence (Nolte et al. 2004), magnitude squared coherence, the phase lag index (Stam et al. 2007), amplitude envelope correlations (Brookes et al. 2011), and the general lagged coherence (Pascual-Marqui et al. 2011). Efficient algorithms enable the computation of interactions of all-to-all voxels on standard single computers. The highly multidimensional connectivity datasets can be interactively visualized together with structural brain images. The toolbox is therefore particularly suitable for explorative studies into the function and pathology of brain networks (Guggisberg et al. 2008). Both cortico-cortical as well as cortico-peripheral (e.g., cortico-muscular; Guggisberg et al. (2011)) measures of FC can be calculated. Several utilities for defining anatomical or functional regions of interest are available. The analyses can be applied to resting-state recordings (e.g., Dubovik et al. (2012)) as

well as to event-locked datasets. Moreover, the toolbox offers parametric and non-parametric statistical analysis including correlations with behavioral data. The analyses can be performed either via the intuitive graphical user interface or via the Matlab command line for efficient batch scripting.

6 Extensions and Future Directions

Extensions include support for specific processing steps of (1) EEG data via 'NUTEEG', and (2) intracranial EEG. Incorporation of recently developed statistical thresholding for sparse source reconstruction methods (Owen et al. 2012a) is also planned. Extensions of the code from the MATLAB to Python language are in place and support additional viewing tools via Xipy (https://github.com/miketrumpis/xipy) and integration with other imaging modalities such as DTI. Future directions include further integration with other existing toolboxes.

Acknowledgments We thank Kensuke Sekihara and Mike Trumpis for their contributions to NUTMEG.

References

Aguera PE, Jerbi K, Caclin A, Bertrand O (2011) ELAN: a software package for analysis and visualization of MEG, EEG, and LFP signals. Comput Intell Neurosci 158:970

Brookes MJ, Hale JR, Zumer JM, Stevenson CM, Francis ST, Barnes GR, Owen JP, Morris PG, Nagarajan SS (2011) Measuring functional connectivity using MEG: methodology and comparison with fcMRI. NeuroImage 56(3):1082–1104

Brunet D, Murray MM, Michel CM (2011) Spatiotemporal analysis of multichannel EEG: CARTOOL. Comput Intell Neurosci 813:870

Dalal SS, Zumer JM, Agrawal V, Hild KE, Sekihara K, Nagarajan SS (2004) NUTMEG: A neuromagnetic source reconstruction toolbox. Neurol Clin Neurophysiol 2004:52

Dalal SS, Guggisberg AG, Edwards E, Sekihara K, Findlay AM, Canolty RT, Berger MS, Knight RT, Barbaro NM, Kirsch HE, Nagarajan SS (2008) Five-dimensional neuroimaging: localization of the time-frequency dynamics of cortical activity. NeuroImage 40(4):1686–1700

Dalal SS, Zumer JM, Guggisberg AG, Trumpis M, Wong DDE, Sekihara K, Nagarajan SS (2011) MEG/EEG source reconstruction, statistical evaluation, and visualization with NUTMEG. Comput Intell Neurosci 758:973

Dang HV, Ng KT (2011) Finite difference neuroelectric modeling software. J Neurosci Methods 198(2):359–363

Dubovik S, Pignat JM, Ptak R, Aboulafia T, Allet L, Gillabert N, Magnin C, Albert F, Momjian-Mayor I, Nahum L, Lascano AM, Michel CM, Schnider A, Guggisberg AG (2012) The behavioral significance of coherent resting-state oscillations after stroke. NeuroImage 61(1):249–257

Gouws A, Woods W, Millman R, Morland A, Green G (2009) Dataviewer3D: an open-source, cross-platform multi-modal neuroimaging data visualization tool. Front Neuroinform 3:9

Gramfort A, Papadopoulo T, Olivi E, Clerc M (2010) OpenMEEG: opensource software for quasistatic bioelectromagnetics. Biomed Eng Online 9(1):45

Gramfort A, Papadopoulo T, Olivi E, Clerc M (2011) Forward field computation with OpenMEEG. Comput Intell Neurosci 923:703

Guggisberg AG, Honma SM, Findlay AM, Dalal SS, Kirsch HE, Berger MS, Nagarajan SS (2008) Mapping functional connectivity in patients with brain lesions. Ann Neurol 63(2):193–203. doi:10.1002/ana.21224

Guggisberg AG, Dalal SS, Zumer JM, Wong DD, Dubovik S, Michel CM, Schnider A (2011) Localization of cortico-peripheral coherence with electroencephalography. NeuroImage 57(4):1348–1357

Nagarajan SS, Attias HT, Hild KE, Sekihara K (2007) A probabilistic algorithm for robust interference suppression in bioelectromagnetic sensor data. Stat Med 26(21):3886–3910

Nolte G, Bai O, Wheaton L, Mari Z, Vorbach S, Hallett M (2004) Identifying true brain interaction from EEG data using the imaginary part of coherency. Clin Neurophysiol 115(10):2292–2307

Oostenveld R, Fries P, Maris E, Schoffelen JM (2011) Field trip: open source software for advanced analysis of MEG, EEG, and invasive electrophysiological data. Comput Intell Neurosci 156:869

Owen JP, Sekihara K, Nagarajan SS (2012a) Non-parametric statistical thresholding for sparse magnetoencephalography source reconstructions. Front Neurosci 6:186

Owen JP, Wipf DP, Attias HT, Sekihara K, Nagarajan SS (2012b) Performance evaluation of the Champagne source reconstruction algorithm on simulated and real M/EEG data. NeuroImage 60(1):305–323

Pascual-Marqui RD, Lehmann D, Koukkou M, Kochi K, Anderer P, Saletu B, Tanaka H, Hirata K, John ER, Prichep L, Biscay-Lirio R, Kinoshita T (2011) Assessing interactions in the brain with exact low-resolution electromagnetic tomography. Philos Transact A Math Phys Eng Sci 369(1952):3768–3784

Singh KD, Barnes GR, Hillebrand A (2003) Group imaging of task-related changes in cortical synchronisation using nonparametric permutation testing. NeuroImage 19(4):1589–1601

Spinelli L, Andino SG, Lantz G, Seeck M, Michel CM (2000) Electromagnetic inverse solutions in anatomically constrained spherical head models. Brain Topogr 13(2):115–125

Stam CJ, Nolte G, Daffertshofer A (2007) Phase lag index: assessment of functional connectivity from multi channel EEG and MEG with diminished bias from common sources. Hum Brain Mapp 28(11):1178–1193

Stenroos M, Mäntynen V, Nenonen J (2007) A Matlab library for solving quasi-static volume conduction problems using the boundary element method. Comput Methods Programs Biomed 88(3):256–263

Tadel F, Baillet S, Mosher JC, Pantazis D, Leahy RM (2011) Brainstorm: a user-friendly application for MEG/EEG analysis. Comput Intell Neurosci 879:716

Zumer JM, Attias HT, Sekihara K, Nagarajan SS (2007) A probabilistic algorithm integrating source localization and noise suppression for MEG and EEG data. NeuroImage 37:102–115

Zumer JM, Attias HT, Sekihara K, Nagarajan SS (2008) Probabilistic algorithms for MEG/EEG source reconstruction using temporal basis functions learned from data. NeuroImage 41:924–940

Recent Developments in MEG Network Analysis

Arjan Hillebrand and Cornelis J. Stam

Abstract In this chapter we will describe recent developments in MEG network analysis, where we will focus on the rationale behind, and application in clinical cohorts of, an atlas-based beamforming approach. This approach contains 3 main components, namely (i) the reconstruction of time-series of neuronal activation through beamforming; (ii) the use of a standard atlas, which enables comparisons across studies and modalities; (iii) the estimation of functional connectivity using the Phase Lag Index (PLI), a measure that is insensitive to the effects of field spread/volume conduction. Moreover, we will discuss the use of the minimum spanning tree (MST), which allows for a bias-free characterization of the topology of the reconstructed functional networks. Application of this approach will be illustrated through examples from recent studies in patients with gliomas, Parkinson's disease, and Multiple Sclerosis.

Keywords Resting-state · Network analysis · Graph theory · Minimum spanning tree · Atlas-based beamformer · Phase lag index (PLI) · Clinical applications

1 Functional Brain Networks

The brain consists of billions of interconnecting neurons, forming an extremely complex system (Tononi et al. 1998; Tononi and Edelman 1998) in which clusters of neurons are organized as functional units with more-or-less specific information processing capabilities (e.g. Born and Bradley 2005; Grodzinsky 2000). Yet, cognitive functions require the coordinated activity of these spatially separated

A. Hillebrand (✉) · C. J. Stam
Department of Clinical Neurophysiology and Magnetoencephalography Center, Neuroscience Campus Amsterdam, VU University Medical Center, Amsterdam, The Netherlands
e-mail: a.hillebrand@vumc.nl

S. Supek and C. J. Aine (eds.), *Magnetoencephalography*,
DOI: 10.1007/978-3-642-33045-2_12,

units, where the oscillatory nature of neuronal activity may provide a possible mechanism (Buzsaki and Wang 2012; Engel et al. 2001; Fries 2005; Singer 1999; Varela et al. 2001). These interacting units form a large-scale complex network (Bullmore and Sporns 2012; Schnitzler and Gross 2005). The organization of such complex brain networks can be characterized using concepts from graph theory (Bullmore and Sporns 2009; Reijneveld et al. 2007; Stam and Reijneveld 2007; Watts and Strogatz 1998). Application of graph theoretical tools to human brain networks has shown that the brain is organized according to a highly efficient topology that combines a high level of local integration (i.e. dense local clustering of connections) with a high level of global efficiency (i.e. critical long-distance connections), forming a so-called small-world organization (Bassett and Bullmore 2006; Stam and van Straaten 2012b; Watts and Strogatz 1998). In addition, brain networks in healthy subjects contain a subset of relatively highly connected regions ('hubs') (Achard et al. 2006; Barabasi and Albert 1999). These hubs seem to be mutually and densely interconnected, forming a connectivity backbone or "rich club" crucial for efficient brain communication (van den Heuvel et al. 2012; van den Heuvel and Sporns 2011).

It has been shown that network topology is highly heritable (Smit et al. 2008, 2010), that the network configuration changes during the life span (Smit et al. 2012) and that there are gender differences (Smit et al. 2008; Tian et al. 2011). Moreover, an increasing number of studies has shown that various brain disorders disturb the optimal organization of the functional brain networks (for reviews see Reijneveld et al. 2007; Stam and van Straaten 2012b; van Straaten and Stam 2013), and that these network alterations correlate with cognitive performance, as well as with parameters of disease severity and/or progression.

2 Source-Space Analysis

Magnetoencephalography, with its high temporal resolution, can be used to characterize the functional brain networks that are formed by interacting sources of oscillatory activity. Although such an analysis can be performed directly at the sensor-level, there are several factors that should be considered. Firstly, multiple sensors pick up the signals from a single source due to the nature of the electromagnetic signals (Sarvas 1987), known as field spread, as well as due to volume conduction.[1] Both these phenomena may lead to erroneous estimates of functional connectivity. It is important to realize though that projection of the signals to source-level in itself does not eliminate these effects (Hillebrand et al. 2012). Secondly, the mixture of signals originating from spatially separated brain areas

[1] In a spherically symmetric volume conductor the magnetic fields produced by the volume currents cancel out exactly (Sarvas 1987), but in a realistically shaped volume conductor there are observable effects of volume conduction.

can result in under- or overestimation of functional connectivity (Schoffelen and Gross 2009). Demixing the contribution from spatially separate sources, as well as enabling a more straightforward interpretation of the functional data in relation to its underlying structure, are therefore the main reasons to perform an analysis in source-space. This requires the solution of the inverse problem, i.e. the problem of estimating the electrical current distribution that produced the recorded magnetic flux. This is an ill-posed problem, meaning that there is no unique solution, unless prior knowledge (or constraints) is added. We know, for example, that the cortical current density is small (the moment per unit area is typically of the order of 50 pAm/mm^2; Lü and Williamson 1991), and solutions with estimated source strengths of several Ampere-meter can therefore safely be ignored. Different source reconstruction techniques exist (Baillet et al. 2001), and they vary in the type and number of constraints that are imposed (Hillebrand and Barnes 2005; Wipf and Nagarajan 2009). Constraints might be that there are only a small number of sources active at a specific instant in time (multi-dipole solutions; Supek and Aine 1993), that the whole cortex is active to some degree but with the minimum energy necessary to describe the measured data (minimum norm solutions; Hamalainen and Ilmoniemi 1994), or that there are no perfectly linearly correlated areas of activation within the brain (beamformers; Robinson and Vrba 1999; Sekihara and Nagarajan 2008; van Veen et al. 1997).

In recent years, beamforming has become one of the main source reconstruction approaches for MEG. It has been argued that the uncorrelated-source assumption may be realistic for many empirical datasets (Hillebrand and Barnes 2005), and violations of this assumption can be tolerated to some extent (Hadjipapas et al. 2005). For those cases where strongly correlated sources are encountered, for example during auditory stimulation or parallel processing of visual stimuli, the beamformer formulism can be adapted (Brookes et al. 2007; Dalal et al. 2006; Diwakar et al. 2011; Hui et al. 2010; Quraan and Cheyne 2010). From a practical point of view, there are few parameters to set when performing beamformer analysis, the main ones being the time-frequency window(s) in the data for which to perform the source reconstruction (Dalal et al. 2008). Source reconstruction is achieved in a sequential manner, where for each target location in the brain (typically a grid consisting of $5 \times 5 \times 5$ mm voxels is used; Barnes et al. 2004) neuronal activity is estimated using an optimal set of beamformer weights, $\mathbf{W}$:

$$\hat{Q} = \mathbf{WB}, \tag{1}$$

where $\hat{Q}$ is the estimated source strength in nAm for a source at a given target voxel, and with a certain orientation; $\mathbf{B}$ is a vector containing the recorded magnetic flux at a given latency.

These weights are optimal in the sense that the values of the weights are chosen such that activity would be fully reconstructed for a target location, if this target location happens to be active (this is called the unit-gain constraint), whilst rejecting the contribution from all other sources, be it within or outside the brain.

For a mathematical description we refer the reader to Robinson and Vrba 1999; Sekihara and Nagarajan 2008; van Veen et al. 1997, and for a review see Hillebrand et al. 2005).

Although other source reconstruction approaches also require accurate MEG/MRI co-registration and modeling of the volume conductor, beamforming is particularly sensitive to inaccuracies in the forward solution (Hillebrand and Barnes 2011, 2003; Vrba 2002): the unit-gain constraint described above results in a suppression of source activity if there is a deviation from the correct forward solution.

Equation 1 assumes that the orientation of a source is known. In practice, this is not the case, and the orientation can be set to the one that gives the maximum beamformer output (scalar beamformer; Robinson and Vrba 1999; Sekihara et al. 2004), the orientation of the cortical surface could be used (but see Hillebrand and Barnes 2003), or one could estimate the beamformer output for three orthogonal directions (vector beamformer; van Veen et al. 1997). Finally, the decrease in sensitivity for deeper sources (Hillebrand and Barnes 2002) results in an increase in the (norm of) the beamformer weights with source depth, and a disproportionate amplification of white sensor noise for deeper sources. To compensate for this depth bias, the beamformer weights, or equivalently the reconstructed beamformer image (Cheyne et al. 2006), are typically rescaled using a (projection of) the sensor noise. An estimate of the sensor noise therefore has to be provided. The effects of noise can further be reduced through regularization (Vrba 2002).

Once the beamformer weights have been estimated, one can reconstruct a three-dimensional volumetric image of activity (or of a change in activity in case experimental conditions are contrasted; see also Brookes et al. 2005). The statistical significance of these individual images is difficult to determine (but see Barnes and Hillebrand 2003), yet one can readily perform group-level statistics using tools developed for functional Magnetic Resonance Imaging (fMRI; Singh et al. 2002, 2003). We have recently introduced an atlas-based approach that also enables the comparison of beamformer results across individuals (see Fig. 1; Hillebrand et al. 2012). For each individual, the neuronal activity is reconstructed for a limited set of regions-of-interest (ROIs) that covers almost the entire brain, where the ROIs can be obtained from a standard atlas (Collins et al. 1995; Evans et al. 2012; Lancaster et al. 1997, 2000; Tzourio-Mazoyer et al., 2002). This approach has two main advantages: i) it enables the comparison between different modalities (Bullmore and Sporns 2009); ii) the number of ROIs is always the same across individuals, such that functional networks can more readily be compared (but see below).

3 Functional Connectivity in Source-Space

The recorded MEG data can be projected through the estimated beamformer weights in order to obtain the time-series for each voxel in the brain (Eq. 1), which are often referred to as virtual electrodes. In order to obtain a single time-series for each ROI, we subsequently select the voxel with maximum power as representative

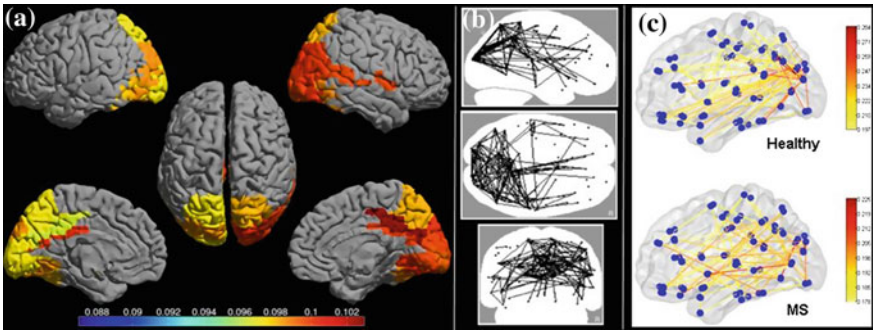

Fig. 1 Examples of recent applications of an atlas-based beamformer in combination with functional network analysis. Panel **a** shows data from a group of 13 healthy controls. The mean alpha band PLI, also known as the weighted degree or node strength in terms of graph theory, for each ROI, is displayed as a color-coded map (thresholded at $p = 0.05$) on a schematic of the parcellated template brain (modified from Hillebrand et al. 2012). Note that the regions in the occipital lobe are most strongly connected, as can be expected for the alpha band. Panel **b** shows the connections (PLI) from each ROI to all other ROIs, using an arbitrary threshold. Again, there is a clear pattern of strong connections between regions in the occipital lobe, with additional connections to areas in the temporal and frontal lobes. The *upper panel* in **c** shows a similar patterns for data from 17 healthy controls from a different study (Tewarie et al. 2014). This figure displays only the connections that formed part of the MST in the alpha2 band (the colorbar indicates PLI values). Interestingly, there seems to be a shift from an occipital to frontal pattern in healthy controls to a more diffuse pattern in 21 patients with Multiple Sclerosis (*lower panel*) (modified from Tewarie et al. 2014). Moreover, Tewarie and colleagues showed that this change in network topology correlated with reduced overall cognitive performance.

for the ROI. These ROI time-series can then be used as input for functional connectivity analysis. A wide range of functional connectivity estimators are available (Pereda et al. 2005), yet most of these measures are sensitive to the effects of volume conduction and field spread. One could remove these biases before performing connectivity analysis (Brookes et al. 2012; Hipp et al. 2012), or estimate the extent of the bias through simulations (Brookes et al. 2011a). Perhaps more straightforward is the use of measures such as the imaginary part of coherency (Nolte et al. 2004), phase-slope index (Nolte et al. 2008), the Phase Lag Index (PLI; Stam et al. 2007) and related lagged phase synchronization (Pascual-Marqui 2007), as these are inherently insensitive to these biases, where the PLI has the additional advantage that it does not directly depend on the amplitude of the signals (but see Muthukumaraswamy and Singh 2011). These measures have therefore gained popularity in recent years (Canuet et al. 2011, 2012; Guggisberg et al. 2008; Ioannides et al. 2012; Martino et al. 2011; Nolte and Muller 2010; Ponsen et al. 2013; Sekihara et al. 2011; Shahbazi et al. 2012; Tarapore et al. 2012).

The PLI is defined as (Stam et al. 2007):

$$\mathrm{PLI} = |\langle \mathrm{sign}[\sin(\Delta\phi(t_k))]\rangle|, \tag{2}$$

where $\Delta\phi$ is the difference between the instantaneous phases for two time-series defined in the interval $[-\pi, \pi]$, t_k are discrete time-steps, and $< >$ denotes the mean. In short, PLI is a measure for the asymmetry of the distribution of phase differences between two signals, and ranges between 0 and 1. A PLI value of 0 indicates no coupling, coupling with a phase difference of $0 \pm n\pi$ radians (with n an integer), or an equal distribution of positive and negative phase differences. Common sources lead to a phase difference of $0 \pm n\pi$ radians between two signals, hence the PLI is insensitive to the influence of common sources (Stam et al. 2007). A PLI > 0 is obtained when the distribution of phase differences is asymmetric and is indicative of functional coupling between two signals. Note that PLI does not indicate which of the signals is leading in phase (but see Stam and van Straaten 2012a) and that it potentially discards true interactions with zero-phase lag. Moreover, a value of 0 for uncoupled sources is only achieved for (infinitely) long time-series, hence the PLI is affected by the length of the time-series. PLI also underestimates connectivity between sources with small-lag interactions. A modification of PLI addresses this issue, albeit at the expense of introducing an arbitrary bias favoring large phase differences and mixing of the estimation of consistency of phase differences with the estimation of the magnitude of the phase difference (Vinck et al. 2011).

4 Topology of the Functional Network

Graph theory provides the mathematical framework to characterize the topology of the functional network that is formed by the interacting sources. For this purpose, each ROI is denoted as a vertex (node) and each connection (e.g. the PLI value) is denoted as an edge between the vertices (see Fig. 1). Various graph-theoretical measures can subsequently be used to characterize the network (e.g. Rubinov and Sporns 2010). Two such measures, the clustering coefficient[2] and the (average shortest) path length,[3] can be used to explain how the brain can fulfill two seemingly contradictory requirements, namely the processing of information in local functional units on the one hand ('segregation') and simultaneous coordination of activity in and between these spatially separated units ('integration') (Sporns et al. 2002, 2004). Watts and Strogatz (1998) famously demonstrated with a simple rewiring model that adding a few long distance connections to a network with many local interconnections results in a high clustering yet small average path length. Many large networks, including the brain, have such a so-called small-world configuration (Bassett and Bullmore 2006; Stam 2004). However, this

[2] The (unweighted) clustering coefficient denotes the likelihood that neighbours of a node are also connected to each other, and characterizes the tendency of nodes to form local clusters.

[3] The average shortest path length is a measure for global integration of the network. It is defined as the harmonic mean of shortest paths between all possible node pairs in the network.

model does not provide a completely satisfactory description of functional brain networks, since it can not explain the occurrence of hubs (Eguiluz et al. 2005). Similarly, the scale-free growth model by Barabasi and Albert (1999), which explains the occurrence of hubs, does not capture the high level of clustering and (hierarchical) modularity observed in experimental data (Meunier et al. 2009). Obviously, we currently lack a model that integrates small-world and scale-free models and fully and elegantly explains the observed functional brain network characteristics (Bullmore and Bassett 2011; Clune et al. 2013; Stam and van Straaten 2012b).

From a practical point of view, although the application of graph theory at the source-level already aids the interpretation of results and the comparability across studies, it is not trivial to compare network topology across individuals, groups, studies or modalities, as was elegantly shown by van Wijk et al. (2010). At the heart of the problem lies the observation that many network properties depend on the size, sparsity (percentage of all possible edges that are present), and the average degree (i.e. the average number of connections per node) of the network. Fixing the number of nodes and average degree in the network (by setting a threshold) does eliminate size effects but may introduce spurious connections or ignore strong connections in the network, and using random surrogates for normalization does not solve this problem either (and may even exuberate it; van Wijk et al. 2010).

A novel approach is to construct the minimum spanning tree (MST) of the original graphs (Boersma et al. 2013; Jackson and Read 2010a, b; Wang et al. 2008). A tree is a sub-graph that does not contain circles or loops and connects all nodes in the original graph, and the MST is the tree that has the minimum total weight (i.e. the sum of all edge values[4]) of all possible spanning trees of the original graph. If the original graph contains N nodes than the MST always has N nodes and $M = N-1$ edges, therefore enabling direct comparison of MSTs between groups and avoiding aforementioned methodological difficulties. Furthermore, if the original network can be interpreted as a kind of transport network, and if edge weights in the original graph possess strong fluctuations, also called the strong disorder limit, then all transport in the original graph flows over the MST (van Mieghem and van Langen 2005), forming the critical backbone of the original graph (van Mieghem and Magdalena 2005; Wang et al. 2008). Interestingly, it seems that for source-reconstructed MEG data for patients with Multiple Sclerosis, as well as for healthy controls, there is a tendency of the weight distribution towards the strong disorder limit (Tewarie et al. 2014). This implies that there is a high probability that the MSTs for both patients and healthy controls can be considered as the critical backbone of the original functional brain networks. Hence, analysis of the minimum spanning tree not only provides a bias free approach to network analysis, but also captures important properties of the original network.

[4] For the construction of the MST, the edge weight is defined as 1/(functional connectivity estimate), e.g. 1/PLI.

5 Applications in Neurology

5.1 Glioma

In a recent MEG study we revealed a relationship between resting-state functional network properties and protein expression patterns in tumor tissue collected during neurosurgery (Douw et al. 2013). In particular, between-module connectivity was selectively associated with two epilepsy-related proteins, namely synaptic vesicle protein 2A (SV2A) and poly-glycoprotein (P-gp), yet only for the ROIs that contained tumor tissue. Moreover, receiver operator characteristic (ROC) analysis revealed that SV2A expression could be classified with 100 % accuracy on the basis of the between-module connectivity, indicating that the role of the tumor area in the brain network may be an excellent marker for molecular features of brain tissue, which may be used clinically to monitor the efficacy of the anti-epileptic drug levetiracetam (de Groot et al. 2011). Moreover, lower between-module connectivity in the tumor area and higher number of seizures significantly predicted higher P-gp expression, which is in line with previous research showing that high seizure proneness is related to increased P-gp expression (Miller et al. 2008), and suggests that local network topology is an intermediate level between molecular tissue features and clinical patient status. A separate study (van Dellen et al. 2014) examined the link between functional network organization and seizure status further in a longitudinal study. Resting-state MEG recordings were obtained for 20 lesional epilepsy patients at baseline (preoperatively; T0), and at 3–7 (T1) and 9–15 months after resection (T2). Functional connectivity in the lower alpha band correlated positively with seizure frequency at baseline, especially in regions where lesions were located. MST leaf fraction, a measure of integration of information in the network, was significantly increased between T0 and T2, yet only for the seizure-free patients. Moreover, MST-based eccentricity and betweenness centrality, which are measures of node importance and hub-status, decreased between T0 and T2 in seizure free patients, also in regions that were anatomically close to lesion locations and resection cavities. These results demonstrate that there is a link between successful epilepsy surgery and changes in functional network topology. These insights may eventually be utilized for optimization of neurosurgical approaches.

5.2 Parkinson's Disease

A longitudinal study involving patients with Parkinson's disease (PD) also revealed a relationship between disease progression and functional brain network topology (Olde Dubbelink et al. 2014). MST analysis revealed a decentralized and less integrated network configuration in early stage untreated PD, which progressed over time. Conventional analysis of clustering and path length also

revealed an initial impaired local efficiency, which continued to progress over time, together with reductions in global efficiency. Importantly, these longitudinal changes in network topology were associated with deteriorating motor function and cognitive performance.

6 Future Developments

Excitingly, network analysis, particularly in combination with a standard parcellation of the brain (e.g. through the use of an anatomical atlas), provides a principled way to compare results across different modalities (Bullmore and Sporns 2009). For example, in recent years there has been an insurgence of research into the functional and cognitive relevance of resting-state functional connectivity as determined using fMRI (van den Heuvel and Hulshoff Pol 2010). Although it is already becoming clear that there is a close link between resting-state networks based on hemodynamic phenomena and the underlying electrophysiological networks (e.g. Brookes et al. 2011b; Niu et al. 2012), we envisage that a bias-free network approach allows for an even more accurate integration of these modalities, leading to a better understanding of brain function. Similarly, this approach enables us to directly link the properties of, and dynamics on, functional networks to the topology of the underlying structural network (Guye et al. 2008; Honey et al. 2007). An interesting direction for future work is the study of the interaction between these two types of networks, i.e. to study how functional plasticity affects the structural network, and vice versa (Assenza et al. 2011). Additionally, the same framework can be used to create anatomically and functionally realistic models that can simulate MEG signals. That is, neural mass models can be placed at each location of the anatomical parcellation scheme, where the anatomical connections between the neural masses can be based on experimental DTI data that were obtained for the same atlas. The parameters in these simulated structural/functional networks can subsequently be adjusted in order to test hypotheses (based on observations in experimental data) about disease mechanisms, or to generate new hypotheses about disease effects that we should be able to observe in experimental studies (de Haan et al. 2012; van Dellen et al. 2013).

The atlas-based beamforming approach itself may be developed further in several aspects. We have proposed to use the voxel with maximum power as representative for a ROI, which can introduce some biases, for example for ROIs that cover a large area of cortex. Indeed, the spatial resolution that is obtainable with MEG varies from millimeters to centimeters across the brain (Hillebrand and Barnes 2002), and depends on factors such as location of the neuronal activity, orientation of the cortex and signal-to-noise ratio (Barnes et al. 2004; Hillebrand and Barnes 2002). Our current hypothesis is that the AAL atlas has a resolution that matches the spatial resolution of MEG resting-state data. However, future research should test whether this hypothesis is valid for all cortical regions, for example through the use of atlases with higher spatial resolution (Evans et al.

2012; Seibert and Brewer 2011). In addition, selection of a single representative voxel might be prone to noise and outliers. However, the optimal method of dealing with multiple voxels within a ROI has not been defined yet, and using for instance an averaging method presents other biases, such as introducing artificial differences in signal-to-noise ratios for different sized ROIs. Similarly, one could argue that a priori selection of a target location within a ROI would speed up the computations. However, beamformer reconstructions vary most around peak activations (Barnes and Hillebrand 2003) and as a consequence, the a priori selection of a target voxel could have the effect that the activity for a ROI is completely missed (Barnes et al. 2004).

Another interesting direction for new research is to study the dynamics of functional networks in more detail (de Pasquale et al. 2012), thereby taking advantage of the strongest attribute of MEG, namely its high temporal resolution. A prerequisite is the development of measures of functional connectivity that have high temporal resolution, yet are insensitive to the effects of volume conduction. This would allow us to study functional networks in more detail, and examine the importance of the evolution of functional networks on short time-scales. For example, it was described above that functional brain networks can be divided into modules; are these modules stable over time (Bassett et al. 2013)? And hubs play an important role in the network, is this also reflected in their dynamics, i.e., do hubs evolve differently than non-hubs? Similarly, how does the formation and re-configuration over time of functional networks relate to cognitive performance? Are these dynamics altered in the diseased brain? And if so, is there a phase-transition that distinguishes the healthy from the diseased brain?

References

Achard S, Salvador R, Whitcher B, Suckling J, Bullmore E (2006) A resilient, low-frequency, small-world human brain functional network with highly connected association cortical hubs. J Neurosci 26:63–72

Assenza S, Gutierrez R, Gomez-Gardenes J, Latora V, Boccaletti S (2011) Emergence of structural patterns out of synchronization in networks with competitive interactions. Sci Rep 1:99

Baillet S, Mosher JC, Leahy RM (2001) Electromagnetic brain mapping. IEEE Signal Process Mag 18:14–30

Barabasi AL, Albert R (1999) Emergence of scaling in random networks. Science 286:509–512

Barnes GR, Hillebrand A (2003) Statistical flattening of MEG beamformer images. Hum Brain Mapp 18:1–12

Barnes GR, Hillebrand A, Fawcett IP, Singh KD (2004) Realistic spatial sampling for MEG beamformer images. Hum Brain Mapp 23:120–127

Bassett DS, Bullmore E (2006) Small-world brain networks. Neuroscientist 12:512–523

Bassett DS, Porter MA, Wymbs NF, Grafton ST, Carlson JM, Mucha PJ (2013) Robust detection of dynamic community structure in networks. Chaos 23:013142

Boersma M, Smit DJ, Boomsma DI, De Geus EJ, Delemarre-van de Waal HA, Stam CJ (2013) Growing trees in child brains: graph theoretical analysis of electroencephalography-derived

minimum spanning tree in 5- and 7-year-old children reflects brain maturation. Brain Connectivity 3: 50–60
Born RT, Bradley DC (2005) Structure and function of visual area MT. Annu Rev Neurosci 28:157–189
Brookes MJ, Hale JR, Zumer JM, Stevenson CM, Francis ST, Barnes GR et al (2011a) Measuring functional connectivity using MEG: methodology and comparison with fcMRI. NeuroImage 56:1082–1104
Brookes MJ, Stevenson CM, Barnes GR, Hillebrand A, Simpson MI, Francis ST et al (2007) Beamformer reconstruction of correlated sources using a modified source model. NeuroImage 34:1454–1465
Brookes MJ, Woolrich M, Luckhoo H, Price D, Hale JR, Stephenson MC et al (2011b) Investigating the electrophysiological basis of resting state networks using magnetoencephalography. Proc Natl Acad Sci USA 108:16783–16788
Brookes MJ, Woolrich MW, Barnes GR (2012) Measuring functional connectivity in MEG: a multivariate approach insensitive to linear source leakage. NeuroImage 63:910–920
Brookes MJ, Gibson AM, Hall SD, Furlong PL, Barnes GR, Hillebrand A et al (2005) GLM-beamformer method demonstrates stationary field, alpha ERD and gamma ERS co-localisation with fMRI BOLD response in visual cortex. NeuroImage 26:302–308
Bullmore E, Sporns O (2009) Complex brain networks: graph theoretical analysis of structural and functional systems. Nat Rev Neurosci 10:186–198
Bullmore E, Sporns O (2012) The economy of brain network organization. Nat Rev Neurosci 13:336–349
Bullmore ET, Bassett DS (2011) Brain graphs: graphical models of the human brain connectome. Annu Rev Clin Psychol 7:113–140
Buzsaki G, Wang XJ (2012) Mechanisms of gamma oscillations. Annu Rev Neurosci 35:203–225
Canuet L, Ishii R, Pascual-Marqui RD, Iwase M, Kurimoto R, Aoki Y et al (2011) Resting-state EEG source localization and functional connectivity in schizophrenia-like psychosis of epilepsy. PLoS ONE 6:e27863
Canuet L, Tellado I, Couceiro V, Fraile C, Fernandez-Novoa L, Ishii R et al (2012) Resting-state network disruption and APOE genotype in Alzheimer's disease: a lagged functional connectivity study. PLoS ONE 7:e46289
Cheyne D, Bakhtazad L, Gaetz W (2006) Spatiotemporal mapping of cortical activity accompanying voluntary movements using an event-related beamforming approach. Hum Brain Mapp 27:213–229
Clune J, Mouret JB, Lipson H (2013) The evolutionary origins of modularity. Proc R Soc B: Biol Sci 280:20122863
Collins DL, Holmes CJ, Peters TM, Evans AC (1995) Automatic 3-D model-based neuroanatomical segmentation. Hum Brain Mapp 3:190–208
Dalal SS, Guggisberg AG, Edwards E, Sekihara K, Findlay AM, Canolty RT et al (2008) Five-dimensional neuroimaging: localization of the time-frequency dynamics of cortical activity. Neuroimage 40:1686–1700
Dalal SS, Sekihara K, Nagarajan SS (2006) Modified beamformers for coherent source region suppression. IEEE Trans Biomed Eng 53:1357–1363
de Groot M, Aronica E, Heimans JJ, Reijneveld JC (2011) Synaptic vesicle protein 2A predicts response to levetiracetam in patients with glioma. Neurology 77:532–539
de Haan W, Mott K, van Straaten EC, Scheltens P, Stam CJ (2012) Activity dependent degeneration explains hub vulnerability in Alzheimer's disease. PLoS Comput Biol 8:e1002582
de Pasquale F, Della PS, Snyder AZ, Marzetti L, Pizzella V, Romani GL et al (2012) A cortical core for dynamic integration of functional networks in the resting human brain. Neuron 74:753–764
Diwakar M, Tal O, Liu TT, Harrington DL, Srinivasan R, Muzzatti L et al (2011) Accurate reconstruction of temporal correlation for neuronal sources using the enhanced dual-core MEG beamformer. NeuroImage 56:1918–1928

Douw L, de Groot M, van Dellen E, Aronica E, Heimans JJ, Klein M et al (2013) Local MEG networks: the missing link between protein expression and epilepsy in glioma patients? NeuroImage 75:203–211

Eguiluz VM, Chialvo DR, Cecchi GA, Baliki M, Apkarian AV (2005) Scale-free brain functional networks. Phys Rev Lett 94:018102

Engel AK, Fries P, Singer W (2001) Dynamic predictions: oscillations and synchrony in top-down processing. Nat Rev Neurosci 2:704–716

Evans AC, Janke AL, Collins DL, Baillet S (2012) Brain templates and atlases. NeuroImage 62:911–922

Fries P (2005) A mechanism for cognitive dynamics: neuronal communication through neuronal coherence. Trends Cogn Sci 9:474–480

Grodzinsky Y (2000) The neurology of syntax: language use without Broca's area. Behav Brain Sci 23:1–21

Guggisberg AG, Honma SM, Findlay AM, Dalal SS, Kirsch HE, Berger MS et al (2008) Mapping functional connectivity in patients with brain lesions. Ann Neurol 63:193–203

Guye M, Bartolomei F, Ranjeva JP (2008) Imaging structural and functional connectivity: towards a unified definition of human brain organization? Curr Opin Neurol 21:393–403

Hadjipapas A, Hillebrand A, Holliday IE, Singh KD, Barnes GR (2005) Assessing interactions of linear and nonlinear neuronal sources using MEG beamformers: a proof of concept. Clin Neurophysiol 116:1300–1313

Hamalainen MS, Ilmoniemi RJ (1994) Interpreting magnetic fields of the brain: minimum norm estimates. Med Biol Eng Compu 32:35–42

Hillebrand A, Barnes GR (2011) Practical constraints on estimation of source extent with MEG beamformers. NeuroImage 54:2732–2740

Hillebrand A, Barnes GR (2002) A quantitative assessment of the sensitivity of whole-head meg to activity in the adult human cortex. NeuroImage 16:638–650

Hillebrand A, Barnes GR, Bosboom JL, Berendse HW, Stam CJ (2012) Frequency-dependent functional connectivity within resting-state networks: an atlas-based MEG beamformer solution. NeuroImage 59:3909–3921

Hillebrand A, Barnes GR (2003) The use of anatomical constraints with MEG beamformers. NeuroImage 20:2302–2313

Hillebrand A, Barnes GR (2005) Beamformer analysis of MEG data. Int Rev Neurobiol (Special volume on Magnetoencephalography) 68:149–171

Hillebrand A, Singh KD, Holliday IE, Furlong PL, Barnes GR (2005) A new approach to neuroimaging with magnetoencephalography. Hum Brain Mapp 25:199–211

Hipp JF, Hawellek DJ, Corbetta M, Siegel M, Engel AK (2012) Large-scale cortical correlation structure of spontaneous oscillatory activity. Nat Neurosci 15:884–890

Honey CJ, Kotter R, Breakspear M, Sporns O (2007) Network structure of cerebral cortex shapes functional connectivity on multiple time scales. Proc Natl Acad Sci USA 104:10240–10245

Hui HB, Pantazis D, Bressler SL, Leahy RM (2010) Identifying true cortical interactions in MEG using the nulling beamformer. NeuroImage 49:3161–3174

Ioannides AA, Dimitriadis SI, Saridis GA, Voultsidou M, Poghosyan V, Liu L et al (2012) Source space analysis of event-related dynamic reorganization of brain networks. Comput Math Methods Med 2012:452503

Jackson TS, Read N (2010a) Theory of minimum spanning trees. I. Mean-field theory and strongly disordered spin-glass model. Phys Rev E: Stat, Nonlin, Soft Matter Phys 81:021130

Jackson TS, Read N (2010b) Theory of minimum spanning trees. II. Exact graphical methods and perturbation expansion at the percolation threshold. Phys Rev E: Stat, Nonlin, Soft Matter Phys 81:021131

Lancaster JL, Rainey LH, Summerlin JL, Freitas CS, Fox PT, Evans AC et al (1997) Automated labeling of the human brain: a preliminary report on the development and evaluation of a forward-transform method. Hum Brain Mapp 5:238–242

Lancaster JL, Woldorff MG, Parsons LM, Liotti M, Freitas CS, Rainey L et al (2000) Automated Talairach atlas labels for functional brain mapping. Hum Brain Mapp 10:120–131

Lü ZL, Williamson SJ (1991) Spatial extent of coherent sensory-evoked cortical activity. Exp Brain Res 84:411–416

Martino J, Honma SM, Findlay AM, Guggisberg AG, Owen JP, Kirsch HE et al (2011) Resting functional connectivity in patients with brain tumors in eloquent areas. Ann Neurol 69:521–532

Meunier D, Lambiotte R, Fornito A, Ersche KD, Bullmore ET (2009) Hierarchical modularity in human brain functional networks. Frontiers Neuroinfo 3:37

Miller DS, Bauer B, Hartz AM (2008) Modulation of P-glycoprotein at the blood-brain barrier: opportunities to improve central nervous system pharmacotherapy. Pharmacol Rev 60:196–209

Muthukumaraswamy SD, Singh KD (2011) A cautionary note on the interpretation of phase-locking estimates with concurrent changes in power. Clin Neurophysiol 122:2324–2325

Niu H, Wang J, Zhao T, Shu N, He Y (2012) Revealing topological organization of human brain functional networks with resting-state functional near infrared spectroscopy. PLoS ONE 7:e45771

Nolte G, Bai O, Wheaton L, Mari Z, Vorbach S, Hallett M (2004) Identifying true brain interaction from EEG data using the imaginary part of coherency. Clin Neurophysiol 115:2292–2307

Nolte G, Muller KR (2010) Localizing and estimating causal relations of interacting brain rhythms. Frontiers Hum Neurosci 4:209

Nolte G, Ziehe A, Nikulin VV, Schlogl A, Kramer N, Brismar T et al (2008) Robustly estimating the flow direction of information in complex physical systems. Phys Rev Lett 100:234101

Olde Dubbelink KTE, Hillebrand A, Stoffers D, Deijen JB, Twisk JWR, Stam CJ et al (2014) Disrupted brain network topology in Parkinson's disease: a longitudinal magnetoencephalography study. Brain 137:197–207

Pascual-Marqui RD (2007) Instantaneous and lagged measurements of linear and nonlinear dependence between groups of multivariate time series: frequency decomposition. arXiv:0711.1455

Pereda E, Quiroga RQ, Bhattacharya J (2005) Nonlinear multivariate analysis of neurophysiological signals. Prog Neurobiol 77:1–37

Ponsen MM, Stam CJ, Bosboom JLW, Berendse HW, Hillebrand A (2013) A three dimensional anatomical view of oscillatory resting-state activity and functional connectivity in Parkinson's disease related dementia: an MEG study using atlas-based beamforming. NeuroImage: Clin 2:95–102

Quraan MA, Cheyne D (2010) Reconstruction of correlated brain activity with adaptive spatial filters in MEG. NeuroImage 49:2387–2400

Reijneveld JC, Ponten SC, Berendse HW, Stam CJ (2007) The application of graph theoretical analysis to complex networks in the brain. Clin Neurophysiol 118:2317–2331

Robinson SE, Vrba J (1999) Functional Neuroimaging by Synthetic Aperture Magnetometry (SAM). In: Kotani M, Kuriki S, Karibe H, Nakasato N, Yoshimoto T (eds) Recent advances in biomagnetism. Tohoku Univ Press, Sendai, pp 302–305

Rubinov M, Sporns O (2010) Complex network measures of brain connectivity: uses and interpretations. NeuroImage 52:1059–1069

Sarvas J (1987) Basic mathematical and electromagnetic concepts of the biomagnetic inverse problem. Phys Med Biol 32:11–22

Schnitzler A, Gross J (2005) Normal and pathological oscillatory communication in the brain. Nat Rev Neurosci 6:285–296

Schoffelen JM, Gross J (2009) Source connectivity analysis with MEG and EEG. Hum Brain Mapp 30:1857–1865

Sekihara K, Nagarajan SS, Poeppel D, Marantz A (2004) Asymptotic SNR of scalar and vector minimum-variance beamformers for neuromagnetic source reconstruction. IEEE Trans Biomed Eng 51:1726–1734

Seibert TM, Brewer JB (2011) Default network correlations analyzed on native surfaces. J Neurosci Methods 198:301–311

Sekihara K, Owen JP, Trisno S, Nagarajan SS (2011) Removal of spurious coherence in MEG source-space coherence analysis. IEEE Trans Biomed Eng 58:3121–3129

Sekihara K, Nagarajan SS (2008) Adaptive Spatial Filters for Electromagnetic Brain Imaging. Springer, Heidelberg

Shahbazi AF, Ewald A, Nolte G (2012) Localizing true brain interactions from EEG and MEG data with subspace methods and modified beamformers. Comput Math Methods Med 2012:402341

Singer W (1999) Neuronal synchrony: a versatile code for the definition of relations? Neuron 24:49–25

Singh KD, Barnes GR, Hillebrand A (2003) Group imaging of task-related changes in cortical synchronisation using non-parametric permutation testing. NeuroImage 19:1589–1601

Singh KD, Barnes GR, Hillebrand A, Forde EME, Williams AL (2002) Task-related changes in cortical synchronization are spatially coincident with the hemodynamic response. NeuroImage 16:103–114

Smit DJ, Boersma M, Schnack HG, Micheloyannis S, Boomsma DI, Hulshoff Pol HE et al (2012) The brain matures with stronger functional connectivity and decreased randomness of its network. PLoS ONE 7:e36896

Smit DJ, Boersma M, van Beijsterveldt CE, Posthuma D, Boomsma DI, Stam CJ et al (2010) Endophenotypes in a dynamically connected brain. Behav Genet 40:167–177

Smit DJ, Stam CJ, Posthuma D, Boomsma DI, De Geus EJ (2008) Heritability of "small-world" networks in the brain: a graph theoretical analysis of resting-state EEG functional connectivity. Hum Brain Mapp 29:1368–1378

Sporns O, Chialvo DR, Kaiser M, Hilgetag CC (2004) Organization, development and function of complex brain networks. Trends Cogn Sci 8:418–425

Sporns O, Tononi G, Edelman GM (2002) Theoretical neuroanatomy and the connectivity of the cerebral cortex. Behav Brain Res 135:69–74

Stam CJ (2004) Functional connectivity patterns of human magnetoencephalographic recordings: a 'small-world' network? Neurosci Lett 355:25–28

Stam CJ, Nolte G, Daffertshofer A (2007) Phase lag index: assessment of functional connectivity from multi channel EEG and MEG with diminished bias from common sources. Hum Brain Mapp 28:1178–1193

Stam CJ, Reijneveld JC (2007) Graph theoretical analysis of complex networks in the brain. Nonlinear Biomed Phys 1:3

Stam CJ, van Straaten EC (2012a) The organization of physiological brain networks. Clin Neurophysiol 123:1067–1087

Stam CJ, van Straaten EC (2012b) Go with the flow: use of a directed phase lag index (dPLI) to characterize patterns of phase relations in a large-scale model of brain dynamics. NeuroImage 62:1415–1428

Supek S, Aine CJ (1993) Simulation studies of multiple dipole neuromagnetic source localization: model order and limits of source resolution. IEEE Trans Biomed Eng 40:529–540

Tarapore PE, Martino J, Guggisberg AG, Owen J, Honma SM, Findlay A et al (2012) Magnetoencephalographic imaging of resting-state functional connectivity predicts postsurgical neurological outcome in brain gliomas. Neurosurgery 71:1012–1022

Tewarie P, Hillebrand A, Schoonheim MM, van Dijk BW, Geurts JJ, Barkhof F et al (2014) Functional brain network analysis using minimum spanning trees in Multiple Sclerosis: an MEG source-space study. NeuroImage 88:308–318

Tian L, Wang J, Yan C, He Y (2011) Hemisphere- and gender-related differences in small-world brain networks: a resting-state functional MRI study. NeuroImage 54:191–202

Tononi G, Edelman GM (1998) Consciousness and complexity. Science 282:1846–1851

Tononi G, Edelman GM, Sporns O (1998) Complexity and coherency: integrating information in the brain. Trends Cogn Sci 2:474–484

Tzourio-Mazoyer N, Landeau B, Papathanassiou D, Crivello F, Etard O, Delcroix N et al (2002) Automated anatomical labeling of activations in SPM using a macroscopic anatomical parcellation of the MNI MRI single-subject brain. NeuroImage 15:273–289

van Dellen E, Hillebrand A, Douw L, Heimans JJ, Reijneveld JC, Stam CJ (2013) Local polymorphic delta activity in cortical lesions causes global decreases in functional connectivity. NeuroImage 83:524–532

van Dellen E, Douw L, Hillebrand A, de Witt Hamer PC, Baayen JC, Heimans JJ et al (2014) Epilepsy surgery outcome and functional network alterations in longitudinal MEG: a minimum spanning tree analysis. NeuroImage 86:354–363

van den Heuvel MP, Hulshoff Pol HE (2010) Exploring the brain network: a review on resting-state fMRI functional connectivity. Eur Neuropsychopharmacol 20:519–534

van den Heuvel MP, Kahn RS, Goni J, Sporns O (2012) High-cost, high-capacity backbone for global brain communication. Proc Natl Acad Sci USA 109:11372–11377

van den Heuvel MP, Sporns O (2011) Rich-club organization of the human connectome. J Neurosci 31:15775–15786

van Mieghem P, Magdalena SM (2005) Phase transition in the link weight structure of networks. Phys Rev E: Stat, Nonlin, Soft Matter Phys 72:056138

van Mieghem P, van Langen S (2005) Influence of the link weight structure on the shortest path. Phys Rev E: Stat, Nonlin, Soft Matter Phys 71:056113

van Straaten EC, Stam CJ (2013) Structure out of chaos: Functional brain network analysis with EEG, MEG, and functional MRI. Eur Neuropsychopharmacol 23:7–18

van Veen BD, van Drongelen W, Yuchtman M, Suzuki A (1997) Localization of brain electrical activity via linearly constrained minimum variance spatial filtering. IEEE Trans Biomed Eng 44:867–880

van Wijk BC, Stam CJ, Daffertshofer A (2010) Comparing brain networks of different size and connectivity density using graph theory. PLoS ONE 5:e13701

Varela F, Lachaux J-P, Rodriguez E, Martinerie J (2001) The brainweb: phase synchronization and large-scale integration. Nat Rev Neurosci 2:229–239

Vinck M, Oostenveld R, van Wingerden M, Battaglia F, Pennartz CM (2011) An improved index of phase-synchronization for electrophysiological data in the presence of volume-conduction, noise and sample-size bias. NeuroImage 55:1548–1565

Vrba J (2002) Magnetoencephalography: the art of finding a needle in a haystack. Physica C 368:1–9

Wang H, Hernandez JM, van Mieghem P (2008) Betweenness centrality in a weighted network. Phys Rev E: Stat, Nonlin, Soft Matter Phys 77:046105

Watts DJ, Strogatz SH (1998) Collective dynamics of 'small-world' networks. Nature 393:440–442

Wipf D, Nagarajan S (2009) A unified Bayesian framework for MEG/EEG source imaging. NeuroImage 44:947–966

Non-parametric Statistical Analysis of Map Topographies on the Epoch Level

Michael Wagner

Abstract In Event-Related Field (ERF) experiments, stimuli—often of several different types—are presented repeatedly, and the subject's brain response is recorded using MEG.

Keywords Magnetoencephalography · Electroencephalography · Event-related fields · Event-related potentials · Mismatch negativity · Mandarin language · Statistical analysis · Randomization statistics · Non-parametrical statistics · Topographical analysis of variance

1 Introduction

In Event-Related Field (ERF) experiments, stimuli—often of several different types—are presented repeatedly, and the subject's brain response is recorded using MEG. After removing artifacts and epoching the data, many repetitions per stimulus type are available, which are later usually averaged and compared. At this stage, though, it is no longer possible to establish whether and for which latencies the averaged waveforms are significantly different between stimulus types, nor whether the trials (epochs) for a given stimulus type are consistent enough to warrant averaging them in the first place. A statistical analysis of all individual epochs can provide exactly this information.

Traditional statistical measures in channel space such as the t-test make disputable assumptions regarding repeatability and independence (Murray et al. 2008; Koenig and Melie-Garcia 2009). Therefore, a new non-parametric family of methods has recently attracted attention as it became computationally feasible for

M. Wagner (✉)
Compumedics Germany GmbH, Heußweg 25, 20255 Hamburg, Germany
e-mail: mwagner@neuroscan.com

S. Supek and C. J. Aine (eds.), *Magnetoencephalography*,
DOI: 10.1007/978-3-642-33045-2_13,

the analysis of Event-Related Potential (ERP) group studies (Murray et al. 2004). Although—misleadingly—referred to as Topographic Analysis of Variance (TANOVA), no analysis of variance is being conducted, but rather a non-parametric randomization test.

In this contribution, a framework is proposed that allows the application of TANOVA not only to individual averages in the context of an ERP group study but to the un-averaged individual epochs themselves, as obtained in a Mismatch Negativity (MMN) MEG experiment.

2 Methods

2.1 Mismatch Negativity Experiment

Three Mandarin syllables were used as auditory stimuli: yi1 ("cloth"), yi2 ("aunt"), and yi3 ("chair"). They share the vowel /i/ but differ in tonal contours. The same set of stimuli was used in Lee et al. (2012), where a complete characterization of the experiment can be found.

In an MMN paradigm, yi3 was used as the standard stimulus, with yi1 and yi2 the deviants. Syllables yi2 and yi3 are harder to discriminate than yi1 and yi3 (Lee et al. 2012). The subject, a healthy adult native Mandarin speaker, lay in a magnetically shielded room and attended to a silent movie while passively listening to the stimuli. Stimuli were delivered binaurally using sound tubing. An initial 20 trials of standards were followed by a randomized presentation of 800 standard stimuli and 100 of each deviant, with at least two successive standards between deviants. The stimulus duration was 250 ms, with an interstimulus interval of 500 ms. MEG data were recorded using a 157-channel axial gradiometer whole-head MEG system (Yokogawa Electric Corporation, Japan) with a sampling frequency of 1 kHz.

Signal processing was performed in the Curry 7 software (Compumedics, Charlotte, NC, USA). Data were filtered from 1 to 40 Hz and epoched from 100 ms before to 600 ms after stimulus onset (Fig. 1). The initial 20 standard stimuli were excluded, as well as any epochs with signals exceeding ± 1.5 pT, since signals of this magnitude are likely due to artifact. The remaining epochs were down-sampled to 200 Hz. Averages for all three stimulus types were computed (Fig. 2).

2.2 Statistical Analysis

In the context of a TANOVA, two different non-parametric randomization tests were performed for all epochs: a consistency test per stimulus type, and a test for differences between stimulus types. Statistical analysis was performed using the Curry 7 software.

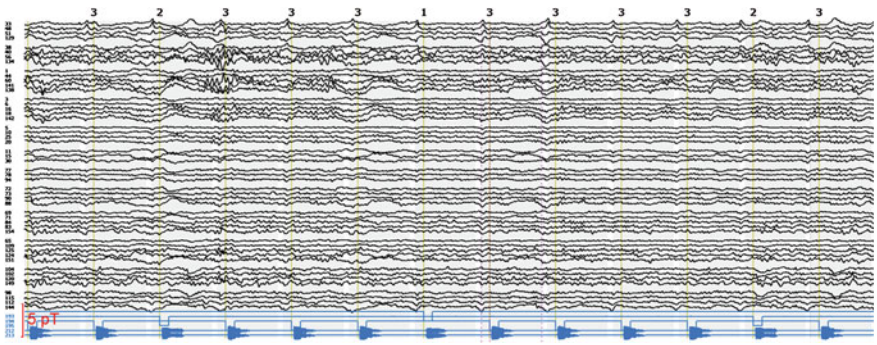

Fig. 1 A 10 s page of ongoing MEG data, filtered at 1 to 40 Hz, with trigger and audio channels. Latency ranges marked in gray were used for epoching, from 100 ms pre- to 600 ms post-stimulus onset

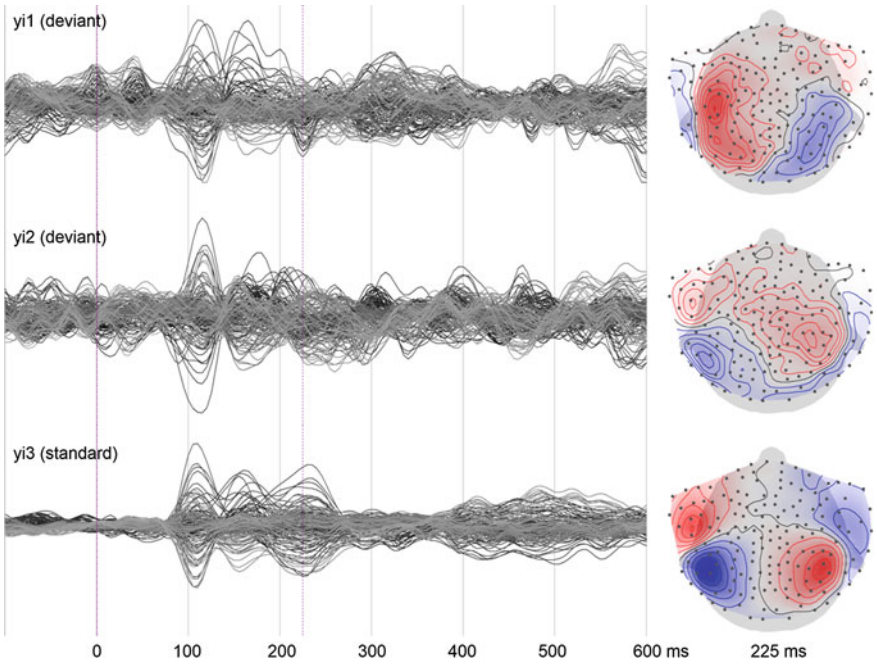

Fig. 2 Averages and field topography maps (shown at 225 ms) for the three stimulus types

The consistency test evaluates field topography (map) similarity across epochs. It is performed independently for each stimulus type and each sample. Here, the Null Hypothesis is that epochs of the same stimulus type are unrelated, i.e. that random maps have been measured. If the Null Hypothesis holds, randomly

perturbing channels *within* each epoch's map should not deteriorate the average map across all epochs.

For each sample s and E_t epochs of stimulus type t, the test is performed as follows: First, the observed mean global field power (MGFP) $P_{s,t,0}$ of the average over all epochs e of the individual maps $\mathbf{d}_{s,t,e}$ is computed as

$$P_{s,t,0} = \mathrm{mgfp}\left(\frac{1}{E_t}\sum_{e=1}^{E_t}\mathbf{d}_{s,t,e}\right) \text{ with } \mathrm{mgfp}(\mathbf{d}) = \sqrt{\frac{1}{M}\sum_{i=1}^{M}\left(d_i - \overline{d}\right)^2} \tag{1}$$

where M is the number of channels.

Then, for a total of R repetitions, the channels within each map are randomly shuffled. For each repetition r, this yields new randomized maps $\mathbf{d}_{s,t,e,r}$, and a new global field power $P_{s,t,r}$ can be computed according to

$$P_{s,t,r} = \mathrm{mgfp}\left(\frac{1}{E_t}\sum_{e=1}^{E_t}\mathbf{d}_{s,t,e,r}\right) \tag{2}$$

The probability $p_{s,t}$ of the Null Hypothesis is the fraction of values $P_{s,t,r}$ that are larger than or equal to $P_{s,t,0}$. Small values of p, traditionally $p < 0.05$, indicate rejection of the Null Hypothesis, or consistency between epochs of the same stimulus type.

The test for differences between stimulus types is again performed independently for each sample. Here, the Null Hypothesis is that there is no difference between stimulus types, i.e. that the same maps occur regardless of stimulus type. If the Null Hypothesis holds, randomly perturbing maps *across* stimulus types should not alter the average maps per stimulus type.

When just two stimulus types are compared, the MGFP of the difference of the averaged maps per stimulus type can serve as the measure. For each sample, the test is performed as follows: In a first step, the observed global field power $P_{s,0}$ of the difference of the averages over all epochs of stimulus types $t = 1$ and $t = 2$ is computed as

$$P_{s,0} = \mathrm{mgfp}\left(\frac{1}{E_1}\sum_{e=1}^{E_1}\mathbf{d}_{s,1,e} - \frac{1}{E_2}\sum_{e=1}^{E_2}\mathbf{d}_{s,2,e}\right) \tag{3}$$

For R repetitions, maps are then randomly shuffled across stimulus types. For each repetition r, randomized maps $\mathbf{d}_{s,t,e,r}$ are obtained and the global field power $P_{s,r}$ can be computed according to

$$P_{s,r} = \mathrm{mgfp}\left(\frac{1}{E_1}\sum_{e=1}^{E_1}\mathbf{d}_{s,1,e,r} - \frac{1}{E_2}\sum_{e=1}^{E_2}\mathbf{d}_{s,2,e,r}\right) \tag{4}$$

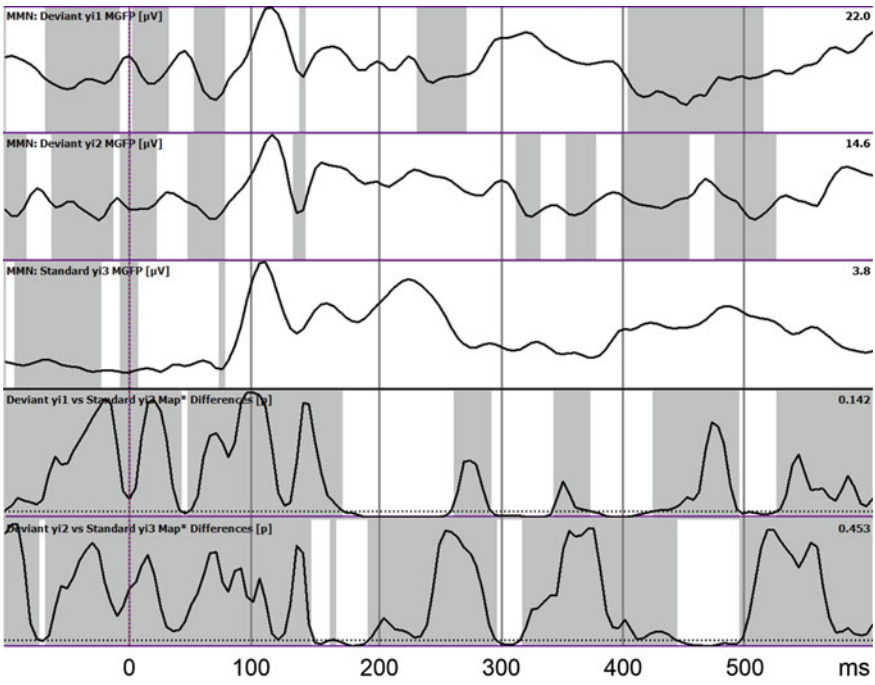

Fig. 3 Rows 1–3 show consistency test results for stimuli yi1, yi2, and yi3. White areas indicate consistency, with $p < 0.05$. Waveforms are MGFPs of the average per stimulus type. Rows 4 and 5 show differences between yi1 and yi3, and between yi2 and yi3. The waveforms here are p values, and white areas indicate significant differences, with $p < 0.05$

Again, the probability p_s of the Null Hypothesis is the fraction of values $P_{s,r}$ that are larger than or equal to $P_{s,0}$. Small values of p indicate significant map differences between stimulus types.

Optionally, averaged maps may be normalized before computing the difference. An extension to more than two and to different categories of stimulus types using a measure called global dissimilarity is described in Murray et al. (2008).

For this paper, the number of repetitions was $R = 5{,}000$ and values of $p < 0.05$ were regarded as significant. Map normalization was used for the difference tests.

3 Results

After excluding epochs with signals exceeding ±1.5 pT, 981 epochs remained and were subjected to TANOVA analysis: 99 of type yi1, 99 of type yi2, and 783 of type yi3. The consistency test for yi1 yielded periods of consistency from 80 to 135 ms, from 145 to 230 ms, from 275 to 400 ms, and from 515 to 600 ms. For yi2, consistency periods were 80–130, 145–310, 335–350, 380–395, 455–470, and

525–600 ms. For yi3, consistency was established for 10–70 and for 80–600 ms (Fig. 3). Pre-trigger consistency periods have not been mentioned as they are likely due to late effects of the previous stimulus.

The test for differences between yi1 and yi3 yielded significant latencies from 175 to 255, 295 to 340, 375 to 425, and 495 to 520 ms. Differences between yi2 and yi3 occurred from 150 to 160, 170 to 190, 300 to 315, and 445 to 490 ms (Fig. 3). The combined computation times of consistency and difference tests with 5,000 randomizations each for 157 channels and 981 epochs, performed for all 140 samples per epoch at 200 Hz were 14 min on a 2 GHz Core i7 CPU.

4 Discussion and Conclusion

Consistent with the behavioral results, the MMN data displayed a more robust statistical difference for the perceptually easier discrimination of the yi3/yi1 contrast compared to yi3/yi2 contrast. It was shown how TANOVA can be applied to the individual epochs obtained in an MMN experiment. This allowed establishing data plausibility and identifying latencies-of-interest for further analysis.

Obviously, this approach is not limited to MEG data analysis but can also be performed on EEG data. It can easily be extended to group or longitudinal studies. In some cases, it is then necessary to shuffle within-subject only. For group or longitudinal studies, either individual averages per stimulus type can be processed, or all acquired epochs of all datasets.

Acknowledgments Michael Wagner thanks Chia-Ying Lee for kindly providing the MMN data and Curtis W. Ponton for data processing advice, as well as Manfred Fuchs and Jörn Kastner for software support.

References

Koenig T, Melie-Garcia L (2009) Statistical analysis of multichannel scalp field data. In: Michel CM, Koenig T, Brandeis D, Gianotti LRR, Wackermann J (eds) Electrical Neuroimaging. Cambridge University Press, Cambridge, pp 169–189

Lee C-Y, Yen H-L, Yeh P-W, Lin W-H, Cheng Y-Y, Tzeng Y-L, Wue H-C (2012) Mismatch responses to lexical tone, initial consonant, and vowel in Mandarin-speaking preschoolers. Neuropsychologia 50:3228–3239

Murray MM, Michel CM, Grave de Peralta R, Ortique S, Brunet D, Gonzalez Andino S et al (2004) Rapid discrimination of visual and multisensory memories revealed by electrical neuroimaging. Neuroimage 21:125–135

Murray MM, Brunet D, Michel CM (2008) Topographic ERP analyses: a step-by-step tutorial review. Brain Topogr 20:249–264

MEG-SIM Web Portal: A Database of Realistic Simulated and Empirical MEG Data for Testing Algorithms

Lori Sanfratello, Julia Stephen, Elaine Best, Doug Ranken and Cheryl Aine

Abstract MEG is a noninvasive measure of electrophysiological brain activity which provides excellent temporal and high spatial resolution. Because of its uniquely high temporal resolution relative to the more commonly used hemodynamic-based measures (fMRI, PET), the usefulness of MEG as a complementary neuroimaging method is becoming more widely recognized, particularly in the investigation of functional connectivity within and between large-scale brain networks. However, the available analysis methods for solving the inverse problem for MEG have yet to be compared and standardized. A comparison of analysis methods is further complicated by the fact that the different MEG systems have different data formats, noise cancellation methods, and sensor configurations. In order to facilitate this process, we established a website containing an extensive series of realistic simulated data for testing purposes (http://cobre.mrn.org/megsim/). In addition, we assert the usefulness of these datasets for training purposes, as they will provide an unambiguous answer to whether a trainee is correctly carrying out analyses. Here we present a brief rationale and description of the testbed created, including cases emphasizing functional connectivity (e.g., oscillatory activity) and the Default Mode Network (DMN). They are suitable for use with a wide assortment of analyses including equivalent current dipole (ECD), minimum norm, beamformers, independent component analysis (ICA), Granger causality/directed transfer function, and single-trial methods.

L. Sanfratello (✉) · C. Aine
Department of Radiology, University of New Mexico School of Medicine, Albuquerque, NM 87131, USA
e-mail: lsanfratello@mrn.org

J. Stephen · E. Best
The Mind Research Network, 1101 Yale Blvd. NE, Albuquerque, NM 87106, USA

D. Ranken
Los Alamos National Laboratory, Los Alamos, NM 87545, USA

S. Supek and C. J. Aine (eds.), *Magnetoencephalography*,
DOI: 10.1007/978-3-642-33045-2_14,

Keywords MEG · Simulations/simulated data · Algorithms · Minimum norm · Beamformer · Dipole modeling

1 Introduction

MEG has the ability to provide information about the temporal activity of brain signaling with excellent temporal resolution (ms), and good spatial resolution (mm range for single source localization and cm range for source discrimination (Supek and Aine 1993, 1997)), and therefore has a unique potential as a tool to investigate brain activity. Furthermore, since MEG offers the capability of providing comprehensive information concerning brain signaling it can also be used for characterizing the fine temporal dynamics of signals underlying cognitive deficits in clinical populations. However, to date, there has been a lack of accepted standards within the MEG community as to what types of analyses are optimal for which types of studies. It is understood that with a given set of assumptions and parameters, the analysis methods each have unique strengths and weaknesses, depending on how they are used (for some examples see (Liljestrom et al. 2005)). Yet a systematic understanding of these methods remains limited. This is in part due to the mathematically ill-posed nature of the inverse problem for source reconstruction of MEG data (i.e., the reconstruction of the current distribution inside the brain based on measurements made outside the head). To solve the inverse problem, constraints need to be applied to obtain a unique solution (Baillet et al. 2001). These constraints vary between analysis methods (Hämäläinen et al. 1993), thereby making certain analysis techniques more appropriate for particular research questions, and making it challenging to choose one or a few analysis methods as "best" in most cases as has occurred in other neuroimaging fields (e.g. fMRI, PET). To further complicate the standardization of MEG data analysis techniques, the various MEG systems have different types of sensor pick-up coils, different number of sensors, and a variety of filtering methods and analysis software, much of which is proprietary.

Of the four broad categories of inverse procedures: equivalent current dipole (ECD), minimum norm (L1 and L2 norms), beamformer, and Bayesian, each has limitations associated with it as discussed below. Critics of the earlier dipole modeling approaches emphasize the difficulties in: (1) accurately localizing more than one or a few point current dipoles; (2) using point current dipoles to localize extended sources; and (3) determining the number of sources to be included in the search a priori (Liu et al. 1998; Fuchs et al. 1999; Uutela et al. 1999; Huang et al. 1998, 2006; Lin et al. 2006; Mattout et al. 2006, Mosher et al. 1992). Our greatest concern for the multidipole, spatiotemporal modeling methods is that under-estimation of the number of true sources can compromise location and timecourse accuracy for the identified sources (Supek and Aine 1997; Greenblatt et al. 2005). This is because multidipole modeling methods attempt to account for the entire measured signal via

a set number of sources, and the omission of one source will generally change the position and/or magnitude of other sources to account for the signal from the omitted source. This is not true for the minimum norm, beamformer, or Bayesian methods. We later discuss a CSST dipole modeling technique, and show how it can accurately localize (mm spatial resolution) simple and complex source configurations.

In contrast, critics of the minimum norm-based (Hämäläinen et al. 1994) approaches state that: (1) the results often appear smeared, even for point current sources and at times may become split across lobes which produce spurious or ghost sources leading to imprecise estimated dynamics (David et al. 2002; Michel et al. 2004; Lin et al. 2006); (2) the solution is biased toward superficial source locations leading to the application of depth weightings by some groups (Ioannides et al. 1990; Lin et al. 2006); (3) the smeared or broadened effect becomes more pronounced with a decrease in signal-to-noise, potentially leading to false positive sources (Wischmann et al. 1995); and (4) it is severely under-determined thereby requiring the use of regularization methods to restrict the range of possible solutions.

Although the linearly-constrained minimum variance (LCMV) beamformer (Vrba and Robinson 2000) has higher spatial resolution than minimum norm-based methods when cortical sources are focal, the underlying assumption is that neural sources are incoherent. Coherent signals will cause the beamformer to fail in finding locations of other coherent sources due to partial cancellation (Hui et al. 2010) which is a potential problem for cognitive data where coherence typically abounds. For example, in working memory studies, activity tends to synchronize across many widespread brain regions for seconds (Aine et al. 2003). Fortunately, several groups have recently introduced variants of the beamformer that can reportedly deal with coherent sources, with some restrictions [e.g. Dalal et al. (2006); Brookes et al. (2007, 2011); Diwakar et al. (2011); Moiseev et al. (2011)visual and auditory studies]. However both beamformer and minimum norm techniques have some difficulty in examining functional connectivity or cortical interactions, given the robust cross-talk present in the data (Hui and Leahy 2006; Hui et al. 2010). But, the general advantages of minimum norm and beamformer methods are that they require less analysis time making them quicker to use.

Finally, there are Bayesian methods (Jun et al. 2005; Schmidt et al. 1999; Wipf et al. 2010). The current drawback of these methods is that they have not yet been widely applied to empirical data. In part this may be due to a need for large computational resources since some versions utilize a Markov Chain Monte Carlo approach to generate sets of activity parameters that are distributed according to the posterior distribution (Schmidt et al. 1999). However proponents of this method state that the Bayesian method combats the issue of ill-posedness by offering a general formulation of regularization constraints. In addition, the Bayesian approach provides statistical performance tools. These tools include the estimation error covariance and the marginal probability density of the measurements (Brooks et al. 2005).

Recently, the strong interest in functional connectivity that has arisen in the MEG field has investigators combining some of the above mentioned localization

methods with other types of analyses to determine which and how sources of activity are temporally related. Functional connectivity has historically been assessed in sensor space (e.g. de Pasquale et al. 2010), but new methods are being developed to determine functional connectivity in source space. For example, Brookes et al. (2011) have used a beamformer localization method, along with a Hilbert transform to derive the analytic signal, to which independent component analysis (ICA) is applied, in order to identify the functional networks of activity. The oscillatory and DMN simulations that have been created and described in Sect. 2.6 could be used to further characterize the strengths of such an analysis procedure.

Given the above, we have established the MEG-SIM website containing both a series of realistic simulated data sets and empirical data sets for testing purposes (http://cobre.mrn.org/megsim/). Through a partnership formed between the Mind Research Network (MRN), Massachusetts General Hospital, University of Minnesota/Veterans Affairs in Minneapolis, University of New Mexico, and Los Alamos National Laboratory, we acquired MEG data using three different MEG systems (VSM MedTech 275, Elekta-Neuromag 306, 4-D Neuroimaging 3,600) and three different sensory paradigms (visual, auditory and somatosensory) for each of 9 participants. A grant from NIMH (R21MH080141) then allowed us to create realistic simulated data derived from the real noise contained in the collected empirical data. A web portal was established so others can access both the simulated and empirical datasets with the hope of furthering algorithm performance assessment and development through the MEG-SIM website. We refer to the testbed as 'realistic' simulated data because: (1) colored noise is used in most examples (i.e., simulations are embedded in spontaneous data containing correlated noise); (2) the simulated timecourses and source locations are based on findings from empirical data; (3) focal and extended cortical patches are created from MRIs of individual participants (i.e., the SNR and orientation of sources differ across participants); and (4) in some cases each of the unique single trials and continuous data, mimicking actual data acquisition, are provided.

We assert that if an algorithm fails to identify the simulated sources and timecourses under realistic conditions (e.g., similar SNR as empirical data with real artifacts occurring at random intervals), then one cannot realistically expect to obtain correct results in empirical data. If an algorithm provides reasonable solutions to simulations then it is standard practice to next apply the algorithm to simple sensory empirical data where the literature provides information on the expected locations and timecourses of sources (e.g., non-human primate studies) before attempting analysis of cognitive datasets, where the literature is not yet well established. We have designed the simulated datasets to provide a wide range of realistic examples emulating brain activity. We specifically tried to design these simulations such that one analysis approach would not be favored. We hope developers will utilize these data to further develop and refine MEG analysis methods. Similarly, we hope that users of the algorithms will compare and contrast their favored approaches with others. Because we are avid users of a semi-automated, multidipole, spatiotemporal approach [Calibrated Start Spatio-Temporal

or CSST; (Ranken et al. 2002, 2004)], many of the solutions shown herein are from the CSST algorithm to demonstrate the efficacy of these simulations. Because the empirical datasets were covered in depth in Aine et al. (2012), we only briefly describe those that are available at the MEG-SIM website in Sect. 3 of this chapter.

2 Simulated Datasets

2.1 Software

The simulated data were primarily created using MRIVIEW and MEGAN software, both of which are made available at the MEG-SIM website. MRIVIEW (Ranken and George 1993; Ranken et al. 2002) is a software tool for integrating volumetric MRI head data with functional information (e.g., EEG, MEG, fMRI—see chapter in this volume by Ranken for further details on MRIVIEW). A Forward Simulator is included in MRIVIEW for creating multiple focal or distributed-source regions of arbitrary size and orientation, allowing users to create a vast array of simulated datasets. We have used these tools previously for simulating epileptic spikes that were then embedded in spontaneous activity from patients (Stephen et al. 2003a, 2005).

MEGAN (E. Best) organizes the data from the different MEG systems into a consistent data format, netMEG, a self-documenting and highly portable file, written using netCDF format. This netCDF file is imported into MRIVIEW. The simulated sensor measurements are obtained by summing the forward fields from all of the simulated sources. White noise, simulated noise or real noise from MEG acquisitions can then be added to the calculated forwards to generate simulations of empirical MEG data. More information about MEGAN can be found in Aine et al. (2012).

CSST (Calibrated Start Spatio-Temporal) is a multidipole, spatiotemporal modeling approach to source localization that has been automated, i.e., it takes the traditional starting parameter guess(es) out of the hands of the investigator. CSST uses the Nelder-Mead non-linear downhill simplex procedure to perform a spatial search (Nelder and Mead 1965) and utilizes information based on a singular value decomposition (SVD) of the data matrix for determining an approximate number of sources to be localized (a range of source models is then chosen by the investigator). CSST runs multiple instances of the downhill simplex search from random combinations of MR-derived starting locations from within the head volume on a Linux PC cluster. CSST has been used extensively with both Neuromag 122 and CTF 275 MEG systems (Stephen et al. 2003a, b, 2005, 2006; Aine et al. 2000, 2010) as well as the Neuromag Vectorview 306-system (Stephen et al. 2012; Susac et al. 2010, 2011; Golubic et al. 2011). CSST has also been thoroughly tested on EEG data.

2.2 Physiologically Plausible Simulations

The initial simulated datasets were constructed using two different-sized patches of cortex determined via MRI ($\sim$4 and $\sim$20 mm^2) and two different source strengths (30 and 50 nAm). We used these values because our previous empirical results suggest that those current strengths are typical of what is encountered in visual and auditory studies [e.g. Table 2 in Aine et al. (2006) and Fig. 4 and Table 3 in (Aine et al. (2005)]. In addition, the empirical visual paradigm used to acquire data at each MRN partner site utilized small and large stimuli (1.0° and 5.0° visual angle) designed to activate $\sim$4 mm^2 of tissue and $\sim$20 mm^2 of tissue in primary visual cortex, according to the cortical magnification factors presented in Rovamo and Virsu (1979). We attempted to equate the simulated and empirical parameters since the goal was to produce both focal and extended activity. This is necessary to evaluate analysis methods where source extent is believed to be dealt with less effectively (e.g. dipole modeling). The somatosensory study used electrical stimulation of the index finger and median nerve, to produce focal versus extended sources. The auditory study used individual pure tones and bursts of white noise to evoke focal versus extended activity. Additional justification for parameter choices can be found in Aine et al. (2012).

2.3 Simulated Visual Data

The locations, timing, and extent of the simulated sources (see Table 1 for Sets 1–5) were generated based on our previous basic visual (Stephen et al. 2002) and visual working memory studies (Aine et al. 2006). Set 3 differs from Set 1 in having synchronous late activity. Set 1.B and 3.B differ from 1.A and 3.A in dipole strengths (i.e., larger cortical patches). Note, these latencies are modeled after empirical visual studies but they were embedded in the noise file so that $\sim$200 ms was treated as prestimulus baseline. DLPFC (dorsolateral prefrontal cortex) and AC (anterior cingulate) were treated as ramping activity peaking later in time. Definitions of areas are: V1 = visual area 1; V2 = visual area 2; V3 = visual area 3; I. LOG = inferior lateral occipital gyrus; IPS = intraparietal sulcus; S. LOG = superior lateral occipital gyrus; RHC = right hippocampus. We varied the synchronicity of sources to allow developers to determine an algorithm's sensitivity to fine temporal changes. Parameters that vary within and across datasets include: number of sources, focal versus extended sources, source strengths, degree of synchrony of sources, and noise level or type of noise (white noise or spontaneous noise). The first 5 sets were produced for 5 participants using individual cortical geometries, different SNRs, and empirical noise data from both the CTF Omega 275 and Neuromag Vectorview 306 MEG systems. Although it was a goal to simulate these cases for the 4-D Neuroimaging Magnus 3,600 system as well, funds for this project ended before we could do so. Timecourses were usually

Table 1 Onset latencies and amplitudes of sources in different visual areas used for each simulated dataset. Reprinted from Aine et al. (2012) with permission from Springer

	VI	V2/V3	I. LOG	IPS	S.LOG	DLPFC	AC	RHC
Set 1.A	80 ms	90 ms		100 ms				
	30 nAm	30 nAm		30 nAm				
1.B	80 ms	90 ms		100 ms				
	50 nAm	50 nAm		50 nAm				
Set 2		90 ms	90 ms	100 ms				
		15 nAm	30 nAm	30 nAm				
Set 3.A	80 ms	90 ms		100 ms				
	30 nAm	30 nAm		30 nAm				
3.B	80 ms	90 ms		100 ms				
	50 nAm	50 nAm		50 nAm				
Set 4		90 ms	90 ms	100 ms	100 ms	300 ms*	400 ms*	
		15 nAm	30 nAm	20 nAm	30 nAm	20 nAm	30 nAm	
Set 5		90 ms	90 ms	100 ms	100 ms	300 ms*	400 ms*	80 ms
		15 nAm	30 nAm	20 nAm	30 nAm	20 nAm	30 nAm	51 nAm

* DLPFC and AC were treated as ramping activity peaking later in time

modeled using 3 Gaussians (e.g., early spike-like activity followed by later slow-wave activity) as typically found in many visual and auditory MEG studies (Portin et al. 1999; Aine et al. 2003, 2005, 2012; Vanni et al. 2004; Kovacevic et al. 2005).

In the simulated example shown in Fig. 1, a Freesurfer-segmented gray matter/white matter boundary for the simulations was imported into MRIVIEW (Fig. 1a), although the segmentation may also be accomplished within MRIVIEW. The simulated activation timecourses (signal) are shown Fig. 1b. In each case, 100 single trials of real spontaneous background activity were averaged together as the noise trial for each of the 5 participants and for each of the MEG systems (Fig. 1c). Then the signal was embedded within the averaged noise file (Fig. 1d). For all simulated datasets on the web portal, a spherical head model was used for the simulations and modeled data; however, a boundary element model (BEM) is also available in MRIVIEW.

Table 2 shows actual source locations, CSST estimated source locations, and errors when either noise was absent (no-noise) or empirical noise was present for visual simulated data Set 4. CTF head-centered coordinate system is used, where -x points out the back of the head, +y points out the left ear, and +z points out the top of the head. Average error across the 6 sources was 0.1 mm for the no-noise condition and 6.8 mm for the real noise condition. Standard deviation (SDev) is shown for estimated solutions for real-noise simulated data. This table demonstrates that the presence of real noise significantly affects source localization accuracy; however, our CSST solution for the real noise condition was still good for this complicated dataset, and inconsistent with previous critiques of dipole-modeling approaches that state dipole methods cannot accurately localize more than a few point sources of activity. Further, Table 3 lists CSST output when

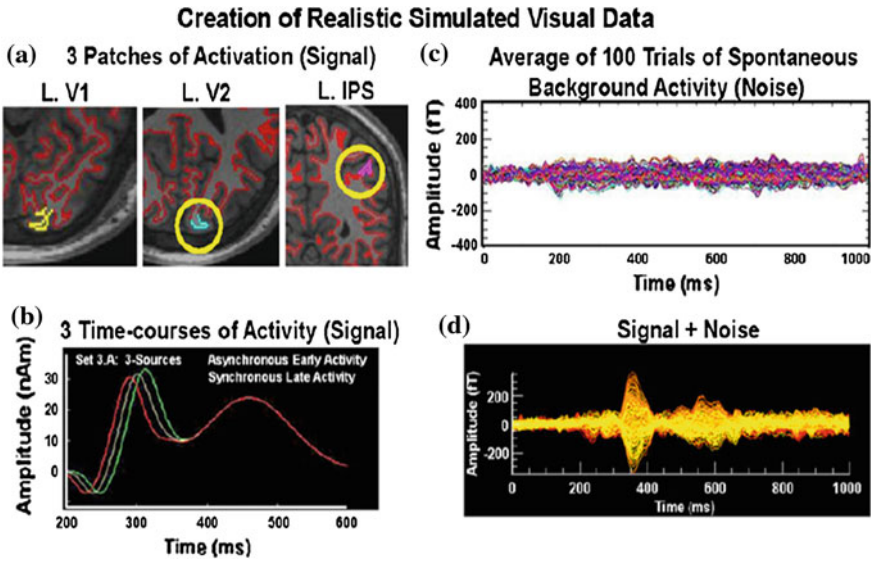

Fig. 1 A Freesurfer-segmented gray matter/white matter boundary for the simulations (shown in *red*) was imported into MRIVIEW from which patches (**a**) of simulated activity (**b**) were generated. 100 passes of spontaneous activity or noise (**c**) were identified using CTF software (Data Editor) and averaged together using MEGAN. The simulated activity was embedded within the averaged noise file (**d**) and saved in netCDF format (i.e., a netMEG file in MEGAN). Reprinted from Aine et al. (2012) with permission from Springer

Table 2 Actual and CSST estimated ("no-noise" and "real-noise") locations for a 6-source, realistic simulation

SET 4 6 sources	Source V3			Error (mm)	Source I. LOG			Error (mm)	Source IPS			Error (nm)
	X	Y	Z		X	Y	Z		X	Y	Z	
Actual	−70.0	5.9	75.8		−59.7	33.2	42.9		−22.1	38.3	82.6	
No noise	−69.7	6.0	75.9	0.3	−59.8	33.3	42.9	0.1	−22.1	38.2	82.7	0.1
Real noise	−61.3	4.3	74.1	9.0	−55.6	31.7	44.5	4.6	−18.7	28.7	71.8	14.8
SDev (Real)	0.3	2.3	1.6		1.6	0.3	0.4		1.5	1.7	0.9	

	Source R. frontal				Source AC				Source S. LOG			
	X	Y	Z		X	Y	Z		X	Y	Z	
Actual	58.1	−41.5	46.2		74.1	−7.0	47.8		−31.3	−40.7	60.3	
No noise	58.1	−41.7	46.2	0.1	74.0	−7.1	47.6	0.2	−31.4	−40.8	60.3	0.1
Real noise	58.5	−43.2	44.0	2.8	72.6	−9.9	46.7	3.4	−27.5	−36.1	59.1	6.1
SDev (Real)	0.1	0.1	0.4		0.5	0.3	0.2		0.5	0.6	0.6	

Table 3 Sample output from an automated routine for determining best-fits to 3-source simulated data

	Source location	Loc error mm (STD)	Peak amplitude error nAm			Peak latency error ms			Avg Loc error mm
			Pk 1	Pk 2	Pk 3	Pk 1	Pk 2	Pk 3	
Real spontaneous noise	1 Dip-V3	17.5 (0.15)	12.4	42.5	19.6	3.0	1.0	18.0	17.5
	2 Dip-Vl	9.25 (0.11)	1.6	4.7	1.0	4.0	2.0	2.0	
	2 Dip-IPS	7.22 (0.08)	5.1	21.5	11.0	7.0	4.0	18.0	8.23
	3 Dip-V1	4.93 (0.13)	1.1	0.45	2.2	5.0	2.0	1.0	
	3 Dip-V3	4.98 (0.12)	1.9	7.1	4.1	13.0	0.0	25.0	
	3 Dip-IPS	2.32 (0.05)	1.3	4.6	2.8	6.0	2.0	15.0	4.08
	4 Dip-V1	3.11 (0.14)	0.03	3.6	0.80	4.0	2.0	6.0	
	4 Dip-V3	3.51 (0.14)	3.2	5.1	2.5	1.0	1.0	29.0	
	4 Dip-IPS	1.56 (0.05)	1.4	5.6	3.6	5.0	2.0	18.0	2.73
	4-Dip-N	Noise	–	–	–	–	–	–	

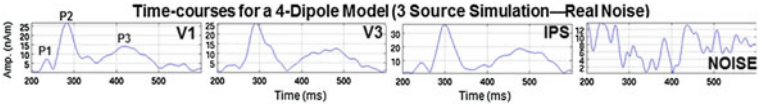

varying the model order (i.e. number of fitted dipoles) for a 3-dipole simulated dataset. The solutions (1–4 Dipoles) shown are for real spontaneous noise. Timecourses (shown as absolute values, bottom) are from the 4-dipole fit to 3-source data. In Table 3 the entries P1, P2, and P3 correspond to the Pk 1, Pk 2, Pk 3 timecourses. Notice that the noise timecourse is low-amplitude and without structure. As this table shows, under-modeling (1- and 2-dipoles) results in large localization errors. In contrast, localization errors are often reduced when over-modeling by 1 dipole (i.e., 4-dipoles for this 3-source dataset). Fortunately, noise sources are often easy to identify by a lack of timecourse structure and low amplitude (lower right panel).

Set 6 (remaining sets are not shown in Table 1) includes late activity (e.g., 400–600 ms) that was synchronous across four cortical sites (V1, I. LOG, IPS, and DLPFC), as is seen in working memory studies (Aine et al. 2006). The upper left panel of Fig. 2 displays the locations of the cortical patches (cortical patches are located at the cross-hairs) while the timecourses assigned to the cortical patches are shown beneath the MRIs. The averaged waveforms (128 trials with signals embedded in real spontaneous noise) seen across the 275 channels of the CTF MEG system are shown in the middle left column. CSST source locations are shown in the upper right panel (see tabled values). The table shows the coordinates of the actual sources, the estimated source locations, and the errors using Euclidean distance. Net source orientation errors were 42.0° for V1, 58.2° for I. LOG, 20.9° for IPS and 48.0° for the DLPFC sources. However, summarizing absolute orientation error is challenging since the original sources consisted of

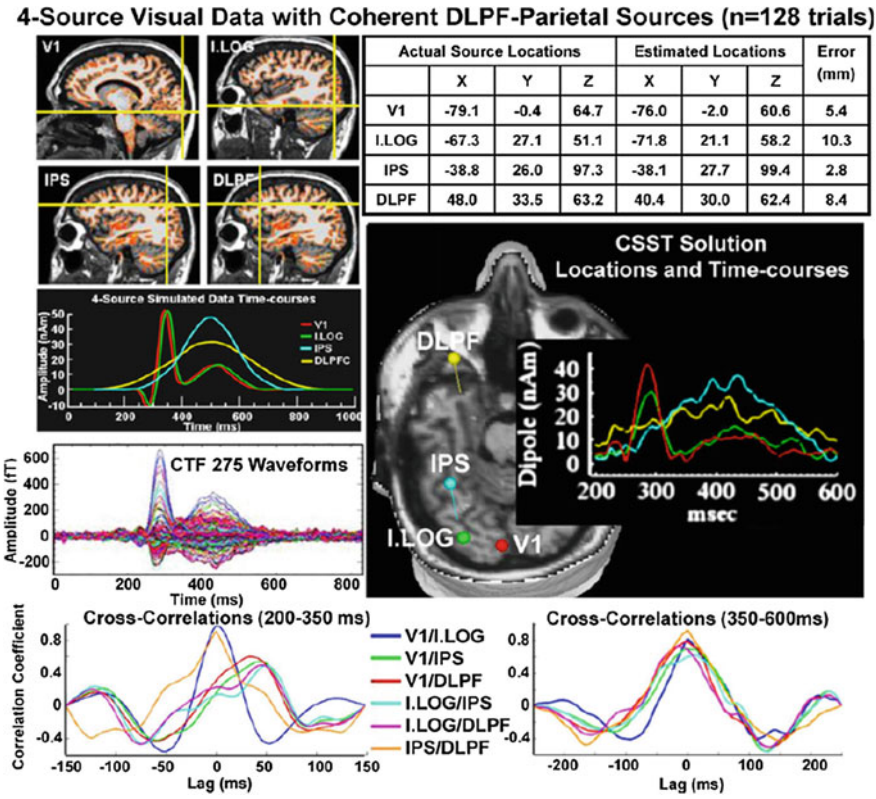

	Actual Source Locations			Estimated Locations			Error (mm)
	X	Y	Z	X	Y	Z	
V1	-79.1	-0.4	64.7	-76.0	-2.0	60.6	5.4
I.LOG	-67.3	27.1	51.1	-71.8	21.1	58.2	10.3
IPS	-38.8	26.0	97.3	-38.1	27.7	99.4	2.8
DLPF	48.0	33.5	63.2	40.4	30.0	62.4	8.4

Fig. 2 Simulation results for a 4-source model (Set 6) where all sources became synchronous during the later interval (see *upper left* panels for source locations (cross-hairs) and timecourses of the sources). Amplitudes and peak latencies were jittered across each of 128 single trials. The averaged waveforms seen at the sensor level for the CTF system are shown beneath the input timecourses. *Upper right* table shows CSST actual locations and errors associated with modeled source locations. The *middle* panel shows location and timecourse plots of the CSST solutions. *Bottom row* shows cross-correlations between source timecourses for an early interval (*left*) when there was some asynchrony across sources and a later interval (*right*) when all sources became synchronous. Adapted from Fig. 5 Aine et al. (2012) with permission from Springer

patches of cortex with the orientation of the patch activity conforming to the cortical folds. The middle right panel shows the estimated timecourses and source locations. The average localization error across all 4 sources was 6.7 mm with the greatest error for the I. LOG source. The cross-correlations between timecourses are shown in the bottom row of Fig. 2. We examined early activity first (200–350 ms–bottom left panel) which shows that V1 activity correlated highly with I. LOG, regions showing the initial spike-like activity ($\sim$280 ms). IPS and DLPF cross-correlations were also highly correlated with near zero-lag. The maximal correlation coefficients of the other pairs of sources were lower in value

and were not near zero-lag. In contrast, the late activity (350–600 ms—bottom right panel) shows higher zero-lag correlation coefficients for activity between the 4 brain regions (i.e., late activity was synchronous across brain regions) with IPS and DLPFC revealing the highest correlation coefficient. This dataset is also suitable for examining coherence either between sensors or between reconstructed sources.

Next, single-trial datasets were created with and without oscillatory activity, with some reflecting functional connectivity in a working memory task, which are suitable for additional types of analyses (i.e., time-frequency analyses, Granger Causality, etc.). In this case, sources embedded within 128 single trials of noise were jittered about their mean latency and amplitude. This dataset (Set 7) is similar to Set 6 (VSM-CTF MEG System). Again, the four cortical sites were: (1) primary visual cortex (V1); (2) inferior lateral occipital gyrus (I.LOG); (3) intraparietal sulcus (IPS); and (4) dorsolateral prefrontal cortex (DLPFC). The cortical patch current strengths were initially assigned values similar to those we observe in our visual working memory studies (30–50 nAm peaks) using the MRIVIEW Forward Simulator (Ranken and George 1993; Ranken et al. 2002) but were then randomly jittered about those values by up to ±50 % across the single trials. Peak latencies were also jittered across each trial by a randomly selected value up to ±FWHM/2. To allow for source analysis of averaged evoked responses, the 128 single trials were then averaged together and written out to the netCDF file format. Therefore each of the 128 single trials plus the averaged file is available at the MEG-SIM website, in netCDF format.

In Set 8, oscillatory activity was added to Set 7 timecourses (Fig. 3). For the time-locked oscillatory activity, V1, I. LOG, and IPS oscillated between 30 and 60 Hz (gamma band) across the 128 trials while IPS and DLPFC oscillated between 14 and 28 Hz (beta band). Oscillatory activity for DLPFC was delayed by 20 ms relative to IPS, and IPS gamma activity was delayed by 10 ms relative to IPS beta activity (see schematic in Fig. 3a). The delays were meant to reflect normal time delays between visual areas (Stephen et al. 2002). Gamma activity mimicked local circuitry activity between V1, I. LOG, and IPS while beta activity mimicked long-range connections between IPS and DLPFC. For both beta and gamma oscillations, the amplitudes were set at 10 nAm and were then jittered between 5 and 15 nAm across the 128 trials. Note that the latencies, and therefore the phase of the oscillations, were kept constant between brain regions, and also between trials. As with the other simulated data sets, the timecourses were constructed within MRIVIEW, however, they had to be constructed independently; i.e., one timecourse contained the evoked response plus real noise while the other timecourse contained the oscillations without noise. The two timecourses were then added together using a Matlab script. Again, to allow for source analysis of the averaged responses, the 128 single trials were averaged together to create a single averaged dataset, and were written out to a netCDF file (datasets for two subjects were created).

Figure 3b shows the input signal at the sensor level across sources before oscillatory activity or noise was added. Sample single trials are shown where peak

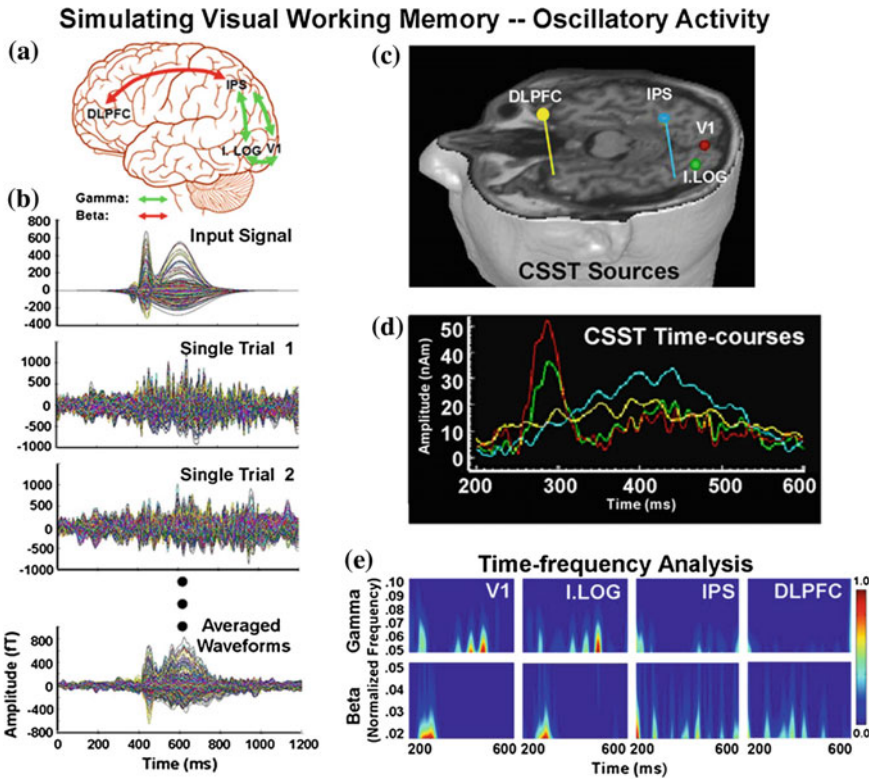

Fig. 3 Simulated visual working memory with long-range beta band and short-range gamma band oscillatory activity (see (**a**) schematic). DLPFC and IPS oscillated at 15–20 Hz while IPS, I. LOG, and V1 oscillated at 30–80 Hz. IPS generated both beta and gamma band oscillations. **a** The averaged input signal without noise is shown followed by sample single-trials and the averaged data as seen at the sensors of the CTF system. **c** CSST location estimates and their associated timecourses (**d**) are shown. **e** Time-frequency representations using Morlet wavelets for the CSST solutions shown above. Frequency was normalized to the Nyquist frequency = ½* sampling frequency (600 Hz). Oscillatory activity was given 10 nAm on average across trials. Reproduced from Aine et al. (2012), with permission from Springer

amplitudes (of both the evoked and oscillatory activity), peak latencies (of the evoked activity only), and frequency of the oscillatory activity were jittered across trials so each single trial is unique. The average of the 128 single trials is shown beneath. Figure 3c and 3d show the output of the CSST algorithm. CSST provides both the locations of the dipoles and the reconstructed timecourses of activity. Table 4 contains the results of this analysis for the two visual/working memory datasets that were created for the first subject (i.e., single trials averaged with and without oscillatory activity). Our results show that CSST can accurately reconstruct both temporal and spatial characteristics of the simulated datasets, even with noisy and oscillating sources. Time-frequency plots are shown in Fig. 3e for

Table 4 CSST results for simulated datasets with 4 visual sources based on averaged waveforms without oscillatory activity (*top*) and with oscillatory activity (*bottom*) for Subject #1

Source	Loc. error (mm)	Lat. error (ms)	Amp. error (nAm)
Single trials (Set 7):			
VI	1.5	6	2.5
I.LOG	9.4	4	3.2
IPS	3.7	3	7.9
DLPF	8.9	13	6.8
Single trials with oscillations (Set 8):			
VI	4.7	6	9.8
I.LOG	9.7	1	4.8
IPS	7.0	1	11.2
DLPF	4.9	16	2.4

gamma and beta bands. Gamma band activity is primarily seen in dipoles located in V1, I.LOG and IPS, which is consistent with the simulated data. No gamma activity was provided to DLPFC and correspondingly, gamma activity during this interval of time is essentially non-existent. It appears that the initial spike-like activity in the timecourse has a predominantly beta component to it as seen in the V1 and I.LOG beta band plots. IPS and DLPFC, in contrast, reveal beta band activity throughout the interval, which is consistent with the simulated data. This shows how our realistic simulated oscillatory activity datasets can be used for testing various frequency analyses and inverse procedures. Again, these data also come with all 128 unique individual trials for investigators wishing to apply single trial analysis methods.

Many MEG/EEG investigators are familiar with more traditional analyses of functional connectivity such as that provided by coherence analysis. Here we show that coherence analysis can be conducted both at the sensor and the source level using our simulated datasets. For example, a sensor near V1 which showed a large evoked response was chosen as the sensor of interest (see Fig. 4a, sensor #273 encircled by a green ring). Next the averaged simulation file (Set 7) was imported into Matlab where "mscohere" was used to determine the coherence of sensor 273 with every other sensor in the MEG array for the frequency range 30–60 Hz. This coherence analysis was repeated for the simulation in which oscillations had been added to the sources as described above (Set 8). Results show a clear increase in coherence between sensors which had gamma band oscillations added to nearby sources. Coherence analyses were also carried out at the source level for Set 8 (Fig. 4b). In this example, coherence in the beta band was examined between sources (i.e., output from CSST). Beta oscillatory activity was added to DLPF and IPS sources and the bottom figure of Fig. 4b shows the resulting coherence between these two sources (IPS is the reference source shown in white and its coherence (normalized magnitude) with DLPF is represented by red color). It turns out that the initial spike-like activity of the timecourses also has a beta band component as indicated by the coherence between reference source V1 (shown in white in the upper Fig. 4b) and I.LOG. Recall that the time-frequency plots shown in Fig. 3e also revealed this information (see Beta activity for V1 and I.LOG).

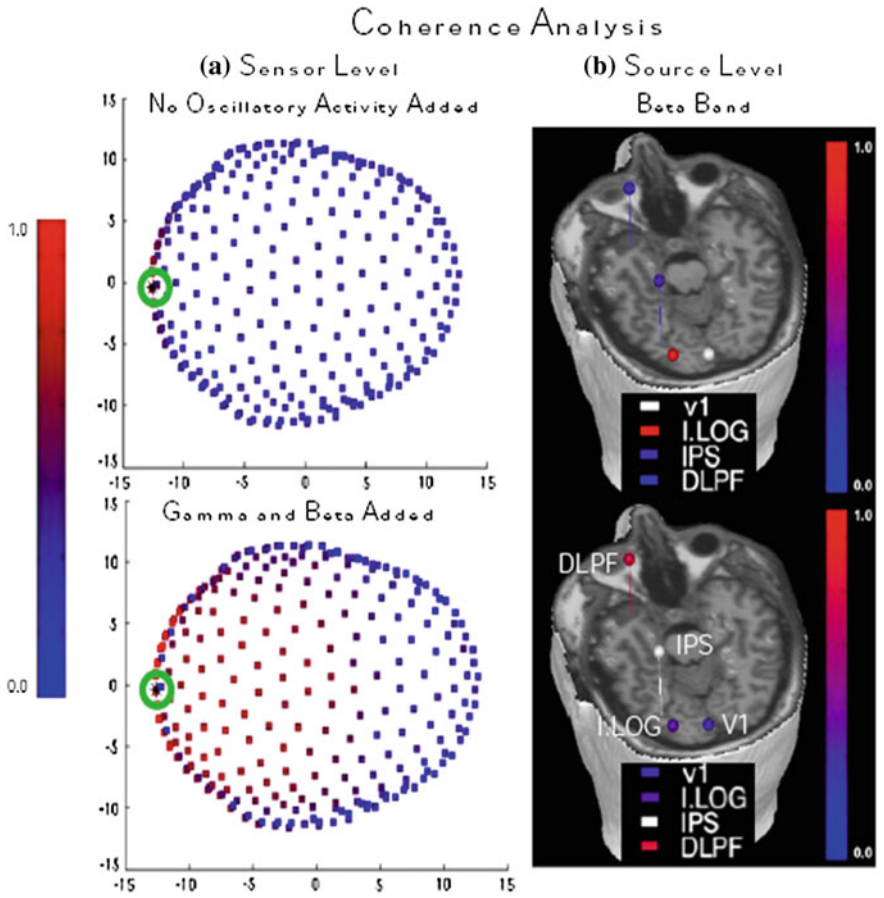

Fig. 4 **a** Sensor level coherence analysis with no oscillatory activity applied to underlying sources (*top*) and with oscillatory activity applied to underlying sources (*bottom*). **b** Source level coherence analysis relative to the white source (V1 *Top*, IPS *Bottom*) of Beta band activity. Level of coherence is indicated by the colorbar

Table 5 CSST results for Subject #2 for both CTF (Set 8) and Neuromag (Set 9) MEG systems

Source	CTF	Neuromag
Single trials and oscillations	Loc. error (mm)	Loc. error (mm)
VI	not found	9.9
I. LOG	7.5	3.7
IPS	4.2	2.8
DLPF	2.1	4.7

For the final visual simulated dataset (Set 9), the same data as Set 8 was created for the Neuromag 306 system with different noise trials and sensor configuration relative to the CTF 275 system. In this case, a Matlab program utilized the netCDF

toolbox for manipulating the opening and closing of the netCDF files containing the individual evoked waveforms and the individual oscillatory waveforms, which were created at cortical locations as similar as possible to Set 7. The simulated data were again created using MRIVIEW and MEGAN. Matlab was used to import the timecourses of the individual areas of evoked activity which were then jittered (in the same way as discussed above) and combined with randomly selected instances of Neuromag 306 noise which was read into Matlab using Fieldtrip functions (http://fieldtrip.fcdonders.nl/). One hundred single trials were created containing evoked and oscillatory activity. This was automated by the process of generating single trials described previously for Set 8. The 100 single trials were then averaged together and saved to a netCDF file, to be used with CSST analyses, and to a Neuromag 306 FIF file to be used with Curry, a commercial software package (Compumedics Neuroscan, Charlotte, NC http://www.neuroscan.com/) for the sLORETA and SWARM analyses (Wagner et al. 2007) discussed below.

2.4 Preliminary Examples of Analysis Algorithm Output for Visual Simulated Data

First, for comparison, multidipole, spatiotemporal source localization was conducted for Subject #2 using the CSST algorithm for simulated data Sets 8 and 9 (CTF and Neuromag systems, respectively). Table 5 shows the results from these analyses. Location was considered "not found" if it was $\geq$50.0 mm from the true source. Once again CSST determines the locations of the active cortical areas with a good degree of accuracy. We do find obvious differences between the results for the CSST dipole fits for the two different subjects (compare Tables 4 and 5) and between the same subject and the two MEG systems (Table 5). This was not surprising since the simulations were (1) created using each subjects' MRI, therefore, the exact location of the cortical patch differs somewhat between subjects which will result in different waveform distributions at the sensor level for the different MEG systems; and (2) the V1 source was given a smaller initial amplitude (30 vs. 50 nAm) in Subject #2, making it more difficult to identify. Furthermore, there is also a slight variation in the noise trials chosen since the noise trials were taken from the empirical datasets (therefore noise varied across the MEG systems).

We next report the results of two L2 minimum norm-based current distribution analyses, sLORETA and SWARM, available in Curry for the datasets made for Subject #2. In current distribution models, the cortex is divided up into a large number of elements, which form the solution space. Since the primary source of the MEG signal is assumed to be associated with postsynaptic currents, a current dipole is assigned to each of the many tens of thousands of tessellation elements (user chooses exact number depending upon desired resolution). Additionally, since the problem is under-determined (i.e. there are fewer equations than

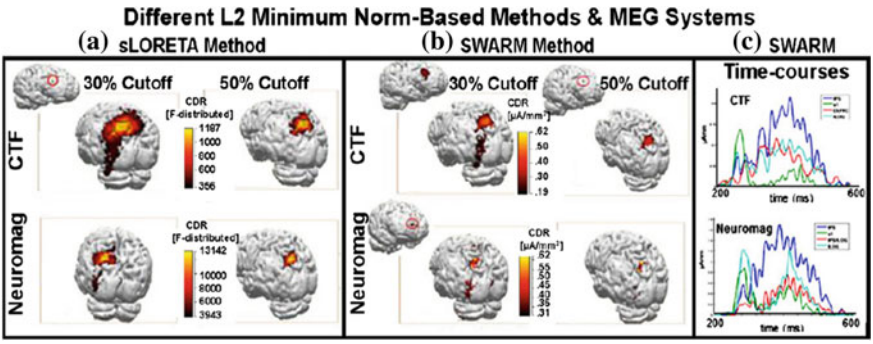

Fig. 5 **a** sLORETA results using Curry at two different cutoff values (30 and 50 %) for the same active cortical areas mixed with spontaneous noise files from the CTF and Neuromag systems. **b** SWARM results using Curry at two cutoff values for the same active cortical areas and noise files used in (**a**). **c** Timecourse reconstructions from SWARM using simulated datasets in (**b**) (both CTF and Neuromag). Reproduced from Aine et al. (2012), with permission from Springer

unknowns), the weighted least-squares criterion requiring that the prediction error is minimized must be augmented with an additional constraint to select the best current distribution among those capable of explaining the data. In the case of the basic L2 minimum norm approach, the mathematical criterion is the solution that minimizes the power (L2-norm) of the dipole moment. After adding noise normalization, statistical significance of current estimates relative to the level of noise can be determined using "dynamic statistical parametric" maps; sLORETA is a variation of this approach (Pascual-Marqui et al. 1994, 1999; Dale et al. 2000; Pascual-Marqui 2002; Wagner et al. 2004, 2008), while SWARM (Wagner et al. 2007, 2008) is an sLORETA-based method that provides current estimates instead of probabilities. Simulated data was read into the Curry software package using either DS files (for the CTF simulations) or FIF files (for the Neuromag simulations). This allowed Curry to assign the correct coordinate system when importing the data and provided access to the digitized fiducials in the files to be used for accurate alignment with the subjects MRI, which was also imported into Curry.

Figure 5 shows preliminary results of the sLORETA and SWARM analyses carried out using the Curry software package. The CTF simulations show results that are more distributed in the IPS/I.LOG/V1 areas in both sLORETA and SWARM in comparison to the simulations made with the Neuromag system, which shows more focal solutions. This is not particularly surprising based on the fact that planar gradiometers are more sensitive to signals directly below the sensors. We additionally provide the results at two different thresholds, to show that some activation may not be seen if the threshold is too high, e.g. compare the CTF sLORETA results in Fig. 5, where the DLPFC area of activity is lost at the higher cutoff. Figure 5 also shows that sLORETA was unable to find DLPFC activity at either cutoff in the Neuromag data. In addition, it is possible to extract

timecourse activation from the SWARM analysis. Although Curry software provides timecourse extraction via "CDR dipoles", an ECD method, it also contains the functionality to save the SWARM results into a Matlab file format for further investigation. We utilized the latter method. As a first step to show how timecourses can be extracted from the SWARM data we chose to identify areas of activation as simply as possible. To this end we used Matlab to identify the areas of highest activation from the SWARM data that Curry created, after importing the Curry output into Matlab. We then plotted the timecourses at those locations (right portion of Fig. 5); the only constraint was that the independent sources be greater than 2.0 cm apart, which we empirically chose such that different sources were resolvable at this separation. Note that the added oscillations (e.g., beta and gamma band activity) can be easily identified. We have less experience with these two L2 minimum norm-based analyses, therefore they should be considered preliminary and no tables of error values are offered. We present a preliminary report here hoping to encourage others to investigate these analyses further using the same simulations. It is clear however that these simulated datasets are already providing a reasonable challenge for a variety of analysis methods.

2.5 Simulated Somatosensory and Auditory Datasets

Simulated somatosensory and auditory datasets are also available at the web portal. Simulating median nerve stimulation provides one of our simplest cases. This activity consists of contralateral primary somatosensory (SIcontra), contralateral secondary somatosensory (SIIcontra), and ipsilateral secondary somatosensory cortex activity (SIIipsi). In addition, an auditory dataset provides a simple example of initial synchronous, bilateral activity in auditory cortex. This set also includes asynchronous activation of the temporo-parietal junction and cingulate cortex (4 cortical sources). For additional details on these datasets please refer to Aine et al. (2012).

2.6 Preliminary Work on a Default Mode Network Dataset

Our newest and most preliminary simulation focuses on resting state data; that is, we have developed a simulated default mode network (DMN) based on what is typically found in the MEG/EEG and fMRI literature. For example we used a low alpha oscillation, and the approximate locations for simulated activity included prefrontal cortex (PFC)/medial prefrontal cortex, posterior cingulate cortex (PCC), and right and left anterior parietal lobes (Brookes et al. 2011; Allen et al. 2014). This first attempt exaggerates the probable size of some of the nodes for initial testing purposes, and may underestimate others. Four 20 mm diameter patches (approximately spherical) were located as shown in Fig. 6a within MRIVIEW.

Each was given a 10 Hz oscillation, with, at this time, no relative phase lag. Simulations with oscillation amplitudes of 20, 100, and 200nAm were created and combined with resting state data from the Neuromag 306 MEG system. The simulations were saved as both continuous files and averaged files, in both netCDF and FIF formats. The simulation with the 100nAm oscillations was then analyzed with three different methods, CSST and SWARM (from within Curry software) which have been discussed previously, and ICA. For the ICA analysis EEGlab (Delorme and Makeig 2004; http://sccn.ucsd.edu/eeglab/) was used to separate the data into 102 independent components (ICs), using only the Neuromag magnetometer data from simulations, due to current capabilities of the EEGlab software. Next, the 5 largest alpha band contributors were determined by the EEGlab software and combined, as shown in the output, Fig. 6b. This is a typical EEG/MEG DMN pattern, as expected (Hui et al. 2010; Brookes et al. 2011).

In addition, as seen in Fig. 6c, SWARM accurately reconstructs the DMN pattern, with some additional sources of activation. And CSST, with a 6 dipole fit, does a good job of accurately locating these distributed sources, although the anterior parietal lobe sources are skewed medially, possibly due to the influence of the large PCC source. SWARM and CSST analyses were conducted on averaged data. As mentioned previously, this simulation and analysis is preliminary.

3 Empirical Datasets

Empirical MEG/MRI data were acquired for 9 participants at MRN, Massachusetts General Hospital and University of Minnesota/Veterans Affairs in Minneapolis. Data from 5 of the participants are available on the MEG-SIM website. Data were acquired using the VSM MedTech 275, Elekta-Neuromag 306, 4-D Neuroimaging 3600 systems and 3 different sensory paradigms (visual, auditory and somatosensory) for each participant. Most participants had repeat testing conducted the following day, which are also available. General characteristics of the sensory studies were mentioned in Sect. 2.2 while detailed information is presented in Aine et al. (2012).

4 Discussion

One objective of the MEG-SIM portal is to offer developers of MEG methods an extensive testbed of realistic simulated and empirical data, established for the purpose of quantifying the strengths and limitations of each analysis method for the purposes of method standardization. This will aid in the refinement and further development of algorithms. Second, we are all aware that some analysis procedures are better-suited for certain types of studies while other analysis procedures are better-suited for other studies. This set of realistic simulated data provided at

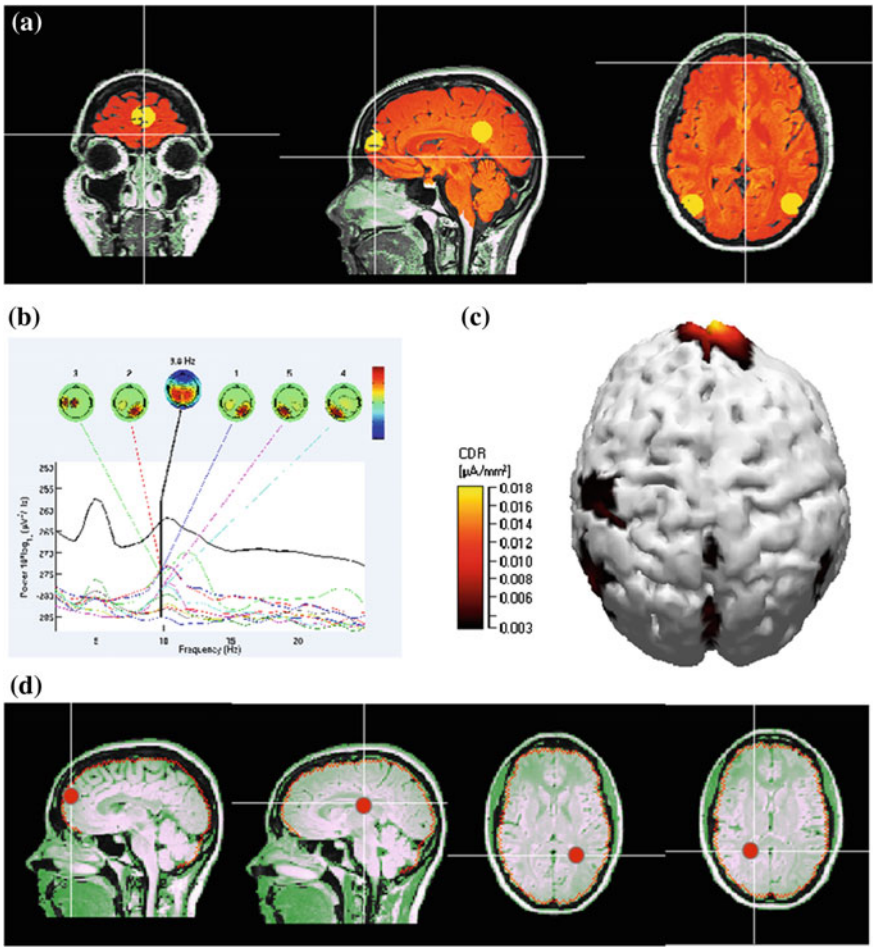

Fig. 6 **a** Distributed source locations created within MRIVIEW to simulate DMN activity. Each was given a 10 Hz oscillation, with a 100 nAm amplitude. **b** ICA analysis showing pattern of activity similar to that seem in the literature for DMN. **c** SWARM analysis using Curry software. **d** CSST analysis

the web portal (http://cobre.mrn.org/megsim/) includes sample datasets emulating sensory and working memory-related processes across visual, auditory, and somatosensory modalities. Users of MEG analysis procedures should be able to make informed decisions as to which analysis tools are best-suited for their research goals by working with these datasets.

The recent creation of continuous and single trial simulated datasets permit testing of a wider variety of MEG analysis tools. Construction of continuous data that mimic the differences between epochs of real data allow the use of analysis techniques such as ICA to be used individually or in conjunction with various

source modeling techniques to identify functional networks. These results can then be compared with traditional source analysis conducted on averaged data, both at the source and sensor levels. With the addition of oscillations to the simulated datasets the accuracy of functional connectivity measures between various brain areas using different analysis methods can also be investigated. Due to requests, system-specific formats have been added, with identical cortical areas and strengths of activation. For example, some of the simulated datasets described here are now available in a variety of file formats, including netCDF, Neuromag FIF, CTF DS and Curry (Compumedics, Neuroscan). Hopefully, the creation of these new datasets and formats, including novel continuous and DMN simulations, will foster algorithm performance comparisons and facilitate cross-site collaborations. We hope that these examples provide sufficient evidence of the flexibility of the simulations we created and we encourage others not only to use the simulations that are currently available but also to suggest additional simulations that may have widespread interest within the community.

Acknowledgment This work was funded by NIH grantsR21MH080141-02, 1P20 RR021938-04, and R01AG029495-04. It was also supported in part by the Department of Energy under Award Number DE-FG02-99ER62764 to the Mind Research Network. We thank M. Weisend, S. Ahlfors, M. Hämäläinen, J. Mosher, A. Leuthold, and A. Georgopoulos for their help when the initial partnership between institutions was established which permitted the acquisition of these data. We also wish to thank J. A. MacArthur, T. Wallace, K. Gilliam, C. H. Donahue, R. Montaño, J. E. Bryant, and A. Scott who aided in the construction of the earlier datasets. The content of this study is solely the responsibility of the authors and does not necessarily represent the official views of the National Institutes of Health.

References

Aine C, Huang M, Stephen J, Christner R (2000) Multistart algorithms for MEG empirical data analysis reliably characterize locations and time courses of multiple sources. NeuroImage 12:159–172

Aine CJ, Stephen JM, Christner R, Hudson D, Best E (2003) Task relevance enhances early transient and late slowwave activity of distributed cortical sources. J Comput Neurosci 15:203–221

Aine C, Adair J, Knoefel J, Hudson D, Qualls C, Kovacevic S et al (2005) Temporal dynamics of age-related differences in auditory incidental verbal learning. Cogn Brain Res 24:1–18

Aine CJ, Woodruff CC, Knoefel JE, Adair JC, Hudson D, Qualls C et al (2006) Aging: compensation or maturation? NeuroImage 32:1891–1904

Aine CJ, Bryant JE, Knoefel JE, Adair JC, Hart B, Donahue CH et al (2010) Different strategies for auditory word recognition in healthy versus normal aging. NeuroImage 49:3319–3330

Aine C, Sanfratello L, Ranken D, Best E, MacArthur J, Wallace T, Gilliam K, Donahue C, Montano R, Bryant J, Scott A, Stephen J (2012) MEG-SIM: a web portal for testing MEG analysis methods using realistic simulated and empirical data. Neuroinformatics 10:141–158

Allen EA, Damaraju E, Plis SM, Erhardt EB, Eichele T, Calhoun VD (2014) Tracking whole-brain connectivity dynamics in the resting state. Cereb Cortex 24:663–676

Baillet S, Mosher J, Leahy R (2001) Electromagnetic brain mapping. IEEE Signal Process Mag 18(6):14–30

Brookes MJ, Stevenson CM, Barnes GR, Hillebrand A, Simpson MI, Francis ST et al (2007) Beamformer reconstruction of correlated sources using a modified source model. NeuroImage 34:1454–1465

Brookes MJ, Woolrich M, Luckhoo H, Price D, Hale JR, Stevenson MC, Barnes GR, Smith SM, Morris PG (2011) Investigating the electrophysiological basis of resting state networks using magnetoencephalography. Proc. Nat Acad Sci USA 108(40):16783–16788

Brooks D, Macleod R (2005) Bayesian solutions and performance analysis in bioelectric inverse problems. IEEE Trans Biomed Eng 52(6):1009–1020

Dalal SS, Sekihara K, Nagarajan SS (2006) Modified beamformers for coherent source region suppression. IEEE Trans Biomed Eng 53:1357–1363

Dale AM, Liu AK, Fischl BR, Buckner RL, Belliveau JW, Lewine JD et al (2000) Dynamic statistical parametric mapping: combining fMRI and MEG for high-resolution imaging of cortical activity. Neuron 26:55–67

David O, Garnero L, Cosmelli D, Varela FJ (2002) Estimation of neural dynamics from MEG/EEG cortical current density maps: application to the reconstruction of large-scale cortical synchrony. IEEE BME 49:975–987

Delorme A, Makeig S (2004) EEGLAB: an open source toolbox for analysis of single-trial EEG dynamics. J Neurosci Methods 134:9–21

Diwakar M, Huang MX, Srinivasan R, Harrington DL, Robb A, Angeles A et al (2011) Dual-Core Beamformer for obtaining highly correlated neuronal networks in MEG. NeuroImage 54:253–263

de Pasquale F, Della Penna S, Snyder AZ, Lewis C, Mantini, D, Marzetti L, Belardinelli P, Ciancetta L, Pizzella V, Romani GL, Corbetta M (2010) Temporal dynamics of spontaneous MEG activity in brain networks. PNAS 107(13):6040–6045

Fuchs M, Wagner M, Kohler T, Wischmann HA (1999) Linear and nonlinear current density reconstructions. J Clin Neurophysiol 16:267–295

Golubic SJ, Susac A, Grilj V, Ranken D, Huonker R, Haueisen J et al (2011) Size matters: MEG empirical and simulation study on source localization of the earliest visual activity in the occipital cortex. Med Biol Eng Compu 49:545–554

Greenblatt RE, Ossadtchi A, Pflieger ME (2005) Local linear estimators for the bioelectromagnetic inverse problem. IEEE Trans Signal Process 53:3403–3412

Hämäläinen MS, Ilmoniemi RJ (1994) Interpreting magnetic fields of the brain: minimum norm estimates. Med Biol Eng Compu 32:35–42

Hämäläinen M, Hari R, Ilmoniemi R, Knuutila J, Lounasmaa O (1993) Magnetoencephalography? theory, instrumentation, and applications to noninvasive studies of the working human brain. Rev Mod Phys 65:413–497

Huang M, Aine CJ, Supek S, Best E, Ranken D, Flynn ER (1998) Multi-start downhill simplex method for spatio-temporal source localization in magnetoencephalography. Electroencephalogr Clin Neurophysiol 108:32–44

Huang MX, Dale AM, Song T, Halgren E, Harrington DL, Podgorny I et al (2006) Vector-based spatial-temporal minimum L1-norm solution for MEG. NeuroImage 31:1025–1037

Hui HB, Leahy RM (2006) Linearly constrained MEG beamformers for MVAR modeling of cortical interactions. In: 3rd IEEE International Symposium on Biomedical Imaging: Macro to Nano, pp 237–240

Hui HB, Pantazis D, Bressler SL, Leahy RM (2010) Identifying true cortical interactions in MEG using the nulling beamformer. NeuroImage 49:3161–3174

Ioannides AA, Bolton JP, Clarke CJS (1990) Continous probabilistic solutions to the biomagnetic inverse problem. Inverse Prob 6:523–542

Jun SC, George JS, Paré-Blagoev J, Plis SM, Ranken DM, Schmidt DM et al (2005) Spatiotemporal Bayesian inference dipole analysis for MEG neuroimaging data. NeuroImage 28:84–98

Kovacevic S, Qualls C, Adair J, Hudson D, Woodruff C, Knoefel J et al (2005) Age-related effects on superior temmporal gyrus activity during an oddball task. NeuroReport 16:1075–1079

Liljestrom M, Kujala J, Jensen O, Salmelin R (2005) Neuromagnetic localization of rhythmic activity in the human brain: a comparison of three methods. NeuroImage 25:734–745

Lin FH, Witzel T, Ahlfors SP, Stufflebeam SM, Belliveau JW, Hämäläinen MS (2006) Assessing and improving the spatial accuracy in MEG source localization by depth-weighted minimum-norm estimates. NeuroImage 31:160–171

Liu AK, Belliveau JW, Dale AM (1998) Spatiotemporal imaging of human brain activity using functional MRI constrained magnetoencephalography data: Monte Carlo simulations. Proc Natl Acad Sci USA 95:8945–8950

Mattout J, Phillips C, Penny WD, Rugg MD, Friston KJ (2006) MEG source localization under multiple constraints: an extended Bayesian framework. NeuroImage 30:753–767

Michel CM, Murray MM, Lantz G, Gonzalez S, Spinelli L, Grave de Peralta R (2004) EEG source imaging. Clin Neurophysiol 115:2195–2222

Moiseev A, Gaspar JM, Schneider JA, Herdman AT (2011) Application of multi-source minimum variance beamformers for reconstruction of correlated neural activity. NeuroImage 58:481–489

Mosher JC, Lewis PS, Leahy RM (1992) Multiple dipole modeling and localization from spatio-temporal MEG data. IEEE Trans Biomed Eng 39:541–557

Nelder J, Mead R (1965) A simplex method for function minimization. Comput J 7:308–313

Pascual-Marqui RD (2002) Standardized low-resolution brain electromagnetic tomography (sLORETA): technical details. Methods Find Exp Clin Pharmacol 24(Suppl D):5–12

Pascual-Marqui RD, Michel CM, Lehmann D (1994) Low resolution electromagnetic tomography: a new method for localizing electrical activity in the brain. Int J Psychophysiol 18:49–65

Pascual-Marqui RD, Lehmann D, Koenig T, Kochi K, Merlo MC, Hell D et al (1999) Low resolution brain electromagnetic tomography (LORETA) functional imaging in acute, neuroleptic-naive, first-episode, productive schizophrenia. Psychiatry Res 90:169–179

Portin K, Vanni S, Virsu V, Hari R (1999) Stronger occipital cortical activation to lower than upper visual field stimuli. Neuromagnetic recordings. Exp Brain Res 124:287–294

Ranken D, George JS (1993) MRIVIEW: an interactive computational tool for investigation of brain structure and function. In: Proceedings of the IEEE visualization '93. IEEE Computer Society Press, pp 324–331

Ranken D, Best E, Schmidt DM, George JS, Wood CC, Huang M (2002) MEG/EEG forward and inverse modeling using MRIVIEW. In Nowak H, Jaueisen J, Giebler F, Huonker R (eds) Proceedings of the 13th international conference on biomagnetism, pp 785–787

Ranken DM, Stephen JM, George JS (2004) MUSIC seeded multi-dipole MEG modeling using the Constrained Start Spatio-Temporal modeling procedure. Neurol Clin Neurophysiol 2004:80

Rovamo J, Virsu V (1979) An estimation and application of the human cortical magnification factor. Exp Brain Res 37:495–510

Schmidt DM, George JS, Wood CC (1999) Bayesian inference applied to the electromagnetic inverse problem. Hum Brain Mapp 7:195–212

Stephen JM, Aine CJ, Christner RF, Ranken D, Huang M, Best E (2002) Central versus peripheral visual field stimulation results in timing differences in dorsal stream sources as measured with MEG. Vision Res 42:3059–3074

Stephen JM, Aine CJ, Ranken D, Hudson D, Shih JJ (2003a) Multidipole analysis of simulated epileptic spikes withreal background activity. J Clin Neurophysiol 20:1–16

Stephen JM, Davis LE, Aine CJ, Ranken D, Herman M, Hudson D et al (2003b) Investigation of the normal proximal somatomotor system using magnetoencephalography. Clin Neurophysiol 114:1781–1792

Stephen JM, Ranken DM, Aine CJ, Weisend MP, Shih JJ (2005) Differentiability of simulated MEG hippocampal, medial temporal and neocortical temporal epileptic spike activity. J Clin Neurophysiol 22:388–401

Stephen JM, Ranken D, Best E, Adair J, Knoefel J, Kovacevic S et al (2006) Aging changes and gender differences in response to median nerve stimulation measured with MEG. Clin Neurophysiol 117:131–143

Stephen JM, Kodituwakku PW, Kodituwakku EL, Romero L, Peters AM, Sharadamma NM, Caprihan A, Coffman BA (2012) Delays in auditory processing identified in preschool children with FASD. Alcohol Clin Exp Res 36(10):1720–1727

Supek S, Aine CJ (1993) Simulation studies of multiple dipole neuromagnetic source localization: model order and limits of source resolution. IEEE Trans Biomed Eng 40:529–540

Supek S, Aine C (1997) Spatio-temporal modeling of neuromagnetic data: I. Multisource location versus timecourse estimation accuracy. Hum Brain Mapp 5:139–153

Susac A, Ilmoniemi RJ, Pihko E, Ranken D, Supek S (2010) Early cortical responses are sensitive to changes in face stimuli. Brain Res 1346:155–164

Susac A, Ilmoniemi RJ, Ranken D, Supek S (2011) Face activated neurodynamic cortical networks. Med Biol Eng Compu 49:531–543

Uutela K, Hämäläinen M, Somersalo E (1999) Visualization of magnetoencephalographic data using minimum current estimates. NeuroImage 10:173–180

Vanni S, Dojat M, Warnking J, Delon-Martin C, Segebarth C, Bullier J (2004) Timing of interactions across the visual field in the human cortex. NeuroImage 21:818–828

Vrba J, Robinson SE (2000) Linearly constrained minimum variance beamformers, synthetic aperturemagnetometry, andMUSIC in MEG applications. IEEE conference record of the 34th Asilomar conference on signals, systems and computers, vol 1, pp 313–317

Wagner M, Fuchs M, Kastner J (2004) Evaluation of sLORETA in the presence of noise and multiple sources. Brain Topogr 16:277–280

Wagner M, Fuchs M, Kastner J (2007) SWARM: sLORETAweighted accurate minimum-norm inverse solutions. Proceedings of the 15th international conference on biomagnetism. Vancouver, BC Canada, Elsevier ICS 1300

Wagner M, Fuchs M, Kastner J (2008) sLORETA, eLORETA, and SWARM in the presence of noise and multiple sources. In Kakigi R, Yokosawa K, Kuriki S (eds) Biomagnetism: interdisciplinary research and exploration. Hokkaido University Press, Tokyo, pp. 74–76

Wipf DP, Owen JP, Attias HT, Sekihara K, Nagarajan SS (2010) Robust Bayesian estimation of the location, orientation, and time course of multiple correlated neural sources using MEG. NeuroImage 49:641–655

Wischmann HA, Fuchs M, Wagner AD, Doessel O (1995) Current density imaging: A time series reconstruction implementing a "best fixed distributions" constraint. In: Baumgartner C, Deecke L, Stroink G, Williamson SJ (eds) Biomagnetism: Fundamental research and clinical applications. Ios Press, Amsterdam, pp 427–432

Analyzing MEG Data with Granger Causality: Promises and Pitfalls

Mingzhou Ding and Chao Wang

Abstract In this chapter we begin by introducing the basic idea of Granger causality and discussing its applications to local field potential data. We then proceed to comment on recent results of applying Granger causality to MEG data. Recognizing that Granger causality is frequently used to examine neural activity recorded during stimulus processing, we point out the adverse effects of the inevitable trial-to-trial variability of stimulus-evoked responses on Granger causality estimation. We end the chapter by discussing the future prospects of using Granger causality in basic and clinical neuroscience research.

Keywords Granger causality · MEG · Local field potential · Trial-to-trial variability · Stimulus-evoked responses

1 Introduction

Cognitive functions are achieved through cooperative neural computation. Multisensor recording and functional imaging afford us the opportunity to study brain mechanisms of cognition from a network perspective. Analytically, cross correlation and ordinary coherence have been the main statistics for assessing the functional connectivity among the monitored nodes of a neuronal network. In the case of MEG, these nodes could be defined either in sensor space or in source space. These measures have the drawback that they do not provide information on the direction of information flow. As neural interactions are mediated by synaptic transmissions which are inherently directional, and the hypotheses concerning the role of network operations in cognitive paradigms become more elaborate, being able to assess the

M. Ding (✉) · C. Wang
The J. Crayton Pruitt Family Department of Biomedical Engineering, University of Florida, Biomedical Sciences Building, 1275 Center Drive, Gainesville FL 32611, USA
e-mail: MDing@bme.ufl.edu

S. Supek and C. J. Aine (eds.), *Magnetoencephalography*,
DOI: 10.1007/978-3-642-33045-2_15,

direction of information flow between neuronal ensembles is becoming increasingly important to better understand the organization and function of complex neural networks. Granger causality has emerged in recent years as a statistically principled way to furnish this capability. The goal of this chapter is to introduce the basic idea of Granger causality and discuss its various applications to local field potential (LFP) and MEG data. Important insights generated by this method are highlighted and a potential issue pointed out.

2 Granger Causality: Basic Idea and Applications to LFP Data

The basic idea of Granger causality can be traced back to Wiener (1956). He proposed that, for two simultaneously measured time series, one series can be called causal to the other if we can better predict the second series by incorporating past knowledge of the first one. This concept was later adopted and formalized by Granger (1969) in the context of linear regression models of stochastic processes. Specifically, if the variance of the prediction error for the second time series at the present time is reduced by including past measurements from the first time series in the linear regression model, then the first time series can be said to have a causal (directional or driving) influence on the second time series. One repeats the process to address the question of driving in the opposite direction by reversing the roles of the two time series. From this definition, it is clear that the flow of time plays an essential role in allowing inferences to be made about directions of causal influences from time series data.

Mathematically, the above idea can be further illustrated as follows. Let the two time series be denoted as $x_1, x_2, \ldots, x_n, \ldots$ and $y_1, y_2, \ldots, y_n, \ldots$. Suppose that one wants to predict the value of x_n from the linear combination of m previous values of the x-series: $a_1 x_{n-1} + a_2 x_{n-2} + \cdots + a_m x_{n-m}$. Because the time series came from a stochastic process, x_n can be written as $x_n = a_1 x_{n-1} + a_2 x_{n-2} + \cdots + a_m x_{n-m} + \varepsilon_n$, where ε_n is the prediction error. This is nothing but a single variable autoregressive (AR) model. The variance of the error series ε_n is a gauge of the prediction accuracy. Now consider the prediction of x_n by including the previous values of both x-series and y-series, namely, $x_n = b_1 x_{n-1} + b_2 x_{n-2} + \cdots + b_m x_{n-m} + c_1 y_{n-1} + c_2 y_{n-2} + \cdots + c_m y_{n-m} + \eta_n$. The variance of the error series η_n is a gauge of the prediction accuracy of the new expanded predictor. If $\mathrm{var}(\eta_n)/\mathrm{var}(\varepsilon_n)$ is less than one in some suitable statistical sense, meaning that the prediction of x_n is improved by incorporating the past knowledge of the y-series, then we say the y-series has a causal influence on the x-series. The role of the x and y series can be reversed to address the influence from x to y.

A comprehensive statistical framework has been developed to estimate Granger causality from experimental data in both the time and frequency domain (Geweke 1982; Ding et al. 2006). A key question is whether Granger causality, a statistically

estimated measure of information flow, reflects physiological information flow mediated by action potential transmission. This question was considered by Bollimunta et al. (2008) in the context of alpha rhythm (8–12 Hz) generation. Alpha oscillations were discovered in the 1920s (Berger 1929). Prior to the 1970s, the thalamus was thought to be the generator of cortical alpha (Andersen and Andersson 1968). More recent studies using in vitro preparations have discovered the role of deep layer pyramidal cells in alpha pacemaking in cortical slice preparations (Silva et al. 1991). We took this finding as the "ground truth" for testing the validity of Granger causality and predicted that if multiple electrodes are placed simultaneously in different layers of the cortical column, because alpha activity measured at middle (layer 4) and superficial layers stems from synaptic transmission of alpha signals from deep layers, one should observe Granger causal influences from deep to middle and superficial layers in the alpha frequency band. Bollimunta et al. (2008) confirmed this prediction by analyzing laminar recordings from V2 and V4 in two awake-behaving monkeys and thereby established the basis for interpreting Granger causality in terms of neuronal information flow. See Fig. 1a.

The crucial role of directional information provided by Granger causality in the formulation of scientific hypotheses was considered in another series of studies in awake-behaving monkeys where local field potentials were recorded simultaneously from multiple sites in the sensorimotor system (Brovelli et al. 2004; Chen et al. 2006; Ding et al. 2006). From power spectral and coherence analysis, it was found that during the prestimulus period in which the monkey anticipated the stimulus onset by attending the computer monitor while holding steady a depressed mechanical lever, there are synchronized beta oscillations in three recording sites: primary motor (M1), primary somatosensory (S1), and posterior parietal area 7b. However, based on power and coherence alone, the functional significance of this oscillation network remains difficult to ascertain. The evaluation of Granger causality, yielding the pattern of causal interactions: (1) S → M1 (2) S1 → 7b, and (3) 7b → M1, shown in Fig. 1b, overcame the problem. The following three reasons led to the hypothesis that the beta oscillation network may exist to support the steady pressure maintenance of the depressed lever. First, steady pressure maintenance is akin to closed loop control and, as such, sensory feedback is expected to provide the input needed for cortical assessment of the current state of behavior. It is well known that the maintenance of sustained motor output is severely impaired when somatosensory input is lacking (Rothwell et al. 1982). This notion is consistent with our observation that S1 serves as the dominant source of causal influence to other areas in the network. Second, posterior parietal area 7b is known to be involved in the control of non-visually guided movement and, as a higher-order association area, it maintains representations pertaining to the current goals of the motor system (Rushworth et al. 1997). This would imply that area 7b receives sensory updates from area S1 and outputs correctional signals to the motor cortex (M1). This conceptualization is consistent with the causality pattern in Fig. 1b. Third, previous data from M1 have already implicated beta range oscillations as a neural correlate of isometric pressure

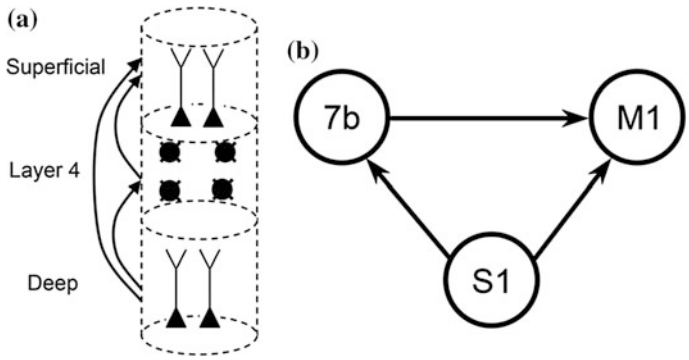

Fig. 1 **a** Granger causality graph for laminar alpha generation. **b** Granger causality graph for sensorimotor beta network

maintenance (Baker et al. 2003). By including S1 and 7b, the relation between M1 and the post-central areas is further clarified. Clearly, in the formulation of the above hypothesis, the vivid computational picture in Fig. 1b derived from Granger causality played a crucial role.

3 Applications to MEG Data

Granger causality is increasingly applied to MEG data. With very few exceptions the analysis is done in the source space. Three examples are considered here to illustrate the diversity of paradigms where this technique has been used to generate insights.

Moratti et al. (2011) analyzed MEG data recorded during the viewing of affective pictures with the goal to study the functional network organization associated with the generation of the magnetic homolog of the emotion-induced late positive potential (mLPP). The research question concerns whether the affective modulation of the mLPP is an automatic bottom-up response to motivationally salient stimuli or a response that reflects both bottom-up and top-down effects. To address this question requires the decomposition of neural interactions into their directional components. Reconstructing the source space time series of cortical activity by using the beamformer technique and computing time-domain Granger causality among predefined regions of interest (ROIs), they found that bidirectional influences between frontal and occipitoparietal cortex were stronger for emotional relative to neutral pictures, lending support to the hypothesis that mLPP reflects a combination of both bottom-up and top-down mechanisms.

Ploner et al. (2009) applied frequency-domain Granger causality to investigate functional integration among pain-related cortical regions. They conducted an MEG study using a simple reaction time paradigm in which painful and nonpainful stimuli were randomly applied to the right hand. Primary (S1) and secondary (S2)

somatosensory cortices as well as primary motor cortex (M1) were source localized from evoked responses by a spatiotemporal source model (Hämäläinen et al. 1993) and were selected as ROIs. Time-courses were computed using a linearly constrained minimum variance beamformer applied to the source locations. The Granger causality analysis revealed that there are causal influences from S1 to S2 during the processing of nonpainful stimuli but such influences are absent in the processing of painful stimuli. These results are taken to be in support of the proposition that there is a partially parallel organization of pain processing in the human brain.

Gow et al. (2008) applied Granger causality to simultaneously recorded MEG and EEG data to study whether the influence of lexical knowledge on speech perception takes the form of direct top-down influences on perceptual processing or it mainly involves feedforward convergence during decision making. In their analyses, the minimum-norm estimate (MNE) and the noise-normalized MNE called dynamic statistical parametric mapping (dSPM) (Dale et al. 2000) were applied to estimate the time-courses of activation across the cerebral cortex. MNE is an estimate of the actual activation time-courses whereas the dSPM provides a statistical measure that indicates regions where the estimated activity exceeds the estimated noise level. Therefore, dSPM was applied for identifying ROIs, but for analysis within and across ROIs, the MNE values were used. In their ROI identification, the 40 Hz gamma band phase synchrony was considered as a mechanism for binding neural populations into transient cell assemblies. Thus a network of ROIs was identified based on the 40 Hz phase locking values across the cortical surface to a reference region. The reference region, consisting primarily of the left posterior superior temporal gyrus (pSTG), was selected as the first area of increased cortical activity after stimulus onset. Within the identified network, the results of Granger causality analysis showed that the left supramarginal gyrus (SMG), known to be associated with wordform representation, influences phonetic processing in the left pSTG during a period of time associated with lexical processing. This finding provided evidence that lexical processes exert top-down influences on lower level phonetic perception.

4 Impact of Stimulus-Evoked Responses on Granger Causality Estimation

The LFP studies reviewed above mainly focus on ongoing neural activity in the absence of a transient sensory stimulus. The three MEG studies reviewed above, however, share a common feature in that they all focus on neural activity in the time period following the presentation of a transient sensory stimulus. Post-stimulus neural activity can be written as the superposition of stimulus-evoked responses, which vary from trial to trial in both amplitude and latency, and ongoing activity which is assumed to be zero-mean (Xu et al. 2009). To estimate

Granger causality from the ongoing activity a common approach is to remove the average stimulus-evoked response from single trial data. Past work has shown that this approach leaves traces of stimulus-evoked response in the ongoing activity which can adversely impact Granger causality estimation (Wang et al. 2008). Without being cognizant of such adverse effects Granger causality analysis can be misconstrued.

Granger causality analysis begins with the fitting of an autoregressive model to data (Ding et al. 2006). The common AR model formulation assumes that the input time series come from a zero-mean stationary stochastic process. To meet the zero-mean requirement one typically computes the average event-related potential (ERP)/event-related field (ERF) and removes it from single trial data. Inherent in this practice is the assumption that ERP/ERF is invariant across trials. It is now clear that this assumption is overly simplistic and trial-to-trial variability of ERP/ERF is substantial (Wang et al. 2008; Liu et al. 2012). This means that removing the average ERP/ERF from single trial data will leave traces of stimulus-evoked response in the residual, which, as the following conceptual model illustrates, can significantly impact Granger causality analysis. A more thorough analysis of this problem can be found in Wang et al. (2008).

Consider two recording channels where ERP/ERFs are represented by sinusoids in Fig. 2a, b. ERP/ERF 2 (channel 2) (Fig. 2b) is 20 ms behind ERP/ERF 1 (channel 1) (Fig. 2a). The amplitude of the evoked response varies from trial to trial and these variations are assumed to be correlated between the two recording sites. Physiologically, one may view ERP/ERF 1 as arising from a primary sensory area while ERP/ERF 2 from an association area. To calculate Granger causality between the two channels, we follow the traditional approach by first obtaining the average ERP/ERF and then subtracting the average from each trial to produce the residual data (Fig. 2c, d), which are then subjected to a sliding window analysis. For the 50 ms window between the two solid lines, the strong activity in channel 1 temporally precedes that in channel 2. Since these activities are correlated, by the definition of Granger causality, we will see a causal influence from channel 1 to channel 2. As the window is moved between the dashed lines, the opposite occurs. Specifically, the temporal precedence of strong activity in channel 2 over that in channel 1 will result in a causal influence from channel 2 to channel 1. In general, as the analysis window is moved through the entire trial, one may observe multiple episodes of causal influence reversals, depending on the morphology of the ERP/ERFs. Such intricate temporal patterns of Granger causality modulations are clearly artifactual and are the result of three factors. First, the event-related responses from two different channels are of a similar shape and have different temporal onsets. Second, the two event-related responses have correlated trial-to-trial variability. Third, the time-frequency analysis of Granger causality is carried out by employing a small moving window. It is worth noting that an analysis with a long time window extending over the entire evoked response will result in a predominantly unidirectional driving from channel 1 to channel 2.

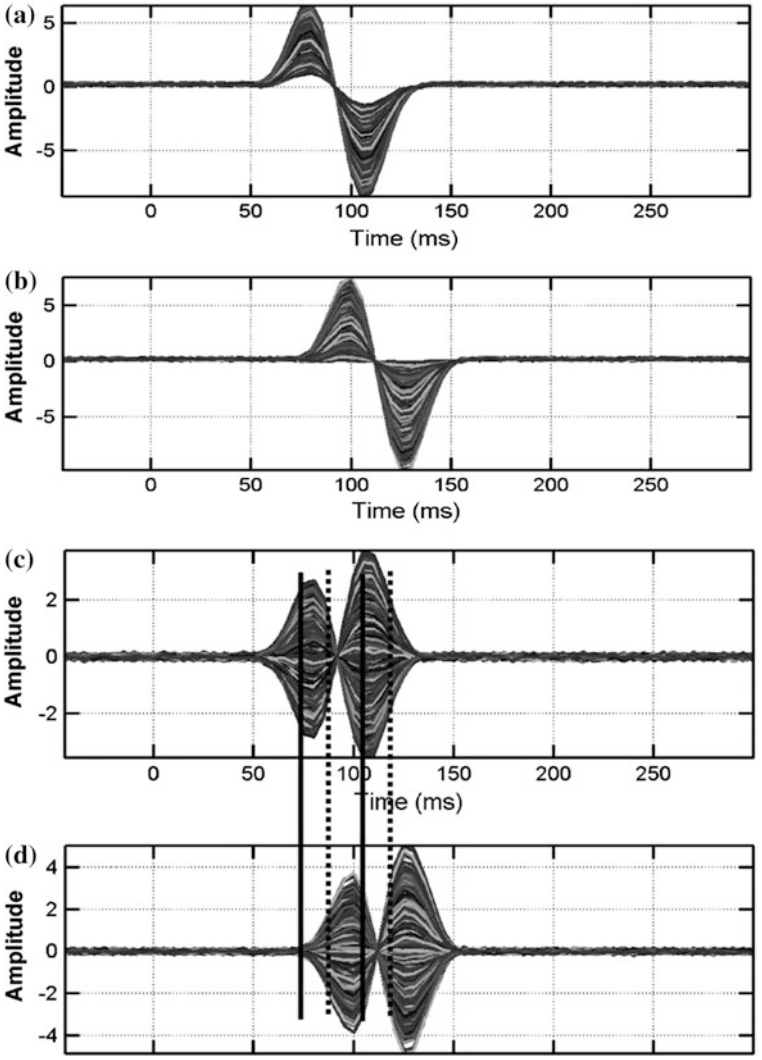

Fig. 2 A conceptual model illustrating the impact of trial-to-trial variability of stimulus-evoked response on Granger causality estimation. **a** and **b** 500 trials of simulated data from channel 1 and 2, respectively. **c** and **d** residuals after subtracting the ensemble averages. Two analysis windows are delineated by the interval between the two *solid lines* and that between the two *dashed lines*. Vertical axis: arbitrary unit. From Wang et al. (2008)

5 Concluding Remarks

Multivariate neural recordings promise unparalleled insights into how different areas of the brain work together to achieve thought and behavior, and how such coordinated brain activity breaks down in disease. While the accumulation of data

continues at an astonishing rate, how to effectively analyze these data to extract information about the workings of the brain remains a key challenge. Work over the past decade has established the importance of Granger causality in dissecting the directional interaction patterns in neuronal networks. As a tool for exploratory analysis, Granger causality is shown to be able to generate physiologically meaningful hypotheses, which can then be tested with further analysis and experimentation (Brovelli et al. 2004; Ding et al. 2006), while as a tool for confirmatory analysis, Granger causality can be used to test physiological hypotheses that are formulated according to consideration and knowledge existing outside the Granger causality analysis framework (Bollimunta et al. 2008).

Despite these promises there are also potential pitfalls associated with the application of Granger causality to MEG/EEG data. Discussions above pointed out the negative impact of the trial-to-trial variability of stimulus-evoked response on Granger causality estimation (Wang et al. 2008). One possible remedy for this problem is to remove evoked responses on a single trial basis (Wang and Ding 2011). Another problem, which is more of a concern in electrophysiological recordings such as LFP, EEG and ECOG, has to do with the negative impact of common reference and volume conduction on connectivity measures. The possible remedy in this case is to perform the analysis in source space or after local referencing such as bipolar derivation to remove or attenuate the effect of common reference and volume conduction (Bollimunta et al. 2009).

These concerns notwithstanding, evidence so far suggests that Granger causality has a useful role to play in both basic and clinical neuroscience, complementing other methods. For many problems the framework for initiating and interpreting a Granger causality analysis is already established by the knowledge accumulated by years of research. For example, the neural substrate of a given behavior is often encapsulated in a network flow diagram with arrows connecting different structures emphasizing their respective roles and their interrelations with one another. An example derived from the literature on sensorimotor control is shown in Fig. 3a (Gazzaniga et al. 2002). Likewise, many neurological and psychiatric disorders involve abnormal cortical and subcortical circuit dynamics. The network mechanisms of these disorders are also expressed in diagrams similar to Fig. 3a. In the case of drug addiction, it has been shown that the nucleus accumbens, amygdala, and hippocampus comprise the mesolimbic system that is important in the reinforcing effects of drugs, whereas the prefrontal cortex, orbitofrontal cortex, and anterior cingulate comprise the mesocortical circuit known to mediate the conscious experience of drug intoxication. These brain areas are hypothesized to interact as illustrated in Fig. 3b (Goldstein and Volkow 2002). These diagrams are compiled from many studies using diverse techniques and could be used to formulate initial hypotheses for a Granger causality analysis and constrain the subsequent interpretation.

As the contributions in this volume demonstrates, MEG, offering superior temporal resolution over fMRI and superior spatial resolution over EEG, can be used to address many basic and clinical neuroscience questions. Because Granger causality can be applied to either sensor or source space MEG has a significant role

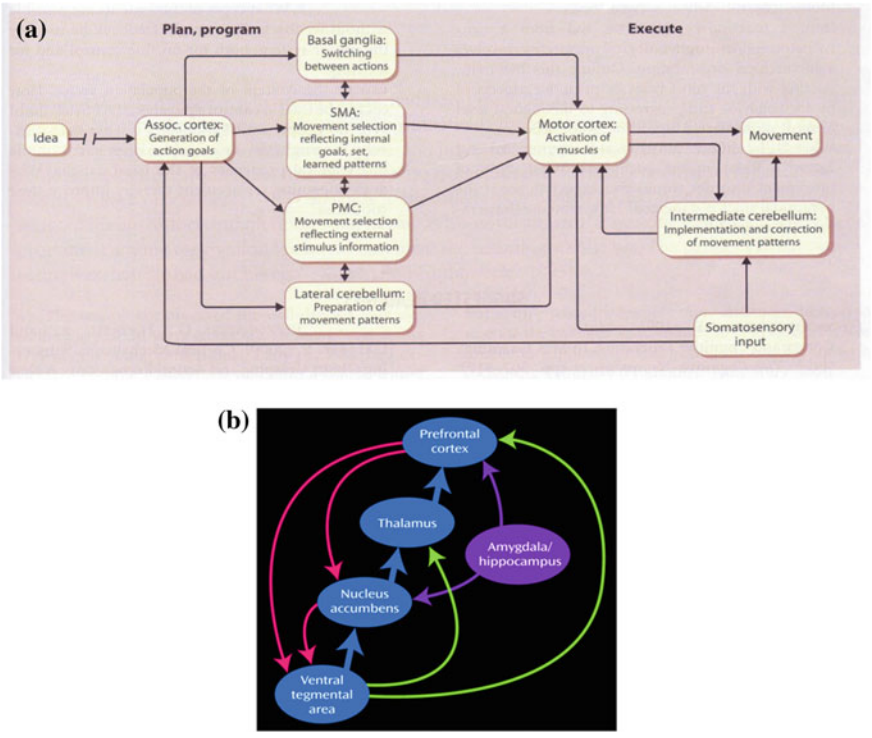

Fig. 3 **a** Diagram showing the functional relations among different brain areas involved in sensorimotor integration. From Gazzaniga et al. (2002). **b** Diagram showing the interactions of the Mesocortical and Mesolimbic circuits in drug addiction. From Goldstein and Volkow (2002)

to play in quantifying the strength of interaction between different brain areas in normal and diseased circuits. It is expected that, with proper care and precaution, principled applications of Granger causality to MEG data will continue to grow, generating insights into the collective computation in the brain not possible with other methods.

References

Andersen P, Andersson SA (1968) Physiological basis of the Alpha Rhythm. Appleton-Century-Crofts, New York

Baker SN, Pinches EM, Lemon RN (2003) Synchronization in monkey motor cortex during a precision grip task. II. Effect of oscillatory activity on corticospinal output. J Neurophysiol 89(4):1941–1953

Berger H (1929) Über das Elektroencephalogramm des Menschen (On the electroencephalogram of man). Arch Psychiatr Nervenkr 87:527–570

Bollimunta A, Chen Y, Schroeder CE, Ding M (2008) Neuronal mechanisms of cortical alpha oscillations in awake-behaving macaques. J Neurosci 28(40):9976–9988

Bollimunta A, Chen Y, Schroeder CE, Ding M (2009) Characterizing oscillatory cortical networks with Granger causality. In: Rubin J, Josic K, Matias M, Romo R (eds) Coherent behavior in neuronal networks. Springer, New York, pp 169–189

Brovelli A, Ding M, Ledberg A, Chen Y, Nakamura R, Bressler SL (2004) Beta oscillations in a large-scale sensorimotor cortical network: directional influences revealed by Granger causality. Proc Natl Acad Sci USA 101(26):9849–9854

Chen Y, Bressler SL, Ding M (2006) Frequency decomposition of conditional Granger causality and application to multivariate neural field potential data. J Neurosci Methods 150(2):228–237

Dale AM, Liu AK, Fischl BR, Buckner RL, Belliveau JW, Lewine JD, Halgren E (2000) Dynamic statistical parametric mapping: combining fMRI and MEG for high-resolution imaging of cortical activity. Neuron 26(1):55–67

Ding M, Chen Y, Bressler SL (2006) Granger causality: basic theory and application to neuroscience. In: Winterhalder M, Schelter B, Timmer J (eds) Handbook of time series analysis. WILEY, Berlin, pp 437–460

Gazzaniga MS, Ivry RB, Mangun GR (2002) Cognitive neuroscience. Norton and Company, New York

Geweke J (1982) Measurement of linear-dependence and feedback between multiple time-series. J Am Stat Assoc 77(378):304–313

Goldstein RZ, Volkow ND (2002) Drug addiction and its underlying neurobiological basis: neuroimaging evidence for the involvement of the frontal cortex. Am J Psychiatry 159(10):1642–1652

Gow DW Jr, Segawa JA, Ahlfors SP, Lin FH (2008) Lexical influences on speech perception: a Granger causality analysis of MEG and EEG source estimates. NeuroImage 43(3):614–623

Granger CWJ (1969) Investigating causal relations by econometric models and cross-spectral methods. Econometrica 37(3):424–438

Hämäläinen M, Hari R, Ilmoniemi RJ, Knuutila J, Lounasmaa OV (1993) Magnetoencephalography—theory, instrumentation, and applications to noninvasive studies of the working human brain. Rev Mod Phys 65(2):413–497

Liu Y, Huang H, McGinnis M, Keil A, Ding M (2012) Neural substrate of the late positive potential in emotional processing. J Neurosci 32(42):14563–14572

Moratti S, Saugar C, Strange BA (2011) Prefrontal-Occipitoparietal Coupling Underlies Late Latency Human Neuronal Responses to Emotion. J Neurosci 31(47):17278–17286

Ploner M, Schoffelen JM, Schnitzler A, Gross J (2009) Functional integration within the human pain system as revealed by Granger causality. Hum Brain Mapp 30(12):4025–4032

Rothwell JC, Traub MM, Day BL, Obeso JA, Thomas PK, Marsden CD (1982) Manual motor-performance in a deafferented man. Brain 105(3):515–542

Rushworth MFS, Nixon PD, Passingham RE (1997) Parietal cortex and movement 1. Movement selection and reaching. Exp Brain Res 117(2):292–310

Silva LR, Amitai Y, Connors BW (1991) Intrinsic oscillations of neocortex generated by layer-5 pyramidal neurons. Science 251(4992):432–435

Wang X, Chen Y, Ding M (2008) Estimating Granger causality after stimulus onset: a cautionary note. NeuroImage 41(3):767–776

Wang X, Ding M (2011) Relation between P300 and event-related theta-band synchronization: a single-trial analysis. Clin Neurophysiol 122(5):916–924

Wiener N (1956) The theory of prediction. In: Beckenbach EF (ed) Modern mathematics for engineers, Chap 8. McGraw-Hill, New York

Xu L, Stoica P, Li J, Bressler SL, Shao X, Ding M (2009) ASEO: a method for the simultaneous estimation of single-trial event-related potentials and ongoing brain activities. IEEE Trans Biomed Eng 56:111–121

Part III
Functional Connectivity and Oscillatory Activity

An Introduction to MEG Connectivity Measurements

Matthew J. Brookes, Mark W. Woolrich and Darren Price

Abstract Researchers are beginning to appreciate the brain as more than a mere collection of loosely connected, highly specialised components. While there is clear specialisation among regions of the cortex, the true power of the brain appears to arise from the ability of those regions to work together across a range of spatial scales as a richly interconnected and complex network. On all levels, the study of brain connectivity seeks to understand how different regions of the cortex communicate, what the emerging networks signify functionally, and why these are important for normal behaviour. The use of MEG in this endeavour is an attempt to understand these processes on the broad, interregional scale, and in that respect MEG is an ideal tool. It has a good deal of spatial resolution, enough to distinguish between brain areas $\sim$1 cm apart, and exquisite temporal resolution, enough to record even the fastest electrical oscillations the brain can generate. This chapter begins with a brief overview of the history of electrophysiological measures and their application to the study of brain connectivity. We then describe some of the core theory underlying the measurement of magnetic fields generated by the brain and practical considerations of measuring correlated activity with MEG. Some notable applications of MEG to the study of brain networks will then be described and a comparison will be made between MEG to other methods such as ECoG. The chapter will also explore some of the principal mathematical techniques used by researchers to probe different aspects of connectivity ranging from simple correlational approaches to more involved concepts such as multivariate autoregressive models (MAR). Finally, we will discuss limitations of using MEG to study connectivity and also give some insight into the exciting prospects the future might hold for MEG connectivity research.

M. J. Brookes (✉) · D. Price
Sir Peter Mansfield Magnetic Resonance Centre, School of Physics,
University of Nottingham, Nottingham, UK
e-mail: Matthew.brookes@nottingham.ac.uk

M. W. Woolrich
Oxford Centre for Human Brain Activity, University of Oxford, Oxford, UK

S. Supek and C. J. Aine (eds.), *Magnetoencephalography*,
DOI: 10.1007/978-3-642-33045-2_16,

1 Introduction

In classical studies of brain function, particularly the study of cytoarchitectonics and neuropsychology, the brain is divided into distinct specialised cortical regions that have some specific functional role in information processing or behavioural control. For example, early studies by Paul Broca in 1861 (Broca 2011) identified a region of the frontal cortex (now known as Broca's area and comprising the pars opercularis and pars triangularis) related to language. There now exists a wealth of literature for almost any area of the cortex that implies some specialisation, some being narrow in scope (e.g. the fusiform face area) and others spanning broad functional domains such as planning and working memory (e.g. prefrontal cortex). This research lends support to hypotheses that information processing subsystems can be related to clear structural and functional modularisation of the cortex. However, whilst it remains clear that there is a degree of specialisation in cerebral architecture, healthy brain function must necessarily rely on communication between those specialist areas. Advances in neuroimaging are beginning to reveal a complex picture of the brain as a dynamic interconnected network, capable of flexible adaptation to the immediate environment (Bressler and Kelso 2001; Engel et al. 2001; Fries 2005; Schnitzler and Gross 2005; Singer 1999; Varela et al. 2001). Recent years have seen rapid progress in this area through the study of network connectivity and MEG has a large part to play in this developing research area. In this chapter we review some of the key concepts and methods related to MEG measurement of network connectivity.

1.1 Types of Connectivity Measurements

On the microscopic scale, investigators are interested in the properties of neurons that allow the binding of neuronal cell assemblies, thought to be important for information processing and remote coordination of cortical regions. This has led to a broad research area that includes animal studies and computational modelling (Rodriguez et al. 1999; Roelfsema et al. 1997; Roopun et al. 2008; Singer and Gray 1995; Whittington et al. 1995). At the systems level (or macroscopic scale), investigators are interested in properties of cortical regions that allow coherent functional systems to form, capable of producing complex behaviour and cognition. This research has wide reaching implications for both normal and abnormal brain function; e.g. neuroimaging research implies that illnesses such as schizophrenia are characterised by disturbances in the recruitment of brain regions, leading to a disconnection hypothesis (Friston 1999; Phillips and Silverstein 2003). Whilst parallels can be drawn between the microscopic and macroscopic scales (Scholvinck et al. 2012), this chapter is concerned with the measurement of connectivity at a macroscopic level.

Using brain imaging techniques such as MRI, fMRI, and MEG, there are three main types of connectivity analysis typically employed: structural, functional and effective. ***Structural connectivity*** can have many definitions depending on the spatial scale at which it is studied. However, at the macroscopic scale it typically involves mapping physical connections between brain regions. A popular methodology to achieve this is diffusion weighted MRI although other methods are now becoming available (Wharton and Bowtell 2012); these techniques allow for mapping of white matter tracts with millimetre precision (Koch et al. 2002; Sakkalis 2011). This approach can give us useful information about the changing structure of the brain's connections during development or illness, but does not tell us much about functional dynamics within and between connected regions. This is the purpose of functional and effective connectivity. **Functional connectivity** (FC) is typically defined by the measurement of a statistical interdependence between functional brain signals measured at two or more spatially separate brain regions. This is distinct from **effective connectivity** (EC) (Friston et al. 2003; Friston et al. 2011), which typically comprises an estimate of directed influence between brain regions (i.e. implying a directionality of information flow) inferred using a generative model. The remainder of this chapter will focus mainly on MEG methodology for functional connectivity, although we will also consider some effective connectivity approaches as well.

1.2 Ways to Measure Functional Connectivity

Functional magnetic resonance imaging (fMRI) has become a popular technique by which to assess functional connectivity following the seminal work of Biswal et al. (1995), who showed temporal correlation between blood oxygen level dependent (BOLD) signals, measured between the left and right motor cortices, in the absence of a task. This study was the first to demonstrate "resting state" (i.e. task independent) long range connectivity in fMRI and this prompted a surge of research in this area. Further use of BOLD temporal correlation, as well as more sophisticated techniques such as independent component analysis (ICA) (Beckmann et al. 2005; Fox et al. 2006; Smith et al. 2009), have led to the somewhat surprising discovery that the resting brain contains a relatively small number of large scale distributed networks, each associated with a specific function or behaviour; for example some networks are associated with sensory action (e.g. visual or somato-motor networks) and others attention or cognition (e.g. the dorsal attention or default mode network). These networks have been shown to be exceptionally robust across subjects and sessions. Furthermore, they are observable during a wide variety of tasks or in the resting state. The field of functional connectivity is, at the time of writing, one of the most rapidly expanding fields in neuroimaging with a fourfold increase in the number of papers published in the last 4 years. fMRI benefits from excellent spatial resolution and reasonably high signal to noise (SNR) (especially at high field; Hale et al. 2010) allowing spatial characterisation of networks at the millimetre scale. However, fMRI

suffers from poor temporal resolution due to the dependence of the BOLD signal on the slow (5–8 s time scale) haemodynamic response. The BOLD response is also indirect, mediated by a poorly understood and convoluted mix of cerebral blood flow, cerebral blood volume, and the cerebral metabolic rate of oxygen uptake. Furthermore, spurious correlations have been identified and attributed to respiratory artefacts, heart rate or vascular organisation (Birn et al. 2006, 2008). In short fMRI network observations can be confounded by haemodynamics; they preclude investigation of the temporal dynamics of functional connectivity, and cannot straightforwardly assess the electrophysiological basis for functional connectivity.

MEG and EEG provide us with excellent tools for studying the electrophysiological signals arising from neural activity. Both have been used extensively to measure functional connectivity (Gow et al. 2008; Gross et al. 2001; Ioannides et al. 2000; Jerbi et al. 2007; Nolte et al. 2004, 2008; Schlögl and Supp 2006; Schoffelen and Gross 2009; Tass et al. 1998) and, as we shall see, there now exists a multitude of different methodologies capable of measuring functional connectivity in MEG or EEG data. A number of studies measure statistical interdependencies between MEG signals at the sensor level; however, scalp based measurements in EEG and MEG are subject to volume conduction or field spread between channels (Schoffelen and Gross 2009) and this has led to development of several techniques designed to probe electrical activity in brain space via source localisation. MEG is significantly advantageous over EEG since magnetic fields are not distorted by the inhomogeneous conductivity profile of the head; this adversely affects the electric field measured in EEG by distorting spatially the electrical potentials measured at the scalp, thus limiting spatial resolution. MEG, therefore, exhibits improved spatial specificity compared to EEG and source localisation techniques such as minimum norm (Hämäläinen and Ilmoniemi 1994), beamforming (Robinson and Vrba 1998), and more recently Bayesian algorithms such as Champagne (Owen et al. 2012) and multiple sparse priors (Friston et al. 2008), facilitate spatial resolution on the millimetre scale. Its exquisite temporal resolution, its good spatial resolution, and its ability to directly assess electrical activity in neural cell assemblies make MEG one of the most attractive techniques for non-invasive measurement of functional connectivity.

1.3 Neural Oscillations

MEG and EEG signals, in the resting and task positive states, are dominated by oscillations over a wide range of frequencies (e.g. 0 to $\sim$1,000 Hz). These neural "oscillations", induced by rhythmic electrical activity in cell assemblies (i.e. clusters of neurons), have been studied non-invasively in humans since Hans Berger (Berger 1929) recorded the 10 Hz alpha ($\sim$8–13 Hz) rhythm using EEG in the 1920s. Modern research into neural oscillations seeks to understand their functional role in the brain and MEG, EEG, and invasive electrocorticography (ECoG) studies in humans and animals show that one typically observes

modulation of the envelope of oscillations across a wide variety of frequency bands in response to stimulation. For example, a visual grating induces changes in alpha, beta (13–30 Hz) and gamma (30–200 Hz) band oscillations. Furthermore, the frequency of induced gamma oscillations has been related to levels of the main inhibitory neurotransmitter, gamma-aminobutyric acid (GABA), in occipital cortex (Muthukumaraswamy et al. 2009). Beta-band oscillations in the human motor cortex are modulated by movement; an effect that has also been related to concentrations of GABA (Gaetz et al. 2011). Such demonstrations show clearly that oscillatory phenomena are mediated by neurochemistry. There is a wealth of computational modelling (Kopell et al. 2000; Kopell et al. 2010) and animal research showing that oscillations have a functional role in the brain, possibly facilitating information transfer via short range and long range synchronisation. One hypothesis is that the efficacy of communication is enhanced via temporal synchronisation (Gray et al. 1989; von Stein et al. 2000; Womelsdorf et al. 2007). Early in vivo studies of the cat brain have shown that inter and intra-regional synchronisation of neuronal firing serves a crucial role in the perception of visual stimuli (Gray et al. 1989). Other researchers suggest that oscillations are a means by which groups of neurons improve the efficacy of information transfer between networks (Kopell et al. 2010; Roopun et al. 2008). There is now emerging literature suggesting that oscillations play a key role in functional connectivity and that via measurement of synchronisation between distant brain regions we can begin to infer the electrophysiological manifestations of functional integration.

In the remainder of this chapter we introduce key concepts that facilitate measurement of functional connectivity, as inferred by neural oscillatory processes, measured using MEG. In Sect. 2 we discuss pre-processing methodology, specifically the procedures required for source space measurement. In Sect. 3 we discuss a number of disparate techniques capable of assessing functional connectivity in brain space and also possible strategies for reducing spurious connectivity introduced as a result of the ill posed inverse problem. In Sect. 4 we introduce some principal findings of current MEG functional connectivity studies, and finally in Sect. 5, we discuss future directions for this important research field.

2 Pre-processing Methodology for Connectivity Measurement in MEG

2.1 Sensor Space Measurements: Volume Conduction and Field Spread

The physics underlying MEG/EEG measurements means that multiple scalp based detectors receive signals from a single source in the brain; the deeper the current source, the more sensors affected (see Fig. 1a). In EEG this is known as volume conduction and is confounded by the low (and inhomogeneous) conductivity of the

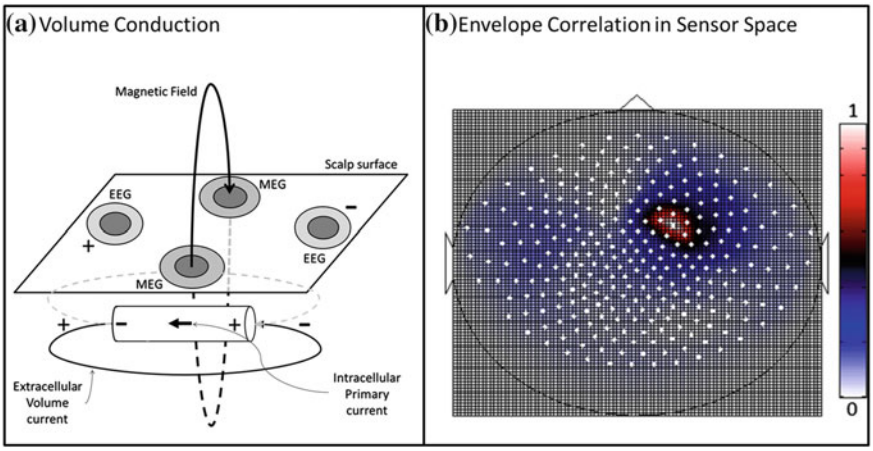

Fig. 1 **a** Schematic showing the physical mechanisms of volume conduction for EEG and MEG. **b** Sensor space representation of *left* and *right* motor cortex envelope correlation. Seed sensor selected over *right* motor cortex

skull which means that the electric field measured at the scalp is spatially broadened and distorted. In MEG the analogous effect is termed field spread and is governed by the Biot-Savart law. As stated above, field spread in MEG is less confounded than it's EEG counterpart since magnetic fields pass relatively undistorted through the skull and it is this fact (coupled with the increased number of sensors) that makes MEG advantageous over EEG in terms of spatial resolution. However, despite this advantage, field spread still means that two spatially separate current sources in the brain can affect the same MEG sensor. This in turn means that in practice, sensor measurements are complex mixtures of many cortical sources making sensor based assessment of long range functional connectivity difficult to interpret. This is highlighted in Fig. 1b where resting state temporal correlation between the amplitude envelopes of beta band oscillations in the left and right sensorimotor regions is represented in sensor space. A 'seed' sensor has been chosen over the right motor area and the result shows temporal correlation between the beta envelope at the seed sensor, and all other sensor locations across the scalp. Note the diffuse pattern of sensors exhibiting correlation with the seed and that, whilst a degree of inter-hemispheric correlation is observed, little spatial information is gained.

Sensor space measurement of connectivity is further complicated by interference measured at multiple sensors. MEG is susceptible to many sources of interference including external environmental noise sources such as computers or 50/60 Hz mains frequency interference as well as biological interference from, for example, the heart or muscles. If such interference sources impact on multiple MEG sensors, then this is likely to generate a spurious increase in sensor space connectivity values. An example (Brookes et al. 2011a) of this is given in Fig. 2: Fig. 2a, shows the measured electrocardiogram (ECG) from a single subject

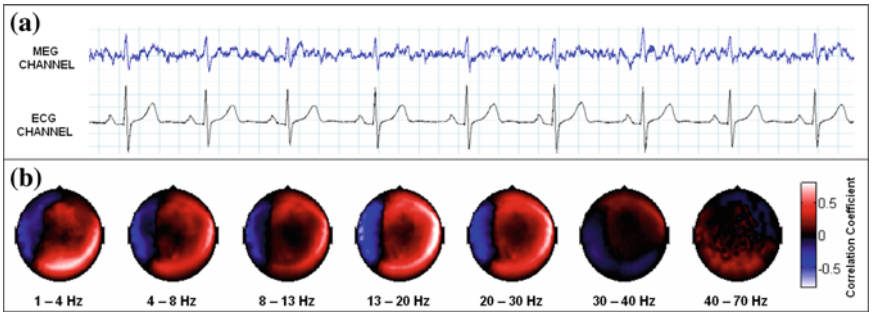

Fig. 2 Cardiac interference in sensor space. **a** The measured ECG and the magnetic field from a single MEG sensor. **b** The sensor space topography of cardiac interference plotted for each frequency band of interest adapted from Brookes et al. (2011a)

plotted alongside the MEG signal from a single sensor; Fig. 2b shows the spatial topography of Pearson correlation between the frequency filtered ECG and the frequency filtered sensor space MEG signals. Note not only the large (>0.5) correlation between MEG and ECG measurements, but also that the cardiac interference affects a large number of MEG sensors and unless adequately dealt with this could lead to spurious connectivity measurement, particularly when using sensor space measurement.

2.2 Projection to Brain Space and Source Leakage

The most useful mechanism to limit confounds associated with field spread is source space projection (Schoffelen and Gross 2009); this means reconstructing timecourses of electrical activity at a set of locations (voxels) in brain space via projection of the MEG/EEG field measurements. The spatial accuracy of such projections is limited since the reconstruction problem (the inverse problem) is mathematically ill-posed; field cancellation means that a single field pattern could result from an infinite number of different current density distributions and so no unique solution exists. However, a rich literature on source space reconstruction shows that, using specific assumption sets, reconstruction is possible with reasonable accuracy (5–8 mm) (Brookes et al. 2010). Figure 3 shows the principal advantage of applying source space projection to MEG data. The left hand panel shows inter-hemispheric functional connectivity measured in sensor space (equivalent to that shown in Fig. 1b) whilst the right hand panel shows inter-hemispheric connectivity, measured using the same data, in source space. Here projection from sensor to source space has been achieved via application of a beamformer spatial filtering approach (Gross et al. 2001; Robinson and Vrba 1998; Sekihara et al. 2006, 2001; van Veen et al. 1997) and the image shows functional connectivity, measured using correlation between band limited power envelopes

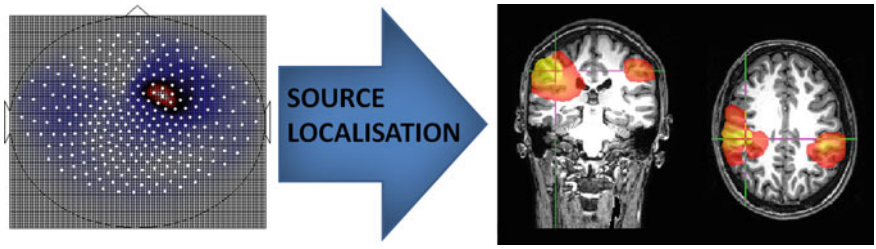

Fig. 3 The effect of projecting MEG data from sensor space to source space of functional connectivity measurement

(Brookes et al. 2011a), between a seed voxel (at the cross hairs) and all other locations in the brain. Note that unlike its sensor space equivalent, source space connectivity measurement facilitates direct interpretation of the image with respect to anatomy. In this example, functional connectivity in the resting state between the left and right sensorimotor areas is shown.

In addition to the advantages summarised by Fig. 3, source space projection offers a second, less obvious advantage over sensor space measurement, specifically a marked improvement in signal to noise ratio. In projecting data from sensor to source space, an estimate of electrical source strength $\hat{Q}_{\psi}(t)$, is made at time t and at a predetermined location and orientation in the brain ($\boldsymbol{\psi}$) using a weighted sum of MEG sensor measurements:

$$\hat{Q}_{\psi}(t) = \mathbf{W}_{\psi}^{T}\mathbf{m}(t) \tag{1}$$

Here, $\boldsymbol{m}(t)$ is a ($N_{sens} \times 1$) vector of magnetic field measurements made at time t, and $\boldsymbol{W}_{\psi}$ is a ($N_{sens} \times 1$) vector of weighting parameters tuned to a specific source space location and current orientation (N_{sens} represents the number of MEG sensors). Superscript T indicates a matrix transpose. Mathematically speaking, most of the commonly used MEG inverse solutions can be formulated in this way, and importantly the weighting parameters can be tuned not only to maintain signals originating at $\boldsymbol{\psi}$, but also to suppress any unwanted interference signals. A good example of such an algorithm is beamforming (Gross et al. 2001; Robinson and Vrba 1998; Sekihara et al. 2006, 2001; van Veen et al. 1997), in which the weighting parameters ($\mathbf{W}_{\psi}$) are derived based on power minimisation: the overall power in $\hat{Q}_{\psi}(t)$ is minimised with a linear constraint that power originating from location/orientation $\boldsymbol{\psi}$ remains. Mathematically:

$$\min_{\mathbf{W}_{\psi}}\left[\varepsilon\left(\hat{Q}_{\psi}^{2}\right)\right] \quad \textit{subject to} \quad \mathbf{W}_{\psi}^{T}\mathbf{L}_{\psi} = 1 \tag{2}$$

where $\mathbf{L}_{\psi}$ is the lead field vector (containing the magnetic fields that would be measured at each of the MEG sensors in response to a dipole source of unit amplitude with location and orientation $\boldsymbol{\psi}$). Note that the minimisation term

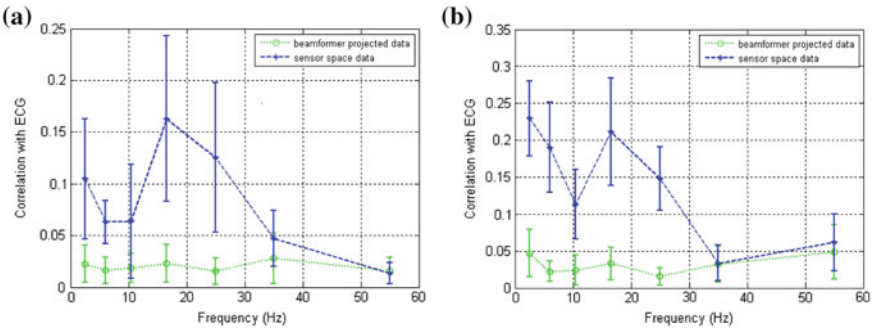

Fig. 4 **a** Correlation between MEG and ECG plotted as a function of frequency; the *blue line* shows correlation with sensors most affected by a source in *left* primary motor cortex; the *green line* shows correlation with a beamformer reconstructed timecourse for the same source in *left* motor cortex. **b** Equivalent to (**a**) but shown for the *right* motor cortex. Notice the significant drop in ECG correlation with application of the spatial filter adapted from Brookes et al. (2011a)

ensures that any signal variance not originating from ψ is minimised. An analytical solution to this problem is:

$$\mathbf{W}_{\psi}^{T} = \left[\mathbf{L}_{\psi}^{T}\{\mathbf{C} + \mu\boldsymbol{\Sigma}\}^{-1}\mathbf{L}_{\psi}\right]^{-1}\mathbf{L}_{\psi}^{T}\{\mathbf{C} + \mu\boldsymbol{\Sigma}\}^{-1} \tag{3}$$

where $\mathbf{C}$ represents the data covariance matrix calculated over a time-frequency window of interest,$\boldsymbol{\Sigma}$ is a diagonal matrix representing the white noise at each of the MEG channels, and μ is a regularisation parameter. In this way, the weights $\boldsymbol{W}_{\psi}$ are derived specifically to reject interference, including that which is correlated across multiple MEG sensors and which might otherwise generate spurious functional connectivity.

Rejection of interference by beamforming is highlighted in Fig. 4 (Brookes et al. 2011a). As shown above in Fig. 2, MEG is highly susceptible to interference generated by the magnetocardiogram. In Fig. 4a, b the blue line shows Pearson correlation between the ECG and the MEG sensors most affected by sources in left (A) and right (B) sensorimotor cortices. In contrast, the green line shows correlation between the ECG and the beamformer reconstructed timecourses from the peak voxel of interest in the left (A) and right (B) sensorimotor cortices. Notice that for sensor space data, high correlation with the ECG is observed, and further that correlation is inhomogeneous with respect to frequency, peaking in the low beta band. However, following application of the beamformer, correlation is significantly reduced across all bands. (Note this example uses the same data as that in Fig. 2.) It is clear that, had sensor space functional connectivity been assessed in these data, it is likely that correlations between left and right hemisphere would have been spuriously increased by the common mode cardiac artifact, particularly in the beta band. However this confound has been reduced by beamforming.

2.3 Source Leakage and Desirable Properties of Inverse Solutions

Despite the advantages of source space projection in measurement of functional connectivity, there remain significant problems which, if not controlled, can lead directly to spurious connectivity measurement. The ill-posed nature of the inverse problem causes a degree of spatial blurring (i.e. a single point dipolar source will be spread across a finite volume). In addition, sources can be mislocalised, for example due to inaccuracies in the MEG forward solution (e.g. representing an extended source as a point dipole) or due to incorrect assumptions made by the inverse localisation algorithm used (e.g. suppression of temporally correlated sources using beamforming). These effects combined mean that MEG assessment of electrical activity made at spatially separate brain sites are not necessarily independent. This means that signals originating from a single brain location can "leak" into the estimated signals from other spatial locations. This manifests as apparent 'signal leakage' between voxels which can lead to spurious functional connectivity measurement. For this reason, it can be instructive to measure the likely effects of signal leakage prior to functional connectivity assessment.

Signal leakage differs depending on the inverse solution employed and brain area studied; for example leakage tends to be worse for deeper sources where the generated field patterns are more spatially diffuse. Furthermore when using adaptive techniques the leakage profile for any given voxel will change depending on the signal to noise ratio of the MEG data. This makes leakage assessment non-trivial. There are many ways to estimate the extent of source leakage and each has its own advantages and disadvantages. In cases where connectivity assessment involves a priori selection of a seed location, a simple but instructive technique is to measure correlation between the source reconstruction weighting parameters, $\boldsymbol{W}_{\psi}$, derived for the seed location, and the equivalent weighting parameters for all other voxels in the brain. In an ideal world, the weights for any one voxel would be a unique combination of MEG sensors, however the underdetermined nature of the inverse problem prevents this and there will necessarily be some correlation between weights for voxels in close proximity. Equation 1 shows that if the weights for two spatially separate voxels are correlated (as is likely to be the case for nearby voxels) then the projected signals will also be correlated and this may appear as spurious functional connectivity in source space. If, however, the weights for two voxels are completely independent, but the timecourses from those voxels are highly correlated, it is more likely that genuine FC exists between those two brain locations.

An example of leakage assessment via weights correlation is given in Fig. 5 (Brookes et al. 2011a). Here we compare the case for a spatial matched filter in which the weighting parameters are simply a scaled version of the lead fields, and two instances of weighting parameters derived using regularised beamforming (Eq. 3; $\mu = 4$). Figure 5a shows a volumetric image of Pearson correlation between lead fields at the seed location (placed at the cross hairs) and lead fields at all other source space voxels. This is shown for a single subject (with the source

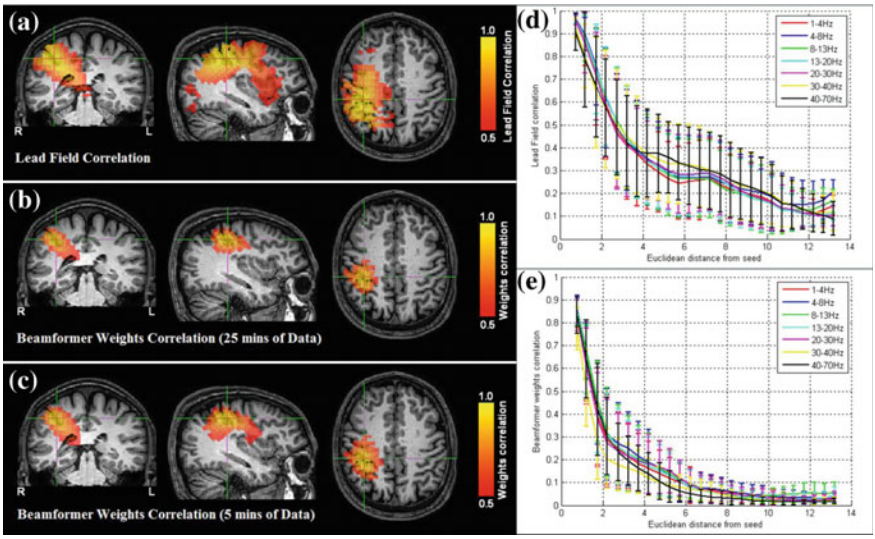

Fig. 5 Signal leakage in beamformer spatial filtering: **a** Correlation between lead fields at the seed location (cross hairs) and all other brain voxels. **b–c** Volumetric images of correlation between beamformer weights at a seed location (cross hairs) and all other test voxels in the brain. **b** Weights computed using 25 min of data ($\mu = 4$; 13–20 Hz band; single subject); **c** Weights computed using 5 min of data only ($\mu = 4$; 13–20 Hz band; single subject); **d** Lead field correlation plotted as a function of Euclidean distance from the seed location. **e** Beamformer weights correlation (Weights computed using 25 min data; $\mu = 4$) plotted as a function of distance from the seed location adapted from Brookes et al. (2011a)

orientation for each voxel derived as the orientation of maximum signal to noise ratio). Pearson correlation coefficients are thresholded at 0.5 for visualisation. Figure 5b, c show volumetric images of correlation between beamformer weights at the seed location and at all other voxels in the brain. (Weights correlation images are computed using 13–20 Hz filtered data.) Figure 5b shows weights correlation in a case where the covariance matrix (**C**) is based on all available MEG data (25 min for this example experiment); Fig. 5c shows weights correlation in a case where covariance is based on the first 5 min of data only. Notice here that weights correlation is far less widespread than lead field correlation, an effect of the adaptive nature of beamforming which shows that, even if lead fields are correlated, beamformer weights can remain independent. Figure 5d, e show lead field correlation and weights correlation as a function of Euclidean distance from the seed location, respectively. Note the improved spatial resolution of beamformer weights correlation with respect to lead field correlation, that is also apparent in Fig. 5a, b. (Separate lead field correlations for different frequency bands appear because the source orientation is computed independently for each frequency band. Lead fields themselves do not change with frequency.)

This simple example highlights some of the desirable properties of inverse problem solutions for functional connectivity measurement. Firstly, the spatial

extent of weights correlation should be as small as possible. In this example we show that the adaptive nature of beamforming limits the spatial extent of weights correlation compared to a spatial matched filter. Note also that for beamforming, data duration has an effect. In this example the total volume of cortex with weights correlated at $r > 0.25$ was 126 ± 15 cm^3 when using 25 min of data; this was compared to 155 ± 17 cm^3 when weights were computed using only the first 5 min (Brookes et al. 2011a). This highlights the importance of judicious experimental design (Brookes et al. 2008), meaning that researchers aiming to assess MEG connectivity based only on 5 min data segments are necessarily going to be more affected by source leakage than those basing measurements on much longer experiments (assuming stationary sources). This is the case for beamforming, however it is not the case for non-adaptive techniques such as certain forms of minimum norm estimation in which weights are based only on system geometry and not the MEG data. Finally, note the inhomogeneous nature of weights correlation. This is particularly notable in Fig. 5a where weights correlation extends asymmetrically from the seed location. For example, here one might spuriously estimate connectivity between the seed in right motor cortex (the cross hairs) and the right insula cortex; however this would be based only on leakage.

In summary, there are significant advantages in measurement of connectivity in source space over sensor space (Schoffelen and Gross 2009) including increased interpretability with respect to anatomy (Fig. 3) and also improved rejection of non-neuronal artifacts (Fig. 4). However, even if connectivity is measured in source space, it is important to note that electrical activity estimated at spatially separate source space locations are not necessarily independent due to signal leakage and care must be taken to ensure that this effect does not impact on measurements. The leakage problem will be further discussed in Sect. 3.3.5.

3 Measuring Functional Connectivity in MEG

Following projection of MEG data from sensor space to source space, which may be achieved using any inverse projection algorithm whose underlying assumptions are reasonable given the experimental design, one aims to assess connectivity between projected signals. To achieve this there are a variety of linear and non-linear methods available. In this section we describe a number of these techniques.

3.1 The Definition of Functional Connectivity

Functional connectivity is based on quantifying statistical dependencies directly from the data (Friston 2011). These statistical measures typically characterize the similarity between a pair of signals (or more) in terms of quantities such as their amplitude or phase in particular frequency bands. This is in contrast to effective

connectivity measures, which are based on generative models of the data, such as Dynamic Causal Modelling (DCM). In fMRI, the term "functional connectivity" has become synonymous with temporal correlation between BOLD signals from spatially separate voxels. However, a number of measures of functional connectivity have also been applied to M/EEG data, with varying levels of success. These include power correlations, mutual information, coherence and phase locking. Unless explicitly stated otherwise, we will assume throughout this chapter that these measures are applied on the timecourses in *brain* (source) space.

At the outset we should be aware that there are potential problems with the use, and in particular in the interpretation, of functional connectivity. One particularly important issue is well exemplified by the increasingly popular approach of using functional connectivity (in fMRI and M/EEG) as a feature to predict or classify the group from which a particular subject was sampled (Craddock et al. 2009). The problem is that changes in functional connectivity, e.g. between conditions or between two population groups, can occur simply due to changes in the signal-to-noise ratio, or due to changes in other parts of a wider network (sometimes known as the "missing node" problem); even when there is no change in the actual neuronal connectivity. This issue has been well documented elsewhere (Friston 2011).

False positive connectivity can also be inferred if correlations caused by the measurement process itself are not accounted for. In particular, as described in Sect. 2.3, artefactual zero-lag correlations are readily caused due to source leakage (Schoffelen and Gross 2009). These phenomena will tend to contaminate all functional connectivity measures unless accounted for.[1] Different ways for accounting for this particular problem will be presented at various points throughout this section, and in particular in Sect. 3.3.5.

Functional connectivity also provides limited insight into the mechanisms of the dynamics that underlie brain activity, and does not directly provide biologically relevant information. In theory, the best way to overcome these limitations is to turn to *effective connectivity*. However effective connectivity approaches arguably still need substantial development and validation before they can be used in earnest on MEG data. Effective connectivity will be discussed further in the "Future Directions" section in this chapter. Until effective connectivity is indeed rendered "effective", functional connectivity will remain the dominant approach in use, with the caveat that considerable care must be taken when interpreting the results.

3.2 Linear Metrics

In this section we will consider linear metrics of statistical dependency, or functional connectivity, between brain areas. Clearly the most straightforward of these

[1] Note, that this problem is avoided when the connectivity to be estimated is between MEG and an externally measured signal such as LFP or EMG recordings.

would be correlation on the raw time series in brain space. However, this is impotent in MEG due to the fact that we do not expect there to be zero lag correlations between distal brain areas. Instead we need turn to more sophisticated measures such as coherence and phase locking.

3.2.1 Coherence and Dynamic Imaging of Coherent Sources

Coherence is a widely used measure of functional connectivity that provides information about the degree of coupling between two signals at a particular frequency. In essence it quantifies linear correlations in the frequency domain. The coherence M_{yz}between a dipole timecourse $y(t)$ and a reference signal $z(t)$ is defined as the magnitude squared cross spectral density of the two signals divided by the autospectral density of each signal:

$$M_{yz} = \frac{\left|C_{yz}(f)\right|^2}{C_{yy}(f)C_{zz}(f)} \tag{4}$$

where C_{yz} is the cross-spectral density between signals y and z, and C_{yy} and C_{zz} are the autospectral densities of signals y and z respectively. The calculation of coherence is a function of frequency, f, and depends on the frequency band over which the cross-spectral density is computed. The cross-spectral density between the two signals may be calculated in the frequency domain as the complex conjugate product of the Fourier transformed data $Y(f)$ and $Z(f)$:

$$C_{yz}(f) = Y(f)Z^{*T}(f) \tag{5}$$

Coherence values lie in the range $0 \leq M \leq 1$, with a value of 1 indicating that the signals are perfectly coupled in frequency. At a given frequency, if the phase of one signal is fixed relative to the other then the signals can have a high coherence at that frequency.

Coherence has been widely used for measuring connectivity in MEG, largely thanks to the popular dynamic imaging of coherent sources (DICS) method (Gross et al. 2001), which uses a frequency domain beamformer to localise sources coherent with a reference signal. The reference signal may be from a cortical location, or an externally measured device (e.g. electrode). This has been shown to work particularly well between cortical sources in MEG and EMG hand movement measurements in motor experiments (Gross et al. 2001), but also between brain regions during a task (Kujala et al. 2007). It should be noted that while DICS computes the cross-spectral density matrix in sensor space, and then applies an adaptive spatial filter (beamformer) to reconstruct source power and coherence for a given frequency bin or band; it can be shown that this is equivalent to using a time-domain beamformer (Woolrich et al. 2011) followed by computation of coherence in source space.

As discussed above, vanilla coherence will be susceptible to false positives due to artefactual zero-lag correlations due to the source leakage problem. A modification to coherence that can overcome this problem is to use ***imaginary coherence*** (Nolte et al. 2004), which works by only using the imaginary terms. These terms cannot be influenced by zero lagged correlations, and so necessarily represent true interactions between brain areas occurring with a certain time (phase) lag:

$$\tilde{M}_{yz} = \frac{\left|Im(C_{yz}(f))\right|^2}{C_{yy}(f)C_{zz}(f)} \tag{6}$$

Measures like imaginary coherence have been used to investigate functional connectivity in patients with brain lesions using resting state MEG (Guggisberg et al. 2008). However, in some resting state MEG studies it is has been shown to be less effective for estimating cortico-cortical interactions than power correlation methods, such as when looking for inter hemispheric connectivity between the left and right motor cortex (Brookes et al. 2011a).

3.2.2 Phase Locking

It has been argued that one of the problems with coherence is that it is not a pure measure of the phase relationship. In other words, it also increases with amplitude covariance, and the relative importance of amplitude and phase covariance in the coherence value is not clear (Lachaux et al. 1999). An alternative is to use a measure that specifically identifies when there is frequency specific transient phase locking. The phase-locking value (PLV) is one example of such a measure.

To estimate PLV, we start by extracting the timecourse of the instantaneous phase of two signals x and y ($\phi_x(t)$ and $\phi_y(t)$, respectively) at the frequency of interest, f. Typically, this is done by band-pass filtering the data, and then computing a time-frequency transform (e.g. Wavelet or Stockwell). We can then compute the phase difference at each time point, $\theta(t) = \phi_x(t) - \phi_y(t)$. The phase locking value (PLV) is then given by:

$$PLV = \frac{1}{T}\sum_{t}^{T} \exp(i\theta(t)) \tag{7}$$

We can look also for phase locking with regards to finding consistent phase difference over repeats of a stimulus in multi-trial (epoched) data at the same time point, t, within trial. In this case we have (Lachaux et al. 1999):

$$PLV(t) = \frac{1}{N}\sum_{n}^{N} \exp j\theta(t,n) \tag{8}$$

where n indexes the N repeated trials. Note that this is related to the Inter-trial Coherence (ITC), which is a univariate measure looking for consistent phase locking over trials in a *single* brain area at a time. When interpreting multi-trial PLV, it is important to be aware that if the two brain areas in question are both separately responding in a stimulus-locked manner (as in an event related field) to the underlying stimulus, then a significant PLV could result even though the two areas are not necessarily directly interacting. Note that this issue of interpretation in the face of what corresponds to the "missing nodes" problem is not specific to PLV, but is a problem inherent to all functional connectivity measures.

One important consideration in the measurement of phase locking is how to choose an appropriate bandwidth. This is a trade-off; the bandwidth needs to be sufficiently specific for the concept of phase to be meaningful, but not too narrow as to make estimation excessively noisy. Like coherence, PLV is a symmetric measure and so does not allow direct inference about directionality between areas. Nonetheless, phase locking measures have been successfully used in task MEG data, notably to detect distributed visuo-motor networks, including structures of the frontoparietal circuit and the cerebello-thalamo-cortical pathway (Jerbi et al. 2007).

Phase lag index (**PLI**) can be thought of as being the same to PLV as imaginary coherence is to coherence (Stam et al. 2007). In other words PLI is a modification of the PLV measure such that it is protected from contamination due to artifactual zero-lag correlations caused by source leakage. PLI works by defining an asymmetry index for the distribution of phase differences. If no phase coupling exists between two time series, then this distribution is expected to be flat. Any deviation from this flat distribution indicates phase synchronization. Pure zero lag phase locking due to field spread will manifest as a *symmetric* distribution around zero phase lag, and so will not adversely influence PLI.

3.3 Nonlinear Metrics

3.3.1 Band Limited Power Correlations

Perhaps the simplest non-linear methodology for measurement of functional connectivity is to assess correlations between either the amplitude or power envelope of band limited oscillations. These envelopes have been shown to exhibit temporal variation over time scales of seconds and in some cases even minutes. Invasive measurements have shown that correlations between band limited power envelopes fall off with distance, yet much more gradually than the correlations in the raw high-frequency local field potentials from which envelopes are derived (Leopold et al. 2003). Spontaneous gamma band limited power fluctuations recorded from depth electrodes in epileptic patients (Nir et al. 2008) revealed correlations between bilateral homotopic brain regions, which is consistent with

numerous fMRI functional connectivity studies. Furthermore a large amount of work has shown a relationship between the BOLD response and changes in MEG oscillatory power during a task (Brookes et al. 2005; Singh et al. 2002; Winterer et al. 2007; Zumer et al. 2009) and this implies that if the haemodynamic networks observed using fMRI are visible to MEG, then assessment of band limited power correlation should be informative.

There are numerous techniques by which to compute either band limited amplitude envelope, or band limited power envelope; here we describe a popular approach based on a Hilbert Transform. In source space, having computed the timecourse of electrical activity in some band of interest, $\hat{Q}_{\boldsymbol{\theta}}(t)$, for each voxel, the *analytic signal* $z_{\theta}(t)$ is given by:

$$z_{\boldsymbol{\theta}}(t) = \hat{Q}_{\boldsymbol{\theta}}(t) + iH(\hat{Q}_{\boldsymbol{\theta}}(t)) \tag{9}$$

where $H(\hat{Q}_{\boldsymbol{\theta}}(t))$ represents the Hilbert transform of $\hat{Q}_{\boldsymbol{\theta}}(t)$ and is given by:

$$H[\hat{Q}_{\boldsymbol{\theta}}(t)] = P\left[\frac{1}{\pi}\int_{-\infty}^{\infty}\frac{\hat{Q}_{\boldsymbol{\theta}}(u)}{t-u}du\right] \tag{10}$$

P denotes the Cauchy principal value of the integral and is used to take account of the singularity at $t = u$. The magnitude of the analytic signal yields the envelope of the measured oscillatory activity thus:

$$E(\hat{Q}_{\boldsymbol{\theta}}(t)) = \sqrt{(\hat{Q}_{\boldsymbol{\theta}}(t))^2 + (H(\hat{Q}_{\boldsymbol{\theta}}(t)))^2} \tag{11}$$

Hilbert envelopes, $E(\hat{Q}_{\boldsymbol{\theta}}(t))$ can be computed for every voxel in the source space.

Following computation of the band limited amplitude envelopes at all locations in the brain, a metric of connectivity between two voxels can be formulated via computation of a Pearson correlation coefficient between Hilbert envelopes at a seed voxel of interest, and some other test voxel (Brookes et al. 2011a). Mathematically, the Pearson product moment correlation coefficient is given by:

$$r(\mathbf{x},\mathbf{y}) = \frac{\varepsilon(E_{\boldsymbol{\theta}_1}E_{\boldsymbol{\theta}_2})}{\sqrt{\varepsilon\left(E_{\boldsymbol{\theta}_1}^2\right)\varepsilon\left(E_{\boldsymbol{\theta}_2}^2\right)}} \tag{12}$$

where $\boldsymbol{\theta}_1$ and $\boldsymbol{\theta}_2$ refer to the seed and test locations/orientations respectively and ε denotes expectation value. Alternatively, in vector notation

$$r(\mathbf{x},\mathbf{y}) = \frac{\mathbf{x}^T\mathbf{y}}{\sqrt{\mathbf{x}^T\mathbf{x}}.\sqrt{\mathbf{y}^T\mathbf{y}}} \tag{13}$$

where we use $\mathbf{x}$ to represent the mean corrected N element envelope timecourse at the seed voxel ($\boldsymbol{\theta}_1$), and $\mathbf{y}$ to represent the mean corrected N element envelope timecourse of the test voxel ($\boldsymbol{\theta}_2$). N is the number of samples in the timecourse which we assume is large. Sequential application of this formula, keeping the seed voxel static and moving the test voxel, enables images of connectivity to be derived. Examples of this are given in Fig. 3.

The reader should note that determining this linear relationship between band limited amplitude envelopes at the seed and test voxel can also be re-cast in the context of a linear regression (Hall et al. 2013). Here, the test envelope timecourse ($\mathbf{y}$) is described by a general linear model (GLM) where $\boldsymbol{x}$ is used to form the design matrix; β represents the regression parameter (or effect size) and $\boldsymbol{\Delta}$ the error.

$$\mathbf{y} = \beta\mathbf{x} + \boldsymbol{\Delta} \tag{14}$$

The regression parameter (or effect size) estimate β is computed via the Moore-Penrose pseudo inverse thus:

$$\beta = [\mathbf{x}^T\mathbf{x}]^{-1}\mathbf{x}^T\mathbf{y} \tag{15}$$

It is possible to show (Hall et al. 2013) that, for the case where only a single column is used in the design matrix, the linear regression framework (Eq. 15) and Pearson correlation (Eq. 13) are directly equivalent other than a constant factor, which itself is reduced to unity if $\mathbf{x}$ and $\mathbf{y}$ are normalised. However, the regression framework has the advantage that the design matrix can be extended to incorporate more columns and thus regress out confounding factors such as motion, heart rate or respiration.

3.3.2 A Note on Full Versus Partial Power Correlations

The technique highlighted above and summarised by Eq. 13 corresponds to full correlation. However, it should be noted that full correlation cannot distinguish between direct and indirect connections, whereas ***partial correlation*** can—at least to some extent. Partial correlation refers to the correlation between two timeseries, after each has been adjusted by regressing out other variables (e.g. activity in other brain regions/network nodes). An efficient way to estimate the full set of partial correlations is via the inverse of the covariance matrix (Marrelec et al. 2006). Under the constraint that this matrix is expected to be sparse, regularisation is often applied, for example, using the Lasso method (Friedman et al. 2008). Partial correlation has been advocated (Marrelec et al. 2006) as a good surrogate for structural equation modelling (SEM). While partial correlation does seem to improve the distinction between direct and indirect connections, it also introduces Berkson's paradox, where there can be artifactual negative correlations between brain regions (Smith et al. 2011).

3.3.3 Independent Component Analysis

One of the disadvantages with seed based approaches to functional connectivity analysis is that they necessarily require selection of *a priori* seed locations. This can prove a limiting factor due to its subjective nature and this has led to the introduction of other methodologies that are not limited in this way. One such technique is ICA which is a commonly used method for the denoising of MEG data and has been used previously with great success in EEG, and in fMRI, particularly for connectivity analysis. ICA itself is a linear decomposition. However, here we consider this as a nonlinear approach as in MEG it is typically (Brookes et al. 2011b; Hall et al. 2013; Luckhoo et al. 2012) applied to the (nonlinear) band-limited power timecourses, rather than raw timecourses.

Although there are many ways in which to apply ICA, the simplest technique for connectivity analysis is first to form a matrix, $\mathbf{X}$, where each row represents the band-limited power (e.g. Hilbert envelope) timecourse, from a single voxel in the brain, temporally concatenated across subjects as shown in Fig. 6, thus:

$$\mathbf{X} = \begin{bmatrix} \mathbf{E}\left(Q_{r_1}^{(subject\ 1)}\right), & \mathbf{E}\left(Q_{r_1}^{(subject\ 2)}\right), & \dots \\ \mathbf{E}\left(Q_{r_2}^{(subject\ 1)}\right), & \mathbf{E}\left(Q_{r_2}^{(subject\ 2)}\right), & \dots \\ \dots & & \\ \mathbf{E}\left(Q_{r_{N_{Voxels}}}^{(subject\ 1)}\right), & \mathbf{E}\left(Q_{r_{N_{Voxels}}}^{(subject\ 2)}\right), & \dots \end{bmatrix} \tag{16}$$

Here $\mathbf{E}\left(Q_{r_i}^{(subject\ k)}\right)$ represents the mean corrected vector envelope timecourse spanning the whole experiment extracted from voxel r using data from subject k. N_{Voxels} is the total number of voxels in standard space. Note that $\mathbf{X}$ represents data from all subjects in all tasks but only a single frequency band, and in practice it is often desirable to temporally smooth and down-sample the voxel timecourses to improve computational efficiency.

Temporal ICA can then be applied such that the measurement matrix, $\mathbf{X}$, is defined as linear mixtures of independent temporal signals $\mathbf{S}$:

$$\mathbf{X} = \mathbf{AS} \tag{17}$$

$\mathbf{A}$ is the mixing matrix which defines the contribution of each independent component to each voxel timecourse. Note temporal ICA is employed since, in MEG, the maximum information is in the temporal domain; this is distinct (typically) from fMRI where spatial ICA is often used because maximum information is to be gained in the spatial domain. The unmixing matrix, $\mathbf{V}$, can be estimated giving the contribution of each voxel timecourse to each independent component:

$$\mathbf{S} = \mathbf{VX} \tag{18}$$

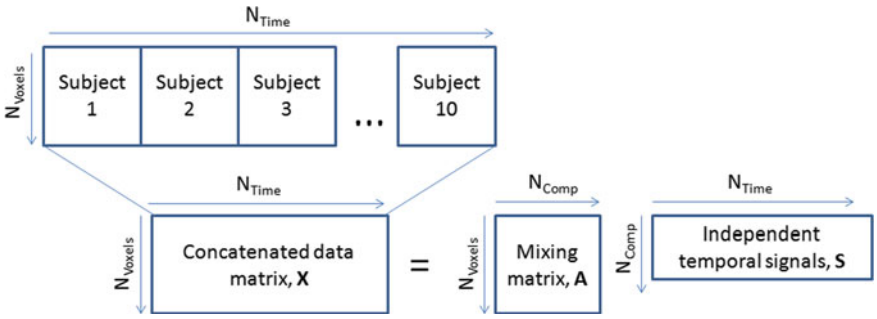

Fig. 6 Schematic representation of ICA on a single frequency band

The spatial signature of each temporal component, for a single frequency band, is represented by the columns of the mixing matrix **A**. This ICA process is depicted schematically in Fig. 6.

Application of ICA in this way typically yields a small number of temporally independent signals, each of which corresponds to a spatial signature in source space. In resting state MEG those spatial signatures have been shown to be similar to spatial signatures of resting state haemodynamic networks observable in fMRI (Brookes et al. 2011b). Further, similar networks have been observed in a task positive state, with network activity significantly altered by the task (Luckhoo et al. 2012; Brookes et al. 2012a, b). Most importantly, derivation of temporally independent timecourses from the data matrix using ICA eliminates the need for *a priori* selection of a seed.

3.3.4 Generalized Synchronization

Coherence or PLV, described above in Sect. 3.2, are only capable of detecting linear relationships, and band-limited power correlation is only capable of detecting linear relationships in the band-limited power timecourses. Furthermore, none of those methods handle temporal non-stationarity in functional connectivity. An alternative approach to detecting synchronization, without these limitations, is generalized synchronization. ***Generalized synchronization*** (GS) exists between two signals, x and y, when the state of one signal y is a repeating function of the other signal x, i.e. $y = f(x)$. The idea is that when signal y plays out a particular pattern, then signal x has a tendency to play out its own specific pattern at the same time; crucially, these patterns in x and y need to be consistently paired up over time, but do not need to resemble each other. But how do we detect these repeating paired patterns? The trick is to convert (embed) x and y into a state-space where we can first detect repeating patterns in x and y individually. Such a state-space corresponds to the values of the time series at different time lags. Figure 7 shows a simple example with x and y plotted (embedded) at just $M = 2$ time lags, t and

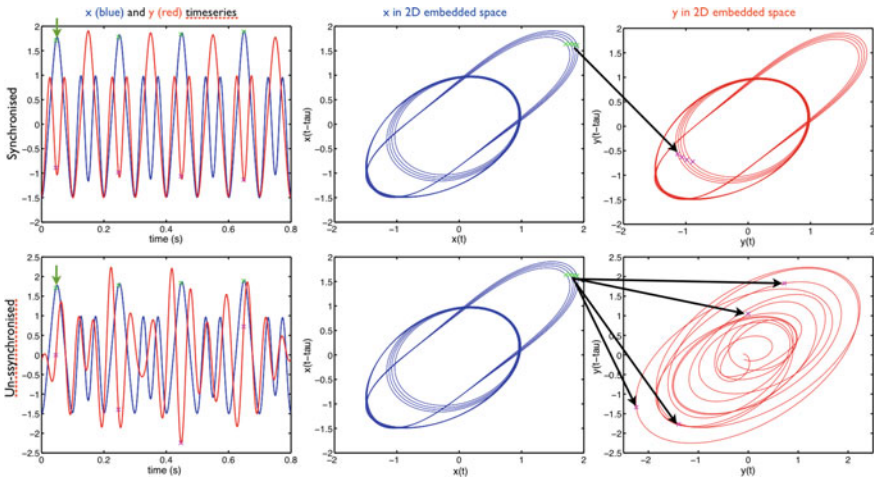

Fig. 7 Illustration of the idea behind Generalised Synchronisation. [*Left*] two timecourses, x (*blue line*) and y (*red line*), for two scenarios: [*top*] synchronised, [*bottom*] unsynchronised (x is the same in both cases). [*Middle*] shows $\boldsymbol{x}$, and [*right*] shows $\boldsymbol{y}$, plotted (*embedded*) at just $\boldsymbol{M} = 2$ time lags, $\boldsymbol{t}$ and $\boldsymbol{t} + \boldsymbol{\tau}$. The idea is that if $\boldsymbol{x}$ and $\boldsymbol{y}$ are synchronized, then the *time points* defined as when points are "close" in the embedded space for x (*green points*), should produce points in the embedded space for y that are also "close" together (*magenta points*). When x and y are unsynchronised, these *magenta points* are spread widely [*bottom-right*]

$t + \tau$. The idea is that if x and y are synchronised, then the time points defined as when points are "close" in the embedded space for x (green points), should produce points in the embedded space for y that are also "close" together (magenta points). This is illustrated for the pattern (time point) indicated with the green arrow; GS is effectively calculated by moving this arrow over all time points and aggregating this measure of "closeness" in the embedded space.

As well as nontrivial interpretation, one of the challenges in using GS is how to choose parameters such as the dimensionality of the embedded space (i.e. the number of lags to look at, M), the lag time step, Δ, and the parameters that determine what is regarded as being "close" in the embedded space. The best choice of parameters will depend on the peculiarities of the attractors (patterns) in x and y. Note that GS can be readily extended to multiple (greater than 2) brain areas (Stam and van Dijk 2002).

3.3.5 Leakage Correction via Linear Regression

We have seen above how techniques such as imaginary coherence or PLI can eliminate source leakage for seed based connectivity estimation by removing zero-phase lag correlation. A related alternative technique, that is perhaps more straightforward, is to remove the zero lag correlations in the raw time series

(Luckhoo et al. 2012; Hipp et al. 2012). It is well known that source leakage gives rise to zero phase lag correlation and so removal of this component suppresses source leakage between a seed and test voxel, albeit at the expense of any genuine zero-phase lag correlation that may exist between the seed and test voxel. To remove the effect of signal leakage between a seed timecourse, $\hat{Q}_{\theta 1}$ and a test timecourse $\hat{Q}_{\theta 2}$, a univariate projection of the vector $\hat{Q}_{\theta 1}$ on $\hat{Q}_{\theta 2}$ is estimated thus:

$$\beta_{UV} = \hat{Q}_{\theta 1}^{+} \hat{Q}_{\theta 2} \tag{19}$$

where $\hat{Q}_{\theta 1}^{+}$ denotes the pseudo-inverse of $\hat{Q}_{\theta 1}$. The linear projection (or estimate of $\hat{Q}_{\theta 2}$ based on vector $\hat{Q}_{\theta 1}$) is removed thus:

$$\hat{Q}_{\theta 2_R} = \hat{Q}_{\theta 2} - \hat{Q}_{\theta 1} \beta_{UV} \tag{20}$$

where $\hat{Q}_{\theta 2_R}$ is the component of $\hat{Q}_{\theta 2}$ that is orthogonal to $\hat{Q}_{\theta 1}$. In this way any linear interaction between the seed and test timecourse is removed. We also note here that this approach can equivalently be used alongside coherence, or PLV, to find non-zero phase lag relationships. An example of the effectiveness of this approach is given in Fig. 8 (Luckhoo et al. 2012; Hipp et al. 2012).

4 Current Findings in MEG Connectivity

Thus far, we have outlined some of the most popular methods for measuring connectivity in MEG. We have also highlighted some of the potential confounds of these metrics, as well as some of the methods by which those confounds might be eliminated. In this section, we will briefly summarise some of the example applications of these methods, and how they are helping neuroscientists understand the functional dynamics of the human brain. The reader should be aware that this section is by no means intended to be an exhaustive list of studies in this area. Instead, some examples are presented that the authors believe are either early key publications or significant recent advances. Throughout, the reader is directed to more comprehensive literature reviews that offer much broader view of specific topics.

4.1 Applications to Pathology

Measurement of network synchronisation has been proposed as a method for the early detection of various forms of neuropathology such as Alzheimer's disease (AD), Parkinson's Disease (PD) and Schizophrenia. For example, EEG has been used as a diagnostic tool in AD for several decades, and is characterised by a

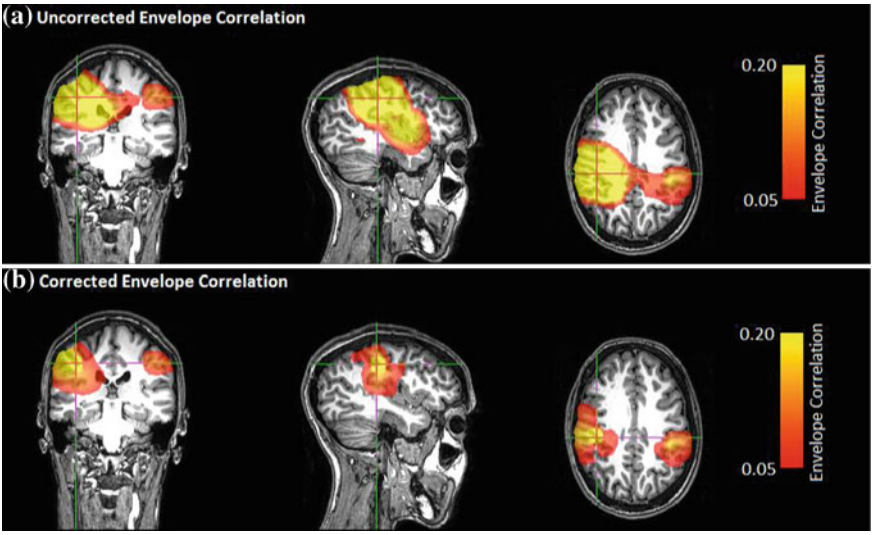

Fig. 8 An illustration of leakage correction. **a** Envelope correlation between a seed in right motor cortex and all other brain locations, prior to correction for leakage. **b** Envelope correlation for the same data post leakage correction. Correction achieved by removing the zero-time lagged components of the raw beta band signal

decrease in synchrony in the alpha and beta bands (Dauwels et al. 2010a, b). This effect is thought to be caused by disconnections between cortical regions leading to decoupling of oscillating networks (Locatelli et al. 1998) (for a review see Jeong et al. 2001). Furthermore, Tass et al. (1998) used MEG to measure phase synchrony between sensors during muscle tremor in PD patients. It was discovered that the temporal evolution of the muscle tremors reflected the timecourses of coherence of abnormal activity between spatially separate motor areas. Bob et al. (2008) investigated disturbed fronto-temporal-central-parietal connectivity in schizophrenia by examining synchronisation patterns using wavelet phase synchronisation (WPS) in 8 EEG electrodes comparing synchrony between all possible pairs. They found significant relationships between symptoms of schizophrenia and phase synchrony. In particular, WPS in frequencies lower than 8 Hz were positively correlated with symptoms, while WPS in bands higher than 8 Hz showed a negative correlation. These studies demonstrate the important clinically evaluative role that synchrony measures may have.

Detection of reduced phase synchrony can be used as an early diagnosis criterion in AD and PD patients potentially improving outcomes for patient's worldwide (Dauwels et al. 2010a; Jeong et al. 2001) by allowing clinicians to begin treatment earlier and potentially prolong quality of life. MEG phase coherence measures have also shown promise as a method to test the disconnection hypothesis of schizophrenia. For example, Maharajh et al. (2010) studied the phase stability of the 40 Hz auditory steady state response (ASSR) using the phase

synchrony index (PSI) with MEG. Results demonstrated reduced phase synchronisation between hemispheres in ipsilateral and contralateral gamma. As well as lending support to the disconnection hypothesis, this might also provide a means to aid drug testing in psychiatric disorders.

For a review on the role of oscillatory communication in the brain during neurodegenerative disorders see (Schnitzler and Gross 2005). At the time of writing there are a multitude of ongoing studies worldwide investigating MEG based metrics of functional connectivity across multiple pathologies, and this is likely to be a fruitful area of future study.

4.2 ECoG

ECoG is an invasive technique used only in pathophysiological conditions such as epilepsy lesion treatment or tumour resection. The most common use of ECoG is as a method to locate the epicentre of epileptiform spike activity in serious cases of epilepsy (Arroyo and Lesser 1993; Wyler et al. 1984) (for a review see Towle et al. 1999). It involves placing an array of electrodes directly on a portion of the brain in order to measure the electric field potentials produced by synchronous neuronal firing; in much the same way as EEG, but with the benefit that no intervening anisotropic conductivity (e.g. from the skull) is present to distort the field potentials. ECoG therefore gives higher spatial resolution than EEG. Numerous studies have highlighted the link between MEG and invasive metrics (Hall et al. 2005) and here we discuss several key connectivity applications that may generalise to MEG.

Connectivity studies have been performed on patients using ECoG although the number of studies and the range of paradigms are generally fairly low. In one notable study, Gevins et al. (1994) used a large ECoG grid (64 electrodes, 8 cm^2) to measure coherence patterns across short distances of the cortex. They detected phase delays of several hundred milliseconds over 7 cm during a behavioural task, which according to Towle et al. (1999) indicates some information transfer between regions. More recently, Matsuzaki et al. (2013) used ECoG to measure cortico-cortical evoked potentials (CCEPs) and stimulation elicited gamma band activity (80–150 Hz) in the medial occipital regions of 10 patients with focal epilepsy. Brain activity was elicited by means of stimulus electrodes with a 3 mA 1 Hz pulse train and wave propagation was tracked across the electrode array. It was found that stimulation of the primary visual areas produce feed forward propagations in high processing areas indicating a direction of information flow from primary to higher order regions of the visual cortex.

It is clear that ECoG is a useful technique for measuring spiking activity and oscillations across relatively large regions of the cortex. The downside of using ECoG as a neuroscientific research tool is that it is only viable in cases where brain damage, or some other disorder, is likely to be present and therefore not viable as a tool to measure healthy function. Furthermore, its usefulness in connectivity research is limited as the brain coverage is generally low, only covering a small

patch of the brain at any one time. However, the increasing utility of MEG connectivity metrics are likely to facilitate non-invasive parallels to these invasive experiments, enabling measurement across a much wider population as well as the whole brain coverage that MEG affords. For a review and in depth discussion of ECoG techniques see Towle et al. (1999).

4.3 Brain Networks and Comparison with fMRI

The recent prevalence of fMRI connectivity measurements have led to obvious questions as to whether the electrophysiological signals measured using MEG mirror the long range interactions observed in distributed fMRI networks. Recent work suggests that significant statistical interdependencies exist between source space reconstructed MEG signals at spatially separate nodes of fMRI networks. Specifically, if one takes the band limited power (BLP) MEG timecourse at a seed location defined within a node of an fMRI network, one generally finds that across the whole brain, the highest correlation often occurs with the BLP MEG timecourses in a separate node of that same network. One of the first demonstrations (de Pasquale et al. 2010) used source space reconstruction and correlations in the BLP timecourses in the theta (3.5–7 Hz), alpha (8–13 Hz), beta (14–25 Hz), gamma (27–70 Hz) bands and broadband (1–150 Hz). By identifying temporally non-stationary periods of particularly high BLP correlation, they found networks in MEG that resembled the default mode and dorsal attention networks, well characterised in fMRI. Further expansion of these findings came from Brookes et al. (2011a) who used a seed based correlation approach to show that temporally down-sampled BLP timecourses are correlated across the left-right motor cortices, mirroring the findings of Biswal et al. (1995). Dependence on frequency band was also investigated with the strongest correlation evident in the beta band. These findings were also mirrored by Hipp et al. (2012), who have extended this to auditory and visual networks, as well as attentional networks that have been previously well characterised by fMRI.

Resting state networks (RSNs) have also been identified independently in MEG data *without* the need to a priori specify (fMRI-derived) seed placement. This has been through the use of temporal ICA applied to BLP timecourses, revealing a number of resting state networks (independent component spatial maps) that significantly spatially correlate with BOLD resting state networks (Brookes et al. 2011b). This ICA approach has also been applied to task positive data (Brookes et al. a, b; Hall et al. 2013; Luckhoo et al. 2012).

Evidence is therefore beginning to suggest that a degree of spatial similarity exists between patterns of haemodynamic and electrophysiological connectivity. However, networks observed in MEG are not perfect spatial matches to those observed in fMRI, and the differences, which are often overlooked, may be just as important as the similarities. Spatial matching of MEG and fMRI networks is inherently confounded due to the fact that both modalities have their own

weaknesses. fMRI is an indirect measure of electrophysiological processes in the brain reflected in the slow hemodynamic response, and while MEG measures electrophysiology more directly, spatial filtering techniques are hampered by the nature of the ill-posed inverse problem that impacts on spatial resolution. However despite this confound, it appears that MEG connectivity measurement will facilitate a useful means by which to investigate the electrophysiological basis of haemodynamic network measurements. For a review of the relationship between electrophysiological and haemodynamic functional connectivity measurements see (Scholvinck et al. 2013).

5 Future Directions

5.1 The Role that Oscillations Play in Long Range Connectivity

Over recent years fMRI has been successful in the mapping of functional networks, for example, using resting state data (Beckmann et al. 2005). However, evidence from MEG suggests that these network interactions are likely underpinned by oscillatory activity in particular frequency bands (Brookes et al. 2011a; Hipp et al. 2012). Understanding these oscillations, and the biophysical models that underpin them, will provide unique and important insights into the function of the brain. For example, one possibility is that long-range connectivity may be mediated by synchronisation of oscillatory activity. To illuminate these models, direct measures of neural activity at high temporal resolution are needed, and such measures are likely to be increasingly provided by MEG.

5.2 Pharmaco-MEG

Given the wealth of data suggesting the role of neural oscillations in connectivity, the development of a true understanding of oscillations and what drives them is likely to be key in our understanding of connectivity. With this in mind, it seems likely that future experiments should aim to probe the relationship between oscillations and neurochemistry. There has been extensive research at the microscopic scale on the role of neurotransmitters such as Glutamate and GABA, and how excitatory and inhibitory neurons interact to produce oscillatory activity (e.g. Bartos et al. 2007; Traub et al. 1996). However, at the macroscopic scale relatively little is known about the role of neurotransmitters in generating the range of oscillatory patterns seen in rest and cognitive tasks in MEG.

Recent studies have measured basal GABA levels and correlated those, across subjects, with task induced neuronal activity measured with MEG (Gaetz et al.

2011; Muthukumaraswamy et al. 2009). However, in such correlation studies it is impossible to infer causality, or rule out the presence of a third hidden covariate. By experimentally manipulating specific variables, the causal effects of neurotransmitter concentration on electrophysiology may be understood more clearly. Hall et al. (2010) demonstrated a novel technique for determining the temporal, spatial and frequency distribution of power changes in the cortex following the administration of any drug that is thought to affect neurotransmission in the brain. They administered the GABAergic modulator diazepam and measured the oscillatory changes in source space using a beamformer approach. Brain wide changes in oscillatory power were observed, mainly in beta band (13–30 Hz), but also in theta, alpha and gamma. These changes were dependent on the region under observation. This technique was later applied to a brain injured patient (Hall et al. 2010) after administration of zolpidem; and it was found that while MRS and MRI showed complete loss of neuronal viability in the peri-infarct region, MEG beamformer analysis showed high amplitude theta and beta band oscillations that were reduced after drug administration.

The use of psychoactive drugs to experimentally alter electrophysiology is not new but until now most of the research was performed with EEG (Bartel et al. 1988; Greenblatt et al. 2004; Loughnan et al. 1987; Restuccia et al. 2002) or fMRI (Bloom et al. 1999; Breiter et al. 1997; Wise and Tracey 2006). The advantage of using MEG is that it offers improved spatial resolution over EEG and is less susceptible to the potential confounds in fMRI such as drug induced changes in baseline blood flow. Hall et al. (2010) point out some limitations of this approach. Firstly, the distribution of receptor sites affected by the drug is inhomogeneous and this might differ between participants, making spatial group averaging difficult. Second, deep sources are generally challenging to observe using MEG and the effects that drugs have on the electrophysiology of subcortical structures is difficult to measure. Multimodal approaches, using MEG/PET for example, could overcome these problems by mapping receptor site distributions and monitoring uptake in subcortical structures. In terms of functional connectivity, pharmacological manipulation offers an exciting new field in which the role of neurotransmitters in cortico-cortical connectivity could be elucidated. At present this field is largely untapped, but may represent a rich area for future investigation.

5.3 Dynamic Connectivity Measurement

In the "resting" brain, one hypothesis is that the resting state can be thought of as a condition of undirected wakefulness in which the mind occupies a number of mental states (Deco et al. 2008). We would therefore expect *dynamic* changes in functional connectivity in the resting state. Indeed a number of recent studies support this. Chang and Glover (2010) applied time-varying measures of pairwise functional connectivity to fMRI time series to show that the brain undergoes fluctuations in connectivity between nodes of the default mode network. High

temporal resolution fMRI (a method of fMRI acquisition that has ~10 times the temporal resolution) used in conjunction with temporal ICA has been shown to reveal multiple temporal modes that appear to break down several well-known RSNs into transient, spatially overlapping subcomponents (Smith et al. 2012), although it should be noted that the method is still limited by the slow haemodynamic response. In MEG, it has been shown that there is temporal non-stationarity in (alpha/beta) band limited power correlations (de Pasquale et al. 2010); along with evidence of a bi-state nature to the power correlations, with periods of zero FC interspersed with periods of high transient FC (Baker et al. 2012). By identifying time points corresponding to high within-network connectivity, it has also been suggested that networks transiently engage with other networks during periods of high internal correlation, with the default mode network (DMN) acting as a hub of cross network interaction (de Pasquale et al. 2012).

However, most of the methods used for investigating time-varying connectivity so far have one fundamental limitation: the fact that they compute time-varying FC using sliding time windows. This limits temporal resolution to the size of the sliding window, which needs to be kept large enough to allow for a good estimate of FC. An attractive alternative is to deploy techniques such as Hidden Markov Models (HMMs), which have already been shown to detect short-lived re-occurring states in resting state MEG data, characterised by repeating multivariate patterns of covariance over channels (Woolrich et al. 2013). Intriguingly, this approach detects states with very short lifetimes on the same timescale as EEG microstates (~100 ms) (van de Ville et al. 2010; Koenig et al. 2005; Britz et al. 2010), and has also been used to perform temporally adaptive MEG source reconstruction.

5.4 Phase Amplitude Coupling

The methodologies for measurement of functional connectivity, as described in Sect. 3, are intended for use within specific frequency bands. However, there is now good evidence from invasive electrophysiological recordings and MEG showing a direct relationship between the phase of some low frequency oscillation, and the amplitude of a higher frequency oscillation. For example, Canolty et al. (2006) show that the phase of theta oscillations is correlated with the amplitude of high frequency oscillations. This form of cross frequency coupling has been observed within single brain regions and also across brain areas (i.e. the phase of low frequency oscillations within one area related to the amplitude of higher frequency oscillations in a second brain area). It is conceivable then that such effects may be a means by which distal cortical regions are synchronised. These measures are in their infancy, however they may provide informative future insights into functional connectivity.

5.5 *Effective Connectivity and Network Models*

Essentially, effective connectivity (EC) is an estimate of directed influence, inferred using a generative model. By attempting to explicitly model the entire network, and accounting for endogenous and exogenous inputs, these can, at least in principle, overcome many of the limitations of functional connectivity. In this section we consider EC techniques such as multivariate autoregressive model, and then more biophysically informed network models, such as Dynamic Causal Modelling.

5.5.1 Multivariate Autoregressive (MAR) Models

The multivariate autoregressive model (MAR) is a generative model that captures the time lagged linear interactions between multiple sources (e.g. brain areas). It is often used to underpin, and provide measures for, Granger Causality. Consider that we have N brain areas (timecourses) with T timepoints, $x_1(t), x_2(t) \ldots x_N(t)$. Then a MAR with model order (maximum lag) P is given by:

$$x(t) = \sum_{p}^{P} A_p x(t-p) + e(t) \tag{21}$$

where $x(t)$ is the $N \times 1$ vector containing $x_n(t)$ for all brain areas, A_p is the $N \times 1$ vector of the autoregressive parameters at lag p, and $e(t)$ is a multivariate Gaussian distribution with zero mean.

To capture the full cross-spectral characteristics of MEG data, MARs can need a large number of parameters. As a result, a particularly useful method of inference is Bayes. This provides a principled framework to regularise the model parameters, at the same time as accounting for their probabilistic uncertainty. These methods can also provide estimates of the Bayesian Model evidence (the probability of the data given the model), which can be used to infer the model order of the MAR, i.e. the number of time lags that need considering (Harrison et al. 2003; Schlögl and Supp 2006).

One of the attractions of working with MAR models, is that the inferred MAR model parameters, A_p, can be used to estimate a wide variety of different functional connectivity measures. These include the cross-spectral density, coherence, partial coherence, directed transfer function (DTF), and partial directed coherence (PDC). Partial coherence and PDC are particularly interesting measures as they effectively find direct connections only, rather than also considering indirect connections as is the case in non-partial approaches. This is analogous to the benefits of partial correlation (e.g. when looking at power correlations), as compared with full correlation, which is discussed above.

Another useful feature of MAR models is that because they are linear, they commute with *linear* source reconstruction methods (e.g. minimum norm). This

means that the MAR can be fit in the relatively low dimensional sensor space, and then be transformed into source space via the linear source reconstruction operation. However, to benefit from the potentially superior rejection of artefacts afforded by *nonlinear* adaptive reconstruction methods (such as beamformers), then the MAR models need to be fit in source space.

MARs have been used to compute measures like DTF and PDC in a number of different applications, particularly in EEG (Astolfi et al. 2005), and spike data (Kaminski and Liang 2005). Recent extensions allow for the computation of time-varying connectivity using adaptive MAR-models (Astolfi et al. 2008). For more information on MAR derived-measures and their mathematical definitions, the reader is referred to (Dauwels et al. 2010b).

5.5.2 Biophysical Network Models

A plausible biophysical model of neuronal interactions should be cyclic, connections should be able to be reciprocal (bi-directional), and the effect of one brain area on another cannot occur instantaneously, due to conduction delays (Woolrich and Stephan 2013). This leads us to the general framework of Dynamic Causal Models (DCM) pioneered by Friston and colleagues (Friston et al. 2003). DCM expresses the interactions between brain regions using differential equations. These equations also allow for known external inputs (experimentally controlled perturbations), and can model both "resting" brain activity and task- or stimulus-related responses:

$$\dot{x} = f(x, \theta, u) + e_x \tag{22}$$

where x is $P \times T_x$ matrix of P hidden neuronal states, $\dot{x}$ is its temporal derivative, T_x is the number of time points, θ are the biophysical neuronal model parameters, u are the known external inputs, and e_x is stochastic neuronal noise. These neuronal models are augmented with an observation model (e.g. incorporating the lead fields) to form a complete generative model of MEG data in sensor space. Typically DCM is inferred upon using Bayesian inference techniques, which allow for the incorporation of biophysical prior knowledge about plausible parameter values, and for model comparison between different hypothesised network models (Penny et al. 2004; Stephan et al. 2007).

In MEG (and EEG) DCM, the form of $f(x, \theta, u)$ is much more biophysically informed and complex than the function used in fMRI DCM, owing to MEG being a more direct neuronal measure with higher temporal resolution. Each brain area in the MEG DCM network is modelled via the combined effects of populations of large numbers of neurons. These neuronal populations can be modelled using *mean-field* or *neural mass* approximations, in which the population behaviour is captured using probability distributions over the neuronal state variables (Deco et al. 2008). Specifically, in M/EEG DCM, there are three sub-populations within each brain area, corresponding to excitatory pyramidal neurons, excitatory spiny

stellate neurons, and inhibitory inter neurons (David et al. 2006). More recently M/EEG DCM has been extended to work with so-called conductance-based models, which model state variables for the transmembrane potentials and for different channel conductances (Marreiros et al. 2010). Note that these conductance-based models are particularly attractive biophysical models to work with, since they are directly related to specific synaptic processes, and can be used to investigate experimental effects of altering specific neurotransmitters (Moran et al. 2011). Arguably, the most successful version of DCM for electrophysiology, has been DCM for steady state responses (Moran et al. 2009), where the temporally stationary frequency response at each brain area in M/EEG or LFP data is modelled directly (rather than the full time series). This includes the demonstration that steady state response DCM can recover known changes in synaptic transmission following neurochemical modulation in rodents (Moran et al. 2008) or MEG in humans (Moran et al. 2011), and that it can track dose-dependent changes in excitation and inhibition, under varying levels of anaesthesia in rodents (Moran et al. 2011).

5.5.3 Kuramoto Oscillators

Coupled mean-field models of neurons tend to produce dynamics that are oscillatory. So an alternative strategy has been to circumvent the complexity of a full neuronal model (albeit at the expense of biophysical interpretability of the parameters), and to model each brain area's population dynamics as a Kuramoto oscillator (Cabral et al. 2011; Shanahan 2010; Breakspear et al. 2010). As in the full biophysical models, these phenomenological models can incorporate endogenous noise, and biophysical parameters such as conduction delays; and have been shown to simulate emergent dynamics, e.g. multistability, similar to those found in "resting" state FMRI (Cabral et al. 2011) and MEG (Cabral et al. 2013) data. A more extensive review of biophysical network models, particularly with regards to their more general role in using multi-modal neuroimaging data to inform human connectomics can be found in (Woolrich and Stephan 2013).

6 Concluding Remarks

In this chapter we have introduced the topic of functional connectivity measurement in MEG. We have discussed source space localisation, the advantages that it brings, and also its limitations in terms of source leakage. We have introduced a multitude of metrics for the measurement of functional connectivity using MEG data; including fixed phase metrics such as coherence or phase locking value, envelope correlation metrics, independent component analysis, and generalised synchronisation. We have also introduced the principles behind reduction of spurious functional connectivity via assessment of the imaginary part of coherence, phase

locking index, and removal of zero-phase-lag interaction via linear regression. The direct nature of the measurements, coupled with exquisite temporal resolution and good spatial resolution make MEG one of the most attractive non-invasive methods for assessment of functional connectivity and this has been evidenced with some of the exciting findings summarised in Sect. 4. Finally we have put forward some ideas for future studies, in particular the introduction of effective connectivity which promises to be an important tool for future research into understanding the temporal dynamics of brain networks.

References

Arroyo S, Lesser RP (1993) PET, MRI, and epilepsy. Neurology 43(10):2156

Astolfi L, Cincotti F, Mattia D, Babiloni C, Carducci F, Basilisco A, Rossini PM, Salinari S, Ding L, Ni Y, He B, Babiloni F (2005) Assessing cortical functional connectivity by linear inverse estimation and directed transfer function: simulations and application to real data. Clin Neurophysiol: Off J Int Fed Clin Neurophysiol 116(4):920–932

Astolfi L, Cincotti F, Mattia D, De Vico Fallani F, Tocci A, Colosimo A, Salinari S, Marciani MG, Hesse W, Witte H, Ursino M, Zavaglia M, Babiloni F (2008) Tracking the time-varying cortical connectivity patterns by adaptive multivariate estimators. IEEE Trans Biomed Eng 55(3):902–913

Baker AH, Luckhoo et al (2012) Investigating the temporal dynamics of resting state brain connectivity using magnetoencephalography. Proceeding of HBM conference

Bartel P, Blom M, van der Meyden C, de Klerk S (1988) Effects of single doses of diazepam, chlorpromazine, imipramine and trihexyphenidyl on visual-evoked potentials. Neuropsychobiology 20(4):212–217

Beckmann CF, DeLuca M, Devlin JT, Smith SM (2005) Investigations into resting-state connectivity using independent component analysis. Philos Trans R Soc Lond B Biol Sci 360(1457):1001–1013

Berger H (1929) Uber das elektrenephalogramm des menschen. Arch Psychiatr Nervenkrankheiten 87:527–570

Birn RM, Diamond JB, Smith MA, Bandettini PA (2006) Separating respiratory-variation-related fluctuations from neuronal-activity-related fluctuations in fMRI. NeuroImage 31(4):1536–1548

Birn RM, Murphy K, Bandettini PA (2008) The effect of respiration variations on independent component analysis results of resting state functional connectivity. Hum Brain Mapp 29(7):740–750

Biswal B, Yetkin FZ, Haughton VM, Hyde JS (1995) Functional connectivity in the motor cortex of resting human brain using echo-planar MRI. Magn Reson Med: Off J Soc Magn Reson Med/Soc Magn Reson Med 34(4):537–541

Bloom AS, Hoffmann RG, Fuller SA, Pankiewicz J, Harsch HH, Stein EA (1999) Determination of drug-induced changes in functional MRI signal using a pharmacokinetic model. Hum Brain Mapp 8(4):235–244

Bob P, Palus M, Susta M, Glaslova K (2008) EEG phase synchronization in patients with paranoid schizophrenia. Neurosci Lett 447(1):73–77

Breakspear M, Heitmann S, Daffertshofer A (2010) Generative models of cortical oscillations: neurobiological implications of the kuramoto model. Front Hum Neurosci 4:190

Breiter HC, Gollub RL, Weisskoff RM, Kennedy DN, Makris N, Berke JD, Goodman JM, Kantor HL, Gastfriend DR, Riorden JP, Mathew RT, Rosen BR, Hyman SE (1997) Acute effects of cocaine on human brain activity and emotion. Neuron 19(3):591–611

Bressler SL, Kelso JA (2001) Cortical coordination dynamics and cognition. Trends Cogn Sci 5(1):26–36

Britz J, Van De Ville D, Michel CM (2010) BOLD correlates of EEG topography reveal rapid resting-state network dynamics. NeuroImage 52(4):1162–1170

Broca P (2011) Remarks on the seat of spoken language, followed by a case of Aphasia (1861). Neuropsychol Rev 21(3):227–229

Brookes MJ, Gibson AM, Hall SD, Furlong PL, Barnes GR, Hillebrand A, Singh KD, Holliday IE, Francis ST, Morris PG (2005) GLM-beamformer method demonstrates stationary field, alpha ERD and gamma ERS co-localisation with fMRI BOLD response in visual cortex. NeuroImage 26(1):302–308

Brookes MJ, Hale JR, Zumer JM, Stevenson CM, Francis ST, Barnes GR, Owen JP, Morris PG, Nagarajan SS (2011a) Measuring functional connectivity using MEG: methodology and comparison with fcMRI. NeuroImage 56(3):1082–1104

Brookes MJ, Liddle EB, Hale JR, Woolrich MW, Luckhoo H, Liddle PF, Morris PG (2012a) Task induced modulation of neural oscillations in electrophysiological brain networks. NeuroImage 63(4):1918–1930

Brookes MJ, Vrba J, Robinson SE, Stevenson CM, Peters AM, Barnes GR, Hillebrand A, Morris PG (2008) Optimising experimental design for MEG beamformer imaging. NeuroImage 39(4):1788–1802

Brookes MJ, Woolrich M, Luckhoo H, Price D, Hale JR, Stephenson MC, Barnes GR, Smith SM, Morris PG (2011b) Investigating the electrophysiological basis of resting state networks using magnetoencephalography. Proc Natl Acad Sci USA 108(40):16783–16788

Brookes MJ, Woolrich MW, Barnes GR (2012b) Measuring functional connectivity in MEG: a multivariate approach insensitive to linear source leakage. NeuroImage 63(2):910–920

Brookes MJ, Zumer JM, Stevenson CM, Hale JR, Barnes GR, Vrba J, Morris PG (2010) Investigating spatial specificity and data averaging in MEG. NeuroImage 49(1):525–538

Cabral J, Hugues E, Sporns O, Deco G (2011) Role of local network oscillations in resting-state functional connectivity. NeuroImage 57(1):130–139

Cabral J, Luckhoo H, et al (2013) Revealing underlying neural mechanisms of spontaneous MEG functional connectivity: oscillatory network interactions can lead to structured band-limited power fluctuations. Under Revision

Canolty RT, Edwards E, Dalal SS, Soltani M, Nagarajan SS, Kirsch HE, Berger MS, Barbaro NM, Knight RT (2006) High gamma power is phase-locked to theta oscillations in human neocortex. Science 313(5793):1626–1628

Chang C, Glover GH (2010) Time-frequency dynamics of resting-state brain connectivity measured with fMRI. NeuroImage 50(1):81–98

Craddock RC, Holtzheimer PE 3rd, Hu XP, Mayberg HS (2009) Disease state prediction from resting state functional connectivity. Magn Reson Med: Off J Society Magn Reson Med/Soc Magn Reson Med 62(6):1619–1628

Dauwels J, Vialatte F, Cichocki A (2010a) Diagnosis of Alzheimer's disease from EEG signals: where are we standing? Curr Alzheimer Res 7(6):487–505

Dauwels J, Vialatte F, Musha T, Cichocki A (2010b) A comparative study of synchrony measures for the early diagnosis of Alzheimer's disease based on EEG. NeuroImage 49(1):668–693

David O, Kiebel SJ, Harrison LM, Mattout J, Kilner JM, Friston KJ (2006) Dynamic causal modeling of evoked responses in EEG and MEG. NeuroImage 30(4):1255–1272

de Pasquale F, Della Penna S, Snyder AZ, Lewis C, Mantini D, Marzetti L, Belardinelli P, Ciancetta L, Pizzella V, Romani GL, Corbetta M (2010) Temporal dynamics of spontaneous MEG activity in brain networks. Proc Natl Acad Sci USA 107(13):6040–6045

de Pasquale F, Della Penna S, Snyder AZ, Marzetti L, Pizzella V, Romani GL, Corbetta M (2012) A cortical core for dynamic integration of functional networks in the resting human brain. Neuron 74(4):753–764

Deco G, Jirsa VK, Robinson PA, Breakspear M, Friston K (2008) The dynamic brain: from spiking neurons to neural masses and cortical fields. PLoS Comput Biol 4(8):e1000092

Engel AK, Fries P, Singer W (2001) Dynamic predictions: oscillations and synchrony in top-down processing. Nat Rev Neurosci 2(10):704–716

Fox MD, Snyder AZ, Zacks JM, Raichle ME (2006) Coherent spontaneous activity accounts for trial-to-trial variability in human evoked brain responses. Nat Neurosci 9(1):23–25

Friedman J, Hastie T, Tibshirani R (2008) Sparse inverse covariance estimation with the graphical lasso. Biostatistics 9(3):432–441

Fries P (2005) A mechanism for cognitive dynamics: neuronal communication through neuronal coherence. Trends Cogn Sci 9(10):474–480

Friston K, Harrison L, Daunizeau J, Kiebel S, Phillips C, Trujillo-Barreto N, Henson R, Flandin G, Mattout J (2008) Multiple sparse priors for the M/EEG inverse problem. NeuroImage 39(3):1104–1120

Friston KJ (1999) Schizophrenia and the disconnection hypothesis. Acta Psychiatr Scand Suppl 395:68–79

Friston KJ (2011) Functional and effective connectivity: a review. Brain Connect 1(1):13–36

Friston KJ, Harrison L, Penny W (2003) Dynamic causal modelling. NeuroImage 19(4):1273–1302

Friston KJ, Li B, Daunizeau J, Stephan KE (2011) Network discovery with DCM. NeuroImage 56(3):1202–1221

Gaetz W, Edgar JC, Wang DJ, Roberts TP (2011) Relating MEG measured motor cortical oscillations to resting gamma-aminobutyric acid (GABA) concentration. NeuroImage 55(2):616–621

Gevins A, Cutillo B, Desmond J, Ward M, Bressler S, Barbero N, Laxer K (1994) Subdural grid recordings of distributed neocortical networks involved with somatosensory discrimination. Electroencephalogr Clin Neurophysiol 92(4):282–290

Gow DW Jr, Segawa JA, Ahlfors SP, Lin FH (2008) Lexical influences on speech perception: a Granger causality analysis of MEG and EEG source estimates. NeuroImage 43(3):614–623

Gray CM, Konig P, Engel AK, Singer W (1989) Oscillatory responses in cat visual cortex exhibit inter-columnar synchronization which reflects global stimulus properties. Nature 338(6213):334–337

Greenblatt DJ, Harmatz JS, von Moltke LL, Wright CE, Shader RI (2004) Age and gender effects on the pharmacokinetics and pharmacodynamics of triazolam, a cytochrome P450 3A substrate. Clin Pharmacol Ther 76(5):467–479

Gross J, Kujala J, Hamalainen M, Timmermann L, Schnitzler A, Salmelin R (2001) Dynamic imaging of coherent sources: Studying neural interactions in the human brain. Proc Natl Acad Sci USA 98(2):694–699

Guggisberg AG, Honma SM, Findlay AM, Dalal SS, Kirsch HE, Berger MS, Nagarajan SS (2008) Mapping functional connectivity in patients with brain lesions. Ann Neurol 63(2):193–203

Hale JR, Brookes MJ, Hall EL, Zumer JM, Stevenson CM, Francis ST, Morris PG (2010) Comparison of functional connectivity in default mode and sensorimotor networks at 3 and 7T. Magn Reson Mater Phy 23(5–6):339–349

Hall EL, Woolrich MW, Thomaz CE, Morris PG, Brookes MJ (2013) Using variance information in magnetoencephalography measures of functional connectivity. NeuroImage 67:203–212

Hall SD, Barnes GR, Furlong PL, Seri S, Hillebrand A (2010) Neuronal network pharmacodynamics of GABAergic modulation in the human cortex determined using pharmacomagnetoencephalography. Hum Brain Mapp 31(4):581–594

Hall SD, Holliday IE, Hillebrand A, Singh KD, Furlong PL, Hadjipapas A, Barnes GR (2005) The missing link: analogous human and primate cortical gamma oscillations. NeuroImage 26(1):13–17

Hämäläinen MS, Ilmoniemi RJ (1994) Interpreting magnetic fields of the brain: minimum norm estimates. Med Biol Eng Comput 32(1):35–42

Harrison L, Penny WD, Friston K (2003) Multivariate autoregressive modeling of fMRI time series. NeuroImage 19(4):1477–1491

Hipp JF, Hawellek DJ, Corbetta M, Siegel M, Engel AK (2012) Large-scale cortical correlation structure of spontaneous oscillatory activity. Nat Neurosci 15(6):884–890

Ioannides AA, Liu LC, Kwapien J, Drozdz S, Streit M (2000) Coupling of regional activations in a human brain during an object and face affect recognition task. Hum Brain Mapp 11(2):77–92

Jeong J, Gore JC, Peterson BS (2001) Mutual information analysis of the EEG in patients with Alzheimer's disease. Clinical Neurophysiol: Off J Int Fed Clin Neurophysiol 112(5):827–835

Jerbi K, Lachaux JP, N'Diaye K, Pantazis D, Leahy RM, Garnero L, Baillet S (2007) Coherent neural representation of hand speed in humans revealed by MEG imaging. Proc Natl Acad Sci USA 104(18):7676–7681

Kaminski M, Liang H (2005) Causal influence: advances in neurosignal analysis. Crit Rev Biomed Eng 33(4):347–430

Koch MA, Norris DG, Hund-Georgiadis M (2002) An investigation of functional and anatomical connectivity using magnetic resonance imaging. NeuroImage 16(1):241–250

Koenig T, Studer D, Hubl D, Melie L, Strik WK (2005) Brain connectivity at different time-scales measured with EEG. Philos Trans R Soc Lond B Biol Sci 360(1457):1015–1023

Kopell N, Ermentrout GB, Whittington MA, Traub RD (2000) Gamma rhythms and beta rhythms have different synchronization properties. Proc Natl Acad Sci USA 97(4):1867–1872

Kopell N, Kramer MA, Malerba P, Whittington MA (2010) Are different rhythms good for different functions? Front Hum Neurosci 4:187

Kujala J, Pammer K, Cornelissen P, Roebroeck A, Formisano E, Salmelin R (2007) Phase coupling in a cerebro-cerebellar network at 8–13 Hz during reading. Cereb Cortex 17(6):1476–1485

Lachaux JP, Rodriguez E, Martinerie J, Varela FJ (1999) Measuring phase synchrony in brain signals. Hum Brain Mapp 8(4):194–208

Leopold DA, Murayama Y, Logothetis NK (2003) Very slow activity fluctuations in monkey visual cortex: implications for functional brain imaging. Cereb Cortex 13(4):422–433

Locatelli T, Cursi M, Liberati D, Franceschi M, Comi G (1998) EEG coherence in Alzheimer's disease. Electroencephalogr Clin Neurophysiol 106(3):229–237

Loughnan BL, Sebel PS, Thomas D, Rutherfoord CF, Rogers H (1987) Evoked potentials following diazepam or fentanyl. Anaesthesia 42(2):195–198

Luckhoo H, Hale JR, Stokes MG, Nobre AC, Morris PG, Brookes MJ, Woolrich MW (2012) Inferring task-related networks using independent component analysis in magnetoencephalography. NeuroImage 62(1):530–541

Maharajh K, Teale P, Rojas DC, Reite ML (2010) Fluctuation of gamma-band phase synchronization within the auditory cortex in schizophrenia. Clin Neurophysiol: Off J Int Fed Clin Neurophysiol 121(4):542–548

Marreiros AC, Kiebel SJ, Friston KJ (2010) A dynamic causal model study of neuronal population dynamics. NeuroImage 51(1):91–101

Marrelec G, Krainik A, Duffau H, Pelegrini-Issac M, Lehericy S, Doyon J, Benali H (2006) Partial correlation for functional brain interactivity investigation in functional MRI. NeuroImage 32(1):228–237

Matsuzaki N, Juhasz C, Asano E (2013) Cortico-cortical evoked potentials and stimulation-elicited gamma activity preferentially propagate from lower- to higher-order visual areas. Clin Neurophysiol: Off J Int Fed Clin Neurophysiol 124(7):1290–1296

Moran RJ, Stephan KE, Dolan RJ, Friston KJ (2011) Consistent spectral predictors for dynamic causal models of steady-state responses. NeuroImage 55(4):1694–1708

Moran RJ, Stephan KE, Kiebel SJ, Rombach N, O'Connor WT, Murphy KJ, Reilly RB, Friston KJ (2008) Bayesian estimation of synaptic physiology from the spectral responses of neural masses. NeuroImage 42(1):272–284

Moran RJ, Stephan KE, Seidenbecher T, Pape HC, Dolan RJ, Friston KJ (2009) Dynamic causal models of steady-state responses. NeuroImage 44(3):796–811

Muthukumaraswamy SD, Edden RA, Jones DK, Swettenham JB, Singh KD (2009) Resting GABA concentration predicts peak gamma frequency and fMRI amplitude in response to visual stimulation in humans. Proc Natl Acad Sci USA 106(20):8356–8361

Nir Y, Mukamel R, Dinstein I, Privman E, Harel M, Fisch L, Gelbard-Sagiv H, Kipervasser S, Andelman F, Neufeld MY, Kramer U, Arieli A, Fried I, Malach R (2008) Interhemispheric correlations of slow spontaneous neuronal fluctuations revealed in human sensory cortex. Nat Neurosci 11(9):1100–1108

Nolte G, Bai O, Wheaton L, Mari Z, Vorbach S, Hallett M (2004) Identifying true brain interaction from EEG data using the imaginary part of coherency. Clin Neurophysiol: Off J Int Fed Clin Neurophysiol 115(10):2292–2307

Nolte G, Ziehe A, Nikulin VV, Schlogl A, Kramer N, Brismar T, Muller KR (2008) Robustly estimating the flow direction of information in complex physical systems. Phys Rev Lett 100(23):234101

Owen JP, Wipf DP, Attias HT, Sekihara K, Nagarajan SS (2012) Performance evaluation of the Champagne source reconstruction algorithm on simulated and real M/EEG data. NeuroImage 60(1):305–323

Penny WD, Stephan KE, Mechelli A, Friston KJ (2004) Comparing dynamic causal models. NeuroImage 22(3):1157–1172

Phillips WA, Silverstein SM (2003) Convergence of biological and psychological perspectives on cognitive coordination in schizophrenia. Behav Brain Sci 26(1):65–82; Discussion 82–137

Restuccia D, Valeriani M, Grassi E, Gentili G, Mazza S, Tonali P, Mauguiere F (2002) Contribution of GABAergic cortical circuitry in shaping somatosensory evoked scalp responses: specific changes after single-dose administration of tiagabine. Clin Neurophysiol: Off J Int Fed Clin Neurophysiol 113(5):656–671

Robinson S, Vrba J (1998) Functional neuroimaging by synthetic aperture magnetometry (SAM). In: Yoshimoto T, Kotani M, Kuriki S, Karibe H, Nakasato N (eds) Recent advances in biomagnetism. Tohoku University Press, Sendai, Japan, pp 302–305

Rodriguez E, George N, Lachaux JP, Martinerie J, Renault B, Varela FJ (1999) Perception's shadow: long-distance synchronization of human brain activity. Nature 397(6718):430–433

Roelfsema PR, Engel AK, Konig P, Singer W (1997) Visuomotor integration is associated with zero time-lag synchronization among cortical areas. Nature 385(6612):157–161

Roopun AK, Cunningham MO, Racca C, Alter K, Traub RD, Whittington MA (2008) Region-specific changes in gamma and beta2 rhythms in NMDA receptor dysfunction models of schizophrenia. Schizophr Bull 34(5):962–973

Sakkalis V (2011) Review of advanced techniques for the estimation of brain connectivity measured with EEG/MEG. Comput Biol Med 41(12):1110–1117

Schlögl A, Supp G (2006) Analyzing event-related EEG data with multivariate autoregressive parameters. Prog Brain Res 159:135–147

Schnitzler A, Gross J (2005) Normal and pathological oscillatory communication in the brain. Nat Rev Neurosci 6(4):285–296

Schoffelen JM, Gross J (2009) Source connectivity analysis with MEG and EEG. Hum Brain Mapp 30(6):1857–1865

Scholvinck ML, Friston KJ, Rees G (2012) The influence of spontaneous activity on stimulus processing in primary visual cortex. NeuroImage 59(3):2700–2708

Scholvinck ML, Leopold DA, Brookes MJ, Khader PH (2013) The contribution of electrophysiology to functional connectivity mapping. NeuroImage 80:297–306

Sekihara K, Hild KE 2nd, Nagarajan SS (2006) A novel adaptive beamformer for MEG source reconstruction effective when large background brain activities exist. IEEE Trans Biomed Eng 53(9):1755–1764

Sekihara K, Nagarajan SS, Poeppel D, Marantz A, Miyashita Y (2001) Reconstructing spatio-temporal activities of neural sources using an MEG vector beamformer technique. IEEE Trans Biomed Eng 48(7):760–771

Shanahan M (2010) Metastable chimera states in community-structured oscillator networks. Chaos 20(1):013108

Singer W (1999) Neuronal synchrony: a versatile code for the definition of relations? Neuron 24(1):49–65, 111–125

Singer W, Gray CM (1995) Visual feature integration and the temporal correlation hypothesis. Annu Rev Neurosci 18:555–586

Singh KD, Barnes GR, Hillebrand A, Forde EM, Williams AL (2002) Task-related changes in cortical synchronization are spatially coincident with the hemodynamic response. NeuroImage 16(1):103–114

Smith SM, Fox PT, Miller KL, Glahn DC, Fox PM, Mackay CE, Filippini N, Watkins KE, Toro R, Laird AR, Beckmann CF (2009) Correspondence of the brain's functional architecture during activation and rest. Proc Natl Acad Sci USA 106(31):13040–13045

Smith SM, Miller KL, Moeller S, Xu J, Auerbach EJ, Woolrich MW, Beckmann CF, Jenkinson M, Andersson J, Glasser MF, van Essen DC, Feinberg DA, Yacoub ES, Ugurbil K (2012) Temporally-independent functional modes of spontaneous brain activity. Proc Natl Acad Sci USA 109(8):3131–3136

Smith SM, Miller KL, Salimi-Khorshidi G, Webster M, Beckmann CF, Nichols TE, Ramsey JD, Woolrich MW (2011) Network modelling methods for FMRI. NeuroImage 54(2):875–891

Stam CJ, Nolte G, Daffertshofer A (2007) Phase lag index: assessment of functional connectivity from multi channel EEG and MEG with diminished bias from common sources. Hum Brain Mapp 28(11):1178–1193

Stam CJ, van Dijk BW (2002) Synchronization likelihood: an unbiased measure of generalized synchronization in multivariate data sets. Physica D 163(3–4):236–251

Stephan KE, Weiskopf N, Drysdale PM, Robinson PA, Friston KJ (2007) Comparing hemodynamic models with DCM. NeuroImage 38(3):387–401

Tass P, Rosenblum MG, Weule J, Kurths J, Pikovsky A, Volkmann J, Schnitzler A, Freund HJ (1998) Detection of n:m phase locking from noisy data: application to magnetoencephalography. Phys Rev Lett 81(15):3291–3294

Towle VL, Carder RK, Khorasani L, Lindberg D (1999) Electrocorticographic coherence patterns. J Clin Neurophysiol 16(6):528–547

Van de Ville D, Britz J, Michel CM (2010) EEG microstate sequences in healthy humans at rest reveal scale-free dynamics. Proc Natl Acad Sci USA 107(42):18179–18184

Van Veen BD, vanDrongelen W, Yuchtman M, Suzuki A (1997) Localization of brain electrical activity via linearly constrained minimum variance spatial filtering. IEEE Trans Biomed Eng 44(9):867–880

Varela F, Lachaux JP, Rodriguez E, Martinerie J (2001) The brainweb: phase synchronization and large-scale integration. Nat Rev Neurosci 2(4):229–239

von Stein A, Chiang C, Konig P (2000) Top-down processing mediated by interareal synchronization. Proc Natl Acad Sci USA 97(26):14748–14753

Wharton S, Bowtell R (2012) Fiber orientation-dependent white matter contrast in gradient echo MRI. Proc Natl Acad Sci USA 109(45):18559–18564

Whittington MA, Traub RD, Jefferys JGR (1995) Synchronized oscillations in interneuron networks driven by metabotropic glutamate-receptor activation. Nature 373(6515):612–615

Winterer G, Carver FW, Musso F, Mattay V, Weinberger DR, Coppola R (2007) Complex relationship between BOLD signal and synchronization/desynchronization of human brain MEG oscillations. Hum Brain Mapp 28(9):805–816

Wise RG, Tracey I (2006) The role of fMRI in drug discovery. J Magn Reson Imaging 23(6):862–876

Womelsdorf T, Schoffelen JM, Oostenveld R, Singer W, Desimone R, Engel AK, Fries P (2007) Modulation of neuronal interactions through neuronal synchronization. Science 316(5831):1609–1612

Woolrich M, Hunt L, Groves A, Barnes G (2011) MEG beamforming using Bayesian PCA for adaptive data covariance matrix regularization. NeuroImage 57(4):1466–1479

Woolrich MW, Baker A, Luckhoo H, Mohseni H, Barnes G, Brookes M, Rezek I (2013) Dynamic state allocation for MEG source reconstruction. NeuroImage 77:77–92

Woolrich MW, Stephan KE (2013) Biophysical network models and the human connectome. NeuroImage 80:330–338

Wyler AR, Ojemann GA, Lettich E, Ward AA (1984) Subdural Strip Electrodes for Localizing Epileptogenic Foci. J Neurosurg 60(6):1195–1200

Zumer J, Stevenson C, Brookes M, Francis S, Morris P (2009) Deconvolved fMRI correlates with source-localised MEG as a function of neural frequency oscillation. In: Proceedings of the international society for magnetic resonance in medicine 2009, p 1672

Human Brain Oscillations: From Physiological Mechanisms to Analysis and Cognition

Ole Jensen, Eelke Spaak and Johanna M. Zumer

Abstract In the cognitive neuroscience community there is a strong and growing interest in the function of oscillatory brain activity. Brain oscillations can readily be detected with MEG, which also allows for indentifying the sources and networks producing the activity. The aim of this chapter is first to describe the physiological mechanisms responsible for generating brain oscillations in various frequency bands and regions. We will focus on insight gained from the animal literature and physiologically realistic computational modeling. Next, we will explain the signal processing tools typically applied to characterize oscillatory brain activity from human electrophysiological data in the context of cognitive paradigms. The final section will address the main ideas on the functional role of brain oscillations in various frequency bands. This discussion will be focused on recent findings applying MEG.

Keywords Magnetoencephalography · Brain oscillations · Signal processing · Time-frequency analysis · Functional and cognitive relevance of oscillations · Computational modelling · Biophysical modelling · Alpha oscillations · Beta oscillations · Gamma oscillations · Delta oscillations · Theta oscillations

1 Introduction

Oscillations in the brain are produced by coordinated electrophysiological activity in large groups of neurons. Human brain oscillations were first discovered in 1929 by Hans Berger by measuring the electrical potentials between two electrodes placed at the scalp (Berger 1938). When the subject was asked to close her eyes,

O. Jensen (✉) · E. Spaak · J. M. Zumer
Radboud University Nijmegen, Donders Institute for Brain, Cognition and Behaviour, Centre for Cognitive Neuroimagin, Nijmegen, The Netherlands
e-mail: o.jensen@donders.ru.nl

S. Supek and C. J. Aine (eds.), *Magnetoencephalography*,
DOI: 10.1007/978-3-642-33045-2_17,

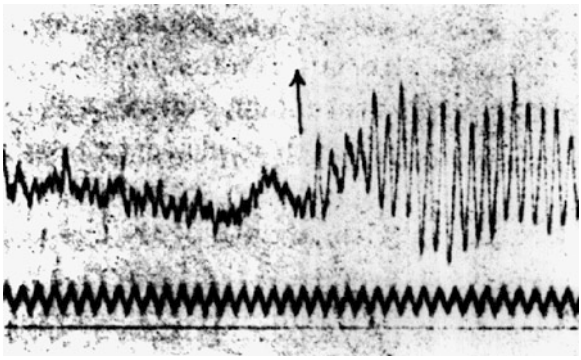

Fig. 1 An early EEG recording performed by Hans Berger. Prior to the arrow the subject is performing a mental arithmetic task. After the task stops, alpha returns. Reproduced from (Niedermeyer 1997)

Berger observed a strong ~10 Hz rhythmic activity in the electrical potential over time. Modulations in the alpha rhythm were also observed in response to simple cognitive manipulations (Fig. 1). The oscillatory activity in the 10 Hz band is termed the *alpha rhythm* or the *Berger rhythm*. Given that such brain oscillations can be readily measured at the scalp and observed with the naked eye, they must be a consequence of thousands of neurons oscillating in synchrony. As such, it is conceivable that brain oscillations will have a strong impact on how neuronal spiking is coordinated in both space and time. The coordination of neuronal spiking by oscillatory brain activity is thus important to investigate in the quest to understand the physiological basis of cognition.

Human brain oscillations have been known for almost a century and have been investigated with various degrees of vigor over the years (Shaw 2003). However, recently there has been a surge in the interest in oscillatory brain activity. This is partly explained by intracranial animal recordings relating spike timing to ongoing oscillations measured in the local electrical field potential. These studies have revealed that spike timing is locked to the phase of the ongoing oscillations in various brain regions and frequency bands (Fries et al. 2001; O'Keefe and Recce 1993; Bollimunta et al. 2008; Pesaran et al. 2002). What also has kindled the interest in brain oscillations is the fact that they are strongly modulated during cognitive tasks. There is now a rich literature reporting on the modulation of brain oscillations by a wealth of tasks spanning from simple perception to higher levels of cognitive processing such as language comprehension (Buzsáki 2006). In particular, MEG recordings using hundreds of sensors have made it possible to identify and locate the source of the brain oscillations (Hari and Salmelin 1997; Siegel et al. 2012; Varela et al. 2001; Tallon-Baudry and Bertrand 1999; Vrba and Robinson 2001; Singh et al. 2002). Further, the theoretical basis of the functional role of neuronal activity coordinated by oscillations is in rapid development (Fries et al. 2007; Jensen et al. 2012a; Fell and Axmacher 2011; Lisman 2005; Mehta 2001). These developments, in combination with improved computer speed and the development of signal-processing tools, have now made human electrophysiological recordings focusing on brain oscillations a strong research area.

The aim of this chapter is first to describe the physiological mechanisms generating oscillations in various frequency bands. We will then describe how these oscillations can be measured and quantified in humans. Finally we will discuss current ideas on the functional role of brain oscillations for cognitive processing. Each section will be organized according to the conventionally defined frequency brands. However, it should be made clear from the onset that these frequency bands are somewhat arbitrarily defined. It is currently debated to what extent distinct brain oscillations should be defined according to frequency band or according to function.

2 Physiological Mechanisms

We have probably all had the following experience: after a play or a concert the audience is applauding. While the audience initially is clapping at a different pace and out of synchrony, they suddenly enter a mode where everybody is clapping in synchrony in a rhythmic manner. What happens is a self-organizing phenomenon where the dynamics emerge from interactions between the individual persons in the audience without external organization. A key requirement for this phenomenon is communication between the individuals in the audience. The communication is constituted by auditory perception of the clapping sounds heard from the other persons. A second key requirement is an inherent drive to clap in pace with the rest of the crowd or, stated differently, the timing of the clapping of an individual is adjusted in phase and frequency according to the summed clapping sound from the audience. Likewise, neurons coupled in a network often show the emergence of spontaneous oscillations (Buzsáki 2006; Traub et al. 1999; Wang 2010). In this case, the communication is constituted by the synaptic interactions between the neurons. The phase- and frequency-adjustments are determined by how the electrical membrane dynamics respond to the synaptic currents. Spontaneous neuronal oscillations have been defined in a wide range of frequency bands. We will here discuss the different physiological mechanisms thought to be responsible for determining the characteristic frequencies of these oscillations and the neuronal synchronization properties underlying them.

2.1 Gamma Oscillations

Neuronal synchronization in the gamma band (30–100 Hz) has been intensively studied via both in vivo and in vitro recordings (Buzsaki and Wang 2012; Traub and Whittington 2010). Further extensive theoretical work has been done in order to understand the dynamical principles creating these oscillations.

Much empirical work has focused on gamma oscillations in various animals and brain regions. For instance there has been a strong interest in the gamma

activity generated in the visual system. In cats, monkeys, and humans, gamma oscillations can be observed in response to visual gratings (Gray et al. 1989; Bosman et al. 2012; Hoogenboom et al. 2006). Another line of research has focused on gamma oscillations in the rat hippocampus (Chrobak and Buzsaki 1996). In particular it has been found that the power in the gamma band is locked to the phase of theta oscillations in the behaving rat (Bragin et al. 1995; Belluscio et al. 2012; Colgin et al. 2009). Importantly, it is also possible to identify the gamma oscillations in slice preparations of the rat and mouse hippocampus. This has allowed for both pharmacological and genetic manipulations aimed at identifying the core mechanism determining neuronal synchronization in the gamma band. This work has then informed computational modeling which has identified the dynamical properties determining both frequency and synchronization properties (Buzsaki and Wang 2012).

The theoretical work has resulted in two key mechanisms which can produce gamma band oscillations, termed the "interneuronal network gamma" (ING) mechanism and the "pyramidal-interneuronal network gamma" (PING) mechanism (Whittington et al. 2000; Tiesinga and Sejnowski 2009).

The ING mechanism (sometimes also referred to as the I-I, inhibitory-inhibitory, model) refers to gamma oscillations produced by interactions between interneurons alone, communicating through gamma-aminobutyric acid (GABA) synapses. These oscillations can be observed in hippocampal slice preparations where the AMPA and NMDA synaptic inputs from pyramidal cells are blocked by CNQX and APV, respectively (Whittington et al. 1995), thus proving that input from pyramidal neurons is not required for the generation of gamma. To observe the oscillations in slice preparations it is essential that the activity of the interneurons is boosted by cholinergic and metabotropic glutamate receptor agonists. The oscillations are abolished if a GABAergic antagonist is applied. The important theoretical insight is that inhibitory interactions alone can serve to synchronize a neuronal population (Van Vreeswijk et al. 1994).

The basic ING mechanism can be understood as follows. Consider one neuron coupled to itself by a GABAergic synapse, receiving some tonic excitatory input. After the neuron fires, the GABAergic feedback will hyperpolarize the membrane potential. The duration of the hyperpolarization is determined by the kinetics of the $GABA_A$ receptor and will typically last 10–20 ms, i.e., the duration of a gamma cycle at 50–100 Hz. When the GABAergic hyperpolarization wanes, the cell will fire again (Fig. 2a). Now consider two inhibitory interneurons mutually coupled with GABAergic connections. If they both fire at about the same time, the GABAergic connections will provide mutual inhibition. When the inhibition wanes, the cells will fire simultaneously (Fig. 2b). Thus zero-lag synchronization emerges. One might also consider the alternative case in which the two neurons fire out of phase. In this case the first neuron might inhibit the second, delaying its firing. When the second neuron fires it will inhibit the first (Fig. 2c). This results in anti-phase synchronization. The conditions for zero-lag and anti-phase synchronization have been studied in the context of physiologically realistic parameters (Van Vreeswijk et al. 1994; Gerstner et al. 1996). As it turns out, the kinetics of the

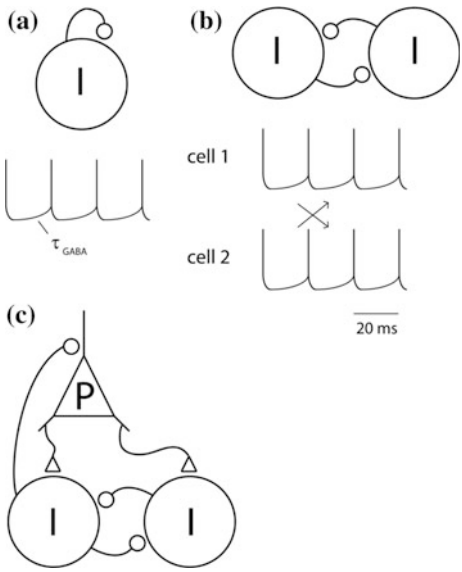

Fig. 2 The ING and PING mechanisms for neuronal synchronization in the gamma band (**a**) Consider one inhibitory neuron coupled to itself with a GABAergic synapse. If sufficiently depolarized, it will fire rhythmically with a frequency determined by the kinetics of the GABAergic feedback. **b** Consider two inhibitory neurons mutually coupled. When coupled they might fire either in phase or in anti-phase. It turns out that synchronized firing (in phase) typically is the most dynamically stable mode given realistic physiological parameters. This constitutes a mechanism for neuronal synchronization in the gamma band that generalizes to larger populations of interneurons. It is termed *interneuronal network gamma* (ING). **c** A second mechanism for the fast oscillations involves pyramidal neurons, and is termed *pyramidal-interneuronal network gamma* (PING). According to this mechanism the pyramidal neurons periodically excite the interneurons, which in return induce synchronized inhibitory post-synaptic potentials (IPSPs) in the pyramidal neurons

$GABA_A$ receptor are a main player in determining the synchronization properties. Importantly, for physiologically realistic parameters, zero-lag synchronization is typically the most stable model (Van Vreeswijk et al. 1994; Wang and Buzsaki 1996). This synchronization scheme is also robust to delays in synaptic transmission. In short, when two interneurons are mutually coupled with GABAergic synaptic input they will typically enter a mode in which they rhythmically synchronize their firing. The frequency of firing is determined by the kinetics of the GABAergic feedback. Now consider what happens when a third or more inhibitory interneurons are added to the network. They will also fire synchronously with the rest. This mechanism explains how gamma oscillations can emerge from a network of interneurons only.

The PING mechanism (also referred to as the E-I, excitatory-inhibitory, model) constitutes another important principle by which neuronal oscillations can emerge in the gamma band. In contrast to the ING mechanism, the PING mechanism

employs two different populations of cells: one excitatory and one inhibitory, reciprocally connected to each other (Whittington et al. 2000; Wilson and Cowan 1972; Ermentrout and Kopell 1998; Borgers and Kopell 2003). In the PING mechanism, AMPAergic projections of the excitatory population onto the inhibitory population provide fast excitation of the latter cells. These inhibitory cells, in turn, provide fast inhibition of the excitatory cells through GABAergic synapses. When the inhibition on the excitatory cells wears off, the excitatory cells fire. The excitatory firing results, a short delay later, in inhibitory firing, thus bringing the network into an oscillatory state. For this oscillatory state to happen, the strength of inhibition and excitation needs to be properly balanced. Note that the short delay between excitatory and inhibitory firing is the crucial factor for determining the oscillatory properties in this network (Borgers and Kopell 2003). This delay is composed of both axonal conduction and synaptic delays (Leung 1982).

For both ING and PING models, GABAergic interneurons are key players, a finding which is corroborated by the observation that GABA concentration in the brain predicts an individual's peak gamma frequency (Muthukumaraswamy et al. 2009). Even though either of these two mechanisms could in principle explain all gamma oscillation phenomena in the brain, there is ample evidence that both of them are at work. For instance, when synaptic inhibition onto inhibitory cells is disabled in the mouse hippocampus, gamma activity is not significantly affected, providing evidence that some mechanism other than ING is at work (Wulff et al. 2009). In contrast, it is known that gamma oscillations are also prominent in structures that do not have dense excitatory-to-inhibitory connections (Brown et al. 2002; Fujisawa and Buzsaki 2011), indicating that PING cannot be the whole story. Thus, whether the PING or the ING mechanism is dominating might depend on the brain region and species (Tiesinga and Sejnowski 2009; Buzsaki and Wang 2012).

Given the likelihood that inhibitory interneurons are crucial for generating gamma oscillations, is anything known about the specific *type* of inhibition involved in this mechanism? Inhibitory interneurons can be broadly classified along two dimensions: fast-spiking versus non-fast-spiking, and soma-targeting versus dendrite-targeting. Several strands of evidence indicate that fast-spiking, soma-targeting basket cell interneurons (specifically, those that express parvalbumin (Kawaguchi et al. 1987)) are crucial in the generation of gamma rhythms (Bartos et al. 2007). These cells are abundant (Freund and Buzsaki 1996), form extensive interconnections amongst one another (Gulyas et al. 1999), and a single basket cell can project onto more than one thousand pyramidal cells (Cobb et al. 1995). These conditions enable basket cells to impose their gamma rhythm onto a pyramidal cell network; the population activity of the pyramidal cells then is reflected in the local field potential (LFP) and MEG signal. Furthermore, gamma activity is associated with strong perisomatic current sinks, consistent with the soma-targeting properties of basket cells (Mann et al. 2005). Finally, fast-spiking basket cells have resonance properties in the gamma range (Pike et al. 2000; Cardin et al. 2009) and typically produce ~ 1 spike per gamma cycle, phase-locked to the population rhythm (Gloveli et al. 2005). Further evidence shows that

gamma-generating interneurons are likely coupled through shunting inhibitory synapses and by gap junctions, which increases their robustness against heterogeneous input (Vida et al. 2006; Bartos et al. 2007).

Apart from gamma oscillations, another high-frequency component of LFP and MEG signals can be distinguished. Sometimes referred to as *high gamma*, relatively broadband high-frequency activity (>85 Hz) is also known as *epsilon* activity (Freeman 2007; Belluscio et al. 2012) or the *chi* band (Miller et al. 2008). It is currently unclear to what extent this activity should be considered a rhythm. The high-frequency broadband spectral components might reflect the spectral fingerprint of neuronal spiking (Manning et al. 2009; Belluscio et al. 2012).

2.2 Beta Oscillations

Typically, beta oscillations (14–30 Hz) are considered to be generated by similar mechanisms as the gamma rhythm. A large-scale simulation of a network generating beta oscillations has been implemented (Traub et al. 1999), based on in vitro observations of hippocampal slices that alternate between gamma and beta states. It has been shown that the essential features of this large-scale network can be reproduced in a much simpler network, which bears strong resemblance to the PING mechanism of gamma generation (Kopell et al. 2000).

Imagine again the PING network described earlier, in which alternating balanced inhibitory and excitatory bursts between two coupled populations result in a network oscillating at gamma frequency. It turns out that only two changes need to be made to this model for it to generate beta oscillations: first, a slow potassium after-hyperpolarization (AHP) conductance is added to the excitatory cells, and, second, the excitatory cells have recurrent connections to themselves. When an excitatory cell has fired in this regime, it cannot fire again in the next gamma cycle, because then the AHP conductance prevents the cell's membrane potential from reaching threshold. Only on the next cycle can the cell fire again. This phenomenon is known as "beat-skipping" and results in the excitatory cells synchronizing at a beta frequency that is half the frequency of the interneuronal gamma rhythm. Note that because the inhibitory cells receive phasic excitatory input from the pyramidal cells, when one pyramidal cell fires, other pyramidal cells on the next gamma cycle will be silenced by the recurrent inhibitory connection. This leads to a regime where, although each individual pyramidal cell fires in a beta rhythm, the population activity is still of gamma frequency. The additional change to the model, the addition of recurrent connections between excitatory cells, ensures the synchronization: because the excitatory cells excite one another, they will fire before the inhibition from the GABAergic cells arrives. The latter route requires two synapses, while the recurrent connection is monosynaptic. Thus, a "PINB" (pyramidal-interneuronal network beta) mechanism might explain the occurrence of beta oscillations in local neuronal networks (Kopell et al. 2000), such as in the hippocampus.

Just as PING is not the whole story for gamma, so PINB is not the whole story for beta. Beta oscillation amplitude over human sensorimotor cortex is increased when benzodiazepines are administered, while the oscillation frequency is decreased (Jensen et al. 2005). Benzodiazepines mainly act by increasing GABAergic conductances. In a PINB-regime, increasing GABAergic conductances has the effect of decreasing the spiking frequency of the inhibitory cells, thus allowing more of the excitatory cells to fire, which in turn then excites the inhibitory cells more, leading to an equilibrium in which the net effect on network frequency is negligible. Therefore, the PINB mechanism cannot explain the robustly observed effect of benzodiazepines on beta oscillations. In contrast, an "INB" mechanism, analogous to ING for gamma, is able to explain these findings: in this mechanism, excitation of the inhibitory cells is tonic, so the period of the inhibitory cells' firing is determined only by the recurrent inhibitory connections. Since these become stronger under administration of benzodiazepines, the period of the inhibition becomes longer, in line with the observed results. As the period increases, a larger fraction of pyramidal cells will be released from inhibition during the refractory period. This explains the increase in beta power and decrease in frequency with benzodiazepines in sensorimotor areas observed in humans (Jensen et al. 2005).

2.3 Theta Oscillations

The mechanisms described above for the generation of gamma and beta oscillations are primarily *local* models: they describe how oscillations of a particular frequency can arise through interaction of neuronal populations within the same brain structure. This allows for related models to account for gamma and beta activity in different structures such as the hippocampus, entorhinal cortex, or neocortex. The lower-frequency theta oscillations (4-8 Hz), primarily (though not exclusively) observed in hippocampus, are typically thought to be generated by an interaction between several brain regions, and might not sufficiently be explained by a local model (Wang 2010).

Classically, the medial septum-diagonal band of Broca (MS-DBB) has been regarded as the crucial brain structure for the generation of the hippocampal theta rhythm, a notion which is corroborated by the observation that lesioning or inactivating the MS-DBB effectively obliterates theta in the rat brain (Stewart and Fox 1990). The MS-DBB provides a tonic cholinergic drive to the hippocampus which greatly influences the amplitude of the hippocampal theta rhythm (Lee et al. 1994). In addition, GABAergic interneurons in the MS-DBB project selectively onto hippocampal interneurons and these projections likely provide the phasic entrainment (Freund and Antal 1988; Buzsaki 2002). Although originally the MS-DBB was regarded as *the* pace-making structure for theta oscillations (i.e., it was thought that the MS-DBB generates theta by itself and then imposes its theta rhythm onto the regions to which it projects), later studies have found that interactions between the MS-DBB and the hippocampus, as well as intra-hippocampal processes, are just as

essential for theta generation. For instance, it turns out that an in vitro preparation of an entire isolated hippocampus is still capable of generating theta oscillations (Goutagny et al. 2009). Furthermore, dendritic inhibition of pyramidal cells by oriens lacunosum-moleculare (OLM) interneurons, the presence of slow $GABA_A$-receptors on hippocampal cells, and the value of several specific active membrane conductances all are important for the occurrence of hippocampal theta oscillations (Buzsaki 2002; Rotstein et al. 2005: Kopell et al. 2010; Wang 2010).

2.4 Alpha oscillations

Alpha oscillations (8-12 Hz) can be robustly observed in both the thalamus and the neocortex. Which of these two regions is the primary pacemaker of the alpha rhythm is still under debate. Generators of the alpha activity have been found with certainty in both thalamus and in neocortex (Lopes da Silva et al. 1980; Bollimunta et al. 2008, 2011). The neocortical alpha activity measured by MEG likely stems from an interaction between the thalamic and neocortical generators.

Most is known about the generation of thalamocortical (TC) alpha oscillations. The lateral geniculate nucleus (LGN) of the thalamus contains a particular set of TC neurons, the high-threshold bursting TC neurons, or HTC neurons. These neurons, coupled through gap junctions, fire bursts of spikes in synchrony with alpha oscillations in the field potential (Hughes and Crunelli 2005). However, this cannot be the whole story of TC alpha, since the main projections conveying visual information from thalamus to cortex are from relay-mode cells (Llinas and Jahnsen 1982), and not HTC cells. So how do the HTC and relay-mode cells interact? Extensive physiological and computational work has converged on the following model (Lorincz et al. 2009; Vijayan and Kopell 2012). HTC cells rhythmically excite thalamically local GABAergic interneurons, probably through axon collaterals. This causes these interneurons to also fire at alpha frequency. Depending on the strength of tonic excitation, the interneurons can fire in one of two modes: a rhythm of single spikes near the trough of an alpha cycle, or a rhythm of spike bursts near the peak of alpha. The interneurons project extensively to the relay-mode cells, thus resulting in an alpha-frequency occurrence of IPSPs on their membrane potential. Because of the two modes of firing of the interneurons, the relay-mode cells can send their information to the cortex in two distinct temporal framing regimes, i.e. at different alpha phases (Lorincz et al. 2009; Vijayan and Kopell 2012).

Apart from alpha activity, sleep spindles are also reflected in the frequency range of 10-15 Hz. These are thought to be generated by mechanisms related to the thalamocortical alpha oscillation, with some important differences: cells of the reticular nucleus are believed to be crucial for the spindle rhythm, and spindle activity emerges only in a regime of widespread (as opposed to sparse) inhibition, as would be expected for a sleep rhythm (Destexhe et al. 1993; Terman et al. 1996).

2.5 Delta Oscillations

Delta oscillations (1–4 Hz) are prominent during sleep, just like the spindle rhythm. A model has been proposed in which these two rhythms are generated by the same neuronal circuitry: an interaction between thalamic reticular (RE) cells, thalamocortical (TC) cells, and neocortical excitation of the reticular cells. In the generation of spindles, RE cells inhibit TC cells through $GABA_A$ and $GABA_B$ receptors. The TC cells project with excitatory connections to the cortex and the RE cells, and the cortex excites the RE cells. A network in this configuration generates spindle activity. When the conductance of the RE cells is changed such that they become less sensitive to the excitatory input of the TC cells, this causes the fast inhibition of the TC cells through $GABA_A$-receptors to be functionally removed. The slow inhibition through $GABA_B$ is unaltered. This gives rise to a rhythm in the delta frequency range during sleep (Terman et al. 1996). Delta activity also occurs during wakefulness (e.g. Lakatos et al. 2008); however, few if any models have been developed for the generation of delta during wakefulness.

2.6 Cross-Frequency Interactions

In addition to observing oscillations in distinct frequency bands, one can also observe *interactions* between those oscillations. In Sect. 3.4, the different types of cross-frequency interactions that can be observed are outlined. The neuronal mechanisms underlying cross-frequency interactions are currently not well understood. One possibility for the observed coupling between the hippocampal theta rhythm and the neocortical gamma rhythm (Sirota et al. 2008) is that the hippocampal theta rhythm is imposed onto fast-spiking interneurons in the neocortex by direct anatomical projections (Tierney et al. 2004; Gabbott et al. 2002). These interneurons are crucial for the generation of the gamma rhythm, as explained in the section on gamma activity above. The number of interneuron network spikes per gamma cycle is proportional to the measured gamma amplitude in the local field potential (and thus the MEG signal). Since the interneuron network spike rate is determined by the input to the network, whenever this input is time-varying at a certain low frequency (e.g., theta), the gamma amplitude will be modulated at the same frequency (Spaak et al. 2012b; Wulff et al. 2009).

3 Methods for Characterizing Oscillations

An oscillation as measured by MEG can most simply be thought of as a stationary sinusoidal signal, varying across time at a particular frequency. However, such pure signals do not exist in the brain, but rather neural data are mixes of sinusoidal

oscillations at varying frequencies whose peak amplitudes vary over time. This section describes how to compute meaningful quantities from these signals that characterize their frequency dependence and dynamics. Although the oscillations are recorded in the time domain (i.e., a signal that varies over time), often they can be better defined in the frequency domain (i.e., a signal whose amplitude and phase vary over frequency). The power spectral density (PSD) of a time series describes how its power (amplitude squared) is distributed with frequency. In this section, first we will describe the transformation of the raw (recorded) time series to the PSD and how the PSD is optimally computed for neuroscience applications. Second, we will describe how oscillations can alternatively be treated in the time domain and lastly, methods for computing within- and cross-frequency interactions. For further references on methods and computation, please see (Muthuswamy and Thakor 1998; Mitra and Pesaran 1999; Gross et al. 2013).

3.1 Power Spectral Density of Oscillatory Activity

Any time series can be re-written as a sum of sine waves with each wave having a frequency at the appropriate amplitude and phase. Vice versa, by knowing the amplitudes and phases of the waves, the original time series can be reconstructed. The amplitude and phase of the sine waves for all relevant frequencies can be determined from the Fourier Transform. Power is defined as the magnitude of the signal squared per time; thus the power spectral density describes how the squared amplitude for a given time window is distributed with frequency.

For discrete, digitized signals, such as those obtained from MEG, EEG, and invasive electrophysiological systems, the discrete Fourier Transform (DFT) is used to compute the amplitude and phase estimates for a finite number of frequencies. Thus, the PSD is the square of the DFT of a given discretized signal. The DFT is typically computed by the Fast Fourier Transform (FFT), a computationally fast and practical algorithm. Limits on the maximum frequency and the spacing of the estimated frequencies exist. First, the maximum frequency possible to be quantified, also called the Nyquist frequency, is half of the temporal sampling rate. For example, using a 1000 Hz sampling rate means that the maximum frequency at which information is estimable is at 500 Hz. If the underlying time signal contains information at a frequency higher than the Nyquist frequency, this information will bleed in at lower frequencies (termed "aliasing"), thus making this information irrecoverable and will corrupt the estimates at lower frequencies. Thus, it is imperative to low-pass filter the analog continuous signals prior to discretizing (Smith 1997). Indeed most commercial data acquisition systems will apply anti-aliasing filters via a lowpass filter at typically 1/4–1/3 of the sampling frequency. The second limit when converting recorded data to the frequency domain is the spacing between discrete frequencies. This spacing is referred to as the Rayleigh frequency and is equal to the inverse of the length of the temporal sampling window. For any finite signal, estimates of oscillatory power can only be

obtained at integer multiples of the Rayleigh frequency (for example, for a 400 ms data segment, estimates will be obtained at 2.5, 5, 7.5 Hz, etc.) (Mitra and Pesaran 1999; Pesaran 2008).

In theory, the estimate of the power spectrum from the FFT of a finite data segment is biased, as the true spectrum can only be obtained from an infinitely long segment. In practice, however, directly applying the FFT to longer segments of data is less desirable for at least three reasons. It will require long computational time, it assumes stationarity of the underlying signal, and also it does not exhibit the expected property of a decrease in variance with increased data length. For a long segment, the noise will be represented at a high spectral resolution determined by the Rayleigh frequency, but not be averaged over nearby frequency bins. As such, while the frequency resolution increases with long data length, the noise variance of the spectral estimate is not improved. *Welch's method* is one way to circumvent these concerns, by first "windowing" (i.e. cutting the data into N shorter equal-length segments) and then computing the power spectra per segment followed by averaging the spectra (Welch 1967). Figure 3 illustrates this, first by showing a long (20 s) time segment of a 20 Hz oscillation with added pink noise (Fig. 3a); a 1 s subset is shown in Fig. 3b. (Pink noise is noise drawn from a signal with a power spectral density following 1/f, in other words inversely proportional to frequency). If the FFT of the 20 s data is calculated (Fig. 3c), the peak at 20 Hz is strong, but also the noise is strong. In contrast, if the Welch method is used, whereby the FFTs of 20 ($N = 20$) segments, each 1 s long, are computed and averaged, the result is a smoothing over N adjacent frequency bins. This smoothing reduces the main peak at 20 Hz, but also reduces the noise, by the expected ratio of $1/\sqrt{N}$. Effectively, one compromises frequency resolution when averaging over N bins, but typically the increased signal-to-noise ratio is preferred over a small Rayleigh frequency, since neural oscillations typically fluctuate in frequency. (Note that in Fig. 3, the short 1 s segments were padded to a length of 20 s prior to FFT; padding is discussed further down).

Segmenting has the further advantage of only assuming/requiring short-time stationarity within one segment, as variation over segments can be examined for non-stationarity. However, care should be taken that the segments do not become too short, as the practical minimal data segment length to sufficiently capture an oscillation is suggested to be about 3–5 times the length of the period of the frequency of interest. Thus, for example, a segment not much shorter than 400 ms should be used to estimate the power and/or phase at 10 Hz. Longer time segments may be advised if characterization of precise frequency estimates are desired (e.g., determining the peak frequency of the alpha oscillation during an eyes-closed resting condition to within 0.5 Hz precision would require a 2 s window). However, at least two concerns become apparent with the use of shorter time windows. The first is the increased Rayleigh frequency. In the example above, sacrificing a Rayleigh frequency of 0.05 Hz from a 20 s window to 1 Hz from a 1 s window is usually acceptable for most research questions; however, a Rayleigh frequency of 5 Hz, resulting from a window length of 200 ms, may not be sufficiently precise. To mitigate this, one may *"pad"* a time window with extra zeros resulting in a

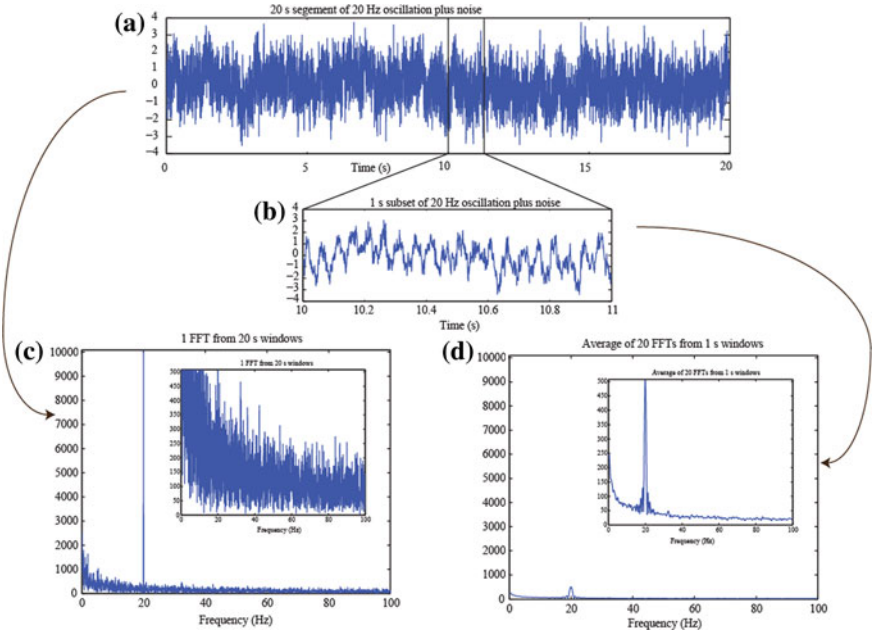

Fig. 3 Illustration of the averaging/smoothing over frequency provided by the Welch method using averaged spectra from shorter time windows. **a** A simulated 20 s long signal created from the addition of a 20 Hz sinusoid plus *pink* noise. **b** A zoomed in view of 1 s of the simulated signal. **c** The FFT of the data in (**a**). The inset is the same figure with a different y-scale. **d** The average of the 20 FFTs obtained from dividing the signal in (**a**) into 20 separate 1 s duration segments, with padding to 20 s length. The inset is the same figure with a different y-scale, but same y-scale as the inset in (**c**)

desired Rayleigh frequency. New information has not been gained at these intermediary frequency bins; the improved frequency resolution is a consequence of spectral interpolation. However, padding allows a spectrally smoothed representation to be depicted. In the situation of unequal time segments, for example due to unequal trial lengths between stimulus and response time, padding each segment to an equal length is necessary if these trials are to be averaged in the frequency domain and thus at the same frequency bins. The effect of padding is illustrated in Fig. 4

A second problem with shorter time windows is that more blurring (spectral leakage) of the PSD can occur. The original Fourier Transform assumes an infinitely long signal with periodic components. However, when a segmented time window is used, this is implicitly the multiplication of a boxcar-shaped window (zeroes everywhere except a segment of ones) with the original signal. Since multiplication in the time domain is equivalent to convolution in the frequency domain, the FFT of a windowed time series appears as the convolution of the FFT of the original signal (for example, a stick, or delta function, at 20 Hz for a pure

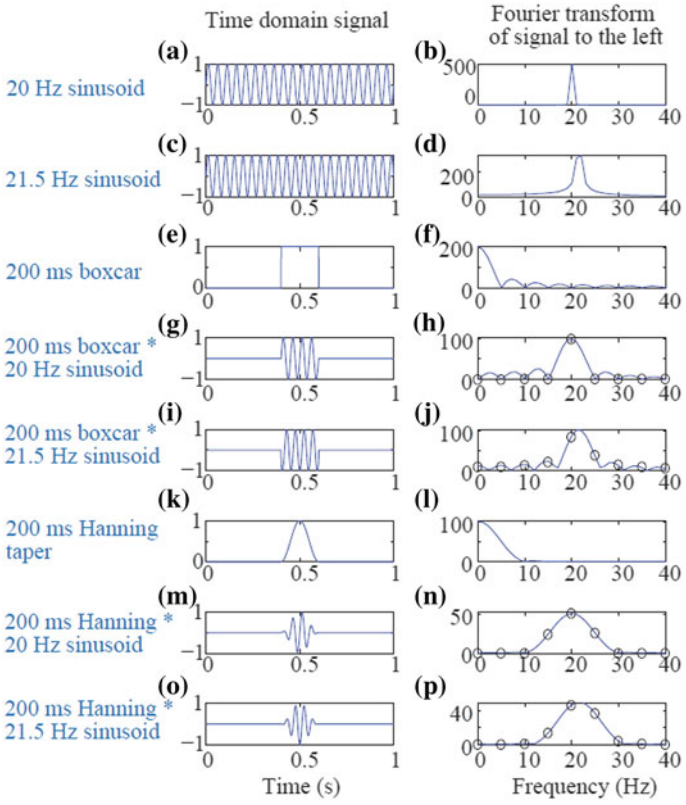

Fig. 4 Effect of window length, zero padding, and tapering on short window Fourier Transform. **a** 20 Hz sinusoid over 1 s. **b** FFT of (**a**). **c** 21.5 Hz sinusoid over 1 s. **d** FFT of (**c**); note the spectral leakage. **e** Boxcar window of length 200 ms. **f** FFT of (**e**). **g** Sinusoid from (**a**) multiplied by boxcar from (**e**). **h** Blue line is the FFT of 1 s padded segment from (**g**); *black circles* are the FFT from the 200 ms segment without padding. **i** Sinusoid from (**c**) multiplied by boxcar from (**e**). **j** Blue line is the FFT of 1 s padded segment from (**i**); *black circles* are the FFT from the 200 ms segment without padding. Again notice the bleeding. **k** Hanning taper of length 200 ms. **l** FFT of (**k**). **m** 20 Hz sinusoid from A multiplied by Hanning taper of (**k**). **n** FFT of (**m**), with the *blue line* resulting from padding to 1 s and the *black circles* from no padding of the 200 ms segment. **o** 21.5 Hz sinusoid from (**c**) multiplied by the Hanning taper of (**k**). **p** FFT of (**o**), with the *blue line* resulting from padding to 1 s and the *black circles* from no padding of the 200 ms segment. The Hanning taper effectively resolved the leakage but with the trade-off of increased spectral smoothing

20 Hz sinusoid) with the FFT of a boxcar, which is a sinc function. The resulting power spectral density contains power in the "tails" of the sinc function, outside the main peak of 20 Hz. This is illustrated in the example in Fig. 4. The time domain (left column) and frequency domain (right column) of several signals are shown. Figure 4a and 4c show sinusoids at 20 Hz and 21.5 Hz, respectively, with a sampling rate of 1000 Hz for duration of 1 s. The Rayleigh frequency is thus 1 Hz and the 20 Hz sinusoid can be well captured in the PSD as a sharp peak at

20 Hz and no power elsewhere (Fig. 4b). However, since the 21.5 Hz sinusoid contains its power at a frequency not at a multiple of the Rayleigh frequency, then the corresponding PSD exhibits a blurred peak near the true frequency but also power in other bands quite some distance from the true peak (Fig. 4d). The situation is worsened by using a shorter time window of 200 ms (sufficiently long to capture at least three periods of oscillation for both 20 Hz and 21.5 Hz), as shown in Fig 4g, i. The Rayleigh frequency is now 5 Hz; the PSD at every 5 Hz is shown in Figs 4h, j indicated by the black circles. The blue lines in these subfigures are computed from "zero padding" the 200 ms signal to a full 1 s length (as depicted in Fig. 4g, i). In Fig. 4h, the PSD of the 20 Hz sinusoid is again well captured with the peak power at 20 Hz and no power at the other sampled frequencies for the time window 200 ms; however, the FFT of the padded signal shows the leakage effects of the boxcar window. Furthermore, in Fig. 4j the bleeding of power to frequencies away from the true 21.5 Hz is strong, both in the unpadded (black circles) and padded (blue line) results.

An operation known as *tapering* can be used to mitigate the effect of the bleeding into far-away frequencies due to shorter time windows. Tapering is the explicit multiplication of the signal with some taper or window function, rather than relying on the implicit multiplication with a boxcar. Smoothing the sharp rise/fall of the boxcar edge leads to reduced leakage into further away frequencies. Tapering results in local smoothing of the peak frequency and thus assumes similarity of power in nearby frequencies (an assumption which is usually justified when analyzing brain signals). A common function used is the Hanning taper. A 200 ms version of the Hanning taper with zeros padded on either side is shown in Fig. 4k and its FFT is shown in Fig. 4l. When multiplying the windowed sinusoids by the Hanning taper (Fig. 4m, o), the resulting FFT of the sinusoids (Fig. 4n, p) now appear as the stick (delta function) at 20 or 21.5 Hz convolved with the smooth curve of Fig. 4l, rather than convolved with the bumpy curve of the sinc function in Fig. 4f. The short window of 200 ms still limits the Rayleigh frequency to 5 Hz and there is still some bleeding at nearby frequencies (e.g. at 15 and 25 Hz); however, the leakage at 10–30 Hz is greatly reduced. It is often recommended to demean before FFT as the baseline (DC) component can leak to other frequency bands.

The choice of which taper to use is based on the assumptions of the underlying true PSD. The Hanning taper illustrated minimizes the spectral leakage in the tails (also referred to as leakage in the side lobes) but results in a fairly wide blur around the true spectral peak (also referred to as a wide main lobe). Ideally, the taper choice should match the expected underlying spectral width. For example, in the alpha band of 8–12 Hz with a 4 Hz bandwidth, the Hanning taper over a 400 ms window gives a suitable match of the width of the main lobe (in fact, one roughly twice as narrow as that depicted in Fig. 4l, since the longer that the Hanning taper is in time, the narrower the lobe is in frequency). Other functions such as the Hamming taper can also be used. The Hanning, Hamming and other tapers differ from each other in their characteristics of relative suppression of the leakage in near and far frequency bands and width of the main lobe. Please see Smith (1997) for a detailed discussion.

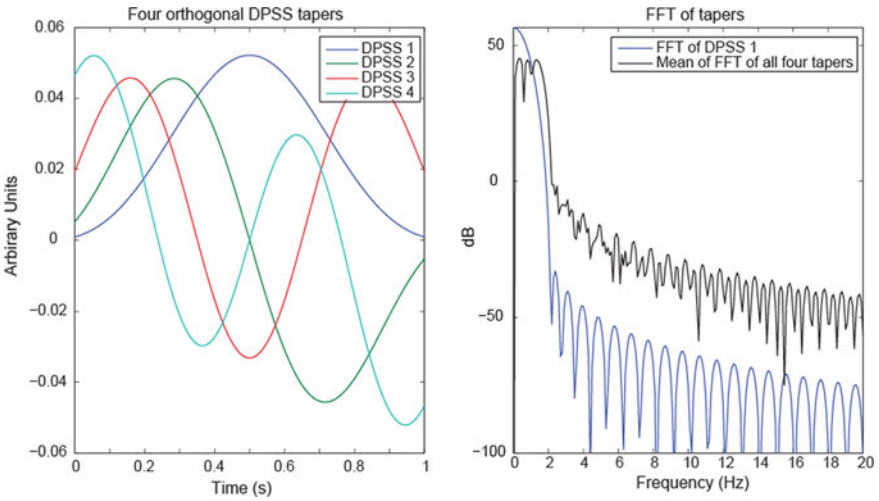

Fig. 5 Orthogonal DPSS tapers over a 1 s window (*left*) and their spectral density (*right*), with zero padding to 10 s length. The *black line* in the *right* figure is the average of the FFT of each taper, which indicates the effective result of using all four together

When considering neural responses in the gamma band, they are often broadband, for example from 60–80 Hz. In this case, one commonly uses a set of tapers, known as the Slepian or discrete prolate spheroidal sequences (DPSS) or simply "multitapers" (Slepian and Pollak 1961), which are a set of mutually orthogonal vectors with optimal desired spectral properties. The number of tapers used is determined by the length of the time window (Δt) and the desired frequency bandwidth (Δf), with the formula: $K = 2*\Delta t*\Delta f - 1$, where K is the number of tapers (Percival and Walden 1993). Ideally at least three tapers should be used. A set of four DPSS are shown in Fig. 5. The result of using the multitaper method is a wider but specific passband with minimal leakage in the stopbands. In other words, the spectral properties are ideal for a broadband but yet band-limited response in the gamma band. The choice of data segment length and desired bandwidth of the multitapers is important, but to advise specific settings that are generally applicable is not possible. Rather, iteration and initial exploration of the data is recommended, for example, to determine whether a wide-band response is actually two distinct bands near each other. Further discussion of Fourier analysis for neural signals can be found in Pesaran (2008).

3.2 Time Domain Characterization of Oscillations

Rather than computing the FFT of a time-windowed signal to obtain its PSD across all frequencies, another option is to band-pass filter the data so as to obtain a time domain signal containing only frequencies of some band of interest. The success of

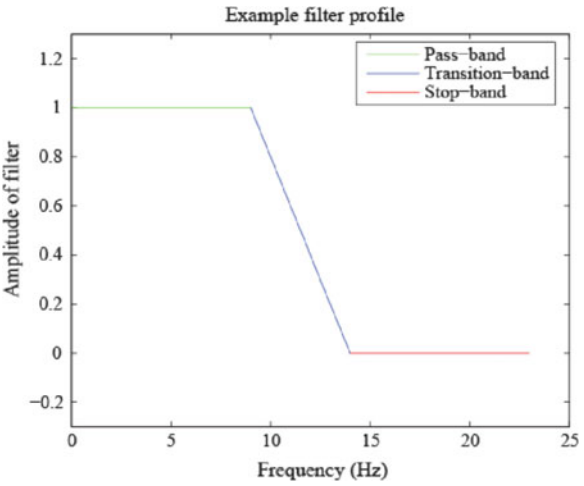

Fig. 6 Portions of a low-pass filter which correspond to the pass-band (unity amplification), transition-band (neither unity amplification nor full suppression), and the stop-band (full suppression). Similarly, a high-pass, band-pass and band-stop filter can be constructed

this method depends on the characteristics of the filter which, similar to the discussion of tapers above, depend on passing the desired frequencies (in the "pass-band") with as close to unity gain as possible and suppressing the non-desired frequencies (in the "stop-band") with as close to full attenuation as possible (see Fig. 6). The "transition-band" refers to the frequencies in between the pass-band and stop-band for which the gain is neither zero nor unity. Four filter types are named according to the relative position(s) of their pass-band and stop-band: low-pass (Fig. 6), high-pass, band-pass and band-reject. In reality, filters are not perfect, and thus three important characteristics of filters are roll-off between the pass-band and reject-band, amount of ripple in the pass-band, and amount of attenuation in the stop-band. For more information on digital filtering, please see Smith (1997).

While the characterization above (low-pass, high-pass etc.) applies to the desired behavior of the filter, another characterization of filters is the type of implementation used: "infinite impulse response" (IIR) or "finite impulse response" (FIR). We do not intend to provide a mathematical explanation of these types and how they differ, but rather to introduce and discuss trade-offs of commonly used filters in neuroscience. For further details please see (Smith 1997). The Butterworth filter is a commonly used IIR filter. Some considerations as to whether to use an IIR or FIR filter are that IIR filters tend to have a flat frequency response but a shallow drop-off in the frequency domain and indirect control over time and frequency resolution, whereas FIR filters tend to have precise control over time and frequency resolution and a sharp drop-off in the frequency domain, but have an "oscillating" response in the frequency stop-band. The order of the filter is important as well, as it relates to the amount of temporal lag of the convolution kernel as well as computation time. One important criterion is to use a filter that will preserve the phase of the signal (a "zero-phase filter") since the phase of the oscillation can be of important functional importance. A zero-phase filter is often implemented by applying two linear-phase

filters in succession, where the second "un-does" the phase shift of the first. However, it is important to know that no filter is perfect and thus by applying the same filter twice to obtain zero-phase, the amplitude is reduced twice as strongly in the pass-band. Thus when comparing amplitudes across conditions, it is imperative to use the same filtering and other preprocessing.

Filters may still have a ringing artifact (Gibbs ringing) of the filtered time series near sharp transitions in the signal, even though optimal filters aim at reducing this artifact. Thus, it is suggested to filter a segment of data longer than needed and discard the transition effects at the edges. The length of the discarded segment depends on the severity of the artifacts, but often 50–100 ms at each end is sufficient. This longer, edge-trimmed segment then can be further cut into shorter segments according to the same guidelines given above (at least 3–5 times the length of the period of oscillation) and a sum of squared amplitudes can be computed for the power of that particular time segment and frequency band according to the filter. Thus, in contrast to the FFT where all frequencies are obtained in one computation and at precise frequencies determined by the window length, this time-domain method allows for power over a window for the breadth of a frequency band to be computed, subject to the precision of the filter used. Note that filtering is for computational reasons often computed in the frequency domain using the FFT approach.

A possibility of probing the data characteristics from the band-pass filtered time domain signal is to compute its instantaneous phase and amplitude envelope (Fig. 7), using the Hilbert Transform (Bruns et al. 2000). In the limit that the time-varying signal is a perfect sinusoid, then the Hilbert transform would provide the same results as the FFT approach at a particular frequency for an infinitely long segment. The Hilbert transform can be useful to obtain the instantaneous phase estimate for an oscillation which, as recorded from a distant sensor as in MEG, may well be a mix of several oscillating neurons at nearly the same frequency. Additionally, the Hilbert amplitude envelope itself may be filtered to assess at what frequency the envelope is modulating (e.g., commonly observed in the range of 0.01–0.1 Hz (Hipp et al. 2012)).

3.3 Computation of Time-Frequency Representations of Oscillations

For many neuroscience applications, it is desired to compute the PSD over a range of frequencies and investigate how the PSD changes over time relative to some aspects of the task. Considering modulations in oscillatory power this way is referred to as a time-frequency representation (TFR) of power. The TFR is computed using a sliding time window. The length of each time segment in the window is determined as discussed before, but the time scale over which the changes in power may occur can be faster than the segment length; thus overlapping segments are often used. For example, 400 ms segments may be computed

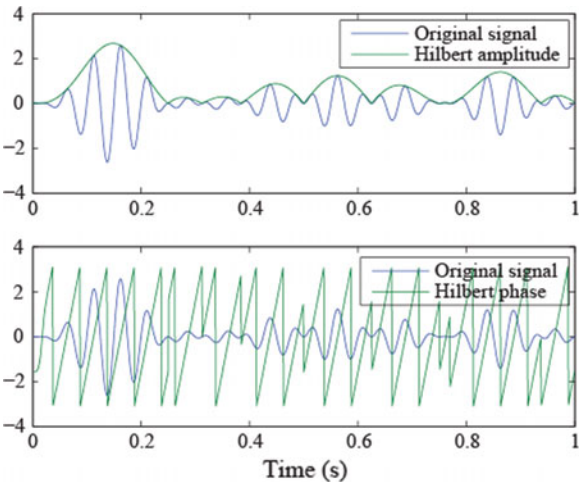

Fig. 7 The *blue line* shows a 20 Hz oscillation modulated by lower frequencies. The *green line* in the *top* panel shows the Hilbert amplitude of this signal and the *green line* in the *bottom* panel shows the Hilbert phase

with the central time point in steps of 50 ms. The overlap helps mitigate the dampening effect that tapering has on the power at the edges of the time segment; the loss of power at the edges of one segment is less of a concern if the edges are the middle of another computed segment. The window length of the segments may be kept the same for all frequencies examined (Fig. 8a) as long as the window length is sufficiently long for the lowest frequency. Alternatively, as shown in Fig. 8b, a different window length may be used for every frequency so that the number of periods of oscillation remains fixed (for example, keeping 4 cycles fixed leads to a 400 ms window for 10 Hz, 200 ms window for 20 Hz, and so on). Keep in mind that if a multitaper approach is used for computing the PSD of broadband gamma, the time window should be kept constant over the frequencies, as the multitapers interact over the range of frequencies. Also due to the difference in spectral width of the generated oscillations, the lower bands (e.g. 1–30 Hz) and higher bands (e.g. 20–100 Hz) are often computed separately using, respectively, Hanning and multitapers.

Wavelets are another computational method which may be used to compute the TFRs of power. They use a set of basis functions across multiple frequencies and times, that qualitatively each look like a burst of oscillatory activity at a given time and frequency, beginning and ending with zero amplitude. The exact shape of the wavelet depends on the type, of which there are many. One common type is the Morlet wavelet created by a sinusoid tapered by a Gaussian window centered at a specific time point (Fig. 9 left panel). The wavelet transform then uses the wavelet basis set (typically optimized for discrete signals with a discrete wavelet transform) to estimate power and phase at each frequency over time (Fig. 9). Wavelets have the property that the product of the bandwidth and window length remains constant, ensuring a constant time-frequency "area" of which the power is computed; the value of this product is user-specified. Note that Fourier analysis using

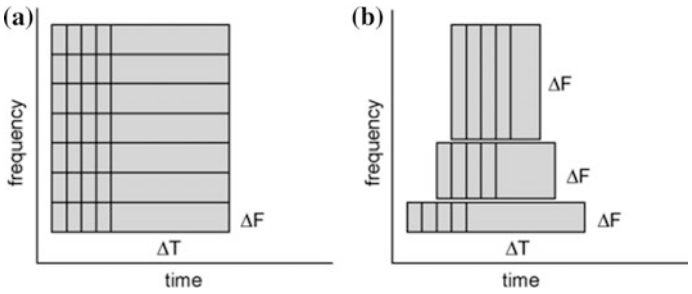

Fig. 8 Illustration of how time-frequency windows may be selected. **a** A fixed time width (ΔT) and fixed frequency width (ΔF) can be used. The *center* of each time window may be shifted in a time shorter than ΔT. **b** Variable time and frequency widths may be used where the area of the time-frequency window remains constant. As the time width (and temporal smoothing) is reduced at higher frequencies, the spectral width and smoothing are increased. This figure is reproduced from the tutorial on time-frequency analysis on the wiki page of the FieldTrip analysis toolbox (http://fieldtrip.fcdonders.nl/tutorial/timefrequencyanalysis)

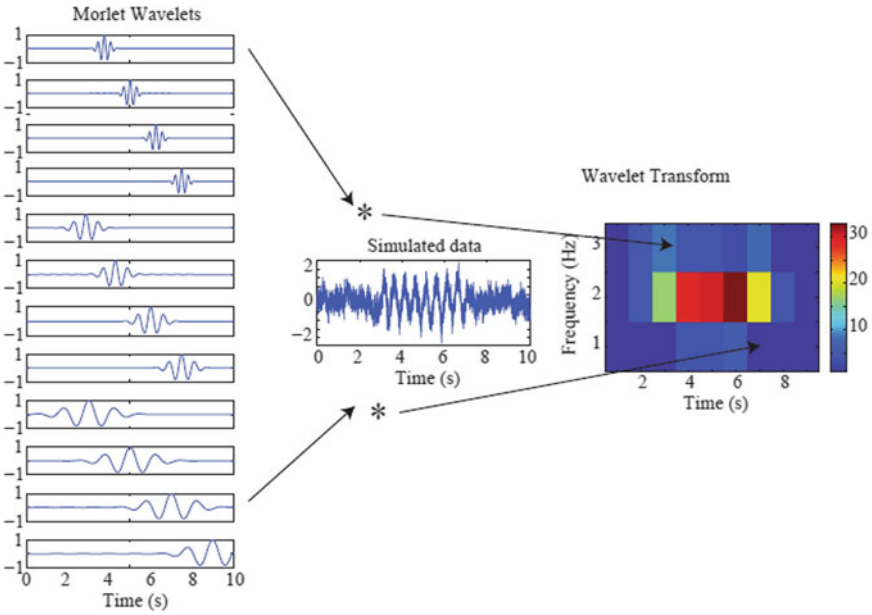

Fig. 9 Morlet wavelets and their use to create a time-frequency representation of data. (*Left*) A set of Morlet wavelets, with four different central points over three different frequencies. (*Middle*) example data with an oscillation at a frequency close to that of the *middle* frequency of the wavelets. (*Right*) The time-frequency representation of the spectral (*vertical*) and temporal (*left* to *right*) variation of each wavelet with the data

sliding time windows, filtering plus Hilbert transform, and the wavelet transform are mathematically equivalent, given specific sets of parameters (Le Van Quyen et al. 2001; Bruns 2004).

3.4 Characterizing Cross-Frequency Interactions

The physiological mechanisms of interactions across frequencies have been briefly described earlier in this chapter and may be quantified in various ways, each emphasizing different aspects of the interaction. Cross-frequency coupling can occur in various ways, involving the phase or amplitude (power) of a lower frequency band and the phase, amplitude or frequency in a higher-frequency band (Colgin et al. 2009; Fig. 10a).

One well-studied type of cross-frequency coupling is phase-amplitude coupling (PAC), i.e., coupling of the phase of the lower frequency (LF) (Fig. 10b–c) to the amplitude of the high frequency (HF) (Fig. 10b–d). Eight metrics to compute PAC are compared in (Tort et al. 2010) and reviewed in (Canolty and Knight 2010), of which we provide here a summary. As shown in Fig. 10b–e, reproduced from (Tort et al. 2010), a phase-amplitude histogram can be computed from the amplitudes of the higher frequency binned according to the phase of the lower frequency. Metric 1 (heights ratio; HR) uses this histogram directly to compute the ratio of the relative difference between the highest and lowest amplitudes; thus the HR metric lies between 0 and 1. Rather than just using the bins with the highest and lowest amplitudes, Metric 2 instead uses the whole distribution to compare against a uniform distribution (Tort et al. 2008, 2009), via a modulation index (MI) computed from the Kullback-Leibler (KL) distance (a method to compute a distance between probability distributions), denoted MI-KL. Metric 3 uses the PSD of the high frequencies to explore for possible PAC with any number of low frequency bands (Cohen 2008). However, note that a simple presence of power at low and high frequencies does not mean that there is phase-coupling in the same bands. Metric 4 uses a complex-valued time series created by the amplitude at high frequencies and the phase of the low frequencies; the mean vector length (MVL) of this new signal in the complex domain then indicates the extent to which amplitudes of high frequency activity are clustered in a particular phase of the low frequency oscillations (Canolty et al. 2006). Metric 5 computes a phase-locking value (PLV) between the phase of the low frequency signal and the phase of the envelope of the high frequency signal (Cohen 2008, Penny et al. 2008). Metric 6 computes the correlation of the high frequency envelope to low frequency signal, referred to as the envelope-to-signal correlation (ESC); this can be modulated to use only the cosine of the phase of the low frequency component removing its amplitude, thus a normalized ESC (NESC). However, ESC and NESC are phase-dependent and cannot detect a 90° phase difference. To get around his problem (Penny et al. 2008) proposed Metric 7, which improves on the phase-specificity of ESC by adding a sine component and using a general linear model (GLM) to determine the dependence of the high frequency envelope on any phase of the low frequency signal. Finally, metric 8 computes a coherence spectrum between the amplitude envelope of the high frequency and the original unfiltered signal (Osipova et al. 2008).

(Tort et al. 2010) compared these eight metrics (see their Table 1) for properties of tolerance to noise, dependence on the amplitude of the low frequency, sensitivity

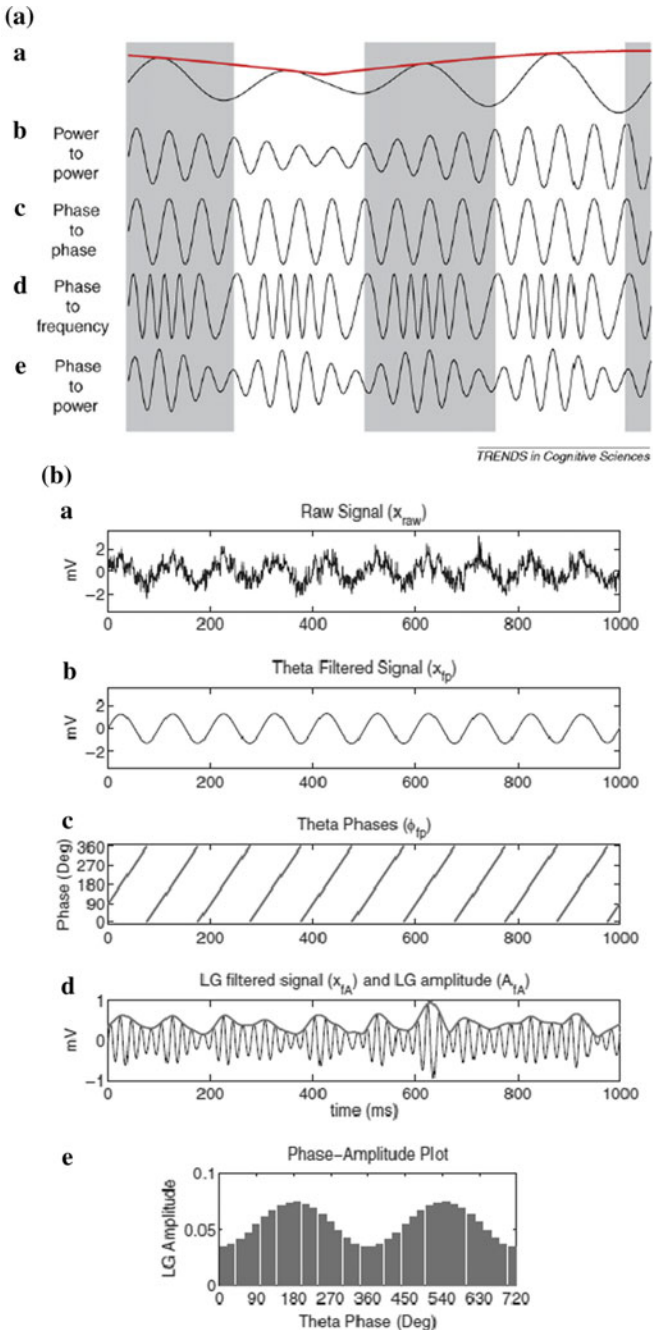

Fig. 10 **a** Demonstration of four ways in which a higher frequency can be modulated by a lower frequency (reproduced from Jensen and Colgin (2007)). **b** Analysis pipeline and example results for computing phase-amplitude coupling, with the lowest panel showing the histogram of amplitudes of the higher frequency binned according to phase of the lower frequency (reproduced from Tort et al. (2010))

to a multimodal histogram distribution, and sensitivity to width of the modulation distribution of the phase-amplitude coupling histogram. Specifically, measures that are only sensitive to the phase-locking will miss out on information of the extent of high frequency envelope modulation. Furthermore, the metric should be independent of the phase at which the high frequency envelope is maximal or minimal or if indeed multimodal. The metric should also have relative tolerance to noise and insensitivity to the absolute amplitudes of the low frequency or envelope of the high frequency signals. They conclude that their method of MI-KL performs optimally on these four considerations, and gives results that match intuitively with quantification of phase-amplitude coupling. The MI-KL metric is limited to examine only one low frequency band at a time, but of course the MI-KL of the same high frequency to several different low frequency bands may be computed independently.

Amplitude-amplitude (or power-power) coupling may be computed in several manners, although not so much variability or flexibility exists as it does for phase-amplitude coupling. One method includes computing the Hilbert amplitude envelope for two different frequencies and correlating them over time or trials. Note that the time series of the Hilbert envelope itself will fluctuate at a frequency much lower than the underlying frequency from which it is computed; thus, in order to compute a correlation, a sufficiently long time window to capture several cycles is needed (e.g., 10 s for the alpha activity). This can be therefore useful in resting state paradigms (de Pasquale et al. 2010; Brookes et al. 2011b; Hipp et al. 2012). Alternatively, it may be desired to assess whether the power at a particular time relative to a task from two different frequencies are co-modulated over trials (de Lange et al. 2008; Mazaheri et al. 2009). In this case, either the frequency domain or time domain methods for computing a PSD may be used.

Phase-phase coupling (PPC) means that the phase of an oscillation in one frequency is coupled to the phase of an oscillation in another frequency; in other words, a fixed number of high frequency cycles occurs every low frequency cycle. Once again, several methods exist to quantify this coupling. Bispectral analysis quantifies how two oscillations can nonlinearly interact to generate a third frequency. This metric has been used successfully in EEG data (Sigl and Chamoun 1994; Shils et al. 1996; Schack et al. 2002). However, like coherence between two signals of the same frequency, the amplitude is involved as well, thus not a strict phase-phase coupling measure. If the two frequencies (n and m) are harmonics of the same fundamental frequency (such that n*f1 = m*f2), then a modified n:m phase synchronization index is computed as $\omega_{n,m} = n*\varphi_1 - m*\varphi_2$ (Tass et al. 1998; Guevara and Glass 1982; Palva et al. 2005).

3.5 Concluding Remarks

We have demonstrated that transforming the original time domain signal to the frequency domain allows for a rich characterization and efficient computation of

the data to obtain a time-frequency representation of power. Considering the time signal as a sum of sinusoids each with its own amplitude and phase can promote a greater conceptual understanding. Considering cross-frequency interactions provides a new and exciting manner for analyzing oscillatory activity. Attention to details such as window length, tapering, spectral leakage and spectral smoothing will ensure an optimal representation of the data.

4 Functional Role of Brain Oscillations

4.1 Gamma Oscillations

Oscillatory activity in the gamma band (30–100 Hz) is typically associated with active neuronal processing of information. We will here first review the theoretical notions for how gamma activity might organize neuronal processing in time. We will then bring forward some examples demonstrating how the gamma activity can be investigated and interpreted in the context of MEG studies on cognition.

One of the key mechanistic ideas of the gamma band activity is related to synaptic integration. Imagine a group of neurons projecting to a downstream region. In order for a single neuron in the receiving region to fire, it must receive synaptic input from several of the neurons in the sending network. However, these inputs need to be somewhat synchronized to add up sufficiently. Typically an excitatory postsynaptic current lasts for about 10–20 ms. This implies that neurons in sending regions that synchronize in the gamma band (1/[20 ms]–1/[10 ms] corresponding to 50–100 Hz) provide a strong feed-forward drive (Tiesinga et al. 2004; Salinas and Sejnowski 2001) (Fig. 11). This framework is supported by the observation that the engagement of a given brain region often is reflected by a gamma band power increase. This has for instance been reported in LFP recordings in animal preparations (Gray et al. 1992). When a visual grating is presented to the monkey, strong gamma band synchronization is observed in visual regions including V1 and V4 (Gail et al. 2000; Fries et al. 2001; Rols et al. 2001; Buffalo et al. 2011; Bosman et al. 2012). Further the timing of neuronal firing is tightly coupled to the phase of the gamma band oscillations. Importantly, the degree of gamma band synchronization might act as a mechanism for gain control (Tiesinga et al. 2004). Tighter synchronization in the sending regions leads to a stronger feed-forward drive. This notion is reflected by an increase in spike-field coherence in the gamma band when covert attention was allocated to the respective visual field (Fries et al. 2001; Buffalo et al. 2011). Further, the tightness of the synchronization will be reflected as an increase in the electrical fields in the gamma band. This has been demonstrated in several human studies using EEG and MEG in which the gamma band activity increases with attention (Bauer et al. 2012; Gruber et al. 1999; Siegel et al. 2008).

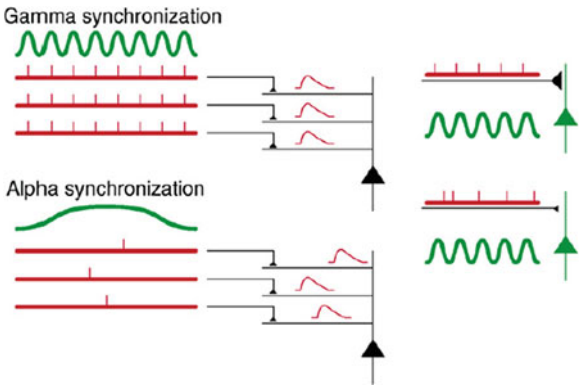

Fig. 11 Neuronal synchronization promotes a stronger feed-forward drive due to the temporal integration of synaptic input. This time-window of temporal integration is determined by the GABAergic feedback and is in the order of 10–20 ms, which makes synchronization in the gamma band optimal for providing a feed-forward drive. A slower rhythm like the alpha rhythm will provide a less tight synchronization and provide a less effective feed forward drive (reproduced from Jensen et al. (2007))

While these findings mainly pertain to the gamma activity in a given region ("the sender") it has also been proposed that communication between regions is a consequence of the dynamics in both the sender and the receiver. This theory is termed "communication through coherence" (Fries 2005). It proposes that to achieve optimal communication, the sender and the receiver need to oscillate coherently such that an incoming synaptic input co-occurs with the maximally excitable gamma phase in a receiving neuron (Fig. 12). Likewise communication between the two regions can be blocked by adjusting the phase relationship such that incoming spikes arrive at the least excitable gamma phase. In general the framework is consistent with the notion that communication between brain regions should be reflected in gamma band coherence (Bressler 1996; Varela et al. 2001). Recently the theory has received some experimental support from intracranial recordings in monkeys (Bosman et al. 2012; Grothe et al. 2012). While these findings are in support of the theory, long-distance coherence in the gamma band has been difficult to reliable identify in human MEG recordings, albeit there are several reports (Siegel et al. 2012). Interestingly there are now several papers on phase-synchronization in the theta and alpha band facilitating long-distance neuronal communication in both animals and humans (Colgin 2011; Liebe et al. 2012; Palva and Palva 2011; Saalmann et al. 2012). More work is required in order to determine the generality of communication through coherence and which frequency bands best reflect communication.

Beyond neuronal communication, it has been proposed that gamma band synchronization is needed for solving the "binding problem" (Gray et al. 1989; Engel and Singer 2001; Engel et al. 1999; Tallon-Baudry and Bertrand 1999). It should be mentioned that this framework pre-dates the ideas on communication by

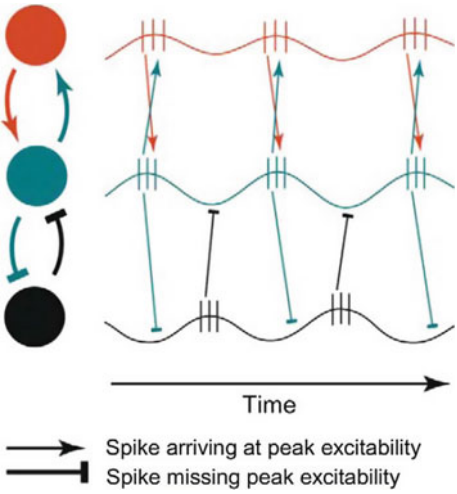

Fig. 12 A schematic illustration explaining communication through coherence. The red and the *green* cells are phase-locked in such a manner that spiking in one set of cells will coincide with the excitation by the gamma phase in the other cells. This allow for the cells to communicate. The phase relationship between the *red* and *black* cells is such that the incoming spikes will be missing the excitable phase. Thus information is only exchanged between the *red* and *green* cells. Reproduced from (Fries 2005)

gamma band synchronization. Typically when we perceive an object it is composed of several parts. In order to perceive the object as one, we need to perceptually combine the parts. Obviously binding needs to be done in a fast and flexible manner. The "binding-by-synchronization" hypothesis proposes that binding is achieved by neuronal synchronization in the gamma band. In other words, neurons coding for different parts will fire synchronously in order to form an ensemble that is perceived as one object (Fig. 13). This theory has received some experimental support (Gray et al. 1989; Engel et al. 1997; Castelo-Branco et al. 2000); however, it has also been criticized (Roelfsema 1998; Burns et al. 2011). One point of criticism pertains to the observation that gamma band activity changes frequency with stimulus contrast (Ray and Maunsell 2010). This poses a challenge to the binding theory since an object can be perceived as one, even if it is composed of parts of different contrast. It is of interest to point out, that a recent paper reported that an ensemble of neurons synchronizing in the beta band ($\sim$30 Hz; also termed lower gamma band) reflected the dynamic formation of representations for rules implementing stimulus-response mappings in prefrontal cortex (Buschman et al. 2012). In this study, the formation of representations seems to be reflected by neuronal synchronization. Although this does not pertain to perceptual binding per se, it does demonstrate that synchronization could play an important role for the dynamic formation of neuronal representations. Further research applying multi-unit and field recordings need to be performed to determine the general importance of gamma synchronization and binding.

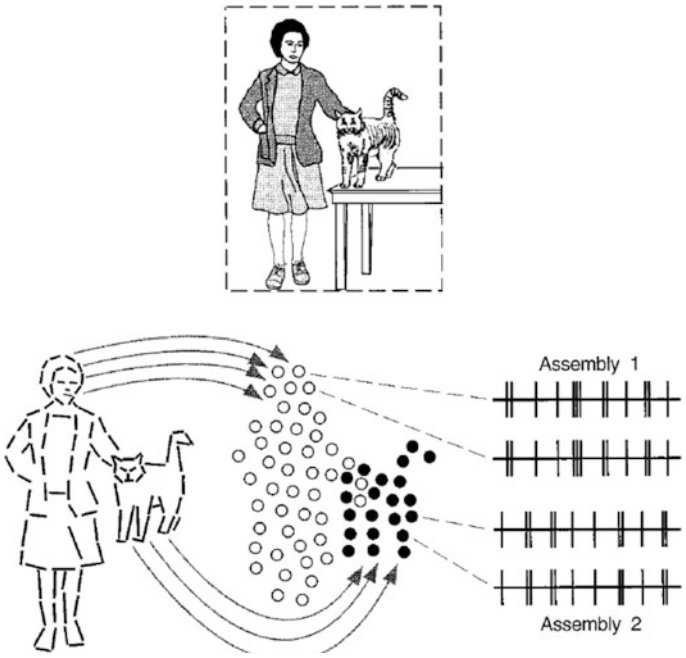

Fig. 13 Perceptual binding by neuronal synchronization in the gamma band (reproduced from Engel 1999). Cells whose receptive fields (RFs) correspond to locations of parts of the same object will synchronize with each other, binding those parts of the visual field together

To summarize, there are several influential theories on the functional role of gamma band oscillations. What these theories have in common is that they implicate gamma band synchronization in neuronal processing. There are now numerous studies demonstrating robust gamma band activity observed with MEG. We will mention a few here. Visual gamma band activity can be induced by gratings presented to the subject (Hoogenboom et al. 2006; Muthukumaraswamy and Singh 2013) (Fig. 14a). This gamma activity is highly robust and remains stable when tested over days (Muthukumaraswamy et al. 2010). Interestingly, the properties of the spectra in the gamma band are highly reproducible over monozygotic twins (van Pelt et al. 2012). This suggests that the frequency and synchronization properties are strongly linked to the physiology in a given subject. Further, sustained gamma band oscillations have been observed in human visual areas during working memory maintenance (Jokisch and Jensen 2007; Roux et al. 2012; Van Der Werf et al. 2009) (Fig. 14b). These findings are consistent with intracranial monkey recordings also demonstrating sustained gamma band activity during working memory maintenance (Pesaran et al. 2002). This was observed in LFP power but also in the coupling between neuronal spiking to the phase of ongoing gamma oscillations. Gamma band activity has also been associated with the successful encoding of long-term memory. Stronger induced gamma activity

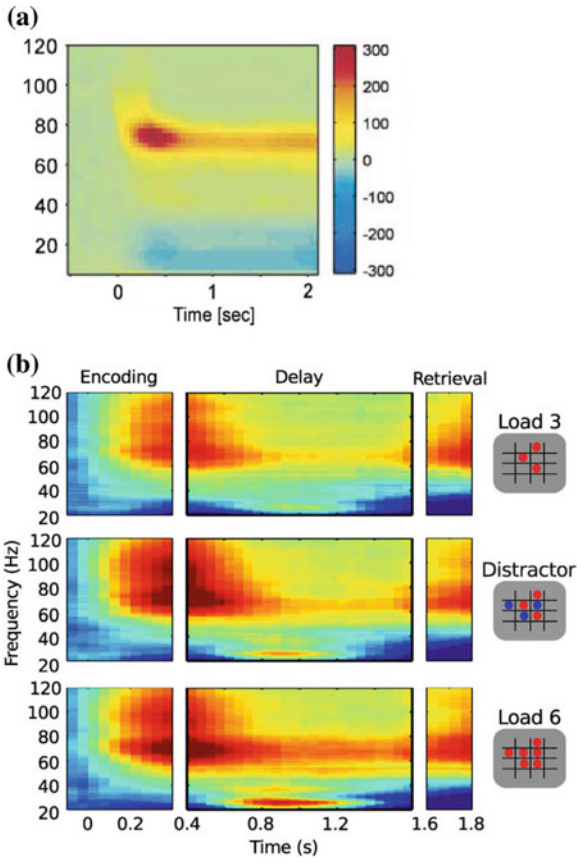

Fig. 14 **a** Robust gamma band oscillations induced by visually presented moving gratings. Their sources were localized to visual cortex (reproduced from Hoogenboom et al. (2006)). **b** Sustained gamma band oscillations observed during working memory maintenance (reproduced from Roux et al. (2012))

was observed in response to the presentation of items that were later remembered compared to forgotten (Gruber et al. 2004; Osipova et al. 2006; Meeuwissen et al. 2011). These findings are possibly linked to the observation that synaptic plasticity (long-term potentiation) can be improved when the inducing stimulus is coupled to the phase of the gamma oscillations (Wespatat et al. 2004). Finally it should be mentioned that MEG studies have found gamma band activity not only in the visual system. Reliable gamma band activity modulated by attention has also been observed in the somatosensory system (Bauer et al. 2006). Also, gamma band activity in the auditory system has been intensively investigated (Knief et al. 2000; Pantev et al. 2003; Kaiser and Lutzenberger 2005).

In conclusion gamma activity can be reliably detected using MEG. Further, the gamma band activity is often observed to be modulated by various cognitive manipulations. Animal recordings indicate that the gamma band activity is a consequence of a temporal organization of neuronal firing. As both theories and experiments develop we will gain further insight into the functional role of gamma oscillations.

Fig. 15 An example of an EEG study in which subjects were asked to shift attention between vision and hearing. The alpha power increased with an increase in attention towards hearing. (Reproduced from Adrian (1944))

4.2 Alpha Oscillations

Oscillatory activity in the alpha band was first reported by Hans Berger in 1929 (Berger 1938). Given that the alpha band activity emerges during rest and increases when subjects close their eyes, it has been associated with a state of rest. It has also been termed an idling rhythm, i.e., reflecting a state in which subjects are not engaged in a particular task but yet wakeful. This notion has recently lost ground in favor of the idea that alpha oscillations reflect active inhibition in a given region, although several indications from older studies actually are in support of this notion. For instance (Adrian 1944) showed that alpha band activity in posterior regions increases when attention was allocated from the visual to the auditory modality (Fig. 15). An EEG study by Ray and Cole (1985) showed a relative increase in alpha band power when attention was allocated to an internal task compared to the environment (Ray and Cole 1985). These types of observations were not consistent with the resting or idling notion of the alpha band activity. As a result of studies manipulating attention between the auditory and visual modality, it has been proposed that the alpha band activity reflected active inhibition of the visual system (Foxe et al. 1998). There are now numerous papers supporting the alpha inhibition hypothesis and we will here mention a few of those (for reviews see Foxe and Snyder (2011); Klimesch (2012); Jensen and Mazaheri (2010)).

There are several lines of direct evidence showing that the alpha activity is associated with a decrease in neuronal activity. When relating spiking neurons to the field potential of ongoing oscillations in monkey recordings, a robust phasic modulation has been shown (Bollimunta et al. 2008; Haegens et al. 2011b; Buffalo et al. 2011; Saalmann et al. 2012). Further it was demonstrated in sensorimotor regions that as firing rate decreases, alpha power increases (Haegens et al. 2011b). In recordings from the monkey visual system, a negative correlation between alpha and gamma power was demonstrated (Spaak et al. 2012a). Combined EEG and fMRI recordings have consistently demonstrated a negative correlation between alpha power and the BOLD signal (Laufs et al. 2003; Goldman et al. 2002). The perception of phosphenes induced by transcranial magnetic stimulation (TMS) has been related to the ongoing EEG signal. It was found that phosphene perception decreases as alpha power increases (Romei et al. 2008). These studies provide direct physiological support for a region specific inhibitory role of the alpha band activity.

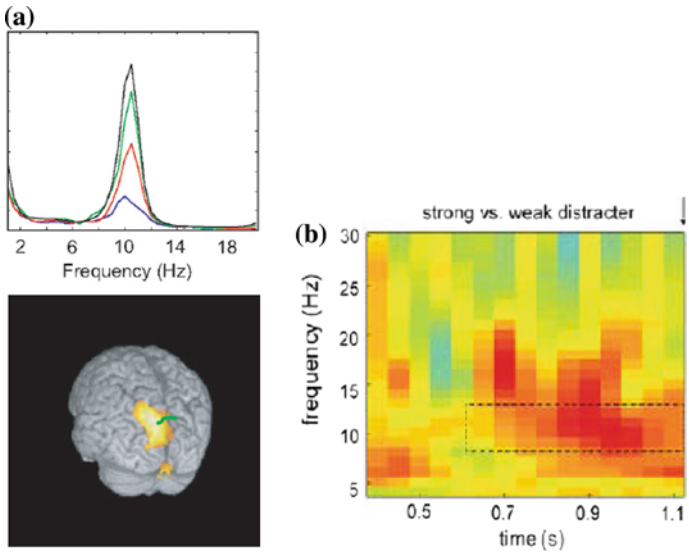

Fig. 16 **a** It has been consistently demonstrated that the posterior alpha activity increase systematically with working memory load. This finding is in contradiction to the resting or idling notion of the alpha activity (reproduced from Tuladhar et al. (2007a)). **b** Distracters were presented in the retention interval of the Sternberg task. The alpha activity increased just prior to the anticipated distracter. This increase was predictive of performance (reproduced from Bonnefond and Jensen (2012))

Considerable effort has also been put into investigating the functional role of the alpha band activity using EEG and MEG. In particular, MEG has allowed studying the region-specific properties of the alpha band activity. One of the challenges to the idling hypothesis stems from working memory paradigms, applying a variation of the Sternberg task. In these studies it has been demonstrated that the alpha activity systematically increases with memory demands (Jensen et al. 1999; Klimesch et al. 1999) (Fig. 16a). This is a highly robust finding that has been shown with EEG, MEG and even concurrent EEG and fMRI recordings using various kinds of stimuli (Tuladhar et al. 2007b; Scheeringa et al. 2009; Park et al. 2011). The increase in the alpha power with working memory demands is in stark contradiction to the resting or idling notion of the alpha activity. It has been proposed that the alpha power increase reflects either the active maintenance of the working memory representations (Palva and Palva 2007) or active inhibition of posterior regions (Klimesch et al. 2007; Foxe and Snyder 2011). This inhibition would serve to decrease the processing of potentially interfering information and thus allocate resources to working memory maintenance. This hypothesis was recently tested in a working memory study in which distracters were presented during the retention interval in a modified Sternberg task (Bonnefond and Jensen 2012). The timing and type of the presented distracters could be anticipated by the subjects. A clear increase in alpha activity was

shown to occur just prior to the arrival of the distracter (Fig. 16b). Furthermore, trials with longer response times to the memory probe were associated with a weaker pre-distracter alpha increase. These findings demonstrate that the posterior alpha activity serves an active role in filtering out distracting information. The alpha activity has also been shown to be strongly modulated with regard to attention allocated to the left or the right hemifield (Worden et al. 2000). When attention is directed to the left hemifield the alpha power is decreased over the right posterior hemisphere. Importantly, the alpha activity is relatively greater in the left hemisphere (and vice versa). These findings suggest that the right hemisphere is engaged while the left is inhibited. This hemispheric lateralization has been shown to have behavioral consequences for visual detection (Thut et al. 2006; Gould et al. 2011; Händel et al. 2010). Importantly, the alpha activity in the hemisphere ipsilateral to the direction of attention predicted performance to a greater extent than the alpha decrease contralateral to the direction of attention.

The functional role of alpha activity generalizes beyond the visual system. The primary sensorimotor system is known to strongly modulate alpha band activity (Pfurtscheller and Neuper 1994; Hari and Salmelin 1997). The somatosensory alpha band rhythm is also referred to as the mu rhythm. Sensorimotor alpha activity is also lateralized hemispherically with respect to attention to left and right hands. This has for instance been observed in a somatosensory working memory task in which subjects had to attend to electrical stimuli presented to one hand. The alpha activity which localized to the primary sensorimotor cortex decreased contralaterally to the stimulated hands, whereas it increased ipsilaterally. Importantly the ipsilateral alpha increase was the best predictor of performance (Haegens et al. 2010). These findings suggest that the active inhibition of task-irrelevant, but potentially interfering, regions is the best predictor of optimal performance. The notion that alpha activity reflects the inhibition of distracting information in the somatasensory system was directly tested in a study where target stimuli were presented to one hand and distracters were presented to the other (Haegens et al. 2012). The alpha activity in the somatosensory cortex contralateral to the hand with the distracters was the best predictor of target detection. Interestingly alpha band activity associated with the inhibition of motor responses has also been identified in the motor system (Sauseng et al. 2009). Alpha activity has also been identified in the auditory cortex using intracranial recordings in humans and MEG (Gomez-Ramirez et al. 2011). In older MEG studies this activity was called the tau rhythm (Lehtela et al. 1997). In more recent studies the functional role of the auditory alpha activity has been investigated (Weisz et al. 2011; Muller and Weisz 2012). These studies suggest that the alpha activity also plays an inhibitory role in the auditory system.

In sum, these studies strongly point to an inhibitory role of the alpha activity. This alpha activity serves to suppress the processing in regions not required for a given task. Importantly, if the suppression is insufficient, performance is suboptimal. While this functional role seems to apply to the visual, somatosensory and auditory sensory systems, it might generalize to other regions. MEG may be particularly sensitive to activity produced in sensory regions. Intracranial recordings

would help to elucidate the generality of the function of alpha oscillations. A recent study reported alpha activity in the prefrontal cortex of monkeys performing a rule-based stimulus-response mapping task (Buschman et al. 2012). Importantly, the alpha band synchronization in prefrontal cortex was associated with the suppression of the rules not to be applied.

The studies mentioned so far have only addressed the functional role of the *amplitude* or *power* of the alpha activity. This functional description is incomplete since the *phase* of the alpha oscillations strongly modulates neuronal firing as well (Bollimunta et al. 2008; Haegens et al. 2011b; Saalmann et al. 2012). Consistently, the BOLD signal evoked by visual stimuli has been shown to depend on the phase of ongoing alpha oscillations (Scheeringa et al. 2011). Several recent studies have investigated how the phase of the alpha oscillations modulates perception. It has been demonstrated that alpha phase in relation to stimulus presentation is predictive of hard-to-detect stimuli (Busch et al. 2009; Mathewson et al. 2009). Also, the detection of phosphenes evoked by TMS is dependent on the phase of ongoing alpha oscillations (Dugue et al. 2011). A recent working memory study demonstrated that alpha phase could be adjusted in anticipation of an incoming stimulus (Bonnefond and Jensen 2012). These studies can all be interpreted as the alpha activity allowing for windows of processing. This notion can be reconciled with the alpha inhibition hypothesis: the stronger the alpha, the shorter the time-window ("duty cycle") of processing. A recent theory has developed these ideas in the context of attention of visual processing (Jensen et al. 2012b). The phasic modulation of processing is also likely to have consequences for communication between brain regions (Palva and Palva 2011). If the information processing is constrained to certain alpha phases in sending regions, a receiving region could benefit in terms of adjusting its phase accordingly. In support of this notion, a recent intracranial monkey study demonstrated phase-synchronization between several visual regions organized by the pulvinar (Saalmann et al. 2012).

4.3 Delta Oscillations

There are several EEG and MEG studies reporting on the modulation of delta oscillations in various tasks (Basar et al. 2001; Handel et al. 2007; Handel and Haarmeier 2009; Knyazev et al. 2009; Knyazev 2012); however, there are only a few explicit ideas on the mechanistic role of the delta oscillations (Lakatos et al. 2005, 2008). One dominating idea is that the phase of the delta oscillations determines the excitability of the network. In tasks where incoming input can be anticipated, the phase of the delta oscillations can change. This provides a gating mechanism allowing for either blocking or facilitating a given anticipated input. This mechanism has been demonstrated in monkey recordings to operate in cross-modal integration paradigms (Lakatos et al. 2008). A monkey received a stream of alternating visual and auditory input spaced at 300 ms. The monkey had to attend to either the visual or the auditory input. As the monkey attended to the visual

input, the delta activity measured in visual cortex adapted in phase to the timing of the visual stream. When attention was allocated to the auditory stream, the delta phase adjusted such that the excitability in visual cortex was no longer high when the input arrived. Further, induced gamma activity reflecting the processing of the input was found to be phase-locked to the delta phase. The demonstration that the phase of the slower delta oscillations control the gamma activity has also been reported in MEG studies (Handel and Haarmeier 2009). In future work it would be interesting to further uncover the mechanistic role of delta oscillations, particularly in tasks where the timing of input can be anticipated.

4.4 Theta Oscillations

Substantial insight on the mechanistic role of theta oscillations has been gained from multi-electrode recordings in behaving rat. It is now possible to record single unit activity from about 100 cells while simultaneously acquiring local field potentials (Wilson and McNaughton 1993). This allows for relating spiking activity of a population of cells to local field oscillations. One of the most important insights from this work is the discovery of phase coding of hippocampal place cells. Place cells code for specific regions in an environment as the rat is exploring. The area in the environment in which a given place cell fires is termed the place field (O'Keefe and Dostrovsky 1971). As the rat enters a place field, the respective place cell will first fire at late phases of the theta cycle. As the rat advances, the firing will occur at earlier and earlier phases. This phenomenon is termed theta phase precession (O'Keefe and Recce 1993). From an ensemble of place cells it is possible to reconstruct the position of the rat; however, when taking the theta phase of firing into account, the reconstruction error is further reduced (Jensen and Lisman 2000; Harris et al. 2003). The evidence for phase coding in the rat hippocampus has promoted the development of biophysical models accounting for the phenomena (Burgess and O'Keefe 2011; Lisman and Redish 2009; Mehta et al. 2002). Several of these models are based on time-compressed representations being activated sequentially within a theta cycle. The principle of phase coding has consequences for communication between regions. A region receiving phase coded information must also receive information about the phase of the theta oscillations in order to make use of the code (Jensen 2001). This can be achieved through theta phase synchronization between regions exchanging a phase code. In support of this notion, phase synchronization between the hippocampus and other regions has been reported in numerous studies. For instance, the hippocampal theta oscillations have been found to be phase-locked to theta activity in prefrontal cortex (Siapas et al. 2005). This phase synchronization is modulated by the memory component in a navigation task (Jones and Wilson 2005; Colgin 2011). Further, the hippocampus has been found to be synchronized to the striatum and the amygdala (Tort et al. 2008; Battaglia et al. 2011; Seidenbecher et al. 2003). Theta oscillations related to information exchange between regions have also been

observed in other animals. For instance, theta phase-synchronization between V4 and prefrontal cortex was reported in a monkey study on working memory maintenance (Liebe et al. 2012). This synchronization was observed both in the local field potentials as well as in the spike trains.

Theta oscillations do not only modulate neuronal spiking, but also oscillations in higher frequency bands. In the rat hippocampus, gamma power in different frequency ranges is modulated by the phase of the theta oscillations (Bragin et al. 1995; Belluscio et al. 2012). Importantly theta modulated gamma band synchronization in different frequency ranges has been shown to route information from either the entorhinal cortex or the CA3 to the CA1 region (Colgin et al. 2009).

Intracranial recordings in humans have also reported theta band activity from both neocortical and hippocampal regions. These recordings are performed using either electrocorticographic or depth electrodes (Kahana et al. 2001; Sederberg et al. 2003; Lega et al. 2012; Burke et al. 2013; Watrous et al. 2013). The intracranial theta band activity has mainly been related to working and long-term memory processing. Interestingly, the intracranial theta activity is also phase-locked to gamma power exactly as seen in the rat (Canolty et al. 2006; Canolty and Knight 2010).

In human extracranial EEG and MEG recordings, the theta band activity is observed most strongly over the frontal midline (Mitchell et al. 2008). In particular, frontal midline theta activity has been reported to increase with memory load in both the N-back and the Sternberg tasks (Scheeringa et al. 2009; Gevins and Smith 2000; Jensen and Tesche 2002).

Frontal midline theta activity has also been associated with error-processing. Several studies using go/no-goparadigms have reported an increase in frontal midline theta after a wrong motor response has been elicited. It remains unclear how the frontal midline theta relates to the error-related negativity, but there might be a tight relation (Luu et al. 2004; Mazaheri et al. 2009; van de Vijver et al. 2011). In general, the frontal midline theta is thought to reflect executive processes related to updating after a perceptual error (Cohen and van Gaal 2013).

It remains unknown to what extent the frontal midline theta activity, associated with working memory maintenance and error processing, relates to the theta activity reported in rats. Nevertheless, both the frontal midline and the hippocampal theta activity are thought to be associated with the temporal coordination of neuronal processing.

4.5 Beta Oscillations

Beta oscillations are strongly associated with the motor system (Baker 2007). They have been recorded both in animals and in humans. Typically beta oscillations decrease in power in anticipation of sensori-motor processing (van Ede et al. 2011). Thus one might think that beta oscillations are associated with suppression. Nevertheless, beta oscillations have also been associated with the exchange of

information between motor cortex and the muscle (Kilner et al. 2000; van Elswijk et al. 2010). During isometric muscle contraction, strong coherence is observed in the beta band between the EMG and the motor cortical EEG or MEG signal (Baker 2007). The motor cortical beta oscillations are not only synchronous with muscle activity but also with basal ganglia areas and the subthalamic nucleus (Hirschmann et al. 2011; Litvak et al. 2011; Jenkinson and Brown 2011). Thus, while it is clear that cortical beta oscillations play an important role for coordinating the timing of spiking between neocortex and motor units, the precise functional role remains elusive. A recent paper proposed that the beta oscillations are involved in setting the *status quo*, i.e. maintaining the state of an extended network (Engel and Fries 2010). This idea is consistent with the observation that restating state networks observed with MEG often are reflected by functional connectivity in the beta band (Hipp et al. 2012; Brookes et al. 2011a).

Higher level cognitive studies in both humans and monkeys point to a role for beta oscillations in decision making. During critical decision periods and updating, beta increases have been observed in prefrontal regions in both monkey and human recordings (Haegens et al. 2011a; Spitzer et al. 2010). Along those lines, the motor cortical beta activity has been proposed to be involved in the accumulation of evidence when perceptual decisions, and motor responses on those decisions, have to be made (Donner et al. 2009). The findings on decision making and beta oscillations give a strong processing connotation to the beta band activity which somehow is in contrast to observed functions of the motor cortical beta activity. Future work is required to determine if activity in the beta band is associated with only one function, or whether beta oscillations in different regions are associated with different functions.

5 Future Perspectives and Conclusions

Hopefully it is clear from this chapter that oscillatory brain activity is observed in a wide range of species. Further, the brain oscillations seem to play an important role in coordinating neuronal processing. This coordination is achieved by a phasic modulation of neuronal firing. The degree of phasic modulation is determined by the magnitude of the oscillations. Further, from human studies, various kinds of cognitive tasks result in reliable modulation of oscillatory activity in different frequency bands. These observations make integration possible in which neuronal firing is related to behavior by considering temporal coordination organized by brain oscillations.

Future work is required to further uncover the functional role of brain oscillations. New technologies and the integration of techniques will facilitate these efforts. For instance, the application of optogenetics will allow for driving oscillatory activity in order to study their causal role (Tiesinga and Sejnowski 2009). Likewise, entrainment can be applied in humans using TMS and transcranial alternating current stimulation (tACS) in association with cognitive paradigms

(Thut et al. 2012). While oscillatory activity is particularly strong in sensory regions, it remains unclear which brain regions are involved in controlling the oscillations. While the fronto-striatal network is likely to play a strong role in the top-down control, the mechanisms by which this control is exercised is unclear. Several approaches can be applied to identify the frontal control network. For instance, EEG combined with fMRI can be applied to identify prefrontal and deep brain regions associated with the modulation of posterior regions. Recording MEG and the structural MRI in the same subjects makes it possible to associate oscillatory modulations with anatomy. Finally, pharmacological manipulations hold a strong promise for isolating the physiological mechanisms associated with top-down control of oscillatory activity. In particular, manipulating the cholinergic and dopaminergic system is of importance (Bauer et al. 2012; Noudoost and Moore 2011). In short, substantial insight has been gained on understanding the functional role of oscillatory brain activity; however, many questions remain open. Integration of evidence where human data are interpreted in the light of animal recordings and the combination of techniques hold a strong promise for making further advances.

References

Adrian ED (1944) Brain rhythms. Nature 153:360–362

Baker SN (2007) Oscillatory interactions between sensorimotor cortex and the periphery. Curr Opin Neurobiol 17:649–655

Bartos M, Vida I, Jonas P (2007) Synaptic mechanisms of synchronized gamma oscillations in inhibitory interneuron networks. Nat Rev Neurosci 8:45–56

Basar E, Basar-Eroglu C, Karakas S, Schurmann M (2001) Gamma, alpha, delta, and theta oscillations govern cognitive processes. Int J Psychophysiol 39:241–248

Battaglia FP, Benchenane K, Sirota A, Pennartz CM, Wiener SI (2011) The hippocampus: hub of brain network communication for memory. Trends Cogn Sci 15:310–318

Bauer M, Kluge C, Bach D, Bradbury D, Heinze HJ, Dolan RJ, Driver J (2012) Cholinergic enhancement of visual attention and neural oscillations in the human brain. Curr Biol 22:397–402

Bauer M, Oostenveld R, Peeters M, Fries P (2006) Tactile spatial attention enhances gamma-band activity in somatosensory cortex and reduces low-frequency activity in parieto-occipital areas. J Neurosci 26:490–501

Belluscio MA, Mizuseki K, Schmidt R, Kempter R, Buzsaki G (2012) Cross-frequency phase-phase coupling between theta and gamma oscillations in the hippocampus. J Neurosci 32:423–435

Berger H (1938) Das Elektrenkephalogramm des Menschen. Geschäftsstelle der Deutschen Akademie der Naturforscher, Halle

Bollimunta A, Chen Y, Schroeder CE, Ding M (2008) Neuronal mechanisms of cortical alpha oscillations in awake-behaving macaques. J Neurosci 28:9976–9988

Bollimunta A, Mo J, Schroeder CE, Ding M (2011) Neuronal mechanisms and attentional modulation of corticothalamic alpha oscillations. J Neurosci 31:4935–4943

Bonnefond M, Jensen O (2012) Alpha oscillations serve to protect working memory maintenance against anticipated distracters. Curr Biol 22:1969–1974

Borgers C, Kopell N (2003) Synchronization in networks of excitatory and inhibitory neurons with sparse, random connectivity. Neural Comput 15:509–538
Bosman CA, Schoffelen JM, Brunet N, Oostenveld R, Bastos AM, Womelsdorf T, Rubehn B, Stieglitz T, De Weerd P, Fries P (2012) Attentional stimulus selection through selective synchronization between monkey visual areas. Neuron 75:875–888
Bragin A, Jando G, Nadasdy Z, Hetke J, Wise K, Buzsaki G (1995) Gamma (40–100 Hz) oscillation in the hippocampus of the behaving rat. J Neurosci 15:47–60
Bressler SL (1996) Interareal synchronization in the visual cortex. Behav Brain Res 76:37–49
Brookes MJ, Hale JR, Zumer JM, Stevenson CM, Francis ST, Barnes GR, Owen JP, Morris PG, Nagarajan SS (2011a) Measuring functional connectivity using MEG: methodology and comparison with fcMRI. Neuroimage 56:1082–1104
Brookes MJ, Woolrich M, Luckhoo H, Price D, Hale JR, Stephenson MC, Barnes GR, Smith SM, Morris PG (2011b) Investigating the electrophysiological basis of resting state networks using magnetoencephalography. Proc Natl Acad Sci USA 108:16783–16788
Brown P, Kupsch A, Magill PJ, Sharott A, Harnack D, Meissner W (2002) Oscillatory local field potentials recorded from the subthalamic nucleus of the alert rat. Exp Neurol 177:581–585
Bruns A (2004) Fourier-, Hilbert- and wavelet-based signal analysis: are they really different approaches? J Neurosci Methods 137:321–332
Bruns A, Eckhorn R, Jokeit H, Ebner A (2000) Amplitude envelope correlation detects coupling among incoherent brain signals. NeuroReport 11:1509–1514
Buffalo EA, Fries P, Landman R, Buschman TJ, Desimone R (2011) Laminar differences in gamma and alpha coherence in the ventral stream. Proc Natl Acad Sci USA 108:11262–11267
Burgess N, O'keefe J (2011) Models of place and grid cell firing and theta rhythmicity. Curr Opin Neurobiol 21:734–744
Burke JF, Zaghloul KA, Jacobs J, Williams RB, Sperling MR, Sharan AD, Kahana MJ (2013) Synchronous and asynchronous theta and gamma activity during episodic memory formation. J Neurosci 33:292–304
Burns SP, Xing D, Shapley RM (2011) Is gamma-band activity in the local field potential of V1 cortex a "clock" or filtered noise? J Neurosci 31:9658–9664
Busch NA, Dubois J, Vanrullen R (2009) The phase of ongoing EEG oscillations predicts visual perception. J Neurosci 29:7869–7876
Buschman TJ, Denovellis EL, Diogo C, Bullock D, Miller EK (2012) Synchronous oscillatory neural ensembles for rules in the prefrontal cortex. Neuron 76:838–46
Buzsaki G (2002) Theta oscillations in the hippocampus. Neuron 33:325–340
Buzsáki G (2006) Rhythms of the brain. Oxford University Press, Oxford
Buzsaki G, Wang XJ (2012) Mechanisms of gamma oscillations. Annu Rev Neurosci 35:203–225
Canolty RT, Edwards E, Dalal SS, Soltani M, Nagarajan SS, Kirsch HE, Berger MS, Barbaro NM, Knight RT (2006) High gamma power is phase-locked to theta oscillations in human neocortex. Science 313:1626–1628
Canolty RT, Knight RT (2010) The functional role of cross-frequency coupling. Trends Cogn Sci 14:506–515
Cardin JA, Carlen M, Meletis K, Knoblich U, Zhang F, Deisseroth K, Tsai LH, Moore CI (2009) Driving fast-spiking cells induces gamma rhythm and controls sensory responses. Nature 459:663–667
Castelo-Branco M, Goebel R, Neuenschwander S, Singer W (2000) Neural synchrony correlates with surface segregation rules. Nature 405:685–689
Chrobak JJ, Buzsaki G (1996) High-frequency oscillations in the output networks of the hippocampal-entorhinal axis of the freely behaving rat. J Neurosci 16:3056–3066
Cobb SR, Buhl EH, Halasy K, Paulsen O, Somogyi P (1995) Synchronization of neuronal activity in hippocampus by individual GABAergic interneurons. Nature 378:75–78
Cohen MX (2008) Assessing transient cross-frequency coupling in EEG data. J Neurosci Methods 168:494–499
Cohen MX, Van Gaal S (2013) Dynamic interactions between large-scale brain networks predict behavioral adaptation after perceptual errors. Cereb Cortex 23:1061–1072

Colgin LL (2011) Oscillations and hippocampal-prefrontal synchrony. Curr Opin Neurobiol 21:467–474
Colgin LL, Denninger T, Fyhn M, Hafting T, Bonnevie T, Jensen O, Moser MB, Moser EI (2009) Frequency of gamma oscillations routes flow of information in the hippocampus. Nature 462:353–357
De Lange FP, Jensen O, Bauer M, Toni I (2008) Interactions between posterior gamma and frontal alpha/beta oscillations during imagined actions. Front Hum Neurosci 2:7
De Pasquale F, Della Penna S, Snyder AZ, Lewis C, Mantini D, Marzetti L, Belardinelli P, Ciancetta L, Pizzella V, Romani GL, Corbetta M (2010) Temporal dynamics of spontaneous MEG activity in brain networks. Proc Natl Acad Sci USA 107:6040–6045
Destexhe A, Mccormick DA, Sejnowski TJ (1993) A model for 8–-10 Hz spindling in interconnected thalamic relay and reticularis neurons. Biophys J 65:2473–2477
Donner TH, Siegel M, Fries P, Engel AK (2009) Buildup of choice-predictive activity in human motor cortex during perceptual decision making. Curr Biol 19:1581–1585
Dugue L, Marque P, Vanrullen R (2011) The phase of ongoing oscillations mediates the causal relation between brain excitation and visual perception. J Neurosci 31:11889–11893
Engel AK, Fries P (2010) Beta-band oscillations–signalling the status quo? Curr Opin Neurobiol 20:156–165
Engel AK, Fries P, Konig P, Brecht M, Singer W (1999) Temporal binding, binocular rivalry, and consciousness. Conscious Cogn 8:128–151
Engel AK, Roelfsema PR, Fries P, Brecht M, Singer W (1997) Role of the temporal domain for response selection and perceptual binding. Cereb Cortex 7:571–582
Engel AK, Singer W (2001) Temporal binding and the neural correlates of sensory awareness. Trends Cogn Sci 5:16–25
Ermentrout GB, Kopell N (1998) Fine structure of neural spiking and synchronization in the presence of conduction delays. Proc Natl Acad Sci USA 95:1259–1264
Fell J, Axmacher N (2011) The role of phase synchronization in memory processes. Nat Rev Neurosci 12:105–118
Foxe JJ, Simpson GV, Ahlfors SP (1998) Parieto-occipital approximately 10 Hz activity reflects anticipatory state of visual attention mechanisms. NeuroReport 9:3929–3933
Foxe JJ, Snyder AC (2011) The role of alpha-band brain oscillations as a sensory suppression mechanism during selective attention. Front Psychol 2:154
Freeman WJ (2007) Definitions of state variables and state space for brain-computer interface: part 1. Multiple hierarchical levels of brain function. Cogn Neurodyn 1:3–14
Freund TF, Antal M (1988) GABA-containing neurons in the septum control inhibitory interneurons in the hippocampus. Nature 336:170–173
Freund TF, Buzsaki G (1996) Interneurons of the hippocampus. Hippocampus 6:347–470
Fries P (2005) A mechanism for cognitive dynamics: neuronal communication through neuronal coherence. Trends Cogn Sci 9:474–480
Fries P, Nikolic D, Singer W (2007) The gamma cycle. Trends Neurosci 30:309–316
Fries P, Reynolds JH, Rorie AE, Desimone R (2001) Modulation of oscillatory neuronal synchronization by selective visual attention. Science 291:1560–1563
Fujisawa S, Buzsaki G (2011) A 4 Hz oscillation adaptively synchronizes prefrontal, VTA, and hippocampal activities. Neuron 72:153–165
Gabbott P, Headlam A, Busby S (2002) Morphological evidence that CA1 hippocampal afferents monosynaptically innervate PV-containing neurons and NADPH-diaphorase reactive cells in the medial prefrontal cortex (Areas 25/32) of the rat. Brain Res 946:314–322
Gail A, Brinksmeyer HJ, Eckhorn R (2000) Contour decouples gamma activity across texture representation in monkey striate cortex. Cereb Cortex 10:840–850
Gerstner W, Van Hemmen JL, Cowan JD (1996) What matters in neuronal locking? Neural Comput 8:1653–1676
Gevins A, Smith ME (2000) Neurophysiological measures of working memory and individual differences in cognitive ability and cognitive style. Cereb Cortex 10:829–839

Gloveli T, Dugladze T, Saha S, Monyer H, Heinemann U, Traub RD, Whittington MA, Buhl EH (2005) Differential involvement of oriens/pyramidale interneurones in hippocampal network oscillations in vitro. J Physiol 562:131–147

Goldman RI, Stern JM, Engel J Jr, Cohen MS (2002) Simultaneous EEG and fMRI of the alpha rhythm. NeuroReport 13:2487–2492

Gomez-Ramirez M, Kelly SP, Molholm S, Sehatpour P, Schwartz TH, Foxe JJ (2011) Oscillatory sensory selection mechanisms during intersensory attention to rhythmic auditory and visual inputs: a human electrocorticographic investigation. J Neurosci 31:18556–18567

Gould IC, Rushworth MF, Nobre AC (2011) Indexing the graded allocation of visuospatial attention using anticipatory alpha oscillations. J Neurophysiol 105:1318–1326

Goutagny R, Jackson J, Williams S (2009) Self-generated theta oscillations in the hippocampus. Nat Neurosci 12:1491–1493

Gray CM, Engel AK, Konig P, Singer W (1992) Synchronization of oscillatory neuronal responses in cat striate cortex: temporal properties. Vis Neurosci 8:337–347

Gray CM, Konig P, Engel AK, Singer W (1989) Oscillatory responses in cat visual cortex exhibit inter-columnar synchronization which reflects global stimulus properties. Nature 338:334–337

Gross J, Baillet S, Barnes GR, Henson RN, Hillebrand A, Jensen O, Jerbi K, Litvak V, Maess B, Oostenveld R, Parkkonen L, Taylor JR, Van Wassenhove V, Wibral M, Schoffelen JM (2013) Good practice for conducting and reporting MEG research. Neuroimage 65:349–363

Grothe I, Neitzel SD, Mandon S, Kreiter AK (2012) Switching neuronal inputs by differential modulations of gamma-band phase-coherence. J Neurosci 32:16172–16180

Gruber T, Muller MM, Keil A, Elbert T (1999) Selective visual-spatial attention alters induced gamma band responses in the human EEG. Clin Neurophysiol 110:2074–2085

Gruber T, Tsivilis D, Montaldi D, Muller MM (2004) Induced gamma band responses: an early marker of memory encoding and retrieval. NeuroReport 15:1837–1841

Guevara MR, Glass L (1982) Phase locking, period doubling bifurcations and chaos in a mathematical-model of a periodically driven oscillator—a theory for the entrainment of biological oscillators and the generation of cardiac dysrhythmias. J Math Biol 14:1–23

Gulyas AI, Megias M, Emri Z, Freund TF (1999) Total number and ratio of excitatory and inhibitory synapses converging onto single interneurons of different types in the CA1 area of the rat hippocampus. J Neurosci 19:10082–10097

Haegens S, Luther L, Jensen O (2012) Somatosensory anticipatory alpha activity increases to suppress distracting input. J Cogn Neurosci 24:677–685

Haegens S, Nácher V, Hernández A, Luna R, Jensen O, Romo R (2011a) Beta oscillations in the monkey sensorimotor network reflect somatosensory decision making. Proc Natl Acad Sci 108:10708

Haegens S, Nacher V, Luna R, Romo R, Jensen O (2011b) alpha-Oscillations in the monkey sensorimotor network influence discrimination performance by rhythmical inhibition of neuronal spiking. Proc Natl Acad Sci USA 108:19377–19382

Haegens S, Osipova D, Oostenveld R, Jensen O (2010) Somatosensory working memory performance in humans depends on both engagement and disengagement of regions in a distributed network. Hum Brain Mapp 31:26–35

Handel B, Haarmeier T (2009) Cross-frequency coupling of brain oscillations indicates the success in visual motion discrimination. Neuroimage 45:1040–1046

Handel B, Lutzenberger W, Thier P, Haarmeier T (2007) Opposite dependencies on visual motion coherence in human area MT + and early visual cortex. Cereb Cortex 17:1542–1549

Händel BF, Haarmeier T, Jensen O (2010) Alpha oscillations correlate with the successful inhibition of unattended stimuli. J Cogn Neurosci 1–9

Hari R, Salmelin R (1997) Human cortical oscillations: a neuromagnetic view through the skull. Trends Neurosci 20:44–49

Harris KD, Csicsvari J, Hirase H, Dragoi G, Buzsaki G (2003) Organization of cell assemblies in the hippocampus. Nature 424:552–556

Hipp JF, Hawellek DJ, Corbetta M, Siegel M, Engel AK (2012) Large-scale cortical correlation structure of spontaneous oscillatory activity. Nat Neurosci 15:884–890
Hirschmann J, Ozkurt TE, Butz M, Homburger M, Elben S, Hartmann CJ, Vesper J, Wojtecki L, Schnitzler A (2011) Distinct oscillatory STN-cortical loops revealed by simultaneous MEG and local field potential recordings in patients with Parkinson's disease. Neuroimage 55:1159–1168
Hoogenboom N, Schoffelen JM, Oostenveld R, Parkes LM, Fries P (2006) Localizing human visual gamma-band activity in frequency, time and space. Neuroimage 29:764–773
Hughes SW, Crunelli V (2005) Thalamic mechanisms of EEG alpha rhythms and their pathological implications. Neuroscientist 11:357–372
Jenkinson N, Brown P (2011) New insights into the relationship between dopamine, beta oscillations and motor function. Trends Neurosci 34:611–618
Jensen O (2001) Information transfer between rhythmically coupled networks: reading the hippocampal phase code. Neural Comput 13:2743–2761
Jensen O, Bonnefond M, Vanrullen R (2012a) An oscillatory mechanism for prioritizing salient unattended stimuli. Trends Cogn Sci 16:200–206
Jensen O, Bonnefond M, Vanrullen R (2012b) An oscillatory mechanism for prioritizing salient unattended stimuli. Trends Cogn Sci 16(4):200–206
Jensen O, Colgin LL (2007) Cross-frequency coupling between neuronal oscillations. Trends Cogn Sci 11:267–269
Jensen O, Gelfand J, Kounios J, Lisman J (1999) 10–12 Hz oscillations increase with memory load in a short-term memory task. Neuroimage 9:951
Jensen O, Goel P, Kopell N, Pohja M, Hari R, Ermentrout B (2005) On the human sensorimotor-cortex beta rhythm: sources and modeling. Neuroimage 26:347–355
Jensen O, Kaiser J, Lachaux JP (2007) Human gamma-frequency oscillations associated with attention and memory. Trends Neurosci 30:317–324
Jensen O, Lisman JE (2000) Position reconstruction from an ensemble of hippocampal place cells: contribution of theta phase coding. J Neurophysiol 83:2602
Jensen O, Mazaheri A (2010) Shaping functional architecture by oscillatory alpha activity: gating by inhibition. Front Hum Neurosci 4:186
Jensen O, Tesche CD (2002) Frontal theta activity in humans increases with memory load in a working memory task. Eur J Neurosci 15:1395–1399
Jokisch D, Jensen O (2007) Modulation of gamma and alpha activity during a working memory task engaging the dorsal or ventral stream. J Neurosci 27:3244–3251
Jones MW, Wilson MA (2005) Theta rhythms coordinate hippocampal-prefrontal interactions in a spatial memory task. PLoS Biol 3:e402
Kahana MJ, Seelig D, Madsen JR (2001) Theta returns. Curr Opin Neurobiol 11:739–744
Kaiser J, Lutzenberger W (2005) Cortical oscillatory activity and the dynamics of auditory memory processing. Rev Neurosci 16:239–254
Kawaguchi Y, Katsumaru H, Kosaka T, Heizmann CW, Hama K (1987) Fast spiking cells in rat hippocampus (CA1 region) contain the calcium-binding protein parvalbumin. Brain Res 416:369–374
Kilner JM, Baker SN, Salenius S, Hari R, Lemon RN (2000) Human cortical muscle coherence is directly related to specific motor parameters. J Neurosci 20:8838–8845
Klimesch W (2012) Alpha-band oscillations, attention, and controlled access to stored information. Trends Cogn Sci 16:606–617
Klimesch W, Doppelmayr M, Schwaiger J, Auinger P, Winkler T (1999) 'Paradoxical' alpha synchronization in a memory task. Brain Res Cogn Brain Res 7:493–501
Klimesch W, Sauseng P, Hanslmayr S (2007) EEG alpha oscillations: the inhibition-timing hypothesis. Brain Res Rev 53:63–88
Knief A, Schulte M, Bertran O, Pantev C (2000) The perception of coherent and non-coherent auditory objects: a signature in gamma frequency band. Hear Res 145:161–168
Knyazev GG (2012) EEG delta oscillations as a correlate of basic homeostatic and motivational processes. Neurosci Biobehav Rev 36:677–695

Knyazev GG, Slobodskoj-Plusnin JY, Bocharov AV (2009) Event-related delta and theta synchronization during explicit and implicit emotion processing. Neuroscience 164:1588–1600

Kopell N, Ermentrout GB, Whittington MA, Traub RD (2000) Gamma rhythms and beta rhythms have different synchronization properties. Proc Natl Acad Sci USA 97:1867–1872

Kopell N, Kramer MA, Malerba P, Whittington MA (2010) Are different rhythms good for different functions? Front Hum Neurosci 4:187

Lakatos P, Karmos G, Mehta AD, Ulbert I, Schroeder CE (2008) Entrainment of neuronal oscillations as a mechanism of attentional selection. Science 320:110–113

Lakatos P, Shah AS, Knuth KH, Ulbert I, Karmos G, Schroeder CE (2005) An oscillatory hierarchy controlling neuronal excitability and stimulus processing in the auditory cortex. J Neurophysiol 94:1904–1911

Laufs H, Kleinschmidt A, Beyerle A, Eger E, Salek-Haddadi A, Preibisch C, Krakow K (2003) EEG-correlated fMRI of human alpha activity. Neuroimage 19:1463–1476

Le Van Quyen M, Foucher J, Lachaux JP, Rodriguez E, Lutz A, Martinerie J, Varela FJ (2001) Comparison of Hilbert transform and wavelet methods for the analysis of neuronal synchrony. J Neurosci Methods 111:83–98

Lee MG, Chrobak JJ, Sik A, Wiley RG, Buzsaki G (1994) Hippocampal theta activity following selective lesion of the septal cholinergic system. Neuroscience 62:1033–1047

Lega BC, Jacobs J, Kahana M (2012) Human hippocampal theta oscillations and the formation of episodic memories. Hippocampus 22:748–761

Lehtela L, Salmelin R, Hari R (1997) Evidence for reactive magnetic 10-Hz rhythm in the human auditory cortex. Neurosci Lett 222:111–114

Leung LS (1982) Nonlinear feedback model of neuronal populations in hippocampal CAl region. J Neurophysiol 47:845–868

Liebe S, Hoerzer GM, Logothetis NK, Rainer G (2012) Theta coupling between V4 and prefrontal cortex predicts visual short-term memory performance. Nat Neurosci 15(456–462):S451–S452

Lisman J (2005) The theta/gamma discrete phase code occuring during the hippocampal phase precession may be a more general brain coding scheme. Hippocampus 15:913–922

Lisman J, Redish AD (2009) Prediction, sequences and the hippocampus. Philos Trans R Soc Lond B Biol Sci 364:1193–1201

Litvak V, Jha A, Eusebio A, Oostenveld R, Foltynie T, Limousin P, Zrinzo L, Hariz MI, Friston K, Brown P (2011) Resting oscillatory cortico-subthalamic connectivity in patients with Parkinson's disease. Brain 134:359–374

Llinas R, Jahnsen H (1982) Electrophysiology of mammalian thalamic neurones in vitro. Nature 297:406–408

Lopes Da Silva FH, Vos JE, Mooibroek J, Van Rotterdam A (1980) Relative contributions of intracortical and thalamo-cortical processes in the generation of alpha rhythms, revealed by partial coherence analysis. Electroencephalogr Clin Neurophysiol 50:449–456

Lorincz ML, Kekesi KA, Juhasz G, Crunelli V, Hughes SW (2009) Temporal framing of thalamic relay-mode firing by phasic inhibition during the alpha rhythm. Neuron 63:683–696

Luu P, Tucker DM, Makeig S (2004) Frontal midline theta and the error-related negativity: neurophysiological mechanisms of action regulation. Clin Neurophysiol 115:1821–1835

Mann EO, Suckling JM, Hajos N, Greenfield SA, Paulsen O (2005) Perisomatic feedback inhibition underlies cholinergically induced fast network oscillations in the rat hippocampus in vitro. Neuron 45:105–117

Manning JR, Jacobs J, Fried I, Kahana MJ (2009) Broadband shifts in local field potential power spectra are correlated with single-neuron spiking in humans. J Neurosci 29:13613–13620

Mathewson KE, Gratton G, Fabiani M, Beck DM, Ro T (2009) To see or not to see: prestimulus alpha phase predicts visual awareness. J Neurosci 29:2725–2732

Mazaheri A, Nieuwenhuis IL, Van Dijk H, Jensen O (2009) Prestimulus alpha and mu activity predicts failure to inhibit motor responses. Hum Brain Mapp 30:1791–1800

Meeuwissen EB, Takashima A, Fernández G, Jensen O (2011) Evidence for human fronto-central gamma activity during long-term memory encoding of word sequences. PLoS ONE 6:e21356
Mehta MR (2001) Neuronal dynamics of predictive coding. Neuroscientist 7:490–495
Mehta MR, Lee AK, Wilson MA (2002) Role of experience and oscillations in transforming a rate code into a temporal code. Nature 417:741–746
Miller KJ, Shenoy P, Den Nijs M, Sorensen LB, Rao RN, Ojemann JG (2008) Beyond the gamma band: the role of high-frequency features in movement classification. IEEE Trans Biomed Eng 55:1634–1637
Mitchell DJ, Mcnaughton N, Flanagan D, Kirk IJ (2008) Frontal-midline theta from the perspective of hippocampal "theta". Prog Neurobiol 86:156–185
Mitra PP, Pesaran B (1999) Analysis of dynamic brain imaging data. Biophys J 76:691–708
Muller N, Weisz N (2012) Lateralized auditory cortical alpha band activity and interregional connectivity pattern reflect anticipation of target sounds. Cereb Cortex 22:1604–1613
Muthukumaraswamy SD, Edden RA, Jones DK, Swettenham JB, Singh KD (2009) Resting GABA concentration predicts peak gamma frequency and fMRI amplitude in response to visual stimulation in humans. Proc Natl Acad Sci USA 106:8356–8361
Muthukumaraswamy SD, Singh KD (2013) Visual gamma oscillations: the effects of stimulus type, visual field coverage and stimulus motion on MEG and EEG recordings. Neuroimage 69:223–230
Muthukumaraswamy SD, Singh KD, Swettenham JB, Jones DK (2010) Visual gamma oscillations and evoked responses: variability, repeatability and structural MRI correlates. Neuroimage 49:3349–3357
Muthuswamy J, Thakor NV (1998) Spectral analysis methods for neurological signals. J Neurosci Methods 83:1–14
Niedermeyer E (1997) Alpha rhythms as physiological and abnormal phenomena. Int J Psychophysiol 26:31–49
Noudoost B, Moore T (2011) The role of neuromodulators in selective attention. Trends Cogn Sci 15:585–591
O'keefe J, Dostrovsky J (1971) The hippocampus as a spatial map. Preliminary evidence from unit activity in the freely-moving rat. Brain Res 34:171–175
O'keefe J, Recce ML (1993) Phase relationship between hippocampal place units and the EEG theta rhythm. Hippocampus 3:317–330
Osipova D, Hermes D, Jensen O (2008) Gamma power is phase-locked to posterior alpha activity. PLoS ONE 3:e3990
Osipova D, Takashima A, Oostenveld R, Fernandez G, Maris E, Jensen O (2006) Theta and gamma oscillations predict encoding and retrieval of declarative memory. J Neurosci 26:7523–7531
Palva JM, Palva S, Kaila K (2005) Phase synchrony among neuronal oscillations in the human cortex. J Neurosci 25:3962–3972
Palva S, Palva JM (2007) New vistas for alpha-frequency band oscillations. Trends Neurosci 30:150–158
Palva S, Palva JM (2011) Functional roles of alpha-band phase synchronization in local and large-scale cortical networks. Front Psychol 2:204
Pantev C, Ross B, Fujioka T, Trainor LJ, Schulte M, Schulz M (2003) Music and learning-induced cortical plasticity. Ann N Y Acad Sci 999:438–450
Park H, Kang E, Kang H, Kim JS, Jensen O, Chung CK, Lee DS (2011) Cross-frequency power correlations reveal the right superior temporal gyrus as a hub region during working memory maintenance. Brain Connect 1:460–472
Penny WD, Duzel E, Miller KJ, Ojemann JG (2008) Testing for nested oscillation. J Neurosci Methods 174:50–61
Percival DB, Walden AT (1993) Spectral analysis for physical applications: multitaper and conventional univeriate techniques. Cambridge, Cambridge University Press
Pesaran B (2008) Spectral analysis for neural signals, In: Mitra P (ed) Society for neuroscience, Washington DC

Pesaran B, Pezaris JS, Sahani M, Mitra PP, Andersen RA (2002) Temporal structure in neuronal activity during working memory in macaque parietal cortex. Nat Neurosci 5:805–811
Pfurtscheller G, Neuper C (1994) Event-related synchronization of mu rhythm in the EEG over the cortical hand area in man. Neurosci Lett 174:93–96
Pike FG, Goddard RS, Suckling JM, Ganter P, Kasthuri N, Paulsen O (2000) Distinct frequency preferences of different types of rat hippocampal neurones in response to oscillatory input currents. J Physiol 529(Pt 1):205–213
Ray S, Maunsell JH (2010) Differences in gamma frequencies across visual cortex restrict their possible use in computation. Neuron 67:885–896
Ray WJ, Cole HW (1985) EEG alpha activity reflects attentional demands, and beta activity reflects emotional and cognitive processes. Science 228:750–752
Roelfsema PR (1998) Solutions for the binding problem. Z Naturforsch C 53:691–715
Rols G, Tallon-Baudry C, Girard P, Bertrand O, Bullier J (2001) Cortical mapping of gamma oscillations in areas V1 and V4 of the macaque monkey. Vis Neurosci 18:527–540
Romei V, Brodbeck V, Michel C, Amedi A, Pascual-Leone A, Thut G (2008) Spontaneous fluctuations in posterior alpha-band EEG activity reflect variability in excitability of human visual areas. Cereb Cortex 18:2010–2018
Rotstein HG, Pervouchine DD, Acker CD, Gillies MJ, White JA, Buhl EH, Whittington MA, Kopell N (2005) Slow and fast inhibition and an H-current interact to create a theta rhythm in a model of CA1 interneuron network. J Neurophysiol 94:1509–1518
Roux F, Wibral M, Mohr HM, Singer W, Uhlhaas PJ (2012) Gamma-band activity in human prefrontal cortex codes for the number of relevant items maintained in working memory. J Neurosci 32:12411–12420
Saalmann YB, Pinsk MA, Wang L, Li X, Kastner S (2012) The pulvinar regulates information transmission between cortical areas based on attention demands. Science 337:753–756
Salinas E, Sejnowski TJ (2001) Correlated neuronal activity and the flow of neural information. Nat Rev Neurosci 2:539–550
Sauseng P, Klimesch W, Gerloff C, Hummel FC (2009) Spontaneous locally restricted EEG alpha activity determines cortical excitability in the motor cortex. Neuropsychologia 47:284–288
Schack B, Vath N, Petsche H, Geissler HG, Moller E (2002) Phase-coupling of theta-gamma EEG rhythms during short-term memory processing. Int J Psychophysiol 44:143–163
Scheeringa R, Mazaheri A, Bojak I, Norris DG, Kleinschmidt A (2011) Modulation of visually evoked cortical FMRI responses by phase of ongoing occipital alpha oscillations. J Neurosci 31:3813–3820
Scheeringa R, Petersson KM, Oostenveld R, Norris DG, Hagoort P, Bastiaansen MC (2009) Trial-by-trial coupling between EEG and BOLD identifies networks related to alpha and theta EEG power increases during working memory maintenance. Neuroimage 44:1224–1238
Sederberg PB, Kahana MJ, Howard MW, Donner EJ, Madsen JR (2003) Theta and gamma oscillations during encoding predict subsequent recall. J Neurosci 23:10809–10814
Seidenbecher T, Laxmi TR, Stork O, Pape HC (2003) Amygdalar and hippocampal theta rhythm synchronization during fear memory retrieval. Science 301:846–850
Shaw JC (2003) The Brain's alpha rhythms and the mind: a review of classical and modern studies of the alpha rhythm component of the electroencephalogram with commentaries on associated neuroscience and neuropsychology. Elsevier, Amsterdam
Shils JL, Litt M, Skolnick BE, Stecker MM (1996) Bispectral analysis of visual interactions in humans. Electroencephalogr Clin Neurophysiol 98:113–125
Siapas AG, Lubenov EV, Wilson MA (2005) Prefrontal phase locking to hippocampal theta oscillations. Neuron 46:141–151
Siegel M, Donner TH, Engel AK (2012) Spectral fingerprints of large-scale neuronal interactions. Nat Rev Neurosci 13:121–134
Siegel M, Donner TH, Oostenveld R, Fries P, Engel AK (2008) Neuronal synchronization along the dorsal visual pathway reflects the focus of spatial attention. Neuron 60:709–719
Sigl JC, Chamoun NG (1994) An introduction to bispectral analysis for the electroencephalogram. J Clin Monit 10:392–404

Singh KD, Barnes GR, Hillebrand A, Forde EM, Williams AL (2002) Task-related changes in cortical synchronization are spatially coincident with the hemodynamic response. Neuroimage 16:103–114

Sirota A, Montgomery S, Fujisawa S, Isomura Y, Zugaro M, Buzsaki G (2008) Entrainment of neocortical neurons and gamma oscillations by the hippocampal theta rhythm. Neuron 60:683–697

Slepian D, Pollak HO (1961) Prolate spheroidal wave functions, fourier analysis and uncertainty. 1. Bell Syst Tech J 40:43–64

Smith SW (1997) The scientist and engineer's guide to digital signal processing. California Technical, San Diego

Spaak E, Bonnefond M, Maier A, Leopold DA, Jensen O (2012a) Layer-specific entrainment of gamma-band neural activity by the alpha rhythm in monkey visual cortex. Curr Biol 22:2313–2318

Spaak E, Zeitler M, Gielen S (2012b) Hippocampal theta modulation of neocortical spike times and gamma rhythm: a biophysical model study. PLoS ONE 7:e45688

Spitzer B, Wacker E, Blankenburg F (2010) Oscillatory correlates of vibrotactile frequency processing in human working memory. J Neurosci 30:4496–4502

Stewart M, Fox SE (1990) Do septal neurons pace the hippocampal theta rhythm? Trends Neurosci 13:163–168

Tallon-Baudry C, Bertrand O (1999) Oscillatory gamma activity in humans and its role in object representation. Trends Cogn Sci 3:151–162

Tass P, Rosenblum MG, Weule J, Kurths J, Pikovsky A, Volkmann J, Schnitzler A, Freund HJ (1998) Detection of n: m phase locking from noisy data: Application to magnetoencephalography. Phys Rev Lett 81:3291–3294

Terman D, Bose A, Kopell N (1996) Functional reorganization in thalamocortical networks: transition between spindling and delta sleep rhythms. Proc Natl Acad Sci USA 93:15417–15422

Thut G, Miniussi C, Gross J (2012) The functional importance of rhythmic activity in the brain. Curr Biol 22:R658–R663

Thut G, Nietzel A, Brandt SA, Pascual-Leone A (2006) Alpha-band electroencephalographic activity over occipital cortex indexes visuospatial attention bias and predicts visual target detection. J Neurosci 26:9494–9502

Tierney PL, Degenetais E, Thierry AM, Glowinski J, Gioanni Y (2004) Influence of the hippocampus on interneurons of the rat prefrontal cortex. Eur J Neurosci 20:514–524

Tiesinga P, Sejnowski TJ (2009) Cortical enlightenment: are attentional gamma oscillations driven by ING or PING? Neuron 63:727–732

Tiesinga PH, Fellous JM, Salinas E, Jose JV, Sejnowski TJ (2004) Synchronization as a mechanism for attentional gain modulation. Neurocomputing 58–60:641–646

Tort AB, Komorowski R, Eichenbaum H, Kopell N (2010) Measuring phase-amplitude coupling between neuronal oscillations of different frequencies. J Neurophysiol 104:1195–1210

Tort AB, Komorowski RW, Manns JR, Kopell NJ, Eichenbaum H (2009) Theta-gamma coupling increases during the learning of item-context associations. Proc Natl Acad Sci USA 106:20942–20947

Tort AB, Kramer MA, Thorn C, Gibson DJ, Kubota Y, Graybiel AM, Kopell NJ (2008) Dynamic cross-frequency couplings of local field potential oscillations in rat striatum and hippocampus during performance of a T-maze task. Proc Natl Acad Sci USA 105:20517–20522

Traub RD, Jefferys JGR, Whittington MA (1999) Fast oscillations in cortical circuits. MIT Press, Cambridge

Traub RD, Whittington MA (2010) Cortical oscillations in health and disease. Oxford University Press, Oxford

Tuladhar AM, Huurne N, Schoffelen JM, Maris E, Oostenveld R, Jensen O (2007a) Parieto-occipital sources account for the increase in alpha activity with working memory load. Hum Brain Mapp 28:785–792

Tuladhar AM, Ter Huurne N, Schoffelen JM, Maris E, Oostenveld R, Jensen O (2007b) Parieto-occipital sources account for the increase in alpha activity with working memory load. Hum Brain Mapp 28:785–792

Van De Vijver I, Ridderinkhof KR, Cohen MX (2011) Frontal oscillatory dynamics predict feedback learning and action adjustment. J Cogn Neurosci 23:4106–4121

Van Der Werf J, Buchholz V, Jensen O, Medendorp W (2009) Neuronal synchronization in human parietal cortex during saccade planning. Behav Brain Res 205:329–335

Van Ede F, De Lange F, Jensen O, Maris E (2011) Orienting attention to an upcoming tactile event involves a spatially and temporally specific modulation of sensorimotor alpha- and beta-band oscillations. J Neurosci 31:2016–2024

Van Elswijk G, Maij F, Schoffelen JM, Overeem S, Stegeman DF, Fries P (2010) Corticospinal beta-band synchronization entails rhythmic gain modulation. J Neurosci 30:4481–4488

Van Pelt S, Boomsma DI, Fries P (2012) Magnetoencephalography in twins reveals a strong genetic determination of the peak frequency of visually induced gamma-band synchronization. J Neurosci 32:3388–3392

Van Vreeswijk C, Abbott LF, Ermentrout GB (1994) When inhibition not excitation synchronizes neural firing. J Comput Neurosci 1:313–321

Varela F, Lachaux JP, Rodriguez E, Martinerie J (2001) The brainweb: phase synchronization and large-scale integration. Nat Rev Neurosci 2:229–239

Vida I, Bartos M, Jonas P (2006) Shunting inhibition improves robustness of gamma oscillations in hippocampal interneuron networks by homogenizing firing rates. Neuron 49:107–117

Vijayan S, Kopell NJ (2012) Thalamic model of awake alpha oscillations and implications for stimulus processing. Proc Natl Acad Sci USA 109:18553–18558

Vrba J, Robinson SE (2001) Signal processing in magnetoencephalography. Methods 25:249–271

Wang XJ (2010) Neurophysiological and computational principles of cortical rhythms in cognition. Physiol Rev 90:1195–1268

Wang XJ, Buzsaki G (1996) Gamma oscillation by synaptic inhibition in a hippocampal interneuronal network model. J Neurosci 16:6402–6413

Watrous AJ, Lee DJ, Izadi A, Gurkoff GG, Shahlaie K, Ekstrom AD (2013) A comparative study of human and rat hippocampal low frequency oscillations during spatial navigation. Hippocampus 23:656–661

Weisz N, Hartmann T, Muller N, Lorenz I, Obleser J (2011) Alpha rhythms in audition: cognitive and clinical perspectives. Front Psychol 2:73

Welch PD (1967) Use of fast fourier transform for estimation of power spectra—a method based on time averaging over short modified periodograms. IEEE Trans Audio Electroacoust Au15: 70–73

Wespatat V, Tennigkeit F, Singer W (2004) Phase sensitivity of synaptic modifications in oscillating cells of rat visual cortex. J Neurosci 24:9067–9075

Whittington MA, Traub RD, Jefferys JG (1995) Synchronized oscillations in interneuron networks driven by metabotropic glutamate receptor activation. Nature 373:612–615

Whittington MA, Traub RD, Kopell N, Ermentrout B, Buhl EH (2000) Inhibition-based rhythms: experimental and mathematical observations on network dynamics. Int J Psychophysiol 38:315–336

Wilson HR, Cowan JD (1972) Excitatory and inhibitory interactions in localized populations of model neurons. Biophys J 12:1–24

Wilson MA, Mcnaughton BL (1993) Dynamics of the hippocampal ensemble code for space. Science 261:1055–1058

Worden MS, Foxe JJ, Wang N, Simpson GV (2000) Anticipatory biasing of visuospatial attention indexed by retinotopically specific alpha-band electroencephalography increases over occipital cortex. J Neurosci 20: RC63

Wulff P, Ponomarenko AA, Bartos M, Korotkova TM, Fuchs EC, Bahner F, Both M, Tort AB, Kopell NJ, Wisden W, Monyer H (2009) Hippocampal theta rhythm and its coupling with gamma oscillations require fast inhibition onto parvalbumin-positive interneurons. Proc Natl Acad Sci USA 106:3561–3566

Studying Dynamic Neural Interactions with MEG

Jan-Mathijs Schoffelen and Joachim Gross

Abstract Interactions between functionally specialized brain regions are crucial for normal brain function. Magnetoencephalography (MEG) is suited to capture these interactions because it provides whole head measurements of brain activity with temporal resolution in the millisecond range. Many different measures of connectivity exist and in order to take the connectivity analysis results at face value one should be aware of the strengths and weaknesses of these measures. Next to this, an important challenge in MEG connectivity analysis lies in the fact that more than one sensor picks up the activity of any underlying source. This field spread severely limits the utility of connectivity measures computed directly between sensor recordings. As a consequence, neuronal interactions should be ideally studied on the level of the reconstructed sources. MEG is well suited for this purpose, since its signal properties and high spatial sampling allows for relatively accurate unmixing of the sensor recordings. This chapter provides some necessary background on connectivity analysis in general, and proceeds by describing the challenges that are associated with the analysis of MEG-based connectivity at the sensor level. Source level approaches are described and some recent advances with respect to MEG-based connectivity during the resting state and graph theoretic approaches are described.

Keywords MEG · Magnetoencephalography · Connectivity · Coherence · Synchronization · Source localization · Field spread · Resting-state networks · Graph theory

J.-M. Schoffelen
Centre for Cognitive Neuroimaging, Donders Institute for Brain, Cognition and Behaviour, Radboud University Nijmegen, Nijmegen, The Netherlands

J.-M. Schoffelen
Max Planck Institute for Psycholinguistics, Nijmegen, The Netherlands

J. Gross (✉)
Department of Psychology, Centre for Cognitive Neuroimaging (CCNi), University of Glasgow, Glasgow, UK
e-mail: Joachim.Gross@glasgow.ac.uk

S. Supek and C. J. Aine (eds.), *Magnetoencephalography*,
DOI: 10.1007/978-3-642-33045-2_18,

1 Introduction

Magnetoencephalography (MEG) as a technique is ideally suited to study activity of the human brain on the time scale of cognitive and behaviorial processes. It provides measurement of brain activity by covering the whole head with a high number of sensors, and is increasingly used to study networks of interacting brain regions. The purpose of this chapter is to provide some background on connectivity analysis with MEG and to highlight some recent methodological developments, which enable researchers to study the interaction between brain regions based on these non-invasively obtained electrophysiological measures of neuronal activity.

The structure of this chapter is as follows: first we review some of the measures that are commonly used to analyze connectivity. Then we will discuss the problems related to electromagnetic field spread in the context of connectivity analysis at the MEG sensor level. Next we will describe approaches that analyze connectivity in source space. Following this, we will discuss the emerging fields of studying connectivity in the brain at rest with MEG and graph theoretic analysis of MEG-based connectivity metrics.

2 Measures of Connectivity

When faced with the possibility to analyse connectivity in MEG, the researcher can employ a vast number of different measures and analysis approaches to quantify this. Each of the different measures of connectivity has its merits and disadvantages with respect to what can be interpreted from those measures, and the ease with which they can be computed. This section provides an overview of the measures most commonly used, without having the intention to be comprehensive. The different metrics that are mentioned are shown in Table 1.

2.1 Connectivity Measures can be Grouped Along Different Dimensions

It may be useful to group the different connectivity measures along several different dimensions. One key distinction which is often made is that of functional versus effective connectivity (Friston 1994). Measures of functional connectivity (undirected interaction measures) quantify statistical dependencies between neuronal signals, without explicitly addressing directed interactions. On the other hand, measures of effective connectivity (or directed interaction measures) quantify the directed influence of one neuronal system over another. This distinction has its implications for the interpretation of the analysis results. Per

Table 1 Overview of different connectivity measures and their main characteristics

	Directed interactions	Freq/time domain	Multi/ bivariate	Linear	Sensitive to field spread
Amplitude envelope correlation	–	f	b	+	+
Coherence	–	f	b	+	+
Cross-correlation function	+	t	b	+	+
Cross-frequency interactions	–	f	b	–	+
Directed transfer function	+	t	m	+	+
Dynamic causal modelling	+	t/f	m	–	+
Granger causality	+	t/f	b	+	+
Imaginary part of coherency	+	f	m	–	–
Mutual information	–	t/f	b	–	+
Partial directed coherence	+	f	m	+	+
Phase lag index	+	f	b	–	–
Phase locking value	–	f	b	–	+
Phase slope index	+	f	b	–	–
Synchronization likelihood	+	t	b	–	–
Transfer entropy	+	t/f	b	–	–

definition, undirected interaction measures do not allow for an interpretation of causality.

Another important distinction is that between time and frequency domain measures of connectivity. This directly refers to the underlying physiological mechanisms by means of which neuronal interactions are thought to occur. One view, which has gained a lot of interest in the past few decades, is that neural interactions are reflected in changes in the synchronization of rhythmic activity between brain regions (Fries 2005). In light of this proposed mechanism of interaction, it makes sense to use connectivity measures that are defined in the frequency domain, and where an estimate of the phase difference is used to compute the connectivity.

Yet another distinction pertains to whether the connectivity measure is a bivariate or a multivariate one. Although typically connectivity measures are estimated between pairs of signals, some measures account for the influence of 'third party signals' on the connection under consideration, yielding a potentially clearer interpretation of the interaction being direct or indirect (e.g. due to common input from a third source of activity).

Some connectivity measures assume the interaction between signals to be linear and/or use linear estimation techniques. Other measures don't rely on these

assumptions. This constrains the interpretation of the estimated connectivity results. Also, in general non-linear measures are often based on estimates of probability distributions and require more computing time, and also more data to be computed reliably.

Finally, in the context of MEG, it is crucial to consider whether the connectivity measure is sensitive to the effects of electromagnetic field spread. This will be outlined and discussed in more detail in Sect. 3.

2.2 Frequency Domain Measures of Undirected Interactions

Amplitude envelope correlation refers to the correlation coefficient between amplitude envelope time courses, which are typically computed on bandpass-filtered data, and as such this measure classifies as a frequency domain connectivity measure.

Coherence (Gross et al. 2001) is the frequency domain analogue of the cross-correlation coefficient, and is usually computed using non-parametric spectral estimation techniques, such as the Fourier transform, or a wavelet transform. As such coherence confounds the estimated consistency of a fixed phase difference with the correlation of the signals' amplitudes. It's a very popular measure, because it's easy to compute and it has a straightforward interpretation in terms of frequency-resolved linear predictions.

Amplitude effects can be disentangled from the consistency of the phase difference by means of the *phase locking value* (PLV). This measure can be obtained by normalising the complex-valued frequency domain single trial values with respect to their amplitudes, prior to estimating the interaction between the signals (Lachaux et al. 1999). This phase synchronisation analysis has been used in source connectivity analysis to complement traditional coherence analysis (Jerbi et al. 2007). Both coherence and PLV are symmetric measures and do not allow direct inference about directionality of information flow between areas. However, time delays can be estimated from the slope of the cross-spectral densities between time series under favourable conditions (Nolte et al. 2008).

Recent years have seen an increased interest in *cross-frequency interactions*, inspired by the notion that neuronal signals typically show rhythmic activity in several distinct frequency bands, and that neuronal interactions thus may also be reflected in statistical dependencies between these frequency bands (Jensen and Colgin 2007). Several types of interactions can be considered here, e.g. amplitude-amplitude coupling (where there is a correlation across observations of the amplitude envelopes of different frequency bands) or phase-amplitude coupling (where the phase of a slow oscillation systematically modulates the amplitude of a fast oscillation).

2.3 Measures of Directed Interactions

Directed interactions can be inferred in one of the following conceptually different ways. The simplest concept is based on estimating the time lag between events occurring in a pair of signals (Nolte et al. 2008; Gross et al. 2000). This is linked to the principle that a cause must precede its effect, but it should be noted that temporal precedence does not provide direct evidence for causal interactions (Atukeren 2008). In the time domain, the cross correlation function can be used to estimate time lags between signals. However, this technique is hardly used in MEG-research. It is more common to explore the time lag in the frequency domain, where one can exploit the principle that a fixed time delay translates into linearly increasing phase differences with increasing frequency. Hence, the slope of the phase difference spectrum is a direct estimate of this time-delay. The *phase slope index* (Nolte et al. 2008; Haufe et al. 2013) is a measure that is based on this principle. The *phase lag index* (PLI) (Stam et al. 2007) quantifies the deviation of the phase difference distribution from 0, thus allowing for the inference of one signal leading (or lagging) the other.

Related to the concept of temporal precedence is the concept of *Wiener-Granger causality* (Bressler and Seth 2011), which is based on the prediction of a signal (let's call this signal A for the time being) based on the past values of itself, and based on the past values of another signal (signal B). If the quality of the prediction of signal A is substantially improved when past values of B are taken into account, signal B is said to cause signal A. This principle has been originally formulated by Wiener (1956), and is operationalized in the measure of Granger causality (Granger 1969). Granger causality in its original formulation is defined in the time domain. It is usually implemented by means of fitting a series of multivariate autoregressive models (MVAR-models) (Schloegl et al. 2006) and by exploring the residuals of the model fit. Based on work by Geweke, frequency-resolved Granger causality can also be computed, and from the Fourier transform of the autoregressive model coefficients a series of related measures can be derived such as the *directed transfer function* (DTF) (Kaminski and Liang 2005) and *partial directed coherence* (PDC) (Baccala and Sameshima 2001). Common to these measures is that they assume that the interaction is linear. *Transfer entropy* (TE Schreiber (2000)) is an implementation of Wiener's principle of causality that is free of an explicit model of the signals and their interaction. A non-linear formulation of Granger causality also exists (Marinazzo et al. 2011).

Finally, rather than using a data-driven approach, one can try and create generative model of the measured data, where the model entails not only the activation patterns of the underlying neural sources, but also their interactions. This approach is implemented in *Dynamic Causal Modelling* (DCM) (Moran et al. 2007; Kiebel et al. 2008; David and Friston 2003). The generative model specifies how input activates a system of pre-specified interconnected neuronal populations, leading to the measured signal. As such DCM provides an estimate of coupling parameters and source parameters in a single step (Kiebel et al. 2008). DCM had originally

been devised for the analysis of evoked responses (Garrido et al. 2007). Recent developments have extended the functionality of this promising technique to induced responses (Chen et al. 2008), steady state responses (Moran et al. 2007) and phase-coupling (Penny et al. 2009).

3 MEG Sensor Level Connectivity Analysis

A central issue in the interpretation of MEG data is the problem of electromagnetic field spread. Although it is a well-known problem and described elsewhere (Winter et al. 2007), it merits discussion in the context of connectivity analysis because it severely confounds many connectivity measures and therefore complicates the correct interpretation of the results. In the following sections we will outline this problem in the context of connectivity analysis, and describe two strategies, which attempt to diminish this problem: the analysis of experimental contrasts, and the use of connectivity measures that are less sensitive to electromagnetic field spread.

3.1 Electromagnetic Field Spread

Field spread refers to the phenomenon that the magnetic fields that are associated with electrical currents (of neural and non-neural origin) are not confined to the vicinity of the current generators, but are measurable far away from their source. For any neuronal source this leads to a widespread representation at the level of the sensor array. As a matter of fact, thanks to this feature, it is possible in the first place to measure MEG extracranially and to build models of the underlying neural sources. Yet, electromagnetic field spread also has important consequences for the interpretability of connectivity measures estimated between pairs or sensors. The reason for this is that any single source of neural (or non-neural) electric activity is visible to many sensors at once. This is illustrated by Fig. 1a. The spatial topography shows the correlation between one channel and the rest, from simulated data containing one single dipole plus uncorrelated sensor noise. Obviously, MEG sensor recordings represent the superposition of the activity of multiple sources, which are either or not functionally connected. Also with multiple sources present, even if the underlying sources are ‘unconnected’, many connectivity measures estimated between pairs of sensors will yield spurious estimates due to the instantaneous mixing process. To illustrate this we simulated the activity of 821 temporally uncorrelated dipoles, with an orientation parallel to the axis between the nasion and the midpoint of the interauricular line, and that were randomly distributed on the cortical sheet. Clearly, the orientations chosen are physiologically not meaningful, but are appropriate to demonstrate the effect of field spread on connectivity analysis. Using FieldTrip (Oostenveld et al. 2011), we simulated 50 s of data for a 275-channel CTF axial gradiometer system, by using a single shell

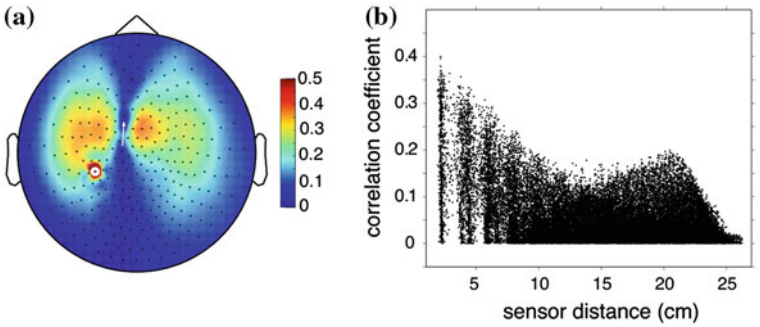

Fig. 1 The effects of field spread confound sensor level estimates of connectivity measures. **a** Sensor-level connectivity between a seed sensor and the rest of the sensor array in the presence of a single underlying source. **b** The absolute value of the correlation coefficient between all pairs of measured signals as a function of sensor distance, where the underlying 821 sources were uncorrelated

volume conductor model (Nolte 2003) and uncorrelated sensor noise. Figure 1b shows the absolute value of the correlation coefficient between all MEG sensor pairs as a function of their distance. Even though the underlying source activities are temporally uncorrelated, many sensor pairs show high values of correlation.

3.2 Addressing Electromagnetic Field Spread with Statistics

In order to reduce the interpretational difficulties caused by field spread, one potential strategy could be to analyze changes in connectivity caused by an experimental manipulation, rather than the strength of the connectivity as such. The rationale for using experimental contrasts in this context is based on the assumption that the effects of electromagnetic field spread are identical across the experimental conditions and therefore subtract out. Unfortunately, the spatial structure of field spread is highly dependent on changes in the signals, and on changes in the noise. As a consequence, estimated modulations in connectivity do not necessarily always reflect modulations in actual connectivity between relevant neuronal sources. Experimental manipulations will most likely always lead to changes in activity of the underlying sources, or in the activation of different sources. Also, in studies that involve the comparison between different groups of subjects (e.g. patients versus controls), it is not unlikely that difference in the distribution and activity of the underlying sources exist. These potential confounds in the interpretation of estimated differences in connectivity should therefore always be taken into account. This is illustrated in Fig. 2. Here, we simulated two dipoles oscillating at 20 Hz in left and right 'motor cortex', at a phase difference of 90°, against a background of 821 uncorrelated dipoles evenly distributed across the cortical sheet. We generated 2 conditions of data where the amplitude of the motor

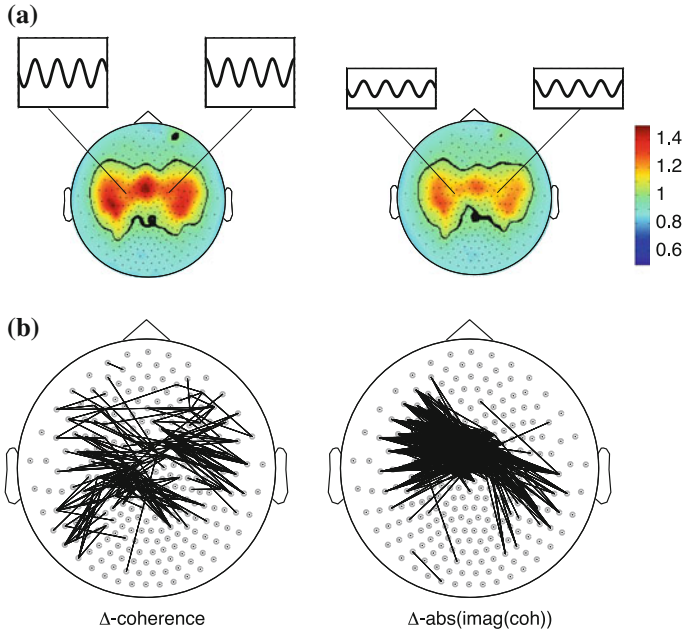

Fig. 2 Changes in source strength yield widespread changes in sensor-level connectivity. **a** spatial topography of simulated activity with 821 randomly distributed, uncorrelated dipoles, and 2 strong, highly correlated dipoles in approximately *left* and *right* motor regions. The amplitude of the 'motor' sources is two times higher in the *left* panel than in the *right* panel. **b** Thresholded differential connectivity patterns (high amplitude condition minus low amplitude condition), where each line represents a sensor pair where the differential connectivity exceeded a threshold of 0.2. Two different connectivity metrices were used: coherence (*left* panel) and the imaginary part of coherency (*right* panel)

cortex dipoles was twice as large in condition 1 compared to condition 2 (Fig. 2a). We computed coherence and the imaginary part of coherency (see Sect. 3.3) across all channel pairs and display the sensor pairs in which the difference in connectivity across the conditions exceeded a certain threshold. Clearly there is interesting spatial structure in the differential coherence and imaginary coherency maps, that cannot be accounted for by a change in actual connectivity (which as a matter of fact in both conditions was simulated to be equal to 1).

For the reasons outlined above, field spread is problematic in the interpretation of sensor-level connectivity estimates, and an important motivation to perform the connectivity analysis at the source level. Also, contrasting connectivity between two experimental conditions in sensor space will likely reduce (but not abolish) negative effects of field spread (Schoffelen and Gross 2009). In addition to this, there are other important motivations to perform the analysis on the source level. First of all, there is a more direct indication of the anatomical location of the interacting brain regions. Secondly, source level analysis facilitates subsequent group analysis because the data can be averaged in a meaningful standardized space.

3.3 Addressing Electromagnetic Field Spread with Clever Measures of Connectivity

Another strategy to address interpretation problems associated with electromagnetic field spread is to use connectivity measures that are insensitive to this effect. In general, this type of measure can be divided into two categories. The first category consists of measures that are derived from conventional linear measures. The imaginary part of coherency (Nolte et al. 2004) is a well-known example of this type of measure. Another example is amplitude-envelope correlation with the zero time-lag correlation removed (Hipp et al. 2012) (see Sect. 5). The other category consists of measures that are derived from the non-linear dynamics framework. This type of measure includes the phase lag index (Stam et al. 2007) synchronization likelihood (Stam and Van Dijk 2002) and transfer entropy (Vicente et al. 2011).

Measures that are insensitive to field spread usually exploit the fact that field spread caused by point sources has an instantaneous effect on the sensors. In other words, field spread causes cross-correlation effects between sensors at a time lag of 0 ms, or equivalently at a phase difference of 0 or 180°. Explicitly removing the zero ms time lag contribution to the estimate of connectivity reduces the risk of falsely interpreting the estimate as true interaction. In the case of the imaginary part of coherency the removal of the 0° phase difference contribution is achieved by projection of the vector representation of the complex-valued coherency onto the imaginary axis.

An important caveat needs to be raised here, which is related to the fact that spurious connectivity is addressed only when contributing sources can be modeled as single point sources (equivalent current dipoles). This is illustrated in Fig. 3 where we present results of an analysis of the weighted phase lag index (WPLI) at 10 Hz (Vinck et al. 2011). For each channel, we computed the average WPLI between that channel and the rest of the channels and represented this in a spatial topography (panel A). Red here means that the underlying channels on average have a positive phase difference with the other channels, blue means that the underlying channels on average have a negative phase difference with the other channels. Thus the picture suggests a fronto-occipital gradient of time-lagged neural oscillations at 10 Hz, where the frontal channels ‘lead’ the occipital channels. However, the data that was used to generate this topography was constructed by back-projecting two independent components that were estimated from a few minutes of resting state MEG data. The time course of these components and their corresponding spatial topographies are shown in panel B. Clearly, these two components mainly represent cardiac activity. The slight time lag between the individual components in combination with the different topographies leads to a non-trivial mixing with significant interaction at non-zero time lag.

For the reasons outlined above it is increasingly acknowledged that the functional interactions should be studied at the level of the neuronal sources.

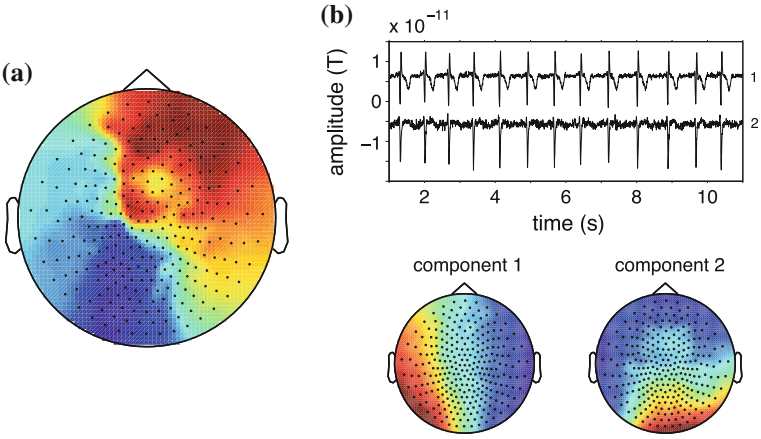

Fig. 3 Sources that cannot be described as a single equivalent dipole yield non-zero phase-lagged connectivity estimates. **a** Spatial topography displaying for each sensor the average of the weighted-phase lag index between that sensor, and the rest of the sensor-array, yielding a distinct pattern of 'information flow' from frontal to posterior sensors. **b** Fragment of the time courses and spatial topographies of the independent components underlying the data that was used to generate the topography in panel (**a**)

4 MEG Source Level Connectivity Analysis

In this section we will provide an overview of the main methods that have been suggested for MEG source connectivity analysis. Most methods essentially adopt a two-step procedure. Firstly, an estimate of the activity of the neuronal sources is obtained by applying an inverse method (for a review, see Baillet et al. (2001)). Secondly, an analysis of connectivity is performed, in which researchers usually restrict themselves to a set of pre-specified seed regions-of-interest (ROIs). A notable exception to this two-step approach is Dynamic Causal Modelling, which will be described below. It is beyond the scope of this chapter to present in a comprehensive discussion the advantages and disadvantages of all connectivity measures and inverse methods; thus we will focus on some applications of connectivity measures in source space.

Typically, MEG source connectivity analysis is performed on the basis of a few selected regions of interest (ROIs). Connectivity measures are computed between all combinations of ROIs or ROIs are used as seeds to compute connectivity between activity at the seed location and all other voxels. Several strategies for the selection of ROIs exist:

A priori selection. A priori knowledge from previous functional imaging studies can be used to select ROIs (Astolfi et al. 2005). These areas can be identified in the individual anatomical MRI or coordinates in Talairach-MNI space can be transformed into individual coordinates. A related approach has been proposed by Haerle et al. (2004). Minimum norm source estimates were computed for 350

voxels to study steady-state auditory responses. Subsequently, coherence was computed between all pairs of voxels.

Cortico-peripheral coherence. In this approach an external signal serves as a reference signal. This can be a kinematic or electromyographic recording or even a continuous stimulus signal (such as speech). Coherence is computed between the reference signal and brain activity reconstructed at a discretized grid. This method allows the identification of brain areas where the activity is modulated by rhythmic processes in the peripheral signal. This strategy has been used successfully for oscillatory components in movements as recorded with electromyography and movement tracking devices (Gross et al. 2001, 2002; Schoffelen et al. 2008), and for localizing activity in auditory cortex using the speech signal as reference signal (Peelle et al. 2012). The local maxima in the cortical coherence map can be used as seed voxels for the analysis of cerebro-cerebral connectivity.

Power maps. Possibly the most widely used strategy is a selection of ROIs based on maps of neural activation or the statistical contrast in activation between experimental conditions. This approach has been successfully applied in a number of studies (David et al. 2002, 2003; Jerbi et al. 2007; Hipp et al. 2011).

Connectivity-based methods. Recently, several studies have performed the computation of connectivity between all pairs of voxels. Palva et al. (2010) computed phase locking on MEG minimum norm estimates to identify networks in a working memory task (see also Sect. 6). Hipp et al. (2011) developed a 6-dimensional cluster method to identify coherent networks from beamformer-localised EEG data. Kujala and co-workers suggested a technique that identifies highly connected areas by computing the connection density throughout the brain (Kujala et al. 2007). These 'hubs' can then be used as ROIs for a more detailed analysis of connectivity.

Source level connectivity analysis has become a powerful tool to identify networks of interacting brain regions and to study task-related changes in these networks. Several consistent findings seem to emerge from these studies. Network interactions seem to be highly specific regarding the frequency band and have modulatory effects on behavioural performance. Phase synchronization in the beta frequency band engaging a fronto-parietal network has been related to successful target detection (Gross et al. 2004). Interestingly, this study also demonstrated that desynchronisation in the network after target detection is important to facilitate detection of a subsequent target. Another study showed beta synchronization in a similar fronto-parietal network related to the perception of ambiguous audiovisual stimuli (Hipp et al. 2011). Again, beta synchronization distinguished between different percepts of the same stimuli. These results are consistent with the involvement of beta band synchronisation in top-down processes.

Another study nicely demonstrates that connectivity between brain areas is task-dependent. Siegel and colleagues studied connectivity between visual, parietal and frontal brain areas in both hemispheres during a visuospatial attention task (Siegel et al. 2008). Interestingly, shifting visuospatial attention to one hemifield (while maintaining central fixation) leads to increased gamma synchronisation between visual, parietal and frontal areas specifically in the contralateral hemisphere. These

findings generalise beyond cognitive processes related to attention and perception. Palva et al. (2010) have studied phase synchronisation in a working memory task. They reported frequency-specific networks with low-frequency phase synchronisation predicting task performance.

5 Resting-State Connectivity

Human electrophysiological brain activity during rest has been studied since 1929, when Hans Berger performed the first human EEG recordings (Berger 1929). He discovered prominent rhythmic fluctuations in the signal at a rate of about 10/s. We now know that this so-called alpha oscillation dominates resting state activity, is strongest over occipital brain areas, and it reflects excitability changes in the generating neuronal populations (Niedermeyer and Silva 2004; Romei et al. 2008).

A vast number of MEG/EEG studies have been performed to study resting state activity in healthy participants and patients. In recent years functional connectivity has been studied in the resting state with MEG/EEG (Stam and van Straaten 2012; Stam 2010). Here, we focus on research that studies resting-state connectivity in source space. First, we present the commonly used methods to study resting-state connectivity and then we proceed to a discussion of the main findings.

5.1 Methodological Overview

It seems surprising that specific methods have been developed to study resting-state connectivity since the overall aim of this analysis is similar to the connectivity analysis for other types of data—namely the identification of significant functional interactions between the time series of different brain areas. However, connectivity analysis in cognitive studies generally relies on the statistical comparison of two conditions, or an 'active' period of time and a baseline—a procedure that is known to reduce (but not abolish) the effect of field spread (see Sect. 3.2). No such comparison is available for resting state data (although surrogate data can be used (Ghuman et al. 2011)). Therefore, researchers have focused on methods that are more robust against contamination by field spread—mostly relying on amplitude correlations.

Most resting state connectivity methods rely on independent component analysis (ICA), albeit at different stages in the processing pipeline. One method has been proposed by Brookes et al. (2011). Beamforming is used to compute time series of activation for individual voxels from bandpass filtered resting-state data (Fig. 4a). ICA is performed on the amplitude envelopes of the band-limited voxel time series to identify independent temporal components with corresponding spatial maps.

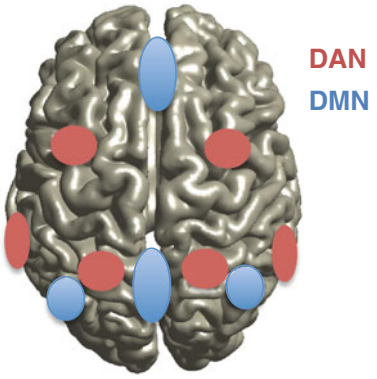

Fig. 4 Schematic illustration of two resting-state networks. *DAN* Dorsal Attention Network, *DMN* Default Mode Network. Locations are taken from (de Pasquale et al. 2010; Brookes et al. 2011)

In a recently proposed method (de Pasquale et al. 2010; Mantini et al. 2011) ICA is used as a first step to decompose the signal into statistically independent components that often correspond to different types of artefacts (e.g. eye blinks and cardiac artefacts) and different activated brain areas (Makeig et al. 2002). In a second step neural generators of non-artifactual components are localised using standard source localisation techniques such as minimum norm or beamforming methods (Fig. 4b). The time series at any voxel in the brain is then computed from the summation of IC timecourses weighted by the amplitude of their source reconstruction at that voxel. A bandpass filter is then applied and the amplitude envelope is computed as the absolute value of the hilbert transform of the filtered signal. Amplitude correlations are computed between a seed voxel and all other voxels.

A promising extension of the seed-based approach has been presented by Hipp et al. (2012). Similar to the approach by Brookes et al. bandpass-filtered data is subjected to beamformer analysis to derive a time series for individual voxels. However, each pair of time series (corresponding to seed voxel and target voxel) was first orthogonalised to remove common components with zero delay—the hallmark of components related to field spread (see Sect. 3).These resting-state methods typically use amplitude correlations based on downsampled amplitude envelopes. The optimal integration window seems to be in the order of 1–4 s (Luckhoo et al. 2012).

Gomez-Herrero et al. combined ICA with multivariate autoregressive (MVAR) models to study directionality in resting-state data (Gomez-Herrero et al. 2008), see also (Haufe et al. 2010). The analysis pipeline (see also Sect. 4) consisted of PCA for dimensionality reduction, followed by estimation of a MVAR model. Residuals of the model were then subjected to ICA decomposition to estimate cortical generators with a source reconstruction method. ICA components were then combined with the coefficients of the MVAR model to compute measures of directed interactions (in this case directed transfer function) in source space.

Alternative approaches have been introduced that do not rely on ICA. Hillebrand et al. (2012) proposed to use beamforming to estimate time series of

activation for regions of interest (ROIs) derived from an anatomical atlas. Spatial normalisation of individual MRIs is used to identify corresponding atlas-based ROIs in the individual brain. The study demonstrated that problems associated with field spread are reduced by using the Phase-Lag Index (Stam et al. 2007). A similar approach was used to study resting-state connectivity based on imaginary coherence in stroke patients (Guggisberg et al. 2008; Westlake et al. 2012).

5.2 Functional Connectivity in Resting-State Networks

The analysis of resting state connectivity in functional MRI has recently attracted significant interest (Beckmann et al. 2005; Deco and Corbetta 2011). This is at least partly due to the seminal study by Biswal and colleagues who demonstrated spatially specific correlations in the temporal activation of brain areas during rest (Biswal et al. 1995). These correlations are driven by slow temporal fluctuations with frequencies around or below 0.1 Hz. However, until recently is has been unclear if and how these correlation patterns are represented in electrophysiological recordings. Recent developments in data analysis methods (reviewed in the previous section) have facilitated the identification of similar spatio-temporal correlation pattern in MEG/EEG signals of the resting brain. Due to their excellent temporal resolution MEG/EEG contribute complementary information to the fMRI-studies of human resting-state connectivity.

De Pasquale and colleagues used a seed-based correlation approach (see previous section) to identify the default mode network (DMN) and the dorsal attention network (DAN) from MEG data (Fig. 5). Both networks showed high spatial overlap with the corresponding networks identified in fMRI data. Interestingly, the high temporal resolution of MEG recordings afforded the investigation of this correlation structure in different frequency bands. DMN and DAN showed strongest amplitude correlations in the alpha (8–13 Hz) and beta (14–25 Hz) frequency bands with correlations that changed significantly over time. These temporal changes were further investigated in a subsequent study by the same authors (de Pasquale et al. 2012). Here, the DMN emerged as the network with strongest cross-network interactions with the posterior cingulate cortex as the most important node in the DMN. The DMN preferentially engages with nodes of another network when the within-network interactions of this other network are low.

Using a data-driven approach that is not based on seed voxels Brookes and colleagues largely corroborated these results by identifying several resting-state networks (including DMN and DAN) with dominant interactions in the beta band (Brookes et al. 2011). The frequency-specific nature of correlations in these (and other) studies convincingly implicates brain oscillations as the basis for these network interactions.

The orthogonalisation introduced by Hipp et al. (2012) improved spatial resolution of correlation maps with interesting results. Significant interhemispheric

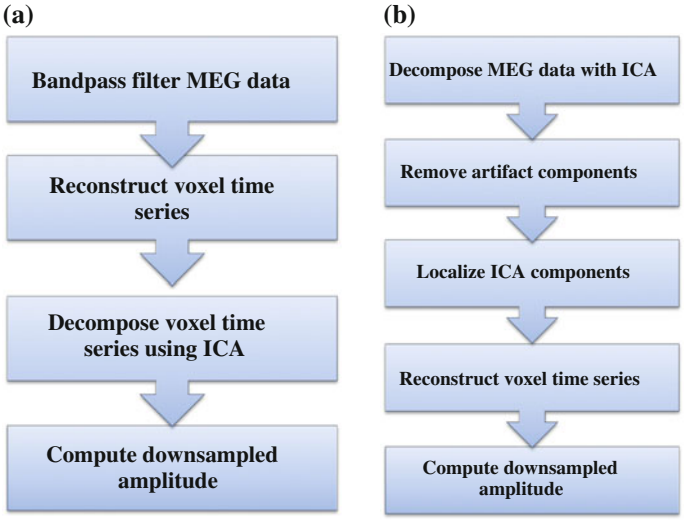

Fig. 5 Two analysis pipelines for resting state MEG data. **a** Analysis approach used by Brookes et al. 2011). **b** Analysis approach used by de Pasquale et al. (2010), (Mantini et al. 2011)

amplitude correlations emerged in the beta frequency band between homologous sensory (auditory, somatosensory, visual) areas.

In summary, recent MEG resting-state connectivity studies in source space independently confirm the existence of resting-state networks previously discovered in fMRI data. Interestingly, MEG studies demonstrate that the correlation pattern in these networks is mediated by brain oscillations (predominantly in the alpha and beta frequency band) and that these correlations show strong temporal modulations that coincide with state transitions of between-network interactions.

6 Graph Theory

Although Graph Theory has been developed decades ago (Erdoes and Renyi 1959) it has only recently found a widespread use in the investigation of brain networks. This interest likely originates from a challenge that researchers face when they investigate anatomical or functional brain connectivity—namely its complexity. Human brain connectivity studies typically work with anatomical or functional data at a spatial resolution of 1–10 mm, leading to thousands of voxels. Each voxel can have anatomical or functional connections to many other voxels. In addition, functional connections are often evaluated in different frequency bands, experimental conditions, and may change over time. A meaningful low-dimensional characterization of this complex, high-dimensional data would greatly facilitate the identification of systematic differences between experimental conditions, or

patients and healthy controls and could lead to a better understanding of the aspects of these complex networks that are essential for the functioning of the human brain. We will first introduce basic concepts of Graph theory, then present applications for MEG connectivity studies and, finally, discuss some limitations.

Networks of interacting brain areas can be represented by graphs. Graphs consist of nodes (or vertices) representing the brain areas, and connections (or edges) that represent the interactions between pairs of brain areas. Furthermore, information about directed information flow can be represented in directed graphs and information about connection strength can be represented in weighted graphs.

The topology of graphs can be characterized in a meaningful way by a number of measures that characterize different aspects of the graph. Here, we describe three important measures and refer the interested reader to more comprehensive material (Sporns 2011; Stam and van Straaten 2012; Ioannides 2007; Bullmore and Basset 2011).

Characteristic path length	This is the average number of nodes on the shortest path between two nodes
Degree distribution	The degree of a node is the number of connected nodes. The distribution of degree across all nodes of a graph is the degree distribution
Clustering coefficient	For a given node the clustering coefficient is the ratio of the number of existing to the number of possible connections between all neighbours of the node

Other measures such as *modularity* or *efficiency* have been introduced to characterise brain networks (Bullmore and Bassett 2011) with the aim to capture basic network characteristics that relate in a meaningful way to aspects of brain function or dysfunction.

Bassett and colleagues have used this approach successfully (Bassett et al. 2009). They demonstrated a positive correlation between performance in a working memory task and cost efficiency of network nodes. Consistent with the majority of MEG/EEG studies in this field individual sensors were taken as nodes. Various connectivity measures (see Sect. 2) can be used to quantify interactions between the signals of sensor pairs. Here, authors used mutual information in different frequency bands ranging from 1–60 Hz. Mutual information between all pairs of sensors signals results in a symmetric connectivity matrix. This matrix (that can also be computed from other connectivity measures such as coherence or phase synchronisation) is then converted into a graph. This conversion involves a thresholding and binarization of the matrix. The binarization sets every element with a value below threshold to zero and every element with a value above threshold to 1. The graph measure used by the authors was cost efficiency, which is inversely related to minimum path length computed at different thresholds. The authors observed significant correlation between cost efficiency and behavioral performance over left temporal and parietal areas and over midline frontal areas. This correlation was strongest in the beta band (12–30 Hz).

The possibility to describe topological aspects of a complex network with a few measures is particularly attractive for clinical studies since some of these measures could potentially be used as biomarkers for pathological changes associated with specific brain dysfunctions. Stam and colleagues have used Synchronization Likelihood (SL), a nonlinear measure of statistical interdependency, to study disease-related changes in functional brain networks. Again, SL values between pairs of MEG signals are used to build an association matrix that is converted into a graph before graph measures are computed. This approach has been used to uncover changes in network topology in different disorders such as Parkinson's and Alzheimer disease and is reviewed in (Stam 2010).

One of the most consistent findings emerging from these studies is that the functional network architecture of the human brain shows small-world properties (Stam 2004; Bassett et al. 2006). Small-worldness refers to networks that are characterised by high clustering but small path length. This is achieved by adding a few long-range connections to networks with predominantly short-range connections.

A limitation of these studies is that they use MEG sensors as graph nodes. This is problematic for at least two reasons (Schoffelen and Gross 2009). First, it is difficult to infer the involvement of specific brain areas from the location of MEG sensors. Second, the signal recorded by any given MEG sensor is typically a linear combination of the activity of several brain areas. Consequently, the topology of graphs constructed from sensor signals can be significantly affected by the sensitivity profile of the MEG sensor type and the specific configuration of active brain areas. Only few studies have addressed this problem by computing graphs from MEG data after source localization. Palva and colleagues studied functional connectivity in source space during visual working memory (Palva et al. 2010) and used graph theory to characterize the network. They localized bandpass filtered single-trial data using cortically constrained minimum-norm estimates. Phase-locking value was computed between pairs of cortical patches to build the association matrix. After thresholding based on group statistics, they used the node degree and related measures to identify hubs in frequency-dependent networks. The alpha-band network showed a hub in frontal cortex whereas for the beta-band hubs emerged in parieto-occipital cortex. Major hubs in the gamma-band were intraparietal sulcus (IPS) and superior parietal gyrus. Phase synchronization between brain areas was shown to correlate with behavioral performance. IPS was again the major hub in these performance-related networks.

This study nicely demonstrates the benefit of performing MEG connectivity analysis together with graph theory at the level of brain areas (as opposed to MEG sensor signals). Since here the graph nodes corresponded to anatomical brain areas results inferred from the functional data increase our understanding of specific brain networks and results can be related to findings from fMRI studies.

Although Graph Theory is a promising approach for the characterization of complex brain networks it has limitations. One main limitation is the loss of information during the computation of graphs (see Fig. 6). Following connectivity analysis the association matrix contains information about the strength of

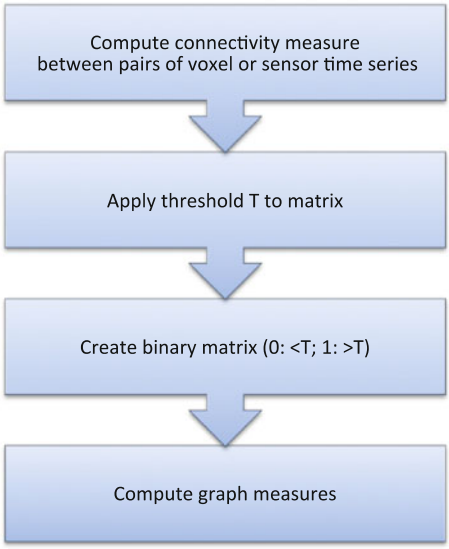

Fig. 6 Typical pipeline for applying Graph Theory to MEG connectivity results

interactions between all pairs of nodes (where nodes could be brain areas or MEG sensors). In addition, some connectivity measures provide information about the direction of information flow (e.g. Granger causality or transfer entropy) leading to a non-symmetric association matrix (different values for the connection from node x−y compared to y−x). Most connectivity studies using graph theory measures however use undirected, unweighted graphs. Converting the association matrix into an undirected, unweighted graph involves thresholding. In most cases there is no objective way for selecting the threshold so one or several arbitrary thresholds are often used. This is problematic since the choice of threshold can affect the results. It is also unclear if different thresholds should be used (e.g. with respect to the distribution of values in the association matrix) when two or more experimental groups are compared.

7 Conclusion and Outlook

MEG connectivity analysis aims to understand the mechanisms underlying information processing in the complex human brain network. This poses a formidable challenge for a number of reasons. Although the location of specialised anatomical areas does not change over time, studies investigating neural plasticity demonstrate that their anatomical and functional properties and their interactions with other brain areas change at different time scales. In addition, connectivity studies have to account for the highly dynamic nature of interactions between brain areas that quickly adapt to changes in incoming sensory information or task

demands. As discussed in this chapter, there is now compelling evidence that functional brain connectivity has to be studied in different frequency bands to account for the potentially different functional roles of these different frequency bands in neural communication. To further add to the complexity, different coupling mechanisms exist both, within and between different frequency bands and may involve phase and/or amplitude dynamics (Jensen and Colgin 2007). Further complications arise from the difficulty in distinguishing real interactions between brain areas from artifacts due to field spread (see Sect. 3).

Despite these challenges, MEG connectivity analysis is a highly active, successful and promising area of research (Palva and Palva 2012; Siegel et al. 2012; Schnitzler and Gross 2005). Significant progress has been made along different dimensions. First, methods have been developed that are more robust against or aim to circumvent the effects of field spread. Second, the development and application of biophysically meaningful generative models such as DCM provide a promising way to model dynamic interactions in brain areas. Third, recent advances of analysing resting-state connectivity with MEG have been able to identify networks that are consistent with results from fMRI studies. Here, MEG can contribute temporally and spectrally resolved information about these networks at a resolution that cannot be achieved with fMRI. Fourth, graph theory has become an increasingly useful tool to characterise the topology of complex anatomical or functional brain networks. This progress has significantly improved our understanding of functional connectivity in the human brain.

References

Astolfi L, Cincotti F, Mattia D, Babiloni C, Carducci F, Basilisco A, Rossini PM, Salinari S, Ding L, Ni Y et al (2005) Assessing cortical functional connectivity by linear inverse estimation and directed transfer function: simulations and application to real data. Clin Neurophysiol 116(4):920–932

Atukeren E (2008) Christmas cards, easter bunnies, and granger-causality. Qual Quant 42(6):835–844

Baccala LA, Sameshima K (2001) Partial directed coherence: a new concept in neural structure determination. Biol Cybern 84(6):463–474

Baillet S, Mosher JC, Leahy RM (2001) Electromagnetic brain mapping. Sig Process Mag IEEE 18(6):14–30

Bassett DS, Bullmore ET, Meyer-Lindenberg A, Apud JA, Weinberger DR, Coppola R (2009) Cognitive fitness of cost-efficient brain functional networks. Proc Natl Acad Sci USA 106(28):11747–11752

Bassett DS, Meyer-Lindenberg A, Achard S, Duke T, Bullmore E (2006) Adaptive reconfiguration of fractal small-world human brain functional networks. Proc Natl Acad Sci USA 103(51):19518–19523

Beckmann CF, DeLuca M, Devlin JT, Smith SM (2005) Investigations into resting-state connectivity using independent component analysis. Philos Trans R Soc Lond B Biol Sci 360(1457):1001–1013

Berger H (1929) Über das elektrenkephalogramm des menschen. Eur Arch Psychiatry Clin Neurosci 87(1):527–570

Biswal B, Yetkin FZ, Haughton VM, Hyde JS (1995) Functional connectivity in the motor cortex of resting human brain using echo-planar MRI. Magn Reson Med Off J Soc Magn Reson Med / Soc Magn Reson Med 34(4):537–541

Bressler SL, Seth AK (2011) Wiener-Granger causality: a well established methodology. NeuroImage 58(2):323–329

Brookes MJ, Woolrich M, Luckhoo H, Price D, Hale JR, Stephenson MC, Barnes GR, Smith SM, Morris PG (2011) Investigating the electrophysiological basis of resting state networks using magnetoencephalography. In: Proceedings of the national academy of sciences of the United States of America

Bullmore ET, Bassett DS (2011) Brain graphs: graphical models of the human brain connectome. Annu Rev Clin Psychol 7:113–140

Chen CC, Kiebel SJ, Friston KJ (2008) Dynamic causal modelling of induced responses. Neuroimage 41(4):1293–1312

David O, Cosmelli D, Hasboun D, Garnero L (2003) A multitrial analysis for revealing significant corticocortical networks in magnetoencephalography and electroencephalography. NeuroImage 20(1):186–201

David O, Friston KJ (2003) A neural mass model for MEG/EEG: coupling and neuronal dynamics. NeuroImage 20(3):1743–1755

David O, Garnero L, Cosmelli D, Varela FJ (2002) Estimation of neural dynamics from MEG/EEG cortical current density maps: application to the reconstruction of large-scale cortical synchrony. IEEE Trans Bio-Med Eng 49(9):975–987

de Pasquale F, Della Penna S, Snyder AZ, Lewis C, Mantini D, Marzetti L, Belardinelli P, Ciancetta L, Pizzella V, Romani GL, Corbetta M (2010) Temporal dynamics of spontaneous MEG activity in brain networks. Proc Natl Acad Sci USA 107(13):6040–6045

de Pasquale F, Della Penna S, Snyder AZ, Marzetti L, Pizzella V, Romani GL, Corbetta M (2012) A cortical core for dynamic integration of functional networks in the resting human brain. Neuron 74(4):753–764

Deco G, Corbetta M (2011) The dynamical balance of the brain at rest. Neuroscientist 17(1):107–123

Erdoes P, Renyi A (1959) On random graphs I. Publ Math 6:290–297

Fries P (2005) A mechanism for cognitive dynamics: neuronal communication through neuronal coherence. Trends Cogn Sci 9(10):474–480

Friston K (1994) Functional and effective connectivity in neuroimaging: a synthesis. Hum Brain Mapp 2:56–78

Garrido MI, Kilner JM, Kiebel SJ, Stephan KE, Friston KJ (2007) Dynamic causal modelling of evoked potentials: a reproducibility study. NeuroImage 36(3):571–580

Ghuman AS, McDaniel JR, Martin A (2011) A wavelet-based method for measuring the oscillatory dynamics of resting-state functional connectivity in MEG. NeuroImage 56(1):69–77

Gomez-Herrero G, Atienza M, Egiazarian K, Cantero JL (2008) Measuring directional coupling between EEG sources. Neuroimage 43(3):497–508

Granger CWJ (1969) Investigating causal relations by econometric models and cross-spectral methods. Econometrica 37:424–438

Gross J, Kujala J, Hamalainen M, Timmermann L, Schnitzler A, Salmelin R (2001) Dynamic imaging of coherent sources: studying neural interactions in the human brain. Proc Natl Acad Sci USA 98(2):694–699

Gross J, Timmermann L, Kujala J, Dirks M, Schmitz F, Salmelin R, Schnitzler A (2002) The neural basis of intermittent motor control in humans. Proc Natl Acad Sci USA 99(4):2299–2302

Gross J, Tass PA, Salenius S, Hari R, Freund HJ, Schnitzler A (2000) Cortico-muscular synchronization during isometric muscle contraction in humans as revealed by magnetoencephalography. J Physiol 527(Pt 3):623–631

Gross J, Schmitz F, Schnitzler I, Kessler K, Shapiro K, Hommel B, Schnitzler A (2004) Modulation of long-range neural synchrony reflects temporal limitations of visual attention in humans. Proc Natl Acad Sci USA 101(35):13050–13055

Guggisberg AG, Honma SM, Findlay AM, Dalal SS, Kirsch HE, Berger MS, Nagarajan SS (2008) Mapping functional connectivity in patients with brain lesions. Ann neurol 63(2):193–203

Haerle M, Rockstroh BS, Keil A, Wienbruch C, Elbert TR (2004) Mapping the brain's orchestration during speech comprehension: task-specific facilitation of regional synchrony in neural networks. BMC Neurosci 5:40

Haufe S, Tomioka R, Nolte G, Müller KR, Kawanabe M (2010) Modeling sparse connectivity between underlying brain sources for EEG/MEG. IEEE Trans Bio-med Eng 57(8):1954–1963

Haufe S, Nikulin VV, Müller KR, Nolte G (2013) A critical assessment of connectivity measures for EEG data: a simulation study. NeuroImage 64:120–133

Hillebrand A, Barnes GR, Bosboom JL, Berendse HW, Stam CJ (2012) Frequency-dependent functional connectivity within resting-state networks: an atlas-based MEG beamformer solution. NeuroImage 59(4):3909–3921

Hipp JF, Engel AK, Siegel M (2011) Oscillatory synchronization in large-scale cortical networks predicts perception. Neuron 69(2):387–396

Hipp JF, Hawellek DJ, Corbetta M, Siegel M, Engel AK (2012) Large-scale cortical correlation structure of spontaneous oscillatory activity. Nature Neurosci 15:884–890

Ioannides AA (2007) Dynamic functional connectivity. Curr Opin Neurobiol 17(2):161–170

Jensen O, Colgin LL (2007) Cross-frequency coupling between neuronal oscillations. Trends Cogn Sci 11(7):267–269

Jerbi K, Lachaux J-P, N'Diaye K, Pantazis D, Leahy RM, Garnero L, Baillet S (2007) Coherent neural representation of hand speed in humans revealed by MEG imaging. Proc Natl Acad Sci USA 104(18):7676–7681

Kaminski M, Liang H (2005) Causal influence: advances in neurosignal analysis. Crit Rev Biomed Eng 33(4):347–430

Kiebel SJ, Garrido MI, Moran RJ, Friston KJ (2008) Dynamic causal modelling for EEG and MEG. Cogn Neurodyn 2(2):121–136

Kujala J, Pammer K, Cornelissen P, Roebroeck A, Formisano E, Salmelin R (2007) Phase coupling in a cerebro-cerebellar network at 8–13 Hz during reading. Cereb Cortex 17(6):1476–1485

Lachaux JP, Rodriguez E, Martinerie J, Varela FJ (1999) Measuring phase synchrony in brain signals. Hum Brain Mapp 8(4):194–208

Luckhoo H, Hale JR, Stokes MG, Nobre AC, Morris PG, Brookes MJ, Woolrich MW (2012) Inferring task-related networks using independent component analysis in magnetoencephalography. NeuroImage 62(1):530–541

Makeig S, Westerfield M, Jung TP, Enghoff S, Townsend J, Courchesne E, Sejnowski TJ (2002) Dynamic brain sources of visual evoked responses. Science (New York, N.Y.) 295(5555):690–694

Mantini D, Della Penna S, Marzetti L, de Pasquale F, Pizzella V, Corbetta M, Romani GL (2011) A signal-processing pipeline for magnetoencephalography resting-state networks. Brain Connect 1(1):49–59

Marinazzo D, Liao W, Chen H, Stramaglia S (2011) Nonlinear connectivity by Granger causality. NeuroImage 58(2):330–338

Moran RJ, Kiebel SJ, Stephan KE, Reilly RB, Daunizeau J, Friston KJ (2007) A neural mass model of spectral responses in electrophysiology. Neuroimage 37(3):706–720

Niedermeyer E, Silva FLD (2004) Electroencephalography: basic principles, clinical applications, and related fields. Lippincott Williams & Wilkins, New York

Nolte G, Bai O, Wheaton L, Mari Z, Vorbach S, Hallett M (2004) Identifying true brain interaction from EEG data using the imaginary part of coherency. Clin Neurophysiol 115(10):2292–2307

Nolte G (2003) The magnetic lead field theorem in the quasi-static approximation and its use for magnetoencephalography forward calculation in realistic volume conductors. Phys Med Biol 48(22):3637–3652

Nolte G, Ziehe A, Nikulin VV, Schlogl A, Kramer N, Brismar T, Müller K-R (2008) Robustly estimating the flow direction of information in complex physical systems. Phys Rev Lett 100(23):234101–234104

Oostenveld R, Fries P, Maris E, Schoffelen JM (2011) FieldTrip: open source software for advanced analysis of MEG, EEG, and invasive electrophysiological data. Comput Intell Neurosci 2011:156869

Palva JM, Monto S, Kulashekhar S, Palva S (2010) Neuronal synchrony reveals working memory networks and predicts individual memory capacity. Proc Natl Acad Sci USA 107(16):7580–7585

Palva S, Palva JM (2012) Discovering oscillatory interaction networks with M/EEG: challenges and breakthroughs. Trends Cogn Sci 16(4):219–230

Peelle JE, Gross J, Davis MH (2012) Phase-locked responses to speech in human auditory cortex are enhanced during comprehension, Cerebral cortex (in press)

Penny WD, Litvak V, Fuentemilla L, Duzel E, Friston K (2009) Dynamic Causal Models for phase coupling. J Neurosci Methods 183(1):19–30

Romei V, Rihs T, Brodbeck V, Thut G (2008) Resting electroencephalogram alpha-power over posterior sites indexes baseline visual cortex excitability. NeuroReport 19(2):203–208

Schloegl A, Supp G, Neuper Christa, Wolfgang K (2006) Analyzing event-related EEG data with multivariate autoregressive parameters. Event-related dynamics of brain oscillations. Elsevier, Amsterdam, pp 135–147

Schnitzler A, Gross J (2005) Normal and pathological oscillatory communication in the brain. Nat Rev Neurosci 6(4):285–296

Schoffelen J-M, Oostenveld R, Fries P (2008) Imaging the human motor system's beta-band synchronization during isometric contraction. NeuroImage 41(2):437–447

Schoffelen J-M, Gross J (2009) Source connectivity analysis with MEG and EEG. Hum Brain Mapp 30(6):1857–1865

Schreiber T (2000) Measuring information transfer. Phys Rev Lett 85(2):461–464

Siegel M, Donner TH, Oostenveld R, Fries P, Engel AK (2008) Neuronal synchronization along the dorsal visual pathway reflects the focus of spatial attention. Neuron 60(4):709–719

Siegel M, Donner TH, Engel AK (2012) Spectral fingerprints of large-scale neuronal interactions. Nat Rev Neurosci 13:121–134

Sporns O (2011) Networks of the brain. MIT Press, Cambridge

Stam CJ, van Straaten EC (2012) The organization of physiological brain networks. Clin Neurophysiol Off J Int Fed Clin Neurophysiol 123(6):1067–1087

Stam CJ (2004) Functional connectivity patterns of human magnetoencephalographic recordings: a 'small-world' network? Neurosci Lett 355(1–2):25–28

Stam CJ (2010) Use of magnetoencephalography (MEG) to study functional brain networks in neurodegenerative disorders. J Neurol Sci 289(1–2):128–134

Stam CJ, Nolte G, Daffertshofer A (2007) Phase lag index: assessment of functional connectivity from multi channel EEG and MEG with diminished bias from common sources. Hum Brain Mapp 28(11):1178–1193

Stam CJ, Van Dijk BW (2002) Synchronization likelihood: an unbiased measure of generalized synchronization in multivariate data sets. Physica D 163(3–4):236–251

Vicente R, Wibral M, Lindner M, Pipa G (2011) Transfer entropy–a model-free measure of effective connectivity for the neurosciences. J Comput Neurosci 30(1):45–67

Vinck M, Oostenveld R, van Wingerden M, Battaglia F, Pennartz CMA (2011) An improved index of phase-synchronization for electrophysiological data in the presence of volume-conduction, noise and sample-size bias. NeuroImage 55(4):1548–1565

Westlake KP, Hinkley LB, Bucci M, Guggisberg AG, Findlay AM, Henry RG, Nagarajan SS, Byl N (2012) Resting state alpha-band functional connectivity and recovery after stroke. Exp Neurol 237(1):160–169

Wiener N (1956) The theory of prediction, Modern mathematics for engineers. McGraw-Hill, New York, pp 165–190

Winter WR, Nunez PL, Ding J, Srinivasan R (2007) Comparison of the effect of volume conduction on EEG coherence with the effect of field spread on MEG coherence. Stat Med 26(21):3946–3957

Thalamocortical Network Dynamics: A Framework for Typical/Atypical Cortical Oscillations and Connectivity

Urs Ribary, Sam M. Doesburg and Lawrence M. Ward

Abstract Recently there has been increased interest in understanding the brain's functional connectivity within local and long-range networks. While structural and functional connectivity at the cortical level has received considerable attention, the structure and functional dynamics of thalamo-cortical interactions are as yet insufficiently integrated with our knowledge of large-scale connectivity and regional function. An important question, yet to be answered in detail, is how typical cognitive functions and their alterations in neuro-psychiatric pathologies are temporally generated across the entire brain space (thalamo-cortical, cortico-cortical, cortico-thalamic) based on intact or altered brain structure and function. We review MEG and related EEG research in the context of multimodal imaging findings, focusing on thalamo-cortical dynamics and their role in functional connectivity across cortico-cortical, and cortico-thalamic circuits, including oscillatory synchronization within and across the various frequency bands underlying cognition. We then further explore the cognitive consequences of various disruptions of thalamo-cortical and cortico-cortical dynamics, including slowing and selective loss of functional network dynamics in particular brain networks related to disabilities or pathologies. We present an overview of current findings and their conceptual implications for how brain imaging technologies can further contribute

U. Ribary (✉) · S. M. Doesburg · L. M. Ward
Behavioral and Cognitive Neuroscience Institute, Simon Fraser University, Burnaby, BC, Canada
e-mail: urs_ribary@sfu.ca

U. Ribary · L. M. Ward
Brain Research Centre, UBC, Vancouver, BC, Canada

S. M. Doesburg
Hospital for Sick Children, Toronto, ON, Canada

S. M. Doesburg
University of Toronto, Toronto, ON, Canada

S. Supek and C. J. Aine (eds.), *Magnetoencephalography*,
DOI: 10.1007/978-3-642-33045-2_19,

to a better understanding of the brain's structural, functional and temporal connectivity dynamics and their relationship to typical and atypical cognition and consciousness.

Keywords Thalamo-cortical · Cortico-cortical · Cortico-thalamic · Synchronization · Functional connectivity dynamics · Alpha · Theta · Gamma · Cognition · Consciousness · Cognitive deficit · Neurology · Psychiatry · Traumatic brain injury

1 Introduction

Recently there has been increased interest in understanding neuronal networks and their connectivity in the human brain (Miller 2010; Sporns et al. 2005), especially regarding structural and functional connectivity at the cortical level using multimodal imaging technologies. Nonetheless, the dynamics of these networks, particularly thalamo-cortical interactions are as yet insufficiently integrated with our knowledge of large-scale connectivity and regional function (Ribary and Ward 2014). This article presents a conceptual overview of current findings from human brain imaging studies that, together with knowledge from animal neurophysiology and neuroanatomy, indicate the significance of thalamo-cortical (TC) network dynamics and connectivity for cognition and perception. We also explore the implications of these findings for how dynamic brain imaging technologies can be further used to probe structural, functional and temporal connectivity across cortical and sub-cortical brain areas. Such potential strategies, as yet sparsely utilized, will provide the possibility of a more detailed and complete understanding of cognition and consciousness, and a better way of diagnosing and treating cognitive disabilities and neuro-psychiatric pathologies, including traumatic brain injury.

Magnetoencephalography (MEG) is particularly well suited for characterizing neural oscillations and their dynamics due to its uniquely good combination of temporal and spatial resolution (Hari and Salmelin 1997). It is very well known that imaging of sub-cortical brain dynamics and connectivity using MEG technologies can be challenging, but by using more advanced state-of-the-art signal processing analysis techniques that are becoming more available over recent years, this challenge can be lessened. Twenty-two years ago, MEG and MFT (Magnetic Field Tomography) technologies were first being combined and they demonstrated coupling of gamma band oscillations within cortical and sub-cortical areas (Ribary et al. 1991), which was later confirmed by animal studies. Eight years ago, Schnitzler and Gross implemented Dynamic Imaging of Coherent Sources (DICS) for the study of Parkinson patients, and were able to successfully image the entire movement-related brain network including thalamus and basal ganglia in relation to the reference primary motor area (Schnitzler and Gross 2005), and again this was similar to the extensively studied motor network reported from many animal

studies. Very recently, Gross, Schnitzler and colleagues provided first evidence for bi-directional causality within the paralimbic network including thalamus, and related such causality to cognition and self-awareness (Lou et al. 2011), further supporting the possibility and significance of studying the thalamo-cortical circuitry and causality within it. In addition, MEG technology is and should be further integrated with multimodal structural and functional brain imaging and combined with knowledge from animal neurophysiology and human neuroanatomy, in order to fully explain MEG data and to better understand cognition and consciousness of the human brain in health and disease.

An important question then arises, that is yet to be answered in detail, namely how typical or atypical cognitive functions and consciousness are temporally generated across the entire brain space, in terms of specific underlying intact or altered brain structure and function across cortical and sub-cortical regions. The challenge in current dynamic brain imaging, using MEG or EEG technologies, is to analyze detailed communication or connectivity dynamics across five dimensions, namely within 3D space across oscillatory frequency and time, and to describe in detail the relation of these connectivity dynamics and causality in relation to cognition and consciousness in health and disease.

2 Thalamo-Cortical Oscillations, Synchronization, Coupling and Connectivity in the Healthy Human Brain

Many investigations over the past 2–3 decades using dynamic brain imaging technologies have indicated the significance of brain dynamics relating to cognition and consciousness (Varela et al. 2001; Ward 2003; Schnitzler and Gross 2005). In addition, the importance of TC network dynamics has also been implicated (Ribary et al. 1991; Victor et al. 2011) in understanding alterations of cognition in disabilities and pathologies (Ribary 2005), including the impact of thalamic damage relating to traumatic brain injuries (TBI) (Schiff et al. 2002). Conversely, surgical intervention at the central thalamus has been shown to improve consciousness in one minimally conscious patient (Schiff et al. 2007). Others have also reported on the significance of the thalamus relating to consciousness (Ward 2011). One striking finding is that the most consistent regional effect produced by general anesthetics at or near loss of consciousness relates to a reduction of thalamic metabolism and blood flow (Alkire et al. 2008), indicating that cortical arousal may occur without the thalamus but that consciousness may not, further explaining why a corticothalamic complex is essential for cognition and consciousness. Recent findings also indicated the importance of imaging the development of functional thalamo-cortical connectivity in humans (Fair et al. 2010), indicating stronger TC functional connectivity in adults than in children, and its weakening with age. Recent MEG findings provided evidence for analyzing and reporting bi-directional causality within the paralymbic TC network related to memory retrieval and self-awareness (Lou et al. 2011). In addition, it has been

recently reported in animals that synchrony of thalamo-cortical inputs maximizes cortical reliability, even though these neurons constitute only about 5 % of the synapses on layer 4 spiny stellate simple cells (Wang et al. 2010), further supporting the importance of TC relations and brain dynamics.

2.1 Thalamo-Cortico-Thalamic Oscillations and Circuitry

It has become evident in recent years that functional connectivity dynamics within the entire brain space and across frequency and time needs to be analyzed in detail in order to better understand the underlying neurophysiology of the typical and atypical brain function. Over the past decade, there is a large and accumulating body of evidence that dynamic human brain imaging using EEG and MEG has revealed many task dependent cortical gamma band activations and connectivities across frequency and time relating to most cognitive brain functions (Tallon-Baudry and Bertrand 1999; Jensen and Vanni 2002; Ward 2003; Ribary 2005; Doesburg et al. 2010).

This recent surge of human neuroimaging research of the oscillatory dynamics during cognitive and perceptual processing is predicated on earlier seminal findings, which indicated that brain rhythms and their coherence were fundamental processes underlying cortical processing. Shortly after Gray and Singer (1989) discovered the 40 Hz synchronized oscillation in cat visual cortex and proposed it as the mechanism to bind visual features into a percept, Crick and Koch (1990) proposed it as the foundation of conscious vision. In parallel, Ribary and Llinás discovered the functional significance of human gamma band oscillations in health and disease, as well as the TC coupling of human gamma-band activations (Ribary et al. 1989; Ribary 2005), and further proposed that TC coupling of gamma-band activity supports the temporal binding mechanism responsible for bringing together information from various sensory modalities into one single percept (Llinás and Ribary 1993). Indeed, MEG recordings on control subjects demonstrated that precise timing of gamma-band TC network activity is associated with sensory processing (Ribary 2005), namely with the minimal interstimulus interval required to identify separate auditory stimuli (Joliot et al. 1994).

Analysis of the origin of transient gamma-band neural activity in humans during early sensory processing using MEG demonstrated specific cortical activations (Pantev et al. 1991) and subcortico-cortical correlations (Ribary et al. 1991), indicating coupling within thalamo-cortical networks and its clinical significance. Specifically, combined MEG and MFT brain imaging results indicated a large-scale coupling of thalamo-cortical gamma-band oscillations, organized in space and time (Ribary et al. 1991), which was altered in Alzheimer patients. These initial MEG findings have stimulated several animal studies confirming the existence of such thalamo-cortical oscillations and rhythmicity using intracellular recordings from cortical interneurons (Llinás et al. 1991) and specific/non-specific thalamic neurons studied in vivo (Steriade et al. 1991, 1993a).

A model for generating and maintaining such thalamo-cortical coupling was then proposed (Llinás and Ribary 1993) allowing the recruiting of sufficient elements to generate the synchronicity observed at both intracellular and extracellular levels in the cortex and thalamus in animals and as observed in human brain imaging (Ribary et al. 1991). Specifically, Llinás and Ribary proposed, based on knowledge from neurophysiology and neuroanatomy, that a co-activation of the specific (via layer IV) and the non-specific (via layer I) TC circuitry is required to initiate and stabilize CC (cortico-cortical) synchronization and functional connectivity among the many brain areas and pathways (see Ribary 2005), including the CT feedback loops. Such a "dialogue" allows (i) to achieve global functional connectivity within the entire brain (ii) the task-dependent integration of well-trained specific local circuits into long-range connectivity across the entire brain, by integrating "content" into "context" (see Llinás and Ribary 1993), and (iii) detailed cortical oscillatory connectivity dynamics at cortical level. Such speculations based on MEG findings and animal neurophysiology have been confirmed by direct recording in animals (Steriade 1993), indicating such specific and nonspecific thalamo-cortical conjunction (Steriade and Amzica 1996). In addition, recent MEG findings provided further evidence for bi-directional causality within the paralimbic network [anterior cingulate/medial prefrontal, posterior cingulate/medial parietal, and pulvinar thalami] related to cognition, namely to autobiographic memory retrieval and self-awareness (Lou et al. 2011), further supporting the importance of thalamo-cortical interactions in cognitive brain function.

In addition, mathematical modeling of the thalamo-cortical system (Babloyantz 1991; Llinás et al. 1994; Wright et al. 2001; Rennie et al. 2002) showed that the dynamics of the system were turbulent and desynchronized when intrinsic thalamic activity was excluded from the model (Babloyantz 1991). The onset of a pacemaker input organized the system into a more coherent spatio-temporal behavior and further provided evidence for the significance of coupling and connectivity of oscillatory activity within thalamo-cortical systems (Steriade and Llinas 1988; Steriade et al. 1993a, b; Llinás et al. 1994; Barth and MacDonald 1996).

Classically, the thalamus is considered to consist mainly of a group of "relay nuclei" (e.g. Sherman and Guillery 2006). Thalamic nuclei such as the lateral and medial geniculate nuclei, which receive input from the peripheral visual and auditory systems, respectively, are examples of such nuclei. These nuclei do indeed relay sensory information into the primary sensory cortical processing areas (V1 and A1 respectively). They also receive massive projections back from cortical layers 5 and 6 that were thought to modify the processing in the thalamic nuclei. This original simple picture of the thalamus as a modulated relay station, however, has changed radically in recent years. First, Guillery and Sherman (e.g. Guillery and Sherman 2002; Sherman and Guillery 2006) argued that the higher-order thalamic nuclei (those that do not receive direct afferent input) function exactly as do the first-order nuclei (those receiving afferent input from sensory receptors, such as the lateral geniculate nucleus from retina, or from subcortical brain areas, such as the medial geniculate nucleus from subcortical auditory

nuclei): they relay information. Sherman and Guillery extended the classical notion of the thalamus as a sensory relay from sensory nuclei such as the lateral geniculate and the medial geniculate, to *all* thalamic nuclei. They did add a twist, however, based on their observation that cortico-thalamic inputs originating in layer 5 of the cortex also branch to motor areas (at least in the visual and somato-sensory systems). Moreover, those inputs from cortical layer 5 do not return to the thalamic nucleus associated with the originating cortical area, but rather to other, "higher" thalamic nuclei (at least for vision), and they are of the "driving" type of inputs (fast, ionotropic synapses, large axons and large synaptic boutons, etc.). Based on these facts, Sherman and Guillery proposed that the higher-order relay neurons relayed *motor* information from one cortical area to other higher areas, basically an efference copy of action-related information sent to motor areas such as the superior colliculus (which controls eye movements), brain stem and spinal cord from these perceptual areas. The scope of their argument is too broad for the present context, but it requires a rethinking of many accepted assumptions about cortical processing of perceptual information.

Other and later important extensions to the classical picture of cortico-thalamic interactions arose from the discovery of two types of thalamic neurons in animals (Jones 2001, 2002, 2009). The "core" and the "matrix" neurons are chemically distinguishable and make very different projections to their targets. All dorsal thalamic nuclei contain matrix neurons and the sensory and motor nuclei in particular also contain many core neurons. Core neurons project to layer IV stellate neurons and layer III, V, and VI pyramidal neurons in sensory- or motor-specific cortical areas, as in the classical picture. Matrix neurons project diffusely to stellate neurons in the superficial layers of several cortical areas, especially in frontal areas. Both types of thalamic neurons receive back projections from layer V pyramidal neurons and the core neurons also receive back projections from layer VI pyramidal neurons. Jones (2001, 2002, 2009) argued that, during thalamic tonic mode, core neurons relay sensory or motor information within specific pathways, whereas matrix neurons bind thalamic and cortical activity and promote thalamo-cortical synchronization, creating consciousness and action. When the thalamus is in burst mode, however, the brainstem arousal system is quiescent and the core and matrix neurons are suppressed by inhibition from the thalamic reticular nucleus (TRN). The TRN, in combination with the brainstem arousal system, thus determines whether the thalamus will promote thalamo-cortical synchronization in the gamma band (consciousness) or at much lower frequencies, in the delta band (sleep). Ward (2011), elaborating on a proposal of Mumford (1991), argued that the sensory thalamus serves as an active blackboard, echoing back to the cortex an integrated impression of diverse cortical inputs. For example, the thalamic neurons associated with visual association areas of the cortex would be integrating "where" information from one, "lower" cortical area with "what" information from another, "higher" cortical area, and sending that integrated information back to their own area. In non-sensory domains, however, in addition to providing a synthetic perceptual construct, the diverse information integrated in thalamic nuclei would be associated with multi-modal association areas. In particular in

those associated with prefrontal cortex, would include that of a non-sensory nature as well, encompassing different facets of information computed by frontal or associative circuits. For example, a perceptual construct of a face is then accompanied by a memory of having seen the face before and the associated person's name, occupation, social standing, and personal relationship to oneself. Ward (2011) argued that the information integration giving rise to primary conscious awareness takes place mostly in the matrix neurons, as these are more common in the non-sensory and non-motor nuclei, rather than in the core neurons. This would explain why the detailed activities of primary and secondary sensory cortical areas do not enter primary awareness, although their outputs are necessary for awareness of specific sensory content.

Indeed, it has been well known for some time that damage to specific brain systems produces loss in the corresponding modality (i.e. vision, sensation, audition, motor functions etc.), while damage of the nonspecific thalamus produces lethargy and coma (Façon et al. 1958; Castaigne et al. 1980) and disturbances in visual perception (Purpura and Schiff 1997) and consciousness (see later section on TBI in this chapter). As such, the resonant gamma-band co-activation (or connectivity dynamics) of both the specific and non-specific TC system, may indeed contribute to awareness and consciousness of a single percept (Llinás and Ribary 1993), and may relate to the well-described integration of sensory information within and across the hemispheres (Gray 1999).

2.2 A Framework for Cortico-Cortical Synchronization and Connectivity Across Alpha, Gamma, and Theta Frequency Bands

As mentioned above, thalamo-cortical interactions are closely related to the initiation and stabilization of dynamic CC connectivity in various frequency bands, which in turn are closely related to cognitive function (see conceptual Fig. 1a). There exist considerable data supporting the view that synchronization of neuronal oscillations both within and between brain regions is an important mechanism mediating formation of and communication within these and other neural networks (Varela et al. 2001; Ward 2003; Palva and Palva 2007; Fries 2005, 2009; Sauseng et al. 2004).

Local alpha oscillations are thought to reflect cortical inhibition (Klimesch et al. 2007) and/or idling (Pfurtscheller et al. 1996), as local alpha power reductions have been observed following stimulus presentation in various sensory modalities (Klimesch et al. 2007) and during cognitive tasks such as selective attention (Snyder and Foxe 2010; Banerjee et al. 2011). Local desynchronization of alpha rhythms over primary cortex is also associated with active motor control (Pfurtscheller and Neuper 1994) and perceptual processing (Hanslmayer et al. 2011). Such results indicate that alpha oscillations reflect fundamental mechanisms of cortical idling and inhibition that directs information flow within brain networks across diverse contexts (Jensen and Mazaheri 2010). It has also been

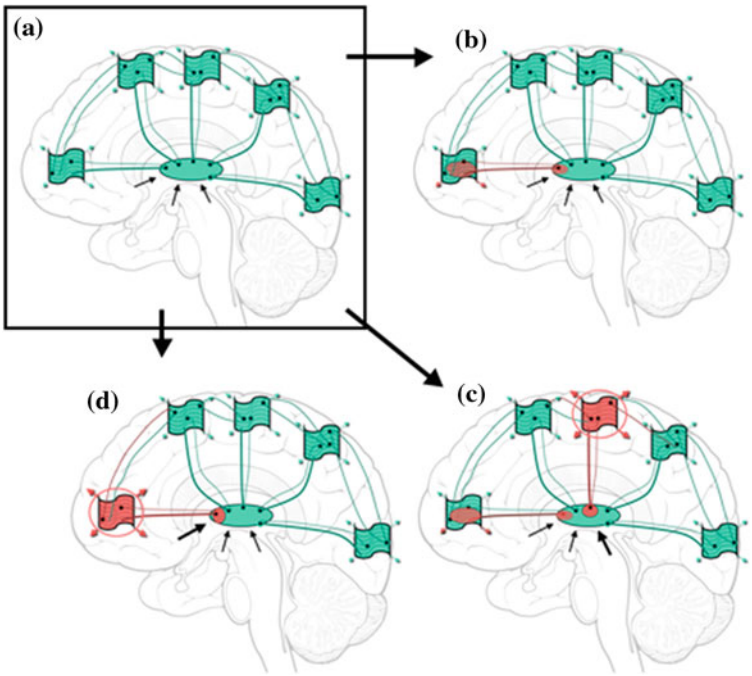

Fig. 1 Conceptual representation of connectivity and dynamics in healthy and challenged brains. *Central ellipse* represents thalamus, *wavy boxes* represent specific cortical regions, *connecting lines* represent both structural and functional connectivity. *Green* is healthy, *red* is damaged or dysfunctional, and represents slow or otherwise compromised functional connectivity. *Black arrows* represent subcortical inputs to thalamus. **a** *Healthy human brain* intact structural, functional and temporal connectivity (shown in *green*) with intact cognition and full consciousness and awareness of external and internal world. **b** *Cognitive disabilities* slight alterations in functional (perhaps structural) connectivity and slight partial slowing (indicated in *red*), otherwise globally intact structural, functional and temporal connectivity, with full consciousness and noticeable but not severe perceptual or cognitive alterations. **c** *Neurology* severe partial and persistent slowing and alterations in structural, functional and temporal connectivity (shown in *red*), mostly related to sensory, motor and cognitive brain areas (TBI patients are excluded here and will be shown in detail in Fig. 2); affecting single or multiple brain networks (probably via inhibition or de-afferentation at thalamic level on TC networks, with additional alterations at CC level). Ranging from intact to altered consciousness depending on pathology, with various and often severe cognitive and sensory-motor alterations. **d** *Psychiatry* severe partial and persistent slowing and alterations in structural, functional and temporal connectivity (shown in *red*), mostly related to limbic and frontal brain areas; affecting single or multiple brain networks (probably via inhibition at thalamic level on TC networks, with additional alterations at CC level). Ranging from intact to distorted consciousness or/and altered emotions depending on pathology, with various and often severe cognitive and sensory-motor alterations and distortions

reported, however, that increases in alpha synchronization among cortical regions may be related to the establishment of long-range networks and further relating to memory retention (Doesburg et al. 2010, 2011a; Palva et al. 2010).

Local increases in gamma-band activity have been linked to active processing within cortex across numerous contexts, supporting the view that they play a critical role in cortical sensory and cognitive processing (Ribary 2005; Fries 2009), including attention and memory (Jensen et al. 2007). Sensory stimulation produces gamma activation (Pantev et al. 1991), as does sensory perception, object recognition and short-term memory retention (Fell et al. 2002; Supp et al. 2007; Tallon-Baudry et al. 1998). Processes that have been reported to reduce local alpha activity are also associated with increased local gamma activation (Fries et al. 2001; Doesburg et al. 2008). As alpha-desynchronization occurs across large areas of cortex relative to the more spatially complex coincident increases in gamma power (Jerbi et al. 2009), transitions of local population dynamics from alpha toward a gamma oscillatory state may mediate segregation of neural populations into functional assemblies relevant for required cortical processing and connectivity.

Further, local theta rhythms have been related to task-dependent processing in both hippocampus and neocortex (Kahana et al. 2001). The relationship between cortical theta oscillations and active processing is perhaps best documented in working memory paradigms (Sauseng et al. 2010). Local theta activity has also been implicated in other cognitive processes including long-term memory processes and selective attention (Osipova et al. 2006; Green et al. 2011). In particular, the coupling of gamma to theta frequency bands has been reported in a variety of cognitive and perceptual processes based on noninvasive recordings (Sauseng et al. 2008; Doesburg et al. 2009, 2012; Griesmayr et al. 2010).

Given the fact that all these oscillations indicate specific individual signatures within the same sensory or cognitive contexts, it is likely that task-dependent activation within a cortical region involves quantifiable cross-frequency relations and connectivity across the entire brain space supported by TC network dynamics, relating to cognition and consciousness (Doesburg, Ward and Ribary, in preparation). More discoveries and reports specifically on cortical oscillatory synchronization and connectivity underlying sensory and cognitive functions in the human brain will be further discussed by several other authors in various other chapters of this book.

3 Persistent Partial Slowing and Altered Functional Network Dynamics in Neurology and Psychiatry

Llinás, Jeanmonod and Ribary (Llinás et al. 1999) suggested that a slowing of spontaneous oscillations and alteration of the functional connectivity dynamics within thalamo-cortical systems could contribute to a better understanding of the brain dysfunctions underlying various pathological behavioral symptoms. While general slowing in clinical populations is well known, earlier MEG results, combined with findings based on electrical recordings from human thalamus (Jeanmonod et al. 1996, 2001; Sarnthein et al. 2003) and physiological findings on

animals (Jahnsen and Llinás 1984; Llinás et al. 2002), indeed indicated that a severe and sustained slowing together with dysrhythmic thalamo-cortical interactions could be related to various positive symptoms observed in a subset of neurological and psychiatric patients (Schnitzler and Gross 2005; Llinás et al. 1999; Volkmann et al. 1996; Llinás et al. 2001; Schulman et al. 2005, 2011; Timmermann et al. 2003; Sarnthein and Jeanmonod 2007, 2008). Compared to control subjects, patients showed increased low frequency theta rhythmicity in conjunction with a widespread and marked increase of power correlation among high and low frequency oscillations, consistent with other reports (John et al. 1988). Such dysrhythmias can be explained by either excess inhibition or disfacilitation on the TC system in those patients, inducing the generation of low threshold calcium spike bursts by thalamic cells as seen in animals (Llinás et al. 2001) and humans (Jeanmonod et al. 1996). The presence of these thalamic bursts then directly relates to thalamic cell hyperpolarization and low frequency oscillation generation within thalamus (Jahnsen and Llinás 1984). This produces a slowing of theta/delta activity as a result of a resonant interaction between thalamus and symptom-specific cortical areas. The etiology of many of these neuropsychiatric pathologies which express these core characteristics of thalamocortical dysrhythmia are of course quite different in nature, but what they all have in common is either an increased inhibition at the thalamic level (i.e. in Parkinson's Disease via pallido-thalamic tract) or a dysfacilitation at the thalamic level (i.e. in amputee patients with neurogenic pain). Such pathological changes in thalamic inhibition or disfacilitation result in such TC slowing, which has been well characterized through animal neurophysiology, and is best observed at the cortical level using MEG or EEG imaging technologies.

Global slowing has been well characterized in the healthy human brain in the context of transition to sleep. Such slowing has also been demonstrated in animal studies, as the brain slows down from resting alpha band frequency (8–12 Hz) to lower frequency theta (6–8 Hz) and then to delta band (2–4 Hz) during deep sleep with a large global coherence across the entire brain (Steriade et al. 1993b). In states of thalamocortical dysrhythmia (TCD) however, partial slowing is persistent with ongoing theta-range (4–8 Hz) thalamic activity, serving as the trigger for cortical dysfunction in which a core region of cortex functions at lowered frequency, surrounded by a region of activation in the normal waking gamma (25–50 Hz) range (Llinás et al. 1999, 2002). In addition, the altered connectivity of the thalamocortical system not only maintains this pathological dynamic, but also causes it to become distributed throughout wide areas of cortex representing a large-scale coupling, which allows such activity to constrain thalamocortical dynamics very efficiently. This strengthens considerably the idea that some of the mild cognitive deficits could arise from varying degrees of a slight dysrhythmia (Llinás et al. 1998b; Ribary 2005).

The challenge for future dynamic brain imaging studies using MEG or EEG technologies is then (i) to precisely localize these persistent slowing TC areas or symptom-specific networks, best observed at the cortical level during "resting state" (ii) to specify the alterations in "resting" connectivity and subsequent

induced altered task-specific activations in functional cortical connectivity dynamics across all frequency bands in precise detail, and (iii) to correlate such altered connectivity and dynamics with clinical symptoms (see conceptual figure: Fig. 1c–d).

4 Slight Partial Slowing and Altered Functional Connectivity Dynamics in Cognitive Disabilities

Altered functional connectivity dynamics, as described in neuropsychiatric populations above, also provides a conceptual framework for evaluating slight alterations in resting brain activity in the normal aging brain or in some cognitive disabilities (see Ribary 2005). These alterations are expected to be minimal compared to severe dysrhythmia in neurological or psychiatric conditions (see conceptual figure: Fig. 1b). Recent behavioral and functional brain imaging studies of some cognitive disabilities indeed suggest slight perceptual and cognitive alterations including slowing in the underlying neurophysiological network connectivity, despite an average or even above average IQ in some of these individuals. In children born very preterm ($\leq$32 weeks gestational age), for example, Grunau, Doesburg, Ribary and colleagues have recently shown a significant alteration in synchronization and network connectivity dynamics within the alpha frequency band (Doesburg et al. 2011a). In particular, a slight slowing of resting alpha band activity towards theta (6–8 Hz), has been correlated with selective developmental difficulties in this group (Doesburg et al. 2011b).

An alteration of precise timing of network dynamics and connectivity has also been reported earlier to be associated with altered behavioral patterns, namely with altered perception of sensory input (Ribary et al. 1999; Ribary 2005). Earlier MEG studies suggested a slight dysrhythmia within thalamo-cortical systems in subjects with Language-Based Learning Disabilities (Llinás et al. 1998a; Nagarajan et al. 1999). Functional imaging data by Ribary, Llinás, Tallal, Miller and colleagues have shown that the minimal interstimulus interval required to identify two separate sensory events was altered and delayed in subjects with Language-Based Learning Disabilities (LLD or dyslexia) (Llinás et al. 1998a; Ribary et al. 2000). This relationship is observable independently by either through psychological tests or by functional MEG imaging. Also, the results from these two different measurement techniques were highly correlated, indicating that MEG imaging can be used as an objective measure of normal and slightly altered sensory cognitive experience, including improvements during intervention (Nagarajan et al. 1999).

Gamma-band connectivity abnormalities were further suggested to be one of the neurophysiological correlates of the temporal deficits recorded in Language-Based Learning Disabilities (LLD or dyslexia) (Llinás 1993). This dyschronia is in fact consistent with other functional and temporal brain imaging findings concerning LLD (Tallal et al. 1993; Tallal 2004; Salmelin et al. 1996; Salmelin 2007; Helenius et al. 1999; Simos et al. 2000; Heim et al. 2000; Benasich and Tallal 2002;

Gabrieli 2009), including the remediation by cognitive interventions (Tallal et al. 1996; Merzenich et al. 1996). MEG findings further suggested the existence of two different sub-groups of LLD subjects, possibly relating to either a delay or an interruption of gamma band connectivity dynamics (Ribary 2005).

Present research on the diagnosis and treatment of dyslexia has accelerated with an increasing focus on identifying biological substrates and potential early precursors (see Benasich and Fitch 2012). A tighter emphasis on precursors, referred to as "predyslexic" populations, should enable earlier identification of those children at highest risk for dyslexia and provide insight into the etiologies, common pathways, neurobiological correlates, and behavioral phenotypes of language learning disorders. Such identification of populations at highest risk is particularly important, given that current remediation relies exclusively on interventional therapies that are most effective at a young age. Therefore, more comprehensive research on cognitive disabilities using structural and functional brain imaging technologies is necessary for better understanding the alterations in structural and functional connectivity and especially the oscillatory connectivity dynamics across subcortical and cortical brain networks (see conceptual figure: Fig. 1b).

5 Alteration and Loss of Functional Network and Connectivity Dynamics in TBI

Schiff, Ribary and colleagues earlier reported a massive dissociation among TC-CC-CT networks in traumatic brain injury in persistent vegetative patients (PVS) who had suffered severe thalamic injury and were unconscious for several months to several years (Schiff et al. 2002). In a series of studies on these PVS patients, using MRI (magnetic resonance imaging), PET (positron emission tomography) and MEG, they reported massive structural damage within thalamocortical systems, combined with a massive shutdown of cortical and sub-cortical brain metabolism, and a massive reduction in functional dynamics indicating abnormal, delayed and incomplete brain activity and gamma band responses (Schiff et al. 1999, 2002; Plum et al. 1998) (see conceptual Fig. 2f). These studies were in accordance with other functional brain imaging studies, demonstrating consistently diffuse and uniformly reduced cerebral metabolic activity (Levy et al. 1987; DeVolder et al. 1990; Tomassino et al. 1995; Rudolf et al. 1999; Laureys et al. 1999), and a selective disappearance of sensory midlatency responses and early-evoked potentials in comatose patients (Pfurtscheller et al. 1983) and during anesthesia (Madler et al. 1991).

In addition, these findings demonstrated for the first time that, although PVS is characterized by massively reduced brain metabolism and functional connectivity, some PVS patients may express isolated meaningless fragments of behavior that can be related to islands of residual metabolic and physiological brain activity (Schiff et al. 2002). An earlier case study described a unique vegetative patient suffering from bilateral thalamic stroke, who randomly produced occasional single

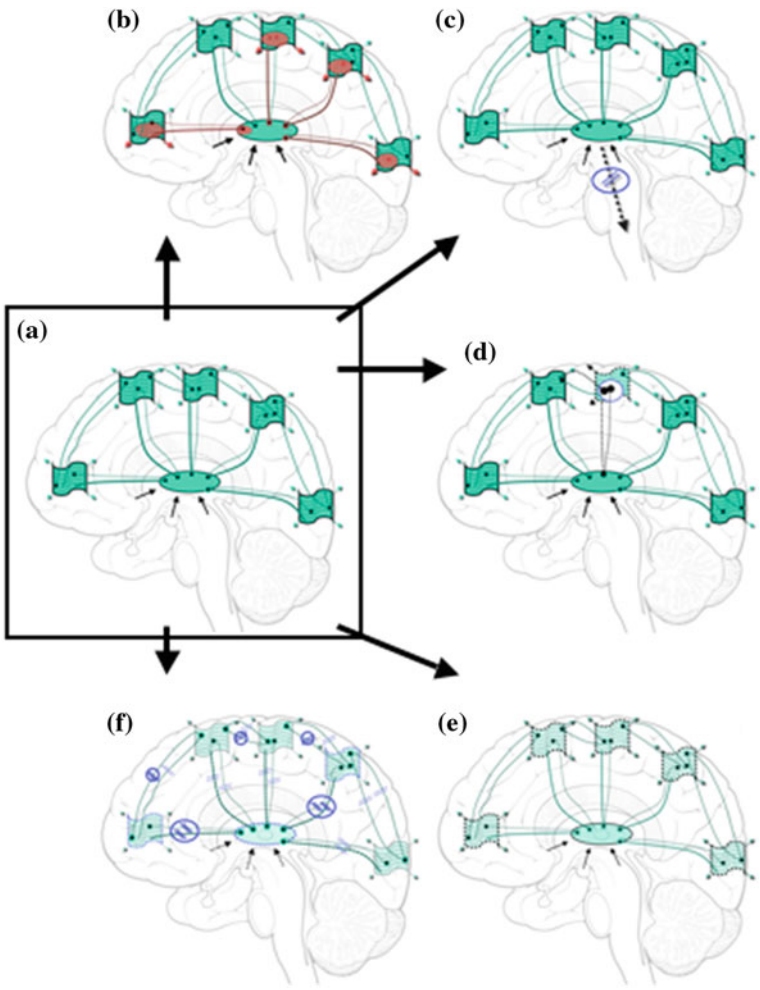

words (Schiff et al. 1999). In this patient, isolated regions of preserved cerebral metabolic activity and thalamocortical transmission were associated with remnants of the human language system. These findings led to the evaluation of additional PVS patients with multi-modal imaging techniques in order to determine in detail what cerebral activity may remain in patients with catastrophic brain injuries. Schiff, Ribary, Llinas, Plum and colleagues reported the first evidence of reciprocal clinical-pathological correlation with regional differences of quantitative cerebral metabolism (Schiff et al. 2002). In addition, these MEG data from the PVS patients indicated partially preserved but abnormal, delayed, incomplete or absent dynamic brain activity. Restricted sensory representations evidenced by slowing evoked magnetic fields and abnormal gamma band activity, were uniquely

◀ **Fig. 2** Effects of traumatic brain injury (TBI). *Central ellipse* represents thalamus, *wavy boxes* represent specific cortical regions, *connecting lines* represent both structural and functional connectivity. *Green* is healthy, *light green* and *red* is loss and dysfunctional, and represents slow or otherwise compromised connectivity. *Blue circles* represent severed connections. *Black arrows* represent subcortical inputs to thalamus. **a** *Healthy human brain* intact structural, functional and temporal connectivity (indicated in *green*) with intact cognition and full consciousness and awareness of external and internal world. **b** *Mild TBI* (mTBI) slight alterations in functional and structural connectivity and slight partial slowing (shown in *red*), affecting frontal, temporal, parietal and/or occipital areas, otherwise globally intact structural, functional and temporal connectivity, with mostly preserved consciousness and noticeable but rather mild perceptual or cognitive alterations. **c** *Locked in syndrome* (LIS) intact structural, functional and temporal connectivity with intact cognition and full consciousness and awareness, but disrupted motor output, with no ability to communicate (except possible eye movements). **d** *Focal lesion* local disruption of structural and functional connectivity (shown in *light green*) accompanied by loss of specific sensory or cognitive function (or neglect); otherwise intact global structural, functional and temporal connectivity with intact cognition and full consciousness and mostly preserved awareness. **e** *Minimally conscious state* (MCS) severe alterations in global functional and temporal connectivity (shown in *light green*) with probably more or less preserved structural connectivity; accompanied by global reduction of consciousness and awareness to a minimal level, and inconsistent ability to follow simple commands. MCS can evolve further with possible restoration of cognitive functions. In one case electrical deep brain stimulation (DBS) of the central thalamus improved cognitive and motor function in an MCS patient (Schiff et al. 2007), probably by activating TC networks and at the same time synchronizing/stabilizing CC-CT circuitry. **f** *Persistent vegetative state* (PVS) disruption in global structural, functional and temporal connectivity (shown in light green with broken lines) (probably mostly affecting thalamus, frontal and parietal TC connectivity, and frontal-parietal pathways), accompanied by complete loss of consciousness and of awareness of the internal or external world with no signs of ability to follow commands or any adaptive behavior. There is a very small chance that PVS, if diagnosed correctly, can evolve further into MCS. However, a subgroup of PVS patients sometimes demonstrate residual and partially preserved local structural, functional and temporal connectivity allowing them to generate some "out of context" behavioral patterns (Schiff, et al. 2002), such as speaking a few "words without mind" (Schiff et al. 1999). Schiff, Ribary and colleagues have further analyzed one particular patient with bilateral thalamic lesion, expressing large arousal and larger brain metabolism at cortical level, which was termed a "free running cortex" (Schiff et al. 2002), probably indicating "uncontrolled" and over-expressive functional and temporal connectivity at the cortical level

expressed in each patient, and correlated with isolated behavioral patterns in two patients (Schiff et al. 2002). The combination of MRI, PET and MEG techniques employed allowed assessment of the residual network properties underlying the expression of meaningless fractional behavior observed in three of the five chronic vegetative patients reported.

In the intact normal healthy brain, modular networks process selective sources of information and are typically integrated into large, coherent or coupled patterns of activity. These initial findings on PVS patients provided an initial foundation for identifying mechanisms underlying complex brain injuries and represented a first step toward characterizing patients with varying degrees of functional recovery beyond the vegetative state (Schiff et al. 2002). These studies also indicated the enormous necessity for further brain imaging studies on such PVS patients. The challenge is to identify such possible isolated network functions within a globally

fractured brain and relating to meaningless fragments of behavior rather than to some conscious awareness. Such findings will further allow one to avoid misdiagnosis and move towards establishing neuroethical guidelines for best possible clinical practice (Lee et al. 2012).

Many other brain imaging studies have been reported recently (Laureys 2005; Owen et al. 2010; Victor et al. 2011). These findings indicate the importance of using multimodal brain imaging technologies to further study, quantify and understand the many forms of traumatic brain injuries (see conceptual figure: Fig. 2b–f), ranging from full consciousness to slowing in mild TBI (Huang et al. 2012), to major connectivity changes in severe TBI and coma. The challenge is to specify its required areas and necessary connectivity (Laureys et al. 2004), including the targeting of central thalamus for surgical interventions in minimally conscious patients (Schiff et al. 2007). These findings are consistent with the view that thalamic and cortiocothalamic systems are critical for conscious experience (Ward 2011; Alkire et al. 2008). In addition, a recent study measured the effective connectivity during a mismatch negativity paradigm and reported impaired backward connections from frontal to temporal cortices in vegetative patients (Boly et al. 2011). These results specifically emphasize the importance of top–down projections in recurrent processing that involve high-order associative cortices for conscious perception. Whereas the loss of cognitive functions and consciousness relates to a breakdown of global structural, functional and temporal connectivity across the TC-CC-CT networks, research findings over recent years further indicated that dysfunction of some brain areas are more damaging than others, such as the thalamus (Façon et al. 1958; Castaigne et al. 1980), or the parietal associative areas (Alkire et al. 2008).

6 Towards Better Understanding Large-Scale Functional Connectivity Dynamics in Health and Disease

Non-invasive brain imaging technologies (MRI, fMRI, PET, MEG, EEG) available today, and combined with highly sophisticated signal processing and analysis techniques are providing complementary and very useful information regarding brain structure and function. A better characterization and detailed analysis of the of underlying structural, functional and temporal connectivity among the TC-CC-CT networks, however, is very important in order to better understand sensory-motor and cognitive human brain function and its alterations in cognitive disabilities and pathologies including its relation to altered consciousness in traumatic brain injury.

The challenge for future structural and functional brain imaging studies will be the quantification and specification of structural, functional and temporal connectivity required to achieve full consciousness and cognition. The various alterations in local and long-range connectivity (see conceptual figures: Figs. 1, 2) can then be statistically specified in five dimensions and attributed to the various brain states in the healthy human brain (wakefulness, deep sleep, REM sleep, etc.)

and to the various cognitive disabilities and neuro-psychiatric pathologies including traumatic brain injury (Laureys et al. 2004; Ribary and Ward 2014). Such imaging and quantification strategies will then allow the determination of truly brain-based and objective diagnostic markers for cognitive disabilities and pathologies, by using the highest neuroethical standards towards best possible clinical practice, and will further allow one to better monitor and improve subject-specific cognitive, pharmacological and surgical interventions.

Acknowledgements Preparation of this chapter was facilitated by funding from the Canadian BC Leading Edge Endowment Fund (BC LEEF) to UR, the Canadian Foundation for Innovation (CFI) and related Operating Funds for the Behavioral and Cognitive Neuroscience Institute (BCNI) to UR, from the Natural Sciences and Engineering Research Council (NSERC) of Canada to LMW and from the Hospital for Sick Children Centre for Brain and Behavior, the Ontario Brain Institute to SMD.

References

Alkire MT, Hudetz AG, Tononi G (2008) Consciousness and anesthesia. Science 322:876–880

Babloyantz A (1991) Self-organization, emerging properties and learning. Plenum Press, New York

Banerjee S, Snyder AC, Molholm S, Foxe JJ (2011) Oscillatory alpha-band mechanisms and the deployment of spatial attention to anticipated auditory and visual target locations: supramodal or sensory-specific control mechanisms? J Neurosci 31:9923–9932

Barth DS, MacDonald KD (1996) Thalamic modulation of high-frequency oscillating potentials in auditory cortex. Nature 383:78–81

Benasich AA, Tallal P (2002) Infant discrimination of rapid auditory cues predicts later language impairment. Behav Brain Res 136:31–49

Benasich AA, Fitch RH (2012) Developmental dyslexia. Paul H Brooks Publishing Co, Baltimore, USA

Boly M, Garrido MI, Gosseries O, Bruno MA, Boveroux P, Schnakers C, et al (2011) Preserved feedforward but impaired top-down processes in the vegetative state. Science 332:858–862

Castaigne P, Lhermitte F, Buge A, Escourolle P, Derouisne C, Der Agopian P et al (1980) Paramedian thalamic and midbrain infarcts: clinical and neuropathological study. Ann Neurol 10:127–214

Crick F, Koch C (1990) Some reflections on visual awareness. Cold Spring Harbor Sympos Quant Biol 55:953–962

DeVolder AG, Goffinet AM, Bol A, Michel C, de Barsy T, Laterre C (1990) Brain glucose metabolism in postanoxic stroke. Arch Neurol 47:197–204

Doesburg SM, Roggeveen AB, Kitajo K, Ward LM (2008) Large-scale gamma-band phase synchronization and selective attention. Cereb Cortex 18:386–396

Doesburg SM, Green JJ, McDonald JJ, Ward LM (2009) Rhythms of consciousness: binocular rivalry reveals large-scale oscillatory network dynamics mediating visual perception. PLoS ONE 4:e6142

Doesburg SM, Herdman AT, Ribary U, Cheung T, Moiseev A, Weinberg H, Liotti M, Weeks D, Grunau RE (2010) Long-range synchronization and local desynchronization of alpha oscillations during visual short-term memory retention in children. Exp Brain Res 4:719–727

Doesburg SM, Ribary U, Herdman AT, Miller SP, Poskitt KJ, Moiseev A, Whitfield MF, Synnes A, Grunau RE (2011a) Altered long-range alpha-band synchronization during visual short-term memory retention in children born very preterm. Neuroimage 54:2330–2339

Doesburg S, Ribary U, Herdman AT, Moiseev A, Cheung T, Miller SP, Poskitt KJ, Weinberg H, Whitfield MF, Synnes A, Grunau RE (2011b) Magnetoencephalography reveals slowing of resting peak oscillatory frequency in children born very preterm. J Paediatr Res 70:171–176

Doesburg SM, Green JJ, McDonald JJ, Ward LM (2012) Theta modulation of inter-regional gamma synchronization during auditory attention control. Brain Res 1431:77–85

Façon E, Steriade M, Wertheim N (1958) Hypersomnie prolongée engendrée par les lésions bilatérales du système activateur médial. Le syndrome thrombotique de la bifurcation du tronc basilaire. Rev Neurol (Paris) 98:117–133

Fair DA, Bathula D, Mills KL, Costa Dias TG, Blythe MS, Zhang D et al (2010) Maturing thalamocortical functional connectivity across development. Front Syst Neurosci 4:1–10

Fell J et al (2002) Suppression of EEG gamma activity may cause the attentional blink. Conscious Cogn 11:114–122

Fries P, Reynolds JH, Rorie AE, Desimone R (2001) Modulation of oscillatory neuronal synchronization by selective visual attention. Science 291:1506–1507

Fries P (2005) A mechanism for cognitive dynamics: Neuronal communication through neuronal coherence. Trends Cog Sci 9:474–480

Fries P (2009) Neuronal gamma-band synchronization as a fundamental process in cortical computation. Ann Rev Neurosci 32:209–224

Gabrieli JDE (2009) Dyslexia: a new synergy between education and cognitive neuroscience. Science 325:280–283

Gray CM, Singer W (1989) Stimulus-specific neuronal oscillations in orientation columns of cat visual cortex. Proc Natl Acad Sci USA 86:1698–1702

Gray CM (1999) The temporal correlation hypothesis of visual feature integration: Still alive and well. Neuron 24:31–47

Green JJ, Doesburg SM, Ward LM, McDonald JJ (2011) Electrical neuroimaging of voluntary audiospatial attention: evidence for a supramodal attention control network. J Neurosci 31:3560–3564

Griesmayr B, Gruber WR, Klimesch W, Sauseng P (2010) Human frontal midline theta and its synchronization to gamma during a verbal delayed match to sample task. Neurobiol Learn Mem 93:208–215

Guillery RW, Sherman SM (2002) The thalamus as a monitor of motor outputs. Phil Trans R Soc Lond 357:1809–1821

Hanslmayer S, Gross J, Klimesch W, Shapiro KL (2011) The role of alpha oscillations in temporal attention. Brain Res Rev 67:331–343

Hari R, Salmelin R (1997) Human cortical oscillations: a neuromagnetic view through the skull. Trends Neurosci 20:44–49

Heim S, Eulitz C, Kaufmann J, Fuchter I, Pantev C, Lamprecht-Dinnesen A et al (2000) Atypical organisation of the auditory cortex in dyslexia as revealed by MEG. Neuropsychologia 38:1749–1759

Helenius P, Uutela K, Hari R (1999) Auditory stream segregation in dyslexic adults. Brain 122:907–913

Huang MX, Nichols S, Robb A, Angeles A, Drake A, Holland M, Asmussen S, D'Andrea J, Chun W, Levy M, Cui L, Song T, Baker DG, Hammer P, McLay R, Theilmann RJ, Coimbra R, Diwakar M, Boyd C, Neff J, Liu TT, Webb-Murphy J, Farinpour R, Cheung C, Harrington DL, Heister D, Lee RR (2012) An automatic MEG low-frequency source imaging approach for detecting injuries in mild and moderate TBI patients with blast and non-blast causes. Neuroimage 61:1067

Jahnsen H, Llinás RR (1984) Electro-physiological properties of guinea-pig thalamic neurones: An in vitro study. J Physiol 349:205–226

Jeanmonod D, Magnin M, Morel A (1996) Low-threshold calcium spike bursts in the human thalamus: common physiopathology for sensory, motor and limbic positive symptoms. Brain 119:363–375

Jeanmonod D, Magnin M, Morel A, Siegemund M, Cancro R, Lanz M, Llinás R, Ribary U, Kronberg E, Schulman JJ, Zonenshayn M (2001) Thalamocortical dysrhythmia II: clinical and surgical aspects. Thal Rel Syst 1:245–254

Jensen O, Vanni S (2002) A new method to identify multiple sources of oscillatory activity. NeuroImage 15:568–574

Jensen O, Kaiser J, Lachaux JP (2007) Human gamma-frequency oscillations associated with attention and memory. Trends Neurosci 30:317–324

Jensen O, Mazaheri A (2010) Shaping functional architecture by oscillatory alpha activity: gating by inhibition. Front Hum Neurosci 4:1–8

Jerbi K, Ossandón T, Hamamé CM, Senova S, Dalal SS et al (2009) Task-related gamma-band dynamics from an intracerebral perspective: review and implications for surface EEG and MEG. Hum Brain Mapp 30:1758–1771

John ER, Prichep LS, Friedman J, Easton P (1988) Neurometrics: Computer assisted differential diagnosis of brain dysfunctions. Science 293:162–169

Joliot M, Ribary U, Llinás R (1994) Human oscillatory brain activity near 40 Hz coexists with cognitive temporal binding. Proc Natl Acad Sci USA 91:11748–11751

Jones EG (2001) The thalamic matrix and thalamocortical synchrony. Trends Neurosci 24:595–601

Jones EG (2002) Thalamic circuitry and thalamocortical synchrony. Phil Trans R Soc Lond 357:1659–1673

Jones EG (2009) Synchrony in the interconnected circuitry of the thalamus and cerebral cortex. In: ND Schiff, S Laureys (eds) Disorders of Consciousness, vol 1157. Annals of the New York Academy of Sciences, New York, pp 10–23

Kahana MJ, Seelig D, Madsen JR (2001) Theta returns. Curr Opin Neurobiol 11:739–744

Klimesch W, Sauseng P, Hanslmayr S (2007) EEG alpha oscillations: the inhibition timing hypothesis. Brian Res Rev 53:63–88

Laureys S, Goldman S, Phillips C, Van Bogaert P, Aerts J, Luxen A et al (1999) Impaired effective cortical connectivity in vegetative state: preliminary investigation using PET. Neuroimage 9:377–382

Laureys S, Owen AM, Schiff N (2004) Brain function in coma, vegetative state, and related disorders. Lancet Neurol 3:537–546

Laureys S (2005) Death, unconsciousness and the brain. Nat Rev Neurosci 6:899–909

Lee G, Byram A, Stables C, Mizgalewicz A, Ribary U, Owen AM, Illes J (2012) A framework for assessing the clinical actionability of functional neuroimaging for disorders of consciousness. Int Neuroethics Soc

Levy DE, Sidtis JJ, Rottenberg DA, Jarden JO, Strother SC, Dhawan V et al (1987) Differences in cerebral blood flow and glucose utilization in vegetative versus locked-in patients. Ann Neurol 22:673–682

Llinás R, Grace AA, Yarom Y (1991) In vitro neurons in mammalian cortical layer 4 exhibit intrinsic activity in the 10 to 50 Hz frequency range. Proc Natl Acad Sci USA 88:897–901

Llinás R (1993) Is dyslexia a dyschronia? Ann NY Acad Sci 682:48–56

Llinás R, Ribary U (1993) Coherent 40-Hz oscillation characterizes dream state in humans. Proc Natl Acad Sci USA 90:2078–2081

Llinás R, Ribary U, Joliot M, Wang XJ (1994) Content and context in temporal thalamocortical binding. In: Buzsaki G, Llinás R, Singer W, Berthoz A, Christen Y (eds) Temporal coding in the brain. Springer, Heidelberg, pp 251–272

Llinás R, Ribary U, Tallal P (1998a) Dyschronic language-based learning disability. In: VonEuler C, Lundberg I, Llinás R (eds) Basic mechanisms in cognition and language. Elsevier, New York, pp 101–108

Llinás R, Ribary U, Contreras D, Pedroarena C (1998b) The neuronal basis for consciousness. Phil Trans R Soc Lond 353:1841–1849

Llinás R, Ribary U, Jeanmonod D, Kronberg E, Mitra PP. (1999) Thalamo-cortical dysrhythmia: a neurological and neuropsychiatric syndrome characterized by magnetoencephalography. Proc Natl Acad Sci USA 96:15222–15227

Llinás R, Ribary U, Jeanmonod D, Cancro R, Kronberg E, Schulman JJ, Zonenshayn M, Magnin M, Morel A, Siegemund M (2001) Thalamocortical dysrhythmia I: functional and imaging aspects. Thal Rel Syst 1:237–244

Llinás RR, Leznik E, Urbano FJ (2002) Temporal binding via cortical coincidence detection of specific and nonspecific thalamocortical inputs: a voltage-dependent dye-imaging study in mouse brain slices. Proc Natl Acad Sci USA 99:449–454

Lou HC, Joensson M, Biermann-Ruben K, Schnitzler A, Ostergaard L, Kjaer TW, Gross J (2011) Recurrent activity in higher order, modality non-specific brain regions: A granger causality analysis of autobiographic memory retrieval. PLoS ONE 6:e22286

Madler C, Keller I, Schwender D, Poeppel E (1991) Sensory information processing during general anaesthesia: effect of isoflurane on auditory evoked neuronal oscillations. Brit J Anaesthes 66:81–87

Merzenich MM, Jenkins WM, Johnston P, Schreiner C, Miller SL, Tallal P (1996) Temporal processing deficits of language-learning impaired children ameliorated by training. Science 271:77–81

Miller G (2010) Neuroscientists grapple with their field's big questions. Science 330:164

Mumford D (1991) On the computational architecture of the neocortex. The role of the thalamocortical loop. Biol Cyber 65:135–145

Nagarajan S, Mahncke H, Salz T, Tallal P, Roberts T, Merzenich MM (1999) Cortical auditory signal processing in poor readers. Proc Natl Acad Sci USA 96:6483–6488

Osipova D, Takashima A, Oostenveld R, Fernandez G, Maris E, Jensen O (2006) Theta and gamma oscillations predict encoding and retrieval of declarative memory. J Neurosci 26:7523–7531

Owen AM, Hampshire A, Grahn JA, Stenton R, Dajani S, Burns AS et al (2010) Putting brain training to the test. Nature 465:775–778

Palva JM, Monto S, Kulashekhar S, Palva S (2010) Neural synchrony reveals working memory networks and predicts individual memory capacity. Proc Natl Acad Sci USA 107:7580–7585

Palva S, Palva JM (2007) New vistas for alpha-frequency band oscillations. Trends Neurosci 30:150–158

Pantev C, Makeig S, Hoke M, Galambos R, Hampson S, Gallen C (1991) Human auditory evoked gamma-band magnetic fields. Proc Natl Acad Sci USA 88:8996–9000

Pfurtscheller G, Schwarz G, Pfurtscheller B (1983) Computer assisted analysis of EEG, evoked potentials, EEG reactivity and heart rate variability in comatose patients. Elektroenzephalogr Elektromyogr Verwandte Geb 14:66–73

Pfurtscheller G, Neuper C (1994) Event-related synchronization of mu rhythm in the EEG over the cortical hand area in man. Neurosci Lett 174:93–96

Pfurtscheller G, Stancak A, Neuper C (1996) Event-related synchronization (ERS) in the alpha-band—an electrophysiological correlate of cortical idling: a review. Int J Psychophysiol 24:39–46

Plum F, Schiff N, Ribary U, Llinás R (1998) Coordinated expression in chronically unconscious persons. Phil Trans R Soc Lond 353:1929–1933

Purpura KP, Schiff ND (1997) The thalamic intralaminar nuclei: role in visual awareness. Neuroscientist 3:8–14

Rennie CJ, Robinson PA, Wright JJ (2002) Unified neurophysiological model of EEG spectra and evoked potentials. Biol Cyber 86:457–471

Ribary U, Llinás R, Kluger A, Suk J, Ferris SH (1989) Neuropathological dynamics of magnetic, auditory, steady-state responses in Alzheimer's disease. In: Williamson SJ, Hoke M, Stroink G, Kotani M (eds) Advances in biomagnetism. Plenum Press, New York, pp 311–314

Ribary U, Ioannides AA, Singh KD, Hasson R, Bolton JPR, Lado F, Mogilner A, Llinás R (1991) Magnetic field tomography (MFT) of coherent thalamo-cortical 40-Hz oscillations in humans. Proc Natl Acad Sci USA 88:11037–11041

Ribary U, Cappell J, Mogilner A, Hund M, Kronberg E, Llinás R (1999) Functional imaging of plastic changes in the human brain. Adv Neurol 81:49–56

Ribary U, Joliot M, Miller SL, Kronberg E, Cappell J, Tallal P, Llinás R (2000) Cognitive temporal binding and its relation to 40 Hz activity in humans: alteration during dyslexia. In: Aine C, Okada Y, Stroink G, Swithenby S, Wood CC (eds) Biomag96. Springer, Berlin, pp 971–974

Ribary U (2005) Dynamics of thalamo-cortical network oscillations and human perception. Progr Brain Res 150:127–142

Ribary U, Ward LM (2014) Synchronization and functional connectivity dynamics across TC-CC-CT networks: Implications for clinical symptoms and consciousness. In: Mishara A (ed) Phenomenological neuropsychiatry: bridging the clinic with clinical neuroscience, Springer

Rudolf J, Ghaemi M, Haupt WF, Szelies B, Heiss WD (1999) Cerebral glucose metabolism in acute and persistent vegetative state. J Neurosurg Anesthesiol 11:17–24

Salmelin R, Service E, Kiesila P, Uutela K, Salonen O (1996) Impaired visual word processing in dyslexia revealed with magnetoencephalography. Ann Neurol 40:157–162

Salmelin R (2007) Clinical neurophysiology of language: the MEG approach. Clin Neurophysiol 118:237–254

Sarnthein J, Morel A, von Stein A, Jeanmonod D (2003) Thalamic theta field potentials and EEG: high thalamocortical coherence in patients with neurogenic pain, epilepsy and movement disorders. Thal Rel Syst 2:231–238

Sarnthein J, Jeanmonod D (2007) High thalamocortical coherence in patients with Parkinson's disease. J Neurosci 27:124–131

Sarnthein J, Jeanmonod D (2008) High thalamocortical coherence in patients with neurogenic pain. NeuroImage 39:1910–1917

Sauseng P, Klimesch W, Doppelmayr M, Hanslmayr S, Schabus M, Gruber WR (2004) Theta coupling in the human electroencephalogram during a working memory task. Neurosci Lett 354:123–126

Sauseng P, Klimesch W, Gruber WR, Birbaumer N (2008) Cross-frequency phase synchronization: a brain mechanism of memory matching and attention. Neuroimage 40:308–317

Sauseng P, Griesmayr B, Freunberger R, Klimesch W (2010) Control mechanisms in working memory: a possible function of EEG theta oscillations. Neurosci Biobehav Rev 34:739–744

Schiff ND, Ribary U, Plum F, Llinás R (1999) Words without mind. J. Cog. Neurosci. 11:650–656

Schiff ND, Ribary U, Moreno DR, Beattie B, Kronberg E, Blasberg R, Giacino J, McCagg C, Fins JJ, Llinas R, Plum F (2002) Residual cerebral activity and behavioural fragments can remain in the persistently vegetative brain. Brain 125:1210–1234

Schiff ND, Giacimo JT, Kalmar K, Victor JD, Baker K, Gerber M et al (2007) Behavioural improvements with thalamic stimulation after severe traumatic brain injury. Nature 448:600–603

Schnitzler A, Gross J (2005) Normal and pathological oscillatory communication in the brain. Nat Rev Neurosci 6:285–296

Schulman JJ, Ramirez RR, Zonenshayn M, Ribary U, Llinás R (2005) Thalamocortical dysrhythmia syndrome: MEG imaging of neuropathic pain. Thal Rel Syst 3:33–39

Schulman JJ, Cancro R, Lowe S, Lu F, Walton KD, Llinás RR (2011) Imaging of thalamocortical dysrhythmia in neuropsychiatry. Front Hum Neurosci 5:1–11

Sherman SM, Guillery RW (2006) Exploring the thalamus and its role in cortical function. MIT Press, Cambridge, MA

Simos PG, Breier JI, Fletcher JM, Bergman E, Papanicolaou AC (2000) Cerebral mechanisms involved in word reading in dyslexic children: a magnetic source imaging approach. Cereb Cortex 10:809–816

Snyder AC, Foxe JJ (2010) Anticipatory attentional suppression of visual features indexed by oscillatory alpha-band power increases: a high-density electrical mapping study. J Neurosci 30:4024–4032

Sporns O, Tononi G, Kötter R (2005) The human connectome: a structural description of the human brain. PLoS Comput Biol 1:e42

Steriade M, Llinas RR (1988) The functional states of the thalamus and the associated neuronal interplay. Physiol Rev 68:649–742

Steriade M, Curro Dossi R, Pare D, Oakson G (1991) Fast oscillations (20–40 Hz) in thalamocortical systems and their potentiation by mesopontine cholinergic nuclei in the cat. Proc Natl Acad Sci USA 88:4396–4400

Steriade M (1993) Central core modulation of spontaneous oscillations and sensory transmission in thalamocortical systems. Curr Opin Neurobiol 3:619–625

Steriade M, Curró Dossi R, Contreras D (1993a) Electrophysiological properties of intralaminar thalamocortical cells discharging rhythmic $\sim$40 Hz spike-bursts at $\sim$1000 Hz during waking and rapid-eye movement sleep. Neurosci 56:1–9

Steriade M, McCormick DA, Sejnowski TJ (1993b) Thalamocortical oscillations in the sleeping and aroused brain. Science 262:679–685

Steriade M, Amzica F (1996) Intracortical and corticothalamic coherency of fast spontaneous oscillations. Proc Natl Acad Sci USA 93:2533–2538

Supp et al (2007) Directed cortical information flow during human object recognition: analyzing induced EEG gamma-band responses in brain's source space. PLoS ONE 2:e684

Tallal P, Miller S, Fitch RH (1993) Neurobiological basis of speech: a case for the preeminence of temporal processing. Ann NY Acad Sci 682:27–47

Tallal P, Miller SL, Bedi G, Byma G, Wang X, Nagarajan SS, Schreiner C, Jenkins WM, Merzenich MM (1996) Language comprehension in language-learning impaired children improved with acoustically modified speech. Science 271:81–84

Tallal P (2004) Improving language and literacy is a matter of time. Nat Rev Neurosci 5:721–728

Tallon-Baudry C, Bertrand O, Peronnet F, Pernier J (1998) Induced γ-band activity during the delay of a visual short-term memory task in humans. J Neurosci 18:4244–4254

Tallon-Baudry C, Bertrand O (1999) Oscillatory gamma activity in humans and its role in object representation. Trends Cogn Sci 3:151–162

Timmermann L, Gross J, Butz M, Kircheis G, Haussinger D, Schnitzler A (2003) Mini-asterixis in hepatic encephalopathy induced by pathologic thalamo-motor-cortical coupling. Neurology 61:689–692

Tomassino C, Grana C, Lucignani G, Torri G, Ferrucio F (1995) Regional metabolism of comatose and vegetative state patients. J Neurosurg Anesthesiol 7:109–116

Varela F, Lachaux JP, Rodriguez E, Martinerie J (2001) The brainweb: phase synchronization and large-scale integration. Nature Rev Neurosci 2:229–239

Victor JD, Drover JD, Conte MM, Schiff ND (2011) Mean-field modeling of thalamocortical dynamics, and a model-driven approach to EEG analysis. Proc Natl Acad Sci USA 108:15631–15638

Volkmann J, Joliot M, Mogilner A, Ioannides AA, Lado F, Fazzini E, Ribary U, Llinás RR (1996) Central motor loop oscillations in Parkinsonian resting tremor revealed by magnetoencephalography. Neurology 46:1359–1370

Wang HP, Spencer D, Fellous JM, Sejnowski TJ (2010) Synchrony of thalamocortical inputs maximizes cortical reliability. Science 328:106–109

Ward LM (2003) Synchronous neural oscillations and cognitive processes. Trends Cog Sci 17:553–559

Ward LM (2011) The thalamic dynamic core theory of conscious experience. Consc Cogn 20:464–486

Wright JJ, Robinson PA, Rennie CJ, Gordon E, Bourke PD, Chapman CL et al (2001) Toward an integrated continuum model of cerebral dynamics: the cerebral rhythms, synchronous oscillation and cortical stability. BioSystems 63:71–88

Temporal and Spectral Signatures of the Default Mode Network

Francesco de Pasquale and Laura Marzetti

Abstract The existence of a structured pattern of neuronal activity in the brain at rest has been consistently reported in the neuroscience literature. Multiple techniques, such as fMRI, MEG and EEG, showed that spontaneous, slow fluctuations of cerebral activity are temporally coherent within distributed functional networks resembling those evoked by sensory, motor, and cognitive paradigms. Among these networks, the Default Mode network gained large interest because of its anatomical and functional architecture. In fact, this network seems to reflect the default brain activity at rest and it has been associated with internal mentation, autobiographical memory, thinking about one's future, theory of mind, self-referential and affective decision making. What processing demands are shared in common across such a variety of tasks is presently unclear, and to disentangle such high level tasks into component processes is challenging. Here, we address some of these aspects by reviewing the current MEG studies on this network. In fact, while MEG data confirm the observed fMRI spatial topography, some new intriguing temporal and frequency properties of this network are revealed. Such findings enrich the original fMRI scenario on the DMN functional roles in terms of internal coupling and cross-network communication in the brain at rest. The Default Mode Network's internal coupling seems to be characterized by slow frequencies in the alpha and beta range and the cross-network interaction reveals that the DMN plays a central role in the communication across many different resting state networks.

F. de Pasquale (✉) · L. Marzetti
Department of Neuroscience and Imaging, "G. d'Annunzio" University Chieti-Pescara, 66100 Chieti, Italy
e-mail: f.depasquale@unich.it

F. de Pasquale · L. Marzetti
Institute for Advanced Biomedical Technologies, "G. d'Annunzio" University Foundation, 66100 Chieti, Italy

S. Supek and C. J. Aine (eds.), *Magnetoencephalography*,
DOI: 10.1007/978-3-642-33045-2_20, © Springer-Verlag Berlin Heidelberg 2014

Keywords Resting state networks · Default mode network · Functional connectivity · Cross-network interaction · Frequency signature · Independent component analysis

1 Introduction

The "resting state" can be defined as a condition in which the subject is engaged in unconstrained stimulus independent thoughts, i.e. the brain is not performing any specific attention-demanding or stimulus dependent task and it switches into a default mode characterized by mental explorations based on personal introspection, autobiographical memories, and thoughts of the future (Buckner et al. 2008). In such an uncontrolled state, brain activations underlying the flow of thoughts would be expected to vary greatly. Despite this intuitive observation, such stimulus independent thought during rest recruits a remarkably consistent neural network—the Default Mode Network (DMN) (Raichle et al. 2001; Shulman et al. 1997).

1.1 Brief History of the Default Mode Network

The discovery of the DMN was an accidental one. The first evidence for the existence of this network came out when measuring brain activity in humans during undirected mental states. Indeed, common practice in studying task driven modulations of brain activity was to acquire passive conditions to be used as experimental controls. However, while comparing activity during different states it was observed in the last decade that specific brain regions were more active during control states than during many goal-directed tasks (Mazoyer et al. 2001; Shulman et al. 1997). These brain regions have gained much attention from the scientific community (Gusnard and Raichle 2001; Raichle et al. 2001). Although the observation of a network of default state was made in the 20th century, the idea that brain activity persists during undirected mental activity was known earlier. Electrophysiological support for this hypothesis was apparent since electroencephalogram (EEG) was discovered and it was evident that electrical oscillations measured by EEG did not stop when the subject was at rest (Berger 1929).

In addition, in 1955, Sokoloff et al. (1955) discovered that cerebral metabolism, measured by using the Kety–Schmidt technique (Kety and Schmidt 1948), did not globally change when going from a quiet rest state to performing a challenging arithmetic problem. Starting from the seventies, Ingvar used regional cerebral blood flow (rCBF) to show that brain activity persists during rest (Ingvar 1979, 1985) and such activity was structured in consistent, regionally specific patterns that prominently include prefrontal cortex.

By the late 20th century, positron emission tomography (PET) became popular, thus allowing for finer spatial resolution and sensitivity to deep-brain structures than earlier methods. Moreover, owing to the development of isotopes with short half-lives, typical PET experiments could include many task and control conditions. This paved the way for performing many imaging studies based on different tasks examining different aspects of brain functioning: language, perception, memory and attention. Within a few years, several dozen experiments were conducted, each comprising scans of different tasks and resting state brain activity as a control condition. The meta-analyses of the passive task data (Mazoyer et al. 2001; Shulman et al. 1997) resulted in the observation that there are brain regions that are consistently active in the passive control condition and show a "deactivation" in the task condition in comparison to control. For review see Andrews-Hanna et al. (2010), Buckner et al. (2008).

1.2 Default Mode Network Functional Roles

Default Mode Network activations have been observed during direct tasks related to internal mentation, autobiographical memory, thinking about one's future, theory of mind, self-referential and affective decision making (Buckner et al. 2008; Ochsner et al. 2004; Spreng et al. 2009). What processing demands are shared in common across such a variety of tasks is presently unclear and to disentangle such high level tasks into component processes is challenging.

Some researchers suggested an involvement of the DMN in scene construction (Hassabis and Maguire 2007), contextual associations and processing (Bar et al. 2007). Others proposed a role for this network in social (Mitchell et al. 2006; Schilbach et al. 2008), self-referential or affective cognition (D'Argembeau et al. 2005; Gusnard et al. 2001; Gusnard and Raichle 2001; Wicker et al. 2003). The divergence across these perspectives, perhaps best exemplified by the different emphasis in Hassabis and Maguire's scene construction model (Hassabis and Maguire 2007) and D'Argembeau and colleagues' emphasis on self-referential cognition (D'Argembeau et al. 2005), suggests that the DMN likely comprises multiple interacting subsystems, e.g., (Buckner et al. 2008). This hypothesis seems to be supported by the identification of distinct and functionally separated DMN subsystems: the dorsal medial prefrontal cortex (dMPFC) and the medial temporal lobe (MTL) systems. The MTL subsystem showed increased activity preferentially when participants made episodic decisions about their future, see Schacter and Addis (2007). The common activation during remembering and prospection implies that a common set of processes underlies these abilities. This evidence hints at the possibility that the MTL subsystem is more sensitive to the act of simulating the future using mnemonic imagery-based processes rather than to temporal aspects of the future per se. In contrast to the constructive function of the MTL subsystem, the dMPFC subsystem seems to be preferentially active when participants consider their present mental states (Gusnard et al. 2001; Lane et al. 1997; Ochsner et al. 2005;

Saxe et al. 2006; Vanderwal et al. 2008; reviewed in Amodio and Frith 2006; Ochsner et al. 2004). Interestingly, regions within the dMPFC subsystem are also activated when participants infer mental states of other people (Gallagher et al. 2000; Ochsner et al. 2004, 2005; Saxe and Kanwisher 2003; Saxe et al. 2006; reviewed in Amodio and Frith 2006; Frith and Frith 2003).

Furthermore, some authors examined how DMN interacts with other networks during memory retrieval and reported a robust functional dissociation within the DMN: whereas angular gyrus and posterior cingulate/precuneus are significantly activated during memory retrieval, an anterior DMN node in medial prefrontal cortex is strongly deactivated. This finding supports a functional heterogeneity rather than homogeneity within the DMN during episodic memory retrieval (Sestieri et al. 2011). The possible neural overlap among affective, self-referential, and social cognitive processes suggests a broader role for this subsystem in either meta-cognition (Ochsner et al. 2004), mental state inference (Frith and Frith 2003; Olsson and Ochsner 2008), social cognition (Mitchell 2006; Mitchell et al. 2006), or the use of one's own mental states as a model for inferring the mental states of others (Goldman 1992). However, the precise interplay between emotion, self-knowledge, and prediction of other's mental states is currently still under investigation, as many stimuli may confound these processes, see Olsson and Ochsner (2008) for a review.

The large scale interactions among the dMPFC and MTL subsystems are realized through a local core set of hubs including the Posterior Cingulate Cortex (PCC) and the anterior medial prefrontal cortex (aMPFC). Consistent with their possible role of integration as default network hubs, the aMPFC and PCC seem to share functional properties of both subsystems exhibiting preferential self-related activity regardless of temporal context.

In general, the presence of such hubs suggests a small-world topology for the DMN architecture, in which separate functional modules are linked through central hubs, and seems to represent a general structure of the brain which allows for the implementation of the two basic principles of functional segregation and dynamic integration (de Pasquale et al. 2012b). This is an attractive model for the organization of brain anatomical and functional networks since it can support both segregated/specialized and distributed/integrated information processing. Small-world networks are efficient, tending to minimize the cost of information flow while supporting high dynamical complexity.

Eventually, a fundamental role for the DMN functions seems to be played by its competitive interactions with other networks (e.g., dorsal attention network-or in general task-positive networks). These DMN interactions have an important cognitive impact: in the healthy brain, greater suppression of the default network is associated with better memory formation (Daselaar et al. 2004, 2009). As a task becomes more difficult, DMN suppression increases (McKiernan et al. 2003; Singh and Fawcett 2008), as if attentional resources are allocated away from intrinsic thoughts and toward difficult extrinsic tasks. On the other hand, greater DMN activation (less task suppression or deactivation) just prior to a stimulus predicts lapses of attention measured as slower and less-accurate performance (Eichele et al. 2008; Betti et al. 2013).

To summarize, the above functional and topological properties of the Default Mode Network raised the interest of the neuroscience community exponentially, thanks to the fascinating idea that this network, rather than simply reflecting a quiescent or idling brain state, represents a window into the brain for the understanding of the basis of free thought from a neuroscience perspective.

2 Methodologies to Study Default Mode Network Interactions at Rest with MEG

Studying the covariance structure of spontaneous cortical activity with MEG at rest is challenging for several reasons. MEG data are often contaminated by several artifacts including physiologic noise (respiration, heart), head and eye movements, and environmental noise. The impact of these artifacts is important in resting state studies because averaging in phase with events cannot be used to improve the signal to noise ratio, which in resting state MEG connectivity studies will always be poor. Moreover, inverse source modeling is inherently uncertain and is especially so when the objective is to recover multiple simultaneously active sources. Most of these factors and their impact on the detection of MEG Resting State Networks (RSNs) have been discussed in Brookes et al. (2011a, b; de Pasquale et al. 2010; Mantini et al. 2011). However, despite these difficulties, a number of studies have employed MEG to measure functional connectivity in both sensor and source space, and a variety of methodologies has been described. Here we summarize some of the most recent and promising approaches based on the MEG band limited power, for a review see Darvas and Leahy (2007).

Several approaches in the frequency domain have been presented to study MEG connectivity. For example, dynamic imaging of coherent sources (Gross et al. 2001) is a technique in which a frequency domain beamformer is employed to project MEG data spectral properties (cross-spectra) onto the source space resulting in coherence maps between brain regions. Other studies have based functional and effective connectivity metrics on the insight that the imaginary part of the cross-spectra cannot be explained as a mixing artifact due to field spread and cross talk (Nolte et al. 2004). From this observation, a series of methods to identify (Ewald et al. 2012; Nolte et al. 2006, 2009) and localize brain interactions (Marzetti et al. 2008, 2013; Shahbazi Avarvand et al. 2012) has been developed. Also the phase slope has been used as a marker for effective connectivity in (Nolte et al. 2008). For a comprehensive review on these methods see also the chapter from Nolte and Marzetti in this book. Other metrics include phase lag index—PLI (Stam et al. 2007)—which quantifies asymmetry in the phase lag distribution based on the observation that field spread and cross talk will cause a symmetric distribution and therefore will not contribute to PLI, and synchronization likelihood (Stam et al. 2002). Essentially, PLI takes two separate electrical signals and looks for isochronous recurrence to a certain part of their (individually different) attractors. Interestingly, in a recent paper (Liu et al. 2010), Liu and colleagues

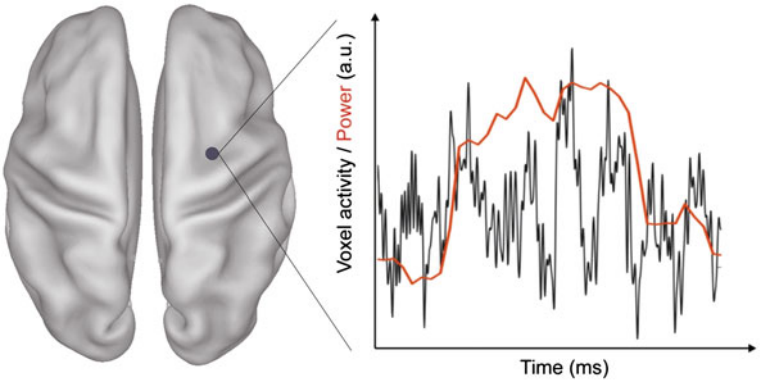

Fig. 1 MEG signal versus power time-scales. Example of time courses of MEG activity (*black*) and power envelope (*red*)

employed a MEG sensor space 'envelope correlation' metric to show that inter-hemispheric connectivity (observed by functional connectivity MRI, fcMRI) is mirrored by interhemispheric neuromagnetic correlation. Other studies (Guggisberg et al. 2008) have also employed time domain beamforming and imaginary coherence to efficiently map connectivity patterns in tumor patients.

Within the framework of source-space connectivity, we will now focus on three methods which have been successfully developed and applied to investigate MEG connectivity at rest and in particular the DMN within and across network interactions. The first method developed by de Pasquale and colleagues, is based on the instantaneous correlation of MEG Band Limited Power (BLP) in the time domain (de Pasquale et al. 2010, 2012a). The second approach, developed by Brookes et al. is based on Independent Component Analysis and MEG power envelope (Brookes et al. 2011b). The third method, developed at the University Medical Center Hamburg-Eppendorf by the group of Andreas Engel, takes advantage of orthogonalized signals to identify delayed interactions thus assuming that all the instantaneous interactions are induced by artificial spurious correlation (Hipp et al. 2012). The different temporal scales of the MEG BLP compared to the MEG signals are shown in Fig. 1 where the two quantities estimated for the same voxel are shown.

Interestingly, all three methods showed important similarities regarding the Default Network interactions' properties. In (Hipp et al. 2012) it is assumed that signal components of the same source measured from different sensors will be characterized by an identical phase while in many cases, different neuron populations have a variable phase relation. This difference can be exploited to remove spurious correlation patterns due to the MEG limited spatial resolution. In particular, every considered pair of signals is orthogonalized before the computation of their power envelopes. This allows one to remove the spurious common correlation leaving a residual 'cleaned' spatial correlation. The activity orthogonalization is performed in the frequency domain on the estimated band limited activity

but this can similarly be done in the time domain where it generalizes to broadband signals. Of practical importance is the selection of the time interval to derive the regression coefficient. This can range from the entire dataset to just a single time window during which the signals' relation should be constant. If such stationarity is fulfilled, longer time intervals provide more robust estimates and may lead to a superior sensitivity of the method. However, it is important to stress that without stationarity, the orthogonalization step may be incomplete. Eventually, the interaction between orthogonalized signals is quantified by means of correlation of the power envelopes obtained by squaring the absolute values of the complex spectral estimates after a logarithmic transform (this makes the power more normally distributed). The correlation with a given seed is considered as significant when it is higher than a baseline value computed as the average correlation with the rest of the brain.

In Brookes et al. (2011a, b) an approach based on Beamforming and the computation of the Hilbert Envelope is presented. MEG data are frequency filtered in the typical physiological bands and covariance matrices are generated independently for each frequency band, using the whole recording session at the subject level. It is important to stress that this corresponds to assuming that sources of interest are stationary throughout the experiment. Following beamformer projection, source-space signals are normalized and Hilbert transformed. The absolute value of the analytic signal, called the "Hilbert envelope", is computed to obtain an amplitude envelope of oscillatory power. Then, data from all subjects are concatenated in the time dimension and temporal Independent Component Analysis (ICA) is applied using the fastICA (http:www.research.ics.tkk.fi/ica/fastica) algorithm. The spatial signature of each IC is measured by Pearson correlation between the temporal IC (tIC) and the time course of each voxel in the concatenated dataset. This process is implemented independently for each frequency band of interest. In addition to the ICA-based approach, the authors also present a seed-based approach for DMN characterization to show that independent temporal signals arise from spatially orthogonal networks. Seed locations in the motor, fronto-parietal, and visual networks are extracted from fMRI data. Down-sampled Hilbert envelopes are extracted for each of these seed locations and in order to generate seed-based correlation maps, data are concatenated across subjects. The Pearson correlation between seed time course and down-sampled Hilbert envelopes for all other brain voxels is computed. In (Brookes et al. 2011b), the validity of correlation measurements are tested using a simulation approach in which two dipolar sources (at the seed and test locations) are repeatedly simulated. To obtain noise data to be added to these simulated data, one empty-room session is recorded (no subject in the scanner). The simulation step is repeated to assess the statistical significance of measured functional connectivity values. Simulated MEG data are projected into the brain using the same beamformer weights derived from and applied to the real MEG data. This interesting approach allows one to check whether the adopted beamformer projection generates spurious correlation due to the volume conduction and signal leakage.

Another interesting aspect of the work of Brookes and colleagues is the different metrics the authors propose to assess the functional connectivity: two are based on envelope correlation—termed Average Envelope Correlation (AEC) and Correlation of Averaged Envelopes (CAE); while two others are based on coherence—termed coherence (Coh) and Imaginary coherence (ICoh). In all cases, connectivity is measured between the projected signal at the seed voxel, and that from all other (test) voxels in the brain.

The approach presented in (de Pasquale et al. 2010, 2012a) is based on the BLP but is different from the previous ones; it is developed to take into account the non-stationarity of brain connections. This temporal non-stationarity represents an important aspect of the DMN internal and across-network interactions. In fact, based on the observation that the coupling among different RSN nodes oscillate over time, de Pasquale et al. propose an approach to estimate time epochs in which the internal connectivity of a network is optimized. In what follows, we describe the basic ingredients of this methodology.

The MEG data are pre-processed by applying a pipeline based on ICA described in (de Pasquale et al. 2010; Mantini et al. 2011), which extends an approach described in (Hironaga and Ioannides 2007). Basically, different from what was described above where each IC was related to a given resting state network, a subset of ICs is classified as artifactual and removed. Importantly, the authors do not assume that a network can be assigned single ICs but rather a combination of them. For this reason, once non-artifactual ICs are identified these are linearly combined to generate the 'cleaned' MEG signal. To this aim, source-space IC maps are reconstructed from the remaining ICs on a Cartesian 3D grid with 4 mm voxel side using a weighted minimum-norm least squares (WMNLS) procedure. For each voxel and each time sample, source-space signals are obtained by linear combination of IC time-courses, each weighted by its source-space map. Then, source-space signals are filtered in the typical physiological frequency bands. From these filtered signals, MEG power time series are obtained by averaging the square of source-space MEG signals.

In order to determine the time scale to adopt for the non-stationary analysis, the total interdependence function, a coherence-based measure of the functional connectivity, is examined from nodes of known network affiliation. The authors report initially for the Default Mode Network and the Dorsal Attention network (de Pasquale et al. 2010), an increase in the vicinity of 0.1 Hz. This result was then extended to the Ventral Attention, Motor and Language networks. Based on this observation the length of 10 seconds, the reciprocal of 0.1 Hz, is selected as the window duration to be used for the evaluation of time-varying node-pair correlation.

Eventually, to identify epochs of high within-RSN correlation or maximal correlation windows (MCWs), de Pasquale and colleagues developed the 'extended maximal correlation window' (EMCW) algorithm. This algorithm accepts as input power time-series spanning an entire MEG run from one seed and two other nodes of known network affiliation. The objective of this algorithm is to identify epochs in which the contrast between within-network, i.e. between the seed and other network

input nodes, versus external node-to-network correlation, i.e. between the seed and an external node, is maximal. Specifically, the algorithm seeks epochs in which the *least* within-network correlation is above a threshold while the external node-to-network is minimal. This is accomplished using an iterative strategy based on the Old Bachelor Acceptance thresholding technique (Hu et al. 1995). The algorithm is run starting with different groups of input nodes to obtain a specific set of MCWs for each network by concatenating the MCWs for each input node group. Additional details on the selection of the threshold and criteria for epoch selection can be found in (de Pasquale et al. 2010, 2012a, b; Mantini et al. 2011).

The network connectivity maps and cross-network interaction matrices are based on the definition of a Z-score obtained from correlation maps computed in all the sessions of all the subjects in all the estimated MCW epochs. To obtain the final RSN connectivity maps, the strengths of the correlations in every voxel of the brain with the seed, compared to the mean correlation in the whole brain, is tested. Then, each connectivity map is corrected for false discovery rate—FDR ($p < 0.05$) and thresholded at a significant level to obtain a binary map. All the binary maps from the different seeds are combined together through a logic AND. This step insures that only regions of significant correlation across all nodes of a network are maintained.

Analogously, the cross-network interaction matrices are also based on Z-scores to is the strengths of the correlations between a pair of RSN nodes compared to the mean correlation of these nodes, with the rest of the brain. It must be stressed that, based on the above definitions, Z-scores are defined on specific temporal epochs including all the MCWs obtained for each specific RSN. This quantity represents the average interaction between one 'fully engaged' network and another network.

In (de Pasquale et al. 2012a) MEG-RSNs interactions are not only characterized on average throughout the recording period by computing matrices of node-to-node or RSN-to-RSN power correlation, but also by characterizing the dynamics of this interaction. This is achieved by computing the degree of temporal overlap between two networks, when each one is respectively in a state of high internal correlation (or MCW). Given two sets of RSN MCWs, we computed the MCW overlap as the average ratio of overlap of all the possible pairs of MCWs from the two networks. It must be noted that differently from the power correlation matrix, this matrix is symmetric by definition. To summarize, in Fig. 2 we report the flowcharts of the described ICA and seed-based approaches.

2.1 Methodological Considerations

The methodologies adopted in the MEG community, due to the intrinsic nature of the MEG signal and the acquisition setup, differ at several levels. The first level is related to the solution of the inverse problem for which different kinds of spatial filters, adaptive or non adaptive, with or without noise normalization, in time or in

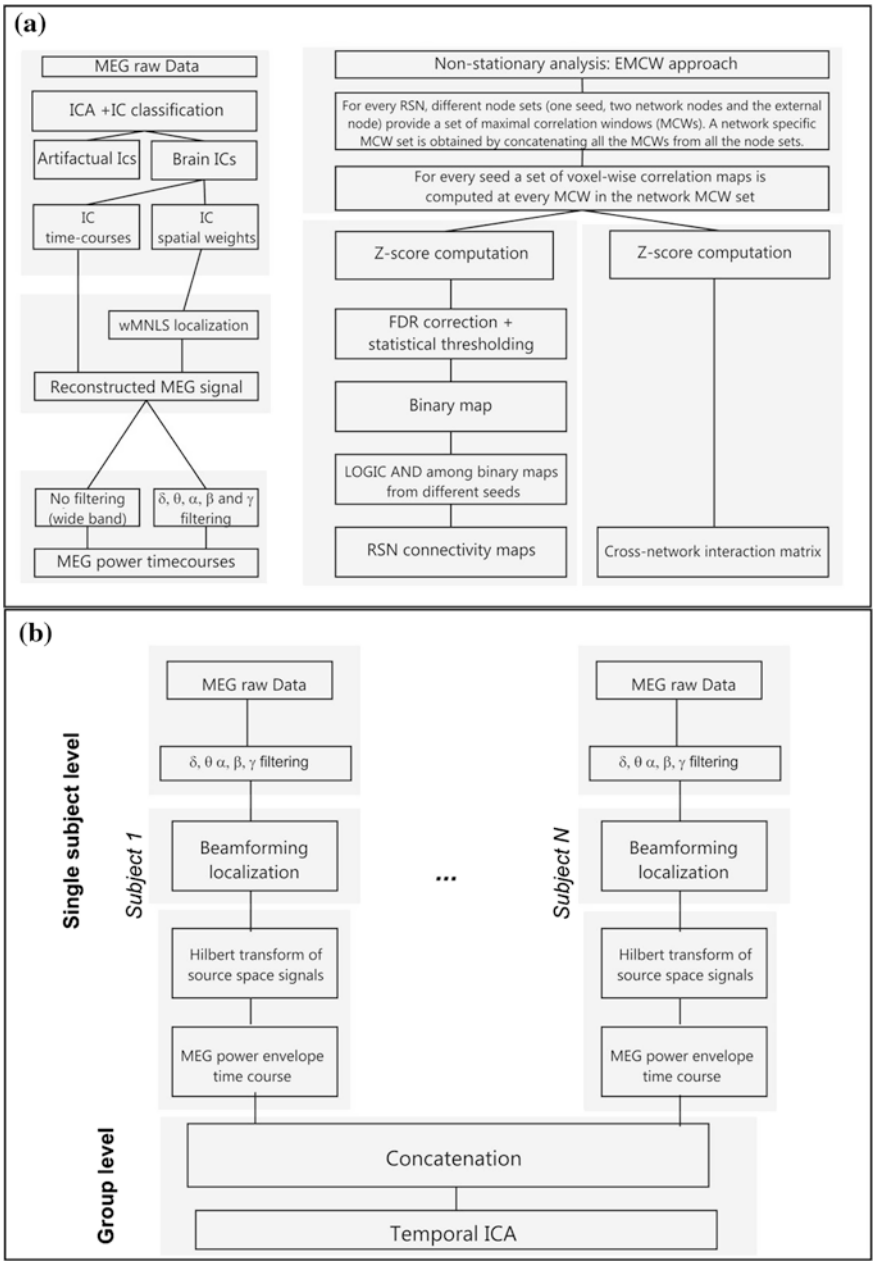

Fig. 2 MEG seed vs ICA based pipelines. **a** Flowchart of the analysis pipeline developed in de Pasquale et al. (2010, 2012a); **b** Flowchart of the analysis pipeline developed in Brookes et al. (2011a, b)

frequency domain, have been developed and employed. The different strategies provide results with different properties (e.g., in terms of field spread) that are related to the different assumptions of the method. Specific metrics have been defined to measure the performance of the inverse strategy used with regard to localization error, presence of ghost sources, point spread function, cross talk function or their combinations (Hauk et al. 2011). Despite the exact choice, all the considerations on the obtained results have to be made without discarding the information on the above characteristics since they basically define the method limitations. This is particularly relevant for connectivity mapping since spurious connectivity can be induced by e.g., mislocalized sources, ghost sources, field spread.

A second level is represented by the particular parameter, i.e. signal vs power or linear vs nonlinear association measures adopted to study the functional connectivity. In fact, a full understanding of brain function requires the investigation of brain interactions at different temporal scales: the slow power fluctuation scale (several seconds) and the faster neuronal communication scale (several milliseconds) see Fig. 1. The first approach has been traditionally pursued with fMRI and more recently also with MEG as extensively discussed above. The second is unique to MEG since it measures the activity of neuronal populations in which communication has been shown to be accomplished in large part via synchronized oscillatory activity (Buzsaki 2009; Fries 2009; Singer 1993). This level of investigation of RSNs offers MEG the privilege and the challenge to provide a unified framework for the relationship between fast oscillatory brain activity and slow temporal dynamics. The exploitation of different connectivity metrics based on signal properties or on power modulation properties represents a first step towards this integration. Also within one temporal scale, the choice of a particular connectivity metric plays a final fundamental role for the characterization of the results. Temporal correlation of BLP is a robust strategy but many other approaches, e.g., non linear measures of interaction or probabilistic ones will provide information on different aspects of the connectivity.

Moreover, seed based approaches are different from ICA based approaches. The main limitation of seed based approaches is that it is assumed that the seed, usually obtained from previous independent experiments, is reproducible across subjects. With ICA this limitation is somehow overcome, but on the other hand, it is assumed that different nodes of the same network are characterized by an identical signal time course. In this way, the hierarchical structure of the network and the different roles played by different nodes cannot be investigated. In addition, the cross-network interaction is somehow limited by the IC independence assumption, i.e. ICs are by definition either spatially or temporally independent. In (Brookes et al. 2011b), since the ICA is run separately on the different frequency bands, the cross-frequency network interaction is presented, i.e. the interaction is computed between ICs extracted from different frequency bands. Seed-based and ICA based approaches also share some similarities: in a seed based approach a seed is considered reproducible across subjects, while in the temporal ICA approach, a similar assumption is made when data from a set of subjects are concatenated together. This assumes that the different subjects are just replications of one subject.

Once a given parameter is chosen to quantify the strength of coupling, a critical question is how to define its statistical significance. A common feature of the different strategies described so far is that they all assume the temporal correlation as a linear measure of coupling among brain areas (Brookes et al. 2011a, b; de Pasquale et al. 2010; Mantini et al. 2011). Then, correlation values are compared to a 'baseline'. In (de Pasquale et al. 2012a; Hipp et al. 2012) this baseline is defined as the average correlation of the seed with the rest of the brain. Such a baseline is subject specific and scales the coupling with a given specific level of 'general' connectivity in the brain during the recording session. In this way, in a group analysis consistent deviations from the average connectivity in the brain are tested. In other studies, however (Brookes et al. 2011b) the baseline value of connectivity is not estimated from the real acquired data but from simulated data obtained by adding synthetic noise to real empty-room data. This threshold is not subject specific and it allows spurious connectivity to be induced by the different pre-processing steps. This approach has the advantage that the coupling is not scaled, i.e. all subjects are tested against the same reference value.

Another common aspect of these approaches is the adoption of ICA based methods. ICs are always used as a classification methodology but the meaning of the estimated ICs is opposite. In one case, the identified temporal ICs are linked to RSNs so that a subset of the estimated ICs are mapped one to one to a subset of resting state networks and the remaining ones are discarded. In the another case, a subset of the identified ICs are linked to artifactual components of the signal and are discarded while the remaining ones are recombined to build a 'cleaned' MEG signal. Thus, the real signal is assumed to be a linear combination of the estimated ICs.

Based on these considerations, it must be stressed that a complete scenario can only be gathered by integrating the properties highlighted by ICA and seed based results. The former will provide important information on the segregation properties of RSNs without any prior information and the latter will provide information on the integration among different RSNs. Interestingly the spatial maps and frequency content obtained by these different approaches are in good agreement.

3 Stationary Connections of the Default Mode Network

There is growing evidence of DMN internal coupling observed with MEG. Typically, a first step in these analyses is to compare the DMN topography with that from fMRI which has been playing the role of golden standard in the identification of RSNs so far. In fact, in Brookes et al. (2011a, b; de Pasquale et al. 2010, 2012a, b) great care is shown in developing techniques to quantify the MEG-fMRI agreement. In Fig. 3 we report the comparison between the nodes of the RSNs usually reported in the fMRI and MEG literature.

This comparison is a very complex and delicate topic since these techniques highlight different properties of the networks under investigation. Apart from the obvious difference between fMRI and MEG spatial and temporal resolution, it

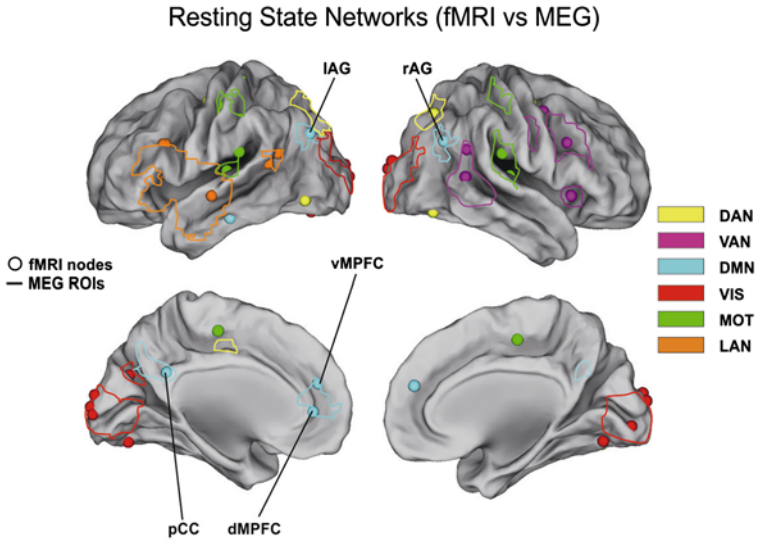

Fig. 3 fMRI versus MEG resting state networks. Location of the consistent nodes of the dorsal attention (*yellow*), ventral attention (*Pink*), default mode (*cyan*), visual (*red*), motor (*green*) and language networks (*brown*) reported in the fMRI literature (*round marks*) as compared to the corresponding regions observed by MEG (*solid lines*)

must be reminded that these techniques are intrinsically different given the different nature of the collected signals. Thus, the observed differences will not claim a superiority of one technique compared to the other but it will simply enrich a multivariate scenario of the considered network. In (Brookes et al. 2011b) good agreement is found between the DMN observed with fcMRI and MEG which corresponds to one of the 25 temporal ICs extracted in the alpha band. In particular, nodes are observed in medial frontal cortex and left/right inferior parietal lobules. The main important difference with fMRI is the absence of the Posterior Cingulate Cortex (PCC), an important node of the DMN which has been consistently reported from other studies and it is hypothesized to play a fundamental role in connectivity at rest (see Fig. 4 panel A). This point is further discussed in the Conclusions section. Of most interest in (Brookes et al. 2011b) is the difference between amplitude and correlation spectra. In the left/right fronto-parietal and the default mode networks clear θ-band components are observed in the amplitude spectra, but not the correlation spectra, indicating that despite the prevalence of θ-oscillations, they are not involved in fronto-parietal or default mode connectivity.

Analogously, also in the motor network, a similar property is observed: despite the prevalence of 8 to 13 Hz oscillatory activity in both primary sensorimotor regions, no significant correlation is observed between the Hilbert envelopes in this frequency band.

Regarding the DMN cross-network interactions, since temporal ICA forces orthoghonality among the networks, this approach cannot be used to study network

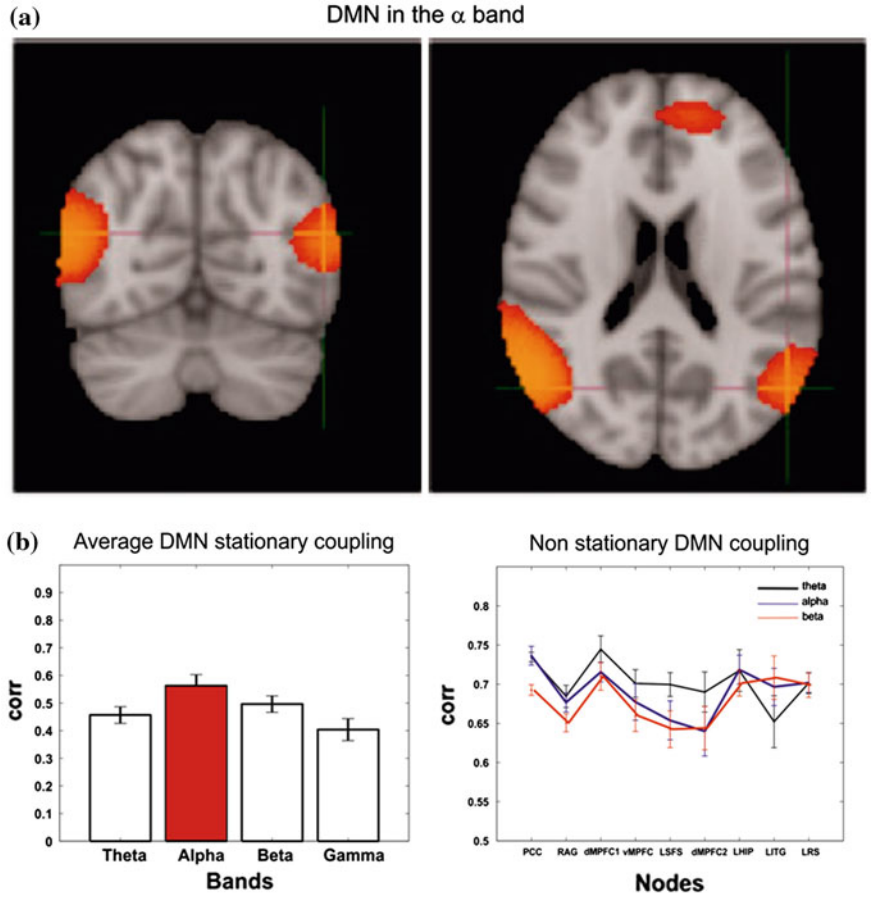

Fig. 4 The internal coupling of the Default Mode Network is consistently observed mainly in the alpha band under the temporal stationarity assumption both from an ICA based approach (*Panel A* modified from Brookes et al. 2011b) and a seed based a one (*Panel B left*—modified from de Pasquale et al. 2010). When the non-stationarity is accounted for a mixed contribution of alpha and theta bands is revealed (*Panel B right*)

cross-coupling within the same frequency band. However, since ICA is adopted independently to each frequency band, cross-network interactions can only be addressed between different frequency bands, in a cross-frequency fashion. In this case, good agreement is reported between fMRI and MEG patterns of interaction between the DMN (for the MEG in the α-band) and the other considered networks (for the MEG in the β-band) such as the left/right frontoparietal, medio-frontal, parietal, visual, motor and cerebellum. These results show some frequency dependence; correlation between nodes of the fonto-parietal, DMN, and motor networks is observed across the 10–30 Hz range, but is strongest in the β-band. This finding agrees with the work by Mantini et al. (Mantini et al. 2007) who used

concurrent EEG/fMRI to show that the envelope of band-limited EEG signals correlates with BOLD signals from separate network nodes. Moreover, these results are in line with (de Pasquale et al. 2012a) in which a strong cross-network interaction of the DMN in the alpha and beta band was found.

By means of BLP seed based connectivity, the picture of the MEG internal coupling of the DMN looks different from the one described so far. As a matter of fact, under the assumption of temporal stationarity, only intra-hemispheric connections, ipsilateral to the seed, are observed in the DMN (when the Left or Right Angular Gyrus are selected as seeds). These connections relate to specific known fMRI DMN nodes such as the Superior Frontal Sulcus, Posterior Cingulate and retrosplenial cortex. This result cannot be attributed to differences between fMRI and MEG in signal temporal frequency content, as shown in (de Pasquale et al. 2010) in which the convolution of the MEG power time series with a canonical hemodynamic response function generated only a spatially blurred version of the original results. However, the identified DMN connections were strongest in the alpha band (see Fig. 4 panel B—left).

4 Dynamic Connections of the Default Mode Network

In (de Pasquale et al. 2010) the comparison of the fMRI and MEG DMN topography revealed a discrepancy showing only ipsilateral connections in the MEG case when a stationary interaction among DMN nodes is assumed. Now, if the same interactions are examined during smaller temporal epochs, a non-stationarity property is revealed, i.e. same nodes alternate periods of high and low synchronization. In this scenario, it seems that a static spatial topography is not sufficient to fully describe the network coupling: the temporal axis must be considered, i.e. the coupling must be considered dynamic over time. Thus, to investigate this dynamic interaction the following properties must be addressed: the temporal scale of interaction, the frequency content of both internal and external network coupling, the degree of non stationarity of the DMN compared to other RSNs and its meaning. In (de Pasquale et al. 2012a), in order to estimate the temporal scale of dynamic interactions the spectral properties of interregional correlations are investigated. Autospectra and total interdependence, a measure of the internodal coherence, are computed for each subject on the principal nodes of DMN (L/R AG;LPCC; LMPFC), and then averaged across subjects. This analysis showed a peak around 0.1 Hz suggesting appropriate time epochs to be as large as 10 s. Of note, in a different study (Luckhoo et al. 2012), although by means of different techniques, a similar range of temporal epochs is proposed to characterize the dynamics. The authors optimize the time-frequency windows for connectivity by estimating the distribution of functional connectivity scores between nodes of known RSNs and contrasting it with a distribution of artefactual scores due to spatial leakage caused by the inverse problem. Interestingly, it is reported that the connectivity is best estimated via correlations in the oscillatory envelope in the

8–20 Hz frequency range. In this work, differently from (de Pasquale et al. 2012a), this result is obtained by assuming that the DMN is both internally and externally coupled to other network nodes in a cross-frequency fashion (alpha–beta synchronization) (Brookes et al. 2011b). Nevertheless, the identified range is in line with (de Pasquale et al. 2012a) which showed the strongest cross-network interactions in the alpha and beta bands.

Now, when the non-stationarity is taken into account, by considering the 10 s temporal scale, MEG activity shows transient formation of complete RSNs, including nodes in the hemisphere contralateral to the seed. In this case, BLP correlations are more bilateral and thus similar to fMRI RSNs (Cordes et al. 2001; Damoiseaux et al. 2006; De Luca et al. 2006; Greicius 2008; Greicius et al. 2003, 2009).

Such similarity is documented via a nonparametric test based on Spearman rank correlation. Thus, a complete set of networks, closely resembling the fMRI ones, can be obtained from MEG. In particular, six RSNs are described: the default mode network (DMN), the dorsal attention network (DAN), the ventral attention network (VAN), plus language (LAN), somatomotor (SOM), and visual (VIS) networks.

The next question is if there is any frequency specificity of this internal coupling. In fact, previous ECoG studies and theoretical considerations suggest that long-range and local synchronization are differentially reflected at low and high frequencies, respectively. For the DMN the most fMRI-like topography is reported in the theta and alpha bands (de Pasquale et al. 2010). Interestingly, stronger correlation with frontal DMN nodes (LMPFC2, LSFS, RMPFC) is observed in theta as compared to alpha or beta bands, see Fig. 4 (panel B—right). Unambiguously, no long-range gamma band power correlations were obtained even when the non-stationarity is taken into account.

Among all RSNs, the DMN also showed the strongest interaction with other networks, and this effect is especially clear in the beta and alpha bands, see (de Pasquale et al. 2012a). Other networks with significant cross-network interactions include the DAN while other networks such as VAN, language, and visual networks appeared relatively segregated on average. When the node-node interactions are investigated, five out of seven nodes of the DMN showed significant interactions with nodes of other networks in the beta band. Among these nodes, the posterior cingulate cortex (PCC) showed the highest mean interaction with all other nodes, see Fig. 5.

Now, a key finding reported in this work, is that the observed strong cross-network interactions of the PCC, and more generally the DMN, are limited to temporal epochs in which this network is strongly internally coherent. The DMN does not exhibit strong correlations with other networks when they are in a state of internal coupling. Importantly, the principle that a network interacts with others when it is in a state of strong internal coherence generalized to both DAN and somatomotor networks, the other two networks with significant cross-network interactions. Thus, these results can be summarized as:

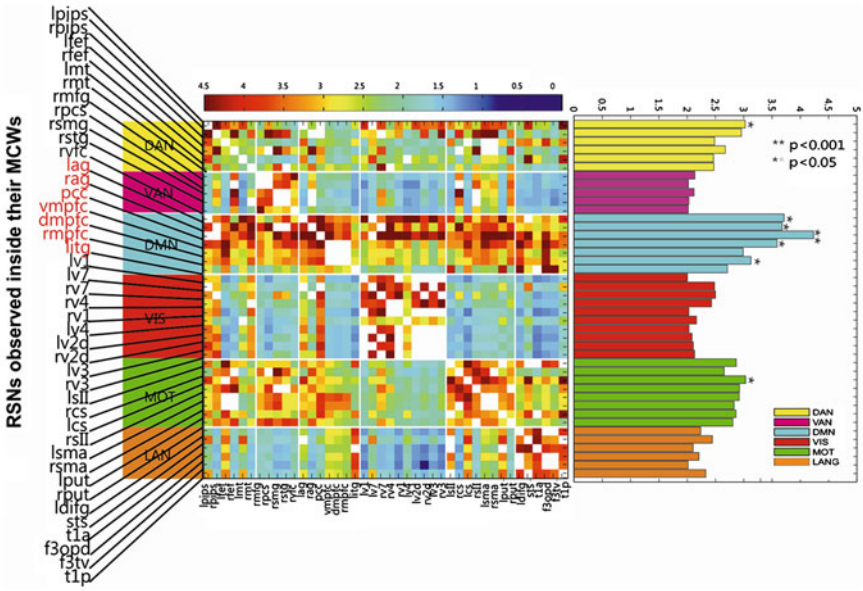

Fig. 5 DMN cross-network interactions. The Default Mode Network plays a central role in the RSN cross-network interactions in the beta band during epochs in which it is highly, internally coupled. In particular, among the DMN nodes, the PCC is statistically more central than the other nodes. (Taken from de Pasquale et al. 2012a)

1. RSNs can be recovered with MEG BLP or power and Hilbert based envelope correlation, especially in the alpha and beta bands, and exhibit large-scale, spatially segregated topographies similar to those obtained with resting state fMRI;
2. RSNs, when internally engaged, differ in the degree with which they interact with other networks;
3. The DMN exhibits the strongest cross-network interactions in the beta and alpha bands;
4. Cross-network interactions are transient: The DMN, and other significantly cross-interacting networks (DAN, somatomotor), do not interact with other networks when they are not internally coupled, nor when correlation in other networks is strong. Cross-network interactions involve one fully engaged network and a subset of nodes of another network, when it is in a state of lower internal correlation. It appears that some nodes can break away from their usual RSN and transiently correlate with one of the networks that tend to cross-interact, especially DMN.
5. Networks spend a variable fraction of time in a state of high internal correlation, and this property seems to inversely relate to their tendency to couple with other networks. Interestingly, the DMN, the most interacting network, spends

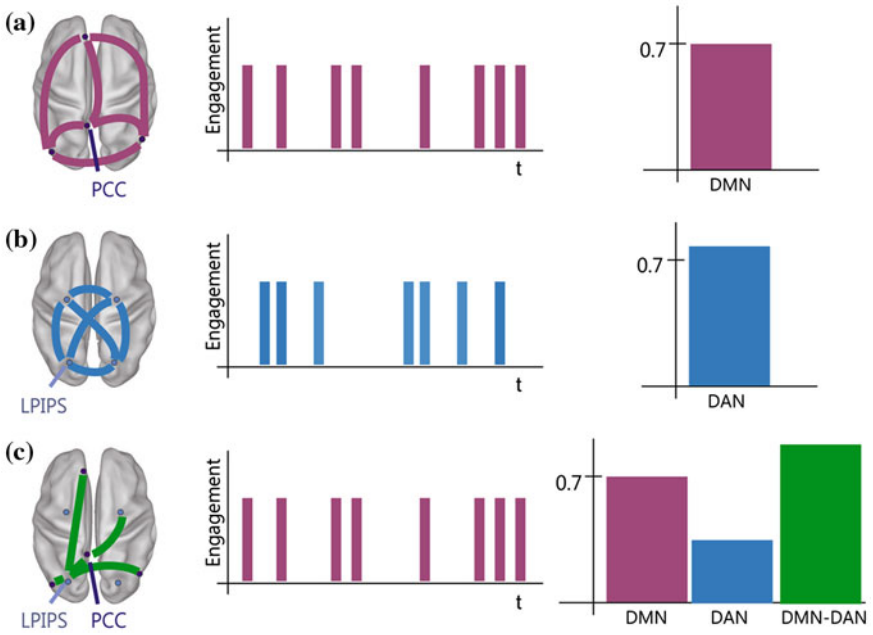

Fig. 6 DMN—DAN cross-network interaction mechanism**. a** Coupling of the Default Mode Network during epochs in which it is highly internally coupled; **b** coupling of the Dorsal Attention Network epochs in which it is highly internally coupled; **c** cross-network coupling between the Default Mode Network and the Dorsal Attention Network during epochs in which the DMN is highly internally coupled. DAN is less internally engaged in favor of cross-network coupling with DMN

on average, less time in a state of high internal correlation (20 % in alpha; 36 % in beta) than the VAN (53 % in alpha; 56 % in beta), the least interacting network. This result is remarkable given these two networks are topographic neighbors yet display very different patterns of temporal interaction (de Pasquale et al. 2010, 2012a). Thus, an intriguing hypothesis is emerging that the observed non stationarity can be interpreted as a mechanism to allow efficient cross-network interactions through the DMN and in particular the PCC. This idea is schematically reported in Fig. 6.

This non-stationarity interpretation could reconcile the distinct spatially separated fMRI networks with the dynamically integrated MEG networks: this strong cross-network interaction happens dynamically in a small fraction of time and therefore when RSN interaction is averaged on long temporal windows (as with fMRI), the internal coupling will weigh more and thus allow only separated networks to emerge.

5 Clinical Applications of the MEG Default Mode Network Connectivity

The complex scenario depicted from MEG connectivity at rest and the central role played by the DMN are paving the way to many clinical applications. For example, the internal coupling and more importantly an abnormal interaction of this network with the other RSNs (e.g., task positive networks) is now being considered a possible biomarker of different mental disorders, see (Broyd et al. 2009) and currently there is a growing literature in which DMN connectivity results are being translated into different clinical fields.

In Castellanos et al. (2010, 2011) the plasticity and reorganization of MEG functional networks are linked to the cognitive recovery of acquired brain injury patients. This provides new evidence of the neurophysiologic mechanisms underlying neuronal plasticity processes after brain injury, and suggests that these changes are related with observed changes at the behavioral level. In the same vein, in (Andrews-Hanna et al. 2010; Stam et al. 2009) the link between RSNs and neurodegenerative disorders such as Alzheimer (AD) and Parkinson Disease (PD) is investigated. These studies show that in PD and AD, characteristic patterns of abnormal oscillatory activity in different frequency bands can be identified as well as distinct patterns of abnormal RSN connectivity in demented and non-demented PD, as well as in AD. In PD, abnormal oscillatory activity and disturbed connectivity may respond differently to dopaminergic treatment.

Moreover, it has been shown that in presence of attention-deficit/hyperactivity disorders (ADHD), DMN functional connectivity between the anterior and posterior aspects is reduced. In particular, in (Wilson et al. 2013) unmedicated adults with ADHD exhibited broadband deficits in medial prefrontal cortices (MPFC), but not in other DMN regions compared to adults without ADHD. Unmedicated patients also showed abnormal cross-frequency coupling in the gamma range between the MPFC and posterior cingulate areas, and disturbed balance within the DMN as activity in posterior regions was stronger than frontal regions at beta and lower frequencies, which dissipated at higher γ-frequencies. Administration of pharmacotherapy significantly increased prefrontal alpha activity (8–14 Hz) in adults with ADHD, and decreased the cross-frequency gamma coupling. These results indicate that neurophysiological aberrations in the DMN of patients with ADHD are not limited to ultra slow oscillations, and that they may be primarily attributable to abnormal broadband activity in the MPFC.

Another clinical application relates to the study of the obesity in which altered functional connectivity in the DMN and temporal lobe network has been shown (Kullmann et al. 2012). In the DMN, obese subjects showed increased functional connectivity bilaterally in the precuneus while the right anterior cingulate revealed decreased functional connectivity strength. Furthermore, in the temporal lobe network, obese subjects showed decreased functional connectivity strength in the left insular cortex. The functional connectivity magnitude significantly correlated with body mass index (BMI). Taken together, these results complement and

expand previous functional neuroimaging findings by demonstrating that obesity and insulin levels influence brain function during rest in networks supporting reward and food regulation.

Another interesting application is the epilepsy in which patients with juvenile absence epilepsy are investigated (Sakurai et al. 2010). Results show strong medial prefrontal activation in all patients, with simultaneous activation in the posterior cingulate and precuneus in three of five patients, or slightly after medial prefrontal activation.

6 Conclusions

Resting State Networks can be recovered with MEG as documented by several papers on this topic which showed a consistent reproducibility of the Default Mode Network obtained using different approaches with similar frequency signatures in the range of alpha and beta bands, see Brookes et al. (2011a, b; de Pasquale et al. 2010, 2012a; Hipp et al. 2012; Luckhoo et al. 2012). Moreover, this network, and in particular PCC, stand out as functional cores of cross-network integration in the awake resting state. This result is in line with previous structural (Hagmann et al. 2008; Sporns et al. 2007) and functional connectivity studies (Buckner et al. 2009; Fransson and Marrelec 2008; Hagmann et al. 2008; Tomasi and Volkow 2011) that have described the centrality of the DMN in terms of graph theory. In (de Pasquale et al. 2010, 2012a), for the first time this property is reported as dynamic on a time scale of seconds which is in agreement with the reported functional significance of these nodes. In fact, PCC is typically reported to serve an important adaptive function and it is implicated in broad-based continuous sampling of external and internal environments (Raichle et al. 2001). This region, together with the retrosplenial cortex, is also associated with the processing of emotionally salient stimuli, and may play a role in emotional processing related to episodic memory (Raichle et al. 2001). Clinical studies showed that this region is implicated in working memory dysfunction (Greicius et al. 2003), it is susceptible to atrophy in Alzheimer disease patients (Buckner et al. 2009) and it shows reduced connectivity with anterior DMN regions in ADHD patients. PCC centrality is apparently in contrast with the work of Brookes (Brookes et al. 2011b) in which this node is not as strongly connected to the other DMN nodes. A possible interpretation could be related to the different approach used for the analysis. In fact, temporal ICA identifies networks by maximizing their independence and thus it will provide networks that are internally coupled, but by definition, segregated from the other networks. Now, if a node is central, thus allowing the communication across multiple networks, its time course will be a mixture of different contributions from the different networks and therefore it will not be identified by the ICA. Another important aspect of this cross-network interactions is that they occur when the DMN is internally engaged, whereas weak or no interactions occur at other times,

even when other networks are internally coupled. This transient functional centrality property of the DMN extends from resting state to goal-driven behavior. In fact, the metabolic activity within the DMN is commonly suppressed (or deactivated) during goal-driven behaviors (Raichle et al. 2001; Shulman et al. 1997) and many different sensory, motor, and associative brain regions also exhibit paradigm-specific deactivations that co-occur with task deactivation of the DMN.

Spectral characterization of network communication is feasible with MEG but not with fMRI because of the sluggish hemodynamic properties of the BOLD signal (Boynton et al. 1996). For the DMN in particular, higher values of cross-network interactions were obtained in the beta band (de Pasquale et al. 2012a). There are also spectral-based distinctions between DMN and DAN, with the former spending more time internally coupled in the beta band, while the latter more in the alpha band. This distinction is consistent with previous work that highlights an attentional role for alpha rhythms (Capotosto et al. 2009; Klimesch 1997), and a complementary role of alpha and beta rhythms in relation to DAN and DMN (Laufs et al. 2003; Mantini et al. 2007). To date, there have been few attempts to characterize the electrophysiological counterparts of fMRI-RSNs. A previous electrocorticography (ECoG) study reported significant spatial correlations between fMRI RSNs and slow cortical potentials in the delta range, as well as interregional BLP correlation in higher frequencies (He et al. 2008). Gamma BLP correlation has been observed in bilateral auditory cortex (Nir et al. 2008) consistent with strong interhemispheric functional connectivity in fMRI. MEG studies have emphasized the importance of alpha and beta BLP in recovering MEG and EEG correspondents of the DMN and the DAN (de Pasquale et al. 2010; Laufs et al. 2003; Mantini et al. 2007). Similarly, Brookes et al. (2011a, b) recovered MEG correlates of the fMRI-sensorimotor RSN and observed that the beta band yielded the closest topographic similarity. Beta rhythms have been reported also to be the main driver of large scale spontaneous neuronal interactions at the MEG sensor level (Liu et al. 2010) and source level examined with ICA (Brookes et al. 2011b). Our results show the importance of beta (and alpha) rhythms not only for within—but also for cross-network interactions in the resting state. A possible interpretation of the dominant role of beta rhythms, in regulating functional interactions at rest, comes from a recent hypothesis by Andreas Engel and Pascal Fries (Engel and Fries 2010), and the observation that the DMN is ubiquitously deactivated across a wide range of cognitive tasks (Shulman et al. 1997). Engel and Fries argue that beta rhythms, even though classically associated with motor tasks, may play a more general role in maintaining the 'status quo' of a current behavioral state. For instance, in the motor system, beta rhythms are strong at rest or during maintenance of a motor set, but are disrupted by a change in motor behavior. Similarly, in perceptual-cognitive tasks, this rhythm is associated with the dominance of the endogenous top–down influences to override the effect of potentially unexpected external events. Beta band oscillations might therefore be important in maintaining the cognitive status quo.

Acknowledgements This work was supported by the European Community's Seventh Framework Programme (FP7/2007–2013), Grant Agreement No. HEALTH-F2-2008-200728 'BrainSynch', NIH grant MH 71920-06, and the Human Connectome Project (1U54MH091657-01) from the 16 National Institutes of Health Institutes and Centers that support the NIH Blueprint for Neuroscience Research.

References

Amodio DM, Frith CD (2006) Meeting of minds: the medial frontal cortex and social cognition. Nat Rev Neurosci 7(4):268–277

Andrews-Hanna JR, Reidler JS, Sepulcre J, Poulin R, Buckner RL (2010) Functional-anatomic fractionation of the brain's default network. Neuron 65(4):550–562

Bar M, Aminoff E, Mason M, Fenske M (2007) The units of thought. Hippocampus 17(6):420–428

Berger H (1929) Über das Elektroenkephalogram des Menschen. Archives fur Psychiatric 87:527–570

Betti V, Della Penna S, de Pasquale F, Mantini D, Marzetti L, Romani GL, Corbetta M (2013) Natural scenes viewing alters the dynamics of functional connectivity in the human brain. Neuron, Available online. http://dx.doi.org/10.1016/j.neuron.2013.06.022. Accessed 25 July 2013, ISSN 0896 6273

Boynton GM, Engel SA, Glover GH, Heeger DJ (1996) Linear systems analysis of functional magnetic resonance imaging in human V1. J Neurosci 16(13):4207–4221

Brookes MJ, Hale JR, Zumer JM, Stevenson CM, Francis ST, Barnes GR, Owen JP, Morris PG, Nagarajan SS (2011a) Measuring functional connectivity using MEG: methodology and comparison with fcMRI. Neuroimage 56(3):1082–1104

Brookes MJ, Woolrich M, Luckhoo H, Price D, Hale JR, Stephenson MC, Barnes GR, Smith SM, Morris PG (2011b) Investigating the electrophysiological basis of resting state networks using magnetoencephalography. Proc Nat Acad Sci USA 108(40):16783–16788

Broyd SJ, Demanuele C, Debener S, Helps SK, James CJ, Sonuga-Barke EJ (2009) Default-mode brain dysfunction in mental disorders: a systematic review. Neurosci Behav Rev 33(3):279–296

Buckner RL, Andrews-Hanna JR, Schacter DL (2008) The brain's default network: anatomy, function, and relevance to disease. Annal NY Acad Sci 1124:1–38

Buckner RL, Sepulcre J, Talukdar T, Krienen FM, Liu H, Hedden T, Andrews-Hanna JR, Sperling RA, Johnson KA (2009) Cortical hubs revealed by intrinsic functional connectivity: mapping, assessment of stability, and relation to Alzheimer's disease. J Neurosci 29(6):1860–1873

Buzsaki G (2009) Rhythms of the brain. Oxford University Press, USA

Capotosto P, Babiloni C, Romani GL, Corbetta M (2009) Fronto-parietal cortex controls spatial attention through modulation of anticipatory alpha rhythms. J Cogn Neurosci 24(12):2363–2371

Castellanos NP, Bajo R, Cuesta P, Villacorta-Atienza JA, Paul N, Garcia-Prieto J, Del-Pozo F, Maestu F (2011) Alteration and reorganization of functional networks: a new perspective in brain injury study. Front Hum Neurosci 5:90

Castellanos NP, Paul N, Ordonez VE, Demuynck O, Bajo R, Campo P, Bilbao A, Ortiz T, del-Pozo F, Maestu F (2010) Reorganization of functional connectivity as a correlate of cognitive recovery in acquired brain injury. Brain 133(Pt 8):2365–2381

Cordes D, Haunghton VM, Arfanakisa K, Wendtz GJ, Turskia PA, Moritza CH, Quigleya MA, Meyeranda ME (2001) Mapping functionally related regions of brain with functional connectivity MR imaging. Am J Neuroradiol 21(9):1636–1644

D'Argembeau A, Comblain C, Van der Linden M (2005) Affective valence and the self-reference effect: influence of retrieval conditions. Br J Psychol 96(Pt 4):457–466

Damoiseaux JS, Rombouts SA, Barkhof F, Scheltens P, Stam CJ, Smith SM, Beckmann CF (2006) Consistent resting-state networks across healthy subjects. Proc Nat Acad Sci USA 103(37):13848–13853

Darvas F, Leahy R (2007) Functional Imaging of Brain Activity and Connectivity with MEG. In: Jirsa V, McIntosh AR (eds) Handbook of brain connectivity. Springer, Berlin Heidelberg, pp 201–220

Daselaar SM, Prince SE, Cabeza R (2004) When less means more: deactivations during encoding that predict subsequent memory. Neuroimage 23(3):921–927

Daselaar SM, Prince SE, Dennis NA, Hayes SM, Kim H, Cabeza R (2009) Posterior midline and ventral parietal activity is associated with retrieval success and encoding failure. Front Hum Neurosci 3:13

De Luca M, Beckmann CF, De Stefano N, Matthews PM, Smith SM (2006) fMRI resting state networks define distinct modes of long-distance interactions in the human brain. Neuroimage 29(4):1359–1367

de Pasquale F, Della Penna S, Snyder AZ, Lewis C, Mantini D, Marzetti L, Belardinelli P, Ciancetta L, Pizzella V, Romani GL, Corbetta M (2010) Temporal dynamics of spontaneous MEG activity in brain networks. Proc Nat Acad Sci USA 107(13):6040–6045

de Pasquale F, Della Penna S, Snyder AZ, Marzetti L, Pizzella V, Romani GL, Corbetta M (2012a) A cortical core for dynamic integration of functional networks in the resting human brain. Neuron 74(4):753–764

de Pasquale F, Sabatini U, Della Penna S, Sestieri C, Caravasso C, Formisano R, Peran P (2012b) The connectivity of functional cores reveals different degrees of segregation and integration in the brain at rest. Neuroimage 69:51–61

Eichele T, Debener S, Calhoun VD, Specht K, Engel AK, Hugdahl K, von Cramon DY, Ullsperger M (2008) Prediction of human errors by maladaptive changes in event-related brain networks. Proc Natl Acad Sci USA 105(16):6173–6178

Engel AK, Fries P (2010) Beta-band oscillations–signalling the status quo? Curr Opin Neurobiol 20(2):156–165

Ewald A, Marzetti L, Zappasodi F, Meinecke FC, Nolte G (2012) Estimating true brain connectivity from EEG/MEG data invariant to linear and static transformations in sensor space. Neuroimage 60(1):476–488

Fransson P, Marrelec G (2008) The precuneus/posterior cingulate cortex plays a pivotal role in the default mode network: Evidence from a partial correlation network analysis. Neuroimage 42(3):1178–1184

Fries P (2009) Neuronal gamma-band synchronization as a fundamental process in cortical computation. Annu Rev Neurosci 32:209–224

Frith U, Frith CD (2003) Development and neurophysiology of mentalizing. Philos Trans R Soc Lond Ser B Biol Sci 358(1431):459–473

Gallagher HL, Happe F, Brunswick N, Fletcher PC, Frith U, Frith CD (2000) Reading the mind in cartoons and stories: an fMRI study of 'theory of mind' in verbal and nonverbal tasks. Neuropsychologia 38(1):11–21

Goldman AI (1992) In defence of the simulation theory. Mind Lang 7(1–2):104–119

Greicius M (2008) Resting-state functional connectivity in neuropsychiatric disorders. Curr Opin Neurol 21(4):424–430

Greicius MD, Krasnow B, Reiss AL, Menon V (2003) Functional connectivity in the resting brain: a network analysis of the default mode hypothesis. Proc Nat Acad Sci USA 100(1):253–258

Greicius MD, Supekar K, Menon V, Dougherty RF (2009) Resting-state functional connectivity reflects structural connectivity in the default mode network. Cereb Cortex 19(1):72–78

Gross J, Kujala J, Hamalainen M, Timmermann L, Schnitzler A, Salmelin R (2001) Dynamic imaging of coherent sources: studying neural interactions in the human brain. Proc Nat Acad Sci USA 98(2):694–699

Guggisberg AG, Honma SM, Findlay AM, Dalal SS, Kirsch HE, Berger MS, Nagarajan SS (2008) Mapping functional connectivity in patients with brain lesions. Annal Neurol 63(2):193–203

Gusnard DA, Akbudak E, Shulman GL, Raichle ME (2001) Medial prefrontal cortex and self-referential mental activity: relation to a default mode of brain function. Proc Natl Acad Sci USA 98(7):4259–4264

Gusnard DA, Raichle ME (2001) Searching for a baseline: functional imaging and the resting human brain. Nat Rev Neurosci 2(10):685–694

Hagmann P, Cammoun L, Gigandet X, Meuli R, Honey CJ, Wedeen VJ, Sporns O (2008) Mapping the structural core of human cerebral cortex. PLoS Biol 6(7):e159

Hassabis D, Maguire EA (2007) Deconstructing episodic memory with construction. Trends Cogn Sci 11(7):299–306

Hauk O, Wakeman DG, Henson R (2011) Comparison of noise-normalized minimum norm estimates for MEG analysis using multiple resolution metrics. Neuroimage 54(3):1966–1974

He BJ, Snyder AZ, Zempel JM, Smyth MD, Raichle ME (2008) Electrophysiological correlates of the brain's intrinsic large-scale functional architecture. Proc Nat Acad Sci USA 105(41):16039–16044

Hipp JF, Hawellek DJ, Corbetta M, Siegel M, Engel AK (2012) Large-scale cortical correlation structure of spontaneous oscillatory activity. Nat Neurosci 15(6):884–890

Hironaga N, Ioannides AA (2007) Localization of individual area neuronal activity. Neuroimage 34(4):1519–1534

Hu TC, Kahng AB, Albert Tsao C-W (1995) Old bachelor acceptance: a new class of non-monotone threshold accepting methods. ORSA J Comput 7:417–425

Ingvar DH (1979) "Hyperfrontal" distribution of the cerebral grey matter flow in resting wakefulness; on the functional anatomy of the conscious state. Acta Neurol Scand 60(1):12–25

Ingvar DH (1985) "Memory of the future": an essay on the temporal organization of conscious awareness. Hum Neurobiol 4(3):127–136

Kety SS, Schmidt CF (1948) The nitrous oxide method for the quantitative determination of cerebral blood flow in man: theory, procedure and normal values. J Clin Invest 27(4):476–483

Klimesch W (1997) EEG-alpha rhythms and memory processes. Int J Psychophysiol 26(1–3):319–340

Kullmann S, Heni M, Veit R, Ketterer C, Schick F, Haring HU, Fritsche A, Preissl H (2012) The obese brain: association of body mass index and insulin sensitivity with resting state network functional connectivity. Hum Brain Mapp 33(5):1052–1061

Lane RD, Reiman EM, Ahern GL, Schwartz GE, Davidson RJ (1997) Neuroanatomical correlates of happiness, sadness, and disgust. Am J Psychiatry 154(7):926–933

Laufs H, Krakow K, Sterzer P, Eger E, Beyerle A, Salek-Haddadi A, Kleinschmidt A (2003) Electroencephalographic signatures of attentional and cognitive default modes in spontaneous brain activity fluctuations at rest. Proc Nat Acad Sci USA 100(19):11053–11058

Liu Z, Fukunaga M, de Zwart JA, Duyn JH (2010) Large-scale spontaneous fluctuations and correlations in brain electrical activity observed with magnetoencephalography. Neuroimage 51(1):102–111

Luckhoo H, Hale JR, Stokes MG, Nobre AC, Morris PG, Brookes MJ, Woolrich MW (2012) Inferring task-related networks using independent component analysis in magnetoencephalography. Neuroimage 62(1):530–541

Mantini D, Della Penna S, Marzetti L, de Pasquale F, Pizzella V, Corbetta M, Romani GL (2011) A signal-processing pipeline for magnetoencephalography resting-state networks. Brain Connect 1(1):49–59

Mantini D, Perrucci MG, Del Gratta C, Romani GL, Corbetta M (2007) Electrophysiological signatures of resting state networks in the human brain. Proc Nat Acad Sci USA 104(32):13170–13175

Marzetti L, Del Gratta C, Nolte G (2008) Understanding brain connectivity from EEG data by identifying systems composed of interacting sources. Neuroimage 42(1):87–98

Marzetti L, Della Penna S, Snyder AZ, Pizzella V, Nolte G, de Pasquale F, Romani GL, Corbetta M (2013) Frequency specific interactions of MEG resting state activity within and across brain networks as revealed by the multivariate interaction measure. Neuroimage 79:172–183

Mazoyer B, Zago L, Mellet E, Bricogne S, Etard O, Houde O, Crivello F, Joliot M, Petit L, Tzourio-Mazoyer N (2001) Cortical networks for working memory and executive functions sustain the conscious resting state in man. Brain Res Bull 54(3):287–298

McKiernan KA, Kaufman JN, Kucera-Thompson J, Binder JR (2003) A parametric manipulation of factors affecting task-induced deactivation in functional neuroimaging. J Cogn Neurosci 15(3):394–408

Mitchell JP (2006) Mentalizing and Marr: an information processing approach to the study of social cognition. Brain Res 1079(1):66–75

Mitchell JP, Macrae CN, Banaji MR (2006) Dissociable medial prefrontal contributions to judgments of similar and dissimilar others. Neuron 50(4):655–663

Nir Y, Mukamel R, Dinstein I, Privman E, Harel M, Fisch L, Gelbard-Sagiv H, Kipervasser S, Andelman F, Neufeld MY, Kramer U, Arieli A, Fried I, Malach R (2008) Interhemispheric correlations of slow spontaneous neuronal fluctuations revealed in human sensory cortex. Nat Neurosci 11(9):1100–1108

Nolte G, Bai O, Wheaton L, Mari Z, Vorbach S, Hallett M (2004) Identifying true brain interaction from EEG data using the imaginary part of coherency. Clin Neurophysiol Official J Int Fed Clin Neurophysiol 115(10):2292–2307

Nolte G, Marzetti L, Valdes Sosa P (2009) Minimum overlap component analysis (MOCA) of EEG/MEG data for more than two sources. J Neurosci Methods 183(1):72–76

Nolte G, Meinecke FC, Ziehe A, Muller KR (2006) Identifying interactions in mixed and noisy complex systems. Phys Rev E Stat Nonlinear Soft Matter Phys 73(5 Pt 1):051913

Nolte G, Ziehe A, Nikulin VV, Schlogl A, Kramer N, Brismar T, Muller KR (2008) Robustly estimating the flow direction of information in complex physical systems. Phys Rev Lett 100(23):234101

Ochsner KN, Beer JS, Robertson ER, Cooper JC, Gabrieli JD, Kihsltrom JF, D'Esposito M (2005) The neural correlates of direct and reflected self-knowledge. Neuroimage 28(4):797–814

Ochsner KN, Ray RD, Cooper JC, Robertson ER, Chopra S, Gabrieli JD, Gross JJ (2004) For better or for worse: neural systems supporting the cognitive down- and up-regulation of negative emotion. Neuroimage 23(2):483–499

Olsson A, Ochsner KN (2008) The role of social cognition in emotion. Trends in cognitive sciences 12(2):65–71

Raichle ME, MacLeod AM, Snyder AZ, Powers WJ, Gusnard DA, Shulman GL (2001) A default mode of brain function. Proc Natl Acad Sci USA 98(2):676–682

Sakurai K, Takeda Y, Tanaka N, Kurita T, Shiraishi H, Takeuchi F, Nakane S, Sueda K, Koyama T (2010) Generalized spike-wave discharges involve a default mode network in patients with juvenile absence epilepsy: a MEG study. Epilepsy Res 89(2–3):176–184

Saxe R, Kanwisher N (2003) People thinking about thinking people. The role of the temporo-parietal junction in "theory of mind". Neuroimage 19(4):1835–1842

Saxe R, Schulz LE, Jiang YV (2006) Reading minds versus following rules: dissociating theory of mind and executive control in the brain. Soc Neurosci 1(3–4):284–298

Schacter DL, Addis, DR (2007) The cognitive neuroscience of constructive memory: remembering the past and imagining the future. Philos Trans R Soc London Ser B Biol Sci 362(1481):773–786

Schilbach L, Eickhoff SB, Rotarska-Jagiela A, Fink GR, Vogeley K (2008) Minds at rest? social cognition as the default mode of cognizing and its putative relationship to the "default system" of the brain. Conscious Cogn 17(2):457–467

Sestieri C, Corbetta M, Romani GL, Shulman GL (2011) Episodic memory retrieval, parietal cortex, and the default mode network: functional and topographic analyses. J Neurosci 31(12):4407–4420

Shahbazi Avarvand F, Ewald A, Nolte G (2012) Localizing true brain interactions from EEG and MEG data with subspace methods and modified beamformers. Comput Math Methods Med 2012:402341

Shulman GL, Fiez JA, Corbetta M, Buckner RL, Miezin FL, Raichle ME, Peterson S (1997) Common blood flow changes acros visual tasks: II Decreases in cerebral cortex. J Cogn Neurosci 9(5):648–663

Singer W (1993) Synchronization of cortical activity and its putative role in information processing and learning. Annu Rev Physiol 55(1):349–374

Singh KD, Fawcett IP (2008) Transient and linearly graded deactivation of the human default-mode network by a visual detection task. Neuroimage 41(1):100–112

Sokoloff L, Mangold R, Wechsler RL, Kenney C, Kety SS (1955) The effect of mental arithmetic on cerebral circulation and metabolism. J Clin Invest 34(7, Part 1):1101–1108

Sporns O, Honey CJ, Kotter R (2007) Identification and classification of hubs in brain networks. PLoS ONE 2(10):e1049

Spreng RN, Mar RA, Kim AS (2009) The common neural basis of autobiographical memory, prospection, navigation, theory of mind, and the default mode: a quantitative meta-analysis. J Cogn Neurosci 21(3):489–510

Stam CJ, de Haan W, Daffertshofer A, Jones BF, Manshanden I, van Cappellen van Walsum AM, Montez T, Verbunt JP, de Munck JC, van Dijk BW, Berendse HW, Scheltens P (2009) Graph theoretical analysis of magnetoencephalographic functional connectivity in Alzheimer's disease. Brain 132 (Pt 1):213–224

Stam CJ, Nolte G, Daffertshofer A (2007) Phase lag index: assessment of functional connectivity from multi channel EEG and MEG with diminished bias from common sources. Hum Brain Mapp 28(11):1178–1193

Stam CJ, van Cappellen van Walsum AM, Pijnenburg YA, Berendse HW, de Munck JC, Scheltens P, van Dijk BW (2002) Generalized synchronization of MEG recordings in Alzheimer's Disease: evidence for involvement of the gamma band. J Clin Neurophysiol Official Publ Am Electroencephalographic Soc 19(6):562–574

Tomasi D, Volkow ND (2011) Functional connectivity hubs in the human brain. Neuroimage 57(3):908–917

Vanderwal T, Hunyadi E, Grupe DW, Connors CM, Schultz RT (2008) Self, mother and abstract other: an fMRI study of reflective social processing. Neuroimage 41(4):1437–1446

Wicker B, Ruby P, Royet JP, Fonlupt P (2003) A relation between rest and the self in the brain? brain research. Brain Res Rev 43(2):224–230

Wilson TW, Franzen JD, Heinrichs-Graham E, White ML, Knott NL, Wetzel MW (2013) Broadband neurophysiological abnormalities in the medial prefrontal region of the default-mode network in adults with ADHD. Hum Brain Mapp 34(3):566–574

Methods to Estimate Functional and Effective Brain Connectivity from MEG Data Robust to Artifacts of Volume Conduction

Guido Nolte and Laura Marzetti

Abstract Due to the high temporal resolution of MEG data they are well suited to study brain dynamics while the limited spatial resolution constitutes a major confounder when one wants the estimate brain connectivity. To very large extent, functional relationships between MEG sensors and also between estimated sources are caused by incomplete demixing of the brain sources. Many measures of functional and effective connectivity are highly sensitive to such mixing artifacts. In this book chapter we review methods which address this problem. They are all based on the insight that the imaginary part of the cross-spectra cannot be explained as a mixing artifact. Several variants of this idea will be presented. We will present three different methods adapted to localize source interactions: (a) minimum overlap component analysis (MOCA) decomposes linear estimates of the P most relevant singular vectors of the imaginary parts of the cross-spectra, (b) the MUSIC algorithm can be applied to this same subspace, and (c) the estimated sources can be analyzed further using multivariate generalizations of the imaginary part of coherency. Finally, a causal relation between these sources can be estimated using the phase slope index (PSI). The methods will be illustrated for empirical MEG data of a single subject under resting state condition.

G. Nolte (✉)
Department of Neurophysiology and Pathophysiology, University Medical Center Hamburg-Eppendorf, Martinistr. 52, 20246 Hamburg, Germany
e-mail: g.nolte@uke.de

L. Marzetti
Department of Neuroscience and Imaging, Institute for Advanced Biomedical Technologies, G. D'nnunzio University Foundation, G. D'Annunzio University, Via dei Vestini, 66100 Chieti, Italy

S. Supek and C. J. Aine (eds.), *Magnetoencephalography*,
DOI: 10.1007/978-3-642-33045-2_21,

1 Introduction

Magnetoencephalography (MEG) and Electroencephalography (EEG) can directly measure ongoing brain activity at the temporal scale of neuronal communication, i.e. frequencies nominally in the range of 1–100 Hz. Although these techniques feature such a millisecond time resolution, their spatial resolution is intrinsically limited by the fact that neuronal signals are recorded from the scalp (Hari and Salmelin 2012). In the past decades the main focus of EEG and MEG research was the analysis of event related fields, i.e. the average brain response to a given stimulus. More recently, the interest of the scientific community has moved towards the understanding of how information is integrated in the brain. Neural oscillations, which are thought to be a direct manifestation of cortical connectivity (Singer 1999; Schnitzler and Gross 2005; Varela et al. 2001), have thus become the focus of the analysis. The ability of MEG (and EEG) to study brain connectivity has been shown by a large number of studies (Fries 2009; Gow et al. 2008; Gross et al. 2002, 2006; Ioannides et al. 2000; Jerbi et al. 2007; Siegel et al. 2008; Womelsdorf and Fries 2006), the great preponderance of this work still concerns coherence induced by task- or stimulus-related events. Nevertheless, strong evidence has been provided by the functional magnetic resonance (fMRI) research in the last fifteen years for the brain as an ensemble of large distributed brain networks that show patterns of coherent activity also in the absence of any imposed task or stimulus, i.e. at rest. Some of these networks are associated with simple sensory processing and others with higher level cognitive function (Buckner and Vincent 2007; Cole et al. 2010; Daglish et al. 2005; Deco and Corbetta 2010; Damoiseaux and Greicius 2009; Fox and Raichle 2007; Miller et al. 2009). Very recently it has been shown that networks can also be detected using MEG (Brookes et al. 2011a, b; de Pasquale et al. 2012; Liu et al. 2010). Despite these promising results, a number of methodological difficulties remain when studying brain connectivity using noninvasive electrophysiological measurements like MEG or EEG. The major challenge is that the data are largely unknown mixtures of activities of brain sources and thus spurious connectivity, which can be estimated by various measures of statistical dependencies (Pereda et al. 2005), can exist that is due entirely to signal leakage rather than to interacting sources (Brookes et al. 2012; Schoffelen and Gross 2009).

To address this issue, we suggest to construct estimates of brain connectivity from quantities that are unbiased by non-interacting sources. For zero mean data[1] the linear statistical signal properties can be determined by the cross-spectral matrices $S(f)$ defined as

$$S_{ij}(f) = \langle x_i(f) x_j^*(f) \rangle \tag{1}$$

[1] In an event related design the mean can be subtracted.

where $x_m(f)$ are the Fourier transforms at frequency f in channel m for a given segment or trial and $\langle\cdot\rangle$ denotes the expectation value which is typically approximated by an average over the segments or trials.

It is straight forward to show that noninteracting sources do not contribute systematically, i.e. apart from random fluctuations around zero to the imaginary part of the cross-spectra, $\Im(S(f))$, regardless of the number of sources and details of the forward mapping (Nolte et al. 2004). The reason is that the forward mapping is essentially instantaneous and does not induce phase delays to excellent approximation (Stinstra and Peters 1998) which would be necessary to yield a nonvanishing imaginary part of $S(f)$.

From the cross-spectra $S(f)$ one can construct coherency matrices $C(f)$, which are a normalized version of $S(f)$, as

$$C_{ij}(f) = \frac{S_{ij}(f)}{\sqrt{S_{ii}(f)S_{jj}(f)}} \tag{2}$$

In contrast to the imaginary parts of the cross-spectra, $\Im(C(f))$ also depends on independent sources through the denominator in Eq. (2). However, independent sources can only lead to a decrease of $\Im(C(f))$ and hence also $\Im(C(f))$ reflects true interaction even though the physiological interpretation is not trivial especially when interpreting differences of $\Im(C(f))$ e.g. between different tasks.

Based on these observations we suggested a series of methods to identify and localize brain interactions (Nolte et al. 2006; Marzetti et al. 2008; Nolte et al. 2009; Ewald et al. 2012; Shahbazi Avarvand et al. 2012). Additionally, we proposed a method to identify causal structures of the dynamical system under study (Nolte et al. 2008). We here give a brief review of some of these methods (Nolte et al. 2006; Marzetti et al. 2008; Ewald et al. 2012, Shahbazi Avarvand et al. 2012; Nolte et al. 2008) to identify interacting brain sources and to estimate causal relationships. All the methods will be demonstrated using real data whose characteristics are defined in the following section.

2 Data Set

For illustrative purposes, and for illustrative purposes only, we will apply the methods, which will be reviewed throughout this chapter, to an emprirical MEG data set. The data set consists of around 20 min MEG data, under resting state, with 10 min eyes closed and 10 min eyes open. We will average across these two conditions. MEG was measured with a CTF system with 273 channels in Hamburg-Eppendorf.

For the subject an anatomical MRI data set was available which was analyzed with fieldtrip/SPM (Oostenveld et al. 2011) for segmentation to get a volume

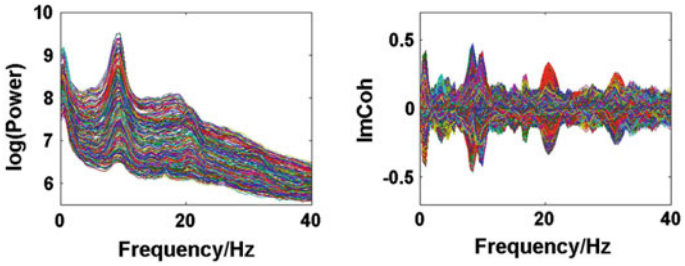

Fig. 1 Power for all channels and ImCoh for all pairs of channels

conductor, which was defined by the inner surface of the skull. Forward calculation was done with an expansion of the magnetic lead field (Nolte 2003).

Spectral analysis was done with a frequency resolution of 0.5 Hz using short-time FFTs of Hanning windowed segments of 2 s duration. In Fig. 1 we show the power for all channels and the imaginary part of coherency (ImCoh) for all pairs of channels as function of frequency. While the peak in the alpha range is very clear it is fairly weak in the beta range and not observable in the gamma range. The rhythms are more clear for ImCoh showing two peaks in the alpha range, at 8 and 10 Hz, a clear peak in the beta range, with a center at 20.5 Hz, and an additional weaker peak at 31 Hz.

In general, subjects can be very different. The present subject has prominent peaks of the imaginary part of coherency at alpha, beta, and gamma frequencies both under eyes closed and eyes open condition. The gamma peak is apparently a (second) higher harmonic of the motor alpha rhythm. At the alpha peak the distinction between central and occipital alpha is not straight forward. The beta-peak, on the other hand, appears to be clearly related to activity in sensory-motor areas, which is also the case for the weaker gamma peak. Since we here show just one example for illustration we decided to discuss in the detail the inverse solutions for the beta-rhythm.

In Fig. 2 we show the imaginary part of coherency at 20.5 Hz. Each of the 50 circles represents one out of the total of 273 channels and shows its ImCoh value to all other channels. The subset of 50 equally distributed channels was chosen to ease visibility. We observe clear dipolar structures over both hemispheres, however, with unclear origin from visual inspection.

3 Methods

3.1 Identifying the Subspace

Below, we will use two different inverse methods to find the sources of the imaginary part of the cross-spectrum. Both methods require the identification of a low dimensional subspace within the channel space. Analogous to the standard

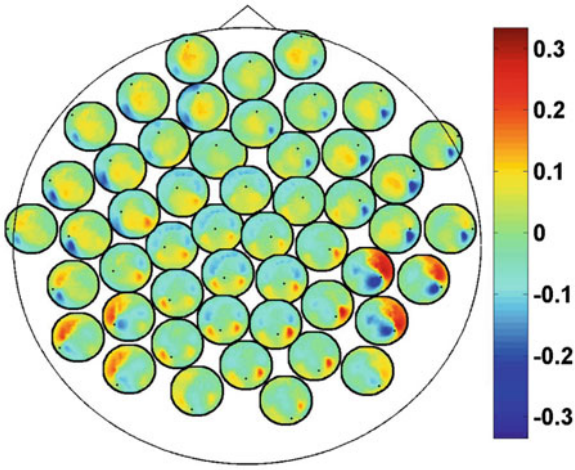

Fig. 2 ImCoh at 20.5 Hz between 50 selected channels and all other channels

PCA decomposition of the full cross-spectrum of a covariance matrix we perform a singular value decomposition of the imaginary part of the cross-spectrum at the signal frequency $f = 20.5\,\mathrm{Hz}$

$$S_{signal} = S(f) \tag{3}$$

For some applications it is convenient to estimate a meaningful contrast, i.e. a cross-spectrum which contains similar background noise but not the rhythmic phenomenon which is under study. We will here construct this as an interpolation between neighboring frequencies:

$$S_{noise} = \frac{1}{2}(S(f + \Delta f) + S(f - \Delta f)) \tag{4}$$

The singular values of $\Im(S_{signal})$ and the ratios of these and the corresponding singular values of $\Im(S_{noise})$ are shown in Fig. 3. Since the imaginary parts of cross-spectra are real valued and antisymmetric, all singular values occur in pairs. (For an odd number of channels the last one is zero.) We observe the presence of four prominent singular values. The ratios of singular values converge roughly to $1.37 \approx \sqrt{2}$, indicating that the background noise is estimated too low. This is expected if the background noise consists essentially of non-interacting sources: the linear interpolation effectively doubles the number of averages and since for non-interacting sources the imaginary part of the cross-spectrum drops with $1/\sqrt{N}$ for N averages, we expect an additional drop by a factor $\sqrt{2}$. The factor is slightly less than $\sqrt{2}$ which is possibly due to the typical $1/f$-decay of the background noise: it is a convex function having the property that linear interpolations are above the true value. Also from this ratio we observe that only 4 singular values are clearly above noise level. In the following we will always analyze this 4-dimensional subspace.

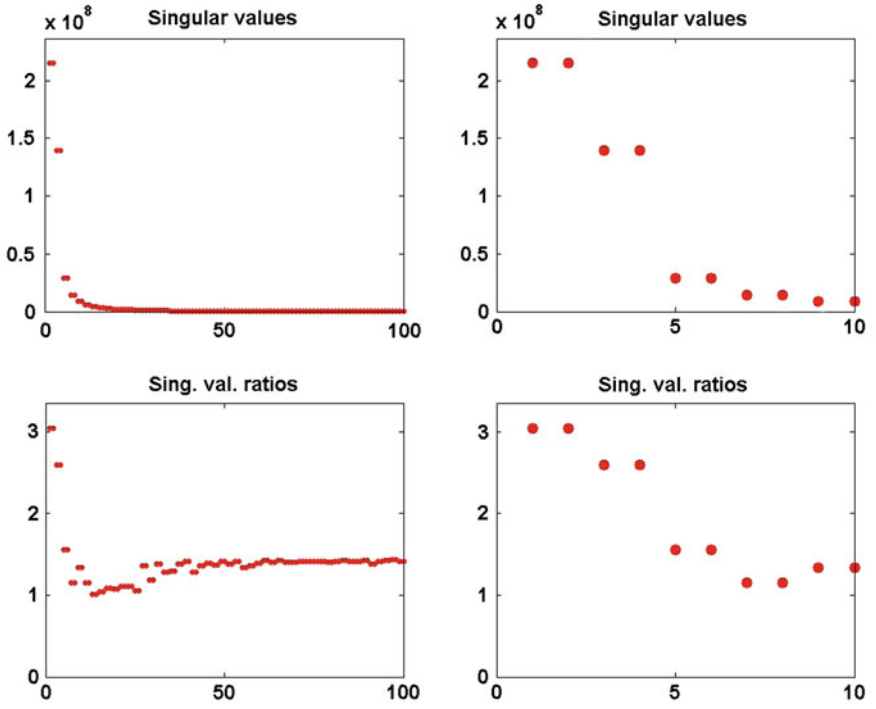

Fig. 3 *Top* singular values of imaginary part of cross-spectrum at 20.5 Hz. *Bottom* ratio of singular values of imaginary part of cross-spectrum at 20.5 Hz and a noise cross-spectrum

The singular vectors are shown in Fig. 4. They roughly have dipole structure, but apparently the dipoles are not well separated. A standard method to demix sources is independent component analysis (ICA), which, however, is not appropriate here, since we are studying interacting sources in sharp contrast to the fundamental assumption of ICA. A separation can still be done using dynamical assumptions if one assumes that all interactions are pairwise using the 'Pairwise Interacting Component Analysis' (PISA) (Nolte et al. 2006). Then the pairs can be separated from each other but a separation of the two sources within each pair is not possible. Also, for such a separation a wide-band analysis of the data is necessary and cannot be done for a single frequency alone. For completeness, we will sketch the theory behind it, but below we will continue with the space spanned by all chosen singular vectors without dynamical separation.

In general, EEG and MEG data are a superposition of many subsystems including (effectively) independent sources but also interacting rhythmic sources of various physiological content. To separate these systems one can assume that (a) all interactions are pairwise and that (b) there are not more interacting sources than channels. These two assumptions are a clear simplification of the true brain dynamics, but they yield a unique decomposition of the data and may capture the most relevant aspects of the interaction observed in EEG/MEG data. These

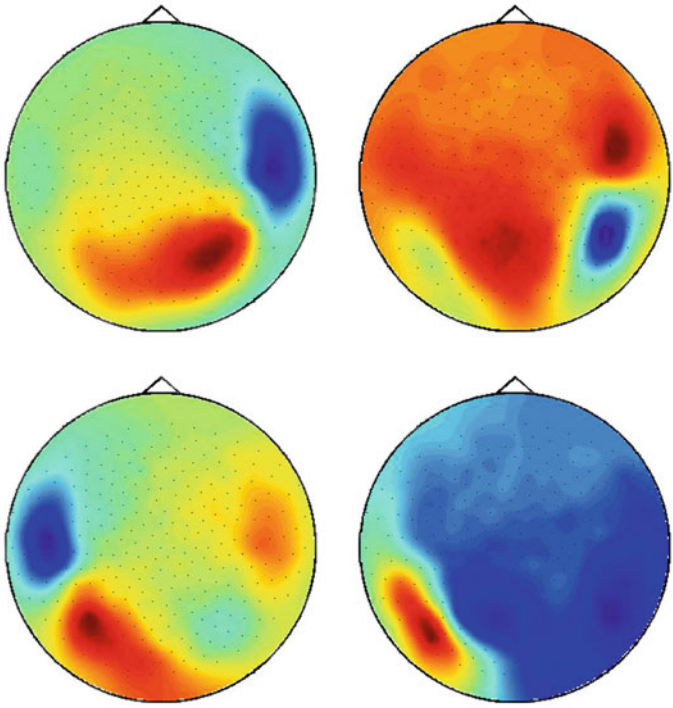

Fig. 4 First four singular vectors of the imaginary of the cross-spectrum at $f = 20.5\,\mathrm{Hz}$

assumptions can be expressed for an even number of N channels as a model for the imaginary part of the cross spectra:

$$\Im(S(f)) = \sum_{k=1}^{N/2} p_k(f)\left(\mathbf{a}_k\mathbf{b}_k^T - \mathbf{b}_k\mathbf{a}_k^T\right) \tag{5}$$

For each k the set of topographies ($\mathbf{a}_k$ and $\mathbf{b}_k$) and the 'interaction spectrum' $p_k(f)$ form a—what we call—PISA-component. We note that this model is only unique up to linear mixing of the two topographies for each k. In other words, the model only identifies the 2D-subspace spanned by the two topographies and not the individual components. For technical details we refer to (Nolte et al. 2006).

3.2 Inverse Method

In order to uniquely decompose the 2D-subspaces found by the singular value decomposition into contributions from individual sources we must introduce further spatial constraints on the nature of the sources. To apply a method designed to

this purpose, outlined in the next section, it is necessary to use a linear inverse method. While in principle the decomposition in sensor space itself does not depend very much on the chosen inverse method, results in source space can vary substantially. We here use eLORETA (Pascual-Marqui et al. 2011), which is a non-adaptive linear inverse solver with a block-diagonal weight matrix adjusted such that the estimated source distribution has maximal power at the true source for a single dipole. The inverse method will be applied for a predefined grid of voxels in the brain. For the mth brain voxel and for the kth dipole direction and for a given forward model, eLORETA defines a spatial filter $\mathbf{G}_{mk}$, which is a column vector of N elements for N channels, such that for the data vector $\mathbf{x}(t)$ in channel space the activity of the kth dipole moment on the mth voxel is given by

$$s_{mk}(t) = \mathbf{G}_{mk}^T \mathbf{x}(t) \tag{6}$$

Due to the linearity of the inverse method, one can directly apply the spatial filters to the cross-spectra to estimate the elements of the 3×3 cross-spectral matrix $P(f, m)$ at the mth voxel at a given frequency

$$P_{kk'}(f, m) = \mathbf{G}_{mk}^T S(f) \mathbf{G}_{mk'} \tag{7}$$

The maximum eigenvalue of $P(f, m)$ is the power of the strongest dipole at that location and the corresponding eigenvector is the orientation.

For the present data, the spectral peak in the beta range is very small. Due to the large noise, meaningful source estimates could not be achieved. Instead, it was necessary, to calculate the power in source space both for the S_{signal} and S_{noise} defined in (3) and (4) and to calculate the ratio of powers shown in Fig. 5.[2] We observe signal peaks in left and right sensory-motor areas as can be expected for central beta-rhythms. We emphasize that for the estimation of the sources of the interaction, to be conducted in the next section, the localization of power is not necessary, but only serves to demonstrate the consistency of the results.

3.3 Minimum Overlap Component Analysis

3.3.1 The Concept

The goal of Minimum Overlap Component Analysis (MOCA) is to decompose sets of topographies based on assumptions about the underlying sources and taking note that orthogonality assumptions, as implicit in PCA or SVD decompositions, are unrealistic (Marzetti et al. 2008). We will explain the concept for two topographies.

[2] We also found that adaptive beamformer performs worse: we could not find convincing inverse solutions for both the signal power and for the power ratios.

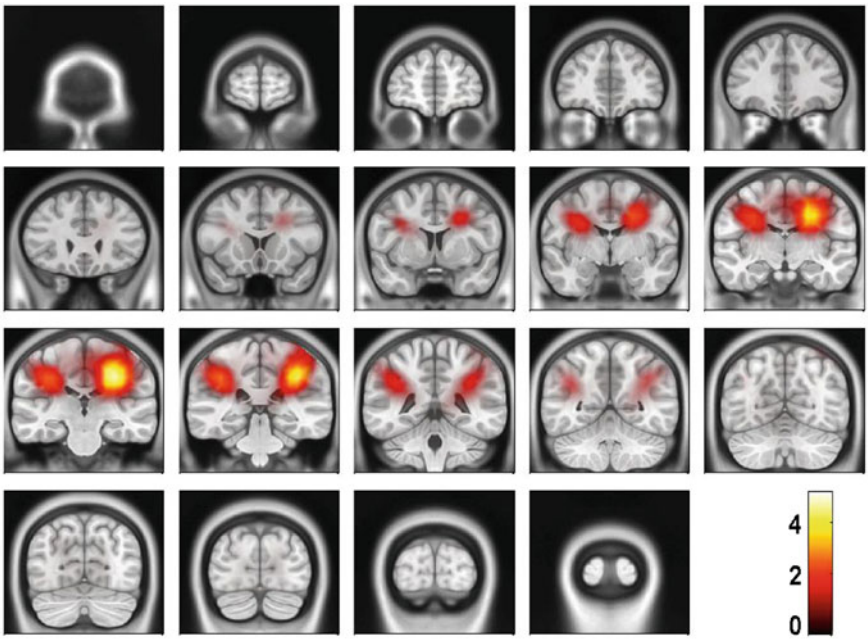

Fig. 5 Power ratio between signal and noise calculated from cross-spectra using eLORETA

We apply a linear inverse operator G onto the singular vectors $\mathbf{x}_1$ and $\mathbf{x}_2$, such that these topographies are mapped into distributions s_i of the source field

$$s_i = G(\mathbf{x}_i) \tag{8}$$

where $s_i = s_i(m,k)$ is a three dimensional vector field calculated in brain voxels $m = 1,\ldots,M$ and in directions $k = 1,\ldots,3$.

The distributions do not represent the sources of the brain, denoted as q_i, but are, within the accuracy of the inverse method, a yet unknown superposition of them:

$$s_i = \sum_{j=1}^{2} W_{ij} q_j \tag{9}$$

for $i = 1, 2$. The 2×2 mixing matrix W can be calculated uniquely under the following constraints

1. The sources are orthonormal:

$$< q_i, q_j > \equiv \sum_{m,k} q_i(m,k) q_j(m,k) = \delta_{ij} \tag{10}$$

2. The sources have minimum overlap:

$$L(q_1, q_2) \equiv \sum_m \left(\sum_k q_1(m,k) q_2(m,k) \right)^2 = min \tag{11}$$

This cost function first squares the scalar product of two dipole moments at each voxel and then sums these squares over all voxels. It vanishes if the two dipole distributions have disjoint support (i.e. disjoint regions of non-vanishing activity), thus measuring overlap. It also vanishes if the orientations at each voxel are orthogonal and therefore corresponds to a weaker form of overlap allowing in principle also activities at the same location as long as the orientations are sufficiently different. Thus, a strong bias towards remote interaction is removed.

The minimization in Eq. (11) can be done analytically (Marzetti et al. 2008). If the concept is generalized to more than two topographies the minimization requires a numerical approach, which, however, is surprisingly fast and robust (Nolte et al. 2009). We note that the spatial constraints (Eqs. 10, 11) and the methods to solve the minimization are similar to those used in ICA in the context of fMRI data analysis (McKeown and Sejnowski 1998; Matsuda and Yamaguchi 2004) with the major difference that we here decompose vector fields rather than scalar ones. To relate to ICA to decompose EEG and MEG data, the orthogonality constraint in Eq. (10) corresponds, mutatis mutandis, to 'sphering' as is used in most ICA methods: the data are transformed to be exactly uncorrelated while independence in higher statistical orders is only forced to be as good as possible.

3.3.2 Illustration

Once the demixing matrix W is found, it can be applied equally to the source distributions and the topographies. If U is an $N \times K$ matrix containing the first K singular vectors as columns, and $H = W^{-1}$ is the demixing matrix, then $\hat{U} = UH^T$ contains as columns the demixed topographies. The demixed topographies for the singular vectors shown in Fig. 4 are presented in Fig. 6. While, of course, the true result is not known for real data, we observe that the apparent mixture of several dipolar structures has been removed.

In Fig. 7 we show the power of the source estimate for all four demixed topographies. We can see that, similar to the result shown in Fig. 5, sources are located in left and right motor-sensory areas. In contrast to the localization of the entire cross-spectrum, for this localization of the interacting sources it is not necessary to visualize power ratios to achieve meaningful results.

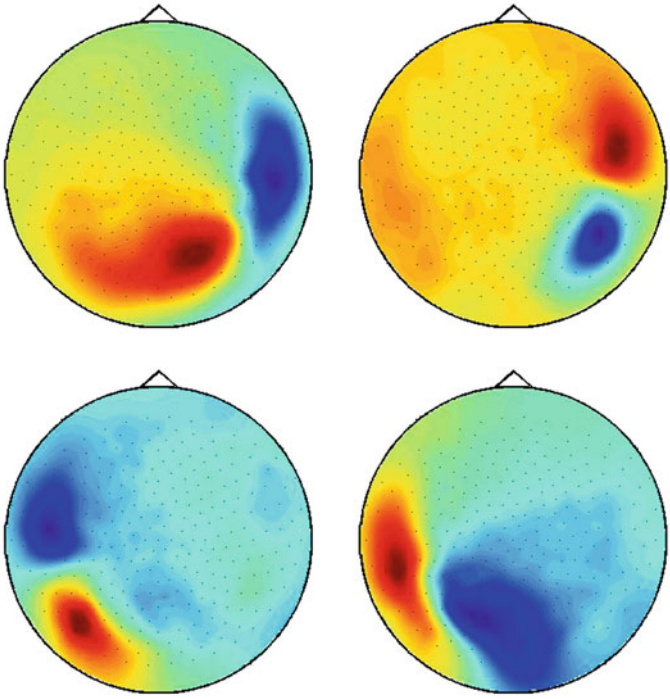

Fig. 6 Demixed singular vectors using MOCA

3.3.3 Minimization of the Cost Function

In this subsection we present the algorithm to solve the minimization problem defined by MOCA. If we only have two source distributions this can be done analytically. To do this we first whiten the distributions s_i to fulfill (10)

$$\hat{s}_i = \sum_j A_{ij} s_j \tag{12}$$

with $A = V^{-1/2}$ and

$$V_{ij} = \sum_{m,k} s_i(m,k) s_j(m,k) \tag{13}$$

In a second step we rotate $\hat{s}_i$ as

$$\begin{pmatrix} q_1 \\ q_2 \end{pmatrix} = \begin{pmatrix} \cos(\phi) & \sin(\phi) \\ -\sin(\phi) & \cos(\phi) \end{pmatrix} \begin{pmatrix} \hat{s}_1 \\ \hat{s}_2 \end{pmatrix} \tag{14}$$

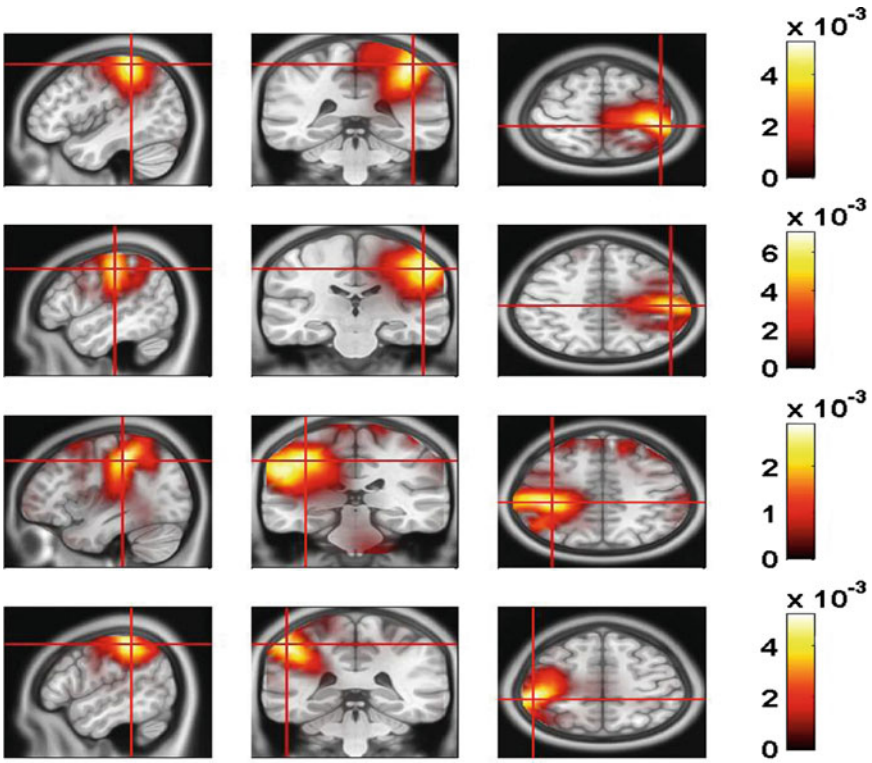

Fig. 7 Sources of demixed singular vectors. Each row displays one source distribution with shown MRI-slices centered at the maximum of the respective power distribution

and find the angle ϕ by minimizing the cost function defined in (11). This minimization can be done analytically in closed form and leads to the solution

$$\phi_0 = \frac{1}{4} tan^{-1}\left(\frac{b}{a-c}\right) \tag{15}$$

with

$$a = \sum_m \left(\sum_k \hat{s}_1(m,k)\hat{s}_2(m,k) \right)^2$$

$$b = \sum_m \left(\sum_k \hat{s}_1(m,k)\hat{s}_2(m,k) \sum_k (\hat{s}_1(m,k)\hat{s}_1(m,k) - \hat{s}_2(m,k)\hat{s}_2(m,k)) \right)$$

$$c = \frac{1}{4} \sum_m \left(\sum_k (\hat{s}_1(m,k)\hat{s}_1(m,k) - \hat{s}_2(m,k)\hat{s}_2(m,k)) \right)^2 .$$

Various solutions arise due to the various branches of the $\tan^{-1}$ function and differ by multiples of $\pi/4$. Minima and maxima are alternating, and we only have to calculate two neighboring solutions with angles ϕ_{max} and ϕ_{min} for the maximum and minimum, and pick the one referring to the minimum out of these two.

For more than two sources the cost function in (11) cannot be solved analytically and must be solved numerically with an iterative procedure using the analytic solution for any given pair of source distributions. These 'sweeps' are repeated over all pairs until convergence is reached. This procedure appears at first sight to be rather naive because such a rotation might affect overlaps between other pairs of sources. This, however, is not the case: all changes between other pairs cancel out exactly in the total cost function which results in a highly efficient algorithm with only few sweeps necessary.

3.4 Music

The multiple signal classification (MUSIC) algorithm is a method which finds sources based on low dimensional subspaces of the entire signals assuming that the topographies of dipoles on true source locations are contained in such a subspace. This is most commonly applied to low dimensional approximations of a covariance matrix defined by the K eigenvectors corresponding to the K largest eigenvalues. Recently, it was suggested to apply this algorithm to the K singular vectors corresponding to the K largest singular values of the imaginary part of the cross-spectrum (Shahbazi Avarvand et al. 2012).

We here recall the essential steps for the MUSIC algorithm. We will at first consider the almost trivial case of fixed dipole orientations with a topography $\mathbf{L}$ and a one-dimensional subspace $\mathbf{U}$, which are both $N \times 1$ vectors. The consistency between dipole field and subspace can be measured by the angle

$$\cos \Theta = \frac{\mathbf{L}^T \mathbf{U}}{\left(\mathbf{L}^T \mathbf{L}\right)^{1/2} \left(\mathbf{U}^T \mathbf{U}\right)^{1/2}} \tag{16}$$

In the general case, the subspace U is an $N \times K$ matrix and L is an $N \times 3$ matrix corresponding to all three dipole orientations. The question then is whether some dipole at a specific location is consistent with the subspace, i.e. whether $L\mathbf{x}$ with unknown dipole moments $\mathbf{x}$ matches a linear combination of the columns of U, which is expressed as $U\boldsymbol{y}$ with $\boldsymbol{y}$ being an unknown $Kx1$ vector. For the minimal angle we have

$$\cos \Theta = \max_{\mathbf{x},\mathbf{y}} \frac{\mathbf{x}^T L^T U \mathbf{y}}{\left(\mathbf{x}^T L^T L \mathbf{x}\right)^{1/2} \left(\mathbf{y}^T U^T U \mathbf{y}\right)^{1/2}} \tag{17}$$

For later use, we express this maximization problem by a gain function $G(\mathbf{x}, \mathbf{y})$ with

$$G(\mathbf{x}, \mathbf{y}) = \frac{\mathbf{x}^T Z \mathbf{y}}{(\mathbf{x}^T X \mathbf{x})^{1/2} (\mathbf{y}^T Y \mathbf{y})^{1/2}} \tag{18}$$

where X and Y are symmetric and positive definite matrices. Maximization, as well as minimization, of G leads to the eigenvalue problem

$$X^{-1/2} Z Y^{-1} Z^T X^{-1/2} \hat{\mathbf{x}} = \lambda \hat{\mathbf{x}} \tag{19}$$

$$Y^{-1/2} Z^T X^{-1} Z Y^{-1/2} \hat{\mathbf{y}} = \lambda \hat{\mathbf{y}} \tag{20}$$

with

$$\hat{\mathbf{x}} = X^{1/2} \mathbf{x} \tag{21}$$

$$\hat{\mathbf{y}} = Y^{1/2} \mathbf{y} \tag{22}$$

The eigenvalues in (19) and (20) are identical, but the eigenvectors are not. If λ_{max} is the maximal eigenvalue, then G is maximized and minimized by the corresponding eigenvectors and it attains the value

$$G^2_{max} = \lambda_{max} \tag{23}$$

Whether a maximum G^2 is a maximum or minimum of G depends on the chosen sign of the eigenvectors which is arbitrary. If we have a maximum for some choice of signs we get a minimum by switching the sign of one of the eigenvectors.

The MUSIC algorithm corresponds to the above case by setting

$$X = L^T L \tag{24}$$

$$Y = U^T U = id_{K \times K} \tag{25}$$

$$Z = L^T U \tag{26}$$

For the minimal angle we get

$$\cos^2 \Theta_{min} = \lambda_{max} \tag{27}$$

and the dipole orientation $\mathbf{x}$ can be calculated from (21). Finally, the topography of the optimized dipole reads

$$\mathbf{v} = L\mathbf{x} \tag{28}$$

For a MUSIC-scan the maximal eigenvalue λ_{max} is calculated for all voxels, and displayed as $1/(1-\lambda_{max})$ which is infinite for a perfect fit.

The MUSIC algorithm can be used to find the location in the brain which is most consistent with the observed subspace as the voxel which maximizes λ_{max} now also over source points. The technical disadvantage of MUSIC is that finding several maxima may be difficult (Mosher et al. 1999). As a remedy, a modification called recursively applied and projected (RAP)-MUSIC was proposed (Mosher et al. 1999). Here, instead of searching simultaneously for several local maxima, only global maxima are determined iteratively. In order to find the next source location, the subspace is updated by projecting out the previously found topographies and then the maximization is repeated. If $V = (\mathbf{v}_1, \ldots, \mathbf{v}_l)$ is the matrix containing as columns the topographies of l sources, then these topographies are projected out both from L and the subspace. Defining a projector as

$$P = id - V\left(V^T V\right)^{-1/2} V^T \tag{29}$$

and in order the find the l-1th location, L is replaced by PL and U is replaced by PU and then the MUSIC algorithm is applied as outlined above.

The result of RAP-MUSIC scans is shown in Fig. 8 for four interations. The red crosses indicate the locations of the maximal eigenvalues which are almost identical to the maxima found by the MOCA inverse solutions. In these figures, the top row corresponds to a 'normal' MUSIC scan without projection. All locations are in principle contained in the scan but only the 'strongest' source is visible in this scan. The ith row corresponds to a MUSIC-scan after the topographies of the i-1 previously found sources is projected out.

3.5 ImCoh in Source Space

To calculate connectivity in source space we first map activities of sensors into sources using eLORETA and then we calculate the imaginary part of coherency between several sources. This is straight forward if the dipole orientation for each voxel is known: the mapping into two voxels leads to a bivariate signal for which ImCoh can be calculated. This is less trivial for unknown dipole orientation, as then each voxel consists of three signals. We will here estimate the directions for each pair voxels as those for which ImCoh is maximized (Ewald et al. 2012; Shahbazi Avarvand et al. 2012; Marzetti et al. 2013). Mathematically, this is very similar to the MUSIC approach presented in the previous section.

Let F_1 and F_2, both of them being $N \times 3$ matrices, be the spatial filters (given here by eLORETA) which map the sensor activity into voxel 1 and voxel 2, respectively. If $\mathbf{x}(t)$ is the activity in the sensors, then the sources activity in the ith voxel reads

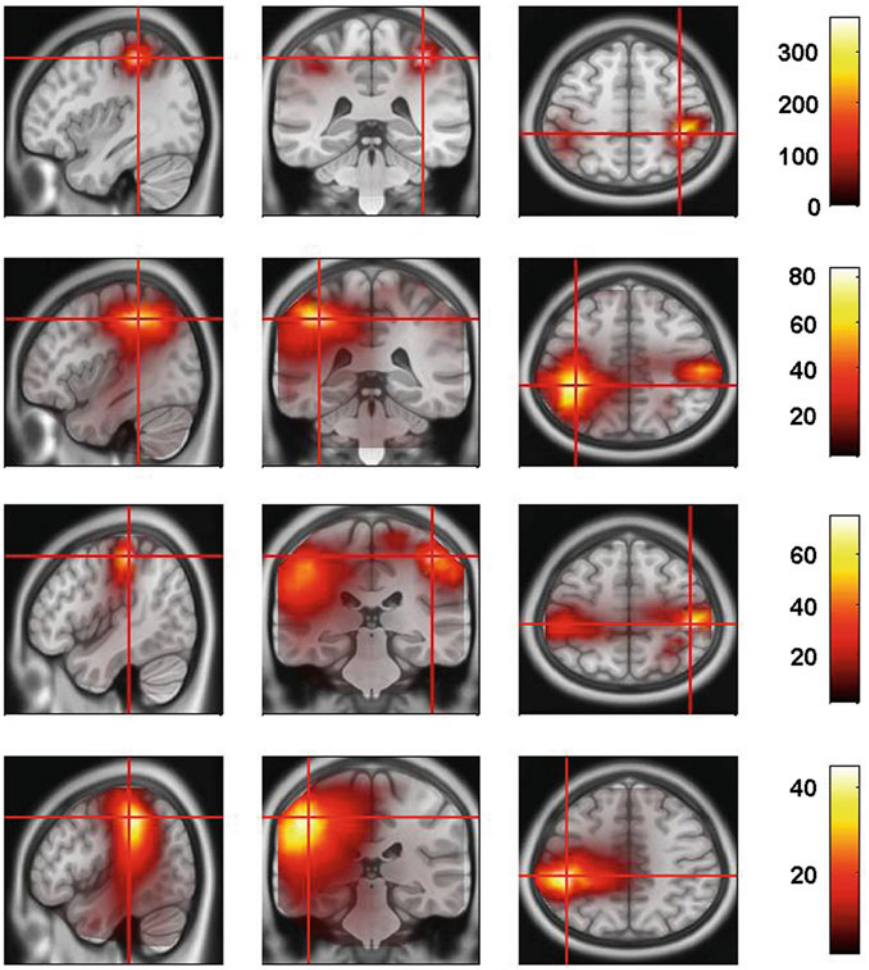

Fig. 8 RAP-MUSIC scan of imaginary part of cross-spectrum. The *k*th row shows the *k*th scan in the three orthogonal views

$$\mathbf{s}_i(t) = F_i^T \mathbf{x}(t) \tag{30}$$

for $i = 1, 2$. Then the cross-spectral matrices within each voxel reads

$$\hat{S}_{ii}(f) = F_i^T S(f) F_i \tag{31}$$

recalling that $S(f)$ is the cross-spectrum in sensor space. The cross-spectral matrices between voxel 1 and voxel 2 reads

$$\hat{S}_{12}(f) = F_1^T S(f) F_2 \tag{32}$$

If $\mathbf{x}_i$ is the dipole moment in the ith voxel, ImCoh between the two dipoles reads

$$ImCoh = \frac{\mathbf{x}_1^T \Im\left(\hat{S}_{12}\right)\mathbf{x}_2}{\left(\mathbf{x}_1^T \hat{S}_{11}\mathbf{x}_1\right)^{1/2}\left(\mathbf{x}_2^T \hat{S}_{22}\mathbf{x}_2\right)^{1/2}} \tag{33}$$

with dependence on frequency f implicit. This, again, has the structure of (18) with the setting $Z = \Im\left(\hat{S}_{12}\right), X = \hat{S}_{11}$, and $Y = \hat{S}_{22}$. The maximal imaginary coherency and the dipole orientations are then given by (19)–(22) with

$$ImCoh_{max} = \sqrt{\lambda_{max}} \tag{34}$$

In Fig. 9 we show this maximizing ImCoh value between between a reference voxels and all other voxels for four different reference voxels, which were found previously from MOCA, and all other voxels. The reference voxels are indicated by blue dots. We observe that ImCoh is maximized in the vicinity of the reference voxels, indicating that the interaction is local.

Local interactions are always trivially observed if one calculates the absolute value of coherency, called coherence, which is a mixing artefact: especially the coherence between a signal and itself is always one and such a result is meaningless. The situation, however, is different when calculating the imaginary part of coherency, which always vanishes between a signal and itself. The interaction can still come out to be local, if the true sources are very close to each other, but have different orientations. Due to the low spatial resolution of EEG/MEG inverse calculations this includes estimated interactions between a voxel and itself if the respective sources are too close to each other to be resolved. Note, that this is also the basis of the 'rotating diple model' which is an effective model for two dipoles which have such a small distance that putting them on the same location is reasonable within the limited spatial resolution of EEG/MEG data.

Had we fixed the orientation according to power, we would not be able to observe such local interactions. In Fig. 10 we show results for the absolute value of imaginary part of coherency for fixed dipole orientations, chosen to the ones which maximize the power for each voxel. For the sources on the right hemisphere we get a qualitatively similar picture but with substantially suppressed values for ImCoh. The local interaction is almost completely lost on the left hemisphere and the remaining interaction appears to be too low and scattered to be considered meaningful.

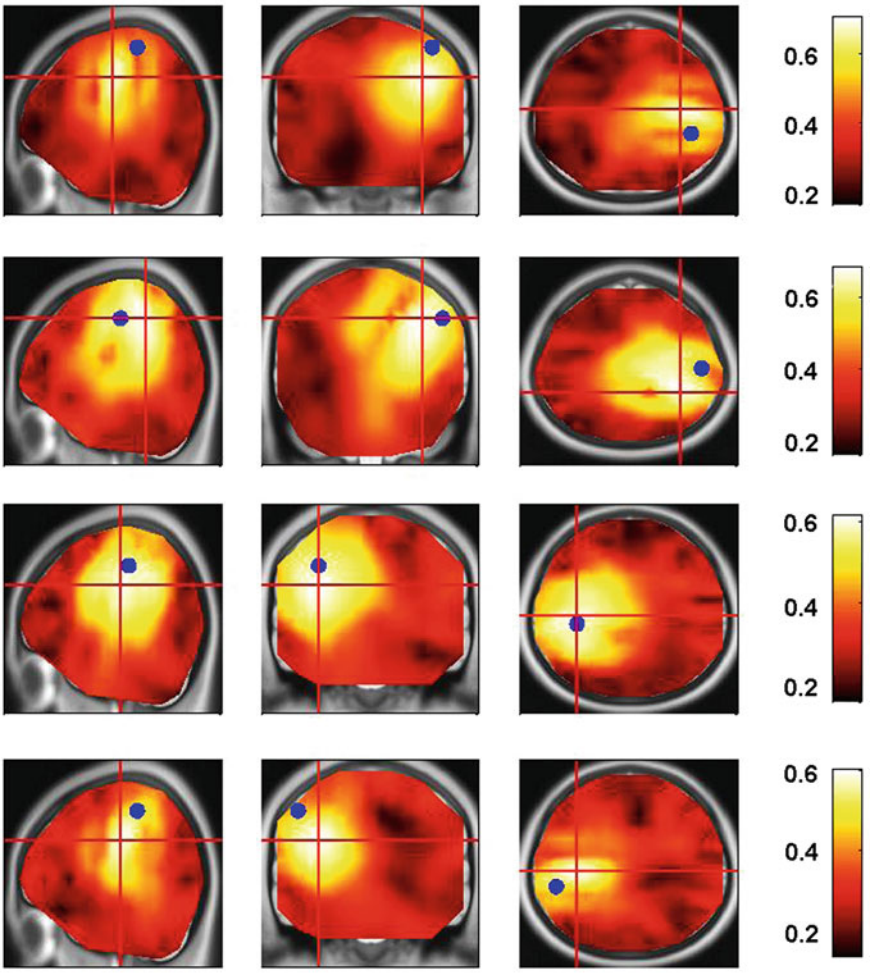

Fig. 9 Maximal ImCoh between reference voxel, calculated from MOCA, and all other voxels for four different reference voxels

3.6 Phase Slope Index

We finally want to estimate causal structures between the estimated sources. The 'Phase Slope Index' (PSI) estimates the causal structure between any two source activities. It is defined as (Nolte et al. 2008)

$$\hat{\Psi}_{ij} = \Im\left(\sum_{f\in F} C_{ij}^{*}(f)C_{ij}(f+\delta f)\right) \tag{35}$$

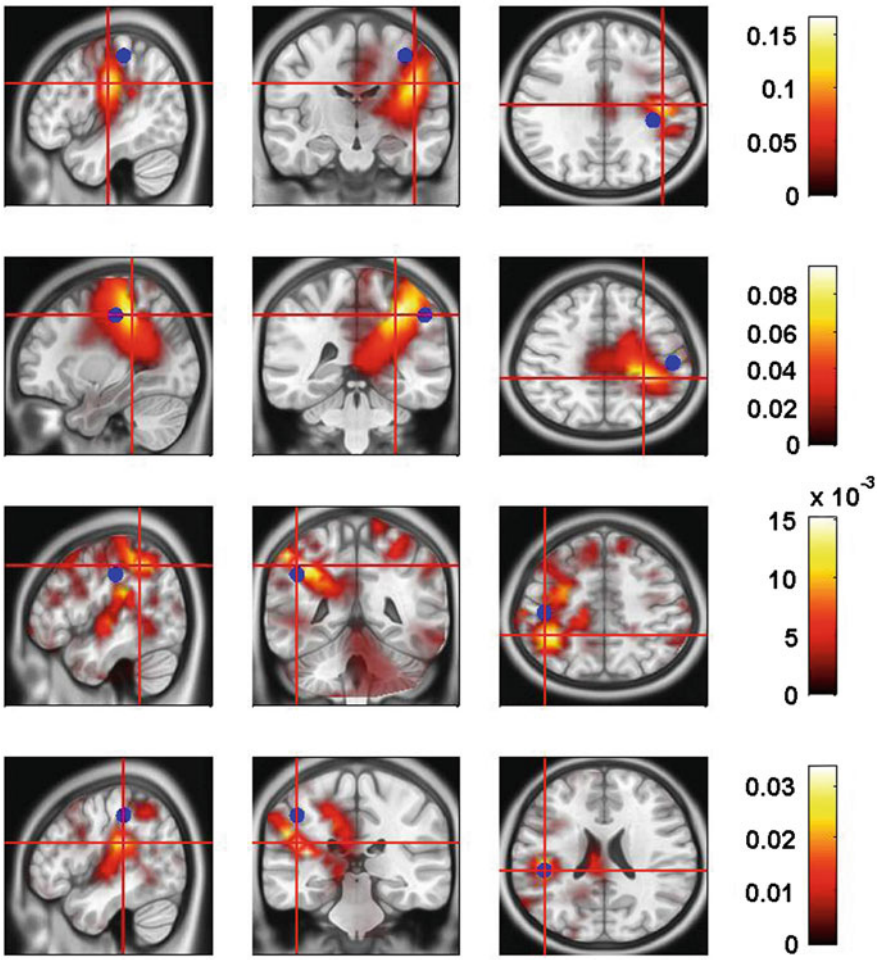

Fig. 10 ImCoh between reference voxel, calculated from MOCA, and all other voxels for four different reference voxels with dipole orientation fixed by power

where $C_{ij}(f)$ is the complex coherency between sources i and j, as given in Eq. (2), and δf is the frequency resolution of the coherency. F is the set of frequencies over which the slope is summed. Usually, F contains all frequencies, but it can also be restricted to a specified band for rhythmic activities.

To see that the definition of $\hat{\Psi}_{ij}$ corresponds to a meaningful estimate of the average slope it is convenient to rewrite it as

$$\hat{\Psi}_{ij} = \sum_{f \in F} \alpha_{ij}(f)\alpha_{ij}(f + \delta f)\sin(\Phi(f + \delta f) - \Phi(f)) \tag{36}$$

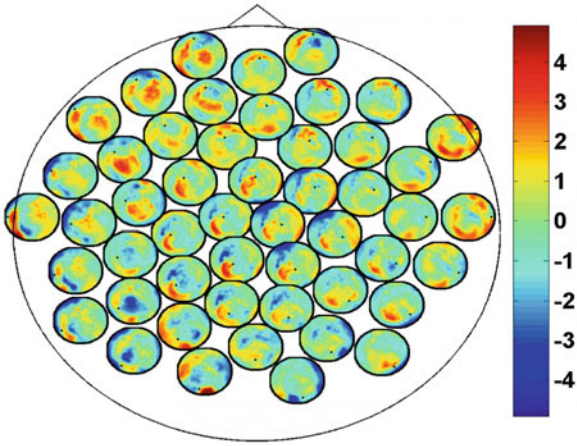

Fig. 11 PSI in channel space

with $C_{ij}(f) = \alpha_{ij}(f)\exp(i\Phi(f))$ and $\alpha_{ij}(f) = |C_{ij}(f)|$ being frequency dependent weights.

For smooth phase spectra, $\sin(\Phi(f+\delta f) - \Phi(f)) \approx \Phi(f+\delta f) - \Phi(f)$ and hence $\hat{\Psi}$ corresponds to a weighted average of the slope.

We list the most important qualitative properties of $\hat{\Psi}$:

1. For an infinite amount of data and for arbitrary instantaneous mixtures of an arbitrary number of independent sources, $\hat{\Psi}$ is exactly zero, because mixtures of independent sources do not induce an imaginary part of coherencies (Nolte et al. 2004)) which in turn is necessary to generate a non-vanishing $\hat{\Psi}$. For finite data, $\hat{\Psi}$ will then fluctuate in this case around zero within error bounds. A special case of this are phase jumps from 0 to $\pm\pi$ which can arise also for mixtures of independent sources.
2. $\hat{\Psi}$ is expressed in terms of coherencies, only. The standard deviation of a coherency is approximately constant and only depends on the number of averages which is equal for all frequencies. Thus, large but meaningless phase fluctuations in frequency bands containing essentially independent signals are largely suppressed.
3. If the phase $\Phi(f)$ is linear in f and provided that the frequency resolution is sufficient (i.e. δf is sufficiently small), the argument in the sum has the same sign across all frequencies and then $\hat{\Psi}$ will have the same sign as the slope of $\Phi(f)$.

It is convenient to normalize $\hat{\Psi}$ by an estimate of its standard deviation

$$\Psi = \frac{\hat{\Psi}}{std(\hat{\Psi})} \tag{37}$$

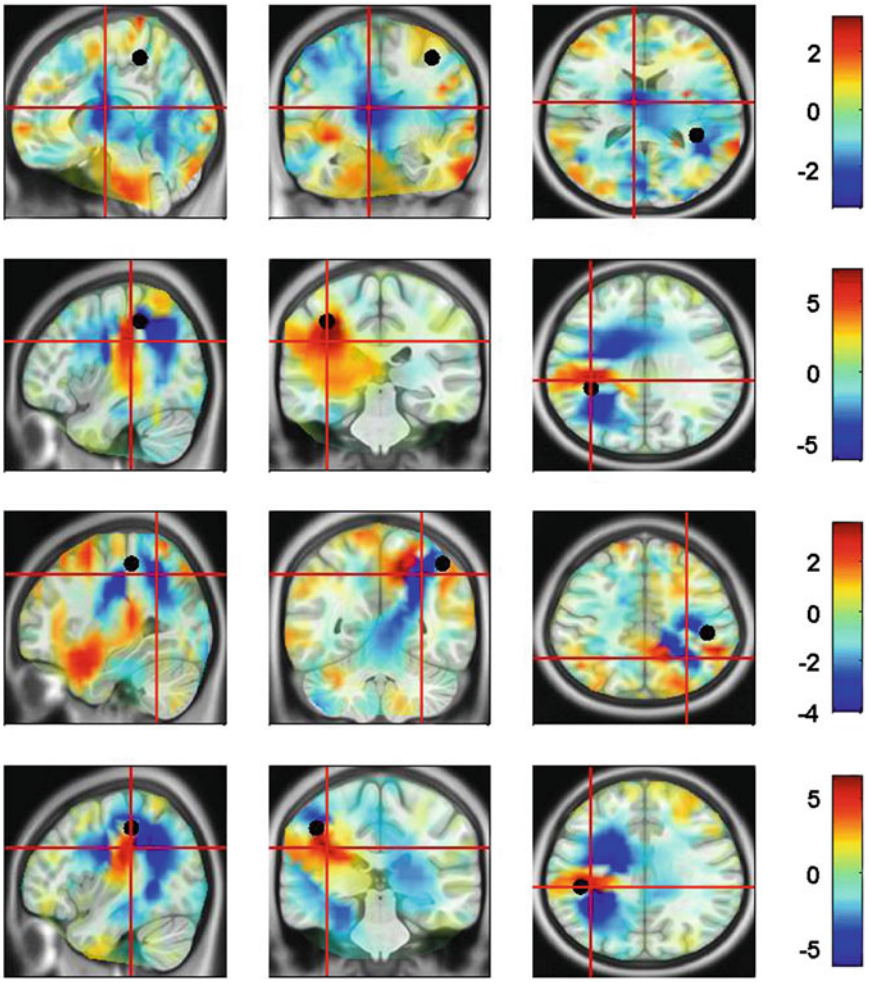

Fig. 12 PSI between reference voxel (*black dot*) and all other voxels for four different references. *Blue color* means the reference is receiving information from these areas and red means the reference is sending information to these areas

with $std(\hat{\Psi})$ being estimated by the Jackknife method. In the examples below we consider absolute values of each larger than 2 as significant.

It is important to point out that the phase of coherency itself is not interpreted in terms of causality. For example, a phase of $\pi/2$ switches to $-\pi/2$ if the sign of one of the signals is reversed, but the PSI measure is invariant with respect to the sign of the signals. Rather than on phase, PSI is based on the slope of the phase as a function of frequency. Note, that a sign change adds a constant to the phase and has no effect on the slope. The method assumes that the studied frequency range properly covers the dynamical range. For purely periodic signals, any causality

estimate would be dubious. In that case Ψ would be insignificant because negative and positive slopes cancel.

To calculate the causal relation for the beta range we calculated PSI in the frequency range around the beta peak $[f - \Delta f, f + \Delta f]$ with $f = 20.5\ Hz$ and $\Delta f = 2$Hz. Results in channel space are shown in Fig. 11. Absolute values of PSI above 2 are significant without correction for multiple comparison with $p \leq .05$. We observe fairly large values up to almost 5 but with highly unclear spatial structure.

To calculate PSI in source space we need to fix an orientation of the dipoles. For each pair of voxels these orientations are chosen to maximize imaginary coherence between the voxels at frequency $f = 20.5$ Hz as explained in the previous section. Results for reference voxels taken from results of the RAP-MUSIC algorithm are presented in Fig. 12. We observe higher (and hence more significant) values than on the sensor level which can mainly be explained by the fact that the source orientation was optimized to observe delayed interactions.

In contrast to ImCoh, for which we displayed the absolute value, the result now has a sign. Such a sign was meaningless for ImCoh at the source level, because it switches if we switch the sign of a source. Since the dipole moment was calculated by an eigenvalue equation with meaningless sign of the eigenvector such a sign was also meaningless for ImCoh. In contrast, PSI does not depend on the sign of the dipole but reflects temporal order. In the figure, blue regions mean that the reference voxel receives information from them, while the reference voxel send information to the red ones. We emphasize, that maximizing ImCoh does not necessarily maximize PSI. It is very well possible that the present approach still misses major effects which are bigger than the ones observed.

4 Conclusion

We presented a series of methods to study functional and effective connectivity from MEG/EEG data in the frequency domain. All presented methods addressed the problem of volume conduction which is by far the most severe confounder when one wants to estimate brain interactions. The basis of the methods is the observation that brain interactions take some time which is much longer than the time needed for the propagation of electromagnetic signals from a source to a sensor which can be considered as quasi-instantaneous for the frequency ranges of interest (Stinstra and Peters 1998). The finite time needed for different neuronal groups to interact with each other makes it possible to find true brain interactions by systematically exploiting time delays between measured signals. This, however, does not mean that for any brain interaction the time delay is observable. If, e.g. an interaction is totally symmetric all net phase/time delays vanish and the interaction cannot be studied with these methods.

We presented two different methods, MOCA and RAP-MUSIC, to localize interacting sources both based on a singular value decomposition of the imaginary part the cross-spectrum at some frequency. The crucial step is to determine a low

dimensional subspace of the signal space spanned by the singular vectors corresponding to the largest P singular values. The choice of P, which corresponds here to the chosen number of sources, is the only free parameter of the methods. For the chosen data set we observed a drop of the kth singular value to a noise floor for $k > 4$ and set $P = 4$ accordingly. The evaluation of other or the development of new techniques to choose P is beyond the scope of this book chapter.

Both presented inverse method only depend on the subspace spanned by the singular vectors and not on the vectors themselves. It is therefore irrelevant whether the singular vectors themselves correspond to topographies of the single sources. The first method, MOCA, is based on some linear inverse method for which we chose eLORETA, but other choices are also possible. MOCA demixes the singular vectors based on assumptions in source space. The second method was RAP-MUSIC applied to this subspace and it assumes that the interacting sources are dipoles. We then found final results to be almost identical for the two methods for the data at hand. Interactions between voxels in the brain were estimated using a multivariate method, with optimized source orientation for each voxel, which was capable of detecting both local and non-local interactions. A comparison with a bivariate method for which source orientation was fixed by power showed that the latter procedure suppresses local interactions. This could lead to a potential bias towards remote interaction. We finally estimated causal relations using the Phase Slope Index in source space with reference voxels chosen from the preceding localization of interacting sources. We observed clear and significant structures in source space which could not be expected from sensor space results.

This book chapter is not an attempt to review all methods addressing the problem of volume conduction. We concentrated on own methods, covering these only partly and totally ignoring a couple of new approaches from other researchers (Pascual-Marqui et al. 2011; Vinck et al. 2011; Stam et al. 2007; Hipp et al. 2012; Meinecke et al. 2005; Sekihara et al. 2011). The relation between our work and the nonlinear measures presented in (Vinck et al. 2011) and the multivariate measures in (Pascual-Marqui et al. 2011) were presented in (Ewald et al. 2012). A more complete survey and comparison of all methods will be addressed in the future.

Acknowledgments This work was supported by grants from the EU (ERC-2010-AdG-269716), the DFG (SFB 936/A3), the BMBF (031A130) and from the Human Connectome Project (1U54MH091657-01) from the 16 National Institutes of Health Institutes and Centers that support the NIH Blueprint for Neuroscience Research.

References

Brookes MJ, Hale JR, Zumer JM, Stevenson CM, Francis ST, Barnes GR, Owen JP, Morris PG, Nagarajan SS (2011a) Measuring functional connectivity using MEG: methodology and comparison with fcMRI. NeuroImage 56:1082–1104

Brookes MJ, Woolrich M, Luckhoo H, Price D, Hale JR, Stephenson MC, Barnes GR, Smith SM, Morris PG (2011b) Investigating the electrophysiological basis of resting state networks using MEG. Proc Natl Acad Sci USA 108:16783–16788

Brookes MJ, Woolrich M, Barnes GR (2012) Measuring functional connectivity in MEG: a multivariate approach insensitive to linear source leakage. NeuroImage 63:910–920
Buckner RL, Vincent JL (2007) Unrest at rest: default activity and spontaneous network correlations. NeuroImage 37:1091–1096
Cole DM, Smith SM, Beckmann CF (2010) Advances and pitfalls in the analysis and interpretation of resting-state FMRI data. Front Syst Neurosci 4:8
Daglish M, Lingford-Hughes A, Nutt D (2005) Human functional neuroimaging connectivity research in dependence. Rev Neurosci 16(2):151–157
Damoiseaux JS, Greicius MD (2009) Greater than the sum of its parts: a review of studies combining structural connectivity and resting-state functional connectivity. Brain Struct Funct 213(6):525–533
Deco G, Corbetta M (2010) The dynamical balance of the brain at rest. Neuroscientist 17:107–123
de Pasquale F, Della Penna S, Snyder AZ, Marzetti L, Pizzella V, Romani GL, Corbetta M (2012) A cortical core for dynamic integration of functional networks in the resting human brain. Neuron 74:753–764
Ewald A, Marzetti L, Zappasodi F, Meinecke FC, Nolte G (2012) Estimating true brain connectivity from EEG/MEG data invariant to linear and static transformations in sensor space. NeuroImage 60(1):476–488
Fox MD, Raichle ME (2007) Spontaneous fluctuations in brain activity observed with functional magnetic resonance imaging. Nat Rev Neurosci 8:700–711
Fries P (2009) Neuronal gamma-band synchronization as a fundamental process in cortical computation. Annu Rev Neurosci 32:209–224
Gow DW, Segawa JA, Ahlfors SP, Lin FH (2008) Lexical influences on speech perception: a Granger causality analysis of MEG and EEG source estimates. NeuroImage 43:614–623
Gross J, Timmermann L, Kujala J, Dirks M, Schmitz F, Salmelin R, Schnitzler A (2002) The neural basis of intermittent motor control in humans. Proc Natl Acad Sci USA 99:2299–2302
Gross J, Schmitz F, Schnitzler I, Kessler K, Shapiro K, Schnitzler A (2006) Anticipatory control of long range phase synchronization. Europ J Neurosci 24:2057–2060
Hari R, Salmelin R (2012) Magnetoencephalography: from SQUIDs to neuroscience. NeuroImage 61:386–396
Hipp JF, Hawellek DJ, Corbetta M, Siegel M, Engel AK (2012) Large-scale cortical correlation structure of spontaneous oscillatory activity. Nat Neurosci 15:884–890
Ioannides AA, Liu LC, Kwapien J, Drozdz S, Streit M (2000) Coupling of regional activations in a human brain during an object and face affect recognition task. Hum Brain Mapp 11:77–92
Jerbi K, Lachaux JP, N'Diaye K, Pantazis D, Leahy RM, Garnero L, Baillet S (2007) Coherent neural representation of hand speed in humans revealed by MEG imaging. Proc Natl Acad Sci USA 104:7676–7681
Liu Z, Fukunaga M, de Zwart JA, Duyn JH (2010) Large-scale spontaneous fluctuations and correlations in brain electrical activity observed with magnetoencephalography. NeuroImage 51:102–111
Marzetti L, Del Gratta C, Nolte G (2008) Understanding brain connectivity from EEG data by identifying systems composed of interacting sources. NeuroImage 42:87–98
Marzetti L, Della Penna S, Snyder AZ, Pizzella V, Nolte G, de Pasquale F, Romani GL, Corbetta M (2013) Frequency specific interactions of MEG resting state activity within and across brain networks as revealed by the multivariate interaction measure. NeuroImage 79:172–183
Matsuda Y, Yamaguchi K (2004) Semi-invariant function of Jacobi algorithm in independent component analysis. In: Proceedings of the International Joint Conference on Neural Networks
McKeown MJ, Sejnowski TJ (1998) Independent component analysis of fMRI data: examining the assumptions. Hum Brain Mapp 6:368–372
Meinecke F, Ziehe A, Kurths J, Müller KR (2005) Measuring phase synchronization of superimposed signals. Phys Rev Lett 94:084102

Miller KJ, Weaver KE, Ojemann JG (2009) Direct electrophysiological measurement of human default network areas. Proc Natl Acad Sci USA 106:12174–12177

Mosher JC, Baillet S, Leahy RM (1999) EEG source localization and imaging using multiple signal classification approaches. J Clin Neurophysiol 16(3):225–238

Nolte G (2003) The magnetic lead field theorem in the quasi-static approximation and its use for magnetoencephalography forward calculation in realistic volume conductors. Phys Med Biol 21;48(22):3637–3652

Nolte G, Bai U, Weathon L, Mari Z, Vorbach S, Hallet M (2004) Identifying true brain interaction from EEG data using the imaginary part of coherency. Clin Neurophysiol 115:2294–2307

Nolte G, Meinecke FC, Ziehe A, Müller KR (2006) Identifying interactions in mixed and noisy complex systems. Phys Rev E 73:051913

Nolte G, Ziehe A, Nikulin VV, Schlögl A, Krämer N, Brismar T, Müller KR (2008) Robustly estimating the flow direction of information in complex physical systems. Phys Rev Lett 100:234101

Nolte G, Marzetti L, Valdes Sosa P (2009) Minimum overlap component analysis (MOCA) of EEG/MEG data for more than two sources. J Neurosci Methods 183:72–76

Oostenveld R, Fries P, Maris E, Schoffelen JM (2011) FieldTrip: open source software for advanced analysis of MEG, EEG, and invasive electrophysiological data. Computat Intell Neurosci 2011, Article ID 156869

Pascual-Marqui RD, Lehmann D, Koukkou M, Kochi K, Anderer P, Saletu B, Tanaka H, Hirata K, John ER, Prichep L, Biscay-Lirio R, Kinoshita T (2011) Assessing interactions in the brain with exact low-resolution electromagnetic tomography. Philos Trans A Math Phys Eng Sci 13; 369(1952):3768–3784

Pereda E, Quiroga RQ, Bhattacharya J (2005) Nonlinear multivariate analysis of neurophysiological signals. Prog Neurobiol 77(1–2):1–37

Schnitzler A, Gross J (2005) Normal and pathological oscillatory communication in the brain. Nat Rev Neurosci 6(4):285–296

Schoffelen JM, Gross J (2009) Source connectivity analysis with MEG and EEG. Hum Brain Mapp 30:1857–1865

Sekihara K, Owen JP, Trisno S, Nagarajan SS (2011) Removal of spurious coherence in MEG source-space coherence analysis. IEEE Trans Biomed Eng 58:3121–3129

Shahbazi Avarvand F, Ewald A, Nolte G (2012) Localizing true brain interactions from EEG and MEG data with subspace methods and modified beamformers. Comput Math Methods Med 2012:402341

Siegel M, Donner TH, Oostenveld R, Fries P, Engel AK (2008) Neuronal synchronization along the dorsal visual pathway reflects the focus of spatial attention. Neuron 60(4):709–719

Singer W (1999) Neuronal synchrony: a versatile code for the definition of relations? Neuron 24:49–65

Stam CJ, Nolte G, Daffertshofer A (2007) Phase lag index: assessment of functional connectivity from multi channel EEG and MEG with diminished bias from common sources. Hum Brain Mapp 28:1178–1193

Stinstra JG, Peters MJ (1998) The volume conductor may act as a temporal filter on the ECG and EEG. Med Biol Eng Comput 36:711–716

Varela F, Lachaux J, Rodriguez E, Martinerie J (2001) The brain web: phase synchronization and large-scale integration. Nat Rev Neurosci 2:229–239

Vinck M, Oostenveld R, van Wingerden M, Battaglia F, Pennartz CM (2011) An improved index of phase-synchronization for electrophysiological data in the presence of volume-conduction, noise and sample-size bias. NeuroImage 55:1548–1565

Womelsdorf T, Fries P (2006) Neuronal coherence during selective attentional processing and sensory-motor integration. J Physiol Paris 100:182–193

Neural Decoding and Brain Machine Interfaces Based on Electromagnetic Oscillatory Activities: A Challenge for MEG

Masayuki Hirata

Abstract One of the technological challenges in neuromagnetism is to establish a method for neuromagnetic measurement of high gamma band activities on a sigle trial basis. This would enables not only accurate neural decoding using MEG, but would also allow phase analyses revealng coupling phenomena between the gamma and other bands.

Keywords Neural decoding · Brain machine interfaces · Electrocorticography · Magnetoencephalography · Oscillations

1 Functional Mapping Using the Magnetoencephalogram

Electromagnetic measurements and analyses of cerebral oscillatory activities have spawned the new field of neuromagnetism. The electroencephalographic analyses conducted by Pfurtscheller on event-related desynchronizations and synchronizations during finger movements was the first study in this field (Pfurtscheller and Aranibar 1977). Since then, a number of studies have established that desynchronization in the alpha to low gamma bands well reflects functional localization of motor, somatosensory and language functions (Hirata et al. 2010, 2002; Taniguchi et al. 2000). Language dominance and localization may also be evaluated noninvasively and can now be investigated as a pre-surgical evaluation (Hirata et al. 2010, 2004). Sliding time window analyses have also revealed temporal profiles of language processing (Goto et al. 2011). However, it is still difficult to record

M. Hirata (✉)
Department of Neurosurgery, Osaka University Medical School,
2-2 Yamadaoka, Suita, Osaka, Japan
e-mail: mhirata@nsurg.med.osaka-u.ac.jp

S. Supek and C. J. Aine (eds.), *Magnetoencephalography*,
DOI: 10.1007/978-3-642-33045-2_22,

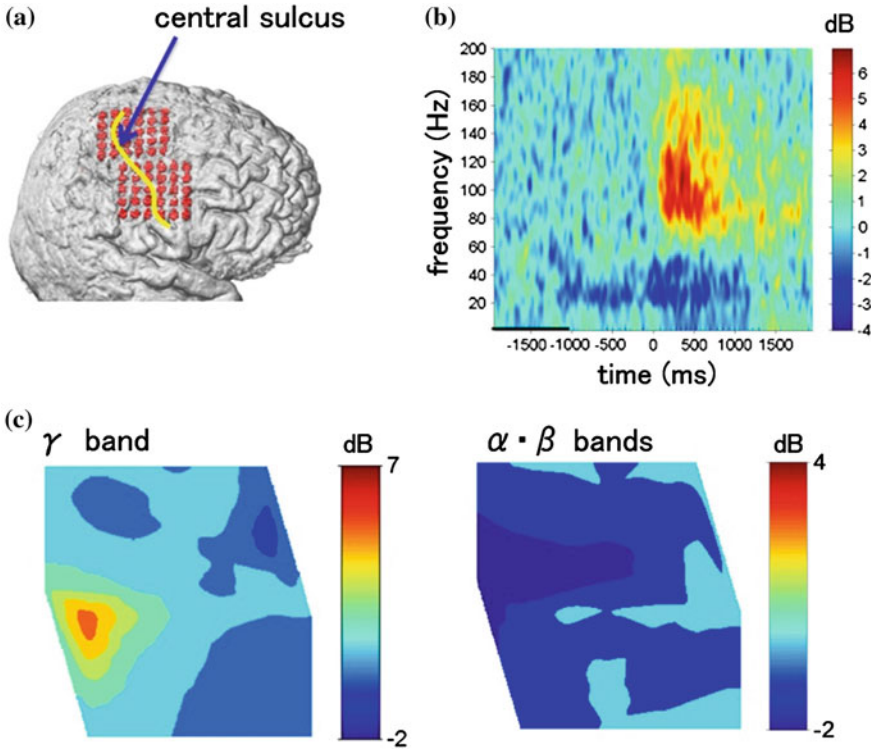

Fig. 1 Spatiotemporal distribution of oscillatory changes during hand grasping, **a** the location of the implanted electrodes, **b** a time-frequency spectrogram, **c** spatial distribution of high gamma band activities (*left*) and alpha and beta desynchronizations (*right*)

neuromagnetic high gamma activities with stability on a single trial basis, and high gamma band activities are not consistently visible on MEG without time-locked stimulation and multi-trial data (Hirata et al. 2002).

2 Brain Machine Interfaces Using the Electrocorticogram

Electrocorticograms provide us with high gamma band activities on a single trial basis. The spatial distribution of high gamma band activities is more focal than that of alpha and beta desynchronizations, and well reflects somatotopic representations (Fig. 1) (Yanagisawa et al. 2011). Using electrocorticographic high gamma activities, we can perform accurate neural decoding as well as the real time control of a robotic arm (Yanagisawa et al. 2011, 2012a). More recently, electrocorticographic phase analyses have revealed cross frequency coupling and phase amplitude coupling in the motor cortex (Yanagisawa et al. 2012b).

3 Neuromagnetic Neural Decoding

Neural decoding using neuromagnetic signals is still a relative newcomer compared to electrocorticographic decoding. Magnetic amplitude as a parameter decodes upper limb movements with high accuracy, while decoding using oscillatory activities does not allow for high accuracy (Sugata et al. 2012a, b). This is probably because it is difficult to pick up weak gamma band activities using MEG. Therefore, one of the technological challenges in neuromagnetism is to establish a method for neuromagnetic measurement of high gamma band activities on a single trial basis. This would enable not only accurate neural decoding using MEG, but would also allow phase analyses revealing coupling phenomena between the gamma and other bands.

References

Goto T, Hirata M, Umekawa Y, Yanagisawa T, Shayne M, Saitoh Y, Kishima H, Yorifuji S, Yoshimine T (2011) Frequency-dependent spatiotemporal distribution of cerebral oscillatory changes during silent reading: a magnetoencephalograhic group analysis. NeuroImage 54:560–567

Hirata M, Goto T, Barnes G, Umekawa Y, Yanagisawa T, Kato A, Oshino S, Kishima H, Hashimoto N, Saitoh Y, Tani N, Yorifuji S, Yoshimine T (2010) Language dominance and mapping based on neuromagnetic oscillatory changes: comparison with invasive procedures. J Neurosurg 112:528–538

Hirata M, Kato A, Taniguchi M, Ninomiya H, Cheyne D, Robinson SE, Maruno M, Kumura E, Ishii R, Hirabuki N, Nakamura H, Yoshimine T (2002) Frequency-dependent spatial distribution of human somatosensory evoked neuromagnetic fields. Neurosci Lett 318:73–76

Hirata M, Kato A, Taniguchi M, Saitoh Y, Ninomiya H, Ihara A, Kishima H, Oshino S, Baba T, Yorifuji S, Yoshimine T (2004) Determination of language dominance with synthetic aperture magnetometry: comparison with the Wada test. NeuroImage 23:46–53

Pfurtscheller G, Aranibar A (1977) Event-related cortical desynchronization detected by power measurements of scalp EEG. Electroencephalogr Clin Neurophysiol 2:817–826

Sugata H, Goto T, Hirata M, Yanagisawa T, Shayne M, Matsushita K, Yoshimine T, Yorifuji S (2012a) Movement-related neuromagnetic fields and performances of single trial classifications. Neuro Rep 23:16–20

Sugata H, Goto T, Hirata M, Yanagisawa T, Shayne M, Matsushita K, Yoshimine T, Yorifuji S (2012b) Neural decoding of unilateral upper limb movements using single trial MEG signals. Brain Res 1468:29–37

Taniguchi M, Kato A, Fujita N, Hirata M, Tanaka H, Kihara T, Ninomiya H, Hirabuki N, Nakamura H, Robinson SE, Cheyne D, Yoshimine T (2000) Movement-related desynchronization of the cerebral cortex studied with spatially filtered magnetoencephalography. NeuroImage 12:298–306

Yanagisawa T, Hirata M, Saitoh Y, Goto T, Kishima H, Fukuma R, Yokoi H, Kamitani Y, Yoshimine T (2011) Real-time control of a prosthetic hand using human electrocorticography signals. J Neurosurg 114:1715–1722

Yanagisawa T, Hirata M, Saitoh Y, Kishima H, Matsushita K, Goto T, Fukuma R, Yokoi H, Kamitani Y, Yoshimine T (2012a) Electrocorticographic control of a prosthetic arm in paralyzed patients. Ann Neurol 71:353–361

Yanagisawa T, Yamashita O, Hirata M, Kishima H, Saitoh Y, Goto T, Yoshimine T, Kamitani Y (2012b) Regulation of motor representation by phase-amplitude coupling in the sensorimotor cortex. J Neurosci 32:15467–15475

Part IV
Neurodevelopment Across Lifespan

Fetal Magnetoencephalography (fMEG)

Jana Muenssinger, Hari Eswaran and Hubert Preissl

Abstract The human brain is one of the most complex organs which develops and adapts continuously over lifetime. Until now, neurophysiological research is mainly related to brain development from birth to adulthood and neurophysiological research concerning prenatal human brain development only started in the last decades. Magnetoencephalography (MEG) is especially suited for fetal investigation, because it is completely noninvasive and not affected by the biological tissue separating the fetus from the outside. The first successful fetal MEG (fMEG) recording was reported in 1985 (Blum et al. 1985). Since the human brain in utero is highly vulnerable to internal and external influences, prenatal brain research is highly important to understand its development during that time period. Therefore, measurement techniques were improved and basic research concerning brain development in utero was conducted. So far, mainly auditory and visual stimulation was used to assess fetal brain development by means of changes in signal processing speed or the development of basic forms of learning. The goal of basic fMEG research is to understand healthy fetal brain development and enable an early detection of possible deviations from it. In the future this may allow the development of early, even prenatal treatments and reduce the risk of adverse outcomes. This chapter gives an overview over structural and functional brain development and introduces the fMEG, a measurement technique to non-invasively assess functional fetal brain development in utero. Moreover, current fMEG studies are introduced and the potential of the method of fMEG is illustrated and discussed.

Keywords Auditory evoked response (AER) · Visual evoked response (VER) · Fetal brain maturation · Magnetoencephalography (MEG)

J. Muenssinger (✉) · H. Preissl
Institute for Medical Psychology and Behavioral Neurobiology, fMEG Center,
University of Tuebingen, Tuebingen, Germany
e-mail: jana.muenssinger@uni-tuebingen.de

H. Eswaran
Department of Obstetrics and Gynecology,
University of Arkansas for Medical Sciences, Little Rock, USA

S. Supek and C. J. Aine (eds.), *Magnetoencephalography*,
DOI: 10.1007/978-3-642-33045-2_23,

1 Introduction

The human brain changes constantly during lifetime and shows high plasticity especially during early development. While the brain's high plasticity is advantageous concerning the rehabilitation of functions after brain damage, unfortunately it also makes the brain vulnerable to external influences, especially during prenatal brain development. In addition to the "normal" differences between age groups, external influences during fetal development can also cause alterations in brain development leading to impairments in individual cognitive processes. During the last decades, augmented research has been done concerning "fetal programming", showing that maternal stress (Talge et al. 2007), exposure to lead (Jedrychowski et al. 2009) or cocaine (Singer et al. 2008) as well as maternal undernutrition (Szitanyi et al. 2003) or obesity (Muhlhausler et al. 2008) during pregnancy can negatively influence cognitive development or increase the risk of developing diseases such as type 2 diabetes in later life.

Since human brain development is such a fragile process, which can be influenced by many different internal and external factors, evaluation of this process especially before birth can give first indications of possible deficits. This might serve as a first step towards an even faster and more adequate treatment and therefore help in the future to decrease the risk of negative outcomes for later life. To evaluate healthy cognitive development in utero, basic research is needed. Only by knowing the developmental steps of the healthy brain, modifications from this process can be detected and treatment initiated.

The fetal magnetoencephalography (fMEG) is a non-invasive technique which enables the investigation of human brain development in utero by evaluating spontaneous fetal brain activity, fetal brain reactions to auditory or visual stimulation, and change detection between stimuli or habituation to repetitively presented stimuli. In this chapter we provide an overview of human central nervous system (CNS) development during the fetal period. Subsequently, the fMEG and its possible applications are introduced and discussed and an overview of the current state of the art in fMEG research is given.

2 Background on Human CNS Development

Shortly after conception, the human brain starts to develop. Already after 18 days post conception, the neural plate, built of tissue developing into the human nervous system, is visible and developing to form a neural tube after 24 days. Around this time, cell proliferation starts. Due to cell division, the number of cells in the neural tube increases substantially. Once created, the cells leave their place of origin to migrate to their place of destination and align themselves with other neurons in the same area (aggregation). These processes build the foundation for the formation of different structures of the human nervous system. However, to enable the newly built brain structures to function appropriately, cells need to be connected to enable

interaction between different structures. This cell connection is initiated immediately after cell aggregation and is characterized by axon growth and synapse formation. However, due to a neuronal overproduction of about 50 % of neurons, a selection takes place, which seems to be related to the integrity of the associated axon and its projection. The decay of neurons takes place either actively (apoptosis) or passively (necrosis) and is regulated by neurotrophins. To ensure the appropriate function of brain structures, axons of the surviving neurons sprout to occupy gaps, which arose through death of neighboring cells. The process of neuronal development and migration is terminated at approximately 7 months of prenatal development. However, the development of the human brain is not "finished" at this point in time or at birth. In contrary, development continues postnatally and proceeds throughout late adolescence. The postnatal period is characterized by an intensified development of new synapses (synaptogenesis), myelination and an increase in dendrite branching as well as synaptic loss. During the long period of brain development between conception and adulthood, different brain regions mature at different time points. While primary visual and auditory cortices are among the first to mature, reaching their maximal synapse density already in the seventh or eighth postnatal month, the prefrontal cortex (PFC) is known to be one of the last brain regions to mature, reaching its maximal synapse density in the second year after birth. Similarly, myelination and synaptic loss occur first in the primary auditory and visual cortices and continue into adolescence in the PFC (Casey et al. 2000; Pinel 2003).

Historically, knowledge about brain development was originally gained through post-mortem examinations; in vivo evaluations became possible with the invention of brain imaging techniques like magnetic resonance imaging (MRI) (for a review about developmental MRI studies see Lenroot and Giedd (2006)). In the last decades, several studies used MRI to evaluate brain development in neonates and children (Huppi et al. 1998; Giedd et al. 1996; Casey et al. 2000). Examining 78 premature and mature newborns at the ages between 29 and 41 postconceptional weeks, Huppi et al. (1998) showed an increase in total brain tissue volume of 22 ml/week during that period. Accordingly, also total gray matter volume increased at approximately 15 ml/week. The highest increment was found in cortical rather than sub-cortical grey matter. In the first two years, synapse formation in the brain was found to be highest and by the age of 2 years, the human brain reached about 75 % of its adult weight. Moreover, no significant increment of cerebral or cerebellar volume could be found during the time period between 4 and 18 years of age (Giedd et al. 1996; Kretschmann et al. 1986; Casey et al. 2000).

2.1 Development of the Auditory System

Human hearing is a process that requires the cooperation of different parts including the ear, auditory nerve, thalamus, and primary auditory cortex. Only a flawless interaction of these systems enables the perception of sounds. The fetal outer ear can already be observed after 10 weeks of gestational age (GA)

(Arabin and van Straaten 2006). The tympanic membrane and ring, which are the transition between the outer and the middle ear, are developed at 16 weeks GA. The adult size of the pinna is reached at about 19–20 weeks GA (Counter 2010). The three ossicles of the middle ear begin to develop between the 4th and the 6th week GA and reach their full size at an gestational age of 18 weeks (Counter 2010; Arabin and van Straaten 2006). In the inner ear, the hair cells can be detected after 14 weeks. At about 20 weeks of GA, the morphology of the cochlea is found to be already similar to the stage when its first function is detected. However, cochlear development was found to proceed after the 20th week GA and to mature around the 30–35th week GA (Pujol et al. 1991). Leaving the ear, the "sound waves" travel further to the auditory pathways, which undergo myelination between the 26th and 29th week of gestation. Nevertheless, myelination further progresses until the age of approximately one year after birth (Arabin and van Straaten 2006).

With a slight delay in comparison to the anatomical development of the fetal auditory system, first auditory experiences can be expected starting at the 20th week GA. Monitoring blink-startle reflexes in response to vibro-acoustic stimulation, Birnholz and Benacerraf (1983) detected first responses in fetuses between the 24th and 25th week GA, however, stable responses across the study group were found at the gestational age of 28 weeks. Using pure tone stimulation of different frequencies, Hepper and Shahidullah (1994) found that responses to different frequencies are observable at different gestational ages. First responses have been detected for 500 Hz stimulation. For this frequency, they were detected even at an age of 19 weeks GA and at the age of 27 weeks GA, 96 % of the participating fetuses showed responses for frequencies of 250 and 500 Hz. Responses to higher frequencies showed a developmental delay with the fetuses responding to a frequency of 1,000 Hz at 33 weeks GA and to a 3,000 Hz tone at 35 weeks GA (Hepper and Shahidullah 1994). Similar gestational ages for the occurrence of fetal responses to external auditory stimulation have also been reported by others (Querleu et al. 1988). During the last trimester of gestation, the intensity of stimulation needed to elicit a fetal response was found to decrease, also indicating developmental progress (Hepper and Shahidullah 1994).

After birth, neonates' auditory system undergoes further development, which enables the localization of sound sources in the environment at about 2 months of age. At an age of around 6 months, localization is even possible in horizontal and vertical planes. In general, an improvement concerning the acuity of hearing as well as the discrimination of different speech sounds progresses over the first three years of life.

2.2 Development of the Visual System

Similar to the auditory system, the visual system consists of multiple parts which have to cooperate to enable human vision. This development starts in early fetal life and progresses through the first postnatal years. One of the first structures to

develop is the physical structure of the eye (early phase of fetal life), while the different necessary neuronal structures and connections develop during later fetal and early neonatal life (Graven and Browne 2008). The development of the retina and its layers commences at around 24 weeks GA and is not finished until 2 or 3 months of postnatal life. This long period is determined by the development of the retinal substructures. While the rod receptors important for scotopic vision develop without any influence of light during the latter period of fetal life and are functional at term, the cone receptors important for photoptic vision are not functional when the baby is born. Photoptic vision develops during the first months of neonatal life. Other retinal cells mature during the period of 22–30 weeks GA. Moreover, random firing of retinal ganglion cells activates the growth of axons which become the optic nerve, the connection between the retina and the lateral geniculate nucleus (LGN). Also retinal amacrine cells start to fire to stimulate axon growth between the retina and the LGN as well as between the LGN and the visual cortex. Amacrine cell activity starts around the fetal age of 28–30 weeks GA and becomes more regular when development progresses. This regularization of activity is accompanied by the beginning of the first organized sleep states which are important for the configuration of ocular dominance columns in visual cortex (Graven and Browne, 2008). First fibers reaching the LGN were detected as early as 7 weeks GA (Cooper 1945). However, at this stage, the LGN is in the beginning of its development and consists of homogeneous cell arrangements while the 6-layer-structure seen in mature LGN develops around the 22th week GA (Hitchcock and Hickey 1980; Cooper 1945). First connections between the LGN and the visual cortex, which is also organized in 6 layers, begin to evolve before the mid-gestational period (Henver 2000). Ocular dominance columns in the visual cortex are built in the last 8–10 weeks of gestation (Graven and Browne 2008).

While not all parts of the visual system are mature before birth and continue developing during the first years of neonatal life, much development takes place in the prenatal period between around 24 and 40 weeks GA. For example, scotopic vision becomes functional during the late prenatal period. Moreover, studies investigating fetal brain maturation showed reactions to light flashes as early as 28 weeks GA (Eswaran et al. 2004).

3 Introduction of the Fetal MEG

Since human brain development in utero is such a complex and fragile process, its anatomical as well as functional evaluation provides important information about healthy brain development. However, because the fetal head is covered by the maternal abdomen and not accessible from outside, the investigation of fetal brain function is accompanied with many challenges. Nevertheless, advances in the technology of brain imaging in the last decades made the evaluation of prenatal brain development possible. During this time, two brain imaging techniques have been developed, which showed promising results in the research of fetal brain

Fig. 1 156-channel fMEG device SARA II (SQUID Array for Reproductive Assessment, VSM MedTech Ltd., Port Coquitlam, Canada) installed at the fMEG Center in Tübingen (© University Hospital Tübingen)

development and function: functional MRI (fMRI) (Belliveau et al. 1991) and fetal magnetoencephalography (fMEG) (Blum et al. 1985). While fMRI has the advantage of high spatial resolution, it also involves many difficulties concerning fetal measurements. During an fMRI measurement, fetuses are exposed to high sound levels and magnetic fields, which mainly restrict the usage to fetuses presenting with clinical measurement indications. In contrast, the fMEG is a noninvasive technique, which makes it a suitable tool for basic research as well (Preissl et al. 2004, 2005). So far, the fMEG is mainly used to evaluate fetal heart signals and brain function as measured by fetal auditory evoked responses (AERs) elicited by tone stimulation, fetal visual evoked responses (VERs) elicited by light stimulation and spontaneous fetal brain activity (for a review see Preissl et al. (2004)).

The fMEG uses the same technique as the MEG but combines this technique with the special requirements needed for fetal and neonatal measurements. To ensure a good detection of the fetal heart and brain signals and enable the mother to have a comfortable position on the device, the sensor array is shaped to fit the maternal abdomen. Worldwide, only two dedicated fMEG devices—also called SARA systems (SQUID Array for Reproductive Assessment)—are operational so far. The first one was developed and installed in Little Rock, Arkansas, USA while an advanced version was installed at the fMEG Center in Tübingen in the year 2008.

The fMEG device installed at the MEG Center in Tübingen (SARA II, VSM MedTech Ltd., Port Coquitlam, Canada) includes 156 primary sensors and 29 reference sensors (see Fig. 1). Four localization coils are used to localize the maternal body and the fetal head in relation to the sensor array. One is attached

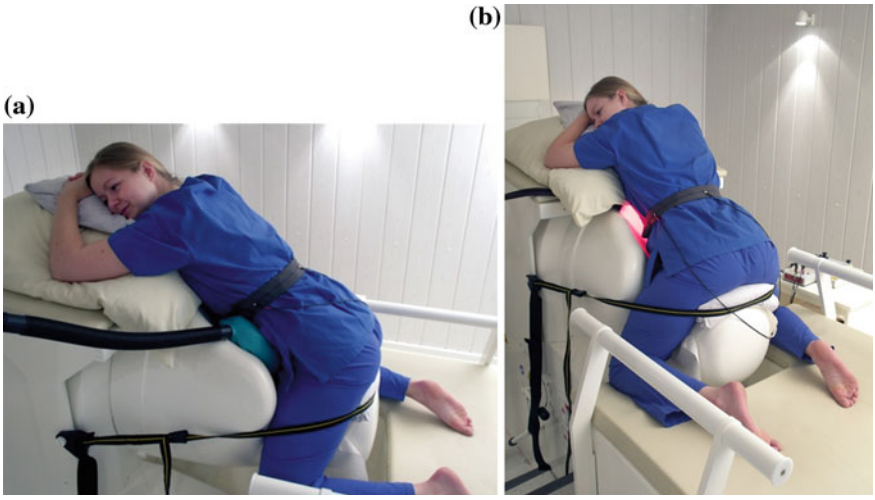

Fig. 2 Fetal measurement with (**a**) auditory and (**b**) visual stimulation. Tones are produced outside the shielded room and transmitted through air-filled tubes to a balloon located directly above the maternal abdomen. Light flashes are produced by a panel of light emitting diodes (© University Hospital Tübingen)

directly to the maternal abdomen above the fetal head, one at the left and right side of the mother respectively and one at the maternal spine. To ensure that the measurement is not influenced by magnetic fields from the surrounding environment, the device is located within a magnetically shielded room (Vakuumschmelze, Hanau, Germany).

3.1 Fetal Measurements

Before each fetal measurement, the head position of the fetus has to be determined. Therefore, an ultrasound is performed immediately before the measurement and fetal head position is marked on the maternal abdomen. After finding a comfortable position on the device, localization coils are attached as described above. During the entire measurement session, contact between the subject and the researcher is ensured through a camera and an intercom. Immediately after the measurement, a second ultrasound is performed to check for changes in the fetal position.

For auditory stimulation during a measurement, stimuli are produced by loudspeakers outside the shielded room and led through air-filled tubes to a balloon which is located directly above the maternal abdomen (Fig. 2a). For visual stimulation, light stimuli are produced by a panel of light emitting diodes (Fig. 2b).

Fig. 3 Neonatal measurement with auditory stimulation. Tones are produced outside the shielded room and transmitted through air-filled tubes to small earphones especially designed for neonatal measurements (© University Hospital Tübingen)

3.2 Neonatal Measurements

For neonatal measurements, a cradle is attached to the fMEG device, which ensures that the newborn is lying comfortably and safely during the measurement. Generally, measurements are performed while the newborn is sleeping or lying quietly.

For auditory stimulation, the newborn is lying on one side with its contralateral temporal lobe resting on the sensor array. Stimulation is produced outside the shielded room, conducted through air filled tubes and presented to the left ear using a headphone which is especially developed for neonatal measurements (Fig. 3). For visual stimulation, the newborn is lying on its back with its occipital lobe resting on the sensor array. The light pad is fixed at approximately 1 m above the neonatal head.

4 State of the Art in Functional Fetal Brain Research Using fMEG

In the year 1985, the first fetal AERs were detected using a one-channel MEG device (Blum et al. 1985). Since then, the technology was improved and measurements with more channels were made possible. In the last decades, mainly auditory evoked responses (AERs) and visual evoked responses (VERs) were recorded and their change over gestational age was investigated (Holst et al. 2005; Eswaran et al., 2002a, b; Schleussner and Schneider 2004). Moreover, auditory change detection (e.g., change in frequencies) was evaluated (Draganova et al. 2005, 2007) and response decrement (i.e., habituation) after repetitive auditory and visual stimulation has been investigated (Sheridan et al. 2008; Matuz et al. 2012; Muenssinger et al. 2013).

4.1 State of the Art in Auditory fMEG Research

As described above, the first human auditory experiences can be expected at 20 weeks GA. In fMEG studies using pure tone stimulation, AERs were detected reliably at a GA of 28 weeks (Lengle et al. 2001; Schleussner and Schneider, 2004; Eswaran et al. 2002a). While response detection rates were highly variable, an AER detection rate of around 80 % could be reached in fetuses between 28 and 40 weeks GA (Schleussner and Schneider 2004; Holst et al. 2005) and 30 and 40 weeks GA (Eswaran et al. 2002a). Moreover, longitudinal studies evaluated the development of AER responses over GA. Therefore, fetuses between 27 and 40 weeks GA were included and measured at least twice with an interval of approximately 2 weeks between measurements (Holst et al. 2005). Results showed that the AER latencies decreased with increasing GA, indicating a gradual maturation of auditory processes and therefore an increase in the speed of auditory signal processing during the last trimester of pregnancy (Holst et al. 2005). These results are also in accordance with those of Schleussner and Schneider (2004), who showed decreasing latencies of the P2 pm and N2 pm components with increasing GA. These findings are first steps toward the understanding of healthy brain maturation in utero and might in the future be helpful in detecting deviant brain development. Moreover, in addition to pure sound detection, fetuses in the last trimester of pregnancy are also able to detect changes in sound frequencies (Draganova et al. 2005). To investigate this ability, an oddball paradigm was used. 500 Hz (88 %) tones were intermixed with 750 Hz (12 %) tones and mismatch negativity responses (MMN), which are an indicator for change detection (in this case a change in frequency), were evaluated. It could be shown that in 48 % of the fetal recordings, an MMN response was found. In a follow-up study, detection rates of MMN responses increased to 66 % in fetuses between the GA of 28 and 39 weeks and 89 % in newborns (Draganova et al. 2007). These results strongly indicate that the fetal brain in the last trimester of pregnancy is able to process auditory stimuli and detect changes in stimulus frequencies. This is an important prerequisite for language development and processing. Also concerning habituation, the most basic form of learning, an auditory fMEG study was performed (Muenssinger et al. 2013). Fetuses were measured using an auditory short-term habituation paradigm consisting of trains of tones including five 500 Hz tones, one 750 Hz tone (dishabituator) and another two 500 Hz tones each. After response sensitization resulting in a response increment between tones one and two, the expected response decrement for the four repetitively presented 500 Hz tones could be observed (Fig. 4).

This response decrement could either be due to sensory adaptation (fatigue) or to habituation. Therefore, not only dishabituation (response increment between last tone before and first tone after the dishabituator) but also stimulus specificity (response increment between last tone before dishabituator and dishabituator itself) were evaluated. Additionally, MMN responses between the last tone before the dishabituator (standard) and the dishabituator itself (deviant) have been

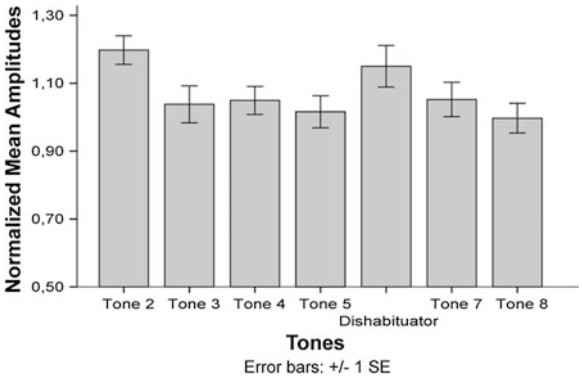

Fig. 4 Normalized fetal amplitudes to tones 2–8 of an auditory habituation paradigm. Mean and standard error are displayed. Figure with permission from Muenssinger et al. (2013)

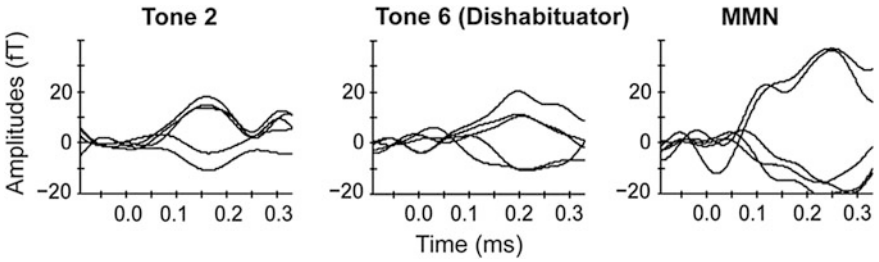

Fig. 5 Amplitude example of tone 2, tone 6 (dishabituator) and the MMN response of one fetus at the gestational age of 36 weeks. The five channels with the highest amplitudes are shown. Figure with permission from Muenssinger et al. (2013)

investigated. Both stimulus specificity and the presence of MMN responses would be an indicator for habituation as reason for response decrement, because sensory fatigue would be stimulus independent. Significant stimulus specificity was found and MMN responses were detected in 50 % of the fetuses (Fig. 5). This indicates that already fetuses in the last trimester of pregnancy are able to show habituation, a basic form of learning.

4.2 State of the Art in Visual fMEG Research

Similar to AERs, VERs have been detected in fetuses as early as in the 28th week GA. In their preliminary study, Eswaran et al. (2002b) presented 180 light flashes to ten fetuses between the GA of 28 and 36 weeks and could show that four of the ten fetuses showed evoked responses to the light stimulation. Using longer

stimulus durations, the response rates could be strongly enhanced. By presenting light flashes with a duration of 100 ms or 500 ms to fetuses starting at 28 weeks GA, a response detection rate of 60 % was found in fetuses between 28 and 32 weeks GA and even a response detection rate of 70 % was found in fetuses between 32 and 36 weeks GA. In the oldest fetuses (36–40 weeks GA), the response detection rate was rather low (28 %). However, different than in responders, it was reported that the position of most of the non-responders was in a way that the eyes were not visible with ultrasound which means that they were turned away from the visual stimulation. Concerning the development of VERs in fetuses over GA, it could be shown that the latencies of the fP200 component decreased with increasing GA. No changes for GA were found for the fP300 component (Eswaran et al. 2004). These results show the possibility to use fMEG to monitor fetal brain development not only using auditory stimulation but also using visual stimulation (Fig. 6).

However, for a clinical setting, the response detection rates are still not high enough. By combining both stimulation types (i.e., by presenting auditory as well as visual stimulation to the fetus), the response detection rate could be enhanced to 91 % (criteria that the fetus showed a response to either one of the stimuli) (Eswaran et al. 2005). In addition to the development of stimulus processing, also studies concerning habituation have been performed using fMEG. Sheridan et al. (2008) investigated the decrement of VERs elicited by trains of four light flashes in fetuses between the GA of 29 and 37 weeks as well as in newborns between 6 and 22 days of age. Newborns showed response decrement from the first to the last light flash. In fetal recordings the response rate was low (29 %), which may be caused by the low signal to noise ratio of visual evoked responses. However, for the fetuses who showed responses, either a decrement from flash one to two or a response for flash one followed by no detectable response for the following flashes were detected. This might at least indicate that response decrement to visual stimuli can be detected in utero. Similar results have also been shown by Matuz et al. (2012), who presented four light flashes to fetuses and neonates but also included an auditory dishabituator in the trains of light stimuli, which was presented after the fourth light flash. Neonatal results showed response decrement between the first and the last light flash as well as response recovery for the dishabituator. For fetal measurements, a low detection rate was found, but a decrement between the VER of flashes one and two could be detected in those fetuses showing VERs. These two studies indicate that newborns born at term show visual response decrement as well as response recovery when an array of repetitive stimuli is interrupted by a novel stimulus. Moreover, there are first indications, that already the fetal brain might be capable of showing visual habituation. However, further research is needed to clearly show visual response decrement in utero and to gain more information about the question if visual response decrement is due to habituation, a basic form of learning, or sensory adaptation/fatigue.

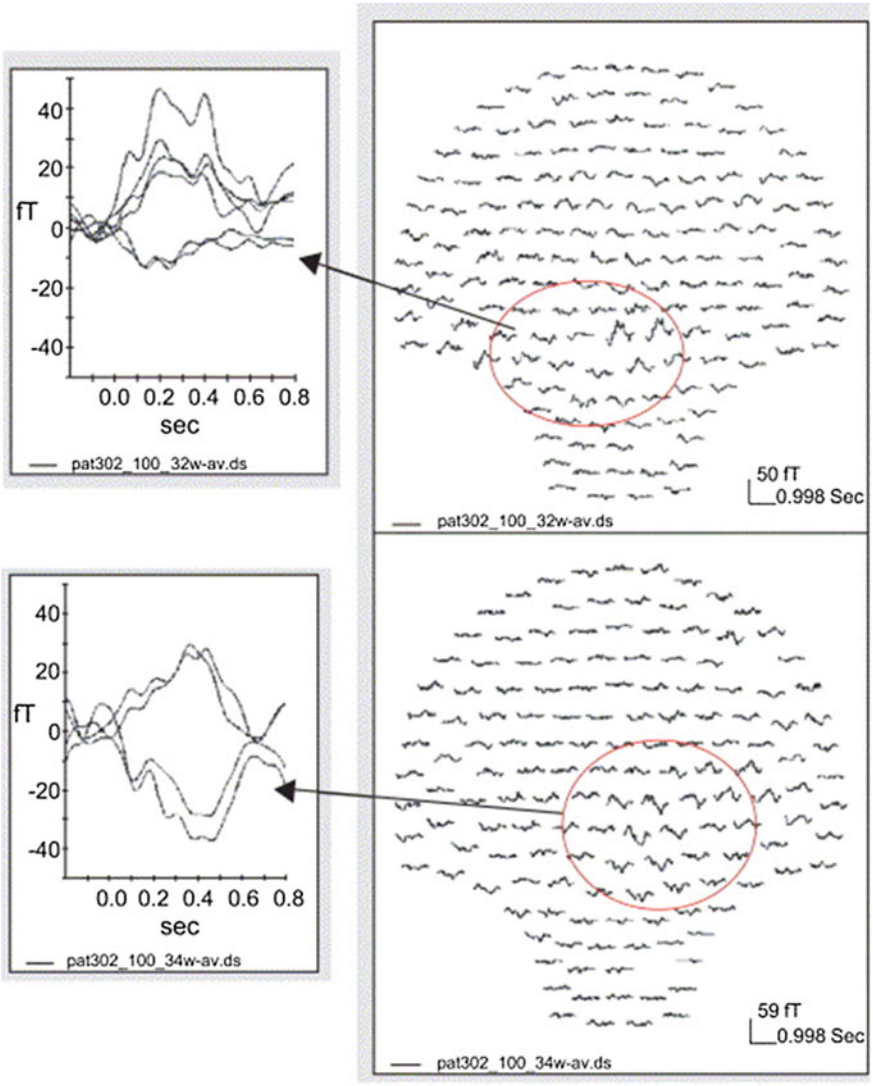

Fig. 6 Averaged VER responses and their locations on the 151 sensor array map from a fetus at 32 (*top*) and 34 (*bottom*) weeks of gestation. The flash duration was 100 ms. Figure with permission from Eswaran et al. (2004)

4.3 State of the Art in Clinical fMEG Research Using Auditory and Visual Stimulation

The knowledge obtained from fMEG research with healthy fetuses and neonates was used to assess clinical questions. In utero, there are different factors which can

influence fetal brain maturation. Intrauterine growth restriction (IUGR) is one factor known to increase the risk for neurologic damage due to oxygen deprivation of the fetal brain as a consequence of placental insufficiency. Therefore, the developmental course of IUGR fetuses is expected to be delayed. Kiefer et al. (2008) used fMEG to investigate fetal brain maturation in fetuses (≥27 weeks GA) who were small for gestational age (SGA), a state defined by a weight below the 10th percentile of the GA age group. In this group, placental insufficiency was expected and validated in 12 of 14 cases through the use of Doppler scans. Results of the SGA group were compared to results of a group of healthy fetuses to assess possible delays in stimulus processing. Both groups were presented with tone burst and AER latencies were evaluated. Results showed longer AER latencies for the group of SGA fetuses in comparison to the group of healthy fetuses. In line with prior studies (Schleussner and Schneider 2004; Holst et al. 2005), a decrement of AER latencies with increasing GA was found in both groups. These fMEG results are a strong indicator for delayed brain maturation in SGA fetuses.

Another factor which may influence fetal brain development is the administration of medication to the mother. Steroids are often administered to the mother to induce fetal lung maturation if premature birth is suspected. However, animal models showed that antenatal steroids involve a delay in fetal brain myelination as well as a delay in fetal brain growth (Whitelaw and Thoresen 2000). Schneider et al. (2011) investigated the fetuses of mothers who received a steroid treatment for medical reasons. Steroids were given at two consecutive days and fMEG measurements were conducted before the first as well as not later than 3 h after the second administration. All fetuses were presented with pure tone stimulation. Results showed a delay in AER responses after steroid administration. Even though steroid administration has been proven to be lifesaving, the results of this study emphasize that they should only be administered when the benefits outweigh the risks.

5 Summary

In the last decades, fMEG opened a new possibility to investigate fetal functional brain development by enabling the direct evaluation of fetal brain responses to different kinds of stimulation. Since the fetal brain is especially vulnerable to internal as well as external influences during that period, knowledge about healthy brain development in utero is needed. Only by knowing how the healthy brain develops, it is possible to detect deviations or delays. Early detection of developmental deviation or delays could enable faster postnatal treatment and therefore improve treatment outcome. Moreover, by examining the harmful effects to the fetus which are induced by maternal medication, the advantages and disadvantages of drug administration can be better weighted, which in turn could also decrease negative neonatal outcomes. Taken together, the fMEG is a promising tool to investigate functional brain development in utero.

References

Arabin B, van Straaten HLM (2006) Fetal and neonatal hearing. In: Kurjak A, Chervenak FA (eds) Textbook of perinatal medicine, 2nd edn. Informa UK Ltd., UK, pp 955–972

Belliveau JW, Kennedy DN, McKinstry RC, Buchbinder BR, Weisskoff RM, Cohen MS, Vevea JM, Brady TJ, Rosen BR (1991) Functional mapping of the human visual cortex by magnetic resonance imaging. Science 254(5032):716–719

Birnholz JC, Benacerraf BR (1983) The development of human fetal hearing. Science 222(4623):516–518

Blum T, Saling E, Bauer R (1985) First magnetoencephalographic recordings of the brain activity of the human fetus. Br J Obstet Gynaecol 92(12):1224–1229

Casey BJ, Giedd JN, Thomas KM (2000) Structural and functional brain development and its relation to cognitive development. Biol Psychol 54(1–3):241–257

Cooper ERA (1945) The development of the human lateral geniculate body. Brain 68:222–239

Counter SA (2010) Fetal and neonatal development of the auditory system. In: Lagerkrantz H, Hanson MA, Ment LR, Peebles DM (eds) The newborn brain: neuroscience and clinical applications, 2nd edn. Cambridge University Press, Cambridge 163–184

Draganova R, Eswaran H, Murphy P, Huotilainen M, Lowery C, Preissl H (2005) Sound frequency change detection in fetuses and newborns, a magnetoencephalographic study. Neuroimage 28(2):354–361

Draganova R, Eswaran H, Murphy P, Lowery C, Preissl H (2007) Serial magnetoencephalographic study of fetal and newborn auditory discriminative evoked responses. Early Human Dev 83(3):199–207

Eswaran H, Lowery CL, Wilson JD, Murphy P, Preissl H (2004) Functional development of the visual system in human fetus using magnetoencephalography. Exp Neurol 190:S52–S58

Eswaran H, Lowery CL, Wilson JD, Murphy P, Preissl H (2005) Fetal magnetoencephalography—a multimodal approach. Dev Brain Res 154:57–62

Eswaran H, Preissl H, Wilson JD, Murphy P, Robinson SE, Rose D, Vrba J, Lowery CL (2002a) Short-term serial magnetoencephalography recordings of fetal auditory evoked responses. Neurosci Lett 331:128–132

Eswaran H, Wilson J, Preissl H, Robinson S, Vrba J, Murphy P, Rose D, Lowery C (2002b) Magnetoencephalographic recordings of visual evoked brain activity in the human fetus. Lancet 360(9335):779–780

Giedd JN, Snell JW, Lange N, Rajapakse JC, Casey BJ, Kozuch PL, Vaituzis AC, Vauss YC, Hamburger SD, Kaysen D, Rapoport JL (1996) Quantitative magnetic resonance imaging of human brain development: ages 4–18. Cereb Cortex 6(4):551–560

Graven SN, Browne JV (2008) Visual development in the human fetus, infant, and young child. Newborn Infant Nurs Rev 8(4):194–201

Henver RF (2000) Development of connections in the human visual system during fetal mid-gestation: a dil-tracing study. J Neuropathol Exp Neurol 59(5):385–392

Hepper PG, Shahidullah BS (1994) Development of fetal hearing. Arch Dis Child 71(2):F81–F87

Hitchcock PF, Hickey TL (1980) Prenatal development of the human lateral geniculate nucleus. J Comp Neurol 194:395–411

Holst M, Eswaran H, Lowery C, Murphy P, Norton J, Preissl H (2005) Development of auditory evoked fields in human fetuses and newborns: a longitudinal MEG study. Clin Neurophysiol 116(8):1949–1955

Huppi PS, Warfield S, Kikinis R, Barnes PD, Zientara GP, Jolesz FA, Tsuji MK, Volpe JJ (1998) Quantitative magnetic resonance imaging of brain development in premature and mature newborns. Ann Neurol 43(2):224–235

Jedrychowski W, Perera FP, Jankowski J, Mrozek-Budzyn D, Mroz E, Flak E, Edwards S, Skarupa A, Lisowska-Miszczyk I (2009) Very low prenatal exposure to lead and mental development of children in infancy and early childhood: Krakow prospective cohort study. Neuroepidemiology 32(4):270–278

Kiefer I, Siegel E, Preissl H, Ware M, Schauf B, Lowery C, Eswaran H (2008) Delayed maturation of auditory-evoked responses in growth-restricted fetuses revealed by magneto-encephalographic recordings. Am J Obstet Gynecol 199(5):503.e501–503.e507

Kretschmann HJ, Kammradt G, Krauthausen I, Sauer B, Wingert F (1986) Brain growth in man. Bibl Anat 28:1–26

Lengle JM, Chen M, Wakai RT (2001) Improved neurpmagnetic detection of fetal and neonatal auditory evoked responses. Clin Neurophysiol 112:785–792

Lenroot RK, Giedd JN (2006) Brain development in children and adolescents: Insights from anatomical magnetic resonance imaging. Neurosci Biobehav Rev 30:718–729

Matuz T, Govindan RB, Preissl H, Siegel ER, Muenssinger J, Murphy P, Ware M, Lowery CL, Eswaran H (2012) Habituation of visual evoked responses in neonates and fetuses: a MEG study. Dev Cogn Neurosci 2(3):303–316

Muenssinger J, Matuz T, Schleger F, Kiefer-Schmid I, Goelz R, Wacker-Gussmann A, Birbaumer N, Preissl H (2013) Auditory habituation in the fetus and neonate - a fMEG study. Dev Sci 16(2):287–295

Muhlhausler BS, Adam CL, McMillen IC (2008) Maternal nutrition and the programming of obesity: the brain. Organogenesis 4(3):144–152

Pinel JP (2003) Development of the nervous system. In: Pinel JP (ed) Biopsychology, 5th edn. Allyn and Bacon, Boston, pp 221–239

Preissl H, Lowery CL, Eswaran H (2004) Fetal magnetoencephalography: current progress and trends. Exp Neurol 190(Suppl 1):S28–S36

Preissl H, Lowery CL, Eswaran H (2005) Fetal Magnetoencephalography: viewing the developing brain in utero. In: Preissl H (ed) Magnetoencephalography. Elsevier Academic Press, San Diego, pp 2–20

Pujol R, Lavigne-Rebillard M, Uziel A (1991) Development of the human cochlea. Acta Otolaryngol Suppl 482:7–12; discussion 13

Querleu D, Renard X, Versyp F, Paris-Delrue L, Crepin G (1988) Fetal hearing. Eur J Obstet Gynecol Reprod Biol 28(3):191–212

Schleussner E, Schneider U (2004) Developmental changes of auditory-evoked fields in fetuses. Exp Neurol 190(Suppl 1):S59–S64

Schneider U, Arnscheidt C, Schwab M, Haueisen J, Seewald HJ, Schleussner E (2011) Steroids that induce lung maturation acutely affect higher cortical function: a fetal magnetoencephalography study. Reprod Sci 18(1):99–106

Sheridan CJ, Preissl H, Siegel ER, Murphy P, Ware M, Lowery CL, Eswaran H (2008) Neonatal and fetal response decrement of evoked responses: a MEG study. Clin Neurophysiol 119(4):796–804

Singer LT, Nelson S, Short E, Min MO, Lewis B, Russ S, Minnes S (2008) Prenatal cocaine exposure: drug and environmental effects at 9 years. J Pediatr 153(1):105–111

Szitanyi P, Janda J, Poledne R (2003) Intrauterine undernutrition and programming as a new risk of cardiovascular disease in later life. Physiol Res 52(4):389–395

Talge NM, Neal C, Glover V (2007) Antenatal maternal stress and long-term effects on child neurodevelopment: how and why? J Child Psychol Psychiatry 48(3–4):245–261

Whitelaw A, Thoresen M (2000) Antenatal steroids and the developing brain. Arch Dis Child Fetal Neonatal 83:F154–F157

Pediatric MEG: Investigating Spatio-Temporal Connectivity of Developing Networks

Kristina R. Ciesielski and Julia M. Stephen

Abstract The extended development of the human brain provides a unique opportunity to study the maturation of cortical networks that subserve sensory and cognitive functions using noninvasive functional neuroimaging techniques. However, considerable challenges have limited the number of functional neuroimaging studies in children. MEG addresses a number of those limitations. MEG provides high temporal and spatial resolution to assess the development of dynamic cortical networks. The technique provides a secure, peaceful testing environment, requires minimal preparation of the child and offers technology to compensate for head movement during scans. We contrast MEG with other functional neuroimaging techniques and describe effective MEG paradigms for testing children. We present MEG as the technique of choice for testing the dynamics of healthy and disordered brain networks.

Keywords Pediatric · Magnetoencephalography (MEG) · Cortical development · Long-range connectivity · Cortical oscillations · Experimental design

K. R. Ciesielski (✉)
Department of Radiology, Athinoula A. Martinos Center for Biomedical Imaging, Massachusetts General Hospital, Harvard Medical School, Charlestown, MA, USA
e-mail: ktc@nmr.mgh.harvard.edu

K. R. Ciesielski
Department of Psychology, University of New Mexico, Albuquerque, NM, USA

J. M. Stephen
The Mind Research Network and Lovelace Biomedical and Environmental Research Institute, Albuquerque, NM, USA

S. Supek and C. J. Aine (eds.), *Magnetoencephalography*,
DOI: 10.1007/978-3-642-33045-2_24,

1 Introduction

Human brain development is a primary focus of research in cognitive neuroscience. The functional imaging technique of magnetoencephalography (MEG), with its superior, millisecond temporal resolution, good spatial resolution and totally noninvasive nature displays all the merits of becoming a leading tool in cognitive studies with children, and yet MEG is rarely used and, as we perceive, undervalued. In this chapter we present evidence that by applying MEG in studies on the developing brain we will attain real-time tracking of distributed long-range cognitive networks and thus gain better insight into brain interconnectivity serving our perceptions, thoughts, feelings and actions (Jaffee and Price 2007; Kandel et al. 2000; Rutter 2006). Since the spatial-temporal distribution of brain signals is a sensitive correlate of brain maturation in health and disease (Bunge and Wright 2007; Casey et al. 2005; Khundrakpam et al. 2012; Stiles et al. 2003; Uddin et al. 2010; Vogel et al. 2010), MEG may provide unique insights into the development of diagnostic, therapeutic and preventive measures (Buzsaki 2006; Hamalainen and Hari 2002).

Magnetic resonance imaging (MRI and fMRI) has been the primary neuroimaging technology used for developmental brain research in children 0–18 years over the last two decades. It has provided a range of findings about brain development including differential development of white and gray matter trajectories (Stiles 2008). It also provided solid evidence of developmental changes across brain regions associated with sensory and cognitive processing (Ciesielski et al. 2006; Durston and Casey 2006; Gao et al. 2009; Tamm et al. 2002). Here, we review outcomes of some of these studies and suggest the possibility for original, complementary contributions from MEG to developmental neuroscience. Recently, developmental studies have shifted towards a dynamic concept of interactive neural connectivity (Atkinson and Adolphs 2011; Johnson 2010; Poldrack 2010). Questions are now asked about the development of long-range neural networks, driven by the principle of non-linear rise-fall of tissue in specialized gray matter modules (Giedd and Rapoport 2010; Sowell et al. 2004), and by concurrent development of white matter that increases monotonically both in volume and density throughout adolescence (Gordon et al. 2011; Hagmann et al. 2010; Loenneker et al. 2011; Paus et al. 2001; Yakovlev and Lecours 1967).

In this chapter we present MEG as a unique tool for studying the developing human brain by direct examination of the temporal characteristics of complex networks that underlie brain function. MEG is a neuroimaging technique that measures the magnetic field generated by the ionic currents primarily within populations of synchronously activated neurons in the brain and the signal arises from the same source as the electroencephalogram (EEG). Both, EEG and MEG, are directly tied in time to neuronal information processing. MEG, however, is unaffected by scalp, skin and, to a large degree, brain tissue inhomogeneities and is, therefore, ideal for testing complex networks in different stages of ontogeny. Since the main attribute of the brain is its dynamic temporal pattern of interactions

between specialized neural modules, the high temporal resolution (millisecond) of MEG offers unprecedented detail for investigation of complex interactive networks. Thus, for this chapter we present a dynamic view of the developing brain as a *spatio-temporal connectome of networks*. In the following sections we first provide neuroimaging evidence supporting such a view of the developing brain and we discuss the use of MEG in several studies targeting long-range functional networks. Then, we describe an optimal MEG data acquisition session with children and discuss the predominant merits of MEG for pediatric research. Finally, we propose future directions for MEG studies with children.

2 The Developing Brain as a Spatio-Temporal Connectome of Networks: Potential of MEG for a Unique Contribution to Developmental Neuroscience

Developmental neuroimaging studies, mostly MRI and fMRI, have demonstrated that the maturation of cognitive functions during ontogeny may result from the fine-tuning of the structural and functional organization of long-range neural networks (Khundrakpam et al. 2012). The majority of MRI research has shown marked structural and functional brain changes between infancy and young adulthood (Stiles 2008). Longitudinal MRI studies of normative children demonstrate a systematic increase of white matter volume but a nonlinear change (rise-fall) in gray matter volume (Gogtay et al. 2004; Paus 2005; Sowell et al. 2002). The tuning of functional networks, first suggested by Changeux and Danchin (1976) and Huttenlocher (1979) was considered an adaptive mechanism for eliminating redundant neural connections. The earliest maturation of cortical layers (as measured by pruning synaptic connections) was first reported in the primary sensory-motor cortex, and only later in higher order association areas, thus suggesting developmental progress in the cortical connections through regressive pruning (Evans 2006; Kuhn 2006). In contrast, the white matter's progressive myelination of axons (Hagmann et al. 2010; Imperati et al. 2011; Tamnes et al. 2010) reflects increased conductivity and speed of information transfer. New studies document coherent changes in cerebral cortical development (Raznahan et al. 2011).

In line with structural findings, functional studies (fMRI) have demonstrated segregation and weakening of short-range local networks, and increasing connectivity and integration of distant regions into functional networks (Dosenbach et al. 2010; Fair et al. 2009). Supportive evidence from fMRI studies with task-evoked activity paradigms mostly conducted in the visual modality (Bunge et al. 2002b; Bunge and Zelazo 2006; Church et al. 2010; Schlaggar et al. 2002; Tamm et al. 2002) have been outnumbered in recent years by studies using resting-state fMRI. The latter reports spontaneous BOLD signal fluctuations in the range 0.01–0.1 Hz that occur without task performance. Often just 4–12 min of data is acquired from each subject. Consistent with Biswal's seminal report on resting

state networks (Biswal et al. 1995) various resting state time-courses reveal connectivity within and between captured networks. For example, significant connectivity is displayed between distant regions of the frontal-parietal network, default mode network, the control attention networks, memory networks (Greicius et al. 2003), and lexical networks (Koyama et al. 2010). The conceptual basis is that certain correlations appear to be strongest between functionally related regions, and this may reflect the past history of co-activation between brain regions and their functional familiality (Van Dijk et al. 2010). Those regions that activate and deactivate at the same time, and therefore show functional time-courses with a significant statistical dependency have been considered to form "a network".

A growing number of studies have utilized the resting state fMRI signal to examine age-dependent changes in well-defined brain networks, both in normative children [e.g. (Fair et al. 2007, 2009; Fransson et al. 2010; Kelly et al. 2009; Stevens et al. 2009; Supekar et al. 2009)], atypical children [e.g. (Gozzo et al. 2009; Myers et al. 2010; Smyser et al. 2010)], and in disease states [e.g. (Church et al. 2009; Cullen et al. 2009; Hampson et al. 2009; He et al. 2007; Jones et al. 2010)]. Since fMRI has low temporal resolution (200–2,000 ms), such a "defined network" remains at a general level of description, raising questions about the phenomena underlying resting-state activity (Kelly et al. 2012). Insight into the temporal interplay between the nodes that form the resting-state network using MEG may greatly improve our understanding of the formation of long-range networks.

We are currently conducting a resting state study on interactions between dorsal and ventral visual networks in young healthy children and children at risk from OCD families, using coherence of MEG oscillatory activity within alpha band [(8–13 Hz) (Ciesielski et al., study in progress)]. Coherence is a frequency-indexed measure commonly used to estimate the power transfer between input and output of a linear system. Thus, coherence between two regions measures the linear relationship between the signals across all time points at a specific frequency. In order for this measure to be relevant, the signals must be stationary, which is not, in general, the case with MEG signals. That is why we epoch our signal in smaller time segments, during which the assumption of stationarity is better justified.

There is a challenge in interpreting MEG data in terms of brain connectivity because of the limited spatial resolution of the inverse solution, activity in one brain region may spread over to other areas in the source estimates. The method proposed by Nolte et al. (2004), focusing on the imaginary part of coherency, effectively overcomes this problem. The imaginary part of coherence is insensitive to 'self-interaction' caused by volume conduction. The imaginary part of coherence is only sensitive to synchronization of two signals, which are time-lagged to each other, whereas estimated signals in two regions that are due to spatial spread caused by the inverse solution will always have zero lag, and thus the imaginary part of the coherence for those signals will vanish. Using our preliminary data on 5 healthy children, age 6–12, and children "at risk", we computed, using measures of alpha-band oscillatory activity (8–13 Hz) the imaginary coherence between

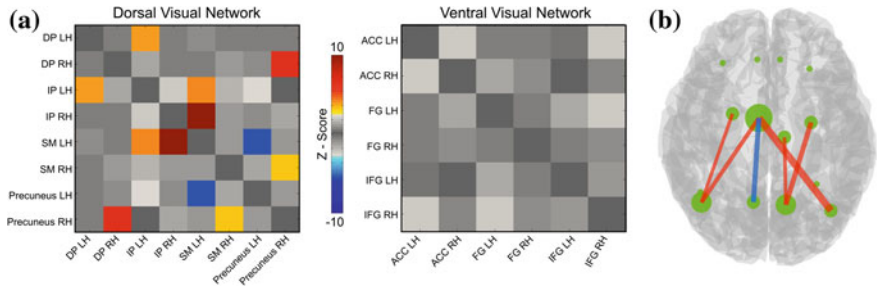

Fig. 1 Resting state MEG for alpha-band oscillatory activity in healthy children and children "at risk" for OCD age 6–12 y (Ciesielski et al. 2013, study in progress)

16 nodes, 8 nodes related to ventral visual network and 8 to dorsal visual network (all derived from fMRI studies). Custom matlab scripts are used for visualization [Khan et al. 2013]. As shown on Fig. 1 the resting-state connectivity is prominent in the posterior cortical regions, where strong alpha power is typically observed in adults (Buzsaki 2006) engaging more significantly cortical nodes (inferior parietal, premotor, dorsal prefrontal, precuneus) within the dorsal visual network, irrespective of age. The preliminary observations suggest also a hypothesis of more prominent maturational differences between healthy children and children "at risk" for OCD within the dorsal visual attentional network as compared to ventral. However, more evidence on the interaction between dorsal and ventral visual networks along the ontogenetic course is needed to verify this observation.

Furthermore, the developmental changes, in both gray and white matter, may be captured by measuring MEG latency in task-related networks. Based on recent studies, it is suggested that nesting oscillations by phase or amplitude of a lower frequency (theta, 3–7 Hz, or alpha, 8–13 Hz) may modulate phase or amplitude of a higher frequency (beta, 13–30 or gamma, 30–60 Hz). It is also suggested that phase-amplitude coupling interacts with local and long-range functional connectivity to integrate information across-networks. A study, employing perception of emotional and neutral faces, has reported reduced local and long-range functional connectivity in autism-spectrum disorders using this approach [Khan et al. 2013].

In summary, although resting-state fMRI studies have provided consistent evidence of correlated changes in spontaneous neural activity within long-range networks, fMRI allows only indirect evidence of brain connectivity. MEG, however, measures the ongoing physiological neural activity in vivo. Because of the high temporal resolution and measurement of specific spectral frequencies, MEG (and EEG) is uniquely suited for measurements of connectivity of groups of neurons within a small envelope of time, thus providing valuable insight into the rapid and complex changes in developing networks.

3 Developmental MEG Studies of Long-Range Networks

3.1 MEG Studies of Stimulus Evoked Responses

This chapter aims to facilitate the use of MEG for investigating network connectivity in children. Below, we present several examples of MEG studies in children. Each study is concluded with a synopsis regarding the contribution of MEG technology in attaining the aims of the study. It is important to realize that most of the studies employing MEG in pediatric populations are used with a clinical aim and focus on neurological conditions, such as mapping focal or multifocal interictal epilepsy. In this capacity MEG is routinely used for preoperative assessment of somatosensory, auditory, visual and language areas for presurgical mapping. The main goal is to improve postoperative patient outcome (Schwartz et al. 2010). There are numerous MEG reports from clinical studies in epilepsy. These are the focus of another chapter in this volume (see Ivasaki and Nakasato, Chap. 39).

Early pediatric MEG studies focused on sensory processing. For example, Paetau et al. (1995) evaluated the characteristics of the auditory M100 in typically developing children in response to speech and non-speech stimuli. The reported reduction of the M100 latency in children age 3–15 years was suggested to be due to a longer refractory time in the auditory cortex, mostly over the right hemisphere (Rojas et al. 1998). The maturational changes in latency of M100 have also been used to investigate processing of low and high frequency tones in children with Autism Spectrum Disorder (ASD) and in healthy children (Gage et al. 2003a, b). A delayed activation in the auditory cortex in ASD as compared to controls was found. The annual rate of latency reduction with age was slower in the ASD group than in controls, suggesting a continued maturational deficit in autism. Furthermore, we have recently identified a systematic delay in auditory processing in children with fetal alcohol spectrum disorders (Stephen et al. 2012). This finding suggests that sensory processing deficits may be a nonspecific marker of atypical brain development across developmental disorders. The above studies indicate that timing of cortical processing is a critical marker of brain maturational progress and therefore millisecond resolution of MEG measures is invaluable here. In agreement, Roberts (2009) provided evidence for a direct link between white matter development in the auditory white matter tracts and decreases in MEG latency with increasing age. Our results from a younger cohort of children aged 6–50 months provides additional evidence of a linear decrease in latency and evolution of the morphology of auditory evoked responses in very young children (see Fig. 2).

MEG studies have also characterized the development of the somatosensory response across age. Most notably Pihko et al. (2009), Pihko and Lauronen (2004) described the emergence of the characteristic peaks of the somatosensory response in infants relative to children and adults. Additional studies indicate atypical brain development based on abnormal somatosensory responses in children with autism spectrum disorders (Marco et al. 2012), children with cerebral palsy (Kurz and Wilson 2011), and in children born prematurely (Rahkonen et al. 2013).

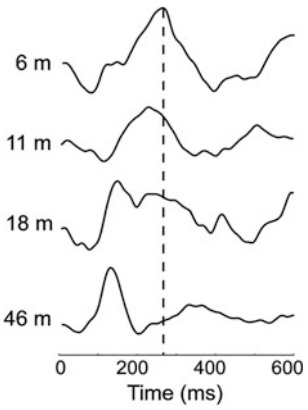

Fig. 2 Auditory evoked responses during sleep in children aged 6–50 months. A linear progression of decreasing latency was observed across 35 healthy children. (Stephen et al. Developmental Neuroscience, submitted)

Most of the reported pediatric MEG studies focused on cognitive development search for magnetic sources of cortical activity associated with a task. The scalp location of magnetic signals and their coherent changes in distant cortical regions inform researchers about interacting components of cognitive networks. In one study facial stimuli were employed to examine preferences to faces from early childhood (6 y) through young (20–30 y) adulthood (Taylor et al. 2011). Over 200 faces were presented within a 1-back working memory task. The high temporal resolution of MEG permitted careful control of time of onset for cortical components (including face-specific M100 and M170). Contrast between those signals synchronized in time offered an important insight into the location of cortical activity associated with developmental changes in memorizing facial stimuli. The M250–600 ms peak was prominent for repeated faces across all ages and all frequency windows, and larger in the right temporal region including the hippocampus. Thus, well-developed facial recognition is present early in childhood. The engagement of the ventral prefrontal cortex, well documented in memory processing in adults, only became significant in later childhood. Generally consistent with these findings are results from another MEG study pointing to protracted development of face processing until adolescence (Kylliainen et al. 2006). The authors presented stimuli of faces and motorbikes in a visual consecutive matching task in boys 8–11 and young adult men. Although MEG activation in the right ventral occipital-temporal region was engaged in both groups at 100 and 135 ms (M100, M135), the primary evidence for face sensitivity in this region came only from a consistent and narrow timing difference between the responses to faces and motorbikes.

3.2 MEG Studies of Brain Oscillatory Activity in Children

Research by others and by our team indicates that neural oscillations are critical for understanding developmental processes within and between brain networks. Indeed, spectral analysis has long been used to characterize brain development in

children mostly using EEG (Case 1992; Klimesch et al. 2001; Krause et al. 2007). A change in amplitude or phase of a single oscillation reflects a change in local neural processing, while amplitude and/or phase correlations (e.g. synchronization) between two distant oscillations reflect the functional connectivity between two neural populations (Buzsaki 2006). An important theta-alpha-beta EEG study in children and adolescents revealed an age-dependent pattern of oscillatory changes (Uhlhaas et al. 2009). These changes involve gradually increasing neural synchrony across childhood followed by an unexpected decrease in synchrony in later adolescence, paralleled by lower performance. The finding is of significance for diagnostic and treatment approaches in child psychopathology, and needs to be further investigated using MEG. Although a considerable number of studies have been completed on oscillatory activity in children using EEG, very few were done with MEG. The general consensus is that the MEG signal is more pure as it is not distorted by skull or skin artifacts, has the advantage of better spatial localization (Papanicolaou et al. 2005a, b) and is superior in analysis of coherence within and between networks (Hamalainen and Hari 2002; Srinivasan et al. 2007). It offers, therefore, unique insight into the mechanism of brain development. For example, our recent MEG study showed a clear increase of mu rhythm frequency in children from 3 months to 5 years of age relative to adults with the most rapid development occurring in the first year of life (Berchicci et al. 2011). This is in line with earlier spectral EEG studies in children (Orekhova et al. 2006; Yordanova and Kolev 1996). Fewer EEG studies have been performed on the sensorimotor mu rhythm, in part because it is only sporadically identified with consistent identification in standard clinical EEG in only 10 % of individuals (Fisch 1991). It has been observed that the generators of the mu rhythm are oriented in the cortex in such a way that MEG is more sensitive than EEG to the sensorimotor mu rhythm. However, further research is needed to explain the developmental significance of this increase in frequency with age and the mu rhythm's role in the development of imitation skills in young children.

Even more rare are studies investigating developmental changes in spectral oscillatory activity in children performing visual working memory tasks. Among different oscillatory spectra the alpha band is the earliest to develop, most robust in children and displays a clear relationship to the inhibitory brain network (Klimesch et al. 2007; Kolev et al. 2002; Krause et al. 2007; Yordanova et al. 2001; Yordanova and Kolev 1996). Alpha oscillations have been associated in adults with top-down inhibitory control and the frontal–parietal network. We recently examined developmental differences in top-down cognitive control by monitoring MEG event-related desynchronization (ERD) and event-related synchronization (ERS) of alpha-band oscillatory activity (8–13 Hz) during the anticipation stage, target detection stage and post-response stage using a visual working memory task, the Categorical N-Back [CNBT; (Ciesielski et al. 2004, 2006, 2010)]. CNBT was validated in our fMRI studies (Ciesielski et al. 2006), which revealed prime activation in the inferior frontal cortex in adults, but significantly less prominent in children. Children, however, had stronger activation than adults in the striatum and posterior cerebellum (Fig. 3a). For details on CNBT see Sect. 6.4. in this chapter.

Full head MEG was recorded from healthy 10-year-old children and young adults, and analyzed with a focus on the frontal-parietal attention network. Figure 3b illustrates the alpha modulation at different temporal stages of the CNBT in children as compared to adults. Whereas adults showed a modulation of the ERD at the anticipatory stages of CNBT and ERS at the post-response stage, children displayed only some anticipatory modulation of ERD but no ERS at the post-response stage, with the alpha-band magnitude remaining in a desynchronized state. Since prior neuroimaging findings indicate that the prefrontal–parietal networks are not fully developed in 10-year olds, and since the children performed as well as the adults on CNBT and yet displayed different patterns of ERD/ERS at different time points of the categorical n-back task (Fig. 3c), it has been suggested that children may be using different top-down cognitive strategies and, hence, different, developmental-stage appropriate neuronal networks (Ciesielski et al., 2006, 2010). One needs to emphasize that top-down cognitive control develops as a result of interaction between top-down and bottom-up networks (Friston and Price 2011; van Essen et al. 1992), and thus new MEG paradigms integrating both measures need to be developed for testing children.

Banaschewski and Brandeis (2007) have recently summarized the findings on developmental patterns in oscillatory brain activity noting a decrease in low frequency activity (delta and theta) and an increase in alpha and beta activity with increasing age. Developmental aspects of gamma have been studied less, but are reliably implicated in feature binding (Csibra et al. 2000; Taylor and Baldeweg 2002). Many of the developmental studies have focused on the evolution of sleep patterns throughout development (Danker-Hopfe 2011). Despite differences in spectral patterns across multiple developmental disorders, EEG measures have not reached the threshold to definitively differentiate disorders or to predict long-term outcome (Cantor and Chabot 2009; Rothenberger 2009).

A new focus on spectral analysis in fMRI and the additional temporal resolution afforded by MEG/EEG has led to an increased interest in spectral analysis in EEG and MEG studies to better understand the interaction between resting brain rhythms and cognitive functioning. Recent MEG and EEG studies have also emphasized the importance of accounting for resting brain rhythms in the context of evoked responses (Fujioka and Ross 2008; Kolev et al. 2002). Fujioka and Ross (2008) reported hemispheric differences in alpha desynchronization following pure tones or musical stimuli suggesting that the amount of desynchronization may provide a hemisphere specific measure of brain development. Rojas (2006) also identified an exponential increase in the auditory 40 Hz steady-state response in children providing a potential marker for normal brain development. Recent reviews (Cantor and Chabot 2009; Rothenberger 2009) report evidence that EEG oscillatory measures may play an important role in guiding diagnosis, prevention and treatment of developmental disorders. We postulate that MEG can further facilitate these translational efforts, by better identifying deficits in the spatio-temporal connectome of networks to improve brain functioning in individual

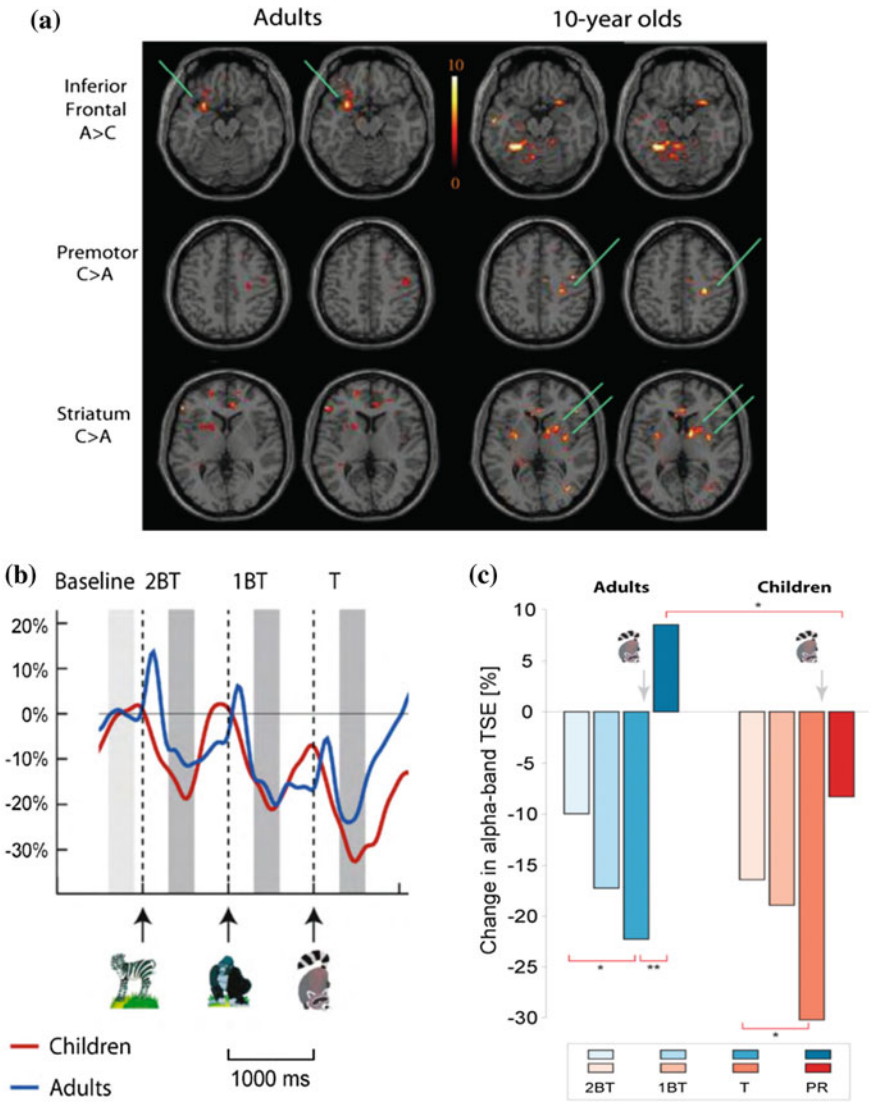

Fig. 3 **a** CNBT has been validated in fMRI studies with adults (*A*) and children (*C*); Of note are the age-dependent differences in task-related networks; **b** Changes in MEG alpha-band Temporal-Spectral Evolution TSE [%]. The normalized TSE waveforms show task-related changes in alpha-band activity; **c** Changes in alpha band: BT-before the target, *T*-Target-raccoon; *PR*-Post-Response; TSE changes calculated in relation to the Pre-2BT baseline; *$p < 0.05$; **$p < 0.001$. Ciesielski et al. (2006, 2010)

children. Future studies will also continue the work linking genetics with cortical oscillatory activity (Begleiter and Porjesz 2006) to identify endophenotypes of developmental disorders.

4 MEG Studies: Challenges Specific to Studies with Children

4.1 MEG: Preparation and Acclimation of Children for Testing: Significance of Parent-Researcher-Child Relationship

MEG has now been used for over a decade to perform clinical diagnostic evaluations in children, but only recently for pediatric research. Excellent communication and trust between the parent, researcher, and child are the prime markers of success in neuroimaging research with children. We, therefore, schedule additional time at the beginning of each MEG session to familiarize both the parent and the child with the study details and testing environment. We describe below several strategies we employ in our pediatric neuroimaging studies to optimize testing for children.

4.2 MEG: Data Acquisition and Processing

Data acquisition is the most important part of any neuroimaging study, since errors committed at this stage are irreversible. Often the participating child is available just for one session. Among the factors that determine whether relevant and valid data have been collected include: clarity of the scientific question and hypothesis, and the pre-selection of a representative subject population. Helpful discussions of those and other factors relevant to studies with children have been published in recent years (Burack et al. 2004; Byars et al. 2002; Cheour et al. 2004; Gaillard et al. 2001; Hansen et al. 2010; Karmiloff-Smith 2010; Kotsoni et al. 2006; Picton et al. 2000; Poldrack 2010; Taylor and Baldeweg 2002; Taylor et al. 2012).

4.3 MEG: Data Acquisition in Infancy

In infants and toddlers [age 6–24 months], an optimal data acquisition is performed during sleep. Multiple studies have confirmed that sensory responses can be probed during sleep with some changes in peak latencies and a reduction in amplitude of later peaks [(Lutter et al. 2004; Pihko et al. 2004)]. Neonatal studies are presented in a separate chapter in this volume (Münbinger et al. in Chap. 23). Importantly, sleep stages mature towards an adult pattern by 6 months of age making it feasible to perform developmental studies across children >6 months while maintaining a constant arousal level across groups and participants. The parent is actively involved and a number of strategies are used for attaining sleep

in young children, all aimed at comfort and safety. Infant/child safety must be ensured to reduce the risk of a child rolling off the MEG system beds as only a few are designed with barriers. Some infants may fall asleep better while being held. It is important that the study begins promptly when sensitivity to touch is reduced, as sleep cycles are short in infants ($\sim$20 min before they rouse/reposition).

If the MEG study is to be performed while the infant is awake, it is important to schedule the time of day when the infant is most alert with a feeding scheduled immediately prior to the study. Infants are sensitive to diurnal patterns and therefore optimizing the chance for an attentive infant is well worth the effort. Patience of the researchers and parents is a valuable determinant of successful data acquisition. Optimization of the study procedures by eliminating unnecessary steps and having well-trained staff is essential.

4.4 MEG: Data Acquisition in Early Childhood

Young children [ages 3–10 years] are apprehensive of new experiences. Thus, providing the parent, in the presence of a listening child, with comprehensive and friendly study information provides important comfort for a child. To secure child collaboration we designed a specific neuroimaging protocol, for both, MEG and MRI laboratory environments. The protocol reduces movement artifacts and remains enjoyable for the child across the testing sessions. The main highlights of our protocol are: (i) acclimation session conducted a couple of hours prior to MEG or MRI scanning; (ii) relaxation session conducted directly before entering MEG or MRI testing rooms, and (iii) information session with a parent and child about safety and the meaning of MEG and MRI technology. In relation to acclimation, some laboratories use a mock MRI scanner a day or two before testing. In our experience mock MRI may not always work well for young children as upon detecting the difference between the mock and the real scanner, the youngsters may refuse participation. Thus, we conduct the acclimation session in the same MRI scanner the day the study is run. There are no mock MEG helmets, thus exposing the young participant to the actual MEG laboratory environment is the most effective priming technique. Muscle relaxation session is conducted immediately before entering the scanner. Children respond well to instructions of control of targeted groups of muscles. The playful approach to the study effectively substitutes the child's fear with curiosity, and develops trust to the experimenter. Imaginary play is typical in young children, and the testing session may be turned into a game with the children imagining themselves as astronauts, etc.

The influence of emotional state, and in particular the level of anxiety in a child and his/her parent are powerful confounds during testing. It is our experience that healthy children who evaluate the laboratory visit as less enjoyable generate higher activation in prefrontal brain regions, despite having comparable performance accuracy to children who enjoyed the study. The relaxation session with children leads to reduction of generalized frontal activity (KRC unpublished data from

MEG and fMRI studies). We agree with Hinton (2002) about the importance of maintaining high ethical standards in performing pediatric neuroimaging studies. The consent to participate by the parent and child frequently needs individualized explanations.

4.5 Time-Table for MEG Studies with Children Age 5 and Older

To benefit also from the spatial sensitivity of MEG, a range of available source estimation methods can be used to map MEG sensor data to the source-cortex in each child individually, thereby requiring an MRI in addition to the MEG data. The optimal course of events in MEG studies is to schedule both MEG and a short MRI session within proximity of a couple of hours, with an MEG session *always* conducted first. It is preferable to schedule neuropsychological testing, for the following day. The novelty of the MEG and MRI imaging environment is often taxing to a child and they need to relax before attending to multiple tasks of a neuropsychological battery. Thus, a 2-day schedule appears optimal for a pediatric MEG study: ***First day***: (i) Study consent and assent; (ii) Acclimation sessions for MEG ~10 min and for MRI ~10 min; (iii) Development of child/parent/researcher rapport [including sensory evaluation, demographics, and question/answer session] takes ~30 min; (iv) MEG data acquisition (with preparation) ~40–60 min; (v) Break 30 min; (vi) Anatomical MRI (with preparations) ~30 min; ***Second day***: (i) Psychiatric/clinical evaluation ~1 h; (ii) Resting break ~1 h; and (iii) Neuropsychological testing ~2 h with resting breaks; (iv) Debriefing session with parents and a child.

5 MEG in Children: Technical Considerations

5.1 Helmet Positioning

It is a continuous challenge to optimize signal strength in pediatric studies since the adult MEG systems are not optimized for children. For example, children find it uncomfortable to keep their head back in the helmet and may compromise data quality in the posterior cortex by bringing their head forward. MEG studies in infants are conducted mostly in the supine position. Alternatively, infants 6–18 months of age may sit in an MEG compatible child seat (Imada et al. 2006). We have found that the supine position works well for children up to 5 years of age (Stephen et al. 2012) by allowing the child to better see investigators in the room in addition to the benefit that the head naturally lays in approximately the same position between transient movements due to the concave shape of the helmet.

Finally, continuous head position monitoring provides an important advantage for pediatric studies (Stephen et al. 2012; Wehner et al. 2008). By approximately 5 years of age, MEG data may be collected in the upright position, in agreement with the child's preference.

5.2 Head Position Indicator Coils

Use of head position indicator (HPI) coils is important to determine where the head is relative to the sensor array in all MEG studies. However, placement of the HPI coils is a greater challenge in children. HPI coils placed on the forehead or neck in young children may be located below the sensor array making the HPI coil position unreadable during data collection. Therefore, we place the HPI coils on the EEG cap, in the case of simultaneous MEG and EEG data collection, or HPI coils are taped to a snug fitting cap that is secured to the head. The cap must be sufficiently taut to ensure that the relative position of the HPI coils does not change with child movement. Beginning from age 5 a child can comfortably sit in the MEG with the HPI coils generally taped along the hairline.

5.3 Bipolar EEG Channels

Bipolar EEG electrodes are used to monitor eye movement, cardiac signal and chin movement in young infants to monitor sleep stage (Fisch 1991). Additional bipolar EEG channels can be used to monitor muscle activity. Based on the robust eye movements and cardiac signals, only mild removal of skin oils is sufficient in infants and young children. We use medical paper tape for attaching facial electrodes so that it can be removed from the skin without distress. Baby oil or commercially-available tape removal swabs provide the best means for removing tape. For older children standard electrode placement is sufficient. However, in childhood disorders with sensory sensitivities electrode placement should be minimized.

6 Examples of Tasks Useful in Pediatric MEG Studies

6.1 Design of Passive Paradigms for Infants

Since infants cannot follow explicit instructions, MEG protocols for infants need to encourage natural behaviors or employ a passive design. Passive designs have been used to track sensory development during sleep in young neonates (see chapter on Designing MEG Experiments by J. Stephen in Chap. 5). Other work

has been performed in older infants in the awake state [e.g. (Imada et al. 2006; Johnson et al. 2010, 2013; Wakai et al. 2007)]. Our approach is to track the child's behavior during the task using: (i) MEG-synchronized video recording to allow for post-processing of behavior with respect to task stimuli and brain function, and (ii) Physiological monitoring, such as monitoring respiration, heartbeat, and supplementary bipolar EEG electrode placements. Standard sleep electrodes are recommended for sleep stage characterization in children who sleep during the protocol. Protocols for young children can include explicit tasks, but require succinct tasks that are designed with young children in mind.

6.2 Sensory Tasks

With some modifications of adult protocols, standard sensory tasks can be presented very efficiently when a child is alert and cooperative. Since cortical processing in children is slower than adults, the inter stimulus interval must be longer to obtain the full sensory response (including the later components). For example, Pihko et al. (2004) recommends an ISI $\sim$2 s for young children. One approach to record data for longer periods of time employed in both child and adult studies is to present a silent video [children: (Oram Cardy et al. 2008; Stephen et al. 2012); adults: (Huttunen et al. 1999; Korvenoja et al. 1999)]. The silent movie while passively activating the visual system is not synchronized to auditory or somatosensory stimuli. It is now recognized that attention impacts even basic sensory responses (Donohue et al. 2011), therefore attention components may be modulated by observation of a video. Our experience is that videos help to calm children and allow for 15 min of data collection in children as young at 2–3 years of age.

Very few basic visual MEG studies have been performed in children. While visual stimuli can be engaging for infants, they become fast disinterested in repetitious stimulus presentation. However, basic visual studies are important for investigating both healthy and disordered brain development. For example, an increase in occipital cortex sensitivity to visual stimulus onset asynchrony has been reported in young children with autism relative to healthy control participants using MEG (Falter et al. 2012). In another study, significant delays in the primary visual cortex response in adolescents with fetal alcohol spectrum disorders (FASD) are reported during a pro-saccade task with greater delays to peripherally versus centrally presented stimuli (Coffman et al. 2012). These results indicate basic sensory processing deficits in developmental disorders and thus encourage studies of the visual system using MEG. Refinement of remote MEG-compatible eye-tracking systems, that accommodate head movement, may provide the necessary technical support to enable future visual studies in children aged 3 and younger.

6.3 Motor Tasks

Among motor tasks, a standard finger lift task can be implemented to study the motor network displaying beta and gamma oscillations (Wilson et al. 2010, 2011). Huo et al. (2011) describe high gamma in children through a simple unilateral finger lift task. Furthermore, we have employed an imitation, squeezing task in infants and young children (Berchicci et al. 2011), which allows the infant to make use of their natural tendency to reach and grasp presented objects. By making this a game with the child, one can monitor mu rhythm ($\sim$10 Hz) modulations based on the child's motor activity and their observations of the investigator performing a similar task. We also use bipolar EEG electrodes to monitor arm muscle activity in the infant to help determine when the child is resting or actively responding. Despite these studies, very few motor studies have been designed for MEG because muscle activity contaminates the MEG signal. Therefore, children must be carefully trained to limit their movement to the chosen hand/finger during the task.

6.4 Cognitive Top-Down Control Tasks

Effective working memory is a fundamental marker of healthy cognitive development. Working memory refers to time-limited processing of an active representation of information, which is accessible for recall or for further manipulation (Baddeley 1986). In other words it is an outcome of sustained attentional focus on task-relevant mental representations and on suppression of competing distracting events (Engle et al. 1999). Effective use of mental representations, actively held "on line", has been found to be critical for behavioral and cognitive flexibility (Gevins and Smith 2000; Goldman-Rakic 1987) and is a sensitive marker of cognitive development. A variety of working memory tasks have been used in classical developmental studies and more recently in pediatric neuroimaging, mostly fMRI (Berl et al. 2006; Bunge et al. 2002b; Gabrieli et al. 1998; Nelson et al. 2000; Owen et al. 2005; Taylor et al. 2011). The major aim has been identification of cortical activation maps over the course of development, and in particular the contribution of late maturing prefrontal networks. However, dynamic changes of the developing brain could be specifically examined through the temporal properties of the cortical long-rage networks and their spatio-temporal engagement at each stage of the working memory task: encoding, retention with distractor and retrieval. Here the role of MEG with its total noninvasiveness and high time resolution is unique and invaluable. Event-related MEG recordings provide an accurate timing of different sensory and cognitive processes, and increase our insight into the temporal organization of different stages of the working memory task.

Among tasks conducive to the MEG environment we suggest two in particular: the Delayed Matching-to-Sample Task (DMST) and the N-Back working memory task, both permitting accurate timing of attentional and memory processes that are

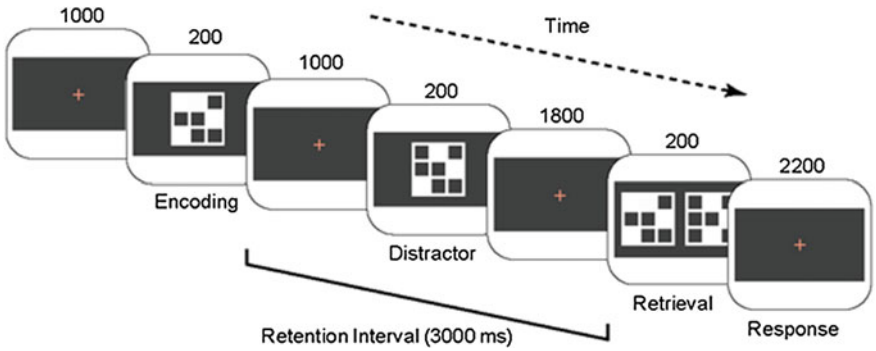

Fig. 4 DMST-WD: Visual-Spatial Delayed Matching-to-Sample Task with distractor (Ciesielski et al. 2005, 2007, 2012)

changing during developmental course. Distinct stages of DMST (encoding, retention and retrieval) belong to these memory processes and attentional processes include top-down inhibitory control of interference and set-shifting. For DMST two variants of the task are available: DMST with distracter (DMST-WD) and without distracter (DMST-ND). Figure 4 presents the DMST-WD sequence of events. Classified by the leading cognitive processes involved, DMST is sometimes labeled as a "delayed recognition" task. We found the following time parameters as the most effective in using the DMST-ND in older children (age 8+) and adolescents: (1) Encoding phase with presentation of a black and white checkerboard sample-stimulus for 200 ms duration and 1.5 × 1.5 visual angle; (2) Retention of about 3,000 ms, and (3) Retrieval involving presentation of two checkerboard patterns (200 ms duration), one identical to sample stimulus. The child is to indicate which of the two patterns is matching the sample-stimulus by pressing a button with the right index finger as fast as possible. The response is counted, if the button is pressed before the beginning of the next trial (2,000 ms window). The DMST-WD is identical to the above version with ND, except that a distracter pattern (200 ms duration), very similar to the stimulus-sample, is presented at the beginning of the Retention phase, 1,000 ms post presentation of the sample-stimulus. The total duration of the Retention phase in DMST-WD is 3,200 ms.

DMST requires effective top-down inhibitory control of events to empty the memory buffer after each single sample-stimulus trial is presented in order to be able to encode the new complex sample-stimulus and to refrain from processing any interfering stimuli during the retention period (e.g. the distracter stimulus) and to correctly identify the sample-stimulus (Ciesielski et al. 2005, 2007, 2012). Thus, MEG with its high temporal resolution (ms) is well suited to examine cortical responses related to the three consecutive phases of the DMST, encoding of the sample-stimulus, retention, and retrieval. In estimating the current brain sources underlying the MEG responses in the DMST task, we employ the minimum-norm

estimates constrained to the cerebral cortex (Dale et al. 2000; Dale and Sereno 1993; Hamalainen and Ilmoniemi 1994). This approach allows user-independent automatic computation of the source estimates and is especially suitable for analyzing complex patterns of activation expected in a multistage cognitive task like DMST.

The network of areas activated by DMST include the lateral and ventral occipital areas, the insular region extending towards the prefrontal orbital cortex, superior temporal sulcus, dorsolateral prefrontal cortex (BA6/8/9 and SFS) and posterior–inferior parietal cortex. It is remarkable that the ROIs which we have chosen for investigation based on adult human fMRI studies of visual–spatial working memory tasks (Courtney et al. 1998; Haxby et al. 2000; Smith and Jonides 1998), showed such a close correspondence to the MEG activation by DMST in adolescents. Moreover, the network of regions (prefrontal, parietal, insula, superior temporal sulcus) related to executive control in adults (Bunge et al. 2002a; Cohen et al. 1997; D'Esposito and Postle 1999; Jonides et al. 1998; Petrides 2000) is crucial to understanding the development of the inhibitory mechanism in developmental disorders.

The N-back working memory task remains one of the most inspirational and most frequently used paradigms in cognitive neuroscience. The simple, elegant design of the task reflects the working memory concept as an integral cognitive operation with an active "on-line" short-term information storage that is cueing the cognitive process and the behavioral response (Gevins and Cutillo 1993). We designed a variant of the classical N-Back task, the Categorical N-Back task [CNBT] (Ciesielski et al. 2004, 2006, 2010). CNBT contains the challenging component of fast "on-the-go" categorical concept formation, a process that may be tracked in time. CNBT performance requires a two-step executive process, first the formation of a categorical concept by comparing each object to a categorical prototype, and second, a comparison between the categorical properties of objects presented consecutively within n-trials prior to the designated target. The memory demands in CNBT, therefore, in contrast to the classical N-Back, remain constant, while the challenge to mental flexibility is emphasized.

Figure 5 illustrates the object Categorical N-Back Task (CNBT). Images of animals and non-animated objects were presented sequentially. Each consecutive image was presented for 500 ms, except for a blank screen that lasted 1,000 ms. The subjects were asked to press one of two buttons whenever an image of a raccoon (target, T) appeared: right button if the two images preceding the target (2BT) belonged to the category of animals, and left button if they belonged to other categories of stimuli. The total time available for the subjects to respond to the target is 2,000 ms. CNBT is appreciated by children, as it has the primary characteristics of an interesting computer game.

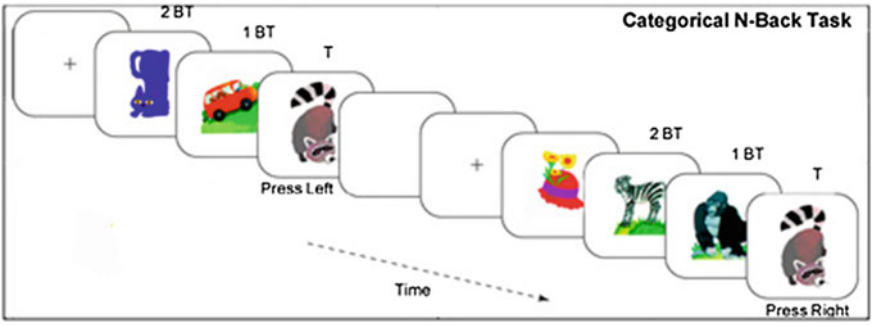

Fig. 5 CNBT *Categorical N-Back Task* (Ciesielski et al. 2006, 2010)

7 MEG: Processing of Pediatric Data

Although the approach to MEG data processing in pediatric studies depends on the question that is being posed, the standard stream of data processing is applied first in most pediatric studies. Therefore, signal averaging is required if one is characterizing the evoked response to one stimulus or a set of stimuli. This requires that the paradigm be designed in such a way that one can present a sufficient number of trials for each condition that the child can enjoy the task and yet allow the researcher to obtain a good signal to noise ratio of the evoked response for each condition.

7.1 MEG: Analysis of Source Activity in Children

Descriptions of source analysis techniques are covered in detail in other chapters in this volume. These will include minimum-norm estimation (MNE) using Statistical Parametric Mapping (Dale 2000; Hamalainen and Ilmoniemi 1994) and dipole modeling. One challenge for source analysis is obtaining individual MRIs due to the severe restrictions on movement during the MRI scan. Although it is optimal to obtain individual MRIs for MEG source analysis, a number of studies have used template MRIs and many source analysis packages provide template MRIs (e.g. Brainstorm, Besa, Curry). Furthermore, pediatric MRI templates are available for research purposes through NIH Pediatric MRI database [4–18 years] http://pediatricmri.nih.gov/nihpd/info/index.html—also available at: http://www.nitrc.org/projects/pediatric_mri/; Neurodevelopmental MRI Database [infant–4 years] http://jerlab.psych.sc.edu/NeurodevelopmentalMRIDatabase/.

Employing source analysis in pediatric studies allows one to fully utilize the strength of MEG by obtaining information about the location *and* the timing of activity. This is important for both normative studies in normal children and for

understanding developmental disorders. For example, developmental studies of auditory processing have identified peaks with different latencies across the pediatric age span (Paetau et al. 1995). While this progression is consistent with the process of white matter myelination, it appears that MEG components within a specified latency window may represent different activations across age and may be differentially impacted by stimulus parameters (e.g. interstimulus interval, auditory stimuli characteristics, language vs. tonal stimuli). With such variability, it is challenging to generalize findings across studies and across developmental disorders. Source analysis helps to clarify these differences by identifying the cortical source associated with waveform peaks to determine if the auditory cortex is exclusively involved in auditory processing or if other areas are also involved (Kotecha et al. 2009; Lutter et al. 2006; Roberts et al. 2009). Similar challenges are apparent across the sensory [e.g. somatosensory (Pihko et al. 2009)] and cognitive domains (Ciesielski et al. 2006; Horiguchi et al. 2003; Trainor 2012). MEG source analysis has improved our understanding of language processing and reading difficulties in pediatric studies [e.g. (Heim et al. 2000; Simos et al. 2011; Wehner et al. 2007)]. Furthermore, the improved techniques of MEG source analysis have increased successful treatment in pediatric epilepsy (Pataraia et al. 2008; Stefan et al. 2003).

7.2 MEG: Analysis of Oscillatory Activity in Children

The analysis of pediatric oscillatory activity is performed using the same tools applied in adult data including standard spectral analysis, coherence analysis, time-frequency analysis, and phase locking (Jensen et al. in Chap. 17). However, oscillatory activity develops rapidly across childhood, requiring that time and frequency windows and oscillatory power must be accounted for during the analysis and interpretation of results from children of different ages. For example, a developmental study designed to assess resting brain rhythms (e.g. occipital alpha or central mu rhythm) will benefit from employing a paradigm that assesses oscillatory reactivity (eyes open/eyes closed for occipital alpha or rest vs. active for sensorimotor mu rhythm). This has been addressed in our recent mu rhythm study by first empirically identifying the subject-specific mu rhythm based on motor reactivity from active to rest conditions (Berchicci et al. 2011). Caution is advised in interpretation as other processes or resting brain rhythms may overlap due to differential development of oscillatory rhythms or spatial congruency between the resting brain rhythm of interest and other confounding oscillatory activity. Finally, applying source analysis to the spectral data (e.g. using a Beamformer approach) will provide important insights into the role of resting state brain rhythms in developmental disorders.

8 MEG Versus Other Measures for Tracking Brain Development in Children: PET, fMRI, EEG

Here we assert that MEG is the most effective functional neuroimaging technique for pediatric studies as it balances the factors of safety, comfort and provides unique insight into temporal characteristics of MEG data, essential for developmental research. The two factors that we consider to be of utmost importance in pediatric studies are: (1) Low stress environment; it is important that the technique does not introduce sustained anxiety. Some apprehension in children is normal in new environments, however, one needs to be able to reliably redirect the child's attention to the task at hand across patient groups to obtain meaningful data. (2) Safety. The technique must be non-invasive. To fully study development it is important to obtain data not only from children with a specific developmental disorder, but also from healthy control children. As a protected population, children can only participate in studies that present a minimal to no-risk environment.

PET as a technique provides important information about the functioning and chemical makeup of the brain. Furthermore, it provides absolute measures of blood flow. However, PET exposes study participants to ionizing radiation and therefore cannot be used in healthy children, thereby limiting the generalizability of pediatric PET studies. Due to this limitation, only a few pediatric studies have been performed in children with developmental disabilities [e.g. (Chugani et al. 1987)], based on the prediction that the individual children may directly benefit.

fMRI is considered a minimally invasive imaging technique. Although there is no evidence of harm associated with participating in MRI scans, the high magnetic field environment generates a risk from metallic projectiles. Additionally, regional heating may occur if the child crosses their arms or legs. Very strict rules must be maintained in MRI laboratories. Furthermore, the MRI scanner generates considerable noise that is anxiety-evoking for many children. To date, most MRI studies are performed on young infants during sleep or children old enough to reliably control movement during the scan (children >5 years of age (Byars et al. 2002; Leach and Holland 2010)]. O'Shaughnessy et al. (2008) reported that children as young as 4 years of age could successfully participate in an fMRI scan with proper behavioral training. However, fMRI studies in awake children under 4 years of age have not been reported, to the best of our knowledge.

EEG is the complement to MEG and similarly noninvasive. However, several factors limit the use of EEG in pediatric studies. First, the preparation required for EEG studies and the requirement that electrodes be placed directly on the scalp make EEG impossible for some study populations due to tactile sensitivity (Baranek et al. 2006). Second, the preparation time may make the study unfeasible. With traditional EEG systems, only a 10–20 system with sparse electrode density is used in children up to 10 years of age. While this provides a measure of brain function, it does not provide sufficient spatial sampling for source analysis. The recently developed high-density, high-impedance EEG systems provide an important alternative to traditional EEG without requiring the intensive EEG

preparation for each electrode site (Ferree et al. 2001), however, it still requires that the child tolerate the high density sensor array placed directly on their head. Third, the changes in the skull that occur across childhood may also impact longitudinal and cross-sectional EEG findings in young children. The skull of young infants contains both superior and posterior fontanels that close at approximately one year of age. Further, the skull plates do not fully fuse until 8–10 years of age. The skull has a noticeable impact on the measured EEG signal with the largest change over the fontanels, whereas there are no detectable differences in the MEG signal (Flemming et al. 2005). Finally, realistic estimates of skull conductivity are required to obtain accurate source localization results (Richards 2005). MEG is resistant to the above factors allowing investigators to use simpler head models for source analysis and, thus, eliminate the risk of misinterpretation of developmental MEG data.

9 Unique Attributes of MEG for Studies of Developmental Connectome in Healthy and Disordered Brain

MEG, with its high temporal and spatial resolution provides unprecedented evidence of changes in the dynamics of cortical networks underlying sensory and cognitive development. Further, MEG provides a non-threatening environment for parents and children, thereby allowing acquisition of data not confounded by fear or discomfort. The peaceful, unobtrusive nature of MEG is welcomed by children who have high levels of anxiety or sensory oversensitivity. These exceptional attributes of MEG provide an opportunity to address crucial questions about the developing brain, related to characteristics of resting-state networks from infancy to adulthood, the role of sensory function in development of healthy cognitive abilities, or the emergence of key cognitive abilities in healthy development and in brain disorders of early childhood. This in vivo time-tracking technique enables exploration of how resting brain activity interacts or interferes with task-related activation.

Previous research has demonstrated the ability of MEG to identify subtle changes in the cortical network dynamics underlying sensory and cognitive functions in children with various developmental disorders. It is estimated that 1 out of 6 children in the United States suffers from a developmental disability (US Center for Disease Control) with the estimated lifetime cost of caring per child reaching $5 million and significant human cost of emotional distress on the children and their families. There is a great need for studies that may help to understand when in ontogeny and why brain development is different in these children. At present, diagnosis of many developmental disorders is made late in development, thus depriving children of early intervention with the best long-term outcomes. The attributes of MEG described above render this technique ideal as a very early testing tool.

In summary, considering the superb time resolution, high spatial resolution, total noninvasiveness, including a quiet testing environment, and the rich insight that MEG offers into the temporal causality and directionality of functional connectivity in developing networks, this technique is uniquely suited for brain studies with children. MEG has all the attributes to become the prime reliable technology for defining the pattern of the developmental connectome of the human brain.

Acknowledgments This work was supported in part by the National Institute of Neurological Disorders and Stroke (R21NS072729), the National Institute on Alcohol, Abuse and Alcoholism (P20AA017068), the National Center for Research Resources (5P20RR021938), the National Institute of General Medical Sciences (8P20GM103472).

References

Atkinson AP, Adolphs R (2011) The neuropsychology of face perception: beyond simple dissociations and functional selectivity. Philos Trans R Soc Lond B Biol Sci 366(1571): 1726–1738

Baddeley A (1986) Modularity, mass-action and memory. Q J Exp Psychol A 38(4):527–533

Banaschewski T, Brandeis D (2007) Annotation: what electrical brain activity tells us about brain function that other techniques cannot tell us—a child psychiatric perspective. J Child Psychol Psychiatry 48(5):415–435

Baranek GT, David FJ, Poe MD, Stone WL, Watson LR (2006) Sensory experiences questionnaire: discriminating sensory features in young children with autism, developmental delays, and typical development. J Child Psychol Psychiatry 47(6):591–601

Begleiter H, Porjesz B (2006) Genetics of human brain oscillations. Int J Psychophysiol 60(2):162–171

Berchicci M, Zhang T, Romero L, Peters A, Annett R, Teuscher U, Bertollo M, Okada Y, Stephen J, Comani S (2011) Development of mu rhythm in infants and preschool children. Dev Neurosci 33(2):130–143

Berl MM, Vaidya CJ, Gaillard WD (2006) Functional imaging of developmental and adaptive changes in neurocognition. NeuroImage 30(3):679–691

Biswal B, Yetkin FZ, Haughton VM, Hyde JS (1995) Functional connectivity in the motor cortex of resting human brain using echo-planar MRI. Magn Reson Med 34(4):537–541

Brookes MJ, Woolrich M, Luckhoo H, Price D, Hale JR, Stephenson MC, Barnes GR, Smith SM, Morris PG (2011) Investigating the electrophysiological basis of resting state networks using magnetoencephalography. Proc Natl Acad Sci USA 108(40):16783–16788

Bunge SA, Zelazo PD (2006) A brain-based account of the development of rule use in childhood. Curr Dir Psychol Sci 15(3):118–121

Bunge SA, Wright SB (2007) Neurodevelopmental changes in working memory and cognitive control. Curr Opin Neurobiol 17(2):243–250

Bunge SA, Hazeltine E, Scanlon MD, Rosen AC, Gabrieli JD (2002a) Dissociable contributions of prefrontal and parietal cortices to response selection. NeuroImage 17(3):1562–1571

Bunge SA, Dudukovic NM, Thomason ME, Vaidya CJ, Gabrieli JD (2002b) Immature frontal lobe contributions to cognitive control in children: evidence from fMRI. Neuron 33(2):301–311

Burack JA, Iarocci G, Flanagan TD, Bowler DM (2004) On mosaics and melting pots: conceptual considerations of comparison and matching strategies. J Autism Dev Disord 34(1):65–73

Buzsaki G (2006) Rhythms of the Brain. Oxford University Press, USA

Byars AW, Holland SK, Strawsburg RH, Bommer W, Dunn RS, Schmithorst VJ, Plante E (2002) Practical aspects of conducting large-scale functional magnetic resonance imaging studies in children. J Child Neurol 17(12):885–890

Cantor DS, Chabot R (2009) QEEG studies in the assessment and treatment of childhood disorders. Clinical EEG Neuroscience 40(2):113–121

Case R (1992) The role of the frontal lobes in the regulation of cognitive development. Brain Cogn 20(1):51–73

Casey BJ, Galvan A, Hare TA (2005) Changes in cerebral functional organization during cognitive development. Curr Opin Neurobiol 15(2):239–244

Changeux JP, Danchin A (1976) Selective stabilisation of developing synapses as a mechanism for the specification of neuronal networks. Nature 264(5588):705–712

Cheour M, Imada T, Taulu S, Ahonen A, Salonen J, Kuhl P (2004) Magnetoencephalography is feasible for infant assessment of auditory discrimination. Exp Neurol 190(Suppl 1):S44–S51

Chugani HT, Mazziotta JC, Engel J Jr, Phelps ME (1987) The Lennox-Gastaut syndrome: metabolic subtypes determined by 2-deoxy-2[18F]fluoro-D-glucose positron emission tomography. Ann Neurol 21(1):4–13

Church JA, Petersen SE, Schlaggar BL (2010) The "Task B problem" and other considerations in developmental functional neuroimaging. Hum Brain Mapp 31(6):852–862

Church JA, Fair DA, Dosenbach NU, Cohen AL, Miezin FM, Petersen SE, Schlaggar BL (2009) Control networks in paediatric Tourette syndrome show immature and anomalous patterns of functional connectivity. Brain 132(Pt 1):225–238

Ciesielski KT, Harris RJ, Cofer LF (2004) Posterior brain ERP patterns related to the go/no-go task in children. Psychophysiology 41(6):882–892

Ciesielski KT, Hamalainen MS, Lesnik PG, Geller DA, Ahlfors SP (2005) Increased MEG activation in OCD reflects a compensatory mechanism specific to the phase of a visual working memory task. NeuroImage 24(4):1180–1191

Ciesielski KT, Lesnik PG, Savoy RL, Grant EP, Ahlfors SP (2006) Developmental neural networks in children performing a Categorical N-Back Task. NeuroImage 33(3):980–990

Ciesielski KT, Ahlfors SP, Bedrick EJ, Kerwin AA, Hamalainen MS (2010) Top-down control of MEG alpha-band activity in children performing Categorical N-Back Task. Neuropsychologia 48(12):3573–3579

Ciesielski KT, Hamalainen MS, Geller DA, Wilhelm S, Goldsmith TE, Ahlfors SP (2007) Dissociation between MEG alpha modulation and performance accuracy on visual working memory task in obsessive compulsive disorder. Hum Brain Mapp 28(12):1401–1414

Ciesielski KT, Rauch SL, Ahlfors SP, Vangel ME, Wilhelm S, Rosen BR, Hamalainen MS (2012) Role of medial cortical networks for anticipatory processing in obsessive-compulsive disorder. Hum Brain Mapp 33(9):2125–2134

Coffman BA, Kodituwakku P, Kodituwakku EL, Romero L, Sharadamma NM, Stone D, Stephen JM (2012) Primary visual response (M100) delays in adolescents with FASD as measured with MEG. Hum Brain Mapp (In print)

Cohen JD, Perlstein WM, Braver TS, Nystrom LE, Noll DC, Jonides J, Smith EE (1997) Temporal dynamics of brain activation during a working memory task. Nature 386(6625): 604–608

Courtney SM, Petit L, Maisog JM, Ungerleider LG, Haxby JV (1998) An area specialized for spatial working memory in human frontal cortex. Science 279(5355):1347–1351

Csibra G, Davis G, Spratling MW, Johnson MH (2000) Gamma oscillations and object processing in the infant brain. Science 290(5496):1582–1585

Cullen KR, Gee DG, Klimes-Dougan B, Gabbay V, Hulvershorn L, Mueller BA, Camchong J, Bell CJ, Houri A, Kumra S, Lim KO, Castellanos FX, Milham MP (2009) A preliminary study of functional connectivity in comorbid adolescent depression. Neurosci Lett 460(3):227–231

D'Esposito M, Postle BR (1999) The dependence of span and delayed-response performance on prefrontal cortex. Neuropsychologia 37(11):1303–1315

Dale AM, Sereno MI (1993) Improved localization of cortical activity by combining EEG and MEG with MRI cortical surface reconstruction: a linear approach. J Cogn Neurosci 5:162–176

Dale AM, Liu AK, Fischl BR, Buckner RL, Belliveau JW, Lewine JD, Halgren E (2000) Dynamic statistical parametric mapping: combining fMRI and MEG for high-resolution imaging of cortical activity. Neuron 26(1):55–67

Danker-Hopfe H (2011) Growth and development of children with a special focus on sleep. Prog Biophys Mol Biol 107(3):333–338

Donohue SE, Roberts KC, Grent-'t-Jong T, Woldorff MG (2011) The cross-modal spread of attention reveals differential constraints for the temporal and spatial linking of visual and auditory stimulus events. J Neurosci 31(22):7982–7990

Dosenbach NU, Nardos B, Cohen AL, Fair DA, Power JD, Church JA, Nelson SM, Wig GS, Vogel AC, Lessov-Schlaggar CN, Barnes KA, Dubis JW, Feczko E, Coalson RS, Pruett JR Jr, Barch DM, Petersen SE, Schlaggar BL (2010) Prediction of individual brain maturity using fMRI. Science 329(5997):1358–1361

Durston S, Casey BJ (2006) What have we learned about cognitive development from neuroimaging? Neuropsychologia 44(11):2149–2157

Engle RW, Tuholski SW, Laughlin JE, Conway AR (1999) Working memory, short-term memory, and general fluid intelligence: a latent-variable approach. J Exp Psychol Gen 128(3):309–331

Evans AC (2006) The NIH MRI study of normal brain development. NeuroImage 30(1):184–202

Fair DA, Cohen AL, Power JD, Dosenbach NU, Church JA, Miezin FM, Schlaggar BL, Petersen SE (2009) Functional brain networks develop from a "local to distributed" organization. PLoS Comput Biol 5(5):e1000381

Fair DA, Dosenbach NU, Church JA, Cohen AL, Brahmbhatt S, Miezin FM, Barch DM, Raichle ME, Petersen SE, Schlaggar BL (2007) Development of distinct control networks through segregation and integration. Proc Natl Acad Sci USA 104(33):13507–13512

Falter CM, Braeutigam S, Nathan R, Carrington S, Bailey AJ (2012) Enhanced Access to Early Visual Processing of Perceptual Simultaneity in Autism Spectrum Disorders. J Autism Dev Disord

Ferree TC, Luu P, Russell GS, Tucker DM (2001) Scalp electrode impedance, infection risk, and EEG data quality. Clin Neurophysiol 112(3):536–544

Fisch B (1991) Spehlmann's EEG Primer, 2nd edn. Elsevier, Amsterdam

Flemming L, Wang Y, Caprihan A, Eiselt M, Haueisen J, Okada Y (2005) Evaluation of the distortion of EEG signals caused by a hole in the skull mimicking the fontanel in the skull of human neonates. Clin Neurophysiol 116(5):1141–1152

Fransson P, Aden U, Blennow M, Lagercrantz H (2010) The functional architecture of the infant brain as revealed by resting-state fMRI. Cereb Cortex 21(1):145–154

Friston KJ, Price CJ (2011) Modules and brain mapping. Cogn Neuropsychol 28(3–4):241–250

Fujioka T, Ross B (2008) Auditory processing indexed by stimulus-induced alpha desynchronization in children. Int J Psychophysiol 68(2):130–140

Gabrieli JD, Poldrack RA, Desmond JE (1998) The role of left prefrontal cortex in language and memory. Proc Natl Acad Sci USA 95(3):906–913

Gage NM, Siegel B, Roberts TP (2003a) Cortical auditory system maturational abnormalities in children with autism disorder: an MEG investigation. Brain Res Dev Brain Res 144(2):201–209

Gage NM, Siegel B, Callen M, Roberts TP (2003b) Cortical sound processing in children with autism disorder: an MEG investigation. NeuroReport 14(16):2047–2051

Gaillard WD, Grandin CB, Xu B (2001) Developmental aspects of pediatric fMRI: considerations for image acquisition, analysis, and interpretation. Neuroimage 13(2):239–249

Gao Y, Glenn AL, Schug RA, Yang Y, Raine A (2009) The neurobiology of psychopathy: a neurodevelopmental perspective. Can J Psychiatry 54(12):813–823

Gevins A, Cutillo B (1993) Spatiotemporal dynamics of component processes in human working memory. Electroencephalogr Clin Neurophysiol 87(3):128–143

Gevins A, Smith ME (2000) Neurophysiological measures of working memory and individual differences in cognitive ability and cognitive style. Cereb Cortex 10(9):829–839

Giedd JN, Rapoport JL (2010) Structural MRI of pediatric brain development: what have we learned and where are we going? Neuron 67(5):728–734

Gogtay N, Giedd JN, Lusk L, Hayashi KM, Greenstein D, Vaituzis AC, Nugent TF 3rd, Herman DH, Clasen LS, Toga AW, Rapoport JL, Thompson PM (2004) Dynamic mapping of human cortical development during childhood through early adulthood. Proc Natl Acad Sci USA 101(21):8174–8179

Goldman-Rakic PS (1987) Development of cortical circuitry and cognitive function. Child Dev 58(3):601–622

Gordon EM, Lee PS, Maisog JM, Foss-Feig J, Billington ME, Vanmeter J, Vaidya CJ (2011) Strength of default mode resting-state connectivity relates to white matter integrity in children. Dev Sci 14(4):738–751

Gozzo Y, Vohr B, Lacadie C, Hampson M, Katz KH, Maller-Kesselman J, Schneider KC, Peterson BS, Rajeevan N, Makuch RW, Constable RT, Ment LR (2009) Alterations in neural connectivity in preterm children at school age. NeuroImage 48(2):458–463

Greicius MD, Krasnow B, Reiss AL, Menon V (2003) Functional connectivity in the resting brain: a network analysis of the default mode hypothesis. Proc Natl Acad Sci USA 100(1):253–258

Hagmann P, Sporns O, Madan N, Cammoun L, Pienaar R, Wedeen VJ, Meuli R, Thiran JP, Grant PE (2010) White matter maturation reshapes structural connectivity in the late developing human brain. Proc Natl Acad Sci USA 107(44):19067–19072

Hamalainen M, Hari R (2002) Magnetoencephalographic characterization of dynamic brain activation: basic principles, and methods of data collection and source analysis. In: Toga AW, Mazziotta JC (eds) Brain mapping: the methods. Academic Press, Amsterdam

Hamalainen MS, Ilmoniemi RJ (1994) Interpreting magnetic fields of the brain: minimum norm estimates. Med Biol Eng Comput 32(1):35–42

Hampson M, Tokoglu F, King RA, Constable RT, Leckman JF (2009) Brain areas coactivating with motor cortex during chronic motor tics and intentional movements. Biol Psychiatry 65(7):594–599

Hansen PC, Kringelbach ML, Salmelin R (eds) (2010) MEG: an introduction to methods. Oxford University Press, New York

Haxby JV, Petit L, Ungerleider LG, Courtney SM (2000) Distinguishing the functional roles of multiple regions in distributed neural systems for visual working memory. NeuroImage 11(2):145–156

He BJ, Snyder AZ, Vincent JL, Epstein A, Shulman GL, Corbetta M (2007) Breakdown of functional connectivity in frontoparietal networks underlies behavioral deficits in spatial neglect. Neuron 53(6):905–918

Heim S, Eulitz C, Kaufmann J, Fuchter I, Pantev C, Lamprecht-Dinnesen A, Matulat P, Scheer P, Borstel M, Elbert T (2000) Atypical organisation of the auditory cortex in dyslexia as revealed by MEG. Neuropsychologia 38(13):1749–1759

Hinton VJ (2002) Ethics of neuroimaging in pediatric development. Brain Cogn 50(3):455–468

Hipp JF, Hawellek DJ, Corbetta M, Siegel M, Engel AK (2012) Large-scale cortical correlation structure of spontaneous oscillatory activity. Nat Neurosci 15(6):884–890

Horiguchi T, Ohta K, Nishikawa T (2003) An MEG study of P300 activity during a color discrimination task 2: source localization study. Brain Dev 25(4):241–244

Huo X, Wang Y, Kotecha R, Kirtman EG, Fujiwara H, Hemasilpin N, Degrauw T, Rose DF, Xiang J (2011) High gamma oscillations of sensorimotor cortex during unilateral movement in the developing brain: a MEG study. Brain Topogr 23(4):375–384

Huttenlocher PR (1979) Synaptic density in human frontal cortex—developmental changes and effects of aging. Brain Res 163(2):195–205

Huttunen J, Wikstrom H, Salonen O, Ilmoniemi RJ (1999) Human somatosensory cortical activation strengths: comparison between males and females and age-related changes. Brain Res 818(2):196–203

Imada T, Zhang Y, Cheour M, Taulu S, Ahonen A, Kuhl PK (2006) Infant speech perception activates Broca's area: a developmental magnetoencephalography study. NeuroReport 17(10):957–962

Imperati D, Colcombe S, Kelly C, Di Martino A, Zhou J, Castellanos FX, Milham MP (2011) Differential development of human brain white matter tracts. PLoS ONE 6(8):e23437

Jaffee SR, Price TS (2007) Gene-environment correlations: a review of the evidence and implications for prevention of mental illness. Mole Psychiatry 12(5):432–442

Johnson BW, Crain S, Thornton R, Tesan G, Reid M (2010) Measurement of brain function in pre-school children using a custom sized whole-head MEG sensor array. Clin Neurophysiol 121(3):340–349

Johnson BW, McArthur G, Hautus M, Reid M, Brock J, Castles A, Crain S (2013) Lateralized auditory brain function in children with normal reading ability and in children withdyslexia. Neuropsychologia 51(4):633–641

Johnson MH (2010) Interactive specialization: a domain-general framework for human functional brain development? Dev Cogn Neurosci 1(1):7–21

Jones DT, Mateen FJ, Lucchinetti CF, Jack CR Jr, Welker KM (2010) Default mode network disruption secondary to a lesion in the anterior thalamus. Arch Neurol 68(2):242–247

Jonides J, Schumacher EH, Smith EE, Koeppe RA, Awh E, Reuter-Lorenz PA, Marshuetz C, Willis CR (1998) The role of parietal cortex in verbal working memory. J Neurosci 18(13):5026–5034

Kandel E, Schwartz J, Jessell T (2000) Principles of neural science, 4th edn. McGraw-Hill, New York

Karmiloff-Smith A (2010) Neuroimaging of the developing brain: taking "developing" seriously. Hum Brain Mapp 31(6):934–941

Kelly C, Biswal BB, Craddock RC, Castellanos FX, Milham MP (2012) Characterizing variation in the functional connectome: promise and pitfalls. Trends Cogn Sci 16(3):181–188

Kelly C, de Zubicaray G, Di Martino A, Copland DA, Reiss PT, Klein DF, Castellanos FX, Milham MP, McMahon K (2009) L-dopa modulates functional connectivity in striatal cognitive and motor networks: a double-blind placebo-controlled study. J Neurosci 29(22):7364–7378

Khan S, Gramfort A, Shetty NR, Kitzbichler MG, Ganesan S, Moran JM, Lee SM, Gabrieli JD, Tager-Flusberg HB, Joseph RM, Herbert MR, Hamalainen MS, Kenet T (2013) Local and long-range functional connectivity is reduced in concert in autism spectrum disorders. Proc Natl Acad Sci USA 110(8):3107–3112

Khundrakpam BS, Reid A, Brauer J, Carbonell F, Lewis J, Ameis S, Karama S, Lee J, Chen Z, Das S, Evans AC (2012) Developmental changes in organization of structural brain networks. Cereb Cortex 23(9):2072–2085

Klimesch W, Sauseng P, Hanslmayr S (2007) EEG alpha oscillations: the inhibition-timing hypothesis. Brain Res Rev 53(1):63–88

Klimesch W, Doppelmayr M, Wimmer H, Gruber W, Rohm D, Schwaiger J, Hutzler F (2001) Alpha and beta band power changes in normal and dyslexic children. Clin Neurophysiol 112(7):1186–1195

Kolev V, Yordanova J, Basar-Eroglu C, Basar E (2002) Age effects on visual EEG responses reveal distinct frontal alpha networks. Clin Neurophysiol 113(6):901–910

Korvenoja A, Huttunen J, Salli E, Pohjonen H, Martinkauppi S, Palva JM, Lauronen L, Virtanen J, Ilmoniemi RJ, Aronen HJ (1999) Activation of multiple cortical areas in response to somatosensory stimulation: combined magnetoencephalographic and functional magnetic resonance imaging. Hum Brain Mapp 8(1):13–27

Kotecha R, Pardos M, Wang Y, Wu T, Horn P, Brown D, Rose D, deGrauw T, Xiang J (2009) Modeling the developmental patterns of auditory evoked magnetic fields in children. PLoS ONE 4(3):e4811

Kotsoni E, Byrd D, Casey BJ (2006) Special considerations for functional magnetic resonance imaging of pediatric populations. J Magn Reson Imaging 23(6):877–886

Koyama MS, Kelly C, Shehzad Z, Penesetti D, Castellanos FX, Milham MP (2010) Reading networks at rest. Cereb Cortex 20(11):2549–2559

Krause CM, Pesonen M, Hamalainen H (2007) Brain oscillatory responses during the different stages of an auditory memory search task in children. NeuroReport 18(3):213–216

Kuhn D (2006) Do cognitive changes accompany developments in the adolescent brain? Perspect Psychol Sci 1:59–67

Kurz MJ, Wilson TW (2011) Neuromagnetic activity in the somatosensory cortices of children with cerebral palsy. Neurosci Lett 490(1):1–5

Kylliainen A, Braeutigam S, Hietanen JK, Swithenby SJ, Bailey AJ (2006) Face and gaze processing in normally developing children: a magnetoencephalographic study. Eur J Neurosci 23(3):801–810

Leach JL, Holland SK (2010) Functional MRI in children: clinical and research applications. Pediatr Radiol 40(1):31–49

Loenneker T, Klaver P, Bucher K, Lichtensteiger J, Imfeld A, Martin E (2011) Microstructural development: organizational differences of the fiber architecture between children and adults in dorsal and ventral visual streams. Hum Brain Mapp 32(6):935–946

Lutter WJ, Maier M, Wakai RT (2006) Development of MEG sleep patterns and magnetic auditory evoked responses during early infancy. Clin Neurophysiol 117(3):522–530

Lutter WJ, Wakai RT, Maier MM, Baryshnikov BV (2004) MEG sleep pattern dependence of auditory evoked fields in young infants. Neurol Clin Neurophysiol 2004:77

Marco EJ, Khatibi K, Hill SS, Siegel B, Arroyo MS, Dowling AF, Neuhaus JM, Sherr EH, Hinkley LN, Nagarajan SS (2012) Children with autism show reduced somatosensory response: an MEG study. Autism Res 5(5):340–351

Myers EH, Hampson M, Vohr B, Lacadie C, Frost SJ, Pugh KR, Katz KH, Schneider KC, Makuch RW, Constable RT, Ment LR (2010) Functional connectivity to a right hemisphere language center in prematurely born adolescents. NeuroImage 51(4):1445–1452

Nelson CA, Monk CS, Lin J, Carver LJ, Thomas KM, Truwit CL (2000) Functional neuroanatomy of spatial working memory in children. Dev Psychol 36(1):109–116

Nolte G, Bai O, Wheaton L, Mari Z, Vorbach S, Hallett M (2004) Identifying true brain interaction from EEG data using the imaginary part of coherency. Clin Neurophysiol 115(10):2292–2307

O'Shaughnessy ES, Berl MM, Moore EN, Gaillard WD (2008) Pediatric functional magnetic resonance imaging (fMRI): issues and applications. J Child Neurol 23(7):791–801

Oram Cardy JE, Flagg EJ, Roberts W, Roberts TP (2008) Auditory evoked fields predict language ability and impairment in children. Int J Psychophysiol 68(2):170–175

Orekhova EV, Stroganova TA, Posikera IN, Elam M (2006) EEG theta rhythm in infants and preschool children. Clin Neurophysiol 117(5):1047–1062

Owen AM, McMillan KM, Laird AR, Bullmore E (2005) N-back working memory paradigm: a meta-analysis of normative functional neuroimaging studies. Hum Brain Mapp 25(1):46–59

Paetau R, Ahonen A, Salonen O, Sams M (1995) Auditory evoked magnetic fields to tones and pseudowords in healthy children and adults. J Clin Neurophysiol 12(2):177–185

Papanicolaou AC, Castillo EM, Billingsley-Marshall R, Pataraia E, Simos PG (2005a) A review of clinical applications of magnetoencephalography. Int Rev Neurobiol 68:223–247

Papanicolaou AC, Pataraia E, Billingsley-Marshall R, Castillo EM, Wheless JW, Swank P, Breier JI, Sarkari S, Simos PG (2005b) Toward the substitution of invasive electroencephalography in epilepsy surgery. J Clin Neurophysiol 22(4):231–237

Pataraia E, Feucht M, Lindinger G, Aull-Watschinger S, Baumgartner C (2008) Combined electroencephalography and magnetoencephalography of interictal spikes in benign rolandic epilepsy of childhood. Clin Neurophysiol 119(3):635–641

Paus T (2005) Mapping brain maturation and cognitive development during adolescence. Trends Cogn Sci 9(2):60–68

Paus T, Collins DL, Evans AC, Leonard G, Pike B, Zijdenbos A (2001) Maturation of white matter in the human brain: a review of magnetic resonance studies. Brain Res Bull 54(3):255–266

Petrides M (2000) Dissociable roles of mid-dorsolateral prefrontal and anterior inferotemporal cortex in visual working memory. J Neurosci 20(19):7496–7503

Picton TW, Bentin S, Berg P, Donchin E, Hillyard SA, Johnson R Jr, Miller GA, Ritter W, Ruchkin DS, Rugg MD, Taylor MJ (2000) Guidelines for using human event-related potentials to study cognition: recording standards and publication criteria. Psychophysiology 37(2):127–152

Pihko E, Lauronen L (2004) Somatosensory processing in healthy newborns. Exp Neurol 190(Suppl 1):S2–S7

Pihko E, Nevalainen P, Stephen J, Okada Y, Lauronen L (2009) Maturation of somatosensory cortical processing from birth to adulthood revealed by magnetoencephalography. Clin Neurophysiol

Pihko E, Lauronen L, Wikstrom H, Taulu S, Nurminen J, Kivitie-Kallio S, Okada Y (2004) Somatosensory evoked potentials and magnetic fields elicited by tactile stimulation of the hand during active and quiet sleep in newborns. Clin Neurophysiol 115(2):448–455

Poldrack RA (2010) Interpreting developmental changes in neuroimaging signals. Hum Brain Mapp 31(6):872–878

Rahkonen P, Nevalainen P, Lauronen L, Pihko E, Lano A, Vanhatalo S, Pesonen AK, Heinonen K, Raikkonen K, Valanne L, Autti T, Andersson S, Metsaranta M (2013) Cortical somatosensory processing measured by magnetoencephalography predicts neurodevelopment in extremely low gestational age infants. Pediatr Res 73(6):763–771

Raznahan A, Lerch JP, Lee N, Greenstein D, Wallace GL, Stockman M, Clasen L, Shaw PW, Giedd JN (2011) Patterns of coordinated anatomical change in human cortical development: a longitudinal neuroimaging study of maturational coupling. Neuron 72(5):873–884

Richards JE (2005) Localizing cortical sources of event-related potentials in infants' covert orienting. Dev Sci 8(3):255–278

Roberts TP, Khan SY, Blaskey L, Dell J, Levy SE, Zarnow DM, Edgar JC (2009) Developmental correlation of diffusion anisotropy with auditory-evoked response. NeuroReport 20(18):1586–1591

Rojas DC, Walker JR, Sheeder JL, Teale PD, Reite ML (1998) Developmental changes in refractoriness of the neuromagnetic M100 in children. NeuroReport 9(7):1543–1547

Rojas DC, Maharajh K, Teale PD, Kleman MR, Benkers TL, Carlson JP, Reite ML (2006) Development of the 40 Hz steady state auditory evoked magnetic field from ages 5 to 52. Clin Neurophysiol 117(1):110–117

Rothenberger A (2009) Brain oscillations forever–neurophysiology in future research of child psychiatric problems. J Child Psychol Psychiatry 50(1–2):79–86

Rutter M (2006) Implications of resilience concepts for scientific understanding. Ann NY Acad Sci 1094:1–12

Schlaggar BL, Brown TT, Lugar HM, Visscher KM, Miezin FM, Petersen SE (2002) Functional neuroanatomical differences between adults and school-age children in the processing of single words. Science 296(5572):1476–1479

Schwartz ES, Edgar JC, Gaetz WC, Roberts TP (2010) Magnetoencephalography. Pediatr Radiol 40(1):50–58

Simos PG, Rezaie R, Fletcher JM, Juranek J, Passaro AD, Li Z, Cirino PT, Papanicolaou AC (2011) Functional disruption of the brain mechanism for reading: effects of comorbidity and task difficulty among children with developmental learning problems. Neuropsychology 25(4):520–534

Smith EE, Jonides J (1998) Neuroimaging analyses of human working memory. Proc Natl Acad Sci USA 95(20):12061–12068

Smyser CD, Inder TE, Shimony JS, Hill JE, Degnan AJ, Snyder AZ, Neil JJ (2010) Longitudinal analysis of neural network development in preterm infants. Cereb Cortex 20(12):2852–2862

Sowell ER, Trauner DA, Gamst A, Jernigan TL (2002) Development of cortical and subcortical brain structures in childhood and adolescence: a structural MRI study. Dev Med Child Neurol 44(1):4–16

Sowell ER, Thompson PM, Leonard CM, Welcome SE, Kan E, Toga AW (2004) Longitudinal mapping of cortical thickness and brain growth in normal children. J Neurosci 24(38):8223–8231

Srinivasan R, Winter WR, Ding J, Nunez PL (2007) EEG and MEG coherence: measures of functional connectivity at distinct spatial scales of neocortical dynamics. J Neurosci Methods 166(1):41–52

Stefan H, Hummel C, Scheler G, Genow A, Druschky K, Tilz C, Kaltenhauser M, Hopfengartner R, Buchfelder M, Romstock J (2003) Magnetic brain source imaging of focal epileptic activity: a synopsis of 455 cases. Brain 126(Pt 11):2396–2405

Stephen J, Kodituwakku P, Kodituwakku EL, Romero L, Peters AM, Sharadamma NM, Caprihan A, Coffman BA (2012) Delays in auditory processing identified in preschool children with FASD. Alcohol Clin Exp Res 36(10):1720–1727

Stevens MC, Pearlson GD, Calhoun VD (2009) Changes in the interaction of resting-state neural networks from adolescence to adulthood. Hum Brain Mapp 30(8):2356–2366

Stiles J (2008) The fundamentals of brain development: integrating nature and nurture. Harvard University Press, Cambridge

Stiles J, Moses P, Passarotti A, Dick FK, Buxton R (2003) Exploring developmental change in the neural bases of higher cognitive functions: the promise of functional magnetic resonance imaging. Dev Neuropsychol 24(2–3):641–668

Supekar K, Musen M, Menon V (2009) Development of large-scale functional brain networks in children. PLoS Biol 7(7):e1000157

Tamm L, Menon V, Reiss AL (2002) Maturation of brain function associated with response inhibition. J Am Acad Child Adolesc Psychiatry 41(10):1231–1238

Tamnes CK, Ostby Y, Walhovd KB, Westlye LT, Due-Tonnessen P, Fjell AM (2010) Intellectual abilities and white matter microstructure in development: a diffusion tensor imaging study. Hum Brain Mapp 31(10):1609–1625

Taylor MJ, Baldeweg T (2002) Application of EEG, ERP and intracranial recordings to the investigation of cognitive functions in children. Dev Sci 5(3):318–334

Taylor MJ, Mills T, Pang EW (2011) The development of face recognition; hippocampal and frontal lobe contributions determined with MEG. Brain Topogr 24(3–4):261–270

Taylor MJ, Donner EJ, Pang EW (2012) fMRI and MEG in the study of typical and atypical cognitive development. Clin Neurophysiol 42(1–2):19–25

Trainor LJ (2012) Musical experience, plasticity, and maturation: issues in measuring developmental change using EEG and MEG. Ann NY Acad Sci 1252:25–36

Uddin LQ, Supekar K, Menon V (2010) Typical and atypical development of functional human brain networks: insights from resting-state FMRI. Front Syst Neurosci 4:21

Uhlhaas PJ, Roux F, Singer W, Haenschel C, Sireteanu R, Rodriguez E (2009) The development of neural synchrony reflects late maturation and restructuring of functional networks in humans. Proc Natl Acad Sci USA 106(24):9866–9871

Van Dijk KR, Hedden T, Venkataraman A, Evans KC, Lazar SW, Buckner RL (2010) Intrinsic functional connectivity as a tool for human connectomics: theory, properties, and optimization. J Neurophysiol 103(1):297–321

Van Essen DC, Anderson CH, Felleman DJ (1992) Information processing in the primate visual system: an integrated systems perspective. Science 255(5043):419–423

Vogel AC, Power JD, Petersen SE, Schlaggar BL (2010) Development of the brain's functional network architecture. Neuropsychol Rev 20(4):362–375

Wakai RT, Lutter WJ, Chen M, Maier MM (2007) On and Off magnetic auditory evoked responses in early infancy: a possible marker of brain immaturity. Clin Neurophysiol 118(7):1480–1487

Wehner DT, Ahlfors SP, Mody M (2007) Effects of phonological contrast on auditory word discrimination in children with and without reading disability: a magnetoencephalography (MEG) study. Neuropsychologia 45(14):3251–3262

Wehner DT, Hamalainen MS, Mody M, Ahlfors SP (2008) Head movements of children in MEG: quantification, effects on source estimation, and compensation. NeuroImage 40(2):541–550

Wilson TW, Slason E, Asherin R, Kronberg E, Reite ML, Teale PD, Rojas DC (2010) An extended motor network generates beta and gamma oscillatory perturbations during development. Brain Cogn 73(2):75–84

Wilson TW, Slason E, Asherin R, Kronberg E, Teale PD, Reite ML, Rojas DC (2011) Abnormal gamma and beta MEG activity during finger movements in early-onset psychosis. Dev Neuropsychol 36(5):596–613

Yakovlev PI, Lecours A-R (1967) The myelogenetic cycles of regional maturation of the brain. In: Minkowski A (ed) Regional development of the brain in early life. Blackwell Scientific, Oxford, pp 3–70

Yordanova J, Kolev V, Polich J (2001) P300 and alpha event-related desynchronization (ERD). Psychophysiology 38(1):143–152

Yordanova JY, Kolev VN (1996) Developmental changes in the alpha response system. Electroencephalogr Clin Neurophysiol 99(6):527–538

MEG and Cognitive Developmental Studies

Margot J. Taylor and Elizabeth W. Pang

Abstract Human social, executive and language functions are complex and known to follow a prolonged developmental course from childhood through to early adulthood. These processes rely on the integrity and maturity of the frontal lobes, which also show protracted maturation into adulthood. MEG is the ideal modality to determine the development of these intricate and multi-faceted cognitive abilities; its exquisite temporal and spatial resolution allows investigators to track the age-related changes in both neural timing and location. The challenge for MEG has been two-fold: to develop appropriate tasks to capture the neurodevelopmental trajectory of these functions; and, to develop appropriate analysis strategies that can capture the subtle, often rapid, frontal lobe activity. In this chapter, we will review our MEG research on social, executive and language functions controlled by the frontal lobes in typically developing children and clinical groups. The studies include the examination of facial emotional processing, inhibition and verb generation. We end with a discussion on the challenges of testing young children in the MEG environment and the development of age-appropriate technologies and paradigms.

Keywords Frontal lobe · Faces · Inhibition · Language · Development · ASD

M. J. Taylor (✉)
Diagnostic Imaging, The Hospital for Sick Children, University of Toronto,
555 University Avenue, Toronto, ON M5G 1X8, Canada
e-mail: margot.taylor@sickkids.ca

M. J. Taylor · E. W. Pang
Neuroscience and Mental Health Programme, The Hospital for Sick Children,
University of Toronto, 555 University Avenue, Toronto, ON M5G 1X8, Canada

E. W. Pang
Neurology, The Hospital for Sick Children, University of Toronto,
555 University Avenue, Toronto, ON M5G 1X8, Canada

S. Supek and C. J. Aine (eds.), *Magnetoencephalography*,
DOI: 10.1007/978-3-642-33045-2_25,

1 Development of Executive Functions and the Frontal Lobes

The frontal lobes are among the last brain regions to mature, with myelination continuing into the third decade of life (Yakolev and Lecours 1967). The frontal lobes are essential for executive functions and perturbations in their development can have devastating effects on executive processes (Powell and Voeller 2004). Social cognitive function, which falls within the rubric of executive functions and describes the ability to adjust and manage successfully in social settings, also relies on intact frontal lobe structure and function. Social cognitive aptitude increases in parallel with frontal lobe maturation. Current models conceptualise executive processes as reliant on a network of frontal lobe regions with strong reciprocal connections to subcortical and parietal areas (Elliott 2003). Social cognitive functions have been linked more specifically with the medial prefrontal and anterior cingulate cortex (Bush et al. 2000; Radke et al. 2011; Telzer et al. 2011) inter-connected with dorsolateral and inferior frontal regions (Hall et al. 2010), with connections to the superior temporal sulcus (STS) (Carter and Pelphrey 2008; Kramer et al. 2010) and subcortical regions including the amygdalae and basal ganglia (Satpute and Lieberman 2006, Jackson et al. 2008, Mehta et al. 2010). This cognitive network is activated to a range of social and emotional tasks, including social judgement, facial affect, inhibition (Go/No-go) and empathy protocols. The medial prefrontal cortex is activated in all of these tasks and is also known to be the last region to mature (Shaw et al. 2008). We focus on the development of two aspects of social cognitive function—emotional processing and inhibition—and the advantages of MEG studies in our understanding of these abilities.

1.1 Social Cognitive Processing Assessed Using Emotional Faces

The most critical visual stimulus in human social interactions is the human face. Faces convey a vast amount of information, and the skill in differentiating and recognizing faces and their emotional content has an extended developmental course through to adulthood (see (Kolb et al. 1992) for review). Although posterior brain areas are involved in face processing, frontal cortices are critical in understanding the social significance of facial expressions and in directing appropriate attention (Adolphs et al. 2002, Kilts et al. 2003). Perception of emotional facial expressions involves an extensive network that includes the amygdalae, frontal lobes, anterior cingulate, STS and fusiform gyri (McCarthy et al. 1999; Allison et al. 2000; Haxby et al. 2000).

Despite the numerous neuroimaging studies on face processing in adults, there are fewer developmental studies and even fewer that investigate emotional processes. Differences in frontal activation between adolescents and adults, however,

have been reported in emotional regulation tasks (Burnett et al. 2009; Passarotti et al. 2009), as well as changes across childhood in frontal activation related to emotional tasks of self-regulation and empathy (Lamm and Lewis 2010). We have demonstrated marked developmental changes in emotional face processing throughout childhood and adolescence with event-related potentials (ERP) (Batty and Taylor 2003) and atypicalities in ERPs to emotional faces in children with autism spectrum disorder (ASD) (Batty et al. 2011). We have extensive developmental data on the spatio-temporal patterns of neutral face processing in MEG recognition paradigms (Taylor et al. 2008, 2010, 2011a, b, 2012). With emotional faces in an explicit recognition task, we showed an early frontal activation that reflected implicit emotional processing, whereas later insula and fusiform activity was related to explicit emotional recognition (Bayle and Taylor 2010). This task, however, was too difficult to be completed in children; therefore we turned to implicit emotional face processing tasks.

An initial adult study provided novel timing information on implicit brain processing to happy and fearful facial emotions (Hung et al. 2010). The faces were presented rapidly and concurrently with a scrambled pattern, one on each side of a central fixation cross. Participants responded as quickly as possible (left or right) to the side of the scrambled pattern; thus attention was not directed to the faces or the emotions. With this implicit processing task, we found that at 100 ms, left amygdala activation was seen to fearful versus neutral faces, and concurrently there was increased activation in the dorsal ACC. The very rapid timing of amygdala-ACC activity suggested a specialized frontal-limbic network that could facilitate early response to a potential threat. This study also demonstrated that MEG source analyses could accurately measure both the location and time course of neurocognitive events in deep brain structures, as confirmed with simulated and real data analyses (Quraan et al. 2011, Mills et al. 2012).

We also determined the development of MEG responses associated with the implicit processing of fearful and happy facial emotions, using the same protocol in two groups of children—school-aged children (7–10 years) and young adolescents (12–15 years) (Hung et al. 2012). In the younger children, there was right lateralised amygdala activation to both happy and fearful faces while no ACC activity passed threshold. For the young teenagers, the pattern was similar to that seen with the adult cohort—only left amygdala activity was seen in response to the fearful faces, and ACC activation was apparent, also to fearful faces only. The results suggest that the processing of emotions first engaged the earlier-developing amygdalae, but was non-specific in regards to the emotion, and then by the teenaged years, involved the later-maturing ACC system. With increasing age there was also a shift in lateralisation of amygdala responses sensitive to the fearful faces. The findings are important to our understanding of the development of functional specialisation of fear perception over childhood; this is a late-maturing process involving the frontal-limbic emotion system. This study also suggests that there may be developmentally time-sensitive periods that influence the normal functioning of these brain regions.

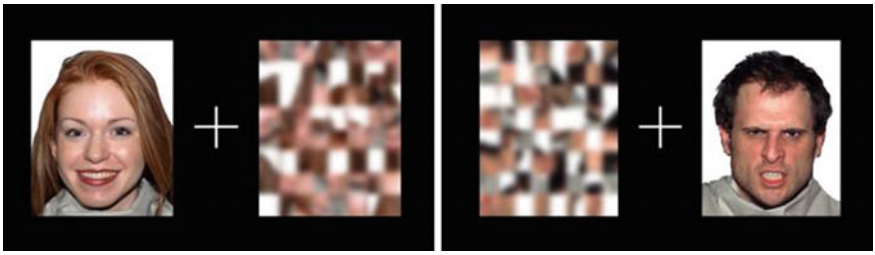

Fig. 1 Examples of the stimuli in the emotional faces task. Happy, angry or neutral faces were presented to the *left* or *right* of fixation, with their matched scrambled faces. Children responded with a *left* or *right* button press to indicate the side of the scrambled pattern, as quickly as possible

A subsequent study used angry faces rather than fearful faces, as anger is an emotional expression that is more commonly experienced in childhood (Todd et al. 2012), and is one with which children with autism have particular difficulties (e.g., Kuusikko et al. 2009). Seventeen adults (23.0 + 1.9 years) and 14 adolescents (14.4 + 1.1 years) were tested. Happy, neutral and angry male and female faces were used from the NimStim Face Stimulus Set (Tottenham et al. 2009) (Fig. 1). Emotional faces and scrambled versions of each were presented concurrently on either side of a central fixation cross. Participants responded as quickly as possible to indicate the left or right location of the scrambled pattern by pressing the left or right button on a response button box. The stimuli were presented for 80 ms to avoid saccadic eye movement.

We conducted event-related beamforming analyses (Quraan and Cheyne 2010) on the MEG data in early time windows (60–200 ms). Happy and angry faces appeared to activate largely distinct brain regions (consistent with fMRI studies e.g., Kesler/West et al. 2001), and the patterns also differed with age group. In response to happy faces, we found that adults showed greater activity than adolescents, particularly at 100–140 ms, in left inferior frontal and inferior parietal lobule, as well as right middle temporal gyrus and superior parietal lobule (Fig. 2). At the same latency, adolescents showed greater activation in bilateral middle frontal regions. Adolescents showed greater activation to happy faces at 140–180 ms, with regions including bilateral inferior frontal, left superior frontal, and right superior temporal and middle frontal gyri. To angry faces, adults showed greater early (60–100 ms) activity in left inferior and right superior frontal regions while adolescents showed greater right middle frontal activation. Between 100–140 ms, adults showed greater right frontal and temporal activation to angry faces, whereas adolescents showed only greater left frontal and temporal activity (Fig. 2). This right hemisphere bias for adults, and left hemisphere bias for adolescents continued until 180 ms.

Early emotion-specific processing has been shown by Peyk et al. (2008) consistent with our findings of bilateral medial frontal activation in response to angry faces (140–180 ms) in adults, but no significant frontal activations to happy faces in this latency window. A number of studies have reported that the right

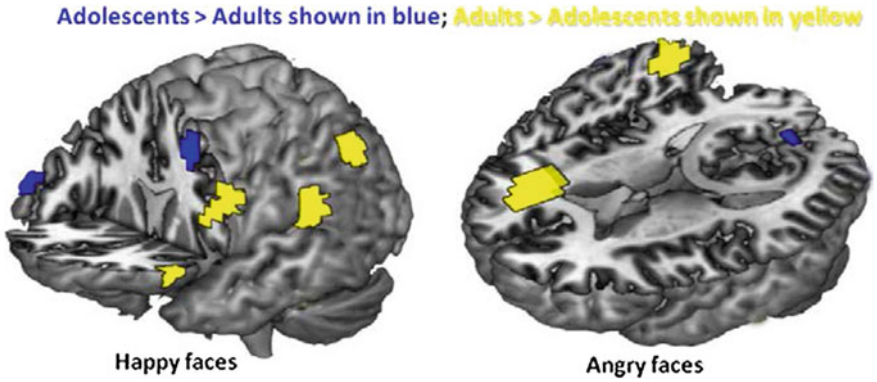

Fig. 2 Frontal and parietal activation to emotional faces differed between adults and adolescents between 100–140 ms—Adolescents > Adults shown in *blue*; Adults > Adolescents shown in *yellow*; happy (*left*) and angry (*right*). There was greater activation to the Happy than Angry faces in both age groups, and greater frontal activity to emotional faces in adults than in adolescents (in the *left* hemisphere for happy face, and the *right* for angry faces)

hemisphere may be dominant for processing negative emotional stimuli (Killgore and Yurgelun-Todd 2007, Fournier et al. 2008); the current data suggest that if this is the case, this lateralisation of function is not complete even in the teenage years. Thus, these MEG data demonstrate that in adolescence the neural mechanisms underlying the development of rapid, implicit and emotion-specific processing are distinct from those seen in adults, suggesting that these processes are continuing to mature.

1.2 Inhibition Skills and Imaging Studies

Inhibition is a key process underlying social cognitive function, as inhibition of context-inappropriate behaviour is critical for successful social functioning. Behavioural studies of inhibition indicate reliable improvements from early childhood to adulthood (Luna et al. 2004), and the ability to produce sustained inhibitory control continues to improve through adolescence. Inhibitory control is supported by a widely-distributed circuitry in which frontal cortex plays a primary role (Rubia et al. 2007).

fMRI investigations in adults have identified a distributed network of brain areas involved in inhibition including striatal and thalamic structures, motor areas, anterior cingulate, parietal lobes and the inferior and dorsolateral frontal gyri (Rubia et al. 2001; Watanabe et al. 2002; Mostofsky and Simmonds 2008). The frontal cortex has been shown to play a major role in inhibition by studies that employed Go/No-go tasks where contrasts were made between the activations of No-go (successful response inhibition) to Go trials (response execution) (see

review in (Dillon and Pizzagalli 2007)). Brain imaging findings in typical development, using Go/No-go tasks, vary extensively but have demonstrated a role for dorsolateral and inferior frontal regions in inhibition, although this involvement was not always reliably reported over childhood (e.g., Durston et al. 2002a; Tamm et al. 2004; Rubia et al. 2007).

Relatively few MEG studies have been conducted on inhibition and most included only a small number of sensors and/or subjects. We have tested adolescents and adults using MEG to determine the spatiotemporal brain dynamics of inhibitory control during the period of significant maturational changes over the teenage years. We used visual Go/No-go tasks that included a baseline condition with many more No-go than Go trials, allowing us to contrast only the No-go trials in the two runs, avoiding the confound of motor activity to the Go trials (Vidal et al. 2012). In this Go/No-go task, the Go stimuli were solid black shapes and No-go stimuli were the same shapes with a superimposed grey 'X' (Fig. 3). Similar to a recent ERP study (Bokura et al. 2001) we found right-lateralised frontal activity starting at 200 ms for the adults in the inhibition condition. Brain activations underlying inhibition in adolescents were slower, more superior and more bilateral in the frontal lobes compared to adults (Vidal et al. 2012). However, the low percentage (7 %) of Go trials in the control condition raised the possibility that the findings were influenced by an oddball effect. Thus, we ran a second study which also included two conditions, but the tasks contained inverse frequencies of Go to No-go trials for the experimental (67–33 %) and control (33–66 %) conditions to avoid an oddball confound and still allowed analysis of only trials pertinent to inhibition: the No-go trials (Vara et al. 2014). Only correct No-go trials from the two conditions were analysed.

The spatiotemporal brain profiles involved in inhibition were examined in 15 adolescents and 15 adults with this Go/No-go task. Contrasting brain activation during No-go trials using vector event-related beamformer (Quraan and Cheyne 2010) showed recruitment of the right inferior frontal gyrus in adults (BA 45; 200–250 ms), but bilateral and delayed recruitment of similar locations in adolescents (BA 45/9; 250–300 ms) (Fig. 4). Activity near the hand motor region in the left hemisphere (BA 6) was present in both groups but persisted for a longer time in adults, suggesting that adolescents relinquished more rapidly the preparation to respond following the No-go stimuli. Adolescents also recruited the right temporal (BA 21) and inferior parietal (BA 40) regions during inhibition, likely reflecting increased attention-related resources being recruited (Durston et al. 2002b, Hampshire et al. 2010) to perform at adult levels. The findings of both delayed frontal and additional cortical recruitment in the teenagers compared to adults (Vidal et al. (2012), Vara et al. 2014) underline the immaturity of the inhibitory network in adolescence. These studies also highlight the importance of MEG to determine the temporal and spatial changes in brain processes related to the late maturation of inhibitory control over adolescence and into adulthood.

In summary, the frontal lobes are critical for cognitive processes underlying social as well as other executive functions; disturbances in their development have long-term, profound consequences. As the development of the frontal lobes

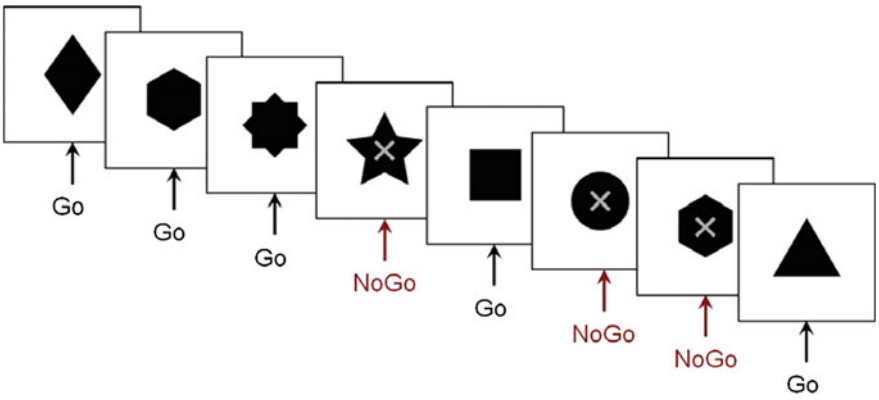

Fig. 3 Figure of Go/No-go protocol. An example of the stimuli in the Go/No-go tasks. Participants responded as quickly as possible to the stimuli except when there was a superimposed 'X'

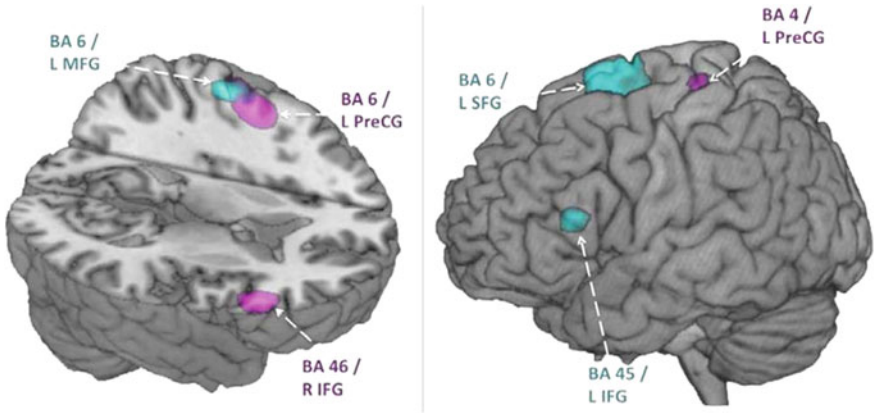

Fig. 4 Early activation in inhibition condition in adults and adolescents. Within group activations overlaid on brain images for 200–250 ms (*left*) and 250–300 ms (*right*). Inhibition condition > baseline condition, in adults shown in *magenta* ($p < 0.005$, uncorrected). Inhibition condition > baseline condition in adolescents shown in *blue* ($p < 0.005$, uncorrected). Note the early *right* IFG activation in adults, but the later *left* IFG in the teenagers. *L* Left, *R* Right, *MFG* Middle Frontal Gyrus, *SFG* Superior Frontal Gyrus, *IFG* Inferior Frontal Gyrus, *PreCG,* Precentral Gyrus

continues into adulthood, their functions are the most susceptible to developmental disturbances; they are also the most amenable to modification with interventions, making the investigation of abilities dependent on the frontal lobes of considerable importance in atypical development.

2 MEG Studies of Executive Functions in Autism Spectrum Disorder (ASD)

Autism is described as a disorder encompassing abnormal social reciprocity, abnormal language use and an intense desire for sameness. While current definitions of ASD encompass varying degrees of difficulties in these three spheres, impairments in social interaction are the most striking feature which even affects individuals with high communication and cognitive functioning abilities (Frith 2004).

Despite considerable evidence of abnormalities of brain development in ASD, there is little consensus on how these findings lead to clinical and behavioural manifestations of ASD. Some findings suggest that some young children with ASD have a 5–10 % abnormal enlargement in total brain volume (Sparks et al. 2002, Courchesne 2004, Hazlett et al. 2005); the most reliable increases are reported in the frontal lobes, particularly in dorsolateral and medial frontal cortices (Carper and Courchesne 2005), which are areas strongly implicated in social cognitive function (Lewis et al. 2011, Telzer et al. 2011). Our own work with children 6–14 years of age found a trend for decreasing grey matter in typical children, but increasing grey matter in children with ASD (Mak-Fan et al. 2012). ASD children also show reduced measures of white matter integrity as assessed with DTI that are particularly marked in the long-range fibres and areas linked to social cognition (Cheng et al. 2010; Shukla et al. 2011; Mak-Fan et al. 2013).

2.1 Deficits in Social Cognition as Assessed with Emotional Faces in ASD

Face processing is central to much of social cognition. The behavioural literature has long reported face processing dysfunction in ASD; people with ASD exhibit poor eye contact (Hobson and Lee 1998) and look less at others' faces (Langdell 1978). Many of the cognitive neuroimaging studies in ASD have focused on face processing, frequently finding atypical activation patterns in the fusiform gyri and/or amygdalae (Pierce et al. 2001; Amaral et al. 2003). In an ERP study we found that early responses to emotional faces were delayed and smaller in children with ASD (Batty et al. 2011), emphasising the need for the use of neuroimaging techniques with high temporal and spatial resolution, such as MEG, to investigate these issues. Face affect protocols in ASD participants have reported reduced activation in the medial prefrontal and STS regions (Pelphrey et al. 2007; Wang et al. 2007), key areas of the social brain network.

Emotional faces are arguably the most critical visual emotional stimuli and the ability to perceive, recognize, and interpret emotions is central to social interaction and communication. As impaired social interaction is one of the hallmarks of ASD, studies on the neural and cognitive mechanisms underlying emotional face

processing in ASD are critical. Using an implicit emotional face processing task while acquiring MEG data (as detailed above), we examined spatiotemporal differences in neural activation during angry and happy emotional face processing in adolescents with and without ASD. The study included 12–15 year-olds, 14 in each group, with the controls being age- and sex-matched with the ASD teenagers. Both groups completed the Affect Recognition subtest of the NEPSY-II (Korkman et al. 2007); the scores on this test and response latencies on the emotional face task during MEG acquisition did not differ between groups. This argues that group differences found in neural activity on the emotional face task were not due to differences in perceived task difficulty. We focused on the MEG responses in the frontal lobes.

Early significant between-group differences to happy faces occurred at 80–120 ms, during which adolescents with ASD exhibited greater right superior and inferior frontal activation relative to controls. In contrast, controls showed greater superior temporal activation, relative to the ASD group, which is consistent with earlier findings of reduced superior temporal activation in individuals with ASD to faces (Pierce et al. 2001) and during social processing (Castelli et al. 2002) in a task that involved attributing mental states to geometric objects.

In response to the angry faces from 160–240 ms, we found greater left middle temporal activation in adolescents with ASD, relative to controls, consistent with the results of an emotional face matching task (Wang et al. 2004). This was in contrast, however, to greater left middle temporal activation seen in controls during explicit emotional face processing (Critchley et al. 2000), suggesting the involvement of different neural structures during explicit and implicit emotional face processing, also confirmed by our group (Bayle and Taylor 2010). In adolescents with ASD, greater activation occurred in the left BA 10 (superior frontal gyrus) while in typically developing controls, greater activation occurred in the right BA 10 (middle frontal gyrus). Our within-group analyses of orbitofrontal activation in controls to angry faces are consistent with evidence in the literature of the orbitofrontal cortex playing a role in anger processing (Blair et al. 1999; Luo et al. 2007). In controls, left orbitofrontal activation was first observed in BA10 from 120–160 ms, bilateral activation during 160–200 ms, which continued into 200–240 ms (right only). In contrast, adolescents with ASD show a delayed trend, with left BA10 activation starting at 200–240 ms, then bilateral activation from 240–280 ms. An atypical pattern of orbitofrontal activity to angry faces was seen in the adolescents with ASD compared to the controls; it was temporally shifted and had a different lateralization pattern Furthermore, between 200–240 ms, between-group comparisons showed greater left orbitofrontal activation in adolescents with ASD while controls showed greater right orbitofrontal activation. As left and right hemisphere advantages have been indicated for holistic and featural face processing, respectively, these findings are consistent with the notion that individuals with ASD utilise alternative face processing strategies, endorsing feature-based rather than holistic information processing (Hillger and Koenig 1991).

Of particular interest was the finding of similar MEG activity during happy, but not angry, face processing, suggesting more typical processing of happy faces in individuals with ASD. In response to angry faces, we found temporally delayed and contralateral activation of the orbitofrontal cortex, an area that has been implicated in anger processing. These data are also consistent with behavioural studies that show high functioning ASD participants perform comparably to controls on tasks involving happy faces, but have the most difficulty with angry faces (Kuusikko et al. 2009; Rump et al. 2009). Furthermore, our data suggest different emotional face processing strategies in individuals with ASD, who may use more local, feature-based processing strategies compared to typically developing individuals, who endorse more holistic strategies when processing emotional faces.

2.2 Difficulties with Inhibitory Control in ASD

Inhibitory control is often deficient in people with ASD, underlying in part their difficulties with emotional outbursts and inappropriate social behaviour. Given its protracted developmental course (Luna et al. 2010; Vidal et al. 2012), inhibition is an important area of investigation in teenagers with ASD, as they are adapting to increasing social demands. Luna et al. (2004) proposed that deficits in inhibitory capacities increase with age in autism, as the inhibitory demands increase in adolescence, a period of critical social development.

Some studies have investigated inhibition tasks in ASD. Adults with ASD show activation with notable differences in the patterns from that seen in controls, e.g., greater left frontal activity (Schmitz et al. 2006), reduced anterior cingulate activity (Kana et al. 2007), as well as in the timing of the brain activation within the frontal network. However, as inhibition is largely dependent upon the slowly maturing frontal lobes, the results from these adult studies cannot be used to generalise to a younger population. To date, there has been little research conducted on the period of brain maturation through adolescence in ASD, when adult levels of inhibition are being established in typically developing individuals which are critical to the establishment of normal social relationships.

To better understand the maturation of inhibition skills in ASD, we acquired MEG measures of brain activity during a Go/No-go task with adolescents and adults with ASD and age- and sex-matched controls (see Vara et al. 2014). There were 15 participants in each of the four groups. During the tasks participants responded to Go stimuli and withheld their response to No-go stimuli (as detailed above). Inhibition (MEG responses to the No-go trials) was compared between individuals with and without ASD. In the comparison between the adult groups, lateralisation differences were found: adults with ASD activated the left inferior prefrontal cortex and control adults recruited the right inferior prefrontal cortex. Adolescents with ASD recruited predominantly frontal regions, unlike their matched controls who showed bilateral frontal activation, as well as activity in temporal and parietal regions (Fig. 5). Implications include immature and deficient

processing in adolescents with ASD, whose false alarm rate was also higher than the control groups, demonstrating poorer inhibitory control. This may be partially accounted for by their failure to recruit distal cortical regions to supplement poor frontal lobe function.

Comparisons of the four groups showed that adults with ASD recruited the left inferior frontal gyrus, similar to typically developing adolescents, but adults with ASD recruited this frontal region at an earlier time than typical adolescents. However, the adults with ASD also activated areas similar to control adults. Although ASD adolescents recruited an inhibitory neural network that differed from age-matched controls, in adulthood functional activity was more comparable, which may suggest some resiliency in the development of this network in ASD adults.

3 MEG Studies of Language Production

While language is a complex phenomenon that requires the integration of distributed brain regions, research in language relies on a framework that emphasises two key areas responsible for core language function. This framework, based on classic neuropsychological data, is referred to as the Wernicke-Geschwind model of language organization (Geschwind 1970). This model suggests that in a typical adult brain, language is located primarily in the left hemisphere with receptive language subsumed in Wernicke's area at the left temporo-parietal junction, and expressive language controlled by Broca's area in the left inferior frontal gyrus (Broca 1861; Wernicke 1874). These two regions have complex and reciprocal connections between primary sensory, secondary sensory and association areas which are incorporated into more specific and complex models, but the basic Wernicke-Geschwind structure is helpful for framing neuroimaging studies (Demonet et al. 2005)

Receptive language has been well studied with MEG (see (Salmelin 2007) for a review). Protocols exist that localize Wernicke's area, and these have been confirmed in healthy (Papanicolaou et al. 2006) and clinical subjects (Simos et al. 1999; Kamada et al. 2007; Breier et al. 2009) and validated against other imaging modalities (Billingsley-Marshall et al. 2007).

Expressive language has been more difficult to study with MEG, for a number of reasons. The large muscle artefact from mouth and tongue movements with speech is problematic, as is the trial-by-trial variability inherent to a complex exogenous response such as speech production (Salmelin 2007). To address these issues, many groups have developed expressive language paradigms that do not require an overt verbal response. For example, Dhond et al. (2001) used a silent word stem completion task, while others used picture/object naming or reading (Vihla et al. 2006; Herdman et al. 2007; Liljestrom et al. 2009; Wheat et al. 2010), and imaginary speech articulation (Kato et al. 2007); others have implemented delayed response paradigms (Breier and Papanicolaou 2008).

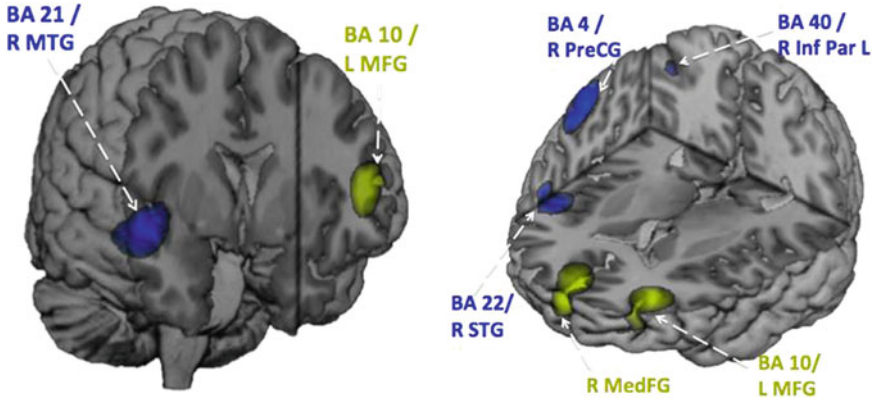

Fig. 5 Inhibition activation in adolescents with and without ASD. Significant ($p < 0.005$) neural activations for ASD (*yellow*) and control adolescents (*blue*), where the inhibition condition was greater than the baseline condition, at 300–350 ms (*left*) and 350–400 ms (*right*). *L* Left, *R* Right, *MTG* Middle Temporal Gyrus, *MFG* Middle Frontal Gyrus, *STG* Superior Temporal Gyrus, *PreCG* Precentral Gyrus, *MedFG* Medial Frontal Gyrus, *Inf Par L* Inferior Parietal Lobule

3.1 Localizing Expressive Language Areas in Children

We have developed an expressive language paradigm that can be used to lateralize and localize frontal language areas in young children. The stimuli consist of high-quality colour pictures of objects familiar to a typically developing 5 year old child (Fig. 6). Children, depending on their ability, are instructed to complete a verb generation task. If unable to do this, they are asked, instead, to name the object in the picture. To ensure that children are alert and attending to stimulus presentation, a 'vigilance trial' is presented with a frequency of 10 %. When children see this stimulus, they are instructed to press a button; these button presses are monitored as a surrogate measure of task attention. After MEG testing, the children are shown the images outside the scanner and asked to complete the task again, overtly. Differential synthetic aperture magnetometry analyses (Robinson and Vrba 1999; Vrba and Robinson 2001) identified task-related low beta desynchronization in left inferior frontal cortex in a group of healthy children aged 13–18 years and in a small clinical series in children with epilepsy and brain tumours (Kadis et al. 2008). We then extended this series to include children as young as 5 years of age, and in all subjects we were successful in identifying Broca's area (Kadis et al. 2011) (Fig. 7). However, the intriguing finding was a significant positive correlation between left hemisphere lateralization and age. This suggested that the left hemisphere frontal language dominance, seen in adults, emerges with development and is, in fact, bilateral in young children.

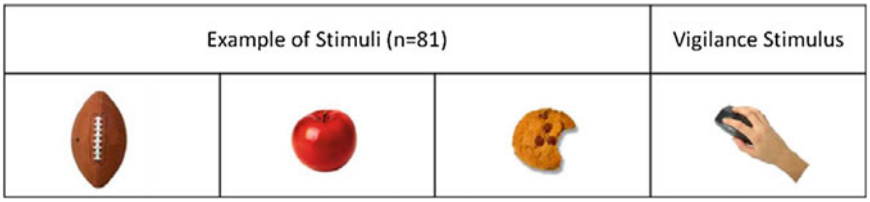

Fig. 6 Sample of stimuli used in MEG verb generation task

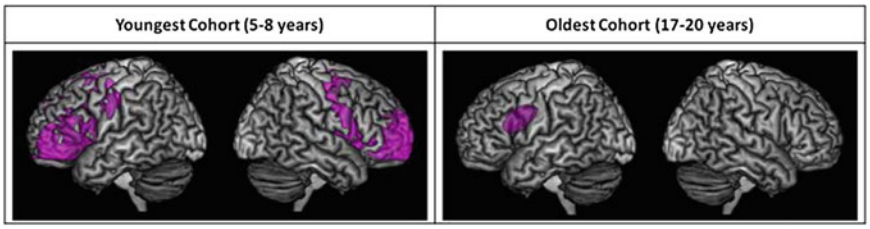

Fig. 7 Event-related desynchronization localizes inferior frontal areas involved in verb generation. In the youngest cohort, the localization is bilateral; whereas in the oldest cohort, the typical *left* lateralization is seen

3.2 fMRI Validation of MEG Expressive Language Task

To validate this expressive language paradigm, we conducted an MEG-fMRI study where the same group of adolescents completed the same tasks in both modalities on the same day. Resultant images from MEG and fMRI analyses were normalized into Talairach space and overlaid onto each individual's structural MRI. After significance testing, the number of remaining voxels from both MEG and fMRI were counted; as well, the number of voxels that overlapped in both modalities was counted. MEG and fMRI showed 100 % concordance for laterality and 79.6 % voxel overlap. We concluded that our MEG paradigm showed high concordance with fMRI verb generation, which is the current clinical gold standard for pre-surgical evaluation of language; thus, MEG is a promising alternative method for the non-invasive localization of frontal language (Pang et al. 2011).

3.3 Sex Differences in Language Lateralization in Young Children

To further examine the bilateral involvement of the frontal lobes in expressive language across development, we conducted a large-scale MEG study where 80 typically developing children (aged 4–18; 48 girls) completed our picture verb

generation task (Yu et al. 2012). MEG data were analyzed for each subject and then grouped by age and sex. The magnitude of event-related desynchronization (ERD) in canonical language areas was calculated as a percentage of total ERD. Boys and girls exhibited significantly different patterns of ERD magnitude in the youngest age groups, and these became increasingly similar as the groups approached the teenage years. Specifically, a strong left lateralization was seen in the boys in the youngest age group, and this was maintained through all age groups. The girls, however, showed a bilateral activation in the youngest groups, which progressively became more left lateralized with age, but did not become predominantly left lateralized until around 16 years. Furthermore, boys showed a significantly greater percentage of ERD activation in canonical language areas during childhood and adolescence, while girls showed lower ERD in canonical language areas and this pattern changed to become more comparable to the boys at around age 10 years. This is interesting as behavioural studies have reported that young boys and girls use different strategies when completing verbal learning and word recall tasks (Kramer et al. 1997); our MEG findings may be capturing these sex-related preferences for different language strategies. Our study suggests, however, the laterality differences do not persist into adulthood, and this is consistent with what is reported in the adult literature. These data emphasize the need to look carefully at age-related and sex-related factors when testing young children, especially as MEG is sensitive enough to capture subtle processing differences that index strategy differences despite similar performance.

3.4 Connectivity Within the Frontal Language Network

Having demonstrated that MEG can localize the left inferior frontal regions involved in language production, we were interested in examining how this region communicates with other regions in the language network. It is thought that low-gamma band (<30 hz) synchronization between neural regions is the underlying mechanism for the integration of functional cortical networks while theta-band oscillations (4–8 Hz) are the key to local regional integration (Ward 2003; Canolty and Knight 2010). Using MEG data from a covert picture verb generation task, we examined inter-regional phase locking between left inferior frontal gyrus and other brain areas, and computed the modulation of inter-regional gamma synchronization by theta phase. We found task-related transient gamma-band long-range synchronization was modulated by the phase of regional theta oscillations (Fig. 8). This was the first evidence of gamma-band synchronization and theta-band modulation within the expressive language network (Doesburg et al. 2012). Furthermore, these findings revealed the extensive connectivity of the left inferior frontal gyrus and confirm the long-held belief that this brain region plays a pivotal role in expressive language control.

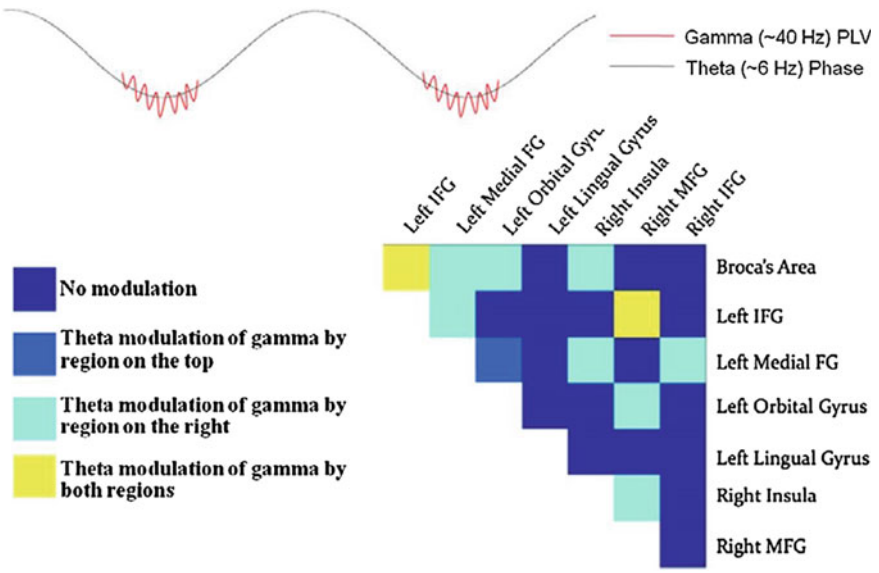

Fig. 8 Neural areas where gamma oscillations induced by verb generation were modulated by regional theta oscillations

4 Practical Considerations for Testing Children in the MEG

We hope, in this review, that we have demonstrated the value of developmental studies and testing children along the age spectrum. Many of the results that we have described show surprising and dramatic changes across age, not just in childhood, but into the teenage and young adult years. Furthermore, the language study reported sex differences only in the youngest age groups which disappeared by the adolescent years; again, emphasizing what may be missed if all stages of the developmental spectrum are not given full scrutiny. Having said this, running developmental studies requires many practical considerations. This last section will describe some of the challenges involved in testing children and provide commentary on some technical and task issues to consider prior to embarking on a developmental study. The reader is referred to Pang (2011) for a more extensive discussion.

When testing children, the most challenging technical factor to overcome is that of movement artefact. While voluntary movement of the head and eyes can be addressed by training, researchers need to be aware that paradigms may need to be lengthened and trial numbers increased to allow for rejection of trials containing unacceptable muscle artefacts. New MEG systems with continuous head localization hold good promise for addressing head movements, but these solutions are valid within a small range and cannot correct for the activities of an agitated, hyperactive or uncooperative child.

Smaller, child-sized, MEG helmets may be very helpful in dealing with head movement, as there is less room for the child to move. These child-sized MEG systems have the further benefit of placing the sensors much closer to the head surface, resulting in significant improvement to the signal to noise ratio, but unfortunately leave some frontal areas without sensor coverage. Institutions owning one of the systems would still need an adult system as the helmets will fit a typical child until the early school years (approximately 4–5 years of age), but would not fit a pre-teen or teenaged individual.

In the studies we have described in this review, our primary strategies for dealing with head movement have been training and subject preparation. The laboratory staff, who are responsible for running these studies, ensure that all subjects, clinical or control, understand the importance of staying still, and subjects are monitored and reminded of this throughout the testing. Furthermore, subjects are offered breaks as often as necessary to ensure compliance with staying still. In addition, our teams have had good success with applying padding into the dewar to stabilize the head, as well as covering the child with a blanket to reduce body movement and thus head movement.

The other important consideration for developmental studies is task design. Tasks need to be age-appropriate, simple, understandable, engaging and quick. In this review, we have presented a variety of tasks which we have found to be effective in children. What may not be obvious to the reader, since the tasks and stimuli look very simple, is the amount of work required to develop, pilot and validate stimuli and tasks for children. Often we start with an adult version of the task and ask what the core function is that we would like to test, then we pare the task down to this core function and develop a paradigm around it. This reduces, but does that eliminate, the possibility that children use different strategies, and that these strategies may differ at different ages, and maybe even between sexes.

There is no guarantee, but an awareness of the challenges and issues unique to testing children increases the likelihood of obtaining valid and reliable data.

5 Summary

We have shown some of the detailed spatial and temporal data available from MEG studies examining the development of social, executive and language skills in typically developing children and children with autism spectrum disorders. The results of these studies emphasize the importance of developmental research as there are variable and subtle changes in brain function that are related to age, sex and clinical condition. Furthermore, we hope that these studies highlight the potential for using MEG as a research tool to examine the spatiotemporal involvement of important brain areas, with an emphasis in this chapter on the frontal lobes. Finally, we hope that our brief discussion of practical considerations for developmental research will help guide labs to explore the possibility of testing children and looking specifically at the maturation of the brain and its corresponding behaviour.

References

Adolphs R, Damasio H, Tranel D (2002) Neural systems for recognition of emotional prosody: a 3-D lesion study. Emotion 2:23–51

Allison T, Puce A, McCarthy G (2000) Social perception from visual cues: role of the STS region. Trends Cogn Sci 4:267–278

Amaral DG, Bauman MD, Schumann CM (2003) The amygdala and autism: implications from non-human primate studies. Genes, Brain Behav 2:295–302

Batty M, Meaux E, Wittemeyer K, Roge B, Taylor MJ (2011) Early processing of emotional faces in children with autism. J Exp Child Psychol 109:430–444

Batty M, Taylor MJ (2003) Early processing of the six basic facial emotional expressions. Cogn Brain Res 17:613–620

Bayle DJ, Taylor MJ (2010) Attention inhibition of early cortical activation to fearful faces. Brain Res 1313:113–123

Billingsley-Marshall RL, Clear T, Mencl WE, Simos PG, Swank PR, Men D, Sarkari S, Castillo EM, Papanicolaou AC (2007) A comparison of functional MRI and magnetoencephalography for receptive language mapping. J Neurosci Methods 161:306–313

Blair RJ, Morris JS, Frith CD, Perrett DI, Dolan RJ (1999) Dissociable neural responses to facial expressions of sadness and anger. Brain 122(5):883–893

Bokura H, Yamaguchi S, Kobayashi S (2001) Electrophysiological correlates for response inhibition in a Go/NoGo task. Clin Neurophysiol 112:2224–2232

Breier JI, Juranek J, Maher LM, Schmadeke S, Men D, Papanicolaou AC (2009) Behavioral and neurophysiologic response to therapy for chronic aphasia. Arch Phys Med Rehabil 90:2026–2203

Breier JI, Papanicolaou AC (2008) Spatiotemporal patterns of brain activation during an action naming task using magnetoencephalography. J Clin Neurophysiol 25:7–12

Broca P (1861) Perte de la parole, ramolissement chronique et destruction partielle du lobe anteriéur gauche du cerveau. Bulletin et Memoires de la Societe d'Anthropologie de Paris 2:235–238

Burnett S, Bird G, Moll J, Frith C, Blakemore SJ (2009) Development during adolescence of the neural processing of social emotion. J Cogn Neurosci 21:1736–1750

Bush G, Luu P, Posner MI (2000) Cognitive and emotional influences in anterior cingulate cortex. Trends Cogn Sci 4:215–222

Canolty RT, Knight RT (2010) The functional role of cross-frequency coupling. Trends Cogn Sci 14:506–515

Carper RA, Courchesne E (2005) Localized enlargement of the frontal cortex in early autism. Biol Psychiatry 57:126–133

Carter EJ, Pelphrey KA (2008) Friend or foe? Brain systems involved in the perception of dynamic signals of menacing and friendly social approaches. Soc Neurosci 3:151–163

Castelli F, Frith C, Happe F, Frith U (2002) Autism, Asperger syndrome and brain mechanisms for the attribution of mental states to animated shapes. Brain 125(8):1839–1849

Cheng Y, Chou KH, Chen IY, Fan YT, Decety J, Lin CP (2010) Atypical development of white matter microstructure in adolescents with autism spectrum disorders. Neuroimage 50:873–882

Courchesne E (2004) Brain development in autism: early overgrowth followed by premature arrest of growth. Mental Retard Dev Disabil Res Rev 10:106–111

Critchley HD, Daly EM, Bullmore ET, Williams SC, Van Amelsvoort T, Robertson DM, Rowe A, Phillips M, McAlonan G, Howlin P, Murphy DG (2000) The functional neuroanatomy of social behaviour: changes in cerebral blood flow when people with autistic disorder process facial expressions. Brain 123(11):2203–2212

Demonet JF, Thierry G, Cardebat D (2005) Renewal of the neurophysiology of language: functional neuroimaging. Physiol Rev 85:49–95

Dhond RP, Buckner RL, Dale AM, Marinkovic K, Halgren E (2001) Spatiotemporal maps of brain activity underlying word generation and their modification during repetition priming. J Neurosci 21:3564–3571

Dillon DG, Pizzagalli DA (2007) Inhibition of action, thought, and emotion: a selective neurobiological review. Appl Prev Psychol 12:99–114

Doesburg SM, Vinette SA, Cheung MJ, Pang EW (2012) Theta-modulated gamma-band synchronization among activated regions during a verb generation task. Front Psychol 3:195

Durston S, Thomas KM, Worden MS, Yang Y, Casey BJ (2002a) The effect of preceding context on inhibition: an event-related fMRI study. Neuroimage 16:449–453

Durston S, Thomas KM, Yang Y, Ulu AM, Zimmerman RD, Casey BJ (2002b) A neural basis for the development of inhibitory control. Dev Sci 4:9–16

Elliott R (2003) Executive functions and their disorders. Br Med Bull 65:49–59

Fournier NM, Calverley KL, Wagner JP, Poock JL, Crossley M (2008) Impaired social cognition 30 years after hemispherectomy for intractable epilepsy: the importance of the right hemisphere in complex social functioning. Epilepsy Behav 12:460–471

Frith U (2004) Emanuel Miller Lecture: confusions and controversies about Asperger syndrome. J Child Psychiatry 45:672–686

Geschwind N (1970) The organization of language and the brain. Science 170:940–994

Hall J, Whalley HC, McKirdy JW, Sprengelmeyer R, Santos IM, Donaldson DI, McGonigle DJ, Young AW, McIntosh AM, Johnstone EC, Lawrie SM (2010) A common neural system mediating two different forms of social judgement. Psychol Med 40:1183–1192

Hampshire A, Chamberlain SR, Monti MM, Duncan J, Owen AM (2010) The role of the right inferior frontal gyrus: inhibition and attentional control. Neuroimage 50:1313–1319

Haxby JV, Hoffman EA, Gobbini MI (2000) The distributed human neural system for face perception. Trends Cogn Sci 4:223–233

Hazlett HC, Poe M, Gerig G, Smith RG, Provenzale J, Ross A, Gilmore J, Piven J (2005) Magnetic resonance imaging and head circumference study of brain size in autism: birth through age 2 years. Arch Gen Psychiatry 62:1366–1376

Herdman AT, Pang EW, Ressel V, Gaetz W, Cheyne D (2007) Task-related modulation of early cortical responses during language production: an event-related synthetic aperture magnetometry study. Cereb Cortex 17:2536–2543

Hillger LA, Koenig O (1991) Separable mechanisms in face processing: evidence from hemispheric specialization. J Cogn Sci 3:42–58

Hobson RP, Lee A (1998) Hello and goodbye: a study of social engagement in autism. J Autism Dev Disord 28:117–127

Hung Y, Smith ML, Bayle DJ, Mills T, Cheyne D, Taylor MJ (2010) Unattended emotional faces elicit early lateralized amygdala-frontal and fusiform activations. Neuroimage 50:727–733

Hung Y, Smith ML, Taylor MJ (2012) Development of ACC-amygdala activations in processing unattended fear. Neuroimage 60:545–552

Jackson MC, Wolf C, Johnston SJ, Raymond JE, Linden DE (2008) Neural correlates of enhanced visual short-term memory for angry faces: an FMRI study. PLoS ONE 3:e3536

Kadis DS, Pang EW, Mills T, Taylor MJ, McAndrews MP, Smith ML (2011) Characterizing the normal developmental trajectory of expressive language lateralization using magnetoencephalography. J Intern Neuropsychol Soc 17:896–904

Kadis DS, Smith ML, Mills T, Pang EW (2008) Expressive language mapping in children using MEG; MEG localization of expressive language cortex in healthy children: Application to paediatric clinical populations. Down Syndr Q 10:5–12

Kamada K, Sawamura Y, Takeuchi F, Kuriki S, Kawai K, Morita A, Todo T (2007) Expressive and receptive language areas determined by a non-invasive reliable method using functional magnetic resonance imaging and magnetoencephalography. Neurosurgery 60:296–305

Kana RK, Keller TA, Minshew NJ, Just MA (2007) Inhibitory control in high-functioning autism: decreased activation and underconnectivity in inhibition networks. Biol Psychiatry 62:198–220

Kato Y, Muramatsu T, Kato M, Shintani M, Kashima H (2007) Activation of right insular cortex during imaginary speech articulation. NeuroReport 18:505–509

Kesler West ML, Andersen AH, Smith CD, Avison MJ, Davis CE, Kryscio RJ, Blonder LX (2001) Neural substrates of facial emotion processing using fMRI. Cogn Brain Res 11:213–226

Killgore WD, Yurgelun-Todd DA (2007) The right-hemisphere and valence hypotheses: could they both be right (and sometimes left)? Soc Cogn Affect Neurosci 2:240–250

Kilts CD, Egan G, Gideon DA, Ely TD, Hoffman JM (2003) Dissociable neural pathways are involved in the recognition of emotion in static and dynamic facial expressions. Neuroimage 18:156–168

Kolb B, Wilson B, Taylor L (1992) Developmental changes in the recognition and comprehension of facial expression: implications for frontal lobe function. Brain Cogn 20:74–84

Korkman M, Kirk U, Kemp S (2007) NEPSY-II: a developmental neuropsychological assessment. The Psychological Corporation, San Antonio

Kramer JH, Delis DC, Kaplan E, O'Donnell L, Prifitera A (1997) Developmental sex differences in verbal learning. Neuropsychology 11:577–584

Kramer UM, Mohammadi B, Donamayor N, Samii A, Munte TF (2010) Emotional and cognitive aspects of empathy and their relation to social cognition–an fMRI-study. Brain Res 1311:110–120

Kuusikko S, Haapsamo H, Jansson-Verkasalo E, Hurtig T, Mattila ML, Ebeling H, Jussila K, Bolte S, Moilanen I (2009) Emotion recognition in children and adolescents with autism spectrum disorders. J Autism Dev Disord 39:938–945

Lamm C, Lewis MD (2010) Developmental change in the neurophysiological correlates of self-regulation in high- and low-emotion conditions. Dev Neuropsychol 35:156–176

Langdell T (1978) Recognition of faces: an approach to the study of autism. J Child Psychol Psychiatry 19:225–268

Lewis PA, Rezaie R, Brown R, Roberts N, Dunbar RI (2011) Ventromedial prefrontal volume predicts understanding of others and social network size. NeuroImage 57:1624–1629

Liljestrom M, Hulten A, Parkkonen L, Salmelin R (2009) Comparing MEG and fMRI views to naming actions and objects. Hum Brain Mapp 30:1845–1856

Luna B, Garver KE, Urban TA, Lazar NA, Sweeney JA (2004) Maturation of cognitive processes from late childhood to adulthood. Child Dev 75:1357–1372

Luna B, Padmanabhan A, O'Hearn K (2010) What has fMRI told us about the development of cognitive control through adolescence? Brain Cogn 72:101–113

Luo Q, Holroyd T, Jones M, Hendler T, Blair J (2007) Neural dynamics for facial threat processing as revealed by gamma band synchronization using MEG. Neuroimage 34:839–847

Mak-Fan K, Taylor MJ, Roberts W, Lerch JP (2012) Measures of cortical grey matter structure and development in children with Autism Spectrum Disorder (ASD). J Autism Dev Disord 42(3):419–427

Mak-Fan K, Morris D, Anagnostou E, Roberts W, Taylor MJ (2013) White matter and development in children with an Autism Spectrum Disorder (ASD). Autism 17(5):541–557

McCarthy G, Puce A, Belger A, Allison T (1999) Electrophysiological studies of human face perception. II: Response properties of face-specific potentials generated in occipitotemporal cortex. Cereb Cortex 9:431–444

Mehta MA, Gore-Langton E, Golembo N, Colvert E, Williams SC, Sonuga-Barke E (2010) Hyporesponsive reward anticipation in the basal ganglia following severe institutional deprivation early in life. J Cogn Neurosci 22:2316–2325

Mills T, Lalancette M, Moses SN, Taylor MJ, Quraan MA (2012) Techniques for detection and localization of weak hippocampal and medial frontal sources using beamformers in MEG. Brain Topogr 25:248–263

Mostofsky SH, Simmonds DJ (2008) Response inhibition and response selection: two sides of the same coin. J Cogn Neurosci 20:751–761

Pang EW (2011) Practical aspects of running developmental studies in the MEG. Brain Topogr 24(3–4):253–260

Pang EW, Wang F, Malone M, Kadis DS, Donner EJ (2011) Localization of Broca's area using verb generation tasks in the MEG: validation against fMRI. Neurosci Lett 490:215–219

Papanicolaou AC, Pazo-Alvarez P, Castillo EM, Billingsley-Marshall RL, Breier JI, Swank PR, Buchanan S, McManis M, Clear T, Passaro AD (2006) Functional neuroimaging with MEG: normative language profiles. Neuroimage 33:326–342

Passarotti AM, Sweeney JA, Pavuluri MN (2009) Neural correlates of incidental and directed facial emotion processing in adolescents and adults. Soc Cogn Affect Neurosci 4:387–398

Pelphrey KA, Morris JP, McCarthy G, Labar KS (2007) Perception of dynamic changes in facial affect and identity in autism. Soc Cogn Affect Neurosci 2:140–149

Peyk P, Schupp HT, Elbert T, Junghofer M (2008) Emotion processing in the visual brain: a MEG analysis. Brain Topogr 20:205–215

Pierce K, Muller RA, Ambrose J, Allen G, Courchesne E (2001) Face processing occurs outside the fusiform 'face area' in autism: evidence from functional MRI. Brain 124:2059–2073

Powell KB, Voeller KK (2004) Prefrontal executive function syndromes in children. J Child Neurol 19:785–797

Quraan MA, Cheyne D (2010) Reconstruction of correlated brain activity with adaptive spatial filters in MEG. Neuroimage 49:2387–2400

Quraan MA, Moses SN, Hung Y, Mills T, Taylor MJ (2011) Detection and localization of evoked deep brain activity using MEG. Hum Brain Mapp 32:812–827

Radke S, de Lange FP, Ullsperger M, de Bruijn ER (2011) Mistakes that affect others: an fMRI study on processing of own errors in a social context. Exp Brain Res 211:405–413

Robinson SE, Vrba J (1999) Functional neuroimaging by synthetic aperture magnetometry. In: Yoshimoto T. et al. (eds) Recent advances in biomagnetism. Tohoku University Press, Sendai, pp 305–305

Rubia K, Russell T, Overmeyer S, Brammer MJ, Bullmore ET, Sharma T, Simmons A, Williams SC, Giampietro V, Andrew CM, Taylor E (2001) Mapping motor inhibition: conjunctive brain activations across different versions of go/no-go and stop tasks. Neuroimage 13:250–261

Rubia K, Smith AB, Taylor E, Brammer M (2007) Linear age-correlated functional development of right inferior fronto-striato-cerebellar networks during response inhibition and anterior cingulate during error-related processes. Hum Brain Mapp 28:1163–1177

Rump KM, Giovannelli JL, Minshew NJ, Strauss MS (2009) The development of emotion recognition in individuals with autism. Child Dev 80:1434–1447

Salmelin R (2007) Clinical neurophysiology of language: the MEG approach. Clin Neurophysiol 118:237–254

Satpute AB, Lieberman MD (2006) Integrating automatic and controlled processes into neurocognitive models of social cognition. Brain Res 1079:86–97

Schmitz N, Rubia K, Daly E, Smith A, Williams S, Murphy DG (2006) Neural correlates of executive function in autistic spectrum disorders. Biol Psychiatry 59:7–16

Shaw P, Kabani NJ, Lerch JP, Eckstrand K, Lenroot R, Gogtay N, Greenstein D, Clasen L, Evans A, Rapoport JL, Giedd JN, Wise SP (2008) Neurodevelopmental trajectories of the human cerebral cortex. J Neurosci 28:3586–3594

Shukla DK, Keehn B, Muller RA (2011) Tract-specific analyses of diffusion tensor imaging show widespread white matter compromise in autism spectrum disorder. J Child Psychol Psychiatry 52:286–295

Simos PG, Breier JI, Maggio WW, Gormley WB, Zouridakis G, Willmore LJ, Wheless JW, Constantinou JE, Papanicolaou AC (1999) Atypical temporal lobe language representation: MEG and intraoperative stimulation mapping correlation. NeuroReport 10:139–142

Sparks BF, Friedman SD, Shaw DW, Aylward EH, Echelard D, Artru AA, Maravilla KR, Giedd JN, Munson J, Dawson G, Dager SR (2002) Brain structural abnormalities in young children with autism spectrum disorder. Neurology 59:184–192

Tamm L, Menon V, Ringel J, Reiss AL (2004) Event-related FMRI evidence of frontotemporal involvement in aberrant response inhibition and task switching in attention-deficit/hyperactivity disorder. J Am Acad Child Adolesc Psychiatry 43:1430–1440

Taylor MJ, Bayless SJ, Mills T, Pang EW (2011a) Recognising upright and inverted faces: MEG source localisation. Brain Res 1381:167–174

Taylor MJ, Donner EJ, Pang EW (2012) fMRI and MEG in the study of typical and atypical cognitive development. Clin Neurophysiol 42:19–25

Taylor MJ, Mills T, Pang EW (2011b) The development of face recognition; hippocampal and frontal lobe contributions determined with MEG. Brain Topogr 3–4:261–270

Taylor MJ, Mills T, Smith ML, Pang EW (2008) Face processing in adolescents with and without epilepsy. Int J Psychophysiol 68:94–103

Taylor MJ, Mills T, Zhang L, Smith ML, Pang EW (2010) Face processing in children: novel MEG findings. In: Supek S, Susac A (eds) IFMBE Proceedings, vol 28, Springer, New York, pp 314–321

Telzer EH, Masten CL, Berkman ET, Lieberman MD, Fuligni AJ (2011) Neural regions associated with self control and mentalizing are recruited during prosocial behaviors towards the family. NeuroImage 58:242–249

Todd RM, Evans JW, Morris D, Lewis MD, Taylor MJ (2012) The changing face of emotion: age related patterns of amygdala activation to salient faces. Soc Cogn Affect Neurosci 6:12–23

Tottenham N, Tanaka JW, Leon AC, McCarry T, Nurse M, Hare TA, Marcus DJ, Westerlund A, Casey BJ, Nelson C (2009) The NimStim set of facial expressions: judgments from untrained research participants. Psychiatry Res 168:242–249

Vara, AS, Pang EW, Vidal J, Anagnostou E, Taylor MJ (2014) Go or No-go: the question of neural activations during inhibitory control from adolescence to adulthood

Vidal J, Mills T, Pang EW, Taylor MJ (2012) Response inhibition in adults and teenagers: spatiotemporal differences in the prefrontal cortex. Brain Cogn 79:49–59

Vihla M, Laine M, Salmelin R (2006) Cortical dynamics of visual/semantic versus phonological analysis in picture confrontation. Neuroimage 33:732–738

Vrba J, Robinson SE (2001) Signal processing in magnetoencephalography. Methods 25:249–271

Wang AT, Dapretto M, Hariri AR, Sigman M, Bookheimer SY (2004) Neural correlates of facial affect processing in children and adolescents with autism spectrum disorder. J Am Acad Child Adolesc Psychiatry 43(4):481–490

Wang AT, Lee SS, Sigman M, Dapretto M (2007) Reading affect in the face and voice: neural correlates of interpreting communicative intent in children and adolescents with autism spectrum disorders. Arch Gen Psychiatry 64:698–708

Ward LM (2003) Synchronous neural oscillations and cognitive processes. Trends Cogn Sci 7:553–559

Watanabe J, Sugiura M, Sato K, Sato Y, Maeda Y, Matsue Y, Fukuda H, Kawashima R (2002) The human prefrontal and parietal association cortices are involved in NO-GO performances: an event-related fMRI study. Neuroimage 17:1207–1216

Wernicke C (1874) Der Aphasiche symptomencomplex. Cohn & Weigert, Breslau

Wheat KL, Cornelissen PL, Frost SJ, Hansen PC (2010) During visual word recognition, phonology is accessed within 100 ms and may be mediated by a speech production code: evidence from magnetoencephalography. J Neurosci 30:5229–5233

Yakolev PI, Lecours AR (1967) The myelogenetic cycles of regional maturation of the brain. In: Minkowski A (ed) Regional development of the brain in early life. Blackwell, Oxford, pp 3–70

Yu VY, MacDonald MJ, Hua G, Oh A, Kadis DS, Pang EW (2012) Boys and girls show different developmental trajectories on a MEG language lateralization task. In: 18th international conference, BioMag Paris, France

Language Processing in Atypical Development: Looking Below the Surface with MEG

Maria Mody

Abstract Neurodevelopmental disorders like dyslexia and autism have witnessed an explosion of research in recent years, leading to detailed characterization of these conditions and paving the way for the identification of phenotypes. Common to both these disorders is an impairment of the language system. Deficits in phonological processing have been the single most consistent finding in individuals with dyslexia, affecting the acquisition of reading skills. In contrast, children and adults with autism spectrum disorder (ASD) have difficulty using semantic information, evident in their idiosyncratic vocabulary and excessively literal interpretation of statements. However, as the term implies, ASD is associated with very heterogeneous profiles and poor language may be related to a broader deficit in social reciprocity and motivation. Regardless, given the important prognostic value of early language abilities in later developmental outcomes, there has been a tremendous drive to better understand the neurobiological basis of language impairments in developmental disorders. Over the years, a growing appreciation of the workings of the human brain has pushed to the forefront noninvasive neuroimaging. Methods like electroencephalography (EEG) and magnetoencephalography (MEG) are providing useful insights into connectivity patterns in the brain by yielding information about temporal coupling in the millisecond time scale across brain regions and frequency bands of neural oscillations. The resulting "spectral-temporal-spatial" patterns of brain activity, characteristic of different cognitive processes, are providing meaningful probes for use in neuroscience and genetic studies toward an improved understanding, assessment and treatment of developmental disorders.

Keywords Children · Dyslexia · Autism · Language · Phonology · Semantics · Speech perception · Reading · Magnetoencephalography · Electroencephalography ·

M. Mody (✉)
Athinoula A. Martinos Center for Biomedical Imaging, Harvard Medical School and Massachusetts General Hospital, Harvard-MIT Division of Health Sciences and Technology, 149 13th Street, Charlestown, MA 02129, USA
e-mail: maria@nmr.mgh.harvard.edu

S. Supek and C. J. Aine (eds.), *Magnetoencephalography*,
DOI: 10.1007/978-3-642-33045-2_26,

Event-related potentials · Brain oscillations · Magnetic resonance imaging · Diffusion tensor imaging

1 Introduction

Dyslexia (or specific reading disability) is one of the most common learning disabilities, with prevalence rates ranging from 5 to 17.5 % of school-aged children. It affects about 80 % of all individuals identified as learning disabled (Shaywitz et al. 2007). Dyslexia is characterized by an unexpected difficulty in learning to read despite normal intelligence, motivation, and educational opportunity. Hallmarks of the disorder include poor word recognition, slow and/or inaccurate decoding and difficulties with spelling. Dyslexia represents the tail end of normal reading distribution and is a life-long condition. At the core of the problem is believed to be a deficit in phonological processing (Mody 2003a, for review). Specifically, poor readers lack phonological awareness, i.e., awareness of the segmentability of the speech stream into smaller units such as syllables and phonemes. Importantly, this deficit is evident in pre-school years, and hence serves as a risk factor for early identification and remediation of reading failure.

Autism spectrum disorder (ASD), like dyslexia, is both familial and heritable (Pennington and Gilger 1996; Ronald and Hoekstra 2011). It is considered to be the fastest growing category of developmental disorders, with recent estimates placing it at 1 in 161 children worldwide (Elsabbagh et al. 2012). ASD affects more boys than girls (4–1) and is diagnosed through the presence of deficits in social communication, repetitive behaviors and restricted interests; it falls along a continuum, varying widely in severity as well as in IQ and linguistic skill (Constantino et al. 2004). Despite the heterogeneity of ASD, a characteristic feature of children and adults on the spectrum is their limited use of language in social context (i.e., to request information, describe an event, or to comment). They also tend not to orient to speech from an early age (Klin 1991; Kuhl et al. 2005). There appears to be a growing belief that the communication impairment in autism may be secondary to a deficit in social reciprocity and motivation (Dawson et al. 1998; Swettenham et al. 1998; Schultz et al. 2000). In a simple sense, the absence of communicative intent may be due to a social deficit that disguises itself as an expressive language impairment (Happe and Frith 1996).

From a neurodevelopmental perspective, disorders like dyslexia and autism tend to be complex, having unknown or multiple etiologies. Unlike Fragile-X Syndrome and Down Syndrome that may be confirmed by genetic testing, the diagnosis of dyslexia and autism depend on standardized cognitive assessments, which tend to suffer from poor sensitivity and low specificity (Byrne et al. 2006; Risi et al. 2006). Particularly troublesome is the fact that whereas these disorders are considered life-long conditions, their diagnosis are far from stable. The varying severity and/or profile of language impairment with age and across subtypes of the

disorder add to the heterogeneity of the subjects across different studies, thereby contributing to the inconsistent findings. Results of structural and functional brain studies with dyslexia and autism suffer from similar criticisms, thereby making it difficult to interpret the many different areas in the brain that have been implicated, as well as identify a core neurobiological profile for each of these disorders.

Despite the issues of complexity and comorbidity of dyslexia and autism with specific language impairment (Kjelgaard and Tager-Flusberg 2001; Messaoud-Galusi and Marshall 2010), recent efforts to identify endophenotypes (i.e., cognitive markers that are inheritable and consistent at all stages of the disorder) along with advances in functional imaging of infants hold tremendous potential for early identification and remediation of neurodevelopmental disorders involving language.

Children's linguistic progress in early years, especially if there is a family history of speech and language difficulties, has important implications for later literacy development (Tomblin 1989). Catts et al. (1999) found that 70 % of their poor readers in second grade had a history of language and phonological processing problems in kindergarten. In fact, phonological awareness is the single best predictor of learning to read (Liberman and Shankweiler 1991) and correlates highly with word recognition; reading comprehension, however, is best predicted by oral language comprehension (namely, vocabulary and grammatical understanding) (Oakhill et al. 2003; Catts et al. 2006). Of particular relevance here is a characteristic difference between autism and dyslexia: whereas phonological deficits are at the core of developmental dyslexia, individuals with ASD appear to be unimpaired on phonological tasks but have deficits in semantic processing. This difference offers interesting points of interaction and divergence for linguistic exploration in these populations (Ricketts 2011). We focus below on language-related MEG findings in autism and dyslexia. First, however, we present a brief overview of the characteristic profiles and related theories of these disorders.

2 Historical Perspective

Over the years, deficits in phonological processing have been found to be the single most consistent finding in dyslexia (Ramus et al. 2003). According to the dual route account (Coltheart 2005), reading engages two routes: a phonological route, which involves decoding, especially for unfamiliar words and nonwords, and a lexical route, which involves word recognition of familiar regular words and irregular words. The achievement of reading mastery is characterized by highly automated phonological processing and increasing use of the lexical route. Findings suggest that dyslexics' difficulties with phonological processing may be traced to weak categorical perception of speech (Godfrey et al. 1981; Mody et al. 1997; Nittrouer 1999) related to their poor coding of phonetic distinctions in the speech stream. While the auditory versus speech-specific basis of the deficit has been a point of controversy (Studdert-Kennedy and Mody 1995; Mody 2003b, for

review), language-based intervention targeting phonological skills have yielded the most promising outcomes (Simos et al. 2002; Blachman et al. 2004). Importantly, despite improvements in decoding, adult dyslexic readers often struggle to achieve reading fluency (Shaywitz et al. 2003), which adversely affects their reading comprehension (Shankweiler et al. 1999). In summary, a deficit in phonological processing in early years may permeate the larger language system affecting later academic performance.

Individuals with dyslexia typically have IQ in the normal range. In contrast, at least half of all children who have autism are intellectually disabled. As such, language abilities may range from being non-verbal to highly idiosyncratic language with echolalia and unusual prosody. For the most part, children with ASD have receptive and expressive language impairments. Theories attempting to explain these deficits in individuals on the spectrum (excluding sensory impairment or other comorbid medical conditions) typically implicate social impairments and/or cognitive impairments. According to the social deficit account, an impaired theory of mind (Baron-Cohen 1995) would affect the acquisition of language. Problems with joint attention and shared referencing early in development at 9–12 months of age would lead to missed learning opportunities for building object-word associations due to a failure to infer the speaker's intention (Parish-Morris et al. 2007; Preissler 2008). The cognitive impairment theories, on the other hand, conceptualize language impairment in ASD as a type of or comorbid with specific language impairment (Kjelgaard and Tager-Flusberg 2001; Walenski et al. 2006; Whitehouse et al. 2007). As such, there appear to be ASD subtypes with and without language impairment.

Despite the shared linguistic features and cognitive markers across ASD with language impairment (ASD/LI+) and SLI, neuroimaging and genetic studies have found significant differences between the two disorders suggesting that they may only be loosely related (Williams et al. 2008).

3 Structural-Functional Language Network in the Brain: A Framework for Examining Language Impairment in Atypical Development

Prior to the introduction of non-invasive neuroimaging, post-mortem studies were the primary source of evidence of alterations in global brain morphology including cortical thinning, gyral atrophy, and total brain weight with normal aging, as well as in disease (Kemper 1994). Today, magnetic resonance imaging (MRI) allows us to examine and quantify the changes in vivo, providing in exquisite detail the evolving anatomy of the pathologic brain in various stages of a disease. This has had a tremendous impact on early detection and diagnosis of neurological conditions.

Over the years, functional neuroimaging studies of individuals with normal and impaired reading have implicated three language areas in reading: the inferior frontal gyrus (IFG), the occipitotemporal (OT) and temporoparietal (TP) junctions (Rumsey et al. 1992; Salmelin et al. 1996; Fiez and Petersen 1998; Shaywitz et al. 1998). The occipito-temporal area known as the Visual Word Form Area (VWFA; Cohen et al. 2000) responds differentially to real words and legal pseudowords versus illegal pseudowords and false-font strings (Petersen et al. 1988; Price et al. 1996). The temporo-parietal region is sensitive to phonological and semantic processing as in word recognition and sentence comprehension (Helenius et al. 1998; Simos et al. 2000). The IFG, on the other hand, is typically activated under phonologically-demanding conditions as in nonword reading (Pugh et al. 2000). A number of structural imaging studies of voxel-based morphometry (VBM) have shown reduced cortical gray matter in these areas in individuals with developmental dyslexia (Eckert et al. 2003; Brambati et al. 2004; Silani et al. 2005; Kronbichler et al. 2008). Of relevance is that the gray matter in OT and TP regions correlates positively with measures of real and/or pseudoword reading, phonological processing, and/or rapid automatized naming.

Newer MRI methods like diffusion tensor imaging (DTI) take advantage of the differences in brain tissue composition to distinguish gray (i.e., cortex) from white matter (i.e., myelinated axons). This has made it possible to visualize and measure white matter (WM) connections in the living brain. Measures of white matter integrity such as fraction anisotropy (FA) and mean diffusivity (MD) have become increasingly important in studies of the intactness of brain circuits for different functions like attention, language, memory and reading that are frequently implicated in cognitive dysfunction. Whereas WM changes are influenced by age (Lebel et al. 2008; Moon et al. 2011), training can also impact white matter structure highlighting the plasticity of different brain systems (Steele et al. 2013). The rate of myelination of frontal and temporo-parietal fiber tracts appears to coincide with the development of working memory and reading ability, respectively (Nagy et al. 2004). Several studies have found (FA) in the left temporo-parietal white matter to be positively correlated with measures of reading and spelling in individuals with and without dyslexia, indicative of an advantage of increased WM in this area (Klingberg et al. 2000; Niogi and McCandliss 2006), and further validating its role in reading.

Insofar as reading involves multiple brain regions, efficient communication between these areas would appear to be important for the achievement of skilled reading. Support for this view comes from the reduced or absent functional connectivity within the reading network in dyslexic readers (Horwitz et al. 1998; Cao et al. 2008; van der Mark et al. 2011). Importantly, the left arcuate fasciculus, a perisylvian WM bundle that connects Wernicke's with Broca's area (Catani and Thiebaut de Schotten 2008) and which corresponds to the dorsal reading route (responsible for mapping graphemes to phonemes during word access) has shown reduced FA in dyslexic readers (Rimrodt et al. 2010; Vandermosten et al. 2012). In the same study, Vandermosten et al. also found a correlation between orthographic processing and FA in left inferior fronto-occipital fasciculus which corresponds to

the ventral (i.e., direct "orthographic to meaning" lexical) route in reading. These findings open up exciting opportunities to combine DTI measures with functional connectivity measures (e.g., phase-locking values (PLV), cross-frequency coupling (CFC) from time-frequency analysis of EEG and MEG data, given the ability of the latter to identify temporally coupled frequency bands and brain areas that could then serve as meaningful targets for white matter tractography in developmental disorders involving language.

The field of autism has seen a surge in the number of neuroimaging studies, but unlike dyslexia, few have examined the neurobiology of speech and language in autism. An inability to stay still, comply with task demands and follow instructions have contributed to the challenges of functional neuroimaging in autism. Consequently, most of the studies have focused on structural imaging and participants in these studies have been adults or high-functioning children with autism. However, recent technical advances and computational modeling are making it easier to study cognitive functions in hard-to-test populations.

One of the most replicated anatomical findings in ASD is the presence of enlarged overall brain volume (Petersson et al. 1999; Courchesne et al. 2011), which is thought to be related to an accelerated rate of growth in total brain volume in the first 2 years of life. Regional variations in brain volume have also been found and seem to be related to differences in white matter volume (Herbert et al. 2004), which appears to be increased in fronto-temporal regions important for language and social cognition (Radua et al. 2010). Others, though, have found gray matter abnormalities in these regions (Abell et al. 1999; McAlonan et al. 2008). Studies using DTI in autism have revealed WM disruptions in the arcuate fasciculus and superior longitudinal fasciculus (SLF) which connect fronto-temporal language areas (Barnea-Goraly et al. 2004; Alexander et al. 2007; Sahyoun et al. 2010a), similar to the findings in dyslexia as mentioned earlier. The results point to the vulnerability of this structure in language impairment.

In a recent study, Wolff et al. (2012) found evidence of blunted white matter development in very young, high-risk infants, 6–24 months of age, who went on to develop autistic symptoms. These results are particularly exciting in light of the late age of diagnosis (>2 years) and the potential for earlier identification and neuroprognosis. As early as 6–12 months of age, infants recruit traditional speech areas in the superior temporal gyrus (STG) as well as motor areas in the frontal lobe in response to speech sounds (Imada et al. 2006). Studies have found 2–3 year olds activate multiple areas including front-temporal and cerebellar regions while listening to bedtime stories during sleep fMRI (Redcay and Courchesne 2008). In summary, WM connections between anterior and posterior brain regions appear to be the locus of structural disruptions in neurodevelopmental disorders involving language. MEG with its exquisite time resolution allows for a deeper interrogation of the causal nature and direction of these disruptions as they relate to functional behaviors.

4 Using MEG to Relate Core Language Symptoms to Neural Bases in Dyslexia and Autism

Over the years, functional neuroimaging methods like electroencephalography, magnetoencephalography, and functional magnetic resonance imaging (fMRI) have helped provide important insights about the functional architecture of language in the brain by disentangling domain-general from language-specific activation patterns. Creative experimental paradigms that combine behavioral measures with brain imaging tools provide a means to temporally and spatially segregate and interrogate component processes in language. Hemodynamic techniques such as PET and fMRI have high spatial resolution (in mm) (Logothetis et al. 2001) but their coarse temporal resolution (in sec) lack sensitivity to the dynamic and millisecond nature of the changes in the brain that are characteristic of language processing, which lend themselves better to study by EEG and MEG. Additionally, a key question in language-based research is whether the component processes of language (viz., phonology, semantics, and syntax) are accessed simultaneously or serially (Friederici 2002; Hagoort 2003) which has consequences for understanding differences across age- and clinical groups (Wehner et al. 2007b; Mody et al. 2008; Han et al. 2012).

4.1 Dyslexia

Findings from a number of studies suggest that the initial steps of language processing are serial with interactions in later stages involving lexical integration. In individuals with dyslexia the deficit appears to be early on in phonological processing evident in tasks like categorical perception of speech. Studies using mismatch negativity (MMN), a pre-attentive index of the brain's capacity to discriminate between two auditory stimuli (Naatanen 1995), have revealed language-specific memory traces in infants as young as 6 months of age (Cheour et al. 1998). It is not surprising then, that auditory event-related potentials (ERP; viz., N1, N2, and P2) recorded with EEG to speech and nonspeech sounds in newborn infants correctly classified 81 % of the subjects as normal, or impaired readers at 8 years of age (Molfese 2000), given that dyslexia is a language-based disorder. In fact, ERP measures in pre-reading children with a family history of reading difficulties were similarly found to be predictive of later reading ability (Maurer et al. 2009).

Studies using MMN have shown that very early on in the auditory pathways, the brain has access to phonological categories (Schulte-Korne et al. 1998; Phillips et al. 2000). Hence a poor MMN response in children with specific language and/or reading impairment may well reflect their difficulties with poor neurophysiological encoding of acoustic-phonetic distinctions and not merely with auditory-acoustic processing. Using an oddball paradigm, Wehner et al. (2007a) tested good and poor readers, 7–13 years of age, with MEG, on auditory discrimination of words varying

in their degree of phonetic contrast. Both groups took longer to discriminate the phonologically similar (PS; e.g. /pat/-/cat/) than phonologically dissimilar (PD; /pat-/rat/) contrast. However, whereas good readers showed a significant difference in activation between the conditions in the STG between 140–190 ms post-stimulus, the poor readers did not, reflecting the latter's reduced sensitivity to phonological contrast. In a follow-up study with the same subjects, Mody et al. (2008) further examined auditory discrimination but within a sentence context. Using a sentence anomaly paradigm containing sentence-terminal incongruent words that were phonologically similar or dissimilar to the target congruent words (e.g., At the restaurant, he offered to pay the bill/pill/hill), the authors found no performance difference between the groups. Both, normal and impaired readers were able to process the sentences correctly. However, the two groups differed significantly in their neural activation patterns with poor readers revealing delayed, and less left-lateralized responses to the PS than PD stimuli in the superior temporal region. The findings are consistent with a reduced response to phonological repetition that has been seen in superior temporal areas (Wei et al. 2007) and thereby support a weak phonological processing account of reading disability especially under perceptually challenging conditions in a semantically-conflicting sentence context (see Fig. 1).

Salmelin et al. (1996, 2000) found that good readers show a strong response to reading words relative to nonwords 150–200 ms post-stimulus in OT area, a region known to be sensitive to letter-strings. Dyslexic readers did not display this early response, which may account for the subsequently weaker and delayed activation in semantic processing in temporo-parietal areas (Helenius et al. 1999). These studies suggest that a disruption in the grapheme-to-phoneme translation interface can have consequences for comprehension. In fact, the temporal profiles of the activity in language-implicated frontal, temporal and parietal areas reflect near-simultaneous peaks in children with reading difficulties compared to the distinct temporal progression of activity associated with component reading processes in these areas, in a typical reader (Rezaie et al. 2011). It is important to note that phonological processing skills continue to develop into mid childhood, as evidenced by changes in underlying speech perception skills. Parviainen et al. used MEG to record neural responses to speech and nonspeech sounds in 7–8 year olds and adults (Parviainen et al. 2011). Whereas both groups activated the superior temporal cortex, the differentiation between the cortical response to the two types of sounds was later (250 ms after sound onset), more prolonged and evident in both hemispheres in children; adults showed a corresponding effect though earlier, at 100 ms post-stimulus, and specifically in the left hemisphere which was linked to superior reading skills. Findings of less lateralized responses to auditory stimuli in children with dyslexia may suggest a problem in balance of auditory functions between the two hemispheres (Johnson et al. 2013).

In a recent study, Han et al. (2012) used MEG to investigate neural oscillatory activity associated with auditory sentence processing in reading impaired adolescents and age and IQ-matched controls. Insofar as auditory comprehension involves the integration of sensory, cognitive, and linguistic processes to arrive at

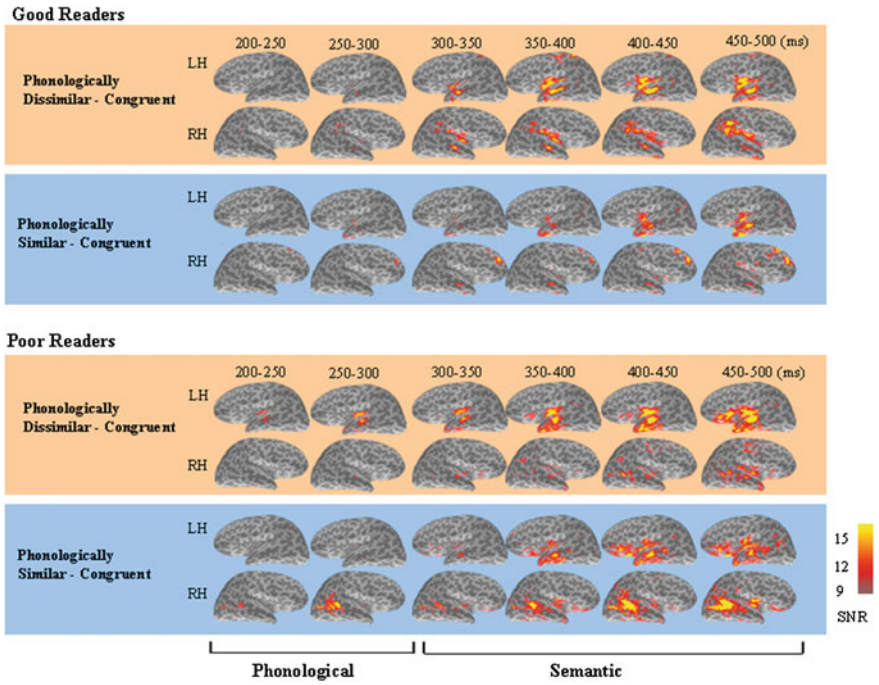

Fig. 1 MEG source estimates. Dynamic Statistical Parametric Maps (*dSPM*) averaged in sequential 50 ms time bins from 200 to 500 ms for the good reader group (*top*) and the poor reader group (*bottom*). The group-averaged dSPM for the two subtraction contrasts (phonologically similar (*PS*) and phonologically dissimilar (*PD*)) are shown on the reconstructed cortical surfaces of one child. The lateral surfaces have been inflated for better visualization of activation within the sulci (*dark gray*) as well as the gyri (*light gray*). Both *left* and *right* hemispheres are shown for all time points. Note, delayed and less lateralized response to PS compared to PD condition in poor readers (Mody et al. 2008)

the meaning of a word or sentence, neural synchrony may be a promising target mechanism for the study of higher-level language. The authors used an N400 task from a previous study with younger dyslexic readers (Mody et al. 2008) to examine top-down and bottom-up interactions in integrating sentence-terminal phonologically similar (PS) versus dissimilar (PD) incongruent words into preceding context. Similar to the results from the previous study, older good and poor readers also differed in their brain activation as a function of the degree of phonological contrast but in the time range of semantic processing (400–600 ms). Specifically, the functional coupling between auditory and superior temporal cortices in the right hemisphere as measured by PLV, was greater in the PS than PD condition for good readers. The results were interpreted as reflecting good readers' superior coding of subtle phonetic differences between perceptually confusable terminal words in a semantically conflicting context. In contrast, for poor readers, who were selected on the basis of impaired decoding abilities, the

PLV was lower in the PS than in the PD condition. This may relate to the group's weak speech perception of subtle phonological differences exacerbated under conflicting semantic cues. That the group difference in phase-locking was significant in the gamma band is in keeping with existing studies that have indicated that gamma-band oscillations may play an important role in spoken language comprehension (Shahin et al. 2009; Obleser and Kotz 2011).

According to a recent study, poor readers' difficulties may arise in part because of impaired phase locking to the slower modulation in the speech signal (<10 Hz), which could affect syllable segmentation abilities key to processing phonological aspects of speech (Hamalainen et al. 2012). To the extent that the responses patterns of the dyslexic and unimpaired readers in the study by Han et al. (2012) was modulated by the degree of phonological contrast, the results appear to be consistent with a phonological rather than an auditory temporal account of the disorder. The findings are also in keeping with the lack of a consistent auditory brainstem response to complex speech-like sounds and not to simple clicks in impaired readers, seen in EEG (Hornickel and Kraus 2013), which was taken as evidence of poor neurophysiological coding and may be viewed as further support of weak and underspecified speech sound representations in dyslexia.

4.2 Autism

Unlike dyslexia, which is primarily a written language disorder, individuals with autism have spoken language problems (Hudry et al. 2010). Early on the problem takes the form of a lack of orientation to speech and to their name when called (Osterling et al. 2002; Nadig et al. 2007). These behaviors have been found to be predictive of broader receptive language problems. However, the apparent difficulty with auditory comprehension may also be reflective of difficulties with testing this population due to a lack of social motivation.

Despite the absorption of language deficits under the broad umbrella of social communication deficits in the new DSM-5, language impairment remains a striking feature of ASD. In general, semantic deficits are among the few consistent language findings in autism (Rutter et al. 1992; Tager-Flusberg and Joseph 2003; Vogindroukas et al. 2003). While the number of functional neuroimaging studies of speech and language in autism has been limited, recent auditory event-related potential studies have begun to yield some important insights into the nature of the language impairment in ASD. Measures like the MMN response, which is larger for between- than within-category phonetic differences, has the potential to reveal abnormalities in auditory perception which have been implicated in autism and dyslexia. Čeponiene et al. (2003) used EEG with an oddball paradigm to examine the MMN for speech (viz., vowels) and non-speech stimuli (viz., simple tones, complex tones) each with a corresponding frequency deviant (created by raising all

the frequencies of the original token by 10 %) in high-functioning children with autism and age-matched controls. Whereas the authors found that there was no difference in the MMN between the groups for all three stimulus types, revealing intact auditory processing in ASD, some studies have yielded delayed MMN responses to speech and non-speech in autism (Oram Cardy et al. 2005; Roberts et al. 2011), similar to that observed in children with specific language impairment (Roberts et al. 2012), and indicative of language impairment in autism. In these latter studies, the speech stimuli consisted of two different vowels, /a/and/u/; Čeponieni et al. however, used a standard vowel paired with an acoustic deviant that was not phonologically different, which might explain the different results. Nevertheless, it is interesting, then, that the ASD participants while showing a normal MMN response, lacked the P3a response (a neural index of involuntary orienting to a novel or salient stimulus) in the speech condition, though not in the tone conditions. In keeping with the literature, the ASD participants did not orient to speech which may account for difficulties in auditory comprehension and an apparent preoccupation with their own world.

In older individuals on the spectrum, abnormal functional organization in fronto-temporal areas has been consistently observed in fMRI tasks of spoken and written language comprehension. These semantic tasks have included priming, categorization, fluency, and sentence processing. Activation is typically reduced in the left hemisphere (Just et al. 2004; Harris et al. 2006; Gaffrey et al. 2007) and increased responsiveness is evident in the right hemisphere (Wang et al. 2006; Knaus et al. 2008; Mason et al. 2008). Studies of reading in high-functioning autism suggest that individuals on the spectrum do not take advantage of contextual cues (Happe 1996). Using a sentence anomaly paradigm, Braeutigam et al. (2008) found that the neuromagnetic N400 response following incongruous words was weaker over left temporal cortices in individuals with autism. The incongruent sentence terminal words also elicited long-lasting gamma oscillations above 40 Hz in the ASD group but not in the controls. While the latter finding is hard to interpret, the results point to atypical semantic processing in ASD. Interestingly, access to semantics via pictures as well as picture naming appears to be less affected in autism (Kamio and Toichi 2000; Walenski et al. 2008; Sahyoun et al. 2010b) supporting an apparent dichotomy between visuo-spatial and linguistic abilities in autism (Tager-Flusberg and Joseph 2003; Behrmann et al. 2006). In separate fMRI and DTI studies, Sahyoun et al. used a three-condition pictorial problem solving task designed to vary the linguistic processing demands across the conditions (Sahyoun et al. 2010a, b). The authors found no difference in behavioral performance between high-functioning children with autism (HFA) and age- and IQ-matched controls regardless of linguistic demands; however, the control group relied more on frontal and temporal language areas whereas the HFA group activated occipito-parietal and ventral temporal areas. Taken together with findings of reduced white matter integrity of the connections between inferior frontal and middle/ventral temporal areas, the results appear to support HFAs' preference

for visuo-spatial strategies in the face of linguistic weaknesses. They also provide connectivity patterns that lend themselves to further fine-grained probing by MEG through use of language tasks that implicate temporal coupling of the same brain areas.

To date, studies of language processing with MEG in autism are limited. While there have been several studies of basic auditory processing in autism, few have examined higher level language processing. The auditory studies involving speech have, for the most part, looked at sound discrimination early in the auditory pathways using the MMN. The results have been mixed, with some reporting abnormal MMN responses (Jansson-Verkasalo et al. 2003; Roberts et al. 2011), yet others finding no abnormalities (Kemner et al. 1995; Čeponiene et al. 2003). Additionally troublesome is the lack of reliability in determining an MMN response, which raises questions as to its usefulness in clinical screening (Kurtzberg et al. 1995). Recent findings of abnormalities in gamma-band oscillatory responses during a continuous word recognition task in parents of children with ASD suggest a possible role for neural oscillatory responses in the search for a heritable neurophysiological biomarker of ASD (McFadden et al. 2012).

5 Future Directions

Findings from a number of behavioral and MEG studies appear to be converging on core abnormalities in dyslexia and autism. Evoked responses and neural synchrony measures in basic and intervention research appear to support a phonological core deficit in developmental reading disability. In later years, the problem of accuracy, frequently gives way to one of fluency, with "slow but accurate" reading frequently being the hallmark of the remediated adult dyslexic reader (Shaywitz et al. 2003). EEG and MEG with their superior temporal resolution are ideally suited to temporally unravel the interactions between top-down and bottom-up processes in reading. Such an approach could be tremendously powerful in a comparison, for example, of reading comprehension in dyslexia versus autism, insofar as a large number of individuals on the spectrum tend to be hyperlexic (i.e., precocious decoders). The findings from such contrasting disorders would move us closer to understanding the neurocognitive architecture of language, as well as the nature and locus of speech and language deficits critical to solving the disconnection puzzle that appears to be characteristic of neurodevelopmental disorders like autism and dyslexia (Mody et al. 2013). Finally, the development of passive task paradigms that reliably capture language processing will go a long way in extending the use of MEG and EEG to the study of minimally verbal ASD, a much needed area of research.

References

Abell F, Krams M, Ashburner J, Passingham R, Friston K, Frackowiak R, Happe F, Frith C, Frith U (1999) The neuroanatomy of autism: a voxel-based whole brain analysis of structural scans. NeuroReport 10:1647–1651

Alexander AL, Lee JE, Lazar M, Boudos R, DuBray MB, Oakes TR, Miller JN, Lu J, Jeong EK, McMahon WM, Bigler ED, Lainhart JE (2007) Diffusion tensor imaging of the corpus callosum in Autism. Neuroimage 34:61–73

Barnea-Goraly N, Kwon H, Menon V, Eliez S, Lotspeich L, Reiss AL (2004) White matter structure in autism: preliminary evidence from diffusion tensor imaging. Biol Psychiatry 55:323–326

Baron-Cohen S (1995) Mindblindness: an essay on autism and theory of mind. MIT Press, London

Behrmann M, Thomas C, Humphreys K (2006) Seeing it differently: visual processing in autism. Trends Cogn Sci 10:258–264

Blachman BA, Schatschneider C, Fletcher JM, Francis DJ, Clonan SM, Shaywitz BA, Shaywitz SE (2004) Effects of intensive reading remediation for second and third graders and a 1 year follow-up. J Educ Psychol 96:444–461

Braeutigam S, Swithenby SJ, Bailey AJ (2008) Contextual integration the unusual way: a magnetoencephalographic study of responses to semantic violation in individuals with autism spectrum disorders. Eur J Neurosci 27:1026–1036

Brambati SM, Termine C, Ruffino M, Stella G, Fazio F, Cappa SF, Perani D (2004) Regional reductions of gray matter volume in familial dyslexia. Neurology 63:742–745

Byrne B, Olson RK, Samuelsson S, Wadsworth S, Corley R, DeFries JC, Willcutt E (2006) Genetic and environmental influences on early literacy. J Res Reading 29:33–49

Cao F, Bitan T, Booth JR (2008) Effective brain connectivity in children with reading difficulties during phonological processing. Brain Lang 107:91–101

Catani M, Thiebaut de Schotten M (2008) A diffusion tensor imaging tractography atlas for virtual in vivo dissections. Cortex 44:1105–1132

Catts HW, Adlof SM, Weismer SE (2006) Language deficits in poor comprehenders: a case for the simple view of reading. J Speech Lang Hear Res 49:278–293

Catts HW, Fey ME, Zhang X, Tomblin JB (1999) Language basis of reading and reading disabilities: evidence from a longitudinal investigation. Sci Stud Read 3:331–362

Čeponiene R, Lepisto T, Shestakova A, Vanhala R, Alku P, Naatanen R, Yaguchi K (2003) Speech-sound-selective auditory impairment in children with autism: they can perceive but do not attend. Proc Natl Acad Sci USA 100:5567–5572

Cheour M, Ceponiene R, Lehtokoski A, Luuk A, Allik J, Alho K, Naatanen R (1998) Development of language-specific phoneme representations in the infant brain. Nat Neurosci 1:351–353

Cohen L, Dehaene S, Naccache L, Lehericy S, Dehaene-Lambertz G, Henaff MA, Michel F (2000) The visual word form area: spatial and temporal characterization of an initial stage of reading in normal subjects and posterior split-brain patients. Brain 123(Pt 2):291–307

Coltheart M (2005) Modeling reading: the dual route approach. In: Snowling M, Hulme C (eds) The science of reading: a handbook. Blackwell Synergy, Boston, pp 2–23

Constantino JN, Gruber CP, Davis S, Hayes S, Passanante N, Przybeck T (2004) The factor structure of autistic traits. J Child Psychol Psychiatry 45:719–726

Courchesne E, Campbell K, Solso S (2011) Brain growth across the life span in autism: age-specific changes in anatomical pathology. Brain Res 1380:138–145

Dawson G, Meltzoff AN, Osterling J, Rinaldi J, Brown E (1998) Children with autism fail to orient to naturally occurring social stimuli. J Autism Dev Disord 28:479–485

Eckert MA, Leonard CM, Richards TL, Aylward EH, Thomson J, Berninger VW (2003) Anatomical correlates of dyslexia: frontal and cerebellar findings. Brain 126:482–494

Elsabbagh M, Divan G, Koh YJ, Kim YS, Kauchali S, Marcin C, Montiel-Nava C, Patel V, Paula CS, Wang C, Yasamy MT, Fombonne E (2012) Global prevalence of autism and other pervasive developmental disorders. Autism Res 5:160–179

Fiez JA, Petersen SE (1998) Neuroimaging studies of word reading. Proc Natl Acad Sci USA 95:914–921

Friederici AD (2002) Towards a neural basis of auditory sentence processing. Trends Cogn Sci 6:78–84

Gaffrey MS, Kleinhans NM, Haist F, Akshoomoff N, Campbell A, Courchesne E, Muller RA (2007) Atypical [corrected] participation of visual cortex during word processing in autism: an fMRI study of semantic decision. Neuropsychologia 45:1672–1684

Godfrey JJ, Syrdal-Lasky AK, Millay KK, Knox CM (1981) Performance of dyslexic children on speech perception tests. J Exp Child Psychol 32:401–424

Hagoort P (2003) How the brain solves the binding problem for language: a neurocomputational model of syntactic processing. Neuroimage 20(Supplement 1):S18–S29

Hamalainen JA, Rupp A, Soltesz F, Szucs D, Goswami U (2012) Reduced phase locking to slow amplitude modulation in adults with dyslexia: an MEG study. Neuroimage 59:2952–2961

Han J, Mody M, Ahlfors SP (2012) Gamma phase locking modulated by phonological contrast during auditory comprehension in reading disability. NeuroReport 23:851–856

Happe F, Frith U (1996) The neuropsychology of autism. Brain 119(Pt 4):1377–1400

Happe FG (1996) Studying weak central coherence at low levels: children with autism do not succumb to visual illusions. A research note. J Child Psychol Psychiatry 37:873–877

Harris GJ, Chabris CF, Clark J, Urban T, Aharon I, Steele S, McGrath L, Condouris K, Tager-Flusberg H (2006) Brain activation during semantic processing in autism spectrum disorders via functional magnetic resonance imaging. Brain Cogn 61:54–68

Helenius P, Salmelin R, Service E, Connolly JF (1998) Distinct time courses of word and context comprehension in the left temporal cortex. Brain 121(Pt 6):1133–1142

Helenius P, Salmelin R, Service E, Connolly JF (1999) Semantic cortical activation in dyslexic readers. J Cogn Neurosci 11:535–550

Herbert MR, Ziegler DA, Makris N, Filipek PA, Kemper TL, Normandin JJ, Sanders HA, Kennedy DN, Caviness VS Jr (2004) Localization of white matter volume increase in autism and developmental language disorder. Ann Neurol 55:530–540

Hornickel J, Kraus N (2013) Unstable representation of sound: a biological marker of dyslexia. J Neurosci 33:3500–3504

Horwitz B, Rumsey JM, Donohue BC (1998) Functional connectivity of the angular gyrus in normal reading and dyslexia. Proc Natl Acad Sci USA 95:8939–8944

Hudry K, Leadbitter K, Temple K, Slonims V, McConachie H, Aldred C, Howlin P, Charman T (2010) Preschoolers with autism show greater impairment in receptive compared with expressive language abilities. Int J Lang Commun Disord 45:681–690

Imada T, Zhang Y, Cheour M, Taulu S, Ahonen A, Kuhl PK (2006) Infant speech perception activates Broca's area: a developmental magnetoencephalography study. NeuroReport 17:957–962

Jansson-Verkasalo E, Ceponiene R, Kielinen M, Suominen K, Jantti V, Linna SL, Moilanen I, Naatanen R (2003) Deficient auditory processing in children with Asperger Syndrome, as indexed by event-related potentials. Neurosci Lett 338:197–200

Johnson BW, McArthur G, Hautus M, Reid M, Brock J, Castles A, Crain S (2013) Lateralized auditory brain function in children with normal reading ability and in children with dyslexia. Neuropsychologia 51:633–641

Just MA, Cherkassky VL, Keller TA, Minshew NJ (2004) Cortical activation and synchronization during sentence comprehension in high-functioning autism: evidence of underconnectivity. Brain 127:1811–1821

Kamio Y, Toichi M (2000) Dual access to semantics in autism: is pictorial access superior to verbal access? J Child Psychol Psychiatry 41:859–867

Kemner C, Verbaten MN, Cuperus JM, Camfferman G, van Engeland H (1995) Auditory event-related brain potentials in autistic children and three different control groups. Biol Psychiatry 38:150–165

Kemper TL (1994) Neuroanatomical and neuropathological changes during aging and dementia. In: Knoefel JE, Albert ML (eds) Clinical neurology of aging. Oxford University Press, New York, pp 3–67

Kjelgaard MM, Tager-Flusberg H (2001) An investigation of language impairment in autism: implications for genetic subgroups. Lang Cogn Process 16:287–308

Klin A (1991) Young autistic children's listening preferences in regard to speech: a possible characterization of the symptom of social withdrawal. J Autism Dev Disord 21:29–42

Klingberg T, Hedehus M, Temple E, Salz T, Gabrieli JD, Moseley ME, Poldrack RA (2000) Microstructure of temporo-parietal white matter as a basis for reading ability: evidence from diffusion tensor magnetic resonance imaging. Neuron 25:493–500

Knaus TA, Silver AM, Lindgren KA, Hadjikhani N, Tager-Flusberg H (2008) fMRI activation during a language task in adolescents with ASD. J Int Neuropsychol Soc 14:967–979

Kronbichler M, Wimmer H, Staffen W, Hutzler F, Mair A, Ladurner G (2008) Developmental dyslexia: gray matter abnormalities in the occipitotemporal cortex. Hum Brain Mapp 29:613–625

Kuhl PK, Coffey-Corina S, Padden D, Dawson G (2005) Links between social and linguistic processing of speech in preschool children with autism: behavioral and electrophysiological measures. Dev Sci 8:F1–F12

Kurtzberg D, Vaughan HG Jr, Kreuzer JA, Fliegler KZ (1995) Developmental studies and clinical application of mismatch negativity: problems and prospects. Ear Hear 16:105–117

Lebel C, Walker L, Leemans A, Phillips L, Beaulieu C (2008) Microstructural maturation of the human brain from childhood to adulthood. Neuroimage 40:1044–1055

Liberman IY, Shankweiler D (1991) Phonology and beginning to read: a tutorial. In: Rieben L, Perfetti CA (eds) Learning to read: basic research and its implications. Lawrence Erlbaum, Hillsdale

Logothetis NK, Pauls J, Augath M, Trinath T, Oeltermann A (2001) Neurophysiological investigation of the basis of the fMRI signal. Nature 412:150–157

Mason RA, Williams DL, Kana RK, Minshew N, Just MA (2008) Theory of mind disruption and recruitment of the right hemisphere during narrative comprehension in autism. Neuropsychologia 46:269–280

Maurer U, Bucher K, Brem S, Benz R, Kranz F, Schulz E, van der Mark S, Steinhausen HC, Brandeis D (2009) Neurophysiology in preschool improves behavioral prediction of reading ability throughout primary school. Biol Psychiatry 66:341–348

McAlonan GM, Suckling J, Wong N, Cheung V, Lienenkaemper N, Cheung C, Chua SE (2008) Distinct patterns of grey matter abnormality in high-functioning autism and Asperger's syndrome. J Child Psychol Psychiatry 49:1287–1295

McFadden KL, Hepburn S, Winterrowd E, Schmidt GL, Rojas DC (2012) Abnormalities in gamma-band responses to language stimuli in first-degree relatives of children with autism spectrum disorder: an MEG study. BMC Psychiatry 12:213–231

Messaoud-Galusi S, Marshall CR et al (2010) Exploring the overlap between dyslexia and SLI: the role of phonology. Sci Stud Read 14:1–7

Mody M (2003a) Phonological basis in reading disability: a review and analysis of the evidence. Read Writ 16:21–39

Mody M (2003b) Rapid auditory processing deficits in dyslexia: a commentary on two differing views. J Phonetics 31:529–539

Mody M, Studdert-Kennedy M, Brady S (1997) Speech perception deficits in poor readers: auditory processing or phonological coding? J Exp Child Psychol 64:199–231

Mody M, Wehner DT, Ahlfors SP (2008) Auditory word perception in sentence context in reading-disabled children. NeuroReport 19:1567–1571

Mody M, Manoach D, Gunther F, Kenet T, Bruno K, McDougle C, Stigler KA (2013) Speech and language in autism spectrum disorder: through the lens of behavior and brain imaging. Neuropsychiatry 3(2):1–10

Molfese DL (2000) Predicting dyslexia at 8 years of age using neonatal brain responses. Brain Lang 72:238–245

Moon WJ, Provenzale JM, Sarikaya B, Ihn YK, Morlese J, Chen S, DeBellis MD (2011) Diffusion-tensor imaging assessment of white matter maturation in childhood and adolescence. Am J Roentgenol 197:704–712

Naatanen R (1995) The mismatch negativity: a powerful tool for cognitive neuroscience. Ear Hear 16:6–18

Nadig AS, Ozonoff S, Young GS, Rozga A, Sigman M, Rogers SJ (2007) A prospective study of response to name in infants at risk for autism. Arch Pediatr Adolesc Med 161:378–383

Nagy Z, Westerberg H, Klingberg T (2004) Maturation of white matter is associated with the development of cognitive functions during childhood. J Cogn Neurosci 16:1227–1233

Niogi SN, McCandliss BD (2006) Left lateralized white matter microstructure accounts for individual differences in reading ability and disability. Neuropsychologia 44:2178–2188

Nittrouer S (1999) Do temporal processing deficits cause phonological processing problems? J Speech Lang Hear Res 42:925–942

Oakhill JV, Cain K, Bryant PE (2003) The dissociation of single-word reading and text comprehension: evidence from component skills. Lang Cogn Process 18:443–468

Obleser J, Kotz SA (2011) Multiple brain signatures of integration in the comprehension of degraded speech. Neuroimage 55:713–723

Oram Cardy JE, Flagg EJ, Roberts W, Roberts TP (2005) Delayed mismatch field for speech and non-speech sounds in children with autism. NeuroReport 16:521–525

Osterling JA, Dawson G, Munson JA (2002) Early recognition of 1-year-old infants with autism spectrum disorder versus mental retardation. Dev Psychopathol 14:239–251

Parish-Morris J, Hennon EA, Hirsh-Pasek K, Golinkoff RM, Tager-Flusberg H (2007) Children with autism illuminate the role of social intention in word learning. Child Dev 78:1265–1287

Parviainen T, Helenius P, Poskiparta E, Niemi P, Salmelin R (2011) Speech perception in the child brain: cortical timing and its relevance to literacy acquisition. Hum Brain Mapp 32:2193–2206

Pennington BF, Gilger JW (1996) How is dyslexia transmitted? In: Chase C, Rosen G, Sherman G (eds) Neural and cognitive mechanisms underlying speech, language, and reading. York Press, Baltimore, pp 41–62

Petersen SE, Fox PT, Posner MI, Mintun M, Raichle ME (1988) Positron emission tomographic studies of the cortical anatomy of single-word processing. Nature 331:585–589

Petersson S, Pedersen NL, Schalling M, Lavebratt C (1999) Primary megalencephaly at birth and low intelligence level. Neurology 53:1254–1259

Phillips C, Pellathy T, Marantz A, Yellin E, Wexler K, Poeppel D, McGinnis M, Roberts T (2000) Auditory cortex accesses phonological categories: an MEG mismatch study. J Cogn Neurosci 12:1038–1055

Preissler MA (2008) Associative learning of pictures and words by low-functioning children with autism. Autism 12:231–248

Price CJ, Wise RJ, Frackowiak RS (1996) Demonstrating the implicit processing of visually presented words and pseudowords. Cereb Cortex 6:62–70

Pugh KR, Mencl WE, Shaywitz BA, Shaywitz SE, Fulbright RK, Constable RT, Skudlarski P, Marchione KE, Jenner AR, Fletcher JM, Liberman AM, Shankweiler DP, Katz L, Lacadie C, Gore JC (2000) The angular gyrus in developmental dyslexia: task-specific differences in functional connectivity within posterior cortex. Psychol Sci 11:51–56

Radua J, Via E, Catani M, Mataix-Cols D (2010) Voxel-based meta-analysis of regional white-matter volume differences in autism spectrum disorder versus healthy controls. Psychol Med 41:1539–1550

Ramus F, Rosen S, Dakin S, Day B, Castellote J, White S, Frith U (2003) Theories of developmental dyslexia: insights from a multiple case study of dyslexic adults. Brain 126:841–865

Redcay E, Courchesne E (2008) Deviant functional magnetic resonance imaging patterns of brain activity to speech in 2–3-year-old children with autism spectrum disorder. Biol Psychiatry 64:589–598

Rezaie R, Simos PG, Fletcher JM, Juranek J, Cirino PT, Li Z, Passaro AD, Papanicolaou AC (2011) The timing and strength of regional brain activation associated with word recognition in children with reading difficulties. Front Hum Neurosci 5:45

Ricketts J (2011) Research review: reading comprehension in developmental disorders of language and communication. J Child Psychol Psychiatry 52:1111–1123

Rimrodt SL, Peterson DJ, Denckla MB, Kaufmann WE, Cutting LE (2010) White matter microstructural differences linked to left perisylvian language network in children with dyslexia. Cortex 46:739–749

Risi S, Lord C, Gotham K, Corsello C, Chrysler C, Szatmari P, Cook EH Jr, Leventhal BL, Pickles A (2006) Combining information from multiple sources in the diagnosis of autism spectrum disorders. J Am Acad Child Adolesc Psychiatry 45:1094–1103

Roberts TP, Cannon KM, Tavabi K, Blaskey L, Khan SY, Monroe JF, Qasmieh S, Levy SE, Edgar JC (2011) Auditory magnetic mismatch field latency: a biomarker for language impairment in autism. Biol Psychiatry 70:263–269

Roberts TP, Heiken K, Kahn SY, Qasmieh S, Blaskey L, Solot C, Parker WA, Verma R, Edgar JC (2012) Delayed magnetic mismatch negativity field, but not auditory M100 response, in specific language impairment. NeuroReport 23:463–468

Ronald A, Hoekstra RA (2011) Autism spectrum disorders and autistic traits: a decade of new twin studies. Am J Med Genet B Neuropsychiatr Genet 156:255–274

Rumsey JM, Andreason P, Zametkin AJ, Aquino T, King C, Hamburber SD, Pikus A, Rapoport JL, Cohen RM (1992) Failure to activate the left temporoparietal cortex in dyslexia. Arch Neurol 49:527–534

Rutter M, Mawhood L, Howlin P (1992) Language delay and social development. In: Fletcher P, Hall D (eds) Specific speech and language disorders in children: correlates, characteristics and outcomes. Whurr Publishers, London, pp 63–78

Sahyoun CP, Belliveau JW, Mody M (2010a) White matter integrity and pictorial reasoning in high-functioning children with autism. Brain Cogn 73:180–188

Sahyoun CP, Belliveau JW, Soulieres I, Schwartz S, Mody M (2010b) Neuroimaging of the functional and structural networks underlying visuospatial vs. linguistic reasoning in high-functioning autism. Neuropsychologia 48:86–95

Salmelin R, Helenius P, Service E (2000) Neurophysiology of fluent and impaired reading: a magnetoencephalographic approach. J Clin Neurophysiol 17:163–174

Salmelin R, Service E, Kiesila P, Uutela K, Salonen O (1996) Impaired visual word processing in dyslexia revealed with magnetoencephalography. Ann Neurol 40:157–162

Schulte-Korne G, Deimel W, Bartling J, Remschmidt H (1998) Auditory processing and dyslexia: evidence for a specific speech processing deficit. NeuroReport 9:337–340

Schultz RT, Gauthier I, Klin A, Fulbright RK, Anderson AW, Volkmar F, Skudlarski P, Lacadie C, Cohen DJ, Gore JC (2000) Abnormal ventral temporal cortical activity during face discrimination among individuals with autism and Asperger syndrome. Arch Gen Psychiatry 57:331–340

Shahin AJ, Picton TW, Miller LM (2009) Brain oscillations during semantic evaluation of speech. Brain Cogn 70:259–266

Shankweiler D, Lundquist E, Katz L, Stuebing KK, Fletcher JM, Brady S, Fowler A, Dreyer LG, Marchione KE, Shaywitz SE, Shaywitz BA (1999) Comprehension and decoding: patterns of association in children with reading difficulties. Sci Stud Read 3:69–94

Shaywitz S, Shaywitz B, Pugh K, Fulbright R, Constable R, Mencl W, Shankweiler D, Liberman A, Skudlarski P, Fletcher J, Katz L, Marchione K, Lacadie C, Gatenby C, Gore J (1998)

Functional disruption in the organization of the brain for reading in dyslexia. Proc Natl Acad Sci USA 95:2636–2641

Shaywitz SE, Gruen JR, Shaywitz BA (2007) Management of dyslexia, its rationale, and underlying neurobiology. Pediatr Clin North Am 54:609–623

Shaywitz SE, Shaywitz BA, Fulbright RK, Skudlarski P, Mencl W, Constable R, Pugh KR, Holahan JM, Marchione KE, Fletcher JM, Lyon G, Gore JC (2003) Neural systems for compensation and persistence: young adult outcome of childhood reading disability. Biol Psychiatry 54:25–33

Silani G, Frith U, Demonet JF, Fazio F, Perani D, Price C, Frith CD, Paulesu E (2005) Brain abnormalities underlying altered activation in dyslexia: a voxel based morphometry study. Brain 128:2453–2461

Simos PG, Breier JI, Fletcher JM, Bergman E, Papanicolaou AC (2000) Cerebral mechanisms involved in word reading in dyslexic children: a magnetic source imaging approach. Cereb Cortex 10:809–816

Simos PG, Fletcher JM, Bergman E, Breier JI, Foorman BR, Castillo EM, Davis RN, Fitzgerald M, Papanicolaou AC (2002) Dyslexia-specific brain activation profile becomes normal following successful remedial training. Neurology 58:1203–1213

Steele CJ, Bailey JA, Zatorre RJ, Penhune VB (2013) Early musical training and white-matter plasticity in the corpus callosum: evidence for a sensitive period. J Neurosci 33:1282–1290

Studdert-Kennedy M, Mody M (1995) Auditory temporal perception deficits in the reading impaired: a critical review of the evidence. Psychon Bull Rev 2:508–514

Swettenham J, Baron-Cohen S, Charman T, Cox A, Baird G, Drew A, Rees L, Wheelwright S (1998) The frequency and distribution of spontaneous attention shifts between social and nonsocial stimuli in autistic, typically developing, and nonautistic developmentally delayed infants. J Child Psychol Psychiatry 39:747–753

Tager-Flusberg H, Joseph RM (2003) Identifying neurocognitive phenotypes in autism. Philos. Trans. R. Soc. B Biol Sci 358:303–314

Tomblin JB (1989) Familial concentration of developmental language impairment. J Speech Hear Disord 54:287–295

van der Mark S, Klaver P, Bucher K, Maurer U, Schulz E, Brem S, Martin E, Brandeis D (2011) The left occipitotemporal system in reading: disruption of focal fMRI connectivity to left inferior frontal and inferior parietal language areas in children with dyslexia. Neuroimage 54:2426–2436

Vandermosten M, Boets B, Poelmans H, Sunaert S, Wouters J, Ghesquiere P (2012) A tractography study in dyslexia: neuroanatomic correlates of orthographic, phonological and speech processing. Brain 135:935–948

Vogindroukas I, Papageorgiou V, Vostanis P (2003) Pattern of semantic errors in autism: a brief research report. Autism 7:195–203

Walenski M, Mostofsky SH, Gidley-Larson JC, Ullman MT (2008) Brief report: enhanced picture naming in autism. J Autism Dev Disord 38:1395–1399

Walenski M, Tager-Flusberg H, Ullman MT (2006) Language in autism. In: Moldin S, Rubenstein J (eds) Understanding autism: from basic neuroscience to treatment. CRC Press/ Taylor & Francis Group LLC, New York, pp 175–203

Wang AT, Lee SS, Sigman M, Dapretto M (2006) Neural basis of irony comprehension in children with autism: the role of prosody and context. Brain 129:932–943

Wehner DT, Ahlfors SP, Mody M (2007a) Effects of phonological contrast on auditory word discrimination in children with and without reading disability: a magnetoencephalography (MEG) study. Neuropsychologia 45:3251–3262

Wehner DT, Ahlfors SP, Mody M (2007b) The influence of semantic processing on phonological decisions in children and adults: a magnetoencephalography (MEG) study. J Speech Lang Hear Res 50:716–731

Wei Q, Ihara A, Hayakawa T, Murata T, Matsumoto E, Fujimaki N (2007) Phonological influences on lexicosemantic processing of kanji words. NeuroReport 18:1775–1780

Whitehouse AJ, Barry JG, Bishop DV (2007) The broader language phenotype of autism: a comparison with specific language impairment. J Child Psychol Psychiatry 48:822–830

Williams D, Botting N, Boucher J (2008) Language in autism and specific language impairment: where are the links? Psychol Bull 134:944–963

Wolff JJ, Gu H, Gerig G, Elison JT, Styner M, Gouttard S, Botteron KN, Dager SR, Dawson G, Estes AM, Evans AC, Hazlett HC, Kostopoulos P, McKinstry RC, Paterson SJ, Schultz RT, Zwaigenbaum L, Piven J (2012) Differences in white matter fiber tract development present from 6 to 24 months in infants with autism. Am J Psychiatry 169:589–600

Whole-Head Child MEG System and Its Applications

Yoshiaki Adachi and Yasuhiro Haruta

Abstract Whole-head magnetoencephalography (MEG) systems to study cognitive processing in young children have recently been developed. The child MEG system has a helmet-shaped sensor array designed to fit child-sized heads. The sensor array comprises 64 or more LTS-SQUID axial-type gradiometric magnetometers with a baseline length of 50 mm, arranged about 100 mm from the center of the child's head. The sensor array is installed in a helmet of a horizontal dewar with a head circumference of about 530 mm, which was determined on the basis of a preliminary investigation on the standard size of preschool children's heads. In this chapter, the details of the child MEG system and its applications to auditory brain functions such as language acquisition are described.

Keywords Magnetoencephalography · MEG · SQUID · Child MEG · Auditory evoked field · Brain connectivity · Language acquisition · Brain development

1 Introduction

We developed a whole-head magnetoencephalography (MEG) system to study cognitive processing in young children. This child MEG system contrasts with conventional systems that have a helmet-shaped sensor array designed to fit adult-sized heads. When adult MEG systems are used with young children, it is difficult to achieve a sufficient signal-to-noise (S/N) ratio because children's head sizes are much smaller than those of adults, and the distance between the sensors and the

Y. Adachi (✉) · Y. Haruta
Applied Electronics Laboratory, Kanazawa Institute of Technology, Ishikawa, Japan
e-mail: adachi.y@gmail.com

Y. Haruta
Department of MEG, Yokogawa Electric Corporation, Tokyo, Japan

S. Supek and C. J. Aine (eds.), *Magnetoencephalography*,
DOI: 10.1007/978-3-642-33045-2_27,

magnetic sources in the brain is significant. Therefore, the use of a conventional MEG system to study child cognitive processing requires compromises that are less than ideal, such as positioning the child's head to one side of the helmet and then the other, which increases data acquisition times.

The child MEG system is expected to become an effective tool for investigating children's brain functions, especially that related to language acquisition and brain development, given its noninvasiveness and high temporal and spatial resolution. An additional advantage is that the MEG system is "acoustically silent" in general. The child MEG system does not make acoustic noise that could sometimes scare child participants during the measurement, unlike other brain functional imaging devices such as functional MRI (fMRI) or positron emission tomography (PET). In this chapter, the details of the developed child MEG system and its applications are described.

2 Instrumentation

2.1 System Configuration

Figure 1 shows the configuration of the child MEG system. SQUID sensors inside the dewar are connected to the SQUID driving electronics outside the magnetically shielded room (MSR). The SQUID signals are amplified and filtered by analog signal processing electronics and are then digitally recorded for visualization and further analysis.

The appearance of the child MEG system installed in an MSR at the Australian Hearing Hub at Macquarie University is shown in Fig. 2. The MSR is made of three mu-metal layers, and it houses two MEG systems. The child MEG system is to the left and a conventional adult MEG system is to the right in the figure. Like the adult MEG, the child MEG system has the gantry-free structure designed for subjects in a supine position (Kado et al. 1999). The supine position is effective for suppressing the movement of the subject's head during the measurement. Similar child MEG and adult MEG systems are installed in an MSR at the Department of MEG, Yokogawa Electric Corp.

2.2 Sensor Array and Dewar

The sensor array comprises 64 LTS-SQUID axial-type first-order gradiometric magnetometers. Niobium-based LTS-SQUIDs known as Ketchen type (Jaycox and Ketchen 1981; Ketchen and Jaycox 1982) are used. The pick-up coil made of niobium thin wire with a 15.5-mm diameter and 50-mm baseline length is wound around a bobbin and coupled with the input coil of each LTS-SQUID mounted at the

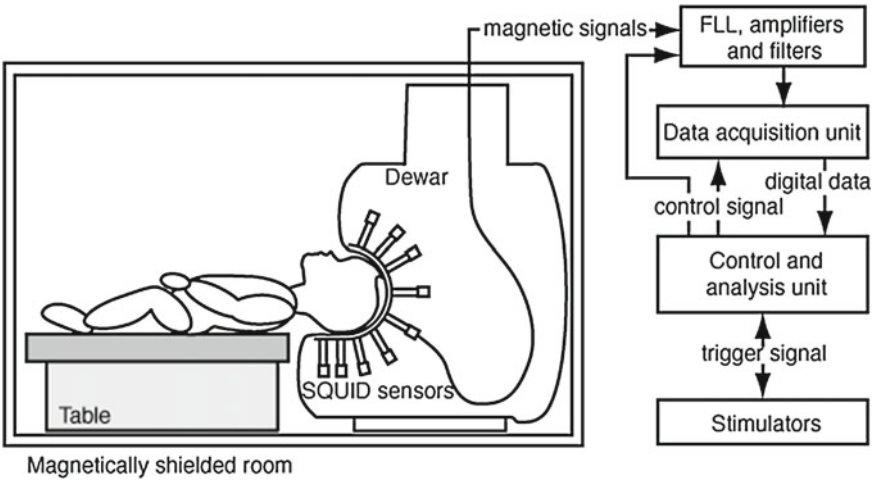

Fig. 1 System configuration of the child MEG

Fig. 2 Appearance of the child MEG system (*left*) and the conventional MEG system (*right*)

top of the bobbin. The typical noise characteristics of the sensor are less than 10 fT/$Hz^{1/2}$ at 1 Hz and less than 5 fT/$Hz^{1/2}$ at 100 Hz. The number of SQUID sensors is expandable up to more than one hundred by reconfiguration with additional sensors. The sensor array is helmet-shaped and its size is about 200 mm in diameter and about 530 mm in circumference. These dimensions were determined on the basis of a preliminary investigation of the standard size of preschool children's heads. This size was about 20 % less than the size of the conventional adult MEG sensor array.

The dewar to store liquid helium is of a horizontal type and is optimized for the measurement in the supine mode. The sensor array described above is positioned

inside the dewar at the helmet side. The size of the helmet for the child MEG system is shown in Fig. 3 in comparison with that for the conventional adult MEG system. The angle of view was designed to be wider than that for the adult MEG system to broaden the field of vision during the measurement. This wide angle of view is effective for preventing the children from feeling claustrophobic. The cool-to-warm separation at the helmet-shaped part is 20 mm. The liquid helium capacity of the dewar is roughly 100 L, and the helium consumption rate is less than 6 L/day. The sensor array is assembled using the *ship-in-a-bottle approach* (Kado 1999), a method used to assemble our adult MEG systems. This technique enables the diameter of the opening to access the dewar to be kept smaller than the total size of the sensor array and, as a result, to reduce the liquid helium consumption rate.

The dewar and the sensor array are made of glass-fiber reinforced plastic (GFRP). It is non-magnetic and effective in preventing magnetic artifacts. However, it is known that GFRP can be mechanically distorted when it is cooled in liquid helium, and a sensor can inevitably be dislocated from its originally designed position. The displacement is not predictable before cooling and it is not negligible in view of the accuracy of magnetic source analysis. Therefore, the positioning and calibration of each sensor is performed after cooling using a precisely machined array of coils and standard electric current to produce standard magnetic fields (Higuchi et al. 1989).

2.3 Flux Locked Loop (FLL) and Data Acquisition Unit

A double-integrator-type FLL based on a direct offset integration technique (DOIT) (Drung et al. 1990; Adachi et al. 2007) is adopted to linearize the flux-voltage characteristics and to improve the dynamic range of the SQUID signal. The second feedback loop of the FLL provides an automatic offset adjustment. Consequently, the effective frequency range of the FLL is 0.16 Hz–5 kHz. Therefore, this FLL is also called a band-pass type FLL.

3 Comparison with the Conventional MEG System

Pioneering works using the whole-head child MEG system were reported by Johnson et al. (2010). Measurements of the auditory evoked field (AEF) from preschool children were performed using both the child MEG system and the conventional MEG system. The position of the child's head relative to the sensor array was obtained by marker coil measurement prior to each MEG measurement (Erné et al. 1987). The conformity of the children's heads to the child MEG helmet and the conventional MEG helmet was evaluated based on the analysis of the sensor-head center distance. The fit of the child MEG helmet to the children's heads was comparable to or better than that typically achieved for adult heads with

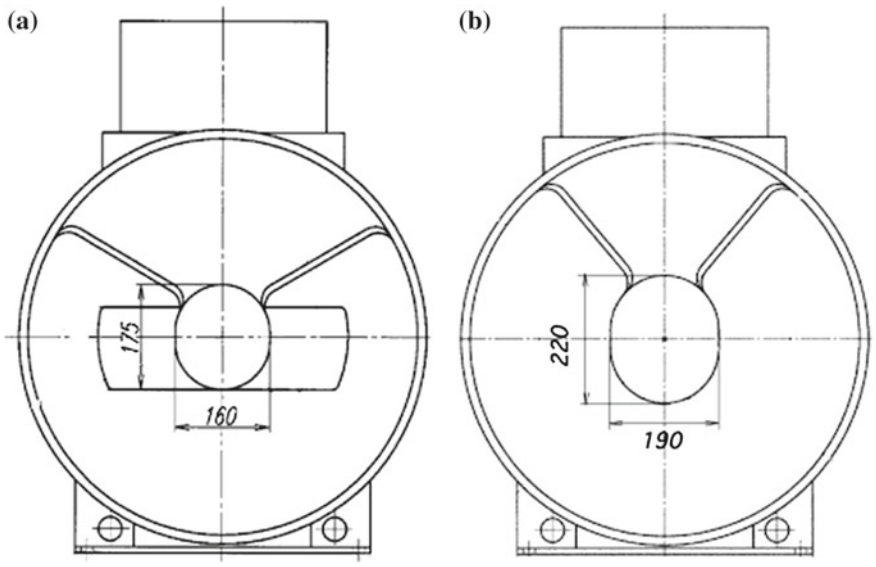

Fig. 3 Front view of the dewars (**a**) for the child MEG and (**b**) conventional MEG systems

a conventional MEG system. The head of a 4-year-old child could not be fully inserted into the adult helmet owing to the smaller crown-neck distance, and symmetrical lateral positioning in the adult helmet could not be achieved and maintained without the insertion of shim pads in the temporal regions.

The AEF was recorded from seven healthy children aged between 4 and 5 years of age using the child MEG system. The repetitive broadband noise stimuli were binaurally presented via plastic tubes with a random interstimulus interval. Subsequent AEF recordings from three of the participants were attempted using the conventional MEG system with the same stimulus conditions.

It is sometimes impossible for young children to perform the demanding tasks that are commonly employed for healthy adult participants. Therefore, acoustic stimuli were delivered to child participants while they viewed a silent video program projected through a hole at the MSR wall onto a screen mounted above them from a video projector placed outside the MSR. The video aided the continued engagement of the child in the MEG environment and also helped minimize the movement artifacts during the experiment.

Using the child-friendly data acquisition technique described above (i.e., silent video), AEFs were obtained from all seven children with the child MEG system. The maximum amplitude response, termed child P100 m, had a mean amplitude of 101.0 fT and a mean latency of 121 ms. The pattern of the P100 m distribution was oppositely directed to that of the adult M100.

In contrast, when children were placed in the conventional MEG system, no AEFs were successfully recorded. This was mainly because of two difficulties associated with the poor fit of children's head to the adult helmet. The first was

positioning of children in the adult helmet. It took about 10 min for placement of shim padding to reduce the children's head movement and it made the recording session longer. Two children were placed in the conventional MEG system, but measurements were terminated before completion owing to considerable movement or by a request by the child. This indicated that the length of the recording session became a strain for child participants. The second difficulty was that the head of a 4-year-old child could not be fully inserted into the adult helmet because of the smaller crown-neck distance. One child completed a recording session in the conventional MEG system, but no AEF was discernible in the recorded data.

Figure 4 shows an example of the AEF obtained from a healthy 4-year-old male child using the child MEG system (Adachi et al. 2010). A numerical experiment was performed to estimate a hypothetical child's AEF distribution obtained by using a conventional MEG system based on the equivalent current dipoles (ECDs) shown in Fig. 4c. When AEF amplitudes in children were compared between the child MEG system and conventional MEG systems, amplitudes were reduced to 74 % in the conventional system, compared to the child MEG system. This result indicated that although it may be possible to record child MEG signals using a conventional MEG system, the amplitude of the detected signals would most likely be lower than that recorded using a child MEG system. It would be necessary to increase the number of repetitive epochs to be averaged by almost a factor of two in order to achieve the same S/N ratio achieved with the child MEG system. This implies that the recording session also has to be extended. A prolonged MEG experiment would be tedious and uncomfortable even for the adult participants. Therefore, it is beneficial for the child participants and researchers to shorten the measurement time using the child MEG system.

4 Applications to Pediatric Neuroscience Research

The child MEG system is currently being used for the functional neuroimaging of children. Unlike other functional neuroimaging devices such as fMRI and PET, MEG is "acoustically silent." This is a large advantage for pediatric neuroscience research because the substantial acoustic noise from the device sometimes scares child participants and disturbs their concentration during MEG measurements. In this section, recent studies of cognitive functions in children using the child MEG system are presented.

Yoshimura et al. (2012) investigated 63 children in an attempt to reveal the linkage between the AEF response to speech syllable stimulation and their language performance using the child MEG system. ECDs were estimated for the P50 m component, between 40 and 150 ms in latency. The results of the AEF measurement indicated that the amplitudes of the ECDs in the left hemisphere were positively correlated with the language performance index obtained by the Kaufman Assessment Battery for Children (K-ABC).

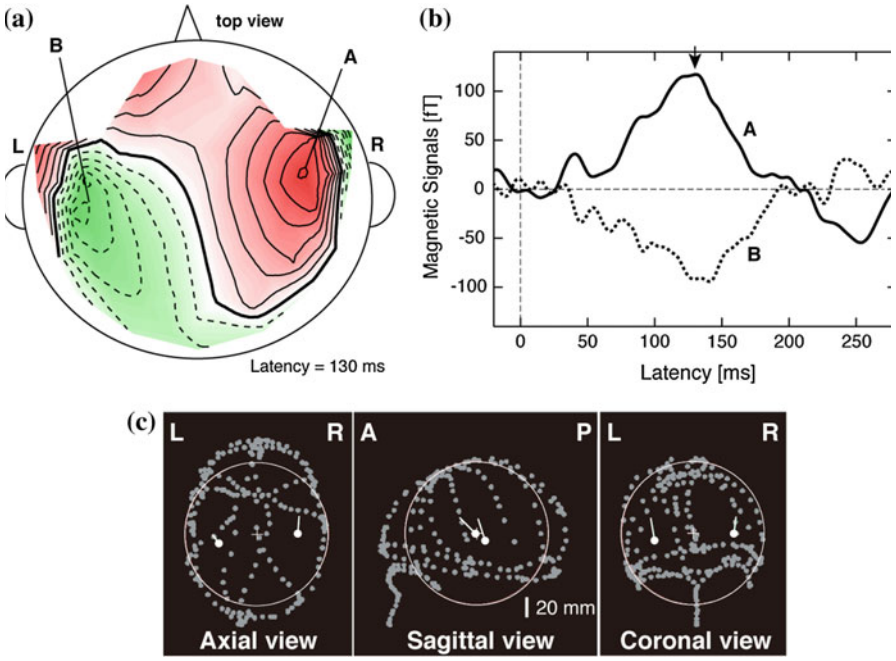

Fig. 4 An example of the AEF recording using the child MEG. **a** Isofield contour map at 130 ms in latency **b** waveforms obtained at the sites indicated in the contour map and **c** the positions of estimated equivalent current dipoles

The analysis of spontaneous MEG signals in children is also useful because it is sometimes difficult to get child participants to perform specific tasks in order to obtain event-related MEG signals. Sophisticated analysis techniques for the oscillatory spontaneous MEG signals in the frequency domain are also important for investigating connectivity within the brain network. In contrast with evoked response recordings, the S/N ratio of spontaneous signals cannot be improved by averaging. Therefore, the acquisition of larger MEG signals, accomplished by using a helmet fitted to a child's head in the child MEG system, is especially effective.

The child MEG system was recently applied to research on brain connectivity to reveal language development in preschool children (Kikuchi et al. 2011). The spontaneous MEG signals were recorded from 78 preschool children while they watched narrative videos. MEG spectra at each sensor obtained with the fast Fourier transform were separated into eight bands; delta (0.7–3.9 Hz), theta-1 (4.2–5.9 Hz), theta-2 (6.4–7.8 Hz), alpha-1 (8.3–9.8 Hz), alpha-2 (10.0–12.0 Hz), beta-1 (12.2–19.8 Hz), beta-2 (20.0–29.8 Hz), and gamma (30.0–57.9 Hz). The coherence and relative power among the sensors were calculated in each band. Their linkages with language-related, cognitive performance acquired by the K-ABC were investigated. A positive correlation between the left dominant

parietotemporal theta band coherence and higher performance scores of language related tasks was indicated. According to this result, it was suggested that the left-lateralized connectivity via theta oscillation activity, not the left dominance in the theta band itself, is linked to the development of language ability.

The foregoing connectivity analysis conducted using spontaneous MEG data, to investigate information flow and interactions between brain areas, is currently becoming more prevalent. A source reconstruction method based on a beam-forming technique is compatible with the analysis of the spontaneous MEG data. Source-level connectivity analysis should become the dominant method, rather than sensor-level connectivity analysis because source-level connectivity analysis can be easily related to the neuroscientific data obtained by other functional brain mapping devices such as fMRI (Gross et al. 2013).

In recent studies on sensorimotor rhythms, data acquired by the child MEG system also revealed that the oscillatory activity pattern evident in young children's brains, induced by a videogame-like task, differs from the typical adult pattern (Cheyne 2012). This result implies that cortical motor networks reveal developmental changes for preferred oscillation frequencies, possibly owing to changes in cortico-subcortical or intracortical connectivity.

5 Conclusion

We developed a whole-head MEG system for young children. To improve the fit of the MEG helmet to the size of a child's head, the size of the helmet-shaped sensor array was reduced by about 20 % compared to a conventional adult MEG system. In addition, because the sensor array is fitted to a child's head, the amplitude of the MEG signals obtained by the child MEG system is higher than that obtained by the conventional MEG system. Consequently, the recording session time to achieve the adequate S/N ratio is shortened, and this is a significant advantage both for the child participants and experimenters using the child MEG system.

The child MEG system will become an effective tool in pediatric neurology. Recently, the child MEG data was effectively used to investigate language acquisition of preschool children. The significance of studying children's brain function is increasing in terms of the early detection of developmental disorders or high-functioning autism. The importance of the child MEG will grow rapidly in the future.

References

Adachi Y, Kawai J, Uehara G, Miyamoto M, Tomizawa S, Kawabata S (2007) A 75-ch SQUID biomagnetometer system for human cervical spinal cord evoked field. IEEE Trans Appl Supercond 17(4):3867–3873

Adachi Y, Miyamoto M, Kawai J, Kawabata M, Higuchi M, Ogata D, Uehara G, Ogata H, Kado H, Haruta Y, Tesan G (2010) Development of a whole-head child MEG system. IFMBE Proc 28:35–38

Cheyne DO (2012) MEG studies of sensorimotor rhythms: A review. Exp Neurol. doi:10.1016/j.expneurol.2012.08.030

Drung D, Cantor R, Peters M, Scheer HJ, Koch H (1990) Low-noise high-speed dc superconducting quantum interference device magnetometer with simplified feedback electronics. Appl Phys Lett 57(4):406–408

Erné SN, Narci L, Pizzella V, Romani G (1987) The positioning problem in biomagnetic measurements: a solution for array of superconducting sensors. IEEE Trans Mag MAG-23:1319–1322

Gross J, Baillet S, Barnes GR, Henson RN, Hillebrand A, Jensen O, Jerbi K, Litvak V, Maess B, Oostenveld R, Parkkonen L, Taylor JR, Wassenhove V, Wibral M, Schoffelen JM (2013) Good practice for conducting and reporting MEG research. Neuroimage 65:349–363

Higuchi M, Chinone K, Ishikawa N, Kado H, Kasai N, Nakanishi M, Koyanagi M, Ishibashi Y (1989) The position of magnetometer pick up coil in dewar by artificial signal source, in advance in Biomagnetism. In: Proceedings of the 7th international conference on Biomagnetism. New York, pp 701–704

Jaycox JM, Ketchen MB (1981) Planar coupling scheme for ultra low noise DC SQUIDs. IEEE Trans Mag M-17:400–403

Johnson BW, Crain S, Thornton R, Tesan G, Reid M (2010) Measurement of brain function in pre-school children using a custom sized whole-head MEG sensor array. Clin Neurophysiol 121:340–349

Kado H (1999) Method of assembling a magnetomeasuring apparatus, US patent, Patent number 5,896,645

Kado H, Higuchi M, Shimogawara M, Haruta Y, Adachi Y, Kawai J, Ogata H, Uehara G (1999) Magnetoencephalogram system developed at KIT. IEEE Trans Appl Supercond 9(2):4057–4062

Ketchen MB, Jaycox JM (1982) Ultra-low noise tunnel junction dc SQUID with a tightly coupled planar input coil. Appl Phys Lett 40:736–738

Kikuchi M, Shitamichi K, Yoshimura Y, Ueno S, Remijn G, Hirosawa T, Munesue T, Tsubokawa T, Haruta Y, Oi M, Higashida H, Minabe Y (2011) Lateralized theta wave connectivity and language performance in 2- to 5-year-old children. J Neurosci 31(42):14984–14988

Yoshimura Y, Kikuchi M, Shitamichi K, Ueno S, Remijn GB, Haruta Y, Oi M, Munesue T, Tsubokawa T, Higashida H, Minabe Y (2012) Language performance and auditory evoked fields in 2- to 5-year-old children. Eur J Neurosci 35:644–650

Towards the Understanding of Healthy and Pathological Aging Through MEG

Fernando Maestú, Elena Solesio-Jofre and Ricardo Bajo

Abstract The study of healthy and pathological aging with Magnetoencephalography (MEG) has become more widespread in recent years. This is mainly due to its excellent temporal resolution which allows the evaluation of functional connectivity in the frequency domain. These characteristics make MEG unique for the study of the organization of the neurophysiological mechanisms supporting cognitive capabilities in the aging brain. In this chapter we will review MEG findings in normal and pathological aging. In normal aging, we will go through the mechanisms of forgetting and the assessment of the default mode network organization. In the field of pathological aging, the literature has mainly focused on Alzheimeŕs Disease (AD). These studies assess sensory memory, short-term and long-term memory, indicating decreased activity and connectivity in AD patients but increased activity at early stages such as Mild Cognitive Impairment (MCI). Finally, there is extensive literature using resting state recordings to characterize the brain networks of patients with dementia in a non-task context. All these topics will be discussed in the context of the literature of cognitive neuroscience of aging. Potential new approaches and recommendations for future research will be provided.

Keywords MEG · Aging · Mild cognitive impairment · Alzheimer's disease · Memory loss · Functional connectivity

F. Maestú (✉) · R. Bajo
Laboratory of Cognitive and Computational Neuroscience, Center for Biomedical Technology, Madrid, Spain
e-mail: fernando.maestu@ctb.upm.es

F. Maestú
Department of Basic Psychology II, Complutense University of Madrid, Madrid, Spain

E. Solesio-Jofre
Motor Control Laboratory, Research Centre for Movement Control and Neuroplasticity
Department of Biomedical Kinesiology, Katholieke Universiteit Leuven, Leuven, Belgium

S. Supek and C. J. Aine (eds.), *Magnetoencephalography*,
DOI: 10.1007/978-3-642-33045-2_28,

1 Introduction

There is growing interest in studying the neurophysiological mechanisms associated with the process of aging. This is mainly due to the progressive increase in the elderly population in developed societies over the last few decades. In fact, the number of elderly people is projected to represent 34 % of the entire population by the year 2050, in more developed regions of the world (world population prospects 2011). In the case of dementia and particularly Alzheimer's disease (AD), which accounts for 50–70 % of all dementia cases (Kukull and Bowen 2002), the incidence is at 35.6 million worldwide and is predicted to rise to 115 million by 2050. These numbers alone illustrate the importance of the study of aging and the need to develop cognitive and neurophysiological models to increase our understanding of the aging process.

Cognitive neuroscience provides an excellent framework from which to develop models that combine information from the behavioral and the neurophysiological levels of analysis. To achieve a more complete understanding of the origin of cognitive decline, it is important to investigate the organization of the aging brain and the intrinsic neurophysiological profiles underlying performance of cognitive tasks.

The process of healthy aging leads to a progressive decline in cognitive abilities such as memory, executive function, visuo-spatial skills, and orientation. All of this seems to be associated with some changes at the neurophysiological level that underlie dysfunctions at the behavioral level. Biochemical changes affect catecholamine circuits such as acetylcholine, dopamine or noradrenalin. Each of these neurotransmission systems has been associated with different behavioral processes that are partially impaired in elderly subjects, such as the ability to encode and remember information (acetylcholine), modulate emotional responses (noradrenalin) or establish some executive mechanisms such as the maintenance and manipulation of information (dopamine). These changes at the biochemical level are somehow associated with modifications at the morphological level. From a neuroanatomical point of view, several changes have been described in the process of normal aging such as the decline in the total brain volume and in both grey and white matter (Hutton et al. 2009). Specific regions seem to be particularly affected by the normal aging process such as the medial temporal lobe (hippocampus, entorhinal cortex), cingulate cortex (anterior and posterior), and the cerebellum (Raz et al. 2005). These morphological changes are probably expressing the loss of cells as well as changes in synaptic efficiency and loss of synaptic connections (Terry et al. 2001).

Functional MRI studies have provided important information regarding the functioning of the aging brain. Based on these findings, some models have emerged aiming to interpret different profiles of brain activity in elderly subjects. Cabeza et al. (2002), taking into account several previous papers reporting the recruitment of the right prefrontal cortex during performance of verbal tasks, developed the

HAROLD model (hemispheric asymmetry reduction in older adults). This model suggests that prefrontal activity during performance of cognitive tasks tends to be less lateralized in older adults than in younger adults. As indicated by Cabeza, this phenomenon is consistent during the performance of a variety of memory (episodic, semantic, working memory), executive (inhibition) and perceptual tasks. This neurophysiological phenomenon seems to be reflecting compensatory mechanisms in response to the lack of efficiency of certain brain networks. However, other authors interpret this finding as a progressive loss of brain functional distinctiveness, termed the dedifferentiation hypothesis (Park et al. 2004). This hypothesis claims that reduced asymmetry in elderly adults may reflect an age-related difficulty in recruiting specialized neural mechanisms (Lindenberger and Baltes 1994). Cabeza et al. (2002) tried to evaluate which of the two hypotheses was more plausible by comparing the brain activity of two groups of healthy elderly subjects: low and high performers of a memory task. Low performers showed unilateral activity while high performers showed bilateral activity of prefrontal cortex. Thus, these data appear to confirm the compensation hypothesis as the most plausible interpretation for the lack of asymmetrical prefrontal activity in elderly subjects.

Another interesting model that accounts for the activation changes in elderly subjects is the PASA model (posterior anterior shift in aging; Davis et al. 2008). This model reflects the fact that elderly subjects tend to recruit the frontal lobe more than younger subjects (Cabeza et al. 1997). The PASA model maintains the idea of hyperactivation as a compensation mechanism based on the following observations: (1) in some tasks elderly subjects achieve a similar performance as young subjects while exhibiting greater brain activity; and (2) when high and low elderly performers were compared to each other, high performers tended to show higher activation levels.

Another approach is the ELSA model, which accounts for the shift from an early- to late-onset cognitive control strategy linked with temporally extended activity in the prefrontal cortex and medial temporal lobe regions (Dew et al. 2012; Velanova et al. 2007). Velanova et al. (2007) showed how elderly subjects tend to delay their strategies until a later stage while young subjects tend to use proactive strategies.This proactive (young subjects) versus reactive (elderly subjects) pattern difference indicates an inefficient use of cognitive strategies, which affects the temporal profile of brain activation in the elderly.

Finally, a phenomenon that is important to bear in mind when attempting to account for the differences in brain activation between young and elderly subjects is the fact that elders tend to show higher activation in low-load tasks and lower activation in high-load tasks. This phenomenon called CRUNCH (compensation-related utilization of neural circuit hypothesis; Reuter-Lorenz and Capell 2008) is, again, in favor of compensatory mechanisms that can only be recruited when elderly subjects can handle the information necessary to perform the task.

These cognitive neuroscience models have addressed the question of hyperactivation as a balance between compensation and dedifferentiation. However, the majority of these interpretations are based on fMRI studies; therefore time-frequency information has not been considered.

In addition to the peculiarities in brain activation of elderly subjects, research into healthy and pathological aging should take into account several variables such as biomolecular issues. A phenomenon associated with the aging process is the progressive accumulation of beta-amyloid protein (Pike et al. 2007), a mechanism frequently associated with dementia. Another factor related to a higher degree of cognitive decline is the APOE 4 genotype. Nichols et al. (2012) found that elderly carriers of the APOE4 showed increased medial temporal lobe (MTL) hemodynamic response compared to APOE 3 or 2 carriers. Furthermore, middle age and elder carriers of APOE 4 showed increased synchronization at the MTL (Westlye et al. 2011). These findings reveal a pathophysiological sign of abnormal MTL functioning in elderly subjects with a strong genetic risk factor for the development of dementia.

So far, we have provided a general overview of functional neuroimaging activity and biomolecular influences in healthy aging. However, the majority of the studies mentioned above have been carried out using fMRI, a technique with high spatial resolution but very low temporal resolution. A combination of good temporal and spatial resolution is necessary for the study of neuroscience since brain networks have a dynamic organization in which information processing can occur in parallel. Different networks process information at different band frequencies, in very short periods of time, in response to environmental demands. Thus, limiting the study of the aging brain to just one of the dimensions (e.g., space) could lead to an erroneous interpretation of the mechanisms underlying cognitive processes in elderly subjects. Magnetoencephalography (MEG) is able to overcome some of the limitations of techniques based on hemodynamic response changes. Some advantages of using MEG are: (1) it is a non-invasive procedure; (2) spatial-time-frequency information of the physiological signals can be obtained and combined with other measures; and (3) it is an absolute measure (e.g., a reference is not required). These advantages make MEG unique in comparison with other procedures such as fMRI, PET and EEG.

So, now the question is, what can MEG add to the study of healthy and pathological aging? Its temporal resolution could be an advantage for studying the speed of processing and for testing ideas that suggest that there are delays in the activation of certain brain regions, such as the prefrontal cortex, in elderly subjects. The exquisite frequency resolution, could add fundamental information regarding the multiple functional networks that are co-activated with time-frequency differences. Finally, the connectivity dimension will be enriched by combining space-time-frequency information that could provide new insights into the hyperactivation phenomena (compensation/dedifferentation) reported in elderly subjects.In the following sections of this chapter we will review the fundamental MEG literature emerging over the last 15 years regarding healthy and pathological aging with MEG.

2 The Study of Normal Aging with Magnetoencephalography

During the last decades cognitive neuroscience has placed special emphasis on the identification of the neural correlates that occur with age-related changes in cognition. The brain is an open system and cognitive development across the lifespan is a dynamic, cumulative process that shapes the neurocognitive representations of ongoing interactions with the environment through experiences. Therefore, not only feed-upward effects from neural mechanisms to cognition and behavior, but also downward contextual and experiential influences on neurocognitive processing have to be investigated (Li et al. 2005).

As stated in the introduction section of this chapter, many models, based on different theoretical assumptions, have been developed to give a plausible explanation to the age-related declines in certain cognitive domains. Such is the case of the Global Factor Models, which postulate the presence of a general slowing-down process in cognition (Salthouse 1996); Cognitive Processes Models, referred to as prefrontal declines (West 1996) and their relation with impairments in inhibition (Hasher and Zacks 1988); the Brain Activation Models, which establish differential brain activation patterns of hemispheric asymmetry in the elderly (HERA Model, Tulving 1994; HAROLD Model, Cabeza 2002; Reuter-Lorenz Model 2005; PASA Model, Davis 2008) and the Neurocomputational Models, which examine the relation between age-related cognitive deficits and the attenuation of neuromodulation affecting neurotransmission (Li et al. 2001). Nevertheless, the aim of this section is not devoted to a comprehensive review of models in cognitive aging that, in the major part of the cases, have been reported with fMRI. Our aim is devoted to those models from the cognitive neuroscience of aging in which MEG reveals very valuable information regarding age-related differences in the temporal dynamics of brain function that other neuroimaging techniques are unable to provide. In this regard, work in the field has focused primarily on memory, which reflects the large behavioral literature existing on memory disruptions in older adults, particularly in terms of episodic memory (Coane et al. 2011) and working memory (Hasher and Zacks 1988). Hence, in the next section we will review research studies using MEG with the aim to explain age-related deficits in memory and the emergent use of MEG as a powerful tool to explore resting state functional connectivity.

2.1 Why do the Elderly Forget? MEG Contributions to Assess the Inhibitory Deficit Hypothesis

Forgetting occurs when items leave the focus of attention and must compete with other items to regain the focus (interference) or when the fidelity of the representation declines over time (decay). This gives rise to two major explanations for

forgetting, often placed in opposition; time-based decay and similarity-based interference. Both of them may ultimately result from the same underlying principles. The central claim of decay theory is that memory fades over time without additional identifiable causal agents, and information is less available for later retrieval (Lewandowsky 2008). There has been strong criticism of decay models, questioning whether it plays any role at all (Nairne 2002; Lewandowsky et al. 2004). Interference is a theoretical notion that refers to memory impairment that occurs due to interfering representations. The basic principle is that items in memory compete with the amount of interference determined by the similarity, number, and strength of the competitors. Interference may occur at multiple stages (encoding, retrieval, and storage) and levels (the representation itself or its association with a cue or a response). Interference from the past (proactive interference, PI) may affect both the encoding and the retrieval of new items, and it often increases over time. By contrast, interference from new items onto older memories (retroactive interference, RI) frequently decreases over time and may not be as reliant on similarity (Wixted 2004).

Interference effects are the dominant explanation of forgetting in the elderly. It is common to use the terms interference and inhibition interchangeably. Instead, it would be preferable to reserve the term interference for an empirical phenomenon in which performance decreases, relative to a baseline, because of processing of some irrelevant information. The term inhibition would be considered as the mechanism to potentially explain that interference. We characterize inhibition as an executive, active, goal-directed process that controls the contents of consciousness. Hence, executive control is necessary to override the retrieval of unwanted memories. It induces a lasting suppression of the unwanted memories, making them more difficult to recall later even when we want to return to them (Anderson 2005). In this regard, one must stop a prepotent response to a stimulus, either because that response must be withheld or because an alternative, a more weakly learned response to that stimulus, is desired. This ability to stop prepotent responses is critical to the flexible control of behavior.

In this context, the inhibitory deficit hypothesis (Hasher and Zacks 1988) provides a theoretical framework to understand cognitive decline during aging. According to this hypothesis, age-related impairments in multiple domains, such as attention, working memory or episodic memory, are the result of an inability to reduce interference from task-irrelevant information due to inefficient inhibitory control mechanisms (May et al. 1999; Zacks et al. 1999; Grady 2000). Age-related decrements in working memory performance have been reported (Salthouse et al. 1991; Grady et al. 2000; Cowan 2008), especially in tasks where subsequent events interfere with previous ones during the maintenance of information (Buckner 2004). This phenomenon termed retroactive interference reduces the ability to down-regulate relevant information and also leads to declines in bottom-up mechanisms.

Two main sources of retroactive interference might affect mainly inhibitory mechanisms, distractions and interruptions. On the one hand, distractions refer to the irrelevant information that should be ignored and are related to top-down

suppression signals from the prefrontal cortex (Chao and Knight 1998; Clapp et al. 2010). Top-down modulation is believed to be the neural mechanism underlying the enhancement of relevant information and the suppression of irrelevant distractions. It is mediated by higher-order regions in multimodal association cortices (prefrontal and parietal), with projections to sensory cortices (Gazzaley et al. 2005, 2007, 2008). On the other hand, interruptions refer to information encountered secondarily, and managing them involves the reallocation of cognitive resources to reactivate the disrupted representations; this process is mediated by the medial temporal lobe and the prefrontal cortex (Sakai and Passingham 2004; Clapp et al. 2010).

Despite the widespread cognitive literature regarding age-related inhibitory deficits, physiological evidence characterizing their neural underpinnings is controversial and has yet to be clearly established. Specifically, a question needs clarification: Is age-related increased susceptibility to interference from task-irrelevant information accompanied by changes in neural activity patterns? In this regard, Solesio-Jofre et al. (2011) investigated with MEG, age-related changes in brain activity during the active maintenance of information ascribed to the presentation of two types of RI, interruptions and distractions (see Fig. 1). To explore age-related and interference-related changes, as well as to assess differences in behaviour, young and older adults performed a delayed paired-associate (DPA) task for faces in which interruptions and distractions were presented during the maintenance stage. These investigators examined the temporal dynamics during the first 1000 ms after the onset of the interfering stimulus, restricted to those trials followed by a correct response in the subsequent probe period. Behaviourally, both types of RI significantly impair memory accuracy at recognition more in older adults than in young adults. MEG results revealed the presence of differential age-related and interference-related neural patterns.

Specifically, time-modulated activations in posterior-frontal regions were increased in young compared to older adults. Additionally, young adults exhibited greater posterior-frontal activations for the interrupting compared to the distracting condition. These results suggest that age-related deficits in inhibitory mechanisms were associated with under-recruitment in posterior-frontal regions. On the other hand, the absence of differential interference-related neural recruitments suggests that both types of interference affect the elderly equally. In a subsequent study, Solesio-Jofre et al. (2012) investigated age-related changes in brain activity during recognition and after the presentation of two types of RI, interruptions and distractions, by using the same DPA task for faces as in the previous study. These investigators, examined the temporal dynamics of brain magnetic activity during the first 1000 ms after the onset of each correct response at recognition. MEG results revealed the presence of differential age-related neural patterns. Specifically, time-modulated activations in temporo-occipital and superior parietal regions were higher in young adults compared to older adults for the interrupting condition. They suggested that age-related deficits in inhibitory mechanisms may be associated with neural under-recruitment in a highly interfering task. Finally, García-Pacios et al. (2013) reported on activity related to the encoding process of

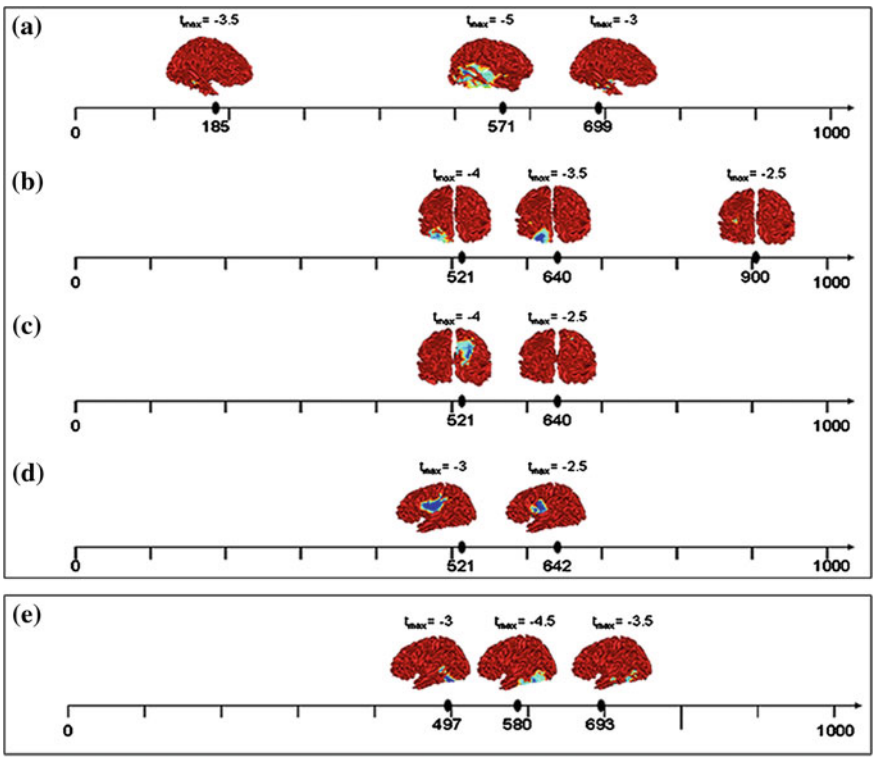

Fig. 1 Statistical maps refer to the largest clusters (*LC*) at the source space indicating significant increased activity for the young adults group relative to the older adults group in the IC [(A) (B) (C) (D)], and in the DC (E). Only statistical differences are shown considering the corresponding minimum Monte Carlo p-value (in text). A time axis (in milliseconds) is included to mark the temporal dynamics of neural differences

this DPA task. They found increased activity over prefrontal regions for elderly participants compared to young adults. This result indicates that elderly subjects needed higher executive control resources during encoding in order to achieve adequate performance on the task.

Altogether, this suggests that the Inhibitory deficit hypothesis provides an appropriate theoretical framework in which to understand age-related declines in memory function. Different studies show that MEG is an ideal tool to test the temporal dynamics of brain activity related to such cognitive deficits. The emerging MEG literature confirms that age-related under-recruitment, together with lower performance on memory tasks, reflect deficient inhibitory mechanisms. Specifically, deficient inhibitory mechanisms result from top-down control processing that regulates goal-directed behaviour and the suppression of irrelevant information when different responses compete for limited working memory resources.

2.2 The Neural Correlates of Age-related Inhibitory Deficits: The Frontal Deficit Hypothesis

Extensive literature suggests that cognitive decline in aging is accompanied by degeneration of tissue and functional reserves (Cabeza et al. 2002; Reuter-Lorenz and Lusting 2005). Converging evidence comes from lesion, anatomical and functional neuroimaging studies. The former show that lesions in dorsolateral prefrontal regions are associated with poorer performance on working memory, executive attention, and inhibitory control (Grasby et al. 1994; D' Esposito et al. 1995; Muller and Knight 2006). Different anatomical approaches have reported linear declines in gray matter in prefrontal regions starting during young adulthood (Gogtay et al. 2004; Hutton et al. 2009). Declines in white matter tracts connecting prefrontal and temporal lobes present the same linear pattern starting from 45 years (Bartzokis et al. 2001; Sullivan et al. 2001). Both gray and white matter declines with advancing age are supportive of the disconnection hypothesis (Geschwind 1965; O'Sullivan et al. 2001) that proposes that functional disruptions of large-scale brain networks account for the cognitive decline across the lifespan. Finally, most functional neuroimaging studies of aging have investigated the relationships between behaviour and brain activation patterns comparing young and older adults. It has been commonly reported that during the performance of memory recognition tasks, older adults show bilateral prefrontal activity while young adults show more lateralized prefrontal activity (Cabeza et al. 2002).

Although inconclusive, these findings showing age-related over-recruitment in the frontal lobes, together with those showing under-recruitment by Solesio-Jofre et al. (2011, 2012) are consistent with the frontal deficit hypothesis. It postulates that cognitive deficits in older adults are primarily caused by the anatomical and functional deterioration of the frontal lobes (e.g., Moscovitch and Winocur 1995; West 1996). Two main mechanismsfor age-related over-recruitment of the PFC have been proposed. On one hand, the compensation model (Madden et al. 1999; Reuter-Lorenz et al. 2000; Cabeza et al. 2002; Grady et al. 2006) postulates that older adults engage some brain areas, particularly the frontal lobes, above the level seen in younger adults to compensate for reduced activity in visual processing regions (PASA, Davis et al. 2008 see above for a detailed explanation). On the other hand, the dedifferentiation model also seems to characterize the increased bilateral prefrontal activity found in older adults (Colcombe et al. 2005; Aine et al. 2010; Park et al. 2010; see introduction section). One MEG study in support of the PASA Model was conducted by Aine et al. (2006). These investigators examined spatial working memory in young and older participants with a delayed-match-to-sample (DMS) task. Correlations between MEG responses and behavioural performance suggested that two different strategies were used by the different age groups while maintaining the same overall performance levels; young adults relied on posterior brain regions while the elderly relied on inferior frontal and supramarginal regions.

To determine the aging effects of brain activity on behaviour and differentiate between compensation and dedifferentiation, Grady (2008) summarized the most relevant findings to date and described four distinctive patterns in order to select the most appropriate explanation. First, older adults show more brain activity but the same performance level as younger adults as evidence of inefficient neural processing. Second, older adults reveal equal or greater brain activity but worse performance which is evidence of inefficient neural processing. Third, older adults recruit a brain region that is not active in young adults but they show equivalent performance, as evidence of compensation or dedifferentiation. Fourth, older adults recruit a brain region that is not active in young adults and it is positively correlated with performance in older adults and not in the young as evidence of compensation.

However, in a recent review (2011), Aine et al. brilliantly suggest an alternative explanation for such under-recruitment and over-recruitment discrepancies commonly shown in brain aging research. Prefrontal differences observed between young and older adults do not necessarily refer to aging impairments but brain maturation as a dynamic process that might improve cognitive abilities through later decades in life. It emphasizes the importance of brain flexibility and development throughout the lifespan in order to differentiate between adaptive changes that occur with age in opposition to brain dysfunction. There is growing interest in the neurosciences on exploring brain development from infancy through childhood, adulthood and aging (Pascual-Leone 2011). It is important to understand the processes underlying aging and how do they shape brain structure and function until death. It is crucial to conduct longitudinal lifespan studies or to, at least, include middle-aged subjects in cross-sectional studies in order to detect the continuous changes from the first to the last stages in life. Additionally, Aine et al. (2011) also highlight the necessity to better define aging and differentiate healthy successful aging from normal and pathological aging with objective measures, instead of subjective self-reports. It will enable the identification of additional risk factors that may lead to cognitive decline.

Finally, it is important to consider that the abovementioned discrepancies across studies regarding age-related neural differences (under-recruitment or over-recruitment) and their relationship with behaviour (compensation, or dedifferentiation) may be affected by different factors (Aine et al. 2011) such as the differences in experimental designs (Daselaar et al. 2003); analysis procedures (ROIs vs. whole brain approaches); and the heterogeneous variability of different measures across lifespan (e.g., white matter tracts in DTI studies, Aine et al. 2010; neurovascular coupling in fMRI studies, Kannurpati et al. 2011). In this regard, resting state functional connectivity emerges as a powerful tool that overcomes some of the limitations derived from task-related experiments. We describe the basic notions and current developments in the use of MEG in resting state studies in the following section.

2.3 Future Directions in the Study of Normal Aging with MEG: Resting State Functional Connectivity

Resting state functional connectivity is a useful tool to investigate the large-scale functional organization of the human brain. This method is based on the discovery that functionally related brain areas have correlated signal oscillations in low frequency ranges, something that was first described (Biswal et al. 1995; Fox et al. 2005) for blood oxygen level-dependent (BOLD) fluctuations measured with fMRI. The advantages of resting state recordings include the ease in acquiring data without any complicated task design, which makes resting state recordings ideal for children, elders, and patients.

Resting state has been used to explore the default activity of different brain networks involved in motor (Biswal et al. 1995), language (Hampson et al. 2002), sensory (De Luca et al. 2005), memory (Greicius et al. 2003), attention (Fox et al. 2006) and reading (Koyama et al. 2010) systems. Most of the studies in the field have measured the integrity of the large-scale system that involves frontal and posterior brain regions (Shulman et al. 1997; Mazoyer et al. 2001; Andrews-Hanna et al. 2007). This is commonly referred to as the default network (DMN, Raichle et al. 2001) which is associated with internally directed mental states, including memory and executive functions, during rest (Greicius et al. 2003; Fransson 2005; Vincent et al. 2006) and characterized by coherent neuronal oscillations (<0.1 Hz). During high demanding cognitive tasks, the DMN is deactivated and a task-positive network (TPN) is activated. Both the DMN and TPN can be considered elements of a single default network with anti-correlated components (Fox et al. 2005). Specifically, a set of frontal and parietal cortical regions routinely exhibit task-related activity increases, whereas a different set of regions including posterior cingulate, medial and lateral parietal, and medial prefrontal cortex routinely exhibit activity decreases. Extensive literature (Park et al. 2004; Gazzaley et al. 2005; Andrews-Hanna et al. 2007) has shown that cognitive decline in normal aging arises from functional disruptions in the large-scale brain systems, especially between anterior and posterior components of the DMN.

The study of age-related changes in the DMN by means of MEG is an emerging approach with great advantages. Resting state MEG extends and complements resting state fMRI (R-fMRI) by providing high temporal resolution that covers major bands of oscillatory brain activity (Schlee et al. 2012). Additionally, MEG offers a useful way to measure connectivity between brain regions with a direct measure of brain activity, that is, the magnetic fields associated with electrophysiological brain activity (Brooks et al. 2011a). A recent study by Schlee et al. (2012), exploring aging effects within the DMN with MEG, found significant age-related alterations of functional resting-state connectivity. Specifically, they found reduced information input into the posterior cingulum/precuneus region together with enhanced information flow to the medial temporal lobe. The authors concluded that resting state functional connectivity in the elderly is driven by attention to internal processes rather than attention to external stimulation and this is associated with

reduced performance in cognitive tasks. In another study, Schlee et al. (2012) focused on large-scale DMN organization across the lifespan. They found that slow frequencies were associated with larger networks compared to higher frequencies. In addition, decreases in visual memory and visuo-constructive functions were associated with an age-dependent enhancement of functional connectivity in both temporal lobes. It led them to conclude the usefulness of resting MEG recordings as a measure of the brain's baseline activity of functional networks.

In general, the utility of MEG to investigate different resting state networks has been shown in recent papers; de Pasquale et al. (2010) showed a correlation between resting state temporal MEG signals in the DMN and the TPN or dorsal attention network (DAN). Liu et al. (2010) examined correlations between oscillatory power modulations at the sensor level showing that significant correlations could be measured across hemispheres. Brookes (2011b) used seed-based correlation in conjunction with beamformer spatial filtering methods to show interhemispheric motor cortex connectivity in source space.

Altogether, these reports provide evidence that results from resting MEG replicate those from fMRI, suggesting that MEG is a powerful tool in the study of age-related changes of resting state functional connectivity. It is also important to emphasize that a better understanding of the age-related changes in resting state networks may provide information on the neural substrates underlying the inevitable functional decline in advanced aging and help in the early diagnosis and therapy of neurodegenerative disorders (Wang et al. 2012).

3 MEG in Pathological Aging

3.1 Evoked Fields in the AD Continuum

3.1.1 Preconscious Auditory/Somatosensory Processing and Sensory Memory

In a very elegant series of studies, Pekkonen and his colleagues were the first to use MEG to show impaired profiles of magnetic brain activity at early stages of auditory processing in AD. For example, they recorded auditory evoked magnetic fields (AEFs) elicited by monaurally presented tone stimuli from ten healthy young and ten elderly participants (Pekkonen et al. 1995). These AEFs are the result of averaged brain signals and provide information aboput the polarity ("P" for positive or "N" for negative) and latency (expresed in miliseconds after the stimulus onset). As an example P50 m will express a positive component with a latency around 50 ms after the stimulus onset. The "m" is indicating their magnetic origin to differentiate it from the EEG P50. Pekkonen et al. found that the amplitude of the P50 m component in primary auditory cortex was larger in older participants. Regarding the N100 m response, interhemispheric latency difference

(ipsilateral peak latency minus contralateral peak latency) increased as a function of age. The authors concluded that early auditory processing in the ipsilateral hemisphere is progressively delayed with increasing age. This study established a normative profile for subsequent studies in AD. Thus, Pekkonen et al. (1996) used similar methodology to record AEFs in AD patients and healthy elders. Peak latencies for P50m and N100m responses were significantly longer in AD patients in the ipsilateral, but not in the contralateral auditory cortex. This finding was replicated in a subsequent study with a larger sample of patients (Pekkonen et al. 1999). No inter-group differences in amplitude were found for N100m or P50m. Notably, scores on standardized language tests correlated with N100m latency recorded in the left (presumably dominant for language functions) hemisphere in the AD group.

To demonstrate that these profiles were related to a cholinergic system dysfunction, Pekkonen et al. (2001a, 2005) injected 0.3 mg of scopolamine (a cholinergic antagonist) prior to the recording session in healthy young (Pekkonen et al. 2001a) and older adults (Pekkonen et al. 2005). The scopolamine effect was associated with increased P50 amplitude in young subjects and a delayed latency of the P50m and N100m in response to tone stimuli in healthy elderly subjects. Another set of studies—using the Mismatch Negativity (MMN) paradigm—indicated that neurophysiological processes associated with sensory memory may be impaired in normal aging as well as in AD. This response takes place within the first 200 ms or so after stimulus onset and originates within the auditory cortex on the supratemporal plane. MMNm was significantly delayed in the left hemisphere ipsilaterally to the stimulated ear in AD patients (Pekkonen et al. 2001b). A subsequent report, however, indicates that MMNm was not affected by scopolamine injection in older healthy adults (Pekkonen et al. 2005). Recently, Cheng et al. (2012) assessed the M50 and MMNm responses during a passive oddball paradigm. The results showed larger cortical activation of standard-evoked M50 in AD patients compared to young and elderly controls. In contrast, the MMNm latency was longer in AD patients than in elderly controls. Thus, this report complements the scopolamine findings by Pekkonen et al., by providing support for the increased power of the signal found at early stages of processing as an indicator of disruption. Finally, Osipova et al. (2006), using a steady-state paradigm, showed that auditory stimulation at 40 Hz generates increased steady-state response in AD patients.

All these findings suggest that alterations in brain function in AD may take place at much more basic stages of stimulus processing. Together with the link established between early magnetic responses and cholinergic function, opens up the possibility of assessing the efficacy of new drugs, by evaluating their ability to modify the delay of this early response in AD patients.

Finally, Stephen et al. (2010) reported on differences in the early somatosensory magnetic response. MCI patients exhibited a larger amplitude response than healthy elders or patients with AD. These investigators also reported a relationship between neuropsychological test results and the amplitude of primary somotosensory responses. This report generalizes the idea that multiple sensory systems can be affected at early stages of the disease.

3.1.2 Memory Task

In a series of studies, comparing AD and age-matched healthy participants, using a modified version of the Sternberg paradigm (a continuous recognition memory task), Maestu et al. prospectively determined biomagnetic profiles that differentiated AD from healthy controls (Maestu et al. 2001) and elderly patients with major depression (Maestu et al. 2004). In these studies, patients with AD showed lower numbers of activity sources over the left parieto-temporal regions between 400 and 800 ms after stimulus onset. These findings correlated with performance on neuropsychological tests; the lower the number of dipoles for the posterior regions, the lower the score on the Minimental State Examination. In addition, the spatio-temporal profiles of neuromagnetic activity correlated with the degree of atrophy in MTL (Maestu et al. 2003), and with the metabolic changes detected by MR-Spectroscopy (Maestu et al. 2005). Thus, the greater the atrophy in MTL, the lower the number of activity sources over parieto-temporal regions in that particular time window. Furthermore, when an ROI for the analysis of MR-Spectroscopy was placed over these parieto-temporal regions, AD patients showed an increased ratio between myoinositol/N-acetyl-aspartate, indicating an increased glial proliferation and a loss of neurons over these regions. This biochemical finding correlates, in this sample of participants, with the loss of activity sources in these brain regions. In fact, the combination of biochemical and biomagnetic profiles was a better predictor of scores on the neuropsychological tests than either of these approaches separately. This series of studies made possible a description of particular MEG profiles that differentiated between AD and healthy elders. More importantly, the comparison between atrophy of the MTL and the biochemical profiles provided new insights about the interpretation of the MEG profiles. Thus, it seems as though the reduction of biomagnetic activity over the parieto-temporal regions could be due to a disconnection between the MTL and these neocortical regions, as well as due to a loss of neurons, as suggested by MR-spectroscopy.

Along similar lines, Walla et al. (2005) conducted a study in which participants were given an incidental verbal learning task (i.e., they were not instructed to learn the items), under two conditions (shallow and deep processing of the stimuli). After a short delay, their memory of previously presented items was tested, using a recognition memory paradigm. Recordings obtained over posterior brain regions revealed clear differences between correctly recognized repeated words (hits) and correctly rejected new words (correct rejections) in healthy elderly participants in the time window between 300 and 400 ms after stimulus onset. AD patients did not show differences between conditions for any brain region.

In two subsequent studies, Maestú et al. evaluated whether biomagnetic profiles could differentiate between MCI patients and controls. Contrary to their initial expectations, the MCI patients showed higher activity over the ventral pathway between 600 and 900 ms (Maestu et al. 2008). The ventral pathway consists of the ventral prefrontal region, the MTL, the mid-temporal gyrus and the inferior parietal lobe. This pathway is well known for its involvement in recognition memory; thus, hyperactivation of this pathway appears to be related to a

compensatory mechanism in the initial stages of the disease. A similar interpretation was developed by Dickerson et al. (2005) in an fMRI study where they describe an increased hemodynamic response in the MTL of MCI patients, in comparison to a control group. In a subsequent study, five control participants that developed MCI after two years of follow-up showed lower numbers of activity sources in the medial temporal lobe (Maestu et al. 2006). These results indicate that brain activity is reduced at a very preliminary stage of the disease. They also imply that when elders progress to MCI their activity is increased as a compensatory mechanism for the progressive lack of efficiency of the memory networks. It is of great interest to note that an independent study found similar results using MEG. Püregger et al. (2003) recorded brain magnetic activity from 10 MCI patients and 10 controls during a shallow (nonsemantic) and deep (semantic) word encoding task. Between 250 and 450 ms after stimulus onset, brain magnetic activity associated with nonsemantic and semantic word encoding differed significantly mainly over left frontal and left temporal regions. MCI patients showed increased activity during shallow encoding as compared to deep encoding. Controls did not show such a profile of activation. The authors interpreted this hyperactivation as a compensatory mechanism. Thus, the increased profile of activation seems to be a general finding that could constitute a biomarker for the early stages of the disease that can be found as well in elders with subjective memory complaints (SMC) as reported by Maestú et al. (2011a). However, in this last study MCI patients and SMC did not show differences between them suggesting that similar physiological mechanisms may underlie SMC and MCI. Later we shall see how the use of functional connectivity measures allows one to detect clear differences between these two groups. Aine et al. (2010) showed that enhanced activity in a group of MCI/AD patients correlated with lower IQs and poorer performance on verbal/visual memory tests. Thus, correlations could indicate that increasing brain activity does not indicate better functioning.

Two recent studies have evaluated memory related activity in the frequency domain using a modified version of Sternberg's paradigm in AD (Kurimoto et al. 2012) and in MCI (Aurtenetxe et al., 2013) patients. Kurimoto et al. (2012) found significant differences in the beta and gamma frequency bands. Patients with AD showed reduced beta event-related desynchronization (ERD) in the right central area compared to controls. Aurtenetxe et al. (2013) showed increased theta, lower beta reduction and decreased alpha and gamma power in frontal, temporal and parietal areas of MCI subjects, during early and late latencies. Their results point towards a dual pattern of activity (increase and decrease of frequency power) in MCI patients which is specific to certain time windows, frequency bands and brain regions. It may be that these results represent two neurophysiological sides of MCI. These two papers indicate that, along the AD process, a common neurophysiological disruption exists—the lack of beta band desynchronization (an electrophysiological phenomenon associated with successful memory performance). This neurophysiological sign is already present at the MCI stage and seems to be underlying early cognitive impairment. However, at the MCI stage,

theta band increases and predicts memory test performance. This phenomenon does not seem to be present at the AD stage, indicating that compensatory mechanisms are present for a limited period of time.

3.2 Resting State Activity

Along with the approach for studying profiles of brain magnetic activity during memory tasks there is also an approach for looking at the spontaneous brain activity (resting state). The studies focusing on resting state examine brain activity mainly in the frequency domain. In a seminal study, Berendse et al. (2000) showed that the absolute low frequency magnetic power was significantly increased in fronto-central regions. Conversely, high frequency power values were decreased over the occipital and temporal areas.

In a series of studies, Fernandez et al. reported specific profiles of increased and decreased oscillatory activity in AD patients. Fernandez et al. (2002) showed an increase of delta and theta activity over the temporal and parietal lobes bilaterally. Notably, increased slow wave activity in these regions was associated with reduced performance in neuropsychological and daily living measures. In parallel with the memory studies carried out by Maestú et al. (2003, 2005), Fernandez et al. characterized the spontaneous findings in relation to MR-volumetry and MR-spectroscopy. A relationship between the presence of focal low-frequency magnetic activity and left hippocampal volume was found (Fernandez et al. 2003). When MEG and MR-volumetry were combined, left medial temporal lobe volume and the left temporal theta activity, correctly classified 87.1 % of the participants in their respective diagnostic groups. Furthermore, myoInositol/N-acetyl-aspartate rate scores in combination with MEG slow magnetic activity classified AD patients and controls with 90 % sensitivity and 100 % specificity (Fernandez et al. 2005). Osipova et al. (2005) found that the lower alpha rhythm was enhanced over the right temporal lobe in AD patients, while in age-matched controls alpha sources were found near the parieto-occipital sulcus. To evaluate whether this effect is due to a cholinergic deafferentation, it is useful to consider some classical studies (Riekkinen et al. 1991) in which a significant correlation between AChE activity of the cerebrospinal fluid (CSF) and delta power in patients with AD was detected. This correlation was further supported by EEG and MEG studies where scopolamine infusions generated changes in background activity, including reduced alpha and beta and increased delta and theta, that mirrored those found in AD patients (Osipova et al. 2003; Kikuchi et al. 2000). Thus, it might be proposed that low-frequency activity may function as an early indicator of neural dysfunction in AD and cognitive impairment. Besga et al. (2010) evaluated the combined contribution of MR-volumetry and MEG in MCI and AD patients. As expected, there were between groups differences in the volume of the medial temporal lobe. MEG showed inter-group differences, with AD patients exhibiting higher theta and delta activity than MCI and controls. Thus, left parietal theta

classified controls versus MCIs with an accuracy of 78.3 %. Right occipital theta and the left parietal delta allowed the discrimination of controls versus ADs, with 81.8 % rate of correct classification. Left parietal theta discriminated between ADs and MCIs with 56.6 % accuracy rate. Finally, the combination of MEG and MR-volumetry significantly improved the rate of correct classification, indicating that use of multidisciplinary techniques may improve diagnostic capabilities.

Findings were not always limited to the slow frequency bands. Ishii et al. (2010; see also Kurimoto et al. 2008), revealed that the averaged alpha event-related synchronization (ERS) after eye closing was enhanced over prefrontal regions in AD patients (Kurimoto et al. 2008). An interesting finding that supports the interpretation of this result was the fact that this frontal ERS source in the alpha band was negatively correlated with Mini-Mental State Examination scores in the AD patient group (Ishii et al. 2010).

3.3 Functional Networks in the Alzheimeŕs Continuum

A breakthrough for MEG and dementia was the introduction of functional connectivity measures and the use of graph theory metrics to better understand AD as a disconnection syndrome. The first study with MEG showing loss of connectivity between brain regions was published by Berendse et al. (2000). In this early study, AD patients present lower inter- and intrahemispheric coherence in all frequency bands compared to controls. Stam et al. (2002) used a non-linear method to evaluate functional connectivity (synchronization likelihood) and showed lower synchronization values in AD patients in the upper alpha band (10–14 Hz), the upper beta band (18–22 Hz), and the gamma band (22–40 Hz) (see Verdoorn et al. 2011 for a different finding). Again, differences between groups were mainly found in posterior regions. In a subsequent confirmatory study (Stam et al. 2006), AD patients showed a loss of left fronto-temporal/parietal long distance intrahemispheric interactions in the alpha1 and beta band. However, local connections were preserved in AD showing a local increase in synchronization in the theta band (centro-parietal regions), beta and gamma bands (occipito-parietal regions). All these changes could be related to reduced cholinergic activity. To assess this hypothesis, Osipova et al. (2003) recorded MEG activity before and after the injection of scopolamine in healthy elders. Scopolamine administration resulted in a desynchronization of the alpha band (8–13 Hz), in the posterior regions. In addition, interhemispheric and left intrahemispheric coherence was significantly decreased in the theta band (4–8 Hz). Another interesting study that assesses connectivity in AD is one published by Franciotti et al. (2006). They showed that coherence in the alpha band was disrupted in AD and Lewy Body Dementia patients, which mainly involved long connections. This paper is still one of the few comparing biomagnetic activity in different types of dementia syndromes (see Babiloni et al. 2005).

One study that had a major impact on current thinking was carried out by Stam et al. (2009). This study was the first to apply graph theory to MEG data in AD patients. On this occasion the investigators used Phase Lag Index to evaluate functional connectivity to avoid crosstalk in sensor space (spurious synchronization) due to volume conduction effects. They then characterized the functional network by calculating the mean clustering coefficient and path length. AD patients showed a decrease in the clustering coefficient and path length in the lower alpha band. This was an indication of the loss of small world architecture, which represents the most efficient functional organization. Through a computational model, Stam et al. were able to demonstrate that these network changes in the lower alpha band were explained by attacking targeted links in the network. As a conclusion, the authors highlight the idea that the functional architecture of the lower alpha band in AD showed a more random structure than age-matched controls. This result can be attributed to the loss of densely connected regions (hubs) as explained by the computational model.

In a subsequent study (De Haan et al. 2012a), the same group of investigators assessed the role of functional sub-networks (modules) in AD patients. The overall modular strength and the number of modules changed significantly in Alzheimer patients. The parietal cortex showed the strongest intramodular losses; however, intermodular connectivity losses were strongly related to cognitive impairment. In line with the previous study, De Haan et al. (2012b) assessed network connectivity, synchronizability, and node centrality. Their results demonstrate a global loss of network connectivity and disrupted synchronizability. Centrality analysis indicates disruption of hubs at parietal and temporal regions. More specifically, the low centrality of the left temporal region in the theta band in AD patients was strongly related to the mini mental state examination. Finally, De Haan et al. (2012c) recently developed a functional network computational model based on the notion that increased brain activity in certain cortical hubs could be a risk factor for the accumulation of beta amyloid. This model aims to evaluate whether increased activity in hub regions can induce hub vulnerability in AD. The model confirms the existence of high hub region activity, and the authors associate this finding with the high resting state activity in the Default Mode Network. Another interesting insight from this study was the modeling of what they term 'Activity dependent degeneration' (ADD), which was achieved by lowering synaptic strength and comparing the result to random degeneration. The model was able to mirror the majority of the previous findings in the literature of MEG-AD, such as oscillatory slowing, loss of spectral power and long-range synchronization, hub vulnerability, and disrupted functional network topology. This series of robust studies by De Haan et al. highlights the importance of viewing the AD continuum as a functional network disorder.

Based on these ideas, Bajo et al. (2010) assess the integrity of functional networks in the early stages of the disease; Mild Cognitive Impairment (MCI) and Subjective Memory Complaints (SMC). All these studies examine the functional

connectivity profiles during performance of a memory task. They showed increased synchronization over the prefrontal and central regions in several frequency bands in MCI patients (Bajo et al. 2010). It is of interest that 16 out of 19 MCI patients showed this pattern of increased synchronization over prefrontal cortex, indicating that this profile was not just a group effect. In fact, this increased synchronization pattern achieved 82 % correct classification of the MCI patients in the beta band. Whether or not this increased synchronization represents compensatory activity was tested by evaluating the functional architecture of the functional network by using a graph theory approach. MCI subjects show an enhancement of the strength of connections, together with an increase in the outreach parameter, suggesting that memory processing in MCI subjects is associated with higher energy expenditure and a tendency toward random structure, which breaks the balance between integration and segregation. All features were reproduced by an evolutionary network model that simulates the degenerative process from a healthy functional network to that associated with MCI (Buldú et al. 2011). This study provides a new interpretation of the hypersynchronization found in MCI patients. The organization of the functional network in MCI patients reveals a tendency toward a random structure with a high energy cost which is not ideal architecture for information processing and it suggests an early network disruption in the continuum of AD. In a subsequent study, Bajo et al. (2012a; see also Maestú et al. 2011a) went one step beyond evaluating functional connectivity in "healthy" elders with SMC, that is, elderly people who complain about their memory but achieve normal performance on neuropsychological memory tests. The question here was whether MEG functional connectivity profiles reveal an early sign of network disruption that cannot be seen by neuropsychological tests alone. The study included three groups: MCI patients with memory complaints and memory impairment revealed by a neuropsychological assessment; healthy elders with memory complaints but without memory impairment as evaluated by performance on memory test; and healthy elders without memory complaints and without memory impairment. The three groups showed differences relative to each other. MCI showed higher synchronization in comparison to the other two groups mirroring the findings described in Bajo et al. (2010). More importantly, the comparison between the two groups of "healthy" elders revealed weaker synchronization in the alpha 2, beta 1 and beta 2 frequency bands in frontal regions of the SMC participants as well as along the left hemisphere. These findings permit the development of a functional connectivity model of the AD continuum as expressed in Fig. 2. Thus, it seems that at the early stages of the disease, when neuropsychological test results are still not able to detect cognitive impairment, the network experienced diminished synchronization values followed by a random increase in synchronization, at the MCI stage, which ultimately resulted in a loss of synchronization when diagnosed as AD.

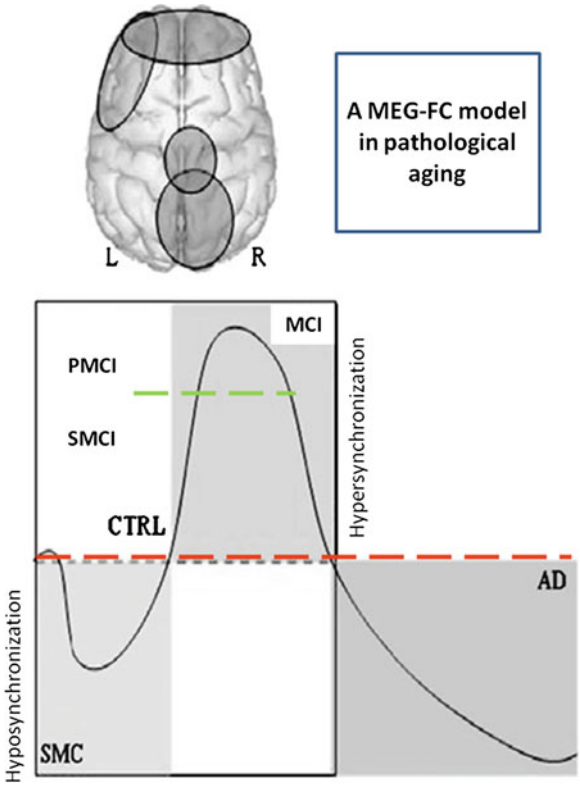

Fig. 2 This figure represents a functional connectivity model of the Alzheimer disease process. *Upper panel* indicates sensors where the profile represented in the *lower panel* was mainly found. *Dashed red line* in the lower panel represents the average synchronization value for the healthy elders. The *solid line* represents the increased or decreased synchronization values in comparison to controls values (*dashed line*) in different stages of the disease: Subjective Memory Complaints (*SMC*), Mild Cognitive Impairment (*MCI*) and Alzheimer Disease (*AD*) stage. PMCI indicates Progressive MCI and SMCI Stable MCI. *Dashed green line* indicates differences between PMCI and SMCI. Note that PMCI showed higher synchronization in comparison to the control group. (Modified from Bajo et al. 2012a,b, Age)

3.4 Profiles Leading to the Prediction of the Development of Dementia

One remaining question that needs to be answered is whether MEG profiles can predict who will develop dementia. Three MEG papers have addressed this question using different signal analysis approaches. Maestú et al. (2011b) used the technique of evoked fields to longitudinally follow MCI patients and tested them to determine who did and did not develop dementia. Thus, by using a retrospective analysis they were able to look for certain brain activity profiles that were different

at the time that Progressive MCI (PMCI) and Stable MCI (SMCI) constituted a single MCI group. This procedure made the development of a prospective model possible. The comparison of the PMCI and SMCI showed reduced power activity during performance on a memory task over the posterior regions of the brain. A higher degree of activation for the PMCI group was evident in the right prefrontal (between 0 and 100 ms after stimulus onset), right inferior parietal lobe (between 100 and 300 ms), left parieto-occipital cortex (between 300 and 400 ms) and ventral prefrontal regions (between 600 and 900 ms). The PMCI participants also showed differences between the AD group, which indicates that at the time of testing they showed a non-AD neurophysiological profile. SMCI showed higher activity than the AD and control groups but lower activity than the PMCI group. Thus, it seems that the higher the degree of the activity, the higher the likelihood of the development of AD-type dementia. Fernandez et al. (2006), who examined slow frequency activity during a resting state condition, indicate that the left parietal delta dipole density permitted a reliable classification of AD and MCI patients. Thus, the MCI patients were divided into 2 groups based on the median left parietal delta dipole density, and were followed for 2 years. The estimated relative risk of conversion to AD was increased by 350 % in those MCI patients with high left parietal delta dipole density scores. Finally, Bajo et al. (2012b) analyzed data recorded during a memory task using a functional connectivity approach. They reported increased synchronization values in the alpha 1 and 2 frequency bands over the posterior parieto-occipital regions and in prefrontal regions in the PMCI group, in comparison with SMCI. These three studies provide converging evidence about the role of the parieto-occipital regions, in PMCI and SMCI, by showing increased activity or synchronization during a memory task or increased slow frequency activity during resting state. During a memory task, an additional profile emerged—bilateral hyperactivity of the prefrontal regions. This excessive activation-synchronization over regions that are considered as anatomical-functional hubs is consistent with the findings achieved by investigators using other imaging modalities, in which atrophy or high accumulation of amyloid in the precuneus predicts who will developed dementia (Forsberg et al. 2008). Additionally, these posterior regions revealed the loss of hub structure in AD patients. Thus, these MEG profiles could serve as a potential biomarker for the prediction of the development of dementia.

4 Conclusion

The use of MEG in the study of healthy and pathological aging emerged in the mid-nineties and has continued to become more widespread to this day (based on the number of publications). This field continues to develop due to the clear evidence indicating that MEG is a powerful method for evaluating the integrity of functional networks.

To date, studies describing the neurophysiological mechanisms underlying progressive cognitive decline in healthy elders have mainly focused on memory functions. More specifically, they focused on mechanisms of forgetting. Solesio-Jofre et al. (2011, 2012) demonstrate in a series of studies that, although elderly people show increases of frontal lobe activity at the encoding stage, interference with the memory trace during the maintenance stage acts to disrupt this potential compensatory mechanism, thereby resulting in a decline in brain activity in posterior and frontal regions during the maintenance and recognition stages. These results suggested that age-related deficits in inhibitory mechanisms were associated with under-recruitment of posterior-frontal networks. On the other hand, the absence of differential interference-related neural recruitment (distraction and interruption), at least at the maintenance stage, suggests that both types of interference affect the elderly equally. These findings need to be compared with the models in the field of cognitive neuroscience of aging. However, these cognitive neuroscience models have been developed based on findings using fMRI. fMRI and MEG would not necessarily be expected to obtain similar findings. The higher temporal resolution of MEG allows cognitive processes to be tracked in a more detailed manner, thus providing a more complete understanding of all dynamic brain activity associated with cognitive processing. In a DMS task in which three different stages of cognitive processing (encoding-maintenance/interference-recognition) occur in a short period of time, fMRI cannot track all the millisecond activity noted across parallel sub-networks that underlie good performance. Thus, MEG is opening up new possibilities in terms of highlighting the neurophysiological mechanisms associated with the aging process. In the future, a detailed examination of functional networks should provide useful new information regarding differences between young and elderly subjects. With regards to this, Schlee et al. (2012) began examining such parameters in a resting state condition. They found decreased and increased inflow of activity in some posterior regions which correlated with cognitive performance. Concerning the field of pathological aging, the advances achieved in the last ten years have been considerable. MEG was used successfully to describe impaired information processing in primary-sensory and in higher-cognitive functions; from sensory to working and declarative memory. In addition, MEG was used to describe different profiles of impairment at different stages of the disease from SMC to MCI and AD. These profiles may prove very useful for: (1) tracking the progression of the disease; (2) providing evidence of disease at the neurophysiological level even when neuropsychological tests are unable to detect memory impairment; (3) providing a measure of neuronal dysfunction; (4) evaluating pharmacological and non-pharmacological treatments; and (5) providing new insights into the pathophysiology of the disease by examining the disruption of pertinent functional networks.

A common finding among the literature of MEG and pathological aging is the fact that at early stages of the disease there appears to be increased activity in some brain regions (Dickerson et al. 2005). For example, during memory tasks, MCI subjects showed increased activation over different brain regions including anterior and posterior cortex (Puregger et al. 2003; Maestú et al. 2008; Aine et al. 2010;

Maestú et al. 2011a). Frequency analysis also revealed an increase of theta power at the right frontal pole in MCI patients, associated with better memory test performance (Aurtenetxe et al. 2013). Connectivity analysis reflected increased synchronization of the prefrontal regions for MCI during performance of a memory task. fMRI models of cognitive neuroscience of aging predict an increase of activity over the anterior regions of the brain which is interpreted as reflecting compensatory activity (HAROLD, PASA, see introduction section for a detailed description of these models). Following the perspective proposed by these models, the increased activation found in MEG studies could be compensatory(i.e. MCI patients are overusing a network activated as well by healthy elders; see García-Pacios et al. 2013). However, there are some findings that argue against this hypothesis. Buldú et al. (2011) demonstrated that the increase of synchronization in MCI patients leads to a random network structure. Furthermore, Bajo et al. (2012a,b) demonstrated that those MCI showing higher synchronization over parietal and frontal regions were those that developed dementia within two years of follow-up. Finally, at the initial stages of the disease, SMC subjects showed an opposite response; decreasing connectivity (Bajo et al. 2012a). Thus, it is hard to say that this increased activity improved the efficiency of the information processing. It may be part of a dedifferentiation process or a non-successful compensatory mechanism (Grady 2012). Aine et al. (2011) provided an interesting alternative explanation involving the idea of a maturation process rather than a compensatory or a dedifferentiation process.It is difficult to say which of these interpretations is correct. However, recent findings in animal models provide new insights into the pathological nature of this increased activity. Cirrito et al. (2008; also see Bero et al. 2011) showed that the hyperactivation of certain brain regions facilitates the accumulation of amyloid in animal models of the disease. Furthermore, the reduction of this hyperactivation by antiepileptic drugs improves cognition (Sanchez et al. 2012). Thus, it seems that this hyperactivation is underlying a pathological process and that it is not improving the functioning of the cognitive system. Instead, it seems to be facilitating the pathophysiological process of the disease. If MEG were able to detect this early sign of impairment (hypersynchronization) it would be a very useful tool for identifying candidates for early cognitive or pharmacological treatment.

Although all these MEG findings may be important clinical biomarkers linked with the pathophysiology of the disease, there is still much left to do before MEG is used in daily clinical practice in the field of dementia. This is our view for the following reasons. First, 90 % of the findings have been found by two or three groups studying different stages of the disease or using different signal analysis approaches. Thus, it seems necessary to establish a multicenter study to assess whether profiles of magnetic activity are reproducible across centers and to establish a blinded protocol with classification carried out on a single subject basis instead of depending on group effects. Second, it is necessary to evaluate the sensitivity and specificity of the MEG profiles found in AD in direct comparison with other types of dementia. Third, MEG should be compared with measures of amyloidosis (cerebrospinal fluid, CSF and/or PET-PIB) and brain injury as required by the new criteria (Sperling et al. 2011). Fourth, it would be necessary to

test whether a relationship exists between magnetic profiles and genotypes of the disease. Fifth, an extensive evaluation of very early stages of the disease such as SMC is required, since there is still a discrepancy between clinical symptoms and an objective measure of impairment (neuropsychological test). Sixth, the ability to detect changes induced by pharmacological and non-pharmacological treatments should be demonstrated. Seventh, a robust model must be found for the prediction of the development of dementia, or at least for the detection of converters from MCI to AD. Eighth, an easy protocol needs to be established for the recording and analysis of brain activity, and this must be accessible to PhDs and MDs, who do not have an extensive background in computer programming.

It is useful to consider the progress made to date regarding each of the eight points raised above. First regarding a multicenter study, there have been at least two independent initiatives that have tried to fill this gap. Verdoorn et al. (2011), in a two-center study, provided evidence for the benefits of a multicenter approach and interesting test / retest results. However, it seems that a much larger consortium would be necessary to obtain enough cross-center reliability and a fully blinded study with patients enrolled from different countries and continents. A different initiative "The MagnetoencephaloGraphy International Consortium for the study of AD" (MAGIC-AD), has been working over the last two years to achieve the aims declared in a position paper (see Zamrini et al. 2011). This consortium involves eight MEG centers from three different continents. The consortium has already conducted a preliminary analysis of blinded data and the results will be shared with the community soon. Second, profiles of biomagnetic activity have been described in other types of dementia such as Parkinson disease (see Stam et al. 2010 for a review), Lewy Body Dementia (Francciotti et al. 2006) or vascular dementia (Babiloni et al. 2005). However, there is still a lack of direct comparison between multiple dementia subtypes to test sensitivity and specificity.

Regarding the rest of the items listed above none or few achievements has been made. Although genetics have been compared with electrical profiles in the EEG field, there is still a lack of such comparison for MEG, at least in AD patients. There is one report indicating the relations between APOE and MEG. Deeny et al. (2008) assessed whether physical exercise level modifies the relationship between APOE genotype and neurocognitive function in a single group comprised of young adults and healthy elderly people (50–70 years old). Regarding the pharma-MEG or the evaluation of the effects of a particular medication is a field that is rapidly developing (Hall et al. 2011). However, there are still no reports about the effects of medication on biomagnetic profiles of AD/MCI/SMC subjects., MEG signal analysis is still difficult for researchers that are not involved in the field (and still for some who are). There is a lack of agreement regarding: types of sensors to record brain activity; source reconstruction techniques; and methods for establishing functional or effective connectivity. Even more importantly, the application of the majority of these methods requires some background on signal processing—a field not frequently covered at institutions granting health-related degrees. This makes MEG a non-accessible method for many, which continues to be a great barrier for the general use of this technique.

It is probably true that connectivity analysis and characterization of the functional networks of the brain represent both the present and future of MEG. As our understanding of aging points more and more towards a process of progressive synaptic and neuronal malfunctioning, MEG could be an ideal tool for evaluating the progressive loss of efficiency of the neuronal networks in normal aging and the dysfunctions at the synaptic level that occur at early stages of pathological aging. One example that illustrates the usefulness of all of this rather well is the computational model provided by De Haan et al. (2012), which is based on MEG findings. The increased interhemispheric synchronization in MCI patients (Bajo et al. 2010) and the prediction of subjects who will develop dementia (Bajo et al. 2012a,b), in conjunction with the characterization of the functional networks at the early (Buldu et al. 2011) and late (Stam et al. 2009) stages of AD, are all increasing the knowledge of the pathophysiology of this disease and providing new non-invasive biomarkers.

MEG has a long road ahead in the study of aging, but every step forward will be better than providing multiple pieces of an impossible jigsaw puzzle. To ensure sustained progress in our understanding, a model of aging based on MEG findings is clearly needed.

References

Aine CJ, Woodruff CC, Knoefel JE, Adair JC, Hudson D, Qualls C, Bockholt J, Best E, Kovacevic S, Cobb W, Padilla D, Hart B, Stephen JM (2006) Aging: compensation or maturation? Neuroimage 32:1891–1904

Aine CJ, Bryant JE, Knoefel JE, Adair JC, Hart B, Donahue CH, Montano R, Hayek R, Qualls C, Ranken D, Stephen JM (2010) Different strategies for auditory word recognition in healthy versus normal aging. Neuroimage 49:3319–3330

Aine CJ, Sanfratello L, Adair JC, Knoefel JE, Caprihan A, Stephen JMBrain (2011) Development and decline of memory functions in normal, pathological and healthy successful aging. Brain Topogr 24(3–4):323–339

Anderson MJ, Riccio DC (2005) Ontogenetic forgetting of stimulus attributes. Learn Behav 4:444–453

Andrews-Hanna JR, Snyder AZ, Vincent JL, Lustig C, Head D, Raichle ME, Buckner RL (2007) Disruption of large-scale brain systems in advanced aging. Neuron 56(5):924–935

Aurtenetxe S, Castellanos NP, Moratti S, Bajo R, Gil P, Beitia G, Del-Pozo F, Maestú F (2013) Dysfunctional and compensatory duality in mild cognitive impairment during a continuous recognition memory task. Int J Psychophysiol. 87(1):95–102

Babiloni C, Cassetta E, Chiovenda P, Del Percio C, Ercolani M, Moretti DV, Moffa F, Pasqualetti P, Pizzella V, Romani GL, Tecchio F, Zappasodi F, Rossini PM (2005) Alpha rhythms in mild dements during visual delayed choice reaction time tasks: a MEG study. Brain Res Bull 65(6):457–470

Bajo R, Maestú F, Nevado A, Sancho M, Gutiérrez R, Campo P, Castellanos NP, Gil P, Moratti S, Pereda E, Del-Pozo F (2010) Functional connectivity in mild cognitive impairment during a memory task: implications for the disconnection hypothesis. J Alzheimers Dis 22(1):183–193

Bajo R, Castellanos NP, López ME, Ruiz JM, Montejo P, Montenegro M, Llanero M, Gil P, Yubero R, Baykova E, Paul N, Aurtenetxe S, Del Pozo F, Maestu F (2012a) Early dysfunction

of functional connectivity in healthy elderly with subjective memory complaints. Age (Dordr) 34(2):497–506

Bajo R, Castellanos NP, Cuesta P, Aurtenetxe S, Garcia-Prieto J, Gil-Gregorio P, del-Pozo F, Maestu F (2012b) Differential patterns of connectivity in progressive mild cognitive impairment. Brain Connectivity 2(1):21–24

Bartzokis G, Beckson M, Lu PH, Nuechterlein KH, Edwards N, Mintz J (2001) Age-related changes in frontal and temporal lobe volumes in men: a magnetic resonance imaging study. Arch Gen Psychiatry 58:461–465

Berendse HW, Verbunt JP, Scheltens P, van Dijk BW, Jonkman EJ (2000) Magnetoencephalographic analysis of cortical activity in Alzheimer's disease: a pilot study. Clin Neurophysiol 111(4):604–612

Bero AW, Yan P, Roh JH, Cirrito JR, Stewart FR, Raichle ME, Lee JM, Holtzman DM (2011) Neuronal activity regulates the regional vulnerability to amyloid-β deposition. Nat Neurosci 14(6):750–756 (Epub 2011 May 1)

Besga A, Ortiz L, Fernández A, Maestu F, Arrazola J, Gil-Gregorio P, Fuentes M, Ortiz T (2010) Structural and functional patterns in healthy aging, mild cognitive impairment, and Alzheimer disease. Alzheimer Dis Assoc Disord 24(1):1–10

Biswal B, Yetkin FZ, Haughton VM, Hyde JS (1995) Functional connectivity in the motor cortex of resting human brain using echo-planar MRI. Magn Reson Med 34(4):537–541

Brookes MJ, Woolrich M, Luckhoo H, Price D, Hale JR, Stephenson MC, Barnes GR, Smith SM, Morris PG (2011) Investigating the electrophysiological basis of resting state networks using magnetoencephalography. Proc Natl Acad Sci USA 108(40):16783–16788

Brookes MJ (2011) Measuring functional connectivity using MEG: methodology and comparison with fcMRI. Neuroimage 56:1082–1104

Buckner RL (2004) Memory and executive function in aging and AD: multiple factors that cause decline and reserve factors that compensate. Neuron 44(1):195–208

Buldú JM, Bajo R, Maestú F, Castellanos N, Leyva I, Gil P, Sendiña-Nadal I, Almendral JA, Nevado A, del-Pozo F, Boccaletti S (2011) Reorganization of functional networks in mild cognitive impairment. PLoS ONE 6(5):e19584 Epub 2011 May 23

Cabeza R, Grady CL, Nyberg L, McIntosh AR, Tulving E, Kapur S, Jennings JM, Houle S, Craik FI (1997) Age-related differences in neural activity during memory encoding and retrieval: a positron emission tomography study. J Neurosci 17(1):391–400

Cabeza R (2002) Hemispheric asymmetry reduction in older adults: the HAROLD model. Psychol Aging 17:85–100

Cabeza R, Anderson ND, Locantore JK, McIntosh AR (2002) Aging gracefully: compensatory brain activity in high-performing older adults. Neuroimage 17(3):1394–1402

Cirrito JR, Kang JE, Lee J, Stewart FR, Verges DK, Silverio LM, Bu G, Mennerick S, Holtzman DM (2008) Endocytosis is required for synaptic activity-dependent release of amyloid-beta in vivo. Neuron 58(1):42–51

Chao LL, Knight RT (1998) Contribution of human prefrontal cortex to delay performance. J Cogn Neurosci 10(2):167–177

Cheng CH, Wang PN, Hsu WY, Lin YY (2012) Inadequate inhibition of redundant auditory inputs in Alzheimer's disease: an MEG study. Biol Psychol 89(2):365–373

Clapp WC, Rubens MT, Gazzaley A (2010) Mechanisms of working memory disruption by external interference. Cereb Cortex 20(4):859–872

Coane JH, Balota DA, Dolan PO, Jacoby LL (2011) Not all sources of familiarity are created equal: the case of word frequency and repetition in episodic recognition. Mem Cogn 39(5):791–805

Colcombe SJ, Kramer AF, Erickson KI, Scalf P (2005) The implications of cortical recruitment and brain morphology for individual differences in inhibitory function in aging humans. Psychol Aging 20:363–375

Cowan N (2008) What are the differences between long-term, short-term, and working memory? Prog Brain Res 169:323–338

Daselaar SM, Veltman DJ, Rombouts SA, Raaijmakers JG, Jonker C (2003) Neuroanatomical correlates of episodic encoding and retrieval in young and elderly subjects. Brain 126:43–56

Davis SW, Dennis NA, Daselaar SM, Fleck MS, Cabeza R (2008) Que PASA? the posterior-anterior shift in aging. Cereb Cortex 18(5):1201–1209

Deeny SP, Poeppel D, Zimmerman JB, Roth SM, Brandauer J, Witkowski S, Hearn JW, Ludlow AT, Contreras-Vidal JL, Brandt J, Hatfield BD (2008) Exercise, APOE, and working memory: MEG and behavioral evidence for benefit of exercise in epsilon4 carriers. Biol Psychol 78(2):179–187

De Haan W, van der Flier WM, Koene T, Smits LL, Scheltens P, Stam CJ (2012a) Disrupted modular brain dynamics reflect cognitive dysfunction in Alzheimer's disease. Neuroimage 59(4):3085–3093

De Haan W, van der Flier WM, Wang H, Van Mieghem PF, Scheltens P, Stam CJ (2012b) Disruption of functional brain networks in Alzheimer's disease: what can we learn from graph spectral analysis of resting-state magnetoencephalography? Brain Connectivity 2(2):45–55

De Haan W, Mott K, van Straaten EC, Scheltens P, Stam CJ (2012c) Activity dependent degeneration explains hub vulnerability in Alzheimer's disease. PLoS Comput Biol 8(8):e1002582. doi: 10.1371/journal.pcbi.1002582

De Luca M, Smith S, De Stefano N, Federico A, Matthews PM (2005) Blood oxygenation level dependent contrast resting state networks are relevant to functional activity in the neocortical sensorimotor system. Exp Brain Res 167:587–594

De Pasquale F (2010) Temporal dynamics of spontaneous MEG activity in brain networks. Proc Natl Acad Sci USA 107:6040–6045

D'Esposito M, Detre JA, Alsop DC, Shin RK, Atlas S, Grossman M (1995) The neural basis of the central executive system of working memory. Nature 378:279–281

Dew IT, Buchler N, Dobbins IG, Cabeza R (2012) Where is ELSA? The early to late shift in aging. Cereb Cortex 22(11):2542–2553

Dickerson BC, Salat DH, Greve DN, Chua EF, R and Giovannetti E, Rentz DM, Bertram L, Mullin K, Tanzi RE, Blacker D, Albert MS, Sperling RA (2005) Increased hippocampal activation in mild cognitive impairment compared to normal aging and AD. Neurology 65:404–411

Fernández A, Maestu F, Amo C, Gil P, Fehr T, Wienbruch C et al (2002) Focal temporoparietal slow activity in Alzheimer's disease revealed by magnetoencephalography. Biol Psychiatry 52(7):764–770

Fernández A, Arrazola J, Maestú F, Amo C, Gil-Gregorio P, Wienbruch C, Ortiz T (2003) Correlations of hippocampal atrophy and focal low-frequency magnetic activity in Alzheimer disease: volumetric MR imaging-magnetoencephalographic study. AJNR Am J Neuroradiol 24(3):481–487

Fernández A, García-Segura JM, Ortiz T, Montoya J, Maestú F, Gil-Gregorio P, Campo P, Viaño J (2005) Proton magnetic resonance spectroscopy and magnetoencephalographic estimation of delta dipole density: a combination of techniques that may contribute to the diagnosis of Alzheimer's disease. Dement Geriatr Cogn Dis 20(2–3):169–177

Fernández A, Turrero A, Zuluaga P, Gil P, Maestú F, Campo P, Ortiz T (2006) Magnetoencephalographic parietal delta dipole density in mild cognitive impairment: preliminary results of a method to estimate the risk of developing Alzheimer disease. Arch Neurol 63(3):427–430

Forsberg A, Engler H, Almkvist O, Blomquist G, Hagman G, Wall A, Ringheim A, Långström B, Nordberg A (2008) PET imaging of amyloid deposition in patients with mild cognitive impairment. Neurobiol Aging 29(10):1456–1465

Fox MD, Corbetta M, Snyder AZ, Vincent JL, Raichle ME (2006) Spontaneous neuronal activity distinguishes human dorsal and ventral attention systems. Proc Natl Acad Sci USA 103:10046–10051

Franciotti R, Iacono D, Della Penna S, Pizzella V, Torquati K, Onofrj M, Romani GL (2006) Cortical rhythms reactivity in AD, LBD and normal subjects: a quantitative MEG study. Neurobiol Aging 27(8):1100–1109

Fransson P (2005) Spontaneous low-frequency BOLD signal fluctuations: an fMRI investigation of the resting-state default mode of brain function hypothesis. Hum Brain Mapp 26:15–29

García-Pacios J, Gutierrez R, Solesio-Jofre E, Moratti S, Ruiz-Vargas JM, López-Frutos JM, Lorenzo-López L, Del-Pozo F, Maestú F (2013) Early prefrontal activation as a mechanisms to prevent forgetting in the context of interference. Am J Geriatr Psychiatry 21(6):580–588. doi: 10.1097/JGP.0b013e31824bdf47

Gazzaley A, Cooney JW, Rissman J, D'Esposito M (2005) Top-down suppression deficit underlies working memory impairment in normal aging. Nat Neurosci 8:1298–1300

Gazzaley A, D'Esposito M (2007) Top-down modulation and normal aging. Annuals N Y Acad Sci 1097:67–83

Gazzaley A, Clapp W, Kelley J, McEvoy K, Knight RT, D'Esposito M (2008) Age-related top-down suppression deficit in the early stages of cortical visual memory processing. Proc Natl Acad Sci USA 105(35):13122–13126

Geschwind N (1965) Disconnexion syndromes in animals and man: part I. Brain 88(3):585–644

Grady CL (2000) Functional Brain imaging and age-related changes in cognition. Biol Psychol 54(1–3):259–281

Grady CL, McIntosh AR, Horwitz B, Rapoport SI (2000) Age-related changes in the neural correlates of degraded and nondegraded face processing. Cogn Neuropsychol 17:165–186

Grady CL, Springer MV, Hongwanishkul D, McIntosh AR, Winocur G (2006) Age-related changes in brain activity across the adult lifespan. J Cogn Neurosci 18:227–241

Grady CL (2008) Cognitive neuroscience of aging. Annu N Y Acad Sci 1124:127–144

Grady C (2012) The cognitive neuroscience of ageing. Nat Rev Neurosci 13(7):491–505

Grasby PM, Frith CD, Friston KJ, Simpson J, Fletcher PC, Frackowiak RS, Dolan RJ (1994) A graded task approach to the functional mapping of brain areas implicated in auditory-verbal memory. Brain 117(Pt 6):1271–1282

Gogtay N, Giedd JN, Lusk L, Hayashi KM, Greenstein D, Vaituzis AC, Nugent TF III, Herman DH, Clasen LS, Toga AW, Rapoport JL, Thompson PM (2004) Dynamic mapping of human cortical development during childhood through early adulthood. Proc Natl Acad Sci USA 101:8174–8179

Greicius MD, Krasnow B, Reiss AL, Menon V (2003) Functional connectivity in the resting brain: a network analysis of the default mode hypothesis. Proc Natl Acad Sci USA 100:253–258

Hall SD, Stanford IM, Yamawaki N, McAllister CJ, Rönnqvist KC, Woodhall GL, Furlong PL (2011) The role of GABAergic modulation in motor function related neuronal network activity. Neuroimage 56(3):1506–1510

Hampson M, Peterson BS, Skudlarski P, Gatenby JC, Gore JC (2002) Detection of functional connectivity using temporal correlations in MR images. Hum Brain Mapp 15:247–262

Hasher L, Zacks RT (1988) Working memory, comprehension, and aging: a review and a new view. In: Bower, GH (ed) The psychology of learning and motivation Academic Press, New York, pp 193–225

Hutton LC, Abbass M, Dickinson H, Ireland Z, Walker DW (2009a) Neuroprotective properties of melatonin in a model of birth asphyxia in the spiny mouse (Acomys cahirinus). Dev Neurosci 31(5):437–451

Hutton C, Draganski B, Ashburner J, Weiskopf NA (2009) Comparison between voxel-based cortical thickness and voxel-based morphometry in normal aging. Neuroimage 48(2):371–380

Ishii R, Canuet L, Kurimoto R, Ikezawa K, Aoki Y, Azechi M, Takahashi H, Nakahachi T, Iwase M, Kazui H, Takeda M (2010) Frontal shift of posterior alpha activity is correlated with cognitive impairment in early Alzheimer's disease: a magnetoencephalography-beamformer study. Psychogeriatrics 10(3):138–143

Kannurpatti SS, Motes MA, Rypma B, Biswal BB (2011) Increasing measurement accuracy of age-related BOLD signal change: minimizing vascular contributions by resting-state-fluctuation-of-amplitude scaling. Hum Brain Mapp 32(7):1125–1140

Kikuchi M, Wada Y, Koshino Y, Nanbu Y, Hashimoto T (2000) Effects of scopolamine on interhemispheric EEG coherence in healthy subjects: analysis during rest and photic stimulation. Clin Electroencephalogr 31(2):109–115

Koyama MS, Kelly C, Shehzad Z, Penesetti D, Castellanos FX et al (2010) Reading networks at rest. Cereb Cortex 10:2549–2559

Kukull WA, Bowen JD (2002) Dementia epidemiology. Med Clin N Am 86(3):573–590

Kurimoto R, Ishii R, Canuet L, Ikezawa K, Azechi M, Iwase M, Yoshida T, Kazui H, Yoshimine T, Takeda M (2008) Event-related synchronization of alpha activity in early Alzheimer's disease and mild cognitive impairment: an MEG study combining beamformer and group comparison. Neurosci Lett 443(2):86–89

Kurimoto R, Ishii R, Canuet L, Ikezawa K, Iwase M, Azechi M, Aoki Y, Ikeda S, Yoshida T, Takahashi H, Nakahachi T, Kazui H, Takeda M (2012) Induced oscillatory responses during the Sternberg's visual memory task in patients with Alzheimer's disease and mild cognitive impairment. Neuroimage 59(4):4132–4140

Lewandowsky S, Duncan M, Brown GDA (2004) Time does not cause forgetting in short-term serial recall. Psychon Bull Rev 11:771–790

Lewandowsky S, Oberauer K (2008) The word-length effect provides no evidence for decay in short-term memory. Psychon Bull Rev 15(5):875–888

Li SC, Lindenberger U, Sikström S (2001) Aging cognition: from neuromodulation to representation. Trends Cogn Sci 5(11):479–486

Li SC, Naveh-Benjamin M, Lindenberger U (2005) Aging neuromodulation impairs associative binding: a neurocomputational account. Psychol Sci16(6):445–450

Lindenberger U, Baltes PB (1994) Sensory functioning and intelligence in old age: a strong connection. Psychol Aging 9:339–355

Liu Z, Fukunaga M, de Zwart JA, Duyn JH (2010) Large-scale spontaneous fluctuations and correlations in brain electrical activity observed with magnetoencephalography. Neuroimage 51(1):102–111

Maestú F, Fernandez A, Simos PG, Gil-Gregorio P, Amo C, Rodriguez R, Arrazola J, Ortiz T (2001) Spatio-temporal patterns of brain magnetic activity during a memory task in Alzheimer's disease. NeuroReport 12:3917–3922

Maestú F, Arrazola J, Fernandez A, Simos PG, Amo C, Gil-Gregorio P, Fernandez S, Papanicolaou A, Ortiz T (2003) Do cognitive patterns of brain magnetic activity correlate with hippocampal atrophy in Alzheimer's disease? J Neurol Neurosurg Psychiatry 74:208–212

Maestú F, Fernandez A, Simos PG, López-Ibor MI, Campo P, Criado J, Rodríguez-Palancas A, Ferre F, Amo C, Ortiz T (2004) Profiles of brain magnetic activity during a memory task in Alzheimeŕs disease and non-demented elderly subjects with or without depression. J Neurol Neurosurg Psychiatry 75:1160–1162

Maestú F, Garcia-Segura J, Ortiz T, Montoya J, Fernandez A, Gil-Gregorio P, Campo P, Fernandez S, Viano J, Portera A (2005) Evidence of biochemical and biomagnetic interactions in Alzheimer's disease: an MEG and MR spectroscopy study. Dement Geriatr Cogn Disord 20:145–152

Maestú F, Campo P, Gil-Gregorio P, Fernandez S, Fernandez A, Ortiz T (2006) Medial temporal lobe neuromagnetic hypoactivation and risk for developing cognitive decline in elderly population: a 2-year follow-up study. Neurobiol Aging 27:32–37

Maestú F, Campo P, Del Rio D, Moratti S, Gil-Gregorio P, Fernandez A, Capilla A, Ortiz T (2008) Increased biomagnetic activity in the ventral pathway in mild cognitive impairment. Clin Neurophysiol 119:1320–1327

Maestu F, Baykova E, Ruiz JM, Montejo P, Montenegro M, Llanero M, Solesio E, Gil P, Yubero R, Paul N, Pozo F, Nevado A (2011a) Increased biomagnetic activity in healthy elderly with subjective memory complaints. Clin Neurophysiol 122(3):499–505

Maestú F, Yubero R, Moratti S, Campo P, Gil-Gregorio P, Paul N, Solesio E, del Pozo F, Nevado A (2011b) Brain activity patterns in stable and progressive mild cognitive impairment during working memory as evidenced by magnetoencephalography. J Clin Neurophysiol 28(2):202–209

Madden DJ, Turkington TG, Provenzale JM, Denny LL, Hawk TC, Gottlob LR, Coleman RE (1999) Adult age differences in the functional neuroanatomy of verbal recognition memory. Hum Brain Mapp 7:115–135

May CP (1999) Synchrony effects in cognition: the costs and a benefit. Psychon Bull Rev 6:142–147
Mazoyer B, Zago L, Mellet E, Bricogne S, Etard O, Houde O, Crivello F, Joliot M, Petit L, Tzourio-Mazoyer N (2001) Cortical networks for working memory and executive functions sustain the conscious resting state in man. Brain Res Bull 54:287–298
Moscovitch M, Winocur G (1995) Frontal lobes, memory, and aging. Proc Natl Acad Sci USA 769:119–150
Muller NG, Knight RT (2006) The functional neuroanatomy of working memory: contributions of human brain lesion studies. Neuroscience 139:51–58
Nairne JS (2002) Remembering over the short-term: the case against the standard model. Annu Rev Psychol 53:53–81
Nichols LM, Masdeu JC, Mattay VS, Kohn P, Emery M, Sambataro F, Kolachana B, Elvevåg B, Kippenhan S, Weinberger DR, Berman KF (2012) Interactive effect of apolipoprotein e genotype and age on hippocampal activation during memory processing in healthy adults. Arch Gen Psychiatry 69(8):804–813. doi: 10.1001/archgenpsychiatry.2011.1893
O'Sullivan M, Jones DK, Summers PE, Morris RG, Williams SC, Markus HS (2001) Evidence for cortical "disconnection" as a mechanism of age-related cognitive decline. Neurology 57(4):632–638
Osipova D, Ahveninen J, Kaakkola S, Jääskeläinen IP, Huttunen J, Pekkonen E (2003) Effects of scopolamine on MEG spectral power and coherence in elderly subjects. Clin Neurophysiol 114(10):1902–1907
Osipova D, Ahveninen J, Jensen O, Ylikoski A, Pekkonen E (2005) Altered generation of spontaneous oscillations in Alzheimer's disease. Neuroimage 27(4):835–841
Osipova D, Pekkonen E, Ahveninen J (2006) Enhanced magnetic auditory steady-state response in early Alzheimer's disease. Clin Neurophysiol 117(9):1990–1995
Park DC, Polk TA, Park R, Minear M, Savage A, Smith MR (2004) Aging reduces neural specialization in ventral visual cortex. Proc Natl Acad Sci USA 101:13091–13095
Park J, Carp J, Hebrank A, Park DC, Polk TA (2010) Neural specificity predicts fluid processing ability in older adults. J Neurosci 30:9253–9259
Pascual-Leone A, Freitas C, Oberman L, Horvath JC, Halko M, Eldaief M, Bashir S, Vernet M, Shafi M, Westover B, Vahabzadeh-Hagh AM, Rotenberg A (2011) Characterizing brain cortical plasticity and network dynamics across the age-span in health and disease with TMS-EEG and TMS-fMRI. Brain Topogr 24(3–4):302–315
Pike KE, Savage G, Villemagne VL, Ng S, Moss SA, Maruff P, Mathis CA, Klunk WE, Masters CL, Rowe CC (2007) Beta-amyloid imaging and memory in non-demented individuals: evidence for preclinical Alzheimer's disease. Brain 130(Pt 11):2837–2844
Pekkonen E, Huotilainen M, Virtanen J, Sinkkonen J, Rinne T, Ilmoniemi RJ, Näätänen R (1995) Age-related functional differences between auditory cortices: a whole-head MEG study. Neuroreport. 6(13):1803–1806
Pekkonen E, Huotilainen M, Virtanen J, Naatanen R, Ilmoniemi RJ, Erkinjuntti T (1996) Alzheimer's disease affects parallel processing between the auditory cortices. NeuroReport 7(8):1365–1368
Pekkonen E, Jaaskelainen IP, Hietanen M, Huotilainen M, Naatanen R, Ilmoniemi RJ et al (1999) Impaired preconscious auditory processing and cognitive functions in Alzheimer's disease. Clin Neurophysiol 110(11):1942–1947
Pekkonen E, Hirvonen J, Jaaskelainen IP, Kaakkola S, Huttunen J (2001a) Auditory sensory memory and the cholinergic system: implications for Alzheimer's disease. Neuroimage 14(2):376–382
Pekkonen E, Jaaskelainen LP, Erkinjuntti T, Hietanen M, Huotilainen M, Ilmoniemi RJ et al (2001b) Preserved stimulus deviance detection in Alzheimer's disease. NeuroReport 12(8):1649–1652
Pekkonen E, Jaaskelainen IP, Kaakkola S, Ahveninen J (2005) Cholinergic modulation of preattentive auditory processing in aging. Neuroimage 27(2):387–392
Puregger E, Walla P, Deecke L, Dal-Bianco P (2003) Magnetoencephalographic–features related to mild cognitive impairment. Neuroimage 20(4):2235–2244

Raichle ME, MacLeod AM, Snyder AZ, Powers WJ, Gusnard DA, Shulman GL (2001) A default mode of brain function. Proc Natl Acad Sci USA 98:676–682

Raz N, Lindenberger U, Rodrigue KM, Kennedy KM, Head D, Williamson A, Dahle C, Gerstorf D, Acker JD (2005) Regional brain changes in aging healthy adults: general trends, individual differences and modifiers. Cereb Cortex 15(11):1676–1689

Reuter-Lorenz PA, Jonides J, Smith EE, Hartley A, Miller A, Marshuetz C, Koeppe RA (2000) Age differences in the frontal lateralization of verbal and spatial working memory revealed by PET. J Cogn Neurosci 12:174–187

Reuter-Lorenz PA, Lustig C (2005) Brain aging: Reorganizing discoveries about the aging mind. Curr Opin Neurobiol 15:245–251

Reuter-Lorenz PA, Cappell KA (2008) Neurocognitive aging and the compensation hypothesis. Curr Dir Psychol Sci 17:177–182

Riekkinen P, Buzsaki G, Riekkinen P, Soininen H, Partanen J (1991) The cholinergic system and EEG slow waves. Electroencephalogr Clin Neurophysiol 78:89–96

Sanchez PE, Zhu L, Verret L, Vossel KA, Orr AG, Cirrito JR, Devidze N, Ho K, Yu GQ, Palop JJ, Mucke L (2012) Levetiracetam suppresses neuronal network dysfunction and reverses synaptic and cognitive deficits in an Alzheimer's disease model. Proc Nat Acad Sci USA 109(42):E2895–E2903

Sakai K, Passingham RE (2004) Prefrontal selection and medial temporal lobe reactivation in retrieval of short-term verbal information. Cereb Cortex 14:914–921

Salthouse TA (1991) Mediation of adults age differences in cognition by reductions in working memory and Speedy processing. Psychol Sci 2:179–183

Salthouse TA (1996) The processing-speed theory of adult age differences in cognition. Psychol Rev 103:403–428

Schlee W, Leirer V, Kolassa IT, Weisz N, Elbert T (2012) Age-related changes in neural functional connectivity and its behavioral relevance. BMC Neurosci 14(13):16

Shulman GL, Fiez JA, Corbetta M, Buckner RL, Miezin FM, Raichle ME, Petersen SE (1997) Common blood flow changes across visual tasks: II: decreases in cerebral cortex. J Cogn Neurosci 9:648–663

Solesio-Jofre E, Lorenzo-López L, Gutiérrez R, López-Frutos JM, Ruiz-Vargas JM, Maestú F (2011) Age effects on retroactive interference during working memory maintenance. Biol Psychol 88(1):72–82

Solesio-Jofre E, Lorenzo-López L, Gutiérrez R, López-Frutos JM, Ruiz-Vargas JM, Maestú F (2012) Age-related effects in working memory recognition modulated by retroactive interference. J Gerontol A Biol Sci Med Sci 67(6):565–572

Sperling RA, Aisen PS, Beckett LA, Bennett DA, Craft S, Fagan AM, Iwatsubo T, Jack CR Jr, Kaye J, Montine TJ, Park DC, Reiman EM, Rowe CC, Siemers E, Stern Y, Yaffe K, Carrillo MC, Thies B, Morrison-Bogorad M, Wagster MV, Phelps CH (2011) Toward defining the preclinical stages of Alzheimer's disease: recommendations from the National Institute on Aging-Alzheimer's Association workgroups on diagnostic guidelines for Alzheimer's disease. Alzheimers Dement 7(3):280–292

Stam CJ, van Cappellen van Walsum AM, Pijnenburg YA, Berendse HW, de Munck JC, Scheltens P, et al. (2002) Generalized synchronization of MEG recordings in Alzheimer's Disease: evidence for involvement of the gamma band. J Clin Neurophysiol 19(6):562–574

Stam CJ, Jones BF, Manshanden I, van Cappellen van Walsum AM, Montez T, Verbunt JP, de Munck JC, van Dijk BW, Berendse HW, Scheltens P (2006) Magnetoencephalographic evaluation of resting-state functional connectivity in Alzheimer's disease. Neuroimage 32(3):1335–1344

Stam CJ, de Haan W, Daffertshofer A, Jones BF, Manshanden I, van Cappellen van Walsum AM, Montez T, Verbunt JP, de Munck JC, van Dijk BW, Berendse HW, Scheltens P(2009) Graph theoretical analysis of magnetoencephalographic functional connectivity in Alzheimer's disease. Brain 132(Pt 1):213–224

Stam CJ (2010) Use of magnetoencephalography (MEG) to study functional brain networks in neurodegenerative disorders. J Neurol Sci 289(1–2):128–134. (Epub 2009 Sep 2)

Stephen JM, Montaño R, Donahue CH, Adair JC, Knoefel J, Qualls C, Hart B, Ranken D, Aine CJ (2010) Somatosensory responses in normal aging, mild cognitive impairment, and Alzheimer's disease. J Neural Transmision 117(2):217–225

Sullivan EV, Adalsteinsson E, Hedehus M, Ju C, Moseley M, Lim KO, Pfefferbaum A (2001) Equivalent disruption of regional white matter microstructure in ageing healthy men and women. NeuroReport 12(1):99–104

Terry RD, Katzman R (2001) Life span and synapses: will there be a primary senile dementia? Neurobiol Aging 22(3):347–348

Tulving E, Kapur S, Craik FI, Moscovitch M, Houle S (1994) Hemispheric encoding/retrieval asymmetry in episodic memory: positron emission tomography findings. Proc Natl Acad Sci USA 91(6):2016–2020

Velanova K, Lustig C, Jacoby LL, Buckner RL (2007) Evidence for frontally mediated controlled processing differences in older adults. Cereb Cortex 17(5):1033–1046

Verdoorn TA, McCarten JR, Arciniegas DB, Golden R, Moldauer L, Georgopoulos A, Lewis S, Cassano M, Hemmy L, Orr W, Rojas DC (2011) Evaluation and tracking of Alzheimer's disease severity using resting-state magnetoencephalography. J Alzheimers Dis 26(Suppl 3):239–255

Vincent JL, Snyder AZ, Fox MD, Shannon BJ, Andrews JR, Raichle ME, Buckner RL (2006) Coherent spontaneous activity identifies a hippocampal-parietal memory network. J Neurophysiol 96:3517–3531

Wang L, Su L, Shen H, Hu D (2012) Decoding lifespan changes of the human brain using resting-state functional connectivity MRI. PLoS One 7(8): e44530. doi: 10.1371/journal.pone.0044530. (Epub 2012 Aug 30)

Walla P, Puregger E, Lehrner J, Mayer D, Deecke L, Dal Bianco P (2005) Depth of word processing in Alzheimer patients and normal controls: a magnetoencephalographic (MEG) study. J Neural Transmision 112(5):713–730

West RL (1996) An application of prefrontal cortex function theory to cognitive aging. Psychol Bull 120:272–292

Westlye ET, Lundervold A, Rootwelt H, Lundervold AJ, Westlye LT (2011) Increased hippocampal default mode synchronization during rest in middle-aged and elderly APOE ε4 carriers: relationships with memory performance. J Neurosci 31(21):7775–7783

Wixted JT (2004) The psychology and Neuroscience of forgetting. Annu Rev Psychol 55:235–269

Zacks RT, Hasher L, Li KZH (1999) Human memory. In: Craik FIM, Salthouse TA, Mahwah NJ (eds.), The Handbook of aging and cognition Erlbaum, Mahwah, pp 200–230

Zamrini E, Maestu F, Pekkonen E, Funke M, Makela J, Riley M, Bajo R, Sudre G, Fernandez A, Castellanos N, Del Pozo F, Stam CJ, van Dijk BW, Bagic A, Becker JT (2011) Magnetoencephalography as a putative biomarker for Alzheimer's disease. Int J Alzheimers Dis 2011:280–289

Fox MD, Snyder AZ, Vincent JL, Corbetta M, Van Essen DC, Raichle ME (2005) The human brain is intrinsically organized into dynamic, anticorrelated functional networks. Proc Natl Acad Sci USA 102(27):8–9673

Current Status and Future Prospects of Perinatal MEG

Ronald T. Wakai

Abstract Neurodevelopment is a vast and critically important area of neuroscience, yet there is a paucity of functional imaging research during the perinatal and infant period when development is most rapid and significant. MEG offers compelling advantages over EEG and other neuroimaging methods for perinatal research. Over the last few decades, interest in this area has vacillated, but it is likely to reemerge in the coming years as neurodevelopmental disorders attract greater attention. This short contribution comments on the current status and future prospects of fetal and neonatal MEG, and highlights the SERF (spin exchange relaxation-free) magnetometer as an important new technology.

Neurodevelopment is a vast and critically important area of neuroscience, yet there is a paucity of functional imaging research during the perinatal and infant period when development is most rapid and significant. There are several reasons for this. First, the studies are difficult to perform due to the inability of the subjects to cooperate and the need to make serial measurements. Second, only techniques believed to be completely safe and noninvasive can be used.

MEG offers compelling advantages over EEG and other neuroimaging methods for perinatal research, and has the potential to become the preferred technique. Over the last few decades, interest in this area has vacillated, but it is likely to reemerge in the coming years as neurodevelopmental disorders attract greater attention. This short contribution comments on the current status and future prospects of fetal and neonatal MEG, and highlights the (SERF) spin exchange relaxation-free magnetometer as an important new technology.

R. T. Wakai (✉)
Department of Medical Physics, University of Wisconsin-Madison,
Madison, WI 53705, USA
e-mail: rtwakai@wisc.edu

S. Supek and C. J. Aine (eds.), *Magnetoencephalography*,
DOI: 10.1007/978-3-642-33045-2_29,

1 Fetal MEG

Intrauterine evaluation of human fetal brain function has been a long-standing and elusive goal, due largely to the inaccessibility of the fetal brain. The main approaches have been indirect. Researchers have studied such outputs of brain function as fetal heart rate variability, fetal body and fetal breathing movements; however, there is little evidence that any method in current use has the specificity to be employed as an effective screening tool for detection of abnormal fetal neurological functioning. The impetus to make progress in this area is the dire prognosis of babies born with cerebral palsy and severe mental retardation, which afflicts more than 10,000 babies per year in the US.

Fetal MEG is one of the few functional brain imaging technologies that can be applied to the fetus, and it is more direct than other techniques. It also provides one of the best examples of the potential advantages of magnetic, versus electric, detection. Fetal electric signals are much weaker than one would expect due to the presence of the *vernix caseosa*, which forms on the fetal skin and impedes the transmission of electrical currents to the maternal surface. Fetal magnetic signals, in contrast, are much less dependent on volume conduction and thus are relatively unaffected. A number of groups have demonstrated the feasibility of using MEG to detect evoked and spontaneous fetal brain activity. But despite the aforementioned advantages of MEG, the modest quality and success rate of fetal recordings preclude routine clinical application and limit the veracity of basic studies. Further advancement will likely require technological improvements. Research in this area, however, should not be abandoned.

2 Neonatal MEG

The neonatal period is a fascinating time to study electrical brain activity. The developmental changes are so rapid that they can be seen from week to week. Furthermore, brain activity in neonates can exhibit striking differences, compared to what is seen in adults. In neonates, the auditory evoked response is dominated by a single component that corresponds to surface positivity of the evoked potential, whereas in adults the response is biphasic and the dominant component, the N1, corresponds to surface negativity. In neonates, the auditory "off" response can be larger than the "on" response, whereas in adults the "off" response is always smaller. In early infancy, sleep spindles are strongly associated with slow wave sleep, whereas in adults spindling exhibits a negative association with slow wave sleep.

The true value of MEG for neonatal studies lies in its high sensitivity to developmental changes in brain activity, combined with its ability to serially track changes in the underlying sources with high spatiotemporal resolution. In principle, EEG is also capable of high resolution source localization in the neonate. In practice, however, the localization accuracy is confounded by the fontanels,

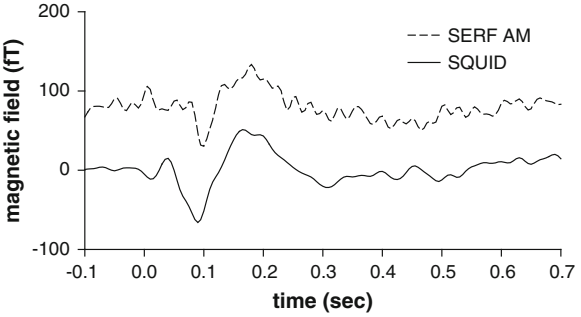

Fig. 1 Comparison of auditory evoked responses obtained from the same subject by a SQUID and a SERF magnetometer. The stimuli consisted of 50 ms, 1 kHz tones; 150 trials were averaged

which effect EEG topography much more than MEG topography. Thus, the simple transmission properties of magnetic signals again confer a significant advantage to MEG.

The neonatal brain provides an invaluable opportunity to study the development of brain rhythms. Some brain rhythms, such as sleep spindles, can be studied from their genesis. Over the last decade, connectivity has become a popular area of brain research. Neonatal studies may allow researchers to observe of the formation of brain networks and to correlate changes in connectivity with changes in evoked and spontaneous MEG activity and behavior.

3 The SERF Magnetometer: A Major Breakthrough

Since the introduction of whole-head systems, MEG has not benefitted from any major advances in sensor technology. Although the magnetic field resolution of SQUID magnetometers is sufficient for the vast majority of applications, the cost has remained stubbornly high. A recent advance that seems likely to have a major impact on MEG and other areas of biomagnetism is the so-called SERF atomic magnetometer (AM), which has achieved a breakthrough in sensitivity. The main advantage of AMs is low cost, which can make MEG much more affordable and widely available. For neonatal MEG, an additional advantage is that the positions of the channels can be adjusted to accommodate different head shapes and sizes. This is not possible with SQUID arrays because the channels are confined within a cryogenic dewar.

Several groups have used AMs to record brain evoked responses, but the results shown were obtained by averaging many more trials than is typically required using a SQUID magnetometer. Recently, we recorded adult auditory evoked responses using an AM fabricated by Vishal Shah at QuSpin, Inc. The recordings were made in a standard shielded room and were compared with recordings made during the same session with a SQUID magnetometer, using the same stimuli (50 ms, 1 kHz tones, 1–3 s ISI) and acquisition parameters. As exemplified in Fig. 1, which shows the average of 150 trials for the AM and a representative

SQUID channel, the responses were remarkably similar in quality and appearance. Although development of a commercial system may take several or more years, there are no fundamental obstacles that prevent the realization of low-cost, high-performance AM systems for MEG.

Technological Challenges of Pediatric MEG and Potential Solutions: The Aston Experience

Caroline Witton, Paul L. Furlong and Stefano Seri

Abstract Magnetoencephalography (MEG) offers significant opportunities for the localization and characterization of focal and generalized epilepsies, but its potential has so far not been fully exploited, as the evidence for its effectiveness is still anecdotal. This is particularly true for pediatric epilepsy. MEG recordings on school-age children typically rely on the use of MEG systems that were designed for adults and children's smaller head-size and stature can cause significant problems. Reduced signal-to-noise ratio when recording from smaller heads, increased movement, reduced sensor coverage of anterior temporal regions and incomplete insertion into the MEG helmet can all reduce the quality of data collected from children. We summarize these challenges and suggest some practical solutions.

Keywords MEG · Children · Pediatric epilepsy · Clinical applications · Brain maturation

1 Introduction

The magnetoencephalography (MEG) community has seen a slow but steady increase in the number of laboratories taking up the challenge of translating the significant wealth of technological and scientific developments of recent years into clinically viable protocols and paradigms. The principal clinical application in

C. Witton · P. L. Furlong · S. Seri (✉)
School of Life and Health Sciences, Aston Brain Centre, Wellcome Trust Laboratory for MEG Studies, Aston University, Birmingham B4 7ET, UK
e-mail: s.seri@aston.ac.uk

S. Seri
Department of Clinical Neurophysiology and Pediatric Epilepsy Surgery Program, The Birmingham Children's Hospital NHS Foundation Trust, Birmingham, UK

S. Supek and C. J. Aine (eds.), *Magnetoencephalography*,
DOI: 10.1007/978-3-642-33045-2_30,

which MEG has established itself as a useful technique capable of offering non-redundant diagnostic information is in the pre-surgical evaluation of patients with refractory epilepsy. In these patients, MEG offers the unsurpassed temporal resolution that is necessary to deconvolve the rapidly spreading nature of paroxysmal epileptiform discharges combined with high spatial sampling and localization accuracy.

Children are at a substantially higher risk for epilepsy than young and middle-aged adults (Hauser 1995) and are most likely to benefit from access to MEG investigations. This is because, in children, neocortical epilepsies associated with cortical dysplasia and low-grade neoplasms are most prevalent. For these patients, one of the main positive prognostic factors is complete resection of the epileptogenic lesion and MEG can make a significant contribution to the accurate characterization of seizure generation and propagation that is critical for the decision of surgical amenability (Jeha et al. 2007). Preliminary evidence also suggests that MEG may be superior to existing diagnostic tools in the characterization of eloquent cortex for pre-surgical assessment (Gaetz et al. 2009). By measuring direct neural processes, MEG does not suffer from the limitations in reliability of fMRI measures of eloquent cortex function due to the distortion of BOLD signal associated with some structural lesions in patients with epilepsy (Wellmer et al. 2009).

Noninvasive measures are of particular potential importance in pediatric patients, where lack of compliance affects the reliability of WADA assessment, cortical stimulation during awake craniotomy or other invasive techniques, and therefore limits the likelihood of early surgical intervention. But despite the increased risk for epilepsy in children, and the enhanced benefits of surgical intervention in reducing cognitive impairment and delayed educational milestones, reports characterizing the application and value of MEG in pediatric age remain scarce. Based on our experience of recording over 300 children in the period 2004–2013 with two different whole-head MEG systems designed for use with adults (a 275-channel VSM-MedTech system, and more recently with a 306-channel Elekta Triux system), we will discuss how the evidence-base for the use of MEG in assessment of pediatric epilepsy has been restricted by some of the limitations of currently available technology, propose some practical solutions and discuss how future developments could significantly enhance the application of MEG in this and other pediatric clinical groups.

2 Key Challenges of Recording from School-Age Children

In this section, we describe some of the main difficulties associated with recording good-quality MEG data from children. We focus on those in ‘school-age’, i.e., between the ages of about 4 and 11 years. Tailored MEG systems for infant recordings have been designed and marketed (Okada et al. 2006; Johnson et al. 2010), but recordings from children above the age of 4 typically rely on the use of an MEG system designed to accommodate adults.

2.1 Head Size

Head size reaches approximately adult-like proportions at a relatively young age. This has led to the assumption that an adult MEG system will provide equivalent signal-to-noise ratio for pediatric recordings. However experience shows that this is not the case. In our laboratory we systematically digitize the shape of the head with a Polhemus 3-D Space Tracker™ system for coregistration purposes. These data have offered us invaluable insight in evaluating differences between adult and children positioning and the overall fit within the MEG helmet. Data suggest that typically developing 9-year-old children do not differ from adults in head width, with a mean of 15.3 and 15.5 cm respectively. But the children's heads are significantly smaller than adults' in the anterior-posterior dimension (16.6 vs. 19 cm; $p < 0.001$, $n = 35$) and younger patients have even smaller head measurements. Helmet dimensions of the most common adult MEG systems are broadly similar to each other; our current Elekta MEG system measures about 22 cm in the anterior-posterior dimension, and about 18 cm from left to right. So it is clear that our pediatric patients—and to a lesser extent our adult patients—have room to spare, in both the anterior-posterior dimension and from left to right. This observation has at least 3 implications; increased margin for head movement, reduced sensor coverage especially in anterior regions, and reduced signal to noise ratio for the smallest heads.

Firstly, head movement: with plenty of extra space in the helmet, a child has much more freedom to move around during the recording than an adult. Child patients often find that they can twist their head from right to left and tilt their head back and forwards quite freely, unlike an adult who experiences a physical restriction by the boundaries imposed by the helmet. This additional freedom of movement makes software systems for tracking and compensating for head-movements extremely valuable in pediatric clinical MEG. Elekta's signal-space separation method provides one framework for head movement compensation (Nenonen et al. 2012) and a different implementation for CTF MEG systems (Wilson 2004) has also been made available. Head position is usually tracked during a MEG recording through the positions of at least 3 small active coils affixed to the patient's head. Without movement compensation, it is typical to reject any dataset in which the coils move more than 5 mm from their starting positions. In practical terms, depending on the age and compliance of the child, this could mean rejecting a significant proportion of datasets with the net effect of prolonging the duration of a recording session beyond tolerable limits, which in turn further reduces the chance of the child to remain completely still. Prior to the availability of head movement-correction software, for clinical patients in the seated position, we rarely recorded more than 2 min at any one time, to ensure that valuable data containing epileptiform activity were not spoiled by head movements which would have compromised localization accuracy. A downside of this practice is the introduction of gaps in the acquisition during which interictal abnormalities or even seizures can occur. With young children we have used a hat with inflatable cushions to restrict head position within the MEG helmet, but this

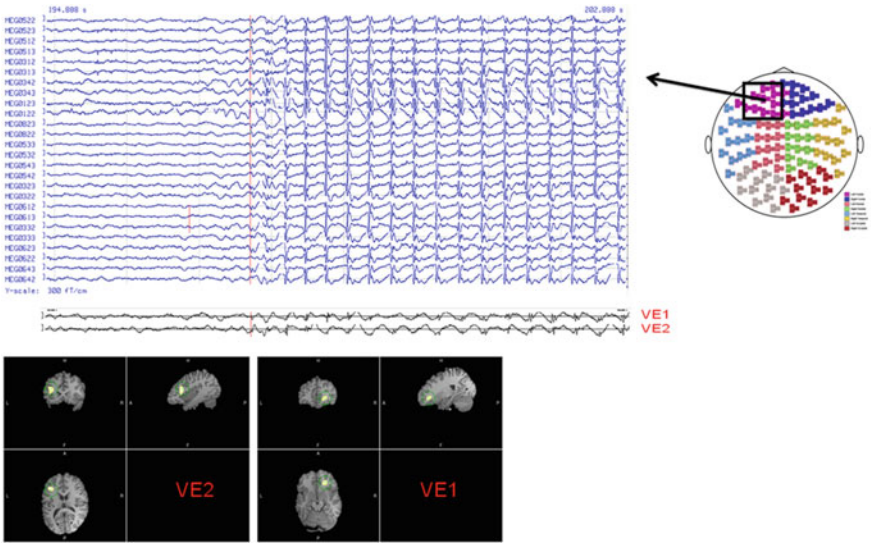

Fig. 1 An absence seizure recorded during hyperventilation. *Top* 8 s of MEG data maxfiltered using tSSS with motion correction, displayed on *left* frontal channels showing seizure onset during hyperventilation. The sources of MEG activity at seizure onset was calculated using a joint minimum-variance beamformer and spike-detection algorithm, a procedure called SAM(g_2) (Kirsch et al. 2006). The beamformer output at a target location has the same temporal resolution as the recorded MEG signals, and is therefore often referred to as a *virtual electrode* (Robinson and Vrba 1999) and can be seen as a morphologic characterization of the regional electrical activity. Spike-like activity is identified from the estimated source data in terms of excess kurtosis. Two virtual electrodes yielded by this analysis (VE1 and VE2) are displayed beneath. *Bottom* Source localization of the two virtual electrodes showing regions of high kurtosis bilaterally in the frontal lobe is shown

has not usually been well tolerated. Our current system, due to the benefit of head-movement compensation, allows recording longer epochs and we have in some cases encouraged the patient to move, to enhance signal-to-noise in different areas of cortex during the recording. We routinely encourage our children to hyperventilate, using toy windmills to encourage participation. In the event that the child becomes drowsy, we also allow them to doze or sleep. Both processes are intended to facilitate the occurrence of interictal activity, but without movement compensation technology it would be challenging or impossible to retain spatial accuracy of localization. Importantly, we can also record brain activity during a seizure such as the example in Fig. 1, providing valuable information about seizure onset and propagation—something that has been extremely challenging to achieve in the past in patients with seizures characterized by significant concomitant motor manifestations.

To make the best of head movement-compensation systems during recordings, it is important to ensure that the coils remain within the MEG sensor-space and as close to the sensors as possible. This can be challenging when working with the

youngest children. When inserted as far as possible into the MEG system, children may find that their vision is obscured by the front of the helmet, and have a tendency to lean forwards and downwards, resting their upper forehead against the forward edge of the helmet, in order to see out. In doing so, they may bring any coils been placed on the forehead outside of the sensor space, making head position estimation, and therefore correction, impossible. Encouraging the child to 'keep their chin up' is therefore important; future modifications to proprietary head motion correction systems should aim to account for this.

The second implication of recording from smaller heads in addition to an increased distance is a reduction in sensor coverage of the anterior temporal lobes, and this also provides another reason to encourage a school-age patient to lean back in the MEG helmet. The anterior temporal lobes lie only a few centimeters behind the eyes, and are easily brought outside the sensors if the head is pitched forward and down. Figure 2 shows examples of auditory N1 field patterns recorded from an adult, and from two children using a CTF MEG system with axial gradiometers, illustrating this loss of signal from the smaller heads. The source of the auditory N1 is in the planum temporale, just posterior to the Heschl's gyrus, yet half of the field pattern is lost. Clearly, depending on its orientation, temporal-lobe epileptiform activity could be lost in the same way and this problem may at least in part explain the reported relative low sensitivity in the mesial temporal lobe (e.g. Agirre-Arrizubieta et al. 2009; Leijten et al. 2003).

The most critical implication of recording from smaller heads is that if the brain surface is further from the sensors, the recorded signal will be smaller. Acknowledging that overall head growth incorporates changes in the size of the cranium as well as of brain-size, we can safely assume that the cerebral cortex is several millimeters, often centimeters, further from the MEG sensors in our youngest patients compared to the adults for whom the system was designed. This can affect signal-to-noise quite considerably (Gaetz et al. 2008). Simulated data have previously shown that whilst superficial MEG sources have in general a high detection probability, the maximum detection probability starts to fall off very dramatically when the minimum source-sensor distance is larger than 6.5 cm (Hillebrand and Barnes 2002). Thus, signal from the anterior and inferior frontal and temporal lobes are sub-optimal in adult heads and may become undetectable in smaller children.

2.2 Stature

Children's smaller stature poses some additional problems for successful MEG recordings, including the suitability of seating arrangements, and the ability to fully insert the child's head into the MEG helmet. Recording while seated, rather than supine, has many benefits, most importantly that the child can feel much more at ease. The child can see the room around them and be reassured by the ease of making eye contact with a parent or other adult figure accompanying them in the

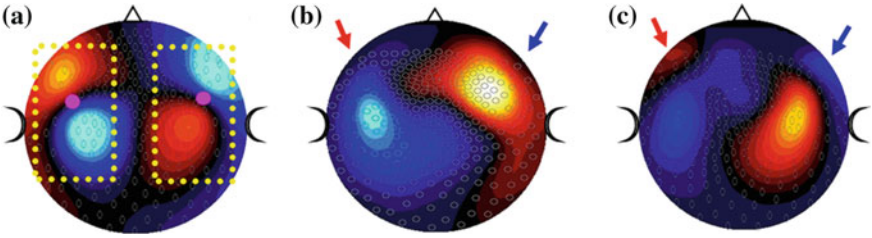

Fig. 2 Three field patterns from a CTF 275-channel MEG system, for evoked responses elicited by an auditory click. The field patterns reflect the activity at about 100-ms after presentation, for the response known as the N1m which originates in planum temporale, just posterior to primary auditory cortex and about mid-way along the temporal lobe. '**a**' shows data for a typical adult, with *red* and *blue* mirror-image dipolar field patterns in the *left* and *right* hemisphere, highlighted by the *yellow* box. In '**b**', the recording is from a child and the anterior portion of the field pattern in each hemisphere is lost (indicated by the *red* and *blue arrows*). '**c**' shows another child recording, where the field patterns are also incomplete. These field patterns illustrate the relative lack of sensitivity to temporal lobe sources in child patients, compared to adults, when recorded in an adult MEG system

magnetically shielded room. When the patient is seated, it is also much easier for them to use response-devices such as joysticks or button-boxes, which can be placed on a table in front of them and easily visible.

However, like MEG helmet sizes, the adjustable chairs supplied with MEG systems were designed with adult patients in mind. With both the MEG systems we have used at Aston, limits to the maximum height of the seat meant that our younger school-age patients, with the seat at maximum height, are not fully inserted into the MEG helmet. The addition of cushions is not ideal, because cushions have a tendency to compress with time, so the child sinks below the sensors during the recording. Booster seats intended for use in cars have offered some success, but are not always comfortable, because we are using them with children much older than those for whom the seats were designed. Improved seating arrangements should be easy to achieve and a cost-effective priority for MEG manufacturers seeking to optimize their systems for use with children.

Whether seated or supine, children of very small stature may also be impossible to insert fully into the helmet for anatomical reasons (Fig. 3). The depth of the helmet, around 22—24 cm (depending on the manufacturer) may be longer than the distance between a very young child's shoulders and the crown. This means that, as the child's head is positioned within the helmet, their shoulders will come into contact with the lower limits of the helmet before their head reaches the top of the helmet, leaving a gap between the top of their head and the upper MEG sensors (see Fig. 3a). Our calculations based on population-level anthropometric data (Snyder et al. 1975) suggest that this is a problem even for the shallowest MEG helmets (22 cm) for typically developing children between about 4 and 6 years of age (Fig. 3b).

A very important observation, in relation to the design of MEG systems and accessories for use with children, is that pediatric patients are smaller than

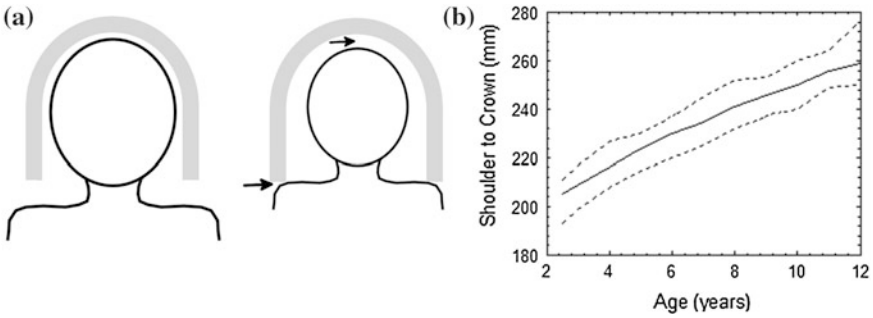

Fig. 3 *Panel A* Illustration of how stature affects insertion into the MEG helmet. An adult, on the *left* panel, can be fully inserted into the helmet; but for a child, the shoulders touch the lower edge of the helmet before the crown of the head reaches the *top* (*arrows*). *Panel B* The distance from shoulder to crown in TD children, as a function of age: data from Snyder et al. (1975). The Elekta MEG system helmet has a depth of about 22 cm and the CTF of about 23.5 cm. Children with a smaller shoulder-crown distance than this depth will not be fully inserted into the helmet.

typically developing children—often considerably so. Figure 4 shows how pediatric epilepsy patients referred for presurgical assessment at the Birmingham Children's Hospital for MEG investigations compare to typically developing children of the same age. Some of the patients' heights fall in the range expected for children who are 2 or even 3 years younger. A lower age limit, based on size, of about 4 years in typically developing children could translate in a lower age limit of up to 7 years for this patient group.

2.3 Compliance and Engagement

A frequent challenge in obtaining good quality data from school-age children is ensuring that the child is compliant enough to tolerate the recording process and engage with any task at hand. Minimizing preparation time is a key strategy to maximize compliance during the MEG recording. MEG compares very favorably with EEG in terms of preparation time. The longest preparation time is due to the need to affix coils to the patient's head and record their positions (i.e., coil positions are digitized prior to the recording) for localization and movement tracking. In our laboratory we use a surface-matching process for coregistration with a structural MRI (Adjamian et al. 2004), which provides improved accuracy compared to coregistration methods based on fiducials, but requires the digitization of the head surface as well as other key positions. This is time consuming and necessitates personal contact of staff with the child. During this procedure the child is required to sit still and we often find that compliance with this process is more challenging than that with the MEG recording itself. In the future, non-contact digital imaging may afford a valuable alternative (Woods et al. 2012) which, combined with alternative methods of locating and digitizing the position of head

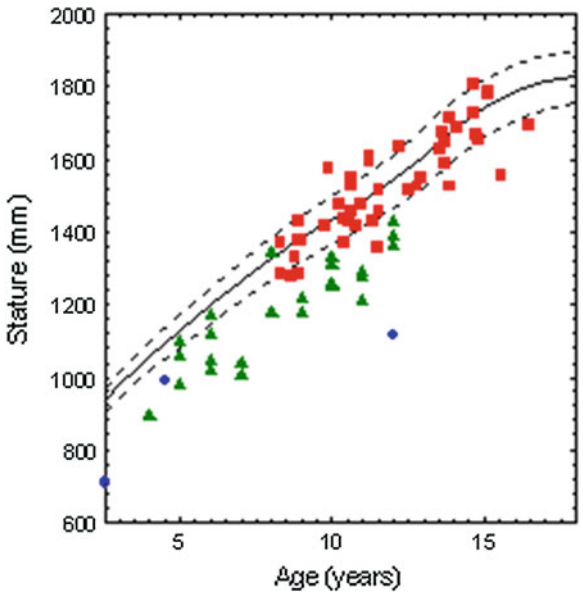

Fig. 4 A graph showing the ages and heights of three groups of our pediatric MEG participants (not selected on any basis other than their participation in MEG recordings between January and December 2010), plotted with mean and standard deviation for the population (www.dined.com). The *red squares* show participants with developmental dyslexia, who are not expected to differ in stature from typically developing children. They fall within the expected normal range and indicate that the norms are an appropriate comparison for our British patient groups. The *green triangles* show children from our epilepsy pre-surgical mapping program, and many of these patients are significantly below the mean height for their age group. The *blue diamonds* indicate children with liver disease who also participated in MEG recordings, and are also significantly smaller than typically developing children

tracking coils, may significantly reduce the time required and improve the reliability of head tracking and subsequent coregistration with MRI data.

Task engagement is a final challenge. While a passive recording with low levels of arousal or even during sleep may provide ideal recording conditions for localizing epileptiform abnormalities, mapping eloquent cortex requires the patient to actively engage with a task. Obtaining good-quality evoked or induced responses depends in part on an optimal level of arousal and compliance, over a number of stimulus or response repetitions. This can be challenging when working with young children, particularly those with cognitive impairments or behavioral difficulties. However this challenge has already been addressed in other fields of research, where good-quality data depend on the active participation of young children. In "Rocket Ship Psychophysics", Abramov et al. (1984) describe how children as young as 5 years of age can be engaged in a series of challenging visual psychophysics experiments through the use of a narrative about astronaut training, complete with space-noises, 'space-rations', and a 'space-pass' where

points were accumulated. Simple computer games are now routinely used for measuring sensory thresholds in the behavioral context (Sutherland et al. 2012; Barry et al. 2010), and their adaptation for use in the context of MEG recordings can provide a useful tool for clinicians needing to encourage task participation.

3 Implications

In the previous sections we have outlined the key challenges of recording good-quality clinical data from school-age children, and some solutions. Here we consider how these challenges may impact on the evidence-base for MEG in clinical applications. The benefits of MEG over EEG for epilepsy work in adults, particularly in the frontal lobe (Ossenblok et al. 2007; Knowlton et al. 1997), are attributed to MEG's significantly improved signal-to-noise-ratio for sources in this region (de Jongh et al. 2005). For temporal lobe spikes the reported value of MEG detection is varied. Recent studies have reported a high level of accuracy in spike detection in lateral and basal temporal lobe validated with ECoG (Agirre-Arrizubieta et al. 2009) or in comparison with simultaneous EEG (Lin et al. 2003). Data on detection rate for spikes located in mesial temporal lobe are still controversial. Some authors have reported poor detectability (Agirre-Arrizubieta et al. 2009; Wennberg et al. 2011), whereas one study has reported that 16 % of patients with mesial temporal lobe epilepsy with non-localizing ictal scalp EEG had well-localized spikes on MEG (Kaiboriboon et al. 2010). Leijten et al. (2003) attributed poor spike yield in mesial temporal lobe epilepsy to inadequate coverage of the temporal lobes by the MEG helmet. There are no equivalent systematic comparisons of spike detection and yield in pediatric patients. Given the increased distance of inferior frontal and temporal lobe sources from sensors in children (see Fig. 2), detection rates and yield are likely to be impoverished in comparison to adult evaluation, but further study in this domain are necessary to accurately characterize the relative detection rates of spikes in pediatric age from the key cortical structures for which current adult MEG systems are sub-optimal.

4 Conclusions and Future Developments

An optimal MEG system designed for school-aged children would ideally incorporate a smaller head shell design with a shallower profile to enable full head insertion and optimize sensor coverage for accurate source reconstruction in frontal and temporal lobes. The prohibitive costs of re-engineering a system make it unlikely that a mainstream MEG manufacturer will develop their device for this purpose, at least in the near future. On the other hand, new software developments are likely to bring about significant improvements in signal to noise ratio for all types of recording. A likely focus on reducing noise (especially sensor-noise),

rather than increasing signal, constitutes an alternative approach to improving detection of brain activity from small children recorded in adult MEG systems (Elekta Neuromag, personal communication), and should have considerable benefits for clinicians working with this age group. Other developments in head-motion compensation, particularly focused on the problem created by small heads, which can easily move beyond the limits of the sensor array (Elekta Neuromag, personal communication), will also be beneficial.

The recent refinement of motion correction algorithms has enabled the incorporation of standard diagnostic protocols such as hyperventilation and recording during spontaneous sleep to become part of routine MEG evaluations. Furthermore, reliable measures can now be made at the onset of most convulsive seizures using MEG (Kakisaka et al. 2012) and the time-locked video-MEG recording of ictal events may well further improve the sensitivity and clinical value of MEG studies (Medvedovsky 2012) and lead to the future adoption of MEG as a gold-standard for pediatric epilepsy work-up.

References

Abramov I, Hainline L, Turkel J, Lemerise E, Smith H, Gordon J, Petry S (1984) Rocket-ship psychophysics. assessing visual functioning in young children. Invest Ophthalmol Vis Sci 25:1307–1315

Adjamian P, Barnes GR, Hillebrand A, Holliday IE, Singh KD, Furlong PL, Harrington E, Barclay CW, Route PJG (2004) Coregistration of magnetoencephalography with magnetic resonance imaging using bite-bar-based fiducials and surface-matching. Clin Neurophysiol 115:691–698

Agirre-Arrizubieta Z, Huiskamp GJ, Ferrier CH, Van Huffelen AC, Leijten FS (2009) Interictal magnetoencephalography and the irritative zone in the electrocorticogram. Brain 132(11): 3060–3071

Barry JG, Ferguson MA, Moore DR (2010) Making sense of listening: the imap test battery. J Visualized Exp 11:e2139

De Jongh A, De Munck JC, Goncalves SI, Ossenblok P (2005) Differences in MEG/EEG epileptic spike yields explained by regional differences in signal-to-noise ratios. J Clin Neurophysiol 22:153–158

Gaetz W, Cheyne D, Rutka JT, Drake J, Benifla M, Strantzas S, Widjaja E, Holowka S, Tovar-Spinoza Z, Otsubo H, Pang EW (2009) Presurgical localization of primary motor cortex in pediatric patients with brain lesions by the use of spatially filtered magnetoencephalography. Neurosurgery 64:177–185

Gaetz W, Otsubo H, Pang EW (2008) Magnetoencephalography for clinical pediatrics: the effect of head positioning on measurement of somatosensory-evoked fields. Clin Neurophysiol 119:1923–1933

Hauser WA (1995) Epidemiology of epilepsy in children. Neurosurg Clin N Am 6:419–429

Hillebrand A, Barnes GR (2002) A quantitative assessment of the sensitivity of whole-head MEG to activity in the adult human cortex. Neuroimage 16:638–650

Jeha LE, Najm I, Bingaman W, Dinner D, Widdess-Walsh P, Luders H (2007) Surgical outcome and prognostic factors of frontal lobe epilepsy surgery. Brain 130:574–584

Johnson BW, Crain S, Thornton R, Tesan G, Reid M (2010) Measurement of brain function in pre-school children using a custom sized whole-head MEG sensor array. Clin Neurophysiol 121(3):249–340

Kaiboriboon K, Nagarajan S, Mantle M, Kirsch HE (2010) Interictal MEG/MSIin intractable mesial temporal lobe epilepsy: spike yield and characterization. Clin Neurophysiol 121(3): 325–331

Kakisaka Y, Wang ZI, Mosher JC, Dubarry AS, Alexopoulos AV, Enatsu R, Kotagal P, Burgess RC (2012) Clinical evidence for the utility of movement compensation algorithm in magnetoencephalography: successful localization during focal seizure. Epilepsy Res 101(1–2): 191–196

Kirsch HE, Robinson SE, Mantle M, Nagarajan S (2006) Automated localization of magnetoencephalographic interictal spikes by adaptive spatial filtering. Clin Neurophysiol 117(10):2264–2267

Knowlton RC, Laxer KD, Aminoff MJ, Roberts TP, Wong ST, Rowley HA (1997) Magnetoencephalography in partial epilepsy: clinical yield and localization accuracy. Ann Neurol 42:622–631

Leijten FS, Huiskamp GJ, Hilgersom I, Van Huffelen AC (2003) High-resolution source imaging in mesiotemporal lobe epilepsy: a comparison between MEG and simultaneous EEG. J Clin Neurophysiol 20(4):227–238

Lin YY, Shih YH, Hsieh JC, Yu HY, Yiu CH, Yeh TC, Wong TT, Kwan SY, Ho LT, Yen DJ, Wu ZA, Chang MS (2003) Magnetoencephalographic yield of interictal spikes in temporal lobe epilepsy. Comparison with scalp EEG recordings. Neuroimage 19(3):1115–1126

Medvedovsky M, Taulu S, Gaily E, Metsähonkala El, Mäkelä JP, Ekstein D, Kipervasser S, Neufeld MY, Kramer U, Blomstedt G, Fried I, Karppinen A, Veshchev I, Roivainen R, Ben-Zeev B, Goldberg-Stern H, Wilenius J, Paetau R (2012) Sensitivity and specificity of seizure-onset zone estimation by ictal magnetoencephalography. Epilepsia 53(9):1649–1657

Okada Y, Pratt K, Atwood C, Mascarenas A, Reineman R, Nurminen J, Paulson D (2006) BabySQUID: a mobile, high-resolution multichannel magnetoencephalography system for neonatal brain assessment. Rev Sci Instrum 77:1–9

Ossenblok P, De Munck JC, Colon A, Drolsbach W, Boon P (2007) Magnetoencephalography is more successful for screening and localizing frontal lobe epilepsy than electroencephalography. Epilepsia 48:2139–2149

Robinson SE, Vrba (1999) Functional neuroimaging by synthetic aperture magnetometry (SAM). In: Yoshimoto T (ed) Recent advances in biomagnetism. Tohoku University Press, Sendai, pp 302–305

Snyder RG, Spencer ML, Owings CL, Schneider LW (1975) In: Physical characteristics of children as related to death and injury for consumer product safety design. UM-HSRI-Bi-75-5. Consumer Product Safety Commission (USA). Available via DIALOG. http://Ovrt.Nist.Gov/Projects/Anthrokids/

Sutherland ME, Zatorre RJ, Watkins KE, Hervé PY, Leonard G, Pike BG, Witton C, Paus T (2012) Anatomical correlates of dynamic auditory processing: relationship to literacy during early adolescence. Neuroimage 60:1287–1295

Nenonen J, Nurminen J, Kičić D, Bikmullina R, Lioumis P, Jousmäki V, Taulu S, Parkkonen L, Putaala M, Kähkönen S (2012) Validation of head movement correction and spatiotemporal signal space separation in magnetoencephalography. Clin Neurophysiol 123:2180–2191

Wennberg R, Valiante T, Cheyne D (2011) EEGand MEG in mesial temporal lobe epilepsy: where do the spikes really come from? Clin Neurophysiol 122(7):1295–1313

Wilson HS (2004) Continuous head-localization and data correction in a whole-cortex MEG sensor. Neurol Clin Neurophysiol 30:56

Woods W, Gouws A, Green GGR (2012) Stereo camera MEG-MRI coregistration and head tracking. Poster presented at Biomag 2012, 18th international conference on biomagnetism, Paris, 26–30 August 2012

Wellmer J, Weber B, Urbach H, Reul J, Fernandez GE (2009) Cerebral lesions can impair fMRI-based language lateralization. Epilepsia 50(10):2213–2224

Cognitive Decline Associated with Aging, Alzheimer's Disease and Cerebrovascular Risk: Advantages of Dynamic Imaging with MEG

Cheryl J. Aine, John C. Adair, Janice E. Knoefel, Lori Sanfratello and Julia M. Stephen

Abstract Recent studies examining Alzheimer's disease (AD) and aging have noted a strong association between cerebrovascular risk and cognitive decline, and suggest that AD may in part be attributed to vascular insufficiency. Based on our recent results we suggest that cognitive decline associated with cerebrovascular pathology should be characterized and if possible separated from neurodegeneration caused by amyloid plaques and neurofibrillary tangles (i.e., traditional AD-related pathology) since the progression of cerebrovascular pathology can be stopped or slowed down. Furthermore, because cerebrovascular pathology (e.g., hypertension and type 2 diabetes) co-exists in most AD patients, neuroimaging techniques dependent on 'uncompromised' neurovascular coupling (e.g., fMRI) will have more potential confounds to deal with in this area of study, in addition to difficulties associated with being an indirect measure of neural activity. We assert that functional measures (e.g., dynamic cortical networks, oscillatory activity and cross-frequency coupling), as opposed to structural measures (e.g., diffusion tensor imaging–DTI), will enable earlier diagnosis of AD and mild cognitive impairment (MCI) and that MEG in particular can make important contributions to this field. A new potential area of study that relates MEG single trial results to models of diffusion parameters in extracellular space is introduced.

C. J. Aine (✉) · L. Sanfratello
Radiology, University of New Mexico School of Medicine, Albuquerque, NM, USA
e-mail: aine@unm.edu

J. C. Adair
Neurology, University of New Mexico School of Medicine, Albuquerque, NM, USA

J. E. Knoefel
Internal Medicine, University of New Mexico School of Medicine, Albuquerque, NM, USA

J. M. Stephen
The Mind Research Network, Albuquerque, NM, USA

S. Supek and C. J. Aine (eds.), *Magnetoencephalography*,
DOI: 10.1007/978-3-642-33045-2_31,

Keywords Mild cognitive impairment (MCI) · Alzheimer's disease (AD) · Aging · Metabolic syndrome · Hypertension · MEG · Memory · Oscillatory · Frequency · Neurodegenerative · White matter hyperintensities (WMHs) · Dementia · Neurovascular coupling · Cerebrovascular

1 Introduction

One goal of our research effort is to accurately differentiate between Alzheimer's disease (AD), mild cognitive impairment (MCI), normal aging, and healthy successful aging. Interest in this area was motivated by our previous neuroimaging studies demonstrating that a majority of a sample of MCI and AD patients revealed moderate to severe MRI abnormalities [e.g., white matter hyperintensities (WMHs), suggestive of chronic white matter ischemia, and volume loss], as determined by a board-certified neuroradiologist (Aine et al. 2010). In addition, approximately 1/3 of our elderly control group also had moderate to severe MRI abnormalities and they generally performed worse on the behavioral tasks and neuropsychological tests of memory, compared to elderly with no or mild MRI abnormalities. Recent literature on WMHs indicate that their presence is typically associated with hypertension and/or type 2 diabetes (Inzitari 2000; Dufouil et al. 2001; Cook et al. 2002; De Groot et al. 2002; Awad et al. 2004; Kuo and Lipsitz 2004; Manschot et al. 2006).

Indeed, numerous epidemiological studies have recently linked cardiovascular risks in midlife (e.g., hypertension) with increased likelihood of developing dementia, including AD, later in life [see review by Qiu et al. (2005)]. DeCarli and colleagues (2001), for example, found that individuals with MCI had an increased prevalence of WMHs and elevated midlife diastolic blood pressure that increased the risk for MCI to at least the same degree as apolipoprotein E ε4 (APOE-4) genotype. Schmidt and colleagues (2000) showed that individuals who developed AD had higher systolic blood pressure than nondemented counterparts 10–15 years prior to disease onset. It has even been shown that antihypertensive medication can protect against dementia in some cases (Forette et al. 2002). And finally, recent results from a meta-analysis (Debette and Markus 2010) suggest that WMHs should be used as an intermediate biomarker of brain health since they are usually associated with small vessel disease. Consequently, careful documentation of brain health for studies of aging and AD is very important because: (1) we need to separate pathological aging (e.g., cognitive decline associated with cerebrovascular risk) from healthy successful aging in order to better understand aging processes per se; and (2) we need to sort out effects due to cerebrovascular pathology from those attributed to AD processes (e.g., plaques and tangles) in order to better understand and treat this disease. Cerebrovascular-related cognitive decline (e.g., due to hypertension and/or type 2 diabetes) can usually be prevented or controlled by changes in lifestyle (diet and exercise) or medication, thereby providing patients

with a possible opportunity to delay the progression of dementia-like symptoms or cognitive decline and enhance the quality of their lives.

The clinical syndrome called dementia consists of an acquired memory impairment and impairment in at least one other cognitive domain, which diminishes the sufferer's ability to cope with activities of daily living for at least 6 months (Eschweiler et al. 2010). AD, the most common form of dementia, ranks among the top public health problems confronting developed countries (Arrieta and Artalejo 1998), with an estimated 14.5 million people in the U.S. to become afflicted with the disease by the middle of next century. Although there is general consensus on the clinical course and neuropathology of AD, there is limited information on its causes and pathogenesis. Current data suggest that various possible causes and predisposing factors most likely reflect an interaction of biological and environmental influences (Small 1998). The gene coding for the amyloid precursor protein (APP), whose cleavage product (beta amyloid) forms the cores of senile plaques in AD, was localized to chromosome 21 (Walker 1997; Small 1998). However, it was soon discovered that APP mutations rarely caused AD. Other genetic mutations causing early-onset familial AD have been identified, but they account for a very small proportion of AD cases. For late-onset AD (dementia beginning after age 60), APOE-4 has been confirmed to be a major susceptibility gene for AD (Hof et al. 1992; Small and Leiter 1998; Small 1998). However, the genes identified thus far for late-onset AD account for only 50 % of the genetic variability in AD. More recently, AD and other dementias have been linked to cardiovascular problems since AD and other dementias typically co-exist with hypertension (60 %), coronary heart disease (30 %), congestive heart failure (28 %) and diabetes (21 %) [2008 Alzheimer's disease Facts and Figures, Alzheimer's Association].

Interestingly, when Alois Alzheimer first described AD, dementia was most often attributed to vascular insufficiency or syphilis (Iadecola 2010) and Scheibel (1989) even referred to AD as a capillary dementia. Regardless of its etiology, early detection strategies for AD are essential since any soon-to-be-developed anti-dementia treatments are not likely to reverse existing neuronal damage, but rather slow further progression. Unfortunately, many studies indicate that significant medial temporal lobe atrophy occurs before the diagnosis of mild AD and that neurofibrillary changes and plaque deposition may begin even before age 30 (Braak and Braak 1997; Price and Morris 1999; Petersen et al. 2006).

2 Neurobiological Changes in Normal Aging and AD

Normal Aging. There is a wealth of cross-validation studies relating measures of cognitive performance to neurodegenerative markers (e.g., changes in microscopic structure, decreases in synaptic density, neuronal density, mean neuronal size, the number of neuritic plaques, etc.), or rather, microscopic brain changes (Huttenlocher 1979; Anderson et al. 1983; Kemper 1984; Burke and Barnes 2006). However, a

broad range of similar neuropathological findings can also be observed in older people with normal cognitive performance (Klunk et al. 2004; Aizenstein et al. 2008; Jack et al. 2009). Generally speaking, brain weight declines with age (by about 10 % from early adult life to the ninth decade); the ventricles and sulci enlarge in volume; and both gray (GM) and white matter (WM) volumes appear to shrink [see review (Kemper 1984)]. Atrophic changes have been reported most frequently in the convexities of the frontal lobes, parasagittal regions and the temporal and parietal lobes. Although past studies reported substantial neuronal loss (Coleman and Flood 1987; Kemper 1993; Rosene 1993; Albert and Moss 1996) recent investigations suggest that there is only an overall loss of $\sim$9.5 % of neurons with age (Voytko 1998; Peters and Rosene 2003) and that it is a misconception to think that dramatic cell loss and morphological changes in neurons occur in normal aging (Burke and Barnes 2006). Instead, age-related changes result in myelin loss and structural changes within the myelin sheaths which has the potential to disrupt communication among neurons (Willott 1997; Peters et al. 2000). WM fiber tracts provide high-density connectivity between cortical and subcortical GM structures, thereby coordinating activity across disparate GM regions and creating widely distributed, functionally integrated circuitry. Similarly, a decrease in number of dendritic branches and reduction in dendritic lengths have also been noted in elderly humans (Scheibel et al. 1975), which affects the number of synaptic contacts that can be made with other neurons (Willott 1997).

AD. The pathologic hallmarks of AD are senile plaques and neurofibrillary tangles which are selectively distributed; their concentrations are highest in the temporal-parietal regions, hippocampus, entorhinal cortex, and the amygdala (Hyman et al. 1984; Katzman 1986; Van Hoesen and Damasio 1987; Hof et al. 1992; Steffens 1997; Willott 1997; Jack et al. 1998; Small 1998). Synaptophysin, a marker of neuronal connections, is decreased in areas that are affected by the disease (e.g., hippocampus) but not in regions that are behaviorally or neuropathologically uninvolved (Honer et al. 1992). Dementia severity of AD patients correlated with synapse counts in biopsy tissue and synaptophysin concentration in postmortem tissue (DeKosky and Scheff 1990; Terry et al. 1991) suggesting that synapse loss is the major correlate of cognitive impairment (Terry et al. 1991). Quantitative MRI studies in AD have documented a general increase in CSF volume in the sulci, ventricles and the combination of sulci and ventricles (Alavi et al. 1993). Other MRI studies showed a regionally specific decrease in volume of the medial temporal lobe and hippocampal formation (Kesslak et al. 1991; Jack et al. 1992; Murphy et al. 1993; Steffens 1997). MCI patients, who are at risk for developing AD (Petersen 2004), are believed by some to have AD neuropathology and that medial temporal atrophy in these patients predicts subsequent progression to AD (Jack et al. 1999).

Jack and colleagues (2010) recently summarized five of the most widely studied biomarkers of AD pathology and ordered the temporal relationships among the biomarkers with clinical disease stage. Amyloid (Aß) imaging (PET-PIB) abnormalities, for example, may precede clinical/cognitive symptoms by as much as 2–3 decades since approximately 20–40 % of cognitively normal elderly have evidence

of significant brain Aß deposition. Other biomarkers included CSF $Aß_{42}$, another index of Aß deposition, CSF tau, a putative marker of neuronal damage, and FDG-PET, an indicator of synaptic dysfunction. Unfortunately, these tests are either prohibitively expensive (i.e., requiring a PET scanner and cyclotron) or invasive (i.e., requiring lumbar puncture or exposing patients to ionizing radiation) so that their use is limited in clinical practice and restricted mainly to research studies. Structural MRI, listed as the 5th biomarker, provides a good measure of medial temporal volume loss that coincides with cognitive symptoms. While more clinically practical, structural MRI changes appear later in the temporal sequence than other biomarkers. Therefore, we need to identify neural signatures earlier, within the 2–3 decades that amyloid burden accumulates, in order to stop or defer disease progression.

3 Posterior Versus Anterior Patterns of Effects Differentiate Between AD and Normal Aging

Since AD is characterized by the presence of cortical amyloid plaques and neurofibrillary tangles in entorhinal and parahippocampal cortex in mild stages of AD, it is generally believed that the pathology has a more posterior distribution. The medial temporal lobe (MTL), a site where neurofibrillary tangles dominate first, is densely interconnected with posterior regions such as parietal cortex (Klunk et al. 2004; Buckner et al. 2005). Consequently, recall and recognition memory (e.g., recognizing a list of words) become increasingly impaired as the number of tangles increases. In contrast, there is a separate anterior pattern of changes associated with normal aging. Cognitive processes such as working memory and executive control are supported by the prefrontal lobes, and are among the first to decline with age [e.g. (Moscovitch and Winocur 1995; West 1996; Tisserand and Jolles 2003)]. Similarly, WM degenerates with an anterior-to-posterior gradient (i.e., prefrontal lobe dysfunction occurs first) (Head et al. 2005; Delano-Wood et al. 2012). Therefore, neuroimaging studies originally focused on differentiating between these anterior changes associated with normal aging (working memory/executive function deficits) versus posterior patterns associated with MCI/AD (word recall/recognition deficits).

However, a meta-analysis conducted by Gunning-Dixon and Raz (2000), along with other studies (Oosterman et al. 2004; Tullberg et al. 2004), have also shown that WMHs are: (1) more abundant in frontal regions; (2) associated with cognitive decline (e.g., executive dysfunction); and (3) associated with hypertension and type 2 diabetes (DeCarli et al. 1999; Gunning-Dixon and Raz 2000; Artero et al. 2004; Awad et al. 2004; Elias et al. 2004; Kuo and Lipsitz 2004; Schmidt et al. 2004; Qiu et al. 2005; Nordahl et al. 2006; Pantoni et al. 2007; Helzner et al. 2009). This cerebrovascular-related cognitive decline is believed to be due to demyelination and axonal degeneration (van Swieten et al. 1991; Taylor et al. 2003) in regions connecting frontal cortex and subcortical structures (Kuo and Lipsitz 2004).

Consequently, cerebrovascular-related cognitive decline also has an anterior pattern of changes since frontal areas are the first to reveal WMHs, followed by periventricular and parietal regions (Artero et al. 2004; Head et al. 2004). In each stage, the density of lesions increases until finally temporal and occipital regions are involved (creating an anterior-posterior gradient). Working memory and executive control functions are targeted first in this group. Since normal aging is also known to affect frontal lobe structures supporting working memory and executive functions, then cerebrovascular-related cognitive decline appears to be a serious confound for aging studies in general and certainly for studies attempting to differentiate between AD and normal aging.

In our most recent ongoing studies, we postulated that cerebrovascular risk factors (e.g., hypertension, hyperglycemia, hypercholesterolemia) underlie at least some of the apparent frontal lobe deficits seen in normal aging (Aine et al. 2011, 2013). This is similar to conclusions reached by Kennedy and Raz (2009) who suggested that: (1) elevation of arterial pulse pressure is linked to deterioration of WM tract integrity in frontal regions and (2) vascular risk may drive the expansion of WM damage from anterior to posterior regions. Burgmans and colleagues (2010) also examined effects of hypertension on white matter integrity (DTI, WMHs, WM volume) and concluded that diffusion-based indices of WM integrity may be more sensitive indicators of global and regional declines in the aging brain. Our initial results [behavioral and MRI/DTI; Aine et al. (2013)] show highly significant effects between cerebrovascular-related health status and cognitive decline. Cerebrovascular risk factors account for at least some, so-called normal aging effects. At least two issues remain: (1) how can we diagnose AD earlier in time; and (2) what do neuroimaging results tell us about the etiology of cognitive decline associated with aging and MCI/AD?

4 Advantages of Functional Neuroimaging with MEG

Currently, it is believed that neurodegenerative diseases and neuropsychiatric illnesses target specific networks, causing disruption and consequent cognitive decline (Seeley et al. 2009). Thus the elucidation of neuroimaging methods that can uniquely characterize these networks across anatomical and functional levels for each of the pathologies facilitates clinical diagnosis. While it is useful to know lesion localization via structural imaging, functional measures should be able to provide information about cognitive decline earlier than anatomical measures. The temporal evolution of biomarkers in AD discussed earlier asserts that changes in activity levels (e.g., FDG-PET hypometabolism) occurs months or years before structural changes within the brain are detectable. As noted above, structural MRI was listed as the 5th biomarker that provides a good measure of hippocampal volume that coincides with cognitive symptoms. However, we need to identify neural signatures prior to significant volume loss or symptom onset to maintain quality of life for those who are susceptible to AD-related cognitive decline.

Recently, Hedden and colleagues (2009) and Sheline and colleagues (2010) examined network connectivity in the default mode network (DMN) using fMRI in a group of cognitively normal elderly who were either classified as PIB+ or PIB− from the PET amyloid imaging exam (i.e., they either showed evidence of amyloid deposition when imaged with ^{11}C-labeled Pittsburgh Compound B or not). The PIB+ groups from both studies revealed a disruption of functional connectivity within the DMN that could not be explained by increased age or structural atrophy. The pattern of disruption was similar to that shown in AD patients in other studies (Greicius et al. 2004; Zhang et al. 2009). For example, connectivity between precuneus and hippocampus (i.e., a posterior pattern of effects) was significantly lower in individuals with amyloid deposition versus those without cerebral amyloid. We suggest that functional connectivity measures are far more likely to provide sensitive measures of disease processes, and earlier in time than structural measures. In addition, by using functional measures with enhanced timescales (i.e., milliseconds rather than seconds) that are less affected by neurovascular coupling issues (e.g., MEG/EEG) should increase the chances for successful differential diagnosis.

Issues Associated with Neurovascular Coupling for fMRI Studies of Age-related and AD Pathology. As mentioned previously even Alois Alzheimer attributed AD to vascular insufficiency or syphilis (Iadecola 2010). Later, AD was associated primarily with posterior degenerative pathology. Thus, it appears that views of AD are beginning to come around full circle since recently there are numerous studies indicating interaction between neurodegenerative and vascular factors in the pathogenesis of dementia (Farrall and Wardlaw 2009; Iadecola 2010; Warsch and Wright 2010) and some are outright suggesting that AD is a microvascular disorder [reviewed in (Jellinger 2002; Zlokovic 2005; Bell and Zlokovic 2009; Schneider and Bennett 2010)]. In a study of 300 AD autopsy cases, 98 % were found to have cerebral amyloid angiopathy (CAA) (i.e., deposition of Aß in arteries, arterioles, and less frequently in capillaries and veins) and 100 % showed microvascular degeneration (Kalaria and Ballard 1999). It is rather interesting that amyloid burden is most prevalent in frontal lobes even though AD is thought of as predominantly affecting medial temporal lobes. For example, a recent study examining cognitively normal elderly with PIB+ suggests that a frontal network associated with working memory was affected first by amyloid deposits (Oh et al. 2011). Theories that suggest cerebrovascular dysfunction precedes cognitive decline and the onset of neurodegenerative changes in AD [e.g. (Zlokovic 2005, 2008; Bell and Zlokovic 2009)] indicate that cerebral hypoperfusion impairs the clearance of Aß from the brain, which is normally performed by the cells in the neurovascular unit. Therefore, Aß accumulates on blood vessels (i.e., CAA) and in brain parenchyma. In support of this hypothesis, MR-based arterial spin labeling (ASL) showed widespread hypoperfusion in AD (Johnson et al. 2005). There is also increasing evidence that the effect of vascular lesions are more pronounced in the early stages of AD (Esiri et al. 1999) and that ischemic lesions and vascular risk factors accelerate disease progression of dementia (Helzner et al. 2009).

A recent meta-analysis covering aging, vascular dementia, AD, lacunar stroke, and leukoaraiosis indicates that the blood-brain-barrier (BBB) permeability in these conditions is altered (Farrall and Wardlaw 2009). In other words, the neurovascular unit itself is altered [e.g. Bell and Zlokovic (2009)]. Therefore, one potential barrier to using fMRI methods for examining AD is that neurovascular coupling may be altered in these groups and consequent interpretations of the BOLD changes may be incorrect (D'Esposito et al. 2003). Neurovascular coupling is defined as the relationship between a change in neuronal activity and the subsequent hemodynamic response reflected by a BOLD signal change. The primary determinant of the BOLD signal, deoxyhemoglobin within each voxel, is dictated by the venous blood volume, arterial blood flow and blood oxygenation, and any disease or medication that modifies the responsiveness or the baseline values of these parameters are likely to modify BOLD contrast even in absence of any modulation of neural activity (Iannetti and Wise 2007). Unfortunately, Lee and colleagues (2009) found patterns of hypo- and hyper-perfusion for their group of 38 healthy elderly leading them to believe that there are problems with neurovascular coupling in many elderly as well. Therefore, Iannetti and Wise (2007) offer several suggestions/steps for improving the interpretability of BOLD fMRI results in cases where the neurovascular coupling may be compromised. For one, they suggest acquiring an independent measure such as electrophysiological responses (e.g., EEG and MEG).

Figure 1 shows the utility of using MEG time-course information derived from inverse procedures to capture differences between diagnostic categories. As mentioned above, MCI and AD have a more posterior pattern of deficits (i.e., temporal lobe). Several recent studies have noted the importance of mapping anterior temporal (ANT) lobe activity as well. Studies monitoring cortical atrophy rates for MCI and AD in longitudinal designs consistently note early changes in the anterior MTL (Bozzali et al. 2006; Smith et al. 2007; Whitwell et al. 2007). Whitwell and colleagues (2007), for example, found changes in the anterior temporal lobe that occurred three years previous to a diagnosis of AD. At the time of diagnosis of AD, atrophy in the temporal lobes had spread to include the middle temporal gyrus and the entire extent of the hippocampus. Our auditory delayed verbal recognition task (Aine et al. 2010) is good for evoking activity in the anterior temporal lobe since this region has been identified as an auditory word form area (Cohen et al. 2004). Most healthy controls showed activation in ANT (blue tracing in top portion of Fig. 1 is the average time-course across participants which show ANT activity). MCI and some AD patients also revealed activity in ANT (red tracing), but they showed hyperactivity in this region. However, we could not localize activity in this region for some AD patients. Dickerson and colleagues (2008) reviewed three fMRI studies that also demonstrated greater MTL activation in MCI patients compared to controls. They consider hyperactivation as a predictive marker in MCI. Hypoactivation of MTL occurs at a later stage of the disease resulting in an inverted U-shaped curve describing blood oxygenation changes in MTL with progression from MCI to AD [(Dickerson and Sperling 2008) see also Maestú et al., this volume]. That is, hyperactivation of MTL circuits occurs early in the course of MCI

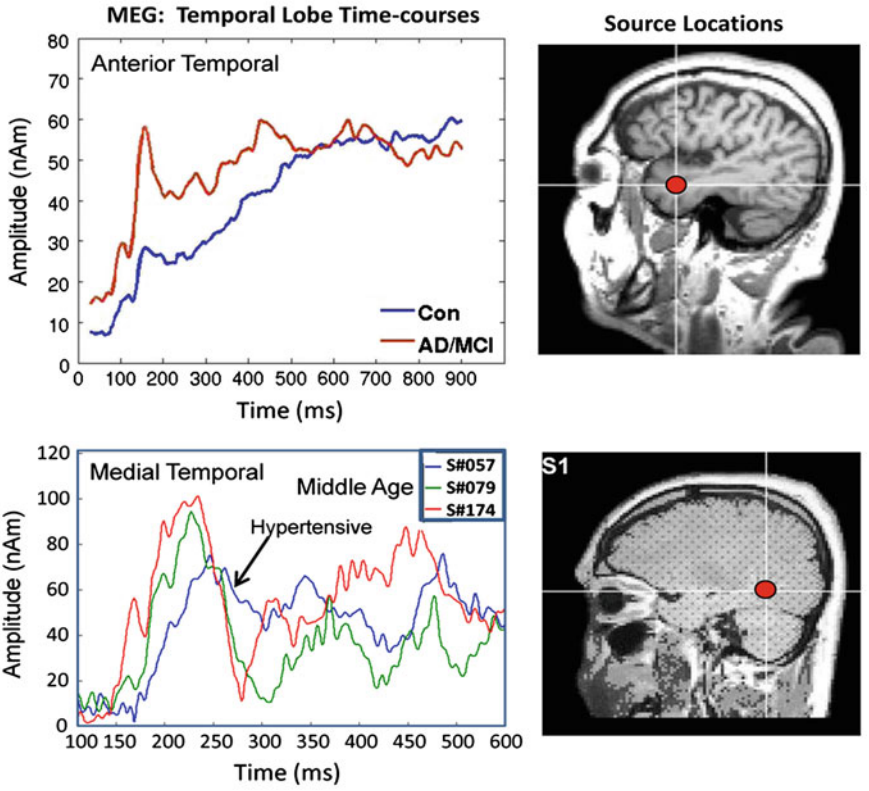

Fig. 1 *Top* MEG time-courses of sources localized to anterior temporal lobe, averaged together for the healthy controls (*blue* tracing) and MCI/AD patients (*red*) tracing. MRI at right reveals anterior temporal lobe. *Bottom* Time-courses of sources for 3 middle-aged participants localized to medial temporal lobe (see MRI at the *right*). Participants denoted by *red* and *green* tracings were healthy controls. *Blue* tracing denotes a hypertensive participant. These time-courses appear noisy because we did not want to eliminate high frequency activity (e.g., gamma band) superimposed on the slower activity

while these same regions failed to activate in AD. It was suggested that entorhinal and perirhinal cortices were most likely devastated by neurofibrillary pathology and cell loss early in the course of AD, effectively disconnecting the hippocampal formation from neocortical afferents and efferents. Our averaged MEG evoked response data corroborate these fMRI findings.

The bottom portion of Fig. 1 shows time-course effects associated with hypertension. In this case we used a visual working memory task (Sternberg variant) to evoke activity in MTL. Single-subject data are shown for two healthy middle-aged controls (red and green tracings) and one middle-aged hypertensive patient (blue tracing). All participants were 35–45 years of age. In contrast with

the ANT activity shown above, the hypertensive patient, representative of our hypertensive group, revealed lower amplitude signals and prolongation of peak activity. In this case, MCI and hypertension appear to operate in opposite directions (MCI have greater amplitude signals and no peak delays in ANT), at least initially, but AD and hypertension may have a similar trajectory (reduced amplitude, delayed peaks until activity in this region can no longer be localized). This is just one example of how MEG source locations and time-courses can be used to characterize various diseases and disorders. It should also be emphasized that MEG easily permits the examination of single subject data, a necessity for clinical intervention.

MEG/EEG: Oscillatory Activity and Frequency Domain Analyses. Certainly, we are interested in finding alternative ways of analyzing data for our clinical research on aging and dementia, that may be faster and/or geared toward very specific questions (e.g., slowing of activity in temporal regions). Characterizing altered neural oscillations and synchrony in pathophysiology as a potential biomarker provides an additional way to achieve classification specificity for brain disorders (Uhlhaas and Singer 2010). Recently, there has been increased interest in understanding oscillating networks since they appear to provide important links between single neuron activity, population activity, and behavior. The existence of an oscillatory hierarchy, which controls neuronal excitability (Buzsaki and Draguhn 2004; Lakatos et al. 2005), has been described in animal studies where higher frequency oscillations are nested within lower frequencies. Lakatos and colleagues (2005), for example, nicely show in monkey auditory cortex that a succession of negative and positive voltage fluctuations, comprising the oscillation, reflected an underlying 7 Hz alternation of net inward and outward transmembrane current flow, which produced extracellular current sinks and sources, respectively. The corresponding multiunit activity indicated that current flow alternation reflected shifts between net depolarized and hyperpolarized states in the local neuronal ensemble (i.e., increases in firing and decreases in firing). Studies on cross-frequency coupling in the hippocampus and other brain regions suggest that these nested oscillatory patterns may be capable of storing multiple memories within a single network (Lisman and Idiart 1995). In addition, there is a correlation between the distance over which synchronization is observed and the frequency of the oscillations such that higher frequency oscillations (gamma band activity) are believed to be confined within small neuronal space (i.e., shorter distance) whereas slower oscillations such as beta band activity carry information over longer distances (e.g., large networks) (Kopell et al. 2000; Buzsaki and Draguhn 2004; Uhlhaas et al. 2010). Only coherently oscillating neuronal groups (i.e., phase locked) can interact effectively across distance. In sum, oscillations constitute rhythmic modulations in neuronal excitability that affects both the likelihood of spike output and sensitivity to input, which also permits coherently oscillating neuronal groups across regions to communicate effectively and efficiently with each other (Fries 2005).

Unfortunately, after decades of research on oscillatory activity there is no unified theory on oscillatory activity as seen in surface EEG or MEG, although

there have been numerous studies attempting to determine the role of oscillations in perceptual binding (Engel et al. 1992; Singer and Gray 1995; Roelfsema et al. 1997). However, MEG recordings are better suited for examining oscillatory activity for two reasons. First, the abnormal MEG patterns noted for AD are very specific to sensor groupings (e.g., temporal regions) rather than being generalized across the head (EEG). This is important since much of the abnormal activity is in the same frequency range as muscle and other related artifacts. MEG can separate out abnormal brain activity from muscle artifact based on different spatial patterns. Second, we have noticed bursts of high frequency signals associated with WMHs and bursts of slow-waves associated with volume loss. Luckily, the skull does not act as a low-pass filter for MEG as it does for EEG (Hamalainen et al. 1993). Clearly this is an exciting area where MEG/EEG studies have a definite advantage over fMRI measures. For those interested in learning more about oscillatory activity and frequency domain analyses, please see chapters (this volume) by Schoeffelen and Gross, Brookes and colleagues, and de Pasquale and Marzetti.

What makes cortical frequencies change? Some frequency changes are associated with development [see Uhlhass et al. for a review (2010)]. But, pathology can also affect regional frequencies. For example, Fernandez and colleagues (2002) found abnormal slow wave activity for AD patients in temporoparietal regions (see a review by Maestú and colleagues—this volume). In general, diffusion parameters of the extracellular space such as volume fraction and diffusion barriers modulate neuronal signaling, neuron-glia communication and extrasynaptic volume transmission (Sykova 2004). Significant decreases in extracellular space volume fraction (e.g., due to astrocytosis) and increases in diffusion barriers (e.g., plaques) may occur in AD as the result of pathology. If ion homeostasis is not maintained in the extracellular space, increased neuronal excitability and synchronization may occur, as noted in epileptiform spike generation (Broberg et al. 2008). Interestingly, several neurodegenerative diseases such as AD are associated with increased incidence of seizures (Palop et al. 2006). Cell swelling and concomitant reduction of extracellular space volume occurs in a number of pathologic conditions, causing an imbalance in the neuronal environment. Plaques, in contrast, disrupt the synchrony of convergent inputs thereby reducing the successful integration and propagation of information by neurons (Stern et al. 2004); it affects network properties and causes an increase in response variability with a net result of reduced synchrony of converging synaptic inputs.

It is clear that pathology affects neuronal signaling but how exactly the deposition of plaques, cell volume changes and changes in the extracellular ion concentration affect signal generation and propagation remain unclear. Our single-trial MEG data shown in Fig. 2 suggest at least 3 different patterns of activity associated with pathology: (1) bursts of slow-wave activity some of which are time-locked to the stimulus; (2) bursts of high frequency spike-like activity that is not time-locked to the stimulus; and (3) abnormal rhythmic patterns (see Fig. 3: a fronto-temporal dementia case). High frequency bursts were often seen in single-trial data from participants who revealed moderate to severe WMHs on their MRIs (bottom panel of left column) resulting in source time-courses that were extremely

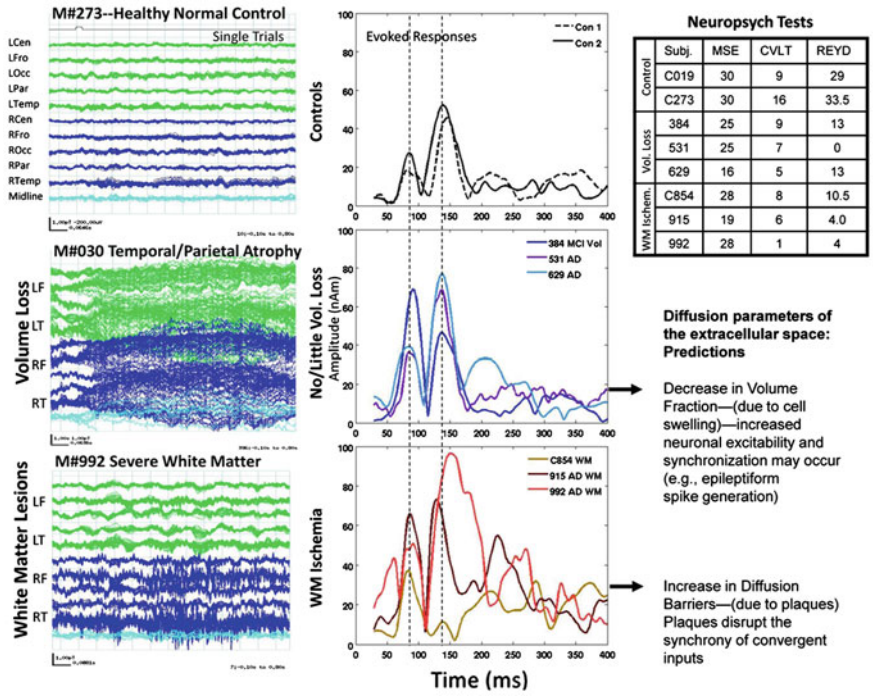

Fig. 2 *Left Column* (*Top*) Single-trial MEG responses from a healthy control evoked by a tone. This 1,000 ms segment (100 ms pre-stimulus and 900 ms post-stimulus) shows low-amplitude, de-synchronized activity from 275 sensors grouped by head regions; *green* and *blue* tracings represent *left* and *right* hemispheres, respectively. *Middle* Slow-wave activity is evident for this participant with MR abnormalities. *Bottom* High frequency activity over right temporal and frontal regions for another participant with MRI abnormalities. *Middle Column* Averaged time-courses localized to the superior temporal gyrus (STG) for (*Top*) 2 healthy controls and (*Middle*) 3 patients revealing moderate-severe volume loss and (*Bottom*) for 3 patients revealing moderate-severe white matter ischemia. *Right Column* (*Top*) Sample neuropsychological test results are shown for each patient and control. *Bottom* Predictions relating diffusion parameters of extracellular space to characteristics seen in the MEG data. *MSE* mini-mental status exam; *CVLT* Trial 5 of the California Verbal Learning Test; *REYD* Delayed recall on the Rey complex Figure Test

variable across participants in terms of peak latencies and amplitudes (bottom panel of middle column). In contrast, bursts of slow-wave patterns were evoked by auditory stimuli from participants with evidence of volume loss on their MRIs (middle panel of left column "M#030 Temporal/Parietal Atrophy"). Their corresponding averaged time-courses showed enhanced amplitudes, but the peak latencies were similar to those seen in normal controls (compare middle and top panels of middle column). As this longitudinal study progressed across years, it became possible to predict the MRI and neuropsychological results based on the number of epochs evidencing slow-wave bursts or high frequency activity in the

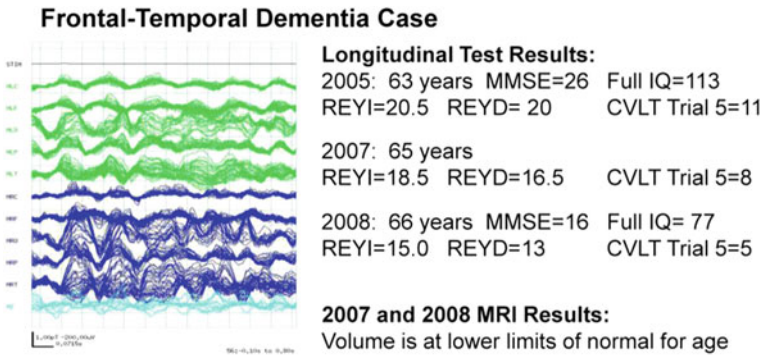

Fig. 3 Abnormal Rhythmic Patterns in Frontal-Temporal Dementia. *MMSE* Mini-mental status Exam; *REYI* Immediate recall on the Complex Figure Test; *REYD* Delayed recall on the Complex Figure Test; *CVLT* Trial 5 of the California Verbal Learning Test. MRI results were still within normal limits

single-trial data (unpublished results). We also see cases where both high frequency bursts and slow-wave activity are present within the same individual and their MRIs show the presence of both WMHs and volume loss. Relating single-trial data to models of diffusion parameters in extracellular space is likely to provide new information on the etiology of cortical pathology and cognitive decline associated with aging, MCI and AD. This is an untapped area of research that is uniquely suited for MEG.

5 Conclusions

If various causes and predisposing factors of AD reflect an interaction of biological and environmental influences (Small 1998), then health of the elderly, in addition to those suspected of probable AD, should be documented in research studies. Yet, most research participants do not complete neurological exams, blood tests, and even when the protocol requires the acquisition of MRIs, they are often not read by a neuroradiologist nor are subjects excluded from the study when MRIs reveal abnormalities for studies of healthy aging. Certainly, many more insults could have occurred in the brains of the elderly group, compared to the young, and in the brains of those suffering from cognitive impairment compared to normal elderly. At minimum, perhaps a structured interview could help determine the suitability of potential applicants for each study by asking a standard set of questions (e.g., have you ever experienced loss of consciousness for greater than 5 min? Did your doctor ever tell you that you have high blood pressure?).

As mentioned earlier, several recent studies found that WMHs associated with cardiovascular disease (e.g., hypertension and diabetes) target prefrontal cortex and affect working memory (DeCarli et al. 1999; Gunning-Dixon and Raz 2000;

Artero et al. 2004; Jeerakathil et al. 2004; Kuo and Lipsitz 2004; Schmidt et al. 2004; Tullberg et al. 2004; Nordahl et al. 2006; Pantoni et al. 2007; Burgmans et al. 2010). WM lesions, for example, affect performance on higher cognitive tasks via the disruption of neural transmission in functional networks (Peters and Rosene 2003; Filley 2005). The use of MEG-derived oscillatory characterizations should help tease out subtle differences in the spatio-temporal patterns of connectivity noted between cerebrovascular-related cognitive decline, neurodegenerative cognitive decline and normal cognition in healthy elderly. For example, it is likely that frequency differences associated with the nodes of the networks and cross-frequency coupling between nodes in the circuit will be evident earlier in time than structural or hemodynamic changes. Appropriate timing within the circuit is critical for proper functional connectivity. This is an area ripe for new studies, particularly if it can be related to models of diffusion parameters in extracellular space. In addition, this new area of research represents a unique niche for MEG methods.

Acknowledgments This work was supported by a grant from the National Institute on Aging, award number R01 AG029495. This work was also supported in part by: (1) National Institute of General Medical Sciences 2P20GM103472-06; (2) National Institute on Aging award number R01AG020302; (3) The Radiology Department at UNM SOM; and (4) The New Mexico VA Healthcare System. The content is solely the responsibility of the authors and does not necessarily represent the official views of the National Institutes on Aging or the National Institutes of Health. We thank Selma Supek for her insightful comments on an earlier version of this commentary.

References

Aine CJ, Bryant JE, Knoefel JE, Adair JC, Hart B, Donahue CH, Montano R, Hayek R, Qualls C, Ranken D, Stephen JM (2010) Different strategies for auditory word recognition in healthy versus normal aging. Neuroimage 49:3319–3330

Aine CJ, Sanfratello L, Adair JC, Knoefel JE, Caprihan A, Stephen JM (2011) Development and decline of memory functions in normal, pathological and healthy successful aging. Brain Topogr 24:323–339

Aine C, Sanfratello L, Adair J, Knoefel J, Qualls C, Lundy S, Caprihan A, Stone D, Stephen J (2014) Characterization of a normal control group: are they healthy? Neuroimage 84:796−809

Aizenstein HJ, Nebes RD, Saxton JA, Price JC, Mathis CA, Tsopelas ND, Ziolko SK, James JA, Snitz BE, Houck PR, Bi W, Cohen AD, Lopresti BJ, DeKosky ST, Halligan EM, Klunk WE (2008) Frequent amyloid deposition without significant cognitive impairment among the elderly. Arch Neurol 65:1509–1517

Alavi A, Newberg AB, Souder E, Berlin JA (1993) Quantitative analysis of PET and MRI data in normal aging and Alzheimer's disease: atrophy weighted total brain metabolism and absolute whole brain metabolism as reliable discriminators. J Nucl Med 34:1681–1687

Albert M, Moss M (1996) Neuropsychology of aging: findings in humans and monkeys. In: Schneider E, Rowe JW (eds) Handbook of the biology of aging. Academic Press, San Diego, pp 217–233

Anderson JM, Hubbard BM, Coghill GR, Slidders W (1983) The effect of advanced old age on the neurone content of the cerebral cortex. Observations with an automatic image analyser point counting method. J Neurol Sci 58:235–246

Arrieta J, Artalejo F (1998) Methodology, results and quality of clinical trials of tacrine in the treatment of Alzheimer's disease: a systematic review of the literature. Age Ageing 27:161–179

Artero S, Tiemeier H, Prins ND, Sabatier R, Breteler MM, Ritchie K (2004) Neuroanatomical localisation and clinical correlates of white matter lesions in the elderly. J Neurol Neurosurg Psychiatry 75:1304–1308

Awad N, Gagnon M, Messier C (2004) The relationship between impaired glucose tolerance, type 2 diabetes, and cognitive function. J Clin Exp Neuropsychol 26:1044–1080

Bell RD, Zlokovic BV (2009) Neurovascular mechanisms and blood-brain barrier disorder in Alzheimer's disease. Acta Neuropathol 118:103–113

Bozzali M, Filippi M, Magnani G, Cercignani M, Franceschi M, Schiatti E, Castiglioni S, Mossini R, Falautano M, Scotti G, Comi G, Falini A (2006) The contribution of voxel-based morphometry in staging patients with mild cognitive impairment. Neurology 67:453–460

Braak H, Braak E (1997) Frequency of stages of Alzheimer-related lesions in different age categories. Neurobiol Aging 18:351–357

Broberg M, Pope KJ, Lewis T, Olsson T, Nilsson M, Willoughby JO (2008) Cell swelling precedes seizures induced by inhibition of astrocytic metabolism. Epilepsy Res 80:132–141

Buckner RL, Snyder AZ, Shannon BJ, LaRossa G, Sachs R, Fotenos AF, Sheline YI, Klunk WE, Mathis CA, Morris JC, Mintun MA (2005) Molecular, structural, and functional characterization of Alzheimer's disease: evidence for a relationship between default activity, amyloid, and memory. J Neurosci 25:7709–7717

Burgmans S, van Boxtel MP, Gronenschild EH, Vuurman EF, Hofman P, Uylings HB, Jolles J, Raz N (2010) Multiple indicators of age-related differences in cerebral white matter and the modifying effects of hypertension. Neuroimage 49:2083–2093

Burke SN, Barnes CA (2006) Neural plasticity in the ageing brain. Nat Rev Neurosci 7:30–40

Buzsaki G, Draguhn A (2004) Neuronal oscillations in cortical networks. Science 304:1926–1929

Cohen L, Jobert A, Le Bihan D, Dehaene S (2004) Distinct unimodal and multimodal regions for word processing in the left temporal cortex. Neuroimage 23:1256–1270

Coleman PD, Flood DG (1987) Neuron numbers and dendritic extent in normal aging and Alzheimer's disease. Neurobiol Aging 8:521–545

Cook IA, Leuchter AF, Morgan ML, Conlee EW, David S, Lufkin R, Babaie A, Dunkin JJ, O'Hara R, Simon S, Lightner A, Thomas S, Broumandi D, Badjatia N, Mickes L, Mody RK, Arora S, Zheng Z, Abrams M, Rosenberg-Thompson S (2002) Cognitive and physiologic correlates of subclinical structural brain disease in elderly healthy control subjects. Arch Neurol 59:1612–1620

De Groot JC, De Leeuw FE, Oudkerk M, Van Gijn J, Hofman A, Jolles J, Breteler MM (2002) Periventricular cerebral white matter lesions predict rate of cognitive decline. Ann Neurol 52:335–341

Debette S, Markus HS (2010) The clinical importance of white matter hyperintensities on brain magnetic resonance imaging: systematic review and meta-analysis. BMJ 341:c3666

DeCarli C, Miller BL, Swan GE, Reed T, Wolf PA, Garner J, Jack L, Carmelli D (1999) Predictors of brain morphology for the men of the NHLBI twin study. Stroke 30:529–536

DeCarli C, Miller BL, Swan GE, Reed T, Wolf PA, Carmelli D (2001) Cerebrovascular and brain morphologic correlates of mild cognitive impairment in the National Heart, Lung, and Blood Institute Twin Study. Arch Neurol 58:643–647

DeKosky ST, Scheff SW (1990) Synapse loss in frontal cortex biopsies in Alzheimer's disease: correlation with cognitive severity. Ann Neurol 27:457–464

Delano-Wood L, Stricker NH, Sorg SF, Nation DA, Jak AJ, Woods SP, Libon DJ, Delis DC, Frank LR, Bondi MW (2012) Posterior cingulum white matter disruption and its associations with verbal memory and stroke risk in mild cognitive impairment. J Alzheimers Dis 29:589–603

D'Esposito M, Deouell LY, Gazzaley A (2003) Alterations in the BOLD fMRI signal with ageing and disease: a challenge for neuroimaging. Nat Rev Neurosci 4:863–872

Dickerson BC, Sperling RA (2008) Functional abnormalities of the medial temporal lobe memory system in mild cognitive impairment and Alzheimer's disease: insights from functional MRI studies. Neuropsychologia 46:1624–1635

Dufouil C, de Kersaint-Gilly A, Besancon V, Levy C, Auffray E, Brunnereau L, Alperovitch A, Tzourio C (2001) Longitudinal study of blood pressure and white matter hyperintensities: the EVA MRI Cohort. Neurology 56:921–926

Elias PK, Elias MF, Robbins MA, Budge MM (2004) Blood pressure-related cognitive decline: does age make a difference? Hypertension 44:631–636

Engel AK, Konig P, Kreiter AK, Schillen TB, Singer W (1992) Temporal coding in the visual cortex: new vistas on integration in the nervous system. Trends Neurosci 15:218–226

Eschweiler GW, Leyhe T, Kloppel S, Hull M (2010) New developments in the diagnosis of dementia. Dtsch Arztebl Int 107:677–683

Esiri MM, Nagy Z, Smith MZ, Barnetson L, Smith AD (1999) Cerebrovascular disease and threshold for dementia in the early stages of Alzheimer's disease. Lancet 354:919–920

Farrall AJ, Wardlaw JM (2009) Blood-brain barrier: ageing and microvascular disease–systematic review and meta-analysis. Neurobiol Aging 30:337–352

Fernandez A, Maestu F, Amo C, Gil P, Fehr T, Wienbruch C, Rockstroh B, Elbert T, Ortiz T (2002) Focal temporoparietal slow activity in Alzheimer's disease revealed by magnetoencephalography. Biol Psychiatry 52:764–770

Filley CM (2005) Neurobehavioral aspects of cerebral white matter disorders. Psychiatr Clin North Am 28:685–700, 697–698

Forette F, Seux ML, Staessen JA, Thijs L, Babarskiene MR, Babeanu S, Bossini A, Fagard R, Gil-Extremera B, Laks T, Kobalava Z, Sarti C, Tuomilehto J, Vanhanen H, Webster J, Yodfat Y, Birkenhager WH (2002) The prevention of dementia with antihypertensive treatment: new evidence from the Systolic Hypertension in Europe (Syst-Eur) study. Arch Intern Med 162:2046–2052

Fries P (2005) A mechanism for cognitive dynamics: neuronal communication through neuronal coherence. Trends Cogn Sci 9:474–480

Greicius MD, Srivastava G, Reiss AL, Menon V (2004) Default-mode network activity distinguishes Alzheimer's disease from healthy aging: evidence from functional MRI. Proc Natl Acad Sci USA 101:4637–4642

Gunning-Dixon FM, Raz N (2000) The cognitive correlates of white matter abnormalities in normal aging: a quantitative review. Neuropsychology 14:224–232

Hamalainen M, Hari R, Ilmoniemi R, Knuutila J, Lounasmaa O (1993) Magnetoencephalography? Theory, instrumentation, and applications to noninvasive studies of the working human brain. Rev Mod Phys 65:413–497

Head D, Buckner RL, Shimony JS, Williams LE, Akbudak E, Conturo TE, McAvoy M, Morris JC, Snyder AZ (2004) Differential vulnerability of anterior white matter in nondemented aging with minimal acceleration in dementia of the Alzheimer type: evidence from diffusion tensor imaging. Cereb Cortex 14:410–423

Head D, Snyder AZ, Girton LE, Morris JC, Buckner RL (2005) Frontal-hippocampal double dissociation between normal aging and Alzheimer's disease. Cereb Cortex 15:732–739

Hedden T, Van Dijk KR, Becker JA, Mehta A, Sperling RA, Johnson KA, Buckner RL (2009) Disruption of functional connectivity in clinically normal older adults harboring amyloid burden. J Neurosci 29:12686–12694

Helzner EP, Luchsinger JA, Scarmeas N, Cosentino S, Brickman AM, Glymour MM, Stern Y (2009) Contribution of vascular risk factors to the progression in Alzheimer disease. Arch Neurol 66:343–348

Hof PR, Bierer LM, Perl DP, Delacourte A, Buee L, Bouras C, Morrison JH (1992) Evidence for early vulnerability of the medial and inferior aspects of the temporal lobe in an 82-year-old patient with preclinical signs of dementia. Regional and laminar distribution of neurofibrillary tangles and senile plaques. Arch Neurol 49:946–953

Honer WG, Dickson DW, Gleeson J, Davies P (1992) Regional synaptic pathology in Alzheimer's disease. Neurobiol Aging 13:375–382

Huttenlocher PR (1979) Synaptic density in human frontal cortex—developmental changes and effects of aging. Brain Res 163:195–205
Hyman BT, Van Hoesen GW, Damasio AR, Barnes CL (1984) Alzheimer's disease: cell-specific pathology isolates the hippocampal formation. Science 225:1168–1170
Iadecola C (2010) The overlap between neurodegenerative and vascular factors in the pathogenesis of dementia. Acta Neuropathol 120:287–296
Iannetti GD, Wise RG (2007) BOLD functional MRI in disease and pharmacological studies: room for improvement? Magn Reson Imaging 25:978–988
Inzitari D (2000) Age-related white matter changes and cognitive impairment. Ann Neurol 47:141–143
Jack CR Jr, Petersen RC, O'Brien PC, Tangalos EG (1992) MR-based hippocampal volumetry in the diagnosis of Alzheimer's disease. Neurology 42:183–188
Jack CR Jr, Petersen RC, Xu Y, O'Brien PC, Smith GE, Ivnik RJ, Tangalos EG, Kokmen E (1998) Rate of medial temporal lobe atrophy in typical aging and Alzheimer's disease. Neurology 51:993–999
Jack CR Jr, Petersen RC, Xu YC, O'Brien PC, Smith GE, Ivnik RJ, Boeve BF, Waring SC, Tangalos EG, Kokmen E (1999) Prediction of AD with MRI-based hippocampal volume in mild cognitive impairment. Neurology 52:1397–1403
Jack CR Jr, Lowe VJ, Weigand SD, Wiste HJ, Senjem ML, Knopman DS, Shiung MM, Gunter JL, Boeve BF, Kemp BJ, Weiner M, Petersen RC (2009) Serial PIB and MRI in normal, mild cognitive impairment and Alzheimer's disease: implications for sequence of pathological events in Alzheimer's disease. Brain 132:1355–1365
Jack CR Jr, Knopman DS, Jagust WJ, Shaw LM, Aisen PS, Weiner MW, Petersen RC, Trojanowski JQ (2010) Hypothetical model of dynamic biomarkers of the Alzheimer's pathological cascade. Lancet Neurol 9:119–128
Jeerakathil T, Wolf PA, Beiser A, Massaro J, Seshadri S, D'Agostino RB, DeCarli C (2004) Stroke risk profile predicts white matter hyperintensity volume: the Framingham Study. Stroke 35:1857–1861
Jellinger KA (2002) Alzheimer disease and cerebrovascular pathology: an update. J Neural Transm 109:813–836
Johnson NA, Jahng GH, Weiner MW, Miller BL, Chui HC, Jagust WJ, Gorno-Tempini ML, Schuff N (2005) Pattern of cerebral hypoperfusion in Alzheimer disease and mild cognitive impairment measured with arterial spin-labeling MR imaging: initial experience. Radiology 234:851–859
Kalaria RN, Ballard C (1999) Overlap between pathology of Alzheimer disease and vascular dementia. Alzheimer Dis Assoc Disord 13(Suppl 3):S115–S123
Katzman R (1986) Alzheimer's disease. N Engl J Med 314:964–973
Kemper T (1984) Neuroanatomical and neuropathological changes in normal aging and in dementia. In: Albert M (ed) Clinical neurology of aging. Oxford University Press, New York, pp 9–52
Kemper TL (1993) The relationship of cerebral cortical changes to nuclei in the brainstem. Neurobiol Aging 14:659–660
Kennedy KM, Raz N (2009) Pattern of normal age-related regional differences in white matter microstructure is modified by vascular risk. Brain Res 1297:41–56
Kesslak JP, Nalcioglu O, Cotman CW (1991) Quantification of magnetic resonance scans for hippocampal and parahippocampal atrophy in Alzheimer's disease. Neurology 41:51–54
Klunk WE, Engler H, Nordberg A, Wang Y, Blomqvist G, Holt DP, Bergstrom M, Savitcheva I, Huang GF, Estrada S, Ausen B, Debnath ML, Barletta J, Price JC, Sandell J, Lopresti BJ, Wall A, Koivisto P, Antoni G, Mathis CA, Langstrom B (2004) Imaging brain amyloid in Alzheimer's disease with Pittsburgh Compound-B. Ann Neurol 55:306–319
Kopell N, Ermentrout GB, Whittington MA, Traub RD (2000) Gamma rhythms and beta rhythms have different synchronization properties. Proc Natl Acad Sci USA 97:1867–1872
Kuo HK, Lipsitz LA (2004) Cerebral white matter changes and geriatric syndromes: is there a link? J Gerontol A Biol Sci Med Sci 59:818–826

Lakatos P, Shah AS, Knuth KH, Ulbert I, Karmos G, Schroeder CE (2005) An oscillatory hierarchy controlling neuronal excitability and stimulus processing in the auditory cortex. J Neurophysiol 94:1904–1911

Lee C, Lopez OL, Becker JT, Raji C, Dai W, Kuller LH, Gach HM (2009) Imaging cerebral blood flow in the cognitively normal aging brain with arterial spin labeling: implications for imaging of neurodegenerative disease. J Neuroimaging 19:344–352

Lisman JE, Idiart MA (1995) Storage of 7 ± 2 short-term memories in oscillatory subcycles. Science 267:1512–1515

Manschot SM, Brands AM, van der Grond J, Kessels RP, Algra A, Kappelle LJ, Biessels GJ (2006) Brain magnetic resonance imaging correlates of impaired cognition in patients with type 2 diabetes. Diabetes 55:1106–1113

Moscovitch M, Winocur G (1995) Frontal lobes, memory, and aging. Ann N Y Acad Sci 769:119–150

Murphy DG, DeCarli CD, Daly E, Gillette JA, McIntosh AR, Haxby JV, Teichberg D, Schapiro MB, Rapoport SI, Horwitz B (1993) Volumetric magnetic resonance imaging in men with dementia of the Alzheimer type: correlations with disease severity. Biol Psychiatry 34:612–621

Nordahl CW, Ranganath C, Yonelinas AP, Decarli C, Fletcher E, Jagust WJ (2006) White matter changes compromise prefrontal cortex function in healthy elderly individuals. J Cogn Neurosci 18:418–429

Oh H, Mormino EC, Madison C, Hayenga A, Smiljic A, Jagust WJ (2011) Beta-Amyloid affects frontal and posterior brain networks in normal aging. Neuroimage 54:1887−1895

Oosterman JM, Sergeant JA, Weinstein HC, Scherder EJ (2004) Timed executive functions and white matter in aging with and without cardiovascular risk factors. Rev Neurosci 15:439–462

Palop JJ, Chin J, Mucke L (2006) A network dysfunction perspective on neurodegenerative diseases. Nature 443:768–773

Pantoni L, Poggesi A, Inzitari D (2007) The relation between white-matter lesions and cognition. Curr Opin Neurol 20:390–397

Peters A, Rosene DL (2003) In aging, is it gray or white? J Comp Neurol 462:139–143

Peters A, Moss MB, Sethares C (2000) Effects of aging on myelinated nerve fibers in monkey primary visual cortex. J Comp Neurol 419:364–376

Petersen RC (2004) Mild cognitive impairment as a diagnostic entity. J Intern Med 256:183–194

Petersen RC, Parisi JE, Dickson DW, Johnson KA, Knopman DS, Boeve BF, Jicha GA, Ivnik RJ, Smith GE, Tangalos EG, Braak H, Kokmen E (2006) Neuropathologic features of amnestic mild cognitive impairment. Arch Neurol 63:665–672

Price JL, Morris JC (1999) Tangles and plaques in nondemented aging and "preclinical" Alzheimer's disease. Ann Neurol 45:358–368

Qiu C, Winblad B, Fratiglioni L (2005) The age-dependent relation of blood pressure to cognitive function and dementia. Lancet Neurol 4:487–499

Roelfsema PR, Engel AK, Konig P, Singer W (1997) Visuomotor integration is associated with zero time-lag synchronization among cortical areas. Nature 385:157–161

Rosene DL (1993) Comparing age-related changes in the basal forebrain and hippocampus of the rhesus monkey. Neurobiol Aging 14:669–670

Scheibel ME, Lindsay RD, Tomiyasu U, Scheibel AB (1975) Progressive dendritic changes in aging human cortex. Exp Neurol 47:392–403

Scheibel AB, Duong TH, Jacobs R (1989) Alzheimer's disease as a capillary dementia. Ann Med 21:103–107

Schmidt R, Schmidt H, Fazekas F (2000) Vascular risk factors in dementia. J Neurol 247:81–87

Schmidt R, Scheltens P, Erkinjuntti T, Pantoni L, Markus HS, Wallin A, Barkhof F, Fazekas F (2004) White matter lesion progression: a surrogate endpoint for trials in cerebral small-vessel disease. Neurology 63:139–144

Schneider JA, Bennett DA (2010) Where vascular meets neurodegenerative disease. Stroke 41:S144–S146

Seeley WW, Crawford RK, Zhou J, Miller BL, Greicius MD (2009) Neurodegenerative diseases target large-scale human brain networks. Neuron 62:42–52

Sheline YI, Raichle ME, Snyder AZ, Morris JC, Head D, Wang S, Mintun MA (2010) Amyloid plaques disrupt resting state default mode network connectivity in cognitively normal elderly. Biol Psychiatry 67:584–587

Singer W, Gray CM (1995) Visual feature integration and the temporal correlation hypothesis. Annu Rev Neurosci 18:555–586

Small GW (1998) The pathogenesis of Alzheimer's disease. J Clin Psychiatry 59(Suppl 9):7–14

Small G, Leiter F (1998) Neuroimaging for diagnosis of dementia. J Clin Psychiatry 59(Suppl 11):4–7

Smith CD, Chebrolu H, Wekstein DR, Schmitt FA, Jicha GA, Cooper G, Markesbery WR (2007) Brain structural alterations before mild cognitive impairment. Neurology 68:1268–1273

Steffens DC (1997) MRI and MRS in dementia. In: Krishnan KR, Doraiswamy PM (eds) Brain imaging in clinical psychiatry. Marcel Dekker Inc, New York, pp 503–532

Stern EA, Bacskai BJ, Hickey GA, Attenello FJ, Lombardo JA, Hyman BT (2004) Cortical synaptic integration in vivo is disrupted by amyloid-beta plaques. J Neurosci 24:4535–4540

Sykova E (2004) Extrasynaptic volume transmission and diffusion parameters of the extracellular space. Neuroscience 129:861–876

Taylor WD, MacFall JR, Provenzale JM, Payne ME, McQuoid DR, Steffens DC, Krishnan KR (2003) Serial MR imaging of volumes of hyperintense white matter lesions in elderly patients: correlation with vascular risk factors. AJR Am J Roentgenol 181:571–576

Terry RD, Masliah E, Salmon DP, Butters N, DeTeresa R, Hill R, Hansen LA, Katzman R (1991) Physical basis of cognitive alterations in Alzheimer's disease: synapse loss is the major correlate of cognitive impairment. Ann Neurol 30:572–580

Tisserand DJ, Jolles J (2003) On the involvement of prefrontal networks in cognitive ageing. Cortex 39:1107–1128

Tullberg M, Fletcher E, DeCarli C, Mungas D, Reed BR, Harvey DJ, Weiner MW, Chui HC, Jagust WJ (2004) White matter lesions impair frontal lobe function regardless of their location. Neurology 63:246–253

Uhlhaas PJ, Singer W (2010) Abnormal neural oscillations and synchrony in schizophrenia. Nat Rev Neurosci 11:100–113

Uhlhaas PJ, Roux F, Rodriguez E, Rotarska-Jagiela A, Singer W (2010) Neural synchrony and the development of cortical networks. Trends Cogn Sci 14:72–80

Van Hoesen G, Damasio A (1987) Neuronal correlates of cognitive impairment in Alzheimer's disease. In: Mountcastle V et al (eds) Handbook of physiology: the nervous system, vol V. American Physiological Society, Bethesda, pp 871–898

van Swieten JC, van den Hout JH, van Ketel BA, Hijdra A, Wokke JH van Gijn J (1991) Periventricular lesions in the white matter on magnetic resonance imaging in the elderly. A morphometric correlation with arteriolosclerosis and dilated perivascular spaces. Brain 114 (Pt 2):761–774

Voytko ML (1998) Nonhuman primates as models for aging and Alzheimer's disease. Lab Anim Sci 48:611–617

Walker LC (1997) Animal models of cerebral beta-amyloid angiopathy. Brain Res Brain Res Rev 25:70–84

Warsch JR, Wright CB (2010) The aging mind: vascular health in normal cognitive aging. J Am Geriatr Soc 58(Suppl 2):S319–S324

West RL (1996) An application of prefrontal cortex function theory to cognitive aging. Psychol Bull 120:272–292

Whitwell JL, Petersen RC, Negash S, Weigand SD, Kantarci K, Ivnik RJ, Knopman DS, Boeve BF, Smith GE, Jack CR Jr (2007) Patterns of atrophy differ among specific subtypes of mild cognitive impairment. Arch Neurol 64:1130–1138

Willott J (1997) Neurogerontology: the aging nervous system. In: Ferraro K (ed) Gerontology: perspectives and issues. Springer, New York, pp 68–96

Zhang HY, Wang SJ, Xing J, Liu B, Ma ZL, Yang M, Zhang ZJ, Teng GJ (2009) Detection of PCC functional connectivity characteristics in resting-state fMRI in mild Alzheimer's disease. Behav Brain Res 197:103–108

Zlokovic BV (2005) Neurovascular mechanisms of Alzheimer's neurodegeneration. Trends Neurosci 28:202–208

Zlokovic BV (2008) New therapeutic targets in the neurovascular pathway in Alzheimer's disease. Neurotherapeutics 5:409–414

Part V
Basic and Clinical Studies

MEG Auditory Research

Alexander Gutschalk

Abstract This chapter reviews auditory research performed with magnetoencephalography (MEG) in normal listeners, with an emphasis on the auditory cortex. The first section provides an overview of basic characteristics of auditory evoked fields and their classification. The second section reviews the relationship between a selection of basic auditory features—including lateralization, periodicity, and spectral content—and auditory evoked fields generated in auditory cortex. The final section highlights recent MEG research in the field of auditory scene analysis, focusing specifically on auditory stream segregation, selective attention, and informational masking.

Keywords Auditory cortex · Auditory evoked fields · Selective adaptation · Pitch · Sound lateralization · Vowel · Auditory scene analysis · Stream segregation · Selective attention · Informational masking · Perceptual awareness

1 Introduction

Acoustic signals unfold on a multitude of timescales, ranging from the sub-millisecond processes supporting sound localization to the multi-second intervals necessary for music perception and speech comprehension. Sounds impinging on the ear are transformed into a frequency-specific neural code in the cochlea. This neural code in the auditory nerve has a sub-millisecond temporal precision and can phase-lock to periodic sound waves up to 5,000 Hz (Young and Sachs 1979). Frequency specificity is maintained in the ascending auditory pathway up to the auditory cortex, with an orderly mapping of frequency that is called tonotopy.

A. Gutschalk (✉)
Department of Neurology, University of Heidelberg,
Im Neuenheimer Feld 400, 69120 Heidelberg, Germany
e-mail: Alexander.Gutschalk@med.uni-heidelberg.de

S. Supek and C. J. Aine (eds.), *Magnetoencephalography*,
DOI: 10.1007/978-3-642-33045-2_32, © Springer-Verlag Berlin Heidelberg 2014

While the ability to phase lock to the acoustic stimulus degrades along the ascending auditory pathway, some aspects of coding in human primary auditory cortex still maintain a millisecond precision and phase-locking capability up to at least 100 Hz (Brugge et al. 2009).

MEG is an excellent tool for studying the human auditory system for several reasons. First and foremost, MEG's temporal resolution matches the resolution with which the brain responds to sound. Second, owing to the situation of auditory cortex on the superior temporal plane, with dipole sources oriented primarily tangential to the head surface, MEG is particularly sensitive to activity generated there and can straight-forwardly discriminate activity arising from the left and right hemispheres. Third MEG acquisition is silent, a clear advantage when compared with modern fMRI acquisition sequences. The first auditory evoked response in MEG was published in the late 1970s (Reite et al. 1978). Using dipole source analysis, other early studies clearly demonstrated that these auditory-evoked fields were generated in the auditory cortex (Hari et al. 1980), and demonstrated tonotopy in the human auditory cortex (Romani et al. 1982). Today, more than 1,000 published studies of the auditory system have used MEG.

This review summarizes aspects of basic auditory neuroscience using MEG in healthy adult listeners. The chapter focuses on activity in the auditory cortex, with less focus on activity in other brain areas. The chapter starts in Sect. 2 with a classification of the different aspects of activity evoked by auditory stimuli as seen by MEG. Section 3 reviews the relationship between specific acoustic features and the MEG response, while Sect. 4 focuses on the perception of more complex auditory scenes. The selection of studies reviewed here is strongly biased towards studies using MEG because of the scope of this book; studies using EEG, a method very related to MEG, as well as intracranial EEG and fMRI studies, are mentioned only occasionally.

2 Classification of Auditory Evoked MEG Activity

The classification of auditory responses used in this chapter is primarily one that is based on the anatomical site of their generation, and as such is a view from source space. Three sites are dissociated: brainstem, auditory cortex, and multi-modal areas beyond auditory cortex. Most auditory studies using MEG have focused on auditory cortex, and therefore activity generated there comprises the largest part of this section. Traditionally, auditory evoked (magnetic) fields (AEF) have been subdivided into three latency ranges, in accordance with the classification of auditory evoked potentials (AEP) in EEG (Picton et al. 1974). In this chapter, the division of auditory evoked fields into early (up to 8 ms), middle (15–50 ms), and long-latency (>50 ms) ranges is introduced alongside the generator-based view. Still other types of activity are not covered by the latency classification, such as steady-state responses and induced activity (i.e., activity that is not precisely phase locked to

stimulus presentation). Each of these classifications has its own limitations, but some basic knowledge of how they have been used is helpful before discussing research that addresses questions of auditory neuroscience more specifically.

2.1 Brainstem

Occurring in the first 8 ms post stimulus onset, the early auditory-evoked field (EAEF) is also referred to as the auditory brainstem response (ABR). The ABR typically comprises five subsequent peaks, known as waves I–V. These components are small relative to either the ongoing MEG or later auditory evoked components, and therefore require large numbers of trials (thousands) in order to achieve an adequate signal to noise ratio. The typical stimuli used to evoke the ABR are clicks presented with inter-stimulus intervals (ISI) in the range of 50–100 ms. Waves I–V of the ABR have prominent spectral power in the range from 700 to 1,200 Hz. High sampling rates are therefore required to record the ABR and the low-pass filter should not be set below 1,000 Hz (better still 1,500 Hz). Highpass filters up to 200 Hz are typically used to suppress the low-frequency components of the later cortical responses that overlap the ABR because of the short ISI. There exist only a few published studies that have used MEG to study the ABR (Lütkenhöner et al. 2000; Parkkonen et al. 2009). These studies show that waves I–V can be recorded in MEG and that the estimated generators are consistent with their EEG counterparts (Scherg and von Cramon 1985). In brief, waves I and II are thought to be generated in the auditory nerve just beyond the cochlea, while wave V, with a latency of 5–6 ms post stimulus, is generated below the inferior colliculus, the obligatory auditory-midbrain nucleus, and probably reflects neuronal input to this structure.

2.2 Auditory Cortex

Both the middle- and long-latency AEF (MAEF and LAEF, respectively) are primarily generated in the auditory cortex (Fig. 1), and their separation at 50 ms is arbitrary. Historically, the MAEF peaks have been denoted with letters (e.g., N_am, P_am, N_bm, and P_bm), and the LAEF peaks with numbers (P_1m, N_1m, and P_2m). Alternatively, these peaks are labeled with their prototypical peak latency. In this nomenclature, the MAEF peaks are N19m, P30m, N40m and P50m; the LAEF peaks are known as P50m, N100m, and P200m. Denoting these peaks as negative (N) or positive (P) was originally in reference to the scalp vertex in EEG, but can be easily adopted with reference to the surface of the auditory cortex in MEG. The P50m has been considered both middle- (P_bm) and long-latency (P_1m), indicating one of the limitations of the latency-based nomenclature. Nevertheless, the dissociation of MAEF and LAEF is often useful and therefore these peaks will be introduced in separate paragraphs below.

2.2.1 Middle-Latency Auditory Evoked Fields

Most of the spectral energy of the early MAEF lies in the (lower) gamma band around 30–60 Hz, with a maximum around 40 Hz. For recording of the MAEF, the low-pass filter cutoff should therefore not be set below 100 Hz. A high-pass filter with cutoff frequencies in the range of 10–30 Hz is often used to suppress overlapping LAEF components (Fig. 2), because the typical ISI to record the MAEF is around 100–200 ms, and thus shorter than the LAEF. The most prominent peak of the MAEF is the P30m (Pelizzone 1987; Mäkelä et al. 1994; Pantev 1995). The preceding N19m is smaller, but has been consistently localized in Heschl's gyrus and close to the generator of the P30m (Hashimoto et al. 1995; Gutschalk et al. 1999; Rupp et al. 2002b; Parkkonen et al. 2009). It has been suggested that the N19m and the P30m share the same macroscopic generator in medial Heschl's gyrus, whereas the P50m is generated more lateral along Heschl's gyrus (Scherg et al. 1989; Yvert et al. 2001), a view that is supported by depth electrode recordings in patients with epilepsy (Liegeois-Chauvel et al. 1991; Liegeois-Chauvel et al. 1994).

With reference to microscopic anatomy, the sources of the N19m and P30m are in the auditory core area (Galaburda and Sanides 1980), most likely in the primary auditory cortex field A1. A less-likely alternative is that the N19m and the P30m are generated in the more medial core field CM (Hackett et al. 2001). The more lateral localization of the P50m would better match with a generator in the lateral core field R, but this is more speculative, and it is likely that other fields additionally contribute to the P_1m peak measured in MEG (Yvert et al. 2001). Laminar recordings of click-evoked activity in monkey A1 show a peak N8 that is generated in deep cortical layers (4 and 5), and a subsequent P24 which is generated predominantly in layer 3 (Steinschneider et al. 1992). One hypothesis is that human N19m is also generated by thalamocortical input into the granular layer 4.

2.2.2 Long-Latency Auditory Evoked Fields

Traditionally, the earliest peak of the LAEF is the P_1m, which has already been mentioned in the context of the MAEF. The earliest latency of the P_1m in response to pure-tone stimuli is typically in the range of 50 ms—hence P50m—(Pantev et al. 1996b). There is at least a second subcomponent of the P1 m with a peak latency around 70 ms (Yvert et al. 2001), and for clicks-train stimuli P_1m latencies around 60–80 ms are typically observed (Gutschalk et al. 2004a). One reason for P_1m variability is that the peak, especially when it is later than 50 ms, overlaps with the onset of the larger N_1m, which may reduce the P_1m amplitude and latency (Königs and Gutschalk 2012).

By far the most prominent peak of the AEF is the N_1m, which comprises a number of subcomponents (Näätänen and Picton 1987) whose specific features are reviewed in more detail below. Optimal recording of the N_1m requires an ISI of 500 ms or longer. The spectral content of the N_1m lies primarily in the theta band and the lower alpha band (approximately 3–10 Hz), such that low-pass filters

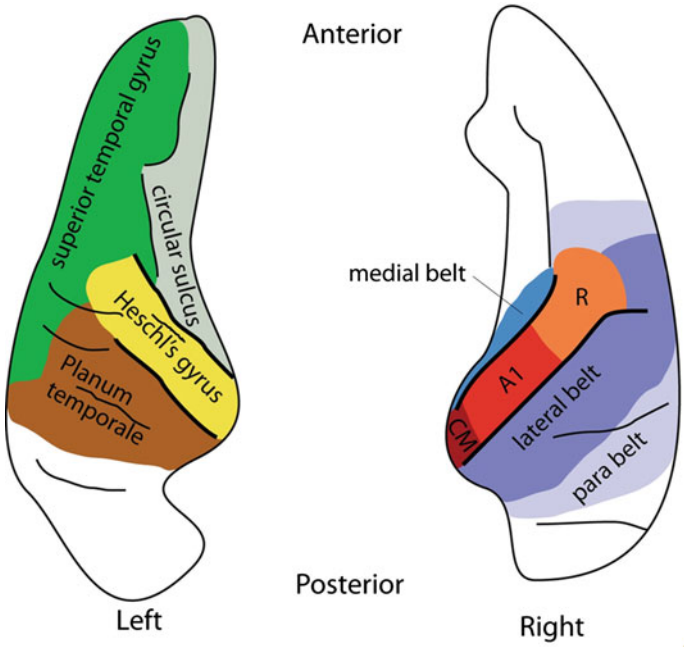

Fig. 1 Schematic of the human auditory cortex. The view is from the *top* on the superior temporal plane, which is buried inside the Sylvian fissure in the intact brain. The macroscopic anatomy is labeled on the *left*: Most lateral is the superior temporal gyrus (STG), most of whose surface extends to the lateral surface not seen in this view. Heschl's gyrus extends from postero-medial to anterior-lateral, where it meets the STG. The border between Heschl's gyrus and the STG is not sharply defined, and in some brains it appears as if the anterior STG is the continuation of Heschl's gyrus. Many subjects have more than one Heschl's gyrus, especially in the lateral part. The Planum temporale starts posterior from Heschl's gyrus and extends up to the temporo-parietal junction. There is no sharp border between the Planum temporale and the STG.A simplified schematic of histological auditory cortex fields is provided on the right: The core area (also primary auditory cortex, koniocortex, or Brodman Area 41) roughly coincides with the borders of Heschl's gyrus. Most anatomists subdivide the core region in at least two to three subregions. The nomenclature used here is adopted from the nomenclature used in the monkey (Hackett et al. 2001). The most medial field CM is not always considered a core field. The field A1 is often considered "primary auditory cortex" sensu stricto, but cannot be easily separated from the more lateral field R based on histology. These two fields have opponent tonotopic organizations (Formisano et al. 2003); in A1, high frequencies are localized postero-medially and low frequencies more antero-laterally, and vice versa in R, so that both fields share a common low-frequency border. An alternative nomenclature for the core fields is, from medial to lateral, Te1.1, Te1.0, and Te1.2 (Morosan et al. 2001). The lateral belt is located in the Planum temporale and extends to the lateral surface of the STG (Braak 1978). It can also be subdivided in at least two to three subfields oriented parallel to the core region, but there is only little information available from human anatomy (Rivier and Clarke 1997). Alternative names for areas that overlap with the lateral-belt definition are parakoniocortex, Brodman Area 42, or Te2 (Morosan et al. 2005). The anterior belt field is located in the circular sulcus, anterior from Heschl's gyrus. This area is also referred to as Prokoniokortex (Galaburda and Sanides 1980). The belt cortex is probably surrounded by the putative parabelt, which includes but may not be limited to Brodman Area 22 or Field Te3 (Morosan et al. 2005); these fields extend far into the lateral STG not seen on the view used here. Note that the different nomenclatures don't map on each other easily and that there is considerable inter-individual variability

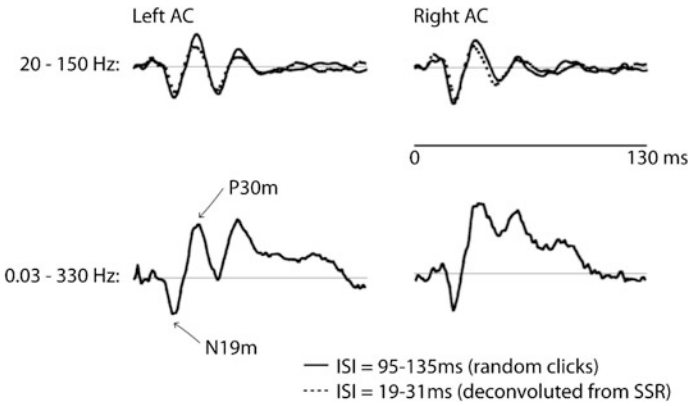

Fig. 2 Middle-latency auditory-evoked fields (MAEF). The data shown are source waveforms based on dipoles in medial Heschl's gyrus—supposedly in A1—averaged across six listeners. The stimuli were clicks presented with a randomized ISI in the range 95–135 ms (for the data plotted in solid lines). A comparison of two filter settings is shown for the upper (20–150 Hz) and lower (0.03–330 Hz) traces. As can be seen, the peaks N19m and P30m are clearly observed with both setting. The subsequent peaks N41m and P50m are elevated by a slower positivity; the latter is not clearly definable and because of the fast repetition rate might comprise a mixture of slower components. This positive shift has been removed by high-pass filtering in the upper traces. The dotted lines show the waveforms deconvolved from a steady-state response (SSR) with seven different rates (19–31 ms) in the same listeners. Note the high similarity between the early peaks and the traditionally obtained MAEF (Gutschalk et al. 1999)

down to 20 Hz cutoff frequency can usually be applied without any appreciable effect on component morphology (Fig. 3). High-pass filters are typically chosen in the range of 0.3–3 Hz, depending on the low-frequency noise level and whether later, slower components are also of interest.

The best-studied subcomponent of the N_1m, termed the N100m, peaks at a latency around 100 ms and is generated on the superior temporal plane (Hari et al. 1980). Based on co-registration with anatomical MRI, both Heschl's gyrus (Eulitz et al. 1995) and the planum temporale, just posterior to Heschl's gyrus (Lütkenhöner and Steinstrater 1998), are thought to be generators of this subcomponent. One important feature of the N100m is the large ISI range—up to 10 s—below which it will not reach its maximal amplitude (Hari et al. 1982; Pantev et al. 1993; Sams et al. 1993b; McEvoy et al. 1997). This effect is diminished for other N_1m subcomponents, which peak at slightly longer latencies (130–150 ms). One subcomponent was localized to the superior temporal gyrus (STG) (Lü et al. 1992), and might be identical to a radial N150 component described in EEG (Scherg and Von Cramon 1986). Another N_1m subcomponent has been consistently observed about 1 cm anterior to the main N100m peak and with a latency around 130 ms (Sams et al. 1993b; Loveless et al. 1996; McEvoy et al. 1997; Gutschalk et al. 1998). Note that the latencies of these N_1m subcomponent are not fixed but vary considerably with the onset and fine-structure of the stimuli used.

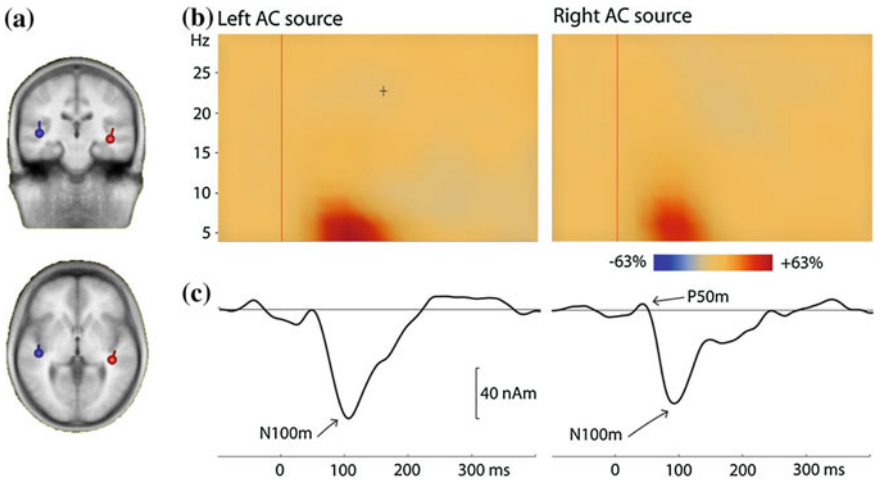

Fig. 3 Long-latency auditory-evoked fields (LAEF) from a single listener. The stimuli were 100-ms long pure tones with frequencies in the range 500–3,000 Hz, presented with a fixed ISI of 800 ms; frequency was randomly changed after 10 s. **a** Two dipoles were fitted to the averaged data in the time range 80–100 ms. **b** Time-frequency plots for the time range −100–400 ms and the frequency range 4–30 Hz. The plot shows the enhancement of power in comparison to the baseline in the time interval 100 ms before tone onset. Most of the signal power is in the theta band. **c** The averaged evoked response is shown for the same time range as the time-frequency analysis (low-pass filter = 30 Hz, no high-pass filter). The most prominent component is the N100m. These source waveforms as well as the time-frequency plots are based on the dipoles shown in (**a**)

The latency of the subsequent P_2m is around 150–250 ms (P200m). Sometimes the P_2m has been studied together with the N_1m by using a peak-to-peak measure. The few studies that specifically studied the P_2m found that the generator of the response is typically located anterior to the N100m (Hari et al. 1987; Pantev et al. 1996a).

For tones longer than about 50 ms, the P_2m is followed by a negative wave—the so-called sustained field—whose duration is directly linked to the stimulus duration. To obtain sustained fields, high-pass filters below 0.5 Hz or direct-coupled recordings should be used. The sustained field can be fitted by a dipole source that is typically located anterior to the N100m in auditory cortex (Hari et al. 1980; Hari et al. 1987; Pantev et al. 1994; Pantev et al. 1996a). Based on parametrical variation of sound features such as temporal regularity (see Sect. 3.4) or sound intensity, at least two subcomponents of the sustained field can be separated in lateral Heschl's gyrus and the planum temporale, similar to the N_1m subcomponents (Gutschalk et al. 2002). With respect to microscopic anatomy, the sources of the N_1m and the sustained field subcomponents are probably distributed across core and belt fields (Fig. 1).

Importantly, components of the N_1m are not only evoked at sound onset from silence, but by all kinds of changes within an ongoing sound (Mäkelä et al. 1988; Sams et al. 1993a). Finally, sounds that are played for a second or longer will also evoke an offset response. This offset response comprises mainly peaks N_1m and

P_2m, whose amplitude varies with sound duration like the onset peaks vary with the silent ISI (Hari et al. 1987; Pantev et al. 1996a).

2.2.3 Selective Adaptation and the Mismatch Negativity

As was briefly noted in the previous paragraph, the N_1m amplitude is determined in part by the ISI between the serial tones that are used to evoke the response (Hari et al. 1982; Imada et al. 1997). This observation is based on simple paradigms, where the same sound is repeated once or continuously. The response to each tone is reduced or adapted by the previous tone(s) of the sequence, and more so when the ISI is short. When two different tones are alternated instead, the adaptation of the N_1 depends additionally on how different these tones are from each other, as has been shown by several EEG studies (Butler 1968; Näätänen et al. 1988): when pure tones are used, the adaptation is strong when the frequencies of the two tones are near to each other; much less adaptation is observed when the tones are an octave or more apart. This phenomenon is referred to as *selective* or *stimulus-specific* adaptation. Selective adaptation is not limited to the N_1m, and has more recently been demonstrated for the P_1m (Gutschalk et al. 2005).

Another classical auditory stimulus paradigm that uses two tones dissociated by their tone frequency (or other features) is the auditory oddball paradigm (Näätänen et al. 1978). In contrast to the paradigm used to evaluate selective adaptation, the two tones are not simply alternated, but are presented at different probabilities. The more frequent tone is referred to as the standard, whereas the rare tone is referred to as the deviant. The ISI between subsequent tones is typically chosen around 300 ms, where the N_1m is almost completely suppressed. In this setting, a prominent negative response with peak latency around 130–200 ms is evoked by the rare deviants, but not by the frequent standard tones. This negative wave, called the mismatch negativity (MMN), is separated from other response components by subtracting the response to standards from the response to deviants. Many studies have examined the MMN and cannot be reviewed here in detail; extensive reviews on this component are already available (Garrido et al. 2009; May and Tiitinen 2010; Näätänen et al. 2011). Briefly, the MMN is not only evoked by differences in tone frequency, but by any sound difference between standard and deviant that is above the listener's threshold. Originally, the MMN was considered to be a component that is distinct from the other LAEF components reviewed in the previous section. However, this view has recently been challenged: a number of studies suggest that the MMN is identical to the anterior N_1m subcomponent, which is reduced in response to the standards but not in response to the deviants due to selective adaptation (May et al. 1999; Jääskeläinen et al. 2004; May and Tiitinen 2010). This view is supported by microelectrode studies in monkey, which suggest that—at least in A1—there is no evidence of an additional evoked component in the context of deviants presented in an oddball paradigm (Fishman and Steinschneider 2012). The associated debate of whether the MMN reflects (bottom-up) selective adaptation (May and Tiitinen 2010), or

(top-down) predictive coding (Garrido et al. 2009; Wacongne et al. 2012) is ongoing.

Finally, the MMN itself is not a single component with a stable topography, but comprises at least two subcomponents in the auditory cortex (Imada et al. 1993; Kretzschmar and Gutschalk 2010). Moreover, it has been suggested that the MMN receives contributions from generators in the frontal cortex (Schönwiesner et al. 2007). Second, a subsequent slow negativity that persists for 600 ms is additionally evoked by the oddball paradigm, which is also generated in the more anterior aspect of the auditory cortex along with the generator of the classical MMN (Kretzschmar and Gutschalk 2010).

2.2.4 Auditory Steady-State Responses

The auditory cortex is able to time-lock to periodic stimuli, a phenomenon that has been studied in particular at rates around 40 Hz (Romani et al. 1982; Mäkelä and Hari 1987) (Fig. 4). A periodic brain response that is imposed by a periodic stimulus is referred to as steady- state response (SSR) in EEG and MEG research. Steady-state responses require an evoked component whose inherent spectral power overlaps with the rate of the periodic repetition. As a result, the spectral representation of an SSR is a narrow band at the frequency of the periodic stimulus and sometimes its harmonics. Accordingly, a relationship between the 40-Hz SSR and the early MAEF peaks, whose spectral maximum is close to 40 Hz, was suggested early on (Galambos et al. 1981; Hari et al. 1989), and steady-state responses in the range of 30–50 Hz can be explained by assuming an identical response convolved with the periodic pulse train used as the stimulus. Conversely, when the underlying response is deconvolved on the basis of this assumption (Gutschalk et al. 1999), it shows high similarity with the early MAEF peaks recorded with a transient stimulus paradigm (Fig. 2). The main source of the 40-Hz SSR is in the medial half of Heschl's gyrus, and thus most likely in the primary area A1 (Fig. 1). This has been demonstrated by source analysis of MEG data (Pantev et al. 1996b; Gutschalk et al. 1999; Brookes et al. 2007), and was confirmed by intracranial recordings (Brugge et al. 2009) and fMRI (Steinmann and Gutschalk 2011). Note that other aspects of the 40-Hz SSR are not readily explained by ongoing, non-refractory MAEF activity. For example, the 40-Hz SSR shows a buildup of activity over about 250 ms before it reaches its constant amplitude (Ross et al. 2002), and this process starts over when, for example, a short sound in another frequency band is presented in parallel (Ross et al. 2005b). Potentially, these effects are related to secondary, more lateral generators of the 40-Hz SSR along Heschl's gyrus (Gutschalk et al. 1999) up to the superior temporal gyrus (Nourski et al. 2013).

Steady-state responses are not limited to the 40-Hz range: Higher frequency SSRs are observed in relationship to the ABR, known as the frequency following response, but this application has so far been limited to EEG research. In the lower frequency range, it has been demonstrated that SSRs power decreases with increasing modulation rate between 1.5 and 30 Hz (Wang et al. 2012); at the single

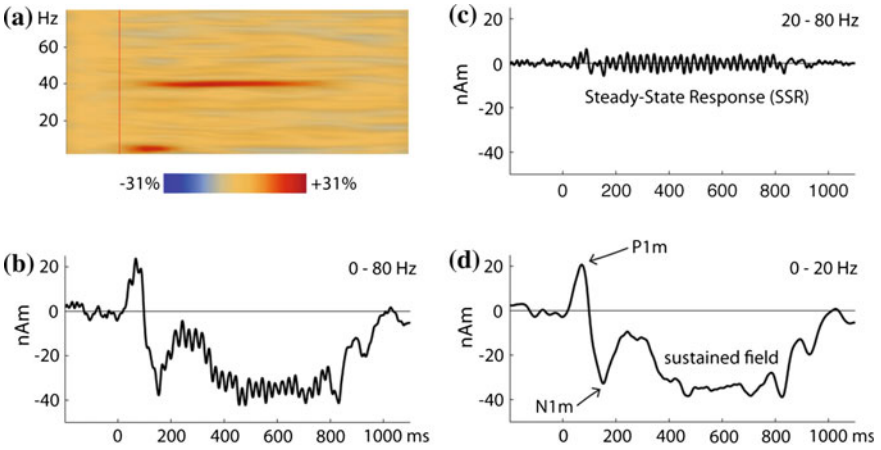

Fig. 4 Auditory 40-Hz steady-state response (SSR) from a single listener. The stimuli were 800-ms long trains of short tone pulses (500 Hz or 1,000 Hz) presented at a rate of 40 Hz. The waveforms are estimated for a dipolar source in the left auditory cortex; highly similar responses were observed on the right (not shown). **a** Time-frequency plots for the time range −200–1,100 ms and the frequency range 1–80 Hz. The plot shows the enhancement of power in comparison to the baseline in the time interval 200 ms before the train onset. The SSR is seen as narrow activity band at 40 Hz, which persists for the whole stimulus duration. The onset response is reflected by a transient increase of power in the theta band. **b** Source waveform for the averaged evoked response filtered from 0–80 Hz. In this setting, the LAEF and the SSR are mixed. Because of the broad frequency separation between these components demonstrated in A, they are separated well with different filter settings. **c** SSR in the frequency range 20–80 Hz, otherwise identical to B. **d** LAEF in the frequency range 0–20 Hz. Note the strong sustained field that is not captured by the time-frequency analysis

subject level, a reliable SSR was generally obtained at 1.5, 3.5, and 31.5 Hz, but only variably at 7.5 and 15.5 Hz stimulation rate. The apparently latency was in the range of 100–150 ms, and there was only a weak dependence on the bandwidth of the stimulus carrier. For an SSR at 4 Hz, it was independently demonstrated that the SSR is stronger for stimuli with a non-sinusoidal amplitude modulation and a more rapid sound onset (Prendergast et al. 2010).

2.2.5 Auditory Non-phase-locked Activity

Separating auditory evoked fields from the background activity by response averaging is based on the assumption that there is little or no jitter between subsequent trials. Stronger jitter may blur the shape of the evoked response in the lower frequency (theta) range. In the higher frequency (gamma) range, jitter may easily exceed the phase duration of a single cycle, such that the variable phase relationship between stimulus and response may results in a cancelation of the response by the averaging procedure. Similar response cancelation by averaging occurs for rhythmic activity that appears in a circumscribed time window but not

tightly locked to the auditory stimulus. Techniques other than response averaging are required to evaluate such non-phase-looked activity. One possibility is to perform time-frequency analysis on a single-trial level and remove phase information before summation across trials. The increase in response power is typically plotted relative to a pre-stimulus baseline (Figs. 3 and 4). This technique is equally sensitive for phase-locked and non-phase locked activity.

Traditionally, gamma activity in the auditory cortex has been evaluated in a narrow frequency band around 40 Hz (Pantev 1995). More recently, activity in the auditory cortex has been observed in a wide frequency range of 70–250 Hz: this high-gamma activity in human auditory cortex has been clearly demonstrated in intracranial recordings on the superior temporal gyrus (Crone et al. 2001; Edwards et al. 2005; Dykstra et al. 2011) as well as in medial Heschl's gyrus (Brugge et al. 2009). It has been suggested that high-gamma activity covaries more closely with spiking activity than with evoked potentials in the lower spectral range (Steinschneider et al. 2008; Ray and Maunsell 2011). Measuring gamma activity in the auditory cortex with MEG is more difficult than in the visual system (Kahlbrock et al. 2012; Millman et al. 2013). However, some recent MEG studies raise hope that high-gamma activity can indeed be evaluated non-invasively based on MEG recordings (Todorovic et al. 2011; Sedley et al. 2012).

2.3 Beyond the Auditory Cortex

While activity in the auditory cortex is modulated by active listening, as discussed in more detail in Sect. 4, all response components reviewed so far are readily recorded in a passive mode, where the subject is not attending to the auditory stimulation and may even be involved into reading a book, watching a silent movie, or another task unrelated to the auditory stimulation. Once a task is added that is directly related to the auditory stimulation, however, additional activity can be elicited, the generators of which are supposedly located in multimodal areas beyond the auditory cortex. The most-frequently-studied response elicited during auditory tasks is the P3 or P300. Sources of the P3 have been studied with depth electrodes in patients suffering from epilepsy (Halgren et al. 1998), and in combined EEG-fMRI studies (Linden 2005), suggesting, amongst others, generators in parietal, prefrontal, and cingulate cortex. So far, only a few MEG studies have explored the generators of the P_3m, suggesting mostly sources in the temporal and frontal lobes (Rogers et al. 1991; Anurova et al. 2005; Halgren et al. 2011). It remains to be determined, whether P3 generators in other sites are also accessible to MEG. Cortical activity related to auditory cognition beyond the auditory cortex is certainly not limited to the P3, but an extensive review of this topic is beyond the scope of this chapter. The near future will likely bring a wealth of new contributions on the functional relationship between the auditory cortex and areas in the frontal and parietal lobe for auditory cognition.

3 Stimulus Specificity of Auditory MEG Activity

This section reviews a selection of basic sound features and how they are reflected in MEG activity originating in the auditory cortex. Only a brief introduction to the background and psychophysics is provided along with each paragraph, and the reader is referred to the available textbooks on psychological acoustics (Moore 2012), phonetics (Stevens 2000), or auditory physiology (Schnupp et al. 2011) for more details and references to the original publications.

3.1 Temporal Resolution and Integration

Temporal coding of sound is differently reflected in the MAEF and LAEF. The early MAEF peaks are very robust to fast stimulus repetition: When two pulses are repeated at ISIs between 1–14 ms (Rupp et al. 2000), a clear response to the second pulse is observed at ISIs >= 4 ms, and the response is nearly completely recovered at ISIs >= 14 ms. The continuous time-locking capability of the MAEF is also demonstrated by the 40-Hz SSR (Gutschalk et al. 1999; Brugge et al. 2009), which shows phase-locking to inter-click intervals of less than 20 ms.

A classical psychoacoustic paradigm to test temporal resolution is gap detection, where a short interruption in an ongoing sound is used as the stimulus. For example, listeners are able to detect interruptions of few milliseconds duration in a continuous broadband noise. When this stimulus is applied in MEG, gaps as short as 3 ms are sufficient to evoke a significant MAEF response (Rupp et al. 2002a), which is in accordance with psychoacoustic thresholds. Moreover, the higher perceptual thresholds observed at the beginning of a noise burst (5 or 20 ms after onset) are paralleled by a lack of MAEF (Rupp et al. 2004).

The subsequent P_1m and N_1m are distinctly different with regard to their suppression at short ISI: when periodic click trains are interrupted by omission of one or more clicks, the onset response after the interruption does not show a significant P_1m when the interruption is 12 and 24 ms. At gap durations of 48 ms, the P_1m is partly recovered, and it has regained almost completely at gaps of 196 ms (Gutschalk et al. 2004b). The time interval required for complete recovery is even longer for the N_1m: Some recovery, especially of the anterior N_1m generator, is observed between 70–150 ms in a two-tone paradigm (Loveless et al. 1996). With ongoing stimulation, the N_1m is reliably observed at ISIs of 300 ms and more (Carver et al. 2002), but some reduction of the response is observed up to 5–10 s (see Sect. 2.2.2). Note that the N_1m can also be evoked by all sorts of transients and transitions in ongoing sound, and not only by sound onset. For example, short gaps of 6 ms in an ongoing noise produce not only a P30m, but also a prominent N_1m (Rupp et al. 2002a). This should not be mistaken as evidence that the N_1m shows similarly fine and fast time-locking as the P30m, but rather reflects the perceptual salience of the transient gap. In contrast to the N19m-P30m, the

N_1m may also reflect auditory events integrated over longer time intervals. Early studies suggested that the N_1m integrates over a time interval of approximately 30–50 ms (Joutsiniemi et al. 1989), because the response amplitude increases with the tone duration for intervals up to this length. More recent studies indicate that temporal integration at the level of the N_1m is not captured by a fixed time window and depends on parameters such as the onset dynamics (Biermann and Heil 2000) and temporal structure of the eliciting stimulus (Krumbholz et al. 2003).

3.2 Stimulus Lateralization

Spatial hearing in the horizontal plane is based on two main cues: one is the difference of sound intensity between the ears caused by the head shadow, the interaural level difference (ILD). The other is the timing difference between the ears, or interaural time difference (ITD). For humans, ITD is predominantly used for lower frequencies, whereas ILD is more important for higher frequencies. The relationship between perceived lateralization and the exact physical parameters is variable, depending on the shape and size of the head and ears. To produce spatial hearing perception, arrays of speakers grouped in some distance around the listener in an anechoic room are the gold standard. In MEG, insert earphones are typically used, in which case one relies on direct manipulation of ITD and ILD. Note, however, that this sound delivery produces somewhat non-ecological percepts of sound sources inside of the head. More exact perceptual lateralization with earphones can be achieved with head-related transfer functions, for which the exact physical parameters are measured with microphones placed at the position of the ears. The simplest method of sound lateralization with earphones is monaural presentation, which is again not an ecological stimulus for normal hearing subjects, but can be viewed as an extreme variant of ILD. Moreover, monaural presentation is easy to implement and has a long tradition in experimental psychology and audiology.

Important processing steps of binaural lateralization cues occur early in the brainstem, and are not readily accessible by MEG. Many MEG studies of sound lateralization have instead focused on its effect on the inter-hemispheric balance between the left and right auditory cortex. It was established early on that the N_1m evoked by monaural sounds is around 15–30 % larger for contralateral compared to isopilateral stimulation, and that the latency of the N_1m is 7–12 ms shorter for contralateral stimulation (Reite et al. 1981; Pantev et al. 1986; Mäkelä et al. 1993). For the P_1m, similar amplitude but smaller latency differences in the range of 1–5 ms were reported (Mäkelä et al. 1994). A stronger modulation of response amplitude in the range of 50 % for contra- in comparison to ipsilateral ear stimulation has been observed for the P30m at the sensor level (planar gradiometers), although the effect was smaller in dipole source waveforms (Mäkelä et al. 1994). However, an EEG source analysis study of the N19-P30 found only an amplitude lateralization in the

range of 6 % and no latency difference (Scherg and Von Cramon, 1986). Currently, little additional data is available to resolve this discrepancy.

ITDs around the maximal physiological range (700 μs) produce lateralization of N_1m-peak amplitudes that can be almost as strong as with monaural presentation (McEvoy et al. 1993; Gutschalk et al. 2012). Moreover, earlier N_1m latencies are observed in the auditory cortex contralateral to the perceptual lateralization (McEvoy et al. 1993). In contrast, no significant effect of ITD is observed for the P30m (McEvoy et al. 1994). Recent MEG studies on the coding of ITD in the auditory cortex support a model with a population rate code for opponent left and right channels, in accordance with earlier work in cat (Stecker et al. 2005), by demonstrating that selective adaptation of the N_1m depended more strongly on whether the adapter and probe were in the same hemifield than on the actual difference in azimuth (Salminen et al. 2009).

So far, the review of contralateral representation in the auditory cortex is simplified, because the balance of activity between the left and right auditory cortex is not symmetric for left- and right-ear stimulation. An amplitude bias towards the right hemisphere has been observed first for the N_1m (Mäkelä et al. 1993), but is even more prominent for the 40-Hz SSR and the sustained field (Ross et al. 2005a): lateralization by ear modulates these responses more strongly in the right AC, and as a result the hemispheric bias is strongly lateralized towards the right auditory cortex for left-ear stimulation and almost counterbalanced for right-ear stimulation (Ross et al. 2005a; Gutschalk et al. 2012). This lateralization bias is not limited to monaural presentation. For example, a combination of ILD and ITD cues, or the use of head-related transfer functions, produces stronger effects on N_1m lateralization than either cue alone (Palomaki et al. 2005), but most prominently in the right auditory cortex. Potentially, this right-hemisphere bias is related to a dominant role of the right hemisphere for spatial processing (Kaiser et al. 2000; Spierer et al. 2009). On the other hand, the bias towards the right may be limited to situations where stimuli are presented in quiet, whereas a lateralization bias towards the left has been observed when sounds are presented under perceptual competition (Okamoto et al. 2007a; Elhilali et al. 2009; Königs and Gutschalk 2012). Finally, the interpretation of hemispheric balance is complicated by anatomical asymmetry in the auditory cortex: stronger cortical folding in the left hemisphere produces stronger signal cancelation in left auditory cortex. The cancelation reduces the MEG signal over the left auditory cortex and biases the MEG response towards larger right-hemisphere responses when in fact equally strong generators can be assumed in both sides (Shaw et al. 2013).

3.3 Sound Frequency

The spectral content of sound is decomposed during sensory transformation in the cochlea, and the resulting tonotopic representation is maintained throughout the ascending auditory pathway, including the auditory cortex. The first demonstration

of a tonotopic map in human auditory cortex made use of MEG, applying dipole source analysis to 32-Hz SSRs evoked by amplitude-modulated pure tones (Romani et al. 1982). This study revealed that the source of the SSR is more medial for higher, and more lateral for lower tone frequencies. The direction of tonotopy, as well as the mapping of dipole locations on structural MRI (Pantev et al. 1996b), is in accordance with a generator of the 40-Hz SSR in the primary auditory cortex field A1. Tonotopy has also been studied for other response components. Studies of the N_1m (Pantev et al. 1988; Pantev et al. 1996b) and the sustained field (Pantev et al. 1994) revealed similar high-low frequency gradients from medial to lateral cortex, as was demonstrated for the SSR. However, it is likely that current source localization techniques are insufficient for modeling synchronous activity in multiple tonotopic fields of the auditory cortex. While the 40-Hz SSR is probably generated in an area focal enough to reflect only one tonotopic gradient, LAEF components are more likely generated in multiple regions of the auditory cortex.

Another reflection of stimulus frequency is by the peak latency of the AEF: because of the propagation delay in the cochlea, AEF latencies are shorter for higher compared to lower stimulus frequencies (Scherg et al. 1989; Roberts and Poeppel 1996). Chirp stimuli (frequency glides from low to high) have been designed to compensate for the propagation delay of the cochlea (Dau et al. 2000). The N19m-P30m evoked by such a chirp is larger than the response evoked by a click or a reversed chirp, because the chirp synchronizes the activity in high and low frequency channels (Dau et al. 2000; Rupp et al. 2002b).

Finally, MEG allows for studying the interaction between stimuli, depending on their frequency separation. One approach that has already been mentioned (Sect. 2.2.3), frequency-selective adaptation, reveals the frequency specificity of cortical processing by reduced adaptation between serial tones when the adapter and probe tones are different in frequency. Another involves tagging simultaneously-presented tones with different amplitude-modulation rates (John et al. 1998). Applying this technique to record the SSR at multiple amplitude-modulation rates around 40-Hz revealed a reduction of amplitude that is more broadly tuned than would have been predicted based on cochlea tuning (Ross et al. 2003). This interaction between simultaneous tones may persist for alternating tones presented at fast repetition rates (20–40 Hz): the alternation of two different tones produces a smaller SSR when the tones are separated by more than a critical band compared to the repetition of identical tone bursts (Gutschalk et al. 2009). Note that the latter finding is opposite to selective adaptation of the P_1m and N_1m, where stronger responses are observed for larger frequency separation between alternating tones. A potential source of the SSR reduction is lateral inhibition. However, a study that explored evidence of lateral inhibition in the auditory cortex found evidence for it only at the level of the N_1m, but not for the SSR (Pantev et al. 2004).

3.4 Pitch and Sound Regularity

Pitch perception is associated with periodic sounds, such as those typically produced by the human voice or musical instruments. In music, pitch is the basic perception required to form melodies. While pure tones evoke a unique pitch percept directly corresponding to their sound frequency, the situation is more complex for everyday periodic sounds in our environment. Briefly, two neural mechanisms supporting pitch perception have been proposed: temporal models that are based on phase-locked neural discharges, primarily in the auditory nerve and spectral-based models relying on distinct loci of maximal displacement of the basilar-membrane. While temporal models assume that pitch is extracted purely in the temporal domain, spectral models estimate pitch based on regular spacing of basilar-membrane maxima from a periodic stimulus' harmonic structure. Many present-day models rely on both spectral and temporal sound features.

One approach to study pitch specificity is to compare regular, periodic sounds with irregular, non-periodic sounds that are otherwise matched in their spectral and temporal envelope. For example, regular click trains are associated with a salient pitch; this pitch can be reduced when the interval between successive clicks is jittered, to the degree that the pitch perception is even completely suppressed (Gutschalk et al. 2002): Regular click trains evoke a much more prominent sustained field than irregular click trains, and source analysis shows that the sustained field evoked by irregular click trains is best explained by dipoles in the planum temporale. Assuming that the components of the sustained field evoked by irregular click trains are also evoked by regular click trains, the pitch-specific component of the sustained field can be separated by calculating the difference between the responses evoked by regular and irregular click trains. This pitch-specific difference response is best explained by dipoles in lateral Heschl's gyrus. In addition to the anatomical separation, these two sources reveal a functional double dissociation: Manipulation of sound intensity predominantly modulates sustained activity in the more posterior source in planum temporale. Conversely, manipulation of click-train regularity predominantly modulates activity in the more anterior source in Heschl's gyrus (Fig. 5).

Another stimulus used to study pitch is so-called iterated rippled noise (Yost et al. 1996); here, a noise is repeatedly copied to itself with a fixed time delay, which equals the inverse of the fundamental frequency (f_0). At the transition from a matched noise to an iterated rippled noise stimulus, a prominent N_1m-like response is evoked, whose peak latency is longer for lower f_0 (Krumbholz et al. 2003); this response has been referred to as the pitch-onset response (POR). The same transient response is evoked at the transition from irregular to regular click trains (Gutschalk et al. 2004a), at the onset of a binaural (Huggins) pitch (Chait et al. 2006), or at the transition between different types of IRN (Ritter et al. 2005). The source of the pitch-onset N_1m is also located in lateral Heschl's gyrus, whereas the sound-onset N_1m observed for irregular click trains or noise maps to the planum temporale. This dissociation is similar to the source configuration of the sustained field, mentioned

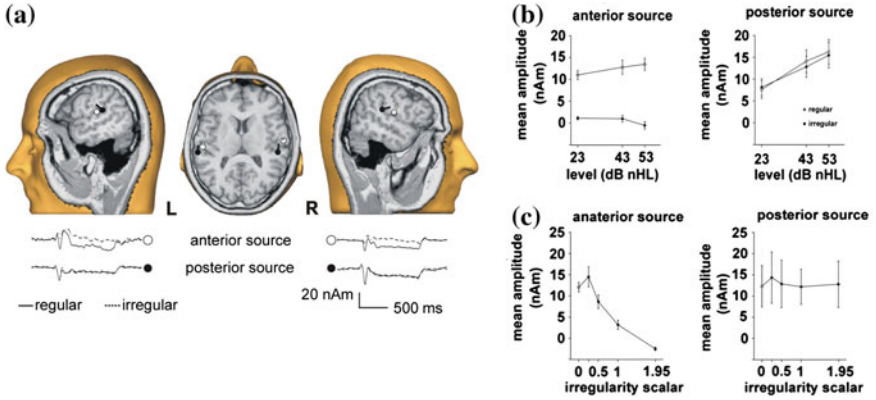

Fig. 5 **a** Influence of click-train regularity—and supposedly pitch salience—on the sustained field and N_1m (exemplary listener). The 1000-ms long click trains were either regular (inter-click interval 5 ms) or irregular (inter-click interval 2.5–7.5 ms); only the regular click trains produce a salient periodicity pitch. One set of dipoles was fitted to the sustained field evoked by irregular click trains (*black*, in Planum temporale). The other set of dipoles was fitted to the difference between the sustained fields evoked by regular minus irregular click trains (*white*, in lateral Heschl's gyrus), supposedly representing pitch- or regularity-specific activity. As can be seen in the source waveforms, the N_1m and sustained field imaged by the anterior source are only observed for regular click trains, whereas the N_1m and sustained field in the posterior source are identical for regular and irregular click trains. **b** Effect of click train intensity on the sustained-field strength in the anterior (*left*) and posterior (*right*) sources (mean ± standard error, N = 12). Intensity only affects activity in the posterior source significantly. **c** Effect of click train regularity (ISI range = 5 ms ± 5 ms * irregularity scalar) on the sustained-field strength in the anterior (*left*) and posterior (*right*) sources (mean ± standard error, N = 11). Regularity only affects activity in the anterior source significantly. Panels A and B reproduced with permission from Elsevier (Gutschalk et al. 2002); panel C represents unpublished data obtained in the same listeners

earlier. Moreover, spatio-temporal dipole modeling allows for separating the pitch-onset and sound-onset components of the N_1m in situations where the periodic sound is presented out of silence (Gutschalk et al. 2004a). Both, the pitch-onset N_1m as well as the sustained pitch response reflect the stimulus history. The amplitude of the pitch-onset N_1m increases with the directly preceding ISI; the sustained field varies depending on the ratio of regular and irregular stimuli occurring in a stimulus sequence on a time scale of seconds to minutes (Gutschalk et al. 2007b).

Specificity for pitch in lateral Heschl's gyrus had also been suggested based on fMRI (Patterson et al. 2002), but this has recently been questioned because it was shown that the fMRI signal evoked by iterated rippled noise is dominated by the presence of temporal fluctuations that are unrelated to pitch (Barker et al. 2012). Note, that these fluctuations evoke ongoing activity in the theta-band in MEG, whereas the N_1m and sustained field components evoked by periodicity are similar for click trains and iterated rippled noise (Steinmann and Gutschalk 2012).

As a final note, it should be mentioned that the interpretation of these regularity-specific responses in terms of pitch perception might be too exclusive.

A number of studies suggest that these responses could also be related to a more general processing of stimulus regularity: a prominent N_1m is, for example, evoked at the transition from random tones (duration = 15, 30 or 60 ms) to a constant tone, whereas a much weaker response was observed when the transition was from constant to random (Chait et al. 2007). With respect to the sustained field, it was demonstrated that the periodic repetition of frozen noise evokes stronger sustained fields than random white noise down to repetition rates of 5 Hz (Keceli et al. 2012), which is well below the lower limit where musical pitch is typically observed (Pressnitzer et al. 2001).

3.5 Vowels and Other Speech Sounds

Vowels are one of the basic elements of speech, and their classification for speech is determined by formants, which are basically peaks in certain parts of the spectrum. The spectral shape of the human voice in general, and thus also of vowels, is formed by the upper vocal tract. MEG studies demonstrated that the N_1m evoked by vowel onset cannot be explained by a linear superposition of their frequency content (Diesch and Luce 2000). It has been suggested instead that the source localization and latency of the N_1m represent abstract phonological features such as place of articulation (Obleser et al. 2004).

As mentioned in Sect. 3.4, the human voice is a prototype of a periodic sound source, due to the periodic pulsations of the vocal folds during voiced speech. Speech periodicity may be disturbed, for example in whispering, or in hoarse, pathological speech, and in this case the sustained field is reduced (Yrttiaho et al. 2009). However, the sustained field does not only reflect the vowels' periodicity, but is also enhanced by spectral formant features that determine the phonological vowel quality: This was first shown with the comparison of pure tones and sine vowels (Eulitz et al. 1995). Using damped sine pulses, the periodicity pitch and the vowels formant structure can be separately violated, producing sounds that have periodicity pitch and/or vowel quality or neither. This way, the sustained field components evoked by pitch, formant structure, and the control sound can be separately evaluated. The source-analysis results showed that the sustained field evoked by the periodicity pitch and the one evoked by the formant structure are co-located in lateral Heschl's gyrus, whereas the residual sustained field was located more posterior (Gutschalk and Uppenkamp 2011). This result raises the possibility that lateral Heschl's gyrus plays a general role in speech sound extraction, or is alternatively related to a more general mechanism of regularity extraction (see Sect. 3.4). This question is of considerable interest, because fMRI studies typically do not find enhanced activity in auditory cortex for speech in contrast to non-speech sounds; for example, the same vowel and non-vowels stimuli evaluated in fMRI evoke enhanced activity only in the superior temporal sulcus (Uppenkamp et al. 2006). This discrepancy between MEG and fMRI can probably be explained by the

finding that sustained fields in MEG have only a weak (Gutschalk et al. 2010) or no (Steinmann and Gutschalk 2012) correlate at all in BOLD fMRI.

Vowels are only one category of speech-specific (phonetic) elements. Topographical differences between N_1m responses have also been found for different consonants, which depended not only on the physical sound's structure but also on its intelligibility (Obleser et al. 2006). In summary, findings accumulated with MEG and other techniques indicate that the transformation of sound into basic speech-specific (phonological) categories starts in the auditory cortex on the superior temporal plane, and it remains to be determined how much of this process is already completed there.

4 Auditory Scene Analysis

Most of the studies reviewed so far explored the processing of sounds emanating sequentially from a single source. This is not the most frequent constellation in ecological environments, where multiple sounds sources are often active interleaved or at once. The title of the seminal monograph "auditory scene analysis" (Bregman 1990) provides the heading for research that explores how the brain separates multiple sound sources. The subsequent sounds emanating from one source, for example the speech from one person, or the melody played on a musical instrument, are herein referred to as auditory streams. Auditory streams are of similar importance for auditory cognitive neurosciences as the conception of objects for the visual neurosciences.

4.1 Auditory Stream Segregation

One of the basic and most commonly used paradigms to study auditory scene analysis is the stream-segregation or streaming paradigm. In the simplest version of this paradigm, two pure tones *A* and *B* are alternated (*ABAB*...) at a rate of around 5–10 Hz with the frequency separation Δf. When Δf is small (up to a few semitones), the sequence is heard as a stream of alternating tones, a trill (Miller and Heise 1950). The streaming phenomenon is observed at larger Δf: here, *A* and *B* tones are perceived as two separate streams, each with its own beat and rhythm. This can be well demonstrated with the *ABA*_ triplet paradigm (Van Noorden 1975), where the underscore stands for a pause whose duration is equal to the tones. When the triplets are heard as one stream, they are associated with a characteristic galloping rhythm. In contrast, two isochronous streams are perceived in the case of streaming. When *ABA*_ tone triplets are presented in MEG, the response strength of *B* tones depend on the Δf (Gutschalk et al. 2005): the P_1m is strongly suppressed by the preceding *A* tone when the tones are close in frequency. For $\Delta f = 4$–6 semitones, there is less adaptation (or suppression) caused by the *A* tones, and the P_1 m evoked at $\Delta f = 12$

semitones is almost the size of the P_1m evoked by *B* tones in the absence of any *A* tones (Fig. 6). This effect is similar to the selective-adaptation phenomenon discussed in Sect. 2.2.3 for the N_1m. In fact, selective adaptation of the N_1m was also observed, but for the fast repetition rates typically used for streaming, the N_1m remains relatively small overall. Importantly, selective adaptation of the response in auditory cortex was correlated with the listeners rating of how easy it was for them to hold to the two-stream perception, suggesting that the selective adaption observed in MEG is linked to neurophysiological processes important for streaming perception. Similar results were obtained by other investigators (Snyder et al. 2006; Chakalov et al. 2012).

Selective adaptation of the P_1m in streaming contexts is not limited to situations where Δf is the segregation cue. Selective release of P_1m adaptation has also been observed when streaming was based on periodicity pitch, using stimuli that were prepared such that they did not provide spectral cues that can be resolved by frequency analysis in the cochlea (Gutschalk et al. 2007a). Finally, selective release of P_1m adaptation was observed with streaming based on lateralization by ITD and was stronger for conditions where streaming was more frequently observed (Carl and Gutschalk 2013). In both cases, for streaming based on pitch and based on ITD, the sources of selective adaption are located in the same area around Heschl's gyrus including core as well as belt areas of the auditory cortex (Schadwinkel and Gutschalk 2010). It therefore appears that the separation of sound sources based on different segregation cues converges at the level of the auditory cortex, potentially providing a general mechanism for sound source separation.

A more direct way to study the relationship between neurophysiology and perception is based on perceptual bistability. The relationship between for example Δf and streaming perception is not deterministic; the same sequence can alternatively be perceived as one or two streams, especially in the intermediate Δf range (Van Noorden 1975), and the perception may flip back and forth between the two perceptual organizations. When listeners indicate the reversal towards one stream with one key, and the reversal towards two streams with another key, the MEG activity evoked by an ongoing sequence with fixed Δf can be averaged with respect to the perception. The results show that the response evoked by the *B* tones is stronger in intervals where listeners heard two streams compared to intervals where they heard one stream (Gutschalk et al. 2005). This result is similar to the growth of the P_1m evoked by *B* tones with larger Δf, albeit the effect size in the bistability experiment was smaller than in the Δf experiment.

4.2 Auditory Selective Attention

Two separate streams of tones are also presented in another classical paradigm, but with a different focus: the ISI between subsequent tones is randomized and one stream is presented to the left and another one to the right ear. Within each stream

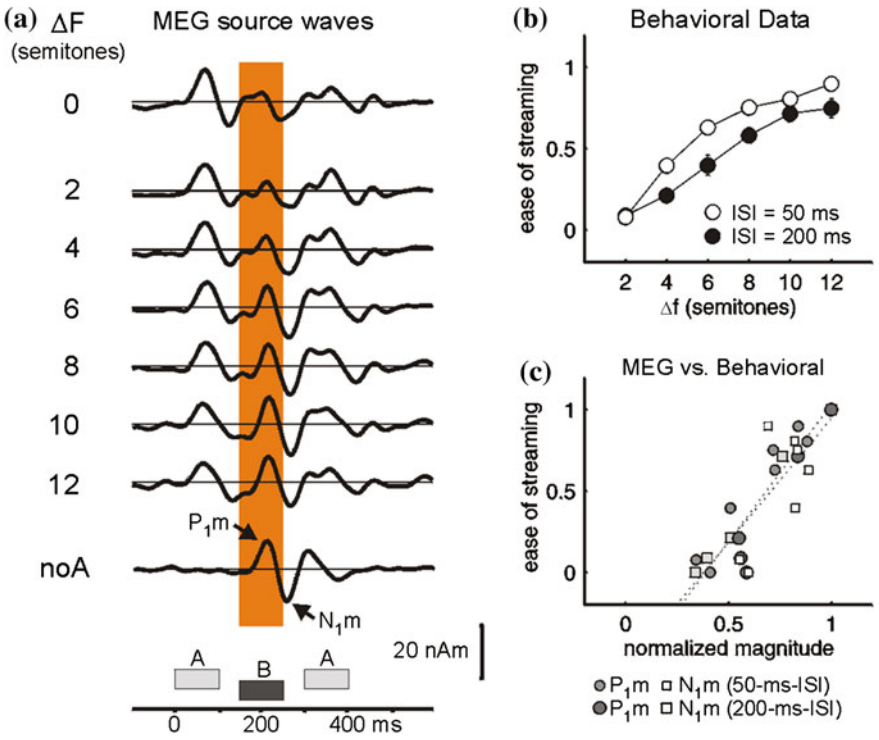

Fig. 6 Relationship between streaming perception and frequency selective adaptation of the P_1m and N_1m (modified from Gutschalk et al. 2005). **a** Auditory cortex source waveforms of the response evoked by sequences of repetitive *ABA_* triplets (average across listeners; n = 14). The frequency (Δf) difference between *A* and *B* is indicated on the *left*. The P_1m and N_1m evoked by *B* tones are strongly suppressed for Δf = 0 and 2 semitones, which were not perceived as two streams. There is a marked release of this adaptation for Δf = 4 semitones and beyond, which can be perceived as one or two streams. At Δf = 10 semitones, the amplitude of the response is almost the same size as the response evoked by *B* tones without any interfering *A* tones. **b** Ease of streaming for the sequences used in panel a and similar sequences with a longer ISI (n = 13). Listeners tried to hear two streams and indicated after the end of the sequence how easy it was to hear two streams on a continuous scale between 0 and 1 (0 = impossible, 1 = very easy). **c** Scatter plot of the average, normalized MEG amplitudes (P_1m and N_1m) versus the average ease of streaming. The correlation was r = 0.91 ($p < 0.0001$) for the P_1m and r = 0.83 ($p < 0.001$) for the N_1m

there are standards and deviants, like in the oddball paradigm introduced in Sect. 2.2.3, and the listeners task is to monitor the occurrence of deviants in only one of the two streams. This paradigm has not been used to study if one or two streams are perceived—the latter was rather implicitly assumed by the setup—but to evaluate how selectively listening to one of the streams modulates the auditory evoked activity. An early EEG study demonstrated that the N_1 is prominently

larger for the tones (standards as well as deviants) in the ear that the listener attended to (Hillyard et al. 1973). Later on, it was demonstrated in MEG that the attentional enhancement of vertex-negative responses originates in the auditory cortex (Rif et al. 1991; Woldorff et al. 1993). One of these studies (Rif et al. 1991) used a setup where the two streams were not separated by ear, but only by their frequency (1,000 vs. 3,000 Hz). The enhancement of surface-negative activity in the auditory cortex was observed in the time interval of the N_1m, or alternatively in the latency range of the P_2m when a longer ISI was used (Rif et al. 1991). There has been some discussion of whether the enhanced negative response evoked by attended streams reflects enhancement of the N_1m or a separate response component called the processing negativity (Näätänen 1982) or the late negative difference wave (Hansen and Hillyard 1980). In any case, there is no doubt that auditory cortex activity in the N_1m latency range can be enhanced by selectively listening to one stream in certain stimulus configurations.

It is less well settled whether attention also modulates response components that are associated with earlier processing stages, such as the P_1m and the 40-Hz SSR. In the P_1m interval, one study found that the response in this interval was more negative with attention, supposedly reflecting the early onset of N_1m enhancement (Rif et al. 1991). Two other studies found an enhanced positive response in the time interval 20–50 ms (Woldorff et al. 1993; Poghosyan and Ioannides 2008), potentially reflecting enhancement of processes related to the P_1m. A few reports also suggest that the 40 Hz SSR is modulated by intra-modal auditory versus visual attention (Ross et al. 2004; Saupe et al. 2009). However, the effect size of attentional amplitude enhancement for the 40-Hz SSR is generally small, and it has been pointed out that the effect is much stronger for the N_1m and the sustained field (Okamoto et al. 2011). One intracranial study suggests that the 20-Hz SSR is modulated when one of two concurrent amplitude-modulated tones is selectively attended (Bidet-Caulet et al. 2007). A recent dichotic MEG study found that the 40-Hz SSR in right auditory cortex was reduced for attended targets in the ispilateral, right ear, and non-significantly enhanced for attended targets in the contralateral, left ear (Weisz et al. 2012). In summary, these studies suggest that the 40 Hz SSR in primary auditory cortex can be modulated by attention in certain contexts, but that the effect size of the attentional modulation is small in comparison to the response amplitude, as well as compared to the modulation observed at later processing stages.

Response enhancement by selective attention is not limited to simple tone stimuli, but can also be observed for more complex sounds, for example when two competing speakers are played to the left and right ear, and the listeners are instructed to report the information from one ear only. This classical dichotic paradigm (Cherry 1953), typically cited in the context of the cocktail party phenomenon, was recently adapted for MEG with an elegant analysis method: instead of averaging from tone onset, Ding and Simon extracted the envelope of each speaker and deconvolved the time course of activity in the auditory cortex using crosscorrelation between the signal envelope and the MEG time series (Ding and Simon, 2012b). The results revealed a response similar to the classical evoked

response with peaks P1 m and N_1m. Moreover, when the listeners selectively listened to one of the speakers, the associated N_1m like response was prominently enhanced. This effect is not limited to the dichotic paradigm, but was also observed when two speakers, for example a male and a female, were presented to both ears without spatial separation, and the listeners were instructed to selectively listen to one of the speakers (Ding and Simon 2012a).

One model for the selective response enhancement observed for attended streams is a simple gain model, which assumes that the response to the attended signal is enhanced. However, the response modulation in the auditory cortex by attention may be more selective. For example, it has been shown that selectively attending to a spatial cue modulates activity in more posterior areas of the auditory cortex, whereas attention to phonetic content predominantly modulates activity in more anterior areas of the auditory cortex (Ahveninen et al. 2006). It has also been suggested that attention towards a tone sharpens the spectral tuning in auditory cortex: When a pure tone is presented in a notch-filtered noise, the attentional enhancement is larger for narrow than for broader notches (Okamoto et al. 2007b), and no response enhancement is observed for tones presented without a concurrent masker (Ahveninen et al. 2011). The authors of the study suggested that this is because the notched noise adapts the broadly tuned activity evoked by pure tones in the absence of attention, but not the sharpened, more focal activation when the tone is attended to.

Directing attention involves a number of areas outside the auditory cortex, such as the frontal eye fields and the temporo-parietal junction (Larson and Lee 2012), as well as more dorsal parietal areas (Sieroka et al. 2003). The exact role of each of these areas is still being explored, and is not reviewed here in detail.

4.3 Auditory Perceptual Awareness

The streaming and attention paradigms reviewed above are typically designed such that the presence of each stream is easily noted, even though smaller details or changes of the target stream may sometimes be missed because of interference from the competing streams. Thus, listeners are typically able to deploy their attention towards a specific stream without major efforts. The situation may be different when more complex soundscapes are used, where multiple streams compete for the listeners processing capacity, such that the listener is not aware of each stream's presence at a time. This phenomenon is known as informational masking (Durlach et al. 2003). In contrast to energetic masking, where two sounds that overlap in their spectrum compete for sensory transformation in the cochlea, informational masking is thought to originate in the central nervous system. To avoid additional energetic masking, a spectral separation between target and masker (the protected region) is typically used. Accordingly, once a stream has been detected in the presence of an informational masker, the perception of the stream is salient, because the target tones are clearly above the sensory threshold.

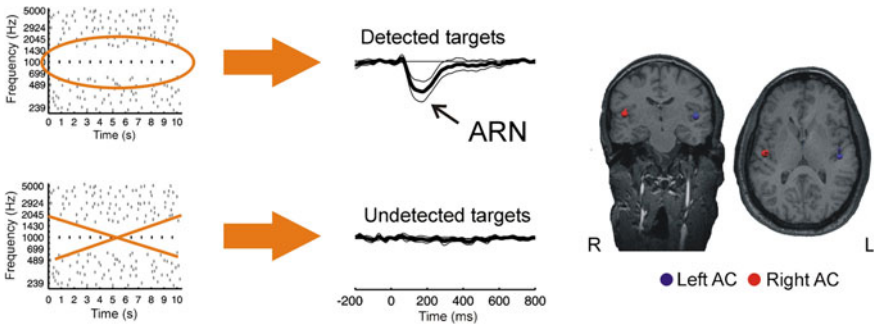

Fig. 7 Relationship between auditory perceptual awareness versus informational masking and MEG activity in the auditory cortex. Streams of target tones are presented for 10.4 s with a stimulus-onset asynchrony of 800 ms and in the context of a random multi-tone masker. The target-tone frequency was randomly chosen for each 10 s sequence (range 489–2924 Hz). Listeners indicated with a mouse button when they detected a regular target stream. Considering that at least two tones were heard before each button press, about half of the target tones were heard and the other half was masked. When the response time locked to target tones was averaged, no significant evoked response was observed for undetected targets (*lower trace*). In contrast, detected targets evoked a prominent negative response in auditory cortex in the time interval 50–250 ms, the awareness related negativity (ARN). Example stimuli are available along with the original, open access online publication (Gutschalk et al. 2008)

An informational masking stimulus that has been adapted for MEG research is illustrated in Fig. 7 (Gutschalk et al. 2008): the target is a regular tone stream, with fixed frequency and ISI. The masker comprises multiple tones, which are arranged in several frequency bands and whose ISI is independently randomized. This type of masker is called a multi tone masker; the randomization of the masker onsets was introduced for application in MEG, to cancel out responses that are phase locked to masker tones, and be able to evaluate selectively the neural response evoked by targets. Because the target frequency varied in subsequent trials, listeners cannot simply monitor a fixed frequency region, but need to listen (search) for the regular target stream. Listeners were instructed to press a mouse button whenever they heard out the regular target stream, and these behavioral responses were used to dissociate epochs where the listeners were aware of the target stream, and those where they were not aware of the target's presence. MEG revealed a prominent negative response in the auditory cortex in the latency range 50–250 ms, with apeak latency around 120–200 ms after tone onset. No late negativity was evoked by target tones in epochs where listeners were not aware of their presence.

In contrast, the 40 Hz SSR (Gutschalk et al. 2008) and the P_1m (Königs and Gutschalk 2012) were evoked by detected and undetected target tones alike. Moreover, the results from an fMRI and MEG study show that stronger activity for detected compared to undetected targets is observed in medial Heschl's gyrus, and thus most probably in the primary auditory cortex (Wiegand and Gutschalk 2012). These results suggest that there is a coexistence of two types of neural activity in the (primary)

auditory cortex: one type (40 Hz SSR) is more closely related to the physical stimulus and the other type (ARN) reflects the perception rather than the sound input.

The source location of the ARN was not statistically different from the N_1m evoked passively when the targets were presented in silence in one study (Gutschalk et al. 2008) and only about 5 mm apart in another study (Königs and Gutschalk 2012). Moreover, the hemispheric balance of both, the ARN and the N_1m, is modulated to similar amounts by sound lateralization (Königs and Gutschalk 2012). It is therefore possible, that the generators of the ARN and N_1m are—at least in part—identical. As has been noted in the previous sections, the N_1m is an automatic response and shows little or no modulation by attention in situations where tones are presented without competing auditory stimuli e.g. (Ahveninen et al. 2011). In contrast, the ARN is not evoked at all when attention is distracted to a different task, e.g. in a dichotic paradigm (Gutschalk et al. 2008). Another study that applied informational masking in MEG found that the SSR evoked by a 4 Hz target stream was enhanced when listeners detected frequency deviants within that stream, but not when they detected a temporal elongation of tones within the multi-tone masker (Elhilali et al. 2009).

While a clear attentional modulation of the N_1m is already observed, for example, when one of two interleaved streams is selectively attended (Rif et al. 1991) or when an attended tone is presented within a simultaneous noise masker (Okamoto et al. 2007b), the N_1m is still evoked automatically by the unattended stream in these cases, and the listener is typically aware of the unattended stream's presence. One explanation for these different observations could be that processes reflected by the N_1m/ARN are only modulated by attention under sensory competition (Desimone and Duncan 1995; Lavie 2006), and that at high levels of sensory competition the reduction of these neural processes is so prominent that they are insufficient for perceptual awareness. The latter case would then produce informational masking. At this point, we don't know if informational masking can already be overcome by bottom-up activity in the auditory cortex, or if the deployment of attentional resources directed by the frontal lobe is additionally required. The relative role of modality specific sensory cortex on the one hand, and activity in prefrontal areas for perceptual awareness, on the other hand, is still diversely discussed across sensory modalities (Dehaene & Changeux 2011; Meyer 2011), and remains an important topic for future research.

Acknowledgements The author is grateful to Andrew Dykstra for many helpful comments and suggestions on the manuscript. Supported by Bundesministerium für Bildung and Forschung (BMBF, grant 01EV0712).

References

Ahveninen J, Hämäläinen M, Jääskeläinen IP, Ahlfors SP, Huang S, Lin FH, Raij T, Sams M, Vasios CE, Belliveau JW (2011) Attention—driven auditory cortex short—term plasticity helps segregate relevant sounds from noise. Proc Nat Acad Sci USA 108:4182–4187

Ahveninen J, Jääskeläinen IP, Raij T, Bonmassar G, Devore S, Hämäläinen M, Levanen S, Lin FH, Sams M, Shinn-Cunningham BG, Witzel T, Belliveau JW (2006) Task-modulated "what" and "where" pathways in human auditory cortex. Proc Nat Acad Sci USA 103:14608–14613

Anurova I, Artchakov D, Korvenoja A, Ilmoniemi RJ, Aronen HJ, Carlson S (2005) Cortical generators of slow evoked responses elicited by spatial and nonspatial auditory working memory tasks. Clin Neurophysiol 116:1644–1654

Barker D, Plack CJ, Hall DA (2012) Reexamining the evidence for a pitch-sensitive region: a human fMRI study using iterated ripple noise. Cereb Cortex 22:745–753

Bidet-Caulet A, Fischer C, Besle J, Aguera PE, Giard MH, Bertrand O (2007) Effects of selective attention on the electrophysiological representation of concurrent sounds in the human auditory cortex. J Neurosci 27:9252–9261

Biermann S, Heil P (2000) Parallels between timing of onset responses of single neurons in cat and of evoked magnetic fields in human auditory cortex. J Neurophysiol 84:2426–2439

Braak H (1978) The pigment architecture of the human temporal lobe. Anat embryol (Berlin) 154:213–240

Bregman AS (1990) Auditory scene analysis. MIT Press, Cambridge

Brookes MJ, Stevenson CM, Barnes GR, Hillebrand A, Simpson MI, Francis ST, Morris PG (2007) Beamformer reconstruction of correlated sources using a modified source model. Neuroimage 34:1454–1465

Brugge JF, Nourski KV, Oya H, Reale RA, Kawasaki H, Steinschneider M, Howard MA 3rd (2009) Coding of repetitive transients by auditory cortex on Heschl's gyrus. J Neurophysiol 102:2358–2374

Butler RA (1968) Effect of changes in stimulus frequency and intensity on habituation of the human vertex potential. J Acoust Soc Am 44:945–950

Carl D, Gutschalk A (2013) Role of pattern, regularity, and silent intervals in auditory stream segregation based on inter-aural time differences. Exp Brain Res 224:557–570

Carver FW, Fuchs A, Jantzen KJ, Kelso JA (2002) Spatiotemporal analysis of the neuromagnetic response to rhythmic auditory stimulation: rate dependence and transient to steady-state transition. Clin Neurophysiol 113:1921–1931

Chait M, Poeppel D, de Cheveigne A, Simon JZ (2007) Processing asymmetry of transitions between order and disorder in human auditory cortex. J Neurosci 27:5207–5214

Chait M, Poeppel D, Simon JZ (2006) Neural response correlates of detection of monaurally and binaurally created pitches in humans. Cereb Cortex 16:835–848

Chakalov I, Draganova R, Wollbrink A, Preissl H, Pantev C (2012) Modulations of neural activity in auditory streaming caused by spectral and temporal alternation in subsequent stimuli: a magneto encephalographic study. BMC Neuroscience 13:72

Cherry C (1953) Some experiments on the recognition of speech, with one and two ears. J Acoust Soc Am 25:975–981

Crone NE, Boatman D, Gordon B, Hao L (2001) Induced electrocorticographic gamma activity during auditory perception. Clin Neurophysiol 112:565–582

Dau T, Wegner O, Mellert V, Kollmeier B (2000) Auditory brainstem responses with optimized chirp signals compensating basilar-membrane dispersion. J Acoust Soc Am 107:1530–1540

Dehaene S, Changeux JP (2011) Experimental and theoretical approaches to conscious processing. Neuron 70:200–227

Desimone R, Duncan J (1995) Neural mechanisms of selective visual attention. Annu Rev Neurosci 18:193–222

Diesch E, Luce T (2000) Topographic and temporal indices of vowel spectral envelope extraction in the human auditory cortex. J Cogn Neurosci 12:878–893
Ding N, Simon JZ (2012a) Emergence of neural encoding of auditory objects while listening to competing speakers. Proc Nat Acad Sci USA 109:11854–11859
Ding N, Simon JZ (2012b) Neural coding of continuous speech in auditory cortex during monaural and dichotic listening. J Neurophysiol 107:78–89
Durlach NI, Mason CR, Kidd G Jr, Arbogast TL, Colburn HS, Shinn-Cunningham BG (2003) Note on informational masking. J Acoust Soc Am 113:2984–2987
Dykstra AR, Halgren E, Thesen T, Carlson CE, Doyle W, Madsen JR, Eskandar EN, Cash SS (2011) Widespread brain areas engaged during a classical auditory streaming task revealed by intracranial EEG. Front Hum Neurosci 5:74
Edwards E, Soltani M, Deouell LY, Berger MS, Knight RT (2005) High gamma activity in response to deviant auditory stimuli recorded directly from human cortex. J Neurophysiol 94:4269–4280
Elhilali M, Xiang J, Shamma SA, Simon JZ (2009) Interaction between attention and bottom-up saliency mediates the representation of foreground and background in an auditory scene. PLoS Biol 7:e1000129
Eulitz C, Diesch E, Pantev C, Hampson S, Elbert T (1995) Magnetic and electric brain activity evoked by the processing of tone and vowel stimuli. J Neurosci 15:2748–2755
Fishman YI, Steinschneider M (2012) Searching for the mismatch negativity in primary auditory cortex of the awake monkey: deviance detection or stimulus specific adaptation? J Neurosci 32:15747–15758
Formisano E, Kim DS, Di Salle F, van de Moortele PF, Ugurbil K, Goebel R (2003) Mirror-symmetric tonotopic maps in human primary auditory cortex. Neuron 40:859–869
Galaburda A, Sanides F (1980) Cytoarchitectonic organization of the human auditory cortex. J Compar Neurol 190:597–610
Galambos R, Makeig S, Talmachoff PJ (1981) A 40-Hz auditory potential recorded from the human scalp. Proc Nat Acad Sci USA 78:2643–2647
Garrido MI, Kilner JM, Stephan KE, Friston KJ (2009) The mismatch negativity: a review of underlying mechanisms. Clin Neurophysiol 120:453–463
Gutschalk A, Brandt T, Bartsch A, Jansen C (2012) Comparison of auditory deficits associated with neglect and auditory cortex lesions. Neuropsychologia 50:926–938
Gutschalk A, Hämäläinen MS, Melcher JR (2010) BOLD responses in human auditory cortex are more closely related to transient MEG responses than to sustained ones. J Neurophysiol 103:2015–2026
Gutschalk A, Mase R, Roth R, Ille N, Rupp A, Hähnel S, Picton TW, Scherg M (1999) Deconvolution of 40 Hz steady-state fields reveals two overlapping source activities of the human auditory cortex. Clin Neurophysiol 110:856–868
Gutschalk A, Micheyl C, Melcher JR, Rupp A, Scherg M, Oxenham AJ (2005) Neuromagnetic correlates of streaming in human auditory cortex. J Neurosci 25:5382–5388
Gutschalk A, Micheyl C, Oxenham AJ (2008) Neural correlates of auditory perceptual awareness under informational masking. PLoS Biol 6:e138
Gutschalk A, Oldermann K, Rupp A (2009) Rate perception and the auditory 40-Hz steady-state fields evoked by two-tone sequences. Hear Res 257:83–92
Gutschalk A, Oxenham AJ, Micheyl C, Wilson EC, Melcher JR (2007a) Human cortical activity during streaming without spectral cues suggests a general neural substrate for auditory stream segregation. J Neurosci 27:13074–13081
Gutschalk A, Patterson RD, Rupp A, Uppenkamp S, Scherg M (2002) Sustained magnetic fields reveal separate sites for sound level and temporal regularity in human auditory cortex. Neuroimage 15:207–216
Gutschalk A, Patterson RD, Scherg M, Uppenkamp S, Rupp A (2004a) Temporal dynamics of pitch in human auditory cortex. Neuroimage 22:755–766
Gutschalk A, Patterson RD, Scherg M, Uppenkamp S, Rupp A (2007b) The effect of temporal context on the sustained pitch response in human auditory cortex. Cereb Cortex 17:552–561

Gutschalk A, Patterson RD, Uppenkamp S, Scherg M, Rupp A (2004b) Recovery and refractoriness of auditory evoked fields after gaps in click trains. Eur J Neurosci 20:3141–3147
Gutschalk A, Scherg M, Picton TW, Mase R, Roth R, Ille N, Klenk A, Hähnel S (1998) Multiple source components of middle and late latency auditory evoked fields. In: Kakigi R, Hashimoto I (eds) Recent advances in human neurophysiology. Elsevier, Amsterdam, pp 270–278
Gutschalk A, Uppenkamp S (2011) Sustained responses for pitch and vowels map to similar sites in human auditory cortex. Neuroimage 56:1578–1587
Hackett TA, Preuss TM, Kaas JH (2001) Architectonic identification of the core region in auditory cortex of macaques, chimpanzees, and humans. J Compar Neurol 441:197–222
Halgren E, Marinkovic K, Chauvel P (1998) Generators of the late cognitive potentials in auditory and visual oddball tasks. Electroencephalogr Clin Neurophysiol 106:156–164
Halgren E, Sherfey J, Irimia A, Dale AM, Marinkovic K (2011) Sequential temporo-fronto-temporal activation during monitoring of the auditory environment for temporal patterns. Hum Brain Mapp 32:1260–1276
Hansen JC, Hillyard SA (1980) Endogenous brain potentials associated with selective auditory attention. Electroencephalogr Clin Neurophysiol 49:277–290
Hari R, Aittoniemi K, Jarvinen ML, Katila T, Varpula T (1980) Auditory evoked transient and sustained magnetic fields of the human brain. Localization of neural generators. Exp Brain Res 40:237–240
Hari R, Hämäläinen M, Joutsiniemi SL (1989) Neuromagnetic steady-state responses to auditory stimuli. J Acoust Soc Am 86:1033–1039
Hari R, Kaila K, Katila T, Tuomisto T, Varpula T (1982) Interstimulus interval dependence of the auditory vertex response and its magnetic counterpart: implications for their neural generation. Electroencephalogr Clin Neurophysiol 54:561–569
Hari R, Pelizzone M, Mäkelä JP, Hallstrom J, Leinonen L, Lounasmaa OV (1987) Neuromagnetic responses of the human auditory cortex to on- and offsets of noise bursts. Audiology 26:31–43
Hashimoto I, Mashiko T, Yoshikawa K, Mizuta T, Imada T, Hayashi M (1995) Neuromagnetic measurements of the human primary auditory response. Electroencephalogr Clin Neurophysiol 96:348–356
Hillyard SA, Hink RF, Schwent VL, Picton TW (1973) Electrical signs of selective attention in the human brain. Science 182:177–180
Imada T, Hari R, Loveless N, McEvoy L, Sams M (1993) Determinants of the auditory mismatch response. Electroencephalogr Clin Neurophysiol 87:144–153
Imada T, Watanabe M, Mashiko T, Kawakatsu M, Kotani M (1997) The silent period between sounds has a stronger effect than the interstimulus interval on auditory evoked magnetic fields. Electroencephalogr Clin Neurophysiol 102:37–45
Jääskeläinen IP, Ahveninen J, Bonmassar G, Dale AM, Ilmoniemi RJ, Levanen S, Lin FH, May P, Melcher J, Stufflebeam S, Tiitinen H, Belliveau JW (2004) Human posterior auditory cortex gates novel sounds to consciousness. Proc Nat Acad Sci USA 101:6809–6814
John MS, Lins OG, Boucher BL, Picton TW (1998) Multiple auditory steady-state responses (MASTER): stimulus and recording parameters. Audiology 37:59–82
Joutsiniemi SL, Hari R, Vilkman V (1989) Cerebral magnetic responses to noise bursts and pauses of different durations. Audiology 28:325–333
Kahlbrock N, Butz M, May ES, Schnitzler A (2012) Sustained gamma band synchronization in early visual areas reflects the level of selective attention. Neuroimage 59:673–681
Kaiser J, Lutzenberger W, Preissl H, Ackermann H, Birbaumer N (2000) Right-hemisphere dominance for the processing of sound-source lateralization. J Neurosci 20:6631–6639
Keceli S, Inui K, Okamoto H, Otsuru N, Kakigi R (2012) Auditory sustained field responses to periodic noise. BMC Neuroscience 13:7
Königs L, Gutschalk A (2012) Functional lateralization in auditory cortex under informational masking and in silence. Eur J Neurosci 36:3283–3290
Kretzschmar B, Gutschalk A (2010) A sustained deviance response evoked by the auditory oddball paradigm. Clin Neurophysiol 121:524–532

Krumbholz K, Patterson RD, Seither-Preisler A, Lammertmann C, Lütkenhoner B (2003) Neuromagnetic evidence for a pitch processing center in Heschl's gyrus. Cereb Cortex 13:765–772

Larson E, Lee AK (2012) The cortical dynamics underlying effective switching of auditory spatial attention. Neuroimage 64:365–370

Lavie N (2006) The role of perceptual load in visual awareness. Brain Res 1080:91–100

Liegeois-Chauvel C, Musolino A, Badier JM, Marquis P, Chauvel P (1994) Evoked potentials recorded from the auditory cortex in man: evaluation and topography of the middle latency components. Electroencephalogr Clin Neurophysiol 92:204–214

Liegeois-Chauvel C, Musolino A, Chauvel P (1991) Localization of the primary auditory area in man. Brain 114(Pt 1A):139–151

Linden DE (2005) The p300: where in the brain is it produced and what does it tell us? Neuroscientist 11:563–576

Loveless N, Levanen S, Jousmaki V, Sams M, Hari R (1996) Temporal integration in auditory sensory memory: neuromagnetic evidence. Electroencephalogr Clin Neurophysiol 100:220–228

Lü ZL, Williamson SJ, Kaufman L (1992) Human auditory primary and association cortex have differing lifetimes for activation traces. Brain Res 572:236–241

Lütkenhöner B, Lammertmann C, Ross B, Pantev C (2000) Brain stem auditory evoked fields in response to clicks. NeuroReport 11:913–918

Lütkenhöner B, Steinstrater O (1998) High-precision neuromagnetic study of the functional organization of the human auditory cortex. Audiol Neurootology 3:191–213

Mäkelä JP, Ahonen A, Hämäläinen M, Hari R, Ilmoniemi R, Kajola M, Knuutila J, Lounasmaa OV, McEvoy L, Salmelin R, Salonen O, Sams M, Simola J, Tesche C, Vasama JP (1993) Functional differences between auditory cortices of the two hemispheres revealed by whole-head neuromagnetic recordings. Hum Brain Mapp 1:48–56

Mäkelä JP, Hämäläinen M, Hari R, McEvoy L (1994) Whole-head mapping of middle-latency auditory evoked magnetic fields. Electroencephalogr Clin Neurophysiol 92:414–421

Mäkelä JP, Hari R (1987) Evidence for cortical origin of the 40 Hz auditory evoked response in man. Electroencephalogr Clin Neurophysiol 66:539–546

Mäkelä JP, Hari R, Leinonen L (1988) Magnetic responses of the human auditory cortex to noise/square wave transitions. Electroencephalogr Clin Neurophysiol 69:423–430

May P, Tiitinen H, Ilmoniemi RJ, Nyman G, Taylor JG, Näätänen R (1999) Frequency change detection in human auditory cortex. J Comput Neurosci 6:99–120

May PJ, Tiitinen H (2010) Mismatch negativity (MMN), the deviance-elicited auditory deflection, explained. Psychophysiology 47:66–122

McEvoy L, Hari R, Imada T, Sams M (1993) Human auditory cortical mechanisms of sound lateralization: II. Interaural time differences at sound onset. Hear Res 67:98–109

McEvoy L, Levanen S, Loveless N (1997) Temporal characteristics of auditory sensory memory: neuromagnetic evidence. Psychophysiology 34:308–316

McEvoy L, Mäkelä JP, Hämäläinen M, Hari R (1994) Effect of interaural time differences on middle-latency and late auditory evoked magnetic fields. Hear Res 78:249–257

Meyer K (2011) Primary sensory cortices, top-down projections and conscious experience. Prog Neurobiol 94:408–417

Miller GA, Heise GA (1950) The trill threshold. J Acoust Soc Am 22:637–638

Millman RE, Prendergast G, Hymers M, Green GG (2013) Representations of the temporal envelope of sounds in human auditory cortex: Can the results from invasive intracortical "depth" electrode recordings be replicated using non-invasive MEG "virtual electrodes"? Neuroimage 64:185–196

Moore BCJ (2012) An introduction to the psychology of hearing. Emerald, Bingley

Morosan P, Rademacher J, Schleicher A, Amunts K, Schormann T, Zilles K (2001) Human primary auditory cortex: cytoarchitectonic subdivisions and mapping into a spatial reference system. Neuroimage 13:684–701

Morosan P, Schleicher A, Amunts K, Zilles K (2005) Multimodal architectonic mapping of human superior temporal gyrus. Anat embryol (Berlin) 210:401–406

Näätänen R (1982) Processing negativity: an evoked-potential reflection of selective attention. Psychol Bull 92:605–640
Näätänen R, Gaillard AW, Mantysalo S (1978) Early selective-attention effect on evoked potential reinterpreted. Acta Psychologica (Amsterdam) 42:313–329
Näätänen R, Kujala T, Winkler I (2011) Auditory processing that leads to conscious perception: a unique window to central auditory processing opened by the mismatch negativity and related responses. Psychophysiology 48:4–22
Näätänen R, Picton T (1987) The N1 wave of the human electric and magnetic response to sound: a review and an analysis of the component structure. Psychophysiology 24:375–425
Näätänen R, Sams M, Alho K, Paavilainen P, Reinikainen K, Sokolov EN (1988) Frequency and location specificity of the human vertex N1 wave. Electroencephalogr Clin Neurophysiol 69:523–531
Nourski KV, Brugge JF, Reale RA, Kovach CK, Oya H, Kawasaki H, Jenison RL, Howard MA 3rd (2013) Coding of repetitive transients by auditory cortex on posterolateral superior temporal gyrus in humans: an intracranial electrophysiology study. J Neurophysiol 109:1283–1295
Obleser J, Lahiri A, Eulitz C (2004) Magnetic brain response mirrors extraction of phonological features from spoken vowels. J Cogn Neurosci 16:31–39
Obleser J, Scott SK, Eulitz C (2006) Now you hear it, now you don't: transient traces of consonants and their nonspeech analogues in the human brain. Cereb Cortex 16:1069–1076
Okamoto H, Stracke H, Bermudez P, Pantev C (2011) Sound processing hierarchy within human auditory cortex. J Cogn Neurosci 23:1855–1863
Okamoto H, Stracke H, Ross B, Kakigi R, Pantev C (2007a) Left hemispheric dominance during auditory processing in noisy environment. BMC Biol 5:52
Okamoto H, Stracke H, Wolters CH, Schmael F, Pantev C (2007b) Attention improves population-level frequency tuning in human auditory cortex. J Neurosci 27:10383–10390
Palomaki KJ, Tiitinen H, Mäkinen V, May PJ, Alku P (2005) Spatial processing in human auditory cortex: the effects of 3D, ITD, and ILD stimulation techniques. Cogn Brain Res 24:364–379
Pantev C (1995) Evoked and induced gamma-band activity of the human cortex. Brain Topogr 7:321–330
Pantev C, Elbert T, Makeig S, Hampson S, Eulitz C, Hoke M (1993) Relationship of transient and steady-state auditory evoked fields. Electroencephalogr Clin Neurophysiol 88:389–396
Pantev C, Eulitz C, Elbert T, Hoke M (1994) The auditory evoked sustained field: origin and frequency dependence. Electroencephalogr Clin Neurophysiol 90:82–90
Pantev C, Eulitz C, Hampson S, Ross B, Roberts LE (1996a) The auditory evoked "off" response: sources and comparison with the "on" and the "sustained" responses. Ear Hear 17:255–265
Pantev C, Hoke M, Lehnertz K, Lütkenhöner B, Anogianakis G, Wittkowski W (1988) Tonotopic organization of the human auditory cortex revealed by transient auditory evoked magnetic fields. Electroencephalogr Clin Neurophysiol 69:160–170
Pantev C, Lütkenhöner B, Hoke M, Lehnertz K (1986) Comparison between simultaneously recorded auditory-evoked magnetic fields and potentials elicited by ipsilateral, contralateral and binaural tone burst stimulation. Audiology 25:54–61
Pantev C, Okamoto H, Ross B, Stoll W, Ciurlia-Guy E, Kakigi R, Kubo T (2004) Lateral inhibition and habituation of the human auditory cortex. Eur J Neurosci 19:2337–2344
Pantev C, Roberts LE, Elbert T, Ross B, Wienbruch C (1996b) Tonotopic organization of the sources of human auditory steady-state responses. Hear Res 101:62–74
Parkkonen L, Fujiki N, Mäkelä JP (2009) Sources of auditory brainstem responses revisited: contribution by magnetoencephalography. Hum Brain Mapp 30:1772–1782
Patterson RD, Uppenkamp S, Johnsrude IS, Griffiths TD (2002) The processing of temporal pitch and melody information in auditory cortex. Neuron 36:767–776
Pelizzone M, Hari R, Mäkelä JP, Huttunen J, Ahlfors S, Hämäläinen M (1987) Cortical origin of middle-latency auditory evoked responses inman. Neurosci. Lett. 82:303–307

Picton TW, Hillyard SA, Krausz HI, Galambos R (1974) Human auditory evoked potentials. I. Evaluation of components. Electroencephalogr Clin Neurophysiol 36:179–190
Poghosyan V, Ioannides AA (2008) Attention modulates earliest responses in the primary auditory and visual cortices. Neuron 58:802–813
Prendergast G, Johnson SR, Green GG (2010) Temporal dynamics of sinusoidal and non-sinusoidal amplitude modulation. Eur J Neurosci 32:1599–1607
Pressnitzer D, Patterson RD, Krumbholz K (2001) The lower limit of melodic pitch. J Acoust Soc Am 109:2074–2084
Ray S, Maunsell JH (2011) Different origins of gamma rhythm and high-gamma activity in macaque visual cortex. PLoS Biol 9:e1000610
Reite M, Edrich J, Zimmermann JT, Zimmerman JE (1978) Human magnetic auditory evoked fields. Electroenceph Clin Neurophysiol 45:114–117
Reite M, Zimmerman JT, Zimmerman JE (1981) Magnetic auditory evoked fields: interhemispheric asymmetry. Electroencephalogr Clin Neurophysiol 51:388–392
Rif J, Hari R, Hämäläinen MS, Sams M (1991) Auditory attention affects two different areas in the human supratemporal cortex. Electroencephalogr Clin Neurophysiol 79:464–472
Ritter S, Dosch HG, Specht HJ, Rupp A (2005) Neuromagnetic responses reflect the temporal pitch change of regular interval sounds. Neuroimage 27:533–543
Rivier F, Clarke S (1997) Cytochrome oxidase, acetylcholinesterase, and NADPH-diaphorase staining in human supratemporal and insular cortex: evidence for multiple auditory areas. Neuroimage 6:288–304
Roberts TP, Poeppel D (1996) Latency of auditory evoked M100 as a function of tone frequency. NeuroReport 7:1138–1140
Rogers RL, Baumann SB, Papanicolaou AC, Bourbon TW, Alagarsamy S, Eisenberg HM (1991) Localization of the P3 sources using magnetoencephalography and magnetic resonance imaging. Electroencephalogr Clin Neurophysiol 79:308–321
Romani GL, Williamson SJ, Kaufman L (1982) Tonotopic organization of the human auditory cortex. Science 216:1339–1340
Ross B, Draganova R, Picton TW, Pantev C (2003) Frequency specificity of 40-Hz auditory steady-state responses. Hear Res 186:57–68
Ross B, Herdman AT, Pantev C (2005a) Right hemispheric laterality of human 40 Hz auditory steady-state responses. Cereb Cortex 15:2029–2039
Ross B, Herdman AT, Pantev C (2005b) Stimulus induced desynchronization of human auditory 40-Hz steady-state responses. J Neurophysiol 94:4082–4093
Ross B, Picton TW, Herdman AT, Pantev C (2004) The effect of attention on the auditory steady-state response. Neurol Clin Neurophysiol 2004:22
Ross B, Picton TW, Pantev C (2002) Temporal integration in the human auditory cortex as represented by the development of the steady-state magnetic field. Hear Res 165:68–84
Rupp A, Gutschalk A, Hack S, Scherg M (2002a) Temporal resolution of the human primary auditory cortex in gap detection. NeuroReport 13:2203–2207
Rupp A, Gutschalk A, Uppenkamp S, Scherg M (2004) Middle latency auditory-evoked fields reflect psychoacoustic gap detection thresholds in human listeners. J Neurophysiol 92: 2239–2247
Rupp A, Hack S, Gutschalk A, Schneider P, Picton TW, Stippich C, Scherg M (2000) Fast temporal interactions in human auditory cortex. NeuroReport 11:3731–3736
Rupp A, Uppenkamp S, Gutschalk A, Beucker R, Patterson RD, Dau T, Scherg M (2002b) The representation of peripheral neural activity in the middle-latency evoked field of primary auditory cortex in humans(1). Hear Res 174:19–31
Salminen NH, May PJ, Alku P, Tiitinen H (2009) A population rate code of auditory space in the human cortex. PLoS ONE 4:e7600
Sams M, Hämäläinen M, Hari R, McEvoy L (1993a) Human auditory cortical mechanisms of sound lateralization: I. Interaural time differences within sound. Hear Res 67:89–97
Sams M, Hari R, Rif J, Knuutila J (1993b) The human auditory sensory memory trace persists about 10 s: neuromagnetic evidence. J Cogn Neurosci 5:363–370

Saupe K, Schröger E, Andersen SK, Müller MM (2009) Neural mechanisms of intermodal sustained selective attention with concurrently presented auditory and visual stimuli. Front Hum Neurosci 3:58

Schadwinkel S, Gutschalk A (2010) Activity associated with stream segregation in human auditory cortex is similar for spatial and pitch cues. Cereb Cortex 20:2863–2873

Scherg M, Hari R, Hämäläinen MS (1989) Frequency-specific sources of the auditory N19-P30-P50 response detected by a multiple source analysis of evoked magnetic fields and potentials. In: Williamson SJ, Hoke M, Sroink G, Kotani M (eds) Advances in biomagnetism. Plenum Press, New York

Scherg M, von Cramon D (1985) A new interpretation of the generators of BAEP waves I-V: results of a spatio-temporal dipole model. Electroencephalogr Clin Neurophysiol 62:290–299

Scherg M, Von Cramon D (1986) Evoked dipole source potentials of the human auditory cortex. Electroencephalogr Clin Neurophysiol 65:344–360

Schnupp JW, Nelken I, King AJ (2011) Auditory neuroscience: making sense of sound. MIT Press, Cambridge, MA

Schönwiesner M, Novitski N, Pakarinen S, Carlson S, Tervaniemi M, Näätänen R (2007) Heschl's gyrus, posterior superior temporal gyrus, and mid-ventrolateral prefrontal cortex have different roles in the detection of acoustic changes. J Neurophysiol 97:2075–2082

Sedley W, Teki S, Kumar S, Overath T, Barnes GR, Griffiths TD (2012) Gamma band pitch responses in human auditory cortex measured with magnetoencephalography. Neuroimage 59:1904–1911

Shaw ME, Hämäläinen MS, Gutschalk A (2013) How anatomical asymmetry of human auditory cortex can lead to a rightward bias in auditory evoked fields. Neuroimage 74:22–29

Sieroka N, Dosch HG, Specht HJ, Rupp A (2003) Additional neuromagnetic source activity outside the auditory cortex in duration discrimination correlates with behavioural ability. Neuroimage 20:1697–1703

Snyder JS, Alain C, Picton TW (2006) Effects of attention on neuroelectric correlates of auditory stream segregation. J Cogn Neurosci 18:1–13

Spierer L, Bellmann-Thiran A, Maeder P, Murray MM, Clarke S (2009) Hemispheric competence for auditory spatial representation. Brain 132:1953–1966

Stecker GC, Harrington IA, Middlebrooks JC (2005) Location coding by opponent neural populations in the auditory cortex. PLoS Biol 3:e78

Steinmann I, Gutschalk A (2011) Potential fMRI correlates of 40-Hz phase locking in primary auditory cortex, thalamus and midbrain. Neuroimage 54:495–504

Steinmann I, Gutschalk A (2012) Sustained BOLD and theta activity in auditory cortex are related to slow stimulus fluctuations rather than to pitch. J Neurophysiol 107:3458–3467

Steinschneider M, Fishman YI, Arezzo JC (2008) Spectrotemporal Analysis of Evoked and Induced Electroencephalographic Responses in Primary Auditory Cortex (A1) of the Awake Monkey. Cereb Cortex 18:610–625

Steinschneider M, Tenke CE, Schroeder CE, Javitt DC, Simpson GV, Arezzo JC, Vaughan HG Jr (1992) Cellular generators of the cortical auditory evoked potential initial component. Electroencephalogr Clin Neurophysiol 84:196–200

Stevens KN (2000) Acoustic phonetics. MIT Press, Cambridge

Todorovic A, van Ede F, Maris E, de Lange FP (2011) Prior expectation mediates neural adaptation to repeated sounds in the auditory cortex: an MEG study. J Neurosci 31:9118–9123

Uppenkamp S, Johnsrude IS, Norris D, Marslen-Wilson W, Patterson RD (2006) Locating the initial stages of speech-sound processing in human temporal cortex. Neuroimage 31:1284–1296

Van Noorden LPAS (1975) Temporal coherence in the perception of tone sequences. University of Technology, Eindhoven

Wacongne C, Changeux JP, Dehaene S (2012) A neuronal model of predictive coding accounting for the mismatch negativity. J Neurosci 32:3665–3678

Wang Y, Ding N, Ahmar N, Xiang J, Poeppel D, Simon JZ (2012) Sensitivity to temporal modulation rate and spectral bandwidth in the human auditory system: MEG evidence. J Neurophysiol 107:2033–2041

Weisz N, Lecaignard F, Müller N, Bertrand O (2012) The modulatory influence of a predictive cue on the auditory steady-state response. Hum Brain Mapp 33:1417–1430
Wiegand K, Gutschalk A (2012) Correlates of perceptual awareness in human primary auditory cortex revealed by an informational masking experiment. Neuroimage 61:62–69
Woldorff MG, Gallen CC, Hampson SA, Hillyard SA, Pantev C, Sobel D, Bloom FE (1993) Modulation of early sensory processing in human auditory cortex during auditory selective attention. Proc Nat Acad Sci USA 90:8722–8726
Yost WA, Patterson R, Sheft S (1996) A time domain description for the pitch strength of iterated rippled noise. J Acoust Soc Am 99:1066–1078
Young ED, Sachs MB (1979) Representation of steady-state vowels in the temporal aspects of the discharge patterns of populations of auditory-nerve fibers. J Acoust Soc Am 66:1381–1403
Yrttiaho S, Alku P, May PJ, Tiitinen H (2009) Representation of the vocal roughness of aperiodic speech sounds in the auditory cortex. J Acoust Soc Am 125:3177–3185
Yvert B, Crouzeix A, Bertrand O, Seither-Preisler A, Pantev C (2001) Multiple supratemporal sources of magnetic and electric auditory evoked middle latency components in humans. Cereb Cortex 11:411–423

MEG Studies on Music

Sibylle C. Herholz and Christo Pantev

Abstract In this chapter we describe and discuss studies that have used musical stimuli or musically trained subjects in order to investigate different aspects of sensory processing and cognition, including auditory and sensorimotor function and multisensory integration. We also include studies that have used music and musical training to study human neuronal plasticity, and clinical applications in conditions such as tinnitus. We highlight the methodological advantages of MEG that are specific for research on auditory processing and for detecting changes through training.

Keywords MEG · Music · Auditory processing · Mismatch negativity · Mental imagery · Multisensory integration · Training-related plasticity · Tinnitus

1 Music and the Brain: A New Field of Research

In the last decades the neuroscience of music and musical training has developed into a thriving research field probing various aspects of human sensation, cognition, and training-related plasticity (Pantev and Herholz 2011; Zatorre 2005). MEG as a method is particularly well-suited for auditory neuroscience for several reasons. It has high temporal resolution allowing for investigation of the time course of neuronal responses to stimuli. The localization of sources of neuronal activity can be estimated, allowing conclusions about neuroanatomical correlates

S. C. Herholz
Deutsches Zentrum für Neurodegenerative Erkrankungen e.V. (DZNE), Bonn, Germany

C. Pantev (✉)
Institut für Biomagnetismus und Biosignalanalyse, Westfälische Wilhelms- Universität, Münster, Germany
e-mail: pantev@uni-muenster.de

S. Supek and C. J. Aine (eds.), *Magnetoencephalography*,
DOI: 10.1007/978-3-642-33045-2_33,

of brain functions and behavior and about lateralization of activity. Furthermore, its complete non-invasiveness allows testing various populations as well as repeated measurements. Finally, it is especially suited for the investigation of auditory and music processing, because the technique is acoustically noise-free. While the aim of this chapter is to give an overview on music neuroscience research using MEG, we will also touch upon many related topics of cognitive neuroscience such as memory, learning, multisensory integration and lateralization of cognitive functions. Music and neuroscience have the potential to be mutually informative for each respective field of research. By using music as a stimulus for neuroscience research, we can improve our understanding of neuronal function and its interaction with the environment. Conversely, by investigating how music is processed in the human brain, we can also arrive at a better understanding of music and musical structures, for example why certain sequences of tones and chords might be perceived as more pleasing than others.

Music is typically considered more than a simple sequence of tones. For example, a classical musical performance that is aesthetically pleasing and emotionally rewarding isn't a strict execution of what is notated on the sheet. Expressive music relies on subtle variations in timbre, timing and pitch, and on dynamics and on interactions between performers. However, for methodological reasons in the research on the cognitive processes underlying music perception and performance, this huge variability in the stimulus material has to be reduced. Therefore, in most cases researchers focus on certain aspects of music that are under investigation while keeping other variables as constant as possible, for example by means of a series of notes presented by a computer in a regular sequence. Thus far, in many studies in the field of music neuroscience, the stimuli that are used can be quite different from everyday music.

2 Melody and Rhythm: On Knowing and Breaking the Rules

Imagine the beginning of a very popular piece of music, Ludwig van Beethoven's sonata no. 14 for piano, also known as the moonlight sonata. Its initial bars in the right hand consist of a repeated triplet of tones, a broken c sharp minor chord, accompanied by bass octaves in the left hand (c.f. Fig. 1). After the first four repetitions of the triplet, several subtle changes in the accompaniment and in the triplet pattern are introduced. These deviations from the previous pattern of tones create tension and elicit an emotional response in many people.

Unexpected deviations from a regular sound pattern are a powerful tool in musical composition, but they are also common in everyday life and often convey important information. Consider a crack of a branch standing out in the acoustic environment of a nightly scene in the woods that might indicate the approach of a predator, or a sudden change in the ongoing, regular noise of a car engine that might indicate an engine malfunction. Research on the encoding of sounds at the

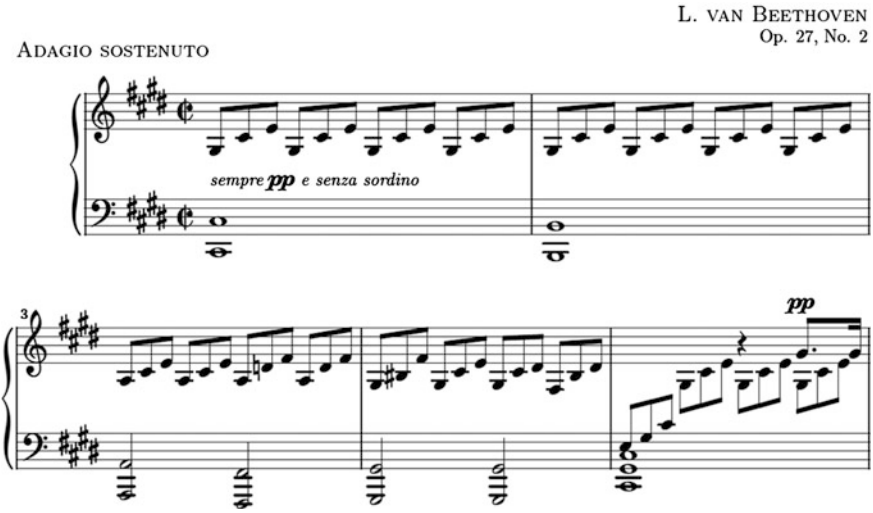

Fig. 1 First five bars of the first movement of sonata no. 14 ("Moonlight") by Ludwig van Beethoven (Op. 27, No. 2). The excerpt shows the characteristic triplet pattern in the right hand and the deviations from the pattern within the first bars. (Music typeset and published in the public domain by Chris Sawer, www.mutopia-project.org)

level of the auditory cortices has shown that we automatically encode various types of regularities in our acoustic environment, and that neuronal networks automatically detect deviations from regularities (Kujala et al. 2007; Näätänen et al. 2007). The mismatch negativity (MMN or MMNm) is a component of auditory evoked responses in EEG and MEG, respectively, that is sensitive to such deviant sounds in a sequence of regular sounds and to violations of expectancies that have been created by the preceding acoustic context. It occurs approximately 150–250 ms after the onset of the deviant sound, with a similar field distribution as the N1m component (auditory evoked response at approx. 100 ms latency), and it is superimposed on the auditory evoked field elicited by the sound. The MMN is a widely used tool in basic and clinical neuroscience that is also useful for research on music processing (Kujala et al. 2007; Näätänen et al. 2007).

Several MEG studies have looked at how we process short melodies that consist of a few consecutive tones. By using the MMN as an indicator, we can investigate which types of sound changes are detected at the level of the auditory cortices. We can also deduce what information from the stimulus is encoded, because the violation of a rule or regularity can only be detected if the underlying rule that is being broken was encoded in the first place. Classic MMN studies employ so-called oddball paradigms, in which one sound is presented with high probability and another sound is presented more rarely (Näätänen and Alho 1995). This deviant sound can be a tone of different pitch, duration, timbre, loudness or another physical parameter. If the difference between the standard and deviant sounds is large enough, a MMN response is observed in the magnetic field in response to the

deviant event. For research on music, this basic approach can be adapted to more complex stimuli such as tone sequences. Here, the standard that is being repeated is not a single tone, but a short melody, and the deviant melody differs in some aspect. Both unfamiliar tone sequences (Boh et al. 2011; Fujioka et al. 2004) and familiar melodies (Hashimoto et al. 2000; Yasui et al. 2009) have been used in melody mismatch studies, and these studies have shed light on the complexity of material that can be stored, on the types of deviations that can be detected and on the capacity of the memory store underlying the deviance detection mechanism.

Fujioka et al. (2004) investigated the processing of melodies under passive listening conditions while participants watched a soundless movie. They presented simple five note melodies that varied in key from trial to trial. Deviant melodies either contained notes that changed the contour of the melody, or that differed only in the size of the musical interval between the tones, without a contour change. They found that while musicians showed clear MMN responses to both types of changes, nonmusicians only showed very weak responses. This was not due to a generally lower MMN response though, since both groups showed a similar MMN response in a simple oddball paradigm, indicating that the complexity of the material was a challenge for the automatic encoding in the nonmusicians.

In order to estimate the capacity of the auditory short-term memory storage underlying the mismatch detection mechanism for unfamiliar material in both musicians and nonmusicians, we designed a melody oddball study using unfamiliar melodies (Boh et al. 2011). In several conditions, we presented melodies of different lengths ranging from 4 to 8 tones. Deviant tones were equally likely to occur at all positions of the melody, and therefore the whole melody had to be encoded and stored in order to detect the deviants. We found that under such challenging circumstances the average capacity of auditory memory underlying the mismatch detection for musically untrained people is approximately 4 tones. For musicians however, this capacity was at least 8 tones, since they showed significant MMN responses to deviants even in the longest melodies (Fig. 2). The improved detection of melody deviants in complex, unfamiliar musical material is most probably due to their long-term musical training.

Even people without musical training automatically encode repeatedly presented short familiar melodies without having to attend to the stimuli. Hashimoto et al. (2000) presented participants without musical background with familiar melodies. Half of the melodies contained an incorrect note that was out of key of the original melody. These notes elicited an early mismatch response that was recorded with a limited number of channels over right auditory areas. Yasui et al. (2009) also used familiar melodies as stimuli. In a series of three experiments they differentiated the processing of lyrics and melody in familiar songs, and elucidated the role of long-term memory in the detection of unexpected events. They were able to show a respective right- and left-lateralization for melody and lyrics deviants in mismatch responses that were similar, but not identical in latency and source location compared to pitch MMN. Additionally, they asked participants to memorize new melodies and again they found the same mismatch responses to unexpected tones in these newly memorized melodies as in the melodies that

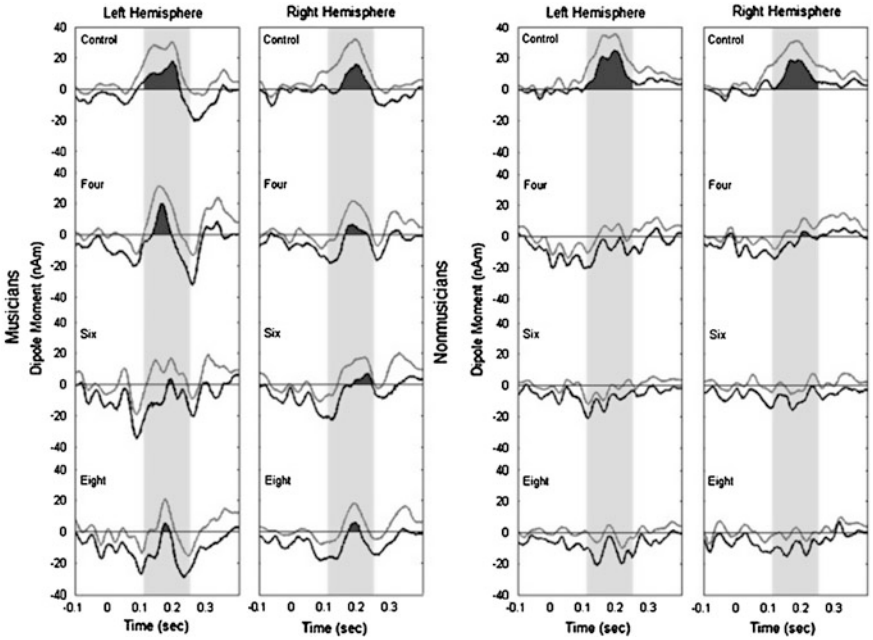

Fig. 2 MMN responses to pitch deviants in melodies of different lengths in musicians and nonmusicians in an MEG study by Boh et al. (2011). The *grey traces* show the group averaged source waveforms in both hemispheres, and the *black traces* show the lower confidence intervals as estimated from a bootstrap procedure. Nonmusicians show significant MMN responses only in the control condition (standard oddball paradigm) and in response to deviants in the four tone melody, whereas musicians show significant responses in all conditions. This result suggests that long-term musical training might lead to an increase of the capacity of auditory short-term memory for complex auditory patterns (Boh et al. 2011)

were familiar from childhood. These findings indicate that not only short-term knowledge about regularities gained from the most recent auditory context but also long-term familiarity with melodies can be the basis for automatic deviance detection.

Some investigators have also looked at processing of musical chords and chord progressions using MEG. In most musical cultures and styles musical harmonies are organized in a musical syntax. People acquire knowledge about these rules via passive exposure in everyday life. This is evident from findings indicating that no special musical training is required to automatically detect untypical chords (Maess et al. 2001) and to distinguish major from minor chords (Brattico et al. 2009). Brattico et al. (2009) investigated the processing of chords in an MMN paradigm, where general musical context, in terms of mostly consonant major Western chords, was presented, but without a particular music-syntactic sequence or order of the chords. In this context, both musically trained and untrained participants showed a MMN response to rarely presented minor chords, indicating that even without a context of musically meaningful chord progressions such

distinctions are automatically made. Maess et al. (2001) presented their subjects sequences of chords that followed Western musical rules of harmony. Infrequently, they presented chords that were consonant but did not quite fit at this position of the chord sequence. Such chords elicited the magnetic equivalent of another early response to unexpected sounds, the early right anterior negativity (ERAN). Importantly, the sources of the mERAN were estimated to be located in Broca's area and its right homologue, and thus differed from typical sources of the MMN in the temporal lobes. This indicates that the syntactic processing and the detection of deviations in a musically meaningful harmonic context relies—at least partly—on a different network than the detection of deviant tones in unfamiliar tone sequences.

Another MEG study using the MMN as a marker for auditory processing investigated musical versus phonological processing (Tervaniemi et al. 1999). MEG provided the possibility to disentangle the respective contributions of the two hemispheres for processing of the two different stimulus types. Tervaniemi et al. (1999) showed that in the right hemisphere, the MMN to an unexpected chord was stronger than the MMN to a phoneme change, whereas there was no difference between the MMN amplitudes in the two stimulus categories in the left hemisphere. Furthermore, in an analysis of the source locations of the corresponding equivalent current dipoles, they found that the MMN sources of the two stimulus categories were distinct, indicating a specific neuronal network for processing of musical versus speech stimuli.

Apart from the spectral and pitch aspect of music that is most evident in the instrumental timbres and in the melodic and harmonic structure of music, another crucial component of music is the rhythmic and metrical structure of a piece. Vuust et al. (2005) investigated rhythm and meter processing in jazz musicians and in persons without musical background. They found that jazz musicians are especially sensitive to subtle deviations in a rhythmic sequence of percussion sounds that did not change the meter underlying the rhythm, whereas nonmusicians were only able to detect the more obvious violation of the meter. Interestingly, the deviance detection was right-lateralized in nonmusicians, but left-lateralized in musicians, again most probably due to the long-term musical training that resulted in changes in functional brain organization.

In summary, these studies demonstrate automatic detection mechanisms on the level of the auditory cortices that respond to unexpected or deviant auditory input. These mechanisms might also be related to some of the effects that make music interesting and beautiful. Although this has not been shown directly, the early and automatic detection of expectancy violations might contribute to emotional responses to unexpected changes in melody, harmony, dynamics or orchestration in music. However, more work is required to fully understand how the processes that detect regularities and expectancy violations have been shaped by nonmusical survival requirements, how music might rely on these evolutionary old mechanisms, and how it interacts with other systems such as language and cognitive systems that model regularities in our environment as a basis for expectancies and planning that are needed for adaptive behavior.

3 Higher-Order Cognition: Music in the Mind

In the beginning of the previous section we invited you to imagine some familiar music as an illustration of repeated tone patterns in music. If you know the piece or if you were able to sight-read it from the score, then you probably had an auditory impression that was a different experience from actual listening to music, but that nevertheless contained important aspects of the musical piece, such as the melody and accompanying chords, the piano timbre, the tempo and the dynamics, maybe even characteristic details of a particular recording that you remember.

Several MEG studies investigated what happens in the brain during higher-order musical cognition such as imagining and remembering music. In one study on auditory imagery (Herholz et al. 2008), we used a musical imagery task that involved listening to the beginnings of familiar melodies and then continuing them mentally in order to investigate musical imagery. The challenge in investigating phenomena such as mental imagery lies in the requirement of an overt behavior that indicates if the participant is doing the task. We tested participants' musical imagery by presenting another tone after the silent imagery period that was either a correct or an incorrect continuation of the imagined melody at that point in time. The participant had to judge this tone and could give a correct answer only if he or she had correctly imagined the melody during the silent gap. Our results showed that musicians were able to detect the incorrect tones behaviorally and that they had a different auditory evoked response to incorrect than to correct continuations of the melody. Since it had also been evoked in response to an expectancy violation, we termed this response imagery MMN (iMMN), in analogy to the classic MMN that had a very similar latency and field distribution. The differential response indicated correct mental imagery of the melody, probably based on cortical activity in networks including the auditory cortices that was strong enough to serve as a basis for the neural comparison mechanism underlying the MMN (Herholz et al. 2008). In a recent replication of our imagery MMN study using more simple tone patterns, we observed a classic MMN to deviants in tone patterns when they were actually presented, but we did not replicate our finding of an iMMN that was based on previous imagery of the tone sequence (Kuchenbuch et al. 2012). This indicates that the stimulus material plays an important role in the investigation of auditory and music imagery. Familiar melodies that elicit more semantic and musical associations, episodic memories and a lyrics component might be better suited for musical imagery tasks.

Gunji et al. (2007) investigated the neuronal processes occurring during mental imagery of music in comparison to musical production. They compared mental imagery to overt speaking, singing and humming of the tune "Happy Birthday" in the MEG scanner. The authors used synthetic aperture magnetometry (SAM) to analyze both event-related synchronization and desynchronization in different frequency bands, and showed similar patterns of activity both in the singing,

humming and imagining conditions, indicating overlapping brain networks for perception, action and imagery, in line with studies using other neuroimaging techniques (Zatorre and Halpern 2005).

4 Sensorimotor Integration and Training-Induced Plasticity

Playing a musical instrument involves processing within and coordination among several sensory, motor and cognitive systems. This multimodality integration is a crucial aspect of music and music making, and several studies have used MEG to understand the multimodal interactions as well as their influence on learning and plasticity. We have previously mentioned several MEG studies on auditory cognition in which musicians show advantages, including processing of tone sequences (Boh et al. 2011; Fujioka et al. 2004) and rhythm (Vuust et al. 2005). The most plausible explanation for these differences is that the long-term musical training has led to lasting changes in the networks for auditory processing. However, in a cross-sectional design such as the comparison of musicians and nonmusicians, other factors like genetic predisposition or socioeconomic confounds cannot be excluded. In order to investigate the causal relationship of musical training and auditory discrimination abilities we conducted two short-term training studies (Lappe et al. 2008, 2011). Participants were randomly assigned to two groups, a piano training group, and an auditory group. Whereas the piano group learned to play a short musical piece over the course of 8 training sessions, the auditory group merely listened attentively to the recordings of a participant in the piano group, and they had to detect errors in the performance in order to ensure their attention. Before and after the training period participants performed melody discrimination tasks and the melody MMN was measured with MEG, as shown in Fig. 3. Piano training resulted in stronger increases in the melody MMN both regarding pitch deviants (Lappe et al. 2008) and rhythmic deviants (Lappe et al. 2011). Interestingly, the enhanced effects of piano training were right-lateralized for the training focusing on pitches (Lappe et al. 2008), whereas no lateralization of the effects were found for the rhythmic training (Lappe et al. 2011). Since the auditory input was the same in both the auditory and the piano training groups, we were able to conclude that the multisensory aspect of musical training is crucial for enhancing training-related plasticity in the auditory domain.

Auditory-motor interactions in music and musical performance have been investigated using various methods (Zatorre et al. 2007). In MEG, coactivation of auditory and motor areas during perception of music has been shown in pianists (Haueisen and Knösche 2001), and during isochronous beat perception in nonmusicians (Fujioka et al. 2012). Another recent study by Krause et al. (2010) used a sensorimotor integration task that involved finger tapping in synchrony to an auditory stimulus. While all subjects showed activity in an auditory-motor

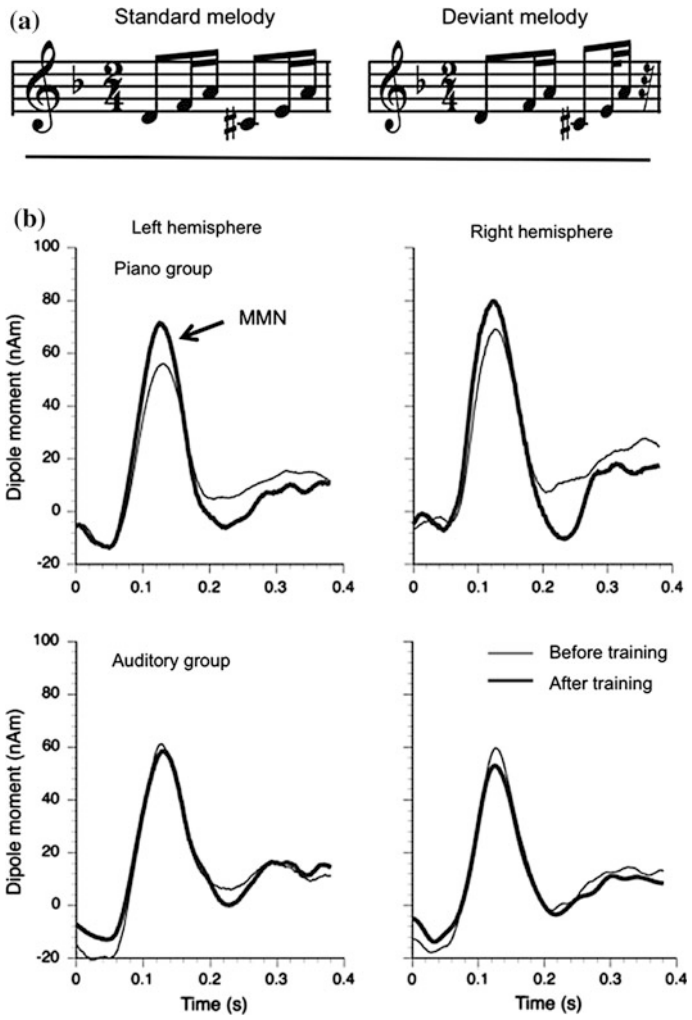

Fig. 3 Illustration of the effect of two weeks of piano training compared to auditory training on neural correlates of rhythm discrimination, from an MEG study by Lappe et al. (2011). Participants passively listened to a melody oddball paradigm with a short standard melody (*panel A*, *left*) and a more rarely presented deviant melody (*panel A*, *right*). The MMN response to the rhythmic deviation was enlarged after training compared to before training in the piano training group whereas the auditory group showed no such increase due to training, although both groups received identical auditory input during the training (*panel B*). This result demonstrates that multimodal (sensorimotor-auditory) training results in stronger MMN responses, suggestive of greater functional plasticity, than unimodal (auditory) training (Figure adapted from Lappe et al. 2011)

network, drummers and pianists showed increased synchronization compared to nonmusicians in a network involving premotor cortex, thalamus and posterior parietal cortex (Krause et al. 2010).

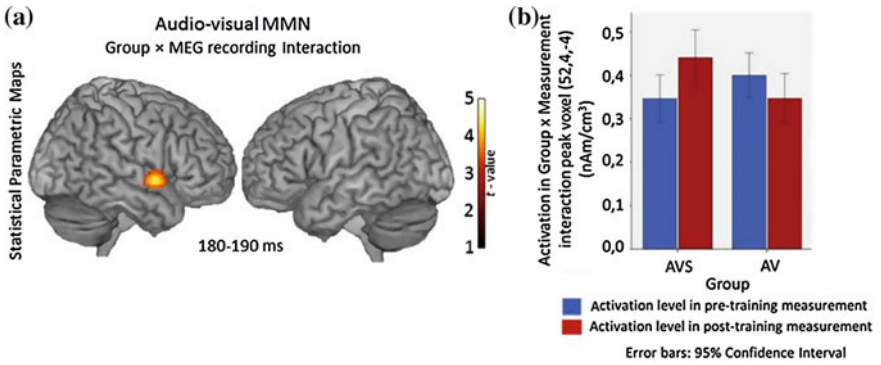

Fig. 4 Illustration of an effect of short-term piano training on neuronal correlates of audiovisual integration, from an MEG study by Paraskevopoulos et al. (2012a). Participants who received audio-visual-sensorimotor piano training (AVS group) showed stronger training-related changes, indicating stronger functional plasticity in auditory association cortex in the right superior temporal gyrus (as seen in *panel A*) compared to participants who received audiovisual training only (AV group). The statistical interaction is shown in panel B. MEG responses elicited by audiovisual incongruencies were analyzed using the LORETA method. The data show that active musical training results in stronger functional changes in correlates of multisensory processing in the human cortex than mere audiovisual sensory training (Paraskevopoulos et al. 2012a)

Not only auditory-motor, but also other multimodal integration processes are enhanced in musicians. Schulz et al. (2003) tested processing of simultaneously presented tactile and auditory stimuli in trumpet players and in nonmusicians. They showed that the neural response in trumpeters to a combined trumpet tone and touch on the lips was larger than the sum of the single-modality responses, indicating enhanced processing of the combined stimulus. We have recently shown that musicians also show increased audio-visual integration compared to nonmusicians as evidenced by an increased response to audio-visual incongruence in short melodies that were simultaneously presented as visual symbols (Paraskevopoulos et al. 2012b). In another recent study we aimed at testing experimentally whether multisensory musical training enhances multisensory processing (Fig. 4). To this end, we again compared two groups that underwent different kinds of musical training (Paraskevopoulos et al. 2012a). One group of randomly assigned participants learned to play melodies on the piano from simple visual representations, while the other group merely listened to the playing while viewing the visual representations. Thus, both groups learned about the audio-visual rules but only one group actively performed the music. In pre- and post-training MEG sessions we measured the MMN to audio-visual incongruities of the learned rules. Participants of the piano group showed stronger increases, indicating that active multisensory training not only enhances unisensory processing as shown in our previous training studies (Lappe et al. 2008, 2011), but also multisensory processing (Paraskevopoulos et al. 2012a).

MMN studies can also inform us on how we gradually acquire knowledge about the acoustic environment during passive listening. In typical oddball studies, the standard sound or sequence is presented very frequently, with typical percentages of standards of 80 % and higher. However, in music as in other acoustic environments, regularities can be much more subtle and hidden. We were interested if a regular pattern of tones could be detected even if its relative frequency among other stimuli was relatively low. Three recent studies from our lab indicate that musicians might be at an advantage for such short-term auditory learning. In order to study the acquisition of knowledge about rules and regularities in auditory processing, we used stimuli where the regularities inherent in a presented tone sequence were not evident right away. For two studies we created stimulus sequences within which the probability of the standard was low (Herholz et al. 2009, 2011), and in another study we presented several short tone patterns in a randomized sequence, resulting in a relatively low probability for each of these individual patterns among the others (Paraskevopoulos et al. 2012c). Importantly, the regularities underlying the tone sequences in each of these studies were not based on familiar musical motives from Western musical repertoire or based on rules of harmony. Therefore, knowledge about the regularities had to gradually emerge from listing to the actual tone sequence. Musicians showed enlarged MMN (Herholz et al. 2009, 2011) and P1 responses (auditory evoked response at approx. 50 ms latency; Paraskevopoulos et al. 2012c) to violations of these regularities that appeared within the sequences, indicating that they were better able to pick up the underlying rules. Such enhancement of short-term learning by previous experience has been labeled meta-plasticity to indicate that plasticity or learning is altered at a different rate, and that the potential for new learning is dependent on the previous learning history (Abraham 2008). It has also been described in the context of motor plasticity (Rosenkranz et al. 2007) and tactile learning (Ragert et al. 2004) that are enhanced in musicians. While we don't know yet which mechanisms underlie these observations in the context of auditory learning and musical training, further exploring and investigating the interactions of short- and long-term learning and plasticity is a promising avenue for future research.

5 Clinical Applications: Music as a Cure

Musical training or music listening can be used in the rehabilitation of neurological disorders and in aging (Wan and Schlaug 2010). One example of successful transfer of basic neuroscience studies to clinical application is the use of notch-filtered music listening to alleviate tinnitus (Okamoto et al. 2010). The finding that ultimately led to a new treatment to tinnitus stemmed from two threads of basic research. On the one hand, animal models had shown that tinnitus goes along with maladaptive reorganization of neuronal networks in auditory cortex, and that tinnitus patients show similar pathological changes in the neural responses to their tinnitus frequency (Eggermont 2007). On the other hand, the cortical responses to

specific pitches are plastic and can be modulated by altered acoustic input. Pantev et al. (1999) had shown that three hours of exposure to notch-filtered music that was modified to exclude specific frequency bands reduced the amplitude of auditory evoked responses that lay within the missing frequency bands. This modulation of neuronal responses in healthy young subjects was short lasting and reverted to baseline over night, but it opened a perspective for a treatment of tinnitus using musical stimulation. In a longitudinal study over twelve months, Okamoto et al. (2010) showed that listening to notch-filtered music that was tailored to the individual tinnitus frequency improves both the subjective suffering and the neural correlates of tinnitus as measured by means of auditory evoked fields to tinnitus and to other control frequencies. Control group subjects that received placebo treatment showed no such improvements. These findings open the door for future clinical use and studies of music listening to alleviate tinnitus, for example involving active music making, with MEG measurements as a means for objective evaluation of the changes on a neuronal level that accompany the subjective improvements.

References

Abraham WC (2008) Metaplasticity: tuning synapses and networks for plasticity. Nat Rev Neurosci 9(5):387–399

Boh B, Herholz SC, Lappe C, Pantev C (2011) Processing of complex auditory patterns in musicians and nonmusicians. PLoS ONE 6(7):e21458

Brattico E, Pallesen KJ, Varyagina O, Bailey C, Anourova I, Jarvenpaa M, Eerola T, Tervaniemi M (2009) Neural discrimination of nonprototypical chords in music experts and laymen: an MEG study. J Cogn Neurosci 21(11):2230–2244

Eggermont JJ (2007) Pathophysiology of tinnitus. Prog Brain Res 166:19–35

Fujioka T, Trainor LJ, Large EW, Ross B (2012) Internalized timing of isochronous sounds is represented in neuromagnetic beta oscillations. J Neurosci 32(5):1791–1802

Fujioka T, Trainor LJ, Ross B, Kakigi R, Pantev C (2004) Musical training enhances automatic encoding of melodic contour and interval structure. J Cogn Neurosci 16(6):1010–1021

Gunji A, Ishii R, Chau W, Kakigi R, Pantev C (2007) Rhythmic brain activities related to singing in humans. Neuroimage 34(1):426–434

Hashimoto T, Hirata Y, Kuriki S (2000) Auditory cortex responds in 100 ms to incongruity of melody. NeuroReport 11(12):2799–2801

Haueisen J, Knösche TR (2001) Involuntary motor activity in pianists evoked by music perception. J Cogn Neurosci 13(6):786–792

Herholz SC, Boh B, Pantev C (2011) Musical training modulates encoding of higher-order regularities in the auditory cortex. Eur J Neurosci 34(3):524–529

Herholz SC, Lappe C, Knief A, Pantev C (2008) Neural basis of music imagery and the effect of musical expertise. Eur J Neurosci 28(11):2352–2360

Herholz SC, Lappe C, Pantev C (2009) Looking for a pattern: An MEG study on the abstract mismatch negativity in musicians and nonmusicians. BMC Neurosci 10(1):42

Krause V, Schnitzler A, Pollok B (2010) Functional network interactions during sensorimotor synchronization in musicians and non-musicians. Neuroimage 52(1):245–251

Kuchenbuch A, Paraskevopoulos E, Herholz SC, Pantev C (2012) Electromagnetic correlates of musical expertise in processing of tone patterns. PLoS ONE 7(1):e30171

Kujala T, Tervaniemi M, Schröger E (2007) The mismatch negativity in cognitive and clinical neuroscience: theoretical and methodological considerations. Biol Psychol 74(1):1–19
Lappe C, Herholz SC, Trainor LJ, Pantev C (2008) Cortical plasticity induced by short-term unimodal and multimodal musical training. J Neurosci 28(39):9632–9639
Lappe C, Trainor LJ, Herholz SC, Pantev C (2011) Cortical plasticity induced by short-term multimodal musical rhythm training. PLoS ONE 6(6):e21493
Maess B, Koelsch S, Gunter TC, Friederici AD (2001) Musical syntax is processed in Broca's area: an MEG study. Nat Neurosci 4(5):540–545
Näätänen R, Alho K (1995) Mismatch negativity–a unique measure of sensory processing in audition. Int J Neurosci 80(1–4):317–337
Näätänen R, Paavilainen P, Rinne T, Alho K (2007) The mismatch negativity (MMN) in basic research of central auditory processing: a review. Clin Neurophysiol 118(12):2544–2590
Okamoto H, Stracke H, Stoll W, Pantev C (2010) Listening to tailor-made notched music reduces tinnitus loudness and tinnitus-related auditory cortex activity. Proc Natl Acad Sci USA 107(3):1207–1210
Pantev C, Herholz SC (2011) Plasticity of the human auditory cortex related to musical training. Neurosci Biobehav Rev 35(10):2140–2154
Pantev C, Wollbrink A, Roberts LE, Engelien A, Lütkenhöner B (1999) Short-term plasticity of the human auditory cortex. Brain Res 842(1):192–199
Paraskevopoulos E, Kuchenbuch A, Herholz SC, Pantev C (2012a) Evidence for training-induced plasticity in multisensory brain structures: an MEG study. PLoS ONE 7(5):e36534
Paraskevopoulos E, Kuchenbuch A, Herholz SC, Pantev C (2012b) Musical expertise induces audio-visual integration of abstract congruency rules. J Neurosci 32(50):18196–18203
Paraskevopoulos E, Kuchenbuch A, Herholz SC, Pantev C (2012c) Musical training effects on statistical learning of melodies: an MEG study. Neuropsychologia 50(2):341–349
Ragert P, Schmidt A, Altenmuller E, Dinse HR (2004) Superior tactile performance and learning in professional pianists: evidence for meta-plasticity in musicians. Eur J Neurosci 19(2): 473–478
Rosenkranz K, Williamon A, Rothwell JC (2007) Motorcortical excitability and synaptic plasticity is enhanced in professional musicians. J Neurosci 27(19):5200–5206
Schulz M, Ross B, Pantev C (2003) Evidence for training-induced crossmodal reorganization of cortical functions in trumpet players. NeuroReport 14(1):157–161
Tervaniemi M, Kujala A, Alho K, Virtanen J, Ilmoniemi RJ, Naatanen R (1999) Functional specialization of the human auditory cortex in processing phonetic and musical sounds: A magnetoencephalographic (MEG) study. Neuroimage 9(3):330–336
Vuust P, Pallesen KJ, Bailey C, van Zuijen TL, Gjedde A, Roepstorff A, Ostergaard L (2005) To musicians, the message is in the meter pre-attentive neuronal responses to incongruent rhythm are left-lateralized in musicians. Neuroimage 24(2):560–564
Wan CY, Schlaug G (2010) Music making as a tool for promoting brain plasticity across the life span. Neuroscientist 16(5):566–577
Yasui T, Kaga K, Sakai KL (2009) Language and music: differential hemispheric dominance in detecting unexpected errors in the lyrics and melody of memorized songs. Hum Brain Mapp 30(2):588–601
Zatorre RJ (2005) Music, the food of neuroscience? Nature 434(7031):312–315
Zatorre RJ, Chen JL, Penhune VB (2007) When the brain plays music: auditory-motor interactions in music perception and production. Nat Rev Neurosci 8(7):547–558
Zatorre RJ, Halpern AR (2005) Mental concerts: musical imagery and auditory cortex. Neuron 47(1):9–12

Sensorimotor Integration

Toshiaki Wasaka and Ryusuke Kakigi

Abstract A motor program for controlling one's own movement requires sensory signals from the target body parts. The information for movement is provided by sensory feedback, as well as the integration of sensory information and motor command, all of which are critical for motor control. Recent studies suggested that cortical activity related to sensory response and perception is modified by movement executing mechanisms. However, this raises the question of how this system integrates motor command and sensory information whenever the intended movement is in progress. In this chapter, we review findings of sensorimotor integration and introduce results of our own studies using magnetoencephalography.

Keywords Corollary discharge · Efference copy · Motor command · Somatosensory information · Visual information

1 Introduction

Movement is the only way of interacting with the world. Indeed, all communication, including speech, gestures and writing, is mediated via the motor system. The motor areas play a crucial role in the coordination of movement, and the sensory areas have a functional role in monitoring the state of movement. To control our action, the human brain uses sensory signals to determine future actions. The existence of

T. Wasaka (✉)
Nagoya Institute of Technology, Gokiso, Syowa, Nagoya, Aichi 466-8555, Japan
e-mail: wasaka.toshiaki@nitech.ac.jp

T. Wasaka · R. Kakigi
Department of Integrative Physiology, National Institute for Physiological Sciences, 38 Nishigonaka, Myodaiji, Okazaki, Aichi 444-8585, Japan

S. Supek and C. J. Aine (eds.), *Magnetoencephalography*,
DOI: 10.1007/978-3-642-33045-2_34,

interactions between motor commands and sensory information processing has been investigated using electroencephalography, magnetoencephalography (MEG) and functional magnetic resonance imaging (fMRI).

Sensory feedback from body parts is used to adjust and correct movement in course to the varying environmental constraints. Preceding and during movement, the motor and higher-order brain systems regulate sensory information at several processing stages. This chapter will begin with an explanation of the neural model concerning sensorimotor integration. This will be followed by research topics of neural modulation in the sensory system, especially somatosensory areas, during execution of voluntary movement including our own recent findings. Finally, the functional role of sensorimotor integration will be discussed.

2 The Neural Mechanism of Sensorimotor Integration

Cortical mechanisms such as corollary discharge (Sperry 1950) and efference copy (von Holst and Mittelstaedt 1950) modify sensory information processing during movement generation and execution. These mechanisms are used to keep track of the expected result of the motor command, and to update the current state. The central idea of corollary discharge is that the oculomotor system sends some information about the motor signal to the visual system when it initiates a movement, and this signal blocks the transient shift of the retinal image of the visual world during saccadic periods. Corollary discharge also plays an important role in auditory, vocalization, skeletomotor and somatosensory systems (Crapse and Sommer 2008). Human studies have provided insights into its functional role in two operations: resolving ambiguity in the origin of sensory information and enabling proper motor performance.

Corollary discharge transiently modulates self-generated sensory responses and can help distinguish between self-generated and externally generated sensory information. Recently, interesting research was conducted on the somatosensory system. Everyone knows you cannot tickle yourself, yet if someone else touches your side, you may suddenly feel ticklish. The neural mechanism of this phenomenon was examined using brain imaging techniques. Compared to self-produced stimuli, more activity in somatosensory areas was found when the stimulus was externally delivered (Blakemore et al. 1998). When a movement is self-produced, its sensory consequences can be accurately predicted, and this prediction can be used to attenuate the sensory effects of the movement. The sensory prediction is made by an internal forward model of the motor system (Wolpert et al. 1998). By comparing the predicted with the actual sensory feedback, it is possible to distinguish the sensory consequences of our movements from sensory signals due to changes in the outside world. This neural mechanism has a functional role in controlling voluntary movement based on sensory information.

3 Sensorimotor Integration in the Somatosensory Areas

When we execute voluntary movement, somatosensory information processing, during its course from the peripheral to the somatosensory areas, is influenced by many mechanisms mediated by a network comprising motor and higher-order brain systems. This phenomenon has been reported as changes in the short- and long-latency components of somatosensory evoked potentials (SEPs) and somatosensory evoked magnetic fields (SEFs).

Sensorimotor integration in the somatosensory areas occurs via two major mechanisms: (1) modulation of SEPs/SEFs can be carried out by inhibitory interaction between the given sensory signals and the efferent signals induced by the motor command from the motor related areas (centrifugal mechanism), and (2) modulation can be exerted by interaction between the given sensory afferents that produce SEPs/SEFs and the afferent signals evoked by the movement, i.e., afferent signals from the muscles and joints (centripetal mechanism) (Jones et al. 1989).

With regard to the modulation of somatosensory cortices produced by voluntary movement, change in SEP/SEF amplitude was found not only during movement (Rushton et al. 1981; Kakigi et al. 1995; Nakata et al. 2003; Nakajima et al. 2006) but also just prior to it (preparatory period) (Cohen and Starr 1987; Kida et al. 2004, 2006). In previous studies, pre-movement modulation of somatosensory information processing has been investigated using reaction time tasks (Starr and Cohen 1985; Bocker et al. 1993; Murase et al. 2000). However, a reaction time task evokes various cognitive brain activities, such as expectancy, motivation and attention, which may change the sensorimotor activities. In fact, the neuronal effect of attention on somatosensory information processing has been addressed with various methods, including single unit recordings in monkeys (Hyvarinen et al. 1980; Iriki et al. 1996), SEPs/SEFs (Desmedt and Tomberg 1989; Garcia-Larrea et al. 1995; Mauguiere et al. 1997; Mima et al. 1998) and fMRI (Johansen-Berg et al. 2000; Staines et al. 2002). By using a self-initiated voluntary movement task without external cues, one can observe the temporal modulation of somatosensory cortical activities with respect to movement onset and elucidate the neural interactions between somatosensory and motor areas in detail.

Our research has focused on the neural mechanisms of sensorimotor integration in the somatosensory areas, especially the centrifugal modulation in the primary somatosensory area (SI) and the secondary somatosensory area (SII), during the preparatory period of self-initiated voluntary movement. The hypothesis is that if motor commands interact with sensory inputs in the central nervous system, neurons in the motor and sensory areas should show a change of activities when these commands are issued.

4 Modulation in the SI During the Preparatory Period of Voluntary Movement

Previously, we reported differential pre-movement modulation of SEP components estimated to be in the SI. There was no significant change in amplitude for the M20, the primary component associated with SI, but there was attenuation of the M35, a subsequent component localized to SI, just before movement onset (Fig. 1) (Wasaka et al. 2003). The change in the amplitude of the M20 during the preparatory period has been controversial. Some authors reported that the amplitude did not change before movement (Starr and Cohen 1985; Murase et al. 2000), while others reported attenuation just before movement (Hoshiyama and Sheean 1998). In contrast, attenuation of the amplitude of the M35 just before movement has consistently been reported (Starr and Cohen 1985; Cohen and Starr 1987; Hoshiyama and Sheean 1998). In general, the M20 is considered to be generated in Brodmann's area 3b of the SI (Desmedt et al. 1987; Allison et al. 1991; Inui et al. 2004). However, the generator for the M35 remains unknown. Inui et al. (2004) reported overlapping activities among multiple cortical areas such as Brodmann's areas 3b, 4 and 1, around 20–30 ms following stimulation of the dorsum of the hand. Source modeling analysis suggested that area 4 of the primary motor area (MI) was involved in generating the M35 (Kawamura et al. 1996). Furthermore, the modulation of SEF components caused by the effect of the interstimulus interval suggested that another potential mechanism responsible for the M35 was inhibitory postsynaptic potentials in the deeper layers in area 3b (Wikstrom et al. 1996). Although we estimated the source of M35 around the SI, further study will be needed to elucidate the generator.

Interestingly, the time course of the M35 modulation, starting from 1500 ms before the movement and the remarkable attenuation just prior to the movement, was similar to that of the activities of movement-related cortical potentials that reflected the neural activities of movement preparation in motor-related areas. In addition, our previous study showed that the extent of the centrifugal mechanism for SEPs was dependent on the amplitude of the negative slope. This result suggested that the centrifugal modulation in the SI was related to the activities of motor related areas (Wasaka et al. 2005b). Subdural recording showed that the supplementary motor area (SMA) and the MI activities in this period were recorded from the cortex of humans (Ikeda et al. 1992). Motor related areas, such as SMA and MI, have extensive cortico-cortical connections to other cortices such as the SI (Jones et al. 1978) and possibly other sensory associated cortices. Intracortical microstimulation of the neurons in the MI in monkeys caused a profound decrease in the magnitude of the short-latency component of somatosensory evoked potentials (Jiang et al. 1990), suggesting that the activities in the motor related areas just before movement could modulate the response in the SI, especially the generator for the M35 component. It is assumed that these electrophysiological changes are associated with a decrease in tactile sensitivity commonly observed before the onset of movement of the limb that received the sensory stimulation (Schmidt et al. 1990).

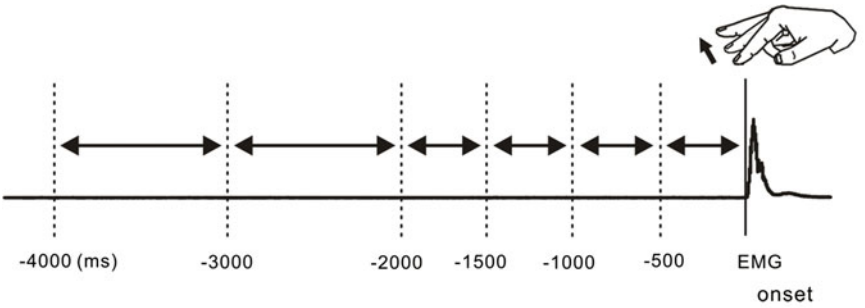
-4000 (ms)
-3000
-2000
-1500
-1000
-500
EMG onset

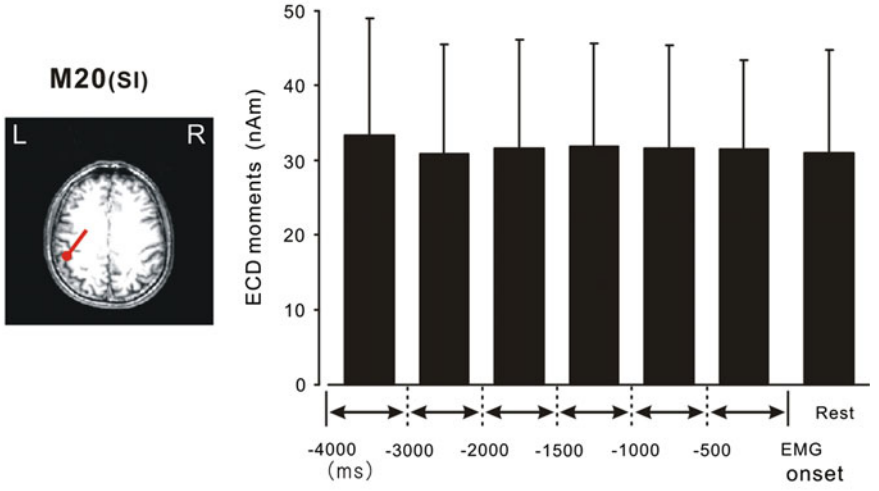
M20(SI)
L
R
ECD moments (nAm)
50
40
30
20
10
0
Rest
-4000 (ms)
-3000
-2000
-1500
-1000
-500
EMG onset

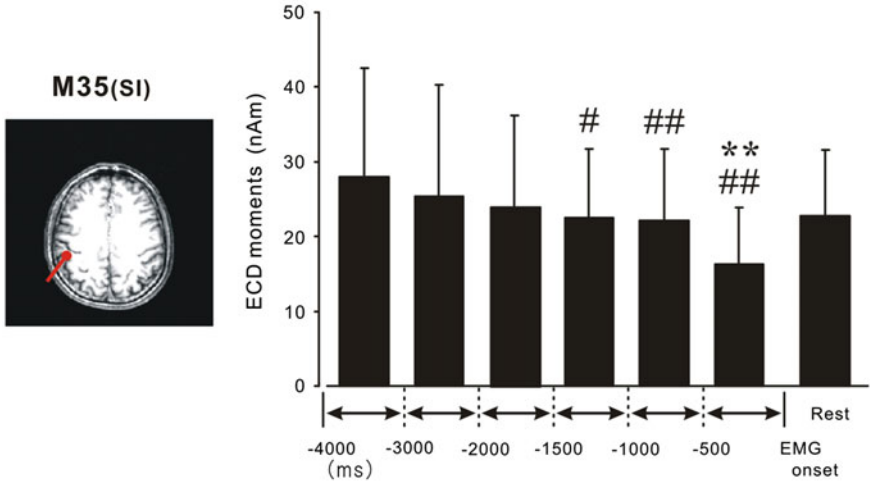
M35(SI)
ECD moments (nAm)
50
40
30
20
10
0
#
##
**
##
Rest
-4000 (ms)
-3000
-2000
-1500
-1000
-500
EMG onset

◀ **Fig. 1** The premovement subperiods and the onset of the rectified EMG. The preparatory period was divided into five subperiods from the onset of EMG to 4000 ms before movement. The time scale is expressed in minus values before the onset of movement. Stimulation of the median nerve was applied at random and the MEG signals following stimulation were averaged separately depending on each subperiod to obtain the premovement somatosensory evoked magnetic fields (SEFs). The sources were located in the posterior bank of the central sulcus in the hemisphere contralateral to the side stimulated. The graphs show the mean and standard deviation of the ECD moments of the M20 and M35 components in the rest condition and premovement subperiods. ** $p < 0.01$; Statistical significance compared with the values in the rest condition, # $p < 0.05$, ## $p < 0.01$; Statistical significance compared with the values for the 4,000–3,000 ms subperiod before EMG onset. Two periods for the M35 showed a significant reduction as compared with the rest condition and/or the 4,000–3,000 ms subperiod before EMG onset. The M20 showed no significant change. Adapted from Wasaka et al. (2003)

5 Modulation in the SII During the Preparatory Period of Voluntary Movement

There is no consensus as to the function of the SII concerning sensorimotor integration during voluntary movement. Enhancement of SII activation was observed (Huttunen et al. 1996; Forss and Jousmaki 1998; Lin et al. 2000) and it was assumed that this phenomenon reflects tuning of the SII neurons to relevant somatosensory information from the regions of contracting muscle. On the other hand, some researchers reported an attenuation of SII activation (Avikainen et al. 2002; Inoue et al. 2002). Using a self-initiated movement task to investigate the preparatory period, whereby the centripetal effect on the SEF response can be eliminated, one can mainly examine the centrifugal effect. We showed an enhancement of SII activation in the 0 to –500 ms sub-period (Fig. 2) (Wasaka et al. 2005a).

It is generally agreed that attention to somatosensory information enhances activation of the SII cortex (Hari et al. 1990; Mauguiere et al. 1997; Fujiwara et al. 2002). Although it is hard to eliminate the attentional effect, we instructed the subjects to concentrate on self-initiated finger extension and not to pay attention to electrical stimulation. Subjects reported that they concentrated on the finger extension and did not turn their mind to the electrical stimulation throughout the recording session. Therefore, although it is possible that attention contributed in a small way to the enhancement of SII activation, the activation of motor related areas prior to voluntary movement enhances the cortical effects of the SII either by increasing synchronicity or by increasing the number of neurons active via the centrifugal process.

6 Differential Modulation in the SI and SII Preceding Voluntary Movement

In the period of 500 ms before the onset of self-initiated movement, an attenuation of activation in the SI and enhancement in the SII was found. The opposite effects of movement on SI and SII cortices indicated that the motor and higher-order brain

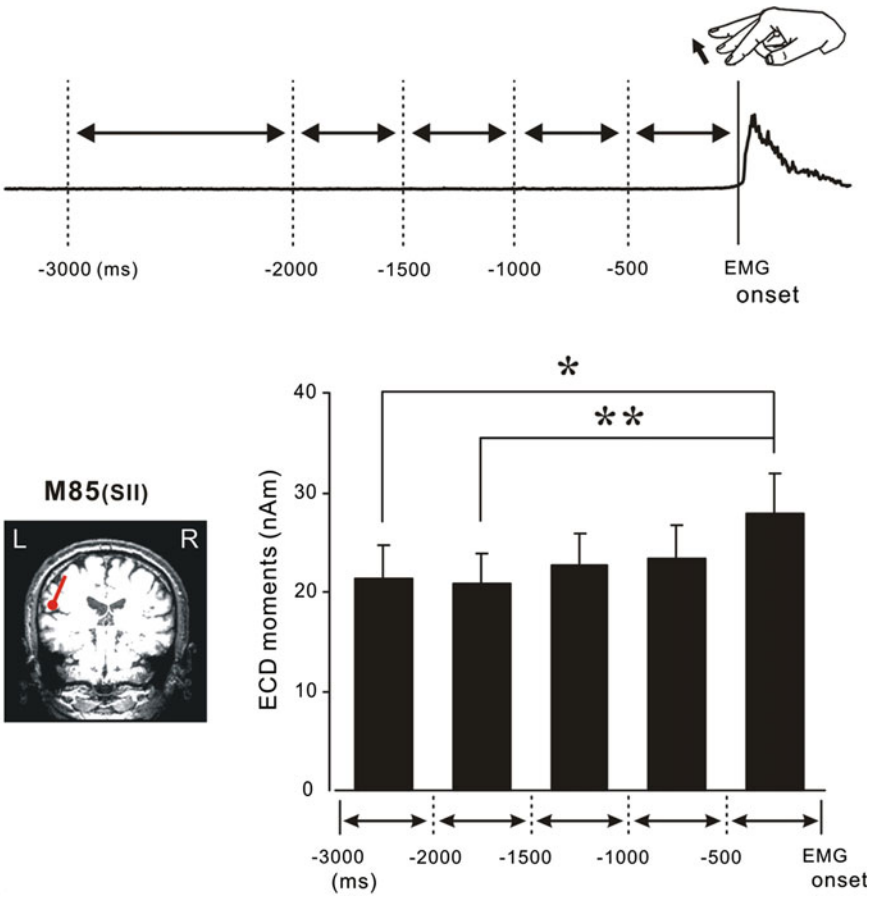

Fig. 2 The premovement subperiods and the onset of the rectified EMG. The preparatory period was divided into five subperiods from the onset of EMG to 3000 ms before movement. The time scale is expressed in minus values before the onset of movement. The dipole for the 80 ms response was identified in the temporal region, corresponding to the SII cortices. The graph shows the mean and standard error of the dipole moment of the SII contralateral to electrical stimulation in the premovement subperiods. * $p < 0.05$, ** $p < 0.01$; Statistical significance within two pairs. The dipole moment for the SII was significantly larger in the 0–500 ms subperiod than the 1500–2000 ms or 2000–3000 ms subperiod before EMG onset. Adapted from Wasaka et al. (2005a)

systems regulate sensory information at several processing stages by the centrifugal process. Motor commands can facilitate or suppress sensory responsiveness and, thus, probably perception, depending on temporal and behavioral constraints.

Removal of the SI area seriously impaired the processing of tactile information in the SII in macaques (Pons et al. 1987). However, deactivation of the SI did not have clear effects on the responsiveness of the SII (Zhang et al. 1996). In addition, tactile information could be directly conveyed to both SI and SII cortices from overlapping

regions within the ventral posterior nucleus of the thalamus (Zhang et al. 2001). In humans, MEG responses from SII increased with active attention, while little effect of attention was observed in the SI (Mima et al. 1998; Fujiwara et al. 2002). Moreover, the responses in the SI and SII are modulated differently depending on the intensity of the electrical stimulation (Torquati et al. 2002; Lin et al. 2003). From these results, it appears that somatosensory information processing, concerning sensorimotor integration in SII, may be independent of that in SI.

Our sensory systems are constantly bombarded by numerous sensory stimuli, from which we must extract the few stimuli important to the control of our movement. One can therefore recognize that an attenuation of SI activation is involved in filtering information. Although much attention has been given to sensorimotor integration in the SI, there is little evidence of such a phenomenon in the SII and the role of the SII in motor execution has not been fully elucidated in humans. Compared with the SI, SII is speculated to serve a higher level of cognitive function in somatosensory information processing, such as attention, decision-making, object recognition, and the integration of nociceptive and non-nociceptive inputs (Mima et al. 1998; Steinmetz et al. 2000; Romo et al. 2002; Inui et al. 2003; Qiu et al. 2004). Our results showed that these cortical areas play a different functional role in sensorimotor integration. When we are moving, the sensory threshold is attenuated. By contrast, exploration using fingertips is sensitive during movement execution (active touch). This neural mechanism can be explained by an enhancement of SII activation. To clarify the function of SII concerning sensorimotor integration, we conducted further research.

7 Crossmodal Interaction Between Somatosensory and Visual Information

Crossmodal interaction occurs when neural activity from one sensory modality modulates activity in another (Macaluso et al. 2000; Kida et al. 2007). Crossmodal links between visual and somatosensory information have shown the critical role of vision in determining limb position and localizing tactile sensations (vanBeers et al. 1996; Botvinick and Cohen 1998; Graziano 1999). For example, viewing a body part improves tactile perception and facilitates the amplitude of long-latency components of event-related potentials (Taylor-Clarke et al. 2002; Cardini et al. 2011). In addition, there is evidence that vision of the body is crucial for localization of tactile stimuli (Eimer et al. 2004; Sambo et al. 2009).

Although less attention has been devoted to the effect of observation of movement on information processing in somatosensory areas, some studies have reported neural modulation in SI and SII. Previous studies showed that viewing another person's gestures modulates the excitability of somatosensory areas (Avikainen et al. 2002; Rossi et al. 2002; Mottonen et al. 2005; Pihko et al. 2010). These results indicate that the somatosensory areas are involved in the mirroring of actions.

8 Somatosensory and Visual Interaction During the Execution of Voluntary Movement

Recognizing one's own movement is essential to the control of voluntary movement. Movement causes changes to sensory inflow as well as changes in the position of body parts. The movement of one's body parts is perceived not only by visual information but also by somatosensory feedback from muscles, skin and tendons which provide information on the status of each part being moved in a moment. Under normal conditions, the visual estimate of limb position is congruent with the somatosensory estimate and motor command, and movement is usually achieved automatically without awareness of the component processes. By contrast, in novel motor tasks or situations which produce conflict or incongruence between intentions and sensorimotor consequences, the mismatch between the actual sensory feedback and predicted movement of the body part disrupts motor execution. A crucial issue is elucidating the brain mechanisms that integrate the multi-sensory information and motor commands for motor control.

It has been suggested that a copy of the motor signal, known as an efference copy, is created so that sensory signals generated from external stimuli can be distinguished from reafferent signals from body movement (von Holst and Mittelstaedt 1950; Wolpert et al. 1998). Corollary discharges are produced only if the motor commands interact with unpredicted sensory inputs and inhibit the neural response to self-generated sensory signals (Sperry 1950). More activity in somatosensory areas was found when an unpredicted stimulus was externally delivered (Hesse et al. 2010). Since crossmodal interaction between somatosensory and visual inputs exists in the somatosensory areas, there is considerable validity to the notion that the prediction of visual feedback of movement modulates the somatosensory areas.

We investigated whether activation in somatosensory areas was affected by discordance between an intended and executed action. A mirror box creates unintended visual feedback of body movement (Fig. 3). Subjects inserted their hands into the mirror box with the forearm supine (Mirror condition). The position of the right hand was adjusted so that the mirror image precisely overlapped the view of the masked left hand. Since the actual visual information on the left hand was masked by the mirror, a mirror image of the right hand was provided. In the Normal and Mirror conditions, subjects experienced the appropriate somatosensory feedback, but in the Mirror condition, what they watched was incongruent with the expected visual feedback which produced a state of cognitive conflict. The motor task was a self-paced thumb movement of the left hand. Electrical stimulation for the recording of somatosensory responses was delivered to the median nerve at the left wrist. Subjects watched the stationary image of the hand while they performed the self-paced movement of the left thumb. In this situation, subjects felt that the movement was not controlled by themselves or the moving body part did not belong to them. The cortical response showed that neural activation in the SII and parietal cortex was strongly affected by the unexpected visual

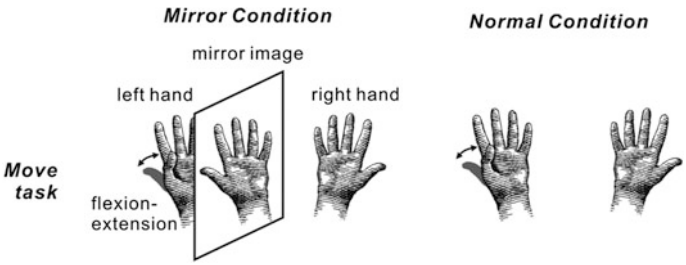

Fig. 3 Schema of the experimental paradigm. In the Mirror condition, subjects inserted their hands into a mirror box with the forearm supine. The position of the *right hand* was adjusted so that the mirror image precisely overlapped the view of the masked *left hand*. A mirror image of the *right hand* was presented instead of the *left hand*. Subjects performed self-paced continuous and repetitive flexion-extension of the *left thumb* in the normal visual feedback (*Normal condition*) and the incongruent non-veridical visual feedback condition (*Mirror condition*). Electrical stimulation for the recording of somatosensory responses was delivered to the median nerve at the *left wrist*. Adapted from Wasaka et al. (2012a)

feedback (Fig. 4) (Wasaka and Kakigi 2012a; Wasaka and Kakigi 2012b). The SII showed significantly higher activation with unpredicted visual feedback of movement, whereas the opposite was true of the parietal activation. These results provide evidence that the visual information modulates activation in somatosensory areas during voluntary movement.

The parietal cortex has been implicated in mediating multisensory integration in different modalities (Andersen et al. 1997) while a fronto-parietal network has been shown to be involved in selecting behaviorally relevant stimuli (Posner and Petersen 1990; Corbetta et al. 1998; Burton et al. 1999). The parietal area integrates the predicted proprioceptive and visual feedback to calculate how the commands affected the state of the body (Shadmehr and Krakauer 2008). The new finding was that the SII had crossmodal functions in the somatosensory and visual modalities during motor execution, and the visual information plays a crucial role in sensorimotor integration of the SII during motor execution. Modulation in the SII during conflicting visual feedback might be involved in computing the motor errors by comparing the actual hand location to the estimated location for controlling movement.

The forward model of the motor system predicts the behavior of a body segment in response to a motor command. In this model, a motor plan is updated continuously by internal feedback loops, and the parietal cortex and cerebellum appear to play a crucial role. In the Mirror condition, subjects faced the surprise of seeing their hand not responding as expected, and our results showed a modulation of activation in the parietal area. We assume that this modulation during conflicting visual feedback might be involved in computing the motor errors by comparing the actual hand location to the estimated location for controlling movement.

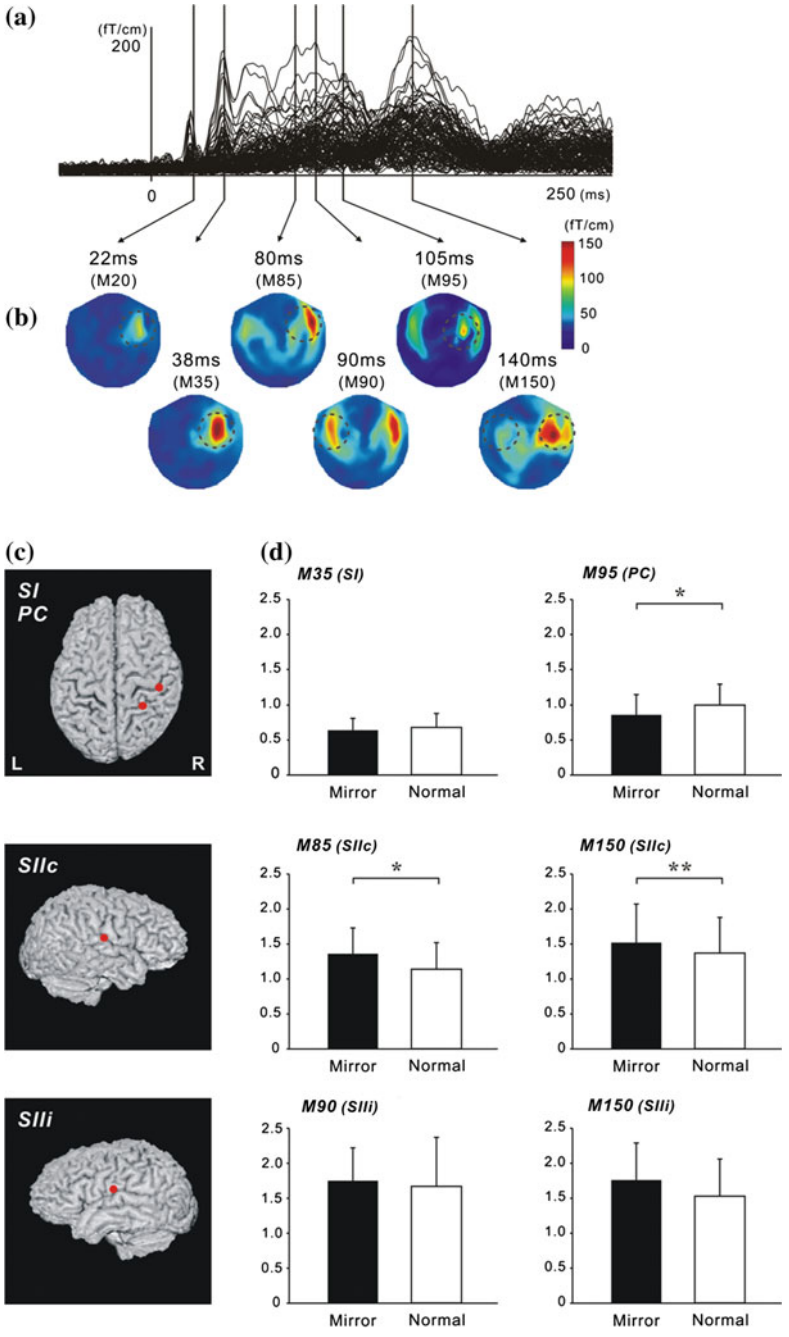
(a)
(fT/cm)
200
0
250 (ms)
(fT/cm)
150
100
50
0
(b)
22ms
(M20)
80ms
(M85)
105ms
(M95)
38ms
(M35)
90ms
(M90)
140ms
(M150)
(c)
SI
PC
L
R
SIIc
SIIi
(d)
M35 (SI)
M95 (PC)
M85 (SIIc)
M150 (SIIc)
M90 (SIIi)
M150 (SIIi)
Mirror
Normal
*
**

◀**Fig. 4** Superimposed MEG waveforms and topographical maps. **a** Superimposed root sum square (RSS) waveforms from 102 sensors. **b** Map of the topography of the RSS at the peak components. The first cortical activation was identified around the central area contralateral to the hemisphere of the side stimulus (M20 and M35). Then, bilateral activations were identified in temporal areas at around 80–100 ms (SII). PC activity was identified in the centro-parietal area located posterior to the SI activity. **c** The location of equivalent current dipoles in each component superimposed on 3D images. **d** The modulation of RSS components with voluntary movement in the Mirror and Normal conditions. A significant difference was observed in the components in the SIIc (M85 and M150) and PC (M95). The ratios of the M85 and M150 in the SIIc were significantly larger in the Mirror than Normal Condition. By contrast, the ratio of the M95 was significantly smaller in the Mirror condition than Normal condition. * $p < 0.05$, ** $p < 0.01$; Statistical significance within two pairs. Adapted from Wasaka et al. (2012a)

9 Sensorimotor Integration Related to the Feeling of Agency

There is evidence that humans are normally not consciously aware of sensory feedback from movement (Fourneret and Jeannerod 1998), and are aware that their arms and legs belong to them through somatosensory and visual inputs. This feeling of self-attribution is impaired when the predicted sensory information estimated from motor intention does not match the actual sensory information. In our study, the Mirror condition corresponded to this situation. Some subjects reported feeling that movement was not controlled by themselves or the body did not belong to them in the Mirror condition. We showed a significant enhancement of a SII component at around 150 ms and reduction of parietal activation in the non-veridical visual feedback of movement (Wasaka and Kakigi 2012a). Our group reported simultaneous activation in the SII and insula peaking at 90 to 160 ms after electrical stimulation. We assumed that the late component peaking at 150 ms in the SII may involve the activity of the neighboring insula (Inui et al. 2003). Studies in patients and recent neuroimaging results in healthy subjects suggest a prominent role for the posterior parietal cortex (Farrer et al. 2008) and insula (Farrer et al. 2003; Karnath et al. 2005) in the sense of limb ownership as well as the self-awareness of limb actions, the sense of agency. Further study will be needed to clarify the functional role of these areas in sensorimotor integration.

10 Conclusions

The sensory information for movement is provided by visual and somatosensory feedback. It has been postulated that the integration between motor commands and sensory information plays an important role in motor control. Efferent neural signals created by central motor networks in parallel with the motor commands are used to predict the sensory consequences of own motor acts. In this process, this signal modulates information processing in sensory areas. Preceding and during voluntary movement, it has been reported that information processing in

somatosensory areas is modulated by the effect of efferent signals. Activities in the SI show a reduction with voluntary movement, whereas those in the SII are enhanced. The functional role for this difference in modulation in somatosensory areas may be the regulation of motor control by facilitating the appropriate information and/or suppressing inappropriate information. Compared with SI, SII is speculated to serve a higher level of somatosensory information processing, such as decision-making, objective recognition and integration of nociceptive and non-nociceptive inputs. Our research showed that neural responses in SII was strongly affected by the unexpected visual feedback during movement execution. This result provides evidence that the visual information plays a crucial role in sensorimotor integration in the SII.

References

Allison T, McCarthy G, Wood CC, Jones SJ (1991) Potentials evoked in human and monkey cerebral cortex by stimulation of the median nerve. a review of scalp and intracranial recordings. Brain 114:2465–2503

Andersen RA, Snyder LH, Bradley DC, Xing J (1997) Multimodal representation of space in the posterior parietal cortex and its use in planning movements. Annu Rev Neurosci 20:303–330

Avikainen S, Forss N, Hari R (2002) Modulated activation of the human SI and SII cortices during observation of hand actions. Neuroimage 15(3):640–646

Blakemore SJ, Goodbody SJ, Wolpert DM (1998) Predicting the consequences of our own actions: the role of sensorimotor context estimation. J Neurosci 18(18):7511–7518

Bocker KB, Forget R, Brunia CH (1993) The modulation of somatosensory evoked potentials during the foreperiod of a forewarned reaction time task. Electroencephalogr Clin Neurophysiol 88(2):105–117

Botvinick M, Cohen J (1998) Rubber hands 'feel' touch that eyes see. Nature 391(6669):756

Burton H, Abend NS, MacLeod AM, Sinclair RJ, Snyder AZ, Raichle ME (1999) Tactile attention tasks enhance activation in somatosensory regions of parietal cortex: a positron emission tomography study. Cereb Cortex 9(7):662–674

Cardini F, Longo MR, Haggard P (2011) Vision of the body modulates somatosensory intracortical inhibition. Cereb Cortex 21(9):2014–2022

Cohen LG, Starr A (1987) Localization, timing and specificity of gating of somatosensory evoked potentials during active movement in man. Brain 110:451–467

Corbetta M, Akbudak E, Conturo TE, Snyder AZ, Ollinger JM, Drury HA, Linenweber MR, Petersen SE, Raichle ME, Van Essen DC, Shulman G (1998) A common network of functional areas for attention and eye movements. Neuron 21(4):761–773

Crapse TB, Sommer MA (2008) Corollary discharge circuits in the primate brain. Curr Opin Neurobiol 18(6):552–557

Desmedt JE, Nguyen TH, Bourguet M (1987) Bit-mapped color imaging of human evoked potentials with reference to the N20, P22, P27 and N30 somatosensory responses. Electroencephalogr Clin Neurophysiol 68(1):1–19

Desmedt JE, Tomberg C (1989) Mapping early somatosensory evoked potentials in selective attention: critical evaluation of control conditions used for titrating by difference the cognitive P30, P40, P100 and N140. Electroencephalogr Clin Neurophysiol 74(5):321–346

Eimer M, Forster B, Fieger A, Harbich S (2004) Effects of hand posture on preparatory control processes and sensory modulations in tactile-spatial attention. Clin Neurophysiol 115(3):596–608

Farrer C, Franck N, Georgieff N, Frith CD, Decety J, Jeannerod M (2003) Modulating the experience of agency: a positron emission tomography study. Neuroimage 18(2):324–333

Farrer C, Frey SH, Van Horn JD, Tunik E, Turk D, Inati S, Grafton ST (2008) The angular gyrus computes action awareness representations. Cereb Cortex 18(2):254–261

Forss N, Jousmaki V (1998) Sensorimotor integration in human primary and secondary somatosensory cortices. Brain Res 781(1–2):259–267

Fourneret P, Jeannerod M (1998) Limited conscious monitoring of motor performance in normal subjects. Neuropsychologia 36(11):1133–1140

Fujiwara N, Imai M, Nagamine T, Mima T, Oga T, Takeshita K, Toma K, Shibasaki H (2002) Second somatosensory area (SII) plays a significant role in selective somatosensory attention. Brain Res Cogn Brain Res 14(3):389–397

Garcia-Larrea L, Lukaszewicz AC, Mauguiere F (1995) Somatosensory responses during selective spatial attention: the N120-to-N140 transition. Psychophysiology 32(6):526–537

Graziano MSA (1999) Where is my arm? The relative role of vision and proprioception in the neuronal representation of limb position. Proc Nat Acad Sci USA 96(18):10418–10421

Hari R, Hamalainen H, Hamalainen M, Kekoni J, Sams M, Tiihonen J (1990) Separate finger representations at the human second somatosensory cortex. Neuroscience 37(1):245–249

Hesse MD, Nishitani N, Fink GR, Jousmaki V, Hari R (2010) Attenuation of somatosensory responses to self-produced tactile stimulation. Cereb Cortex 20(2):425–432

Hoshiyama M, Sheean G (1998) Changes of somatosensory evoked potentials preceding rapid voluntary movement in Go/No-go choice reaction time task. Brain Res Cogn Brain Res 7(2):137–142

Huttunen J, Wikstrom H, Korvenoja A, Seppalainen AM, Aronen H, Ilmoniemi RJ (1996) Significance of the second somatosensory cortex in sensorimotor integration: enhancement of sensory responses during finger movements. NeuroReport 7(5):1009–1012

Hyvarinen J, Poranen A, Jokinen Y (1980) Influence of attentive behavior on neuronal responses to vibration in primary somatosensory cortex of the monkey. J Neurophysiol 43(4):870–882

Ikeda A, Luders HO, Burgess RC, Shibasaki H (1992) Movement-related potentials recorded from supplementary motor area and primary motor area. Role of supplementary motor area in voluntary movements. Brain 115:1017–1043

Inoue K, Yamashita T, Harada T, Nakamura S (2002) Role of human SII cortices in sensorimotor integration. Clin Neurophysiol 113(10):1573–1578

Inui K, Wang X, Qiu Y, Nguyen BT, Ojima S, Tamura Y, Nakata H, Wasaka T, Tran TD, Kakigi R (2003) Pain processing within the primary somatosensory cortex in humans. Eur J Neurosci 18(10):2859–2866

Inui K, Wang X, Tamura Y, Kaneoke Y, Kakigi R (2004) Serial processing in the human somatosensory system. Cereb Cortex 14(8):851–857

Iriki A, Tanaka M, Iwamura Y (1996) Attention-induced neuronal activity in the monkey somatosensory cortex revealed by pupillometrics. Neurosci Res 25(2):173–181

Jiang W, Chapman CE, Lamarre Y (1990) Modulation of somatosensory evoked responses in the primary somatosensory cortex produced by intracortical microstimulation of the motor cortex in the monkey. Exp Brain Res 80(2):333–344

Johansen-Berg H, Christensen V, Woolrich M, Matthews PM (2000) Attention to touch modulates activity in both primary and secondary somatosensory areas. NeuroReport 11(6):1237–1241

Jones EG, Coulter JD, Hendry SH (1978) Intracortical connectivity of architectonic fields in the somatic sensory, motor and parietal cortex of monkeys. J Compative Neurol 181(2):291–347

Jones SJ, Halonen JP, Shawkat F (1989) Centrifugal and centripetal mechanisms involved in the 'gating' of cortical SEPs during movement. Electroencephalogr Clin Neurophysiol 74(1):36–45

Kakigi R, Koyama S, Hoshiyama M, Watanabe S, Shimojo M, Kitamura Y (1995) Gating of somatosensory evoked responses during active finger movements magnetoencephalographic studies. J Neurol Sci 128(2):195–204

Karnath HO, Baier B, Nagele T (2005) Awareness of the functioning of one's own limbs mediated by the insular cortex? J Neurosci 25(31):7134–7138

Kawamura T, Nakasato N, Seki K, Kanno A, Fujita S, Fujiwara S, Yoshimoto T (1996) Neuromagnetic evidence of pre- and post-central cortical sources of somatosensory evoked responses. Electroencephalogr Clin Neurophysiol 100(1):44–50

Kida T, Inui K, Wasaka T, Akatsuka K, Tanaka E, Kakigi R (2007) Time-varying cortical activations related to visual-tactile cross-modal links in spatial selective attention. J Neurophysiol 97(5):3585–3596

Kida T, Nishihira Y, Wasaka T, Sakajiri Y, Tazoe T (2004) Differential modulation of the short- and long-latency somatosensory evoked potentials in a forewarned reaction time task. Clin Neurophysiol 115(10):2223–2230

Kida T, Wasaka T, Inui K, Akatsuka K, Nakata H, Kakigi R (2006) Centrifugal regulation of human cortical responses to a task-relevant somatosensory signal triggering voluntary movement. Neuroimage 32(3):1355–1364

Lin YY, Shih YH, Chen JT, Hsieh JC, Yeh TC, Liao KK, Kao CD, Lin KP, Wu ZA, Ho LT (2003) Differential effects of stimulus intensity on peripheral and neuromagnetic cortical responses to median nerve stimulation. Neuroimage 20(2):909–917

Lin YY, Simoes C, Forss N, Hari R (2000) Differential effects of muscle contraction from various body parts on neuromagnetic somatosensory responses. Neuroimage 11(4):334–340

Macaluso E, Frith CD, Driver J (2000) Modulation of human visual cortex by crossmodal spatial attention. Science 289(5482):1206–1208

Mauguiere F, Merlet I, Forss N, Vanni S, Jousmaki V, Adeleine P, Hari R (1997) Activation of a distributed somatosensory cortical network in the human brain: a dipole modelling study of magnetic fields evoked by median nerve stimulation. Part II: effects of stimulus rate, attention and stimulus detection. Electroencephalogr Clin Neurophysiol 104(4):290–295

Mima T, Nagamine T, Nakamura K, Shibasaki H (1998) Attention modulates both primary and second somatosensory cortical activities in humans: a magnetoencephalographic study. J Neurophysiol 80(4):2215–2221

Mottonen R, Jarvelainen J, Sams M, Hari R (2005) Viewing speech modulates activity in the left SI mouth cortex. Neuroimage 24(3):731–737

Murase N, Kaji R, Shimazu H, Katayama-Hirota M, Ikeda A, Kohara N, Kimura J, Shibasaki H, Rothwell JC (2000) Abnormal premovement gating of somatosensory input in writer's cramp. Brain 123:1813–1829

Nakajima T, Wasaka T, Kida T, Nishimura Y, Fumoto M, Sakamoto M, Takashi E (2006) Changes in somatosensory evoked potentials and Hoffmann reflexes during fast isometric contraction of foot plantarflexor in humans. Percept Mot Skills 103(3):847–860

Nakata H, Inui K, Wasaka T, Nishihira Y, Kakigi R (2003) Mechanisms of differences in gating effects on short- and long-latency somatosensory evoked potentials relating to movement. Brain Topogr 15(4):211–222

Pihko E, Nangini C, Jousmaki V, Hari R (2010) Observing touch activates human primary somatosensory cortex. Eur J Neurosci 31(10):1836–1843

Pons TP, Garraghty PE, Friedman DP, Mishkin M (1987) Physiological evidence for serial processing in somatosensory cortex. Science 237(4813):417–420

Posner MI, Petersen SE (1990) The attention system of the human brain. Annu Rev Neurosci 13:25–42

Qiu Y, Inui K, Wang X, Nguyen BT, Tran TD, Kakigi R (2004) Effects of distraction on magnetoencephalographic responses ascending through C-fibers in humans. Clin Neurophysiol 115(3):636–646

Romo R, Hernandez A, Zainos A, Lemus L, Brody CD (2002) Neuronal correlates of decision-making in secondary somatosensory cortex. Nat Neurosci 5(11):1217–1225

Rossi S, Tecchio F, Pasqualetti P, Ulivelli M, Pizzella V, Romani GL, Passero S, Battistini N, Rossini PM (2002) Somatosensory processing during movement observation in humans. Clin Neurophysiol 113(1):16–24

Rushton DN, Rothwell JC, Craggs MD (1981) Gating of somatosensory evoked potentials during different kinds of movement in man. Brain 104(3):465–491

Sambo CF, Gillmeister H, Forster B (2009) Viewing the body modulates neural mechanisms underlying sustained spatial attention in touch. Eur J Neurosci 30(1):143–150
Schmidt RF, Schady WJ, Torebjork HE (1990) Gating of tactile input from the hand. I. Effects of finger movement. Exp Brain Res 79(1):97–102
Shadmehr R, Krakauer JW (2008) A computational neuroanatomy for motor control. Exp Brain Res 185(3):359–381
Sperry RW (1950) Neural basis of the spontaneous optokinetic response produced by visual inversion. J Compar Physiol Psychol 43(6):482–489
Staines WR, Graham SJ, Black SE, McIlroy WE (2002) Task-relevant modulation of contralateral and ipsilateral primary somatosensory cortex and the role of a prefrontal-cortical sensory gating system. Neuroimage 15(1):190–199
Starr A, Cohen LG (1985) 'Gating' of somatosensory evoked potentials begins before the onset of voluntary movement in man. Brain Res 348(1):183–186
Steinmetz PN, Roy A, Fitzgerald PJ, Hsiao SS, Johnson KO, Niebur E (2000) Attention modulates synchronized neuronal firing in primate somatosensory cortex. Nature 404(6774):187–190
Taylor-Clarke M, Kennett S, Haggard P (2002) Vision modulates somatosensory cortical processing. Curr Biol 12(3):233–236
Torquati K, Pizzella V, Della Penna S, Franciotti R, Babiloni C, Rossini PM, Romani GL (2002) Comparison between SI and SII responses as a function of stimulus intensity. NeuroReport 13(6):813–819
vanBeers RJ, Sittig AC, vanderGon JJD (1996) How humans combine simultaneous proprioceptive and visual position information. Exp Brain Res 111(2):253–261
von Holst E, Mittelstaedt H (1950) Das Reafferenzprinzip: Wechselwirkungen Zwischen Zentralnervensystem und Peripherie. Natursissenschaften 37:464–476
Wasaka T, Hoshiyama M, Nakata H, Nishihira Y, Kakigi R (2003) Gating of somatosensory evoked magnetic fields during the preparatory period of self-initiated finger movement. Neuroimage 20(3):1830–1838
Wasaka T, Kakigi R (2012a) Conflict caused by visual feedback modulates activation in somatosensory areas during movement execution. Neuroimage 59(2):1501–1507
Wasaka T, Kakigi R (2012b) The effect of unpredicted visual feedback on activation in the secondary somatosensory cortex during movement execution. BMC Neurosci 13(1):138
Wasaka T, Nakata H, Akatsuka K, Kida T, Inui K, Kakigi R (2005a) Differential modulation in human primary and secondary somatosensory cortices during the preparatory period of self-initiated finger movement. Eur J Neurosci 22(5):1239–1247
Wasaka T, Nakata H, Kida T, Kakigi R (2005b) Changes in the centrifugal gating effect on somatosensory evoked potentials depending on the level of contractile force. Exp Brain Res 166(1):118–125
Wikstrom H, Huttunen J, Korvenoja A, Virtanen J, Salonen O, Aronen H, Ilmoniemi RJ (1996) Effects of interstimulus interval on somatosensory evoked magnetic fields (SEFs): a hypothesis concerning SEF generation at the primary sensorimotor cortex. Electroencephalogr Clin Neurophysiol 100(6):479–487
Wolpert DM, Miall RC, Kawato M (1998) Internal models in the cerebellum. Trends Cogn Sci 2(9):338–347
Zhang HQ, Murray GM, Coleman GT, Turman AB, Zhang SP, Rowe MJ (2001) Functional characteristics of the parallel SI- and SII-projecting neurons of the thalamic ventral posterior nucleus in the marmoset. J Neurophysiol 85(5):1805–1822
Zhang HQ, Murray GM, Turman AB, Mackie PD, Coleman GT, Rowe MJ (1996) Parallel processing in cerebral cortex of the marmoset monkey: effect of reversible SI inactivation on tactile responses in SII. J Neurophysiol 76(6):3633–3655

Organizational Neuroscience: A New Frontier for Magnetoencephalography?

Sven Braeutigam

Abstract Organizational neuroscience is an emerging field of research aimed at the neuro-scientific study of human behavior in organizations. The purpose of this short chapter is to provide a brief overview of the field and to make an informed guess about the role magnetoencephalography might play by exploiting the strengths of this technology. Also, some of the broader conceptual challenges and ethical considerations are touched upon that have been raised by recent neuro-technologies and that will most likely be relevant to organizational neuroscience as well.

Keywords Organizational neuroscience · Neuroeconomics · Neuromarketing · Magnetoencephalography · Decision making

1 Introduction

Organizational neuroscience, ON for short, is an emerging, highly interdisciplinary area of research that explores the implications of brain science for workplace behavior. ON builds on key theories and methods of behavioral, cognitive, and social psychology and attempts to incorporate advances in neuroscience that have failed to reach organizational and/or business research as yet. The broad aim is a better understanding, explanation and prediction of human behavior in organizational relevant situations, which might ultimately provide evidence-based recommendations for practice. It is hoped that neuroscience methodology will help to push organizational research in exciting new directions such as how and why managers make appropriate decisions or how serial entrepreneurs might perceive and act upon risk differently than others (Becker et al. 2011; Senior et al. 2011; Lee et al. 2012).

S. Braeutigam (✉)
Oxford Centre for Human Brain Activity, University of Oxford,
Oxford OX3 7JX, UK
e-mail: sven.braeutigam@psych.ox.ac.uk

S. Supek and C. J. Aine (eds.), *Magnetoencephalography*,
DOI: 10.1007/978-3-642-33045-2_35,

As an area of research, ON is distinct from but nevertheless related to two established neuro-technologies, namely neuroeconomics and neuromarketing. The former combines neuroscience, psychology and economics for the study of how people evaluate gains, losses and rewards in economic decision-making (Camerer 2008). The latter specifically adopts imaging tools to investigate customer choices for marketing purposes such as TV commercials (Ariely and Berns 2010). Note some protagonists refer to OCN (organizational cognitive neuroscience) in order to emphasize the role of cognitive processes, however, this distinction is not made in this paper.

2 A Role for MEG

From a neurophysiological perspective, organizational researchers are intrigued by the superior temporal resolution of MEG, which, in conjunction with powerful source estimation approaches, allows the detailed mapping of brain activity associated with complex cognitive processes. In particular, rapid responses that occur at the edge between perception and cognition are deemed powerful markers in the quest for better models of decision-making and judgment under uncertainty (Senior et al. 2011). As an illustrative example taken from the neuroeconomics literature, a recent study utilized MEG to study the neural mechanisms associated with buying decisions that have potentially long-term consequences (Hedgcock et al. 2010).

In a real estate scenario, the subjects were given the choice to buy an expensive apartment (high monthly mortgage) located in a safe neighborhood or to buy a cheap apartment located in a less safe area with a modest crime rate. The authors found that neural responses over frontal and parietal cortices correlated with trial outcome as early as a 500 ms after presentation of choice options, and several seconds before the buying decision was communicated. The significance of such early neuronal activity is currently unresolved, as to what processes may be occurring during the time between divergence of neuronal response and the decision. These neuronal responses, however, appear to reflect higher-order cognitive processes outside awareness, raising the possibility that economically relevant behavior is, to some extent, decided upon long before it becomes manifest. If so, a deeper understanding of these neuronal systems might yield insight into why individuals often seem unaware of the relative importance of different choice attributes that affect their perceptions regarding the attractiveness of their choice options (Dhar and Simonson 2003; Braeutigam 2012).

From an organizational perspective, research on leadership and associated management training programs have been highlighted as areas of particular interest to ON. A relevant scenario might be to use MEG in order to study the neuronal mechanisms supporting the interaction and relationship aspects of a leader and his/her team (Becker et al. 2011). Clearly, it would be impossible to reduce leader-team interactions to individual brains, however, contextual effects

can be reliably quantified at the level of neuronal processes with the help of well known marker signals such as the N400 response. This response is observed at about 400 ms after stimulus onset and can be elicited by a broad range of meaningful stimuli, including but not restricted to auditory and visual words, pictures, sign language, faces and environmental sounds (Kutas and Federmeier 2011). It is generally assumed that the N400 indexes neuronal processes related to semantic memory. Moreover, it has been suggested that neuronal responses at 400 ms reflect gender specific cognitive strategies in choice making in real life situations (Braeutigam et al. 2004). Thus, it is conceivable that MEG could build towards a better understanding of how the human brain responds to and utilizes contextual information within an organizational setting. In particular, one might be able to shed some light on why a declaration of intent of a leader may in some situations be taken as invigorating, while in others as merely ridiculous.

3 Challenges

Important challenges have been posed regarding the validity and generalizability of the insight gained from neuroscience-based approaches such as neuroeconomics and neuromarketing. It is likely that organizational neuroscientists, as time progresses, will have to face similar conceptual issues, but will also be able to draw on accepted methods in order to overcome limitations.

Specifically, a criticism has been made that all that neuroeconomic research has been able to identify so far has been the brain regions that appear to be activated in response to certain decisions and choices, or responses to reward stimuli. Accordingly, the evidence is of correlation, making the interpretation of causality difficult, if not impossible (Harrison 2008; Birnberg and Granguly 2012). Despite this being a deeply fundamental even philosophical issue, a mathematical framework known as Bayesian inference can be utilized in order to maximize the insight gained from individual studies. Accordingly, a large number of correlations, if available, can be exploited to support reverse inference, i.e., inferring the likelihood of a cognitive process from a pattern of brain activity (Poldrack 2011; Braeutigam 2012). An example often cited in the neuroeconomics literature is the probability that a reward process is present given nucleus accumbens activation.

The nucleus accumbens is part of the ventral striatum implicated in the processing of reward, novelty, and salience. Using meta-analytical techniques based on over 1,000 studies in conjunction with Bayesian inference, it can be shown that there is a moderate, almost strong, evidence to infer reward-related processes when observing nucleus accumbens activation, although nucleus accumbens activation is not necessarily observed in studies utilizing a reward task (Poldrack 2011). In general, Bayesian approaches are strong, meaning that, under suitable conditions, unknown or difficult to estimate quantities become irrelevant and final inferences robust. This is important as, for example, there is a plethora of N400 studies (many using MEG) that could potentially be exploited for leadership studies indicated above.

The issue of ecological validity is also relevant. Invariably, most of the neuroimaging results will be produced under controlled laboratory conditions, and it might not be straightforward to extrapolate to a genetically and culturally diverse population of people in a vast variety of organizational situations. It is likely that OCN will follow a recent trend and make use of virtual-reality technologies in order to boost generalizability of the insight gained from MEG studies. Strongly related to this will be an increased reliance on paradigms with broader real-life content as already employed in some areas of neuroeconomics and neuromarketing. Of particular interest are approaches addressing the issue of drawing conclusions about real decisions based on hypothetical reports of intended behavior often utilized in experiments when implementing real choice is considered impractical or unethical.

A relevant example is a functional magnetic resonance imaging study that required the subjects to make hypothetical (trial did not count) and real (trial would be implemented as real) purchasing decisions (Jeong-Kang et al. 2011). Interestingly, the authors observed neuronal activity in the orbitofrontal cortex and the ventral striatum that correlated with behavioral measures of the stimulus value of the consumer goods in both types of decision. Despite apparent differences in other regions, the substantial overlap in neural activity between the two conditions suggests that conclusions about neural circuitry drawn from hypothetical choice might generalize to real choice when making purchasing decisions.

4 Ethical Considerations

It is important to note that existing neuromarketing and, to a lesser degree neuroeconomics research has been subject to controversy within the scientific press, including editorials in high impact journals such as Lancet Neurology (2004, 3:71) and Nature Neuroscience (2004, 7:683). There is no doubt that brain-imaging technology will increasingly be used in commercial, organizational and governmental settings raising concerns neuroscience methodologies might be used in ways that infringe on personal privacy to an unacceptable degree. In response, researchers have begun to outline guidelines and recommendations aimed at the protection of individual autonomy, averting harm and exploitation caused by the research and maintaining public trust in neuroscience. The ethical issues at hand are non-trivial, however, it has been argued that there is currently no evidence that any advanced neuroscience-based technology permits the types of insights and subsequent manipulations that critics envisage. Ultimately, one has to observe and consider the implications that such a development might have and by which means it might be sensibly managed or regulated (Murphy et al. 2008; Fisher et al. 2010).

5 Conclusion

Despite challenges, concerns and possible adverse implications, the potential role MEG can play in new applications aimed at the level of groups, organizations or even societies appears huge. ON is still in its nascent state but it is likely to gain momentum rapidly offering an excellent opportunity for MEG researchers to be at the forefront of charting new territory. Importantly, neuroeconomics and, to a lesser degree neuromarketing are increasingly recognized by clinicians as potentially powerful frameworks for investigating, amongst others, mental disorders, addiction and ageing (Brown and Ridderinkhof 2009; Hasler 2012). Assuming this trend continues, embarking on the ON venture is likely to strengthen the standing of MEG in clinical sciences.

Acknowledgements This work was supported by the Department of Psychiatry, University of Oxford, UK.

References

Ariely D, Berns GS (2010) Neuromarketing: the hope and hype of neuroimaging in business. Nat Rev Neurosci 11:284–292

Becker WJ, Cropanzano R, Sanfey AG (2011) Organizational neuroscience: taking organizational theory inside the neural black box. J Manag 37(4):933–961

Birnberg JG, Ganguly AR (2012) Is neuroaccounting waiting in the wings? An essay. Acc Organ Soc 37:1–13

Braeutigam S, Rose SPR, Swithenby SJ, Ambler T (2004) The distributed neuronal systems supporting choice-making in real-life situations: differences between men and women when choosing groceries detected using magnetoencephalography. Eur J Neurosci 20:293–302

Braeutigam S (2012) Neural systems supporting and affecting economically relevant behavior. Neurosci Neuroecon 1:11–23

Brown SBRE, Ridderinkhof KR (2009) Aging and the neuroeconomics of decision making: a review. Cogn, Affect Behav Neurosci 9(4):365–379

Camerer CF (2008) Neuroeconomics: opening the grey box. Neuron 60:416–419

Dhar R, Simonson I (2003) The effect of forced choice on choice. J Mark Res 40:146–160

Fisher CE, Chin L, Klitzman R (2010) Defining neuromarketing: practices and professional challenges. Harvard Rev Psychiatry 18(4):230–237

Harrison GW (2008) Neuroeconomics: A critical reconsideration. Econ Philos 24:303–344

Hasler G (2012) Can the neuroeconomics revolution revolutionize psychiatry? Neurosci Behav Rev 36:64–78

Hedgcock WM, Crowe DA, Leuthold AC, Georgopoulos AP (2010) A magnetoencephalography study of choice bias. Exp Brain Res 202:121–127

Jeong-Kang MJ, Rangel A, Camus M, Camerer CF (2011) Hypothetical and real choice differentially activate common valuation areas. J Neurosci 31(2):461–468

Kutas M, Federmeier KD (2011) Thirty years and counting: finding meaning in the N400 component of the event related potential. Annu Rev Psychol 62:621–647

Lee N, Senior C, Butler M (2012) The domain of organizational cognitive neuroscience: theoretical and empirical challenges. J Manag 38(4):921–931

Murphy ER, Illes J, Reiner PB (2008) Neuroethics of neuromarketing. J Consum Behav 7:293–302

Poldrack RA (2011) Inferring mental states from neuroimaging data: from reverse inference to large-scale decoding. Neuron 72:692–697

Senior C, Lee N, Butler M (2011) Organizational Cognitive Neuroscience. Organ Sci 22(3):804–815

Pain- and Itch-Related Magnetic Fields

Hideki Mochizuki, Koji Inui and Ryusuke Kakigi

Abstract Pain and itch are unpleasant somatic sensations, and, in particular, severe problems for patients with chronic pain and itch. It is important to understand how these sensations are perceived/modulated in the brain in order to develop treatments for chronic pain and itch. Magnetoencephalography (MEG) can be used to investigate pain- and itch-related cerebral processing with high temporal resolution (ms). Many pain researchers have investigated the temporal profiles of cortical activities evoked by noxious stimuli and discussed how neural signals associated with pain are processed in the brain. In addition, pain modulation by physical and physiological factors has also been of interest for pain researchers and has been investigated to understand the pain modulation system in the brain. Until recently, it was considered impossible to measure itch-related processing in the brain using MEG, because no itch stimulus was shown to be useful for MEG. However, a new stimulus to evoke the itch sensation by applying electrical stimuli to the skin was developed. This electrical method is reproducible and produces a steep rise in the itch sensation and, therefore, it is suitable for MEG recording. A MEG study using electrical itch stimuli demonstrated that the temporal profile of cortical activity evoked by itch stimuli was partly different from that evoked by pain.

Keywords Pain · Itch · Pain modulation · Magnetic response · Oscillation activity · Alpha oscillation · Gamma oscillation · The primary somatosensory cortex · The secondary somatosensory cortex · The precuneus

H. Mochizuki (✉) · K. Inui · R. Kakigi
Department of Integrative Physiology, National Institute for Physiological Sciences, Okazaki, Japan
e-mail: motiz@nips.ac.jp

S. Supek and C. J. Aine (eds.), *Magnetoencephalography*,
DOI: 10.1007/978-3-642-33045-2_36,

1 Introduction

Pain and itch are unpleasant somatic sensations. Why do we have such sensations? What happens if these sensations are lost? There are patients who cannot perceive pain sensations, referred to as congenital analgesia and congenital pain insensitivity. Even if a part of the body, for example the back, is burned, a patient with this disorder cannot perceive it. As a result, these patients can have severe burns, and a worst case scenario, it can result in death. The itch sensation was also shown to be affected (little or not perceived) in most patients with this disorder (Tomioka et al. 2002). Thus, the perception of pain and itch sensations are important warning signals to become aware of dangers that occurred in the body in order to avoid further damage of the body. Thus, these sensations are necessary functions. On the other hand, pain and itch are serious problems for patients with chronic pain and itch (pain: including neuropathic pain, cancer pain, hernia, and cingulum; itch: including allergic diseases, liver diseases, and neuropathic itch). The unpleasantness caused by pain and itch evoke negative emotions and stress, which decrease activities in daily life, work, and education and sometimes lead to depression and suicidal thoughts. Moreover, itch evokes not only unpleasantness, but also the desire to scratch. Scratching itchy skin causes damage. This damage worsens the skin condition, resulting in the exacerbation of itch. However, chronic itch patients can not stop scratching. The phenomenon is called the itch-scratch-cycle. Therefore, it is important to control itch and pain in these patients. The unpleasantness of pain and itch and the desire to scratch are generated in the brain. How are these mental events generated in the brain? These issues have been the focus of study for researchers. Positron emission tomography (PET), functional magnetic resonance imaging (fMRI), electroencephalography (EEG), and magnetoencephalography (MEG) can noninvasively observe or visualize physiological activity such as neural activity and/or the activity of neurotransmitters in living human brains. Thus, the development of these apparatuses has markedly changed and expanded the understanding of the cerebral mechanisms of itch and pain. The merit of MEG and EEG is higher temporal resolution (unit: ms) than PET and fMRI (unit; min or s). Since neural signals are processed and transmitted in the order of ms, MEG and EEG are strong tools for visualizing information flow in the brain. Pain studies using MEG started in the 1980's (Hari et al. 1983; Huttunen et al. 1986; Kakigi et al. 1995). Since then, many researchers have investigated the cerebral mechanisms of pain sensation. In contrast, itch studies using MEG began in 2009 (Mochizuki et al. 2009). In this chapter, we have introduced what high spatial resolution apparatuses, mainly MEG, have unveiled regarding the cerebral mechanisms of pain and itch.

2 Noxious Stimuli-Evoked Magnetic Responses

2.1 Source Localization

The pain sensation is mediated by Aδ- and C-fibers. The activation of Aδ-fibers evokes a sharp pain sensation while that of C-fibers evokes a burning sensation. The ideal pain stimulation for MEG is pain-specific, controllable, safe, and repeatable. Laser beam stimulation such as CO_2 and Tm: YAG to the skin and electrical stimulation satisfy all of the above. Thus, they have frequently been used in pain studies using MEG. Figure 1 shows the typical magnetic responses while the dorsum of the left hand was stimulated by laser. The source location of the magnetic responses observed in the central area (Fig. 1A) was estimated to be the primary somatosensory cortex (SI). Since laser stimuli were applied to the left hand, the contralateral SI (i.e., the right SI) was activated. The source location of the magnetic responses observed in the bilateral fronto-temporal areas (Fig. 1B and C) was estimated to be the secondary somatosensory cortex (SII). Kakigi et al. (1995) reported that dipoles for stimulating the arm and those for the leg were located in the Sylvian fissure including SII and insula (IC), although there was no consistency in somatotopical organization for the arm and leg among subjects in the Sylvian fissure, their locations differed by less than 2 cm, which suggested the existence of somatotopy in the Sylvian fissure for noxious processing. A precise investigation was performed by Baumgärtner et al. (2010) using high spatial resolution fMRI. They found hand-foot somatotopy in the contralateral anterior and posterior IC and in the contralateral parietal operculum for heat stimuli.

SI consists of three cytoarchitectural subdivisions, areas 3, 2, and 1. Anatomical studies have demonstrated that information from the deep body tissues such as muscles and joints reach areas 3a and 2, while areas 3b and 1 receive information from the skin (Hyvärinen and Poranen 1978; Iwamura et al. 1993; Powell and Mountcastle 1959; Kandel 2000). Consistent with these anatomical studies, MEG studies showed that source localizations in SI for tactile stimuli were estimated to be area 3b and 1 (Ploner et al. 2000; Kakigi et al. 2000; Kida et al. 2007). Area 3b responded to innocuous somatosensory stimuli 20–30 ms after the stimulus onset (Wood et al. 1985; Allison et al. 1989a, b; McCarthy et al. 1991) and area 1 responded later than area 3b (Ploner et al. 2000; Inui et al. 2003). In contrast, pain studies using MEG reported that only area 1 responded to noxious stimuli (Ploner et al. 1999; Kanda et al. 2000; Inui et al. 2003). However, single unit recordings in monkeys showed nociceptive SI neurons in areas 3b and 1 (Kenshalo and Isensee 1983). One possibility to explain why the magnetic response in area 3b was not observed in previous MEG studies may be due to the lower number of neurons in area 3b than in area 1 (Chudler et al. 1990). In previous MEG studies that observed area 3b response to tactile stimuli, median nerve stimulation was used as the tactile stimuli. On the other hand, pain studies using MEG used laser stimuli. The area to be stimulated was a tiny spot for laser stimuli, while a much larger skin area was stimulated for the median nerve stimulation. Thus, the total number of neurons in

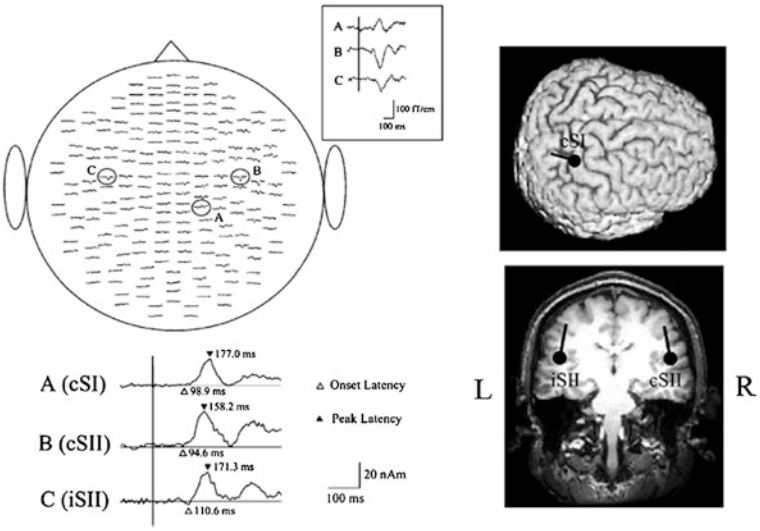

Fig. 1 Typical magnetic responses obtained when noxious stimuli were applied and their source localizations (Single subject). Adopted from Nakata et al. (2004). *cSI* contralateral *SI*, *cSII* contralateral *SII*, *iSII* ipsilateral SII, *L* left, *R* right. This figure has been reproduced with the permission of the International Association for the Study of Pain (IASP). The figure may not be reproduced for any other purpose without permission

area 3b that responded to the nerve stimulation may have been much higher than that responding to the laser stimuli. This may be another reason for the lack of a clear response in area 3b to noxious stimuli. Unfortunately, there is currently no clear evidence to explain the discrepancy between single unit recordings and pain studies using MEG.

2.2 Peak Latency

The peak latency of painful stimuli-evoked magnetic responses in the contralateral SI, contralateral SII, and ipsilateral SII reported in previous MEG studies were 164–217, 160–212, and 169–213 ms, respectively (Ploner et al. 1999, 2000, 2002; Kanda et al. 2000; Nakata et al. 2004). A human microneurography study demonstrated that the conduction velocity (CV) of Aδ-fibers was about 19 ms (Adriaensen et al. 1983). In a monkey study, the CV of the spinothalamic tract (STT) was found to be 8.0 ms by determining STT neurons with antidromic activation in the contralateral posterior part of the ventral medial nucleus in the thalamus (Dostrovsky and Craig 1996). Similar CVs were reported in a human study in which the CV of the STT using laser-evoked potentials was estimated to be approximately 8–10 ms (Kakigi and Shibasaki 1991). In addition, the CV of

thalamocortical fibers was estimated to be 33 ms based on the somatosensory evoked potentials of electric stimulation (Desmedt and Cheron 1980). Based on CVs, it takes over 110 ms for the signals evoked by laser to be transmitted from the hand to the cerebral cortex. On the other hand, the CV of C-fibers and STT associated with C-fibers are 1.2–2.4 ms (Towell et al. 1996; Magerl et al. 1999; Tran et al. 2001) and 2.9 ms (Tran et al. 2002), respectively, based on laser-evoked potential studies. Thus, it takes over 500 ms for signals to be transmitted from the hand to the cerebral cortex. The peak latency of the magnetic responses observed in the previous MEG studies was about 200 ms. Thus, magnetic responses are suggested to be derived from the excitation of Aδ-fibers. Kakigi et al. (1995) compared the peak latency and source location (i.e., dipole) of painful stimuli-evoked magnetic responses when a CO_2 laser was applied to the arm compared to when it was applied to the leg. They observed that the peak latency for the stimulation of the leg was 50 ms longer than that of the arm. This difference was attributed to the distance between the leg and brain being longer than that between the arm and brain. In all previous pain studies using MEG, peak latency was shorter for the contralateral SII than for the ipsilateral SII (e.g., Yamasaki et al. 1999; Ploner et al. 2000, 2002; Kanda et al. 2000; Nakata et al. 2004, 2008, 2009). The difference in latency between contralateral and ipsilateral SII was 1–25 ms (mean: 13.8 ms) in these studies. Ploner et al. (2000) reported that differences in peak latency between the contralateral and ipsulateral SII for tactile and laser stimuli were 11 and 15 ms, respectively. Similar values were also observed in other MEG studies (e.g., Mauguière et al. 1997). The difference in peak latency has been interpreted to reflect the time to transmit a neural signal from the contralateral SII to the ipsilateral side.

2.3 Intensity Coding of SI and SII

Pain is a complex sensation composed of sensory-discriminative and motivational-affective components. SI and SII are considered to be the main regions for the sensory-discriminative component. Animal studies have demonstrated that there are neurons responsive to nociceptive stimuli in SI and most of the neurons encode the stimulus intensity of noxious stimuli (Chudler et al. 1990; Kenshalo and Isensee 1983; Kenshalo et al. 1988). Unit recoding studies in monkeys have demonstrated that the intensity coding of neurons responsive to noxious stimuli in SII appeared to be poorer than that in SI (Dong et al. 1989, 1994). Analogous to these animal studies, a MEG study observed that the relationship between SI activity and stimulus intensity closely matched the subjects' pain ratings, while SII activity exhibited an S-shaped function with a sharp increase in amplitude only at a stimulus intensity well above the pain threshold (Timmermann et al. 2001). Similar results were also reported in human fMRI and intracranial recoding studies (Bornhövd et al. 2002; Frot et al. 2007).

2.4 Parallel or Serial Processing?

Noxious stimuli, as well as innocuous tactile stimuli, activate SI and SII. However, the temporal profiles of SI and SII activations for noxious stimulation clearly differ from those for tactile stimulation. Intracranial and MEG recordings have demonstrated that the activation of SI precedes the activation of SII in innocuous tactile processing (Allison et al. 1989a, b; Hari et al. 1993; Mima et al. 1998; Schnitzler et al. 1999). These temporal patterns of SI and SII activations for tactile stimulation are not inconsistent with anatomical projections from SI to SII (Gardner and Kandel 2000). Thus, SI and SII have been suggested to have serial processing for innocuous tactile stimuli. In pain studies using MEG, the activation of SI was almost the same as that of SII (e.g., Ploner et al. 1999; Kanda et al. 2000; Nakata et al. 2004, 2009). Thus, serial processing cannot explain the activations of SI and SII for noxious stimuli. Ploner et al. (1999) described that the simultaneous activation of SI and SII for noxious stimuli contributed to independent anatomical and functional pathways from the thalamus to SI and SII, such as the pathways from the ventroposterior lateral thalamic nucleus (VPL) to SI and from the ventroposterior inferior thalamic nucleus (VPI) to SII (Gingold et al. 1991; Friedman and Murray 1986; Stevens et al. 1993; Apkarian and Hodge 1989; Apkarian and Shi 1994; Dong et al. 1989; Kenshalo and Willis 1991). Thus, some researchers have proposed that SI and SII have parallel processing for noxious stimuli. However, Inui et al. (2003) reported that the activation of SI for noxious stimuli occurred earlier than that of SII. The peak latency of SI in previous MEG studies reported the simultaneous activations of SI and SII for noxious stimuli were later than 160 ms (Ploner et al. 1999, 2000, 2002; Kanda et al. 2000; Nakata et al. 2004). Inui et al. (2003) observed magnetic responses for noxious stimuli in SI at not only around 160 ms, but also 88–100 ms after the stimulus onset. Source localizations for the earlier (i.e., 88–100 ms) and later (i.e., around 160 ms) responses were estimated to be area 1. In other words, the responses originated from the same area. Interestingly, the peak latency of the first response in SI was earlier than that of the response in the contralateral SII, indicating that serial processing cannot simply be ruled out. Another MEG study suggested that the magnetic response in SI reported in previous pain studies using MEG may be the response in the posterior parietal cortex (PPC) (Nakata et al. 2008). In most previous MEG studies, noxious stimuli were applied to the hand. One of the magnetic responses to noxious stimuli is commonly observed from MEG sensors around the top of the head (Fig. 1). Previous MEG studies estimated the source location of the response to be SI. Anatomically, SI and PPC are located adjacent to each other. Therefore, it is not easy to distinguish the magnetic response in SI from that in PPC. In a MEG study conducted by Nakata et al. (2008), noxious stimuli were applied to the thigh, which is easier to distinguish anatomically from PPC. The distribution of the magnetic responses in the central areas when noxious stimuli were applied to the hand (Fig. 1) was clearly different from when noxious stimuli were applied to the thigh (Fig. 2a). As shown in Fig. 2b, two dipoles were

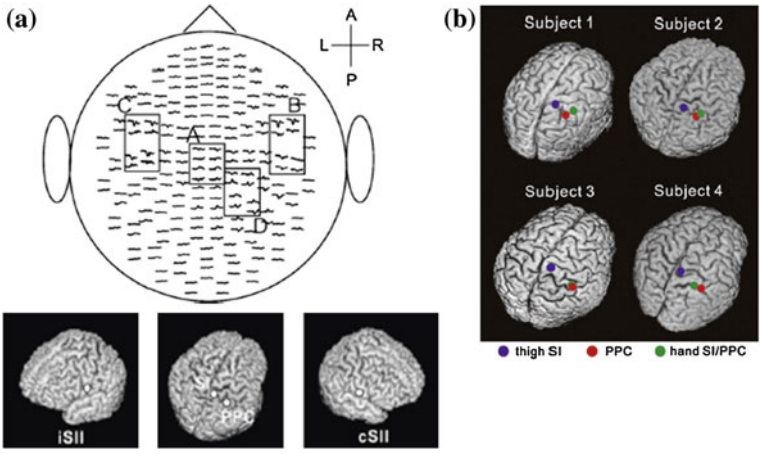

Fig. 2 Magnetic responses when noxious stimuli were applied to the thigh. **a** The grand average of magnetic responses and their source localizations. *A* anterior, *P* posterior, *L* left, *R* right, *iSII* ipsilateral secondary somatosensory cortex, *cSII* contralateral secondary somatosensory cortex. **b** Source localizations in the post central gyrus. Adopted from Nakata et al. (2008)

observed in the post central gyrus when the thigh was stimulated. On the other hand, only one dipole was observed when the hand was stimulated. These results indicate that the activation of SI and PPC cannot be distinguished when the hand is stimulated. Interestingly, in the thigh stimulation condition, the peak latency of the magnetic response in SI was 151 ms and significantly shorter than that in SII, while that in PPC was 183 ms, which was almost the same latency as that in SII. Based on this finding, they suggested that there may be serial processing for noxious stimuli and the findings of previous MEG studies may not be SI, but PPC. It has not yet been clarified whether noxious processing is parallel or serial.

2.5 Magnetic Responses to Noxious Stimuli Associated with C-Fibers

The pain sensation induced by the excitations of C-fibers evokes aching, burning, throbbing and dull sensations. They are clearly different perceptions from the pain induced by the excitation of Aδ-fibers, which evokes sharp and pricking sensations. Noxious stimuli using laser stimuli and electrical stimuli activate both Aδ- and C-fibers or selectively activate Aδ-fibers. However, the cerebral responses to noxious stimuli that can be measured are commonly associated with Aδ-fibers. Thus, findings observed in the pain studies discussed in the previous sections were all associated with the pain sensation mediated by Aδ-fibers. It is difficult to measure cerebral responses to noxious stimuli associated with C-fibers by just

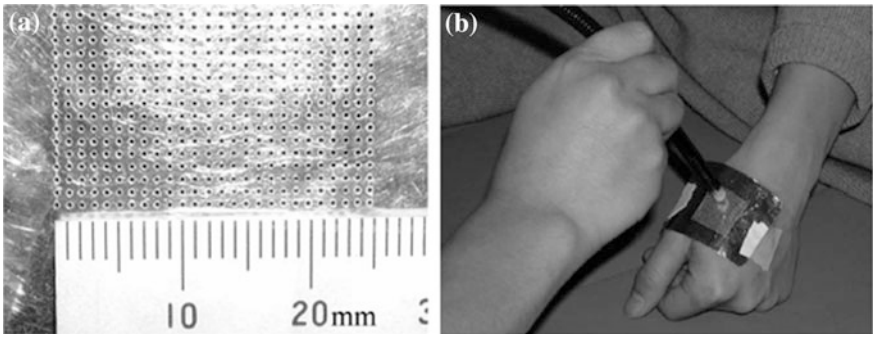

Fig. 3 The aluminum plate used for evoking C-fiber pain using laser. **a** Thin (0.1 mm in depth) aluminum plate (40 mm in length and 60 mm in width) with many tiny holes. **b** The plate was attached to the skin and laser stimuli were applied to the skin through the plate. The array of holes allowed the 2 mm laser beam to pass through one to four holes to reach the skin. Adopted from Kakigi et al. (2003)

applying laser and electrical stimuli to the skin because of the suppression of cortical responses associated with C-fibers by those associated with Aδ-fibers. One of the methods used to investigate the cerebral processing of C-fiber pain has been a physical block of the conduction of A-fibers by the compression of nerve fibers. Ploner et al. (2002) used this method and observed the activations associated with C-fiber pain in bilateral SII and ACC. Meanwhile, a novel method using CO_2 and YAG lasers to selectively stimulate C-fibers was developed (Tran et al. 2001, 2002; Qiu et al. 2003; Qiu et al. 2006). This method involves placing an aluminum plate with many tiny holes on the skin where laser stimuli are applied (Fig. 3).

The peak latencies of the magnetic responses in SI and SII were longer than 700 ms when the stimuli were applied to the hand (Kakigi et al. 2003), which was clearly a different latency from noxious stimuli associated with Aδ-fibers. A microneurographic study confirmed that the novel method selectively excited C-fibers (Qiu et al. 2003). Forss et al. (2005) compared cortical processing between Aδ-fiber-and C-fiber-related pain. They reported that the peak latencies of the magnetic response to laser stimuli were much shorter for Aδ-fiber pain than for C-fiber pain, while the source localizations were not significantly different. Thus, they suggested that nociceptive inputs mediated by Aδ- and C-fibers are processed in a common cortical network in different time windows. A pain study using fMRI reported significant differences in the activities in the anterior cingulate cortex (ACC) and IC between Aδ- and C-fibers (Qiu et al. 2006). These different perceptions between Aδ- and C-fibers may contribute to motivational-affective components such as ACC and IC rather than sensory-discriminative components such as SI and SII.

3 Pain Modulation

The pain sensation can be modulated by psychological factors such as the manipulation of attention to pain, relaxation, and mental stress or physiological factors such as the interference of pain perception by applying noxious and innocuous somatosensory stimuli or movements. Qiu et al. (2004) investigated the underlying mechanism of pain inhibition by distracting attention from pain using MEG and EEG. To distract attention from pain, subjects were asked to perform a mental arithmetic task while noxious laser stimuli were applied to the dorsum of their hands. All subjects reported that the subjective pain sensation decreased during the distraction task. They observed that noxious stimuli-related responses in the contralateral SI, bilateral SII, cingulate cortex, and medial temporal areas were markedly diminished while subjects performed the distraction task. Similar results were also reported in other studies (Yamasaki et al. 1999; Schlereth et al. 2003). It has been demonstrated that attention such as shifting attention between stimuli and sustaining attention to or distracting attention from stimuli, is controlled by several brain regions, such as the prefrontal, cingulate, and parietal cortices, thalamus, and reticular formation (the attention control system) (Coull 1998; Raz 2004). Thus, these regions are considered to play important roles in attention-related neural activity changes in the brain regions associated with pain (Peyron et al. 2000; Lenz and Treede 2002; Villemure and Bushnell 2002). Some researchers reported that the analgesic effect by distraction was associated with the activation of descending inhibitory control (Tracey et al. 2002; Valet et al. 2004). Simply said, descending inhibitory control is accomplished by inhibiting the pain-related ascending neural signal at the spinal level by descending neural signals from the periaqueductal grey and rostral medulla (Millan 2002). However, since the task to distract attention from pain modulates not only attention, but also stress and mood levels, it is still controversial whether high cognitive demanding tasks are an appropriate method to investigate the neural mechanism of pain modulation by attention (e.g., Villemure and Bushnell 2002). Another well-known pain modulation system is the gate control theory, in which excitation of the thin fibers conducting the tactile sensation (e.g., Aβ-fibers) inhibits nociceptive ascending signals conducted by thick fibers (e.g., Aδ- and C-fibers) in the spinal cord through the interneurons of substantia gelatinosa. Following this model, pain sensation is not inhibited if noxious ascending signals pass through the spinal dorsal horn before ascending signals mediating the tactile sensation reach there or noxious stimuli are applied after ascending signals mediating tactile sensation reach the brain. Inui et al. (2006) investigated the issue using MEG. They attached electrodes for noxious electrical stimuli and tactile stimuli to the right side of the back 4 cm lateral to the ninth thoracic vertebral spinous process. The electrical noxious stimulus (i.e., intra-epidermal electrical stimulation (IES)) was current constant double pulses at 100 Hz with a 0.5 ms duration (Inui et al. 2002). The tactile stimulus (TS) was double pulses at 100 Hz with 0.5 ms duration. They randomly changed the timing to apply the conditioning stimulus (i.e., the tactile stimulus) relative to the test stimulus (i.e., IES). The

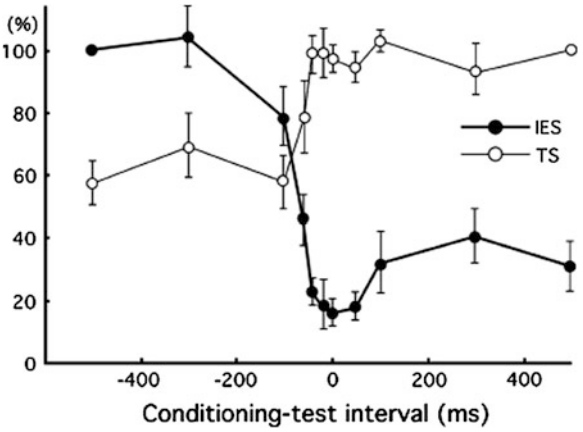

Fig. 4 Amplitude changes in the IES- and TS-evoked responses. Each value is the percentage of the area under the curve during a latency period of 50–300 ms relative to that in the control condition (500 ms condition for TS and −500 ms condition for IES). Adopted from Inui et al. (2006)

conditioning-test intervals (CTIs) were −500, −300, −100, −60, −40, −20, 0, 50, 100, 300, and 500 ms. Interestingly, the pain sensation was reduced when TS was applied 20–60 ms earlier than IES and even when IES was applied much later (e.g., 500 ms) than TS. The magnetic response supported the behavioural results. As shown in Fig. 4, the magnetic response associated with IES was reduced to less than 60 % of the control (IES 500 s before TS). They suggested that cortical responses to noxious stimuli can also be inhibited by innocuous tactile stimuli at the cortical level. These findings strongly demonstrate that the underlying mechanism of pain inhibition by tactile stimuli is not only the gate control theory.

4 Oscillatory Activity and Pain

It has recently been demonstrated that time frequency information (i.e., oscillatory activity) encodes or reflects several mental states such as cognition, emotion, perception, and thought. For example, several researchers reported an association between alpha oscillation (around 10 Hz) and pain perception. Kakigi et al. (2005a, b) reported that the power of the alpha band increased while a Yoga master in meditation did not feel the pain sensation. Nir et al. (2010) reported that subjects with higher frequency, which was maximum in power within the alpha range (i.e., 8–12 Hz) during the resting state, perceived noxious stimuli as being more intense. Other studies demonstrated that the gamma frequency range (40–100 Hz) reflected pain perception. Gross et al. (2007) showed that gamma power at a frequency between 60 and 95 Hz in the contralateral SI (i.e., SI in the left hemisphere) increased when laser stimuli were applied to the right hand. Pain-induced gamma oscillations were observed around 100–300 ms after the stimulus onset, indicating the excitation of Aδ-fibers. The power of gamma oscillations increased with increments in stimulus intensity and subjective pain sensation. Interestingly, they reported that laser-evoked magnetic responses in SI were observed regardless of

whether subjects perceived stimuli as painful or not, whereas the power of gamma oscillations in the region was observed only when stimuli were painful for subjects. It was reported that the power of gamma oscillations was modulated by the manipulation of subjects' attention to pain (Hauck et al. 2007). Alpha and gamma oscillations are not specific to pain. These oscillations are also observed in other modalities. However, at least, these oscillations may be useful for the evaluation of subjective pain sensation and assessment of chronic pain.

5 Itch Stimuli-Evoked Magnetic Responses

Itch is an unpleasant sensation with the desire to scratch. It has been hypothesized for a long time that itch is induced by the low-frequency excitation of nociceptors also mediating the pain sensation. However, phenomena conflicting this hypothesis have also been reported such as morphine used for pain relief evoking itch sensation. Several researchers recently reported direct evidence that itch is not just a weak pain. For example, Schmelz et al. (1997, 2003) found C-fibers selective for histamine, which is a representative substrate to evoke itch. Andrew and Craig (2001) reported that some STT neurons responded to the application of histamine, but not to mustard oil which evokes the pain sensation. More recently, it was found that STT neurons expressing gastrin- releasing peptide receptor transfer neural signals associated with itch to the brain (Sun et al. 2009). Thus, it is generally accepted in the itch and pain research fields that itch is a sensation independent of pain and has a different mechanism from pain. In fact, ones can distinguish them as different sensations such as "itch" and "pain". Several researchers have attempted to identify how the brain distinguishes these sensations. To the best our knowledge, the first study to investigate the brain mechanism of itch perception was reported by Hsieh et al. in 1994. It was a PET study. Since then, several researchers have conducted PET and fMRI studies and reported that histamine- or cowhage-induced itch activates several brain regions including the prefrontal cortex, primary motor cortex, supplementary motor area, premotor cortex, parietal cortex, SI and SII, cingulate cortex, IC, basal ganglia, and cerebellum (Darsow et al. 2000; Drzezga et al. 2001; Leknes et al. 2007; Mochizuki et al. 2007; Herde et al. 2007; Papoiu et al. 2012). However, it was still unclear how these regions interact with each other. To visualize itch-related information flow in the brain, it was necessary to measure neural activity in the brain in the order of ms, since neural signals are transmitted in that order. However, it was necessary to develop an itch stimulus which could repeatedly evoke short duration-itch sensations (i.e., ∼a few s) to measure itch-related brain activity using EEG and MEG. Histamine or cowhage do not satisfy these conditions. The application of electrical stimulus to the skin can evoke the itch sensation (Edwards et al. 1976; Shelley and Arthur 1957; Tuckett 1982). Ikoma et al. (2005) then established a stimulus condition to evoke the itch sensation with an electrical current. The stimulus can easily control the duration of the itch sensation and repeatedly apply itch stimuli.

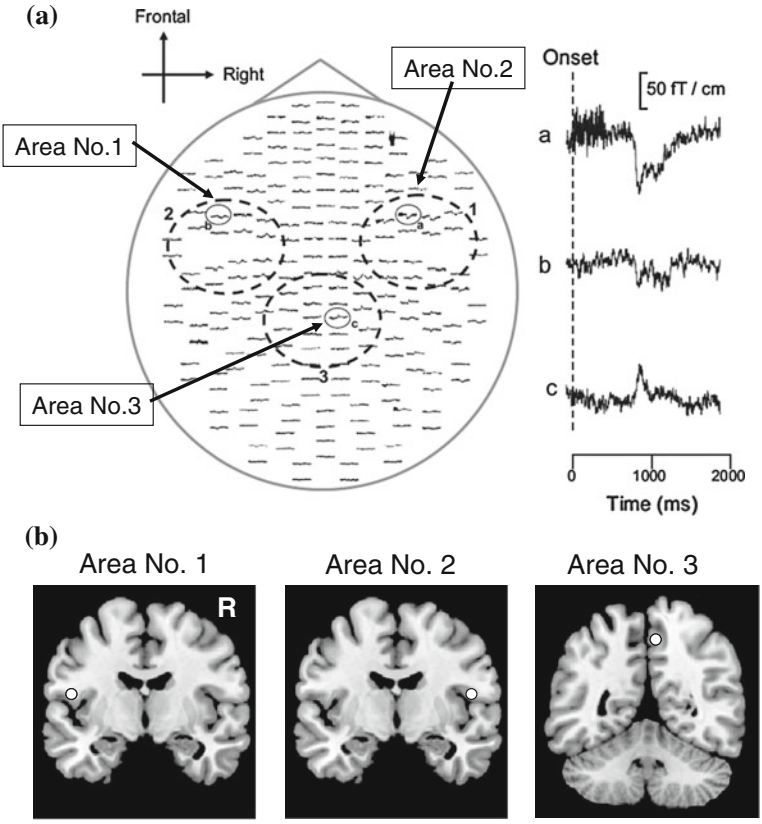

Fig. 5 Magnetic responses and source localizations for itch. **a** The typical magnetic responses when electrical itch stimuli were applied (single subject). Adopted from Mochizuki et al. (2009). **b** Mean coordinate of the dipole of each magnetic response on the MNI brain template. *R* right hemisphere

Thus, Mochizuki et al. (2008) developed electrodes for the electrical itch stimulus and confirmed that the itch sensation evoked by electrical itch stimuli is associated with C-fibers and the cerebral responses to the electrical itch stimuli can be measured using EEG. Using the stimulus and MEG, Mochizuki et al. (2009) first visualized cerebral responses to the itch stimuli in the order of ms. They reported that magnetic responses to the itch stimuli were mainly observed in the bilateral fronto-temporal areas and centro-parietal area (Fig. 5a). The mean source localizations of the magnetic responses obtained from subjects were the bilateral opercular cortex (OPC) and precuneus (Fig. 5b). The peak latency of the magnetic responses in the contralateral OPC was significantly shorter than that in the ipsilateral OPC (contralateral side: 740 ± 76 ms, ipsilateral side: 785 ± 76 ms). This difference in latency would reflect the transmission of neural signals from the contralateral to ipsilateral OPC. The peak latency of the magnetic response in the precuneus was between the contralateral and ipsilateral OPC. Interestingly, no

previous pain or tactile studies using MEG and EEG reported dipoles in the precuneus (e.g., Forss et al. 2005; Inui et al. 2003; Kakigi et al. 2005a, b; Kanda et al. 2000; Nakata et al. 2008; Opsommer et al. 2001; Ploner et al. 1999, 2000), which implied that some differences exist in parietal processing between itch and pain. However, some pain and tactile studies using PET and fMRI also observed activation of the precuneus (de Leeuw et al. 2006; Iadarola et al. 1998; Kitada et al. 2005; Niddam et al. 2008). Thus, activation of the precuneus is not specific to itch in somatosensory processing. Unfortunately, the precise role of the precuneus in somatosenory processing is not fully understood. Some neuroimaging studies concerning pain reported that the precuneus was associated with empathy for pain, pain hallucination, and the modulation of pain by hypnosis, and speculated that the precuneus may play some role in the interaction between internal or psychological states and somatic sensations (Bär et al. 2002; Faymonville et al. 2006; Jackson et al. 2006; Ochsner et al. 2008; Schulz-Stübner et al. 2004).

6 Conclusion

MEG is a strong tool to investigate information flow in the brain with high temporal resolution. Several aspects of the cerebral processing of pain have been unveiled. For example, SI and SII respond to noxious stimuli mediated by Aδ-fibers about 100–200 ms after the stimulus onset, while those mediated by C-fibers respond much later. Pain inhibition by tactile stimuli occurs not only in the spinal cord (i.e., the gate control theory), but also in the brain. The intensities of the responses of SI and SII to noxious stimuli are closely related to the stimulus intensity and subjective pain rating, which supported these regions being associated with the sensory-discriminative component of pain. Oscillation studies have reported that oscillation activity is a good indicator to evaluate subjective pain sensation. At the same time, new questions have also been raised. For example, it is still unclear whether SI and SII have a serial or parallel pathway, what mechanism underlies pain inhibition by tactile stimuli, and why is subjective pain sensation reflected by oscillation activity? Studies investigating the itch sensation using MEG have been too few to discuss the cerebral processing of itch. There are still many questions that remain to be answered in the pain and itch research fields.

References

Adriaensen H, Gybels J, Handwerker HO, Van Hees J (1983) Response properties of thin myelinated (A-delta) fibers in human skin nerves. J Neurophysiol 49(1):111–122

Allison T, McCarthy G, Wood CC, Darcey TM, Spencer DD, Williamson PD (1989a) Human cortical potentials evoked by stimulation of the median nerve. I. Cytoarchitectonic areas generating short-latency activity. J Neurophysiol 62(3):694–710

Allison T, McCarthy G, Wood CC, Williamson PD, Spencer DD (1989b) Human cortical potentials evoked by stimulation of the median nerve. II. Cytoarchitectonic areas generating long-latency activity. J Neurophysiol 62(3):711–722

Andrew D, Craig AD (2001) Spinothalamic lamina I neurons selectively sensitive to histamine: a central neural pathway for itch. Nat Neurosci 4(1):72–77

Apkarian AV, Hodge CJ (1989) Primate spinothalamic pathways: II. The cells of origin of the dorsolateral and ventral spinothalamic pathways. J Comp Neurol 288(3):474–492

Apkarian AV, Shi T (1994) Squirrel monkey lateral thalamus. I. Somatic nocicresponsive neurons and their relation to spinothalamic terminals. J Neurosci 14(11 Pt 2): 6779–6795

Baumgärtner U, Iannetti GD, Zambreanu L, Stoeter P, Treede RD, Tracey I (2010) Multiple somatotopic representations of heat and mechanical pain in the operculo-insular cortex: a high-resolution fMRI study. J Neurophysiol 104(5):2863–2872

Bär KJ, Gaser C, Nenadic I, Sauer H (2002) Transient activation of a somatosensory area in painful hallucinations shown by fMRI. NeuroReport 13:805–808

Bornhövd K, Quante M, Glauche V, Bromm B, Weiller C, Büchel C (2002) Painful stimuli evoke different stimulus-response functions in the amygdala, prefrontal, insula and somatosensory cortex: a single-trial fMRI study. Brain 125(6):1326–1336

Chudler EH, Anton F, Dubner R, Kenshalo DR Jr (1990) Responses of nociceptive SI neurons in monkeys and pain sensation in humans elicited by noxious thermal stimulation: effect of interstimulus interval. J Neurophysiol 63(3):559–569

Coull JT (1998) Neural correlates of attention and arousal: insights from electrophysiology, functional neuroimaging and psychopharmacology. Prog Neurobiol 55(4):343–361

Darsow U, Drzezga A, Frisch M, Munz F, Weilke F, Bartenstein P, Schwaiger M, Ring J (2000) Processing of histamine-induced itch in the human cerebral cortex: a correlation analysis with dermal reactions. J Invest Dermatol 115(6):1029–1033

Desmedt JE, Cheron G (1980) Central somatosensory conduction in man: neural generators and interpeak latencies of the far-field components recorded from neck and right or left scalp and earlobes. Electroencephalogr Clin Neurophysiol 50(5–6):382–403

Drzezga A, Darsow U, Treede RD, Siebner H, Frisch M, Munz F, Weilke F, Ring J, Schwaiger M, Bartenstein P (2001) Central activation by histamine-induced itch: analogies to pain processing: a correlational analysis of O-15 H_2O positron emission tomography studies. Pain 92(1–2):295–305

Dong WK, Salonen LD, Kawakami Y, Shiwaku T, Kaukoranta EM, Martin RF (1989) Nociceptive responses of trigeminal neurons in SII-7b cortex of awake monkeys. Brain Res 484(1–2):314–324

Dong WK, Chudler EH, Sugiyama K, Roberts VJ, Hayashi T (1994) Somatosensory, multisensory, and task-related neurons in cortical area 7b (PF) of unanesthetized monkeys. J Neurophysiol 72(2):542–564

Dostrovsky JO, Craig AD (1996) Cooling-specific spinothalamic neurons in the monkey. J Neurophysiol 76(6):3656–3665

Edwards AE, Shellow WV, Wright ET, Dignam TF (1976) Pruritic skin diseases, psychological stress, and the itch sensation. A reliable method for the induction of experimental pruritus. Arch Dermatol 112(3):339–343

Faymonville ME, Boly M, Laureys S (2006) Functional neuroanatomy of the hypnotic state. J Physiol (Paris) 99(4–6):463–469

Forss N, Raij TT, Seppä M, Hari R (2005) Common cortical network for first and second pain. Neuroimage 24(1):132–142

Friedman DP, Murray EA (1986) Thalamic connectivity of the second somatosensory area and neighboring somatosensory fields of the lateral sulcus of the macaque. J Comp Neurol 252(3):348–373

Frot M, Magnin M, Mauguière F, Garcia-Larrea L (2007) Human SII and posterior insula differently encode thermal laser stimuli. Cereb Cortex 17(3):610–620

Gardner EP, Kandel ER (2000) Touch. In: Kandek ER, Schwartz JH, Jessell TM (eds) Principles of neural science. McGraw-Hill, New Yrok, pp 451–471

Gingold SI, Greenspan JD, Apkarian AV (1991) Anatomic evidence of nociceptive inputs to primary somatosensory cortex: relationship between spinothalamic terminals and thalamocortical cells in squirrel monkeys. J Comp Neurol 308(3):467–490

Gross J, Schnitzler A, Timmermann L, Ploner M (2007) Gamma oscillations in human primary somatosensory cortex reflect pain perception. PLoS Biol 5(5):e133

Hari R, Kaukoranta E, Reinikainen K, Huopaniemie T, Mauno J (1983) Neuromagnetic localization of cortical activity evoked by painful dental stimulation in man. Neurosci Lett 42(1):77–82

Hari R, Hämäläinen M, Knuutila J, Salonen O, Sams M, Vilkman V (1993) Functional organization of the human first and second somatosensory cortices: a neuromagnetic study. Eur J Neurosci 5(6):724–734

Hauck M, Lorenz J, Engel AK (2007) Attention to painful stimulation enhances gamma-band activity and synchronization in human sensorimotor cortex. J Neurosci 27(35):9270–9277

Herde L, Forster C, Strupf M, Handwerker HO (2007) Itch induced by a novel method leads to limbic deactivations a functional MRI study. J Neurophysiol 98(4):2347–2356

Huttunen J, Kobal G, Kaukoranta E, Hari R (1986) Cortical responses to painful CO_2 stimulation of nasal mucosa; a magnetoencephalographic study in man. Electroencephalogr Clin Neurophysiol 64(4):347–349

Hyvärinen J, Poranen A (1978) Receptive field integration and submodality convergence in the hand area of the post-central gyrus of the alert monkey. J Physiol (Lond) 283:539–556

Iadarola MJ, Berman KF, Zeffiro TA, Byas-Smith MG, Gracely RH, Max MB, Bennett G (1998) Neural activation during acute capsaicin-evoked pain and allodynia assessed with PET. Brain 121(5):931–947

Ikoma A, Handwerker H, Miyachi Y, Schmelz M (2005) Electrically evoked itch in humans. Pain 113(1–2):148–154

Inui K, Tran TD, Hoshiyama M, Kakigi R (2002) Preferential stimulation of Adelta fibers by intra-epidermal needle electrode in humans. Pain 96(3):247–252

Inui K, Wang X, Qiu Y, Nguyen BT, Ojima S, Tamura Y, Nakata H, Wasaka T, Tran TD, Kakigi R (2003) Pain processing within the primary somatosensory cortex in humans. Eur J Neurosci 18(10):2859–2866

Inui K, Tsuji T, Kakigi R (2006) Temporal analysis of cortical mechanisms for pain relief by tactile stimuli in humans. Cereb Cortex 16(3):355–365

Iwamura Y, Tanaka M, Sakamoto M, Hikosaka O (1993) Rostrocaudal gradients in the neuronal receptive field complexity in the finger region of the alert monkey's postcentral gyrus. Exp Brain Res 92(3):360–368

Jackson PL, Brunet E, Meltzoff AN, Decety J (2006) Empathy examined through the neural mechanisms involved in imagining how I feel versus how you feel pain. Neuropsychologia 44(5):752–761

Kakigi R, Shibasaki H (1991) Estimation of conduction velocity of the spino-thalamic tract in man. Electroencephalogr Clin Neurophysiol 80(1):39–45

Kakigi R, Koyama S, Hoshiyama M, Kitamura Y, Shimojo M, Watanabe S (1995) Pain-related magnetic fields following painful CO_2 laser stimulation in man. Neurosci Lett 192(1):45–48

Kakigi R, Hoshiyama M, Shimojo M, Naka D, Yamasaki H, Watanabe S, Xiang J, Maeda K, Lam K, Itomi K, Nakamura A (2000) The somatosensory evoked magnetic fields. Prog Neurobiol 61(5):495–523

Kakigi R, Tran TD, Qiu Y, Wang X, Nguyen TB, Inui K, Watanabe S, Hoshiyama M (2003) Cerebral responses following stimulation of unmyelinated C-fibers in humans: electro- and magneto-encephalographic study. Neurosci Res 45(3):255–275

Kakigi R, Inui K, Tamura Y (2005a) Electrophysiological studies on human pain perception. Clin Neurophysiol 116(4):743–763

Kakigi R, Nakata H, Inui K, Hiroe N, Nagata O, Honda M, Tanaka S, Sadato N, Kawakami M (2005b) Intracerebral pain processing in a Yoga Master who claims not to feel pain during meditation. Eur J Pain 9(5):581–589

Kanda M, Nagamine T, Ikeda A, Ohara S, Kunieda T, Fujiwara N, Yazawa S, Sawamoto N, Matsumoto R, Taki W, Shibasaki H (2000) Primary somatosensory cortex is actively involved in pain processing in human. Brain Res 853(2):282–289

Kandel ER (2000) From nerve cells to cognition: the internal cellular representation required for perception and action. In: Kandek ER, Schwartz JH, Jessell TM (eds) Principles of neural science. McGraw-Hill, New York, pp 381–403

Kenshalo DR Jr, Isensee O (1983) Responses of primate SI cortical neurons to noxious stimuli. J Neurophysiol 50(6):1479–1496

Kenshalo DR Jr, Chudler EH, Anton F, Dubner R (1988) SI nociceptive neurons participate in the encoding process by which monkeys perceive the intensity of noxious thermal stimulation. Brain Res 454(1–2):378–382

Kenshalo DR, Willis WD (1991) The role of the cerebral cortex in pain sensation. In: Jones EG, Peter A (eds) Cerebral cortex, normal and altered states of function. Plenum, New York, pp 153–212

Kida T, Inui K, Wasaka T, Akatsuka K, Tanaka E, Kakigi R (2007) Time-varying cortical activations related to visual-tactile cross-modal links in spatial selective attention. J Neurophysiol 97(5):3585–3896

Kitada R, Hashimoto T, Kochiyama T, Kito T, Okada T, Matsumura M, Lederman SJ, Sadato N (2005) Tactile estimation of the roughness of gratings yields a graded response in the human brain: an fMRI study. NeuroImage 25(1):90–100

de Leeuw R, Davis CE, Albuquerque R, Carlson CR, Andersen AH (2006) Brain activity during stimulation of the trigeminal nerve with noxious heat. Oral Surg Oral Med Oral Pathol Oral Radiol Endod 102(6):750–757

Leknes SG, Bantick S, Willis CM, Wilkinson JD, Wise RG, Tracey I (2007) Itch and motivation to scratch: an investigation of the central and peripheral correlates of allergen- and histamine-induced itch in humans. J Neurophysiol 97(1):415–422

Lenz FA, Treede RD (2002) Attention, novelty, and pain. Pain 99(1–2):1–3

Magerl W, Ali Z, Ellrich J, Meyer RA, Treede RD (1999) C- and A delta-fiber components of heat-evoked cerebral potentials in healthy human subjects. Pain 82(2):127–137

Mauguière F, Merlet I, Forss N, Vanni S, Jousmäki V, Adeleine P, Hari R (1997) Activation of a distributed somatosensory cortical network in the human brain. A dipole modelling study of magnetic fields evoked by median nerve stimulation. Part I: location and activation timing of SEF sources. Electroencephalogr Clin Neurophysiol 104(4):281–289

McCarthy G, Wood CC, Allison T (1991) Cortical somatosensory evoked potentials. I. Recordings in the monkey Macaca fascicularis. J Neurophysiol 66(1):53–63

Millan MJ (2002) Descending control of pain. Prog Neurobiol 66(6):355–474

Mima T, Nagamine T, Nakamura K, Shibasaki S (1998) Attention modulates both primary and secondary somatosensory cortical activities in humans: a magnetoencephalographic study. J Neurophysiol 80(4):2215–2221

Mochizuki H, Sadato N, Saitoh D, Toyoda H, Tashiro M, Okamura N, Yanai K (2007) Neural correlates of perceptual difference between itching and pain using functional magnetic resonance imaging. NeuroImage 36(3): 706–717. (Erratum: Neuroimage. 2008; 39: 911–912)

Mochizuki H, Inui K, Yamashiro K, Ootsuru N, Kakigi R (2008) Itching-related somatosensory evoked potentials. Pain 138(3):598–603

Mochizuki H, Inui K, Tanabe HC, Akiyama LF, Otsuru N, Yamashiro K, Sasaki A, Nakata H, Sadato N, Kakigi R (2009) Time course of activity in itch-related brain regions: a combined MEG-fMRI study. J Neurophysiol 102(5):2657–2666

Nakata H, Inui K, Wasaka T, Tamura Y, Tran TD, Qiu Y, Wang X, Nguyen TB, Kakigi R (2004) Movements modulate cortical activities evoked by noxious stimulation. Pain 107(1–2):91–98

Nakata H, Tamura Y, Sakamoto K, Akatsuka K, Hirai M, Inui K, Hoshiyama M, Saitoh Y, Yamamoto T, Katayama Y, Kakigi R (2008) Evoked magnetic fields following noxious laser stimulation of the thigh in humans. Neuroimage 42(2):858–868

Nakata H, Sakamoto K, Honda Y, Mochizuki H, Hoshiyama M, Kakigi R (2009) Centrifugal modulation of human LEP components to a task-relevant noxious stimulation triggering voluntary movement. Neuroimage 45(1):129–142

Niddam DM, Chan RC, Lee SH, Yeh TC, Hsieh JC (2008) Central representation of hyperalgesia from myofascial trigger point. Neuroimage 39(3):1299–1306

Nir RR, Sinai A, Raz E, Sprecher E, Yarnitsky D (2010) Pain assessment by continuous EEG: association between subjective perception of tonic pain and peak frequency of alpha oscillations during stimulation and at rest. Brain Res 1344:77–86

Ochsner KN, Zaki J, Hanelin J, Ludlow DH, Knierim K, Ramachandran T, Glover GH, Mackey SC (2008) Your pain or mine? Common and distinct neural systems supporting the perception of pain in self and other. Soc Cogn Affect Neurosci 3(2):144–160

Opsommer E, Weiss T, Plaghki L, Miltner WH Opsommer E, Weiss T, Plaghki L, Miltner WH (2001) Dipole analysis of ultralate (C-fibres) evoked potentials after laser stimulation of tiny cutaneous surface areas in humans. Neurosci Lett 298:41–44. (Erratum: Neurosci Lett 2001; 314: 156)

Papoiu AD, Coghill RC, Kraft RA, Wang H, Yosipovitch G (2012) A tale of two itches. Common features and notable differences in brain activation evoked by cowhage and histamine induced itch. Neuroimage 59(4):3611–3623

Peyron R, Laurent B, García-Larrea L (2000) Functional imaging of brain responses to pain. A review and meta-analysis (2000). Neurophysiol Clin 30(5):263–288

Ploner M, Schmitz F, Freund HJ, Schnitzler A (1999) Parallel activation of primary and secondary somatosensory cortices in human pain processing. J Neurophysiol 81(6):3100–3104

Ploner M, Schmitz F, Freund HJ, Schnitzler A (2000) Differential organization of touch and pain in human primary somatosensory cortex. J Neurophysiol 83(3):1770–1776

Ploner M, Gross J, Timmermann L, Schnitzler A (2002) Cortical representation of first and second pain sensation in humans. Proc Natl Acad Sci U S A 99(19):12444–12448

Powell TPS, Mountcastle VB (1959) Some aspects of the functional organization of the cortex of the postcentral gyrus of the monkey: a correlation of findings obtained in a single unit analysis with cytoarchitecture. Bull. Johns Hopkins Hosp 105:133–162

Qiu Y, Fu Q, Wang X, Tran TD, Inui K, Iwase S, Kakigi R (2003) Microneurographic study of C fiber discharges induced by CO_2 laser. Neurosci Lett 353(1):25–28

Qiu Y, Inui K, Wang X, Nguyen BT, Tran TD, Kakigi R (2004) Effects of distraction on magnetoencephalographic responses ascending through C-fibers in humans. Clin Neurophysiol 115(3):636–646

Qiu Y, Noguchi Y, Honda M, Nakata H, Tamura Y, Tanaka S, Sadato N, Wang X, Inui K, Kakigi R (2006) Brain processing of the signals ascending through unmyelinated C fibers in humans: an event-related functional magnetic resonance imaging study. Cereb Cortex 16(9):1289–1295

Raz A (2004) Anatomy of attentional networks. Anat Rec B New Anat. 281(1):21–36

Schlereth T, Baumgärtner U, Magerl W, Stoeter P, Treede RD (2003) Left-hemisphere dominance in early nociceptive processing in the human parasylvian cortex. Neuroimage 20(1):441–454

Schmelz M, Schmidt R, Bickel A, Handwerker HO, Torebjörk HE (1997) Specific C-receptors for itch in human skin. J Neurosci 17(20):8003–8008

Schmelz M, Schmidt R, Weidner C, Hilliges M, Torebjork HE, Handwerker HO (2003) Chemical response pattern of different classes of C-nociceptors to pruritogens and algogens. J Neurophysiol 89(5):2441–2448

Schnitzler A, Volkmann J, Enck P, Frieling T, Witte OW, Freund HJ (1999) Different cortical organisation of visceral and somatic sensation in humans. Eur J Neurosci 11(1):305–315

Schulz-Stübner S, Krings T, Meister IG, Rex S, Thron A, Rossaint R (2004) Clinical hypnosis modulates functional magnetic resonance imaging signal intensities and pain perception in a thermal stimulation paradigm. Reg Anesth Pain Med 29(6): 549–556

Shelley WB, Arthur RP (1957) The neurohistology and neurophysiology of the itch sensation in man. AMA Arch Derm. 76(3):296–323

Stevens RT, London SM, Apkarian AV (1993) Spinothalamocortical projections to the secondary somatosensory cortex (SII) in squirrel monkey. Brain Res 631(2):241–246

Sun YG, Zhao ZQ, Meng XL, Yin J, Liu XY, Chen ZF (2009) Cellular basis of itch sensation. Science 325(5947):1531–1534

Timmermann L, Ploner M, Haucke K, Schmitz F, Baltissen R, Schnitzler A (2001) Differential coding of pain intensity in the human primary and secondary somatosensory cortex. J Neurophysiol 86(3):1499–1503

Towell AD, Purves AM, Boyd SG (1996) CO_2 laser activation of nociceptive and non-nociceptive thermal afferents from hairy and glabrous skin. Pain 66(1):79–86

Tomioka T, Awaya Y, Nihei K, Sekiyama H, Sawamura S, Hanaoka K (2002) Anesthesia for patients with congenital insensitivity to pain and anhidrosis: a questionnaire study in Japan. Anesth Analg 94(2):271–274

Tracey I, Ploghaus A, Gati JS, Clare S, Smith S, Menon RS, Matthews PM (2002) Imaging attentional modulation of pain in the periaqueductal gray in humans. J Neurosci 22(7):2748–2752

Tran TD, Lam K, Hoshiyama M, Kakigi R (2001) A new method for measuring the conduction velocities of Ab-, Ad- and C-fibers following electric and CO_2 laser stimulation in humans. Neurosci Lett 301(3):187–190

Tran TD, Inui K, Hoshiyama M, Lam K, Kakigi R (2002) Conduction velocity of the spinothalamic tract following CO_2 laser stimulation of C-fibers in humans. Pain 95(1–2):125–131

Tuckett RP (1982) Itch evoked by electrical stimulation of the skin. J Invest Dermatol 79(6):368–373

Villemure C, Bushnell MC (2002) Cognitive modulation of pain: how do attention and emotion influence pain processing? Pain 95(3):195–199

Valet M, Sprenger T, Boecker H, Willoch F, Rummeny E, Conrad B, Erhard P, Tolle TR (2004) Distraction modulates connectivity of the cingulo-frontal cortex and the midbrain during pain—an fMRI analysis. Pain 109(3):399–408

Wood CC, Cohen D, Cuffin BN, Yarita M, Allison T (1985) Electrical sources in human somatosensory cortex: identification by combined magnetic and potential recordings. Science 227(4690):1051–1053

Yamasaki H, Kakigi R, Watanabe S, Naka D (1999) Effects of distraction on pain perception: magneto- and electro-encephalographic studies. Brain Res Cogn Brain Res 8(1):73–76

Selection of Stimulus Parameters for Visual MEG Studies of Sensation and Cognition

Cheryl J. Aine, Selma Supek, Lori Sanfratello and Julia M. Stephen

Abstract Historically, MEG investigations of the visual system either attempted to: (1) corroborate findings from invasive monkey or basic psychophysical studies as an indirect way to validate MEG results or (2) enhance previously demonstrated clinical event-related potential findings (ERPs) (e.g., multiple sclerosis patients reveal longer ERP peak latencies). We focused on the former with the ultimate goal of developing/testing new stimulus paradigms and clinical applications for assessing cognitive functions such as working memory since several neuropsychiatric and neurological disorders such as schizophrenia and dementia reveal deficits in working memory circuits. However, characterization of neural circuits involved in disorders of the nervous system (i.e., neuromagnetic mapping of networks of regions and their temporal dynamics) presents a tremendous technical challenge. In this chapter we will discuss some of the technical issues we encountered while developing and testing paradigms for basic vision, attention and working memory, and will highlight ways to avoid some of these potential confounds. We will also briefly review the organization of the visual system to provide an overall appreciation for the intricacies of the visual system as well as providing some historical context for the manner in which certain studies have been designed.

C. J. Aine (✉) · L. Sanfratello
Department of Radiology, University of New Mexico School of Medicine, Albuquerque, NM 87131, USA
e-mail: aine@unm.edu

S. Supek
Department of Physics, Faculty of Science, Bijenicka cesta 32, 10000 Zagreb, Croatia

J. M. Stephen
The MIND Research Network, 1101 Yale Blvd. NE, Albuquerque, NM 87106, USA

S. Supek and C. J. Aine (eds.), *Magnetoencephalography*,
DOI: 10.1007/978-3-642-33045-2_37,

Keywords Visual system · Visual field · Visual areas · Retinotopy · Striate · Extrastriate · Sensory · Cognition · Working memory · Attention · Synchronicity · Oscillations · Cross-correlation · On-response · Off-response · Averaging · Stimulus size · Stimulus parameters · Cortical magnification · Source localization · Feedback · ERPs · ERFs · FMRI · Extended sources

1 Overview of the Functional Organization of the Visual System: Sensation to Cognition

Considerable knowledge of the visual system has been gained from the numerous anatomical, electrophysiological, and lesion studies in monkeys, thereby providing a rich database from which to formulate new and interesting hypotheses for MEG studies, including clinical studies in cognition. But, MEG investigations of the human visual system are challenged by the overwhelming complexity of this system in terms of the number of visual areas active (Fig. 1), the overlapping nature of the signals across brain regions (both synchronous and asynchronous), and the almost complete reciprocity between the connections (feedforward and feedback activity). Felleman and Van Essen (1991) identified 32 different visual areas in monkey brains and each of these visual areas are believed to provide representations of the visual field that process information in slightly different ways (Zeki 1978). For example, visual area 4 (V4) in monkeys contains a large proportion of color selective cells from the central visual field while the medial temporal area (MT) is quite sensitive to moving stimuli particularly in the peripheral field (Albright 1984; Maunsell and van Essen 1983; Zeki 1973, 1978, 1980). While it remains unclear how many visual areas exist in human brains, discoveries of commonalities between human and nonhuman primate brains continue to grow. Measures of regional cerebral blood flow and positron emission tomography (PET) in monkeys during working memory tasks suggest that the same general areas in monkeys and humans are involved in spatial working memory (Inoue et al. 2004). Spectral analysis in monkeys reveals spatially tuned elevated power in the gamma band during working memory (Pesaran et al. 2002), similar to human studies. MRI conducted in humans and the great apes indicate that humans do not have disproportionately larger frontal lobes in comparison to the great apes when equating for size of the primates (Semendeferi et al. 2002) and great apes even reveal a left hemisphere asymmetry in BA 44 which is a part of Broca's area in humans (Cantalupo and Hopkins 2001). While it has been difficult in the past to relate global MEG measures in humans to single unit activity in monkeys, more neuroimaging studies are currently being conducted in monkeys and great apes which will greatly aid in understanding the differences between these scales of measurement.

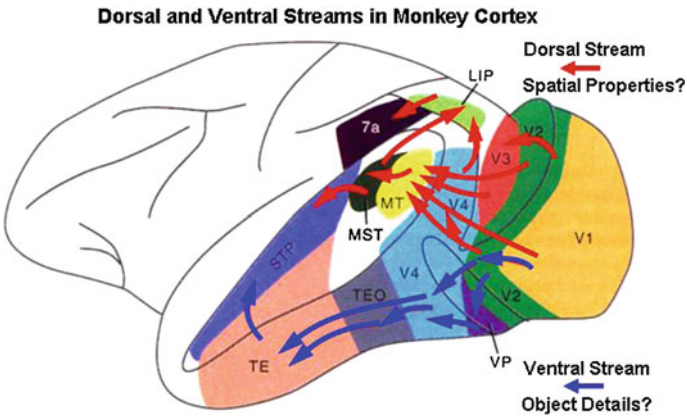

Fig. 1 Multiple visual areas in monkey cortex and two processing streams, dorsal and ventral. Adapted from Farah et al. (1999)

Most early MEG studies of basic vision [see review by Aine and Stephen (2002)] focused on examining properties (e.g., spatial or temporal frequency tuning properties) of a single visual area (e.g., primary visual cortex or V1) or have examined the retinotopic organization of visual areas (i.e., the point-to-point projection of visual field onto cortical areas). By carefully selecting stimulus parameters (e.g., color, size, motion), it is possible to identify and characterize different visual areas in the human brain similar to the methods employed in monkey studies. More recently, visual MEG studies have examined cognitive processes such as the representation of language in the brain, as well as memory and imagery. These studies rely less on the invasive results in monkeys and more on results from other functional neuroimaging methods such as PET and functional magnetic resonance imaging (fMRI) for corroboration [See review of fMRI visual studies in Courtney and Ungerleider (1997)].

Contemporary views of higher cognitive functions (e.g., cognitive neuroscience) date back to the late 1980s which emphasize that a number of different neural systems participate in the representation of an object or event (Kosslyn 1988; Squire 1986). A paradigm shift occurred away from the predominant view at that time that feature integration relies on convergent hierarchical processing, i.e., the visual system can be viewed as a series of processing stages that represent a progressive increase in complexity of neuronal representations that are dependent upon the output of preceding stages (De Yoe et al. 1994; Van Essen 1985; Van Essen and Maunsell 1983; Zeki 1978). While no investigator would argue that serial hierarchical processing does not occur within the visual system, a new emphasis was placed on "networks" or "systems." The earliest example of a systems approach was the overwhelming evidence for the existence of *at least* two functionally specialized processing streams in the visual system (e.g., "dorsal" and "ventral"—see Fig. 1) operating in parallel (De Yoe and Van Essen 1988;

Merigan and Maunsell 1993; Ungerleider 1995; Ungerleider and Mishkin 1982; Van Essen and Maunsell 1983). Basically, attributes of stimuli are not believed to be stored as a unified percept in a single cortical location; but rather, appear to be stored in a distributed cortical system in which information about specific features are stored close to the regions of cortex that mediate the perception of those features (Goldman-Rakic 1988; Mesulam 1998; Ungerleider 1995). Memory retrieval, therefore, means that a cue triggers a pattern of neural activity which is the same as the one elicited during the initial processing of the retrieved material (Alvarez and Squire 1994; Damasio 1989; Fuster 2001; Mesulam 1998; Mishkin 1982; Squire and Zola-Morgan 1991; Tulving 1995; Wheeler et al. 2000). Memories essentially consist of networks ranging from simple sensory memories or cell assemblies in sensory or parasensory areas to perceptual-motor associations consisting of reciprocal long-fiber connections linking perceptual memory networks of the posterior cortex with the prefrontal motor networks (Fuster 1997). The current results demonstrating consistent networks of activity during rest (e.g., default mode network or DMN) underline this view that brain activity during rest and task related activities involve broad cortical network activation.

Prefrontal cortex (PFC) was shown to be a key player in maintaining perceptual representations during working memory tasks and providing feedback to posterior cortex, thereby biasing activity in favor of behaviorally relevant stimuli (Baylis and Rolls 1987; Fuster 1973; Goldman-Rakic 1995). In monkeys, an elevated discharge in PFC during a delay interval was the most characteristic effect of the 'sample' stimulus (during encoding) on prefrontal cells suggesting that short-term memory basically consists of the continued facilitation of neural activity in cerebral structures recently engaged in sensory processing (Fuster 1973; Fuster and Jervey 1981; Miller et al. 1991; Richmond et al. 1983; Wilson et al. 1993). The monkey studies also showed that cooling of either PFC or inferotemporal cortex (ITC) interrupted loops of reverberating activity between them, a likely mechanism of the continued facilitation (Fuster 2001). Chafee and Goldman-Rakic (2000) found similar patterns of neuronal activity in PFC and parietal neurons in monkeys and demonstrated their interdependence via cortical cooling. These studies and others (Tomita et al. 1999) indicate that PFC-parietal and PFC-ITC regions share reciprocal projections and that these circuits are necessary for the transmission of receptive field properties and other dimensions of task-related activity when these areas are recruited to a common task. Our earliest memory study (Aine et al. 2003), designed to parallel the Delayed-Match-to-Sample (DMS) working memory studies conducted in monkeys, revealed strikingly similar results as those obtained in monkeys. Figure 2 (top row) shows similar time-courses for V1 in the monkey and humans. Walsh Stimuli (upper right) were used in both cases. The bottom row (left) shows an example from monkey area V4 when the monkey was attending a preferred stimulus versus attending a non-preferred stimulus. At the right, an effect of attention or working memory in humans also reveals elevated and sustained activity in several brain regions including the prefrontal region (Aine et al. 2003).

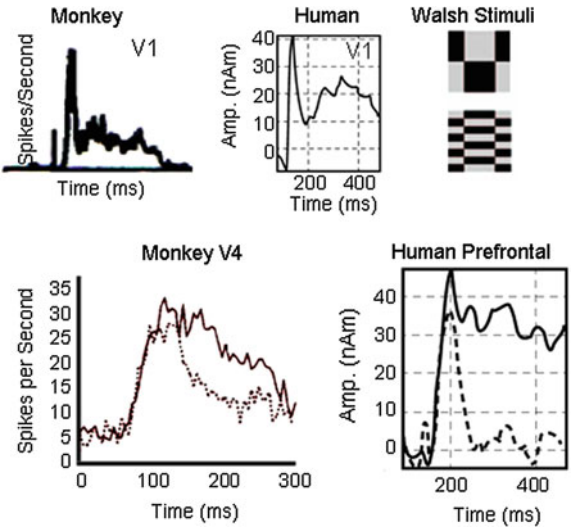

Fig. 2 *Top row* Monkey V1 responses are compared to time-courses localized to occipital cortex in a human participant. Sample stimuli (Walsh patterns) used in both studies are shown in the *upper right panel*. *Bottom row* Effects of attention are shown for monkey V4 and for human prefrontal cortex. Activity in both monkey and human participants was elevated and sustained. Compare *solid lines* (attended) with *dashed lines* (not attended). Each tracing in the human time-course represents an average of 250 responses. Adapted from (a) Richmond et al. (1990); (b) Reynolds and Desimone (1999); and (c) Aine et al. (2003)

Cortical Feedback Connections. Although little is known about the physical nature or development of feedback connections, many believe that feedback projections from prefrontal cortex play a major role in modifying responses in lower-order brain regions during controlled or effortful processing, such as that required for attention and working memory tasks. Studies in nonhuman primates have revealed the existence of massive feedback projections that carry information from higher-order to lower-order regions. Although feedback connections can theoretically modulate early portions of the initial visual response (Hupe et al. 2001), most studies show that attentional modulations lag the earliest response ($\sim$250–300 ms in monkeys) (Haenny and Schiller 1988; Lamme et al. 1998; Mehta et al. 2000a; Motter 1994; Roelfsema et al. 1998; Seidemann and Newsome 1999). The late sustained activity allows information from feedback connections to be incorporated into the response to increase and sharpen the neural responses (Gilbert et al. 2001; Lamme and Roelfsema 2000). Our early attention studies using MEG were the first to suggest that attention can modulate V1 of humans via feedback from higher-order areas (Aine et al. 1995). These conclusions were based on the observations that: (1) attention-related effects in area V1 occurred later in time ($\sim$150 ms) than the earliest V1 activity and (2) this later attention-related activity showed a $\sim 180^{\circ}$ difference in net direction of current flow relative to the initial feedforward response around 80 ms. Previously, when ERPs were utilized

to examine visual selective attention, concepts of "early in time" were often confused with "early levels of the visual system" suggesting that if attention had its effect early in time, then it must have occurred at the level of V1 or V2 and that if the attention-related effect occurred later in time, then it must have occurred at a higher level within the visual system (e.g., extrastriate regions). More recently, the attention effect in V1 was examined using both ERPs and fMRI (Di Russo et al. 2003; Martinez et al. 1999; Noesselt et al. 2002) and these studies supported the conclusions reached in Aine et al. (1995), as well as providing more definitive evidence. Additionally, fMRI studies (Brefczynski and DeYoe 1999; Tootell et al. 1998a) routinely show that attention can affect activity at the level of primary visual cortex and invasive studies show that it is via feedback influence which occurs later in time (Lamme and Roelfsema 2000; Mehta et al. 2000a, b). In general, MEG provides a unique tool for characterizing the spatio-temporal dynamics of neuronal activity that can even be used in certain circumstances (e.g., imagery) to differentiate feedforward activation sequences from feedback activity (Aine et al. 2003). Feedback connections are crucial for the establishment of neural circuits.

Feature Integration. How features and attributes of stimuli become integrated across widespread cortical regions has been an issue of intense interest and debate. Evidence indicates that (1) local field potentials (LFPs), which provide a measure of mainly postsynaptic dendritic responses, show strong sub-threshold synchrony of ongoing fluctuations in the cell's membrane potentials (Lampl et al. 1999) and (2) coordinated sub-threshold excitability changes have been demonstrated to modulate local networks (Engel et al. 2001). From this perspective, induced oscillations are part of different cell assemblies that are activated to temporally bind different stimulus characteristics or to bind the activation of a system of distributed areas necessary for the task at hand. While the specific roles these rhythmic activities play are still debated (i.e., is it an epiphenomenon?), the existence of oscillatory activity is not (Salinas and Sejnowski 2001; Tallon-Baudry et al. 2004). But, as Tallon-Baudry et al. (2004) suggest, it is important to establish the behavioral relevance of oscillatory activity by showing that it is associated with behavior such as correct performance. Along these lines, Jensen and Tesche (2002) presented a list of digits similar to the original Sternberg design and found that MEG theta band activity over frontal regions increased parametrically with the number of items retained in working memory and there was stronger theta during the memory task compared to a control task. There was also a systematic increase in RT with increase in memory load. EEG and fMRI studies also suggest that an increase in frontal theta, associated with an increase in memory load, corresponds to a decrease in BOLD in DMN regions (Scheeringa et al. 2009). These studies suggest a functional role for oscillatory activity, but the conditions under which gamma, theta, beta or alpha activity is involved as well as their specific roles is still unclear. For example, does synchronization in theta band reflect episodic memory encoding (Klimesch 1999) or does it play a role in holding a stimulus in mind over the course of a brief delay (Lee et al. 2005)? MEG methods are uniquely suited for this exciting area of study.

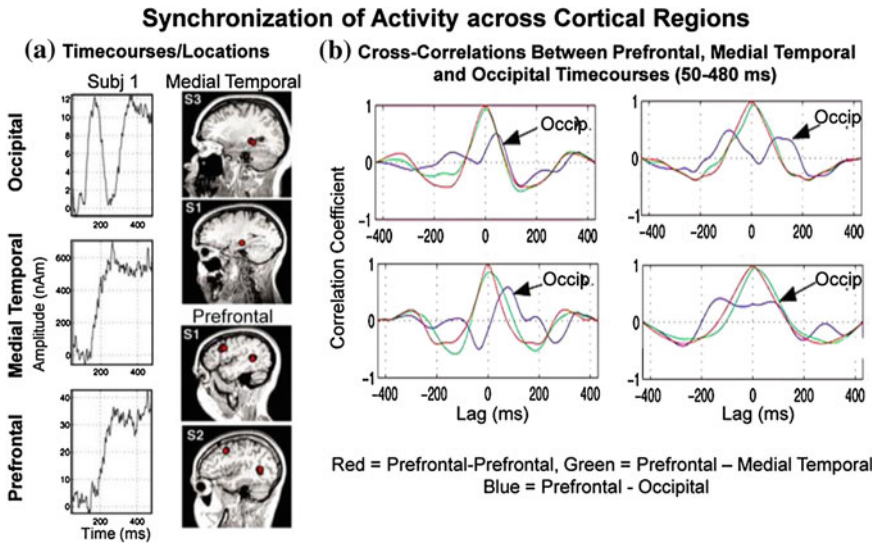

Fig. 3 Cross-correlation plots for three cortical regions. Post hoc comparisons revealed that the maximum cross-correlation value for medial temporal and prefrontal time-courses were significantly greater than the other two comparisons [occipital and medial temporal time-courses ($p < 0.05$) and the occipital and prefrontal time-courses ($p < 0.01$)]

As mentioned above, memories are formed through associations; brain regions or neural systems that are repeatedly active at the same time will tend to become associated (i.e., the principle of synchronous convergence) (Aertsen et al. 1989; Fuster 1997). Some investigators refer to the correlated activity across cortical areas as *functional connectivity* (Friston 1994) and others refer to it as temporal binding (Engel et al. 1992; Gray 1999; Roelfsema et al. 1997; Singer and Gray 1995). The former emphasizes the observed temporal correlation between two neurophysiological measurements from different parts of the brain (Gerstein and Perkel 1969) and the latter denotes the linking together of different features and attributes of stimuli through the selective synchronization of distributed neuronal activities (Bressler 1995; Gray 1999; Milner 1974; Singer and Gray 1995). Attention has been shown to enhance synchronization across different areas of cat brain (visual, parietal and motor cortex); with close to zero time lag (Roelfsema et al. 1997). While most studies in humans examine connectivity via coherence analysis using sensor measurements (sensor space), we have used our localized time-courses (source space) for cross-correlational analyses. Figure 3 shows a cross-correlation analysis (50–480 ms) conducted on the DMS data for three brain regions (medial occipital, medial temporal lobe or MTL, and PFC) and 4 participants. Similar to the Roelfsema study, attention or task relevance increases synchronicity across distributed cortical regions in healthy human participants (Aine et al. 2003). Activity in MTL and PFC regions covaried with each other (e.g., compare time-courses for one participant at left for MTL and PFC and cross-correlation plots for 4 participants at

the right—green tracings). The maximum peak of the PFC and MTL correlation is near the zero lag while the maximum peak of the PFC and occipital correlation (shown in blue in the plots at the right) is not near zero. Lags and cross-correlation coefficients can be compared with behavioral performance measures to determine the relatedness of these brain regions. For a more thorough review of the functional organization of the visual system and of visual MEG studies in general, please refer to Aine and Stephen (2002).

2 Basic Differences Between ERPs and ERFs

Although some ERP manuals readily provide normative values for amplitudes and peak latencies of ERP waveforms, similar tables will not be created here since: (1) the shape of MEG waveforms change dramatically across small cortical distances and (2) net amplitudes depend critically upon the net orientation of the sources of activity. Newcomers to MEG from the ERP field will notice immediately that averaged event-related fields (ERFs) do not look the same across subjects even though the same stimuli were presented to evoke them (Fig. 4). Investigators using ERPs know that whole-head ERP topography maps appear quite similar across participants and consequently, averaging data across subjects was used as an easy data-reduction approach. However, as Fig. 5 shows, MEG is extremely sensitive to the primary source of neuronal activity, in particular the orientation of sources, which is why it is not justified to average ERFs across subjects. In Fig. 5, the averaged ERFs, superimposed across 122 sensors for 2 subjects, appear different. However, once sources are localized to occipital cortex and other brain areas, then time-courses and locations can appear remarkably similar across participants, as in this example (see Fig. 5b and c, respectively). Consequently, our data reduction strategy has been, in some studies, to localize the sources of activity first, and then average time-courses from similar brain regions across participants.

Because MEG signal strength is sensitive to net dipole orientation, signals may appear to have reduced amplitudes for some subjects relative to others which do not necessarily indicate pathology. Figure 6 shows an example where the source moment is the same for three subjects in our realistic simulated data but the resultant waveform amplitudes are not (Stephen et al. 2003). Two spikes (upper right plot) separated by 10 ms were generated in left and right premotor cortices (shown in yellow on the MRI at the left) and embedded in real spontaneous activity from each participant. Considerable differences in signal-to-noise ratio (SNR) can be seen across patients as a result of: (1) cancellation of signals across gyri and sulci and (2) the net orientation of the active patch (radial vs. tangential). The background activity in each case is fairly similar in this example. It was the differences in the cortical geometry of the sources that contributed to these overall differences in SNR.

Figure 7a shows how cortical geometry differences can exist across participants even for a prominent fissure in cortex such as the calcarine fissure. Sample MRIs

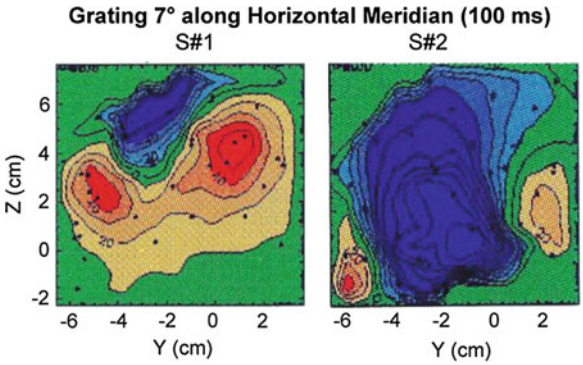

Fig. 4 A grating stimulus presented to the same position in the visual field for 2 subjects reveals radically different field distributions for this small region at the back of the head. Aine et al. (1995)

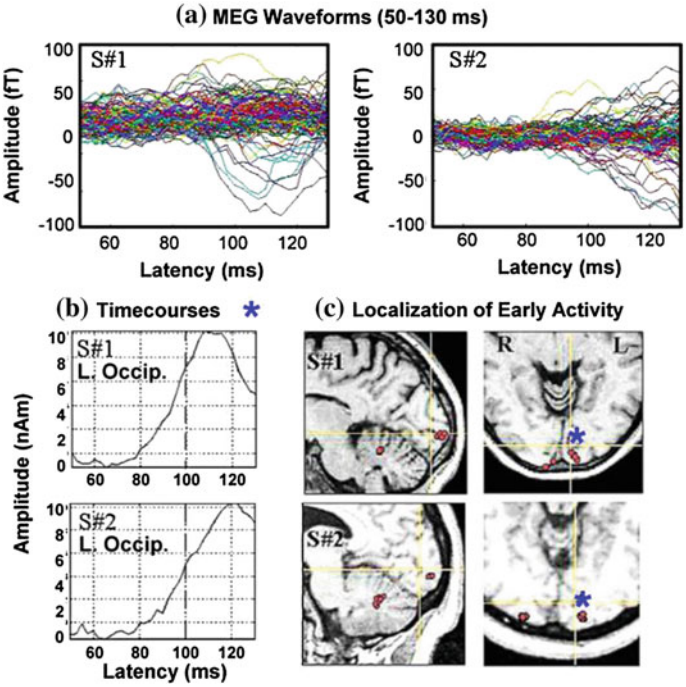

Fig. 5 **a** MEG waveforms are shown for 2 subjects. **b** Time-courses localized to left medial occipital cortex are shown. **c** Locations of active sources for 2 participants. Time-courses were taken at source locations marked with *blue asterisks*

for two participants show how the fissures differ (i.e., follow the fissure from the black arrows starting at the occipital pole up to the parieto-occipital sulcus). In this example, the MRIs were placed into Talairach space, a space used for roughly

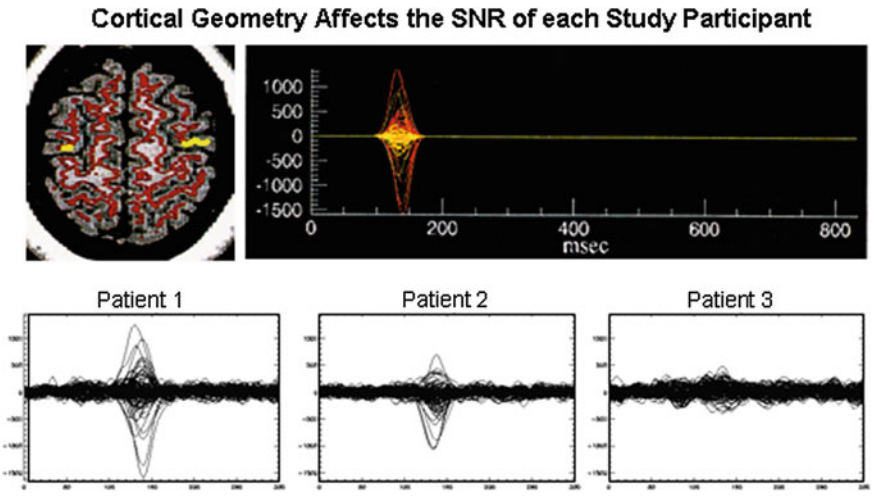

Fig. 6 Realistic simulated data for 3 study participants using the same source moment (135 nAm) for *left* and *right* premotor sources (1 cm^2 patches on the MRI). The first and second sources were separated by 10 ms as shown in the *upper right plot*. Adapted from Stephen et al. (2003)

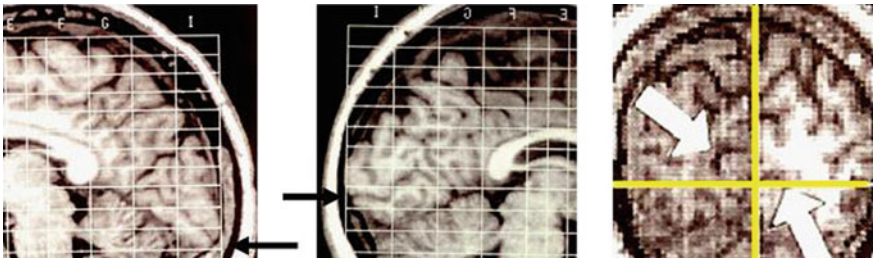

Fig. 7 MRIs from 2 subjects show Talairach bounding boxes to reveal differences in calcarine fissures. The *black arrows* show where the calcarine fissures meet at the occipital pole. The *right panel* shows that even within a single subject, calcarine fissures can be very asymmetric across hemispheres (see *white arrows*)

equating brain regions across subjects. However, there is about a 2 cm difference, between subjects, in terms of where the calcarine fissure meets the occipital pole (black arrows). The MRI at right shows that even within a single participant, MEG waveforms and contour plots may appear radically different across hemispheres given the asymmetry of some calcarine fissures. In general, the pattern of summation and cancellation may differ across hemispheres and participants.

Do ERP methods share similar problems with ERFs regarding amplitude measures? Both EEG and MEG are source orientation dependent (i.e., scalar product and vector product, respectively of two vector quantities). It holds only for

a spherical volume conductor assumption that EEG "sees" only radial sources and MEG "sees" only tangential sources. In realistic head volumes the two techniques have preferential but not exclusive sensitivity to radial and tangential sources, respectively. However, because MEG primarily measures intracellular current flow rather than return currents, significant differences in field patterns across sensor locations from subject to subject is usually evident due to the variable orientations of the sources contributing to the field patterns. EEG, reflecting primarily volume currents, tends to show a more similar pattern of activity across subjects, regardless of differences in functional neuroanatomy across subjects.

In general, EEG and MEG are both sensitive to differences in cortical geometry across subjects and cancellation/summation of potentials/fields within active cortical patches. EEG and MEG are also both sensitive to the stimulating parameters used to evoke responses. Camisa and Bodis-Wollner (1982) report, for example, that using a horizontal grating instead of a vertical grating or by changing the luminance of the stimulus changed the number of subjects classified as being normal using ERPs. As a general strategy, when one wishes to compare amplitude measures across subjects one could make within-subject comparisons across different experimental conditions first (e.g., attend versus not attend or passive versus active tasks). In this way, within-subject comparisons act as a control for individual absolute amplitude measures since one is comparing relative effect sizes across subjects (e.g., the effect of attention). As a final note, normative ERP measures for one laboratory are typically not used by other laboratories since ERP amplitudes (and ERF amplitudes) are dependent upon the stimulus parameters and equipment used to evoke them. When one adds the variability of cortical geometry normally witnessed across individuals to the above, it becomes very difficult to defend the use of absolute ERP/ERF peak amplitudes as a clinical diagnostic measure.

ERP Peaks. Early ERP studies labeled peaks in the evoked responses either as components 1, 2, and 3 (CI, CII, CIII) or as peaks denoted by polarity (negative versus positive) and latency (N70, P100, N200, P200, P300), depending on the type of stimulation (e.g., pattern reversal, pattern onset, flash stimulation) and the country in which in the studies were conducted (e.g., UK vs. USA). Considerable effort was expended on attempts at localizing the source of each individual peak either qualitatively (Jeffreys and Axford 1972a, b; Michael and Halliday 1971) or quantitatively via source localization procedures [e.g. Butler et al. (1987), Darcey et al. (1980), Maier et al. (1987), Ossenblok and Spekreijse (1991)], but it eventually became clear that single peaks/components in the waveforms (e.g., P100) do not necessarily reflect activity from a single cortical area. Each peak can reflect activity from a number of different sources.

ERF Peaks and Origins. The neural origin of the P100 visual response, which was so elusive in the ERP studies, became a focus of several early MEG studies. Seki et al. (1996) used a single-dipole model to account for activity occurring within a 90–135 ms time window to pattern reversals of full-field, half-field, and quadrant-field stimulation. In each of these cases, the MEG correlate of P100 localized to the bottom of the calcarine fissure. However, source locations were

often variable in these early studies since peaks were analyzed using single-dipole models even though many investigators were aware that multiple generators contribute to the peaks in the MEG waveforms even as early as 130 ms (Ahlfors et al. 1992; Aine et al. 1995). Most MEG studies focused on localizing the sources of different components of the visual ERPs and showed various localizations around the calcarine fissure for the 1st through 3rd components (Harding et al. 1994, 1991; Hashimoto et al. 1999; Seki et al. 1996; Shigeto et al. 1998).

In Supek et al. (1999) we set out to determine if we could find evidence for retinotopic organization of extrastriate areas in humans, as documented by invasive monkey studies, and to examine the linearity of the evoked magnetic fields. In the latter case, it was assumed that responses to paired stimuli should equal the sum of responses evoked by single stimulus presentations, at least for retinotopically organized visual areas. Two-dimensional, difference of Gaussians (DOGs), as shown in the top portion of Fig. 8a, was used to test this hypothesis. In general, the paired presentation of stimuli reflected superposition of the responses evoked by single stimuli but only for early activity up to 150 ms poststimulus; undersummation was evident later in time. This study also nicely demonstrated the retinotopic organization of 3 brain regions, using multidipole modeling, the first MEG study to do so (Fig. 8b). Later we moved away from using DOG stimuli in order to evoke additional visual areas simultaneously using circular sinusoids (e.g., bulls-eye targets); higher-order areas such as area V4 prefer stimuli that contain higher spatial frequency content. In addition, the circular sinusoids allowed us to examine spatial frequency without having to use large stimulus sizes (e.g., grating stimuli); i.e., in order to examine spatial frequency, stimuli should contain at least 2 cycles.

The results of Stephen et al. (2002) helped confirm that the human visual system is as complicated as the monkey visual system by identifying many of the homologous visual areas including, V1, V2/V3, V4, putative MT, intraparietal sulcus (IPS), medial parietal cortex and frontal eye fields, using circular sinusoids. The timing and onset of the different visual areas are consistent with previous monkey results suggesting that cortical areas in the dorsal visual stream are activated more quickly than cortical areas along the ventral visual stream. The results also suggested that stimuli with characteristics that are preferred by the dorsal or ventral visual stream still activate both dorsal and ventral visual areas with the largest difference appearing to be timing associated with that activation. This study is discussed more completely under “Retinotopy.”

More recently, Aine et al. (2003) characterized temporal response profiles from several cortical areas during a working memory task. Response profiles from primary visual cortex revealed initial “spike-like” activity followed by “slow-wave” activity. Similar to findings by Hashimoto and colleagues (Hashimoto et al. 1999), the “spike-like” activity appeared to have different physiological properties than the “slow-wave” activity even though both of these activities were generated from the same cortical region; it was hypothesized that the former predominantly reflects afferent or feedforward activity and the latter reflects a mixture of afferent and efferent activity. As suggested in recent monkey studies, the late sustained activity

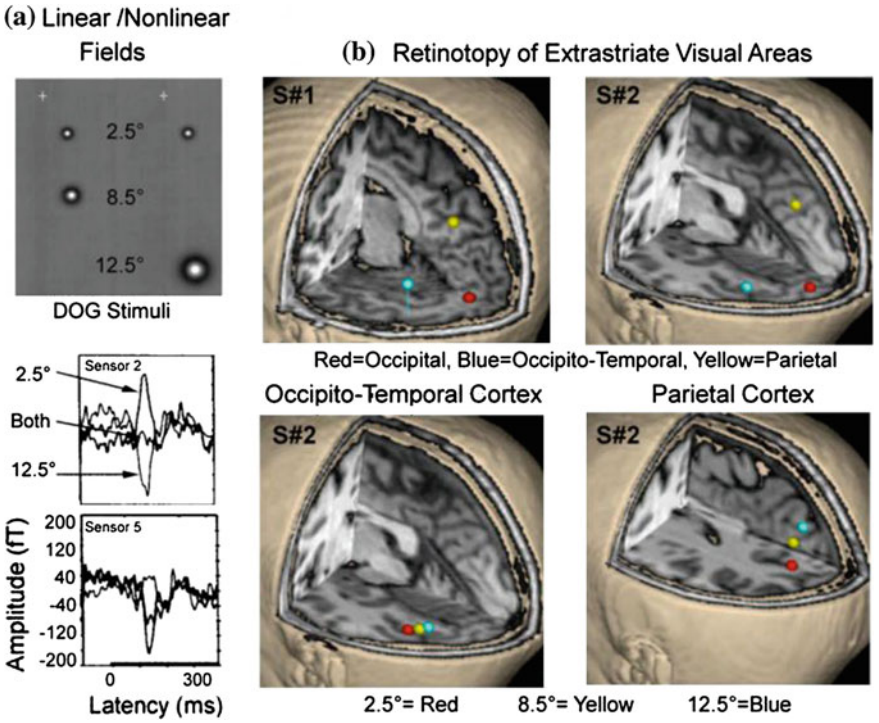

Fig. 8 **a** DOG stimuli were presented individually to 3 locations in the *lower right field* as well as in pairs to examine both retinotopy of extrastriate regions and superposition of evoked fields. Fixation point is shown as a *white* "+". The lower portion reveals 2 sensor locations showing the averaged evoked fields to the 2.5° and 12.5° stimuli, when presented individually, and when the two were presented as pair. Every subject revealed sensor locations where the response to the paired stimuli were nulled (sensor 2) and showed the opposite relationship between stimulus conditions (sensor 5). **b** Two subjects reveal 3 regions of activation in response to DOG stimuli when a multidipole model was used and each region showed a systematic shift in brain location as a function of location in the visual field (i.e., retinotopy). Adapted from Supek et al. (1999)

does indeed allow information from feedback connections to be incorporated into the response to increase and sharpen the neural responses (Gilbert et al. 2001; Lamme and Roelfsema 2000). Effects of attention are also typically found later when feedback into lower cortical regions is evident. The overall shape of the visual time-courses in the working memory task was quite different than the time-courses identified in Stephen et al. (2002), when there was no task associated with the visual stimuli. The simple sensory responses tend to have more peaks with an overall shorter duration response than visual responses evoked by a memory task suggesting again that the visual system is inherently involved in memory tasks.

ERF Norms. Armstrong et al. (1991) attempted to establish norms for MEG responses to visual stimuli similar to what had been done with ERPs, using a 2nd-order gradiometer in an unshielded environment. They studied 100 subjects

aged 18–87 years and found that pattern reversal stimuli evoked a major positive component between 90 and 120 ms while flash stimulation produced a major positive component between 90 and 140 ms. They noted that the latencies were considerably more variable in MEG than in EEG. This may be due to the fact that MEG primarily measures intracellular current flow rather than the return currents, which can cause significant differences from subject to subject in the field patterns at each sensor location, due to the variable orientations of the sources contributing to these components. Alternatively, some investigators suggest that MEG sees fewer sources than EEG. If several sources contribute to a given component and MEG does not see all of them, then it is possible that the overall latency would be more variable for MEG than EEG. In addition to the possible contributors to variability mentioned above, ERP signals are generally more distributed across the head, due to the conductivity properties of the skull and scalp, whereas MEG responses tend to be more focal. Therefore, every source is more likely to be seen in more of the sensors using ERPs leading to less variability to timing in the overall waveforms. However, every source will not contribute to every sensor in MEG. If the multiple sources are not accounted for when modeling the MEG data, then there will be more variability in reported onset times, overall. In addition to the fact that some sources may have a larger or smaller contribution to the waveform due to differences in cortical geometry, this will also lead to variability in the timing for MEG. These factors can be better accounted for using a proper source model to differentiate the timing of individual sources.

3 Experimental Design Parameters

Stimulus Location–Retinotopy. Figure 9 reveals a portion of the classical model of V1 retinotopic organization. V1 in monkeys contain a point-to-point representation of the entire contralateral visual hemifield (Felleman and Van Essen 1991; Van Essen 1979). This is true for humans as well, as shown initially from lesion studies (Holmes 1945; Horton and Hoyt 1991; Spector et al. 1981) and then by noninvasive neuroimaging studies (Engel et al. 1997; Fox et al. 1987; Maclin et al. 1983; Tootell et al. 1998b). The classical model of retinotopy based on lesion data suggests that the representation of the horizontal meridian (HM) is at the base of the calcarine fissure (see white arrow in Fig. 9a—HM is represented along the fold of the calcarine fissure). Lower field stimuli are expected to activate regions in the upper bank of the calcarine fissure and vice versa. Furthermore, there is a systematic relationship between the depths of sources in the calcarine fissure and the eccentricity of stimuli in the visual field (i.e., peripheral placements activate regions deeper within the fissure). Finally, left hemifield stimuli project to the right hemisphere and vice versa. Figure 9c shows a hypothetical stimulus located at 20° eccentricity in the lower right visual field (see small circle at 315°). Figure 9b shows its theoretical representation in flattened visual areas V1, V2, and V3.

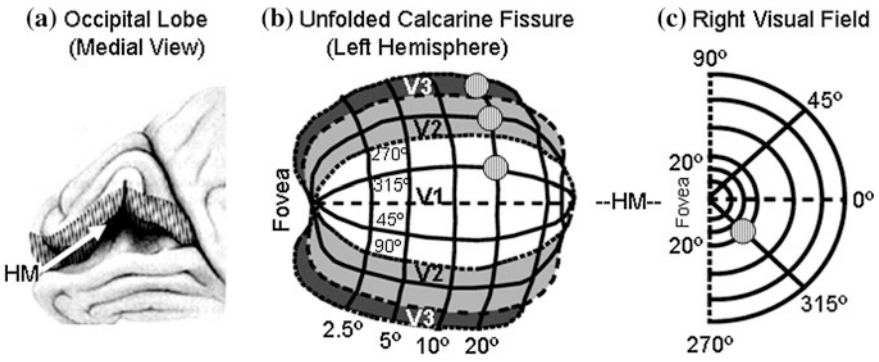

Fig. 9 **a** Left medial view of occipital lobe with idealized V1 superimposed. Horizontal meridian (HM) is located along the fold of the calcarine fissure (see *white arrow*). **b** Calcarine fissure is unfolded and three visual areas are demarcated, both upper and lower fields. **c**. There is a systematic point-to-point representation between the visual field and it's projections onto areas V1, V2 and V3. A theoretical stimulus (*small circle*) is positioned in the *lower right* field and it's projections to the upper portions of V1, V2 and V3 can be seen in B. HM is denoted by *dashed lines* and vertical meridians are denoted by *dotted lines*. The representations of V1 and V2 are mirror images of each other as are the representations of V2 and V3. Adapted from Horton and Hoyt (1991)

In our MEG retinotopy studies (Aine et al. 1996), we found that area V1 is not synonymous with the calcarine fissure as many investigators assume. In essence, the classical model is a simplified depiction of retinotopic organization. Human anatomical studies on cadavers have identified V1 via the stria of genari and these studies showed that only 55 % of V1 was found in the calcarine fissure of 52 human hemispheres (Stensaas et al. 1974) and that the anterior boundary of V1 is ordinarily found in the lower lip of the fissure (Polyak 1957). The latter finding suggests that in some cases, particularly for more eccentric placements in the lower field paralleling HM, lower field stimuli do not activate regions above the calcarine fissure. Areas V2 and V3 (shown in Fig. 9b also have retinotopic organization that are mirror images of each other. However, these areas cannot be identified by anatomical features. Retinotopic and functional mapping must be conducted for each individual, which is likely to be quite variable when using MEG due to differences in the folding of cortex. In addition, the process itself is tedious when multiple sites within the visual field have to be stimulated and analyzed. While our MEG studies demonstrated retinotopic organization of extrastriate cortex (Supek et al. 1999), extensive retinotopic mapping can be accomplished more easily using fMRI (Sereno et al. 1995); however, the time-courses of these regions will not be characterized as well as they could be via the use of MEG methods and appropriate modeling strategies.

Stimulus Location—Differences in Onset Latencies. At least two parallel streams of visual processing begin as early as the level of the retina and continue through primary and higher-order visual areas. The dorsal stream (Fig. 1) is characterized primarily by faster conducting large cell types (magnocellular)

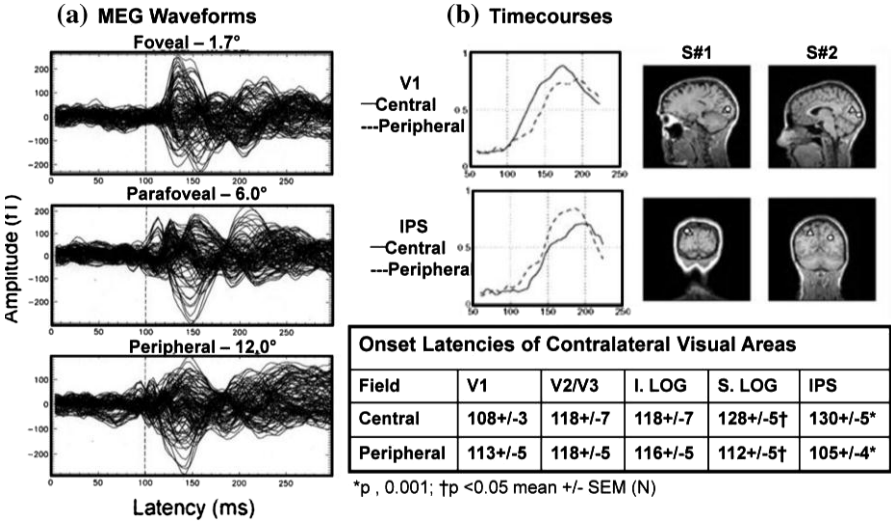

Onset Latencies of Contralateral Visual Areas

Field	V1	V2/V3	I. LOG	S. LOG	IPS
Central	108+/-3	118+/-7	118+/-7	128+/-5†	130+/-5*
Peripheral	113+/-5	118+/-5	116+/-5	112+/-5†	105+/-4*

*p , 0.001; †p <0.05 mean +/- SEM (N)

Fig. 10 **a** Eccentric placements in the visual field yield earlier onset latencies as demonstrated in the surface waveforms obtained from lower field stimulation. The *vertical dashed line* marks 100 ms. **b** Onset latencies of time-courses of sources localized to V1 and intraparietal sulcus (IPS—a dorsal stream structure) differ depending upon whether stimuli are presented to central (2.3°) or peripheral locations (24°). The table below shows quantified values and statistical differences

which are more pronounced in the peripheral retina and project primarily to MT and posterior parietal cortex while the ventral stream is characterized primarily by slowly conducting small cell types (parvocellular) which are more pronounced in the central retina and project to inferior temporal areas (De Monasterio and Gouras 1975; De Yoe and Van Essen 1988; Livingstone and Hubel 1987; Nowak and Bullier 1997; Shipp and Zeki 1985; Ungerleider and Desimone 1986). Figure 10a shows averaged MEG waveforms indicating earlier onsets associated with more eccentric or peripheral placements of the stimulus in the visual field (compare onset of activity for 1.7 versus 12 degrees along the dashed vertical line demarcating 100 ms poststimulus).

In general, dorsal stream structures have been related to motion processing or spatial vision and ventral stream structures have been related to the processing of features such as color and spatial frequency or object and face processing. Because peripheral stimulation may excite more large cell types than central field stimulation and peripheral field representations have more direct projections to parietal cortex, we hypothesized that peripheral stimulation would result in earlier onset latencies in dorsal stream structures than central stimulation (Stephen et al. 2002). Figure 10b shows that activation of IPS and the superior lateral occipital gyrus or S. LOG (dorsal stream structures) onset earlier for peripheral field stimulation. The table shown below indicates that visual areas reveal a systematic increase in onset latency for central field stimulation as one progresses from V1 to inferior lateral

occipital gyrus (I. LOG) through IPS. In contrast, peripheral field stimulation results in similar onset latencies throughout the structures with IPS and S. LOG onsetting earlier, compared to when central field stimulation evoked the activity. These results are consistent with results from nonhuman studies (Nowak and Bullier 1997).

Stimulus Location—Cortical Magnification Factor. Stimulus location is usually described as retinal eccentricity which is the angle between the primary visual axis (fixation point) and the line of sight from the eye to the object. If stimuli are to be placed in different locations of the visual field then the cortical magnification factor should be considered since in monkey striate cortex there is at least a 10-fold reduction in the area of cortex representing a corresponding area of the retina $\geq 15^{\circ}$ from the fixation point (Daniel and Whitteridge 1961). For example, if the goal of the study is to place a 2° square at different eccentricities of the visual field (e.g., 5° and 10°) and to compare responses, then squares placed in more peripheral locations should be scaled larger in size in order to activate the same amount of tissue in primary visual cortex that is activated by a square placed in more central areas (Perry and Cowey 1985; Rovamo and Virsu 1979). Cortical magnification describes the scale of retinotopic mapping by indicating how many millimeters of cortex represent 1° of visual angle at any given eccentricity. Unfortunately, the cortical magnification factor based on cell densities in the retina of monkeys and humans has been estimated for primary visual cortex only. Cell densities are greater at the fovea where receptive field sizes are small and they decrease in the periphery as receptive field sizes become larger. In addition, the upper field representation of the retina has fewer cells than lower field. A formula or series of formulas for the different visual field quadrants can be used to estimate the sizes of the stimuli necessary for activating equivalent amounts of tissue. Also, cortical magnification factors for striate and extrastriate cortex in humans have been estimated using fMRI (Sereno et al. 1995). Figure 11 shows an example of stimulus sizes scaled by the cortical magnification factor used in some of our basic visual studies (Stephen et al. 2002, 2006). See also different sizes of DOG stimuli in Fig. 8a.

Stimulus Intensity, Contrast and Spatial Frequency Content—Onset Latencies and Amplitudes. In general, ERP studies have shown that higher intensity and higher contrast stimuli shorten onset and peak latencies and reaction times (Armington 1964a, b; Campbell and Kulikowski 1972; Okada et al. 1982; Robson 1966) and increase amplitudes (e.g., peak to trough) until they reach a saturated level. However, complex interactions may occur when varying contrast, intensity, spatial and temporal frequency, stimulus size and location of the stimulus in the visual field, as discussed below.

Spatial frequency relates to the amount of detail cells can process and is inversely related to cell size (Enroth-Cugell and Robson 1966). Both cat and monkey studies show, as mentioned previously, that the ratio of small versus large cells changes from central to peripheral retina; that is, there are a greater number of small cells in the central retina and a greater number of large cells in the peripheral retina (Stone and Johnston 1981; Wright and Ikeda 1974). This physical

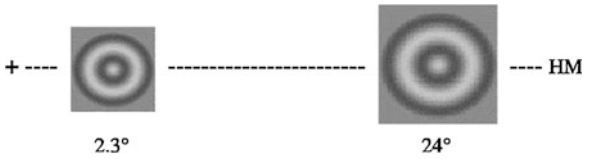

Fig. 11 Example of circular sinusoids scaled by the Cortical Magnification Factor for these right field stimuli. (Note the fixation point at the *left*). Stephen et al. (2002, 2006)

arrangement implies that conduction velocities will vary across the retina as well as preferred temporal and spatial frequencies (larger cell sizes prefer lower spatial frequencies and faster temporal frequencies). ERP studies found that small check sizes for example, evoked the greatest amplitude response when stimuli were presented to the foveal retina and that the check size producing the largest amplitude response increased as the peripheral retina was stimulated (Harter 1971). Okada et al. (1982) systematically examined peak-to-peak amplitudes (e.g., the amplitude from the maximum positive to the maximum negative peak of the initial occipital response) of visual ERPs and ERFs to different spatial frequencies, temporal frequencies and contrast levels using vertical, contrast-reversal gratings. The results showed: (1) greater amplitudes for higher spatial frequencies presented at low temporal frequencies; (2) higher temporal frequencies revealed greater amplitudes to low spatial frequencies; and (3) latencies of the ERFs increased with higher spatial frequency and decreased when contrast was increased. The characteristics of these transfer functions agreed well with both ERPs (Campbell and Kulikowski 1972; Campbell and Maffei 1970; Regan 1978) and the psychophysical contrast function (Kelly 1966; Robson 1966). Although many of these results had been shown previously (Kaufman and Williamson 1980; Williamson et al. 1978), this was the first study to quantitatively document the linear relation between the steady-state magnetic field and electrical potential for both phase and amplitude. Nakamura et al. (2000) also found, similar to many ERP studies, that check size (spatial frequency) significantly affected the latency and amplitude of the 100 ms peak in the transient response (i.e., longer latencies and reduced amplitudes for higher spatial frequencies).

If a proposed study intends to examine the spatial frequency content of stimuli then the use of sinusoidal stimuli (Fig. 11) may be preferable since square wave stimuli contain high spatial frequency content due to the sharp edges (Perry and Childers 1969). Furthermore, the stimuli should contain at least 2 cycles in order for the stimulus to be perceived at the desired spatial frequency (Regan 1989). In addition, psychophysical studies using a constant-luminance patterned stimulus (i.e., pure contrast stimulus) generally keep the mean luminance of the total stimulus field constant (see Fig. 11 for example—the entire background was the same as the gray surrounding the circular sinusoids which equaled the mean luminance of the circular sinusoids). Early ERP studies suggest that using pure contrast patterned stimuli will avoid unnecessary contamination by large luminance-related components (Jeffreys 1977) and will still yield amplitudes as large

as, or larger than those evoked by luminance related or unpatterned stimuli (Regan 1972). These studies suggest that pattern and non-pattern related components have two distinct types of cortical processes contributing to the CI, CII, and CIII components of the evoked response and that they have different sources that are essentially independent of each other. Contrast specific mechanisms (patterned) contribute to CI while luminance related mechanisms (or unpatterned) predominantly contribute to CII and CIII but also contribute to CI. Responses to sinusoidal gratings of less than 1 cycle per degree (cpd) are also considered for the most part to be luminance responses (Kulikowski 1974). Since the early studies focused on careful analysis of waveforms they attempted to simplify the responses as much as possible to eliminate alternative interpretations of the data. Some investigators may be wondering why this information is considered to be important, when they are interested in cognition and not basic vision. If two different stimuli are used in a cognitive study (e.g., high spatial frequency content of a house vs low spatial frequency content of a landscape) then changes in the MEG response may be associated with one condition versus another, due to differences in basic visual properties (e.g., differences in spatial frequency content), rather than being due to the cognitive factors under study. If the cognitive study is not well-controlled, it may lead to an alternative interpretation of the data.

As a final note, if the study involves the examination of spatial frequency and color, then the investigator should become aware of potential artifacts associated with chromatic aberration. A spatial frequency of 4 cpd or lower could be selected rather than a higher spatial frequency in order to minimize artifacts associated with chromatic aberration (Howarth and Bradley 1986).

Stimulus Duration and Temporal Frequency—Off-Response and Overlapping Signals. The visual system is sensitive to changes in luminance over the visual field. When stimuli are turned on, a sequential set of peaks emerge in the response. The visual system is also sensitive to when the stimulus is turned off and again a set of peaks emerge in the response. Although several early ERP studies examined human cortical on- and off-responses, there are no studies that we are aware of that have systematically examined the sources of these responses. However, ERP investigators have hypothesized that the CI component, believed to be generated from V1, is a large contributor of the off-response and they note that the off-response varies less with retinal location (Jeffreys 1977). Also, the resultant response to stimuli presented <25 ms in duration is not a simple linear sum of the onset and off-responses (Regan 1972). Figure 12 shows examples of two stimulus durations and consequent off-responses associated with them. In the top row, long stimulus durations permit one to choose whether or not to include the off-response in the analysis interval. A pronounced off-response in the bottom row makes the waveforms and time-course appear more complicated. The medial occipital region (MO—putative V1) was the only region in this particular analysis to reveal the off-response. Note that off-responses take about 100–150 ms to become evident after the stimulus goes off and they are smaller in amplitude than on-responses.

As stimulus repetition frequency is increased, the responses in both ERPs and ERFs overlap to an increasing extent. Stimulation rates for typical transient ERPs/

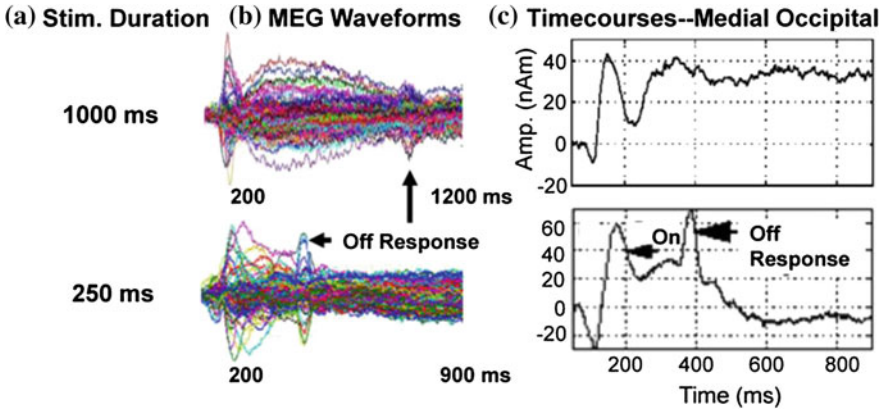

Fig. 12 **a** Effects of 2 different stimulus durations are shown. **b** On- and Off-responses are shown in the averaged MEG waveforms and in the time-courses. **c** Long-duration stimuli permit one to analyze data before the off-response appears (*upper right time-course*) whereas short duration stimuli change the appearance of the time-courses (*lower time-course*)

ERFs range from 1 stimulus per every few seconds to a more common average rate of one per second (1 Hz). At higher repetition rates (e.g., 10 Hz), ERP and ERF waveforms begin to entrain where no individual response cycle can be associated with a particular stimulus cycle (steady-state). When this state is reached it is no longer appropriate to describe the response as amplitudes across time but rather as amplitudes and phases of the various harmonic components of the ERP/ERF versus stimulus repetition frequency (Regan 1972). Fourier analysis decomposes the ERP/ERF waveforms into constituent harmonic components and describes each component by specifying its amplitude and phase. Pattern reversal frequencies exceeding 5 Hz can usually be adequately described by two harmonics. Since our group is interested in localizing sources of activity and understanding the temporal dynamics between brain regions, we used a pseudo steady-state design to determine which visual areas were engaged in frequency following (Stephen et al. 2002). Figure 13 shows waveform and time-course samples (i.e., localized to MO) using our pseudo steady-state design. Although it was hypothesized that dorsal stream structures would follow higher frequencies better than ventral stream structures, these results indicate that MO (putative V1), common to both streams, is very capable of following at low and high frequencies.

In general, careful consideration should be given to the timing of the stimuli. Does it matter if you have overlapping on- and off-responses due to the stimulus duration chosen or residual activity from one stimulus averaged with responses from the next cycle, which occurs with short interstimulus intervals (ISIs)? Early ERP studies of basic vision attempted to assure clean baseline measures (e.g., no overlapping activity from previous trials) since all amplitude measurements were dependent upon these baseline measures and it was assumed that interruption of a response by another stimulus contaminates the response. There is empirical

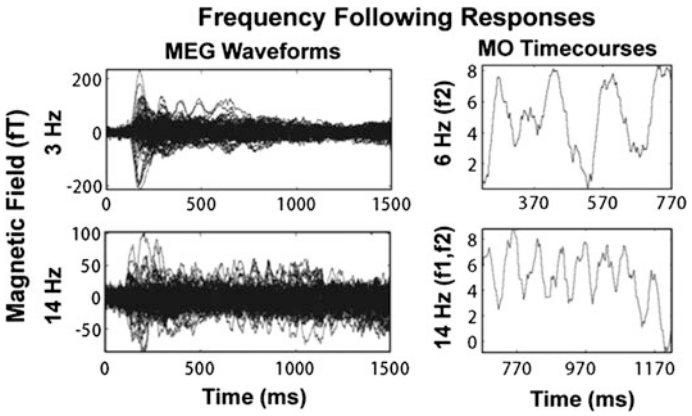

Fig. 13 Circular sinusoids were contrast reversed at different rates for 1 s. The averaged waveforms shown in the *left column* reveal frequency following behavior. Sources localized to medial occipital (MO) cortex also revealed frequency following effects. Stephen et al. (2002, 2006)

evidence that response tails of each response overlap and add as the frequency of stimulation is increased beyond 3 Hz (Perry and Childers 1969).

There are a couple of other ways to help assure that: (1) the baseline returns to a state of rest between successive trials and (2) the SNR is maximal. First, randomization of the ISI (e.g., 500 ms: the ISI varies between 800 and 1200 ms for an average ISI of 1 Hz) helps eliminate an anticipatory response or the contingent negative variation (CNV) which is a slow negative wave identified in ERPs that precedes a stimulus to which a response must be made (Walter et al. 1964). S1, S2 paired designs are notorious for producing slow negative shifts just preceding the presentation of S2. Slow ramping behavior in baselines has been identified in ERFs as well. Second, randomization of the stimulus conditions may also help prevent habituation of the responses (reduction of signal due to repetitive stimulation). Inclusion of short rest breaks also helps. While MEG studies routinely rely on inverse procedures for localizing sources, purity of the data will ultimately help in analysis and consequent interpretation.

Stimulus Size—Focal versus Extended Sources. In the past, many ERP and ERF studies were conducted using full field and half field stimuli. Localization of the sources of activity using inverse algorithms was not a primary goal of these studies. When designing visual studies one should keep in mind the tradeoffs between stimulus size and the ability to localize sources (i.e., spatial resolvability and whether or not the basic assumptions of the localization algorithm are violated). There is an ongoing debate about how much of cortex is activated even when small stimuli are utilized, particularly when higher-order cognitive functions are involved. However, if large stimuli are utilized then it is well known that large extended regions of cortex will be active in multiple brain regions. Resolvability of the sources will be more difficult and appropriate algorithms should be used.

For example, depending on source extent, dipole models have proven to be quite robust. Hillebrand and Barnes (2002) found that when equivalent current dipoles (ECDs) were used to fit a range of source extents, localization error increased from $\sim$2 mm for a 60 mm^2 source area to $\sim$4 mm for a 260 mm^2 source area. Jerbi et al. (2004) examined the ability of ECD and multipole models to fit a range of orientations and source extents. For source depths < 6 cm, localization errors ranged from 2 mm for 50 mm^2 areas to $\sim$6 mm for a 500 mm^2 patch size. If the investigator has good reasons to believe that extended activity will be produced in excess of the sizes enumerated above, then perhaps a distributed current approach should be considered.

The most convincing evidence, however, that higher-cognitive functions such as language are represented as focal and distributed regions of activity, as opposed to extended sources, comes from intracortical recordings of language processing largely carried out by Ojemann et al. (1989). In a study of language localization of 117 left hemisphere dominant patients, during object naming, language centers were found to be very focal (1–2 cm^2). There was a frontal focus as well as one or two in temporoparietal areas. Ojemann suggests that the discrepancy between his results and studies using blood flow or metabolic measurement techniques such as PET (which suggest larger language areas) is likely due to: (1) the large variability in the location of these focal sources across subjects and (2) the fact that functional imaging studies may indirectly indicate where neurons participate in language but not whether these neurons are essential for the language functions. Stimulation and lesion methods indicate areas that are *essential* for language.

Inter-Subject Averaging. Steinmetz and Seitz (1991) compared Ojemann's results with their PET results and they also concluded that the variability in the PET results was due to: (1) variability in the exact location of language function across subjects and (2) strict anatomical variability across subjects. In the former case, variability in the location of function was affected by numerous factors such as gender, verbal intelligence and the strategy used by the subjects during the task. They strongly discouraged inter-subject averaging and strongly encouraged intra-subject averaging as a resolution to this problem.

Figure 7 provides a concrete example of the anatomic variability often witnessed across subjects. In order to average data across subjects, PET methods typically require transforming PET brain coordinates for each individual into coordinates within an anatomical reference such as Talairach space. As discussed previously, the brains in the first two panels of Fig. 7 were placed into Talairach space and the grids show differences in where the calcarine fissure meets the occipital pole. If a small stimulus was presented in the central field, then an average of the active regions around the occipital pole (across subjects) would either reveal no activity due to low SNR for each subject or it would reveal a larger region of activation due to the smearing of foci across subjects. The anatomic variability and variability in functional loci can be enormous. Ojemann and colleagues indicate that some patients revealed only a frontal or only a temporoparietal language module while others showed both a frontal and temporoparietal

module of varying locations. Given the enormous individual variability, is it reasonable to average regions of source activity across subjects?

fMRI and MEG Language Studies. Figure 14 shows recent fMRI and MEG results when examining language functions such as verb or word generation or when participants had to make decisions regarding whether the word presented was concrete or abstract. Unlike many earlier fMRI results, these fMRI results look consistent with each other and with Ojemann's findings, while the MEG results look quite different and are clearly dependent on the type of language task and modeling method used. The two fMRI studies were clinical applications geared toward determining the language dominant hemisphere. In one MEG study, words were presented visually and participants determined whether they were concrete or abstract (Dhond et al. 2007). The second MEG study (Kamada et al. 2007) was a verb generation task to determine which hemisphere was dominant for language (clinically oriented). This figure highlights the importance of task differences, intended purpose of the study (e.g., research versus clinical application), and the modeling approach used (including basic assumptions about the source and head model). The upper right plot reveals results from a research study where the investigators generally believe that higher cognitive functions necessarily result in extended activity across cortex. Therefore, a distributed current model was used to analyze these data. In the lower right plot, a clinical study was conducted and the purpose was to determine the language dominant hemisphere for this patient, similar to a Wada test. The purpose of this figure is not to show how radically different MEG results are, but rather to emphasize that the investigator needs to consider many factors before conducting experiments and choosing an analysis method.

Summary and Conclusions. MEG is very sensitive to even the slightest changes in the stimulus parameters discussed above. As mentioned previously, careful design of the study is important for the consequent ease of analysis and interpretation of the results. In addition, these parameters (intensity, contrast level, pattern or no pattern, spatial frequency, size of stimulus and its relation to the fixation point, stimulus duration and ISI) should be measured and reported for publications and grant applications and most importantly, they need to be consistent across participants.

Some investigators feel that since they are examining higher cognitive functions such as memory, that sensory-related activity is not as important. However, given the recent studies indicating that functional neural circuits are involved (i.e., sensory-related regions involved in the initial perception of a past event are members of this circuit) and attention and working memory help to maintain these activities, there is a good possibility that sensory-related activity affects the overall cognitive response through efferent or feedback activation. In our working memory studies we design the stimuli so that the same set of stimuli is presented for the different experimental conditions so that it is the task instruction that differs between experimental conditions. In this way, if there are differences noted between conditions they are due to task instructions themselves, and not due to any of the stimulus parameters known to affect EEG/MEG responses. For example, our

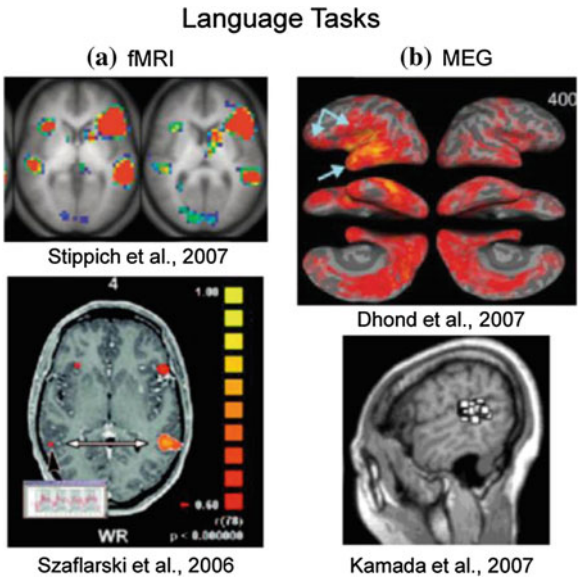

Fig. 14 **a** fMRI studies examining language dominance (verb or word generation tasks). Both reveal bilateral frontal and posterior regions of activation. **b** MEG studies examining language (abstract and concrete words versus verb generation). A distributed current model was used in the *upper plot* while multiple single dipoles were applied in the *lower plot*

delayed-match-to-sample studies used a set of Walsh function stimuli that have been well-characterized in monkey studies (see Fig. 2). The visual stimuli used are members of the 8 × 8 Walsh function set that are composed of black and white squares with the characteristic that each member has an equal amount of black and white allowing for equal luminance across the stimulus set (Richmond and Optican 1987; Richmond et al. 1990). Although the spatial frequency varies across the 64 stimulus set DMS choice pairs were chosen to be within a small and medium range of spatial frequencies to create different levels of difficulty for our aging population. The different experimental conditions are active versus passive tasks with the exact same stimuli being presented in both conditions. In another study, we are examining the neural circuits associated with verbal and spatial working memory (Aine et al. 2011). Again, the same set of stimuli is utilized across experimental conditions (Fig. 15). In the spatial task, subjects attend to the locations of red digits in this variant of the Sternberg task. In the verbal task, subjects attend to the digits. Distracting stimuli may also be placed in the delay interval, but since we are more interested in responses to the "target" stimuli, differences between distracter stimulus types is not an issue. We also keep the matrices relatively small in size ($\leq 4^{\circ}$ visual angle) since we use multi-dipole, spatial temporal modeling which assumes point sources of activity.

Another issue worth mentioning is not actually a problem related to stimulus parameters but rather how individuals utilize stimulus parameters to conduct the task at hand. We have been studying different strategies that individuals use, some of which differ due to changes in health status (e.g., normal aging versus mild cognitive impairment and Alzheimer's disease) and some of which differ for other reasons (Aine et al. 2010, 2011). Steinmetz and Seitz (1991) were also aware of

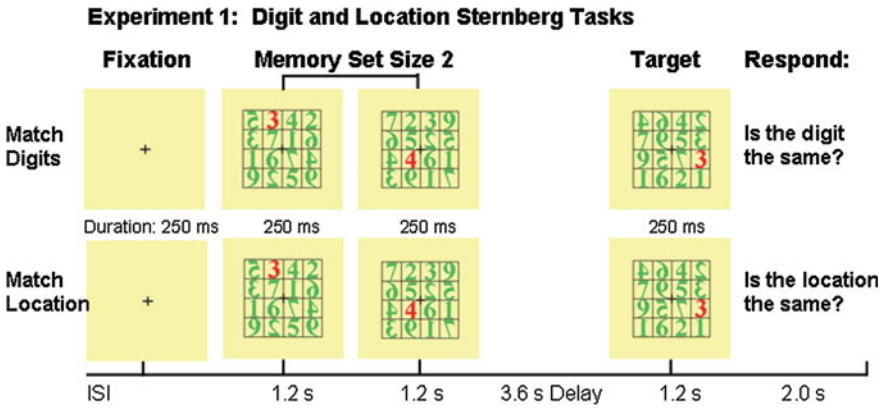

Fig. 15 Matrices (4°) are presented sequentially to the central field

the potential problem associated with averaging hemodynamic based measures across subjects. If participants use different strategies, which there is evidence of, then different neural systems are activated and averaged across subjects leaving a result that isn't characteristic of any one of the strategies utilized (Sanfratello et al. 2014).

4 Averaging MEG Data Across Participants

Pooling Data—Averaging Time-courses in Source Space. Because MEG is sensitive to the cortical geometries of each participant, averaging raw waveform data across participants would cause spurious cancellation/summation across subjects and is, therefore, inappropriate. However, we have found very good consistency in time-course morphology across participants with our analysis methods [CSST: a multidipole, spatio-temporal approach (Ranken et al. 2004): see Sanfratello et al. this volume, for more information on this analysis method] which enable us to average time-courses across subjects for specific brain regions. Figure 16 reveals consistency in morphology across participants and differences in morphology across cortical regions. Similarities across participants, associated with working memory, may also be seen in the left portion of this figure. Blue tracings in the left panel reflect responses to stimuli while participants were actively engaged in the working memory task while red tracings reflect activity evoked by the passive task. We carefully examine the internal consistency of our data on the first few subjects when we begin a new study before continuing with data acquisition (pilot study) in order to be certain that the parameters are what we wanted (e.g., stimulus markers occur where they are supposed to occur) and that the quality of data is appropriate for our analysis methods.

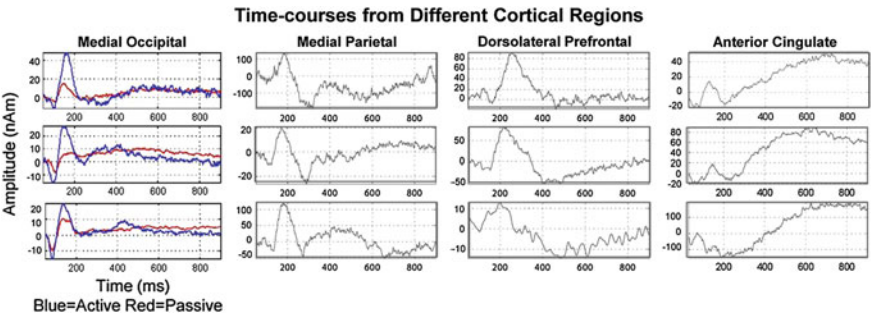

Fig. 16 Time-courses from 3 participants (*rows*) are shown for 4 cortical regions (*columns*). The *upper left panel* superimposes time-courses from "Active" (*blue tracing*) and "Passive" tasks (*red tracing*) during a working memory experiment. Clear differences in time-course morphology can be seen across brain regions while consistency in time-course morphology can be see across subjects during a working memory task

5 Concluding Remarks

We have attempted to highlight the most important issues confronting visual studies gleaned from our 25 + year history of conducting MEG studies. Historically, visual studies were initially avoided since it was clear that sources associated with the multiple visual areas needed to be modeled adequately, in contrast to early studies examining auditory cortex with single dipole models. While it remains true that the visual system is rich in terms of the numbers of active sources, it is also true that many of these sources are reasonably spaced so that the resolvability of the visual sources is not onerous. Furthermore, it later became clear that auditory cortex does not contain a single area of activation but it too consists of multiple regions that are located in a small region of cortex typically situated in the temporal lobe, a region that poses problems when using a spherical head model. The point to be made here is that the complexity of the visual system initiated an early search for methods that went beyond the traditional single dipole model. Consequently, we are now in a position to fully characterize the richness of the visual system in terms of identifying numerous visual areas, characterizing the timing within and between these visual areas, and in assessing the functional integrity of neural circuits hypothesized to be deficient in clinical populations.

However, there are many parameters that should be considered when designing visual protocols that can severely limit the interpretability of the data if they are not controlled. We have illustrated several of these potential confounds. Despite the complexities of MEG data, high quality data and appropriate analysis methods allow MEG to offer both good spatial and excellent temporal resolution, which no other method currently offers. In this chapter, we have demonstrated that MEG studies further our understanding of human sensation and cognition, with sensitivity at a single-subject level, paving the way for individualized medicine and clinical applications.

Acknowledgments This work was supported by NIH grants R01 AG029495, R01 AG020302, R01 EY08610, R21 MH080141, 5P20 RR021938 and 2P20 GM103472, as well as a VA MERIT review grant and Croatian MZOS grant 119-1081870-1252. The content of this chapter is solely the responsibility of the authors and does not necessarily represent the official views of the National Institutes of Health. The authors thank The Mind Research Network (Albuquerque, New Mexico) for the unlimited use of their computing facility, as well as UNM Radiology Department and the Research Office of the New Mexico VA Health Care System. We also thank Yoshio Okada for his insightful comments on an earlier version of this chapter.

References

Aertsen AM, Gerstein GL, Habib MK, Palm G (1989) Dynamics of neuronal firing correlation: modulation of "effective connectivity". J Neurophysiol 61:900–917

Ahlfors SP, Ilmoniemi RJ, Hamalainen MS (1992) Estimates of visually evoked cortical currents. Electroencephalogr Clin Neurophysiol 82:225–236

Aine CJ, Bryant JE, Knoefel JE, Adair JC, Hart B, Donahue CH, Montano R, Hayek R, Qualls C, Ranken D, Stephen JM (2010) Different strategies for auditory word recognition in healthy versus normal aging. Neuroimage 49:3319–3330

Aine CJ, Sanfratello L, Adair JC, Knoefel JE, Caprihan A, Stephen JM (2011) Development and decline of memory functions in normal, pathological and healthy successful aging. Brain Topogr 24:323–339

Aine CJ, Stephen JM (2002) MEG studies of visual processing. In: Zanni A, Proverbio AM (eds) The cognitive electrophysiology of mind and brain, Academic Press, pp 93–142

Aine CJ, Stephen JM, Christner R, Hudson D, Best E (2003) Task relevance enhances early transient and late slow-wave activity of distributed cortical sources. J Comput Neurosci 15:203–221

Aine CJ, Supek S, George JS (1995) Temporal dynamics of visual-evoked neuromagnetic sources: effects of stimulus parameters and selective attention. Int J Neurosci 80:79–104

Aine CJ, Supek S, George JS, Ranken D, Lewine J, Sanders J, Best E, Tiee W, Flynn ER, Wood CC (1996) Retinotopic organization of human visual cortex: departures from the classical model. Cereb Cortex 6:354–361

Albright TD (1984) Direction and orientation selectivity of neurons in visual area MT of the macaque. J Neurophysiol 52:1106–1130

Alvarez P, Squire LR (1994) Memory consolidation and the medial temporal lobe: a simple network model. Proc Natl Acad Sci U S A 91:7041–7045

Armington JC (1964a) Adaptational changes in the human electroretinogram and occipital response. Vision Res 4:179–192

Armington JC (1964b) Relations between electroretinograms and occipital potentials elicited by flickering Stimuli. Doc Ophthalmol 18:194–206

Armstrong RA, Slaven A, Harding GF (1991) Visual evoked magnetic fields to flash and pattern in 100 normal subjects. Vision Res 31:1859–1864

Baylis GC, Rolls ET (1987) Responses of neurons in the inferior temporal cortex in short term and serial recognition memory tasks. Exp Brain Res 65:614–622

Brefczynski JA, DeYoe EA (1999) A physiological correlate of the 'spotlight' of visual attention. Nat Neurosci 2:370–374

Bressler SL (1995) Large-scale cortical networks and cognition. Brain Res Brain Res Rev 20:288–304

Butler SR, Georgiou GA, Glass A, Hancox RJ, Hopper JM, Smith KR (1987) Cortical generators of the CI component of the pattern-onset visual evoked potential. Electroencephalogr Clin Neurophysiol 68:256–267

Camisa J, Bodis-Wollner I (1982) Stimulus parameters and visual evoked potential diagnosis. In: Bodis-Wollner I (ed) Evoked potentials. The New York Academy of Sciences, New York, pp 645–647
Campbell FW, Kulikowski JJ (1972) The visual evoked potential as a function of contrast of a grating pattern. J Physiol 222:345–356
Campbell FW, Maffei L (1970) Electrophysiological evidence for the existence of orientation and size detectors in the human visual system. J Physiol 207:635–652
Cantalupo C, Hopkins WD (2001) Asymmetric Broca's area in great apes. Nature 414:505
Chafee MV, Goldman-Rakic PS (2000) Inactivation of parietal and prefrontal cortex reveals interdependence of neural activity during memory-guided saccades. J Neurophysiol 83:1550–1566
Courtney SM, Ungerleider LG (1997) What fMRI has taught us about human vision. Curr Opin Neurobiol 7:554–561
Damasio A (1989) The brain binds entities and events by multiregional activation from convergence zones. Neurol Comp 1:23–32
Daniel PM, Whitteridge D (1961) The representation of the visual field on the cerebral cortex in monkeys. J Physiol 159:203–221
Darcey TM, Ary JP, Fender DH (1980) Spatio-temporal visually evoked scalp potentials in response to partial-field patterned stimulation. Electroencephalogr Clin Neurophysiol 50:348–355
De Monasterio FM, Gouras P (1975) Functional properties of ganglion cells of the rhesus monkey retina. J Physiol 251:167–195
De Yoe EA, Felleman DJ, Van Essen DC, McClendon E (1994) Multiple processing streams in occipitotemporal cortex. Nature 371:151–154
De Yoe EA, Van Essen DC (1988) Concurrent processing streams in monkey visual cortex. Trends Neurosci 11:219–226
Dhond RP, Witzel T, Dale AM, Halgren E (2007) Spatiotemporal cortical dynamics underlying abstract and concrete word reading. Hum Brain Mapp 28:355–362
Di Russo F, Martinez A, Hillyard SA (2003) Source analysis of event-related cortical activity during visuo-spatial attention. Cereb Cortex 13:486–499
Engel AK, Fries P, Singer W (2001) Dynamic predictions: oscillations and synchrony in top-down processing. Nat Rev Neurosci 2:704–716
Engel AK, Konig P, Kreiter AK, Schillen TB, Singer W (1992) Temporal coding in the visual cortex: new vistas on integration in the nervous system. Trends Neurosci 15:218–226
Engel SA, Glover GH, Wandell BA (1997) Retinotopic organization in human visual cortex and the spatial precision of functional MRI. Cereb Cortex 7:181–192
Enroth-Cugell C, Robson JG (1966) The contrast sensitivity of retinal ganglion cells of the cat. J Physiol 187:517–552
Farah M, Humphreys GW, Rodman HR (1999) Chapter 52: object and face recognition. In: Zigmond MJ, Bloom FE, Landis SC, Roberts JL, Squire LR (eds) Fundamental neuroscience, Academic Press, San Diego
Felleman DJ, Van Essen DC (1991) Distributed hierarchical processing in the primate cerebral cortex. Cereb Cortex 1:1–47
Fox PT, Miezin FM, Allman JM, Van Essen DC, Raichle ME (1987) Retinotopic organization of human visual cortex mapped with positron-emission tomography. J Neurosci 7:913–922
Friston KJ (1994) Statistical parametric mapping. In: Thatcher MHRW, Zeffiro T, John ER, Huerta M (eds) Functional neuroimaging: technical foundations. Academic Press, New York, pp 79–93
Fuster JM (1973) Unit activity in prefrontal cortex during delayed-response performance: neuronal correlates of transient memory. J Neurophysiol 36:61–78
Fuster JM (1997) Network memory. Trends Neurosci 20:451–459
Fuster JM (2001) The prefrontal cortex–an update: time is of the essence. Neuron 30:319–333
Fuster JM, Jervey J (1981) Neuronal firing in the inferotemporal cortex of the monkey in a visual memory task. J Neurosci 2:361–365

Gerstein GL, Perkel DH (1969) Simultaneously recorded trains of action potentials: analysis and functional interpretation. Science 164:828–830
Gilbert CD, Sigman M, Crist RE (2001) The neural basis of perceptual learning. Neuron 31:681–697
Goldman-Rakic PS (1988) Topography of cognition: parallel distributed networks in primate association cortex. Annu Rev Neurosci 11:137–156
Goldman-Rakic PS (1995) Architecture of the prefrontal cortex and the central executive. Ann N Y Acad Sci 769:71–83
Gray CM (1999) The temporal correlation hypothesis of visual feature integration: still alive and well. Neuron 24(31–47):111–125
Haenny PE, Schiller PH (1988) State dependent activity in monkey visual cortex. I. Single cell activity in V1 and V4 on visual tasks. Exp Brain Res 69:225–244
Harding GF, Degg C, Anderson SJ, Holliday I, Fylan F, Barnes G, Bedford J (1994) Topographic mapping of the pattern onset evoked magnetic response to stimulation of different portions of the visual field. Int J Psychophysiol 16:175–183
Harding GF, Janday B, Armstrong RA (1991) Topographic mapping and source localization of the pattern reversal visual evoked magnetic response. Brain Topogr 4:47–55
Harter MR (1971) Visually evoked cortical responses to checkerboard patterns: effects of check size as a function of retinal eccentricity. Electroenceph clin Neurophys 23:48–54
Hashimoto T, Kashii S, Kikuchi M, Honda Y, Nagamine T, Shibasaki H (1999) Temporal profile of visual evoked responses to pattern-reversal stimulation analyzed with a whole-head magnetometer. Exp Brain Res 125:375–382
Hillebrand A, Barnes GR (2002) A quantitative assessment of the sensitivity of whole-head MEG to activity in the adult human cortex. Neuroimage 16:638–650
Holmes G (1945) The organization of the visual cortex in man. Proc R Soc Lond [Biol] 132:348–361
Horton JC, Hoyt WF (1991) The representation of the visual field in human striate cortex. A revision of the classic Holmes map. Arch Ophthalmol 109:816–824
Howarth PA, Bradley A (1986) The longitudinal chromatic aberration of the human eye, and its correction. Vision Res 26:361–366
Hupe JM, James AC, Girard P, Lomber SG, Payne BR, Bullier J (2001) Feedback connections act on the early part of the responses in monkey visual cortex. J Neurophysiol 85:134–145
Inoue M, Mikami A, Ando I, Tsukada H (2004) Functional brain mapping of the macaque related to spatial working memory as revealed by PET. Cereb Cortex 14:106–119
Jeffreys D (1977) The physiological significance of pattern visual evoked potentials. In: Desmedt JE (ed) Visual evoked potentials in man: new developments. Clarendon Press, Oxford, pp 134–167
Jeffreys DA, Axford JG (1972a) Source locations of pattern-specific components of human visual evoked potentials. I. Component of striate cortical origin. Exp Brain Res 16:1–21
Jeffreys DA, Axford JG (1972b) Source locations of pattern-specific components of human visual evoked potentials. II. Component of extrastriate cortical origin. Exp Brain Res 16:22–40
Jensen O, Tesche CD (2002) Frontal theta activity in humans increases with memory load in a working memory task. Eur J Neurosci 15:1395–1399
Jerbi K, Baillet S, Mosher JC, Nolte G, Garnero L, Leahy RM (2004) Localization of realistic cortical activity in MEG using current multipoles. Neuroimage 22:779–793
Kamada K, Todo T, Masutani Y, Aoki S, Ino K, Morita A, Saito N (2007) Visualization of the frontotemporal language fibers by tractography combined with functional magnetic resonance imaging and magnetoencephalography. J Neurosurg 106:90–98
Kaufman L, Williamson SJ (1980) The evoked magnetic field of the human brain. Ann N Y Acad Sci 340:45–65
Kelly DH (1966) Frequency doubling in visual responses. J Opt Soc Am 56:1628–1633
Klimesch W (1999) EEG alpha and theta oscillations reflect cognitive and memory performance: a review and analysis. Brain Res Brain Res Rev 29:169–195

Kosslyn SM (1988) Aspects of a cognitive neuroscience of mental imagery. Science 240:1621–1626
Kulikowski JJ (1974) Proceedings: Human averaged occipital potentials evoked by pattern and movement. J Physiol 242:70P–71P
Lamme VA, Roelfsema PR (2000) The distinct modes of vision offered by feedforward and recurrent processing. Trends Neurosci 23:571–579
Lamme VA, Zipser K, Spekreijse H (1998) Figure-ground activity in primary visual cortex is suppressed by anesthesia. Proc Natl Acad Sci U S A 95:3263–3268
Lampl I, Reichova I, Ferster D (1999) Synchronous membrane potential fluctuations in neurons of the cat visual cortex. Neuron 22:361–374
Lee H, Simpson GV, Logothetis NK, Rainer G (2005) Phase locking of single neuron activity to theta oscillations during working memory in monkey extrastriate visual cortex. Neuron 45:147–156
Livingstone MS, Hubel DH (1987) Psychophysical evidence for separate channels for the perception of form, color, movement, and depth. J Neurosci 7:3416–3468
Maclin E, Okada YC, Kaufman L, Williamson SJ (1983) Retinotopic map on the visual cortex for eccentrically placed patterns: first noninvasive measurement. Il Nuovo Cimento 2:410–419
Maier J, Dagnelie G, Spekreijse H, van Dijk BW (1987) Principal components analysis for source localization of VEPs in man. Vision Res 27:165–177
Martinez A, Anllo-Vento L, Sereno MI, Frank LR, Buxton RB, Dubowitz DJ, Wong EC, Hinrichs H, Heinze HJ, Hillyard SA (1999) Involvement of striate and extrastriate visual cortical areas in spatial attention. Nat Neurosci 2:364–369
Maunsell JH, van Essen DC (1983) The connections of the middle temporal visual area (MT) and their relationship to a cortical hierarchy in the macaque monkey. J Neurosci 3:2563–2586
Mehta AD, Ulbert I, Schroeder CE (2000a) Intermodal selective attention in monkeys. I: distribution and timing of effects across visual areas. Cereb Cortex 10:343–358
Mehta AD, Ulbert I, Schroeder CE (2000b) Intermodal selective attention in monkeys. II: physiological mechanisms of modulation. Cereb Cortex 10:359–370
Merigan WH, Maunsell JH (1993) How parallel are the primate visual pathways? Annu Rev Neurosci 16:369–402
Mesulam MM (1998) From sensation to cognition. Brain 121(Pt 6):1013–1052
Michael WF, Halliday AM (1971) Differences between the occipital distribution of upper and lower field pattern-evoked responses in man. Brain Res 32:311–324
Miller EK, Li L, Desimone R (1991) A neural mechanism for working and recognition memory in inferior temporal cortex. Science 254:1377–1379
Milner PM (1974) A model for visual shape recognition. Psychol Rev 81:521–535
Mishkin M (1982) A memory system in the monkey. Philos Trans R Soc Lond B Biol Sci 298:83–95
Motter BC (1994) Neural correlates of feature selective memory and pop-out in extrastriate area V4. J Neurosci 14:2190–2199
Nakamura M, Kakigi R, Okusa T, Hoshiyama M, Watanabe K (2000) Effects of check size on pattern reversal visual evoked magnetic field and potential. Brain Res 872:77–86
Noesselt T, Hillyard SA, Woldorff MG, Schoenfeld A, Hagner T, Jancke L, Tempelmann C, Hinrichs H, Heinze HJ (2002) Delayed striate cortical activation during spatial attention. Neuron 35:575–587
Nowak LG, Bullier J (1997) The timing of information transfer in the visual system. In: Rockland KS, Kaas JH, Peters A (eds) Cerebral cortex. Plenum Press, New York, pp 205–241
Ojemann G, Ojemann J, Lettich E, Berger M (1989) Cortical language localization in left, dominant hemisphere. An electrical stimulation mapping investigation in 117 patients. J Neurosurg 71:316–326
Okada YC, Kaufman L, Brenner D, Williamson SJ (1982) Modulation transfer functions of the human visual system revealed by magnetic field measurements. Vision Res 22:319–333
Ossenblok P, Spekreijse H (1991) The extrastriate generators of the EP to checkerboard onset. A source localization approach. Electroencephalogr Clin Neurophysiol 80:181–193

Perry JNW, Childers DG (1969) The human visual evoked response: method and theory. Charles C Thomas, Springfield
Perry VH, Cowey A (1985) The ganglion cell and cone distributions in the monkey's retina: implications for central magnification factors. Vision Res 25:1795–1810
Pesaran B, Pezaris JS, Sahani M, Mitra PP, Andersen RA (2002) Temporal structure in neuronal activity during working memory in macaque parietal cortex. Nat Neurosci 5:805–811
Polyak SI (1957) The vertebrate visual system. University of Chicago, Chicago
Ranken DM, Stephen JM, George JS (2004) MUSIC seeded multi-dipole MEG modeling using the constrained start spatio-temporal modeling procedure. Neurol Clin Neurophysiol 2004:80
Regan D (1972) Evoked potentials in psychology, sensory physiology and clinical medicine. Wiley-Interscience, New York
Regan D (1978) Assessment of visual acuity by evoked potential recording: ambiguity caused by temporal dependence of spatial frequency selectivity. Vision Res 18:439–443
Regan D (1989) Human brain electrophysiology: evoked potentials and evoked magnetic fields in science and medicine. Elsevier, New York
Reynolds J, Desimone R (1999) The role of neural mechanisms of attention in solving the binding problem. Neuron 24:19–29
Richmond BJ, Optican LM (1987) Temporal encoding of two-dimensional patterns by single units in primate inferior temporal cortex. II. Quantification of response waveform. J Neurophysiol 57:147–161
Richmond BJ, Optican LM, Spitzer H (1990) Temporal encoding of two-dimensional patterns by single units in primate primary visual cortex. I. Stimulus-response relations. J Neurophysiol 64:351–369
Richmond BJ, Wurtz RH, Sato T (1983) Visual responses of inferior temporal neurons in awake rhesus monkey. J Neurophysiol 50:1415–1432
Robson JG (1966) Spatial and temporal contrast-sensitivity functions of the visual system. J Opt Soc Am 56:1141–1142
Roelfsema PR, Engel AK, Konig P, Singer W (1997) Visuomotor integration is associated with zero time-lag synchronization among cortical areas. Nature 385:157–161
Roelfsema PR, Lamme VA, Spekreijse H (1998) Object-based attention in the primary visual cortex of the macaque monkey. Nature 395:376–381
Rovamo J, Virsu V (1979) An estimation and application of the human cortical magnification factor. Exp Brain Res 37:495–510
Salinas E, Sejnowski TJ (2001) Correlated neuronal activity and the flow of neural information. Nat Rev Neurosci 2:539–550
Sanfratello L, Caprihan A, Stephen JM, Knoefel JE, Adair JC, Qualls C, Lundy SL, Aine CJ (2014) Same task, different strategies: how brain networks can be influenced by memory strategy. Hum Brain Mapp (in press)
Scheeringa R, Petersson KM, Oostenveld R, Norris DG, Hagoort P, Bastiaansen MC (2009) Trial-by-trial coupling between EEG and BOLD identifies networks related to alpha and theta EEG power increases during working memory maintenance. Neuroimage 44:1224–1238
Seidemann E, Newsome WT (1999) Effect of spatial attention on the responses of area MT neurons. J Neurophysiol 81:1783–1794
Seki K, Nakasato N, Fujita S, Hatanaka K, Kawamura T, Kanno A, Yoshimoto T (1996) Neuromagnetic evidence that the P100 component of the pattern reversal visual evoked response originates in the bottom of the calcarine fissure. Electroencephalogr Clin Neurophysiol 100:436–442
Semendeferi K, Lu A, Schenker N, Damasio H (2002) Humans and great apes share a large frontal cortex. Nat Neurosci 5:272–276
Sereno MI, Dale AM, Reppas JB, Kwong KK, Belliveau JW, Brady TJ, Rosen BR, Tootell RB (1995) Borders of multiple visual areas in humans revealed by functional magnetic resonance imaging. Science 268:889–893

Shigeto H, Tobimatsu S, Yamamoto T, Kobayashi T, Kato M (1998) Visual evoked cortical magnetic responses to checkerboard pattern reversal stimulation: a study on the neural generators of N75, P100 and N145. J Neurol Sci 156:186–194
Shipp S, Zeki S (1985) Segregation of pathways leading from area V2 to areas V4 and V5 of macaque monkey visual cortex. Nature 315:322–325
Singer W, Gray CM (1995) Visual feature integration and the temporal correlation hypothesis. Annu Rev Neurosci 18:555–586
Spector RH, Glaser JS, David NJ, Vining DQ (1981) Occipital lobe infarctions: perimetry and computed tomography. Neurology 31:1098–1106
Squire LR (1986) Mechanisms of memory. Science 232:1612–1619
Squire LR, Zola-Morgan S (1991) The medial temporal lobe memory system. Science 253:1380–1386
Steinmetz H, Seitz RJ (1991) Functional anatomy of language processing: neuroimaging and the problem of individual variability. Neuropsychologia 29:1149–1161
Stensaas SS, Eddington DK, Dobelle WH (1974) The topography and variability of the primary visual cortex in man. J Neurosurg 40:747–755
Stephen JM, Aine CJ, Christner RF, Ranken D, Huang M, Best E (2002) Central versus peripheral visual field stimulation results in timing differences in dorsal stream sources as measured with MEG. Vision Res 42:3059–3074
Stephen JM, Aine CJ, Ranken D, Hudson D, Shih JJ (2003) Multidipole analysis of simulated epileptic spikes with real background activity. J Clin Neurophysiol 20:1–16
Stephen JM, Ranken D, Aine CJ (2006) Frequency-following and connectivity of different visual areas in response to contrast-reversal stimulation. Brain Topogr 18:257–272
Stippich C, Rapps N, Dreyhaupt J, Durst A, Kress B, Nennig E, Tronnier VM, Sartor K (2007) Localizing and lateralizing language in patients with brain tumors: Feasibility of routine preoperative functional MR imaging in 81 consecutive patients. Radiology 243:828–836
Stone J, Johnston E (1981) The topography of primate retina: a study of the human, bushbaby, and new- and old-world monkeys. J Comp Neurol 196:205–223
Supek S, Aine CJ, Ranken D, Best E, Flynn ER, Wood CC (1999) Single versus paired visual stimulation: superposition of early neuromagnetic responses and retinotopy in extrastriate cortex in humans. Brain Res 830:43–55
Szaflarski JP, Holland SK, Schmithorst VJ, Byars AW (2006) fMRI study of language lateralization in children and adults. Hum Brain Mapp 27:202–212
Tallon-Baudry C, Mandon S, Freiwald WA, Kreiter AK (2004) Oscillatory synchrony in the monkey temporal lobe correlates with performance in a visual short-term memory task. Cereb Cortex 14:713–720
Tomita H, Ohbayashi M, Nakahara K, Hasegawa I, Miyashita Y (1999) Top-down signal from prefrontal cortex in executive control of memory retrieval. Nature 401:699–703
Tootell RB, Hadjikhani N, Hall EK, Marrett S, Vanduffel W, Vaughan JT, Dale AM (1998a) The retinotopy of visual spatial attention. Neuron 21:1409–1422
Tootell RB, Hadjikhani NK, Vanduffel W, Liu AK, Mendola JD, Sereno MI, Dale AM (1998b) Functional analysis of primary visual cortex (V1) in humans. Proc Natl Acad Sci U S A 95:811–817
Tulving E (1995) Organization of memory: quo vadis. MIT Press, Cambridge
Ungerleider LG (1995) Functional brain imaging studies of cortical mechanisms for memory. Science 270:769–775
Ungerleider LG, Desimone R (1986) Projections to the superior temporal sulcus from the central and peripheral field representations of V1 and V2. J Comp Neurol 248:147–163
Ungerleider LG, Mishkin M (1982) Two cortical visual systems. In: Ingle DJ, Goodale MA, Mansfield RJW (eds) Analysis of visual behavior. MIT Press, Cambridge, pp 549–586
Van Essen DC (1979) Visual areas of the mammalian cerebral cortex. Annu Rev Neurosci 2:227–263
Van Essen DC (1985) Functional organization of primate visual cortex. In: Peters A, Jones EG (eds) Cerebral cortex. Plenum, New York, pp 259–329

Van Essen DC, Maunsell JH (1983) Hierarchical organization and functional streams in the visual cortex. Trends Neurosci 6:370–375
Walter WG, Cooper R, Aldridge VJ, McCallum WC, Winter AL (1964) Contingent negative variation: an electric sign of sensorimotor association and expectancy in the human brain. Nature 203:380–384
Wheeler ME, Petersen SE, Buckner RL (2000) Memory's echo: vivid remembering reactivates sensory-specific cortex. Proc Natl Acad Sci U S A 97:11125–11129
Williamson SJ, Kaufman L, Brenner D (1978) Latency of the neuromagnetic response of the human visual cortex. Vision Res 18:107–110
Wilson FA, Scalaidhe SP, Goldman-Rakic PS (1993) Dissociation of object and spatial processing domains in primate prefrontal cortex. Science 260:1955–1958
Wright MJ, Ikeda H (1974) Processing of spatial and temporal information in the visual system. In: Schmitt FO, Worden FG (eds) The neurosciences. MIT Press, Cambridge, pp 115–122
Zeki S (1980) A direct projection from area V1 to area V3A of rhesus monkey visual cortex. Proc R Soc Lond B Biol Sci 207:499–506
Zeki SM (1973) Colour coding in rhesus monkey prestriate cortex. Brain Res 53:422–427
Zeki SM (1978) Functional specialisation in the visual cortex of the rhesus monkey. Nature 274:423–428

MEG Imaged Pathways of Stuttering

Susan M. Bowyer and Jennifer Peacock

Abstract Knowledge of the underlying mechanism of stuttering may be useful for finding the best individual treatment for this persistent disorder. Stuttering is a disruption in speech production, characterized by repetitions, blocks, and/or prolongations. MEG neuroimaging techniques provide an excellent tool for establishing and evaluating reliable protocols to detect the underlying mechanisms of stuttering which in the future will help clinicians assess responses to treatments. Detection of neuronal network abnormalities in the default mode network of patients who stutter can also provide further brain regions for evaluation of pre and post treatment. This chapter reviews the use of MEG in past and present studies of stuttering. Areas for future research and refinement of MEG protocols for stuttering are also presented.

Keywords Stuttering · Magnetoencephalography (MEG) · Resting state · Evoked responses · Broca's area · Wernicke's area · Fiber tracks · Neuronal networks · Adults who stutter (AWS) · Children who stutter (CWS) · People who stutter (PWS) · Language processing · Treatment · Inferior frontal gyrus · Premotor · Auditory · Visual

1 Introduction

1.1 Stuttering Background

Stuttering is a disorder that disrupts the forward flow of speech. Approximately 5 % of people have stuttered at one point in time in their lives (World_Health_Organization 1992). Approximately 1 % of these children will continue to stutter into

S. M. Bowyer (✉) · J. Peacock
Departments of Neurology and Speech Pathology, Henry Ford Health systems,
2799 West Grand Blvd, Detroit, MI 48202, USA
e-mail: sbowyer1@hfhs.org

S. Supek and C. J. Aine (eds.), *Magnetoencephalography*,
DOI: 10.1007/978-3-642-33045-2_38, © Springer-Verlag Berlin Heidelberg 2014

adulthood (Guitar 1998). In America there are 3 million adults who stutter (AWS) (Bloodstein 1995). Four times more boys than girls are effected by this disorder (Yairi et al. 1996). Although stuttering is a very debilitating communication disorder, many can continue to lead very successful lives. Examples of famous people who stuttered (PWS) include Marilyn Monroe, James Earl Jones, Winston Churchill and of course King George VI of England whose stuttering woes were depicted in the award wining movie "The King's Speech" (Howell 2011).

The primary characteristics of stuttering include repetitions, prolongations and/or blocks. Repetitions typically consist of sounds, syllables or whole words that are repeated ("c-c-c-can", "for-for-forgive", "I…I see you"). Prolongations are characterized as sounds that are pulled out, often in an effortful manner ("I wwwwwwant" or "Lllllllike"). Blocks are complete disruptions in the flow of air as the person attempts to vocalize words. Stuttering also encompasses secondary behaviors, which are the physical components that arise from a person's reaction to the stuttering (Guitar 1998). Secondary behaviors (i.e. eye-blinking, head jerks, body movements, etc.) vary dramatically among individuals in their physical presentation as well as the severity of their effect on communication.

Many children go through a period of normal disfluency as they grow their vocabulary and increase the length and complexity of their sentence structures. The primary characteristics that differentiate developmental stuttering from normal disfluency include: higher number of disfluencies, a higher number of "stuttering-like" disfluencies, higher number of repeated units, and an emergence of secondary behaviors (Zebrowski 1995).

Stuttering most commonly presents in young childhood during language development (developmental stuttering). However, it can also occur as the result of a neurological incident (neurogenic stuttering) or a psychological incident (psychogenic stuttering).

There are many theories about the causes of developmental stuttering, but research has not found one core factor that is both necessary and sufficient to cause stuttering. Instead, stuttering results from a complex interaction of a number of risk factors (Gordon 2002). The risk factors include but are not limited to a combination of neurological, genetic, speech-language functioning, temperament and environment (Anderson et al. 2003; Zebrowski and Buhr 2005).

Of the studies exploring risk factors, genetic studies have shown the most conclusive findings (Bennett 2006). Stuttering has been found in several family members, suggesting that genetic factors are involved (Kang and Drayna 2011). Past studies have revealed genetic predisposition and excess dopamine as potential causes of this developmental disorder (Gordon 2002; Movsessian 2005; Kang and Drayna 2011). Genetic mutations in genes such as GNPTAB and NAGPA, responsible for lysosomal enzyme transport (where digestive enzymes break down toxic substances, digest bacteria that invade the cell, and recycle worn-out cell components), as well as FOXP2 and CNTNAP2, which play critical roles in gene expression, have revealed the inherent flaws in cortical metabolism of PWS (MacDermot et al. 2005; Newbury and Manaco 2010; Drayna and Kang 2011). Excess dopaminergic neurotransmission in the basal ganglia arising from

dysfunctional DRD2 and SLC6A3 genes has also been observed as a contribution to the stuttering condition (Lan et al. 2009). Genetic factors make up a small number of stuttering cases, but this provides an avenue for research investigations into the substrates and mechanisms that underlie stuttering.

Neurogenic stuttering usually occurs after a stroke, head trauma, or other type of brain injury. With neurogenic stuttering, the brain has difficulty coordinating the different components involved in speaking because of signaling problems between the brain and nerves or muscles. In some cases, diseases such as epilepsy, stroke, trauma, brain tumor, and Parkinson's, which interfere with normal frontal lobe and basal ganglia function, lead to acquired stuttering (Theys et al. 2008; Watkins et al. 2008; Kaplan et al. 2011). In other cases, stuttering can often be a secondary manifestation of conditions such as dyslexia, autism, Down's syndrome, and Tourette's syndrome (De Nil et al. 2005; Van Borsel and Tetnowski 2007).

Psychogenic stuttering is caused from long-term stress or an emotional trauma. This type of stuttering is very rare. The stuttering behaviors are similar to those of developmental stuttering, but are often not consistent in speech production. Secondary behaviors tend to be unusual or will be present even when stuttering behaviors are not being displayed (Guitar 1998).

1.2 Models of Neurological Activation in Speech-Language Functions

Researchers have been attempting to identify the neural processes underlying stuttering, with a growing emphasis on brain imaging research. In a review of the literature, Ludlow (2000) suggests a "dynamic interplay among complex cortical and subcortical systems", involving areas of planning, production and monitoring. Ingham (2001), Ingham et al. (2004) supports this claim in his reviews of neuroimaging studies. Although there is agreement that there are likely many neural subsystems that comprise the disorder of stuttering, there has not been agreement about what subsystems are involved and how they are connected (Braun et al. 1997; Salmelin et al. 2000; Ingham 2001; Brown et al. 2005).

1.3 Functional Imaging Language Studies

Ever since the first language models were developed by Wernicke and Geschwind (Geschwind 1970), neurologists and neuropsychologists have been attempting to determine how the brain processes language and which cortical areas underlie specific language functions. A number of theoretical models have been proposed for both language production (Fromkin 1971; Garret 1975, 1980; Shattuck-Hufnagel 1979, 1987; Stemberger 1985; Dell 1986; MacKay 1987; Levelt 1989, 1998) and comprehension in normal readers (Liberman 1967; Marslen-Wilson and Tyler 1980;

McClelland 1986, 1991; Frazier 1987; Friederici 2002; Hagoort 2003). There is ongoing debate about whether the language subprocesses of semantics, syntax, and phonology are accessed simultaneously [e.g. production: Dell (1986); e.g. comprehension: Marslen-Wilson and Tyler (1980)] or in some hierarchical order [production: e.g., Levelt (1999); comprehension: e.g., Friederici (1999, 2002)]. Serial models (hierarchical) rely on a predictable and sequential pattern of processes engaged for successful understanding and production.

A review paper by Heim (2005) explored neuroimaging results from PET, fMRI, EEG and MEG to determine which models of language processing provide a basis for the interpretation of these neuroimaging results. The results are not conclusive, yet they do shed light on the cortical processing steps involved in language processing. They do account for a dual-route model featuring one direct and one indirect route which involve phonological processing.

MEG has been used in a number of studies to study brain activation during normal speech production in a variety of nonverbal and verbal tasks, including overt picture naming (Helenius et al. 1998; Levelt et al. 1998; Simos et al. 1998, 2001; Tarkianine et al. 1999; Hari et al. 2000; Greenwald and Bowyer 2003). These studies all provide a refined view of the dual stream model of language neuroanatomy (Hickok 2009) where the ventral stream, for speech comprehension, is bilateral and flows into the temporal lobes and the dorsal stream, for sensory-motor integration, is left dominant and involves the parietal temporal junction and frontal lobe.

1.4 Differences Seen with Language Processing in People Who Stutter

Many techniques have been used over the years to attempt to localize the brain regions involved in stuttering. Some of the earlier research was completed with positron emission tomography (PET) studies (Fox et al. 1996, 2000; Braun et al. 1997; De Nil et al. 2000; Ingham et al. 2004). Although PET scans give valuable information on localization, they lack the temporal resolution needed to assess the dynamic system of connected speech.

Another neuroimaging technique utilized frequently to study stuttering is functional magnetic resonance imaging (fMRI) (Watkins et al. 2008; Chang et al. 2009; Loucks et al. 2011). Several studies using fMRI have found task-to-brain-area-activation correlations for various stuttering experiments (Fox et al. 2000; De Nil et al. 2008; Chang et al. 2009; Lu et al. 2010). No single region fully responsible for stuttering has been found, but the basal ganglia, cerebellum, and motor cortex are among those suspected. Functional MRI detects oxygen consumption and can measure neural activity that lasts at least tens of milliseconds (Liu et al. 2006). Though fMRI provides higher temporal resolution than PET, it still does not provide the temporal resolution that is necessary for connected speech to be examined.

A meta analysis of speech production studies (PET and fMRI) on controls and AWS (Brown et al. 2005) identified activation in inferior frontal gyrus, superior temporal gyrus, primary motor cortex, premotor cortex, supplementary motor area, Rolandic operculum, lateral cerebellum, and auditory areas during single-word reading by control subjects who did not stutter. In AWS similar areas were involved but the motor areas were over-activated during the same task. These neuroimaging techniques offer an increasingly comprehensive view of brain activity and may point to certain areas of concern during monitored task execution.

Electroencephalographic recordings of event-related brain potentials (ERPs), used by Weber-Fox (2001, 2004) provide excellent temporal resolution of speech production, however, ERPs do not provide good localization information (Liu et al. 2006) due to the complex inverse solution problem.

Magnetoencephalography (MEG) has been used to localize brain regions activated during language processing in normal subjects (Simos et al. 1998; Bowyer et al. 2004; Salmelin 2007), and has been used to evaluate stuttering (Salmelin et al. 1998, 2000; Biermann-Ruben et al. 2005; Bowyer et al. 2010; Beal et al. 2011; Kikuchi et al. 2011; Walla et al. 2004).

The earliest MEG research in stuttering was done by Salmelin et al. (1998). They looked at auditory feedback in people who stuttered (PWS). They showed differences in cortical organization of the auditory response between AWS and fluent speakers. This study used the equivalent current dipole (ECD) method to localize brain activity. They found functional deficits in the auditory system which may affect speech fluency during speech production in AWS.

MEG was then used to detect speech production during reading aloud of single words to detect the cortical processing area differences in AWS compared to controls (Salmelin et al. 2000). Using the ECD method they mapped the cortical activation sequences and found differences in evoked responses time-locked to word presentation and mouth movement onset. Within the first 400 ms after seeing the word, processing in fluent speakers advanced from the left inferior frontal cortex (articulatory programming) to the left lateral central sulcus and dorsal premotor cortex (motor preparation). This sequence was reversed in the AWS, who showed an early left motor cortex activation followed by a delayed left inferior frontal signal (See Fig. 1). This same study found a task-related suppression of the motor cortical 20 Hz oscillations during overt reading, which may indicate mouth movement cortical areas did not develop normally in AWS. Though this study found significant differences in single word reading they acknowledged that more detailed studies (specifically, more realistic speech production conditions) were required to determine the functional roles of the areas affected.

The third MEG study performed on stuttering subjects was by Walla et al. This MEG study looked at the lack of focused anticipation of verbal information in AWS during visually presented single words (Walla et al. 2004). When fluent readers spoke the word aloud, immediately after word presentation, neural activation (in the normalized MEG waveforms) was seen in the motor speech area before speech onset. They used a two-dipole model to approximate the sources for this pre speech activity. Pre speech brain activity was not detected in AWS.

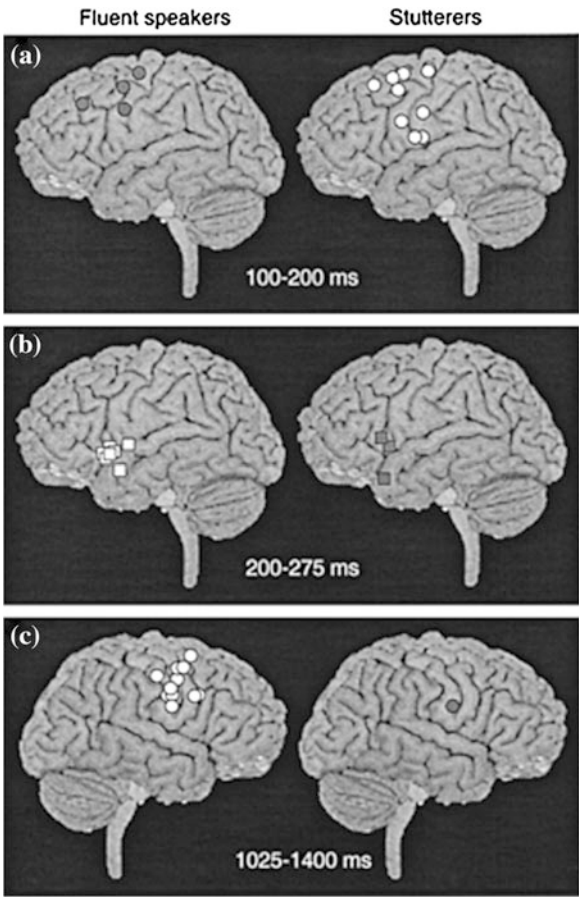

Fig. 1 Source areas of individual subjects showing a positive non-zero signal ($P < 0.001$) within those regions of interest (ROI) and time of interest (TOI) where activation strengths differed significantly between fluent speakers (*left*) and stutterers (*right*). The symbols are filled with grey in that subject group which showed on average less activation in each ROI/TOI (Salmelin et al. 2000)

Indicating that this brain activity (also named Bereutschafts field 2) might reflect preparatory activity known to occur for many other voluntary movements, and may be the link to disfluent speech in AWS.

A fourth MEG study of speech perception indicated language processing in the auditory modality differs for AWS and normally fluent readers. Biermann-Ruben et al. (2005), detected alternate language processing pathways during speech perception prior to overt repetition of a spoken word and sentence, and a sentence transformation task. AWS had greater activation of left inferior frontal areas, thought to be important for speech preparation, during the temporal window of 95–145 ms post-word and sentence onsets. In addition, between 315 and 1,000 ms post-stimulus, activations of the right rolandic areas, thought to be involved in sensorimotor processing, were larger for single-word compared to sentence tasks for the fluent readers, but the opposite pattern was seen for the AWS. Their results suggest that activation in the left inferior frontal and right rolandic areas in AWS differs from that in controls during speech perception. These findings may reflect differences due to

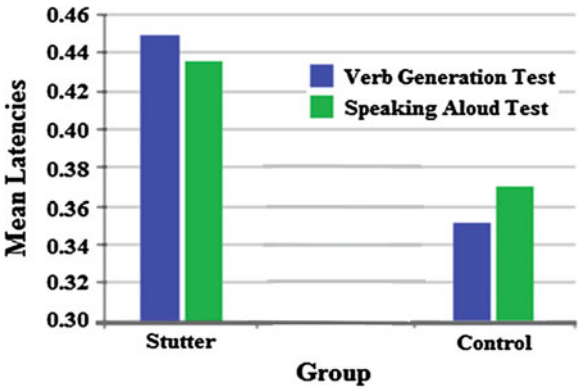

Fig. 2 Mean latencies of the groups during the verb generation task and the speaking aloud task. Broca's activation in AWS was significantly higher than that of control subjects

the paradigm set up as there was a delay prior to speaking. In a previous MEG study in fluent readers, which did not require speaking following speech perception, also did not elicit activation in the temporo-parietal, inferior-frontal, and rolandic areas (Helenius et al. 1998). This suggests the possibility that the differences between the AWS and fluent readers may be just due to activations for preparing to speak.

Our group (Bowyer et al. 2010) identified cortical activity in Wernicke's area (posterior section of the superior temporal gyrus) activated at the same time in controls and AWS. Activation was located in the supramarginal gyrus (SMG) in the latency interval 230 ± 20 ms across all 14 subjects. This indicated that comprehension was normal in both groups during the early language components in a verb generation task. Visual activation was detected in all subjects at 101 ± 10 ms after stimulus onset during all language task runs, indicating that visual processing was normal across all subjects. Using a one word speaking aloud task differences were noted in Broca's activation. AWS had delayed motor speech activation (434 ± 20 ms) compared to normal fluent readers (378 ± 36 ms) in the inferior frontal gyrus [$p < 0.0001$]. Also using an overt Verb Generation task AWS had delayed motor speech activation (450 ± 22 ms) compared to normal fluent readers (350 ± 29 ms) in the inferior frontal gyrus [$p < 0.0001$] (Fig. 2).

This study used a current distribution technique [MR-FOCUSS (Moran et al. 2005)] to localize brain activity during these language tasks. This MEG technique is different from the ECD method used in the previous MEG studies in that it allows the identification of simultaneous brain activity that is occurring across the brain to be displayed, where as the ECD method only allows one location in the brain to be displayed. Figure 3 depicts the MR-FOCUSS results for one individual AWS and one fluent reader. The inferior frontal gyrus in the Left hemisphere is active in both subjects but at different latencies. The MEG waveforms depict a large amplitude wave at ~100 ms representing visual processing. The line is located at the latency where Broca's area (inferior frontal gyrus) was active.

Two recent MEG studies have investigated the auditory system in AWS which has implications for treatment, which we will discuss further later in this chapter. Kikuchi et al. (2011) found auditory sensory gating (P50m suppression) was

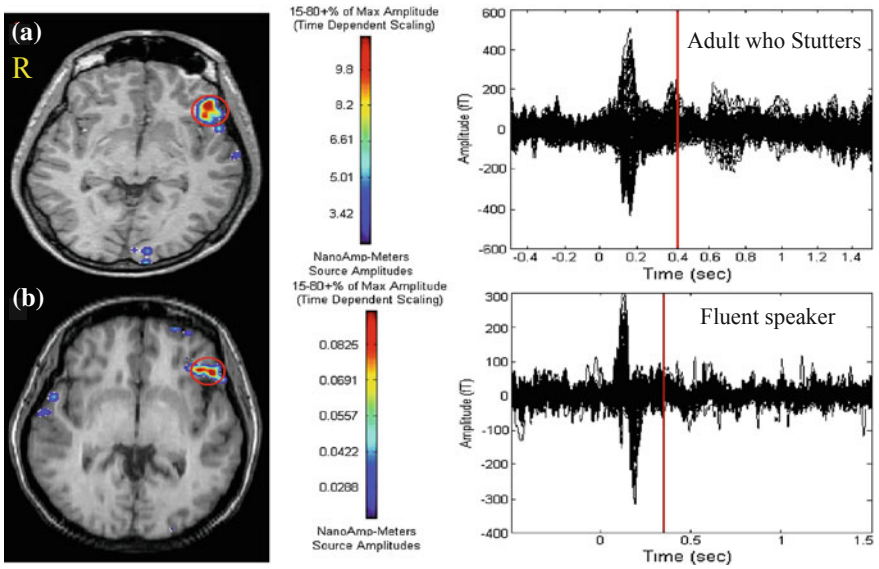

Fig. 3 MEG results during the overt verb generation task. Broca's area activity is indicated by a circle on the MRI. Scale is in nanoAmp-meters. **a** Maximum peak activity was seen at 440 ms in the evoked MEG waveform after word onset in this AWS. **b** Maximum activity was seen at 336 ms after word onset in this fluent reader. AWS had a much high current distribution seen in Broca's area compared to fluent readers

impaired in the left hemisphere during basic auditory input processing and that some error signals in the auditory cortex could result in abnormal speech processing. The tonotopic organization in the right hemisphere of AWS is expanded compared with that of the controls, along with a significant increase in the gray matter volume of the right superior temporal gyrus, consistent with the right tonotopic expansion. This study used the ECD model to localize brain activity. They hypothesize that the functional and structural reorganization of the right auditory cortex maybe a compensatory mechanism for impaired left auditory cortex function in AWS.

Beal et al. (2011) found speech induced suppression of auditory evoked fields in children who stutter (CWS). They examined the auditory P50m response in children as it most likely reflects a motor-to-auditory relation. This group used an event related vector beamformer to localize brain activation. See Fig. 4. Both CWS and those that do not stutter demonstrated speech-induced suppression of the auditory P50m. However, CWS had a delayed auditory M50 peak latency to vowel sounds compared to children who do not stutter indicating a possible deficiency in their ability to efficiently integrate auditory speech information for the purpose of establishing neural representations of speech sounds.

The millisecond temporal resolution and millimeter spatial resolution of these seven MEG studies provided significant information on how the stuttering brain is processing higher order cognitive language functioning differently than fluent

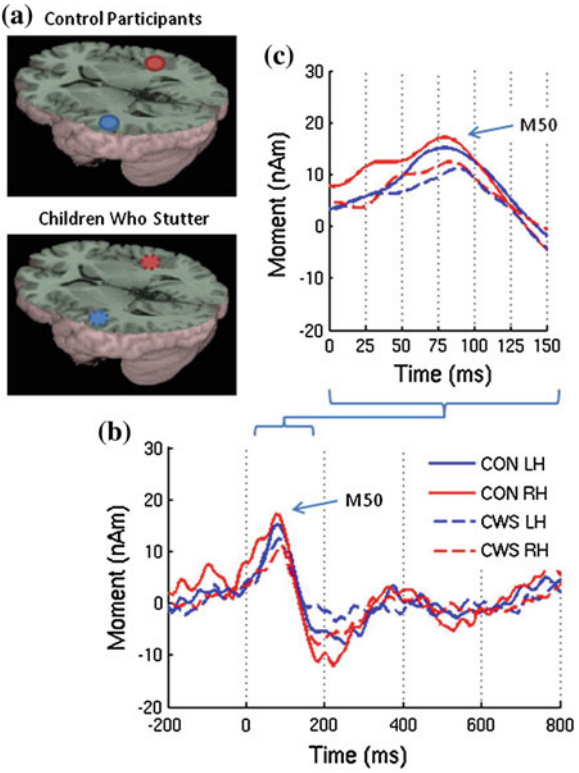

Fig. 4 **a** Group averaged source images of the auditory evoked magnetic fields for the *speak vowel* task overlaid on the MNI canonical brain. **b** Group averaged source magnitude variations from 200 ms prestimulus to 800 ms post stimulus corresponding to those sources and **c** a detailed view of the early components (Beal et al. 2011)

speaking control subjects. Though these studies all used either a single visual or auditory word or sentence task, the results provided a more integrated image of the neuronal processing that underlies stuttering. Advances in MEG signal processing and artifact removal techniques make it easier to collect realistic speech and analyze the location of corresponding brain activity more effectively than 10 yeas ago. The refinement of protocols to look at continuously connected speech will also provide an abundant amount of data to investigate in more detail the underlying brain regions activated in the stuttering process. There is currently no other imaging technique available providing combined high temporal resolution and high spatial resolution in a safe, noninvasive imaging modality for studying children.

1.5 Studying PWS Across Their Development

When studying stuttering it is extremely important to understand how age effects the results. Researchers have been suggesting for many years that drawing conclusions about the cause and nature of developmental stuttering in CWS from studies of AWS is unwise (Conture and Kelly 1991; Yairi 1993) because it

disregards the "influence of development, learning history, and experience" (Conture 1990).

Although limited, there have been some studies exploring the neural processes involved in children. In a study examining CWS (Chang et al. 2008), differences were found in Broca's area but no differences were found in the right hemisphere regions. These findings supported the suggestions from many studies completed with AWS that right hemisphere involvement may be the result of compensatory reactions (De Nil et al. 2000; De Nil and Kroll 2001; Fox and Raichle 2007; Chang et al. 2008; Loucks et al. 2011). Weber-Fox et al. (2008) found that neural processes related to phonological processing in CWS were different than children who do not stutter (CWNS). It is also noteworthy that, when compared to a similar study done with AWS (Weber-Fox et al. 2004), the differences were qualitatively different and more pronounced in the CWS.

Although the research completed by Weber-Fox et al. (2008) and Chang et al. (2008), are steps in the right direction of exploring stutter in children, both studies were completed with school-aged children, with the youngest being 9 years old. The onset of stuttering typically occurs in young children when rapid cognitive, linguistic and motor development is occurring (Fox et al. 2000). This stage typically occurs during the preschool years, between the ages of two and five (Ambrose and Yairi 1999). To explore the underlying neurophysiology of developmental stuttering and the likely causes of it, it is important to study children close to the point of recovery or persistency (Loucks et al. 2011) to avoid contamination "by time-related adjustments to internal and external responses" (Yairi 1993). Many have avoided completing neuroimaging studies with young children, however, because there are many challenges to studying young children, including a reluctance to participate and a shorter time period for tolerance of the protocol (Loucks et al. 2011).

When looking at the above research, it becomes clear that exploring stuttering across the continuum of development is essential to tell the story of the developmental and cortical contributions to stuttering. Studying different age groups in different stages of stuttering will give comparative data on the neurophysiology of stuttering. That data may then be evaluated to give a better picture of the causal versus resultant neural processes involved in stuttering.

1.6 Network Activity Seen in PWS

Recently resting state MEG data has been used to evaluate the default mode network (DMN) in different disorders such as Epilepsy (Elisevich et al. 2011). The DMN is a network of brain regions that are active when the individual is not focused on the outside world and the brain is at wakeful rest. fMRI and MEG provide neuroimaging techniques that can look at the source location of the coherent brain oscillations during rest. Although the DMN has not been a main

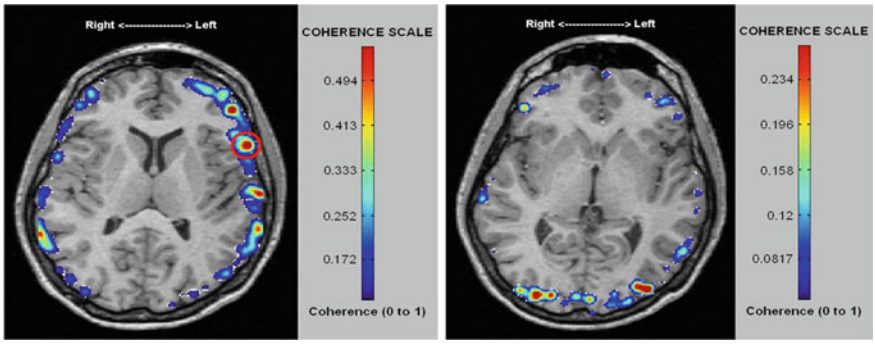

Fig. 5 **a** DMN coherence of a PWS. Highly coherent activity was found in Broca's area (Brodmann's Area 45) during resting state. **b** DMN coherence of a fluent speaking control subject finds little or no coherent activity in Broca's area

area of focus for stuttering research studies in the past, high areas of coherent activity in the inferior frontal gyrus and auditory cortex during the resting state in AWS was hypothesized to create an abnormal DMN and cause decreased efficiency in accessing those areas for AWS (Bowyer et al. 2010).

Guitar (1998) suggested that atypical neurological organization predisposes certain people to stuttering, however, those atypical organizations do not appear to be consistent from person to person. In fact, he hypothesizes that patterns of neural activity develop in unique ways and may account for the wide variety of symptoms seen in people who stutter.

Our group investigated the resting state, when no langauge processing was occurring, and found Broca's areas had significantly higher coherence in PWS (0.31 ± 0.08) compared to controls (0.13 ± 0.04) [$p < 0.0001$]. Figure 5 displays one PWS and one fluent speaking control subject's resting state results. These MEG resting state results possibly indicate continuous brain activity is occurring in the motor speech area thus providing competition for brain resources resulting in stuttering.

This finding was supported by a recent fMRI resting state study in 44 male AWS compared to 46 aged matched fluent speakers. (Xuan et al. 2012). Increased low frequency fluctuations were found in the left Inferior frontal gyrus as well as in the Left auditory and bilateral prefrontal cortices in PWS. This study also found that functional connectivity within anterior and posterior speech- and language-associated areas was increased in PWS compared to controls.

However, more extensive MEG studies will be needed to further explore how these results can be used for diagnois and detection of treatment responses. The nice thing about this type of task is that even infants can preform a task where they lay quietly for a few minutes with their eyes open.

1.7 Treatments

Currently, there are no cures for stuttering, although pharmacological and clinical avenues for potential treatments are being pursued (Bothe et al. 2006a, b; Blomgren 2010; Ratner 2010). The nature of the treatment will differ, based upon a person's age, communication goals, and other factors. Therapy for stuttering is primarily done by a certified speech-language pathologist.

For very young children, early treatment may prevent developmental stuttering from becoming a lifelong problem. Certain strategies can help children learn to improve their speech fluency while developing positive attitudes toward communication. Health professionals generally recommend that a child be evaluated if he or she has stuttered for at least 6 months, exhibits awareness of the stuttering and/or struggle behaviors associated with stuttering, or has a family history of stuttering or related communication disorders.

The two therapy techniques most commonly used for pre-teens though adulthood focus on strategies for improved fluency (fluency enhancing techniques) and strategies for modifying the stutter (stuttering modification techniques). It is widely upheld that a more integrated approach, utilizing a combination of the two techniques to address the behaviors, thoughts and feelings associated with stuttering, is the best practice for clinicians to treat PWS (Bennett 2006).

Drug therapies with Risperidone and Asenapine, which are dopamine-antagonist agents, have been shown to moderately improve a patients' stuttering frequency (Maguire et al. 2011; Tavano et al. 2011). However, better treatment methods are being sought as dopamine antagonists can lead to severe side-effects including Parkinson's disease and other conditions characterized by dopamine-deficiency.

Multiple studies have affirmed that choral speech (speaking in unison with others) and singing can greatly reduce the frequency of stuttering in affected patients (Howell et al. 2004; Toyomura et al. 2011). This finding suggests that timing can play a role in reducing stuttering. Fluency devices have been designed to capitalize on these concepts. These devices use altered auditory feedback (AAF) that digitally replays a slightly delayed or altered version of the wearer's voice into the ear to aid in fluency. Although these devices have been shown to be very effective in many PWS, they are by no means a cure. The devices do not take into consideration any of the emotional or psychological components of the stuttering. Therefore, treatment by a certified speech-language pathologist along with use of any device is essential.

1.8 Imaged Effects of Treatment Responses

One device that uses AAF is called the SpeechEasy®. The SpeechEasy® is an in-the-ear auditory feedback device that is reported to enhance fluency in people who stutter. It combines delayed auditory feedback (DAF) with frequency altered

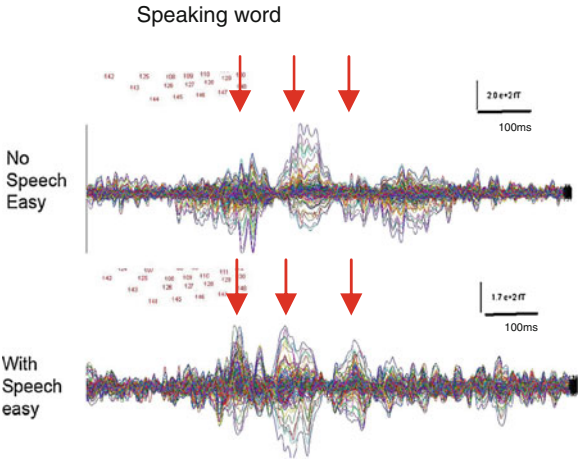

Fig. 6 148 MEG channel butterfly plots. MEG averaged evoked responses during speaking words aloud. *Initial peak* is visual processing, *second peak* is Wernicke's activation, and *third peak* is Broca's activation. Note in *bottom* trace Broca's activation is clearly seen with the use of the SpeechEasy device

feedback (FAF) to create a choral effect. The choral effect occurs when people who stutter speak or sing in unison with others, resulting in dramatically reducing or even eliminating the stutter. The SpeechEasy® is one of the few devices that has been made portable and inconspicuous enough for people to wear outside of the therapy room and in their daily lives.

fMRI research has looked at the results of DAF on cortical functioning. Results suggest that there may be two biological subgroups of AWS, (1) those with anomalous anatomy of the auditory cortex, and (2) those considered to have typical anatomy of the auditory cortex. Those with anomalous anatomy of the auditory cortex were found to have a greater percentage of dysfluencies (Foundas et al. 2004). This same group also showed a greater response to DAF as well.

Our group used MEG to image the location of cortical processes of stuttering with and without the SpeechEasy® device, to determine the latency and sequence of activation of the cognitive neural pathways involved in stuttering. These results indicated that during both the overt verb generation (VG) and reading aloud (RA) task, activation in Wernicke's area, supramarginal gyrus (SMG), was similarly active regardless of the use of the SpeechEasy® device in PWS [with VG: 250 ± 16 ms; RA: 247 ± 7 ms and without VG: 249 ± 25 ms; RA: 245 ± 15 ms].

Broca's area activation was significantly delayed in PWS (434 ± 20 ms) compared to controls (378 ± 36 ms) [$p < 0.0001$] during the reading aloud task, but when the SpeechEasy® device was used the latency of Broca's activation appeared to normalize the in PWS (375 ± 22 ms) to the point that no statistically significant comparison could be achieved with controls [$p < 0.05$]. The same normalization of the latency was found in the overt verb generation task where AWS delayed motor speech activation (450 ± 22 ms) compared to normal fluent readers (350 ± 29 ms) normalized to (373 ± 36 ms) [$p < 0.05$].

When looking at cortical activity in AWS, we found an increase in activity in the inferior frontal gyrus (Broca's area) while using the SpeechEasy® device

compared to the MEG measurement without the SpeechEasy® in place. Without the SpeechEasy®, there was no clear peak in Broca's area, indicating low levels of activation see Fig. 6. When the SpeechEasy® was being used, there was a clear peak, showing higher levels of activation see Fig. 6. It is hypothisized that because AWS showed lower activation in Broca's area, the stuttering is a result of decreased motor speech functioning. Therefore the increased activity with the SpeechEasy®, may help focus the neurons in that area to complete the motor speech tasks necessary for increased levels of fluency.

The increased cortical activation with the SpeechEasy® device in place ($\sim$0.200 nAm) was still lower compared to control subjects ($\sim$0.380 nAm), which explains why, although the SpeechEasy® may improve fluency, it does not create complete fluency and why it has varied effects from person to person.

An additional finding included high areas of coherent activity in the inferior frontal gyrus and auditory cortex during the resting state while the subject was not speaking. This data shows an abnormal default mode network (DMN) involving the inferior frontal gyrus area as well as the auditory cortex. During resting state in AWS, these areas were highly active, where control subjects showed very low levels of activation. Therefore, it is thought that when AWS need to access these areas, they are more difficult to access because they are already being activated (during the resting state) and need to be redirected to the task at hand. Looking at the combination of the resting state data and the evoked data, it appears that AWS may have a defect in the cortical activation of Broca's area. Therefore, it is hypothesized that when the SpeechEasy® is utilized, it may disrupt the DMN, creating the ability to more effectively activate Broca's area for motor speech and creating improved fluency.

1.9 Future Direction and Needs

Currently researchers are working to help speech-language pathologists determine which children are most likely to outgrow their stuttering and which children are at risk for continuing to stutter into adulthood. Advances in the study of the underlying neuronal bases for stuttering may lead to an objective biological marker for clinicians to identify these two groups. Brain imaging studies with PET, fMRI and MEG have indicated that there are connectivity differences in the left inferior frontal and premotor cortices in people who stutter. The deficiencies in these communicating brain regions hinder the efficient planning and execution of sound production.

Biomarkers that can detect changes in children who have recovered from stuttering will provide significant targets for detecting the effects of treatment. Future research on how treatments affect the brain networks and regional activations, in a child who stutters compared to one who has recovered, may lead to treatments that normalize the brain function of stuttering children.

Several research studies have indicated the possibility of subgroups within the stuttering populations. If neuroimaging methods can identify or classify groups of PWS then more focused approaches (i.e. tailored treatments) may be successful. There are clear gender differences within this patient population where males are four times more likely to stutter than their female counterparts. Research has shown females who stutter have more bilateral brain activation during language processing, which may help them recover from stuttering. Research into the influence of genetic factors on brain development patterns may also provide an understanding of the causes of stuttering.

Past studies on stuttering have been performed predominantly on adults or older children who have stuttered for many years. In these studies, neuroimaging techniques may be detecting the compensatory mechanisms that individuals have invoked to cope with their stuttering disorder instead of the cause of the stuttering. Research performed on children close to the onset of the stuttering could provide answers to how the speech processing network differs from those children who do not stutter. This would lead to an understanding how remediation could change the stuttering brain networks.

Understanding developmental stages of language network processing is necessary to identify the point when language processing development veers off the normal path. On the whole a more extensive understanding of normal and aberrant language pathways as well as of regions that are critical for plasticity will be extremely valuable. Further illumination is necessary of brain-behavior relationships and of disorders for which language impairment is central. Autism, speech and language impairment, and prior to epilepsy surgery are examples of clinical ailments where language network changes may have occurred during development of these disorders. Neuroimaging advances will lead to better clinical diagnoses and subgroup classification of stuttering, which in turn will lead to better treatments and hopefully long-term cures for these devastating afflictions.

References

Ambrose NG, Yairi E (1999) Normative disfluency data for early childhood stuttering. J Speech Lang Hear Res 42:895–909

Anderson JD, Pellowski MW, Conture EG, Kelly EM (2003) Temperamental characteristics of young children who stutter. J Speech Lang Hear Res 46(5):1221–1233

Beal DS, Quraan MA, Cheyne DO, Taylor MJ, Gracco VL, De Nil LF (2011) Speech-induced suppression of evoked auditory fields in children who stutter. NeuroImage 54(4):2994–3003

Bennett EM (2006) Working with people who stutter: a lifespan approach. Pearson Education Inc, New Jersey

Biermann-Ruben K, Salmelin R, Schnitzler A (2005) Right rolandic activation during speech perception in stutterers: a MEG study. NeuroImage 25(3):793–801

Blomgren M (2010) Stuttering treatment for adults: an update on contemporary approaches. Semin Speech Lang 31(4):272–282

Bloodstein O (1995) A handbook on stuttering. Singular Publishing Group, San Diego

Bothe AK, Davidow JH, Bramlett RE, Franic DM, Ingham RJ (2006a) Stuttering treatment research 1970–2005: II. Systematic review incorporating trial quality assessment of pharmacological approaches. Am J Speech Lang Pathol 15(4):342–352

Bothe AK, Davidow JH, Bramlett RE, Franic DM, Ingham RJ (2006b) Stuttering treatment research 1970–2005: I. Systematic review incorporating trial quality assessment of behavioral, cognitive, and related approaches. Am J Speech Lang Pathol 15(4):321–341

Bowyer SM, Moran JE, Mason KM, Constantinou JE, Smith BJ, Barkley GL, Tepley N (2004) MEG localization of language-specific cortex utilizing MR-FOCUSS. Neurology 62(12):2247–2255

Bowyer SM, Peacock J, Tepley N, Moran JE (2010) Neuronal effects of the SpeechEasy treatment for stuttering. In: 17th international conference on biomagnetism advances in biomagnetism—BIOMAG2010, vol 28. IFMBE, Dubrovnik, Croatia, pp 342–345

Braun A, Varga M, Stager S, Schulz G, Selbie S, Maisog JM, Carson RE, Ludlow CL (1997) Altered patterns of cerebral activity during speech and language production in developmental stuttering. Brain 120:761–784

Brown S, Ingham RJ, Ingham JC, Laird AR, Fox PT (2005) Stuttered and fluent speech production: an ALE meta-analysis of functional neuroimaging studies. Hum Brain Mapp 25:105–117

Chang S, Erickson KI, Ambrose NG, Hasegawa-Johnson MA, Ludlow CL (2008) Brain anatomy difference in childhood stuttering. NeuroImage 39(3):1333–1344

Chang SE, Kenney MK, Loucks TMJ, Ludlow CL (2009) Brain activation abnormalities during speech and non-speech in stuttering speakers. NeuroImage 46(1):201–212

Conture EG (1990) Childhood stuttering: what is it and who does it? ASHA Rep 18:2–14

Conture EG, Kelly EM (1991) Young stutterers' nonspeech behaviors during stuttering. J Speech Lang Hear Res 34:1041–1056

De Nil LF, Beal DS, Lafaille SJ, Kroll RM, Crawley AP, Gracco VL (2008) The effects of simulated stuttering and prolonged speech on the neural activation patterns of stuttering and nonstuttering adults. Brain Lang 107(2):114–23

De Nil LF, Kroll RM (2001) Searching for the neural basis of stuttering treatment outcome: recent neuroimaging studies. Clin Linguist Phon 15:163–168

De Nil LF, Kroll RM, Kapur S, Houle S (2000) A positron emission tomography study of silent and oral single word reading in stuttering and nonstuttering adults. J Speech Lang Hear Res 43:1038–1053

De Nil LF, Sasisekaran J, Van Lieshout PH, Sandor P (2005) Speech disfluencies in individuals with Tourette syndrome. J Psychosom Res 58(1):97–102

Dell G (1986) A spreading activation theory of retrieval in sentence production. Psychol Rev 93:283–321

Drayna D, Kang C (2011) Genetic approaches to understanding the causes of stuttering. J Neurodev Disord 3(4):374–380

Elisevich K, Shukla N, Moran JE, Smith BJ, Schultz L, Mason KM, Barkley GL, Tepley N, Gumenyuk V, Bowyer SM (2011) An assessment of MEG coherence imaging in the study of temporal lobe epilepsy. Epilepsia 52(6):1110–1119. PMID:21366556

Foundas AL, Bollich AM, Feldman J, Corey DM, Hurley M, Lemen LC, Heilman KM (2004) Aberrant auditory processing and atypical planum temporale in developmental stuttering. Neurology 63(9):1640–1646. PMID:15534249

Fox MD, Raichle ME (2007) pontaneous fluctuations in brain activity observed with functional magnetic resonance imaging. S. Nat Rev Neurosci 8:700–711

Fox PT, Ingham RJ, Ingham JC, Zamarripa F, Xiong J-H, Lancaster JL (2000) Brain correlates of stuttering and syllable production: a PET performance-correlation analysis. Brain 123:1985–2004

Fox PT, Ingham RJ, Ingham JC, Hirsch TB, Downs JH, Matrin C et al (1996) A PET study of the neural systems of stutteing. Nature 382:158–161

Frazier L (1987) Theories of sentence processing. MIT Press, Cambridge

Friederici A (2002) Towards a neural basis of auditory sentence processing. Trends Cogn Sci 6:78–84
Friederici A (1999) The neurobiology of language comprehension. Springer, Berlin
Fromkin V (1971) The non-anomalous nature of anomalous utterances. Language 47:27–52
Garret M (1975) The analysis of sentence production. Academic Press, NewYork
Garrett M (1980) Levels of processing in sentence production. Academic Press, London
Geschwind N (1970) The organization of language and the brain. Science 170(961):940–944
Gordon N (2002) Stuttering: incidence and causes. Dev Med Child Neurol 44(4):278–281
Greenwald M, Bowyer S (2003) MEG studies of speech production. Perspect Neurophysiol Neurogenic Speech Lang Disord 13(3):4–9
Guitar B (1998) Stuttering: an integrated approach to its nature and treatment. Williams & Wilkins, Baltimore
Hagoort P (2003) How the brain solves the binding problem for language: a neurocomputational model of syntactic processing. Neuroimage 20:S18–S29
Hari R, Levanen S et al (2000) Timing of human cortical functions during cognition: role of MEG. Trends Cogn Sci 4(12):455–462
Heim S (2005) The structure and dynamics of normal language processing: insights from neuroimaging. Acta Neurobiol Exp 65:95–116
Helenius P, Salmelin R, Service E, Connolly JF (1998) Distinct time courses of word and context comprehension in the left temporal cortex. Brain 121(Pt 6):1133–1142
Hickok G (2009) The functional neuroanatomy of language. Phys Life Rev 6(3):121–143
Howell P (2004) Effects of delayed auditory feedback and frequency-shifted feedback on speech control and some potentials for future development of prosthetic aids for stammering. Stammering Res 1(1):31–46
Howell P (2011) Listen to the lessons of The King's Speech. Nature 470(7332):7
Ingham RJ (2001) Brain imaging studies of developmental stuttering. J Commun Disord 34:493–516
Ingham RJ, Fox PT, Ingham JC (2004) Brain correlates of stuttering and syllable production: gender comparison and replication. J Speech Lang Hear Res 47:321–341
Kang C, Drayna D (2011) Genetics of speech and language disorders. Annu Rev Genomics Hum Genet 22(12):145–164
Kaplan PW, Stagg R (2011) Frontal lobe nonconvulsive status epilepticus: a case of epileptic stuttering, aphemia, and aphasia—not a sign of psychogenic nonepileptic seizures. Epilepsy Behav 21(2):191–195
Kikuchi Y, Ogata K, Umesaki T, Yoshiura T, Kenjo M, Hirano Y, Okamoto T, Komune S, Tobimatsu S (2011) Spatiotemporal signatures of an abnormal auditory system in stuttering. Neuroimage 55(3):891–899
Lan J, Song M, Pan C, Zhuang G, Wang Y, Ma W, Chu Q, Lai Q, Xu F, Li Y, Liu L, Wang W (2009) Association between dopaminergic genes (SLC6A3 and DRD2) and stuttering among Han Chinese. J Hum Genet 54(8):457–460
Levelt W (1989) Speaking: from intention to articulation. MIT Press, Cambridge
Levelt W (1998) The genetic perspective in psycholinguistics or where do spoken words come from? J Psycholinguist Res 27:167–180
Levelt WJ, Praamstra P, Meyer AS, Helenius P, Salmelin R (1998) An MEG study of picture naming. J Cogn Neurosci 10(5):553–567
Levelt WJM, Roelofs A, Meyer AS (1999) A theory of lexical access in speech production. Behav Brain Sci 22:1–75
Liberman AM, Cooper FS, Shankweiler DP, Studdert-Kennedy M (1967) Perception of the speech code. Psychol Rev 74:431–461
Liu Z, Ding L, He B (2006) Integration of EEG/MEG with MRI and fMRI. IEEE Eng Med Biol Mag 25(4):46–53
Loucks T, Kraft SJ, Choo AL, Sharma H, Ambrose NG (2011) Functional brain activation differences in stuttering identified with a rapid fMRI sequence. J Fluency Disord 36(4): 302–307

Lu C, Chen C, Ning N, Ding G, Guo T, Peng D, Yang Y, Li K, Lin C (2010) The neural substrates for atypical planning and execution of word production in stuttering. Exp Neurol 221(1):146–156
Ludlow CL (2000) Stuttering: dysfunction in a complex and dynamic system. Brain 123(10):1983–1984
MacDermot KD, Bonora E, Sykes N, Coupe AM, Lai CS, Vernes SC, Vargha-Khadem F, McKenzie F, Smith RL, Monaco AP, Fisher SE (2005) Identification of FOXP2 truncation as a novel cause of developmental speech and language deficits. Am J Hum Genet 76(6):1074–1080
MacKay D (1987) The organization of perception and action: a theory for language and other cognitive skills. Springer, New York
Maguire GA, Franklin DL, Kirsten J (2011) Asenapine for the treatment of stuttering: an analysis of three cases. Am J Psychiatry 168(6):651–652
Marslen-Wilson WD, Tyler L (1980) The temporal structure of spoken language understanding. Cognition 8:1–71
McClelland J (1991) Stochastic interactive processes and the effect of context on perception. Cogn Psychol 23:1–44
McClelland JL, Elman J (1986) The TRACE model of speech perception. Cogn Psychol 18:1–86
Moran JE, Bowyer S, Tepley N (2005) Multi-resolution FOCUSS: a source imaging technique applied to MEG data. Brain Topogr 18:1–17
Movsessian P (2005) Neuropharmacology of theophylline induced stuttering: the role of dopamine, adenosine and GABA. Med Hypotheses 64(2):290–297
Newbury DF, Monaco AP (2010) Genetic advances in the study of speech and language disorders. Neuron 68(2):309–320
Ratner NB (2010) Translating recent research into meaningful clinical practice. Semin Speech Lang 31(4):236–249
Salmelin R (2007) Clinical neurophysiology of language: the MEG approach. Clin Neurophysiol 118(2):237–254
Salmelin R, Schnitzler A, Schmitz F, Freund H-J (2000) Single word reading in developmental stutterers and fluent speakers. Brain 123:1184–1202
Salmelin R, Schnitzler A, Schmitz F, Jäncke L, Witte OW, Freund HJ (1998) Functional organization of the auditory cortex is different in stutterers and fluent speakers. NeuroReport 9(10):2225–2229
Shattuck-Hufnagel S (1979) Speech errors as evidence for a serial ordering mechanism in sentence production. Erlbaum, Hillside
Shattuck-Hufnagel S (1987) The role of word-onset consonants in speech production planning: new evidence from speech error patterns. Erlbaum, Hillsdale
Simos PG, Breier JI, Zouridakis G, Papanicolaou AC (1998) Identification of language-specific brain activity using magnetoencephalography. J Clin Exp Neuropsychol 20(5):706–722
Simos PG, Castillo EM et al (2001) Mapping of receptive language cortex in bilingual volunteers by using magnetic source imaging. J Neurosurg 95(1):76–81
Stemberger J (1985) An interactive activation model of language production. Erlbaum, London
Tarkianine A, Helenius P, Hansen PC, Cornelissen PL, Salmelin R (1999) Dynamics of letter sting perception in the human occipitotemporal cortex. Brain 122:2119–2132
Tavano A, Busan P, Borelli M, Pelamatti G (2011) Risperidone reduces tic-like motor behaviors and linguistic dysfluencies in severe persistent developmental stuttering. J Clin Psychopharmacol 31(1):131–134
Theys C, van Wieringen A, De Nil LF (2008) A clinician survey of speech and non-speech characteristics of neurogenic stuttering. J Fluency Disord 33(1):1–23
Toyomura A, Fujii T, Kuriki S (2011) Effect of external auditory pacing on the neural activity of stuttering speakers. Neuroimage 57(4):1507–1516
Van Borsel J, Tetnowski JA (2007) Fluency disorders in genetic syndromes. J Fluency Disord 32(4):279–296

Walla P, Mayer D, Deecke L, Thurner S (2004) The lack of focused anticipation of verbal information in stutterers: a magnetoencephalographic study. Neuroimage 22(3):1321–1327
Watkins KE, Smith SM, Davis S, Howell P (2008) Structural and functional abnormalities of the motor system in developmental stuttering. Brain 131:50–59
Weber-Fox C (2001) Neural systems for sentence processing in stuttering. J Speech Lang Hear Res 44:814–825
Weber-Fox C, Spencer RMC, Spruill JE, Smith A (2004) Phonologic processing in adults who stutter: electrophysiological and behavioral evidence. J Speech Lang Hear Res 47:1244–1258
Weber-Fox C, Spruill JE, Spencer R, Smith A (2008) Atypical neural functions underlying phonological processing and silent rehearsal in children who stutter. Dev Sci 11(2):321–337
World_Health_Organization (1992) International statistical classification of diseases and related health problems. 10th rev. ICD-10. World_Health_Organization, Geneva, p 387
Xuan Y, Meng C, Yang Y, Zhu C, Wang L, Yan Q, Lin C, Yu C (2012) Resting-state brain activity in adult males who stutter. PLoS ONE 7(1):1–11
Yairi E (1993) The early months of stuttering: a developmental study. J Speech Lang Hear Res 36:521–528
Yairi E, Ambrose N, Cox N (1996) Genetics of stuttering: a critical review. J Speech Hear Res 39(4):771–784
Zebrowski P, Buhr A (ed) (2005) Straight talk on stuttering: information, encouragement, and counsel for stutterers, caregivers, and speech-language clinicians. J Fluency Disord 30(2):149–152
Zebrowski PM (1995) The topography of beginning stuttering. J Commun Disord 28(2):75–91

MEG in Epilepsy and Pre-surgical Functional Mapping

Masaki Iwasaki and Nobukazu Nakasato

Abstract Magnetoencephalography (MEG) is routinely used in pre-surgical evaluation of epilepsy. Magnetic source imaging (MSI) of epileptic spikes provides additional information to those provided by other non-invasive measures, including fluorodeoxyglucose-positron emission tomography (FDG-PET) and ictal single-photon emission computed tomography (SPECT), especially in neocortical epilepsy and in MRI-negative epilepsy. MSI may guide additional electrode coverage for intracranial EEG and area of resection when planning surgery; both of these approaches are associated with better seizure outcome. Mono-focal spike localization strongly indicates the epileptogenic zone. Complete removal of the MEG focus often results in the patient being seizure free, post-operatively. Similarities and differences between MEG and EEG should be well recognized when using MEG. Although the overall sensitivity of MEG to epileptic spikes is similar to that of EEG, such sensitivity can depend primarily on the orientation of equivalent current dipoles (ECD) of spikes. Favorable areas for MEG include the orbito-frontal, opercular, interhemispheric, temporo-lateral, and rolandic regions. MEG is less sensitive to deep regions, such as mesial temporal structures. MEG is also utilized for functional brain mapping. Somatosensory evoked fields to median nerve stimulation lead to an accurate, within a few millimeters, identification of the central sulcus. MEG analysis of event-related potentials or event-related de/synchronization in response to language tasks provides more than 80 % sensitivity and specificity in language lateralization for intra-carotid amobarbital procedures. MEG is a non-invasive alternative for pre-surgical determination of the language-dominant hemisphere.

M. Iwasaki (✉)
Department of Neurosurgery, Tohoku University Graduate School of Medicine,
1-1 Seiryo-machi, Aoba-ku, Sendai 980-8574, Japan
e-mail: epinetmi@gmail.com

N. Nakasato
Department of Epileptology, Tohoku University Graduate School of Medicine,
1-1 Seiryo-machi, Aoba-ku, Sendai 980-8574, Japan

S. Supek and C. J. Aine (eds.), *Magnetoencephalography*,
DOI: 10.1007/978-3-642-33045-2_39,

Keywords Magnetic source imaging · Focal epilepsy · Epilepsy surgery · Epileptogenic zone · Interictal spikes · Ictal EEG · Pre-surgical evaluation · Intracranial EEG · MRI · FDG-PET · Ictal SPECT · Hippocampal sclerosis · Cortical dysplasia · Somatosensory evoked potential · Event related potential · Event related desynchronization · Language dominance · Intracarotid amobarbital procedure

1 Introduction

Localization of epileptic discharges and pre-surgical functional brain mapping are the most common clinical applications of magnetoencephalography (MEG). During the last 40 years, MEG instrumentation has evolved from a single-channel sensor system to whole-head systems with more than 300 channels that scan over the entire head surface. Currently, the majority of "MEG centers" provide clinical services (Bagic et al. 2009). In this chapter, the current status of clinical MEG in epilepsy and presurgical mapping is reviewed.

2 Epilepsy

2.1 Role of MEG in Evaluation of Epilepsy

In clinical settings, MEG is used principally to map sources of epileptic activities in pre-surgical evaluation of epilepsy. An epileptic seizure is defined as a transient occurrence of signs and/or symptoms due to abnormal excessive or synchronous neuronal activity in the brain. Epilepsy is a disorder of the brain characterized by an enduring predisposition to generate epileptic seizures (Fisher et al. 2005). Epilepsy has a prevalence of 4–10 per 1,000 individuals in industrialized countries, and the epileptic seizures of approximately 30 % of patients are not adequately controlled by antiepileptic medications (World Health Organization 2009). Surgery is a most important treatment option for such drug-resistant epilepsy, and MEG plays an important role in the pre-surgical evaluation of epilepsy.

The goal of pre-surgical evaluation of epilepsy is to identify the epileptogenic zone. The epileptogenic, or "icto-genic", zone is the brain region that is indispensable for generating a patient's epileptic seizures. Removal of the epileptogenic zone results in total control over or "cure" of a patient's epilepsy. However, we have no gold standard, or single measure, for identifying the epileptogenic zone (Table 1). The epileptogenic zone is usually determined by a consensus among the findings of multiple evaluations, including magnetic resonance imaging (MRI), electroencephalography (EEG), seizure symptomatology, fluorodeoxyglucose positron emission tomography (FDG-PET), MEG and so on. Theoretically, the diagnostic accuracy of MEG itself is hard to assess (Burch et al. 2012). However, it is well accepted that MEG or magnetic source imaging (MSI) of epileptic discharges

Table 1 Six zone concept in pre-surgical evaluation of epilepsy

	Definition	Measures
Irritative zone	Area of cortex that generates interictal spikes	EEG, MEG
Ictal onset zone	Area of cortex where seizures are generated	EEG, MEG
Epileptogenic lesion	Structural abnormality of the brain that is the direct cause of the epileptic seizures	MRI, Tissue pathology
Symptomatogenic zone	Portion of the brain that produces the initial clinical symptomatology	Video monitoring, Patient report
Functional deficit zone	Cortical area of non-epileptic dysfunction	Neurological examination, Neuropsychological testing, EEG, MEG, PET, SPECT
Epileptogenic zone	Area of brain that is necessary and sufficient for initiating seizures and whose removal or disconnection is necessary for abortion of seizures	Theoretical concept

The epileptogenic zone is a theoretical concept, and each evaluation plays a role in the estimation of this zone. MEG primarily measures the irritative zone and measures the ictal onset zone. (Modified from Lüders et al. (1993) with permission)

provides important and additional information for the estimation of the epileptogenic zone. Together with FDG-PET and single-photon emission computed tomography (SPECT), MEG should be considered when MRI is unremarkable or discordant with clinical and EEG data (Duncan 2010). These supplemental imaging data can inform strategies for intracranial EEG evaluations. Comprehensive reviews of the use of MEG in pre-surgical evaluation of epilepsy are also available elsewhere (Barkley and Baumgartner 2003; Baumgartner and Pataraia 2006; Lau et al. 2008; Leijten and Huiskamp 2008; Schwartz et al. 2010; Shibasaki et al. 2007; Stefan et al. 2011a). As MEG/MSI technology was considered sufficiently mature for routine use in pre-surgical evaluations of patients with epilepsy, clinical practice guidelines were issued by the American Clinical MEG Society in 2009 (Bagić et al. 2011a, b, c; Bagić 2011; Burgess et al. 2011a, b).

Although the use of MEG is often limited to pre-surgical evaluation of drug-resistant epilepsy, MEG is occasionally used for "routine" diagnostic purposes in clinical epilepsy. Additional diagnostic information can be provided by MEG, especially in patients with inconclusive routine EEG findings (Colon et al. 2009).

2.2 Added Clinical Value of MSI

Several recent prospective studies have established the added clinical value of MSI. In terms of pre-surgical management of refractory focal epilepsy, MSI

supplies additional information in 20–30 % of cases and offers information crucial to final decision making in 10–20 % of cases (Stefan et al. 2003; Sutherling et al. 2008; De Tiège et al. 2012). One prospective study of patients with non-localizing MRI found that MEG spike localization had 82–90 % positive predictive value for seizure localization in intracranial EEG. Thus, MEG can potentially replace intracranial EEG for seizure localization (Knowlton et al. 2006). Two prospective studies examined whether MSI changed surgical decisions about patients with intractable neocortical epilepsy which potentially required intracranial EEG evaluation. One study showed that MSI provided non-redundant information in 33 % of patients, including 13 % for additional intracranial EEG coverage and 20 % for surgical decisions (Sutherling et al. 2008). Another study showed that MSI indicated additional intracranial EEG coverage in 23 % of patients. In 39 %, the additional coverage indicated by MSI contributed to revealing seizure-onset patterns via intracranial EEG, which significantly contributed to a seizure-free outcome (Knowlton et al. 2009).

2.3 Recording and Source Estimation of Epileptiform Discharges

2.3.1 MEG Recording in Patients with Epilepsy

MEG is used primarily for recording and localizing interictal epileptiform discharges (IEDs), because of limitations caused by recording duration and vulnerability to artifacts due to the subject's movement during seizure (Iwasaki and Burgess 2008). The neural substrates that generate IEDs are not necessarily identical to the epileptogenic zone. However, localization or distribution of IEDs provides an important hint that the epileptogenic zone is nearby. Sedative agents may be used to maintain the immobility of patients, especially children or those with mental retardation, during MEG recording. General anesthesia with propofol, etomidate, sevoflurane or dexmedetomidine is acceptable for recording IEDs (Balakrishnan et al. 2007; König et al. 2009). Etomidate may increase IED frequency (Stefan et al. 2010). Continuous infusion of midazolam may not be appropriate because of suppressive effects (Szmuk et al. 2003).

There are increasing opportunities to use MEG with patients receiving vagus nerve stimulation (VNS). VNS is an adjunctive treatment for patients with intractable epilepsy who are not suitable for resective surgery. An implanted electrical pulse generator and battery cause major magnetic artifacts. Although temporal explantation of VNS had been necessary to record MEG to avoid artifacts (Donahue et al. 2007), MEG can now be recorded in subjects receiving VNS by applying a noise cancellation algorithm such as temporally extended signal-space separation (tSSS) (Carrette et al. 2011; Kakisaka et al. 2013; Song et al. 2009; Tanaka et al. 2009b).

2.3.2 Interictal Spikes

Magnetic fields picked up by the sensor coils are sampled at several hundreds to thousands Hz as discrete time signals, and these constitute multiple traces of "brain waves" measured at each sensor location (Salmelin and Hari 1994). Similar to EEG reading, MEG signals must be "read" in the first step of the analysis to identify epileptic spikes. Epileptic spikes should be appropriately discriminated from artifacts by human interpreters, usually with help from simultaneously recorded EEG. Expertise in EEG and an understanding of clinical neurophysiology are necessary for reliable interpretation (Burgess et al. 2011a). Special knowledge about and experience with the visual inspection of MEG may be important for accurate interpretation (Fernandes et al. 2005).

The generator of the selected spike is estimated by using a source analysis algorithm. It should be recognized that source estimation in MEG requires solving an ill-posed biomagnetic inverse problem with errors (e.g. location, distribution and amplitude) associated with each source estimation algorithm (Iwasaki and Burgess 2008). The classic and most popular method is an equivalent current dipole (ECD) model. This model assumes that epileptic spikes emanate from a single dipole located at a certain point in the brain (a point source). The model can be extended to localizing a few point sources as well (multiple dipoles). It has been empirically established that the ECD model provides a good approximation for localizing epileptic spikes in many cases. However, the ECD model can result in larger errors when attempting to localize multi-focal or extended sources underlying spike activity and, any epileptic spike may be more or less distributed. Moreover, the ECD approach can be biased by the analyzer's guess about the number and location of the initial dipoles selected to start the search algorithm. Objective criteria and automated methods for spike detection and source estimation have been used to try to overcome this problem (Bowyer et al. 2003; Ossadtchi et al. 2004).

A number of distributed source modeling approaches has been developed in addition to the ECD model. Distributed source modeling provides objective (unbiased), but spatially blurred results regarding spike localization (Shiraishi et al. 2005, 2011). Reasonable correlation between the results of distributed source modeling and those of the ECD model have been reported with regard to the localization of epileptic spikes (Slater et al. 2012; Uda et al. 2012). Although a simple calculation of the magnetic field gradient is useful for estimating the location of epileptic spikes (Hashizume et al. 2007; Shirozu et al. 2010), both the localization and the orientation of current sources should be considered when interpreting MEG. The orientation of the ECD provides an important clue for determining the epileptogenic side of opposing cortices in the cerebral sulcus (Salayev et al. 2006). At their peak, epileptic spikes usually generate dipolar current oriented to the basal side of the cortex. For example in rolandic epilepsy, anteriorly oriented dipoles suggest activation of the anterior bank ("frontal or motor side") of the central sulcus, whereas posteriorly oriented dipoles suggest activation of the parietal side; this phenomenon can be diagnostically important (Kakisaka et al. 2009, 2011b).

2.3.3 Ictal MEG

Because long-term recording is technically difficult for MEG, "ictal" MEG recording is limited to patients with frequent seizures (Assaf et al. 2003). However, when recorded, ictal MEG may provide more specific localizing information about the epileptogenic zone. Ictal-onset MEG is localized closer to the seizure onset zone than is interictal MEG (Fujiwara et al. 2012; Medvedovsky et al. 2012). Ictal activities are more distributed than are interictal spikes, rendering distributed source modeling superior to ECD source representation (Tanaka et al. 2009a). Movement compensation algorithms are useful for recording ictal events (Kakisaka et al. 2012b).

2.4 Comparison with Scalp EEG and Intracranial EEG

The neurophysiological processes that generate the MEG signal are essentially the same as that producing the EEG signal (Barth 1993). The clinical value of MEG is often compared with that of scalp EEG in terms of costs and benefits. EEG and MEG are thought to play complementary roles in detecting IEDs (Ebersole and Ebersole 2010). MEG preferentially records tangential sources, whereas EEG is better at recording radial ones. However, sources that are completely tangential or radial are rare; the cortical area to which MEG is sensitive largely overlaps with that to which EEG is sensitive (Hillebrand and Barnes 2002). Therefore, in most cases, epileptic spikes are captured by both MEG and EEG, but the detectability (the number or signal-to-noise ratio of spikes) may differ significantly (Iwasaki et al. 2005). The sensitive volume, the brain volume that a sensor scans, is relatively smaller for whole-head MEG recordings than for scalp EEG recordings using the standard 10–20 electrode placement (Malmivuo et al. 1997), rendering MEG more sensitive to small sources located in the surface brain area. Although MEG is more limited in its sensitivity to deep activity than scalp EEG, one can use magnetometers, which have greater sensitivity to deep sources than gradiometers (Enatsu et al. 2008).

The findings of previous studies comparing MEG with EEG are consistent with the above theoretical differences. When MEG and EEG are simultaneously recorded, the number of epileptic spikes can be higher in either modality (Iwasaki et al. 2005; Lin et al. 2003), but the overall concordance in interpretation is high (85 %) (Kirsch et al. 2007a). In a blinded review of spike detection, more spikes were unique to MEG than to EEG or the combination of both modalities (Ramantani et al. 2006). MEG had slightly higher overall sensitivity for detecting IEDs than did scalp EEG (72 versus 61 %) (Knake et al. 2006).

It is noteworthy that epileptic spikes are detected uniquely by MEG on a few occasions (Fig. 1). Epileptic activities generated in the fissural cortex may produce exclusively tangential dipoles that are not visible on scalp EEG. Such cases have been described in epilepsy of the orbito-frontal lobe and opercular regions, and in Landau-Kleffner syndrome (Iwasaki et al. 2003; Kakisaka et al. 2012a, d; Rodin et al. 2004).

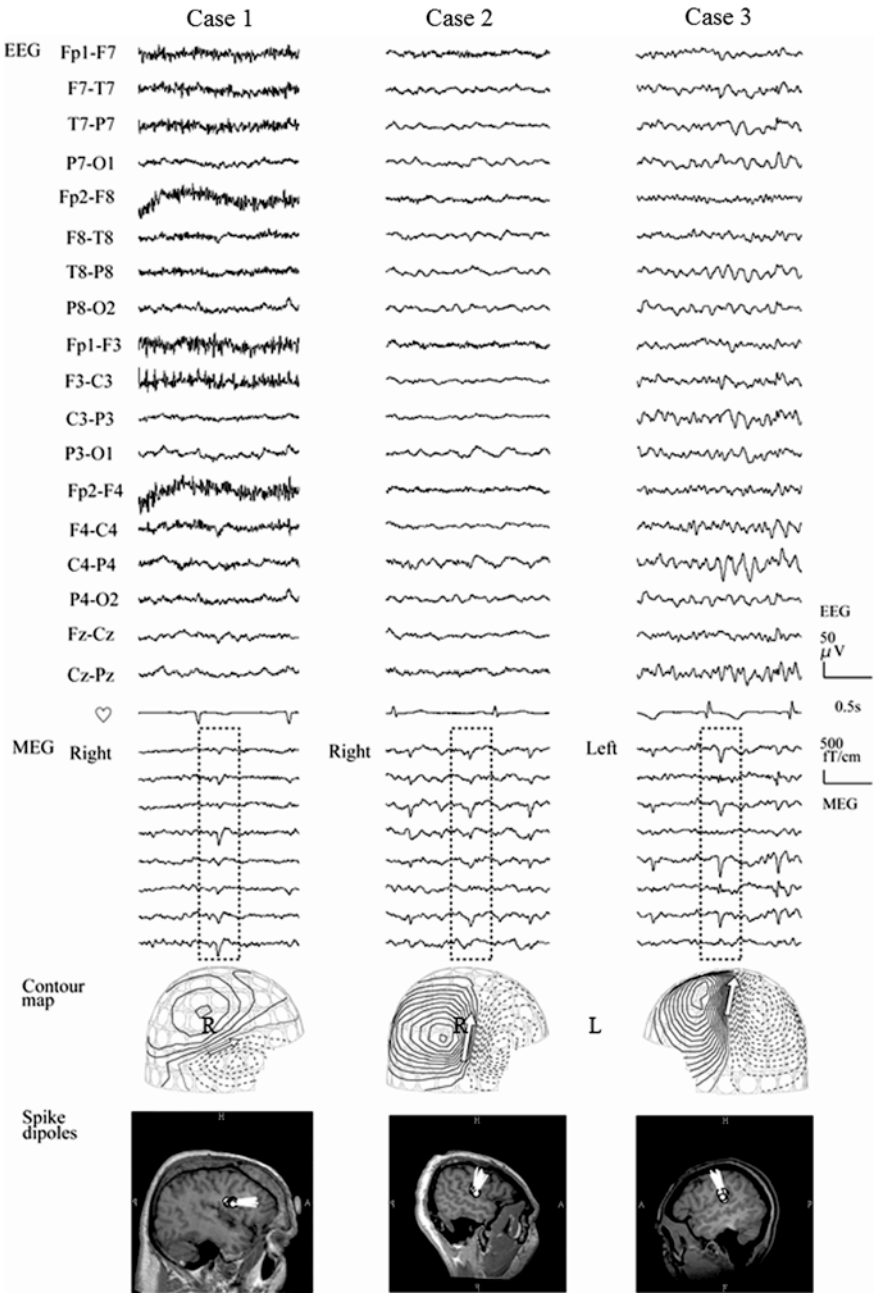

Fig. 1 Case examples of opercular MEG spikes not detected on scalp EEG. Waveforms of simultaneous scalp EEG and MEG (*top*) and corresponding contour maps (*middle*) are shown. ECDs estimated at MEG spike peaks are co-registered on the patient's MRI (*bottom*). *Solid* and *broken lines* on contour maps indicate magnetic field efflux and influx from the head surface, respectively. *Circles* and *bars* on MRI indicate estimated locations and orientations of each individual dipole. Exclusively tangential dipoles generated in the opercular surface can be detectable with MEG, not with scalp EEG (Modified from Kakisaka et al. 2012a)

MEG's sensitivity to epileptic spikes is probably higher in extratemporal or neocortical epilepsy than in temporal lobe epilepsy (TLE). The combination of MEG and EEG is useful for detecting more interictal spikes in patients with extratemporal epilepsy (Park et al. 2004). Simultaneous M/EEG is especially successful in detecting epileptic spikes in patients with MR-negative epilepsy, because of the neocortical predominance of the epileptogenic zone (Heers et al. 2010a). The signal-to-noise ratio of MEG is greater in the frontal lobe, and MEG spike yield and localization is superior to that of EEG in frontal lobe epilepsy (De Jongh et al. 2005; Ossenblok et al. 2007). On the other hand, exclusively vertical dipoles may be missed by MEG. Mislocalization of MEG spikes owing to loss of fissures in the cortical structure has been described in cases of polymicrogyria (Bast et al. 2005). The sensitivity of MEG has also been compared with that of intracranial EEG. Favorable areas for MEG include the orbito-frontal, interhemispheric, temporo-lateral and central regions (Huiskamp et al. 2010). In one study, 56 % of all interictal ECoG spikes had a MEG counterpart. The association between the two was >90 % in the interhemispheric and frontal orbital region, 75 % in the superior frontal, central and lateral temporal regions; and only 25 % in the mesial temporal region (Agirre-Arrizubieta et al. 2009).

MEG is also advantageous in the presence of cranial defects because the magnetic field is not distorted by the inhomogeneity of electrical impedance. MEG has been successfully used in patients with previous craniotomy for purpose of spike localization (Lee et al. 2010a; Mohamed et al. 2007; Yoshinaga et al. 2008).

2.5 Focal Epilepsy

2.5.1 Temporal Lobe Epilepsy

The role of MEG in mesial TLE is relatively limited because MEG spike localization does not pinpoint the epileptogenic zone or seizure-onset zone in the mesial temporal region, including the hippocampus. Simultaneous recordings of intracranial EEG and extracranial EEG/MEG have shown that classical anterior or midtemporal spikes in scalp EEG or MEG were generated in anterior and lateral temporal neocortical structures and did not propagate from or to the mesial temporal region (Fig. 2). Extracranial EEG or MEG, along with their source localization techniques have been unable to detect the true mesial temporal spikes that are detected by intracranial electrodes (Wennberg et al. 2011). Although a debate on the ability of MEG to detect mesial temporal spikes persists (Kaiboriboon et al. 2010; Stephen et al. 2005), MEG source estimation is only partially correlated with electrocorticography findings. Moreover, the whole-head MEG helmet insufficiently covers the basal temporal region (Leijten et al. 2003).

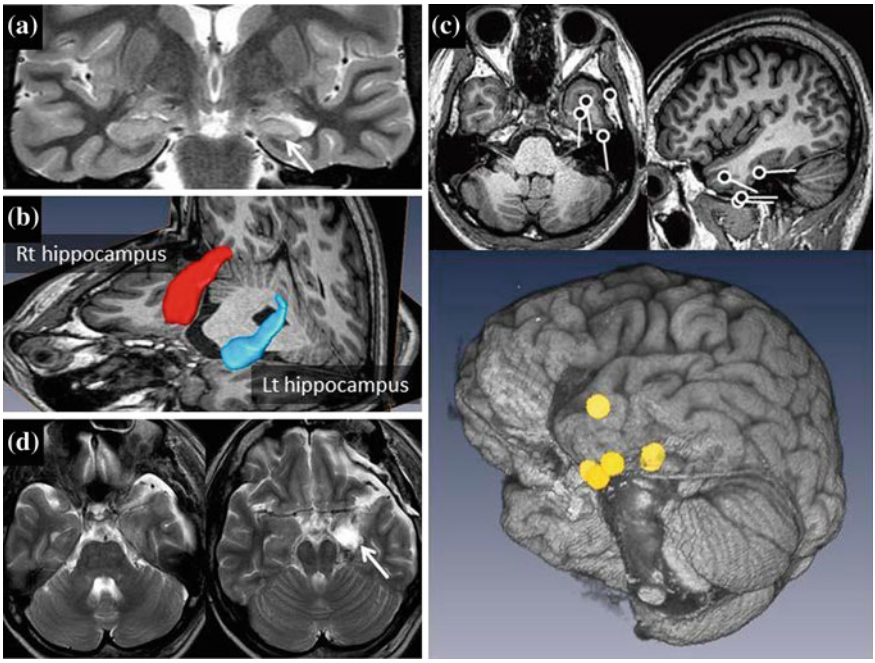

Fig. 2 MSI in a 30 year old female with mesial TLE with left hippocampal sclerosis. **a** Pre-operative T2 weighted image shows atrophy of the left hippocampus (*arrow*) and no other abnormalities. **b** Volume segmentation of the hippocampus shows significant volume loss on the *left side*. **c** Single ECD model was used for source estimation of epileptic spikes. ECDs of her left temporal MEG spikes were localized in the left anterior temporal lobe. *Circles* and *bars* indicate locations and orientations of dipoles. The three-dimensional brain image co-registered with dipoles (*yellow spheres*) shows that spike sources are not localized in the mesial temporal structure, but in the anterior temporal neocortex. This dipole pattern is relatively specific to the mesial TLE, whereas MSI does not pinpoint the epileptogenic zone in the mesial temporal region. **d** Post-operative MRI. The patient received selective amygdalo-hippocampectomy (*arrow*) and became free from seizures. Note that the area of MEG spike localization was not included in the resection

MSI can identify subcompartments of the temporal lobe involved in epileptic activity and may be helpful in non-invasively differentiating among subtypes of TLE (Pataraia et al. 2005). The spikes localized in the anterior temporal neocortex, including those in the temporal tip with a horizontal orientation to the temporal lobe axis, and those in the superior or basal temporal cortex with a vertical orientation, are relatively specific to mesial TLE. Spikes localized vertically in the posterior temporal region are seen frequently in patients with seizures originating from the lateral temporal lobe (Iwasaki et al. 2002). In patients with epileptogenic lesions (lesional TLE), monofocal localization of MEG spikes reliably identifies the epileptogenicity of the lesion (Heers et al. 2010b) (Fig. 3).

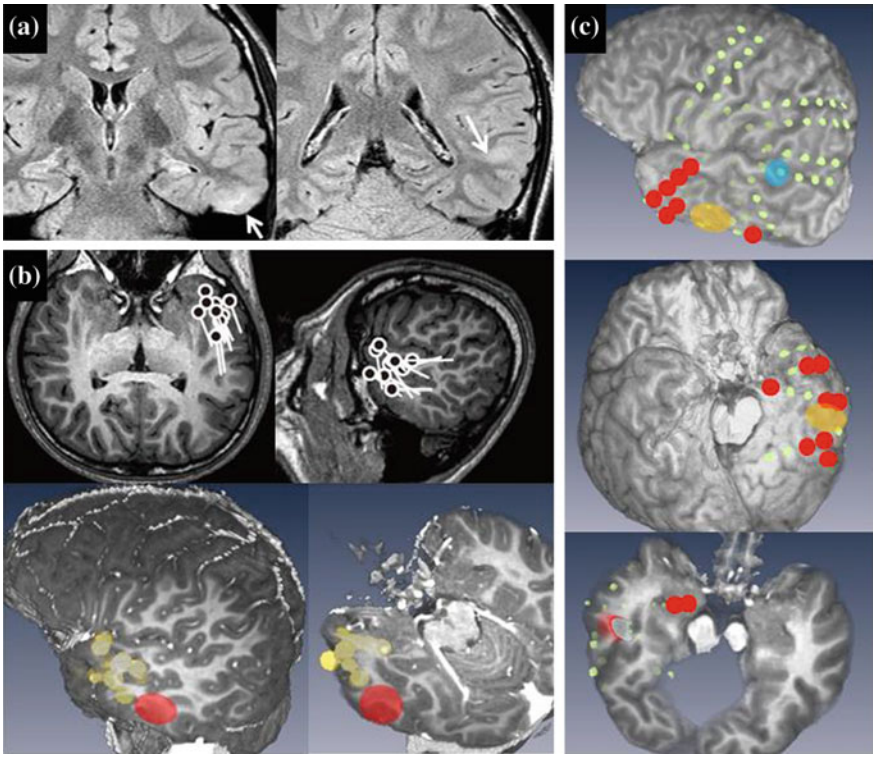

Fig. 3 MSI in a 16 year old female with left TLE with multiple lesions. **a** Pre-operative fluid attenuated inversion recovery (FLAIR) images show atrophy of the left hippocampus and two isolated increased T2 lesions, one anteriorly in the inferior temporal gyrus (*arrow*, *left*) and another posteriorly at the bottom of the superior temporal sulcus (*arrow*, *right*), suggesting cortical dysplasia. **b** ECDs of her left temporal MEG spikes were localized in the anterior part of the left temporal lobe. The ECD location was relatively close to the anterior lesion (*red circles*). **c** Interictal spike map from implanted intracranial electrodes. Four depth electrodes, including two in the hippocampus, one in the anterior lesion, and one in the posterior lesion, were implanted. The subdural electrodes were also implanted to cover the whole temporal lobe and extratemporal region. Electrodes are represented by *green circles*. *Red circles* show locations of epileptic spikes. Epileptic spikes were distributed in the antero-mesial-basal temporal region, corresponding to the MEG findings. No epileptic activities were recorded from depth electrodes inserted in the posterior lesion (*blue circle*). The patient received anterior temporal lobectomy including resection of the inferior temporal gyrus lesion (*orange circles*). The posterior lesion was not removed, but the patient became seizure free

2.5.2 Extratemporal Lobe Epilepsy

In neocortical epilepsy, monofocal MEG spike localization or "a single dipole cluster" is correlated with the ictal onset zone, and complete resection leads to better seizure outcome (Iida et al. 2005a; Stefan et al. 2011b). Multiple clusters of MEG spikes suggest multiple or extensive epileptogenic zones, which should be

completely delineated by intracranial EEG before planning surgery (Oishi et al. 2006). Similarly, a high coverage of MEG spikes by resection volume and a small distance to the resection volume are both correlated with a favorable outcome (Fischer et al. 2005).

MEG is diagnostic in rolandic epilepsy because tangential dipoles generated in the central sulcus are detected and localized by MEG better than by scalp EEG. Epileptic spikes are characterized by anteriorly-oriented dipoles localized in the central sulcus in benign rolandic epilepsy, or benign childhood epilepsy with centro-temporal spikes (BECCT) (Ishitobi et al. 2005). In these patients, spikes originate in the pre-central gyrus, or "motor cortex". Posteriorly oriented spikes are atypical for benign rolandic epilepsy, and are associated with poorer prognosis for seizures and cognitive functioning (Kakisaka et al. 2009). Moreover, dipole localization can differentiate between benign and atypical rolandic epilepsy. Spike dipoles are localized ventro-laterally around the oro-facial level in benign rolandic epilepsy, and dorso-medially around the hand level in atypical rolandic epilepsy (Kakisaka et al. 2011b; Perkins et al. 2008).

2.5.3 MRI-Negative Epilepsy

Surgical treatment is challenging in intractable focal epilepsy with no evident MRI abnormality (MRI-negative epilepsy). Under these circumstances, MEG helps to identify the epileptogenic zone and guide intracranial electrode implantation (Zhang et al. 2011). In combination with SPECT or FDG-PET findings, monofocal MEG spikes suggest an epileptogenic zone with excellent post-operative outcome (Wu et al. 2013). Compared with subtraction ictal SPECT co-registered to MRI (SISCOM), MEG is more advantageous in predicting seizure-free post-operative outcome (Schneider et al. 2013). MEG provides information that is useful over and above that provided by intracranial EEG alone. When sublobar concordance is observed between MEG and intracranial EEG, complete resection of both regions is predictive of post-operative seizure-free outcome (Schneider et al. 2012a). In pediatric populations, MEG and SISCOM are better tools for lobar localization than is SPM analysis of FDG-PET (Seo et al. 2011). Postoperative freedom from seizure is less likely in children with bilateral MEG dipole clusters or only scattered dipoles (Ramachandrannair et al. 2007).

MEG can identify epileptogenic regions associated with cortical dysplasia. Alterations in tissue microstructure beyond the MRI visible cortical dysplasia are revealed by diffusion-tensor imaging at the area of MEG spikes (Widjaja et al. 2009). The best surgical outcome is obtained after complete removal of areas containing clustered MEG spike sources and MR lesions (Widjaja et al. 2008) (Fig. 4).

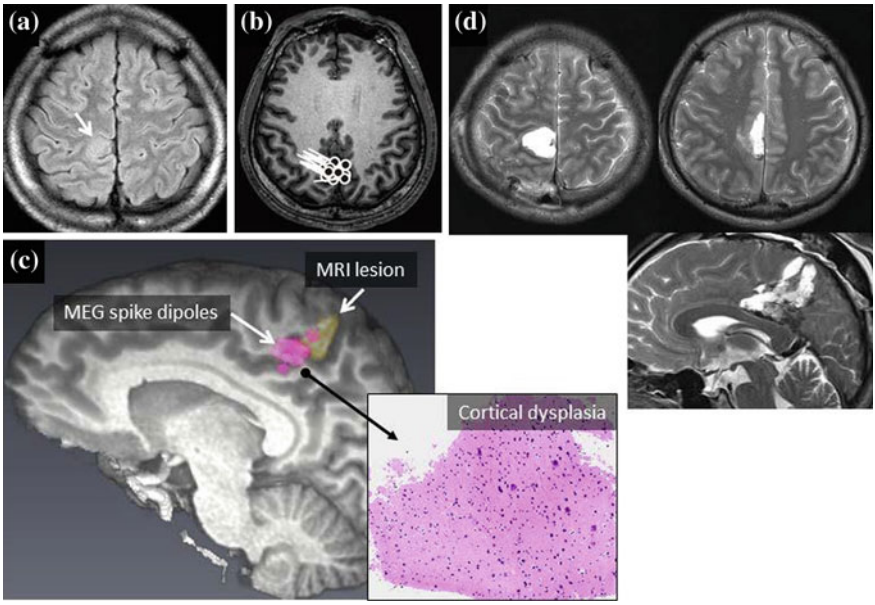

Fig. 4 MSI in a 20 year old male with intractable epilepsy due to cortical dysplasia in the right parietal paracentral lobule. **a** Pre-operative FLAIR image shows increased signal, indicating a lesion in the medial parietal region (*arrow*). **b** ECDs of of the MEG spikes were localized in the parietal interhemispheric area and oriented to the *right side*, suggesting spike sources in the right medial parietal cortex. **c** Co-registration of MRI-identified lesion and MEG spikes on three-dimensional brain image. MEG spikes were located deeper than the MRI-identified lesion. Intracranial EEG revealed epileptic activities distributed in the lesion as well as in the MEG spike area. **d** Post-operative MRI. Tailored cortical resection including both the MRI-identified lesion and the MEG spike area led to significant improvement in his seizures. Histopathological examination of the surgical specimen obtained from the MEG spike area revealed cortical dysplasia with dysmorphic neurons

2.6 Generalized Epilepsy and Other Epilepsy Syndromes

MEG can successfully localize the primary focus of secondary bilaterally synchronized spikes which appear as generalized in scalp EEG (Chang et al. 2009; Yu et al. 2004). MEG may reveal early and focal sources in generalized epileptiform discharges in patients with infantile spasms and Lennox-Gastaut syndrome (Kakisaka et al. 2011a, 2010; Ramachandrannair et al. 2008; Sakurai et al. 2007). In a subset of patients, focal MEG findings may lead to resective surgery followed by excellent seizure outcome (Chang et al. 2009).

Tuberous sclerosis complex often presents as intractable multi-focal or generalized epilepsy due to multiple epileptogenic lesions (cortical tubers). Even when multiple cortical tubers are seen, epileptogenicity may reside in one or few tubers, i.e. epileptogenic tubers, in some patients. Resective epilepsy surgery is often challenging, but MEG has an important role in pre-surgical evaluation, i.e.,

to identify the most epileptogenic tuber (Evans et al. 2012; Iida et al. 2005b; Wu et al. 2006). Epileptogenic sources identified by MEG are closer to the presumed epileptogenic tuber than are similar sources identified by EEG. Moreover, spike consensus is greater with MEG (Jansen et al. 2006).

MEG has been used to reveal the initial focal component of generalized epileptiform discharges in idiopathic or primary generalized epilepsies (Sakurai et al. 2010; Stefan et al. 2009; Westmijse et al. 2009). Local frontal and/or parietal activation is found before the onset of the generalized pattern, and the site of initial activation can be dependent on the type of epilepsy (Stefan et al. 2009).

3 Pre-surgical Functional Mapping

Accurate localization of the functionally "eloquent" cortex is crucial in planning surgical procedures near the functional area. Along with functional MRI, MEG is a non-invasive alternative for mapping brain functions (Mäkelä et al. 2006; Stufflebeam et al. 2009). In a subset of neurosurgical patients, the lesion is located within or near eloquent cortices, causing a distortion of neuroanatomy and hampering topographical localization of eloquent areas in relation to the mass lesion. In these patients, functional mapping of eloquent brain areas is crucial. MEG provides functional mapping with excellent temporal and reasonable spatial accuracy. Central sulcus localization and the mapping of auditory, visual and language cortices are feasible with MEG.

3.1 Somatosensory Evoked Fields for Central Suclus Localization

Somatosensory evoked magnetic fields (SEFs) in response to electrical stimulation of the median nerve at the wrist allows reliable identification of the central sulcus. The first cortical component of the median nerve SEF is called N20m, as it is the magnetic counterpart of the N20 of the somatosensory evoked potentials (SEPs). The ECD of N20m is localized on the posterior bank of the central sulcus with an accuracy of a few millimeters, corresponding to area 3b of the primary somatosensory cortex (Kawamura et al. 1996). Although the central sulcus is usually recognized by the sulcal and gyral pattern on anatomical MRI (Berger et al. 1990), SEF can provide critical information when the central sulcus is anatomically displaced or distorted by a structural lesion or brain edema (Nakasato and Yoshimoto 2000). Spatial accuracy can be increased by combining information from simultaneously-recorded EEGs (Bast et al. 2007).

Somatotopic organization of the primary somatosensory cortex is examined by combining multiple stimulation points in SEFs. The first cortical component of the posterior tibial nerve stimulation at the ankle is called P38m. The ECD of P38m is

localized at the highest part of the central sulcus, corresponding to the "foot-level" primary somatosensory cortex. The first component of lip stimulation identified as N15m, is localized on the lower part of the central sulcus, corresponding to the "face-level" primary somatosensory cortex (Nagamatsu et al. 2001). Knowledge of the somatotopic organization and the locations of critical functions is important for surgical planning especially when maximum brain resection is required such as for malignant gliomas and medically intractable epilepsy. Neurological deficits are minimal or transient after unilateral resection of the oro-facial primary sensorimotor areas because functional compensation by the contralateral cortex can be expected (Kirsch et al. 2007b).

3.2 Auditory Evoked Fields for Presurgical Mapping

Bilateral auditory cortical responses are obtained by applying monaural or binaural stimuli. The most prominent cortical auditory evoked field (AEF) is named N100m, the magnetic counterpart of N100 in AEPs. The ECD of N100m is localized in the posterior part of the superior temporal plane, corresponding to the Heschl's gyrus. Reliable source estimation is possible using a two dipole model for whole-head data. Delayed N100m latency can be observed in patients with brain tumors involving the posterior temporal lobe (Nakasato et al. 1997) or with focal epilepsy arising in the primary auditory cortex (Kubota et al. 2007). Abnormally large-amplitude (giant) N100m is observed in some patients with autosomal dominant lateral temporal lobe epilepsy (ADTLE), possibly reflecting hyperexcitability or loss of inhibition in the pathological temporal cortex (Usui et al. 2009).

3.3 Language Mapping with MEG

When language stimuli are presented acoustically or visually, early responses from the primary auditory and visual areas may be followed by late responses from the language areas, typically after 200 ms and up to 1,000 ms from stimulus onset. Amplitude asymmetry of the late event-related fields can predict the language-dominant hemisphere. The language-related activation can be quantified by the number of fitted ECDs localized near the frontal and posterior temporal language areas (Papanicolaou et al. 2004). Other source modeling is also applicable to language-related source localization, and yields clinically relevant results (Bowyer et al. 2004, 2005; McDonald et al. 2009; Tanaka et al. 2013). Although several language tasks have been proposed, relatively simple tasks, such as those involving passive listening, are sufficient for lateralizing language function (Pirmoradi et al. 2010). Passive auditory language mapping during sleep is possible in children who are not cooperative during conventional language testing (Van Poppel et al. 2012).

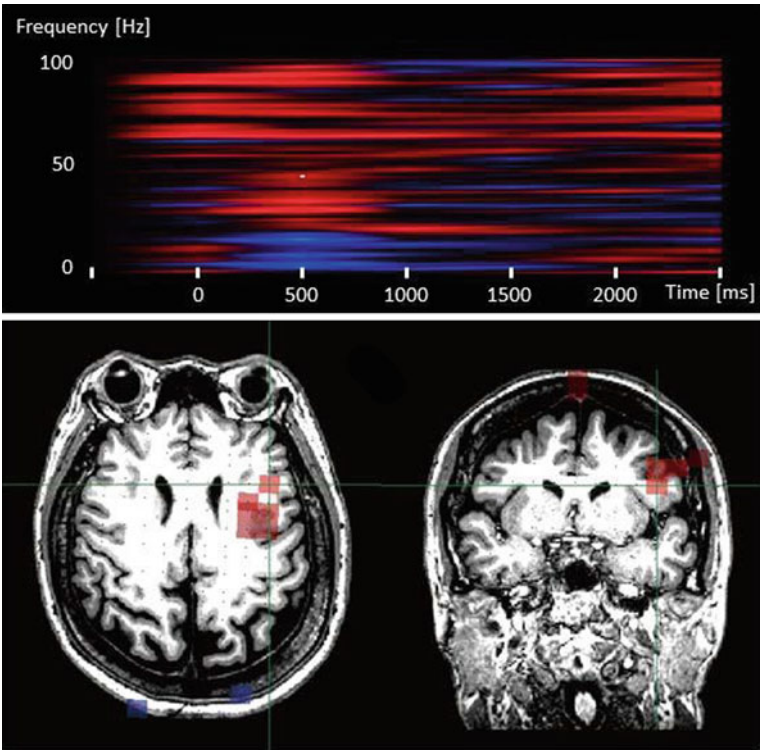

Fig. 5 Event-related synchronization and desynchronization for a silent naming task involving visually presented nouns. Time-frequency representation of signal source strength in the left inferior frontal gyrus (*upper panel*) shows a decrease (*color-coded in blue*) in beta-range activity and an increase (*red*) in gamma-range activity around 500 ms from onset. Voxels showing statistically significant changes in beta desynchronization were mapped onto the left frontal language area (*lower panel*). Left-hemisphere language dominance was suggested

MEG is currently used as a non-invasive alternative for lateralization of the language-dominant hemisphere (Abou-Khalil 2007; Pelletier et al. 2007). In terms of language lateralization, MEG is concordant with the intra-carotid amobarbital procedure (IAP), the gold standard for language lateralization, in 86 % of cases with sensitivity and specificity values of 80 and 100 %, respectively (Doss et al. 2009; Merrifield et al. 2007; Papanicolaou et al. 2004). Good test-retest reliability has also been confirmed (Lee et al. 2006).

Language activation can also be measured as event-related changes in MEG oscillation (i.e., event-related desynchronization, ERD, or event-related synchronization, ERS) (Lee et al. 2010b). Beta to low gamma-range band desynchronization in the left frontal area and alpha to beta-range desynchronization in the left parietotemporal areas show 85 % concordance with IAP (Hirata et al. 2010) (Fig. 5). A recent study showed that power decrease in the beta band was especially sensitive and specific to IAP (Findlay et al. 2012).

4 Conclusions

In pre-surgical evaluation of epilepsy, magnetic source imaging (MSI) of epileptic spikes provides additional information to those provided by other non-invasive measures especially in neocortical epilepsy and in MRI-negative epilepsy. MSI guides additional electrode coverage for intracranial EEG and area of resection when planning surgery. Mono-focal spike localization strongly indicates the epileptogenic zone, and complete removal of the MEG focus often results in the patient being seizure free, post-operatively.

MEG is also utilized for functional brain mapping. Somatosensory evoked fields to median nerve stimulation lead to an accurate, within a few millimeters, identification of the central sulcus. MEG is a non-invasive alternative for pre-surgical determination of the language-dominant hemisphere. MEG analysis of event-related responses to language tasks provides more than 80 % sensitivity and specificity in language lateralization for intra-carotid amobarbital procedures.

References

Abou-Khalil B (2007) An update on determination of language dominance in screening for epilepsy surgery: the Wada test and newer noninvasive alternatives. Epilepsia 48:442–455

Agirre-Arrizubieta Z, Huiskamp GJM, Ferrier CH et al (2009) Interictal magnetoencephalography and the irritative zone in the electrocorticogram. Brain 132:3060–3071

Assaf BA, Karkar KM, Laxer KD et al (2003) Ictal magnetoencephalography in temporal and extratemporal lobe epilepsy. Epilepsia 44:1320–1327

Bagić AI (2011) Disparities in clinical magnetoencephalography practice in the United States: a survey-based appraisal. J Clin Neurophysiol 28:341–347

Bagic A, Funke ME, Ebersole J (2009) American Clinical MEG Society (ACMEGS) position statement: the value of magnetoencephalography (MEG)/magnetic source imaging (MSI) in noninvasive presurgical evaluation of patients with medically intractable localization-related epilepsy. J Clin Neurophysiol 26:290–293

Bagić AI, Barkley GL, Rose DF, Ebersole JS (2011a) American clinical magnetoencephalography society clinical practice guideline 4: qualifications of MEG-EEG personnel. J Clin Neurophysiol 28:364–365

Bagić AI, Knowlton RC, Rose DF, Ebersole JS (2011b) American clinical magnetoencephalography society clinical practice guideline 3: MEG-EEG reporting. J Clin Neurophysiol 28:362–363

Bagić AI, Knowlton RC, Rose DF, Ebersole JS (2011c) American clinical magnetoencephalography society clinical practice guideline 1: recording and analysis of spontaneous cerebral activity. J Clin Neurophysiol 28:348–354

Balakrishnan G, Grover KM, Mason K et al (2007) A retrospective analysis of the effect of general anesthetics on the successful detection of interictal epileptiform activity in magnetoencephalography. Anesth Analg 104:1493–1497

Barkley GL, Baumgartner C (2003) MEG and EEG in epilepsy. J Clin Neurophysiol 20:163–178

Barth DS (1993) The neurophysiological basis of epileptiform magnetic fields and localization of neocortical sources. J Clin Neurophysiol 10:99–107

Bast T, Ramantani G, Boppel T et al (2005) Source analysis of interictal spikes in polymicrogyria: loss of relevant cortical fissures requires simultaneous EEG to avoid MEG misinterpretation. Neuroimage 25:1232–1241

Bast T, Wright T, Boor R et al (2007) Combined EEG and MEG analysis of early somatosensory evoked activity in children and adolescents with focal epilepsies. Clin Neurophysiol 118:1721–1735

Baumgartner C, Pataraia E (2006) Revisiting the role of magnetoencephalography in epilepsy. Curr Opin Neurol 19:181–186

Berger MS, Cohen WA, Ojemann GA (1990) Correlation of motor cortex brain mapping data with magnetic resonance imaging. J Neurosurg 72:383–387

Bowyer SM, Mason K, Tepley N et al (2003) Magnetoencephalographic validation parameters for clinical evaluation of interictal epileptic activity. J Clin Neurophysiol 20:87–93

Bowyer SM, Moran JE, Mason KM et al (2004) MEG localization of language-specific cortex utilizing MR-FOCUSS. Neurology 62:2247–2255

Bowyer SM, Moran JE, Weiland BJ et al (2005) Language laterality determined by MEG mapping with MR-FOCUSS. Epilepsy Behav 6:235–241

Burch J, Marson A, Beyer F et al (2012) Dilemmas in the interpretation of diagnostic accuracy studies on presurgical workup for epilepsy surgery. Epilepsia 53:1294–1302

Burgess RC, Barkley GL, Bagić AI (2011a) Turning a new page in clinical magnetoencephalography: practicing according to the first clinical practice guidelines. J Clin Neurophysiol 28:336–340

Burgess RC, Funke ME, Bowyer SM et al (2011b) American clinical magnetoencephalography society clinical practice guideline 2: presurgical functional brain mapping using magnetic evoked fields. J Clin Neurophysiol 28:355–361

Carrette E, De Tiège X, Op De Beeck M et al (2011) Magnetoencephalography in epilepsy patients carrying a vagus nerve stimulator. Epilepsy Res 93:44–52

Chang EF, Nagarajan SS, Mantle M et al (2009) Magnetic source imaging for the surgical evaluation of electroencephalography-confirmed secondary bilateral synchrony in intractable epilepsy. J Neurosurg 111:1248–1256

Colon AJ, Ossenblok P, Nieuwenhuis L et al (2009) Use of routine MEG in the primary diagnostic process of epilepsy. J Clin Neurophysiol 26:326–332

De Jongh A, De Munck JC, Gonçalves SI, Ossenblok P (2005) Differences in MEG/EEG epileptic spike yields explained by regional differences in signal-to-noise ratios. J Clin Neurophysiol 22:153–158

De Tiège X, Carrette E, Legros B et al (2012) Clinical added value of magnetic source imaging in the presurgical evaluation of refractory focal epilepsy. J Neurol Neurosurg Psychiatr 83:417–423

Donahue D, Sanchez R, Hernandez A et al (2007) Preservation of a subcutaneous pocket for vagus nerve stimulation pulse generator during magnetoencephalography. Technical note. J Neurosurg 107:519–520

Doss RC, Zhang W, Risse GL, Dickens DL (2009) Lateralizing language with magnetic source imaging: validation based on the Wada test. Epilepsia 50:2242–2248

Duncan JS (2010) Imaging in the surgical treatment of epilepsy. Nat Rev Neurol 6:537–550

Ebersole JS, Ebersole SM (2010) Combining MEG and EEG source modeling in epilepsy evaluations. J Clin Neurophysiol 27:360–371

Enatsu R, Mikuni N, Usui K et al (2008) Usefulness of MEG magnetometer for spike detection in patients with mesial temporal epileptic focus. Neuroimage 41:1206–1219

Evans LT, Morse R, Roberts DW (2012) Epilepsy surgery in tuberous sclerosis: a review. Neurosurg Focus 32:E5

Fernandes JM, Da Silva AM, Huiskamp G et al (2005) What does an epileptiform spike look like in MEG? Comparison between coincident EEG and MEG spikes. J Clin Neurophysiol 22:68–73

Findlay AM, Ambrose JB, Cahn-Weiner DA et al (2012) Dynamics of hemispheric dominance for language assessed by magnetoencephalographic imaging. Ann Neurol 71:668–686

Fischer MJM, Scheler G, Stefan H (2005) Utilization of magnetoencephalography results to obtain favourable outcomes in epilepsy surgery. Brain 128:153–157

Fisher RS, Van Emde Boas W, Blume W et al (2005) Epileptic seizures and epilepsy: definitions proposed by the International League Against Epilepsy (ILAE) and the International Bureau for Epilepsy (IBE). Epilepsia 46:470–472

Fujiwara H, Greiner HM, Hemasilpin N et al (2012) Ictal MEG onset source localization compared to intracranial EEG and outcome: improved epilepsy presurgical evaluation in pediatrics. Epilepsy Res 99:214–224

Hashizume A, Iida K, Shirozu H et al (2007) Gradient magnetic-field topography for dynamic changes of epileptic discharges. Brain Res 1144:175–179

Heers M, Rampp S, Kaltenhäuser M et al (2010a) Detection of epileptic spikes by magnetoencephalography and electroencephalography after sleep deprivation. Seizure 19:397–403

Heers M, Rampp S, Kaltenhäuser M et al (2010b) Monofocal MEG in lesional TLE: does video EEG monitoring add crucial information? Epilepsy Res 92:54–62

Hillebrand A, Barnes GR (2002) A quantitative assessment of the sensitivity of whole-head MEG to activity in the adult human cortex. Neuroimage 16:638–650

Hirata M, Goto T, Barnes G et al (2010) Language dominance and mapping based on neuromagnetic oscillatory changes: comparison with invasive procedures. J Neurosurg 112:528–538

Huiskamp G, Agirre-Arrizubieta Z, Leijten F (2010) Regional differences in the sensitivity of MEG for interictal spikes in epilepsy. Brain Topogr 23:159–164

Iida K, Otsubo H, Matsumoto Y et al (2005a) Characterizing magnetic spike sources by using magnetoencephalography-guided neuronavigation in epilepsy surgery in pediatric patients. J Neurosurg 102:187–196

Iida K, Otsubo H, Mohamed IS et al (2005b) Characterizing magnetoencephalographic spike sources in children with tuberous sclerosis complex. Epilepsia 46:1510–1517. doi:10.1111/j.1528-1167.2005.14005.x

Ishitobi M, Nakasato N, Yamamoto K, Iinuma K (2005) Opercular to interhemispheric source distribution of benign rolandic spikes of childhood. Neuroimage 25:417–423

Iwasaki M, Burgess RC (2008) Magnetoencephalography in the evaluation of the irritative zone. In: Lüders HO (ed) Textbook of epilepsy surgery. Informa Healthcare, London, pp 537–543

Iwasaki M, Nakasato N, Shamoto H et al (2002) Surgical implications of neuromagnetic spike localization in temporal lobe epilepsy. Epilepsia 43:415–424

Iwasaki M, Nakasato N, Shamoto H, Yoshimoto T (2003) Focal magnetoencephalographic spikes in the superior temporal plane undetected by scalp EEG. J Clin Neurosci 10:236–238

Iwasaki M, Pestana E, Burgess RC et al (2005) Detection of epileptiform activity by human interpreters: blinded comparison between electroencephalography and magnetoencephalography. Epilepsia 46:59–68

Jansen FE, Huiskamp G, Van Huffelen AC et al (2006) Identification of the epileptogenic tuber in patients with tuberous sclerosis: a comparison of high-resolution EEG and MEG. Epilepsia 47:108–114

Kaiboriboon K, Nagarajan S, Mantle M, Kirsch HE (2010) Interictal MEG/MSI in intractable mesial temporal lobe epilepsy: spike yield and characterization. Clin Neurophysiol 121:325–331

Kakisaka Y, Nakasato N, Haginoya K et al (2009) Sensorimotor seizures of pediatric onset with unusual posteriorly oriented rolandic spikes. Epilepsy Res 84:153–158

Kakisaka Y, Alexopoulos AV, Gupta A et al (2010) Generalized 3-Hz spike-and-wave complexes emanating from focal epileptic activity in pediatric patients. Epilepsy Behav 20:103–106

Kakisaka Y, Gupta A, Wang ZI et al (2011a) Different cortical involvement pattern of generalized and localized spasms: a magnetoencephalography study. Epilepsy Behav 22:599–601

Kakisaka Y, Iwasaki M, Haginoya K et al (2011b) Somatotopic distribution of peri-rolandic spikes may predict prognosis in pediatric-onset epilepsy with sensorimotor seizures. Clin Neurophysiol 122:869–873

Kakisaka Y, Iwasaki M, Alexopoulos AV et al (2012a) Magnetoencephalography in fronto-parietal opercular epilepsy. Epilepsy Res 102:71–77

Kakisaka Y, Wang ZI, Mosher JC et al (2012b) Clinical evidence for the utility of movement compensation algorithm in magnetoencephalography: successful localization during focal seizure. Epilepsy Res 101:191–196

Kakisaka Y, Mosher JC, Wang ZI et al (2013) Utility of temporally-extended signal space separation algorithm for magnetic noise from vagal nerve stimulators. Clin Neurophysiol 124:1277–1282

Kakisaka Y, Wang ZI, Mosher JC et al (2012d) Magnetoencephalography's higher sensitivity to epileptic spikes may elucidate the profile of electroencephalographically negative epileptic seizures. Epilepsy Behav 23:171–173

Kawamura T, Nakasato N, Seki K et al (1996) Neuromagnetic evidence of pre- and post-central cortical sources of somatosensory evoked responses. Electroencephalogr Clin Neurophysiol 100:44–50

Kirsch HE, Mantle M, Nagarajan SS (2007a) Concordance between routine interictal magnetoencephalography and simultaneous scalp electroencephalography in a sample of patients with epilepsy. J Clin Neurophysiol 24:215–231

Kirsch HE, Zhu Z, Honma S et al (2007b) Predicting the location of mouth motor cortex in patients with brain tumors by using somatosensory evoked field measurements. J Neurosurg 107:481–487

Knake S, Halgren E, Shiraishi H et al (2006) The value of multichannel MEG and EEG in the presurgical evaluation of 70 epilepsy patients. Epilepsy Res 69:80–86

Knowlton RC, Elgavish R, Howell J et al (2006) Magnetic source imaging versus intracranial electroencephalogram in epilepsy surgery: a prospective study. Ann Neurol 59:835–842

Knowlton RC, Razdan SN, Limdi N et al (2009) Effect of epilepsy magnetic source imaging on intracranial electrode placement. Ann Neurol 65:716–723

König MW, Mahmoud MA, Fujiwara H et al (2009) Influence of anesthetic management on quality of magnetoencephalography scan data in pediatric patients: a case series. Paediatr Anaesth 19:507–512

Kubota Y, Otsuki T, Kaneko Y et al (2007) Delayed N100m latency in focal epilepsy associated with spike dipoles at the primary auditory cortex. J Clin Neurophysiol 24:263–270

Lau M, Yam D, Burneo JG (2008) A systematic review on MEG and its use in the presurgical evaluation of localization-related epilepsy. Epilepsy Res 79:97–104

Lee D, Sawrie SM, Simos PG et al (2006) Reliability of language mapping with magnetic source imaging in epilepsy surgery candidates. Epilepsy Behav 8:742–749

Lee JW, Tanaka N, Shiraishi H et al (2010a) Evaluation of postoperative sharp waveforms through EEG and magnetoencephalography. J Clin Neurophysiol 27:7–11

Lee S-Y, Kim JS, Chung CK et al (2010b) Assessment of language dominance by event-related oscillatory changes in an auditory language task: magnetoencephalography study. J Clin Neurophysiol 27:263–269

Leijten FSS, Huiskamp G (2008) Interictal electromagnetic source imaging in focal epilepsy: practices, results and recommendations. Curr Opin Neurol 21:437–445

Leijten FSS, Huiskamp GM, Hilgersom I, Van Huffelen AC (2003) High-resolution source imaging in mesiotemporal lobe epilepsy: a comparison between MEG and simultaneous EEG. J Clin Neurophysiol 20:227–238

Lin YY, Shih YH, Hsieh JC et al (2003) Magnetoencephalographic yield of interictal spikes in temporal lobe epilepsy. Comparison with scalp EEG recordings. Neuroimage 19:1115–1126

Lüders HO, Engel JJ, Munari C (1993) General principles. In: Engel JJ (ed) Surgical treatment of epilepsy, 2nd edn. Raven Press, New York, pp 137–153

Mäkelä JP, Forss N, Jääskeläinen J et al (2006) Magnetoencephalography in neurosurgery. Neurosurgery 59:493–510

Malmivuo J, Suihko V, Eskola H (1997) Sensitivity distributions of EEG and MEG measurements. IEEE Trans Biomed Eng 44:196–208

McDonald CR, Thesen T, Hagler DJ et al (2009) Distributed source modeling of language with magnetoencephalography: application to patients with intractable epilepsy. Epilepsia 50:2256–2266

Medvedovsky M, Taulu S, Gaily E et al (2012) Sensitivity and specificity of seizure-onset zone estimation by ictal magnetoencephalography. Epilepsia 53:1649–1657

Merrifield WS, Simos PG, Papanicolaou AC et al (2007) Hemispheric language dominance in magnetoencephalography: sensitivity, specificity, and data reduction techniques. Epilepsy Behav 10:120–128

Mohamed IS, Otsubo H, Ochi A et al (2007) Utility of magnetoencephalography in the evaluation of recurrent seizures after epilepsy surgery. Epilepsia 48:2150–2159

Nagamatsu K, Nakasato N, Hatanaka K et al (2001) Neuromagnetic localization of N15, the initial cortical response to lip stimulus. NeuroReport 12:1–5

Nakasato N, Yoshimoto T (2000) Somatosensory, auditory, and visual evoked magnetic fields in patients with brain diseases. J Clin Neurophysiol 17:201–211

Nakasato N, Kumabe T, Kanno A et al (1997) Neuromagnetic evaluation of cortical auditory function in patients with temporal lobe tumors. J Neurosurg 86:610–618

Oishi M, Kameyama S, Masuda H et al (2006) Single and multiple clusters of magnetoencephalographic dipoles in neocortical epilepsy: significance in characterizing the epileptogenic zone. Epilepsia 47:355–364

Ossadtchi A, Baillet S, Mosher JC et al (2004) Automated interictal spike detection and source localization in magnetoencephalography using independent components analysis and spatio-temporal clustering. Clin Neurophysiol 115:508–522

Ossenblok P, De Munck JC, Colon A et al (2007) Magnetoencephalography is more successful for screening and localizing frontal lobe epilepsy than electroencephalography. Epilepsia 48:2139–2149

Papanicolaou AC, Simos PG, Castillo EM et al (2004) Magnetocephalography: a noninvasive alternative to the Wada procedure. J Neurosurg 100:867–876

Park H-M, Nakasato N, Iwasaki M et al (2004) Comparison of magnetoencephalographic spikes with and without concurrent electroencephalographic spikes in extratemporal epilepsy. Tohoku J Exp Med 203:165–174

Pataraia E, Lindinger G, Deecke L et al (2005) Combined MEG/EEG analysis of the interictal spike complex in mesial temporal lobe epilepsy. Neuroimage 24:607–614

Pelletier I, Sauerwein HC, Lepore F et al (2007) Non-invasive alternatives to the Wada test in the presurgical evaluation of language and memory functions in epilepsy patients. Epileptic Disord 9:111–126

Perkins FF, Breier J, McManis MH et al (2008) Benign rolandic epilepsy—perhaps not so benign: use of magnetic source imaging as a predictor of outcome. J Child Neurol 23:389–393

Pirmoradi M, Béland R, Nguyen DK et al (2010) Language tasks used for the presurgical assessment of epileptic patients with MEG. Epileptic Disord 12:97–108

Ramachandrannair R, Otsubo H, Shroff MM et al (2007) MEG predicts outcome following surgery for intractable epilepsy in children with normal or nonfocal MRI findings. Epilepsia 48:149–157

Ramachandrannair R, Ochi A, Imai K et al (2008) Epileptic spasms in older pediatric patients: MEG and ictal high-frequency oscillations suggest focal-onset seizures in a subset of epileptic spasms. Epilepsy Res 78:216–224

Ramantani G, Boor R, Paetau R et al (2006) MEG versus EEG: influence of background activity on interictal spike detection. J Clin Neurophysiol 23:498–508

Rodin E, Funke M, Berg P, Matsuo F (2004) Magnetoencephalographic spikes not detected by conventional electroencephalography. Clin Neurophysiol 115:2041–2047

Sakurai K, Tanaka N, Kamada K et al (2007) Magnetoencephalographic studies of focal epileptic activity in three patients with epilepsy suggestive of Lennox-Gastaut syndrome. Epileptic Disord 9:158–163

Sakurai K, Takeda Y, Tanaka N et al (2010) Generalized spike-wave discharges involve a default mode network in patients with juvenile absence epilepsy: a MEG study. Epilepsy Res 89:176–184

Salayev KA, Nakasato N, Ishitobi M et al (2006) Spike orientation may predict epileptogenic side across cerebral sulci containing the estimated equivalent dipole. Clin Neurophysiol 117:1836–1843

Salmelin R, Hari R (1994) Characterization of spontaneous MEG rhythms in healthy adults. Electroencephalogr Clin Neurophysiol 91:237–248

Schneider F, Alexopoulos AV, Wang Z et al (2012a) Magnetic source imaging in non-lesional neocortical epilepsy: additional value and comparison with ICEEG. Epilepsy Behav 24:234–240

Schneider F, Irene Wang Z, Alexopoulos AV et al (2013) Magnetic source imaging and ictal SPECT in MRI-negative neocortical epilepsies: additional value and comparison with intracranial EEG. Epilepsia 54:359–369

Schwartz ES, Edgar JC, Gaetz WC, Roberts TPL (2010) Magnetoencephalography. Pediatr Radiol 40:50–58

Seo JH, Holland K, Rose D et al (2011) Multimodality imaging in the surgical treatment of children with nonlesional epilepsy. Neurology 76:41–48

Shibasaki H, Ikeda A, Nagamine T (2007) Use of magnetoencephalography in the presurgical evaluation of epilepsy patients. Clin Neurophysiol 118:1438–1448

Shiraishi H, Ahlfors SP, Stufflebeam SM et al (2005) Application of magnetoencephalography in epilepsy patients with widespread spike or slow-wave activity. Epilepsia 46:1264–1272

Shiraishi H, Ahlfors SP, Stufflebeam SM et al (2011) Comparison of three methods for localizing interictal epileptiform discharges with magnetoencephalography. J Clin Neurophysiol 28:431–440

Shirozu H, Iida K, Hashizume A et al (2010) Gradient magnetic-field topography reflecting cortical activities of neocortical epilepsy spikes. Epilepsy Res 90:121–131

Slater JD, Khan S, Li Z, Castillo E (2012) Characterization of interictal epileptiform discharges with time-resolved cortical current maps using the helmholtz-hodge decomposition. Front Neurol 3:138

Song T, Cui L, Gaa K et al (2009) Signal space separation algorithm and its application on suppressing artifacts caused by vagus nerve stimulation for magnetoencephalography recordings. J Clin Neurophysiol 26:392–400

Stefan H, Hummel C, Scheler G et al (2003) Magnetic brain source imaging of focal epileptic activity: a synopsis of 455 cases. Brain 126:2396–2405

Stefan H, Paulini-Ruf A, Hopfengärtner R, Rampp S (2009) Network characteristics of idiopathic generalized epilepsies in combined MEG/EEG. Epilepsy Res 85:187–198

Stefan H, Heers M, Schmitt HJ et al (2010) Increased spike frequency during general anesthesia with etomidate for magnetoencephalography in patients with focal epilepsies. Clin Neurophysiol 121:1220–1226

Stefan H, Rampp S, Knowlton RC (2011a) Magnetoencephalography adds to the surgical evaluation process. Epilepsy Behav 20:172–177

Stefan H, Wu X, Buchfelder M et al (2011b) MEG in frontal lobe epilepsies: localization and postoperative outcome. Epilepsia 52:2233–2238

Stephen JM, Ranken DM, Aine CJ et al (2005) Differentiability of simulated MEG hippocampal, medial temporal and neocortical temporal epileptic spike activity. J Clin Neurophysiol 22:388–401

Stufflebeam SM, Tanaka N, Ahlfors SP (2009) Clinical applications of magnetoencephalography. Hum Brain Mapp 30:1813–1823

Sutherling WW, Mamelak AN, Thyerlei D et al (2008) Influence of magnetic source imaging for planning intracranial EEG in epilepsy. Neurology 71:990–996

Szmuk P, Kee S, Pivalizza EG et al (2003) Anaesthesia for magnetoencephalography in children with intractable seizures. Paediatr Anaesth 13:811–817

Tanaka N, Cole AJ, Von Pechmann D et al (2009a) Dynamic statistical parametric mapping for analyzing ictal magnetoencephalographic spikes in patients with intractable frontal lobe epilepsy. Epilepsy Res 85:279–286

Tanaka N, Thiele EA, Madsen JR et al (2009b) Magnetoencephalographic analysis in patients with vagus nerve stimulator. Pediatr Neurol 41:383–387

Tanaka N, Liu H, Reinsberger C et al (2013) Language lateralization represented by spatiotemporal mapping of magnetoencephalography. AJNR Am J Neuroradiol 34:558–563

Uda T, Tsuyuguchi N, Okumura E et al (2012) sLORETA-qm for interictal MEG epileptic spike analysis: comparison of location and quantity with equivalent dipole estimation. Clin Neurophysiol 123:1496–1501

Usui K, Ikeda A, Nagamine T et al (2009) Abnormal auditory cortex with giant N100m signal in patients with autosomal dominant lateral temporal lobe epilepsy. Clin Neurophysiol 120:1923–1926

Van Poppel M, Wheless JW, Clarke DF et al (2012) Passive language mapping with magnetoencephalography in pediatric patients with epilepsy. J Neurosurg Pediatr 10:96–102

Wennberg R, Valiante T, Cheyne D (2011) EEG and MEG in mesial temporal lobe epilepsy: where do the spikes really come from? Clin Neurophysiol 122:1295–1313

Westmijse I, Ossenblok P, Gunning B, Van Luijtelaar G (2009) Onset and propagation of spike and slow wave discharges in human absence epilepsy: a MEG study. Epilepsia 50:2538–2548

Widjaja E, Otsubo H, Raybaud C et al (2008) Characteristics of MEG and MRI between Taylor's focal cortical dysplasia (type II) and other cortical dysplasia: surgical outcome after complete resection of MEG spike source and MR lesion in pediatric cortical dysplasia. Epilepsy Res 82:147–155

Widjaja E, Zarei Mahmoodabadi S, Otsubo H et al (2009) Subcortical alterations in tissue microstructure adjacent to focal cortical dysplasia: detection at diffusion-tensor MR imaging by using magnetoencephalographic dipole cluster localization. Radiology 251:206–215

World Health Organization (2009) Epilepsy fact sheet. http://www.who.int/mediacentre/factsheets/fs999/en/index.html. Accessed 16 Feb 2013

Wu JY, Sutherling WW, Koh S et al (2006) Magnetic source imaging localizes epileptogenic zone in children with tuberous sclerosis complex. Neurology 66:1270–1272

Wu X-T, Rampp S, Buchfelder M et al (2013) Interictal magnetoencephalography used in magnetic resonance imaging-negative patients with epilepsy. Acta Neurol Scand 127:274–280

Yoshinaga H, Kobayashi K, Hoshida T et al (2008) Magnetoencephalogram in a postoperative case with a large skull defect. Pediatr Neurol 39:48–51

Yu HY, Nakasato N, Iwasaki M et al (2004) Neuromagnetic separation of secondarily bilateral synchronized spike foci: report of three cases. J Clin Neurosci 11:644–648

Zhang R, Wu T, Wang Y et al (2011) Interictal magnetoencephalographic findings related with surgical outcomes in lesional and nonlesional neocortical epilepsy. Seizure 20:692–700

Towards Brain Connectivity in Epilepsy Using MEG

Seung-Hyun Jin and Chun Kee Chung

Abstract In recent years, there has been a growing interest in the area of brain connectivity. In particular, brain connectivity analyses using either functional or effective connectivity have been performed to look at functional integration between various cortical areas in the field of brain research. MEG has been widely used as a tool for presurgical mapping of epilepsy. But attempts to take advantage of technical advances of brain connectivity have been made and provided valuable information in addition to the conventional technique. Here, we discussed what we have learned from recent studies on the investigation of brain connectivity in epilepsy using MEG and future directions for this field.

Keywords Epilepsy · Presurgical evaluation · Functional segregation · Functional integration · Complex network · Functional connectivity · Effective connectivity · Information flow · Source localization · Interictal spike · Interictal spike free epoch · Focal cortical dysplasia · Electrophysiological biomarker · Epileptogenic zone · Neocortical epilepsy

S.-H. Jin · C. K. Chung (✉)
Department of Neurosurgery, Seoul National University Hospital,
101 Daehak-ro, Jongno-gu, Seoul, Republic of Korea
e-mail: chungc@snu.ac.kr

C. K. Chung
Department of Neurosurgery, Seoul National University College of Medicine,
101 Daehak-ro, Jongno-gu, Seoul, Republic of Korea

C. K. Chung
Department of Brain and Cognitive Sciences, Seoul National University College
of Natural Sciences, 1 Gwanak-ro, Gwanak-gu, Seoul, Republic of Korea

S. Supek and C. J. Aine (eds.), *Magnetoencephalography*,
DOI: 10.1007/978-3-642-33045-2_40,

1 Introduction

MEG has established as a reputation for a presurgical evaluation tool in clinical practice. In particular, there is a large body of evidence showing the feasibility of MEG as a useful tool for presurgical mapping of epilepsy, including localization of the epileptic focus and eloquent cortex evaluation (Stefan et al. 2011a, b; Colon et al. 2009; Stufflebeam et al. 2009). The inherent advantages of MEG over EEG including its being contactless and reference free and having limited influence on the volume conduction effect are well recognized (Stefan et al. 2011a). Yet its greatest advantage of high temporal resolution is still well maintained, which cannot be achieved with other neuroimaging modalities such as fMRI, PET and SPECT.

One of the contributions of this high temporal resolution is that it allows us to investigate connectivity in the brain at a high temporal resolution (Stufflebeam 2011). Let us consider functional segregation and integration. These two concepts are the two major organizational principles of the cerebral cortex (Zeki 1978; Zeki and Shipp 1988; Tononi et al. 1994; Friston 2002, 2005, 2009). They look like two sides of the same coin because we cannot understand brain function looking at only one aspect between these two features (Jin and Chung 2012). Functional segregation implies how a brain region is statistically distinct from another (Friston 2009) and it is a multi-scale phenomenon, ranging from specialized neurons to neuronal populations and cortical areas (Sporns 2011). However, considering that the brain is a large-scale network consisting of millions of neuronal elements that are interconnected in characteristic patterns, analyzing the interactions, that is, looking at the functional integration between various cortical areas, may be essential in understanding brain functions as complex network architecture. Because functional integration can be characterized in terms of functional and effective connectivity (Friston 2009), connectivity analysis has a central role in neuroscience fields such as neuroanatomy, neurodevelopment, electrophysiology, and the neural basis of cognition (Sporns 2011). This chapter will discuss what we have learned from recent studies on the exploration of brain connectivity in epilepsy using MEG.

2 Messages from the Brain Connectivity in Epilepsy Using MEG

2.1 From Functional Connectivity Perspective

Functional connectivity indicates the statistical dependencies among remote neurophysiological events (Sporns 2011) and is believed to reflect communication between different brain areas (Bullmore and Sporns 2009; Reijneveld et al. 2007). Many studies have reported on altered functional connectivity and its network in

mesial temporal lobe epilepsy (Liao et al. 2010), juvenile myoclonic epilepsy (Glerean et al. 2012) and idiopathic generalized epilepsy (Zhang et al. 2011) with the fMRI method. However, brain oscillatory activity from the perspective of functional connectivity can be better reflected with electrophysiological approaches. In fact, patients with tumor-related epilepsy showed altered functional connectivity in the theta band, suggesting the possibility of theta band functional connectivity as a hallmark of tumor-related epilepsy (Douw et al. 2010). In addition, 5 epileptic patients with absence seizures presented a rich connectivity with a clear modular structure in the brain networks, especially in the 5–14 Hz range (Chavez et al. 2010). These studies suggest the possibility of applying functional connectivity and its network to epileptic brain analysis, which might provide an electrophysiological biomarker of epilepsy.

2.2 From Effective Connectivity Perspective

Effective connectivity referring to the causal interaction between distant structures in the brain (Friston et al. 1997; Sporns 2011) is another way to unveil functional integration. Functional and effective connectivity could be considered complementary properties of brain function. Thus, effective connectivity can be viewed as an extension of functional connectivity given some underlying neuroanatomic assumptions. In fact, effective connectivity attempts to go beyond functional connectivity by identifying causal influence among the components of a network, and thus, its beauty comes from the fact that it endeavors to reveal the causes driving observed patterns of neural activity (Jin and Chung 2012). Recently, a study by Jin et al. (2013) showed its possible potential value as a presurgical evaluation of effective connectivity using MEG. The main contribution of this study is that it shows the usefulness of effective connectivity analysis in the detection of the potential epileptogenic focus of multiple MEG interictal spike clusters in focal cortical dysplasia with discordant multimodal presurgical evaluations. Similarly, effective connectivity analysis of MEG in order to estimate the primary sources of epileptiform activities was performed based on directed transfer function (Dai et al. 2012). Through these applications, it seems that effective connectivity could provide important information when determining the epileptogenic zone in terms of information flow in both the interictal spike (Dai et al. 2012) and interictal spike-free MEG signals (Jin et al. 2013).

3 Future Challenges

Although the neuroimaging of connectivity is indicated for the next 20 years as a leading research topic in disclosing the brain architecture (Friston 2011), attempts to use these technical advances in epilepsy research with MEG have not been

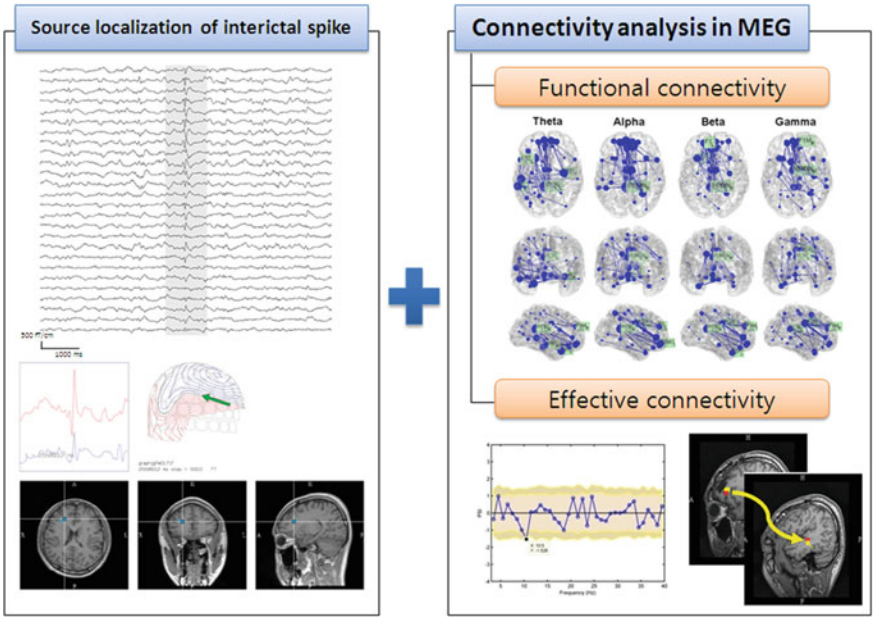

Fig. 1 Conventional MEG technique for source localization of interictal spike (*left panel*) and challengeable approach combining functional and effective connectivity (*right panel*) in epilepsy using MEG

popular as of yet relative to other clinical populations. In order to take advantage of the recent advances in connectivity research, basic studies on how brain connectivity in epilepsy using MEG is reorganized due to the pathologic origin and how brain connectivity is correlated with clinical factors should be done to ensure the feasibility and utility of these methods. Attempts to discover the core elements of functional connectivity and its relation to the epileptogenic zone would be an attractive future research theme. Effective connectivity analysis with core elements revealed by functional connectivity will provide additional information on the relationships among core elements, demonstrating the information source region. Especially, these applications would exert a strong influence in the case of non-lesional neocortical epilepsy because it is a clinical challenge to determine the potential region when surgically resected without a definite MRI lesion, but MEG as a useful diagnostic tool in non-lesional epilepsy has been reported (Funke et al. 2011). Development of a new measure to determine the epileptogenic zone based on brain connectivity would be one of the challenges of a useful clinical application. In particular, an approach combining functional and effective connectivity would allow us to understand the dynamic mechanisms underlying the epileptic brain architecture and the generation of seizures (Fig. 1).

Of course, since structural connectivity referring to a set of anatomical connections liking neural elements (for instance, from DTI) would provide structural

information (Engel et al. 2013), combining structural connectivity and brain connectivity derived from MEG will enhance our understanding of fundamental mechanisms of epilepsy and greatly help in determining the epileptogenic zone using a multi-modal prognostic tool from a connectomics perspective.

4 Conclusion

The conventional source localization technique has been a large part of the clinical application of MEG in epilepsy; however, recent advances in connectivity research with MEG will open a new era in terms of how the epileptogenic focus can interact with other regions from the perspectives of functional and effective connectivity. One of the benefits of using MEG in brain connectivity is that frequency dependent connectivity can be pursued, which is the greatest advantage of the electrophysiological approach using MEG. In summary, brain connectivity studies in epilepsy using MEG have been growing, which are expected to provide a better understanding of the epileptic brain. These studies will eventually contribute to develop the electrophysiological biomarkers of epilepsy in the near future.

References

Bullmore E, Sporns O (2009) Complex brain networks: graph theoretical analysis of structural and functional systems. Nat Rev Neurosci 10(3):186–198

Chavez M, Valencia M, Navarro V, Latora V, Martinerie J (2010) Functional modularity of background activities in normal and epileptic brain networks. Phys Rev Lett 104(11):118701

Colon AJ, Ossenblok P, Nieuwenhuis L, Stam KJ, Boon P (2009) Use of routine MEG in the primary diagnostic process of epilepsy. J Clin Neurophysiol 26(5):326–332

Dai Y, Zhang W, Dickens DL, He B (2012) Source connectivity analysis from MEG and its application to epilepsy source localization. Brain Topogr 25(2):157–166

Douw L, van Dellen E, de Groot M, Heimans JJ, Klein M, Stam CJ, Reijneveld JC (2010) Epilepsy is related to theta band brain connectivity and network topology in brain tumor patients. BMC Neurosci 11:103

Engel J Jr, Thompson PM, Stern JM, Staba RJ, Bragin A, Mody I (2013) Connectomics and epilepsy. Curr Opin Neurol 26(2):186–194

Friston K (2002) Beyond phrenology: what can neuroimaging tell us about distributed circuitry? Annu Rev Neurosci 25:221–250

Friston KJ (2005) Models of brain function in neuroimaging. Annu Rev Psychol 56:57–87

Friston KJ (2009) Modalities, modes, and models in functional neuroimaging. Science 326(5951):399–403

Friston KJ (2011) Functional and effective connectivity: a review. Brain Connect 1(1):13–36

Friston KJ, Buechel C, Fink GR, Morris J, Rolls E, Dolan RJ (1997) Psychophysiological and modulatory interactions in neuroimaging. Neuroimage 6(3):218–229

Funke ME, Moore K, Orrison WW Jr, Lewine JD (2011) The role of magnetoencephalography in "nonlesional" epilepsy. Epilepsia 52(Suppl 4):10–14

Glerean E, Salmi J, Lahnakoski JM, Jaaskelainen IP, Sams M (2012) Functional magnetic resonance imaging phase synchronization as a measure of dynamic functional connectivity. Brain Connect 2(2):91–101

Jin SH, Chung CK (2012) Messages from the brain connectivity regarding neural correlates of consciousness. Exp Neurobiol 21(3):113–122

Jin SH, Jeong W, Chung CK (2013) Information source in multiple MEG spike clusters can be identified by effective connectivity in focal cortical dysplasia. Epilepsy Res 105(1-2):118–124

Liao W, Zhang Z, Pan Z, Mantini D, Ding J, Duan X, Luo C, Lu G, Chen H (2010) Altered functional connectivity and small-world in mesial temporal lobe epilepsy. PLoS ONE 5(1):e8525

Reijneveld JC, Ponten SC, Berendse HW, Stam CJ (2007) The application of graph theoretical analysis to complex networks in the brain. Clin Neurophysiol 118(11):2317–2331

Sporns O (2011) Networks of the brain. MIT Press, Cambridge

Stefan H, Rampp S, Knowlton RC (2011a) Magnetoencephalography adds to the surgical evaluation process. Epilepsy Behav 20(2):172–177

Stefan H, Wu X, Buchfelder M, Rampp S, Kasper B, Hopfengartner R, Schmitt F, Dorfler A, Blumcke I, Zhou D, Weigel D (2011b) MEG in frontal lobe epilepsies: localization and postoperative outcome. Epilepsia 52(12):2233–2238

Stufflebeam SM (2011) Clinical magnetoencephalography for neurosurgery. Neurosurg Clin N Am 22(2):153–167, vii–viii

Stufflebeam SM, Tanaka N, Ahlfors SP (2009) Clinical applications of magnetoencephalography. Hum Brain Mapp 30(6):1813–1823

Tononi G, Sporns O, Edelman GM (1994) A measure for brain complexity: relating functional segregation and integration in the nervous system. Proc Natl Acad Sci USA 91(11):5033–5037

Zeki SM (1978) Functional specialisation in the visual cortex of the rhesus monkey. Nature 274(5670):423–428

Zeki S, Shipp S (1988) The functional logic of cortical connections. Nature 335(6188):311–317

Zhang Z, Liao W, Chen H, Mantini D, Ding JR, Xu Q, Wang Z, Yuan C, Chen G, Jiao Q, Lu G (2011) Altered functional-structural coupling of large-scale brain networks in idiopathic generalized epilepsy. Brain 134(Pt 10):2912–2928

Review of Schizophrenia Research Using MEG

Donald C. Rojas

Abstract Schizophrenia is a severe form of mental illness characterized by hallucinations, delusions, changes in affect and serious cognitive and social dysfunction. MEG has made contributions to our understanding of the disorder in many areas, although the most significant contributions have been in four areas. First, MEG has suggested that schizophrenia may be characterized by alteration in cerebral lateralization, particularly in auditory evoked responses. Second, auditory evoked responses suggest significant impairment in early auditory perceptual processes. Third, in one of these sensory deficits in particular, the underlying source configuration of sensory gating abnormalities has provided us with information about the localization of the deficit that was not apparent from EEG studies. Finally, spectrotemporal abnormalities are evident in the disorder, particularly for low frequency oscillations, and MEG has contributed to our understanding of the regional distribution of those anomalies. These and other interesting, but less well characterized electrophysiological phenomena studied using MEG methods in schizophrenia and related psychopathologies, are reviewed in this chapter.

Keywords Schizophrenia · Bipolar disorder · Psychosis · Cerebral asymmetry · Sensory gating · Delta · Alpha · Beta · Gamma · M100 · M50

1 Introduction to Schizophrenia

Schizophrenia is a serious mental disorder characterized behaviorally by symptoms indicating a disconnection from reality as well as significant cognitive and social disability. Although it had been previously described, the Swiss psychiatrist

D. C. Rojas (✉)
University of Colorado Denver, Anschutz Medical Campus, Denver, USA
e-mail: Don.Rojas@ucdenver.edu

S. Supek and C. J. Aine (eds.), *Magnetoencephalography*,
DOI: 10.1007/978-3-642-33045-2_41,

Eugen Bleuler first named the disorder schizophrenia in 1911 (Bleuler 1911), the Greek origin of the word schizophrenia denoting "split mind". Bleuler's use of this term was meant to suggest a split from reality in the affected individual rather than a split in personalities, as is often unfortunately assumed among laypersons when thinking about the meaning of the disorder's name. Schizophrenia has a worldwide prevalence of 1 % (Gottesman 1991), which makes it more prevalent than other nervous system disorders such as Alzheimer's disease, multiple sclerosis and Parkinson's disease.

Symptoms in schizophrenia are commonly divided into positive and negative symptoms. The positive symptoms of schizophrenia, those typically not present in healthy individuals, include hallucinations and delusions, disorganized behavior and disorganized or illogical speech. Negative symptoms, which are those in which there is an absence of a normal behavior, include flattened affect, alogia and avolition. These symptoms are codified in the Diagnostic and Statistical Manual of Mental Illness, 4th edition (American Psychiatric Association 1994) and International Classification of Disease, version 10 (World Health Organization 1992).

The etiology of schizophrenia is not well understood despite years of dedicated research into the underlying biological and environmental contributions. It is clear that schizophrenia has a significant genetic component, evidenced by twin studies demonstrating 50 % concordance in monozygotic twins and 17 % concordance in dizygotic twins (Gottesman 1991). Although there are a number of mutations that convey risk for the disorder, there are few if any genes with large effects identified. Schizophrenia may be a complex polygenic disorder with many risk genes of small effect, and/or a collection of disorders with shared symptomatology but distinct etiologies perhaps with convergence on particular molecular pathways (Gejman et al. 2011). There are also clearly associated environmental factors, including season of birth effects, perinatal/obstetric risks and associations with viral infection during pregnancy (Tsuang 2000).

Schizophrenia treatment remains essentially unchanged over the past 30 years of drug development. The revolution of the first generation of antipsychotic medications in the 1970s was followed by a subsequent development of so-called second generation, or atypical, antipsychotic medications. Despite differences in receptor affinity profiles, particularly with respect to serotoninergic, 5-HT2A-receptor antagonism, a common mechanism for clinical efficacy shared by all currently approved antipsychotic medications is antagonism of the D2 dopamine receptor. Despite early marketing claims, modern studies have failed to find significant differences in efficacy between first- and second-generation drugs (Lieberman and Stroup 2011), and there has been a call to abandon the terminology altogether (Tyrer and Kendall 2009). Although such medications are generally effective for treatment of positive symptoms in the disorder, few if any have shown promise in treating the cognitive deficits and negative symptoms, which is important since they are more closely associated with prognosis (Rabinowitz et al. 2012; Green 2006). Thus, the search for effective pharmacological and behavioral treatments in schizophrenia has shifted towards cognitive disability.

2 Historical Overview of MEG Applications in Schizophrenia Research

The first MEG paper published on schizophrenia was in 1988 (Reite et al. 1988), which focused on localization of the M50 auditory evoked magnetic field component in six men with schizophrenia. A single channel, second-order gradiometer was used, combined with simultaneous EEG recordings from the scalp vertex. Mapping the topography of the field distribution, which took several days of work for each subject, was accomplished by employing a grid outlined on a swim cap and 28–43 serially repeated measurements of 128 trials per location with the gradiometer positioned over each grid point. There was no comparison group in the study, so it served primarily as a proof of concept study that MEG could be applied to a severely impaired patient population. The first published paper with a direct comparison between schizophrenia patients and a control group appeared the following year, in 1989, from the same group (Reite et al. 1989). Somewhat surprisingly, the observations from these earlier MEG technologies have generally replicated using more modern methods and machines (see Sect. 3.1).

From those earlier studies, MEG publications on schizophrenia slowly increased in the 1990s and is currently showing a strong increasing trend (see Fig. 1), probably reflecting the wider installed MEG system base as well as the relative ease of conducting whole head, high-density MEG recordings, compared to the earlier days of limited channel arrays. The increase in publications using MEG also seems to track the larger overall trend of increasing numbers of published papers in schizophrenia.

3 Evoked Magnetic Fields in Schizophrenia

3.1 Cerebral Lateralization of the Location of Auditory and Somatosensory Evoked Fields

Some of the earliest studies employing MEG in schizophrenia focused on an asymmetry between the left and right hemisphere location of the auditory components of the evoked response. The M100 (also termed the N100 m) is generated within the auditory cortices on the supratemporal plane (Pantev et al. 1998; Reite et al. 1994) and its location is generally relatively more anterior in the right compared to the left hemisphere (Nakasato et al. 1995; Mäkelä et al. 2004). Reite et al. (1989) reported in a preliminary study of 6 male patients and 6 controls that the schizophrenia group exhibited reduced interhemispheric asymmetry compared to controls. Although the original study used repeated measurements of a single-channel MEG instrument, the finding has been replicated using larger array devices, both by the original research group and independently by other investigators using

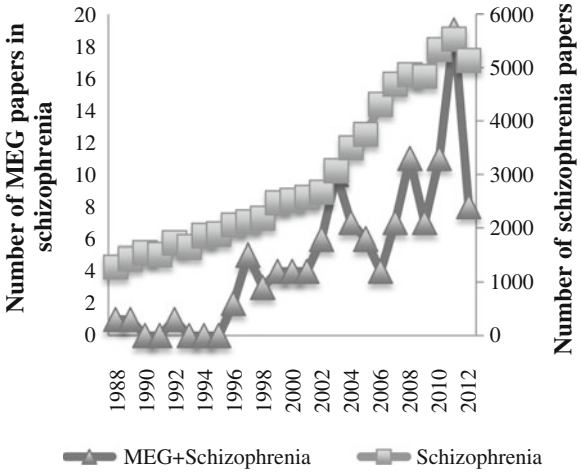

Fig. 1 Studies published by year involving schizophrenia and MEG. A search of pubmed using the terms ("magnetoencephalography", "MEG", "neuromagnetism", OR "neuromagnetic") AND ("schizophrenia", "schizoaffective disorder", "hallucinations" OR "psychosis") was performed (line labeled MEG + Schizophrenia). This was compared to all schizophrenia publications over the same time period

different MEG devices (Tiihonen et al. 1998; Rojas et al. 2002; Rockstroh et al. 2001; Edgar et al. 2006; Reite et al. 1997). Reduced M100 asymmetry has been compared directly between patients with schizophrenia and those with schizoaffective disorder, with both patient groups exhibiting reduced asymmetry compared to controls, but these groups were not significantly different from each other (Teale et al. 2000).

Two studies have compared reduced M100 location asymmetry in schizophrenia directly to samples of persons with dyslexia, a developmental disorder defined by reading disability (Edgar et al. 2006; Heim et al. 2004). In both studies, reduced anterior-posterior asymmetry in both clinical groups was reported relative to control samples, suggesting that the asymmetry reduction might reflect a nonspecific neurodevelopmental biomarker. Supportive of this interpretation, reduced asymmetry has also been observed in other neurodevelopmental disorders, including Fragile X syndrome (Rojas et al. 2001) and autism (Rojas et al. 2008; Schmidt et al. 2009).

It has also been suggested that the reduced asymmetry in schizophrenia may be a finding specific to males (Reite et al. 1997; Rojas et al. 1997). However, other investigators examining gender differences have not observed changes in location in schizophrenia, but have noted gender specific alterations in M100 dipole orientation instead (Hajek et al. 1997a, b). Gender differences, if any, may be important in schizophrenia because of the observation of later onset and possibly less severe psychopathology in women with the disorder (Goldstein 1988; Aleman et al. 2003).

The abnormality in asymmetry is not limited to source locations based on the M100, or even to auditory evoked field locations. The very first schizophrenia paper published suggested reduced asymmetry of the location of the auditory M50 source (Reite et al. 1988), and more recently there has been evidence published that the auditory-steady state source also exhibits this phenomenon in schizophrenia patients (Teale et al. 2003). Outside of the auditory cortex, reduced location asymmetry of the somatosensory M20 and M50 components have been described in schizoaffective disorder and schizophrenia, respectively (Reite et al. 1999b, 2003).

Reduced laterality of the location of auditory and somatosensory responses has also been examined in two studies of early onset psychotic disorders including schizophrenia. Wilson et al. (2008) did not find significant differences in lateralization of the auditory steady state response in children and adolescents with a heterogeneous sample of various early onset psychoses. In a separate study, however, somatosensory M50 dipole location asymmetry was found to be reduced in study of children ages 8–16 years with various early onset psychotic disorders including schizophrenia, mood disorders with psychotic features and psychosis NOS (Wilson et al. 2007). In that study, the location asymmetry for the M50 dipole was left more anterior than right hemisphere for both groups, but this left to right shift was reduced in the psychotic group. Although the increased symptomatic heterogeneity in combined psychotic disorder samples may lead to increased variability in sources, a study in bipolar disorder, directly comparing currently euthymic patient samples with and without a history of psychosis, found that reversed somatosensory M20 anterior-posterior localization was specific to the patients with a positive history psychosis, operationally defined as a history of hallucination and/or delusions (Reite et al. 1999a). In contrast to healthy control subjects and non-psychotic bipolar groups, both of which exhibited right hemisphere locations anterior to the left hemisphere locations, the psychotic bipolar group exhibited right hemisphere M20 locations posterior to the ones in the left hemisphere. This suggests that the dimension of psychosis rather than the specificity of the diagnosis is a key factor. The developmental trajectory of location lateralization for auditory and somatosensory cortices has not yet been studied, however, and more evidence is needed to define both the development and the symptom dimension associations. No studies have yet reported significant correlations between various symptoms of schizophrenia/psychosis and location asymmetry. Reduced M100 amplitude asymmetry to monaural stimulation, between the contralateral and ipsilateral responses, has also been reported (Rockstroh et al. 1998).

Evidence of altered cerebral lateralization in location of auditory and somatosensory function from MEG is part of a larger literature on changes in structural and functional lateralization in schizophrenia. For example, a meta-analysis of various aspects of lateralization in the schizophrenia indicates increased odds ratio of non-right-handedness, increased odds of reduced right-ear advantage in dichotic listening to consonant-vowel sounds, and increased odds of reduced asymmetry of brain structure in schizophrenia, especially in temporal lobe/Sylvian fissure

regions, compared to controls (Sommer et al. 2001). It should be noted, however, that abnormality of the localization of function does not necessarily imply an underlying structural abnormality. In one study comparing locations of the auditory M100 to the location of Heschl's gyrus, asymmetry (right anterior to left) in the location of Heschl's gyrus was observed in both schizophrenia and control samples (Rojas et al. 1997). Although there were no significant differences between groups in anterior-posterior position of the structure, M100 location asymmetry was significantly different between groups (Rojas et al. 1997). MEG information on location of function may be additive, rather than simply a reflection of an underlying anatomical difference.

3.2 MEG Studies of Auditory Processing

Deficient auditory processing is consistently observed in behavioral studies of schizophrenia. Frequency-matching performance, for example, is commonly reported to be worse in subjects with schizophrenia than in comparison groups (Holcomb et al. 1995; Rabinowicz et al. 2000; Javitt et al. 2000). There is an extensive body of EEG and MEG research on impairment of the mismatch negativity (MMN) in schizophrenia (reviewed in Naatanen and Kähkönen 2009). Similar to the widely replicated reduction in MMN observed in schizophrenia patients using EEG, MEG studies of the magnetic analog (variously termed MMNm or MMF), have also revealed smaller mismatch responses in patients (Kircher et al. 2004; Kreitschmann-Andermahr et al. 1999; Pekkonen et al. 2002; Kasai et al. 2003; Jordanov et al. 2011).

Some MEG studies, however, have tended to capitalize more on source localization strategies than EEG studies, and some interesting results have emerged. Kircher et al. (2004) reported that for duration mismatch responses, schizophrenia patients were significantly less right lateralized compared to healthy controls. Pekkonen et al. (2002) found that while patients with schizophrenia had significantly reduced MMNm amplitudes in both hemispheres compared to control subjects, MMNm latency was only significantly delayed in the left hemisphere. Simple dipole analyses of MMNm, however, may not be as likely to succeed for individual patients with schizophrenia as with healthy control subjects, probably due to a reduction in signal strength in the patient group (Yamasue et al. 2004; Ahveninen et al. 2006). To avoid this, one study fixed the dipole location for the MMNm using a priori information on the location of the primary auditory cortex (Thonnessen et al. 2008). In this latter study, MEG and EEG mismatch responses were directly compared using the fixed dipole locations and MEG sources outperformed the EEG sources in terms of significant group differences across a number of experimental manipulations (Thonnessen et al. 2008). In a recent study, Dima et al. (2012) examined connectivity and MMNm in schizophrenia, employing a dynamic causal modeling (Friston et al. 2003) approach to fixed dipole locations within primary auditory, secondary auditory and inferior frontal

cortices. Dima et al. (2012) reported an abnormal reversal of connectivity (i.e., reversal of information directional flow) between frontal and superior temporal sources during the MMNm. Whereas healthy individuals exhibited the predicted negative modulation of temporal lobe from frontal lobe (i.e., bottom up rather than top down), schizophrenia patients exhibited greater bottom up modulation from the temporal lobe to frontal lobe.

MMNm studies have also been published concerning risk for schizophrenia and its genetics. Shin et al. (2009) studied 16 individuals at high risk for schizophrenia based on the presence of attenuated symptoms (i.e., the schizophrenia prodrome) and found that MMNm dipole amplitude was reduced in the right hemisphere and latency was prolonged, relative to 18 healthy controls. Ahveninen et al. (2006) examined MMN and MMNm in a twin design, including monozygotic twins discordant for schizophrenia (N = 10 pairs) and dizygotic twins discordant for schizophrenia (N = 13 pairs) as well as control MZ and DZ twin pairs. Although the EEG MMN component was significantly reduced in the schizophrenia patients and their unaffected twins, the MEG MMNm did not exhibit significant differences between groups, in contrast to the more recent study of Thonnessen et al. (2008), described above. Both EEG and MEG responses exhibited genetic influence relative to the degree of relatedness to schizophrenia (Ahveninen et al. 2006).

Aside from the MMNm component, other evoked magnetic components have been studied with respect to sensory representations and processing in schizophrenia. Two studies have examined tonotopy, or the spatial mapping of frequency to the auditory cortex, using the auditory M100 response (Rosburg et al. 2000b; Rojas et al. 2002). Both found evidence of frequency effects on M100 dipole location location for healthy controls, similar to other MEG studies published using only healthy samples (Romani et al. 1982; Pantev et al. 1995). Although both studies also reported differences in the patient group, the specifics differed between studies. Rosburg et al. (2000b) reported frequency-dependent differences in location in the anterior-posterior coordinate, which were slightly greater in patients than controls in the right hemisphere but much greater in controls than in patients in the left hemisphere. In contrast, Rojas et al. (2002) found frequency differences in location on the medial-lateral coordinate for the M100, as well as a reduction in this difference, in both hemispheres, in patients with schizophrenia. Relative to the head coordinate systems used, Heschl's gyrus, the nominal structural correlate of the primary auditory cortex, has an oblique angle. Frequency gradients along it may be anterior-posterior, medial-lateral, or both, depending on the specific anatomy. Future comparisons may benefit from an accounting of this variability by expressing location coordinates within an anatomically derived framework (Jordanov et al. 2010).

In addition to dipole location, several studies have examined auditory evoked field latency and amplitude in schizophrenia under various experimental manipulations. M100 amplitude is known to exhibit stimulus-specific refractoriness and habituation to repeated stimulation (Hari et al. 1982). Rosburg et al. (2000a) did not find differences in this behavior in 20 patients with schizophrenia when comparing latency and amplitude of the M100 to repeated stimulation over several

trial blocks. Overall both controls and schizophrenia patients showed increased latency and decreased amplitude of the M100 as trial blocks increased. There was, however, a significantly higher degree of habituation in a small sub-group of patients taking clozapine, the dose of which correlated with amplitude habituation. As pointed out by the authors, clozapine may be more effective than other anti-psychotics at relieving a deficit in rapid habituation termed sensory gating in schizophrenia (Adler et al. 2004). Yet another study used M100 refractory behavior to examine frequency specific tuning of the M100 and found reduced frequency specificity of the habituation in M100 amplitude in schizophrenia patients (Rojas et al. 2007). Additional reported findings indicating an impairment of early auditory processes include earlier M50 responses (Pekkonen et al. 1999) and reduced amplitude of the M100 (Kreitschmann-Andermahr et al. 1999; Rojas et al. 2007; Edgar et al. 2012). Reduced M100 amplitude appears to be associated with thinner underlying auditory cortex, both in persons with schizophrenia (Edgar et al. 2012) and in subjects at high risk for the disorder based on having a first degree relative and/or prodromal symptoms (Shin et al. 2012).

3.3 Sensory Gating

One of the most widely replicated and highly studied EEG evoked potential findings in schizophrenia is the so-called sensory gating deficit (Adler et al. 1982). Normally studied using the EEG auditory P50 response to closely spaced paired clicks, healthy individuals tend to exhibit reduced amplitude to the second click (i.e., gating), while individuals with schizophrenia do not exhibit suppression of the second click response amplitude (Patterson et al. 2008). It is sometimes observed that reduced amplitudes of responses to the first, rather than the second click, explain the usual gating ratio for P50 and M50-based sensory gating impairment in schizophrenia (Blumenfeld and Clementz 2001). Impaired sensory gating has been linked to mutations of the cholinergic alpha-7 receptor (CHRNA7) on chromosome 15 (Freedman et al. 2003).

MEG studies have added useful information to this extensive literature. EEG researchers commonly measure P50 sensory gating at vertex (Cz), referenced to linked mastoids or ears and therefore have no information about lateralization of the response. Thoma et al. (2003) first reported that the sensory gating deficit appeared to be lateralized to auditory M50 sources in the left hemisphere. The left, but not right hemisphere gating in MEG was correlated to the vertex P50 gating response. The lateralized left hemisphere M50 gating deficit correlates with negative symptoms (Thoma et al. 2005), attention and working memory deficits (Thoma et al. 2003; Smith et al. 2010) and long-term memory (Smith et al. 2010). A recent study also extended the MEG sensory gating deficit for the M50 to human voices rather than clicks, finding that the left-lateralized deficit was associated with auditory hallucinations (Hirano et al. 2010). Simulations of changes in dipole location, orientation and interhemispheric latency differences have shown that

source configuration is important to consider in sensory gating studies in schizophrenia (Edgar et al. 2003). Indeed, source modeling of the M50 response has also been shown to improve the reliability of sensory gating measures, compared to Cz-only EEG approaches (Lu et al. 2007). An MEG study that did not examine sensory gating per se found that M50 responses had higher signal-to-noise ratios than P50 responses, suggesting another potential advantage to MEG (Thonnessen et al. 2008).

One MEG study examined the proportion of variance in the vertex EEG explained by bilateral auditory dipoles modeled using MEG data. Huang et al. (2003) found that dipoles in the left and right auditory cortices account for approximately 97 % of the variance in healthy individuals observed at a vertex EEG electrode for the time period including the P50 responses, but a smaller amount, 86 %, in persons with schizophrenia. In that study, the residual variance waveform for the dipole had a peak frequency of 40 Hz, suggesting unaccounted for variance in the gamma-band in schizophrenia subjects. Indeed, an early combined EEG and MEG sensory gating paper suggested that the gating effect was stronger for gamma-band signals overlapping the P50/M50 response temporally (Clementz et al. 1997). Other spectrally-focused MEG studies of sensory gating have implicated theta, alpha and beta abnormalities as well (Edgar et al. 2008; Ho et al. 2008; Popov et al. 2011).

Gating is not specific to the auditory M50 response. The M100 response also exhibits reduced amplitude to the second of two paired sounds, although historically this has been considered in the context of refractoriness or habituation (see Sect. 3.2). Hanlon et al. (2005a) reported M100 gating deficits in schizophrenia, in addition to the M50-based deficit. The M100, unlike the M50, showed bilateral deficits in the patients. One MEG study examining M100 suppression effects in schizophrenia found that when using monaural stimulation, instead of the usual binaural stimuli, ipsilateral but not contralateral response gating was worse in patients compared to controls (Blumenfeld and Clementz 1999). Similarly, Dale et al. (2010) found that M100 response suppression to the second of two closely spaced syllables was impaired in schizophrenia. Another study examined the generality of sensory gating deficits across sensory modalities in 27 patients with schizophrenia and 21 control subjects (Edgar et al. 2005). Deficits were replicated for the auditory M50 gating response, but were not present in the somatosensory system using the M20 response to median nerve stimulation. The lack of somatosensory gating deficit in schizophrenia does not imply an intact somatosensory system, however, as another MEG study found abnormalities in evoked responses to median nerve stimulation in schizophrenia in the context of a somatosensory oddball task (Huang et al. 2010). Additionally, a follow-up study of secondary somatosensory cortical responses (the M20 is generated in primary somatosensory cortex) found evidence for gating deficits in these later responses in patients with schizophrenia (Thoma et al. 2007).

As with the M100 response, M50 and gating measures derived from it are correlated with structural changes in the brain in schizophrenia. An early study reported that M50 gating was negatively correlated with anterior hippocampal

volumes in a hemisphere-specific manner, such that gating in the left correlated with left hippocampus and gating in the right correlated with right hippocampus (Thoma et al. 2008). This is an important observation given the putative role for the hippocampus in some models of sensory gating and the general lack of imaging evidence for a hippocampal generator. Other experimental paradigms more specific to hippocampal function have revealed hippocampal deficits in schizophrenia using MEG (Hanlon et al. 2005b, 2011). In addition, Thoma et al. (2004) also found that thinner auditory cortex in schizophrenia subjects was associated with reduced sensory gating of the M50.

Finally, there are two additional points worth considering for MEG measures of sensory gating in schizophrenia. The first is that while most studies do in fact replicate the alteration in response amplitude ratios between first and second stimuli, regardless of whether the specific change is to the first or the second stimulus, at least one study using first-episode, medicated schizophrenia subjects did not find evidence for sensory gating impairment in schizophrenia (Bachmann et al. 2010). A significant number of patients, however, were taking clozapine, which in separate studies has been shown to improve sensory gating in schizophrenia, unlike other antipsychotic medications (Adler et al. 2004). Last, MEG-based sensory gating may be a schizophrenia biomarker amenable to inclusion in clinical trials. Popov et al. (2012) reported preliminary evidence of normalization of M50 and gamma-band measures of sensory gating in a sample of schizophrenia patients assigned to a 4 week cognitive remediation intervention.

3.4 Affect Processing in Schizophrenia

More recently, schizophrenia researchers have been focused on impairments in social cognition in the disorder, and it has long been known that schizophrenia patients have reduced affective expression. Several MEG studies have examined aspects of affect processing in the disorder. Streit et al. (2001) examined visual evoked magnetic fields to standardized pictures of facial affect in patients with schizophrenia (N = 15) and control subjects (N = 12). They reported reduced activations in brain regions including the inferior prefrontal, temporal, parietal and occipital cortices in the schizophrenia group. Inferior prefrontal and fusiform gyrus activity was correlated with behavioral categorization of emotional faces, which was worse in the schizophrenia subjects. A follow-on study of the same dataset examined interregional connectivity using mutual information metrics (Ioannides et al. 2004), observing that schizophrenia subjects had generally weaker linkages between regions involved in the task, including a missing link between right amygdala and primary/secondary visual cortices. Another MEG study employed stimuli from the International Affective Picture System (IAPS) and found that the schizophrenia patients (N = 12) exhibited lower response differences between emotional versus neutral stimuli in frontal and posterior regions of the brain (Rockstroh et al. 2006). They also observed a shift in schizophrenia patients

towards emotional valence responsiveness towards the right, rather than left, hemisphere, compared to healthy control subjects. In a separate study involving only neutral-face perception, patients with schizophrenia exhibited significantly greater right hemisphere activation than left, compared to control subjects (Lopez-Ibor et al. 2008). A final MEG study involved a heterogeneous sample of patients including schizophrenia (N = 15), depression (N = 19), drug addiction (N = 10), and borderline personality disorder (N = 6), as well as healthy controls (Weber et al. 2009). This study, which also employed emotional and neutral pictures from the IAPS, examined the impact of early life stress on affective processing by focusing on the visual early posterior negativity (EPN) between 160 and 210 ms. They reported that the EPN response was smaller overall in patients with borderline personality and depression than in schizophrenia patients. They also reported, however, that schizophrenia patients had reduced EPN sensitivity to arousing stimuli. Overall, early life stress was negatively correlated with EPN responses.

4 Spontaneous MEG in Schizophrenia

4.1 Abnormal Slow Wave Activity

Several studies have examined spontaneous low frequency oscillatory signals in resting MEG recordings from schizophrenia patients. Canive et al. (1996) were the first to report the presence of abnormal slow waves in a small sample of schizophrenia subjects using MEG, reporting the presence of the activity in four unmedicated patients out of 11 studied. Fehr et al. (2001) reported increased slow wave activity (delta and theta band), measured via dipole densities, that tended to cluster in frontal and temporal regions of the cortex in schizophrenia patients. In a follow-on study by the same group that compared different mental states (mental arithmetic and imagery) to rest, schizophrenia patients (N = 30) exhibited higher densities of slow wave related dipoles compared to controls (N = 17) in the temporal and parietal regions. Dipole density was correlated with a measure of negative symptoms in the patient group (Fehr et al. 2003). Another MEG research group replicated the increased slow wave result in schizophrenia patients, but reported a relationship between dipole density and both positive and negative symptoms in their sample (Sperling et al. 2002, 2003).

Three studies have examined the effects of medication on abnormal slow wave activity in schizophrenia patients. In a cross-sectional comparison, Fehr et al. (2003) reported that dipole density measure did not differ between medicated and unmedicated patients, in contrast to the earlier report from Canive et al. (1996), who reported that abnormal slow wave activity found in unmedicated patients was not present in the same subjects after antipsychotic medication for 8 weeks. Studies of medication effects within the context of repeated measurements on

patients in a controlled trial are more convincing than cross-sectional comparisons. One such study by Sperling et al. (2002) demonstrated that treatment with clozapine or haloperidol had no effect on slow wave density, which also contrasted with the Canive et al. (1996) report. Both medication trials had low numbers of patients, however, and a larger trial would be needed to provide a definitive answer to whether antipsychotic medications reduce slow wave dipole density in schizophrenia.

The specificity of increased focal slow wave activity in schizophrenia has also been examined in MEG studies. Wienbruch et al. (2003) published data from 25 patients with schizophrenia compared to 27 with major depressive disorder and 18 healthy controls. While the schizophrenia patients exhibited the same pattern of increased delta/theta density in frontal regions compared to controls, there was a significant reduction in slow wave activity in the depression sample, relative to both the schizophrenia and control groups. A more recent examination by investigators from the same group confirmed these findings. In a very large sample of 76 schizophrenia/schizoaffective disorder patients, compared to 116 healthy subjects and 42 with mood or somatoform disorders, elevation in slow wave activity was seen in the schizophrenia sample but not in a group comprised of mood and somatoform disorders (Rockstroh et al. 2007). In the Rockstroh et al. (2007) study, the mood/somatoform disorder patient group had fewer slow wave dipoles than either the schizophrenia or healthy control groups. Interestingly, however, in both diagnostic groups, there was a relationship between affective symptoms and slow wave activity, the specifics of which differed by diagnosis; in the schizophrenia sample, affective flattening and slow wave activity were positively correlated, while in the mood/somatoform group, higher depression scores were associated with fewer frontal slow waves. This last point is intriguing given the authors' choice to combine schizoaffective patients with the schizophrenia patients in the analyses, since major mood symptoms, including major depressive and/or manic episodes, are more characteristic of the former group. The number of schizoaffective patients was too small in the Rockstroh et al. (2007) sample, but in future studies it would be worth characterizing slow wave activity and symptom relationships separately for schizophrenia and schizoaffective patients, with a goal of further sub-typing the schizoaffective sample by history of depression and mania (i.e., depressive vs. bipolar subtype in the DSM-IV system).

4.2 Other Spectral, Connectivity and Complexity Studies of Spontaneous MEG in Schizophrenia

Aside from the abnormal slow wave studies in schizophrenia, there are a smaller number of papers that have examined spontaneous signals in higher frequency bands. Activity in the alpha (8–12 Hz), beta (12–30 Hz) and gamma (30 Hz and higher) bands has been examined. Sperling et al. (1999, 2002), using the same

dipole density methods employed in the delta/theta studies described above, also reported higher density for beta activity in schizophrenia patients, although no significant differences in the alpha band were noted. A recent eyes-closed resting state MEG study by Hinkley et al. (2011) of 30 patients and 15 controls replicated the lack of group difference in alpha power. In this study, connectivity analyses using coherence in the alpha band were conducted in source space after reconstruction using a beamforming approach. Decreased connectivity in left dorsolateral prefrontal cortex and right superior temporal cortex was seen in the patient group relative to controls. Prefrontal connectivity was inversely related to negative symptoms, such that low connectivity predicted higher symptoms (Hinkley et al. 2011). In a sensor-level analysis of spontaneous activity during rest and a mental arithmetic task, Kissler et al. (2000) found reduced task-related increases in low-gamma (30–45 Hz) power in left frontal regions of schizophrenia patients, and also significantly reduced high-gamma (60–71 Hz) across both task conditions in the patient group. Another study employing beamforming source reconstructions examined changes in a wide range of frequencies from delta to very high gamma (80–150 Hz) in a study of 38 patients, 38 unaffected siblings and 38 healthy controls (Rutter et al. 2009). Reduced gamma, particularly between 30 and 70 Hz, was observed in the schizophrenia group within a large cluster centered primarily in the precuneus region of the medial occipitoparietal cortex. Unaffected siblings demonstrated a similar reduction suggestive of a possible heritable contribution to the deficit. Although the schizophrenia sample was medicated, the presence of the gamma-band deficit in the unaffected, and unmedicated relatives suggests that medication does not explain the observation.

Two additional studies deserving mention in this section did not examine the relative spectral power in different bandwidths directly. Fernandez et al. (2011) calculated a measure of signal complexity (Lempel-Ziv complexity) on MEG signals, in sensor space, that is an approximation of the number of frequency components comprising the signal measured. In this study, 15 patients and 15 control subjects were studied, and the authors reported that the complexity measure was positive correlated with age in controls, but negatively correlated with age in the schizophrenia subjects. This was interpreted as possible evidence for a neurodegenerative process in schizophrenia, although the cross-sectional design was recognized as a limitation in this respect. Longitudinal studies employing complexity measures, as well as more traditional spectral and connectivity metrics, could help answer the controversial question of whether schizophrenia is a neurodegenerative disorder. In an earlier MEG study of complexity using a single channel gradiometer system and a different metric involving non-linearity dimensionality, it was reported that schizophrenia subjects also had lower complexity than healthy controls (Kotini and Anninos 2002).

4.3 Spectral Findings Associated with Hallucinations in Schizophrenia

Tiihonen et al. (1992) first described latency delays in auditory evoked fields during the hallucinating state in two patients with schizophrenia. Subsequent MEG studies, however, have concerned themselves with spectral content rather than evoked effects. One study employing the dipole density methodology described above reported an increase in beta-band dipole density (12–30 Hz) in the left auditory cortex of a single patient compared to a reference group of 13 healthy controls (Ropohl et al. 2004). It was unclear in this study to what extent the recordings were concomitant with the hallucinations, and there was no comparison of the activity in periods of hallucination and no hallucination. A group study involving eight hallucinating and eight non-hallucinating patients reported significantly greater beta-band dipole density in the hallucinating patients in the superior temporal region of both hemispheres (Reulbach et al. 2007). Although Reulbach et al. did have patients indicate periods of hallucination with button-presses, there is no direct, within-group comparison of the hallucinating versus non-hallucinating state in that study (Reulbach et al. 2007). In another $N = 1$ study, Ishii et al. (2000) did examine hallucinating versus non-hallucinating periods in a patient, observing that theta-band activity increased during periods of hallucination. Using a frequency-based beamforming approach, these bursts associated with the hallucinations were localized to posterior, superior temporal areas of the left hemisphere. In a recent study involving 12 hallucinating patients (10 with schizophrenia), van Lutterfield et al. (2012) had the participants indicate periods of auditory hallucination with button-presses. They examined oscillatory activity associated with precise timing to the button press in order to estimate changes related to the onset of hallucinations in the patients. Beamformer images were formed for delta, theta, alpha and beta bands and compared between hallucinating and non-hallucinating segments. During hallucinations, compared to non-hallucination time periods, patients exhibited reduced alpha power in right inferior frontal gyrus and decreases in beta power in the left middle and superior temporal gyrus region. Just prior to the onset of auditory hallucinations, a significant increase in theta power was observed in the hippocampal-amygdala region. No changes in delta were observed. These findings, taken together, suggest that auditory-verbal regions of the cerebral cortex and subcortical regions including the hippocampus are involved in auditory hallucinations, consistent with a larger literature on hallucinations using PET and fMRI methods (see meta-analysis of Jardri 2011). Future studies should continue to explore possible event-related oscillatory state-changes associated with hallucinations to separate hallucination mechanisms from internally driven auditory-verbal perceptual activation, if possible. For interested readers, a more comprehensive review of spontaneous MEG findings in schizophrenia can be found in a recent paper by Siekmeier and Stufflebeam (2010).

5 Event Related Spectral Perturbance (ERSP) in Schizophrenia

In the previous section, we reviewed MEG studies primarily concerned with so-called resting-state, or spontaneous oscillations in schizophrenia. Since the brain is never truly at rest, these studies are in effect examining patients' brain activity during periods of free association or stream of consciousness, in the absence of defined external stimulation. Next, MEG studies of neuromagnetic oscillations during the performance of various tasks are considered. Such studies can be grouped under the term event-related spectral perturbances (Makeig et al. 2004). Studies involving both event-related desynchronization (ERD) and event-related synchronization (ERS) are reviewed in this section.

5.1 Alpha-Band and Working Memory

Several MEG studies have considered alpha-band ERD during performance of working memory tasks in schizophrenia. MEG has been used extensively to examine working memory in healthy individuals, primarily focusing on theta and alpha band oscillations (Kaufman et al. 1992; Jensen and Tesche 2002; Jensen et al. 2002; Rojas et al. 2000; Bonnefond and Jensen 2012). In the first such study in schizophrenia, Reite et al. (1996) found that, during an auditory Sternberg working memory task, schizophrenia participants exhibited reduced left hemisphere duration of alpha suppression (ERD) elicited by memory probe items. No differences were observed in the right hemisphere. This study was inherently limited in spatial coverage by use of a 7-channel gradiometer system, but was prepositioned over the M100 posterior field maximum so that signals might be nominally interpreted as having a temporal lobe origin. Two recent studies using large array systems have been published, however, using a visual rather than auditory Sternberg working memory task. Canuet et al. (2010, 2011) have published two studies involving individuals with schizophrenia and chronic interictal psychosis, or schizophrenia-like psychosis of epilepsy (SLPE). Controversy exists in terms of whether these patient groups can be considered distinct, either etiology- or nosology-wise (Sachdev 1998). During the retention interval of the task, alpha ERD and ERS were observed in both groups as well as in healthy controls and nonpsychotic epilepsy patients. Schizophrenia and SLPE subjects, however, had greater ERD in right dorsolateral prefrontal cortex (DLPFC) compared to healthy controls and nonpsychotic epilepsy patients (Canuet et al. 2010). Subjects with SLPE and schizophrenia were not directly compared. Higher DLPFC activation may indicate relatively higher working memory loading (i.e., difficulty) for the two psychotic clinical groups, as working memory is particularly impaired in persons with schizophrenia compared across neuropsychological domains (Barch and Ceaser 2012; Forbes et al. 2009). A follow-on study involving patients in the SLPE

group from the earlier study showed correlations between DLPFC ERD and symptoms of disorganization (Canuet et al. 2011). Finally, Ince et al. (2008, 2009) have used support vector machine classification of working memory task performance in a schizophrenia study to attempt diagnostic classification. Spectral analysis of the selected classifier features indicated the best classification was obtained in lower frequencies, including delta, theta and alpha.

Several additional studies of alpha ERSP have been published that do not concern working memory directly. A study of visual steady-state responses using stimulation frequencies between 8 and 10.5 Hz found reduced alpha power entrainment across temporal, parietal and occipital, but not frontal sensors (Koudabashi et al. 2004). Koh et al. (2011) studied alpha ERD and selective attention during an auditory oddball task in 10 people with schizophrenia, 17 individuals at higher genetic and/or symptomatic risk for developing schizophrenia, and 18 healthy controls. Alpha ERD to tones (targets and standards were not separated) was reduced in the schizophrenia and high-risk groups relative to control subjects. Source localization was not employed in this study, but the sensors chosen for statistical analysis were parieto-occipital. A separate auditory oddball study observed that rather than showing differences in ERD, schizophrenia patients had reduced ERS between 700 and 1500 ms post-stimulus, compared to controls (Fujimoto et al. 2012). In this study, which did localize the ERS/ERD sources, the alpha ERD activity was localized to occipital and parietal regions. Finally, one study examined alpha reactivity to eyes open and closed in an event-related manner (Ikezawa et al. 2011). They found that the posterior-dominant alpha rhythm ERS on eye-closed events was smaller in the schizophrenia subjects, with source localization suggesting the significant difference was in left posterior temporal cortex. Earlier conceptualizations of the functional significance of alpha synchrony were that it reflected a sort of passive cortical idling rhythm when the cortex was unoccupied by sensory information (Pfurtscheller et al. 1996). More recent evidence, however, suggests that it is associated with top-down, active inhibition of sensory processing in various regions of the cortex in which it is expressed (Klimesch et al. 2007; Bonnefond and Jensen 2012). Thus, differences in alpha synchronization in schizophrenia may reflect inhibitory dysfunction in the disorder, for which there is considerable evidence in the disorder (Lewis et al. 2005).

5.2 Beta-Band

In the same auditory oddball study that found alpha ERS differences (see Sect. 5.1), Fujimoto et al. (2012) described alterations in beta-band in schizophrenia. Significant decreases in beta ERS between 500 and 750 ms were noted in the schizophrenia subjects in occipital cortex, while decreases between 750 and 1500 ms were evident in right frontal and anterior cingulate cortex. Beta ERD was significantly increased in patients in right frontal, temporal and parietal cortices, compared to healthy controls.

With respect to working memory, beta has been explored using graph theoretical measures to examine network efficiency in schizophrenia (Bassett et al. 2009). In an interesting comparison between 28 people with schizophrenia and 29 controls, graph measures were assessed in an n-back working memory task. Findings of the study included significantly lower cost efficiency, but higher global efficiency in the schizophrenia group in the beta band during the task. This suggests a shift in the schizophrenia group towards a more random network wiring rather than a typical small-world network. The authors noted, however, that efficiency was highly correlated with performance, and that when performance differences between groups were accounted for, differences in efficiency remained but were less significant (Bassett et al. 2009). Using a different method, support vector machine classification, Ince et al. (2009) found discriminant features in beta band (as well as lower frequencies) in a Sternberg working memory task.

Wilson et al. (2009) examined beta ERSP to tactile stimulation of the fingertip in a mixed group of children and adolescents with psychoses including schizophrenia, compared to healthy controls. Beta ERD was significantly higher in the psychotic group in motor related regions of the brain including the cerebellum and precentral gyrus. In a separate study with a similar group of patients, beta ERD/ERS was examined during performance of a simple, visually-cued unimanual finger flexion task (Wilson et al. 2011). Beta-band differences in pre-movement ERD, as well as post-movement ERS (also known as the post-movement beta-rebound) were observed. Patients exhibited higher beta ERD in pre-central and cerebellar regions, similar to the findings of the tactile stimulation study. Beta ERS, however, was reduced in patients within the cerebellum, supplementary motor cortex and parietal lobe. Motor coordination deficits are one of the few early life predictors of later psychotic disorder onset (Isohanni et al. 2001), and beta abnormalities may reflect early abnormalities in motor circuitry. One recent MEG study has suggested a relationship between the post-movement beta rebound and GABA concentration in the somatomotor region (Gaetz et al. 2011). GABAergic dysfunction is one of the hottest topics in schizophrenia (Benes 2012; Lewis et al. 2012).

Apart from its potential relationship with GABAergic dysfunction, motor beta rhythms may be related to mirror neuron activity, which are neurons that respond to action observation and are theoretically important to social disability in schizophrenia. The beta rhythm has been shown to be reactive to action observations in addition to actual movements (Muthukumaraswamy and Johnson 2004). Schurmann et al. (2007) studied beta-rhythm reactivity to action observation in 11 twin pairs discordant for schizophrenia. They reported that the post-movement beta rebound was reduced to both action execution and observation in the twins with schizophrenia compared to the twins without the disorder, suggesting that the beta effect, while not specific to action observation, may be important for accurate internal representation of the actions of others (i.e., theory of mind).

5.3 Gamma-Band

Interest in gamma-band oscillations (30–150 Hz) in schizophrenia is very high and relates to the observation that gamma-band activity is highly dependent on inhibitory neurotransmission mediated by GABAergic neurons (Lewis et al. 2005; Uhlhaas 2011). The circuitry for gamma-band generation in the cortex and hippocampus is reasonably well characterized and represents the interaction of pyramidal glutamatergic inputs to fast-spiking GABAergic interneurons that recurrently inhibit the pyramidal cells (Bartos et al. 2007; Hájos and Paulsen 2009). It should be noted that this relationship, between GABA and gamma, is not unique to gamma oscillations, because there is evidence for GABAergic involvement in lower frequencies (e.g., beta-band) as well (Vierling-Claassen et al. 2008; Porjesz et al. 2002). Gamma-band abnormalities have received more attention in this respect, however.

Reduced auditory gamma band activity in schizophrenia was first noted using EEG and have been widely replicated (Kwon et al. 1999; Koenig et al. 2012; Brenner et al. 2009) and is also present in first-degree unaffected relatives (Hong et al. 2004). Auditory stimuli produce two types of gamma-band responses. An early, obligatory transient gamma-band response is seen in typically developing individuals to all types of sound stimuli within the first 30–80 ms post-stimulus (Pantev et al. 1991). When stimuli are modulated in amplitude, either as part of a train of clicks or by amplitude modulation, a later auditory steady-state response (aSSR), beginning around 100 ms is produced at or near the frequency of modulation, peaking around 40 Hz modulatory rates (Hari et al. 1989). Both types of responses are highly phase-locked in typically developing individuals. The aSSR reduction has been extended to magnetic responses in children and adults with schizophrenia (Teale et al. 2008; Maharajh et al. 2010; Wilson et al. 2008; Vierling-Claassen et al. 2008). Reductions in neuromagnetic aSSR have also been shown to be specific to frequency of stimulation. Tsuchimoto et al. (2011) found that 40 and 80 Hz stimulation rates elicited evidence of reduced bilateral auditory power and phase-locking in schizophrenia, but not stimulation at 20 and 30 Hz. This finding was partly replicated by Hamm et al. (2011), who found reduced power at 80 Hz rates in both hemispheres, but only in the right hemisphere at 40 Hz. Auditory steady-state magnetic responses are typically larger in the right than in the left hemispheres (Ross et al. 2005). In an interesting preliminary study that needs replication in a larger sample, schizoaffective disordered patients ($N = 8$) had *higher* 40 Hz aSSR responses in the right hemisphere compared to control subjects, while schizophrenia patients exhibited a bilateral reduction in 40 Hz aSSR power and phase-locking (Reite et al. 2010). Replication of this would be important because many studies combine schizoaffective and schizophrenia groups, although there is some evidence to suggest the two are distinct clinical entities (Abrams et al. 2008).

Transient magnetic gamma-band responses (tGBR) have also been reported as reduced in schizophrenia. Hirano et al. (2008) found reduced evoked tGBR power and phase-locking, as well as longer tGBR peak latency to speech, but not

non-speech sounds in the left hemisphere of persons with schizophrenia (N = 20) compared to healthy controls (N = 23). Teale et al. (2008) reported a trend for reduced pure tone phase-locking of the tGBR specific to the left hemisphere, but no differences in evoked power. In the first study of tGBR in MEG published, Clementz et al. (1997) reported a significant reduction in tGBR suppression in schizophrenia subjects in the context of a classic P50/M50 sensory gating paradigm (discussed previously in Sect. 3.3).

6 Future Directions

Despite having made substantial contribution to our knowledge of the electrophysiology of schizophrenia, more MEG research is still needed. MEG remains advantageous for examining the relatively unexplored area between the spatial resolving power of fMRI and the vast EEG literature in schizophrenia with poor spatial resolution. In particular, combining the strength of high sensor density and/or source analytic techniques with modern connectivity approaches such as mutual information (Ioannides et al. 2004), graph theory (Bassett et al. 2009) and causal modeling (Dima et al. 2012) are of high importance given the significant overall interest in the field about brain network-level impairments in the disorder. The use of machine learning and multivariate classification methods is also potentially important (Ince et al. 2009) and could be used to identify subtle risk factors and applied to populations at high risk for developing schizophrenia. With respect to the latter point, more work with unaffected first degree relatives is recommended (Rutter et al. 2009), both to identify heritable risk factors and to protect the interpretation of findings against medication confounds. Finally, a comment should be made about finding solutions to a significant barrier to MEG research in schizophrenia, which is the relative difficulty of conducting large, multi-site clinical trials due to the relatively low installed user base and differences in technology employed between sites. Efforts to measure and reduce differences between different MEG sites would allow MEG to participate as a technology in future large scale behavioral and pharmacological intervention trials, as well as providing the means to incorporate large samples in general into new and interesting research studies.

References

Abrams DJ, Rojas DC, Arciniegas DB (2008) Is schizoaffective disorder a distinct categorical diagnosis? a critical review of the literature. Neuropsychiatric Dis Treat 4(6):1089–1109

Adler LE et al (1982) Neurophysiological evidence for a defect in neuronal mechanisms involved in sensory gating in schizophrenia. Biol Psychiatry 17(6):639–654

Adler LE et al (2004) Varied effects of atypical neuroleptics on P50 auditory gating in schizophrenia patients. Am J Psychiatry 161(10):1822–1828

Ahveninen J et al (2006) Inherited auditory-cortical dysfunction in twin pairs discordant for schizophrenia. Biol Psychiatry 60(6):612–620
Aleman A, Kahn RS, Selten J-P (2003) Sex differences in the risk of schizophrenia: evidence from meta-analysis. Arch Gen Psychiatry 60(6):565–571
American Psychiatric Association (1994) Diagnostic and statistical manual of mental disorders, 4th edn. Author, Washington, DC
Bachmann S et al (2010) MEG does not reveal impaired sensory gating in first-episode schizophrenia. Schizophr Res 121(1–3):131–138
Barch DMD, Ceaser AA (2012) Cognition in schizophrenia: core psychological and neural mechanisms. Trends Cogn Sci 16(1):8
Bartos M, Vida I, Jonas P (2007) Synaptic mechanisms of synchronized gamma oscillations in inhibitory interneuron networks. Nat Rev Neurosci 8(1):45–56
Bassett DS et al (2009) Cognitive fitness of cost-efficient brain functional networks. Proc Natl Acad Sci 106(28):11747–11752
Benes FMF (2012) A new paradigm for understanding gamma-aminobutyric acid cell pathology in schizophrenia? Biol Psychiatry 72(9):712–713
Bleuler E (1911) Dementia praecox or the group of schizophrenias. International Universities Press, New York
Blumenfeld LD, Clementz BA (1999) Hemispheric differences on auditory evoked response suppression in schizophrenia. NeuroReport 10(12):2587–2591
Blumenfeld LD, Clementz BA (2001) Response to the first stimulus determines reduced auditory evoked response suppression in schizophrenia: single trials analysis using MEG. Clin Neurophysiol 112(9):1650–1659
Bonnefond M, Jensen O (2012) Alpha oscillations serve to protect working memory maintenance against anticipated distracters. Curr Biol 22(20):1969–1974
Brenner CAC et al (2009) Steady state responses: electrophysiological assessment of sensory function in schizophrenia. Brain Res Brain Res Rev 35(6):1065–1077
Canive JM et al (1996) Magnetoencephalographic assessment of spontaneous brain activity in schizophrenia. Psychopharmacol Bull 32(4):741–750
Canuet L et al (2011) Psychopathology and working memory-induced activation of the prefrontal cortex in schizophrenia-like psychosis of epilepsy: evidence from magnetoencephalography. Psychiatry Clin Neurosci 65(2):183–190
Canuet L et al (2010) Working memory abnormalities in chronic interictal epileptic psychosis and schizophrenia revealed by magnetoencephalography. Epilepsy Behav 17(1):109–119
Clementz BA, Blumenfeld LD, Cobb S (1997) The gamma band response may account for poor P50 suppression in schizophrenia. NeuroReport 8(18):3889–3893
Dale CL et al (2010) Timing is everything: neural response dynamics during syllable processing and its relation to higher-order cognition in schizophrenia and healthy comparison subjects. Int J Psychophysiol: Official J Int Organ Psychophysiol 75(2):183–193
Dima D et al (2012) Abnormal intrinsic and extrinsic connectivity within the magnetic mismatch negativity brain network in schizophrenia: a preliminary study. Schizophr Res 135(1–3):23–27
Edgar JC et al (2005) Cross-modal generality of the gating deficit. Psychophysiology 42(3):318–327
Edgar JC et al (2003) Interpreting abnormality: an EEG and MEG study of P50 and the auditory paired-stimulus paradigm. Biol Psychol 65(1):1–20
Edgar JC et al (2006) Reduced auditory M100 asymmetry in schizophrenia and dyslexia: applying a developmental instability approach to assess atypical brain asymmetry. Neuropsychologia 44(2):289–299
Edgar JC et al (2008) Superior temporal gyrus spectral abnormalities in schizophrenia. Psychophysiology 45(5):812–824
Edgar JC et al (2012) Temporal and frontal cortical thickness associations with M100 auditory activity and attention in healthy controls and individuals with schizophrenia. Schizophr Res 140(1–3):250–257

Fehr T et al (2001) Source distribution of neuromagnetic slow waves and MEG-delta activity in schizophrenic patients. Biol Psychiatry 50(2):108–116
Fehr T et al (2003) Source distribution of neuromagnetic slow-wave activity in schizophrenic patients–effects of activation. Schizophr Res 63(1–2):63–71
Fernandez A et al (2011) Lempel-Ziv complexity in schizophrenia: a MEG study. Clin Neurophysiol 122(11):2227–2235
Forbes NF et al (2009) Working memory in schizophrenia: a meta-analysis. Psychol Med 39(6):889–905
Freedman R et al (2003) The genetics of sensory gating deficits in schizophrenia. Curr Psychiatry Rep 5(2):155–161
Friston KJ, Harrison L, Penny W (2003) Dynamic causal modelling. NeuroImage 19(4):1273–1302
Fujimoto T et al (2012) Changes in event-related desynchronization and synchronization during the auditory oddball task in schizophrenia patients. Open Neuroimaging J 6:26–36
Gaetz W et al (2011) Relating MEG measured motor cortical oscillations to resting γ-aminobutyric acid (GABA) concentration. NeuroImage 55(2):616–621
Gejman PVP, Sanders ARA, Kendler KSK (2011) Genetics of schizophrenia: new findings and challenges. Genomics Hum Genet 12:121–144
Goldstein JM (1988) Gender differences in the course of schizophrenia. Am J Psychiatry 145(6):684–689
Gottesman II (1991) Schizophrenia genesis: the origins of madness. W H Freeman/Times Books/ Henry Holt & Co, New York
Green MF (2006) Cognitive impairment and functional outcome in schizophrenia and bipolar disorder. J Clin Psychiatry 67(10):e12
Hajek M, Boehle C et al (1997a) Abnormalities of auditory evoked magnetic fields in the right hemisphere of schizophrenic females. Schizophr Res 24(3):329–332
Hajek M, Huonker R et al (1997b) Abnormalities of auditory evoked magnetic fields and structural changes in the left hemisphere of male schizophrenics–a magnetoencephalographic-magnetic resonance imaging study. Biol Psychiatry 42(7):609–616
Hamm JP et al (2011) Abnormalities of neuronal oscillations and temporal integration to low- and high-frequency auditory stimulation in schizophrenia. Biol Psychiatry 69(10):989–996
Hanlon FM et al (2011) Bilateral hippocampal dysfunction in schizophrenia. NeuroImage 58(4):1158–1168
Hanlon FM, Miller GA et al (2005a) Distinct M50 and M100 auditory gating deficits in schizophrenia. Psychophysiology 42(4):417–427
Hanlon FM, Weisend MP et al (2005b) A specific test of hippocampal deficit in schizophrenia. Behav Neurosci 119(4):863–875
Hari R, Hämäläinen M, Joutsiniemi SL (1989) Neuromagnetic steady-state responses to auditory stimuli. J Acoust Soc Am 86(3):1033–1039
Hari RR et al (1982) Interstimulus interval dependence of the auditory vertex response and its magnetic counterpart: implications for their neural generation. Electroencephalogr Clin Neurophysiol 54(5):561–569
Hájos N, Paulsen O (2009) Network mechanisms of gamma oscillations in the CA3 region of the hippocampus. Neural Networks: Official J Int Neural Network Soc 22(8):1113–1119
Heim S et al (2004) Cerebral lateralization in schizophrenia and dyslexia: neuromagnetic responses to auditory stimuli. Neuropsychologia 42(5):692–697
Hinkley LBN et al (2011) Clinical symptoms and alpha band resting-state functional connectivity imaging in patients with schizophrenia: implications for novel approaches to treatment. Biol Psychiatry 70(12):1134–1142
Hirano S et al (2008) Abnormal neural oscillatory activity to speech sounds in schizophrenia: a magnetoencephalography study. J Neurosci: Official J Soc Neurosci 28(19):4897–4903
Hirano Y et al (2010) Auditory gating deficit to human voices in schizophrenia: a MEG study. Schizophr Res 117(1):61–67

Ho M-HR et al (2008) Time-frequency discriminant analysis of MEG signals. NeuroImage 40(1):174–186
Holcomb HH et al (1995) Tone discrimination performance in schizophrenic patients and normal volunteers: impact of stimulus presentation levels and frequency differences. Psychiatry Res Neuroimaging 57(1):75–82
Hong LE et al (2004) Evoked gamma band synchronization and the liability for schizophrenia. Schizophr Res 70(2–3):293–302
Huang M-X et al (2010) Somatosensory system deficits in schizophrenia revealed by MEG during a median-nerve oddball task. Brain Topogr 23(1):82–104
Huang MX et al (2003) Predicting EEG responses using MEG sources in superior temporal gyrus reveals source asynchrony in patients with schizophrenia. Clin Neurophysiol 114(5):835–850
Ikezawa K et al (2011) Decreased alpha event-related synchronization in the left posterior temporal cortex in schizophrenia: a magnetoencephalography-beamformer study. Neurosci Res 71(3):235–243
Ince NF et al (2009) Classification of schizophrenia with spectro-temporo-spatial MEG patterns in working memory. Clin Neurophysiol 120(6):1123–1134
Ince NF et al (2008) Selection of spectro-temporal patterns in multichannel MEG with support vector machines for schizophrenia classification. In: Conference proceedings: annual international conference of the IEEE engineering in medicine and biology society. IEEE Engineering in Medicine and Biology Society, pp 3554–3557
Ioannides AA et al (2004) Real-time neural activity and connectivity in healthy individuals and schizophrenia patients. NeuroImage 23(2):473–482
Ishii R et al (2000) Theta rhythm increases in left superior temporal cortex during auditory hallucinations in schizophrenia: a case report. NeuroReport 11(14):3283–3287
Isohanni M et al (2001) Early developmental milestones in adult schizophrenia and other psychoses. A 31-year follow-up of the Northern Finland 1966 Birth Cohort. Schizophr Res 52(1–2):1–19
Jardri (2011) Cortical activations during auditory verbal hallucinations in schizophrenia: a coordinate-based meta-analysis. Am J Psychiatry 168(1):73–81
Javitt DC, Shelley A, Ritter W (2000) Associated deficits in mismatch negativity generation and tone matching in schizophrenia. Clin Neurophysiol 111(10):1733–1737
Jensen O, Tesche CD (2002) Frontal theta activity in humans increases with memory load in a working memory task. Eur J Neurosci 15(8):1395–1399
Jensen O et al (2002) Oscillations in the alpha band (9–12 Hz) increase with memory load during retention in a short-term memory task. Cereb Cortex (New York 1991) 12(8):877–882
Jordanov T et al (2010) Local Heschl's gyrus-based coordinate system for intersubject comparison of M50 auditory response modeled by single equivalent current dipole. J Neurosci Methods 192(1):121–126
Jordanov T et al (2011) Reduced mismatch negativity and increased variability of brain activity in schizophrenia. Clin Neurophysiol 122(12):2365–2374
Kasai K et al (2003) Neuromagnetic correlates of impaired automatic categorical perception of speech sounds in schizophrenia. Schizophr Res 59(2–3):159–172
Kaufman L et al (1992) Changes in cortical activity when subjects scan memory for tones. Electroencephalogr Clin Neurophysiol 82(4):266–284
Kircher TTJ et al (2004) Mismatch negativity responses in schizophrenia: a combined fMRI and whole-head MEG study. Am J Psychiatry 161(2):294–304
Kissler J et al (2000) MEG gamma band activity in schizophrenia patients and healthy subjects in a mental arithmetic task and at rest. Clin Neurophysiol 111(11):2079–2087
Klimesch WW, Sauseng PP, Hanslmayr SS (2007) EEG alpha oscillations: the inhibition-timing hypothesis. Brain Res Rev 53(1):63–88
Koenig TT et al (2012) Is gamma band EEG synchronization reduced during auditory driving in schizophrenia patients with auditory verbal hallucinations? Schizophr Res 141(2–3):266–270
Koh Y et al (2011) An MEG study of alpha modulation in patients with schizophrenia and in subjects at high risk of developing psychosis. Schizophr Res 126(1–3):36–42

Kotini A, Anninos P (2002) Detection of non-linearity in schizophrenic patients using magnetoencephalography. Brain Topogr 15(2):107–113
Koudabashi A et al (2004) Spatiotemporal characteristics of MEG and EEG entrainment with photic stimulation in schizophrenia. In: Conference proceedings: annual international conference of the IEEE engineering in medicine and biology society. IEEE Engineering in Medicine and Biology Society, vol 6, pp 4465–4468
Kreitschmann-Andermahr I et al (1999) Impaired sensory processing in male patients with schizophrenia: a magnetoencephalographic study of auditory mismatch detection. Schizophr Res 35(2):121–129
Kwon JS et al (1999) Gamma frequency-range abnormalities to auditory stimulation in schizophrenia. Arch Gen Psychiatry 56(11):1001–1005
Lewis DA et al (2012) Cortical parvalbumin interneurons and cognitive dysfunction in schizophrenia. Trends Neurosci 35(1):57–67
Lewis DA, Hashimoto T, Volk DW (2005) Cortical inhibitory neurons and schizophrenia. Nat Rev Neurosci 6(4):312–324
Lieberman JA, Stroup TS (2011) The NIMH-CATIE Schizophrenia Study: what did we learn? Am J Psychiatry 168(8):770–775
Lopez-Ibor JJ et al (2008) The perception of emotion-free faces in schizophrenia: a magneto-encephalography study. Schizophr Res 98(1–3):278–286
Lu BY et al (2007) Improved test-retest reliability of 50-ms paired-click auditory gating using magnetoencephalography source modeling. Psychophysiology 44(1):86–90
Maharajh K et al (2010) Fluctuation of gamma-band phase synchronization within the auditory cortex in schizophrenia. Clin Neurophysiol: Official J Int Fed Clin Neurophysiol 121(4):542–548
Makeig S et al (2004) Mining event-related brain dynamics. Trends Cogn Sci 8(5):7
Mäkelä JP et al (2004) Functional differences between auditory cortices of the two hemispheres revealed by whole-head neuromagnetic recordings. Hum Brain Mapp 1(1):48–56
Muthukumaraswamy SD, Johnson BW (2004) Primary motor cortex activation during action observation revealed by wavelet analysis of the EEG. Clin Neurophysiol 115(8):1760–1766
Naatanen R, Kähkönen S (2009) Central auditory dysfunction in schizophrenia as revealed by the mismatch negativity (MMN) and its magnetic equivalent MMNm: a review. Int J Neuropsychopharmacol Official Sci J Collegium Int Neuropsychopharmacologicum (CINP) 12(1):125–135
Nakasato N et al (1995) Functional localization of bilateral auditory cortices using an MRI-linked whole head magnetoencephalography (MEG) system. Electroencephalogr Clin Neurophysiol 94(3):183–190
Pantev C et al (1991) Human auditory evoked gamma-band magnetic fields. Proc Natl Acad Sci 88(20):8996–9000
Pantev C et al (1998) Study of the human auditory cortices using a whole-head magnetometer: left versus right hemisphere and ipsilateral versus contralateral stimulation. Audiol Neuro-Otology 3(2–3):183–190. http://eutils.ncbi.nlm.nih.gov/entrez/eutils/elink.fcgi?dbfrom=pubmed&id=9575384&retmode=ref&cmd=prlinks
Pantev CC et al (1995) Specific tonotopic organizations of different areas of the human auditory cortex revealed by simultaneous magnetic and electric recordings. Electroencephalogr Clin Neurophysiol 94(1):26–40
Patterson JVJ et al (2008) P50 sensory gating ratios in schizophrenics and controls: A review and data analysis. Psychiatry Res Neuroimaging 158(2):22
Pekkonen E et al (1999) Altered parallel auditory processing in schizophrenia patients. Schizophr Bull 25(3):601–607
Pekkonen E et al (2002) Impaired temporal lobe processing of preattentive auditory discrimination in schizophrenia. Schizophr Bull 28(3):467–474
Pfurtscheller GG, Stancák AA, Neuper CC (1996) Event-related synchronization (ERS) in the alpha band–an electrophysiological correlate of cortical idling: a review. Int J Psychophysiol 24(1–2):39–46

Popov T et al (2012) Adjusting brain dynamics in schizophrenia by means of perceptual and cognitive training García AV (ed) PLoS One 7(7):e39051
Popov T et al (2011) Evoked and induced oscillatory activity contributes to abnormal auditory sensory gating in schizophrenia. NeuroImage 56(1):307–314
Porjesz B et al (2002) Linkage disequilibrium between the beta frequency of the human EEG and a GABAA receptor gene locus. Proc Natl Acad Sci 99(6):3729–3733
Rabinowicz EF et al (2000) Auditory sensory dysfunction in schizophrenia: imprecision or distractibility? Arch Gen Psychiatry 57(12):1149–1155
Rabinowitz J et al (2012) Negative symptoms have greater impact on functioning than positive symptoms in schizophrenia: analysis of CATIE data. Schizophr Res 137(1–3):147–150
Reite M et al (2003) Anomalous somatosensory cortical localization in schizophrenia. Am J Psychiatry 160(12):2148–2153
Reite M et al (1994) Auditory M100 component 1: relationship to Heschl's gyri. Brain Res Cogn Brain Res 2(1):13–20
Reite M et al (1989) Late auditory magnetic sources may differ in the left hemisphere of schizophrenic patients. A preliminary report. Arch Gen Psychiatry 46(6):565–572
Reite M et al (1997) Magnetic source imaging evidence of sex differences in cerebral lateralization in schizophrenia. Arch Gen Psychiatry 54(5):433–440
Reite M et al (1996) Magnetoencephalographic evidence of abnormal early auditory memory function in schizophrenia. Biol Psychiatry 40(4):299–301
Reite M et al (2010) Schizoaffective disorder - a possible MEG auditory evoked field biomarker. Psychiatry Res Neuroimaging 182(3):284–286
Reite M et al (1988) Source origin of a 50-ms latency auditory evoked field component in young schizophrenic men. Biol Psychiatry 24(5):495–506
Reite M, Teale P, Rojas DC, Arciniegas D et al (1999a) Bipolar disorder: anomalous brain asymmetry associated with psychosis. Am J Psychiatry 156(8):1159–1163
Reite M, Teale P, Rojas DC, Sheeder J et al (1999b) Schizoaffective disorder: evidence for reversed cerebral asymmetry. Biol Psychiatry 46(1):133–136
Reulbach U et al (2007) Specific and unspecific auditory hallucinations in patients with schizophrenia: a magnetoencephalographic study. Neuropsychobiology 55(2):89–95
Rockstroh B et al (2001) Altered hemispheric asymmetry of auditory magnetic fields to tones and syllables in schizophrenia. Biol Psychiatry 49(8):694–703
Rockstroh B et al (2006) Electromagnetic brain activity evoked by affective stimuli in schizophrenia. Psychophysiology 43(5):431–439
Rockstroh B et al (1998) Failure of dominant left-hemispheric activation to right-ear stimulation in schizophrenia. NeuroReport 9(17):3819–3822
Rockstroh BS et al (2007) Abnormal oscillatory brain dynamics in schizophrenia: a sign of deviant communication in neural network? BMC Psychiatry 7:44
Rojas D et al (2008) Reduced neural synchronization of gamma-band MEG oscillations in first-degree relatives of children with autism. BMC Psychiatry 8(1):66
Rojas DC et al (2002) Alterations in tonotopy and auditory cerebral asymmetry in schizophrenia. Biol Psychiatry 52(1):32–39
Rojas DC et al (2001) Auditory evoked magnetic fields in adults with fragile X syndrome. NeuroReport 12(11):2573–2576
Rojas DC et al (2000) Neuromagnetic alpha suppression during an auditory sternberg task. Evidence for a serial, self-terminating search of short-term memory. Brain Res Cogn Brain Res 10(1–2):85–89
Rojas DC et al (2007) Neuromagnetic evidence of broader auditory cortical tuning in schizophrenia. Schizophr Res 97(1–3):206–214
Rojas DC et al (1997) Sex-specific expression of Heschl's gyrus functional and structural abnormalities in paranoid schizophrenia. Am J Psychiatry 154(12):1655–1662
Romani GL, Williamson SJ, Kaufman L (1982) Tonotopic organization of the human auditory cortex. Science 216(4552):1339–1340

Ropohl A et al (2004) Cortical activity associated with auditory hallucinations. NeuroReport 15(3):523–526
Rosburg T, Kreitschmann-Andermahr I, Nowak H et al (2000a) Habituation of the auditory evoked field component N100 m in male patients with schizophrenia. J Psychiatr Res 34(3):245–254
Rosburg T, Kreitschmann-Andermahr I, Ugur T et al (2000b) Tonotopy of the auditory-evoked field component N100 m in patients with schizophrenia. J Psychophysiol 14(3):131–141
Ross B, Herdman AT, Pantev C (2005) Right hemispheric laterality of human 40 Hz auditory steady-state responses. Cereb Cortex (New York 1991) 15(12):2029–2039
Rutter L et al (2009) Magnetoencephalographic gamma power reduction in patients with schizophrenia during resting condition. Hum Brain Mapp 30(10):3254–3264
Sachdev P (1998) Schizophrenia-like psychosis and epilepsy: the status of the association. Am J Psychiatry 155(3):325–336
Schmidt GL et al (2009) Absence of M100 source asymmetry in autism associated with language functioning. NeuroReport 20(11):1037–1041
Schurmann M et al (2007) Manifest disease and motor cortex reactivity in twins discordant for schizophrenia. Br J Psychiatry 191:178–179
Shin KS et al (2012) Neuromagnetic auditory response and its relation to cortical thickness in ultra-high-risk for psychosis. Schizophr Res 140(1–3):93–98
Shin KS et al (2009) Pre-attentive auditory processing in ultra-high-risk for schizophrenia with magnetoencephalography. Biol Psychiatry 65(12):1071–1078
Siekmeier PJ, Stufflebeam SM (2010) Patterns of spontaneous magnetoencephalographic activity in patients with schizophrenia. J Clin Neurophysiol: Official Publ Am Electroencephalographic Soc 27(3):179–190
Smith AK et al (2010) Cognitive abilities and 50- and 100-ms paired-click processes in schizophrenia. Am J Psychiatry 167(10):1264–1275
Sommer I et al (2001) Handedness, language lateralisation and anatomical asymmetry in schizophrenia: meta-analysis. Br J Psychiatry 178:344–351
Sperling W et al (1999) Spontaneous slow and fast MEG activity in male schizophrenics treated with clozapine. Psychopharmacology 142(4):375–382
Sperling W et al (2002) Spontaneous, slow and fast magnetoencephalographic activity in patients with schizophrenia. Schizophr Res 58(2–3):189–199
Sperling W, Kornhuber J, Bleich S (2003) Dipole elevations over the temporoparietal brain area are associated with negative symptoms in schizophrenia. Schizophr Res 64(2–3):187–188
Streit M et al (2001) Disturbed facial affect recognition in patients with schizophrenia associated with hypoactivity in distributed brain regions: a magnetoencephalographic study. Am J Psychiatry 158(9):1429–1436
Teale P et al (2008) Cortical source estimates of gamma band amplitude and phase are different in schizophrenia. NeuroImage 42(4):1481–1489
Teale P et al (2000) Fine structure of the auditory M100 in schizophrenia and schizoaffective disorder. Biol Psychiatry 48(11):1109–1112
Teale P et al (2003) Reduced laterality of the source locations for generators of the auditory steady-state field in schizophrenia. Biol Psychiatry 54(11):1149–1153
Thoma RJ et al (2004) Auditory sensory gating deficit and cortical thickness in schizophrenia. Neurol Clin Neurophysiol NCN 2004:62
Thoma RJ et al (2007) Impaired secondary somatosensory gating in patients with schizophrenia. Psychiatry Res 151(3):189–199
Thoma RJ et al (2003) Lateralization of auditory sensory gating and neuropsychological dysfunction in schizophrenia. Am J Psychiatry 160(9):1595–1605
Thoma RJ et al (2005) M50 sensory gating predicts negative symptoms in schizophrenia. Schizophr Res 73(2–3):311–318
Thoma RJ et al (2008) Schizophrenia diagnosis and anterior hippocampal volume make separate contributions to sensory gating. Psychophysiology 45(6):926–935

Thonnessen H et al (2008) Optimized mismatch negativity paradigm reflects deficits in schizophrenia patients. A combined EEG and MEG study. Biol Psychol 77(2):205–216
Tiihonen J et al (1992) Modified activity of the human auditory cortex during auditory hallucinations. Am J Psychiatry 149(2):255–257
Tiihonen J et al (1998) Reversal of cerebral asymmetry in schizophrenia measured with magnetoencephalography. Schizophr Res 30(3):209–219
Tsuang MM (2000) Schizophrenia: genes and environment. Biol Psychiatry 47(3):210–220
Tsuchimoto R et al (2011) Reduced high and low frequency gamma synchronization in patients with chronic schizophrenia. Schizophr Res 133(1–3):99–105
Tyrer P, Kendall T (2009) The spurious advance of antipsychotic drug therapy. Lancet 373(9657):4–5
Uhlhaas PJ (2011) High-frequency oscillations in schizophrenia. Clin EEG Neurosci: Official J EEG Clin Neurosci Soc (ENCS) 42(2):77–82
van Lutterveld R et al (2012) Oscillatory cortical network involved in auditory verbal hallucinations in schizophrenia. PLoS ONE 7(7):e41149
Vierling-Claassen D et al (2008) Modeling GABA alterations in schizophrenia: a link between impaired inhibition and altered gamma and beta range auditory entrainment. J Neurophysiol 99(5):2656–2671
Weber K et al (2009) Early life stress and psychiatric disorder modulate cortical responses to affective stimuli. Psychophysiology 46(6):1234–1243
Wienbruch C et al (2003) Source distribution of neuromagnetic slow wave activity in schizophrenic and depressive patients. Clin Neurophysiol 114(11):2052–2060
Wilson TW et al (2007) Aberrant functional organization and maturation in early-onset psychosis: evidence from magnetoencephalography. Psychiatry Res Neuroimaging 156(1):59–67
Wilson TW et al (2009) Aberrant high-frequency desynchronization of cerebellar cortices in early-onset psychosis. Psychiatry Res 174(1):47–56
Wilson TW et al (2011) Abnormal gamma and beta MEG activity during finger movements in early-onset psychosis. Dev Neuropsychol 36(5):596–613
Wilson TW et al (2008) Cortical gamma generators suggest abnormal auditory circuitry in early-onset psychosis. Cereb Cortex (New York 1991) 18(2):371–378
World Health Organization (1992) The ICD-10 classification of mental and behavioural disorders: clinical descriptions and diagnostic guidelines. World Health Organization, Geneva
Yamasue H et al (2004) Abnormal association between reduced magnetic mismatch field to speech sounds and smaller left planum temporale volume in schizophrenia. NeuroImage 22(2):720–727

Neuropsychopharmacology: Recent MEG Investigations

Ksenija Marinković

Abstract Neuroimaging methods can play an increasingly important role in a highly complex drug development process by providing sensitive biomarkers of disease state and the effects of therapeutic intervention. Based on the functional mapping of the anatomical specificity of drug effects, neuroimaging methods can illuminate the basic mechanisms of a disease and can assist in guiding the development of drugs with high specificity and sensitivity in the context of clinical applications and the increased reliance on personalized medicine. Magnetoencephalography (MEG) reflects synaptic currents directly, it is free of vascular confounds, and its sources can be modeled with increasingly sophisticated algorithms that often incorporate complementary imaging modalities, making it highly applicable to neuropsychopharmacological investigations. Indeed, numerous MEG studies have examined spontaneous or task-related brain activity in response to neuromodulators and drugs of abuse. With emphasis on the spectral analysis models, this chapter briefly reviews the MEG studies manipulating GABA, acetylcholine, dopamine, glutamate and alcohol in healthy cohorts, as well as the research on Parkinson's disease, attention deficit hyperactivity disorder, and anesthesia in epilepsy. These studies provide unique insight into the spatiotemporal characteristics of the effects of pharmacological agents on different neurofunctional systems in health and disease and can reveal their effects on the oscillatory synchrony in real time and at the level of an interactive multifocal system. The MEG is increasingly relevant for understanding the neuropharmacology of psychoactive substances and for developing realistic neural models of the neuropsychiatric disorders and their sensitivity to pharmacological intervention.

Keywords Pharmacology · Magnetoencephalography · Biomarkers · Neuromodulators · GABA · Benzodiazepines · Tiagabine · Acetylcholine · Physostigmine · Dopamine · Levodopa · Glutamate · Ketamine · Alcohol ·

K. Marinković (✉)
Radiology Department, University of California at San Diego,
9500 Gilman Dr., MC 0841, La Jolla, CA 92093-0841, USA
e-mail: xenia@ucsd.edu

S. Supek and C. J. Aine (eds.), *Magnetoencephalography*,
DOI: 10.1007/978-3-642-33045-2_42,

Parkinson's disease · Amphetamine · Attention deficit hyperactivity disorder · Epilepsy · Anesthesia · Cognition · Attention · Language · Memory · Coherence · Oscillations · Theta alpha · Beta · Gamma · Frequency domain

1 Introduction

Neuropsychiatric conditions are the leading cause of disability and represent a large burden on societies worldwide (WHO 2008; Bass et al. 2012). Despite a remarkable array of existing medications, treatment options for many disorders are currently inadequate (e.g., Alzheimer's disease). Whereas the need for novel and more effective medications is increasing, the pace of new drug development is actually declining and is insufficient to meet the growing demands (Prajapati and Dureja 2012). Reasons for this state of affairs are multidimensional and include complex economic considerations and regulatory constraints bearing on exceedingly long, costly, and safety-minded drug development process impeded by high failure rates at different stages (Honig and Lalonde 2010). Several approaches have been applied in an effort to streamline and accelerate the process, including an intensified search for sensitive and reliable biomarkers. A biomarker is defined as "a characteristic that is objectively measured and evaluated as an indicator of normal biological processes, pathogenic processes, or pharmacologic responses to a therapeutic intervention" (Atkinson et al. 2001). Different biomarkers are used at successive stages of the drug development process. Disease-related biomarkers are essential for monitoring disease progression and for assessing individual predisposition and risks. Drug-related biomarkers are key to validating the specificity and sensitivity of the drug, as well as for evaluating its safety. To the extent that they predict responses to drugs, genetic biomarkers are increasingly used for patient stratification and selecting treatment dosage. They are also helpful in illuminating the basic mechanisms of a disease and in guiding the development of drugs that have high efficacy, optimal pharmacokinetics, and minimal side effects (Marrer and Dieterle 2007; Dieterle and Marrer 2008).

Despite the indispensable contributions of animal research especially in the domain of drug pharmacodynamics and toxicity, human neuroimaging experiments can provide crucial insight into drug effects on cognitive functions and clinical features that are impossible to assess in animal models. Neuroimaging can play a very important role throughout the multistage process of drug development as it can delineate biomarkers of disease progression and the effects of treatment in the context of a clinical presentation. It can provide functional mapping of the anatomical specificity of drug effects in a dose-dependent manner which can serve as sensitive biomarkers that could be targeted by pharmacological agents. Its clinical relevance further derives from its capacity to objectively track the clinical efficacy and outcome of therapeutic interventions over time (Borsook et al. 2009, 2011;

Wong et al. 2009). This aspect is especially powerful when combined with pharmacogenomics, i.e., accounting for the genetic variation in drug response. Tailoring drug selection and titration to the individual characteristics of each patient is the cornerstone of personalized medicine (Lesko and Atkinson 2001). Furthermore, although the development of neuroleptics is of vital importance for the improved treatment of psychiatric disorders, there has been some effort to develop nootropic drugs (i.e., "smart drugs" or cognition enhancers) (Lanni et al. 2008). Evidence suggests that certain cognitive functions such as attention and memory can be improved with pharmacological agents (Lynch et al. 2011; Lanni et al. 2008), although such applications raise ethical issues (Sahakian and Morein-Zamir 2011).

Diverse imaging methods have been applied in the neuropsychopharmacology domain. Positron emission tomography (PET) and single-photon emission computed tomography (SPECT) use molecular imaging tracers and are uniquely useful in investigating neurotransmitter systems in health and disease. They can assess regional differences in receptor densities and the engagement of targeted neural systems by the drugs (Ametamey and Honer 2007). Methods based on magnetic resonance imaging (MRI) methodology are noninvasive, repeatable, and have been used increasingly in neuropharmacological studies (Borsook et al. 2011; Wong et al. 2009). Magnetic resonance spectroscopy (MRS) is sensitive to certain neurotransmitters such as glutamate and GABA and is well-suited to examine the roles played by these major neurotransmitters in cognitive functions and their alterations by the centrally active compounds (Ross et al. 2011). Given that a number of commonly used psychotropic drugs modulate GABAergic and glutamatergic systems, the MRS has been applied in studies investigating a variety of psychiatric disorders (Dager et al. 2008).

Functional MRI (fMRI), also termed pharmacological (phMRI) in the context of pharmacological manipulations, is often used to investigate the effects of drugs on the brain function. This is particularly essential for gaining an insight into the neurophysiology underlying neuropsychiatric disorders. The non-invasive nature of the MRI scans makes it suitable for tracking treatments over time in conjunction with behavioral measures of cognitive functions and clinical features (Tracey 2001). The phMRI can also be applied to validate drug effects during clinical trials as it provides evidence that the targeted neurofunctional system is indeed engaged by the drug in the patient population. If the pharmacological intervention results in a desired clinical outcome, the drug enters a new phase of development and further clinical testing (Honey and Bullmore 2004; Borsook et al. 2009; Wise and Tracey 2006). Due to its high sensitivity and superior spatial resolution, T2*-weighted blood oxygenation level dependent (BOLD) signal is the method of choice in fMRI studies. However, it reflects neural changes only indirectly via neurovascular coupling as it depends on regional changes in blood flow, volume, and oxygenation rate (Buxton 2002). Therefore, the BOLD signal is sensitive to anything that can alter hemodynamic response including pharmacological agents, disease, etc. Even though the fMRI-BOLD is an excellent mapping tool, there is a caveat in interpreting the observed magnitude changes since the neural activity may be confounded with vascular changes when vasoactive drugs are administered. As a

result, pharmacological studies present a particular challenge for functional hemodynamic neuroimaging techniques. Additional imaging methods can be used to provide quantification and validation of the observed magnitude changes and to disentangle the neural from vascular influences (Rickenbacher et al. 2011).

2 Event-Related Potentials (ERPs) and Magnetic Fields (ERFs): Time Domain Investigations

The principal advantage of electrophysiological methods including EEG and MEG is their excellent temporal resolution as they reflect postsynaptic neural currents directly and are free of vascular confounds (Hämäläinen et al. 1993). Numerous pharmacological studies have used EEG methods to investigate effects of psychotropic medications in clinical populations as well as in healthy volunteers with an emphasis on drugs relevant to treatment of psychiatric disorders (Saletu et al. 2002a, 2006; Mucci et al. 2006; Leiser et al. 2011). Increased reliance on the MEG technology has resulted in significant contributions to the field as MEG can provide further insight into the neural basis of the pharmacological effects on brain and behavior. The pharmacodynamic profile of neural activity in the context of sensorimotor or cognitive tasks holds direct relevance for drug development and could be an important dimension in a multimodal biomarker approach (Polikar et al. 2010). Other chapters in the current volume describe MEG signal generation, acquisition, and analysis techniques in greater detail including multimodal imaging approaches (e.g., combination with structural MRI) and a variety of sophisticated source modeling algorithms. Many such models permit estimation of spatiotemporal stages of processing from sensory and perceptual to cognitive integration and motor execution. Time-domain analysis (i.e., averaging across trials in a manner time-locked to a stimulus onset) has been used to investigate the effects of various neurotransmitters on ERFs.

Extant reviews (Kahkonen and Ahveninen 2002; Kahkonen 2006; Kenemans and Kahkonen 2011) encompass studies using pharmacological MEG and EEG and provide excellent and thoughtful overviews of the questions, paradigms, and results of those manipulations. This large body of evidence places particular emphasis on psychotropic compounds that are used to treat psychiatric conditions via their agonist or antagonist effects on one or more neurotransmitter systems. The reviews include studies manipulating dopamine (DA), acetylcholine (ACh), serotonin (5-HT), norepinephrine (NE), glutamate, GABA, and histamine among others, in addition to caffeine and alcohol. These studies mainly used standard paradigms that probe pre-attentional and attentional processing indexed by canonical components such as N100, mismatch negativity (MMN) and P300 because they are impaired in several psychiatric disorders and because they are modulated by pharmacological agents. For the most part, the reviewed studies employed healthy volunteers and

therefore provide insight into the neurophysiological effects of these drugs on normal brain function. In other cases, reviews focused on a specific disorder. For instance, Korostenskaja and Kahkonen (2009) provide a comprehensive review of the effects of antipsychotic treatment in schizophrenia patients on ERPs and ERF as biomarkers of pre-attentional (e.g., MMN) and attention-dependent processing (e.g., P300). The MMN and the mismatch field (the magnetic counterpart to the mismatch negativity, MMNm), have been used extensively to probe involuntary attention drawn to an oddball stimulus in a repetitive sequence of sounds (Naatanen et al. 1994). The evidence indicates that the MMN is relatively insensitive to dopaminergic antipsychotic medications but it is modulated by drugs targeting the glutamatergic system, making it a potential glutamate functional biomarker (Javitt et al. 2008). In a study employing parallel ERP and ERF measures, Korostenskaja et al. (2008) administered methylphenidate (MPH) to healthy volunteers as they took part in a placebo-controlled standard MMN paradigm. MPH is a psychostimulant which is used successfully to treat attention deficit and hyperactivity disorder (ADHD). It augments the availability of catecholamines by reducing DA reuptake and modulating NE release. In this study, MPH did not affect ERPs or ERFs, confirming that catecholamines do not play an essential role in generating MMN (Kahkonen and Ahveninen 2002; Leung et al. 2007).

One of the proposed vulnerability markers for schizophrenia is a deficit in sensory gating of auditory stimuli (Cadenhead 2002). It is reflected in a failure to suppress, or gate out a P50 ERP component to the second click presented in a pair. Glutamatergic mediation of the sensory gating response has been investigated by administering ketamine to healthy participants in a MEG study (Boeijinga et al. 2007). As a NMDA receptor antagonist, ketamine exerts analgesic, anesthetic, and hallucinatory effects (Gunduz-Bruce 2009). Boeijinga et al. (2007) administered three ketamine doses in a repeated measures placebo-controlled study and recorded MEG and EEG during a paired-click sensory gating paradigm. Equivalent current dipoles of the signal sources were estimated to the temporal cortices bilaterally. The results indicate disrupted auditory gating by nonanesthetic doses of ketamine, emulating the effects seen in schizophrenic patients. This suggests that NMDA receptors are involved in auditory gating. In addition, they support other evidence that psychotic symptoms may be mediated by the glutamatergic system. In the clinical context of ketamine treatment of depression (Mathew et al. 2012), Salvadore et al. (2009, 2010) recorded MEG signals from drug-free patients diagnosed with major depression during a working memory task and in response to fearful faces. They observed a correlation between the activity estimated to originate in the anterior cingulate cortex and the antidepressant response to ketamine that was administered subsequent to the MEG recording.

Overall, the application of MEG methodology in psychopharmacological studies is important as it provides insight into the biochemistry of well-known evoked components and can lead to development of physiologically realistic and clinically relevant models of drug effects on the brain.

3 Spectral Analysis of the MEG Signals in the Frequency and Time-Frequency Domain

Rhythmic oscillation is a fundamental characteristic and an emergent property of brain activity (Buzsaki 2006). Different frequency bands have distinct neurofunctional properties and mediate different states in response to cognitive tasks (Schomer and Lopes da Silva 2010; Salmelin and Hari 1994). Neural co-oscillations are believed to reflect interactions between distant brain areas (Varela et al. 2001), making it possible to investigate oscillatory synchrony in real time and at the level of an interactive multifocal system. Numerous EEG studies have outlined effects of different psychotropic drugs on the EEG power spectrum (Saletu et al. 2002b, 2006; Mucci et al. 2006). More recently, however, MEG-based methods relying on multimodal integration and source modeling techniques have emerged, permitting investigations of the spatiotemporal characteristics of different neurofunctional systems under pharmacological challenge. Here we provide a brief overview of recent lines of research focusing on the effects of neuromodulators and an addictive substance in healthy cohorts and in patient populations using different models of MEG spectral analysis. Since a comprehensive and all-encompassing review is beyond the scope of this chapter, it merely endeavors to illustrate more recent developments and applications of MEG in neuropsychopharmacology.

3.1 Gaba

As the primary inhibitory neurotransmitter, GABA exerts widespread effects on neuronal excitability. Benzodiazepines increase GABA's inhibitory effects and are widely used in clinical settings due to their anxiolytic, anticonvulsant, and muscle relaxant properties (Trimble and Hindmarch 2000). Several MEG studies have investigated the effects of benzodiazepines on beta-band oscillations which are associated with sensorimotor neural system (Baker 2007; Neuper and Pfurtscheller 2001). Jensen and colleagues (2005) recorded MEG signal during resting with eyes closed before and after administrating a benzodiazepine to healthy volunteers. Based on the minimum current estimation approach (Uutela et al. 1999), the sources of beta band peaking at $\sim$20 Hz were estimated to be over bilateral sensorimotor cortices and were enhanced by the benzodiazepine. These results suggest that the motor cortex activity is characterized by beta oscillations during rest which are sensitive to GABAergic manipulation. In a similar paradigm, Hall et al. (2010) acquired MEG signals before and after administering a benzodiazepine to healthy controls during isometric contraction and resting with eyes closed. Using the synthetic aperture magnetometry (SAM) beamformer approach Hillebrand and Barnes (2005) confirmed that the benzodiazepine enhanced power of beta band

oscillations estimated to the motor cortex. In a subsequent study, Hall et al. (2011) investigated the nature of motor cortex sensitivity to GABAergic manipulation by recording MEG during a reaction time task and resting. Within the SAM analysis approach, Morlet-wavelet analysis revealed the timecourse of the movement-related power changes in a wide-band spectrum. The benzodiazepine increased spontaneous beta oscillations and event-related desynchronization (beta-ERD) in the motor cortex without affecting post-movement beta rebound, suggesting that GABA differentially modulates these two phenomena. Instead of administering benzodiazepine, Muthukumaraswamy et al. (2012) used tiagabine to enhance GABA modulation in a placebo-controlled, but otherwise similar experiment. Tiagabine binds with GABA reuptake transporter, resulting in increased synaptic GABA levels (Dalby 2000). They recorded MEG signals during a movement task and at regular intervals post-movement and employed the time-frequency SAM beamformer analysis (Fig. 1). Their results indicate that increased GABA results in elevated baseline beta power, augmented beta-ERD and decreased post-movement beta rebound, without affecting movement-related gamma. This study largely confirms previous findings and provides further refinement of the current understanding of the neuromodulatory basis of these two movement-related oscillatory phenomena in beta frequency range. Clinical relevance of these types of insights derives from their applicability to movement disorders such as Parkinson's since the stimulation-induced decrease of beta-band power brings symptomatic relief to patients (Brown et al. 2004).

Even though the effects of benzodiazepines are particularly evident in increased beta power over sensorimotor cortices (Jensen et al. 2005; Hall et al. 2010, 2011), they modulate oscillatory changes in other frequency bands as well. Hall et al. (2010) reported distributed power increases in alpha (7–14 Hz) and gamma (30–80 Hz) bands, as well as theta power decrease (4–7 Hz) in frontal regions. Ahveninen et al. (2007) administered a benzodiazepine drug to healthy controls in a placebo-controlled design and recorded MEG during resting with eyes open or closed. Focusing on the alpha frequency which dominates the resting spectrum, they applied a distributed minimum norm inverse estimate (Lin et al. 2004). The estimates were anatomically constrained with the realistic shape of the cortical mantle obtained from MRI scans on the same subjects (Dale et al. 2000). Benzodiazepine administration reduced power in the alpha band which was estimated to originate in the medial occipital cortex. Indeed, it has been proposed that alpha oscillations are subserved by GABAergic currents and that they play an important role in modulating attentional processing (Mazaheri and Jensen 2010). Taken together, MEG studies manipulating GABA provide important insight into the neurochemistry underlying different functional states (e.g., motor activation and rest) in healthy individuals, and can illuminate how the GABA function is altered in disease when these paradigms are applied to patient cohorts.

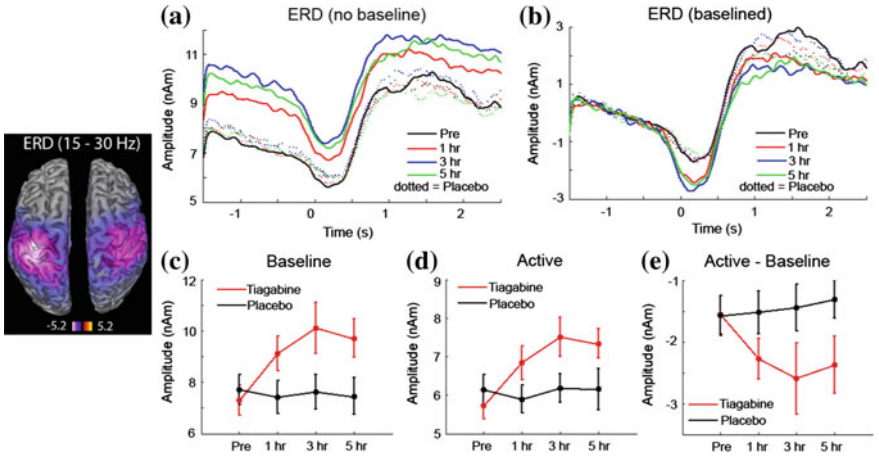

Fig. 1 *Left panel* Grand-averaged source localization of beta-ERD (15–30 Hz) with the main peak estimated to be in the left precentral gyrus (i.e., contralateral to the finger movement. Uncorrected baseline (**a**) and baseline corrected (**b**) beta (15–30 Hz) envelopes time-locked to the movement onset for the location with maximal beta-ERD as shown in the spatial map. Timecourse estimates obtained before (Pre) and 1, 3, and 5 h after administration of tiagabine or placebo are superimposed. Averaged values are plotted for the baseline period (**c**), active period (**b**) and the active–baseline difference (**e**). There was beta power increase in the baseline and a larger ERD (active–baseline) with tiagabine (Muthukumaraswamy et al. 2012, used with permission)

3.2 Acetylcholine

Acetylcholine is a major neurotransmitter in both the central and peripheral nervous systems (Picciotto et al. 2012) with regulatory effects on vigilance, attention, learning, and memory functions (Everitt and Robbins 1997; Sarter et al. 2005; Hasselmo and Sarter 2011). Its contributions to cognition have recently begun to be explored with the MEG. Bauer and colleagues (2012) examined the effects of cholinergic modulation on oscillatory brain activity during a spatial visual attention task. They administered a cholinergic agonist (physostigmine) to healthy volunteers in a placebo-controlled design. The MEG signals were analyzed with a beamformer approach within the SPM environment (Van Veen et al. 1997). Oscillations in lower (alpha and beta) frequency bands were affected by physostigmine in the visual cortex only. In contrast, gamma-band power was selectively enhanced by physostigmine in the prefrontal cortex (Fig. 2). The results suggest that the cholinergic modulation may be expressed in a regionally- and functionally-specific manner across different frequency bands with particular relevance to top-down attentional control. Given the importance of acetylcholine for cognition (Klinkenberg et al. 2011), it is essential to expand and continue this line of research in order to further delineate its functional, anatomical, and neurotransmission specificity. This may be particularly relevant to the development of novel

treatment options for dementia such as Alzheimer's disease whose pathology is linked to cholinergic transmission but which has been rather minimally responsive to the available treatment including many of the currently available cholinergic neuromodulators (Sivaprakasam 2006; Leon et al. 2013). Degeneration of the cholinergic system has been shown to characterize Parkinson's-related dementia as well (Bohnen and Albin 2011). Drugs enhancing the cholinergic function have been shown to ameliorate some of the cognitive and behavioral impairments in Parkinson's patients (Rolinski et al. 2012). Given the increasing prevalence of neurodegenerative diseases and the severity of the accompanying deterioration of cognitive abilities (WHO 2006), it is essential to intensify search for successful biomarkers and treatments (Berg 2008; Caselli et al. 2006).

3.3 Dopamine

Dopamine is associated with memory and cognition functions (Goldman-Rakic 1998; Seamans and Yang 2004) and it plays a critical role in the neural circuitry of reward and addiction (Koob and Volkow 2010). The notion that DA imbalance underlies psychotic symptoms is the basis of the "dopamine hypothesis of schizophrenia" (Curran et al. 2004; Brunelin et al. 2013) lending additional importance to the neuroimaging investigations of DA function.

Modulatory effects of DA on memory have been examined with levodopa administration in a recent pharmacological MEG study (Moran et al. 2011). Levodopa is the catecholamine precursor resulting in increased dopamine availability (Olanow 2008). Moran et al. (2011) recorded MEG signals during a working memory task as healthy volunteers participated in a placebo-controlled acute levodopa (100 mg) challenge. They applied a dynamic causal modeling (DCM) approach in the context of the macrocolumnar architecture framework (Kiebel et al. 2009; Moran et al. 2009). The observed increased theta band activity under levodopa was estimated to the superior frontal gyrus and was related to behavioral performance within the DCM model of multidimensional synaptic signaling. In a study relying on time-domain analysis, Eckart and Bunzeck (2012) acquired MEG signals and administered levodopa (150 mg) or placebo to different groups of healthy volunteers as they were shown images that differed in the degree of novelty/familiarity. Sources of the ERF averages were estimated using the Linearly Constrained Minimum Variance (LCMV) beamformer approach (Van Veen et al. 1997) within the SPM8 environment. Increased levels of DA resulted in short latency (<100 ms) novelty differences that were estimated to originate in the medial temporal lobe. The results underscore prefrontal and temporal contributions to memory as a function of DA levels. Dopaminergic transmission is impaired in Parkinson's disease, additionally giving high relevance to this type of study. MEG techniques can continue to provide insight into the basic mechanisms of the impairment as well as guidance for drug development when employed in healthy cohorts.

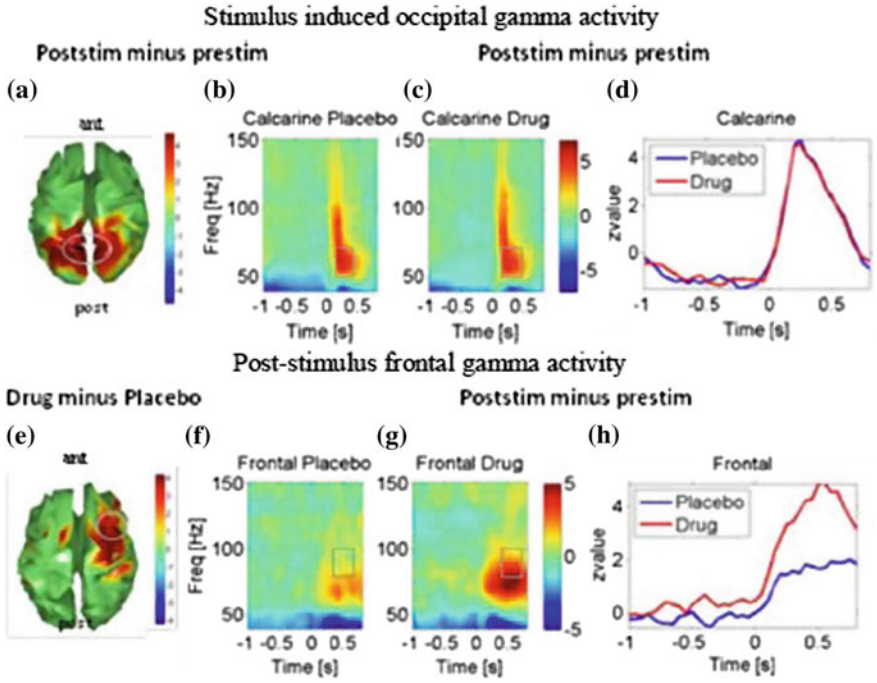

Fig. 2 **a**–**d**: Gamma activity induced by the onset of visual gratings and averaged across both hemispheres. Spatial attention was manipulated by cues indicating which hemifield to attend. **a** Stimulus-induced gamma increases for both drug and spatial attention conditions during the window marked in the time-frequency profiles are shown for the visual (peri-calcarine) cortex in **b** under placebo and in **c** under physostigmine. **d** Shows timecourses of induced 50–70 Hz gamma for the active drug and placebo conditions. **e**–**h** Induced gamma response for the frontal areas that show an enhancement by the cholinergic antagonist. **e** Topography for the statistical comparison between drug and placebo showing an increased gamma response over predominantly right frontal cortex. **f** Time-frequency profile of the response in area as marked in **e** under placebo and in **g** under physostigmine. **b** and **c** clearly show enhanced gamma-band response under physostigmine, which is confirmed with timecourses of induced 50–70 Hz gamma shown in (**h**). Values plotted are z-values for post- versus pre-stimulus power. Topography maps are thresholded at $p < 0.01$. The figure is used with permission (Bauer et al. 2012)

3.4 Parkinson's Disease

PD is a degenerative disease characterized by motor deficits mainly resulting from the loss of DAergic neurons in substantia nigra (Bergman and Deuschl 2002). In addition, there is a progressive deterioration of non-motor abilities such as cognition which seems to be caused by other neurochemical (e.g., cholinergic) deficiencies (Coelho and Ferreira 2012; Bohnen and Albin 2011). The currently available treatment aims to restore DA levels and it commonly includes dopamine agonists and precursors (e.g., levodopa) in conjunction with agents targeting other

neurotransmitter systems to mitigate cognitive dysfunction, psychotic symptoms, and treatment side-effects (Muller 2012).

MEG has been used in a series of "resting state" studies investigating oscillatory activity in PD patients across the span of the disease and as a function of dopaminomimetic and cholinomimetic therapy. Bosboom, Stoffers, and colleagues (Bosboom et al. 2006, 2009a, b; Stoffers et al. 2007, 2008a, b) recorded MEG signals during "eyes closed" resting state from groups of PD patients in their early or late disease stages as well as from healthy controls. The data were analyzed in sensor space with wideband spectral signal decomposition. Evidence from their group, as well as other groups consistently showed diffuse slowing of resting oscillatory activity in Parkinson's patients with and without dementia symptoms (Bosboom et al. 2006; Stoffers et al. 2007; Kotini et al. 2005; Vardy et al. 2011). A longitudinal study revealed that this slowing worsens over time and is related to cognitive decline, but in a manner that is independent of aging effects (Olde Dubbelink et al. 2013). Furthermore, even untreated de novo PD patients showed significant slowing of the resting oscillatory activity that was expressed as a global power increase in the low frequency (<10 Hz) range and a loss of gamma power. These effects were not related to disease stage, duration, or other clinical indices and were only slightly affected by acute administration of dopaminomimetic medication (Stoffers et al. 2007). In contrast, cholinomimetic medication resulted in a shift towards faster frequencies, partially restoring the oscillatory deficit observed in PD patients (Bosboom et al. 2009a). Stoffers et al. (2007) interpreted these observations as evidence against a major role of the DA system in subserving the resting state brain oscillations in PD. Instead, they argue that other neurotransmitter systems including the cholinergic, noradrenergic, and serotonergic systems are involved in oscillatory alterations observed in PD (Bosboom et al. 2003; Brooks 2007). In another study, Stoffers et al. (2008a) examined functional connectivity in patients with PD and healthy controls by calculating temporal correlation between MEG epochs recorded during eyes-closed rest across pairs of sensors topographically grouped into regions of interest (Stam et al. 2002). Compared to healthy controls, PD patients exhibited increased levels of connectivity, which was related to motor symptoms (Stoffers et al. 2008a). Acute administration of dopaminomimetic medications increased the functional connectivity even further, which correlated with improved motor symptoms (Stoffers et al. 2008b).

A study by Pollok et al. (2009) investigated the effects of levodopa on functional connectivity during the parkinsonian resting tremor. They recorded MEG and EMG signals simultaneously from PD patients in their "off-medication" state (i.e., after overnight medication withdrawal) and immediately after an application of a fast-acting levodopa during rest. They examined cerebro-muscular and cerebro-cerebral coherence and applied the Dynamic Imaging of Coherent Sources (DICS) beamforming method (Gross et al. 2001) to estimate the MEG signal sources. The medication reduced the coupling strength within a thalamo-premotor/motor network at 8–12 Hz range, and was accompanied by a decrease in tremor and cerebro-muscular coherence. These results are taken as evidence of the drug-

induced restoration of a normal functional interaction between the cortical and motor cortical regions.

In the clinical context of deep brain stimulation treatment for PD, Litvak and colleagues investigated the role of the basal ganglia and their functional connectivity with cortical areas in a series of multimodal imaging studies. They acquired MEG signals simultaneously with intracranial EEG (iEEG) recorded with depth electrodes implanted in the subthalamic nucleus (STN) (Litvak et al. 2011, 2012; Oswal et al. 2013). One study examined oscillatory synchronization between the signal in the basal ganglia and in cortical networks during resting with eyes open (Litvak et al. 2011). The coherence was estimated with Dynamic Imaging of Coherent Sources (DICS) beamforming method (Gross et al. 2001). A frontal network co-oscillated with the STN in the beta frequency range, whereas the network estimated to be in the temporoparietal area and the brainstem co-oscillated with the STN in alpha band. Acute effects of dopaminomimetic medications were examined by comparing the recording obtained after overnight medication withdrawal (OFF state) and after the usual dosage (ON state). The medication effects were expressed as an increase in beta coherence between the prefrontal cortex and STN. In another study, Litvak and colleagues used the same clinical setup and obtained simultaneous MEG and iEEG recordings during a finger movement task (Litvak et al. 2012). They examined movement-related oscillations estimated to originate in the motor cortex and those recorded from STN and their coherence in PD patients. Power and coherence in the gamma frequency range increased during movement and the increase was more pronounced during the ON state. Furthermore, the medication-induced increase in gamma co-oscillations at 60–90 Hz around the movement correlated with the improvement in motor symptoms, indicating their facilitatory modulation of motor activity. A companion study based on the same cohort and using the same paradigm reported effects in the alpha band that were complementary to the gamma power and coherence (Fig. 3) (Oswal et al. 2013). The coherence between the MEG-recorded alpha oscillations estimated to the right temporal cortex and the alpha in the STN was reduced after movement, particularly in the ON—medication state. Alpha suppression that preceded movement was unaffected by the medication state.

Overall, this type of research can provide essential insight into the neurophysiology of neural disorders and can track the effects of different pharmacological treatments in a spatially- and temporally sensitive way. The rare opportunity to obtain combined MEG and iEEG data is particularly valuable for developing neurophysiologically realistic models of the basic mechanisms underlying motor and cognitive impairments and their sensitivity to pharmacological intervention. In this particular case, simultaneous recordings from the STN and the MEG estimates of cortical activity are especially advantageous for understanding the cortico-subcortical network and its sensitivity to pharmacological modulation in PD patients. In general, studies of patient populations are important for delineating biomarkers of the general and idiosyncratic features of the disease, for predicting treatment efficacy, and for guiding treatment development.

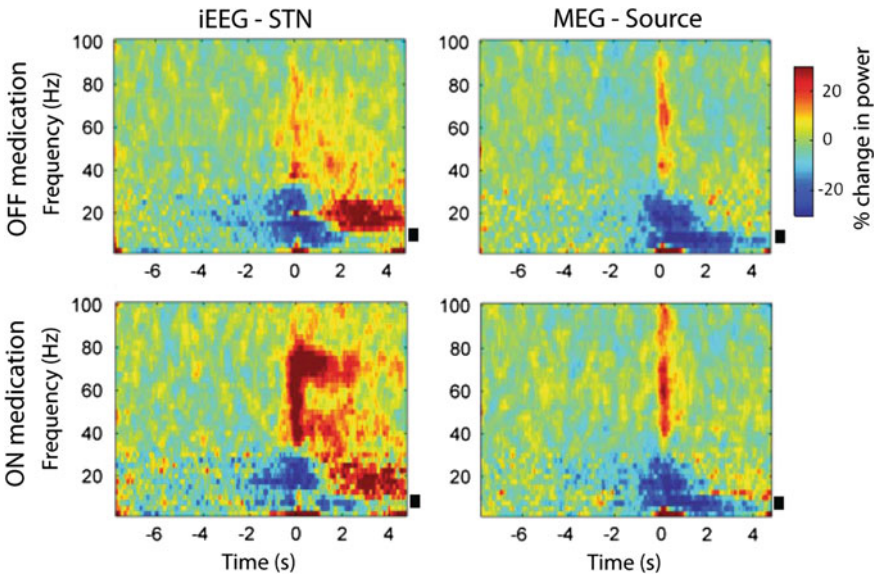

Fig. 3 Time-frequency images of power averaged across subjects for the STN (*left column*) and the right superior temporal MEG source (*right column*) during OFF medication (*top row*) and ON medication state (*bottom row*), recorded contralateral to movement. Power changes are expressed as percentage change calculated with respect to the baseline period from −8 to −5 s prior to movement. There is a beta desynchronization with onset prior to movement and gamma power increase upon movement. Gamma power increase is more marked ON medication. For the STN contacts, there was a significant reduction in alpha power from about 2 s before movement in both drug conditions. The *black bars* indicate alpha band frequencies between 7 and 13 Hz. Used with permission (Oswal et al. 2013)

3.5 Attention Deficit Hyperactivity Disorder (ADHD)

ADHD is one of the most common neurobehavioral developmental disorders affecting ∼5–7 % of children and persisting into adulthood (Willcutt 2012). It is characterized by hyperactivity which is particularly prevalent in children, whereas inattention and executive impairments are observed across the life span (Seidman 2006). Evidence from studies using MRI and EEG methods indicates structural and functional aberrations in individuals with ADHD (Cubillo et al. 2012; Cherkasova and Hechtman 2009; Barry et al. 2003). ADHD is successfully treated with stimulants such as methylphenidate (MPH) and amphetamine (AMP) which are particularly beneficial for immediate symptom relief (Bitter et al. 2012; Wilens et al. 2011), but nonstimulants and antidepressants are also prescribed (Wilens 2006). Both AMP and MPH increase DA synaptic availability but act at different points of the DA release and reuptake sequence (Heal et al. 2012; Challman and Lipsky 2000). They also modulate norepinephrine though to a lesser degree.

In an early MEG study investigating the effects of MPH treatment on resting state activity, Wienbruch et al. (2005) recorded MEG signals from a group of children diagnosed with ADHD. They performed a spectral analysis in sensor space before and after administering MPH and observed an increase in theta power over the left frontal region which correlated with improved scores on a test of attention. The authors suggested that the MPH renders its behavioral effects by increasing motor inhibition in ADHD patients.

In a recent series of studies, Wilson and colleagues (Franzen and Wilson 2012; Wilson et al. 2012, 2013) have explored the neural basis of ADHD, as well as the mechanisms underlying AMP treatment. They recorded MEG signals from adult individuals diagnosed with ADHD in the OFF-medication state (i.e., ~24 h after the last dose), and again after their regular stimulant medication intake (i.e., ON state). This paradigm allowed them to compare neural activity between the ADHD patients and healthy controls in addition to examining effects of AMP. They analyzed the MEG data in the frequency domain and estimated signal sources with a beamformer approach (Van Veen et al. 1997). One study (Wilson et al. 2013) examined broadband oscillations within the Default Mode Network (DMN) (Raichle et al. 2001) during rest. The principal finding was a globally-reduced wide-band power in unmedicated ADHD patients compared to controls in a higher frequency range (i.e., 14–228 Hz) that was estimated to originate in the medial prefrontal region. The only effect of medication was increased alpha power in the medial prefrontal area (Wilson et al. 2013). Another study (Wilson et al. 2012) investigated the neural basis of gamma activity induced by auditory stimuli in adults with ADHD before and after medication administration and in a control cohort. Binaural click trains presented at 40 Hz induced 40-Hz gamma activity estimated to bilateral auditory cortices. The gamma power was significantly attenuated in ADHD patients compared to control participants. However, administration of a regular dose of the AMP-based medication resulted in a significant increase in gamma activity in ADHD patients (Fig. 4). These results suggest that the commonly prescribed stimulant medication normalizes neural activity in response to auditory 40 Hz stimulation. The authors speculated that abnormalities in GABAergic transmission may underlie abnormally low responsivity in ADHD patients in the off-medication state. By the same token, they propose that the beneficial effects of the amphetamine-based medication derive from its modulation of GABAergic circuitry (Wilson et al. 2012).

Employing an auditory oddball paradigm with frequent and target tones, Franzen and Wilson (2012) recorded MEG signals from adult ADHD patients before and after administering a standard dosage of amphetamine salts medication. They again focused on the event-related gamma response (68–88 Hz) which was desynchronized relative to baseline in the off-medication state and was estimated to the medial prefrontal region. The stimulant medication attenuated gamma desynchronization. These results suggest that the ADHD symptomatology may be due in part to impaired coactivation of distributed cortical circuitry that underlies cognitive processes (Uhlhaas et al. 2009). This line of research illustrates the MEG

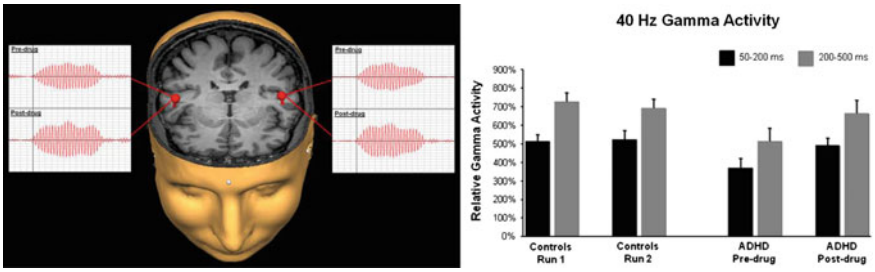

Fig. 4 *Left panel* Generators of the 40 Hz gamma activity were estimated to the auditory cortices and overlaid onto a 3D rendition of a representative ADHD subject. The source time series (nAm) from each session (pre-drug and post-drug) show the stimulus onset (*vertical line*) and the 40-Hz gamma response that is stronger after stimulant administration. *Right panel* Group means of gamma activity. Unmedicated adults with ADHD exhibited significantly less gamma activity relative to their healthy peers during the standard 200–500 ms time window (*grey*), and during an earlier window from 50–200 ms post-stimulus (*black*). The administration of amphetamine significantly increased gamma activity in participants with ADHD during both time windows, and the magnitude of this increase eliminated group statistical differences in Run 2 (ON drug). Control subjects showed no significant effects from Run 1 to Run 2. These data indicate that stimulant medication may modulate cortical gamma activation in adults with ADHD. On the y-axis, gamma activity is shown in normalized unit relative to a −200 to 0 ms pre-stimulus period (Wilson et al. 2012, used with permission)

contributions to a better understanding of the basic mechanisms underlying the ADHD disorder and the neural basis of the effects of a successful therapeutic intervention.

3.6 Epilepsy and Anesthesia

Sophisticated models of the MEG signal source analysis have played a crucial role in the non-invasive functional localization of epileptogenic zones. They have assisted in guiding surgical evaluations and treatment, especially benefitting patients with pharmacoresistant epilepsy (Bagic et al. 2009; Funke et al. 2009; Rampp and Stefan 2007). The MEG is particularly helpful in diagnosing neocortical epilepsy, outlining the eloquent cortex and lesional zones, which is crucial for guiding surgical resections (Baumgartner and Pataraia 2006; Pirmoradi et al. 2010; Stufflebeam 2011; Makela et al. 2006). The debate on the relative advantages of the MEG versus EEG notwithstanding (Barkley 2004; Baumgartner 2004), the two methods provide complementary information, as the MEG is a valuable tool that can furnish unique information in certain clinical cases and guide clinical decisions (Lesser 2004; Cappell et al. 2006). In the context of pharmacological MEG applications, several studies have indicated that anesthesia improves immobility and maintains or even increases rates of the detection of epileptiform activity (Balakrishnan et al. 2007; Stefan et al. 2010). This protocol

has been useful in pediatric seizure patients (Fujimoto et al. 2009; Konig et al. 2009) particularly at lower doses and with certain combinations of anesthetic agents (Szmuk et al. 2003). In addition to the studies of anesthesia in the clinical context, the MEG technique could potentially be instrumental in investigating different levels of consciousness as a function of anesthetic dosage. It could contribute to the evidence obtained with other neuroimaging techniques concerning the neural basis of consciousness and the functional connectivity from which it presumably emerges (Nallasamy and Tsao 2011).

3.7 Alcohol Intoxication

As the most common drug of abuse and a "gateway" to drug addiction, alcohol exerts a costly burden on the society (Kirby and Barry 2012; Bouchery et al. 2011). Although alcohol intoxication affects functioning at multiple levels of the neuraxis, executive abilities in situations of increased complexity and novelty are particularly disrupted (Koelega 1995; Marinković et al. 2001; Ridderinkhof et al. 2002). Alcohol may interfere with cognitive assessment of novel cues and the capacity to inhibit impulsive responses. These impairments may contribute to the socially important effects of acute intoxication such as traffic- or work-related hazards and violence (CDCP 2011; Kuhns et al. 2011). Most of the MEG studies investigating acute effects of alcohol intoxication on brain function focused on ERFs during sensory and cognitive tasks, as well as spontaneous oscillations during rest. This evidence has been included in the excellent and comprehensive reviews of the pharmacological MEG literature (Kenemans and Kahkonen 2011; Kahkonen 2005, 2006). More recently, our group has carried out a series of crossover alcohol challenge studies using an anatomically-constrained MEG approach which combines distributed source modeling with structural MRI yielding estimated maps of oscillatory activity estimates across time (Dale et al. 2000). In a study investigating cognitive control, healthy volunteers performed the Stroop task under moderately low alcohol and placebo conditions (Kovacevic et al. 2012). Acute intoxication selectively affected event-related theta power in the anterior cingulate cortex (ACC) during the high conflict, incongruous condition (Fig. 5). Spatial estimates were in concordance with fMRI-based observations of the ACC importance for conflict processing (Marinković et al. 2012a; Botvinick 2007; Carter and van Veen 2007). The results indicate that the top-down regulatory capacity is selectively vulnerable to alcohol intoxication during conditions that necessitate cognitive control. This evidence supports the view that impaired self-control may underlie the development of alcohol abuse via its effects on the ability to refrain from drinking (Field et al. 2010; Finn 2000; Lyvers 2000).

Another experiment manipulated lexical-semantic retrieval in a visual lexical decision task in healthy participants who took part in both placebo, and alcohol conditions (Marinković et al. 2012b). Event-related theta source power to standard words (SW) and pseudowords (PW), meaningless but word-like pronounceable

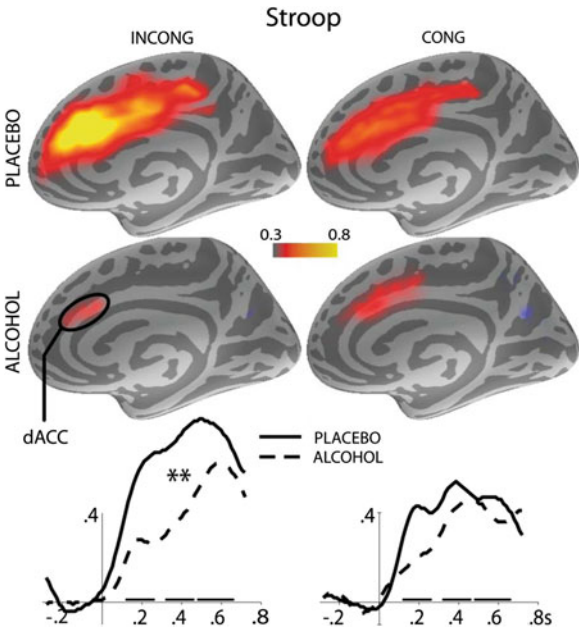

Fig. 5 Group-averaged maps of event-related theta source power estimates in the 320–470 ms time window after word onset under placebo (*top row*) and alcohol conditions (*middle row*). The color scale depicts baseline-corrected noise-normalized source power. *Bottom row* timecourses were estimated to originate in the dorsal anterior cingulate cortex (*dACC*), the strongest source of theta power which was particularly sensitive to conflict. The estimated activity to incongruous (INCONG, high conflict) trials is shown in the *left column* and the activity to congruous (CONG, low conflict) trials in the *right column*. Alcohol may interfere with goal-directed behavior by affecting decision-making, which results in poor self-control (Kovacevic et al. 2012, used with permission)

letter strings, was estimated with the anatomically-constrained MEG approach. Theta oscillations were particularly sensitive to lexical-semantic retrieval (Fig. 6). In contrast to the N400 which is usually larger to PW as it reflects *attempts* to access and integrate a semantic representation into the current context (Halgren 1990; Holcomb et al. 2002; Kutas and Federmeier 2011), theta power was larger to SW. This indicates that theta may be uniquely sensitive to the *outcome* of lexical-semantic retrieval of word meaning, consistent with its engagement in memory (Klimesch et al. 2001). This finding suggests that this measure is well suited for investigating the neural basis of language. Alcohol specifically affected semantic retrieval since it reduced theta to real words but not pseudowords that carry no meaning. This type of study can delineate the neural circuits affected by acute intoxication. In concert with studies on chronic alcoholics and populations at risk, they can help parse out the effects of alcohol neurotoxicity, genetic susceptibility, and environmental factors in vulnerability to addiction. This research could also be

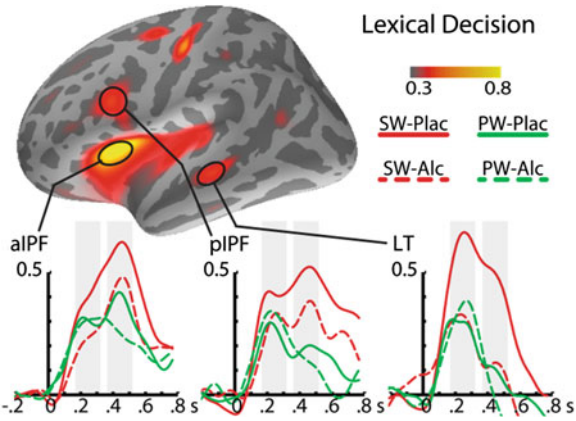

Fig. 6 Group-averaged map of baseline-corrected event-related theta source power estimates in the left hemisphere to standard words (*SW*) in the 370–520 ms time window (*top row*). Group averaged timecourses of theta estimates to SW and pseudowords (*PW*) for alcohol and placebo conditions are shown below for the lateral temporal (*LT*), anteroventral inferior prefrontal cortex bordering the insula (*aIPF*), and posterolateral inferior prefrontal cortex (*pIPF*). Theta power is sensitive to semantic retrieval as indicated by stronger theta to SW compared to PW. Alcohol attenuated only theta to SW, suggesting that it specifically affects lexical-semantic retrieval and not other aspects of verbal processing (Marinković et al. 2012b, used with permission)

relevant to legislative and preventive initiatives regarding driving and it could potentially inform and guide pharmacological research on possible agents that might diminish alcohol's effects by targeting the relevant circuits.

4 Conclusion

Recent developments in MEG methodology that rely on sophisticated source modeling algorithms and multimodal integration have been successfully used to study brain activity in response to pharmacological agents. In many such studies psychotropic medications are administered to healthy volunteers in an effort to delineate the spatiotemporal characteristics of their effects on different neurofunctional systems. This chapter provides a brief overview of studies primarily focusing on the spontaneous and task-related MEG oscillatory activity. This includes pharmacological manipulations of GABA, acetylcholine, and dopamine neurotransmitter systems during resting, motor activity, attention, and memory. Such studies provide important insights into the neurochemistry underlying different functional states. They have also begun to delineate the neuroanatomical specificity of drug effects as they are expressed in a regionally- and functionally-specific manner across different frequency bands. Other lines of research have examined neural responses to alcohol intoxication during cognitive tasks and the

effects of pharmacological interventions in the clinical context of neuropsychiatric disorders including ADHD and Parkinson's disease, as well as the effects of anesthesia administered to epilepsy patients. This type of MEG application can provide essential insight into the basic mechanisms underlying motor and cognitive impairments accompanying neural disorders and can track the effects of drugs in spatially- and temporally-sensitive ways. It can estimate where the drug-induced changes are occurring and elucidate the temporal sequence of the involved neural components. Furthermore, analyses of co-oscillatory activity can estimate the neural underpinnings of the pharmacological effects on the brain in real time and at the level of an interactive multifocal system. Future clinical MEG applications in patient cohorts hold high promise in delineating biomarkers of the general and idiosyncratic features of the disease, for predicting treatment efficacy, and for guiding treatment development.

Acknowledgments I am grateful to the National Institutes of Health (R01AA016624) for their continued support and to Burke Rosen and Sanja Kovacevic for their kind assistance.

References

Ahveninen J, Lin FH, Kivisaari R, Autti T, Hämäläinen M, Stufflebeam S, Belliveau JW, Kahkonen S (2007) MRI-constrained spectral imaging of benzodiazepine modulation of spontaneous neuromagnetic activity in human cortex. Neuroimage 35(2):577–582

Ametamey SM, Honer M (2007) Pharmacological prerequisites for PET ligands and practical issues in preclinical PET research. PET Chemistry 62:317–327

Atkinson AJ Jr, Colburn WA, DeGruttola VG, DeMets DL, Downing GJ, Hoth DF, Oates JA, Peck CC, Schooley RT, Spilker BA, Woodcock J, Zeger SL (2001) Biomarkers and surrogate endpoints: preferred definitions and conceptual framework. Clin Pharmacol Ther 69(3):89–95

Bagic A, Funke ME, Ebersole J (2009) American Clinical MEG Society (ACMEGS) position statement: the value of magnetoencephalography (MEG)/magnetic source imaging (MSI) in noninvasive presurgical evaluation of patients with medically intractable localization-related epilepsy. J Clin Neurophysiol 26(4):290–293

Baker SN (2007) Oscillatory interactions between sensorimotor cortex and the periphery. Curr Opin Neurobiol 17(6):649–655

Balakrishnan G, Grover KM, Mason K, Smith B, Barkley GL, Tepley N, Bowyer SM (2007) A retrospective analysis of the effect of general anesthetics on the successful detection of interictal epileptiform activity in magnetoencephalography. Anesth Analg 104(6):1493–1497

Barkley GL (2004) Controversies in neurophysiology. MEG is superior to EEG in localization of interictal epileptiform activity: Pro. Clin Neurophysiol 115(5):1001–1009

Barry RJ, Clarke AR, Johnstone SJ (2003) A review of electrophysiology in attention-deficit/hyperactivity disorder: I. Qualitative and quantitative electroencephalography. Clin Neurophysiol 114(2):171–183

Bass JK, Bornemann TH, Burkey M, Chehil S, Chen L, Copeland JR, Eaton WW, Ganju V, Hayward E, Hock RS, Kidwai R, Kolappa K, Lee PT, Minas H, Or F, Raviola GJ, Saraceno B, Patel V (2012) A united nations general assembly special session for mental, neurological, and substance use disorders: the time has come. PLoS Med 9(1):e1001159

Bauer M, Kluge C, Bach D, Bradbury D, Heinze HJ, Dolan RJ, Driver J (2012) Cholinergic enhancement of visual attention and neural oscillations in the human brain. Curr Biol 22(5):397–402

Baumgartner C (2004) Controversies in clinical neurophysiology. MEG is superior to EEG in the localization of interictal epileptiform activity: Con. Clin Neurophysiol 115(5):1010–1020
Baumgartner C, Pataraia E (2006) Revisiting the role of magnetoencephalography in epilepsy. Curr Opin Neurol 19(2):181–186
Berg D (2008) Biomarkers for the early detection of Parkinson's and Alzheimer's disease. Neurodegenerative Dis 5(3–4):133–136
Bergman H, Deuschl G (2002) Pathophysiology of Parkinson's disease: from clinical neurology to basic neuroscience and back. Mov Disord 17(Suppl 3):S28–S40
Bitter I, Angyalosi A, Czobor P (2012) Pharmacological treatment of adult ADHD. Curr Opin Psychiatry 25(6):529–534
Boeijinga PH, Soufflet L, Santoro F, Luthringer R (2007) Ketamine effects on CNS responses assessed with MEG/EEG in a passive auditory sensory-gating paradigm: An attempt for modelling some symptoms of psychosis in man. J Psychopharmacol 21(3):321–337
Bohnen NI, Albin RL (2011) The cholinergic system and Parkinson disease. Behav Brain Res 221(2):564–573
Borsook D, Beccera LR, Bullmore ET, Hargreaves RJ (eds) (2009) Imaging in CNS drug discovery and development: implications for disease and therapy. Springer, New York
Borsook D, Hargreaves R, Becerra L (2011) Can functional magnetic resonance imaging improve success rates in CNS drug discovery? Expert Opin Drug Discov 6(6):597–617
Bosboom JL, Stoffers D, Stam CJ, Berendse HW, Wolters E (2009a) Cholinergic modulation of MEG resting-state oscillatory activity in Parkinson's disease related dementia. Clin Neurophysiol 120(5):910–915
Bosboom JL, Stoffers D, Stam CJ, van Dijk BW, Verbunt J, Berendse HW, Wolters E (2006) Resting state oscillatory brain dynamics in Parkinson's disease: an MEG study. Clin Neurophysiol 117(11):2521–2531
Bosboom JL, Stoffers D, Wolters E (2003) The role of acetylcholine and dopamine in dementia and psychosis in Parkinson's disease. J Neural Transm Suppl 65:185–195
Bosboom JL, Stoffers D, Wolters E, Stam CJ, Berendse HW (2009b) MEG resting state functional connectivity in Parkinson's disease related dementia. J Neural Transm 116(2):193–202
Botvinick MM (2007) Conflict monitoring and decision making: Reconciling two perspectives on anterior cingulate function. Cogn Affect Behav Neurosci 7(4):356–366
Bouchery EE, Harwood HJ, Sacks JJ, Simon CJ, Brewer RD (2011) Economic costs of excessive alcohol consumption in the U.S., 2006. Am J Prev Med 41(5):516–524
Brooks DJ (2007) Imaging non-dopaminergic function in Parkinson's disease. Mol Imag Biol 9(4):217–222
Brown P, Mazzone P, Oliviero A, Altibrandi MG, Pilato F, Tonali PA, Di Lazzaro V (2004) Effects of stimulation of the subthalamic area on oscillatory pallidal activity in Parkinson's disease. Exp Neurol 188(2):480–490
Brunelin J, Fecteau S, Suaud-Chagny MF (2013) Abnormal striatal dopamine transmission in schizophrenia. Curr Med Chem 20(3):397–404
Buxton RB (2002) Introduction to functional magnetic resonance imaging. Cambridge University Press, New York
Buzsaki G (2006) Rhythms of the brain. Oxford University Press, New York
Cadenhead KS (2002) Vulnerability markers in the schizophrenia spectrum: Implications for phenomenology, genetics, and the identification of the schizophrenia prodrome. Psychiatr Clin North Am 25(4):837–853
Cappell J, Schevon C, Emerson RG (2006) Magnetoencephalography in epilepsy: tailoring interpretation and making inferences. Curr Neurol Neurosci Rep 6(4):327–331
Carter CS, van Veen V (2007) Anterior cingulate cortex and conflict detection: an update of theory and data. Cogn Affect Behav Neurosci 7(4):367–379
Caselli RJ, Beach TG, Yaari R, Reiman EM (2006) Alzheimer's disease a century later. J Clin Psychiatry 67(11):1784–1800

CDCP (2011) Vital signs: alcohol-impaired driving among adults–United States, 2010. Morb Mortal Wkly Rep 60(39):1351–1356
Challman TD, Lipsky JJ (2000) Methylphenidate: its pharmacology and uses. Mayo Clin Proc 75(7):711–721
Cherkasova MV, Hechtman L (2009) Neuroimaging in attention-deficit hyperactivity disorder: Beyond the frontostriatal circuitry. Can J Psychiatry 54(10):651–664
Coelho M, Ferreira JJ (2012) Late-stage Parkinson disease. Nat Rev Neurol 8(8):435–442
Cubillo A, Halari R, Smith A, Taylor E, Rubia K (2012) A review of fronto-striatal and fronto-cortical brain abnormalities in children and adults with attention deficit hyperactivity disorder (ADHD) and new evidence for dysfunction in adults with ADHD during motivation and attention. Cortex 48(2):194–215
Curran C, Byrappa N, McBride A (2004) Stimulant psychosis: systematic review. Br J Psychiatry 185:196–204
Dager SR, Corrigan NM, Richards TL, Posse S (2008) Research applications of magnetic resonance spectroscopy to investigate psychiatric disorders. Top Magn Reson Imaging 19(2):81–96
Dalby NO (2000) GABA-level increasing and anticonvulsant effects of three different GABA uptake inhibitors. Neuropharmacology 39(12):2399–2407
Dale AM, Liu AK, Fischl BR, Buckner RL, Belliveau JW, Lewine JD, Halgren E (2000) Dynamic statistical parametric mapping: Combining fMRI and MEG for high-resolution imaging of cortical activity. Neuron 26(1):55–67
Dieterle F, Marrer E (2008) New technologies around biomarkers and their interplay with drug development. Anal Bioanal Chem 390(1):141–154
Eckart C, Bunzeck N (2012) Dopamine modulates processing speed in the human mesolimbic system. Neuroimage 66C:293–300
Everitt BJ, Robbins TW (1997) Central cholinergic systems and cognition. Annu Rev Psychol 48:649–684
Field M, Wiers RW, Christiansen P, Fillmore MT, Verster JC (2010) Acute alcohol effects on inhibitory control and implicit cognition: implications for loss of control over drinking. Alcohol Clin Exp Res 34(8):1346–1352
Finn P (2000) Acute effects of alcohol on cognition and impulsive-disinhibited behavior. In: Noronha A, Eckardt M, Warren K (eds) Review of NIAAA's neuroscience and behavioral research portfolio, vol 34., US Department of Health and Human ServicesBethesda, MD, pp 337–356
Franzen JD, Wilson TW (2012) Amphetamines modulate prefrontal gamma oscillations during attention processing. NeuroReport 23(12):731–735
Fujimoto A, Ochi A, Imai K, Chan D, Sharma R, Viljoen A, Chu B, Holowka S, Kemp SM, Chuang SH, Matsumura A, Ayuzawa S, Snead OC 3rd, Otsubo H (2009) Magnetoencephalography using total intravenous anesthesia in pediatric patients with intractable epilepsy: Lesional vs nonlesional epilepsy. Brain Dev 31(1):34–41
Funke M, Constantino T, Van Orman C, Rodin E (2009) Magnetoencephalography and magnetic source imaging in epilepsy. Clin EEG Neurosci 40(4):271–280
Goldman-Rakic PS (1998) The cortical dopamine system: role in memory and cognition. Adv Pharmacol 42:707–711
Gross J, Kujala J, Hämäläinen M, Timmermann L, Schnitzler A, Salmelin R (2001) Dynamic imaging of coherent sources: studying neural interactions in the human brain. Proc Nat Acad Sci USA 98(2):694–699
Gunduz-Bruce H (2009) The acute effects of NMDA antagonism: from the rodent to the human brain. Brain Res Rev 60(2):279–286
Halgren E (1990) Insights from evoked potentials into the neuropsychological mechanisms of reading. In: Scheibel AB, Wechsler AF (eds) Neurobiology of higher cognitive function. Guilford, New York, pp 103–150

Hall SD, Barnes GR, Furlong PL, Seri S, Hillebrand A (2010) Neuronal network pharmacodynamics of GABAergic modulation in the human cortex determined using pharmacomagnetoencephalography. Hum Brain Mapp 31(4):581–594

Hall SD, Stanford IM, Yamawaki N, McAllister CJ, Ronnqvist KC, Woodhall GL, Furlong PL (2011) The role of GABAergic modulation in motor function related neuronal network activity. NeuroImage 56(3):1506–1510

Hämäläinen M, Hari R, Ilmoniemi RJ, Knuutila J, Lounasmaa OV (1993) Magnetoencephalography—theory, instrumentation, and applications to noninvasive studies of the working human brain. Rev Mod Phys 65(2):413–497

Hasselmo ME, Sarter M (2011) Modes and models of forebrain cholinergic neuromodulation of cognition. Neuropsychopharmacology 36(1):52–73

Heal DJ, Smith SL, Findling RL (2012) ADHD: Current and future therapeutics. Curr Top Behav Neurosci 9:361–390

Hillebrand A, Barnes GR (2005) Beamformer analysis of MEG data. Int Rev Neurobiol 68:149–171

Holcomb PJ, Grainger J, O'Rourke T (2002) An electrophysiological study of the effects of orthographic neighborhood size on printed word perception. J Cogn Neurosci 14(6):938–950

Honey G, Bullmore E (2004) Human pharmacological MRI. Trends Pharmacol Sci 25(7):366–374

Honig P, Lalonde R (2010) The economics of drug development: a grim reality and a role for clinical pharmacology. Clin Pharmacol Ther 87(3):247–251

Javitt DC, Spencer KM, Thaker GK, Winterer G, Hajos M (2008) Neurophysiological biomarkers for drug development in schizophrenia. Nat Rev Drug Discovery 7(1):68–83

Jensen O, Goel P, Kopell N, Pohja M, Hari R, Ermentrout B (2005) On the human sensorimotor-cortex beta rhythm: sources and modeling. Neuroimage 26(2):347–355

Kahkonen S (2005) MEG and TMS combined with EEG for mapping alcohol effects. Alcohol 37(3):129–133

Kahkonen S (2006) Magnetoencephalography (MEG): a non-invasive tool for studying cortical effects in psychopharmacology. Int J Neuropsychopharmacol 9(3):367–372

Kahkonen S, Ahveninen J (2002) Combination of magneto- and electroencephalography in studies of monoamine modulation on attention. Methods Find Exp Clin Pharmacol 24(Suppl C):27–34

Kenemans JL, Kahkonen S (2011) How human electrophysiology informs psychopharmacology: from bottom-up driven processing to top-down control. Neuropsychopharmacology 36(1):26–51

Kiebel SJ, Garrido MI, Moran R, Chen CC, Friston KJ (2009) Dynamic causal modeling for EEG and MEG. Hum Brain Mapp 30(6):1866–1876

Kirby T, Barry AE (2012) Alcohol as a gateway drug: a study of US 12th graders. J Sch Health 82(8):371–379

Klimesch W, Doppelmayr M, Stadler W, Pollhuber D, Sauseng P, Rohm D (2001) Episodic retrieval is reflected by a process specific increase in human electroencephalographic theta activity. Neurosci Lett 302(1):49–52

Klinkenberg I, Sambeth A, Blokland A (2011) Acetylcholine and attention. Behav Brain Res 221(2):430–442

Koelega HS (1995) Alcohol and vigilance performance: a review. Psychopharmacology 118(3):233–249

Konig MW, Mahmoud MA, Fujiwara H, Hemasilpin N, Lee KH, Rose DF (2009) Influence of anesthetic management on quality of magnetoencephalography scan data in pediatric patients: a case series. Paediatr Anaesth 19(5):507–512

Koob GF, Volkow ND (2010) Neurocircuitry of addiction. Neuropsychopharmacology 35(1):217–238

Korostenskaja M, Kahkonen S (2009) What do ERPs and ERFs reveal about the effect of antipsychotic treatment on cognition in schizophrenia? Curr Pharm Des 15(22):2573–2593

Korostenskaja M, Kicic D, Kahkonen S (2008) The effect of methylphenidate on auditory information processing in healthy volunteers: a combined EEG/MEG study. Psychopharmacology (Berlin) 197(3):475–486

Kotini A, Anninos P, Adamopoulos A, Prassopoulos P (2005) Low-frequency MEG activity and MRI evaluation in Parkinson's disease. Brain Topogr 18(1):59–63

Kovacevic S, Azma S, Irimia A, Sherfey J, Halgren E, Marinković K (2012) Theta oscillations are sensitive to both early and late conflict processing stages: effects of alcohol intoxication. PLoS ONE 7(8):e43957

Kuhns JB, Wilson DB, Clodfelter TA, Maguire ER, Ainsworth SA (2011) A meta-analysis of alcohol toxicology study findings among homicide victims. Addiction 106(1):62–72

Kutas M, Federmeier KD (2011) Thirty years and counting: finding meaning in the N400 component of the event-related brain potential (ERP). Annu Rev Psychol 62:621–647

Lanni C, Lenzken SC, Pascale A, Del Vecchio I, Racchi M, Pistoia F, Govoni S (2008) Cognition enhancers between treating and doping the mind. Pharmacol Res 57(3):196–213

Leiser SC, Dunlop J, Bowlby MR, Devilbiss DM (2011) Aligning strategies for using EEG as a surrogate biomarker: a review of preclinical and clinical research. Biochem Pharmacol 81(12):1408–1421

Leon R, Garcia AG, Marco-Contelles J (2013) Recent advances in the multitarget-directed ligands approach for the treatment of Alzheimer's disease. Med Res Rev 33(1):139–189

Lesko LJ, Atkinson AJ Jr (2001) Use of biomarkers and surrogate endpoints in drug development and regulatory decision making: criteria, validation, strategies. Ann Rev Pharmacol Toxicol 41:347–366

Lesser RP (2004) MEG: good enough. Clin Neurophysiol 115(5):995–997

Leung S, Croft RJ, Baldeweg T, Nathan PJ (2007) Acute dopamine D(1) and D(2) receptor stimulation does not modulate mismatch negativity (MMN) in healthy human subjects. Psychopharmacology 194(4):443–451

Lin FH, Witzel T, Hämäläinen MS, Dale AM, Belliveau JW, Stufflebeam SM (2004) Spectral spatiotemporal imaging of cortical oscillations and interactions in the human brain. Neuroimage 23(2):582–595

Litvak V, Eusebio A, Jha A, Oostenveld R, Barnes G, Foltynie T, Limousin P, Zrinzo L, Hariz MI, Friston K, Brown P (2012) Movement-related changes in local and long-range synchronization in Parkinson's disease revealed by simultaneous magnetoencephalography and intracranial recordings. J Neurosci 32(31):10541–10553

Litvak V, Jha A, Eusebio A, Oostenveld R, Foltynie T, Limousin P, Zrinzo L, Hariz MI, Friston K, Brown P (2011) Resting oscillatory cortico-subthalamic connectivity in patients with Parkinson's disease. Brain 134(2):359–374

Lynch G, Palmer LC, Gall CM (2011) The likelihood of cognitive enhancement. Pharmacol Biochem Behav 99(2):116–129

Lyvers M (2000) "Loss of control" in alcoholism and drug addiction: a neuroscientific interpretation. Exp Clin Psychopharmacol 8(2):225–249

Makela JP, Forss N, Jaaskelainen J, Kirveskari E, Korvenoja A, Paetau R (2006) Magnetoencephalography in neurosurgery. Neurosurgery 59(3):493–510

Marinković K, Halgren E, Maltzman I (2001) Arousal-related P3a to novel auditory stimuli is abolished by moderately low alcohol dose. Alcohol Alcohol 36(6):529–539

Marinković K, Rickenbacher E, Azma S, Artsy E (2012a) Acute alcohol intoxication impairs top-down regulation of Stroop incongruity as revealed by blood oxygen level-dependent functional magnetic resonance imaging. Hum Brain Mapp 33(2):319–333

Marinković K, Rosen BQ, Cox B, Kovacevic S (2012b) Event-related theta power during lexical-semantic retrieval and decision conflict is modulated by alcohol intoxication: Anatomically-constrained MEG. Front Psychol 3:121

Marrer E, Dieterle F (2007) Promises of biomarkers in drug development–a reality check. Chem Biol Drug Des 69(6):381–394

Mathew SJ, Shah A, Lapidus K, Clark C, Jarun N, Ostermeyer B, Murrough JW (2012) Ketamine for treatment-resistant unipolar depression: Current evidence. CNS Drugs 26(3):189–204

Mazaheri A, Jensen O (2010) Rhythmic pulsing: linking ongoing brain activity with evoked responses. Front Hum Neurosci 4:177
Moran RJ, Stephan KE, Seidenbecher T, Pape HC, Dolan RJ, Friston KJ (2009) Dynamic causal models of steady-state responses. Neuroimage 44(3):796–811
Moran RJ, Symmonds M, Stephan KE, Friston KJ, Dolan RJ (2011) An in vivo assay of synaptic function mediating human cognition. Curr Biol 21(15):1320–1325
Mucci A, Volpe U, Merlotti E, Bucci P, Galderisi S (2006) Pharmaco-EEG in psychiatry. Clin EEG Neurosci 37(2):81–98
Muller T (2012) Drug therapy in patients with Parkinson's disease. Transl Neurodegeneration 1(1):10
Muthukumaraswamy SD, Myers JF, Wilson SJ, Nutt DJ, Lingford-Hughes A, Singh KD, Hamandi K (2012) The effects of elevated endogenous GABA levels on movement-related network oscillations. Neuroimage 66C:36–41
Naatanen R, Ilmoniemi RJ, Alho K (1994) Magnetoencephalography in studies of human cognitive brain function. Trends Neurosci 17(9):389–395
Nallasamy N, Tsao DY (2011) Functional connectivity in the brain: effects of anesthesia. Neuroscientist 17(1):94–106
Neuper C, Pfurtscheller G (2001) Event-related dynamics of cortical rhythms: frequency-specific features and functional correlates. Int J Psychophysiol 43(1):41–58
Olanow CW (2008) Levodopa/dopamine replacement strategies in Parkinson's disease–future directions. Mov Disord 23(Suppl 3):S613–S622
Olde Dubbelink KT, Stoffers D, Deijen JB, Twisk JW, Stam CJ, Berendse HW (2013) Cognitive decline in Parkinson's disease is associated with slowing of resting-state brain activity: a longitudinal study. Neurobiol Aging 34(2):408–418
Oswal A, Brown P, Litvak V (2013) Movement related dynamics of subthalmo-cortical alpha connectivity in Parkinson's disease. Neuroimage 70:132–142
Picciotto MR, Higley MJ, Mineur YS (2012) Acetylcholine as a neuromodulator: cholinergic signaling shapes nervous system function and behavior. Neuron 76(1):116–129
Pirmoradi M, Beland R, Nguyen DK, Bacon BA, Lassonde M (2010) Language tasks used for the presurgical assessment of epileptic patients with MEG. Epileptic Disord 12(2):97–108
Polikar R, Tilley C, Hillis B, Clark CM (2010) Multimodal EEG, MRI and PET data fusion for Alzheimer's disease diagnosis. IEEE Eng Med Biol 2010:6058–6061
Pollok B, Makhloufi H, Butz M, Gross J, Timmermann L, Wojtecki L, Schnitzler A (2009) Levodopa affects functional brain networks in Parkinsonian resting tremor. Mov Disord 24(1):91–98
Prajapati V, Dureja H (2012) Produce lifecycle management in pharmaceuticals. J Med Mark 12(3):9
Raichle ME, MacLeod AM, Snyder AZ, Powers WJ, Gusnard DA, Shulman GL (2001) A default mode of brain function. Proc Nat Acad Sci USA 98(2):676–682
Rampp S, Stefan H (2007) Magnetoencephalography in presurgical epilepsy diagnosis. Expert Rev Med Devices 4(3):335–347
Rickenbacher E, Greve DN, Azma S, Pfeuffer J, Marinković K (2011) Effects of alcohol intoxication and gender on cerebral perfusion: an arterial spin labeling study. Alcohol 45(8):725–737
Ridderinkhof KR, de Vlugt Y, Bramlage A, Spaan M, Elton M, Snel J, Band GP (2002) Alcohol consumption impairs detection of performance errors in mediofrontal cortex. Science 298(5601):2209–2211
Rolinski M, Fox C, Maidment I, McShane R (2012) Cholinesterase inhibitors for dementia with Lewy bodies, Parkinson's disease dementia and cognitive impairment in Parkinson's disease. The Cochrane Database of Systematic Reviews 3:CD006504
Ross B, Tran T, Bhattacharya P, Watterson DM, Sailasuta N (2011) Application of NMR spectroscopy in medicinal chemistry and drug discovery. Curr Top Med Chem 11(1):93–114
Sahakian BJ, Morein-Zamir S (2011) Neuroethical issues in cognitive enhancement. J Psychopharmacol 25(2):197–204

Saletu B, Anderer P, Saletu-Zyhlarz GM (2006) EEG topography and tomography (LORETA) in the classification and evaluation of the pharmacodynamics of psychotropic drugs. Clin EEG Neurosci 37(2):66–80

Saletu B, Anderer P, Saletu-Zyhlarz GM, Arnold O, Pascual-Marqui RD (2002a) Classification and evaluation of the pharmacodynamics of psychotropic drugs by single-lead pharmaco-EEG, EEG mapping and tomography (LORETA). Methods Find Exp Clin Pharmacol 24(Suppl C):97–120

Saletu B, Anderer P, Saletu-Zyhlarz GM, Pascual-Marqui RD (2002b) EEG topography and tomography in diagnosis and treatment of mental disorders: evidence for a key-lock principle. Methods Find Exp Clin Pharmacol 24(Suppl D):97–106

Salmelin R, Hari R (1994) Characterization of spontaneous MEG rhythms in healthy adults. Electroencephalogr Clin Neurophysiol 91(4):237–248

Salvadore G, Cornwell BR, Colon-Rosario V, Coppola R, Grillon C, Zarate CA Jr, Manji HK (2009) Increased anterior cingulate cortical activity in response to fearful faces: a neurophysiological biomarker that predicts rapid antidepressant response to ketamine. Biol Psychiatry 65(4):289–295

Salvadore G, Cornwell BR, Sambataro F, Latov D, Colon-Rosario V, Carver F, Holroyd T, DiazGranados N, Machado-Vieira R, Grillon C, Drevets WC, Zarate CA Jr (2010) Anterior cingulate desynchronization and functional connectivity with the amygdala during a working memory task predict rapid antidepressant response to ketamine. Neuropsychopharmacology 35(7):1415–1422

Sarter M, Hasselmo ME, Bruno JP, Givens B (2005) Unraveling the attentional functions of cortical cholinergic inputs: Interactions between signal-driven and cognitive modulation of signal detection. Brain Res Rev 48(1):98–111

Schomer D, Lopes da Silva FH (eds) (2010) Niedermeyer's Electroencephalography: basic principles, clinical applications, and related fields. Lippincott Williams & Wilkins, Philadelphia

Seamans JK, Yang CR (2004) The principal features and mechanisms of dopamine modulation in the prefrontal cortex. Prog Neurobiol 74(1):1–58

Seidman LJ (2006) Neuropsychological functioning in people with ADHD across the lifespan. Clin Psychol Rev 26(4):466–485

Sivaprakasam K (2006) Towards a unifying hypothesis of Alzheimer's disease: cholinergic system linked to plaques, tangles and neuroinflammation. Curr Med Chem 13(18):2179–2188

Stam CJ, van Cappellen van Walsum AM, Pijnenburg YA, Berendse HW, de Munck JC, Scheltens P, van Dijk BW (2002) Generalized synchronization of MEG recordings in Alzheimer's Disease: evidence for involvement of the gamma band. J Clin Neurophysiol 19(6):562–574

Stefan H, Heers M, Schmitt HJ, Rauch C, Kaltenhauser M, Rampp S (2010) Increased spike frequency during general anesthesia with etomidate for magnetoencephalography in patients with focal epilepsies. Clin Neurophysiol 121(8):1220–1226

Stoffers D, Bosboom JL, Deijen JB, Wolters E, Stam CJ, Berendse HW (2008a) Increased cortico-cortical functional connectivity in early-stage Parkinson's disease: An MEG study. Neuroimage 41(2):212–222

Stoffers D, Bosboom JL, Deijen JB, Wolters EC, Berendse HW, Stam CJ (2007) Slowing of oscillatory brain activity is a stable characteristic of Parkinson's disease without dementia. Brain 130(7):1847–1860

Stoffers D, Bosboom JL, Wolters E, Stam CJ, Berendse HW (2008b) Dopaminergic modulation of cortico-cortical functional connectivity in Parkinson's disease: an MEG study. Exp Neurol 213(1):191–195

Stufflebeam SM (2011) Clinical magnetoencephalography for neurosurgery. Neurosurg Clin N Am 22(2):153–167

Szmuk P, Kee S, Pivalizza EG, Warters RD, Abramson DC, Ezri T (2003) Anaesthesia for magnetoencephalography in children with intractable seizures. Paediatr Anaesth 13(9):811–817

Tracey I (2001) Prospects for human pharmacological functional magnetic resonance imaging (phMRI). J Clin Pharmacol 41:21S–28S
Trimble MR, Hindmarch I (eds) (2000) Benzodiazepines. Wrightson Biomedical Publishing, Petersfield
Uhlhaas PJ, Pipa G, Lima B, Melloni L, Neuenschwander S, Nikolic D, Singer W (2009) Neural synchrony in cortical networks: History, concept and current status. Front Integr Neurosci 3:17
Uutela K, Hämäläinen M, Somersalo E (1999) Visualization of magnetoencephalographic data using minimum current estimates. Neuroimage 10(2):173–180
Van Veen BD, van Drongelen W, Yuchtman M, Suzuki A (1997) Localization of brain electrical activity via linearly constrained minimum variance spatial filtering. IEEE Trans Bio-Medical Eng 44(9):867–880
Vardy AN, van Wegen EE, Kwakkel G, Berendse HW, Beek PJ, Daffertshofer A (2011) Slowing of M1 activity in Parkinson's disease during rest and movement–an MEG study. Clin Neurophysiol 122(4):789–795
Varela F, Lachaux JP, Rodriguez E, Martinerie J (2001) The brainweb: phase synchronization and large-scale integration. Nat Rev Neurosci 2(4):229–239
WHO (2006) Neurological disorders: public health challenges. World Health Organization, Geneva
WHO (2008) The global burden of disease: 2004 update. World Health Organization, Geneva
Wienbruch C, Paul I, Bauer S, Kivelitz H (2005) The influence of methylphenidate on the power spectrum of ADHD children—an MEG study. BMC Psychiatry 5:29
Wilens TE (2006) Mechanism of action of agents used in attention-deficit/hyperactivity disorder. J Clin Psychiatry 67(Suppl 8):32–38
Wilens TE, Morrison NR, Prince J (2011) An update on the pharmacotherapy of attention-deficit/hyperactivity disorder in adults. Expert Rev Neurother 11(10):1443–1465
Willcutt EG (2012) The prevalence of DSM-IV attention-deficit/hyperactivity disorder: a meta-analytic review. Neurotherapeutics 9(3):490–499
Wilson TW, Franzen JD, Heinrichs-Graham E, White ML, Knott NL, Wetzel MW (2013) Broadband neurophysiological abnormalities in the medial prefrontal region of the default-mode network in adults with ADHD. Hum Brain Mapp 34(3):566–574
Wilson TW, Wetzel MW, White ML, Knott NL (2012) Gamma-frequency neuronal activity is diminished in adults with attention-deficit/hyperactivity disorder: a pharmaco-MEG study. J Psychopharmacol 26(6):771–777
Wise RG, Tracey I (2006) The role of fMRI in drug discovery. J Magn Reson Imaging 23(6):862–876
Wong DF, Tauscher J, Grunder G (2009) The role of imaging in proof of concept for CNS drug discovery and development. Neuropsychopharmacology 34(1):187–203

Food Meets Brain

Maike A. Hege, Krunoslav T. Stingl and Hubert Preissl

Abstract Food intake is essential for the survival of a living organism. The brain controls this complex behavior by integrating information of several systems to achieve a stable body weight of the individual. Over the last decades, however, the number of overweight people has been steadily increasing. These individuals are often characterized by increased food consumption and thus, have been associated with alterations in their control of food intake. In this chapter, we will review knowledge about the systems involved in the control of eating behavior and introduce how MEG can be used to learn more about the cognitive aspects of this behavior.

Keywords Categorization · Cognitive inhibition · Eating behavior · Event-related fields · Executive function · Food · Homeostatic control · Insulin · Obesity · Prefrontal cortex · Resting state · Reward · Visual processing · Working memory

1 Introduction

Obesity has become a major health problem with a steady increase in numbers of obese people in our modern society. According to the World Health Organization, more than 1.4 billion adult people are overweight (body mass index (BMI) > 25 kg/m^2) and about 500 million people are obese (BMI > 30 kg/m^2) (WHO 2012). Excessive body weight is associated with various diseases, particularly cardiovascular diseases (Hubert et al. 1983; Rexrode et al. 1997; Vega 2004), diabetes mellitus type 2 (Haslam and James 2005) and certain types of cancer (Calle et al. 2003). For these reasons,

M. A. Hege (✉) · K. T. Stingl · H. Preissl
Institute of Medical Psychology and Behavioral Neurobiology, fMEG Center,
University of Tübingen, Tübingen, Germany
e-mail: maike.hege@med.uni-tuebingen.de

S. Supek and C. J. Aine (eds.), *Magnetoencephalography*,
DOI: 10.1007/978-3-642-33045-2_43,

obesity is associated with reduction of life expectancy and is currently the leading preventable cause of death (Mokdad et al. 2004).

Obesity develops due to a combination of overeating and insufficient physical activity and also shows aspects of a neurobehavioral disorder (Dagher 2012). Several brain imaging studies investigating food-related processing showed changes in brain regions involved in the control of eating behavior which depend on the body mass index (DelParigi et al. 2004; Gautier et al. 2000, 2001; Karhunen et al. 1997; Stoeckel et al. 2008). Eating behavior is a complex process which requires integration of several internal and external signals. Besides the homeostatic regulation of energy balance, the influence on food intake by the hedonic system and the inhibitory control of hedonic feeding has gained considerable attention in the last years. However, integration of information between these systems is still not well understood. A deeper understanding of the interactions between homeostatic and cognitive elements of eating behavior control might be important for dealing with the obesity problem.

In this chapter, we will first introduce current knowledge about the control of eating behavior in humans with the brain posited as being the central region for controlling both homeostatic and cognitive systems. Secondly, we will focus on insulin as a key hormonal signal in the homeostatic control of eating behavior and discuss its role in obesity. This will lead us to establish obesity as a model for cerebral insulin signaling deficiency. Finally, we will present MEG studies that investigated the effects of insulin on cognitive aspects of eating behavior control. Finally, implications for obesity treatment by the observed interaction effects and future directions will be discussed.

2 Control of Eating Behavior

Food intake is a complex behavior, which requires sensing of internal energy-balance signals and external cues of food availability and is determined by the need of an organism to acquire adequate energy and nutrients (Seeley and Woods 2003). The central control region of this behavior is the brain. Different interconnected networks have to integrate homeostatic information about short- and long-term energy stores with higher-level cognitive demands to adjust our eating behavior according to dietary goals (see Fig. 1). Therefore, our eating behavior and the interplay of these networks is modulated by physiological, psychological, and cognitive factors (Dagher 2012).

2.1 Physiology of Homeostatic Control of Food Intake

Most adults are characterized by a relatively stable body weight, even if daily food intake and energy expenditure (in the form of basal metabolism, adaptive thermogenesis, and physical activity) underlie huge variations. The balance between

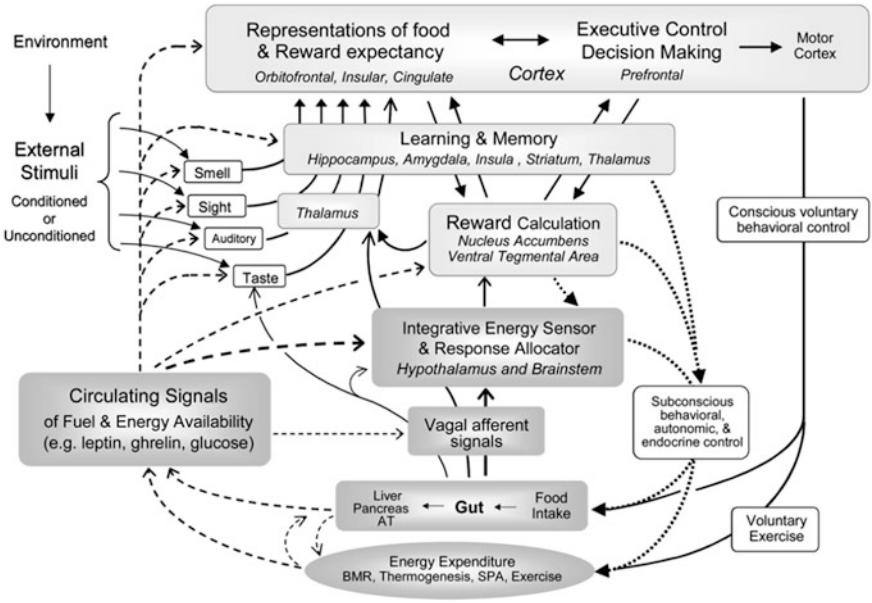

Fig. 1 Schematic diagram showing neural systems and flow of information involved in the control of food intake and regulation of energy balance. Internal regulatory circuitry using neural and hormonal feedback on hypothalamus and brainstem is shown at the *bottom* (*dark grey boxes*). Sensory and cortico-limbic brain areas used for processing information from the environment are shown in the upper half (*light gray boxes*). The extensive influence of circulating and neural internal feedback signals on sensory processing and cortico-limbic systems concerned with reward, emotion, learning and memory is emphasized (*dashed lines*) (Figure with permission from Shin et al. 2009)

energy intake and expenditure is regulated by a complex physiological system with the hypothalamus as a key structure for regulating appetite by integrating signals from central and peripheral pathways (Suzuki et al. 2010; Mayer and Thomas 1967).

The hypothalamic network involved in the control of feeding and energy metabolism is composed of interconnected neuronal populations located in the arcuate nucleus, ventromedial nucleus, paraventricular nucleus, dorsomedial nucleus, and lateral hypothalamus (Saper et al. 2002; Berthoud and Morrison 2008; Dietrich and Horvath 2009). This network receives peripheral signals that can be divided into anorexic (reduction of food consumption) and orexic (increase of food consumption) signals. These signals encode the amount of circulating nutrients, such as glucose, fatty acids, or the amount of stored energy and are conveyed by hormones like insulin, leptin, and ghrelin with their concentrations directly connected to food intake, amount of adipose tissue, or gut peptide concentrations (Cummings et al. 2001; Woods and Seeley 2000). In addition, these peripheral signals can also be conveyed by direct activation of the brainstem by gut peptides via vagal afferents or by arcuate nucleus neurons with the ability of sensing energy-rich nutrients directly (Suzuki et al. 2010). These peripheral signals

are then integrated and the information is encoded by neuropeptides and other neurotransmitters (Meister 2007) connected to circadian rhythm, thermoregulation and arousal (Saper et al. 2002). In principle, the output of the hypothalamic network is two-fold. For one, the hypothalamic network exhibits projections to sympathic and parasympathic nuclei innervating the endocrine organs and the gastrointestinal tract (Williams et al. 2001) to send feedback signals to the periphery. Secondly, the hypothalamic network is interconnected with cortical and mesolimbic control circuits controlling food reward to initiate or terminate food intake (Hommel et al. 2006; Kampe et al. 2009).

2.2 Cognitive Elements of Eating Behavior

Food intake, however, is not regulated by this homeostatic system alone. For actual behavioral activation to pursue food intake, integration of information from other systems like sensory, reward, and cognitive networks is required. This results in complex interactions between the systems, which so far are not well understood.

For a long time in evolution, food and especially high fat, energy-dense, palatable food was scarce. Thus, consumption of such high palatable food had clear homeostatic and social benefits. As a result, reward-driven or "hedonic" feeding has developed. Besides increased motivation for obtaining highly palatable food, hedonic feeding is also characterized by the consumption of this food beyond current needs and saving it in form of fat (Berthoud 2007).

Reward-associated feeding is regulated by a complex reward circuitry, involving interactions between several signaling systems, including opioid, dopaminergic, and cannabinoid systems (Wynne et al. 2005). In hedonic feeding, a differentiation between "liking", the sensory pleasure from eating a palatable food, and the motivational process of "wanting" (an incentive value is attributed to a food stimulus) has been suggested (Berridge 2007). As a neurophysiological basis for liking of palatable food, opioid neurotransmission in the nucleus accumbens has been discussed (Kelley and Berridge 2002). Opioate antagonists reduce food palatability in man (Yeomans et al. 1990) and reduce palatable food intake in animals and their affective facial expressions in response to tasting palatable food (Pecina and Berridge 2005). Wanting is thought to be mediated by the mesolimbic system including dopaminergic projections from the ventral tegmental area to the nucleus accumbens (Kelley and Berridge 2002) and hyperdopaminergic mice have a higher motivation to consume palatable food without changes in the pleasantness perceived for it (Pecina et al. 2003).

Interactions between the homeostatic and hedonic networks have been addressed in several studies, but the picture is far from being complete. Cabanac (1971) showed that sweetness is rated less pleasant after subjects had ingested glucose syrup. Other studies were also able to show that subjective palatability is different in the fed and in the fasted state (Berridge 1991). Therefore, the nutritional status of a subject can influence the rewarding effects of food. Besides direct

action of leptin, insulin, and ghrelin in the hypothalamic structure, they have also been shown to influence neurons in the ventral tegmental area, nucleus accumbens, and amygdale (Kampe et al. 2009, Shin et al. 2009). For instance, leptin can inhibit firing of dopaminergic neurons and feeding-induced dopamine release in the nucleus accumbens (Fulton et al. 2006; Hommel et al. 2006). Ghrelin on the other hand, stimulates firing of dopaminergic neurons and dopamine release in the nucleus accumbens (Abizaid et al. 2006). Functionally, also direct neuronal connections between hypothalamic, cortical, and mesolimbic circuits exist (Hommel et al. 2006). The neurons in the arcuate nucleus project to the insular and anterior cingulate cortex via midline thalamic nuclei, while neurons in the lateral hypothalamus project to the shell of the nucleus accumbens and the cerebral cortex (Kampe et al. 2009).

In our modern society with high energy food easily accessible, hedonic feeding would promote a positive energy balance in the long run. However, most individuals stay at a relatively stable body weight. Consequently, additional mechanisms of executive control and decision making in the control of eating behavior have been suggested (Appelhans 2009). Considered in the context of evolution, cognitive control of hedonic feeding is a valuable mechanism allowing for conservation of food during periods of anticipated food shortage (Polivy and Herman 2006) or in social interactions. The second aspect is still traceable in our modern society. In company of others, individuals match their food intake to those around them, regardless of hunger or satiation (Herman et al. 2003).

Cognitive control of eating behavior is considered to involve networks responsible for cognitive control of behavior in general. The primary neuroanatomical basis for self-regulation and executive function is the prefrontal cortex (PFC). The PFC is considered to exert top-down control over automatic cognitive and affective processes to inhibit responses to environmental cues with unfiltered emotionally driven behaviors (Miller and Cohen 2001). Regarding inhibition of hedonic feeding, the dorsolateral region of PFC (DLPFC) is activated after ingestion of a meal (Gautier et al. 2001; Tataranni et al. 1999). It seems that prefrontal cortex is important for inhibition of hedonic feeding; its interplay with the homeostatic system, however, is not clear.

Finally, sensory processing channels allowing detection and interpretation of environmental food cues interact with and are modulated by these neural systems involved in control of eating behavior. In many cases, food is first perceived by the visual system. The visual stimulus of food signals availability and provides information about palatability and therefore, is a key factor in the initiation of a meal (Cornier et al. 2007). Not only viewing of real food, but also viewing of food pictures has been shown to activate distributed networks of brain regions involved in food categorization and also in reward evaluation, such as amygdale and orbitofrontal cortex as well as the hypothalamus (Berthoud 2004; Rolls 2005; Cornier et al. 2007).

In tasks assessing attention allocation, visual selective attention is preferably directed towards food items (Nummenmaa et al. 2011). Activity in these networks and the degree of attention allocation is highly dependent on motivational states, either by the motivational significance of external cues or by the intrinsic current

need state. For instance, only the attention capture effects of food items, but not non-food items, as well as the memory performance for visually presented food items is strongly modulated by an individual's hunger level (Mogg et al. 1998; Morris and Dolan 2001; Piech et al. 2010). Furthermore, in an electroencephalographic (EEG) study, Stockburger et al. (2008) showed that hunger state modulated brain potentials selectively to food pictures. Food specific correlations between regions involved in processing of visual food cues with states of hunger and calorie content of the food cues were also found by means of functional magnetic resonance imaging (fMRI) (Porubska et al. 2006; Siep et al. 2009; Fuhrer et al. 2008; Cornier et al. 2007). It appears that the hunger state induces a change in the salience of food stimuli as need-related cues.

3 Role of Insulin in Eating Behavior

Although individual systems of eating behavior control have been described to some detail, interactions between them are still rather elusive. Manipulation of a key hormonal signal and investigation of its effects on cognitive elements in eating behavior might shed some light on these interactions in humans.

3.1 Cerebral Insulin Function

As previously described, one of the key signals is the hormone insulin, which regulates the metabolism of carbohydrates, lipids and amino acids. Insulin interferes with the metabolism of all three types of nutrients; however, the most important function of insulin is the regulation of glucose metabolism in peripheral tissues. Since glucose uptake in neurons is independent of insulin, the central nervous system has long been considered an insulin-independent tissue. However, insulin receptors are expressed all over the brain with high concentrations in the olfactory bulb, the primary olfactory cortex, the limbic and paralimbic system and the hypothalamic nuclei (Baskin et al. 1987; Unger et al. 1991; Schulingkamp et al. 2000).

Currently, it is well established that insulin affects eating behavior and metabolism by targeting the hypothalamic nuclei (e.g. ventromedial nucleus, arcuate nucleus) (Woods et al. 1979; Schwartz et al. 2000; Benoit et al. 2002). Furthermore, insulin is an essential neuronal growth factor and stimulator of neuronal protein synthesis during development of the central nervous system (Heidenreich and Toledo 1989; Robinson et al. 1994; Choi et al. 2005; Chiu and Cline 2010). Insulin has also been shown to co-regulate neurotransmitters and/or their receptors including norepinephrine (Boyd et al. 1985; Masters et al. 1987; Figlewicz et al. 1993; Apparsundaram et al. 2001), acetylcholine through glucose utilization (Lechin and van der Dijs 2006), glutamate receptors (Man et al. 2000; Plitzko et al. 2001; Mielke et al. 2005; van der Heide et al. 2005), and GABA-ergic

transmission (Wan et al. 1997; Ma et al. 2003; Vetiska et al. 2007). The majority of these insulin effects on neurotransmission are localized in the hippocampus, prefrontal cortex, and hypothalamus.

Thus, it is not surprising that an important role for insulin in high-level cognition, memory, and synaptic plasticity has been suggested. Animal studies demonstrated that rats which were injected intracerebroventricularly with insulin after a training task showed increase in performance if tested for retention in comparison to control animals (Park et al. 2000). Improvement of memory function by insulin administration was also shown in humans (Craft et al. 2000; Benedict et al. 2004).

3.2 Cerebral Insulin Resistance in Humans

For the investigation of insulin effects on cognitive elements of eating behavior, there are in general two ways for manipulating insulin levels and action in the human brain. One approach is to raise insulin levels in the body either by a hyperinsulinemic euglycemic clamp, which increases the plasma concentration of insulin without changing the glucose level, or by administration of intranasal insulin. The advantage of intranasal insulin is that it raises insulin concentration in the cerebrospinal fluid without relevant absorption in the systemic blood circulation as it enters the brain via the olfactory nerve (Illum 2000; Born et al. 2002). The other approach is to study eating behavior in a model with impaired insulin function. Obesity is associated with peripheral insulin resistance. In addition, the deletion of central insulin receptors in rats and mice is accompanied by hyperphagia and obesity (Bruning et al. 2000; Obici et al. 2002).

In a recent MEG study, we investigated insulin action in resting state networks/spontaneous brain activity to evaluate association of cerebral insulin resistance and BMI in humans. Spontaneous brain activity is characterized by the presence of more or less regular oscillations in various frequency bands (δ = 1–4 Hz, ϑ = 4–8 Hz, α = 8–12 Hz, β = 12–30 Hz, $\gamma > 30$ Hz). These oscillations are generated by specific brain areas and networks and are quite stable at rest. Any input to the system and/or information exchange between spatially separated areas is accompanied by power/and or phase synchronization in specific frequency bands (Schnitzler and Gross 2005). This type of information transfer seems to be affected in different neurological disorders, such as Alzheimer's disease or schizophrenia (Uhlhaas et al. 2008, Stam et al. 2009), as well as in type 1 diabetes (van Duinkerken et al. 2009) and in obesity (Olde Dubbelink et al. 2008). We hypothesized that alterations in insulin signaling may be one cause of dysfunction in oscillatory networks in obese subjects.

Tschritter et al. (2006) used a hyperinsulinemic euglycemic clamp to assess cerebrocortical insulin effects in resting state and modulation by body weight. For lean subjects, we observed an increase in power in theta and beta band for an increase in plasma insulin concentration. For obese subjects, on the contrary, no effect of

insulin on beta activity was observed and even a decrease in theta activity was evident. Furthermore, the insulin-induced changes in theta and beta activity were closely correlated with BMI and percent body fat. Regarding peripheral insulin sensitivity, these changes were positively correlated with insulin sensitivity of glucose disposal. In summary, this means that cerebrocortical insulin action was positively correlated with peripheral insulin sensitivity and negatively with measures of obesity.

Results of this study indicate that an increase in insulin levels in the brain has an effect on resting state brain networks and that this effect is altered in obese subjects. Therefore, we suggest that obese subjects are not only characterized by peripheral, but also by central insulin resistance. This insulin resistance is most likely associated with overeating and the development of obesity and is of special interest when investigating insulin effects on networks involved in eating behavior control.

4 Modulation of Neural Networks Related to Control of Eating Behavior by Insulin and Obesity

Stingl et al. (2010a) explored the effects of intranasally administered insulin on the small world dynamics of resting state magnetoencephalographic brain activity. Insulin induced subject-specific changes of the weighted path length in the theta band were observed. This change again showed a statistically significant positive correlation with the body mass index of individual subjects supporting the hypothesis of cerebral insulin resistance in obese individuals.

Weighted path length is a measure of global interconnectedness of a network and its global efficiency. This confirms that insulin is a strong modulator of global communication of the brain networks involved in satiation and the control of eating behavior. However, this approach is not suitable to elucidate which networks or how the communication between these networks is modulated by insulin.

In general, these networks have a highly complex pattern of correlated activity of multiple brain areas with interconnectivities and existing feedback loops. In this respect, a method with high temporal resolution is advantageous for evaluation of function or malfunction of individual components of these networks. Based on the low sensitivity of MEG for activity in homeostatic control areas, MEG research has to focus on cognitive elements of eating behavior including brain areas involved in sensory processing and categorization and higher-order brain areas involved in executive functions.

4.1 Visual Processing and Categorization

The visual system of the human cortex is hierarchically organized and processing of visual stimuli starts in primary visual areas in the occipital lobe. In the following, two functionally distinct pathways process different information about the stimulus

separately. The dorsal occipito-temporal pathway is mostly concerned with the perception of the spatial locations of objects, the perception of motion and the guidance of movements towards objects. The ventral occipito-temporal pathway is important for the perception of object identity—it has been shown to exhibit category-specific activation (Ungerleider and Haxby 1994; Kawakami et al. 2000; Clark et al. 1996). Categorization processes enable the brain to recognize objects on the basis of common properties independently of their physical differences.

In humans, visual categorization is a very fast process occurring already between 80 and 200 ms after stimulus onset (Thorpe et al. 1996; Antal et al. 2000; Fabre-Thorpe et al. 2001; Thorpe and Fabre-Thorpe 2001; VanRullen and Thorpe 2001; Thierry et al. 2007). Food as a category is very inhomogeneous and differs widely in structure, color, and cultural background. Nevertheless, it was shown that food and non-food pictures result in significantly different cortical activation already in early stages of visual processing with food inducing category-specific activation (Stingl et al. 2010b; Toepel et al. 2009). Stingl et al. (2010b) showed that a difference in brain responses between food and non-food objects were observed already 120 ms after stimulus onset, even though stimuli were controlled for differences in low-level visual features. Source reconstruction of these differences revealed sources of activity in primary visual areas. Additionally, we observed activation differences around 160 ms post-stimulus, which were localized in the inferior-occipital region. We suggested that they were related to categorization of the object. Event-related fields (ERFs) and source reconstruction of food/non-food differences are displayed in Fig. 2.

It has also been shown that not only food versus non-food objects, but also high-energy versus low-energy food stimuli elicit differences related to visual categorization at around 160 ms (Toepel et al. 2009). Thus, information about food as a category as well as the caloric content of it seems to be encoded very early in neural information processing. Furthermore, Stockburger et al. (2008) reported that hunger state modulated brain potentials selectively to food pictures very early in the visual processing stream (already 170 ms post-stimulus). Enhanced processing of food pictures in a hungry state was mainly found in occipito-temporo parietal regions.

This suggests that early visual processing is already influenced by characteristics of external cues and by intrinsic motivational states. To investigate whether this modulation might be related to insulin action in the brain, intranasal insulin was administered to lean and overweight subjects in a placebo controlled study (Guthoff et al. 2011). In lean subjects, again the evoked component at around 160–170 ms, which is related to identification and categorization, was modulated. This modulation was only observed for food pictures and once more source localized to inferior-occipital regions. Modulation of the evoked components by insulin administration is displayed in Fig. 3. This specific insulin-induced modulation was also observed in an fMRI study (Guthoff et al. 2010). In obese individuals, however, the modulation of the magnetic evoked components was absent, giving further support for the hypothesis that obese individuals suffer from cerebral insulin resistance.

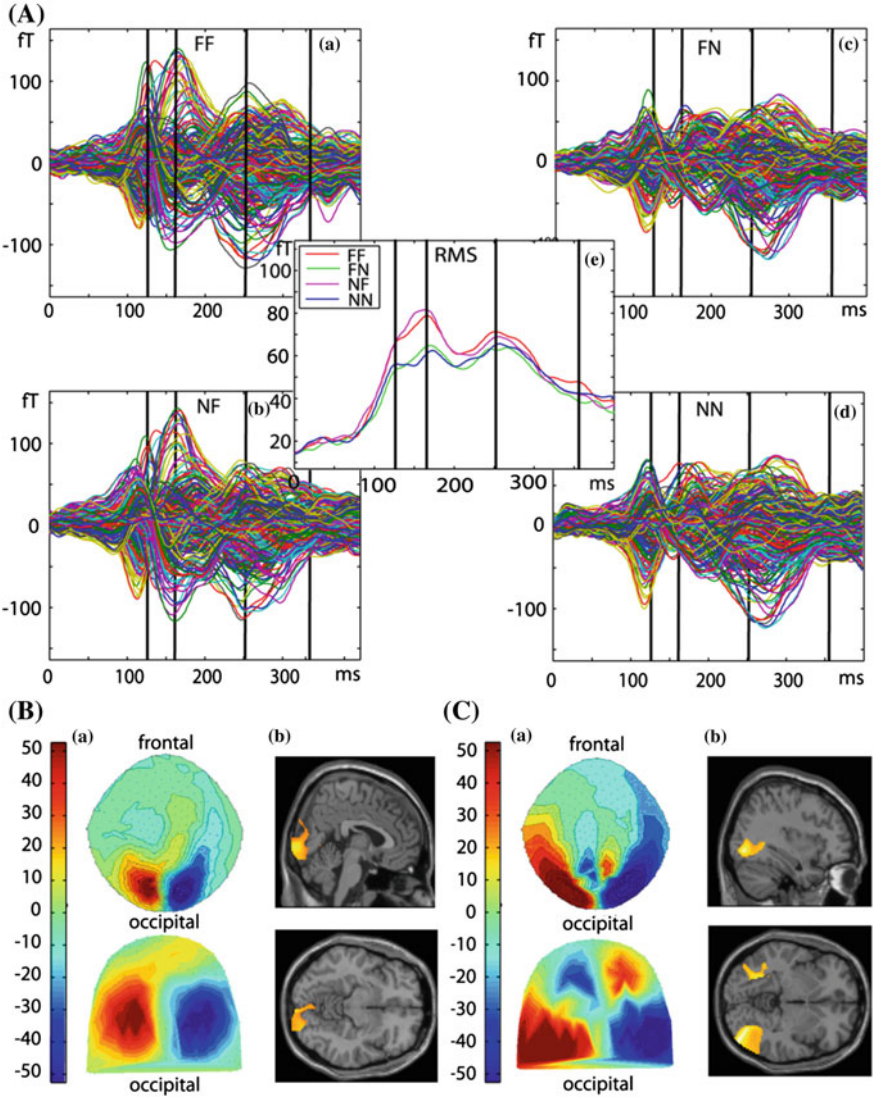
(A)
FF
(a)
FN
(c)
RMS
(e)
FF
FN
NF
NN
NF
(b)
NN
(d)
fT
ms
(B)
(C)
frontal
occipital
(a)
(b)

◀**Fig. 2** Differences in ERFs to food and non-food stimuli. Brain responses were obtained during a one-back working memory task with four conditions depending on current and preceding stimulus. *FF* food as preceding and current stimulus, *FN* food as preceding and non-food as current stimulus, *NF* non-food as preceding and food as current stimulus, *NN* non-food as preceding and current stimulus. **A** The waveforms of the grand average magnetic fields for all experimental conditions (**a** FF, **b** NF, **c** FN, **d** NN). **e** Root mean square values of all channels for all subjects and all conditions (*red* FF; *purple* NF; *green* NN; *blue* FN), quantified magnetic evoked components M1-A, M1-B, M2, and M3. The latency for the maximum in the M1-A response was 123, 162 ms for the M1-B response, 251 ms for the M2 response, and 355 ms for the M3 response. **B** and **C** Topographic maps of the difference between *NF* and *NN* conditions at 123 ms (M1-A) and 162 ms (M1-B), respectively. **a** *top* 2D map of all sensors, *bottom* 3D map of sensors viewed from the back; **b** source localization of the difference between *NF* and *NN* conditions for the time interval between 110 and 130 ms and 150 and 170 ms, respectively. Only activations significant with $P < 0.001$ are shown. Maximal activation was observed in the primary visual areas (**B**) and the left and right fusiform gyri (**C**) (Figure with permission from Stingl et al. 2010b)

In conclusion, all of these studies indicate that our perception of the environment is highly dependent on intrinsic motivation and might be modulated very early by reward and homeostatic control networks. In particular, insulin seems to have an effect not only on the hypothalamus as the homeostatic control region of eating behavior, but also in the regulation of our eating behavior by modulating our perceptions.

4.2 Executive Functions

Executive functions in general are neuropsychological processes (Miller and Cohen 2001) including inhibitory control, attention control, and working memory. As introduced earlier, these processes are also essential for the cognitive control of eating impulses and the ability to maintain energy balance (Cummings 1995; Tataranni et al. 1999; Gautier et al. 2001; Small et al. 2001; Appelhans 2009). Investigation of differential activation of these functions in lean and obese individuals provides the opportunity to explore them in the presence of potential deficiency in insulin signaling.

A well established paradigm for the investigation of executive functions is the working memory task including executive and attention control of short-term memory. In our previously mentioned studies by Stingl et al. (2010b) and Guthoff et al. (2011), visual stimuli were incorporated in a visual working memory task; however, only early effects between food and non-food stimuli were reported so far. As shown in Stingl et al. (2010b), later magnetic components related to the retrieval and encoding of memory representations also showed significant activation differences for food versus non-food objects. When a food stimulus was presented, an increase in activity of later components correlated with an increase in behavioral performance (faster reaction time and higher accuracy).

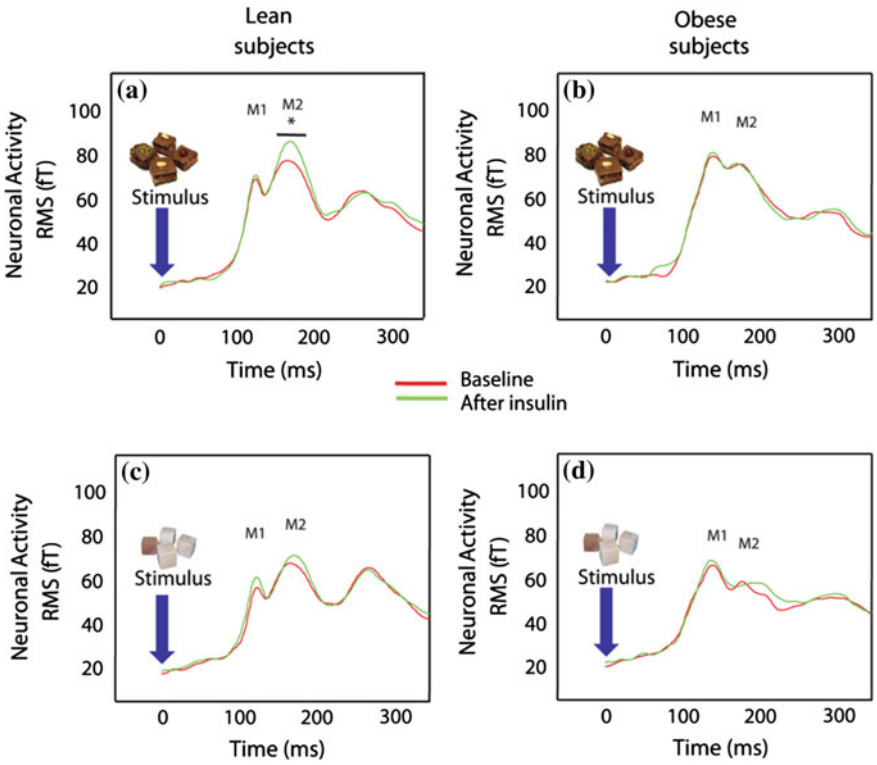

Fig. 3 ERFs to food and non-food stimuli before and after insulin application in lean and obese subjects. Time traces of ERFs quantified by root mean square for the measurements before (*red line*) and after intranasal (*green line*) insulin application. In the *upper row*, the response of lean (**a**) and obese (**b**) subjects to food stimuli are shown. In the *lower row*, the responses to non-food-pictures are shown (**c** lean, **d** obese). Only for lean subjects, a statistically significant difference between basal and insulin in the M2 component was found and only when they were viewing food pictures (Figure with permission from Guthoff et al. 2011)

The same paradigm was used to directly address alterations in working memory performance in obese subjects. Stingl et al. (2012) reported a decrease in performance with elevated BMI. Obese subjects showed an increase in reaction time and a decrease in accuracy independent of stimulus category. Regarding brain activation, BMI correlated negatively with neuronal activity starting as early as 150 ms post-stimulus and localized in occipital areas. In addition, obese subjects showed an increase in activity in right PFC for food objects only (differences in activation between lean and obese individuals are displayed in Fig. 4), a region activated in several tasks involving executive functions and considered to be crucial for cognitive inhibition and control of hedonic feeding.

BMI dependent modulation of PFC has also been observed in previous studies. A structural MRI study showed lower gray matter density in the middle frontal

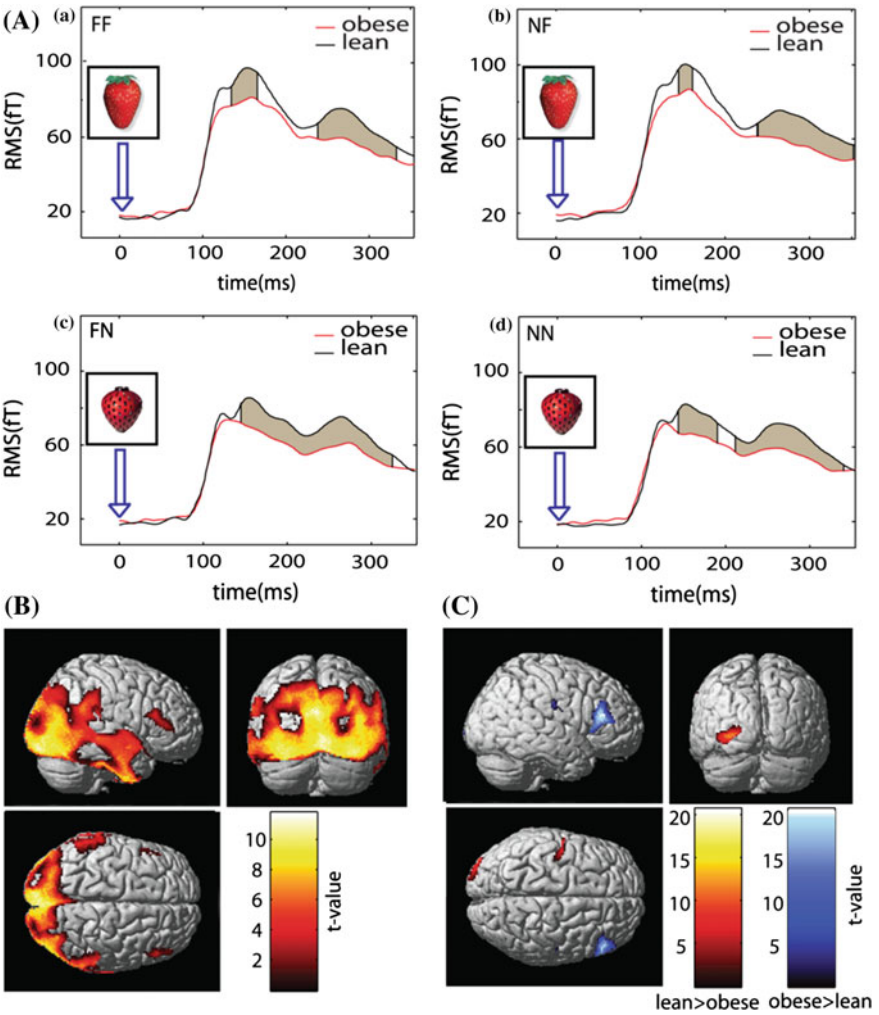

Fig. 4 Differences in brain activity between obese and lean individuals during a one-back working memory task. **A** Root mean square values of all channels for lean (*blue*) and obese group (*red*) for every experimental condition **a** FF, **b** NF, **c** FN, **d** NN (see Fig. 2 for explanation of conditions). Obese in comparison to lean individuals showed decreased root mean square values; the time period in which there was a statistically significant difference between the two groups is marked by *brown color*. **B** Areas activated during the working memory task for the period 100–350 ms for both groups and all conditions. **C** Differential activation for lean and obese group for the period 100–350 ms. Obese individuals showed decreased activation in occipital areas and increased activation in right prefrontal regions. Regression analyses revealed that activation in occipital areas was negatively correlated with body mass index for all conditions, whereas activation in right frontal region was only positively correlated for conditions with food as the current stimulus (*FF*, *NF*). Cortical activity was rendered onto the surface of a standard anatomical brain volume (Montreal Neurological Institute). All regional activations above initial significance threshold $P < 0.05$ (family wise error (FWE) corrected) (Figure with permission from Stingl et al. 2012)

gyrus of the PFC in obese versus lean individuals (Pannacciulli et al. 2006). Similarly, Volkow et al. (2009) showed through the use of positron emission tomography (PET) that greater BMI is correlated with lower baseline metabolism in PFC. Increased recruitment of this area in obese subjects during our working memory task may reflect a functional compensation to deal with deficits in the inhibitory systems observed by lower metabolism at baseline. However, we didn't observe this modulation to correlate with better performance. Thus, it seems that this increase in cortical activity for obese subjects does not present an efficient recruitment of neural circuits form right PFC.

In the working memory task, inhibitory mechanisms are actually crucial to determine which information enters the working memory and to suppress information that is no longer needed (Hasher et al. 1997). Thus, any deficiency in this system will have consequences on working memory performance. Behavioral results from a go/nogo task investigating response inhibition also indicated an inverse relation of BMI and behavioral inhibition (Nederkoorn et al. 2006a, b).

The reported results show specific and quantifiable differences between obese and lean subjects. It seems that obesity is partially related to deficits in executive functions and thus, in cognitive control of eating behavior. This leads to the assumption that insulin has an effect on cognitive control of eating behavior, which is altered in the presence of cerebral insulin resistance.

5 Conclusion and Future Directions

In this chapter, we discussed networks involved in the control of eating behavior and alterations of these networks in obesity. We introduced insulin as a central hormonal signal in the regulation of food intake and discussed evidence pointing to a cerebral insulin resistance in overweight and obese individuals. Finally, we showed that insulin has diverse effects not only on homeostatic control, but also on cognitive elements of eating behavior and that these insulin effects are altered in obese individuals. Insulin affected the cognitive process of food categorization and overweight and obese, in comparison to lean individuals, showed decline in cognitive function which was related to activation differences in brain areas involved in behavioral inhibition.

Regarding the multitude of effects of insulin action, further exploration of its role in eating behavior might reveal new approaches in obesity treatment. In Tschritter et al. (2012), loss of body fat during a lifestyle intervention was associated with high cerebral insulin sensitivity. Results of another MEG study (Hege et al. 2013) indicated that successful weight loss during a diet was associated with increased cognitive control over food intake. In line with cognitive effects of insulin discussed in this chapter, investigation of the pathway connecting behavioral inhibition and insulin resistance of CNS might be especially valuable in developing new strategies for non-responders in weight loss programs.

References

Abizaid A, Liu ZW, Andrews ZB, Shanabrough M, Borok E, Elsworth JD, Roth RH, Sleeman MW, Picciotto MR, Tschop MH, Gao XB, Horvath TL (2006) Ghrelin modulates the activity and synaptic input organization of midbrain dopamine neurons while promoting appetite. J Clin Invest 116(12):3229–3239

Antal A, Keri S, Kovacs G, Janka Z, Benedek G (2000) Early and late components of visual categorization: an event-related potential study. Brain Res Cogn Brain Res 9(1):117–119

Apparsundaram S, Sung U, Price RD, Blakely RD (2001) Trafficking-dependent and -independent pathways of neurotransmitter transporter regulation differentially involving p38 mitogen-activated protein kinase revealed in studies of insulin modulation of norepinephrine transport in SK-N-SH cells. J Pharmacol Exp Therapy 299(2):666–677

Appelhans BM (2009) Neurobehavioral inhibition of reward-driven feeding: implications for dieting and obesity. Obesity (Silver Spring) 17(4):640–647

Baskin DG, Figlewicz DP, Woods SC, Porte D Jr, Dorsa DM (1987) Insulin in the brain. Annu Rev Physiol 49:335–347

Benedict C, Hallschmid M, Hatke A, Schultes B, Fehm HL, Born J, Kern W (2004) Intranasal insulin improves memory in humans. Psychoneuroendocrinology 29(10):1326–1334

Benoit SC, Air EL, Coolen LM, Strauss R, Jackman A, Clegg DJ, Seeley RJ, Woods SC (2002) The catabolic action of insulin in the brain is mediated by melanocortins. J Neurosci 22(20):9048–9052

Berridge KC (1991) Modulation of taste affect by hunger, caloric satiety, and sensory-specific satiety in the rat. Appetite 16(2):103–120

Berridge KC (2007) The debate over dopamine's role in reward: the case for incentive salience. Psychopharmacology 191(3):391–431

Berthoud HR (2004) Mind versus metabolism in the control of food intake and energy balance. Physiol Behav 81(5):781–793

Berthoud HR (2007) Interactions between the "cognitive" and "metabolic" brain in the control of food intake. Physiol Behav 91(5):486–498

Berthoud HR, Morrison C (2008) The brain, appetite, and obesity. Annu Rev Psychol 59:55–92

Born J, Lange T, Kern W, McGregor GP, Bickel U, Fehm HL (2002) Sniffing neuropeptides: a transnasal approach to the human brain. Nat Neurosci 5(6):514–516

Boyd FT Jr, Clarke DW, Muther TF, Raizada MK (1985) Insulin receptors and insulin modulation of norepinephrine uptake in neuronal cultures from rat brain. J Biol Chem 260(29):15880–15884

Bruning JC, Gautam D, Burks DJ, Gillette J, Schubert M, Orban PC, Klein R, Krone W, Muller-Wieland D, Kahn CR (2000) Role of brain insulin receptor in control of body weight and reproduction. Science 289(5487):2122–2125

Cabanac M (1971) Physiological role of pleasure. Science 173(2):1103–1107

Calle EE, Rodriguez C, Walker-Thurmond K, Thun MJ (2003) Overweight, obesity, and mortality from cancer in a prospectively studied cohort of U.S. adults. N Engl J Med 348(17):1625–1638

Chiu SL, Cline HT (2010) Insulin receptor signaling in the development of neuronal structure and function. Neural Dev 5:7

Choi J, Ko J, Racz B, Burette A, Lee JR, Kim S, Na M, Lee HW, Kim K, Weinberg RJ, Kim E (2005) Regulation of dendritic spine morphogenesis by insulin receptor substrate 53, a downstream effector of Rac1 and Cdc42 small GTPases. J Neurosci 25(4):869–879

Clark VP, Keil K, Maisog JM, Courtney S, Ungerleider LG, Haxby JV (1996) Functional magnetic resonance imaging of human visual cortex during face matching: a comparison with positron emission tomography. Neuroimage 4(1):1–15

Cornier MA, Von Kaenel SS, Bessesen DH, Tregellas JR (2007) Effects of overfeeding on the neuronal response to visual food cues. Am J Clin Nutr 86(4):965–971

Craft S, Asthana S, Schellenberg G, Baker L, Cherrier M, Boyt AA, Martins RN, Raskind M, Peskind E, Plymate S (2000) Insulin effects on glucose metabolism, memory, and plasma amyloid precursor protein in Alzheimer's disease differ according to apolipoprotein-E genotype. Ann N Y Acad Sci 903:222–228

Cummings DE, Purnell JQ, Frayo RS, Schmidova K, Wisse BE, Weigle DS (2001) A preprandial rise in plasma ghrelin levels suggests a role in meal initiation in humans. Diabetes 50(8):1714–1719

Cummings JL (1995) Anatomic and behavioral aspects of frontal-subcortical circuits. Ann N Y Acad Sci 769:1–13

Dagher A (2012) Functional brain imaging of appetite. Trends Endocrinol Metab 23(5):250–260

DelParigi A, Chen K, Salbe AD, Hill JO, Wing RR, Reiman EM, Tataranni PA (2004) Persistence of abnormal neural responses to a meal in postobese individuals. Int J Obes Relat Metab Disord 28(3):370–377

Dietrich MO, Horvath TL (2009) Feeding signals and brain circuitry. Eur J Neurosci 30(9):1688–1696

Fabre-Thorpe M, Delorme A, Marlot C, Thorpe S (2001) A limit to the speed of processing in ultra-rapid visual categorization of novel natural scenes. J Cogn Neurosci 13(2):171–180

Figlewicz DP, Bentson K, Ocrant I (1993) The effect of insulin on norepinephrine uptake by PC12 cells. Brain Res Bull 32(4):425–431

Fuhrer D, Zysset S, Stumvoll M (2008) Brain activity in hunger and satiety: an exploratory visually stimulated FMRI study. Obesity (Silver Spring) 16(5):945–950

Fulton S, Pissios P, Manchon RP, Stiles L, Frank L, Pothos EN, Maratos-Flier E, Flier JS (2006) Leptin regulation of the mesoaccumbens dopamine pathway. Neuron 51(6):811–822

Gautier JF, Chen K, Salbe AD, Bandy D, Pratley RE, Heiman M, Ravussin E, Reiman EM, Tataranni PA (2000) Differential brain responses to satiation in obese and lean men. Diabetes 49(5):838–846

Gautier JF, Del Parigi A, Chen K, Salbe AD, Bandy D, Pratley RE, Ravussin E, Reiman EM, Tataranni PA (2001) Effect of satiation on brain activity in obese and lean women. Obes Res 9(11):676–684

Guthoff M, Grichisch Y, Canova C, Tschritter O, Veit R, Hallschmid M, Haring HU, Preissl H, Hennige AM, Fritsche A (2010) Insulin modulates food-related activity in the central nervous system. J Clin Endocrinol Metab 95(2):748–755

Guthoff M, Stingl KT, Tschritter O, Rogic M, Heni M, Stingl K, Hallschmid M, Haring HU, Fritsche A, Preissl H, Hennige AM (2011) The insulin-mediated modulation of visually evoked magnetic fields is reduced in obese subjects. PLoS ONE 6(5):e19482

Hasher L, Quig MB, May CP (1997) Inhibitory control over no-longer-relevant information: adult age differences. Mem Cognit 25(3):286–295

Haslam DW, James WP (2005) Obesity. Lancet 366(9492):1197–1209

Hege MA, Stingl KT, Ketterer C, Haring HU, Heni M, Fritsche A, Preissl H (2013) Working memory-related brain activity is associated with outcome of lifestyle intervention. Obesity (Silver Spring) 21(12):2488–2494

Heidenreich KA, Toledo SP (1989) Insulin receptors mediate growth effects in cultured fetal neurons. II. Activation of a protein kinase that phosphorylates ribosomal protein S6. Endocrinology 125(3):1458–1463

Herman CP, Roth DA, Polivy J (2003) Effects of the presence of others on food intake: a normative interpretation. Psychol Bull 129(6):873–886

Hommel JD, Trinko R, Sears RM, Georgescu D, Liu ZW, Gao XB, Thurmon JJ, Marinelli M, DiLeone RJ (2006) Leptin receptor signaling in midbrain dopamine neurons regulates feeding. Neuron 51(6):801–810

Hubert HB, Feinleib M, McNamara PM, Castelli WP (1983) Obesity as an independent risk factor for cardiovascular disease: a 26-year follow-up of participants in the Framingham Heart Study. Circulation 67(5):968–977

Illum L (2000) Transport of drugs from the nasal cavity to the central nervous system. Eur J Pharm Sci 11(1):1–18

Kampe J, Tschop MH, Hollis JH, Oldfield BJ (2009) An anatomic basis for the communication of hypothalamic, cortical and mesolimbic circuitry in the regulation of energy balance. Eur J Neurosci 30(3):415–430

Karhunen LJ, Lappalainen RI, Vanninen EJ, Kuikka JT, Uusitupa MI (1997) Regional cerebral blood flow during food exposure in obese and normal-weight women. Brain 120(Pt 9):1675–1684

Kawakami O, Kaneoke Y, Kakigi R (2000) Perception of apparent motion is related to the neural activity in the human extrastriate cortex as measured by magnetoencephalography. Neurosci Lett 285(2):135–138

Kelley AE, Berridge KC (2002) The neuroscience of natural rewards: relevance to addictive drugs. J Neurosci 22(9):3306–3311

Lechin F, van der Dijs B (2006) Central nervous system circuitry involved in the hyperinsulinism syndrome. Neuroendocrinology 84(4):222–234

Ma XH, Zhong P, Gu Z, Feng J, Yan Z (2003) Muscarinic potentiation of GABA(A) receptor currents is gated by insulin signaling in the prefrontal cortex. J Neurosci 23(4):1159–1168

Man HY, Lin JW, Ju WH, Ahmadian G, Liu L, Becker LE, Sheng M, Wang YT (2000) Regulation of AMPA receptor-mediated synaptic transmission by clathrin-dependent receptor internalization. Neuron 25(3):649–662

Masters BA, Shemer J, Judkins JH, Clarke DW, Le Roith D, Raizada MK (1987) Insulin receptors and insulin action in dissociated brain cells. Brain Res 417(2):247–256

Mayer J, Thomas DW (1967) Regulation of food intake and obesity. Science 156(773):328–337

Meister B (2007) Neurotransmitters in key neurons of the hypothalamus that regulate feeding behavior and body weight. Physiol Behav 92(1–2):263–271

Mielke JG, Taghibiglou C, Liu L, Zhang Y, Jia Z, Adeli K, Wang YT (2005) A biochemical and functional characterization of diet-induced brain insulin resistance. J Neurochem 93(6):1568–1578

Miller EK, Cohen JD (2001) An integrative theory of prefrontal cortex function. Annu Rev Neurosci 24:167–202

Mogg K, Bradley BP, Hyare H, Lee S (1998) Selective attention to food-related stimuli in hunger: are attentional biases specific to emotional and psychopathological states, or are they also found in normal drive states? Behav Res Therapy 36(2):227–237

Mokdad AH, Marks JS, Stroup DF, Gerberding JL (2004) Actual causes of death in the United States, 2000. JAMA 291(10):1238–1245

Morris JS, Dolan RJ (2001) Involvement of human amygdala and orbitofrontal cortex in hunger-enhanced memory for food stimuli. J Neurosci 21(14):5304–5310

Nederkoorn C, Braet C, Van Eijs Y, Tanghe A, Jansen A (2006a) Why obese children cannot resist food: the role of impulsivity. Eat Behav 7(4):315–322

Nederkoorn C, Smulders FT, Havermans RC, Roefs A, Jansen A (2006b) Impulsivity in obese women. Appetite 47(2):253–256

Nummenmaa L, Hietanen JK, Calvo MG, Hyona J (2011) Food catches the eye but not for everyone: a BMI-contingent attentional bias in rapid detection of nutriments. PLoS ONE 6(5):e19215

Obici S, Feng Z, Karkanias G, Baskin DG, Rossetti L (2002) Decreasing hypothalamic insulin receptors causes hyperphagia and insulin resistance in rats. Nat Neurosci 5(6):566–572

Olde Dubbelink KT, Felius A, Verbunt JP, van Dijk BW, Berendse HW, Stam CJ, Delemarre-van de Waal HA (2008) Increased resting-state functional connectivity in obese adolescents; a magnetoencephalographic pilot study. PLoS ONE 3(7):e2827

Pannacciulli N, Del Parigi A, Chen K, Le DS, Reiman EM, Tataranni PA (2006) Brain abnormalities in human obesity: a voxel-based morphometric study. Neuroimage 31(4):1419–1425

Park CR, Seeley RJ, Craft S, Woods SC (2000) Intracerebroventricular insulin enhances memory in a passive-avoidance task. Physiol Behav 68(4):509–514

Pecina S, Berridge KC (2005) Hedonic hot spot in nucleus accumbens shell: where do mu-opioids cause increased hedonic impact of sweetness? J Neurosci 25(50):11777–11786

Pecina S, Cagniard B, Berridge KC, Aldridge JW, Zhuang X (2003) Hyperdopaminergic mutant mice have higher "wanting" but not "liking" for sweet rewards. J Neurosci 23(28):9395–9402

Piech RM, Pastorino MT, Zald DH (2010) All I saw was the cake. Hunger effects on attentional capture by visual food cues. Appetite 54(3):579–582

Plitzko D, Rumpel S, Gottmann K (2001) Insulin promotes functional induction of silent synapses in differentiating rat neocortical neurons. Eur J Neurosci 14(8):1412–1415

Polivy J, Herman CP (2006) An evolutionary perspective on dieting. Appetite 47(1):30–35

Porubska K, Veit R, Preissl H, Fritsche A, Birbaumer N (2006) Subjective feeling of appetite modulates brain activity: an fMRI study. Neuroimage 32(3):1273–1280

Rexrode KM, Hennekens CH, Willett WC, Colditz GA, Stampfer MJ, Rich-Edwards JW, Speizer FE, Manson JE (1997) A prospective study of body mass index, weight change, and risk of stroke in women. JAMA 277(19):1539–1545

Robinson LJ, Leitner W, Draznin B, Heidenreich KA (1994) Evidence that p21ras mediates the neurotrophic effects of insulin and insulin-like growth factor I in chick forebrain neurons. Endocrinology 135(6):2568–2573

Rolls ET (2005) Taste, olfactory, and food texture processing in the brain, and the control of food intake. Physiol Behav 85(1):45–56

Saper CB, Chou TC, Elmquist JK (2002) The need to feed: homeostatic and hedonic control of eating. Neuron 36(2):199–211

Schnitzler A, Gross J (2005) Normal and pathological oscillatory communication in the brain. Nat Rev Neurosci 6(4):285–296

Schulingkamp RJ, Pagano TC, Hung D, Raffa RB (2000) Insulin receptors and insulin action in the brain: review and clinical implications. Neurosci Biobehav Rev 24(8):855–872

Schwartz MW, Woods SC, Porte D Jr, Seeley RJ, Baskin DG (2000) Central nervous system control of food intake. Nature 404(6778):661–671

Seeley RJ, Woods SC (2003) Monitoring of stored and available fuel by the CNS: implications for obesity. Nat Rev Neurosci 4(11):901–909

Shin AC, Zheng H, Berthoud HR (2009) An expanded view of energy homeostasis: neural integration of metabolic, cognitive, and emotional drives to eat. Physiol Behav 97(5):572–580

Siep N, Roefs A, Roebroeck A, Havermans R, Bonte ML, Jansen A (2009) Hunger is the best spice: an fMRI study of the effects of attention, hunger and calorie content on food reward processing in the amygdala and orbitofrontal cortex. Behav Brain Res 198(1):149–158

Small DM, Zatorre RJ, Dagher A, Evans AC, Jones-Gotman M (2001) Changes in brain activity related to eating chocolate: from pleasure to aversion. Brain 124(Pt 9):1720–1733

Stam CJ, de Haan W, Daffertshofer A, Jones BF, Manshanden I, van Cappellen van Walsum AM, Montez T, Verbunt JP, de Munck JC, van Dijk BW, Berendse HW, Scheltens P (2009) Graph theoretical analysis of magnetoencephalographic functional connectivity in Alzheimer's disease. Brain 132(Pt 1):213–224

Stingl KT, Kullmann S, Guthoff M, Heni M, Fritsche A, Preissl H (2010a) Insulin modulation of magnetoencephalographic resting state dynamics in lean and obese subjects. Front Syst Neurosci 4:157

Stingl KT, Kullmann S, Ketterer C, Heni M, Haring HU, Fritsche A, Preissl H (2012) Neuronal correlates of reduced memory performance in overweight subjects. Neuroimage 60(1):362–369

Stingl KT, Rogic M, Stingl K, Canova C, Tschritter O, Braun C, Fritsche A, Preissl H (2010b) The temporal sequence of magnetic brain activity for food categorization and memorization—an exploratory study. Neuroimage 52(4):1584–1591

Stockburger J, Weike AI, Hamm AO, Schupp HT (2008) Deprivation selectively modulates brain potentials to food pictures. Behav Neurosci 122(4):936–942

Stoeckel LE, Weller RE, Cook EW 3rd, Twieg DB, Knowlton RC, Cox JE (2008) Widespread reward-system activation in obese women in response to pictures of high-calorie foods. Neuroimage 41(2):636–647

Suzuki K, Simpson KA, Minnion JS, Shillito JC, Bloom SR (2010) The role of gut hormones and the hypothalamus in appetite regulation. Endocr J 57(5):359–372
Tataranni PA, Gautier JF, Chen K, Uecker A, Bandy D, Salbe AD, Pratley RE, Lawson M, Reiman EM, Ravussin E (1999) Neuroanatomical correlates of hunger and satiation in humans using positron emission tomography. Proc Natl Acad Sci USA 96(8):4569–4574
Thierry G, Martin CD, Downing P, Pegna AJ (2007) Controlling for interstimulus perceptual variance abolishes N170 face selectivity. Nature neuroscience 10(4):505–511
Thorpe S, Fize D, Marlot C (1996) Speed of processing in the human visual system. Nature 381(6582):520–522
Thorpe SJ, Fabre-Thorpe M (2001) Neuroscience. Seeking categories in the brain. Science 291(5502):260–263
Toepel U, Knebel JF, Hudry J, le Coutre J, Murray MM (2009) The brain tracks the energetic value in food images. Neuroimage 44(3):967–974
Tschritter O, Preissl H, Hennige AM, Sartorius T, Stingl KT, Heni M, Ketterer C, Stefan N, Machann J, Schleicher E, Fritsche A, Haring HU (2012) High cerebral insulin sensitivity is associated with loss of body fat during lifestyle intervention. Diabetologia 55(1):175–182
Tschritter O, Preissl H, Hennige AM, Stumvoll M, Porubska K, Frost R, Marx H, Klosel B, Lutzenberger W, Birbaumer N, Haring HU, Fritsche A (2006) The cerebrocortical response to hyperinsulinemia is reduced in overweight humans: a magnetoencephalographic study. Proc Natl Acad Sci USA 103(32):12103–12108
Uhlhaas PJ, Haenschel C, Nikolic D, Singer W (2008) The role of oscillations and synchrony in cortical networks and their putative relevance for the pathophysiology of schizophrenia. Schizophr Bull 34(5):927–943
Unger JW, Livingston JN, Moss AM (1991) Insulin receptors in the central nervous system: localization, signalling mechanisms and functional aspects. Prog Neurobiol 36(5):343–362
Ungerleider LG, Haxby JV (1994) 'What' and 'where' in the human brain. Curr Opin Neurobiol 4(2):157–165
van der Heide LP, Kamal A, Artola A, Gispen WH, Ramakers GM (2005) Insulin modulates hippocampal activity-dependent synaptic plasticity in a N-methyl-d-aspartate receptor and phosphatidyl-inositol-3-kinase-dependent manner. J Neurochem 94(4):1158–1166
van Duinkerken E, Klein M, Schoonenboom NS, Hoogma RP, Moll AC, Snoek FJ, Stam CJ, Diamant M (2009) Functional brain connectivity and neurocognitive functioning in patients with long-standing type 1 diabetes with and without microvascular complications: a magnetoencephalography study. Diabetes 58(10):2335–2343
VanRullen R, Thorpe SJ (2001) The time course of visual processing: from early perception to decision-making. J Cogn Neurosci 13(4):454–461
Vega GL (2004) Obesity and the metabolic syndrome. Minerva Endocrinol 29(2):47–54
Vetiska SM, Ahmadian G, Ju W, Liu L, Wymann MP, Wang YT (2007) GABAA receptor-associated phosphoinositide 3-kinase is required for insulin-induced recruitment of postsynaptic GABAA receptors. Neuropharmacology 52(1):146–155
Volkow ND, Wang GJ, Telang F, Fowler JS, Goldstein RZ, Alia-Klein N, Logan J, Wong C, Thanos PK, Ma Y, Pradhan K (2009) Inverse association between BMI and prefrontal metabolic activity in healthy adults. Obesity (Silver Spring) 17(1):60–65
Wan Q, Xiong ZG, Man HY, Ackerley CA, Braunton J, Lu WY, Becker LE, MacDonald JF, Wang YT (1997) Recruitment of functional GABA(A) receptors to postsynaptic domains by insulin. Nature 388(6643):686–690
WHO (2012) Obesity and overweight. http://www.who.int/mediacentre/factsheets/fs311/en/. Accessed 20 Feb 2013
Williams G, Bing C, Cai XJ, Harrold JA, King PJ, Liu XH (2001) The hypothalamus and the control of energy homeostasis: different circuits, different purposes. Physiol Behav 74(4–5):683–701
Woods SC, Lotter EC, McKay LD, Porte D Jr (1979) Chronic intracerebroventricular infusion of insulin reduces food intake and body weight of baboons. Nature 282(5738):503–505

Woods SC, Seeley RJ (2000) Adiposity signals and the control of energy homeostasis. Nutrition 16(10):894–902

Wynne K, Stanley S, McGowan B, Bloom S (2005) Appetite control. J Endocrinol 184(2):291–318

Yeomans MR, Wright P, Macleod HA, Critchley JA (1990) Effects of nalmefene on feeding in humans. Dissociation of hunger and palatability. Psychopharmacology (Berl) 100(3):426–432

Presurgical MEG to Forecast Pediatric Cortical Epilepsies

Douglas F. Rose and Hisako Fujiwara

Abstract Although multiple modalities (semiology, EEG, MEG, PET, SPECT, fMRI) are useful for presurgical evaluation of patients with medication resistant epilepsy, only EEG and MEG have the millisecond time resolution to track the onset and spread of interictal discharges and ictal events. For good surgical outcome, both seizure onset zones (SOZ) and regions of immediate spread, the epileptogenic zone (EZ), need to be resected. Although for adults the main preoperative question may be whether seizures arise in left or right mesial temporal lobe, the locations of SOZ can be much more variable in children and adolescents. Recent studies indicate the most common cause of medically intractable epilepsy in pediatrics is cortical dysplasias functioning as epileptogenic regions. A child may have a single circumscribed cortical dysplastic region, multiple regions throughout a lobe, cerebral hemisphere, or even bihemispheric dysplastic regions. Sometimes seizures will start at just one focal cortical dysplastic region and spread throughout the brain. For other patients, multiple cortical dysplastic regions may independently generate seizures, more in the context of a seizure network than a single seizure focus. The difficult task is to anticipate the pattern of locations of cortical dysplasias and functional epileptogenic regions for each pediatric patient. Addressing this task adequately presurgically for each patient allows intracranial electrodes to be placed correctly to verify the locations where seizures start and to observe how the seizures spread in a single patient during different clinical seizure patterns. MEG with mathematical models of the head, brain and current source regions may be able to contribute significantly to the presurgical identification of the pediatric patient's seizure networks and to the prediction of source locations that should be assessed with intracranial EEG recording.

Keywords Beamformer · Cortical dysplasia · Epilepsy · Interictal · Ictal · Magnetoencephalography · Pediatric · Seizure · Surgery

D. F. Rose (✉) · H. Fujiwara
Division of Neurology, MEG Center, Cincinnati Children's Hospital Medical Center, University of Cincinnati, 3333 Burnet Avenue, Cincinnati, OH 45229, USA
e-mail: douglas.rose@cchmc.org

S. Supek and C. J. Aine (eds.), *Magnetoencephalography*,
DOI: 10.1007/978-3-642-33045-2_44,

1 Introduction

In children with medically intractable seizures who are candidates for epilepsy surgery, the most frequent etiology determined by postoperative pathology is abnormal cortical development, termed cortical dysplasia (Becker et al. 2006; Harvey et al. 2008). For evaluation of surgical candidates, no single recording or imaging modality has been able to predict correctly the location of seizure onset zones (SOZ) and epileptogenic zone (EZ) for all patients. Usually multiple modalities (seizure history, seizure semiology, video/EEG, high density EEG, MEG, MRI, EEG-fMRI, ictal SPECT, PET) are utilized to attempt to determine first the hemisphere of seizure onset, then the lobe of onset. If multiple modalities indicate the same hemisphere and lobe, there is some confidence that seizures may start in that lobe. However, each modality has its limitations.

Video/EEG with 10–20 electrode positions can capture seizures with excellent time resolution, but spatial resolution is limited. High density EEG with 128 or 256 scalp electrodes has improved spatial resolution over the scalp, though long recordings of several days are not yet routine. Methods to assess impedance tomography are not readily available to improve source localization with finite element modeling to account for tissue inhomogeneities that alter the measured electrical extracellular currents. MRI can provide superb anatomical resolution to identify certain types of cortical dysplasia, but diffuse cortical dysplasias sometimes escape detection. The anatomical assessment does not indicate which cortical dysplasias may be pathologically relevant for seizure onset or spread. EEG-fMRI combines certainty of localization with timing of interictal discharges, but the blood oxygen level dependent (BOLD) response may occur with a delay of up to 5 s. The relative timing in the rapid evolution and spread of electrical activity during the interictal discharge from one cortical region to another may be blurred and lost by 5 s later. The recording of ictal events may be limited because of associated patient movement at seizure onset. Ictal SPECT has been very successful in highlighting increased blood flow at seizure onset. However, because of timing of injection, the highest signal region may not have been the region of first onset. Multiple regions sometimes are activated, but relative timing can be difficult to ascertain. Finally, if the patient has multiple seizure types, the ictal SPECT may have only captured one of the types unless the test is repeated multiple times. PET scan does not have to capture a seizure and can show hypometabolism in the hemisphere involved in seizures, but spatial resolution may be limited to a lobe or hemisphere. MEG has both excellent time resolution and good spatial resolution, but the generally short recording times of 1–2 h means that primarily interictal discharges, not seizures, are captured. However, if a seizure is captured, MEG may be useful to examine signals at the very beginning of the clinical seizure, before the patient begins to move. Continuous head localization with real time tracking of fiducial sources may be able to track head movement even after the patient begins to move, although presence of scalp muscle artifact can decrease signal to noise ratio (SNR), similar to

EEG. If seizures are not captured, the question becomes how much information can be extracted from captured interictal discharges and how closely the evolution of an interictal discharge recapitulates the spread of a seizure (Lopes da Silva 2008).

2 Application of MEG Analysis to Interictal Discharges for Presurgical Estimation of Seizure Localization: Observations on General Limitations

Unlike adults, pediatric patients often have many interictal discharges captured during a 1–2 h MEG recording session. Nonetheless, the first limitation occurs when the pediatric patient does not have any interictal discharges from the hemisphere from which seizures are recorded by other modalities, such as video/EEG. The second limitation occurs when the patient has frequent interictal discharges from both hemispheres. MEG can provide localizations for the interictal discharges in each hemisphere, but cannot provide fundamental information regarding whether seizures begin in one hemisphere, or independently in each hemisphere. Unless actual seizures have also been captured for that patient by MEG, MEG data must be interpreted in the context of seizures captured by other modalities, such as video/EEG. Finally, both MEG and EEG must deal with the uncertainty of the inverse problem. They must rely on other information such as knowledge of brain anatomy to limit ictal onsets to regions of neurons rather than ventricles or blood vessels, and to cortical surfaces rather than regions of primarily white matter. Thus, interpretation of both modalities are dependent on MRI and known physiologic characteristics regarding most likely locations for epileptiform discharges to arise, either ictal or interictal. If these overall clinical limitations are kept in mind for each patient, it may be possible to attend to interictal discharges in the correct hemisphere to address issues of origin and spread.

3 Characterization of Interictal Discharges to Forecast Ictal Discharges in Pediatric Patients

An on-going debate occurs whether interictal spikes and sharp waves, brief events lasting perhaps 30–200 ms, arise anywhere near or within the SOZ and EZ or only represent irritative zones far removed from the seizure onset zone. Some authors note that interictal discharges, although brief, can spread rapidly through the brain (Alarcon et al. 1994; Ossadtchi et al. 2005; Hara et al. 2007) and suggest that elucidation of these propagation patterns may be similar to the pathways utilized during ictal initiation spread. Other authors note a variability of the propagation patterns during an interictal spike (Lantz et al. 2003; Sabolek et al. 2012), although patients whose seizures seem to begin similarly but evolve in different patterns are

well known. One group studying six patients with mixed patterns of cortical dysplasia with EEG-fMRI, noted that for some types of cortical dysplasia, interictal and ictal activation involved the same MRI lesions, while for patients with other types of cortical dysplasia, interictal discharges showed BOLD changes in the MRI lesion, but ictal discharges showed more activity in the overlying cortex (Tyvaert et al. 2008). Because interictal discharges can arise in the hemisphere opposite to that suggested by the patient's seizure semiology, care must be taken in choosing the interictal discharges to be examined in detail. In addition, as with all evaluative modalities in the patient's presurgical examination, the interpretation of the findings must be considered in light of the results from all the other evaluative modalities. Since the seizure is the event to be treated, every effort should be made to maximize the opportunity to capture one or more ictal events during the MEG study, and particularly the first few seconds before the patient begins to move. The same kinds of analysis for onset and propagation may be applied to the early ictal onset as are applied to interictal discharges.

Ictal onsets recorded with intracranial electrodes often begin with low amplitude high frequency repetitive activity that spreads locally and then more generally as the seizure evolves. The ability to detect these higher frequencies with MEG by examining higher bandwidths may improve analysis of cortical activities from extracranial recordings (Xiang et al. 2009, 2010; Rampp et al. 2010). Simply choosing a bandwidth of 20–70 Hz, instead of 1–70 Hz may eliminate much of the interfering lower frequency activities and improve SNR. The goal then may be to identify established abnormal networks of signal spread that occur in interictal discharges, some of which may occur also as networks of favored signal spread during ictal discharges.

From clinical experience, at least three patterns of cortical dysplasia may be seen in pediatric patients with medically intractable epilepsy: (1) a single focal region of cortical dysplasia from which seizures arise, (2) multiple regions of cortical dysplasia that may seem separate and sometimes distant, albeit in the same lobe, or different lobes in the same hemisphere, or (3) a diffuse region of cortical dysplasia throughout one or more lobes in a hemisphere (the pathologic, rather than functional, classification of cortical dysplasias has become more complex (Blumcke et al. 2011; Kabat and Krol 2012)). The challenge, once MEG signals are acquired at a high digitization rate, is which mathematical analysis algorithms to apply to these signals to best characterize the features of the underlying pathologic cortical activity.

The combination of a single equivalent current dipole (ECD) as a source model and the least squares approximation algorithm was among the first source localization methods used for MEG. Over the past 20 years this ECD algorithm has been the one most often used in clinical epilepsy studies. By definition the single ECD model is a point source. For presurgical evaluation of medically intractable epilepsy, the single ECD model can be very appropriate to localize a single small circumscribed region of abnormal cortex. The neurosurgeon, though, may prefer to have additional information on the spatial extent of the functional pathology.

Spikes are defined as lasting less than 70 ms with a peak amplitude at a halfway point around 35 ms after onset. However, if conduction velocities in cortical axons are such that a single impulse can cross from one hemisphere to another in perhaps 10 ms (Barth et al. 1982), then from onset to peak amplitude enough time has expired for a signal to cross back and forth between the two hemispheres 3½ times. Thus, we should not be surprised if several pathologic cortical regions could become active during a single spike and contribute signals to the overall spike signal recorded extracranially. Examples of spikes that are composites of sequential activations in multiple cortical regions, corroborated by later intracranial EEG recordings, have been published for scalp EEG (Alarcon et al. 1994) and more recently for MEG (Rose et al. 2013).

The single ECD source localization algorithm evaluated at a spike peak, where SNR is best, may identify the 'center of gravity' of a single contiguous cortical activation. However, if the abnormal activity spreads rapidly to several more disparate cortical regions, the single ECD source model would likely identify a point located somewhere in the middle of disparate sources that may be located on separate gyri or in separate lobes, whose activations nonetheless overlap in time during a single spike. In such a case, the single ECD source model might not correctly identify the locations of any of the sources.

The multiple ECD model may resolve this mislocalization. However, since the prior source localizations may change as the model increases from single to multiple dipoles as each new putative dipole is added, the putative locations have been dependent on the examiner's estimate as to how many different sources may be involved, although more recently automated Bayesian approaches have been published (Campi et al. 2011).

Algorithms that assess source signals at multiple evenly spaced locations throughout the brain avoid examiners' biases for number of sources. For example, multiple signal classification, MUSIC (Mosher et al. 1992), scans evenly through the brain at multiple locations and then evaluates results for the best source location. A refinement of this method recursively solves for additional dipole locations in the remaining signal (Mosher and Leahy 1999) and thereby removes the requirement for an a priori choice of number of dipoles. Another approach is to distribute multiple dipoles evenly throughout the brain and simultaneously solve for the combination of sources that best fits the signal. Minimum norm estimation (MNE) was perhaps the earliest method that applied this approach to MEG signals (Hamalainen and Ilmoniemi 1994), but there have been many refinements subsequently (Grech et al. 2008). A third approach, beamformer, essentially tunes the magnetometer to a single location in the brain, obtains and evaluates the signal at that location, repeats the process at locations spaced evenly throughout the brain, then allows comparison of the resulting signals. For each of these approaches, the examined locations or the placement of putative dipole sources can be restricted to cortical surfaces, if the patient's three dimensional magnetic resonance image (MRI) has been constructed and the cortical surface has been segmented.

Although the singe ECD model has historically been most frequently utilized for clinical presurgical epilepsy evaluations and other algorithms have been more

frequently utilized in clinical research, studies have begun to appear comparing the single ECD model to the other algorithms in clinical epilepsy applications (Robinson et al. 2004; Ukai et al. 2004; Shiraishi et al. 2005a, b; Imai et al. 2007; Tanaka et al. 2009; Elisevich et al. 2011; Shiraishi et al. 2011; Zhang et al. 2011; de Gooijer-van de Groep et al. 2012).

4 The Rationale for Noninvasive Delineation of Multiple Onset and Spread Locations in the Presurgical Evaluation of Cortical Dysplasias

In the past 30 years, subdural electrodes became widely used in the United States and elsewhere for intracranial EEG recordings, supplanting prior use of stereotaxic/tactic EEG (SEEG) with depth electrodes at many institutions (Wyler et al. 1984; Ryvlin and Rheims 2008). The subdural grids record primarily from the surfaces of the brain, i.e., the crowns of the gyri. Since the grids are often placed contiguously on the brain surface, perhaps only the perimeter of the surface to be covered needs to be estimated presurgically to facilitate presurgical planning for grid placement. The locations of gyral crowns that show epileptic activity relative to normal gyral crowns are determined after the grids are placed. However, about 60 % of cerebral cortex is buried in sulci (Van Essen 2005) and therefore may not be well sampled by surface grids (Ryvlin and Rheims 2008).

Recently, there has also been recognition that epilepsy arising from cortical dysplasia may involve networks of cortical regions rather than just the prior conception of a single epileptic focus (Kramer et al. 2010; Berg and Scheffer 2011; Varotto et al. 2012; Terry et al. 2012; Bartolomei et al. 2008) and that the SOZs may sometimes arise deep in sulci not well detected by surface grids (Wang et al. 2012). During the presurgical phase of invasive monitoring with intracranial EEG and medication withdrawal, children often have frequent seizures in short time duration. Assessment of possible seizure networks, in addition to determination of the locations of one or more SOZs, must be made often over just several days. Advance knowledge regarding possible epileptogenic regions and possible networks of spread may make complex results from intracranial EEG more easily understood. Non-invasive studies, such as MEG, that can detect multiple sources in interictal or ictal discharges, and the relative timing of activation of each source region, may be helpful in interpreting relative activation of epileptic discharges at the electrodes of cerebral surface grids.

Additionally, there has been a recently renewed interest in using SEEG (Cardinale et al. 2013; Gonzalez-Martinez et al. 2013) for presurgical delineation of SOZ and spread, particularly for patients whose seizure onsets were not well-localized by surface grid recordings. For these studies, both gyral crowns and sulci can be assessed by the depth electrodes. However, the targets for the depth electrodes must be planned in advance, both to avoid the vascular rete of cerebral

arteries and veins and to reach the SOZ and EZ. For this method of intracranial EEG recording, extensive non-invasive recordings and source localization that predict interictal or ictal onset and patterns of spread may be very important for planning the depth electrode placement.

5 The Quest

In summary, children with intractable epilepsy, possibly caused by cortical dysplasias, may have more complex seizure networks than a single epileptogenic cortical focus with local spread. The challenge for researchers and clinicians helping these children is to determine whether there is a single SOZ or multiple SOZs, and whether spread of epileptiform activity is to secondary regions that are otherwise normal cortex, or to regions potentially epileptogenic themselves.

The improvement in MEG source localization algorithms over the past 35 years has been steady and impressive. There are now multiple source localization algorithms available and strategies regarding how best to apply the algorithms clinically to the study of interictal spikes and ictal discharges, when the latter can be captured in an MEG session (Yoshinaga et al. 2004; Yagyu et al. 2010; Fujiwara et al. 2012). These range from independent component analysis (ICA) (Ossadtchi et al. 2004) to spatiotemporal modeling of dipole scanning algorithms such as MUSIC (Huiskamp et al. 2004) or distributed dipole algorithms such as MNE (Tanaka et al. 2010, 2012; Chowdhury et al. 2013). Beamformer algorithms may have special appeal in this regard because the general methodology is well-positioned to improve SNR at multiple source locations throughout the brain and then reconstruct the time series signal at those locations (Sekihara et al. 2001, 2002; Otsubo et al. 2012; Hong and Jun 2012).

Regardless of the algorithm used, the main task is to optimize the algorithm's ability to detect multiple sources, if present, and to delineate the time course of activation of each source within the evolution of the overall interictal or ictal discharge. The time courses of activation of different sources within the interictal or ictal discharge may be sufficiently different that they are distinguishable by visual inspection alone. However, if the timing differences of onset and peak activation are less than 10 ms, visual inspection of the waveforms may be insufficient. Quantitative measures of coherence and phase differences may be required. The beamformer algorithms are known to have difficulty resolving tightly correlated sources that are spatially close (Brookes et al. 2007). However, modifications of these algorithms have been shown to handle correlated sources well (Moiseev and Herdman 2013; Belardinelli et al. 2012; Diwakar et al. 2011). Since the authors of each of the multiple algorithms described above may have used different starting assumptions, the safest approach may be to apply two or more different algorithms to the interictal or ictal discharge and compare the findings.

Perhaps in the future with careful application of these algorithms to localization of interictal and/or ictal events we will attain the quest of non-invasively mapping

SOZs, EZs, and epileptic networks in children with single or multiple regions of cortical dysplasia to guide placement of intracranial electrodes, subdural or SEEG, for improved surgical treatment of their medication resistant epilepsy.

References

Alarcon G, Guy CN, Binnie CD, Walker SR, Elwes RD, Polkey CE (1994) Intracerebral propagation of interictal activity in partial epilepsy: implications for source localisation. J Neurol Neurosurg Psychiatry 57(4):435–449

Barth DS, Sutherling W, Engel J Jr, Beatty J (1982) Neuromagnetic localization of epileptiform spike activity in the human brain. Science 218(4575):891–894

Bartolomei F, Wendling F, Chauvel P (2008) The concept of an epileptogenic network in human partial epilepsies. Neurochirurgie 54(3):174–184

Becker AJ, Blumcke I, Urbach H, Hans V, Majores M (2006) Molecular neuropathology of epilepsy-associated glioneuronal malformations. J Neuropathol Exp Neurol 65(2):99–108

Belardinelli P, Ortiz E, Braun C (2012) Source activity correlation effects on LCMV beamformers in a realistic measurement environment. Comput Math Methods Med 2012:190513

Berg AT, Scheffer IE (2011) New concepts in classification of the epilepsies: entering the 21st century. Epilepsia 52(6):1058–1062

Blumcke I, Thom M, Aronica E, Armstrong DD, Vinters HV, Palmini A, Jacques TS, Avanzini G, Barkovich AJ, Battaglia G, Becker A, Cepeda C, Cendes F, Colombo N, Crino P, Cross JH, Delalande O, Dubeau F, Duncan J, Guerrini R, Kahane P, Mathern G, Najm I, Ozkara C, Raybaud C, Represa A, Roper SN, Salamon N, Schulze-Bonhage A, Tassi L, Vezzani A, Spreafico R (2011) The clinicopathologic spectrum of focal cortical dysplasias: a consensus classification proposed by an ad hoc Task Force of the ILAE Diagnostic Methods Commission. Epilepsia 52(1):158–174

Brookes MJ, Stevenson CM, Barnes GR, Hillebrand A, Simpson MI, Francis ST, Morris PG (2007) Beamformer reconstruction of correlated sources using a modified source model. Neuroimage 34(4):1454–1465

Campi C, Pascarella A, Sorrentino A, Piana M (2011) Highly automated dipole estimation (HADES). Comput Intell Neurosci 2011:982185

Cardinale F, Cossu M, Castana L, Casaceli G, Schiariti MP, Miserocchi A, Fuschillo D, Moscato A, Caborni C, Arnulfo G, Lo Russo G (2013) Stereoelectroencephalography: surgical methodology, safety, and stereotactic application accuracy in 500 procedures. Neurosurgery 72(3):353-366; discussion 366

Chowdhury RA, Lina JM, Kobayashi E, Grova C (2013) MEG source localization of spatially extended generators of epileptic activity: comparing entropic and hierarchical Bayesian approaches. PLoS ONE 8(2):e55969

de Gooijer-van de Groep KL, Leijten FS, Ferrier CH, Huiskamp GJ (2012) Inverse modeling in magnetic source imaging: comparison of MUSIC, SAM(g2), and sLORETA to interictal intracranial EEG. Human brain mapping

Diwakar M, Huang MX, Srinivasan R, Harrington DL, Robb A, Angeles A, Muzzatti L, Pakdaman R, Song T, Theilmann RJ, Lee RR (2011) Dual-Core beamformer for obtaining highly correlated neuronal networks in MEG. Neuroimage 54(1):253–263

Elisevich K, Shukla N, Moran JE, Smith B, Schultz L, Mason K, Barkley GL, Tepley N, Gumenyuk V, Bowyer SM (2011) An assessment of MEG coherence imaging in the study of temporal lobe epilepsy. Epilepsia 52(6):1110–1119

Fujiwara H, Greiner HM, Hemasilpin N, Lee KH, Holland-Bouley K, Arthur T, Morita D, Jain SV, Mangano FT, Degrauw T, Rose DF (2012) Ictal MEG onset source localization compared to

intracranial EEG and outcome: improved epilepsy presurgical evaluation in pediatrics. Epilepsy Res 99(3):214–224
Gonzalez-Martinez J, Bulacio J, Alexopoulos A, Jehi L, Bingaman W, Najm I (2013) Stereoelectroencephalography in the difficult to localize refractory focal epilepsy: early experience from a North American epilepsy center. Epilepsia 54(2):323–330
Grech R, Cassar T, Muscat J, Camilleri KP, Fabri SG, Zervakis M, Xanthopoulos P, Sakkalis V, Vanrumste B (2008) Review on solving the inverse problem in EEG source analysis. J Neuroengineering Rehabil 5:25
Hamalainen MS, Ilmoniemi RJ (1994) Interpreting magnetic fields of the brain: minimum norm estimates. Med Biol Eng Compu 32(1):35–42
Hara K, Lin FH, Camposano S, Foxe DM, Grant PE, Bourgeois BF, Ahlfors SP, Stufflebeam SM (2007) Magnetoencephalographic mapping of interictal spike propagation: a technical and clinical report. Am J Neuroradiol 28(8):1486–1488
Harvey AS, Cross JH, Shinnar S, Mathern BW (2008) Defining the spectrum of international practice in pediatric epilepsy surgery patients. Epilepsia 49(1):146–155
Hong JH, Jun SC (2012) Scanning reduction strategy in MEG/EEG beamformer source imaging. J Appl Math 2012(528469):19. doi:10.1155/2012/528469
Huiskamp G, van Der Meij W, van Huffelen A, van Nieuwenhuizen O (2004) High resolution spatio-temporal EEG-MEG analysis of rolandic spikes. J Clin Neurophysiol Official Publ Am Electroencephalographic Soc 21(2):84–95
Imai K, Otsubo H, Sell E, Mohamed I, Ochi A, RamachandranNair R, Snead OC 3rd (2007) MEG source estimation from mesio-basal temporal areas in a child with a porencephalic cyst. Acta Neurol Scand 116(4):263–267
Kabat J, Krol P (2012) Focal cortical dysplasia—review. Pol J Radiology Pol Med Soc Radiology 77(2):35–43
Kramer MA, Eden UT, Kolaczyk ED, Zepeda R, Eskandar EN, Cash SS (2010) Coalescence and fragmentation of cortical networks during focal seizures. J Neurosci Official J Soc Neurosci 30(30):10076–10085
Lantz G, Spinelli L, Seeck M, de Peralta Menendez RG, Sottas CC, Michel CM (2003) Propagation of interictal epileptiform activity can lead to erroneous source localizations: a 128-channel EEG mapping study. J Clin Neurophysiol Official Publ Am Electroencephalographic Soc 20(5):311–319
Lopes da Silva FH (2008) The impact of EEG/MEG signal processing and modeling in the diagnostic and management of epilepsy. IEEE Rev Biomed Eng 1:143–156
Moiseev A, Herdman AT (2013) Multi-core beamformers: derivation, limitations and improvements. Neuroimage 71:135–146
Mosher JC, Leahy RM (1999) Source localization using recursively applied and projected (RAP) MUSIC. IEEE Trans Signal Process 47(2):332–340
Mosher JC, Lewis PS, Leahy RM (1992) Multiple dipole modeling and localization from spatio-temporal MEG data. IEEE Trans Bio-med Eng 39(6):541–557
Ossadtchi A, Baillet S, Mosher JC, Thyerlei D, Sutherling W, Leahy RM (2004) Automated interictal spike detection and source localization in magnetoencephalography using independent components analysis and spatio-temporal clustering. Clin Neurophysiol Official J Int Fed Clin Neurophysiol 115(3):508–522
Ossadtchi A, Mosher JC, Sutherling WW, Greenblatt RE, Leahy RM (2005) Hidden Markov modelling of spike propagation from interictal MEG data. Phys Med Biol 50(14):3447–3469
Otsubo H, Mohamed IS, Cheyne D (2012) Source localization using event related beamformer of magnetoencephalography for interictal spikes in pediatric neocortical epilepsy. In: ICME international conference on complex medical engineering (CME), 2012. pp 288–291
Rampp S, Kaltenhauser M, Weigel D, Buchfelder M, Ingmar Blumcke I, Dorfler A, Stefan H (2010) MEG correlates of epileptic high gamma oscillations in invasive EEG. Epilepsia 51(8):1638–1642
Robinson SE, Nagarajan SS, Mantle M, Gibbons V, Kirsch H (2004) Localization of interictal spikes using SAM(g2) and dipole fit. Neurol Clin Neurophysiol 2004:74

Rose DF, Fujiwara H, Holland-Bouley K, Greiner HM, Arthur T, Mangano FT (2013) Focal peak activities in spread of interictal-ictal discharges in epilepsy with beamformer MEG: evidence for an epileptic network? Front Neurol 4:56

Ryvlin P, Rheims S (2008) Epilepsy surgery: eligibility criteria and presurgical evaluation. Dialogues Clin Neurosci 10(1):91–103

Sabolek HR, Swiercz WB, Lillis KP, Cash SS, Huberfeld G, Zhao G, Ste Marie L, Clemenceau S, Barsh G, Miles R, Staley KJ (2012) A candidate mechanism underlying the variance of interictal spike propagation. J Neurosci Official J Soc Neurosci 32(9):3009–3021

Sekihara K, Nagarajan SS, Poeppel D, Marantz A, Miyashita Y (2001) Reconstructing spatio-temporal activities of neural sources using an MEG vector beamformer technique. IEEE Trans Bio-med Eng 48(7):760–771

Sekihara K, Nagarajan SS, Poeppel D, Marantz A, Miyashita Y (2002) Application of an MEG eigenspace beamformer to reconstructing spatio-temporal activities of neural sources. Hum Brain Mapp 15(4):199–215

Shiraishi H, Ahlfors SP, Stufflebeam SM, Knake S, Larsson PG, Hamalainen MS, Takano K, Okajima M, Hatanaka K, Saitoh S, Dale AM, Halgren E (2011) Comparison of three methods for localizing interictal epileptiform discharges with magnetoencephalography. J Clin Neurophysiol Official Publ Am Electroencephalographic Soc 28(5):431–440

Shiraishi H, Ahlfors SP, Stufflebeam SM, Takano K, Okajima M, Knake S, Hatanaka K, Kohsaka S, Saitoh S, Dale AM, Halgren E (2005a) Application of magnetoencephalography in epilepsy patients with widespread spike or slow-wave activity. Epilepsia 46(8):1264–1272

Shiraishi H, Stufflebeam SM, Knake S, Ahlfors SP, Sudo A, Asahina N, Egawa K, Hatanaka K, Kohsaka S, Saitoh S, Grant PE, Dale AM, Halgren E (2005b) Dynamic statistical parametric mapping for analyzing the magnetoencephalographic epileptiform activity in patients with epilepsy. J Child Neurol 20(4):363–369

Tanaka N, Cole AJ, von Pechmann D, Wakeman DG, Hamalainen MS, Liu H, Madsen JR, Bourgeois BF, Stufflebeam SM (2009) Dynamic statistical parametric mapping for analyzing ictal magnetoencephalographic spikes in patients with intractable frontal lobe epilepsy. Epilepsy Res 85(2–3):279–286

Tanaka N, Grant PE, Suzuki N, Madsen JR, Bergin AM, Hamalainen MS, Stufflebeam SM (2012) Multimodal imaging of spike propagation: a technical case report. AJNR Am J Neuroradiol 33(6):E82–E84

Tanaka N, Hamalainen MS, Ahlfors SP, Liu H, Madsen JR, Bourgeois BF, Lee JW, Dworetzky BA, Belliveau JW, Stufflebeam SM (2010) Propagation of epileptic spikes reconstructed from spatiotemporal magnetoencephalographic and electroencephalographic source analysis. Neuroimage 50(1):217–222

Terry JR, Benjamin O, Richardson MP (2012) Seizure generation: the role of nodes and networks. Epilepsia 53(9):e166–e169

Tyvaert L, Hawco C, Kobayashi E, LeVan P, Dubeau F, Gotman J (2008) Different structures involved during ictal and interictal epileptic activity in malformations of cortical development: an EEG-fMRI study. Brain J Neurol 131(Pt 8):2042–2060

Ukai S, Kawaguchi S, Ishii R, Yamamoto M, Ogawa A, Mizuno-Matsumoto Y, Robinson SE, Fujita N, Yoshimine T, Shinosaki K, Takeda M (2004) SAM(g2) analysis for detecting spike localization: a comparison with clinical symptoms and ECD analysis in an epileptic patient. Neurol Clin Neurophysiol 2004:57

Van Essen DC (2005) A Population-average, landmark- and surface-based (PALS) atlas of human cerebral cortex. NeuroImage 28(3):635–662

Varotto G, Tassi L, Franceschetti S, Spreafico R, Panzica F (2012) Epileptogenic networks of type II focal cortical dysplasia: a stereo-EEG study. NeuroImage 61(3):591–598

Wang ZI, Jin K, Kakisaka Y, Mosher JC, Bingaman WE, Kotagal P, Burgess RC, Najm IM, Alexopoulos AV (2012) Imag(in)ing seizure propagation: MEG-guided interpretation of epileptic activity from a deep source. Hum Brain Mapp 33(12):2797–2801

Wyler AR, Ojemann GA, Lettich E, Ward AA Jr (1984) Subdural strip electrodes for localizing epileptogenic foci. J Neurosurg 60(6):1195–1200

Xiang J, Liu Y, Wang Y, Kirtman EG, Kotecha R, Chen Y, Huo X, Fujiwara H, Hemasilpin N, Lee K, Mangano FT, Leach J, Jones B, DeGrauw T, Rose D (2009) Frequency and spatial characteristics of high-frequency neuromagnetic signals in childhood epilepsy. Epileptic Disord Int Epilepsy J Videotape 11(2):113–125

Xiang J, Wang Y, Chen Y, Liu Y, Kotecha R, Huo X, Rose DF, Fujiwara H, Hemasilpin N, Lee K, Mangano FT, Jones B, DeGrauw T (2010) Noninvasive localization of epileptogenic zones with ictal high-frequency neuromagnetic signals. J Neurosurg Pediatr 5(1):113–122

Yagyu K, Takeuchi F, Shiraishi H, Nakane S, Sueda K, Asahina N, Kohsaka S, Umeoka S, Usui N, Baba K, Saitoh S (2010) The applications of time-frequency analyses to ictal magnetoencephalography in neocortical epilepsy. Epilepsy Res 90(3):199–206

Yoshinaga H, Ohtsuka Y, Watanabe Y, Inutsuka M, Kitamura Y, Kinugasa K, Oka E (2004) Ictal MEG in two children with partial seizures. Brain Dev 26(6):403–408

Zhang R, Wu T, Wang Y, Liu H, Zou Y, Liu W, Xiang J, Xiao C, Yang L, Fu Z (2011) Interictal magnetoencephalographic findings related with surgical outcomes in lesional and nonlesional neocortical epilepsy. Seizure 20(9):692–700

Future Developments in Clinical MEG and Its Combination with nTMS

Jyrki P. Mäkelä

Abstract Development of clinical MEG will provide biomarkers of neurodegenerative disorders by producing functional and effective connectivity measures within and between distinct functional brain areas. It is highly probable that neurodegenerative disorders damage these connections early in their course and detection of such changes will be feasible with sophisticated signal analysis of MEG data. Combining MEG and nTMS has already proven to be valuable in clinical evaluations. Such combinations will assist us in understanding the complex brain networks and the effective connectivity within them both in the healthy and diseased brains.

Keywords Connectivity · Epilepsy · Neurodegenerative diseases · Navigated transcranial magnetic stimulation (nTMS)

1 MEG in Clinical Connectivity Studies

The trend in the MEG community, as well as in the neuroscience community in general, is to reveal the brain functions creating the unified perceptions of the world, despite the parcellated presentation of its features in our brains. Higher level cognitive functions such as attention, working memory and sensory awareness also arise from activations in widespread cortical networks. The complete view/model of these functional networks will require understanding of anatomical, functional and effective connectivity within and between distinct functional brain areas. MEG, with its excellent temporal and tolerable spatial accuracy will definitively play an important role in this endeavor (e.g., Palva et al. 2010; Hipp et al. 2012).

J. P. Mäkelä (✉)
BioMag Laboratory, HUS Medical Imaging Center, Helsinki University Central Hospital, P.O. Box 340, 00029 Helsinki, Finland
e-mail: jyrki.makela@hus.fi

S. Supek and C. J. Aine (eds.), *Magnetoencephalography*,
DOI: 10.1007/978-3-642-33045-2_45,

The advances of neuroscience and clinical applications of MEG have been linked closely to progress of instrumentation and signal analysis methods. Development of instrumentation provides new possibilities as "hypothesis generating" research, complementing the traditional "hypothesis testing" approaches.

Studies of signal conduction between different brain areas using MEG were first started in patients with epilepsy. Already the early efforts demonstrated that MEG is able to identify source locations of epileptiform activity and map its spread to the opposite hemisphere (Barth et al. 1982). More recent studies have convincingly shown the usefulness of MEG studies in planning epilepsy surgery. MEG improves the treatment plan in about 20–30 % of the patients (Sutherling et al. 2008; Knowlton et al. 2009; de Tiege et al. 2012). However, source localization of the earliest epileptiform activity, not a detailed analysis of its spread, has been the main target of MEG studies in epilepsy (for a review, see, e.g., Mäkelä et al. 2006). The significance of tracking the spread of epileptiform activity may increase along with developments of epilepsy surgery planning, e.g., in increased use of stereotactic EEG as opposed to subdural grid recordings.

Recent developments have made studies of such "clinical connectivity" more precise. New, more comfortable gantries and continuous head position localization have made ictal MEG recordings more convenient, and they localize ictal onset zone with high sensitivity and specificity at the brain lobe level. Sources of ictal onset MEG signals and interictal dipole clusters are essentially equally specific in estimation of the ictal onset zone as defined by ECoG, but ictal MEG is more sensitive (Medvedovsky et al. 2012). A combination of MEG with precisely time-locked video recordings has enhanced the identification of ictal events and eased the recognition of artifacts (Zhdanov et al. 2013). These applications, developed in clinical studies, will also definitively assist sophisticated basic research experiments, e.g., by guiding the data analysis into precisely selected time windows of required behaviors and provide additional information for MEG "metadata" storage.

MEG may also provide tools to improve diagnostics of neurodegenerative disorders. In these conditions, detection of functional disconnection between brain regions will be crucial. For example, early AD pathology results in abnormal interactions between neuronal systems even before the onset of clinical signs and symptoms (Delbeuck et al. 2003; Brier et al. 2012). MEG is a useful tool to identify a "signature" of altered functional connectivity that can distinguish pathological processes from normal cognition (Stam et al. 2009). MEG studies may provide unique information regarding the changes in brain function responsible for the development of clinical dementia. This should help to direct the development of treatment strategies (e.g., as an endpoint in clinical trials), and in the tracking of disease progression. Because MEG is sensitive to dendritic activity at the synaptic level (Murakami and Okada 2006), it may be able to detect pathology even before there is evidence of other "positive" neuroimaging biomarkers (e.g., in vivo amyloid imaging; for a review, see Zamrini et al. 2011).

The present connectivity analysis methods require relatively long recordings of high-quality signals for providing meaningful results. Exquisite experimental setups are needed to avoid problems related to varying vigilance. Moreover,

sophisticated movement correction and artifact suppression are required for complete realization of their clinical value. Fortunately, MEG noise suppression methods have developed rapidly. The signal space separation algorithm (SSS) allows the recognition of magnetic signals from different subspaces, e.g., from the head and its surroundings (Taulu and Simola 2006). The removal of the signals that appear statistically similar in both subspaces strongly suppresses the artifacts generated even in the close vicinity of the sensors, e.g., by electric stimulation of subthalamic electrodes in patients with Parkinson's disease. This expands the MEG applications into studies of effects of deep brain stimulation on spontaneous brain activity in different neurodegenerative diseases (Airaksinen et al. 2012). The present efficacy of the SSS method can probably be enhanced further by optimizing the MEG sensor array to also include elements measuring the tangential components of the extracranial magnetic field (Nurminen et al. 2013). Besides external noise, random sensor noise may also deteriorate data quality. It is possible to use SSS for simultaneous modeling of the correlated signals from the brain and magnetic interference, and the uncorrelated part (from sensor noise) of a multichannel MEG signal, and thus aid in removing the uncorrelated part from the source estimation. This approach decreases the white noise level with a factor of about 2–4 while the physiological spectral peaks remain intact (Taulu et al. 2012). This is particularly important in single-trial analysis of evoked responses, and in analyzing high-frequency signals having relatively poor signal-to noise ratio. The method may also have clinical relevance e.g., in detecting high-frequency epileptiform signals (Helle et al. 2012). These developments will definitely assist in obtaining more crisp data for connectivity analyses, and also aid in applying the new analysis methods in the clinical diagnostics.

Time will tell, whether new MEG analysis methods searching for cortico-cortical spatial (Schnitzler and Gross 2005), phase-related (Palva et al. 2010), and temporal correlations (Montez et al. 2009) of spontaneous MEG networks in signal or source spaces will produce robust biomarkers of disease in individual patients. The complex methods used in data mining and complicated statistics associated with them may be relatively impenetrable for clinical users. In order to further the integration of clinical MEG results into routine patient flow, the analyses also need to be fast and understandable to the clinical teams utilizing them. The hypotheses and presumptions underlying the modeling need to be clear, and the effects of various details of the models required for the completion of the final results need to be thoroughly understood. Clinical decision making is seldom based on one methodology only. Nevertheless, developers of new analysis methods for such purposes may benefit by placing themselves into the clinical situation, i.e., as a target for the planned procedures, or to consider their willingness to use preventive medication for the next 20 years, based on data analysis results conducted by a technician. Although solving such usability problems is not necessarily attractive for researchers in basic neuroscience, it is highly important in clinical research and particularly in MEG clinical applications.

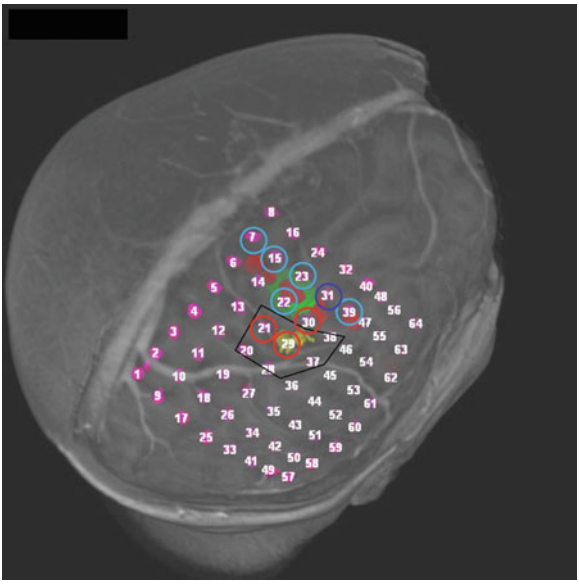

Fig. 1 Comparison of mapping with MEG, nTMS and ECoG in a patient with epilepsy, depicted on a 3-D reconstruction of the patient's brain. Epileptiform region near the motor cortex, as depicted by MEG, is colored *yellow*. *Red dots* indicate sites producing motor evoked potentials in nTMS. *Green dot* indicates the anatomic indicator of the hand motor area. *Red circles* mark electrodes where stimulation elicited typical seizures, *dark blue circle* indicates site producing hand movements and a seizure, and *light blue circles* indicate sites producing hand and arm movements. The surgeon removed the cortical area delineated by *black lines*. After the operation, the patient has remained free of seizures. Modified from Vitikainen et al. (2009)

2 Combination of MEG with Navigated Transcranial Magnetic Stimulation

The physics underlying noninvasive transcranial magnetic stimulation (TMS) can be considered as the reverse of MEG; instead of picking up tiny magnetic signals from the cortex, it utilizes fast, strong (about 2 T) magnetic pulses to modify cortical activity. Navigated TMS (nTMS) displays a dynamic estimate of the stimulus-induced electric field on the patient's individual 3-D brain MRI reconstruction, and enables selection of localized stimulation targets from it. The effects of nTMS can be tested on the source areas selected from MEG. For example, nTMS delivered to secondary somatosensory cortex area, pinpointed by MEG, speeds up somatomotor reactivity (Raij et al. 2008), and rhythmic TMS to the MEG-identified source areas of spontaneous oscillatory activity entrains these oscillations at the stimulation frequency (Thut et al. 2011) (Fig. 1).

In the foreseeable future, TMS devices will develop towards more complex delivery of pulses into multiple sites, monitoring the effects of TMS by electrophysiological measures, and even guiding the TMS properties by the induced

modifications. Although simultaneous TMS and MEG recordings probably will not be feasible, MEG will be a crucial tool in interpreting the electrophysiological connectivity utilized in such studies. Combining MEG and nTMS has already proven to be valuable in clinical evaluations (e.g. Vitikainen et al. 2009; Mäkelä et al. 2013, see also Fig. 1). Such combinations will assist us in understanding the complex brain networks, the effective connectivity within them both in the healthy and diseased brains.

References

Airaksinen K, Butorina A, Pekkonen E, Nurminen J, Taulu S, Ahonen A, Schnitzler A, Mäkelä JP (2012) Somatomotor mu rhythm amplitude correlates with rigidity during deep brain stimulation in Parkinsonian patients. Clin Neurophysiol 123:2010–2017

Barth DS, Sutherling W, Engel J Jr, Beatty J (1982) Neuromagnetic localization of epileptiform spike activity in the human brain. Science 218:891–894

Brier MR, Thomas JB, Snyder AZ, Benzinger TL, Zhang D, Raichle ME, Holltzman DM, Morris JC, Ances BM (2012) Loss of intranetwork and internetwork resting state functional connections with Alzheimer disease progression. J Neurosci 32:8890–8899

Delbeuck X, van der Linden M, Collette F (2003) Alzheimer's disease as disconnection syndrome? Neuropsychol Rev 13:79–91

DeTiege X, Carrette E, Legros B, Vonck K, Op de Beeck M, Bourguignon M, Massager N, David P, Van Roost D, Meurs A, Lapere S, Deblaere K, Goldman S, Van Bogaert P (2012) Clinical added value of magnetic source imaging in the presurgical evaluation of refractory focal epilepsy. J Neurol Neurosurg Psychiatry 83:417–423

Helle L, Parkkonen L, Taulu S, Ahonen A (2012) Suppression of uncorrelated sensor noise and artifacts: demonstration with high-frequency brain signals. Poster in Biomag 2012, Paris

Hipp JF, Hawellek DJ, Corbetta M, Siegel M, Engel AK (2012) Large-scale cortical correlation structure of spontaneous oscillatory activity. Nat Neurosci 15:884–890

Knowlton RC, Radzan SN, Limdi N, Elgavish RA, Killen J, Blount J, Burneo JG, Ver Hoef L, Paige L, Faught E, Kankiratwana P, Bartolocci A, Riley K, Kusniwecky R (2009) Effect of epilepsy magnetic source imaging on intracranial electrode placement. Ann Neurol 65:716–723

Medvedovsky M, Taulu S, Gaily E, Metsähonkala E-L, Mäkelä JP, Ekstein D, Kipervasser S, Neufeld MY, Kramer U, Blomstedt G, Fried I, Karppinen A, Veshchev I, Roivainen R, Ben-Zeev B, Goldberg-Stern H, Wilenius J, Paetau R (2012) Sensitivity and specificity of seizure onset zone estimation by ictal MEG. Epilepsia 53:1649–1657

Montez T, Poil S-S, Jones BF, Manshanden I, Verbunt JPA, van Dijk P, Brussaard AB, van Ooyen A, Stam CJ, Scheltens P, Linkenkaer-Hansen K (2009) Altered temporal correlations in parietal alpha and prefrontal theta oscillations in early-stage Alzheimer disease. PNAS 106:1614–1619

Murakami S, Okada Y (2006) Contributions of principal neocortical neurons to magnetoencephalography and electroencephalography signals. J Physiol 575(3):925–936

Mäkelä JP, Forss N, Jääskeläinen J, Kirveskari E, Korvenoja A, Paetau R (2006) Magnetoencephalography in neurosurgery. Neurosurgery 59:493–510

Mäkelä JP, Vitikainen A-M, Lioumis P, Paetau R, Ahtola E, Kuusela L, Valanne L, Blomstedt G, Gaily E (2013) Functional plasticity of the motor cortical structures demonstrated by navigated TMS in two patients with epilepsy. Brain Stimulat 6:286–291

Nurminen J, Taulu S, Nenonen J, Helle L, Simola J, Ahonen A (2013) Improving MEG performance with additional tangential sensors. IEEE Trans Biomed Eng 60:2559–2566

Palva JM, Monto S, Kulashekrar S, Palva S (2010) Neuronal synchrony reveals working memory networks and predicts individual memory capacity. PNAS 107:7580–7585

Raij T, Karhu J, Kičić D, Lioumis JP, Lin F-H, Ahveninen J, Ilmoniemi RJ, Mäkelä JP, Hämäläinen M, Rosen BR, Belliveau JW (2008) Parallel sensory input makes the brain run faster. NeuroImage 40:1792–1797

Schnitzler A, Gross J (2005) Normal and pathological oscillatory communication in the brain. Nat Neurosci 6:285–296

Stam CJ, de Haan W, Daffertshofer A, Jones BF, Manshanden I, van Cappellen van Walsum AM, Montez T, Verbunt JP, de Munck JC, van Dijk BW, Berendse HW, Scheltens P (2009) Graph theoretical analysis of magnetoencephalographic functional connectivity in Alzheimer's disease. Brain 132:213–224

Sutherling WW, Mamelak AN, Thyerlei D, Maleeva T, Minazad Y, Philpott L, Lopez N (2008) Influence of magnetic source imaging for planning intracranial EEG in epilepsy. Neurology 71:990–996

Taulu S, Simola J (2006) Spatiotemporal signal space separation method for rejecting nearby interference in MEG measurements. Phys Med Biol 51:1759–1768

Taulu S, Simola J, Kajola M, Helle L, Ahonen A, Sarvas J (2012) Suppression of uncorrelated sensor noise and artifacts in multi-channel MEG data. Poster in Biomag 2012, Paris

Thut G, Veniero D, Romei V, Miniussi C, Schyns P, Gross J (2011) Rhythmic TMS causes local entrainment of natural oscillatory signatures. Curr Biol 21:1176–1185

Vitikainen A-M, Lioumis P, Paetau R, Salli E, Komssi S, Metsähonkala L, Paetau A, Kičić D, Blomstedt G, Valanne L, Mäkelä JP, Gaily E (2009) Combined use of non-invasive techniques for improved functional localization for a selected group of epilepsy surgery candidates. NeuroImage 45:342–348

Zamrini E, Maestu F, Funke M, Mäkelä JP, Riley M, Bajo R, Sudre G, Fernandez A, Castellanos NP, Del Pozo F, Stam K, van Dijk B, Bagic A, Pekkonen E, Becker JT (2011) Magnetoencephalography (MEG) as a putative biomarker for Alzheimer's disease. Int J Alzh. Dis., doi:10.4061/2011/280289

Zhdanov A, Wilenius J, Paetau A, Ahonen A, Mäkelä JP (2013) Quantifying the contribution of video in combined video-magnetoencephalographic ictal recordings of epilepsy patients. Epilepsy Res 105:405–409

Part VI
Emerging Technologies

Ultra-Low-Field MRI and Its Combination with MEG

Lauri Parkkonen, Risto J. Ilmoniemi, Fa-Hsuan Lin and Michelle Espy

Abstract Recent progress in SQUID instrumentation has demonstrated the feasibility of using SQUID sensor arrays in MEG helmets to record also MRI data. Here we describe the basic principles of MRI as well as the special requirements and solutions needed to perform ultra-low-field MRI concurrently with MEG. We consider it is feasible to build practical MEG–MRI instruments for scientific experimentation and for clinical use. Acquiring an MRI with 2-mm spatial resolution and sufficient signal-to-noise ratio and contrast appears achievable without essentially lengthening the normal MEG measurement time.

Keywords MEG · MRI · ULF MRI · SQUID MRI · Magnetoencephalography · Magnetic resonance imaging · Ultra-low-field MRI

1 Introduction

The availability of large arrays of highly sensitive SQUID magnetometers in modern MEG devices enables one to measure magnetic fields other than those produced by neuronal electrical activity. Perhaps the most promising such possibility is to measure magnetic resonance imaging (MRI) signals in order to obtain anatomical images of the head concurrently with neuromagnetic experimentation.

L. Parkkonen (✉) · R. J. Ilmoniemi · F.-H. Lin
Department of Biomedical Engineering and Computational Science,
Aalto University School of Science, Espoo, Finland
e-mail: lauri.parkkonen@aalto.fi

F.-H. Lin
Institute of Biomedical Engineering, National Taiwan University, Taipei, Taiwan

M. Espy
Los Alamos National Laboratory, Los Alamos, NM, USA

S. Supek and C. J. Aine (eds.), *Magnetoencephalography*,
DOI: 10.1007/978-3-642-33045-2_46,

As will be explained below, this would bring several benefits such as improved registration of MEG and MRI, improved work flow, structural images with less distortion, and information about the conductivity of the brain.

A combined MEG and MRI device would be highly desirable. Although MRI provides excellent spatial resolution, functional MRI (fMRI) is limited by its poor temporal resolution (>1 s) and by its inability to directly measure neuronal activity. Based on blood volume or oxygenation changes, fMRI is only indirectly related to neuronal function (Logothetis et al. 2001). MEG, on the other hand, has excellent temporal resolution (in the millisecond scale). However, the ill-posed inverse problem limits the spatial accuracy attainable with MEG. This limitation can be mitigated to some extent by combining MEG with anatomical MRI to provide constraints to the inverse problem as well as to visualize the estimated source locations with respect to brain anatomy. Currently, this requires two costly scanners and complex measurement procedures. Even when done carefully, the combination of the MEG and MRI data may result in a biased inverse solution because of errors in the registration of the two coordinate systems.

In principle, combining MEG and MRI is straightforward: simply build a magnet as well as gradient and radiofrequency (RF) coils around an MEG sensor array. The problem is that MEG devices are generally designed to measure femtotesla-level fields and have a dynamic range only up to some tens or hundreds of nanoteslas while in MRI the fields go up to several tesla, i.e., 15 orders of magnitude above the weakest fields measured by SQUIDs. One solution is ultra-low-field MRI: the recordings are performed in a field of about 100 microtesla. If conventional MRI approaches, including tuned inductive receiver coils, would be used at these low fields, the resulting signal-to-noise ratio (SNR) would be very low and the system practically unusable because the amplitude SNR is proportional to the square of the field; the signal at 100 microtesla would be 9 orders of magnitude weaker than at 3 T. Fortunately, we can use three methodologies to counteract this problem. First, unlike tuned receivers, the sensitivity of SQUID sensors is independent of frequency; second, we can use pre-polarization techniques to magnetize the sample before the MRI data acquisition; third, we can gain from parallel data acquisition made available by the large number (up to 306 currently) of SQUID sensors in a typical MEG array.

2 Basic Principles of Ultra-Low-Field MRI

Before we begin a discussion of the recent progress and opportunities in ultra-low-field MRI combined with MEG, it is worth discussing the fundamental principles of nuclear magnetic resonance (NMR) and MRI, paying special attention to the unique features of SQUID-based ultra-low-field MRI. This will help us to better understand the fundamental benefits and unique challenges of combining MEG and MRI in a single device. We will present just a brief overview as there already

are excellent texts on NMR and MRI, such as those by Callaghan (1991) and Abragam (1961).

2.1 NMR

NMR can be performed on any nucleus that possesses a non-zero spin. The simplest case is the spin-½ nucleus of hydrogen (^{1}H), which we discuss here. The ^{1}H found in water is most commonly imaged in MRI. ^{1}H also provides the highest NMR sensitivity of any nuclei.

We can think of the spin as a magnetic moment or a tiny bar magnet. When placed in an external magnetic field, B, two states corresponding to different energy levels are possible: the lower level where the magnetic moment is aligned with B, and the higher energy state where it is oppositely oriented. The energy gap between these states is given by

$$\Delta E = h\gamma B, \tag{1}$$

where h is the Planck's constant ($h = 6.626 \times 10^{-34}$ J s); γ is the nucleus-dependent gyromagnetic ratio (for ^{1}H, $\gamma = 42.6$ MHz/T). We can also write

$$f = \gamma B, \tag{2}$$

where f is the characteristic *Larmor frequency*, a fundamental concept in NMR and MRI; a photon at this frequency can induce a transition from the lower to the higher energy state, or conversely, as we describe later, a nucleus emits a photon at this frequency when switching from the higher to the lower energy state. For a ^{1}H nucleus in a 1-T magnetic field, the Larmor frequency is 42.6 MHz.

The equilibrium distribution of spins in an external magnetic field follows Boltzmann statistics such that we find an excess of spins in the lower energy state. If N_0 is the total number of spins, this excess can be described as

$$\frac{\Delta N}{N_0} = \frac{h\gamma B}{kT}, \tag{3}$$

where k is the Boltzmann constant ($k = 1.381 \times 10^{-23}$ J/K) and T is the absolute temperature.

Here we meet the first challenge of ultra-low-field MRI. At room temperature (300 K) and in the strong magnetic field of 1 T, this excess is only about 0.0007 %. Thus, the resulting magnetization is very small and the signals measured are rather weak. This explains why almost every practical implementation of NMR and MRI involves a large magnetic field, and the overwhelming technological trend is toward higher fields. For example, 3 T is now routinely used in clinical MRI.

When the sample (or subject) is placed in an external magnetic field, the magnetization takes some time to develop. This step is referred to as polarization. To follow the usual NMR convention, we define the magnetic field to be along the z axis. The magnetization will develop toward the equilibrium as

$$M_z(t) = M_{z,\mathrm{eq}}\left(1 - \mathrm{e}^{-t/T_1}\right). \tag{4}$$

The equilibrium magnetization is

$$M_{\mathrm{eq}} = \frac{Nh^2\gamma^2 I(I+1)B}{3kT}, \tag{5}$$

where N is the number of spins being measured, and I is the spin number ($I = ½$ for ^{1}H). For example, for 1 cm^2 of water ($N = 6.69 \times 10^{22}$ proton spins) at 300 K in a 1-tesla field, $M_{\mathrm{eq}} \sim 3.2 \times 10^{-9}$ J/T. Again, if the magnetic field is smaller by a factor of 100, the magnetization (and thus signal amplitude) will also be smaller by a factor of 100. As shown in Eq. (4), the magnetization (or sample polarization) builds up inverse-exponentially. The characteristic time constant of this process is known as the T_1, or spin–lattice, relaxation time. T_1 is a powerful probe of chemical environment, providing means to discriminate between tissue types (e.g., Damadian et al. 1971). As we will discuss later, T_1 depends on the magnetic field strength as well, and hence may contain unique information in the ULF regime.

Once the sample is magnetized, one can manipulate this magnetization to produce a measurable signal. The first step is to orient a proportion of the magnetization off the axis of the magnetic field. Any component of the spins tipped off-axis will begin to rotate, or precess, at the Larmor frequency and emit a signal at that frequency. For example, if the magnetic field is along the z axis, precession will be in the x–y plane. During precession, the spins experience magnetic field inhomogeneities associated with their chemical environment (as well as the local ambient environment) that will slightly shift the local Larmor frequency and thus cause spin dephasing and therefore loss of signal. The rate at which the transverse signal decreases is

$$M_x(t) = M_{x,t=0}\cos(\omega t)e^{-t/T_2}. \tag{6}$$

$M_{x,t=0}$ is the initial magnetic moment transverse to the magnetic field, the cosine term describes rotation at the Larmor frequency($\omega = 2\pi f$), and T_2 is the characteristic dephasing, or spin–spin, relaxation time.

There is a fundamental difference between ULF and high-field (HF: $B > 1$ T for this discussion) NMR and MRI. In HF, the process of polarization, magnetization reorientation, spin evolution, and measurement all occur within a single magnetic field provided (typically) by a large superconducting magnet. At ULF, however, these fields may all be different and produced by different magnets.

Because the magnetization and thus signal is proportional to the field, one strategy is to use pre-polarization in a higher field ($B_p \sim$ 1–200 mT) followed by readout in a much lower measurement field ($B_m \sim$ 1–200 μT). Thus, T_1 in Eq. (4) refers to T_1 in the polarization field (B_p). However, T_2 in Eq. (6) will be that in the B_m field. Also, the values of precession are given by $f = \gamma B_m$, where B_m is the μT-level measurement field.

There are also differences in approaches to spin re-orientation (e.g., how precession is started, or how subsequent manipulations of the magnetization are accomplished) between conventional high-field (HF) MRI and the ULF MRI approaches. In HF MRI, spin re-orientation is typically accomplished by a time-varying magnetic field applied at the Larmor frequency, in a direction orthogonal to the direction of magnetization. This field is usually designated as B_1. The relation between B_1, the duration of its application t_{RF}, and angular tip of the magnetization Θ is given by

$$\Theta = 2\pi\gamma B_1 t_{RF}. \tag{7}$$

Note that in HF MRI, B_1 is chosen to match the fixed Larmor frequency of the scanner. But in ULF MRI, we can either perform the spin flip in B_p or B_m, depending on the pulse sequence we have chosen.

Typically we aim at $\Theta = 90^\circ$ to produce the maximum signal in the x–y plane, where detection occurs. However, there is another method of spin reorientation that takes advantage of the flexibility of ULF MRI magnetic field generation. In many ULF-MRI configurations, B_p and B_m are orthogonal. Thus, one can simply begin precession by a rapid (non-adiabatic, $dB_p/dt \gg \gamma B_m^2$) shut-off of B_p. In a non-adiabatic process, the magnetization cannot follow the field change, and is left aligned orthogonal to B_m. Precession will then begin automatically, without a B_1 pulse. Figure 1 illustrates both approaches.

Once precession has begun, detection of the magnetization can begin. In HF MRI, the typical scanner strengths are 1.5 or 3 T. This translates to a proton Larmor frequency of 64 or 128 MHz. A tuned induction coil is highly sensitive in this range. However, in ULF MRI precession occurs in the B_m field, typically on the order of 100 μT, corresponding to a Larmor frequency of 4.26 kHz.

In conventional MRI with a Faraday coil, the signal scales as B^2, one order arising from the magnetization being proportional to B and one for the induced signal being proportional to the Larmor frequency. However, this relationship no longer holds once we are limited by the body noise, which is typically above about 10 MHz (Myers et al. 2006). While pre-polarization is an approach to improve the former factor (Macovski and Conolly 1993), using an ultra-sensitive detector such as the SQUID is a way to mitigate the latter. SQUIDs, broadband detectors with unsurpassed sensitivity of about 1 fT/$\sqrt{\text{Hz}}$ in the frequency range of ULF MRI, are almost two orders more sensitive than a Faraday coil in this regime (Myers et al. 2006; Matlashov 2011). Because the SQUID is also the detector of choice for MEG, the combination of MEG and ULF MRI in a single device becomes obvious. We should, however, mention that getting a SQUID to work in the dynamic

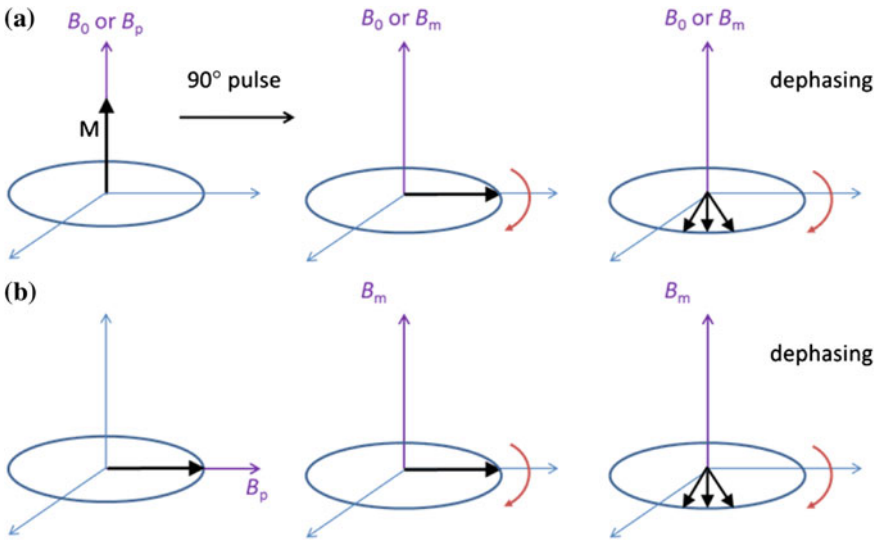

Fig. 1 Two methods for beginning precession. **a** The traditional 90° spin flip, possible both in HF and ULF MRI. In ULF MRI, the fields for polarization, spin flip, and precession may be of different amplitudes (and orientations, not shown here). In HF MRI, the fields are the same. **b** After polarization B_p is removed non-adiabatically and B_m is applied orthogonally. Precession begins immediately

environment of MRI, even at ultra-low fields, is quite challenging. We will discuss some of the basic hardware considerations in Sect. 2.3.

2.2 Basic Principles of Image Acquisition

The physical principles between ULF and HF MR imaging are quite similar. Here we review a few basic concepts that will help us understand the differences. An excellent and far more complete description of imaging principles in the context of conventional MRI is provided by Callaghan (1991).

MRI is the spatial encoding of the NMR properties (e.g., T_1, T_2, or spin density). Encoding is based on the variation of the Larmor frequency within the applied field, see Eq. (2). A magnetic field gradient $G(t)$ (assumed to be spatially linear for these discussions) is applied, causing the local Larmor frequency to vary such that

$$\omega(\mathbf{r}, t) = \omega_0 + 2\pi\gamma\mathbf{G}(t) \cdot \mathbf{r}. \tag{8}$$

The NMR signal $\Delta S(t)$ from a single voxel (ΔV) will be (neglecting relaxation)

$$\Delta S(t) \propto \rho(\mathbf{r}) \exp\left(i \int_0^t \omega\left(\boldsymbol{r}, t'\right) dt' \right) \Delta V, \tag{9}$$

where ρ(r) is the spin density, and $\omega(\mathbf{r},t')$ is the angular Larmor frequency. In Eq. (9), we assume that B_0 does not vary with time or position during the measurement. However, the ability to manipulate the measurement field in strength and orientation *between* measurements to extract different information from the image is a feature of ULF MRI that is typically absent in high-field MRI.

The signal from the whole sample, assuming here uniform detector sensitivity, becomes

$$S(t) = \exp(i\varphi(t)) \iiint q(\mathbf{r}) \exp\left(i \int_0^t 2\pi\gamma \mathbf{G}\left(t'\right) \cdot \mathbf{r} dt' \right) dV, \tag{10}$$

where $q(\mathbf{r})$ is the spin density containing contrast information on local spin density $\rho(\mathbf{r})$ and, when a suitable preparatory sequence is used, relaxation times $T_1(\mathbf{r})$ and $T_2(\mathbf{r})$, and/or diffusion coefficient $D(\mathbf{r})$. The time-varying phase, $\varphi(t)$, is the integral over the main Larmor frequency. Here we assume that the signal is obtained from the entire sample.

We next introduce the concept of the reciprocal space vector (Ljunggren 1983; Twieg 1983)

$$\mathbf{k} \equiv \gamma \int_0^t \mathbf{G}\left(t'\right) dt' \tag{11}$$

and we re-write Eq. 10 as (Callaghan 1991)

$$\mathrm{S}(\mathbf{k}) = \exp(i\varphi(t)) \iiint q(\mathbf{r}) \exp(i2\pi \mathbf{k} \cdot \mathbf{r}) dV \tag{12}$$

and

$$q(\mathbf{r}) = \exp(i\varphi(t)) \iiint \mathrm{S}(\mathbf{r}) \exp(-i2\pi \mathbf{k} \cdot \mathbf{r}) d^3k. \tag{13}$$

Equations (12) and (13) are a fundamental formulation in MRI. They comprise a Fourier transform pair showing that the signal and spin density are mutually conjugate. The MRI pulse sequence can then be thought of as a trajectory through *k*-space, where the gradient is analogous to velocity. How we apply the gradients will determine the course through image acquisition (Callaghan 1991).

Arising from this formulation, we can next consider two concepts that are critical to understanding image quality—spatial resolution and field of view

(FOV). We will see that in addition to lower polarization leading to lower signal, the lower strength of imaging gradients also poses a unique new challenge for ULF MRI in terms of image acquisition time.

The Fourier transform pair (12) and (13) defines the relationship between the spatial and frequency domains. It follows from the Nyquist theorem that for any real signal (using the *x,* or readout, direction as an example)

$$\Delta x = \frac{1}{k_{x,\max} - k_{x,\min}} \tag{14}$$

and

$$\Delta k = \frac{1}{x_{\max} - x_{\min}}. \tag{15}$$

We can re-write (15) as

$$L_x = (x_{\max} - x_{\min}) = \frac{1}{\Delta k}. \tag{16}$$

Equation (14) shows that the spatial resolution is related to the extent ($k_{\min}$ ... $k_{\max}$) of the image in the *k*-space. Equation (16) shows that the spatial extent of the image ($x_{\min}$ ... $x_{\max}$), or FOV, is related to the resolution in the *k*-space.

If the gradient does not change when it is switched on, the acquisition time t_a, Eq. (11) becomes

$$k_{x,\max} - k_{x,\min} = \gamma G_x t_a. \tag{17}$$

Thus we can describe the spatial resolution as

$$\Delta x = (\gamma G_x t_a)^{-1}. \tag{18}$$

Spatial resolution in other directions can be derived similarly. As can be seen from Eq. (18), to improve the spatial resolution, one either has to increase the gradient or the acquisition (or encoding) time. The gradients in ULF MRI are typically on the order of 10^{-4} T/m. This is about 1/100 of those used in HF MRI. Thus, if we want to keep the same resolution as in HF MRI, with these weaker gradients we must increase the acquisition time by a factor of 100.

Why don't we just increase the gradients? There are two reasons, the first being related to concomitant gradients. These are the unwanted magnetic fields, $G_\perp$, that inevitably arise in directions orthogonal to the measurement field B_m and to the gradients which we deliberately apply for imaging, $G_\parallel$. At a location within the imaging volume, these fields shift the frequency by

$$\Delta f \approx \gamma G_{\parallel} + \frac{1}{2}\frac{\gamma}{B_0 + G_{\parallel}} G_{\perp}^2. \tag{19}$$

In HF MRI, these gradients can be neglected because the main magnetic field ($B_0 > 1$ T) is typically much higher than the gradients (10^{-2} T/m) such that $G_{\parallel}/B_0 \ll 1$, $G_{\perp}/B_0 \ll 1$, and thus frequency variations produced by the stray fields are small. However, in ULF MRI the main magnetic field $B_m \approx 10^{-4}$ T and the gradients $G \approx 10^{-4}$ T/m, which generates a magnetic field variation of 0.2×10^{-4} T in a 20-cm FOV. The concomitant fields, not in parallel with B_m, are of similar order of magnitude as $G_{\parallel}$. Thus, the frequency variations are non-negligible and the total magnetic field experienced by the spin system is no longer in a plane orthogonal to B_m. In general, concomitant gradients can be accounted for with some effort (e.g. Volegov et al. 2005; Nieminen et al. 2010; Hsu et al. 2013), but they do pose a constraint.

The other reason that gradients cannot be arbitrarily strong is related to bandwidth. Consider a simple case: a HF MRI system with $B_0 = 1$ T and 10^{-2} T/m gradients. A 20-cm object would have a central frequency of 42.6 MHz and a frequency spread across the object of $\Delta f \sim 85.2$ kHz. However, if $B_m = 10^{-4}$ T and $G = 10^{-4}$ T/m, the central frequency is 4.26 kHz and the frequency spread within a FOV of 20 cm is 852 Hz. If we turn up the gradients, we will further widen the frequency spread across the object and consequently need to measure part of the MRI signal in the challenging concomitant-field regime.

Thus, our only choice to maintain spatial resolution at ULF appears to be longer acquisition times. But at ULF, the T_1 and T_2 times for many interesting tissues are approximately of the length required for t_a (Zotev et al. 2009), so we are also running out of signal at the same time. We note that Eq. (18) is applicable only when the SNR is sufficient, usually >5 (Matlashov et al. 2012). We can write SNR as (Myers et al. 2006)

$$\mathrm{SNR}_{\mathrm{voxel}} \approx C \cdot f(\mathrm{geom}) \cdot B_p \cdot V \cdot \sqrt{\frac{t_a}{2S_B}}, \tag{20}$$

where C comprises the physical constants, f is a function of the geometry, S_B is the magnetic noise spectral density, B_p is the pre-polarization field, and V is the voxel volume. We note again that SNR is proportional to B_p. As we mentioned previously, this is different from HF MRI where it scales as B_p^2 (i.e., ω_0^2). This is also different than pulsed-field MRI using a Faraday coil (Matter et al. 2006), where SNR scales as $B_p B_m$. The reason for this is the broad-band sensitivity of the untuned SQUID. We are again reminded that higher pre-polarization (or lower sensor noise) will increase SNR, and smaller voxels will decrease it.

Let us briefly return to the discussion of field-of-view (FOV). FOV is the spatial extent of our image, and is related to the spatial resolution by the number of steps, N. Again assuming the x-direction, we can write

$$L_x = (N_x - 1)\Delta x \tag{21}$$

A simple way to speed up imaging is provided by parallel imaging methods (Pruessmann et al. 1999). In this approach, the spatial sensitivity of an array of SQUIDs is used to replace spatial encoding steps. Using less encoding steps speeds up the acquisition but usually results in an aliased image. By using, for example, the sensitivity maps from an array of coils, a full image may still be reconstructed. In applications like combined MEG and MRI, where a SQUID array is available, this has been demonstrated as a viable approach (Zotev et al. 2008a). Some of the complications due to inductive coupling between tuned receiver coils in HF MRI parallel imaging are greatly reduced with untuned SQUIDs. However, it should be emphasized that parallel imaging accelerates the MRI acquisition at the cost of SNR, which is already scarce in ULF MRI.

Before we move on to a discussion of the ULF MRI instrumentation, we would like to mention briefly that in addition to providing a new regime of applications due to lower magnetic fields (namely the combination of MEG and MRI), ULF MRI also enables new opportunities for image contrast. As we mentioned, T_1 is a sensitive function of the magnetic field; there is evidence that T_1 contrast at ULF is different, and for some applications superior (Lee et al. 2005) to that at HF MRI. Of course, it is not just contrast but contrast-to-noise that must be considered, as we discuss at the end of Sect. 2.4.

2.3 ULF-MRI Instrumentation

In the discussion below we will generally assume that the application is for the combination of ULF MRI and MEG. Thus, we are assuming that ULF MRI is being done in the presence of a magnetically shielded room (MSR). We will also assume that we have an array of SQUIDs. We note that for applications of ULF MRI that do not include MEG, an MSR may not be required. For example, the Clarke group at UC Berkeley operates in an aluminum eddy current shield only. We also note that there has been progress using sensors other than SQUIDs (namely the atomic magnetometer) both for MEG (Xia et al. 2006) and ULF MRI (Savukov et al. 2009), which we will not discuss here.

In ULF MRI, one aims at the highest pre-polarization that can be tolerated (while maintaining the benefits of the ULF regime) and at the most sensitive sensor. The heart of any ULF MRI instrument is the SQUID sensor array. Large (hundreds of sensors) SQUID arrays have been used for decades for MEG (Hämäläinen et al. 1993). The noise level of a SQUID can be as low as 10^{-15} T, enabling it to detect the very weak (10^{-12}–10^{-15} T) magnetic fields from brain activity from outside the head. A challenge for ULF MRI is that the changing magnetic fields are many orders of magnitude larger than the dynamic range of SQUIDs. Several strategies have been implemented to deal with this. One

approach is to encapsulate the SQUID chips in sealed Pb boxes that have a critical field of about 80 mT. The SQUID can also be locally shielded by Nb plates on the chip (Luomahaara et al. 2011). In either case, the pick-up coil extends outside the shield to detect the fields of interest. Thus, the input coil circuit also needs current limiters. One can use externally controlled superconducting cryo-switches (Zotev et al. 2007), which become resistive when heated above the critical temperature and thereby make the pick-up coil much less sensitive to magnetic fields. Other groups have used arrays of Josephson junctions (Hilbert et al. 1985) that become resistive above the Josephson critical current and thereby limit the current.

To achieve a high pre-polarization field, a variety of magnet designs have been proposed. In some sense, generating B_p is much simpler than at HF because the fields are so much lower and the field homogeneity requirement is less stringent (McDermott et al. 2002; Burghoff et al. 2005). B_p can be relatively (a few percent) inhomogeneous compared to the parts-per-million or better requirement for B_0 in HF MRI.

However, there are considerations to producing (and removing) B_p. In fact, some of the advantages (reduced homogeneity requirement, shorter T_1 times) can be disadvantages if not accounted for. The first consideration is that it is not trivial to make a pulsed field at >50 mT. The coil will heat up, dissipated energy must be removed, and the proximity of a large amount of conductor near the SQUIDs can introduce Johnson noise. The B_p coil should be physically disconnected during the measurement (via a relay) to reduce the antenna effect.

There have been several approaches to producing a pulsed B_p, including water-cooled (Myers 2006), coolant (Fluorinert) and liquid nitrogen (LN) cooled coils (Sims et al. 2010). The LN coil has the benefit of seven times lower resistance, but requires an additional cryostat. Recently, a self-shielded (Nieminen et al. 2011) pulsed superconducting coil (Vesanen et al. 2013) has been demonstrated for ULF MRI; the B_p coil was integrated into the cryostat with the SQUIDs. The choice of materials for B_p can be important. For example, we have found that multi-stranded Litz wire performs much better than solid wire in terms of noise. According to Vesanen et al. (2013), the superconducting wire magnetized if too high of a current (>12 A) was applied, producing spurious gradients that influenced the image quality, limiting B_p in that work to <24 mT.

Perhaps the most challenging aspect of a pulsed B_p is how to turn it off appropriately. When the B_p field changes transient eddy currents will be induced in nearby conductors, which can impose a long dead-time if the magnetic fields from the transients exceed the dynamic range of the SQUIDs.

There are two approaches to switching off B_p: adiabatic and non-adiabatic. In a non-adiabatic ramp-down, $dB_p/dt \gg \gamma B_m^2$ such that the magnetization is left aligned with the original direction of B_p. If B_m is orthogonal to B_p, precession will begin automatically. In principle, this approach can minimize the time between beginning precession and measurement. In reality, however, the faster the ramp-down of B_p, the larger are the transients that are induced in nearby conductors. When measurements are made inside a conductive MSR, these transients can become a serious confound as they may have components that persist for hundreds

of ms (Vesanen et al. 2012) and are inherently low frequency and hard to deconvolve from the MEG. Even in the absence of an MSR, anything conducting nearby will also support transients that may impact the image and/or impose long wait times. One added consideration in the non-adiabatic field removal is the non-uniformity of B_p. Not requiring a uniform B_p greatly simplifies the magnet design, but signal is lost because of this non-uniformity; when precession starts, the spins are not all in phase. In addition, there are technical problems associated with the requirement to dissipate the energy stored in the B_p coil.

If, instead, an adiabatic ramp ($dB_p/dt \ll \gamma B_m^2$) is used, the final magnetization will be aligned with the low B_m field, which is easy to make uniform. Further, phase coherence is typically improved due to lack of transients. A spin-flip pulse is then required to start precession. In an adiabatic ramp, *dB/dt* is lower and thus there is less danger of heating metallic implants or affecting therapeutic electronic devices the subject may be carrying. This is a special consideration when imaging near metal. In an ULF MRI system, B_p is typically 10–200 mT and it is removed within 10–100 ms (depending on the approach). Thus, the field change *dB*/*dt* may range from 0.1 to 20 T/s. Even with relatively high pre-polarization, the *dB*/*dt* in a ULF MRI system is typically lower than that produced by the switching gradients in HF MRI systems. However, the adiabatic ramp-down takes longer, and signal is lost due to T_1 relaxation during that time.

The self-shielded design of Nieminen and colleagues (2011) is an especially appealing approach because it largely eliminates the origin of the transients. The pre-polarization field is reduced only by 10 %, but the fields at the walls of the MSR are reduced by as much as 90 %. This approach is likely critical to achieving successful field pulsing inside an MSR.

Before we leave our discussion of B_p, we note that a pulsed B_p field gives one unique opportunity to access new information. For example, T_1 dispersion (i.e., how T_1 changes with field) can be measured easily compared to HF MRI where the polarization field is fixed. The value of this possibility has already been shown in more traditional field-cycling MRI applications (Ungersma et al. 2006), but ULF MRI provides access to a unique new range of frequencies (Hartwig et al. 2011). Nieminen and colleagues () have also shown that the B_p field could be temporally varied to provide maximum image contrast between two tissues. This is a unique feature of ULF that might hold some promise for future imaging applications.

The generation of the other magnetic fields required for imaging (B_m and gradients) is relatively simple given their low field strengths. Typically, simple wire-wound coils can be utilized. An example of a common coil topology is shown in Fig. 2. A tetra-coil arrangement is used for B_m. The B_p coil is not shown.

An interesting and important aspect regarding the measurement and gradient coils is how we power them. Because the noise level should be as low as possible (~ 1 fT/$\sqrt{\text{Hz}}$ is a typical goal) at the frequencies of interest, the current noise of the power supplies must also be as low as possible. While this sort of noise is not an issue at the frequencies of HF MRI, at ULF it can be a problem. Typically this has been dealt with by the use of batteries and heavily filtered circuits. Unfortunately, these solutions limit the sorts of pulse sequences that can be used. For

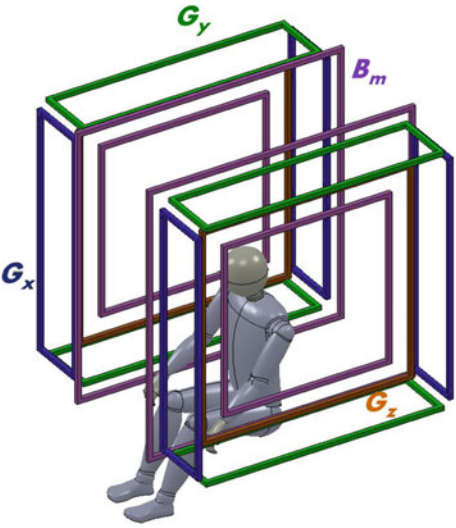

Fig. 2 Schematic of the ULF MRI system for MEG and MRI at Los Alamos. For simplicity, the B_p coil and MEG cryostat are not shown

example, in projection imaging one can use different orientations of the gradient field to traverse *k*-space without lengthy encoding times. However, projection imaging requires B_m and all three gradients to be on. Instead, most ULF MRI applications use a very simple pulse sequence shown in Fig. 3. In this case, only B_m and a single gradient (the readout gradient G_x) are on during acquisition, t_a. This is the lowest-noise approach, but as one can see we must wait the encode time, t_g, for every step. This time is usually 30–50 ms, and valuable signal is being lost due to T_2 relaxation while we are encoding. Thus, it is likely that one critical advance to ULF MRI instrumentation will be developing low-noise electronics that enable flexible pulse sequences. For example, the B_m field could also be oriented in any direction on the fly (enabling a totally new kind of projection imaging that would provide maximum sensitivity in a helmet-like configuration of sensors) but this approach also requires three B_m field coil sets to be on simultaneously.

2.4 Contrast-to-Noise (CNR)

The spin–lattice relaxation time, T_1, can be a sensitive probe of the chemical environment. Only magnetic field fluctuations arising from the local chemical environment at the Larmor frequency can cause T_1 relaxation of the affected spins. Thus, T_1 depends on both the field strength and the chemical environment (via molecular dynamics). In the ULF regime, where Larmor frequencies are on the order of Hz–kHz, one is probing processes on a timescale of seconds to milliseconds. This is an interesting timescale for processes such as intramolecular motion, diffusion, chemical reactions and chemical exchange, protein folding, and

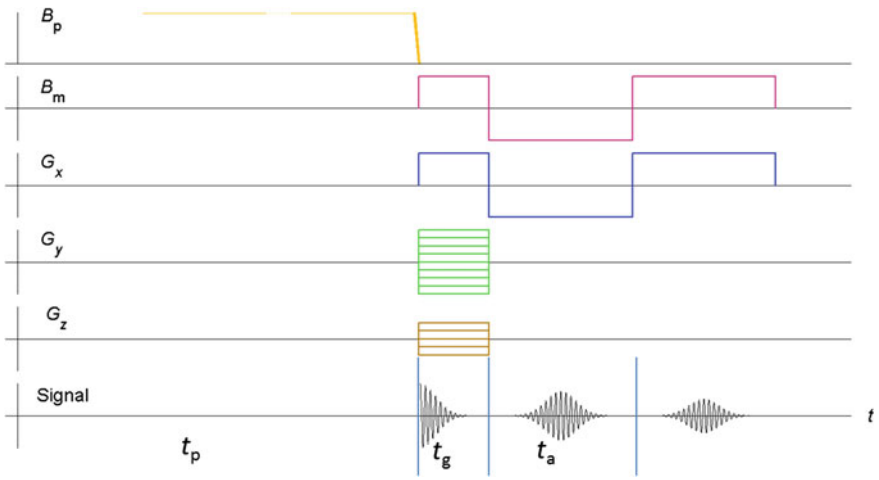

Fig. 3 An example pulse sequence for ULF MRI

even neuronal activity. This domain is different from what can be accessed with high-field MRI where the Larmor frequencies are $\sim$100 MHz, and one is probing processes at the microsecond-to-nanosecond time scales, which are primarily dominated by intramolecular motion. The potential of new contrast information is another driver for the ULF regime. For example, the PTB group observed unexpected relaxation behavior in water at frequencies <100 Hz (Hartwig et al. 2011), and the UC Berkeley group has shown that for some tissues there might be contrast that is only available at ULF (Lee et al. 2005).

But it is not just contrast that one has to consider in image quality. One has to ensure that there is adequate SNR in the image such that the contrast information is meaningful. We refer the reader to the work of Myers and colleagues (2006) for an excellent discussion of how one might predict the SNR obtained with a ULF MRI system. Here we will assume that we do have a notion of what the SNR is between ULF and HF MRI. We assume we are only using thermally limited polarization, so it is given that the SNR for ULF MRI will be lower. The issue at hand is whether the benefit in contrast at ULF outweighs the lower SNR.

To do this, we introduce the notion of contrast-to-noise ratio (CNR). Assuming we have two types of tissue in an image (A and B), we can write the CNR between them as

$$\mathrm{CNR} \propto \frac{(S_\mathrm{A} - S_\mathrm{B})}{\sigma} \left(t_\mathrm{seq}\right)^{\frac{1}{2}}, \tag{22}$$

Table 1 Comparison of CNR (see text for assumptions) at various fields

	$B_0 = 3.0$ T $f =$ 128 MHz (Wright et al. 2008)	$B_0 = 0.23$ T $f = 9.8$ MHz (Fischer et al. 1990)	$B_m = 46$ μT $f = 2.0$ kHz (Zotev et al. 2009)
Grey matter T_1 (s)	1.61	0.667	0.103
White matter T_1 (s)	0.84	0.333	0.075
t_c (s)	1.14	0.462	0.088
CNR_{max}	0.23	0.25	0.12

where t_{seq} is a time factor that depends on the imaging sequence (Hendrick 1987) and the signal for tissue A is

$$S_A = S \cdot e^{-t \cdot R_A} \tag{23}$$

and $R_A \equiv 1/T_{1A}$. The signal from tissue B is defined similarly. The CNR tells us how SNR (S/σ) and relaxation are related. Note that for simplicity here we are neglecting T_2 relaxation for the moment.

Equation (22) also tells us that for any two such tissues there will be some optimal time of maximum contrast (again neglecting T_2 relaxation).

$$t_c = \frac{\ln R_A - \ln R_B}{R_A - R_B}. \tag{24}$$

Now we can imagine a simple example, shown in Table 1, where we make the assumption that for all tissue $SNR \cdot t_{seq} = 1$. We can see that the CNR at 0.23 T is the highest, in agreement with the data of Fischer et al. (1990). However, we made a clearly erroneous assumption. The SNR will not be the same at 3 T, 0.23 T, and 46 μT using $B_p = 30$ mT. For example, the SNR at 3 T will likely be much higher than that at 0.23 T. Naively, one might expect this difference to be over hundredfold if SNR really scales as ω_0^2. However, in 10–128 MHz, the main noise contribution is from the human body (noise spectral density $S_n = \sim 4\text{–}5 \times 10^{-17}$ T $Hz^{-1/2}$; see Myers et al. 2006), not from the pick-up coil. Nevertheless, one could expect the SNR to be at least 10 times higher at 3 T due to the higher polarization field strength, and thus the CNR at 3 T will remain better unless dramatic improvements in the SNR at ULF are made.

However, there are exceptions to the above example. An agarose gel phantom, designed to mimic the relaxation of biological tissue, yielded $R_A = 2.5$ and $R_B = 5$ for 0.25 and 5 % agarose gels, respectively, at ULF ($f = 1000$ Hz); at $f = \sim 12$ MHz, the difference between R_A and R_B vanished (Lee et al. 2005). In such cases, the CNR is always better at ULF, as long as the SNR is high enough to produce a useful image.

3 History of Ultra-Low-Field MRI

Since the discovery of magnetic resonance (MR), in the form of NMR, there has been interest in performing it at ultra-low fields (i.e., the microtesla regime). For example, in their early work, Packard and Varian (1954) demonstrated NMR in the Earth's magnetic field. One can imagine that this was initially driven by the fact that in these early days the generation of strong magnetic fields was a challenge. However, there have always remained scientific drivers for ultra-low-field (ULF) MR, perhaps the most interesting one arising from the magnetic field dependence of T_1 contrast. At low magnetic fields, and hence low Larmor frequencies, there are typically many more mechanisms which can produce T_1 relaxation than at high magnetic fields, which makes ULF-MR a rich area for scientific exploration. For example, a recent measurement of T_1 relaxation at very low Larmor frequencies (<100 Hz) gave new and unexpected insight into chemical exchange processes (Hartwig et al. 2011).

While interest in NMR processes and relaxation contrast at ULF has always persisted from a scientific standpoint, the overwhelming trend for almost all practical applications of NMR and MRI has been towards ever higher magnetic fields because the signal (and chemical shift effects) scales with the applied magnetic field. However, several key developments led to a re-kindling of interest in the ULF regime, even as this trend to higher and higher fields persists.

One such key development was the Macovski effort in pulsed-field MRI with lower-frequency readout (Macovski and Conolly 1993). The motivation was to simplify magnetic field production (and thus reduce cost) while retaining the signal benefits of a higher magnetic field through pulsed pre-polarization. A key observation was that the requirements for magnetic field uniformity scaled with the strength of the absolute magnetic field, and thus by using a lower readout magnetic field, simpler magnets could be utilized. However, the performance of the highly tuned inductive Faraday coils deteriorates when the frequency is lowered. To this end, Seton brought to bear a SQUID sensor for magnetic field detection in a ~400-kHz MRI demonstration (Seton et al. 1995, 1997). While they did not use pulsed-field methods, they did show that the ultra-sensitive SQUID could be used in an MRI environment, and mitigated the poor performance of inductive receivers at lower Larmor frequencies. Then, in the early years of the 2000s, John Clarke's group at UC Berkeley really pulled these advances together and showed that SQUID-detected ULF NMR and MRI was possible using pulsed pre-polarization methods. The work showed the promise of very narrow NMR linewidths, the ability to image through metal, and interesting applications for unique contrast (see, e.g., Clarke et al. 2007). Perhaps one of the most compelling arguments for ULF MRI, however, was the sudden compatibility of anatomical imaging with magnetoencephalography (MEG). Because the sensor for both ULF MRI and MEG was the same, the SQUID, these two complementary but incompatible methods seemed possible to integrate.

The work at UC Berkeley was followed by several proof-of-concept demonstrations at LANL that MEG and ULF MRI could be combined (Zotev et al. 2008b; Magnelind et al. 2011). The effort was quickly picked up by a European project, which has made much progress in combining a full-scale whole-head MEG system with ULF MRI (Vesanen et al. 2013). At the time of this writing, many groups in Asia are also pursuing ULF NMR/MRI, including ULF MRI for small animals which could be combined with MEG (Hatta et al. 2011). In the next section, we will discuss the present state-of-the art in ULF MRI.

4 ULF-MRI Systems

4.1 UC Berkeley

Much of the pioneering work in ULF MRI has been done by the team of John Clarke at UC Berkeley. Although their system is not in a mu-metal MSR, which precludes combination with MEG, the Clarke group was keenly aware of the potential of this application, as demonstrated in their early patent on the work (Clarke et al. 2005). The UC Berkeley system, which operates inside an aluminum shield, has been described extensively by Myers (2006b) and more recently by Busch and others (2011).

The UC Berkeley system is the first one housed inside an aluminum shield to reduce the influence of external magnetic fields down to the kHz range. The walls were originally 6 mm thick but have been redesigned with 2-mm aluminum to reduce the influence of eddy currents after B_p pulsing (Busch et al. 2011). The system compensates the Earth's magnetic field ($\sim$50 μT) in the two directions orthogonal to B_m ($\sim$100 μT). A powerful water-cooled polarization coil can achieve 150 mT. The UC Berkeley system uses an adiabatic ramp-down scheme in which the B_p field is removed such that the spins are left aligned with B_m. As discussed previously, this method reduces the need for homogeneous B_p and improves phase coherence. The system relies on a single 2nd-order axial gradiometer housed in a low-noise cryostat for signal detection. Busch (2011) has an excellent description as well as the schematic of the UCB MRI system shown in Fig. 4. In recent times, the work with this system has focused on utilizing the unique contrast between benign and cancerous tissue to determine the percentage of cancer in prostate tissue by changes in T_1 (Busch et al. 2012).

4.2 PTB

The group at Physikalisch-Technische Bundesanstalt (PTB) in Berlin, Germany, has developed instrumentation for ultra-low-field MRI as well as investigated

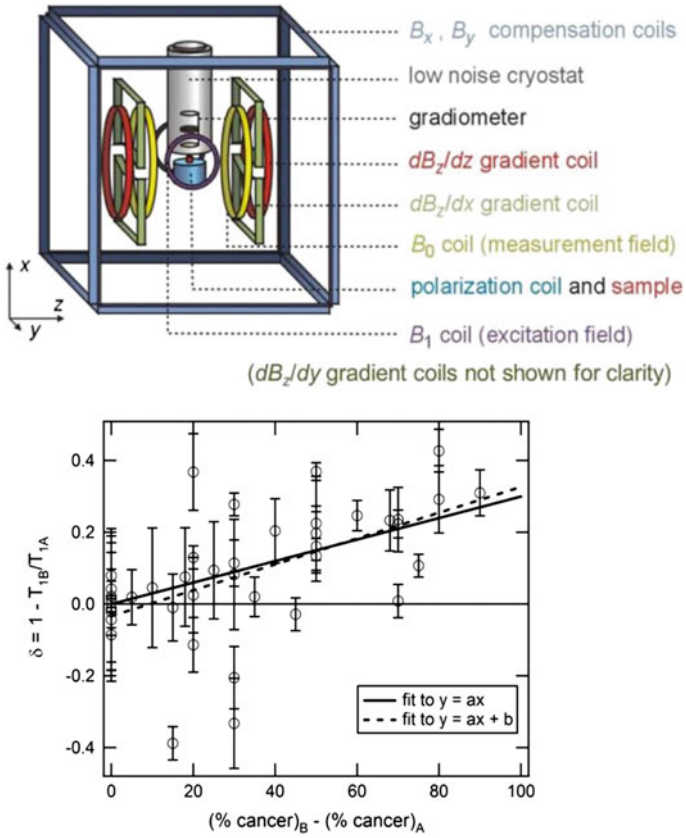

Fig. 4 *Top* The UC Berkeley ULF MRI system. *Bottom* Contrast δ versus percentage cancer for excised prostate tissue

NMR physics at extremely low fields. PTB hosts a very-high-performance magnetically shielded room, which facilitates such studies by providing a shielding factor in excess of 10^8 at frequencies above 6 Hz and a white-noise contribution from the shield less than 1.5 fT $Hz^{-1/2}$ (Bork et al. 2001).

PTB has modified a single-channel biomagnetometer and a 304-channel MEG/MCG system, both based on SQUIDs, for ULF-MRI. The white noise levels are 4.5 and 2.3 fT $Hz^{-1/2}$ for the single- and multichannel systems, respectively (Burghoff et al. 2007). In both systems, the compensated polarization coil system produces a maximum field of 1 mT in the sample. The measurement field is generated by a Helmholtz coil pair and it can be varied from 12 nT to 8.5 μT. A more recent single-channel system reaches a white-noise level of 1.9 fT $Hz^{-1/2}$ at 1 kHz and generates a B_p in excess of 50 mT at the center of the sample (Hilschenz et al. 2013); see Fig. 5. The PTB systems reach spectral line widths well below 1 Hz.

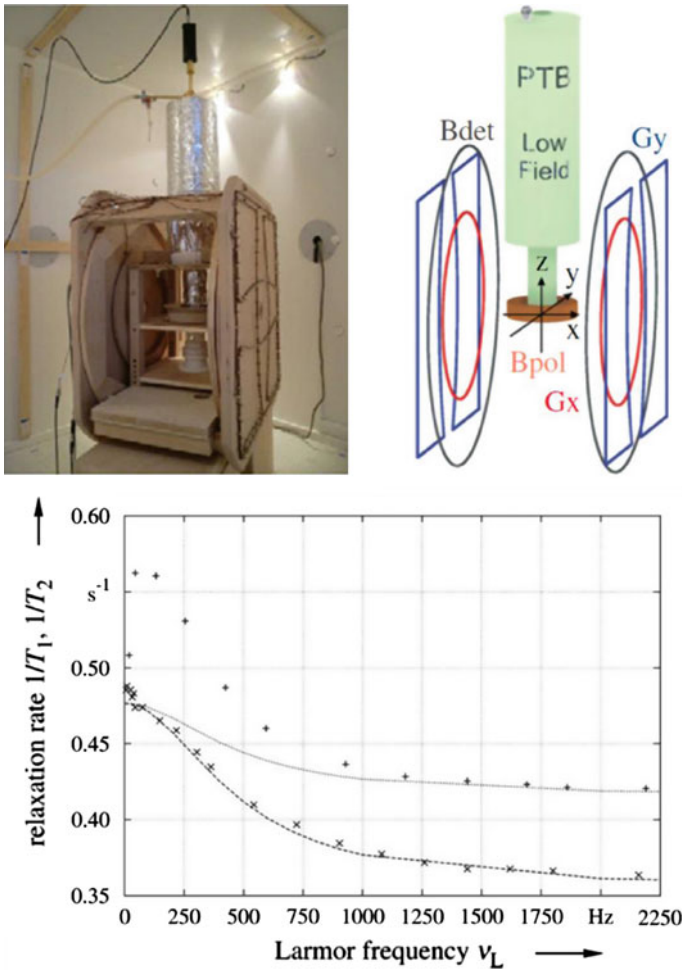

Fig. 5 *Top* The single-channel ULF-MRI system at PTB (Hilschenz et al. 2013). *Bottom* Measured T_1 (x) and T_2 (+) relaxation dispersion of pure water (pH = 7.5). Dashed and solid lines indicate fits of T_1 and T_2 data, respectively, to a conventional model. Reprinted from Hartwig et al. (2011)

The PTB group has exploited their exquisite measurement set-ups to study relaxation and its dispersion at ultra-low fields (Hartwig et al. 2011), pure J-coupling (Bernarding et al. 2006; Trahms and Burghoff 2010), and possibilities of detecting neuronal currents with ULF MRI (Burghoff et al. 2010; Höfner et al. 2011; Hilschenz et al. 2013).

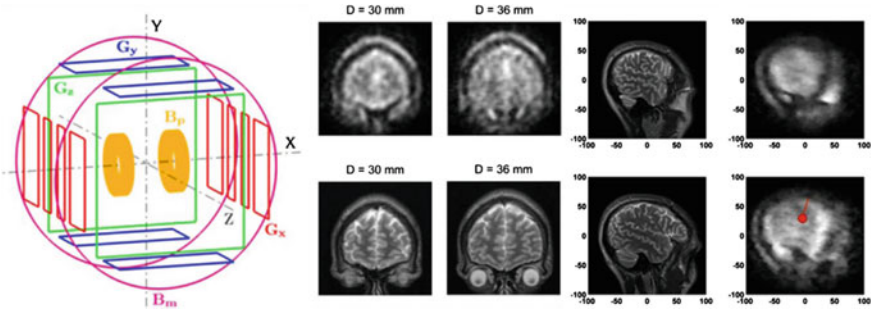

Fig. 6 *Left* Schematic of the LANL ULF-MRI system. *Middle* First ULF-MRI images of the human brain at 46 μT (*upper two*) versus 1.5 T (*lower two*). *Right* Co-registration of auditory MEG (*red dot*) to ULF MRI acquired in a single interleaved session at 94 μT (*right column*) versus 3 T (*left column*)

4.3 LANL

The group at Los Alamos National Laboratory (LANL) was primarily pursuing novel applications and systems for MEG (Kraus et al. 2002) when the first demonstrations of ULF MRI with SQUIDs were made at UC Berkeley. The potential for combined MEG and ULF MRI was immediately obvious. However, at LANL, the first demonstration of MR at ULF was J-coupling spectroscopy to determine enrichment fraction in UF6 (Volegov et al. 2006). Upon the successful demonstration of the ULF NMR signal, the team began to pursue MEG and MRI with early proof-of-concept demonstrations (Volegov et al. 2004). These ultimately led to a single system capable of MEG and MRI (Zotev et al. 2008b), and MEG co-registered to the ULF MRI (Magnelind et al. 2011).

The LANL system, which demonstrated these results, has been described extensively elsewhere (Zotev et al. 2007). A schematic of the coil set and examples of data are shown in Fig. 6. Coming from an MEG motivation, the system operates inside a two-layer mu-metal and aluminum MSR suitable for MEG. The LANL system uses a 7-channel 2nd-order gradiometer array enabling parallel imaging (Zotev et al. 2008a), LN-cooled pre-polarization coils capable of achieving 50–100 mT, and a cryo-switch approach for the management of SQUIDs during the pre-polarization (Matlachov et al. 2005). Most LANL ULF-MRI applications use B_m fields from 50 to 100 μT. At the time of this writing, a second system (Matlashov et al. 2012) is under development to accommodate a Neuromag-122 MEG system (Ahonen et al. 1993) and enable the use of an array of magnetometers separately optimized for MEG and MRI (Burmistrov et al. 2013). The coils for this system are shown schematically in Fig. 2.

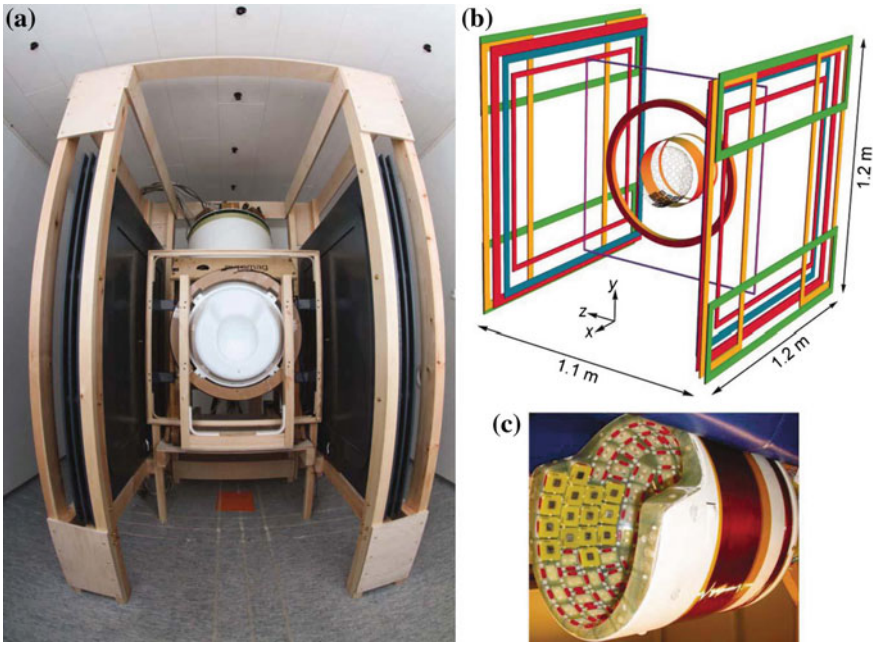

Fig. 7 The Aalto MEG-MRI system. **a** The dewar surrounded by MRI coils in a magnetically shielded room. **b** MRI coil arrangement. The large circular coil is for the compensation of the dipole moment of the superconducting pre-polarization coil (small circular coil). **c** Insert containing the SQUID sensors and the superconducting pre-polarization coil

4.4 Aalto

Figure 7 shows the MEG-MRI prototype developed at Aalto University (Vesanen et al. 2013). This system was built using several components of the Elekta whole-head MEG device such as the dewar, framework for the 102 triple-sensor units, and the data acquisition system. Major novelties, in addition to the helmet structure and large number of channels, included a superconducting pre-polarization coil (Fig. 7c), compensation of the lowest multipole moments of the magnetic field from the pre-polarization coil, and novel sensor-unit structures where the SQUID is shielded with superconducting plates (Luomahaara et al. 2011) against the strong magnetic fields used for MRI. The pre-polarization field was limited to 22 mT because higher fields resulted in field trapping in the superconducting coil with adverse effects on measurement field homogeneity. Figure 8 shows the images (voxel size $4 \times 4 \times 6$ mm^3) obtained with a 3D spin-echo sequence from a human head measured at 50 μT; the measurement time was 92 min.

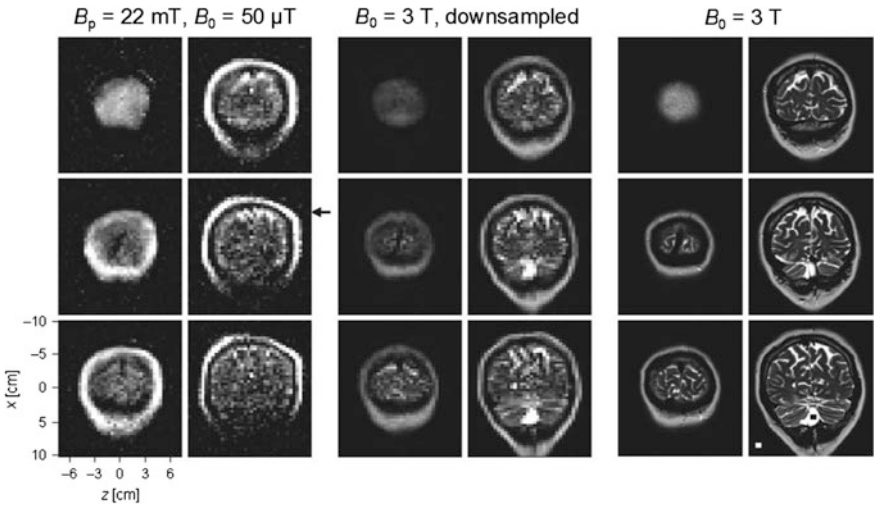

Fig. 8 *Left* First brain images obtained with the Aalto MEG-MRI system. *Right* Corresponding set of T_2 images obtained with a 3-tesla magnet. *Middle* The 3-tesla images down-sampled to the same resolution as on the *left*, confirming some of the details in the ULF-MRI images

4.5 Other Groups

Researchers at the Korean Research Institute of Standards and Science (KRISS) have developed an ULF-MRI system which utilizes a double relaxation oscillation (DROS) SQUID instead of a conventional dc-SQUID (Seok Kang et al. 2011). This system can use measurement fields as low as a few μT. The group has also demonstrated the use of Dynamic Nuclear Polarization (DNP) technique (Lee et al. 2010), which exploits the Overhauser double-resonance effect to increase the effective polarization (Overhauser 1953).

A research team at National Taiwan University and National Taiwan Normal University has successfully explored the use of high-Tc SQUIDs in a compact ULF-MRI set-up (Yang et al. 2006; Chen et al. 2011). Their system is optimized for small objects (sample volume 64 cm^3), and it comprises a shield to enable measurements outside of a conventional magnetically shielded room. The system reaches spectral resolution better than 1 Hz.

Liu and colleagues (2012, 2013) have demonstrated MRI using a high-T_c rf-SQUID with a tuned input circuit. At $B_m = 213$ μT ($f = 9$ kHz), tuning improved sensitivity from 40 to 50 fT $Hz^{-1/2}$ to 6–7 fT $Hz^{-1/2}$. In this system, polarization is achieved using permanent magnets that produce about 1 T in the sample.

Seton and colleagues (2007) have employed tuned low-T_c SQUIDs for signal detection but at a considerably higher measurement field $B_0 = 20$ mT, without a separate pre-polarization field. According to their analysis, at the Larmor

frequency (840 kHz) of their system, a tuned SQUID circuit outperforms both a room-temperature tuned receiver and an unturned SQUID. The group at CEA, France, utilizes "mixed sensors", which combine a superconducting input loop and a giant magnetoresistive element (Pannetier et al. 2004), to perform low-field MRI at $B_0 = \sim 10$ mT (Sergeeva-Chollet et al. 2011).

5 Potential Applications of ULF MRI

Despite rapid progress during the past few years, ultra-low-field MRI is still in its infancy. Although it might be too early to define specific applications other than its combination with MEG, ULF MRI clearly holds promise in many scientific and clinical areas. We outline a few of these in the following.

5.1 Medical Imaging

As discussed in Sect. 2.4, MRI at ultra-low fields shows improved T_1 contrast compared to high fields, which may translate into a unique capability of ULF MRI to help delineate certain tissue types better than high-field MRI. It has already been shown that, for example, biopsies of prostate cancer tissue exhibit a significantly shorter T_1 time at $B_m = 132$ μT than healthy tissue (Clarke et al. 2007) and cancerous versus normal rat liver shows similarly high contrast at $B_m = 100$ μT (Liao et al. 2010). The complex behavior of the proton relaxation dispersion of water when approaching zero field (Hartwig et al. 2011) may be the physical background of the enchancement of T_1 contrast between healthy tissue and tumors at low fields.

The grey–white matter border has a relatively high T_1 contrast. This border is blurred at focal cortical dysplasias (FCDs), malformations generated during cortical development. FCDs are highly epileptogenic and frequently cause intractable epilepsy. Unfortunately, a considerable fraction of FCDs can not be discerned in high-field MRI and are only detected in tissue microscopy after removal of the cortical region. Thanks to its higher T_1 contrast, ULF MRI may be able to visualize FCDs better than high-field MRI.

High-field MRI cannot be applied to patients with pacemakers, stimulators or metal in the body. However, there are no similarly strict restrictions with ULF MRI, which is inherently much safer.

5.2 Temperature Mapping

Vesanen et al. (2012) utilized the dependence of T_1 relaxation time of agarose gel to demonstrate the ability of ULF MRI to measure temperature. Although this method can prove useful in special cases, one must bear in mind that in human tissue, T_1 is influenced much more by the detailed structure of the tissue than by temperature. Therefore, this method can be used only for indicative purposes and to monitor possible changes of temperature when other factors affecting T_1 can be assumed fixed.

5.3 Conductivity Imaging

If electric current is applied to a conducting object using two electrodes, the current will distribute itself between different paths in proportion to the conductivities of the paths. It was shown by Nieminen et al. (2014) and Vesanen et al. (2014) that the direction and amplitude of the current distribution can be measured with low-field MRI, provided, of course, that the SNR is sufficient. This is not possible with a high-field MRI device without the need to turn the head between two measurements. So far, only simulation studies have been done. These indicate excellent reconstruction accuracy but also the fact that the SNR of MRI measurements must be significantly improved before electrical impedance tomography can be done in humans with safe current strengths (on the order of 2 mA as those in transcranial direct current stimulation or tDCS).

6 Future Directions

6.1 Improvements in Instrumentation

The present state of the art is not yet sufficient for scientific and clinical applications of combined MEG and ULF MRI. However, we can predict that ULF MRI can be improved to a level that will provide acceptable image quality and allow accurate registration of MEG and MRI coordinate systems. A great improvement in SNR can be obtained by increasing the pre-polarization field strength and by reducing SQUID and dewar noise further; $B_p > 100$ mT and sensor noise level of 0.5 fT/Hz$^{-1/2}$ seem possible even in a large array. The improvement in SNR may enable us to measure the conductivity structure of the head as well (see Sect. 5.3). However, problems arising from the highly sensitive SQUIDs in strong pulsed magnet fields will become more severe. Thus, the task of building a practical MEG-MRI system is far from trivial. Elaborate methods will be needed to handle problems caused by eddy currents in the system and in nearby structures as well as

the magnetization of materials. Optimized sequences and signal processing will be needed to maximally utilize the recorded data. Next, we will give a glimpse of one approach in developing signal processing.

6.2 Advances in Signal Processing

Conceivably, ULF MRI with up to hundreds of sensors for whole-brain imaging will be developed in the next few years. In high-field MRI, such highly parallel signal detection has been used to improve the spatiotemporal resolution at the cost of SNR (Pruessmann et al. 1999; Sodickson and Manning 1997). The feasibility of 3-fold acceleration has been reported in an ULF-MRI study with a seven-channel SQUID system (Zotev et al. 2008a). Although currently the SNR of ULF MRI is too low to be compromized, we expect that with future SNR improvements offered by higher pre-polarization field and more sensitive SQUID detectors, it might be possible to trade off SNR for a shorter acquisition time. The SNR loss in parallel MRI (pMRI) is the consequence of the loss of data samples and the noise amplification in image reconstruction (Pruessmann et al. 1999). While the former loss is inevitable in acceleration, the latter loss can be compensated for by regularized reconstruction methods (Lin et al. 2004, 2005) and by increasing the number of parallel detectors.

The SNR penalty of accelerated ULF MRI was recently investigated by simulating a helmet-shaped sensor array with up to 306 SQUID sensors (204 gradiometers and 102 magnetometers; VectorView™, Elekta Oy, Helsinki, Finland) (Lin et al. 2012). The g-factor, the SNR ratio between images reconstructed from unaccelerated and accelerated data after normalizing the data samples (Pruessmann et al. 1999), was used to quantify the relative SNR efficiency of accelerated ULF MRI at different acceleration rates and array geometries. Typically, $g > 1$. Four array geometries based on the whole-head Elekta system were studied: 102 magnetometers (planar circular loops, "array102"), 102 gradiometers (planar figure-of-eight loops, "array102x" and "array102y"), and the combination of all three sets ("array306").

It was found that all geometries have high SNR for voxels close to the scalp. The gradiometer arrays (array102x and array102y) show very fast decay of the SNR with distance from the scalp. This is because the gradiometers take the spatial difference between two neighboring measurements and thus they are exquisitely sensitive to the cortical signal (Hämäläinen et al. 1993). The results from arrays using magnetometers only (array102) and magnetometers plus gradiometers (array306) were visually indistinguishable (Fig. 9).

Arrays with gradiometer pick-up coils (array102x and array102y) show a similar g-factor distribution to the array with magnetometer pick-up coils (array102). A combination of both gradiometer and magnetometer pick-up coils (array306) only slightly improves the g-factor at locations close to the sensors. In all geometries, image locations away from pick-up coils show a larger g-factor in

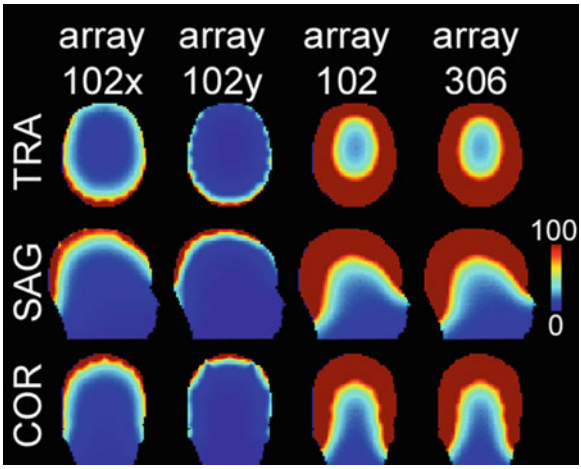

Fig. 9 The spatial distribution of SNR in mid-sagittal, mid-coronal, and one axial slice with array102, array102*x*, array102*y*, and array306 geometries

general (Fig. 10). These numbers suggest that, in a 3D ULF-MRI acquisition with two phase-encoding directions, the highest acceptable acceleration rate R, which is defined as the ratio between the planned accelerated acquisition data sample and the non-accelerated acquisition data sample, may be from 9- to 16-fold (based on an arbitrary threshold of average $g = 1.4$). Consider a 3D ULF-MRI acquisition with $64 \times 64 \times 64$ voxels. It needs 4,096 independent read-outs with 64×64 phase encoding steps. With repetition time TR = 1 s, this amounts to more than an hour of acquisition time. Using an array of 102 sensors and 9-fold acceleration and assuming that the SNR loss due to reduced samples is tolerable, the data acquisition can be completed in approximately 7 min. However, as suggested by these results, spatially varying noise amplifications (i.e., g-factor) could be significant at 9- and 16-fold acceleration, resulting in inhomogeneous image quality deterioration.

In addition to or instead of aiming at achieving a higher resolution or shorter measurement time, parallel MRI can be applied to ULF MRI to improve the SNR by exploiting the redundancy among the receiver channels via enforcing k-space data consistency among them and by adding *a priori* image sparsity constraint to further suppress noise (Lin et al. 2013). Figure 11 shows experimental images of the right hand of a subject. Notably, there was a clear vertical strip artifact in the sum-of-squares (SoS) image, potentially due to elevated SQUID noise at 3 kHz. Using the data consistency constraint alone reduced the vertical strip artifact and the background noise significantly. Applying the data consistency constraint also increased the peak SNR (pSNR) from 7.7 to 14.0. Further, the use of the sparsity prior further improved the peak SNR (pSNR) to 57.6 because of the strong suppression of background noise.

Six coronal slices of brain images from our ULF-MRI system (Vesanen et al. 2013) with 22-mT pre-polarization, 130-μT/m maximum gradient, and 90-min imaging time (eight averages) are shown in Fig. 12. We found that the signal from

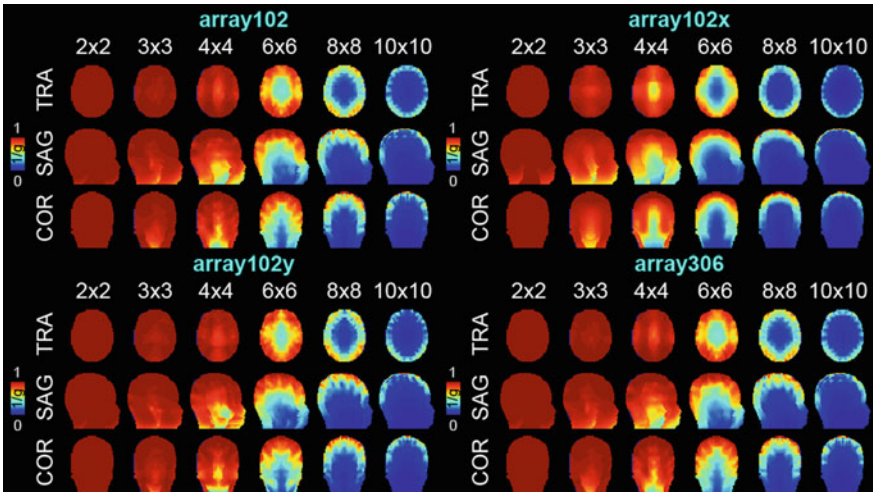

Fig. 10 The spatial distribution of $1/g$-factor in mid-sagittal, mid-coronal, and in one axial slice with array102, array102x, array102y, and array306 geometries at acceleration rates $R = 2 \times 2$, 3×3, 4×4, 6×6, 8×8, and 10×10 in 2D over the FOV of $256 \times 256 \times 256$ mm^3

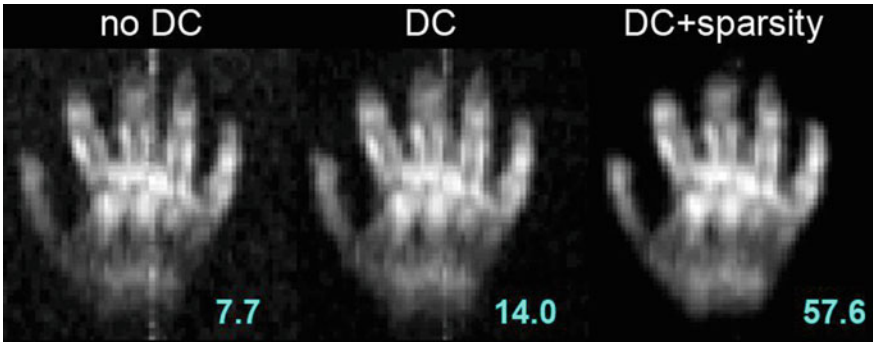

Fig. 11 *Left* A sum-of-squares image of a hand. *Middle* The data consistency (DC) constraint alone significantly reduces the vertical strip artifact. *Right* The sparsity prior improves the reconstruction only marginally. The peak SNR is indicated below each image

gray and white matter increased as the data consistency constraint was applied ($\lambda = 0$); the average pSNR across six images increased from 11 to 26. Furthermore, when the sparsity constraint was added ($\lambda = 0.1$), the average pSNR dramatically increased to 296 due to strong suppression of the background noise. However, applying the sparsity constraint also decreased the image intensity at the FOV center.

These results demonstrate that the use of the data consistency constraint in multi-sensor ULF MRI can increase the peak SNR of the reconstructed images.

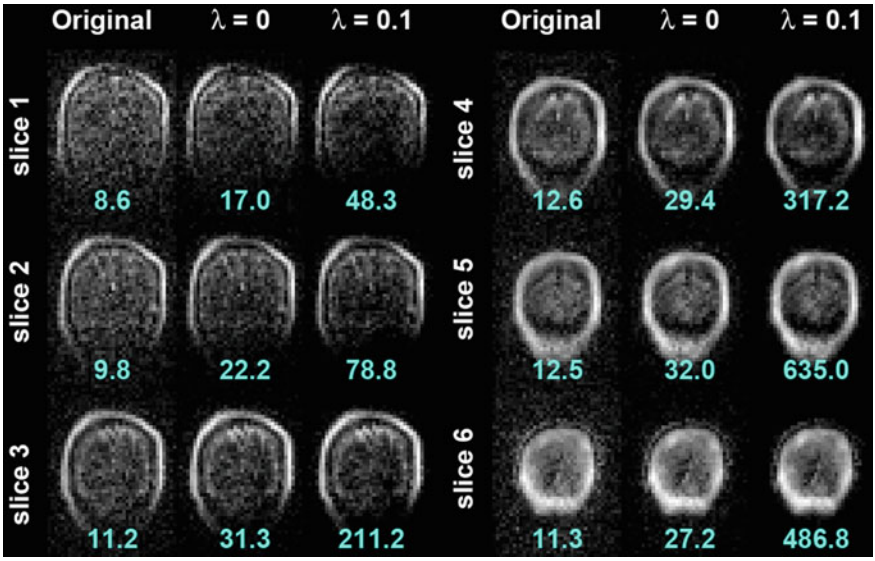

Fig. 12 Brain images reconstructed by the regularized SENSE method with no acceleration (*left columns*). The data consistency constraint ($\lambda = 0$) improves the image by showing a strong signal in the brain parenchyma (*middle columns*). Further, the sparsity prior ($\lambda = 0.1$) suppresses the background noise significantly to better delineate the skull and the brain (*right columns*). The pSNR is indicated below each image

Note that this method is different from the signal-space projection (SSP) (Uusitalo and Ilmoniemi 1997) and signal-space separation (SSS) (Taulu et al. 2004) methods in MEG, both of which are spatial filtering methods to separate measurements into signal and noise components and to remove the latter. The data consistency constraint, however, is based on the *k*-space formulation, which is a unique property in MRI (MEG does not have similar spatial encoding). However, it can be expected that if this method is integrated with SSP and SSS, noise can be suppressed even more, resulting in further improvements in image quality.

7 Conclusions

By performing MRI measurements with the large arrays of SQUID sensors available in MEG helmets, one can realize combined MEG and MRI, which offers unprecedented possibilities to obtain new kinds of information about the human brain. MEG-MRI systems will be quiet, open, and safe. They will enable highly accurate registration of MEG and MRI coordinate systems and, if imaging of injected current density proves practical, the determination of the three-dimensional conductivity distribution. This, in turn, would enable us to solve the inverse problem of MEG (and EEG) using reliable knowledge of both measurement and

conductivity geometry. However, we are still far from constructing practical devices. It will be necessary to improve the SNR considerably to attain MR image quality that is sufficient for clinical and scientific applications.

Acknowledgements LP, RI and FL acknowledge the financial support from the Academy of Finland, TEKES, and the European Community's 7th Framework Programme (FP7/2007–2013); Grant number: 200859. ME would like to acknowledge the financial support of LDRD as well as thank her colleagues and especially Andrei Matlashov for his assistance in writing this chapter.

References

Abragam A (1961) Principles of nuclear magnetism. Clarendon Press, Oxford

Ahonen AI, Hämäläinen MS, Kajola MJ, Knuutila JET, Laine PP, Lounasmaa OV, Parkkonen LT, Simola JT, Tesche CD (1993) 122-channel SQUID instrument for investigating the magnetic signals from the human brain. Phys Scr T49:198–205

Bernarding J, Buntkowsky G, Macholl S, Hartwig S, Burghoff M, Trahms L (2006) J-coupling nuclear magnetic resonance spectroscopy of liquids in nT fields. J Am Chem Soc 128:714–715

Bork J, Hahlbohm HD, Klein R, Schnabel A (2001) The 8-layered magnetically shielded room of the PTB: design and construction. In: Nenonen J, Ilmoniemi R, Katila T (eds) Biomag 2000, proceedings of the 12th international conference on biomagnetism. Helsinki University of Technology, Espoo, pp 970–973

Burghoff M, Hartwig S, Trahms L (2005) Nuclear magnetic resonance in the nanotesla range. Appl Phys Lett 87:054103

Burghoff M, Hartwig S, Kilian W, Vorwerk A, Trahms L (2007) SQUID systems adapted to record nuclear magnetism in low magnetic fields. IEEE Trans Appl Supercond 17:846–849

Burghoff M, Albrecht HH, Hartwig S, Hilschenz I, Korber R, Hofner N, Scheer HJ, Voigt J, Trahms L, Curio G (2010) On the feasibility of neurocurrent imaging by low-field nuclear magnetic resonance. Appl Phys Lett 96:233701

Burmistrov E, Matlachov A, Sandin H, Schultz L, Volegov P, Espy M (2013) Optimization and configuration of SQUID sensor arrays for a MEG-MRI system. IEEE transaction on applied superconductivity, (in press)

Busch S, Hatridge M, Mößle M, Myers W, Wong T, Mück M, Chew K, Kuchinsky K, Simko J, Clarke J (2012) Measurements of T1-relaxation in ex vivo prostate tissue at 132 μT. Magn Reson Med 67:1138–1145

Busch SE (2011) Ultra-low field MRI of prostate cancer using SQUID detection. Ph.D. thesis, UC Berkeley

Callaghan PT (1991) Principles of nuclear magnetic resonance microscopy. Oxford Science Publications, Oxford

Chen HH, Yang HC, Horng HE, Liao SH, Yueh S, Wang LM (2011) A compact SQUID-detected magnetic resonance imaging system under microtesla field in a magnetically unshielded environment. J Appl Phys 110:093903

Clarke J (2005) SQUID detected NMR and MRI at ultralow fields. US patent 6885192, 26 Apr 2005

Clarke J, Hatridge M, Mössle M (2007) SQUID-detected magnetic resonance imaging in microtesla fields. Annu Rev Biomed Eng 9:389–413

Damadian R (1971) Tumor detection by nuclear magnetic resonance. Science 171:1151–1153

Fischer HW, Rinck PA, Van Haverbeke Y, Muller RN (1990) Nuclear relaxation of human brain gray and white matter: Analysis of field dependence and implications for MRI. Magn Reson Med 16:317–334

Hämäläinen M, Hari R, Ilmoniemi RJ, Knuutila J, Lounasmaa OV (1993) Magnetoencephalography—theory, instrumentation, and applications to noninvasive studies of the working human brain. Rev Mod Phys 65:413–497

Hartwig S, Voigt J, Scheer H-J, Albrecht H-H, Burghoff M, Trahms L (2011) Nuclear magnetic relaxation in water revisited. J Chem Phys 135:054201

Hatta J, Miyamoto M, Adachi Y, Kawai J, Uehara G, Kado H (2011) SQUID-based low field MRI system fors animals. IEEE Trans Appl Supercond 21:526–529

Hendrick RE (1987) Sampling time effects on signal-to-noise and contrast-to-noise ratios in spin-echo MRI. Magn Reson Imaging 5:31–37

Hilbert C, Clarke J, Sleator T, Hahn EL (1985) Nuclear quadrupole resonance detected at 30 MHz with a dc superconducting quantum interference device. Appl Phys Lett 47:637–639

Hilschenz I, Körber R, Scheer HJ, Fedele T, Albrecht HH, Cassará A, Hartwig S, Trahms L, Haase J, Burghoff M (2013) Magnetic resonance imaging at frequencies below 1 kHz. Magn Reson Imaging 31:171–177

Hsu YC, Vesanen PT, Nieminen JO, Zevenhoven KCJ, Dabek J, Parkkonen L, Chern IL, Ilmoniemi RJ, Lin FH (2013) Efficient concomitant and remanence field artifact reduction in ultra-low-field MRI using a frequency-space formulation. Magnetic resonance in medicine, (in press)

Höfner N, Albrecht H-H, Cassará AM, Curio G, Hartwig S, Haueisen J, Hilschenz I, Körber R, Martens S, Scheer HJ, Voigt J, Trahms L, Burghoff M (2011) Are brain currents detectable by means of low-field NMR? A phantom study. Magn Reson Imaging 29:1365–1373

Kraus RH Jr, Volegov P, Maharajh K, Espy MA, Matlashov AN, Flynn ER (2002) Performance of a novel SQUID-based superconducting imaging-surface magnetoencephalography system. Physica C 368:18–23

Lee S, Mossle M, Myer W, Kelso N, Trabesinger AH, Pines A, Clarke J (2005) SQUID-detected MRI at 132 μT with T1-weighted contrast established at 10 μT–300 mT. Magn Reson Med 53:9–14

Lee SJ, Kim K, Kang CS, Hwang S, Lee YH (2010) Pre-polarization enhancement by dynamic nuclear polarization in SQUID-based ultra-low-field nuclear magnetic resonance. Supercond Sci Technol 23:115008

Liao SH, Huang KW, Yang HC, Yen CT, Chen MJ, Chen HH, Horng HE, Yang SY (2010) Characterization of tumors using high-Tc superconducting quantum interference device-detected nuclear magnetic resonance and imaging. Appl Phys Lett 97:263701–263703

Lin FH, Huang TY, Chen NK, Wang FN, Stufflebeam SM, Belliveau JW, Wald LL, Kwong KK (2005) Functional MRI using regularized parallel imaging acquisition. Magn Reson Med 54:343–353

Lin FH, Kwong KK, Belliveau JW, Wald LL (2004) Parallel imaging reconstruction using automatic regularization. Magn Reson Med 51:559–567

Lin FH, Vesanen PT, Nieminen JO, Hsu YC, Zevenhoven KC, Dabek J, Parkkonen LT, Zhdanov A, Ilmoniemi RJ (2012) Noise amplification in parallel whole-head ultra-low-field magnetic resonance imaging using 306 detectors. Magn Reson Med. doi:10.1002/mrm.24479

Lin FH, Vesanen PT, Hsu YC, Nieminen JO, Zevenhoven KCJ, Dabek J, Parkkonen LT, Simola J, Ahonen AI, Ilmoniemi RJ (2013) Suppressing multi-channel ultra-low-field MRI measurement noise using data consistency and image sparsity. PLoS ONE 8:e61652

Liu C, Zhang Y, Qiu L, Dong H, Krause HJ, Xie X, Offenhäusser A (2012) Low-field MRI measurements using a tuned HTS SQUID as detector and permanent magnet pre-polarization field. Supercond Sci Technol 25:075013

Liu C, Zhang Y, Dong H, Qiu L, Krause H, Xie X, Offenhäusser A (2013) Tuned HTS SQUID-detected low field MRI using a permanent magnet for pre-polarization with automatic transportation. IEEE Trans Appl Supercond 23:1601104

Ljunggren S (1983) A simple graphical representation of Fourier-based imaging methods. J Magn Reson 54:338–343

Logothetis NK, Pauls J, Augath M, Trinath T, Oeltermann A (2001) Neurophysiological investigation of the basis of the fMRI signal. Nature 412:150–157

Luomahaara J, Vesanen PT, Penttilä J, Nieminen JO, Dabek J, Simola J, Kiviranta M, Grönberg L, Zevenhoven CJ, Ilmoniemi RJ, Hassel J (2011) All-planar SQUIDs and pickup coils for combined MEG and MRI. Supercond Sci Technol 24:075020

Macovski AS, Conolly S (1993) Novel approaches to low cost MRI. Magn Reson Med 30:221–230

Magnelind PE, Gomez JJ, Matlashov AN, Owens T, Sandin JH, Volegov PL, Espy MA (2011) Co-registration of interleaved MEG and ULF MRI using a 7 channel low-Tc SQUID system. IEEE Trans Appl Supercond 21:456–460

Matlachov AN, Volegov PL, Espy MA, Stolz R, Fritzsch L, Zakosarenko V, Meyer HG, Kraus R Jr (2005) Instrumentation for simultaneous detection of low-field NMR and biomagnetic signals. IEEE Trans Appl Supercond 15:676–679

Matlashov AN, Burmistrov E, Magnelind PE, Schultz L, Urbaitis AV, Volegov PL, Yoder J, Espy MA (2012) SQUID-based systems for co-registration of ultra-low field nuclear magnetic resonance images and magnetoencephalography. Physica C 482:19–26

Matlashov AN, Schultz LJ, Espy MA, Kraus RH, Savukov IM, Volegov PL, Wurden CJ (2011) SQUIDs vs. induction coils for ultra-low field nuclear magnetic resonance: experimental and simulation comparison. IEEE Trans Appl Supercond 21:465–468

Matter NI, Scott GC, Grafendorfer T, Macovski A, Conolly SM (2006) Rapid polarizing field cycling in magnetic resonance imaging. IEEE Trans Med Imaging 25:84–93

McDermott R, Trabesinger AH, Mück M, Hahn EL, Pines A, Clarke J (2002) Liquid-state NMR and scalar couplings in microtesla magnetic fields. Science 295:2247–2249

Myers W, Slichter D, Hatridge M, Busch S, Mößle M, McDermott R, Trabesinger A, Clark J (2006) Calculated signal-to-noise ratio of MRI detected with SQUIDs and Faraday detectors in fields from 10 μT to 1.5 T. J Magn Reson 186:182–192

Myers WR (2006b) Potential applications of microtesla magnetic resonance imaging detected using a superconducting quantum interference device. Ph.D. thesis, UC Berkeley. http://escholarship.org/uc/item/19x7q88x

Nieminen JO, Vesanen PT, Zevenhoven KCJ, Dabek J, Hassel J, Luomahaara J, Penttilä JS, Ilmoniemi RJ (2011) Avoiding eddy-current problems in ultra-low-field MRI with self-shielded polarizing coils. J Magn Reson 212:154–160

Nieminen JO, Ilmoniemi RJ (2010) Solving the problem of concomitant gradients in ultra-low-field MRI. J Magn Reson 207:213–219

Nieminen JO, Zevenhoven KCJ, Vesanen PT, Hsu Y-C, Ilmoniemi RJ (2014) Current-density imaging using ultra-low-field MRI with adiabatic pulses. Magn Reson Imaging 32:54–59

Overhauser AW (1953) Polarization of nuclei in metals. Phys Rev 92:411–412

Packard M, Varian R (1954) Phys Rev 93:941

Pannetier M, Fermon C, Le Goff G, Simola J, Kerr E (2004) Femtotesla magnetic field measurement with magnetoresistive sensors. Science 304:1648–1650

Pruessmann KP, Weiger M, Scheidegger MB, Boesiger P (1999) SENSE: Sensitivity encoding for fast MRI. Magn Reson Med 42:952–962

Savukov IM, Zotev VS, Volegov PL, Espy MA, Matlashov AN, Gomez JJ, Kraus RH Jr (2009) MRI with an atomic magnetometer suitable for practical imaging applications. J Magn Reson 199:188–191

Seok Kang C, Kim K, Lee SJ, Hwang S, Kim JM, Yu KK, Kwon H, Lee SK, Lee YH (2011) Application of the double relaxation oscillation superconducting quantum interference device sensor to micro-tesla ^{1}H nuclear magnetic resonance experiments. J Appl Phys 110:053906–053909

Sergeeva-Chollet N, Dyvorne H, Dabek J, Herreros Q, Polovy H, Goff GL, Cannies G, Pannetier-Lecoeur M, Fermon C (2011) Low field MRI with magnetoresistive mixed sensors. J Phys Conf Ser 303:012055

Seton HC, Bussell DM, Hutchison JMS, Lurie DJ (1995) Use of a DC SQUID receiver preamplifier in a low field MRI system. IEEE Trans Appl Supercond 5:3218–3221

Seton HC, Hutchison JMS, Bussell DM (1997) A 4.2 K receiver coil and SQUID amplifier used to improve the SNR of low-field magnetic resonance images of the human arm. Meas Sci Technol 8:198–207

Seton HC, Rieger SW, Hutchison JMS (2007) Tuned SQUID-MRI system with resonant frequency adjustment. IEEE Trans Appl Supercond 17:850–853

Sims JR, Schillig JB, Swenson CA, Gardner DL, Matlashov AN, Ammerman CN (2010) Low-noise pulsed pre-polarization magnet systems for ultra-low field NMR. IEEE Trans Appl Supercond 20:752–755

Sodickson DK, Manning WJ (1997) Simultaneous acquisition of spatial harmonics (SMASH): fast imaging with radiofrequency coil arrays. Magn Reson Med 38:591–603

Taulu S, Kajola M, Simola J (2004) Suppression of interference and artifacts by the signal space separation method. Brain Topogr 16:269–275

Trahms L, Burghoff M (2010) NMR at very low fields. Magn Reson Imaging 28:1244–1250

Twieg D (1983) The k-trajectory formulation of the NMR imaging process with applications in analysis and synthesis of imaging methods. Med Phys 10:610–621

Ungersma S, Matter N, Hardy J, Venook R, Macovski A, Conolly S, Scott G (2006) Magnetic resonance imaging with T1 dispersion contrast. Magn Reson Med 55:1362–1371

Uusitalo MA, Ilmoniemi RJ (1997) Signal-space projection method for separating MEG or EEG into components. Med Biol Eng Comp 35:135–140

Vesanen PT, Nieminen JO, Zevenhoven KCJ, Dabek J, Parkkonen LT, Zhdanov AV, Luomahaara J, Hassel J, Penttilä J, Simola J, Ahonen AI, Mäkelä JP, Ilmoniemi RJ (2013) Hybrid ultra-low-field MRI and magnetoencephalography system based on a commercial whole-head neuro magnetometer. Magn Reson Med 69:1795–1804

Vesanen PT, Nieminen JO, Zevenhoven KCJ, Dabek J, Simola J, Sarvas J, Ilmoniemi RJ (2012) The spatial and temporal distortion of magnetic fields applied inside a magnetically shielded room. IEEE Trans Magn 48:53–61

Vesanen PT, Nieminen JO, Zevenhoven KCJ, Hsu Y-C, Ilmoniemi RJ (2014) Current-density imaging using ultra-low-field MRI with zero-field encoding. Magn Reson Imaging, in press

Volegov P, Matlachov AN, Espy MA, George JS, Kraus RH Jr (2004) Simultaneous magnetoencephalography and SQUID detected nuclear MR in microtesla magnetic fields. Magn Reson Med 52:467–470

Volegov PL, Mosher JC, Espy MA, Kraus RH Jr (2005) On concomitant gradients in ultra-low field MRI. J Magn Reson 175:103–113

Volegov PL, Matlashov AN, Kraus RH Jr (2006) Ultra-low field NMR measurements of liquids and gases with short relaxation times. J Magn Reson 183:134–141

Wright PJ, Mougin OE, Totman JJ, Peters AM, Brookes MJ, Coxon R, Morris PE, Clemence M, Francis ST, Bowtell RW, Gowland PA (2008) Water proton T1 measurements in brain tissue at 7, 3, and 1.5 T using IR-EPI, IR-TSE, and MPRAGE: results and optimization. Magn Reson Mater Phys, Biol Med 21:121–130

Xia H, Ben-Amar Baranga BA, Hoffman D, Romalis MV (2006) Magnetoencephalography with an atomic magnetometer. Appl Phys Lett 89:211104

Yang HC, Liao SH, Horng HE, Kuo SL, Chen HH, Yang SY (2006) Enhancement of nuclear magnetic resonance in microtesla magnetic field with prepolarization field detected with high-Tc superconducting quantum interference device. Appl Phys Lett 88:252505

Zotev VS, Matlashov AN, Volegov PL, Urbaitis AV, Espy MA, Kraus RH Jr (2007) SQUID-based instrumentation for ultra-low-field MRI. Supercond Sci Technol 20:S367–S373

Zotev VS, Volegov PL, Matlashov AN, Espy MA, Mosher JC, Kraus RH Jr (2008a) Parallel MRI at microtesla fields. J Magn Reson 192:197–208

Zotev VS, Matlashov AN, Volegov PL, Savukov IM, Espy MA, Mosher JC, Gomez JJ, Kraus RH (2008b) Microtesla MRI of the human brain combined with MEG. J Magn Reson 194:115–120

Zotev VS, Matlashov AN, Savukov IM, Owens T, Volegov PL, Gomez JJ, Espy MA (2009) SQUID-based microtesla MRI for in vivo relaxometry of the human brain. IEEE Trans Appl Supercond 19:823–826

Neuronal Current Imaging with Ultra-Low-Field NMR Techniques

Rainer Körber, Martin Burghoff and Lutz Trahms

Abstract Neuronal current imaging (NCI) aims at detecting the influence of neuronal magnetic fields on an NMR signal which might be easier at ultra-low fields ($\sim\mu$T) than at high fields ($\sim$T). In the so-called 'DC effect', long-lived neuronal activity shifts the Larmor frequency of the surrounding protons and changes the NMR line-shape. An alternative strategy is to use fast neuronal activity as a tipping pulse. This so-called 'AC effect' requires the proton Larmor frequency to match the frequency of the neuronal activity. Phantom studies validating both principal working mechanisms are described assessing the feasibility of NCI at ultra-low fields. MRI on phantoms taken at Larmor frequencies of 100 and 731 Hz are also shown and discussed in an attempt to combine the AC effect and ULF MRI. These frequencies are examples of brain activity triggered by electrostimulation of the median nerve.

Keywords ULF NMR · ULF MRI · Neuronal currents · AC effect · DC effect · Median nerve · Phantom

1 Introduction

A non-invasive technique for direct and tomographic imaging of neuronal current flow within the brain with adequate temporal and spatial resolution is not available at present. The functional variant of magnetic resonance imaging (fMRI) is an indirect method for imaging neuronal activity as it relies on the cerebral metabolism via the blood-oxygen-level dependent (BOLD) effect and has a temporal delay of the order of seconds (Goense and Logothetis 2008). Electro- and

R. Körber (✉) · M. Burghoff · L. Trahms
Physikalisch-Technische Bundesanstalt, Berlin, Germany
e-mail: rainer.koerber@ptb.de

S. Supek and C. J. Aine (eds.), *Magnetoencephalography*,
DOI: 10.1007/978-3-642-33045-2_47,

magnetoencephalography (EEG and MEG) directly monitor neuronal currents via their accompanying electric and magnetic fields and track neuronal activity down to the millisecond range (Häamäläinen et al. 1993). However, these techniques do not give tomographical images of current distributions but rather infer the current distribution from electric and magnetic field maps, and thus one has to solve the inverse problem to estimate the dynamics and the locations of the brain currents which can result in spatial uncertainties of up to the cm range.

Another approach which seeks to achieve high temporal and spatial resolution is neuronal current imaging (NCI) where magnetic field changes of neuronal currents are mapped directly onto an MR image. This approach relies on the interaction of the precessing magnetization with the field generated by an active neuronal ensemble. For conventional high-field MRI this concept has yielded controversial results due to the obvious enormous difference of about nine orders of magnitude between the applied imaging field in the tesla range and the field generated by the neuronal generators (Hagberg et al. 2006) (hundreds of pT (Burghoff et al. 2010)). Consequently, reducing the imaging field to the ultra-low-field (ULF) regime of μT should alleviate the direct detection of neuronal activity.

The possibility of ULF NMR/MRI has been demonstrated by various groups with imaging systems operating at Larmor frequencies of 2 kHz (Zotev et al. 2007), 5.6 kHz (Clarke et al. 2007), and 425 kHz (Seton et al. 1997). Human brain anatomy was imaged at a frequency of about 2 kHz (Zotev et al. 2008). Here, we describe the instrumentation and ULF-MR studies on phantoms which were performed in order to validate the AC and DC effect and to demonstrate the capability of imaging at Larmor frequencies as low as 100 Hz (Hilschenz et al. 2013). The combination of ULF MRI and MEG (Magnelind et al. 2011; Vesanen et al. 2013) is described elsewhere in this book.

2 Demonstration of the AC and DC Effects

Two different mechanisms were proposed to record the influence of evoked brain currents by means of ULF NMR (Höfner et al. 2011; Cassará et al. 2009; Kraus et al. 2007). For the so-called DC effect, long-lasting neuronal fields shift the Larmor frequency of the protons around a neuronal activity and change the NMR line-shape, whereas for the AC effect, an NMR signal itself is generated by using the AC neuronal field as a tipping pulse. The fact that neuronal activities show spectral components mainly in the frequency range from DC up to 1 kHz implies that the AC effect can only be exploited if the imaging field is reduced to below 20 μT (Larmor frequency of 1 kHz). Note, contrary to the high-field-based NCI modality, for the AC effect an actual change in the spin population of the system forms the basis for the direct detection of the neuronal activity.

A suitable paradigm to exploit these two mechanisms is repetitive electrostimulation of the median nerve above motor threshold. It evokes contralaterally both fast activity, such as the N20 response (20 ms after stimulation) and slow activity

(lasting up to seconds after stimulation), a so-called near -DC response. Equivalent current dipoles (ECDs) are in the range of 15 nAm for the N20 and about 50 nAm for near-DC activity with depths relative to the head surface of $\sim$15 and $\sim$35 mm, respectively (Körber et al. 2011).

Phantom studies were performed in order to demonstrate the mechanism of the two effects (Höfner et al. 2011). To this end, a 10-mm-long current dipole was placed 4 mm away from the inner top surface inside a sphere of 78 mm diameter. It was filled with saline solution (0.9 % NaCl, spin-spin relaxation time $T_2 = 2$ s) for investigating the AC effect. For experiments regarding the DC effect an aqueous solution of $CuSO_4$, NaCl and hydroxyehtylcellulose (HEC) with concentrations of 0.034, 0.166 and 2.0 wt%, respectively, with a T_2 of 190 ms, was used. The phantom was placed directly underneath a dewar containing a 3-channel SQUID magnetometer system. It consists of three fully integrated helium-cooled multi-loop DC SQUIDs (Drung 2003) with an intrinsic white noise of about 4 fT/Hz with a 1/f corner frequency below 2 Hz. The sensors record the magnetic field in the z-direction and have a sensitive area of 3.6 mm in diameter.

In ULF MR two separate magnetic fields are used: a large polarizing field $\vec{B}_P$ (up to tens of mT) to boost the sample magnetization and a much smaller detection field $\vec{B}_D$ ($\sim\mu$T) in which the magnetization precesses. For the DC effect, $\vec{B}_D$ was perpendicular to the current dipole and $\vec{B}_P$ was turned off non-adiabatically. For the AC effect, $\vec{B}_D$ was parallel to the current dipole and $\vec{B}_P$ turned off adiabatically. $\vec{B}_D$ was set to 1.93 μT corresponding to a Larmor frequency of 82 Hz which matches the main frequency band of the evoked N20. A $\vec{B}_P$ of 5 mT was applied in both cases.

In Fig. 1 the results of the DC and AC effect are shown. For the DC effect the amplitude spectra of of the difference of the time domain signals (phantom on–phantom off) are shown. The subtraction is necessary to reveal the minute effect on the NMR line-shape. The amplitude of the residual signal scales with the applied current dipole moment Q and we can infer a resolution limit of $\sim$200 nAm.

For the AC effect, applying two physiological N20 signals consecutively with $Q = 771$ nAm clearly induces an NMR signal at 82 Hz. For a single N20 signal with the same Q a signal cannot be identified reliably and we conclude, that a resolution limit is likely to be about 1 μAm for a single N20 signal. Comparing these resolution limits to the ECDs evoked by electrostimulation of the median nerve it is evident that an increase of the signal to noise ratio (SNR) of at least 4 is necessary to observe neuronal currents based on the DC effect. The AC effect requires an increase in SNR of at least 67 and appears to be more difficult to exploit.

It should be noted that the quoted resolution limits represent lower bounds. The physiological ECDs are in fact deeper than current dipole in the phantom and the NMR relaxation times are significantly longer, in particular for the study regarding the AC effect, than the physiologically observed values for T_2 of 106 ms (gray matter) and 79 ms (white matter) (Zotev et al. 2009). An increase of the noise by a

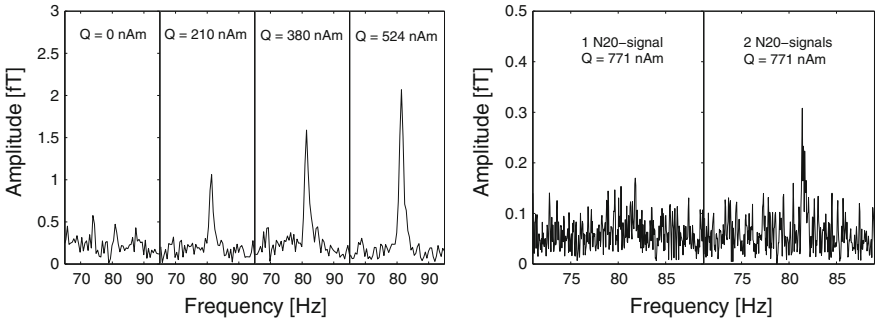

Fig. 1 *Left* Results for the DC effect phantom measurements (4,000 averages, total measurement time: 4 h 27 min). The residual signal scales with Q and a resolution limit of $\sim$200 nAm was obtained. *Right* Results for the AC effect phantom measurements (1,000 averages, total measurement time: 4 h 10 min). Two consecutive N20 signals with $Q = 771$ nAm induced a reliable resonant signal in contrast to the application of a single N20 trace. The resolution limit was estimated to be $\sim$1 μAm

factor of 3 would arise if the excessively long measurement time of about 4.5 h was reduced to 30 min. The final minimum resolution limits are then 600 nAm and 3 μAm for the DC and AC effects, respectively.

3 Imaging Below 1 kHz

For the potential use of the AC effect in ULF MRI, initial 2D MRI experiments were performed inside a custom designed magnetically shielded room (MSR) whose design is based on the commercially available AK3b from Vacuumschmelze. After degaussing the residual field inside the central volume of 1 m^3 is at most 1.5 nT with a gradient below 20 pT/cm. For ULF MRI we used a current sensor SQUID with additional positive feedback (APF) and integrated input coil (Drung et al. 2007) connected to a 1st-order wire-wound axial gradiometer (20 mm diameter and 120 mm baseline) with a noise spectral density of 1.9 fT/Hz.

Cylindrical phantoms with volumes of $\sim$5 ml, as shown at the left in Fig. 2, were imaged at 100 and 733 Hz using a 2D Fourier gradient echo sequence. These frequency ranges correspond to frequency bands stimulated by electrostimulation of the median nerve. Different solutions were chosen to obtain various spin-lattice and spin-spin relaxation times T_1 and T_2 for the phantoms: (a) tap water with a T_2 of $\sim$2.0 s (b) aqueous solution of $CuSO_4$ and NaCl with concentrations of 0.034 wt% and 0.166 wt%, respectively with a T_2 of 220 ms and (c) sample as in (b) but with additional 2 wt% hydroxethylcellulose (HEC) resulting in a T_2 of 190 ms (All T_2-values refer to the field of 17.17 μT). The images of the phantoms are shown in the middle and on the right hand side of Fig. 2. They clearly display the structure and arrangement of the phantom with a two dimensional pixel size of

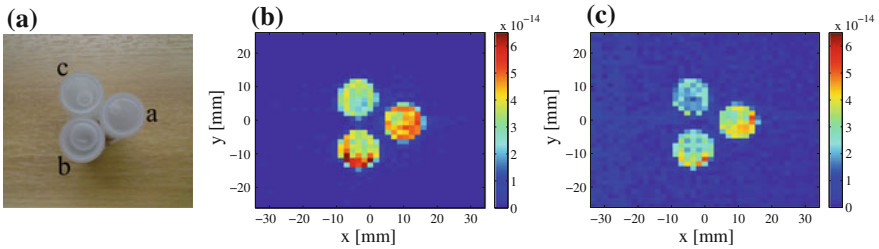

Fig. 2 *Left* The phantoms (**a**) tap water, (**b**) aqueous solution of $CuSO_4$ and (**c**) aqueous solution of $CuSO_4$ and HEC. *Middle* Image at 17.17 μT (731 Hz). *Right* Image at 2.35 μT (100 Hz). The color bar is in units of Tesla. (Reprinted with permission from Ref. (Hilschenz et al. 2013))

1.8×1.4 mm^2. Hence, by careful design imaging at frequencies as low as 100 Hz can be performed which is essential for the combination of the AC effect and ULF MRI.

4 Conclusion

Direct, non-invasive and tomographic imaging of current flow within the brain with adequate spatial and temporal resolution remains a challenge. The AC and the DC effect in ULF MR, which rely on fast and slow activity, respectively may provide a way out of this predicament. In phantom studies both mechanisms were demonstrated and evaluated. The increase in the SNR necessary to apply these techniques to in vivo measurements should be achievable with current technology as for instance by increasing $\vec{B}_P$ from 5 to 50 mT as it was done in the MRI experiments. The direct detection of neuronal currents using ULF-NMR techniques might thereby become possible. In addition, magnetic resonance images taken at Larmor frequencies below 1 kHz show that imaging is possible even at such extremely low fields where the AC effect applies.

Acknowledgements The authors wish to thank Jens Haueisen (TU Ilmenau) for providing the phantom and Gabriel Curio (Charité Berlin) for fruitful discussions regarding somatosensory stimulation. This work was supported by the Federal Ministry of Education and Research of Germany, Bernstein Focus Neurotechnology (grant number 01GQ0852).

References

Burghoff M, Albrecht HH, Hartwig S, Hilschenz I, Körber R, Höfner N, Scheer HJ, Voigt J, Trahms L, Curio G (2010) On the feasibility of neurocurrent imaging by low-field nuclear magnetic resonance. Appl Phys Lett 96:233701

Cassará A, Maraviglia B, Hartwig S, Trahms L, Burghoff M (2009) Neuronal current detection with low-field magnetic resonance: simulations and methods. Magn Reson Imaging 27:1131–1139

Clarke J, Hatridge M, Mößle M (2007) SQUID-detected magnetic resonance imaging in microtesla fields. Annu Rev Biomed Eng 9:389–413

Drung D (2003) High-T_C and low-T_C dc SQUID electronics. Semicond Sci Technol 16:1320–1336

Drung D, Aßmann C, Beyer J, Kirste A, Peters M, Ruede F, Schurig T (2007) Highly sensitive and easy-to-use SQUID sensors. IEEE Trans Appl Supercond 17:699–704

Goense J, Logothetis N (2008) Neurophysiology of the BOLD fMRI signal in awake monkeys. Curr Biol 18:631–640

Hagberg G, Bianciardi M, Maraviglia B (2006) Challenges for detection of neuronal currents by MRI. Magn Reson Imaging 24:483–493

Hämäläinen M, Hari R, Ilmoniemi R, Knuutila J, Lounasmaa O (1993) Magnetoencephalography—theory, instrumentation, and applications to noninvasive studies of the working human brain. Rev Mod Phys 65:413–497

Hilschenz I, Körber R, Scheer HJ, Fedele T, Albrecht HH, Cassará AM, Hartwig S, Trahms L, Haase J, Burghoff M (2013) Magnetic resonance imaging at frequencies below 1 kHz. Magn Reson Imaging 31:171–177

Höfner N, Albrecht HH, Cassará AM, Curio G, Hartwig S, Haueisen J, Hilschenz I, Körber R, Martens S, Scheer HJ, Voigt J, Trahms L, Burghoff M (2011) Are brain currents detectable by means of low-field NMR? A phantom study. Magn Reson Imaging 29:1365–1373

Körber R, Curio G, Hartwig S, Hilschenz I, Höfner N, Scheer HJ, Trahms L, Voigt J, Burghoff M (2011) Simultaneous measurements of somatosensory evoked AC and near-DC MEG signals. Biomed Tech 56:91–97

Kraus RH, Volegov P, Matlachov A, Espy M (2007) Toward direct neuronal current imaging by resonant mechanisms at ultra-low field. Neuroimage 39:310–317

Magnelind P, Gomez J, Matlashov A, Owens T, Sandin J, Volegov P, Espy M (2011) Co-registration of interleaved MEG and ULF MRI using a 7 channel low-T_C SQUID system. IEEE Trans Appl Supercond 21:456–460

Seton H, Hutchinson J, Bussel D (1997) A 4.2 K receiver coil and SQUID amplifier used to improve the SNR of low-field magnetic resonance images of the human arm. Meas Sci Technol 8:198–207

Vesanen P, Nieminen J, Zevenhoven K, Dabek J, Parkkonen L, Zhdanov A, Luomahaara J, Hassel J, Penttilä J, Simola J, Ahonen A, Mäkelä J, Ilmoniemi R (2013) Hybrid ultra-low-field MRI and magnetoencephalography system based on a commercial whole-head neuromagnetometer. Magn Reson Med 69:1795–1804

Zotev V, Matlashov A, Savukov I, Owens T, Volegov P, Gomez J, Espy M (2009) SQUID based microtesla MRI for in vivo relaxometry of the human brain. IEEE Trans Appl Supercond 19:823–826

Zotev V, Matlashov A, Volegov P, Savukov I, Espy M, Mosher J, Gomez J, Kraus R (2008) Microtesla MRI of the human brain combined with MEG. J Magn Reson 194:115–120

Zotev V, Matlashov A, Volegov P, Urbaitis A, Espy M, Kraus R (2007) SQUID-based instrumentation for ultralow-field MRI. Supercond Sci Technol 20:S367–S373

Magnetic Relaxometry: A Comparison to Magnetoencephalography

Edward R. Flynn

Abstract Magnetic relaxometry is a technology utilizing SQUID sensors and superparamagnetic nanoparticles to target various diseases using antibodies or other biomolecules specific to disease cells. The nanoparticles are magnetized in a small field and the SQUID sensors are used to detect the nanoparticle decaying field. The method has high sensitivity, more than 1000 times a mammogram for breast cancer, high contrast as only nanoparticles bound to cells are measured, and high specificity using specific biomarkers conjugated to the nanoparticles. Future directions of magnetic relaxometry include diagnosis of neural diseases using biomarkers specific to these diseases coupled to nanoparticles; this will complement ongoing diagnostic programs using magnetoencephalography.

Keywords SQUID · Magnetic relaxometry · Nanoparticles · Cancer

1 Introduction

The development of superconducting quantum interference detectors (SQUID) sensor technology (Zimmerman 1966) opened up a number of new research areas where the measurement of ultra-low magnetic fields provided new illumination into underlying phenomenon. Some of the earliest of these programs were in the area of measurement of magnetic fields from the heart (MCG) and brain (MEG) by (Cohen 1968) followed by the measurement of evoked responses in the brain by (Brenner 1975). These early efforts have been summarized in the review of (Hämäläinen et al. 1993) where the details of the SQUID sensors and applications

E. R. Flynn (✉)
Senior Scientific LLC, Albuquerque, NM 87111, USA
e-mail: seniorscientific@gmail.com

S. Supek and C. J. Aine (eds.), *Magnetoencephalography*,
DOI: 10.1007/978-3-642-33045-2_48,

are described. These applications are based on the measurements of biomagnetic magnetic fields emanating from currents involved in living tissue.

Magnetic relaxometry, or as defined here as superparamagnetic relaxometry (SPMR) is a more recent emerging technology (Flynn 2005; Kötitz 1995; Romanus et al. 2001) that is similar in many respects to MEG and MCG in its application and in the procedures used to analyze the data. At Senior Scientific, SPMR has been used to investigate various disease states, in particular cancer through the use of biomarkers conjugated to the nanoparticles [NP]. The method has been shown to be very sensitive for detecting cancer; for example, it is more than 1000 times more sensitive than a mammogram for detecting breast cancer. Because of the unique nature of superparamagnetic NP, very high contrast can be obtained between bound and unbound NP, and high specificity to disease using biomarkers. As in MEG, SPMR typically uses SQUID sensors to measure the low magnitude fields emitted by the NP during their magnetic relaxation. Similarly, SPMR uses arrays of SQUID sensors to localize sources of magnetic activity with the analysis normally performed with inverse-theory algorithms of the same type as in MEG and MCG (see for example, the inverse theory described by (Huang et al. 1998) for MEG. The resulting data are also subject to filtering and noise-suppression methods developed for biomagnetism measurements. As in MEG, the use of phantoms to calibrate and test the sensor systems and develop the software analysis methods, is directly applicable to SPMR; both MEG and SPMR taking advantage of the basic principles of electromagnetism.

The principal difference is that SPMR measures the relaxing magnetic fields from magnetic nanoparticles (NP) that have been briefly magnetized in a magnetic field and are not biomagnetic in nature. In MEG and MCG, the sources are described in terms of current dipoles with units corresponding to picoamps, whereas in SPMR, the sources are described in terms of magnetic moments with units corresponding to pJ/T (picoJoule/Tesla). However many of the applications of SPMR are directly related to biological phenomena. In the following discussions, SPMR is applied to the measurement of specificity and sensitivity of various antibodies to various cell types—in particular cancer cells, to the study of incubation rates for attachment of NP to cells, to localization of tumors in living animals, and to measurement of percentage of injected material delivered to tumors and other targeted organs in living animals.

There are two important principals that SPMR methods utilize in their measurements: (1) The high sensitivity of SQUID sensors for detecting extremely small amounts of magnetite—the principal ingredients of NP used, and (2) the special properties of superparamagnetic NP that yield high magnetic moments and high contrast for bound NP. In this regard, the SQUID sensors are exactly the same as used in MEG and the prototype system described here was originally used for MEG measurements. The sensitivity required is somewhat less than MEG and this fact combined with the method of measurement, allows most SPMR measurements to be made without the need for shielded rooms. As in MEG, it is typical to use gradiometers for the sensor configuration. An important difference between MEG and SPMR in the SQUID sensor configuration considerations is that the magnetic NP must be magnetized and this requires the presence of a pulsed magnetic field.

This magnetizing field needs be only some tens of gauss due to the intrinsic saturation properties of the NP and the magnetizing field is only applied for a fraction of a second. However, this requires that the SQUID sensor system be turned on and off during the pulsing and that the components of the system do not respond to this magnetic pulse for any extended duration. The coil configuration producing this magnetizing field also limits the configuration of the sensors such that this field is relatively uniform in strength and direction over the sensor array; thus a whole-head MEG system is not amenable to SPMR measurements whereas a relatively flat array such as used in MCG works quite well.

2 The SPMR Method

In Fig. 1, the system used for SPMR measurements at Senior Scientific is illustrated. The SQUID sensor system, seen here as the dewar at the top with the sensor snout below, is a replica of an early 7-channel 2nd-order gradiometer system used in early MEG studies (Supek et al. 1999) and is operated here in an unshielded environment without any background compensation; this condition along with artifacts induced by the pulsing, limits the sensitivity to 20pT. As described later, this system is being improved by several orders-of-magnitude in sensitivity. The magnetizing field of 50 gauss is applied by the Helmholtz coils seen in this photo and is in the direction parallel to the central gradiometer and relatively uniform over the measurement volume of interest. Samples to be measured are placed on a stage seen just below the sensor snout and can be moved in three dimensions. Samples may consist of live cell cultures, phantom sources, and live animals (normally mice). For single source samples, the 7-channel system is adequate for determining the position and magnetic moment strength of the sample. For multiple sources, such as with animals or phantoms, the stage is moved in the x-y plane in order to obtain sufficient field measurements to solve the inverse problem. An important difference here between MEG and SPMR is that the sources are aligned along the z-direction (along the axis of the central sensor) so that only the coordinates and the magnitude of the moments need be calculated and not the directions. This not only simplifies the inverse-problem calculations but results in a significant increase in spatial resolution over MEG (Flynn 1994) with localizations better than 0.5 mm observed. The field from a magnetic dipole is given by

$$\mathbf{B}(\boldsymbol{\mu}, \mathbf{r}) = (\mu_0/4\pi)\left[\left(3(\boldsymbol{\mu}\cdot\mathbf{r})\,\mathbf{r}\right)/\mathrm{r}^5 - \boldsymbol{\mu}/\mathrm{r}^3\right]$$

and since both $\boldsymbol{\mu}$ and $\mathbf{r}$ lie along the z-axis, this reduces to

$$\mathrm{B_z} = (\mu_0/2\pi)\left(\mu/\mathrm{z}^3\right)$$

where μ is the magnetic moment which may be expressed in units of pJ/T. A typical value of μ observed for high quality NP is 1.27×10^{-07} pJ/T/np.

Fig. 1 Photograph of magnetic relaxometry system used at senior scientific for studying disease using cell cultures and small animals. The *upper structure* is the dewar containing the SQUID sensors with gradiometers in the protruding snout. The Helmholtz coils are shown above and below the measurement stage

To measure the moments using the SPMR method, the sample is placed under the SQUID sensor system and a magnetizing field of approximately 50 gauss is applied for 0.75 s during which time the sensors are turned off. After a short delay, 0.035 s, to allow any induced currents in the system to dissipate, the decaying magnetic moment of the sample is measured by the SQUID sensor array. An example of such a decaying moment is shown in Fig. 2. The initial decay follows an exponential curve as predicted by Néel (1955). The field decay curve is measured for several seconds and the field magnitude calculated at the end of the magnetizing pulse. The field from each sensor position is then used to derive the source positions and magnitudes.

An important attribute of SPMR is that the decay time constants differ substantially between NP that are bound to a cell or some other substance and thus not able to freely rotate, and NP that are unhindered (Adolphi et al. 2009, 2010). This is shown clearly in Fig. 2 where the curve for NP bound to cells decays in seconds whereas effectively no signal is seen for the same NP but not bound to cells. Néel relaxation occurs due to thermal fluctuations of the direction of the magnetic moment relative to the crystal orientation. The rate for Néel is given by

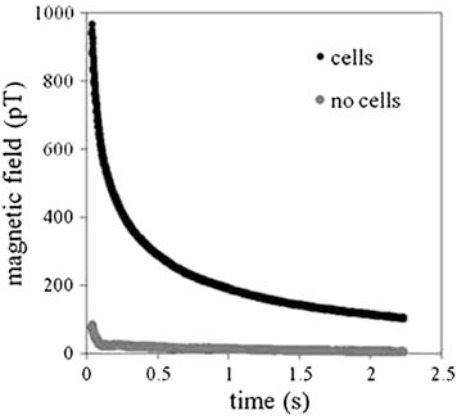

Fig. 2 Magnetic relaxation decay curves for NP bound to cells through antibody interactions and the same NP without cells present

$$\tau_N = \tau_0 e^{KV/kT}$$

where K is a characteristic of the magnetic material, V is the volume of the NP, k is the Boltzmann constant and τ_0 has a value of 10^{-9} s. In contrast, if the NP are not bound, they decay by Brownian motion given by the rate

$$\tau_B = {}^{3\eta V_h}/_{k_B T}$$

where η is the viscosity of the medium, Vh is the hydrodynamic volume, k_B is Boltzmann's constant. The desired decay time for bound NP is several seconds which according to the Néel formula requires a NP with a diameter of 25 nm. Unbound NP of this diameter decaying by Brownian motion decay in less than one msec. This very important feature of SPMR means that very high contrast is achieved in imaging cancer cells in vivo that are targeted by the NP that have been conjugated to antibodies specific to the cancer cells as NP circulating in the blood give no signal in the SQUID sensor time window. There are some similarities in this property of SPMR and MEG. PET is often used for both cancer detection and for brain activity through targeting metabolic activity. However, PET isotopes are decaying whether at the targeted site or anywhere in the blood stream. As stated above this is not true of SPMR and also not true in MEG where only active neuronal clusters are producing measurable magnetic fields.

The first important attribute of SPMR is the high sensitivity of the method for detecting minute amounts of NP, less than ng of Fe required, because of the SQUID sensor capabilities. The second important attribute are the characteristics of the superparamagnetic NP that yield high magnetic moments, substantial difference between bound and unbound NP, and are not ferromagnetic so do not cluster. The Néel time dependence on volume severely restricts the size of the NP that can be used in SPMR since a diameter of just a few nm in either direction from the ideal of 25 nm can be many orders-of-magnitude difference in decay time. For

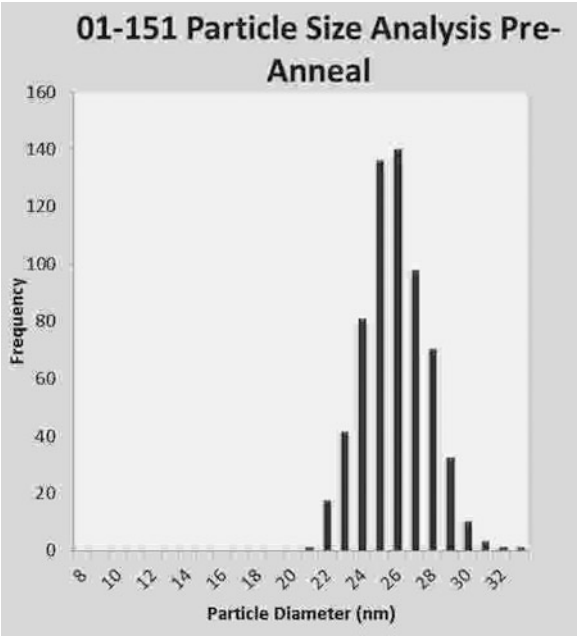

Fig. 3 Plot of NP diameter distribution as obtained from analyzing a transmission electron microscope photo of NP placed on a slide

this reason, substantial effort has gone into methods of producing NP with minimal dispersity in size. Figure 3 is a recent result obtained at The Center for Integrative Nanotechnology (CINT) (Huber 2012).

3 Applications of SPMR to Nanomedicine

The methodology of SPMR has been applied to a number of diseases in the area of nanomedicine. T-cells have been labeled with NP conjugated to an antibody for the specific T-cells responsible for rejecting transplanted organs and used to measure transplant rejection in a mouse model (Flynn et al. 2007; Butler et al. 2013). A study of leukemia Minimal Residual Disease (MRD) has been carried out using NP with antibodies (CD-34) specific to a number of leukemia types (Jaetao et al. 2009). SPMR has also been applied to the study of solid tumors in breast cancer (Hathaway et al. 2011; Adolphi et al. 2012a, b), ovarian cancer (Flynn et al. 2014), and prostate cancer. The results have also been compared to MRI imaging in some detail using an animal model (Adolphi et al. 2012b). A further advantage of the SPMR technique over many other biomedical methods is the transparency of tissue and bone to low frequency magnetic fields. This implies, just as in the case of MEG, that source localization is not affected by intervening tissue. For animal studies this is quite important and is unlike the scattering that occurs in the use of fluorescent markers resulting in loss of localization of source accuracy with depth.

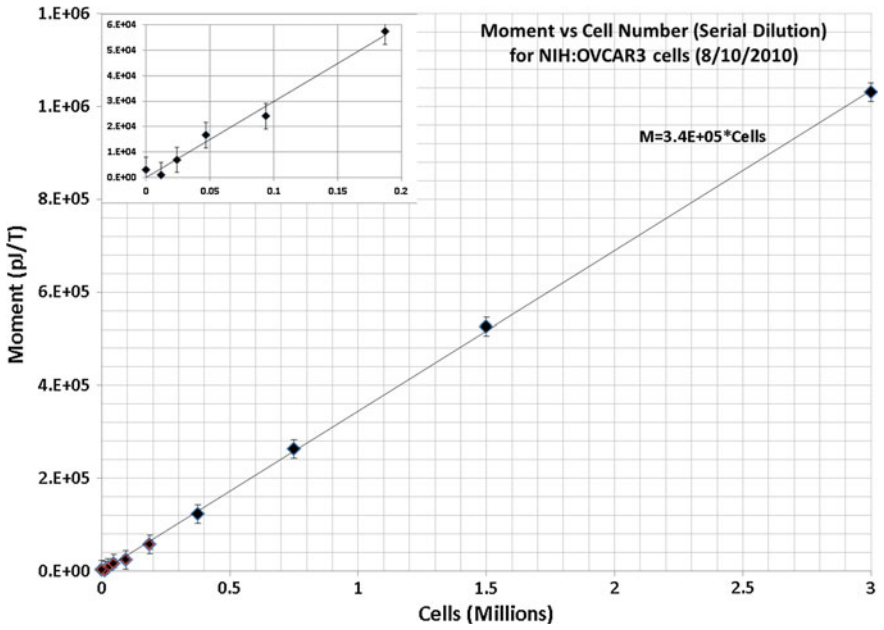

Fig. 4 Plot of the magnetic moment of cell cultures versus the number of cells illustrating the moment is linear with the cell number. The insert is the lower cell count indicating the sensitivity of the SPMR method for these cells

3.1 Linearity of Response

Because the strength of the magnetic field is completely linear in relationship to the source magnetic moment, the SPMR results are directly proportional to the number of bound NP in the source. Again, a similarity to MEG where the magnetic field strength observed can be directly related to the number of neurons involved. This linearity is demonstrated in Fig. 4 for the case of ovarian cancer cells (Flynn et al. 2014). Here the number of live ovarian cells in an in vitro sample was varied with the strength of the magnetic moment measured. The inset to this figure shows that the sensitivity with the present SPMR system shown in (Fig. 1) is 40,000 cells. The present standard for detecting ovarian cancer is trans-vaginal sonography (TVS) which requires over one billion cells indicating the excellent sensitivity of the SPMR method. The linearity shown in this figure is useful for in vivo animal studies of therapy. By using known amounts of cells and NP, it is possible to convert magnetic moments to numbers of cells and then monitor the number of cancer cells in a tumor as a function of applied therapy to see if the therapy is working or not. This is not possible in MRI where saturation of signal occurs and the response is not linear.

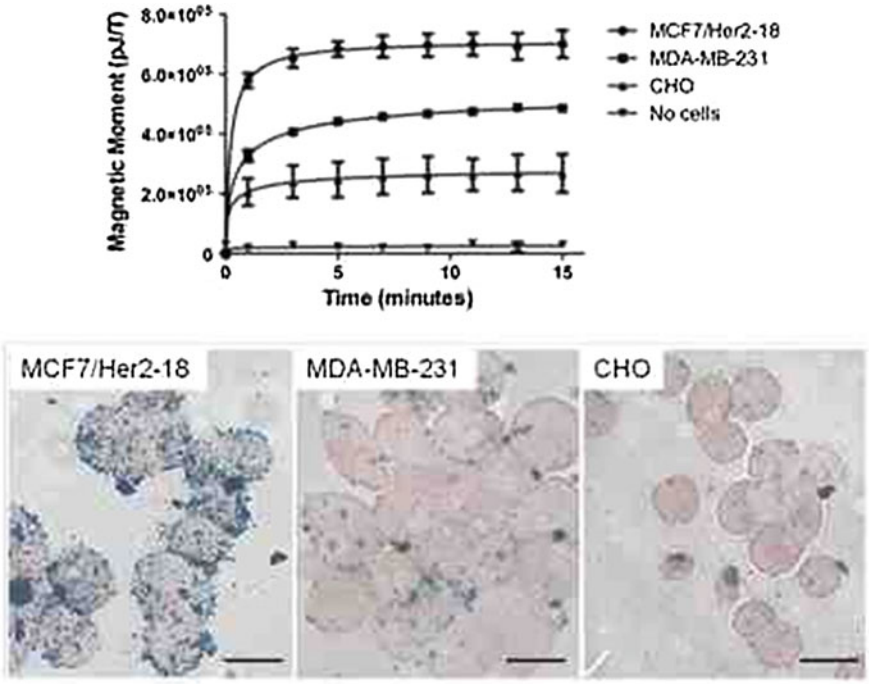

Fig. 5 Specificity of the SPMR method is shown for different cell types in breast cancer depending on the antibody chosen, Her2. The *upper part* of the figure shows incubation curves for three different cell lines and no cells with the magnitude of each curve representing the specificity of the Her2 antibody for that cell line. The *lower part* of the figure verifies this finding by showing that the cells with the highest specificity are covered more completely with the NP as visualized through Prussian Blue staiing

3.2 Specificity

There are many types of antibodies, proteins and other bio-agents that can be linked to the NP used in SPMR through conjugation procedures. By using various live cell lines of cancer or T-cells, it is possible to determine the specificity of these various agents to different cell lines by measuring the magnetic moment as a function of time after mixing the conjugated NP with the cells. The resulting incubation curve can be used for a variety of purposes. From a dynamic perspective, the rate of binding of the antibody to the cells can be used to understand the chemical processes involved. The relative magnitudes of the moments observed indicate the specificity of the particular antibody for the cell line and can be used to determine biomarker efficacy. The results also can be used as a calibration for in vivo studies to determine what type of cancer is present. Figure 5 is an example of such a study using several breast cancer cell lines and the antibody Her2 (Hathaway et al. 2011). The results at the top of the figure show that the cell line MCF7/Her2-18 is significantly more specific to the Her2 antibody than the MDA-MB-231 cell line, and even more so

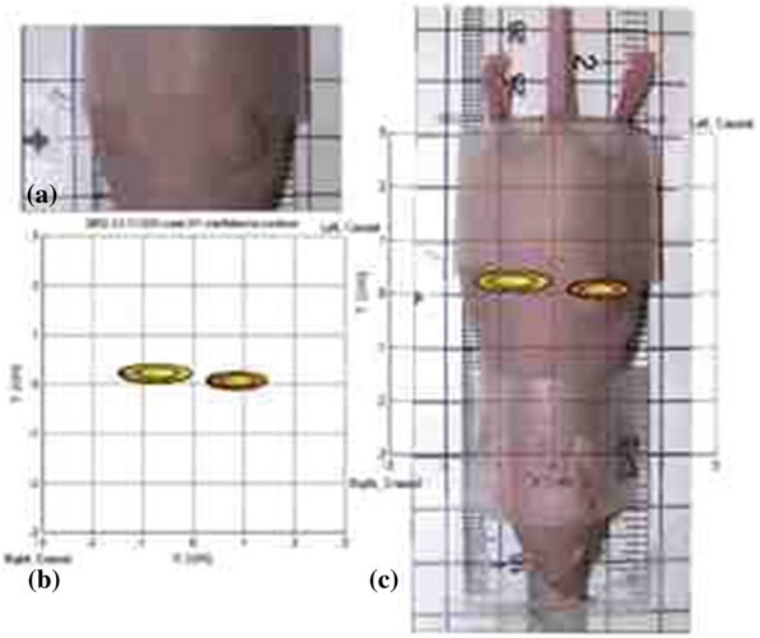

Fig. 6 Superposition of SPMR magnetic moment confidence limits on photographs of small animals showing localization in animals containing xenograft human tumors. A shows the tumors on the animal and C the superposition

than the non-specific cell line CHO. This comparison is verified by the microscopic examination of the cells in the lower part of the figure where Prussian Blue staining has stained the NP on the cell surface. The MCF7.Her2-18 cell line shows considerable more NP are on the surface than the other cell lines. Fitting these curves with a rate equation (Flynn et al. 2014) yields the number of NP/cell which may be several million NP. The sensitivity for detecting these breast cancer cells in the present SPMR system is about 100,000 cells. This may be compared to a mammogram that requires 100 million cells. Because of the specific action of the antibody on the NP, only cancer cells are targeted and not benign tumors.

3.3 In Vivo Detection and Localization

Living animals containing tumors may be placed under the SPMR system and the tumors localized and the number of cells determined. In Fig. 6, an example of such an experiment is shown. The mouse is a xenograft mouse containing two human breast cancer tumors. For this case, the NP + Her2 have been intra-tumorally injected although intra-venous injections also may be used. The mouse was placed under the system and the stage moved to obtain a total of 35 sensor positions. The

inverse problem was solved using a Levenberg-Marquadt algorithm similar to that used in MEG (Huang et al. 1998) and the source locations and magnetic moments extracted. The resulting confidence limits are then superimposed on a photograph of the mouse using a grid to establish the correct geometric relationship. The upper left hand corner of the figure shows the two tumors growing on the mouse; the lower left corner shows the resulting confidence limits x and y coordinates, and the right photo shows the superposition of these two measurements.

Through the use of phantoms containing vials of live cells, it has been shown that spatial resolutions of approximately 0.5 mm for multiple sources can be obtained (Hathaway et al. 2011). This is better than the resolution normally obtained in MEG experiments. The principal reason for this is that in the inverse problem only the coordinates and the magnitude of the source have to be determined since the sources are all aligned with the magnetizing field. In MEG, two more factors are needed that determine the orientation of the source.

4 Future SPMR Systems

The SPMR system described here, and shown in Fig. 1, is limited in sensitivity and resolution capabilities. It has no background sensors and operates in an unshielded environment and is thus subject to considerable interference. It is currently operating at a 20 pT sensitivity level whereas the SQUID sensitivity is better than 5 fT/$\sqrt{\text{Hz}}$. System performing MCG measurements in unshielded environments often exceed 10 fT/$\sqrt{\text{Hz}}$ noise thresholds so it is possible to improve the present system by several orders of magnitude by addition of background sensors. Other considerations to improve the performance of the system are removal of all metal components and induced currents in the system due to the pulsing of the Helmholtz coils which can be accomplished by reengineering the SQUID probe. Finally, improvements in the NP themselves offer additional sensitivity increases due to the dispersity of the size of the NP. Because of the narrow range of NP diameters that fall in the SPMR window, many of the NP coupled to cells fall outside of the window but occupy sites on the cell thus reducing the effective magnetic moment of the cell. Reduced dispersity of the NP is a major goal in the development of SPMR. Figure 7 is an illustration of the next generation system performance for detecting cells. In this T-cells are shown but the performance increase is representative of all of the cell lines for the various cancers being investigated.

5 Combining the Attributes of SPMR and MEG

Although the primary thrust of this manuscript has been on cancer and similar diseases, there are many other diseases with biomarkers known that SPMR can be applied to. These include several diseases of the brain and in the future the

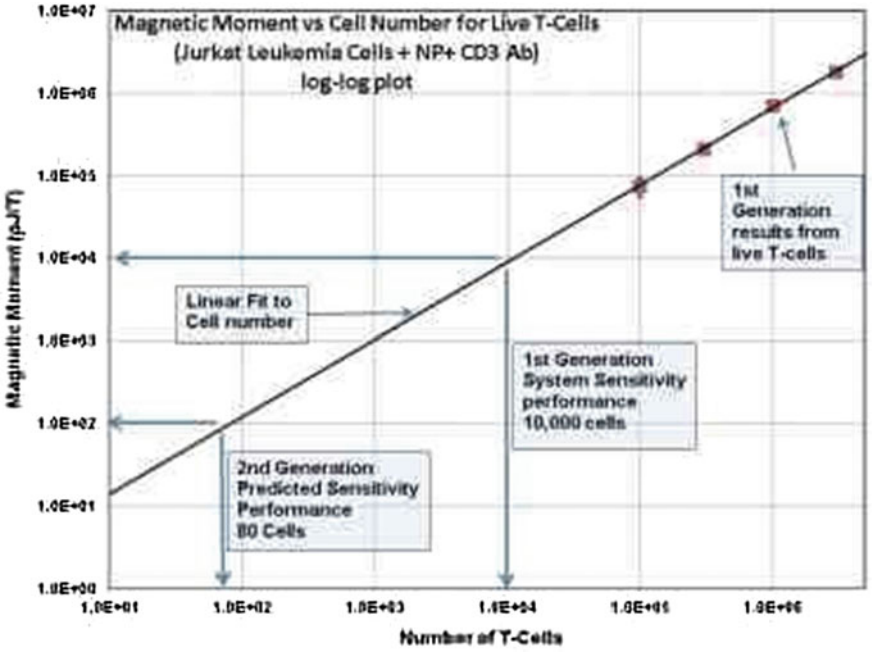

Fig. 7 Extrapolation of the linearity curve for cells versus moment to a SPMR system of much higher sensitivity demonstrating <100 cell detection capability

combining of MEG and SPMR in the diagnosis and treatment of neural diseases will be quite promising. There are a number of biomarkers known for the tau and amyloid plaque that build up in the brain of Alzheimer's patients. There is also increasing evidence for the role of tau in PTSD and CTE and it will be possible to identify this with SPMR using the known biomarkers for tau. Recent MEG research in these areas have identified methods for MEG biomarkers in brain disorders (Georgopoulos et al. 2007), PTSD (Georgopoulos et al. 2010) and traumatic brain injury (Huang et al. 2009). The combination of these approaches could be a significant advance in understanding these increasingly common neural diseases.

References

Adolphi NL, Huber DL, Jaetao JE, Bryant HC, Lovato DM, Fegan DL, Venturini EL, Monson TC, Tessier TE, Hathaway HJ, Bergemann C, Larson RS, Flynn ER (2009) Characterization of magnetite nanoparticles for SQUID-relaxometry and magnetic needle biopsy. JMMM 321:1459–1464

Adolphi NL, Huber DL, Bryant HC, Monson TC, Fegan DL, Lim JK, Jaetao JE, Tessier TE, Lovato DM, Butler KS, Provencio PC, Hathaway HJ, Majetich SA, Larson RS, Flynn ER (2010) Characterization of single-core magnetite nanoparticles for magnetic imaging by SQUID-relaxometry. PMB 55:5985–6012

Adolphi NA, Butler KS, Lovato DM, Tessier TE, Trujillo JE, Hathaway HJ, Fegan DM, Monson TC, Stevens TE, Huber DL, Ramu J, Milne ML, Conradi MS, Altobelli SA, Larson RS, Flynn ER (2012a) Imaging of Her2-targeted magnetic nanoparticles for breast cancer detection, comparison of SQUID-detected magnetic relaxometry and MRI. Contrast Media Mol Imaging 7(3):308–319

Adolphi NA, Butler KS, Lovato DM, Tessier TE, Trujillo JE, Hathaway HJ, Fegan DM, Monson TC, Stevens TE, Huber DL, Ramu J, Milne ML, Conradi MS, Altobelli SA, Larson RS, Flynn ER (2012b) Imaging of Her2-targeted magnetic nanoparticles for breast cancer detection, comparison of SQUID-detected magnetic relaxometry and MRI. Contrast Media Mol Imaging 7(3):308–319

Brenner D, Williamson SJ, Kaufman L (1975) Visually evoked magnetic fields of the human brain. Science 190:480–482

Butler KS, Lovato DM, Adolphi NA, Belfon R, Fegan DM, Monson TC, Hathaway HJ, Huber DL, Tessier TE, Bryant HC, Flynn ER, Larson RS (2013) Development of antibody-tagged nanoparticles for noninvasive detection of transplant rejection using biomagnetic sensors, Cell Transplantation 22:1943–1954

Cohen D (1968) Magnetoencephalography: evidence of magnetic fields produced by alpha-rhythm currents. Science 161:784–786

Flynn ER, Bryant HC (2005) A SQUID based system for in vivo cancer imaging. Phys Med Biol 50:1273–1293

Flynn ER (1994) Factors which affect spatial resolving power in large array biomagnetic sensors. Rev Sci Inst 65:922

Flynn ER, Bryant HC, Bergemann C, Larson RS, Lovato D, Sergatskov DA (2007) Use of a SQUID array to detect T-cells with magnetic nanoparticles in determining transplant rejection. JMMM 311:429–435

Flynn ER, Adolphi NL, Bryant HC, Butler KS, Hathaway HJ, Huber DL, Lovato DM, Tessier TE, Trujillo JE, Larson RS (2014) Applications of magnetic relaxometry in ovarian cancer, to be published

Georgopoulos AP, Karageorgiou E, Leuthold AC, Lewis SM, Lynch JK, Alonso AA, Aslam Z, Carpenter AF, Georgopoulos A, Hemmy LS, Koutlas IG, Langheim FJP, McCarten JR, McPherson SE, Pardo JV, Pardo PJ, Parry GJ, Rottunda SJ, Segal BM, Sponheim SR, Stanwyck JJ, Stephane M, Westermeyer JJ (2007) Synchronous neural interactions assessed by magnetoencephalography: a functional biomarker for brain disorders. J Neural Eng 4:349–355

Georgopoulos AP, Tan HRM, Lewis SM, Leuthold AC, Winskowski AM, Lynch JK, Engdahl B (2010) The synchronous neural interactions test as a functional neuromarker for post-traumatic stress disorder (PTSD): a robust classification method based on the bootstrap. J Neural Eng 7:016011

Hämäläinen M, Hari R, Ilmoniemi RJ, Knuutila J, Lounasmaa OV (1993) Magnetoencephalography—theory, instrumentation, and applications to noninvasive studies of the working human brain. Revs Mod Phys 65:413–497

Hathaway HJ, Butler KS, Adolphi NA, Lovato DM, Belfon R, Fegan DL, Monson TC, Trujillo JE, Tessier TE, Bryant HC, Huber DL, Larson RS, Flynn ER (2011) A novel method for early detection of breast cancer using magnetic nanoparticles and ultra-sensitive magnetic field sensors. Breast Cancer Res 13:R108

Huang M, Aine CJ, Supek S, Best E, Ranken D, Flynn ER (1998) Multi-start downhill simplex methods for spatio-temporal source localization in magnetoencephalography. Electroenceph Clin Neurophys 108:32–44

Huang MX, Theilmann RJ, Robb A, Angeles A, Nichols S, Drake A, D'Andrea J, Levy M, Holland M, Song T, Sheng G, Hwang E, Yoo K, Cui L, Baker D, Trauner T, Coimbra R, Lee R (2009) Integrated imaging approach with MEG and DTI to detect mild traumatic brain injury in military and civilian patients. J Neurotrauma 26:1213–1226

Huber D (2012) Center for integrative nanotechnology, Sandia National Laboratory, private communication

Jaetao JE, Butler KS, Adolphi NL, Lovato DM, H. C. Bryant HC, Rabinowitz I, Winter SS, Tessier TE, Hathaway HJ, Bergemann C, Flynn ER, Larson RS (2009) Enhanced leukemia cell detection using a novel magnetic needle and nanoparticles. Cancer Res 69(21):8310–8316

Kötitz R (1995) Ferrofluid relaxation for biomagnetic imaging, biomagnetism: fundamental research and clinical applications. In: Baumgartner C et al (eds) Elsevier science. IOS Press, Amsterdam, p 785

Néel L (1955) Some theoretical aspects of rock-magnetism. Adv Phys 4:191–243

Romanus E, Huckel M, Gross C, Prass S, Brauer R, Weitsches W, Weber P (2001) Magnetic nanoparticles as a novel tool in vivo diagnostics, ICMF9 MRX poster

Supek S, Aine C, Ranken D, Best E, Flynn ER, Wood C (1999) Single versus paired visual stimulation: superposition of early neuromagnetic responses and retinotopy in exstrastriate cortex in humans. Brain Res 830:43–55

Zimmerman JE (1966) Macroscopic quantum interference effects through superconducting point contacts. Phys Rev 141:367–375

Optically-Pumped Magnetometers for MEG

Svenja Knappe, Tilmann Sander and Lutz Trahms

Abstract Optically-pumped magnetometers (OPMs) have seen rapid progress over the last decade in terms of performance and technology development. As highly sensitive room-temperature magnetometers they present several advantages over superconducting quantum interference device (SQUID) sensors, such as the possibility for conformal geometries and low-maintenance systems. We review the state of the art and different types of low-field OPMs, as well as the first magnetoencephalography (MEG) demonstrations with OPMs. Several challenges remain, such as the demonstration of OPM multichannel systems, their limited dynamic range, and the demonstration of gradiometric operation to name just a few. Certainly OPMs present a promising technology to complement existing SQUID-based installations.

Keywords Optically pumped magnetometer · Magnetoencephalography · Superconducting quantum interference device · Magnetocardiography · Multichannel · Electron spin resonance · Micro-electromechanical system · Alkali-metal vapor cell · Atomic magnetometer · Optical magnetometer

1 Introduction

Rapid advances in atomic physics over the last decade have led to the design of optical magnetometers Optically Pumped Magnetometer (OPM) capable of recording biomagnetic signals; although the first attempts are much older (Livanov

S. Knappe (✉)
National Institute of Standards and Technology, Boulder, CO 80303, USA
e-mail: Svenja.knappe@nist.gov

T. Sander · L. Trahms
Physikalisch-Technische Bundesanstalt, 10587 Berlin, Germany

S. Supek and C. J. Aine (eds.), *Magnetoencephalography*,
DOI: 10.1007/978-3-642-33045-2_49,

et al. 1981). Further motivation to develop room-temperature alternatives to low-temperature SQUID magnetometers comes from the spiraling helium costs, which complicate the operation of MEG systems. Optical magnetometers have demonstrated sensitivities similar to those of the best SQUID magnetometers (Deng et al. 2010), at least over a narrow frequency band. At present, only laboratory prototypes of OPMs exist, and few MEG measurements have been demonstrated (Xia et al. 2006; Johnson et al. 2010; Sander, et al. 2012). Clearly these OPMs cannot compete with sophisticated commercial SQUID-based MEG systems yet. Nevertheless, OPMs have the potential to complement SQUID-based systems or to replace them for certain applications. This might soon be the case in magnetocardiography, where multi-channel OPM systems have been implemented (Bison et al. 2009; Wyllie et al. 2012). Other applications of OPMs that have been demonstrated include magnetic resonance imaging (Xu et al. 2006; Savukov et al. 2009) and magnetic relaxation measurements of nano-particles (Knappe et al. 2010).

OPMs are individually placeable room-temperature sensors, which entail several advantages. First, without the need for a dewar, OPMs allow for a shorter distance between sensor and scalp. This will enhance the MEG signal strength at the location of the sensor, especially for sources at shallow depths beneath the skull and can therefore result in a higher signal-to-noise ratio. Second, sensor placement conformal to the individual scalp reduces the distance between sensor and source further, which can be especially advantageous for MEG measurements on children and for flexible research systems. This would require, however, accurate detection of the sensor arrangement for analysis purposes. Third, open geometries and room-temperature operation simplify the combination with other modalities, such as electroencephalography (EEG) or functional near-infrared spectroscopy in the same system. Fourth, the operation of OPMs does not require a shielded room for the measurements, although the practicability of biomagnetic measurements with OPMs in an unshielded environment still must be demonstrated.

These advantages, nevertheless, come at a price. The OPMs used for MEG so far have much smaller dynamic ranges and bandwidths compared to those of SQUIDs. Furthermore, gradiometers with good common-mode rejection ratios have not yet been demonstrated; cross-talk issues with neighboring sensors need to be resolved, and multichannel devices need to be demonstrated.

2 Principle of Operation

The OPMs used for MEG recordings so far use electron-spin resonances in alkali atoms in the vapor phase. These atoms have a single valence electron that determines most of the properties of interest. Due to their electron spin and magnetic moment, the spin precesses around a magnetic field at a well-defined frequency, the Larmor frequency (see Fig. 1). Furthermore, a large macroscopic

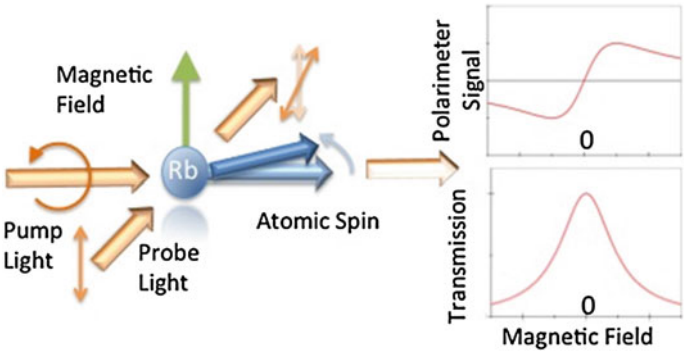

Fig. 1 Light from a circularly polarized laser beam optically pumps the Rb atoms, while light from a second laser beam probes the magnetic field-dependent spin orientation through polarization rotation. Both the transmission and polarimeter signal show a resonance as a function of magnetic field

polarization can be produced in these atoms through optical pumping (Happer 1972). In its simplest form, the spin from near-resonant circularly polarized photons is transferred to the atoms during absorption. Since these incident photons all have spins in a specific direction, the spins of the atoms become oriented. This process is very efficient, and can achieve atomic spin-polarizations close to unity. A magnetic field changes the atomic spin orientation, which can be probed once again with near-resonant light, making use of the absorption or dispersion of the light. The light carries information about the external magnetic field.

For MEG measurements made thus far, only zero-field magnetometers have been used. When operated in a regime of frequent atomic collisions and in low magnetic fields, the decoherence mechanism through spin-exchange collisions can be suppressed (Happer and Tang 1973). This so-called spin-exchange relaxation-free (SERF) regime (Allred et al. 2002) allows for very high magnetometer sensitivities, but limits the dynamic range of the magnetometer. In very small magnetic fields, the spins are tilted by the magnetic field and a static reorientation results from the balance between precession and continuous pumping. Again, the orientation of the spins is measured with near-resonant light by detecting the transmission of resonant light. Often it is more advantageous to monitor the polarization rotation of a slightly detuned light beam, which is usually done with a balanced polarimeter. This method can cancel intensity noise of the laser light and also tolerate much higher optical thickness of the vapor, since the light is detuned from resonance. In order to increase the signal-to-noise ratio, phase-sensitive detection can be implemented. For the zero-field resonances, one parameter, such as the magnetic field or the probe light polarization, is modulated and the same frequency component of the light is detected at a fixed phase with the modulation. Typically, OPMs measure the magnitude of the magnetic field, but the zero-field OPMs used for MEG are operated to measure a magnetic-field component in a certain direction, e.g., through external field modulation with an additional Helmholtz coil pair.

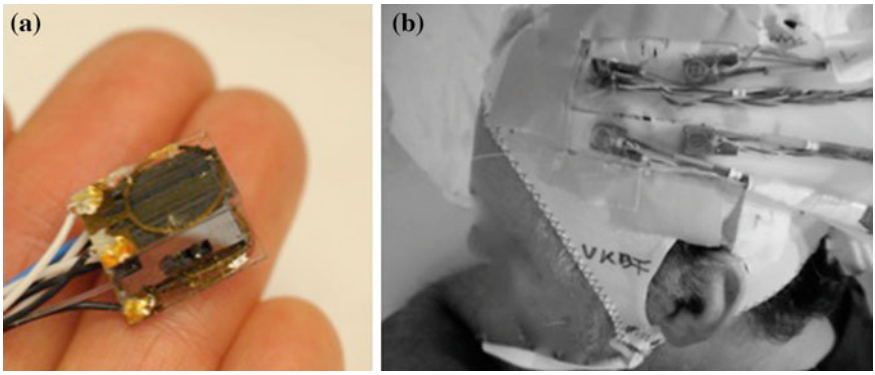

Fig. 2 **a** Photograph of a chip-scale OPM sensor head. **b** Photograph of four chip-scale OPMs attached to an EEG cap for MEG measurements. The fibers and wires needed to drive a sensor are collected in a bundle leaving the head tangentially

All of the devices used for MEG demonstrations have been operated in an open-loop configuration, where the dynamic range was limited by the linewidth of the resonance to below 100 nT. While feedback systems have been demonstrated in principle, they have not yet reached the same sensitivities (Seltzer and Romalis 2004). Furthermore, the response of the magnetometer shows the behavior of a first-order low-pass filter with a width corresponding to the linewidth of the atomic resonance. This usually limits the intrinsic bandwidth to below 1 kHz.

Figure 2a shows a chip-scale high-sensitivity OPM, which was manufactured by use of a micro-electro-mechanical-system (MEMS) process (Mhaskar et al. 2012). In the center of the cube is an alkali-vapor cell, heated to generate a sufficient atomic density of the vapor (Knappe et al. 2005). A laser, on resonance with a transition of the atoms, is circularly polarized and optically pumps the atoms. The same laser is used to monitor the atomic polarization by detecting the transmitted light with a photodiode (Dupont-Roc et al. 1969; Shah et al. 2007). This is only one of many possible configurations with respect to polarization, sensor shape, and beam.

3 MEG with OPMs

Three different demonstrations of MEG measurements with OPMs on human subjects have been published to this date. In the first one, Xia et al. used a $(7.5\ \text{cm})^3$ Pyrex cell filled with potassium vapor and heated to 180° C (Xia et al. 2006). It was placed on the left side of the head at a distance of 6.25 cm between the scalp and center of the cell. The atoms were polarized with 500 mW circularly polarized pump light, and the magnetic field was monitored through the polarization rotation of linearly polarized probe light at a right angle, so that the OPM

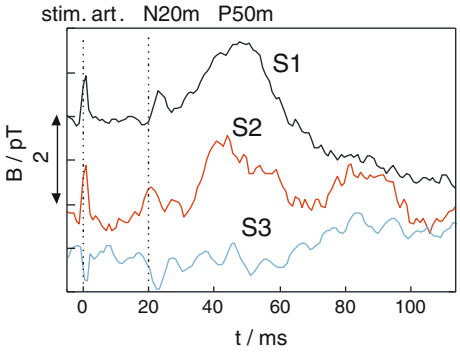

Fig. 3 Exemplary single-channel OPM recordings of the N20 and P50 m brain responses from three subjects (S1–S3). Electrical stimuli were applied to the right median nerve and a total of 5,000 responses were recorded inside a seven-layer magnetically-shielded room. The averaged responses show the stimulus artifact at 0 ms, the N20 m response (20 ms poststimulus), and the P50 m at 50 ms (figure reprinted with permission from Sander et al. 2012, copyright OSA 2012)

was sensitive to the component of the magnetic field normal to the scalp. The probe light was detected by a 16 × 16 photodiode array and 256 parallel channels of roughly 0.4 × 0.4 × 7.5 cm and spacing of 5 mm could be monitored simultaneously. Auditory evoked fields were recorded and the N100 m peak was clearly visible in the data. Six subjects were measured.

In the second paper Johnson et al. demonstrated an OPM with a fiber-coupled sensor head. Pump and probe beams were collinear and passed through a cylindrical Rb vapor cell of diameter 2.5 cm and length 2.5 cm (Johnson et al. 2010). A balanced polarimeter consisted of a photodiode and a quadrant detector, which allowed them to monitor four channels with a spatial distance of 5 mm simultaneously. The distance between cell and scalp was 2 cm, and one component of the magnetic field tangential to the scalp was measured. Evoked fields were recorded after auditory stimulation and after electrical stimulation of the median nerve in a male subject. They were verified by consecutive SQUID measurements.

The third MEG measurement was performed with a fiber-coupled chip-scale OPM (Sander et al. 2012). Here, the Rb vapor cell was of size $(2\ \text{mm})^3$ and the magnetometer was operated with a single laser beam and detection of the transmitted light. The distance to the scalp was 4 mm and the sensor was attached to an EEG cap for ease of placement similar to the four-channel configuration shown in Fig. 2b. The magnetic field component normal to the scalp was measured in three subjects. The sensor was operated with a modulation field of 1.8 kHz and the high-frequency cutoff was optimized to achieve a bandwidth sufficient for the recording of brain signals. By use of a coil to generate an AC magnetic field, it was verified that the − 3 dB cut-off for the sensor was at 150 Hz. This is sufficient to resolve the evoked responses N20 and P50 m due to electrical stimulation of the median nerve at the wrist, as can be seen in the typical MEG results shown in Fig. 3. The same responses in the same subjects were identified in consecutive SQUID measurements.

An OPM very similar to the one used in Xia et al. was demonstrated to measure signals from a dipolar current source immersed in a saline solution MEG phantom (Taue et al. 2010). A $(3\ \mathrm{cm})^3$ potassium cell was used to record the magnetic field at several locations around the phantom with a single channel. From the measured field map the location of the dipolar current source was estimated, and good agreement was obtained with the known position.

4 Conclusions and Outlook

In the last decade several research groups have demonstrated the measurement of MEG signals by use of single OPM sensor units. The head coverage was very limited, but the signals obtained show that OPMs are suitable as MEG sensors. It is still an open question whether multichannel OPM systems will achieve the same sensitivity as the best multichannel SQUID systems with up to 300 sensors. The reduced distance between the cortical source and OPM will certainly allow for stronger signals.

For a rapid advance of OPMs the development focus should be on broadband operation of multichannel devices with self-tuning capabilities. At least two types of multichannel systems appear promising: a standalone multichannel OPM device for weak shielding and a combined SQUID and OPM system for the most demanding studies. A combined system could consist, for example, of a SQUID helmet design with an additional OPM array to cover other positions difficult to reach with a closed dewar, such as the base of the head or the forehead. Development of multichannel devices can utilize experience gathered during the design of multichannel SQUID systems, hopefully reducing development time and cost. On a technical level, OPM gradiometers need to be demonstrated with dynamic ranges high enough to achieve common-mode rejections sufficient to suppress residual magnetic fields fluctuations inside the shielded room. Furthermore, three-axis OPMs would be desirable. It appears sensible to commercialize single-unit OPMs in order that system developers can buy sensors off the shelf to design multichannel systems themselves.

The development of OPMs is accelerated by a current helium shortage, which could also lead to a new generation of closed-cycle refrigeration systems suitable to support SQUID MEG systems. OPMs nevertheless offer the advantage of a flexible geometry, which might allow gathering a more complete picture of brain function (see other chapters in the present book and Brookes and Singh (2013) for more on challenges in MEG research). Overall, OPMs are an attractive candidate for designing inexpensive low-maintenance MEG systems and judging from the initial MEG demonstrations no obvious shortcomings could be identified, which would prevent the successful use of OPMs in large-scale MEG systems.

References

Allred JC, Lyman RN, Kornack TW, Romalis MV (2002) High-sensitivity atomic magnetometer unaffected by spin-exchange relaxation. Phys Rev Lett 89:130801

Bison G, Castagna N, Hofer A, Knowles P, Schenker JL, Kasprzak M, Saudan H, Weis A (2009) A room temperature 19-channel magnetic field mapping device for cardiac signals. Appl Phys Lett 95:173701

Brookes M, Singh K (2013) Methods in mind. Phys World 25:39–44

Dang HB, Maloof AC, Romalis MV (2010) Ultrahigh sensitivity magnetic field and magnetization measurements with an atomic magnetometer. Appl Phys Lett 97:151110

Dupont-Roc J, Haroche S, Cohen-Tannoudji C (1969) Detection of very weak magnetic fields (10–9 gauss) by Rb zero-field level crossing resonances. Phys Lett A 28:628–639

Happer W (1972) Optical pumping. Rev Mod Phys 44:169–249

Happer W, Tang H (1973) Spin-exchange shift and narrowing of magnetic resonance lines in optically pumped alkali vapors. Phys Rev Lett 31:273

Johnson C, Schwindt PDD, Weisend M (2010) Magnetoencephalography with a two-color pump-probe, fiber-coupled atomic magnetometer. Appl Phys Lett 97:243703

Knappe S, Gerginov V, Schwindt PDD, Shah V, Robinson H, Hollberg L, Kitching J (2005) Atomic vapor cells for chip-scale atomic clocks with improved long-term frequency stability,". Opt Lett 30:2351–2353

Knappe S, Sander TH, Kosch O, Wiekhorst F, Kitching J, Trahms L (2010) Cross-validation of microfabricated atomic magnetometers with superconducting quantum interference devices for biomagnetic applications. Appl Phys Lett 97:133703

Livanov MN, Kozolov AN, Sinelnikova SE, Kholodov JA, Markin VP, Gorbach AM, Korinewsky AV (1981) Record of the human magnetocardiogram by the quantum gradiometer with optical pumping. Adv Cardiol 28:78–80

Mhaskar R, Knappe S, Kitching J (2012) A low-power, high-sensitivity micromachined optical magnetometer. Appl Phys Lett 101:241105

Sander TH, Preusser J, Mhaskar R, Kitching J, Trahms L, Knappe S (2012) Magnetoencephalography with a chip-scale atomic magnetometer. Biomed Opt Express 3:981–990

Savukov IM, Zotev VS, Volegov PL, Espy MA, Matlashov AN, Gomez JJ, Kraus RH Jr (2009) MRI with an atomic magnetometer suitable for practical imaging applications. J Mag Resonanace 199:188–191

Seltzer SJ, Romalis MV (2004) Unshielded three-axis vector operation of a spin-exchange-relaxation-free atomic magnetometer. Appl Phys Lett 85:4804–4806

Shah V, Knappe S, Schwindt PDD, Kitching J (2007) Subpicotesla atomic magnetometry with a microfabricated vapour cell. Nat Photonics 1:649–652

Taue S, Sugihara Y, Kobayashi T, Ichihara S, Ishikawa K, Mizutani N (2010) Development of a highly sensitive optically pumped atomic magnetometer for biomagnetic field measurements: a phantom study. IEEE Trans Magn 46:3635–3638

Wyllie R, Kauer M, Wakai RT, Walker TG (2012) Optical magnetometer array for fetal magnetocardiography. Opt Lett 37(12):2247–2249

Xia H, Baranga ABA, Hoffman D, Romalis MV (2006) Magnetoencephalography with an atomic magnetometer. Appl Phys Lett 89:211104

Xu S, Yashchuk VV, Donaldson MH, Rochester SM, Budker D, Pines A (2006) "Magnetic resonance imaging with an optical atomic magnetometer. Proc Natl Acad Sci 103:12668–12671

Spin Electronics Based Magnetic Sensors for Biomagnetic Measurements

M. Pannetier-Lecoeur, C. Fermon, P. Campiglio, Q. Herreros and G. Jasmin-Lebras

Abstract In this short chapter, we present an alternative approach for biomagnetic signals detection using spin electronics based magnetic sensors. The principle of these sensors is first given followed by examples of their use for magnetocardiography and low field MRI.

Keywords Spin electronics · Magneto-cardiography · Magneto-encephalography · MRI

1 Introduction

Magnetic sensors based on spin electronics principle are now used in a wide range of applications due to their large sensitivity and high integration capabilities. Their field equivalent noise is now in the range of tens to hundreds of picotesla at room temperature. The use of mixed sensors, combining superconductivity and spin electronics (Pannetier et al. 2004) has opened the possibility of entering in the femtotesla range suitable for biomagnetism and low field Magnetic Resonance Imaging (MRI). In this short chapter we present the principle of such sensors with their main properties and limitations, and then we give some examples of biomagnetic signal detection and low field MRI images.

M. Pannetier-Lecoeur (✉) · C. Fermon · P. Campiglio · Q. Herreros · G. Jasmin-Lebras
DSM/IRAMIS/SPEC, CEA Saclay and CNRS URA 2464, 91191 Gif sur Yvette, France
e-mail: myriam.pannetier-lecoeur@cea.fr

C. Fermon
e-mail: claude.fermon@cea.fr

S. Supek and C. J. Aine (eds.), *Magnetoencephalography*,
DOI: 10.1007/978-3-642-33045-2_50,

2 Mixed Sensors Principle

Mixed sensors are fabricated from thin film technology, combining a Giant Magneto-Resistive (GMR) element with a superconducting loop, which acts as an efficient flux-to-field transformer (Fig. 1). To date, two types of mixed sensors have been fabricated. The first combines a Niobium (Nb) loop and a GMR, and has to be cooled at 4 K. The second uses a high-T_c superconductor -$YBa_2Cu_3O_{7-\delta}$ (YBCO)- combined with a GMR and can be operated at liquid nitrogen temperature (77 K). The GMR element consists of a spin valve with a hard magnetic layer whose magnetic orientation is fixed, a copper spacer, and a free magnetic bilayer whose magnetization rotates under small in-plane magnetic field. It is designed in a yoke-shape (see Fig. 1) which maximizes the free layer magnetic homogeneity. The superconducting loop is a large loop, 1–2 cm^2 size, with a micron size constriction placed on top or below the GMR element. The response of a mixed sensor is linear up to several microteslas and becomes flat when the critical current in the constriction is reached. The amplification gain of the superconducting loop, i.e. the ratio between the field applied to the loop and the field seen by the GMR element is roughly given by the ratio between the loop size and the constriction width.

3 Detectivity

The detectivity, also called field equivalent noise, is the voltage noise of the sensor given in $V/\sqrt{Hz}$ divided by the sensitivity given in V/T. It represents the field for which a Signal-to-Noise Ratio (SNR) is one. This allows for an easy comparison between the performance of various sensors that are at strengths similar to biomagnetic sources.

The detectivity of SQUIDs used in MEG is in the range of $2-5fT/\sqrt{Hz}$ down to several Hz. High-T_c SQUIDs made with YBCO have a detectivity of the order of 30 fT/sqrt(Hz).

For mixed sensors, the noise is given by the GMR element; the superconducting loop does not contribute to the noise since it operates in the purely non-resistive state. The noise is comprised of two contributions; the thermal noise which is flat in frequency and the low frequency noise (1/f noise) with a power spectral density decreasing as 1/f. For that reason, mixed sensors are more sensitive at high frequencies than at low frequencies. Figure 2 gives the detectivity of a small-size YBCO sensor as function of frequency.

4 MCG and MEG Applications

As seen in the previous section, the detectivity of the present mixed sensors is good enough to perform fast and reliable MCG measurements but is at the limit for the detection of MEG signals. A clinical investigation of MCG recordings on

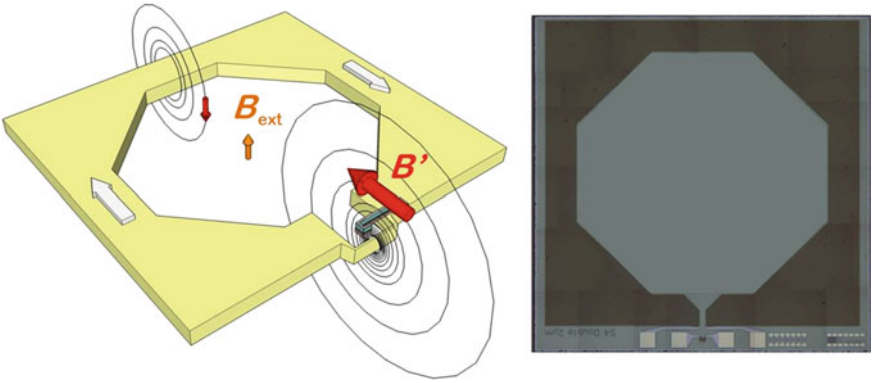

Fig. 1 *Left panel* Mixed sensor schematic; a superconducting loop (*yellow*) containing a constriction reacts to the applied field B_{ext} by generating a supercurrent (*white arrows*) which, passing through a constriction, exhibits an amplified local field B'. This field can be detected by the GMR element (*light blue*) placed on top or below the constriction. The GMR element is designed in a yoke shape which allows reducing the magnetic domain noise. Right panel: Photograph of a YBCO-mixed sensor. The YBCO appears in dark brown; the GMR contact pads can be seen at the bottom of the figure (*light grey squares*)

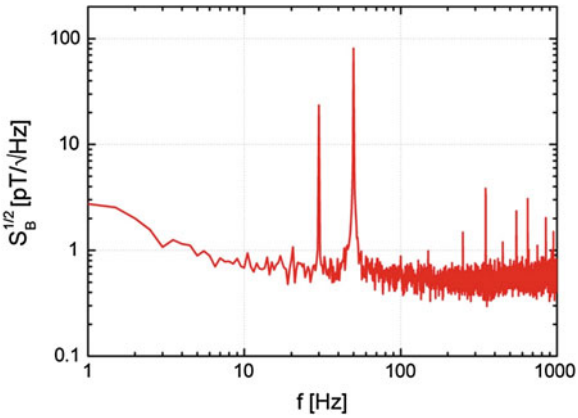

Fig. 2 Equivalent field sensitivity of the Nb-mixed sensor coupled with a flux-transformer obtained from the power spectrum density, calibrated using a test signal of 25 pT at 30 Hz, generated by an external coil. The main power supply (50 Hz) signal is of the order of 80 pT in the MSR. At 10 Hz, the detectivity is around 700 $\mathrm{fT}/\sqrt{\mathrm{Hz}}$

healthy subjects has been performed in the shielded room of Neurospin in Saclay (Pannetier-Lecoeur et al. 2011; Campiglio et al. 2012) with both Nb-based mixed sensors and YBCO-mixed sensors. Figure 3 gives an example of MCG signals recorded during that study.

In order to perform MEG measurements the detectivity of the mixed sensors has to be improved to achieve the fT range at frequencies below 10 Hz. To achieve this goal we choose to couple the mixed sensor with a Nb wire-made flux transformers. First attempts to record an auditory evoked response are encouraging and demonstrate that mixed sensors are capable of detecting MEG signals.

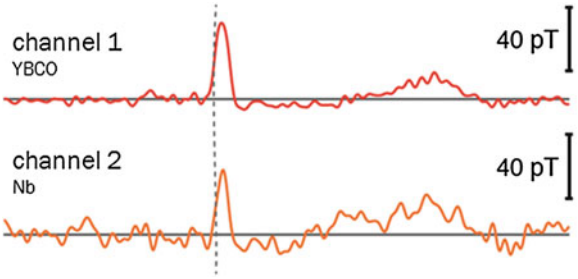

Fig. 3 MCG signals recorded simultaneously using a YBCO (*top*) and a Nb (*bottom*) -mixed sensors. The two sensors are 5 cm apart, center-to-center on a plane parallel to the patient's chest

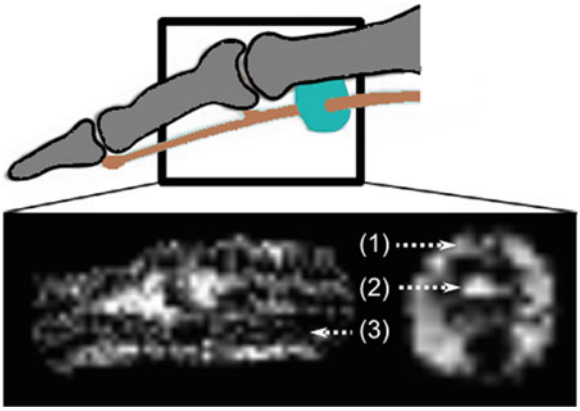

Fig. 4 Sagittal (*left*) and axial (*right*) slice of a finger at 7.4 mT with a resolution of $4 \times 1 \times 1$ mm^3 for a total acquisition time of 15 min. Anatomical details like (1) fat, (2) marrow or (3) tendon can be identified

5 MRI at Very Low Fields

Very low field MRI can offer solutions for portable, silent, open access systems, with a lower price due to the fact that no superconducting coils are required for the static field generation. Besides, spin relaxation mechanisms below 400 kHz offer a new diagnosis perspective through enhanced contrast-to-noise ratio. Due to the weakness of the resonant signal produced, very sensitive sensors, operating at low field/low frequency should be used. Mixed sensors are therefore good candidates because of their high sensitivity and robustness, which allows one to apply RF pulses for NMR sequences without a need to isolate the sensors electrically. Furthermore, the detectability of mixed sensors is much better at the Larmor frequency, 426 kHz at 10 mT, due to the absence of 1/f noise and levels below 10 fT/sqrt (Hz) are achieved in this frequency range.

To avoid using a prepolarizing field, mixed sensors can be used in static fields of 1–10 mT, where the proton spin polarization is not too weak, and using standard NMR sequences, without switching off the static field. This allows the use of fast acquisition sequences. Based on these ideas, we have developed a low field MRI setup operating between 5 and 10 mT with copper coils for both static field and gradients (Dyvorne et al. 2009; Herreros et al. 2013). The detection of the signal is

achieved with a mixed sensor coupled to a copper flux transformer. The cooling system for the sensor is a pulse-tube cryocooler. The field of view is $6 \times 6 \times 6$ cm^3. Voxel resolution of about 1 mm^3 is obtained (Fig. 4).

6 Conclusion and Perspectives

Spin electronics-based sensors offer a new alternative for biomagnetism and low field MRI. They are competitive with SQUIDs at high frequencies but are still limited at low frequencies due to their high 1/f noise. However, this technology is rather new and a lot of improvements are possible. First, the sensitivity of the magnetoresistive elements have been improving regularly, particularly due to the development of tunnel magnetic junctions. This development has resulted in improved sensitivity by a factor of 20, but they are more difficult to incorporate with superconductors. Second, the use of intermediate flux transformers also needs to be optimized for mixed sensors as it has been done for SQUIDs for decades. Finally, switching of supercurrents to modulate the field seen by the GMR element is a way to significantly reduce the 1/f contribution at low frequencies.

References

Campiglio P, Caruso L, Paul E, Demonti A, Azizi-Rogeau L, Parkkonen L, Fermon C, Pannetier-Lecoeur M (2012) GMR-based sensors arrays for biomagnetic source imaging applications, IEEE. Trans Magn 48:3501–3504

Dyvorne H, Fermon C, Pannetier-Lecoeur M, Polovy H, Walliang AL (2009) NMR with superconducting-GMR mixed sensor. IEEE Trans Appl Supercond 19:819–822

Herreros Q, Dyvorne H, Campiglio P, Jasmin-Lebras G, Demonti A, Pannetier-Lecoeur M, Fermon C (2013) Very low field magnetic resonance imaging with spintronics sensors. Rev Sci Instrum 84:095116

Pannetier M, Fermon C, Le Goff G, Simola J, Kerr E (2004) Femtotesla magnetic field measurement with magnetoresistive sensors. Science 304:1648–1650

Pannetier-Lecoeur M, Parkkonen L, Sergeeva-Chollet N, Polovy h, Fermon C, Fowley C (2011) Magnetocardiography with sensors based on giant magnetoresistance. Appl Phys Lett 98:153705

Index

A

Abnormal slow wave activity, 146, 624, 667, 669, 778, 859, 860
Acetylcholine, 610, 878, 882, 892, 906
Active compensation, 14, 44, 47, 62, 63, 66
Adults who stutter (AWS), 802, 805–808, 810, 811, 813, 814
Aging, 147, 439, 458, 526, 582, 610–614, 617–621, 629–631, 633, 658–662, 664, 666, 669, 670, 723, 790, 885
Alcohol, 530, 539, 547, 878, 890–892
Alpha, 30, 130, 168, 216, 218, 221, 222, 224, 228, 231, 267, 301, 311, 324, 343, 347, 360, 367, 373, 381, 387, 389, 390, 418, 419, 421, 435, 437, 439, 463, 465, 468, 471, 528, 529, 533, 534, 624, 625, 759, 857, 862, 881
  Alpha oscillation, 221, 301, 367, 370, 387, 390, 416, 435, 532, 758
Alzheimer's disease, 342, 421, 432, 469, 470, 610, 625, 626, 658, 659, 663, 790, 850, 876, 883, 907, 989
AMICA, 200, 201, 204, 208, 211
Amphetamine, 887–889
Analog signal processing, 10, 11
Anesthesia, 440, 824, 889, 890, 893
Artifact, 15, 19, 23, 24, 37, 40, 50, 56, 60, 61, 65, 130, 132, 134, 135, 137, 138, 140, 144–146, 154, 157, 168, 176, 189, 201, 204, 208, 223, 228, 259, 280, 329, 332, 376, 423, 455, 458, 536, 602, 667, 785, 809, 824, 825, 934, 935, 966
Artifacts of volume conduction, 477–501
Atomic magnetometer, 26–28, 31, 950
Attention, 26, 43, 87, 143, 168, 222, 230, 279, 323, 345, 382, 386, 387, 389, 391, 415, 418, 435, 437, 452, 454, 458, 466, 469, 471, 528, 529, 539–541, 545, 559, 562, 568, 582, 583, 613, 614, 619, 620, 698, 700, 703, 729, 732, 734, 757, 887
Attention deficit hyperactivity disorder, 469, 470, 879, 887–889
Auditory, 1, 19, 28, 130, 131, 137, 143, 151, 156, 164, 172, 188, 287, 290, 301, 303, 345, 361, 387, 390, 510, 511, 517, 519, 530, 539, 544, 585, 585, 588, 589, 620, 642, 649, 664, 666, 688, 691, 715, 717, 718, 724, 805, 811
Auditory cortex, 164, 174, 175, 188, 301, 389, 415, 471, 511, 530, 544, 620, 621, 650, 666, 680, 682, 692, 696, 700, 701, 703, 888, 813, 814, 834, 853, 854, 858, 862
Auditory evoked fields, 19, 28, 174, 602, 603, 680–682, 685, 688, 715, 834, 862
Auditory evoked response (AER), 514, 516, 517, 521
Auditory processing, 530, 544, 589, 590, 620, 621, 718, 720, 854
Auditory scene analysis, 697
Autism, 529, 530, 539, 560, 564, 566, 580, 584, 588, 590, 606, 803, 815, 852
  ASD, 530, 539, 564–568, 580–582, 584, 588–590
Averaging, 19, 25, 130, 136, 142, 145, 147, 168, 248, 272, 370, 455, 543, 643, 689, 700, 788

B

Bayesian inversion, 259, 287
Bayesian methods, 259, 287
Beamforming, 65, 93, 172, 265, 266, 271, 328, 329, 416, 417, 456, 861, 862, 885, 886
  Beamformer, 37, 53, 65, 172, 256, 259, 265, 266, 267, 277, 286, 312, 313, 327, 331, 334, 347, 415, 455, 457, 484, 562, 620, 648, 808, 862, 880, 883, 925, 927
BEM, 96, 111, 112, 114–116, 123, 201, 205, 259, 291
Benzodiazepines, 366, 880

S. Supek and C. J. Aine (eds.), *Magnetoencephalography*,
DOI: 10.1007/978-3-642-33045-2, © Springer-Verlag Berlin Heidelberg 2014

Beta, 222, 297, 471, 835, 864, 865
Beta oscillations, 311, 365, 366, 392, 393, 880, 881
Biomarkers, 421, 469, 623, 629, 631, 63, 658, 660, 662, 814, 845, 852, 876, 879, 886, 893, 935, 980, 986
Biophysical modeling, 185, 346, 350, 351, 391
Bipolar disorder, 853
Brain connectivity, 419, 423, 478
Brain imaging, 164, 169, 170, 172, 174, 185, 248, 253, 430–432, 438–440, 442, 443, 511, 513, 562, 585, 642, 728, 803, 814, 902, 965
Brain oscillations, 359–361, 382, 393, 418, 419, 810, 885
Broca's area, 322, 366, 567, 568, 583, 718, 768, 807, 810, 811, 813–814

C

Calibration accuracy, 50, 52, 59, 61
Categorization, 239, 589, 858, 905, 908, 909, 914
Children, 431, 439, 440, 511, 526–534, 536–540, 546, 559, 568, 571, 580, 582, 585, 589, 602, 646, 650, 808, 814, 831, 853, 865, 926, 927
Children who stutter (CWS), 458, 459, 808–810
Cognition, 26, 219–221, 224, 230, 323, 360, 382, 430, 431, 437, 442, 453, 454, 531, 541, 559, 564, 581, 583, 590, 613, 615, 630, 661, 664, 719, 734, 744, 758, 768, 785, 858, 877, 882, 926, 934, 935
Cognitive deficit, 286, 438, 613, 616, 617, 850
Cognitive inhibition, 912
Coherence, 27, 135, 176, 177, 260, 287, 295, 297, 311, 333, 335, 336, 342, 349, 351, 379, 382, 383, 408, 409, 412, 432, 438, 456, 466, 478, 605, 625, 811, 885, 886, 952, 957
Computational modeling, 322, 325, 584, 626
Connectivity, 30, 123, 175–177, 221, 230, 256, 264, 267, 271, 287, 288, 297, 316, 322, 326, 329, 330, 335, 339, 342, 344, 348, 406, 410, 411, 413, 421, 443, 455, 459, 465, 469, 528, 532, 584, 606, 619, 625, 631, 660, 844, 861, 934
Consciousness, 431, 435, 443, 890
Cooling, 28, 31, 66, 602, 770
Corollary discharge, 728, 735
Correlation, 17, 25, 61, 64, 90, 98, 178, 220, 223, 228, 231, 294, 323, 326, 329–331, 337, 341, 345, 348, 379, 418, 420, 428, 457, 459, 471, 583, 605, 620, 624, 666, 699, 745, 773, 879, 885, 908
Cortical Development, 922
Cortical dysplasia, 646, 830, 831, 832, 845, 922, 924
Cortical magnification factor, 149, 783, 784
Cortical networks, 157, 253, 432, 546, 570, 886, 933
Cortical oscillations, 172, 173
Cortico–cortical, 260, 335, 344, 347, 432, 433, 730
Cortico–thalamic, 434
Cross correlation, 294, 407, 409, 413, 773, 774
Cross–network interaction, 458, 459, 461, 463, 464, 466–468, 471
Cross–talk, 37, 41, 49, 50, 177, 187, 994
Cryocooler, 31, 1005
Current dipole, 6, 20, 22, 58, 74, 78, 86, 87, 92–95, 99, 101, 102, 109, 167, 169, 187, 286, 413, 605, 718, 738, 805, 825, 879, 924, 975, 980

D

Data acquisition, 131, 142, 156, 157, 193, 288, 369, 527, 535, 537, 600, 602, 791, 942, 961
Data fusion, 185, 190
Default Mode Network, 301, 323, 347, 348, 417, 418, 452, 453, 455, 457, 458, 462, 463, 465, 528, 626, 814, 888
Delta, 216, 222, 228, 368, 373, 390, 391, 434, 438, 471, 605, 624, 859, 860, 862, 864
Delta oscillations, 368, 390, 391
Development, 30, 31, 46, 74, 172, 178, 239, 253, 272, 288, 302, 323, 324, 333, 346, 360, 391, 423, 431, 453, 499, 510–514, 517, 519, 521, 526, 527, 530–533, 537–540, 542, 544–546, 558, 559, 561–564, 566–569, 572, 581–584, 590, 600, 605, 606, 613, 618, 627–629, 632, 643, 644, 667, 746, 750, 771, 802, 809, 810, 815, 846, 850, 853, 876–879, 882, 883, 886, 890, 893, 906, 908, 922, 934 , 956, 963, 963, 988, 998, 1005
Dewar, 10–12, 15, 19, 38, 67, 143, 150, 572, 600–603, 643, 961, 964, 981, 984, 988
Diffusion tensor imaging, 583, 831
Digital signal processing, 4, 10, 15, 135
Dipole, 65, 78, 74, 79, 86, 93, 96, 98, 100, 102, 110, 202, 205, 216, 238, 287, 299, 328, 410, 484, 498, 680, 755, 831, 854, 856, 859, 925
Dipole modeling, 117, 287, 290, 543, 695
Dipole analysis, 247, 248

Dopamine, 610, 802, 812, 850, 878, 883, 892, 905
Dyslexia, 439, 440, 580–586, 588, 590, 852

E
Eating behavior, 902, 904–908, 914
EEG/MEG modeling, 210
EEGLAB, 199–204, 211, 302
Electroencephalography (EEG), 39, 61, 63, 64, 74, 75, 78, 80, 86–88, 93, 122, 132, 134, 135, 164, 165, 168, 176, 184, 186, 191, 201, 204, 207, 214, 218, 223, 231, 238, 248, 253, 259, 316, 324, 348, 393, 438, 452, 493, 526, 532, 545, 590, 632, 653, 666, 687, 777, 823, 826, 842, 854, 878, 922, 923, 926, 994, 997
eLORETA, 484, 485, 491, 499
Epilepsy, 24, 85, 122, 131, 270, 344, 470, 530, 568, 646, 652, 653, 803, 810, 815, 822, 824, 846, 926, 934, 963
Epilepsy surgery, 270, 815, 934
Epileptogenic zone, 822–824, 826, 828, 830, 831, 845, 846, 922
Event related desynchronization (ERD), 503, 532, 533, 570, 623, 835, 863, 865, 869, 881, 882
Event-related fields (ERFs), 259, 279, 314, 774, 777, 779, 784, 786, 834, 879, 909, 912
Event-related potentials (ERPs), 146, 202, 203, 207, 227, 230, 280, 314, 515, 559, 564, 585, 734, 771, 772, 774, 777, 784, 785, 805, 878
Evoked responses, 64, 94, 100, 130, 131, 147, 156, 166, 169, 172, 207, 257, 295, 297, 313, 314, 518, 530, 533, 543, 642, 688, 715, 719, 777, 785, 805, 813, 851, 1003
Executive function, 558, 562, 564, 610, 619, 661, 662, 905, 908, 911, 912
Experimental design, 130, 140, 143, 155, 157, 189, 203, 332, 618
Extended sources, 109, 187, 290, 330, 787, 788, 825
Extrastriate, 772, 778, 779, 781, 783

F
Faces, 102, 113, 529, 531, 558–561, 564–566, 615, 745, 858, 879
FDG-PET, 661, 662, 822, 823, 831
Feedback, 8, 9, 37, 41, 44, 49, 62, 63, 143, 311, 362, 363, 433, 602, 728, 735, 736, 738, 739, 768, 770–772, 779, 789, 805, 812, 813, 904, 908, 976, 996
FEM, 112, 116–118, 201, 205, 942
Fetal brain maturation, 513, 521
Fiber tracts, 801
Field computation, 107
Field spread, 264, 267, 324, 325, 326, 327, 336, 406, 408, 410, 411–413, 416–416, 423, 455, 461
Flux-locked loop, 8, 15, 165
fMRI, 132, 134, 149, 164, 175, 176, 184, 185, 186, 189, 190–192, 214, 215–231, 238, 248, 249, 251, 253, 271, 286, 289, 301, 316, 323, 324, 333, 337, 339, 340, 345, 346–351, 387, 394, 418, 419, 421, 423, 443, 457, 461–468, 471, 478, 486, 514, 526–528, 529, 532, 533, 537, 540, 542, 545, 560, 561, 569, 584, 585, 589, 600, 604, 606, 611–613, 618–620, 623, 630, 631, 646, 663–665, 667, 680, 687, 689, 695–697, 702, 728, 729, 750, 751, 753, 756, 759, 761, 769, 772, 781, 783, 789, 804, 805, 810, 811, 813, 814, 844, 845, 862, 867, 877, 890, 906, 909, 922, 924, 942, 973
  BOLD fMRI, 214, 215–218, 220, 221–223, 249, 664, 697
  Functional magnetic resonance imaging, 164, 266, 323, 585, 728, 746, 804
Focal epilepsy, 823, 828, 831
Food, 470, 902, 903, 904–907, 909, 911, 912, 913, 914
Forward models, 36, 119, 166, 239
Forward problem, 73, 74, 78, 108, 122, 123
Forward simulator, 238, 241, 249, 250, 251, 289
Frequency domain, 16, 18, 130, 176, 177, 310, 312, 334, 369, 372, 375, 376, 381, 407, 408, 455, 456, 461, 498, 605, 624, 666, 667, 880, 888
Frequency signature, 470
Frontal lobe, 267, 558, 562–567, 569, 572, 611, 617, 630, 648, 653, 660–663, 689, 703, 768, 803, 804, 826, 828, 855
Functional connectivity, 29, 30, 176, 177, 178, 260, 265, 266, 267, 270–272, 287, 288, 295, 297, 304, 323, 324, 325, 327, 329, 330–334, 336, 337, 339, 340, 344, 346, 347–349, 351, 352, 393, 406, 416, 418, 423, 430–432, 436, 437, 439, 441, 442, 455–457, 458, 465, 469, 470, 471, 532, 613, 618–620, 623, 625, 626, 627, 629, 663, 670, 773, 811, 844–846, 890, 934
  Functional connectivity dynamics, 432, 437, 439

G
GABA, 325, 346, 362, 364, 865, 866, 877, 878, 880, 881, 892, 906
Gamma, 30, 146, 147, 216, 228, 295, 297, 301, 313, 325, 336, 344, 345, 347, 361, 362–366, 368, 374, 377, 382, 383–387, 391, 392, 415, 421, 430, 432, 434, 435, 437–441, 469, 471, 480, 503–505, 506, 529, 533, 540, 570, 588–590, 605, 623, 625, 666, 682, 688, 689, 758, 759, 768, 772, 835, 857, 858, 860, 861, 866, 881, 882, 885, 886, 888, 889
  Gamma oscillation, 364
Glutamate, 346, 362, 877–879, 906
Graph Theory, 264, 268, 269, 419, 420, 421, 422, 423, 470, 625–627, 867
Group statistics, 421

H
Head model, 78, 80, 81, 83, 85, 95, 96, 114, 167, 186, 188, 204, 205, 208, 257, 258, 291, 789, 792
High-temperature SQUID, 4
Hippocampal sclerosis, 829
Homeostatic control, 902, 908, 911, 914

I
Ictal EEG, 823
Ictal SPECT, 831, 922
Imaginary part of coherency, 267, 412, 413, 480, 491, 493, 528
Independent component analysis (ICA), 23, 53, 54, 63, 64, 146, 168, 199, 201, 202–205, 208, 210, 211, 220, 223–228, 231, 288, 302, 303, 323, 339, 340, 345, 348, 351, 416, 417, 456–459, 461–464, 470, 471, 482, 486, 927
Inferior frontal gyrus, 562, 567, 570, 805, 807, 811, 813, 814
Informational masking, 701–703
Inhibition, 351, 362, 364–368, 387–390, 434–439, 438, 558, 561–563, 566, 568, 611, 613, 614, 693, 757, 758, 761, 834, 864, 888, 905, 912, 914
Insulin, 470, 902, 903, 905–909, 911, 914
Interference, 22, 36, 37–42, 44–48, 50–63, 65–68, 165, 168, 170, 172, 174, 184, 326, 327–329, 541, 613–616, 630, 701, 757, 935, 988
Interictal spikes, 825, 826, 828, 923, 927
Intracarotid amobarbital procedure, 835
Intracranial data, 256
Intracranial EEG, 256, 261, 680, 823, 824, 826, 828, 831, 836, 886, 926
Intrinsic connectivity, 230
Inverse method, 414, 483–485, 499
Inverse problem, 86, 88, 92, 102, 169, 184, 190, 265, 286, 325, 346, 459, 465, 825, 923, 942, 974, 981
Inverse procedures, 122, 286, 297, 664, 787
  Algorithms, 36, 48, 50, 116, 123
  Inverse algorithms, 169, 249, 787
Itch, 750, 759–761

K
Ketamine, 879

L
Language, 141, 164, 201, 239, 244, 261, 322, 360, 439–441, 453, 458, 466, 505, 517, 530, 544, 564, 567–571
Language dominance, 568
Language processing, 503, 544, 585, 590, 788, 804–806, 815
Lead field, 45, 46, 48, 86–88, 175, 257, 258, 328, 331, 480
Levodopa, 883, 885
Linear metrics, 333
Localization, 23, 27, 30, 39, 53, 92–94, 96–98, 102, 120, 123, 167–169, 171, 176, 184, 186, 190, 202, 208, 210, 216, 248, 259, 260, 286–289, 291, 293, 294, 299, 987
Long-range Connectivity, 346, 433
Low-field MRI, 942, 943, 956, 957, 963, 964

M
M50, 621, 808, 851, 853, 856–858, 867
M100, 156, 530, 531, 603, 852–857, 863
Magnetic resonance imaging (MRI), 29, 30, 39, 67, 78, 80, 87, 95–97, 103, 119, 120, 132, 134, 137, 140, 150, 164, 168, 185, 188, 215, 228, 238–242, 248, 252, 253, 256–259, 266, 289, 290, 299, 300, 302, 323, 347, 394, 418, 440, 442, 443, 456, 479, 488, 511, 514, 526, 527, 536, 537, 543, 545, 569, 582, 583, 585, 600, 610, 651, 652, 658, 660–662, 665, 668, 669, 684, 693, 728, 746, 768, 769, 774, 776, 804, 808, 822–824, 827, 829, 831–833, 836, 846, 877, 878, 881, 887, 890, 906, 912, 922–925, 936, 941–954, 956–968, 973, 974, 976, 977, 984, 985, 994, 1001, 1004, 1005

Magnetic response, 621, 751, 754–756, 758, 760
Magnetic shielding, 12, 16, 22, 41–44, 75, 68, 165
Magnetic source imaging, 60, 822, 836
Magnetically shielded room, 3, 11, 16, 18, 29, 41, 63, 66, 68, 515, 650, 950, 962, 976
Magnetoencephalography (MEG), 4–20, 23, 26, 27, 30, 31, 36–38, 39–68, 74, 75, 78, 80, 85–89, 92, 94–96, 99, 102, 108, 112, 114, 117, 121, 129–147, 150–152, 154–157, 164–178, 184–193, 200–211, 214–230, 238–253, 256–260, 264–272, 279–284, 286–303, 309–317, 322–351, 360–394, 406–423, 430–443, 455–471, 478–498, 504, 505, 509, 510, 513–516, 526–547, 558–572, 581–590, 599–606, 612–633, 642–644, 645–654, 662–670, 680–703, 713–724, 728–747, 750–761, 768–792, 801–815, 822–836, 844–847, 851–867, 878–893, 902–927, 933–937, 942–969, 974, 979–989, 994–1003
Magnetometer, 4, 6, 14, 18, 26, 27, 29, 31, 39, 40, 46, 48, 56, 62, 202, 641, 643, 925, 950, 965, 975, 995, 996, 997
Maximum likelihood estimation, 88, 89, 169
MEEG, 201–211
MEG-SIM, 249, 288, 289, 295, 302
Memory, 116, 118, 155, 230, 287, 290, 293, 295, 296, 303, 322, 385, 386, 388–392, 415, 416, 420, 421, 431, 433, 435–437, 453, 454, 470, 528, 531, 532, 540–542, 583, 585, 610, 611, 613–617, 619–624, 626–631, 658, 659, 661–663, 665 , 669, 714, 716, 717, 745, 768–772, 778, 789–792, 856, 863–865, 877, 879, 882, 883, 891, 892, 903, 906, 907, 911–914
Mental imagery, 719
Minimum norm, 17, 171, 174, 189, 259, 286, 287, 299–301, 313, 324, 332, 349, 414, 415, 417, 421, 458, 541, 543, 881, 925
  Minimum norm solution, 101, 103
Mismatch negativity, 290, 443, 621, 696, 715, 878, 879
  MMNm, 621, 715, 854, 855, 879
MMF, 854
MOCA, 484, 487, 491, 493–495, 498, 499
Motor, 138, 139, 142, 143, 154, 155, 178, 217, 271, 311, 313, 323, 325, 326, 329, 332, 334–336, 343, 345, 389, 392, 393, 411, 412, 430, 434–436, 442, 443, 457, 458, 463, 464, 471, 480, 484, 486, 503, 504, 527, 540, 544, 561, 562, 584, 606, 619, 620, 648, 720, 722, 723, 727–730, 732–736, 738, 739, 759, 770, 773, 804, 805, 807, 808, 810, 811, 813, 814, 825, 831, 834, 865, 878, 880, 881, 884–886, 888, 892, 893, 936, 974
Motor command, 728, 729, 733, 735, 736, 738
Multi-start minimization, 238, 244, 253
Multichannel measurement, 38
Multimodal, 184, 185, 192, 193, 200, 201, 203, 207, 214, 227, 347, 381, 431, 443, 615, 689, 720–722, 845, 878, 880, 886, 892
Multisensory integration, 134, 714, 736
Multivariate models, 176, 349, 417
Music, 679, 694, 713–720, 722–724
MUSIC, 100, 169, 245–247, 253, 489–492, 498, 499, 925, 927

N

N100m, 621, 681, 684, 685, 834
Networks, 157, 177, 178, 185, 192, 214, 215, 218, 222–225, 230, 231, 253, 260, 264, 266, 268, 269, 271, 272, 288, 304, 310, 316, 323, 325, 336, 337, 340, 343, 345, 346, 348, 352, 365, 393, 406, 415–421, 423, 430, 432, 435, 436, 438, 440, 442, 443, 454, 455, 457–459, 462–464, 466–471, 478, 526–534, 540, 546, 547, 570, 606, 611, 612, 617, 619, 620, 623, 625, 626, 629, 630, 633, 643, 662, 666, 670, 715, 719, 720, 723, 738, 769, 770, 772, 814, 815, 845, 886, 902, 904, 905, 907, 908, 911, 914, 924, 926–928, 933, 935, 937
Neurology, 270, 436, 437, 606, 746
Neuromodulators, 880, 883
Neuronal currents, 86, 87, 94, 176, 959, 974, 975, 977
Neuronal networks, 316, 365, 430, 533, 633, 715, 723
Noise suppression, 64, 68, 935, 990
Non-linear metrics, 336
Nonmagnetic stimuli, 28

O

Obesity, 469, 470, 510, 901, 902, 907, 908, 914
Off-response, 141, 785, 786
On-response, 785
Oscillations, 135, 147, 172, 173, 178, 216, 221, 260, 295, 297, 301, 302, 304, 311, 324–326, 336, 344, 346–348, 359–370, 374, 376, 377 , 379, 381, 382, 387, 394, 413, 418, 419, 430, 437, 438, 452, 463,

469, 478, 529, 606, 666, 758, 759, 761, 805, 810, 835, 849, 863, 866, 882, 890, 907, 936, 962
Functional and cognitive relevance of oscillations, 271
Oscillation activity, 606, 761

P
P50m, 621, 681, 682, 807, 808
Pain, 749, 750–754, 757, 758, 761
Pain modulation, 749, 757
Parkinson's disease, 135, 263, 270, 342, 812, 850, 875, 883, 884, 893, 935
Pediatric, 138, 527, 530, 531, 535, 537, 538, 540, 543–545, 604, 606, 645–647, 650, 653, 654, 831, 890, 921, 923, 924
People who stutter (PWS), 804, 805, 811, 814
Perceptual awareness, 701, 703
Pharmacology, 877, 880
Phonology, 585, 804
Physostigmine, 882
Pitch, 694–696, 698, 714, 718, 720, 724
Precuneus, 454, 469, 470, 529, 619, 629, 663, 760, 761, 861
Prefrontal cortex, 301, 316, 322, 390, 392, 435, 454, 511, 610–612, 615, 669, 770, 771, 882, 886, 905, 907
Premotor, 529, 774, 805, 814, 885
Pre-surgical evaluation, 503, 569, 646, 822, 823, 832, 836
Primary somatosensory cortex, 169, 751, 833, 834
Principal component analysis, 23, 55, 63
Phase slope index (PSI), 153, 344, 477, 494, 497
Psychiatry, 437

Q
Quasistatic approximation, 74–77, 110

R
Radial, 19, 59, 79, 88, 95, 113, 164, 175, 186–188, 202, 204, 205, 208, 214, 684, 774, 777, 826
Reading, 238, 248, 544, 567, 579, 580–586, 589, 590, 619, 689, 805, 852
Resting state, 132, 177, 178, 221–223, 230, 260, 270, 271, 301, 302, 323, 326, 328, 335, 340, 351, 405, 416, 418, 423, 452, 471, 479, 527, 528, 758, 810, 811, 814, 863, 885, 907, 908
Resting State Networks, 451, 455, 458, 462, 470, 546, 620, 907
Retinotopy, 778, 780, 781
Reward, 470, 744, 745, 883, 904, 911

S
Schizoaffective disorder, 853, 860, 866
Schizophrenia, 178, 342, 343, 767, 849–867
Secondary somatosensory cortex, 153, 751, 936
Segmentation, 117, 238, 239, 244, 291, 479, 588
Selective adaptation, 686, 692, 693, 698
Selective attention, 435, 437, 698, 700, 772, 864
Semantics, 585, 589, 804
Sensory, 129, 138, 140, 154, 155, 168, 177, 219, 251, 288, 302, 303, 311, 323, 389, 422, 432–435, 451, 471, 478, 526, 535, 630, 653, 692, 701, 703, 720, 727, 728, 856, 904, 905, 908
Sensory gating, 807, 849, 856, 857, 858, 867, 879
Signal processing, 3, 4, 15, 38, 46, 48, 50, 65, 199, 237, 247, 280, 359, 360, 443, 517, 600, 632, 809, 965
Signal space, 20, 36, 48, 51, 53–55, 58, 59
Signal space projection, 15, 51, 55, 65, 68, 968
Signal space separation, 15, 51, 68, 968
Simulations/Simulated data, 22, 30, 108, 110, 172, 173, 177, 188, 253, 257, 288–293, 295, 297, 299–302, 304, 315, 410, 457, 462, 649, 714, 716, 856
sMRI, 249
Somatosensory, 93, 120, 131, 137, 138, 143, 152, 169, 288, 290, 301, 386, 389, 419, 503, 530, 539, 544, 621, 728, 729, 735, 821
Somatosensory evoked potential, 729, 730, 833
Somatosensory information, 729, 732, 734, 739
Sound lateralization, 691, 703
Source localization, 27, 39, 120, 123, 168, 171, 176, 184, 190, 202, 286, 289, 299, 421, 546, 642, 696, 751, 777, 847, 864, 922, 925, 927, 934, 984
Source reconstruction, 36, 108, 109, 123, 168, 172, 255, 256, 261, 265, 266, 330, 417, 606, 632, 653, 861, 909
Source separation, 63, 204, 222, 224
Source statistics, 260, 266
Spatial filtering, 16, 19, 54, 55, 56, 65, 174, 346, 620, 968

Spatiotemporal, 164, 184, 203, 214, 223, 225, 237, 288, 572, 875, 878, 880, 892, 927, 965
Spatiotemporal dynamics, 218
Speech perception, 586, 588, 806, 807
SQUID, 3–11, 16, 19, 27, 29, 31, 36, 146, 165, 184, 600, 945, 950, 951, 956, 960, 982, 988, 993, 994, 998, 1002, 1005
SQUID MRI, 942
Stimulus integration, 134, 390, 435, 454
Stimulus size, 778, 783, 787
Stream segregation, 679, 697
Striate, 783
Stuttering, 801–805, 808–810, 812, 815
Synchronicity, 290, 433, 732, 773
Synchronization, 170, 177, 219, 267, 336, 340, 361–363, 365, 381, 382, 384, 385, 390–392, 407, 413, 415, 421, 429, 431, 433, 435, 439, 455, 528, 570, 612, 625, 627, 629, 631, 666, 719, 772, 821, 907

T
Tangential, 27, 59, 95, 113, 164, 167, 186, 208, 680, 774, 777, 826, 831, 935, 997
Thalamo-cortical, 429, 430–435, 437, 438
Theta, 216, 228, 345, 347, 368, 435, 466, 772, 860, 862, 864
  Theta oscillations, 348, 362, 366, 391, 392, 891
Theta alpha, 532
Tiagabine, 881
Time-frequency, 50, 147, 169, 172, 199, 257, 259, 329
Time-frequency analysis, 147, 314, 584, 689
Timing Parameters, 136, 142
Tinnitus, 713, 723, 724
Training-related plasticity, 713, 720
Traumatic brain injury, 430, 440, 443, 444
Treatment, 343, 344, 440, 469, 510, 521, 532, 533, 544, 631, 723, 724, 807, 811, 812, 814, 822, 824, 831, 850, 860, 876–879, 883–886, 888, 889, 893, 902, 914, 928, 934, 989

U
Ultra-low-field MRI, 941–943, 956, 957, 963
  ULF MRI, 67, 945, 947–950, 952, 953, 954, 956–960

V
Visual, 53, 129, 131, 135, 138, 143, 148, 207, 245, 290, 463, 509, 518, 700, 734, 735, 825
Visual areas, 189, 221, 295, 344, 419, 768, 781, 786, 909, 911
Visual cortex, 149, 207, 290, 295, 386, 391, 513, 769, 772
Visual evoked response (VER), 514, 516, 519
Visual field, 143, 189, 385, 768, 780, 782
Visual information, 734, 735, 739
Visual processing, 155, 390, 781, 807, 813, 908
Visual system, 1236, 138, 362, 389, 512, 539, 728, 772, 785, 905
Visualization, 30, 199–201, 211, 238, 239, 256, 257, 259, 529, 600
Volume conduction, 123, 176, 214, 216, 263, 272, 316, 324, 457, 498, 499, 528, 626, 642, 844
Vowel, 280, 588, 589, 696, 808, 853

W
Wernicke's area, 567, 807, 813
Working memory, 155, 287, 290, 293, 295, 296, 322, 415, 531, 540, 583, 611, 613, 614, 661, 662, 669, 767, 789, 791, 856, 863, 883, 911, 912, 914, 933